Proceedings of International Conference on
Studies in Engineering, Science, and Technology

NOVEMBER 7-10, 2024   Istanbul/TURKIYE

EDITORS
Prof.Dr. Abid Ali Khan
Prof.Dr. Muhammet Demirbilek
M. Lutfi Ciddi

istes
Organization

www.icsest.net

Volume 1, Pages 1-609

Proceedings of International Conference on Studies in Engineering, Science, and Technology

© 2024 Published by the ISTES

ISBN: 978-1-952092-71-8

Editors: Abid Ali Khan, Muhammet Demirbilek, & M. Lutfi Ciddi

Articles: 1-48

Conference: International Conference on Studies in Engineering, Science, and Technology (ICSEST)

Dates: November 7-10, 2024

Publication Date: December 31, 2024

Location: Istanbul, Turkiye

Conference Chair(s):

Omid Noroozi, Wageningen University and Research, the Netherlands

Stephen Jackowicz, University of Bridgeport, United States

Presidents

Omid Noroozi, Wageningen University and Research, the Netherlands

Stephen Jackowicz, University of Bridgeport, United States

Scientific Board

Janice Fournillier, Georgia State University, United States

Wilfried Admiraal, Leiden University, Netherlands

Elizabeth (Betsy) Kersey, University of Northern Colorado, United States

Anastasios Theodoropoulos, University of Peloponnese, Greece

Abid Ali Khan, Military Technological College (MTC), Oman

Arturo Tobias Calizon, University of Perpetual Help System Dalta, Philippines

Brett Buttliere, Technical University Dresden, Germany

Cara Williams, Emirates College For Advanced Education, United Arab Emirates

Chandra Pratama Syaima, University of Lampung, Indonesia

Chris Plyley, University of the Virgin Islands, Virgin Islands

Claudiu Mereuta, Dunarea De Jos University of Galati, Romania

Dana Aizenkot, Ashkelon Academic College, Israel

El Takach Suzanne, Lebanese University, Lebanon

Farouk Bouhadiba, University of Oran 2, Algeria

Frank Angelo Pacala, Samar State University, Philippines

Hou-Chang Chiu, Fu-Jen Catholic University Hospital, Taiwan

Irena Markovska, Assen Zlatarov University, Bulgaria

Irina Andreeva, Peter The Great St. Petersburg Polytechnic University (SPBPU), Russia

Iwona Bodys-Cupak, Jagiellonian University, Poland

Jaya Bishnu Pradhan, Tribhuvan University, Nepal

Jean-Yves Gantois, ICHEC, Belgium

Kassa Mickael, Addis Ababa University, Ethiopia

Kemmanat Mingsiritham, Sukhothai Thammathirat Open University, Thailand

Kristyna Balatova, University of Zilina, Slovakia

Milan Kubiatko, Jan Evangelista Purkyně University, Czech Republic

Neide Da Fonseca Parracho Sant'anna, Colegio Pedro II, Brazil

Oguz Akturk, Necmettin Erbakan University, Turkey

Ossi Autio, Univertsity of Helsinki, Finland

Philomina Ifeanyi Onwuka, Delta State University, Nigeria

Sharif Abu Karsh, Arab American University, Palestine

Shenglei Pi, Guangzhou University, China

Siew Nyet Moi, Universiti Malaysia Sabah, Malaysia

Sindorela Doli Kryeziu, University of Gjakova, Albania

Siti Sarawati Johar, Universiti Tun Hussein Onn Malaysia, Malaysia

Sodangi Umar, Federal University Gusau, Nigeria

Tayfur Ozturk, Necmettin Erbakan University, Turkey

Theodore Chadjipadelis, Aristotle University of Thessaloniki, Greece

Tryfon Mavropalias, University of Western Macedonia, Greece

Volodymyr Sulyma, Dnipropetrovsk Medical Academy, Ukraine

Organizing Committee

Janice Fournillier, Georgia State University, United States

Wilfried Admiraal, Leiden University, Netherlands

Elizabeth (Betsy) Kersey, University of Northern Colorado, United States

Aehsan Haj Yahya, Beit-Berl College, Israel

Alaa AlDahdouh, University of Minho, Portugal

Augusto Z. Macalalag, Arcadia University, United States

Bhesh Mainali, Rider University, United States

Janez Jamsek, University of Ljubljana, Slovenia

Josiah Zachary Nyangau, Louisiana State University, United States

Kent Löfgren, Umeå University, Sweden

Laurie Murphy, Saint Joseph's College, United States

Marelbi Olmos Perez, Universidad Tecnológica de Bolívar, Colombia

Masood Badri, UAE University, United Arab Emirates

Monica Reichenberg, University of Gothenburg, Sweden

Phu Vu, The University of Nebraska at Kearney, United States

Qian Wang, Manhattan College, United States

Rachid Ait Maalem Lahcen, University of Central Florida, United States

Wei Zakharov, Purdue University, United States

Zhanat Alma Burch, Duke University, United States

Table of Contents

Analysis of the Development of Critical Thinking Skills Research in The Educational Context Physics in Indonesia: Overview from Research Design to Data Analysis

Ogiarto Ate

State University of Malang, Indonesia, https://orcid.org/0009-0003-9813-7039

Parno

State University of Malang, Indonesia, https://orcid.org/0000-0002-1363-0453

Nuril Munfaridah

State University of Malang, Indonesia, https://orcid.org/0000-0002-9114-7100

Abstract: One of the educational efforts in the 21st century is to provide every individual with the skills needed so they can compete and survive. One of the important skills that students have is critical thinking. This research was carried out by analyzing the content of a number of articles that have been published in Physics Education Journals throughout Indonesia from 2018 to 2023 which have been accredited SINTA 1-3 with critical thinking skills as the main focus of the research. The results of this research reveal that in the last 5 years the number of published articles focusing on critical thinking skills has continued to increase. Among these publications, the most dominant research design is research and development, followed by quantitative research. Apart from that, class XI senior high studentsand the material "Temperature and Heat" respectively became the most research subjects and materialsused. Based learning (Inquiry, Problem and Project), Scientific Approach and STEM are the treatments most often used by researchers. Test questions (description and multiple choice) and questionnaires are the most widely used instruments. The N-Gain test and T test are the instruments and data analysis methods most commonly used serially. In connection with the findings of this research, several recommendations can be proposed for future research that base critical thinking skills as the main focus, including increasing the diversity of research designs and selecting more appropriate data analysis techniques. Apart from that, it is important to pay attention to the treatment given so that students' critical thinking becomes more optimal.

Citation: Ate, O., Parno., & Munfaridah, N. (2024). Analysis of the Development of Critical Thinking Skills Research in The Educational Context Physics in Indonesia: Overview from Research Design to Data Analysis. In A. A. Khan, M. Demirbilek, & M. L. Ciddi (Eds.), *Proceedings of ICSEST 2024-- International Conference on Studies in Engineering, Science, and Technology* (p. 1-12), Istanbul, Turkiye. ISTES.

Introduction

We are currently entering the development of the 21st century which is marked by many accelerations changes in science and technology are very fast and have an impact on various aspects of life. In the 21st century, critical thinking skills have become an ability that everyone must have individual (Bao & Koenig, 2019). This capability is recognized as a key element in the entire process problem solving. Moreover, this critical thinking ability can be considered as a basis for strengthening individual competence and community development. Education requires new goals reflecting future requirements. These goals are known as 'future skills', namely knowledge, attitudes, values and skills designed to prepare students for facing the future. The need to educate future skills is driven by the awareness that the future The future brings new challenges for society. (Ziva Sabag, 2018).

Critical thinking skills are one of the 10 main competencies that have been formulated in Assessment and Teaching of 21st Century Skills (ACT21S) (Binkley et al., 2012). LMTF too includes critical thinking skills as a sub-domain of the Global Framework of Learning Domains – 21st century skills framework designed by UNESCO (Learning Metrics Task Force, 2013). Besides that, Wagner (2010) and the Change Leadership Group from Harvard University identified competencies and survival skills needed by students in facing life, the world of work, and citizenship in the 21st century emphasizes the following seven (7) skills: (1) critical thinking skills and problem solving, (2) collaboration and leadership, (3) agility and adaptability, (4) initiative and entrepreneurial spirit, (5) able to communicate effectively both orally and in writing, (6) capable access and analyze information, and (7) have curiosity and imagination. So that it can It is concluded that critical thinking skills must be the main focus in the learning process so that able to deliver students who can compete and produce strategic solutions to problems new in life. One of the long-term targets of education in Indonesia is training critical thinking skills through useful learning, with the aim of preparing students so that you can become a lifelong and independent learner. (Luvia Ranggi et al., 2021).

Emphasis on developing critical thinking in learning is important because of expertise This is very necessary in social interaction. Individuals are faced with situations that require it solution. Thus, critical thinking skills are important to instill in context education, both through formal education at school and through learning experiences outside the classroom. (Graph, 2021). In developing critical thinking skills, students need to consider everything potential that might occur before making a decision. This is due to the information obtained cannot necessarily be used as a guide for taking action. (Rosyidah et al., 2021). Thinking skills Critical thinking is very important to support someone in explaining, analyzing, assessing and rearranging thinking (Oktavianty, 2023).

However, the reality that still occurs today is based on several studies that have been carried out revealed that students' critical thinking abilities are relatively low, especially in physics lessons (Nurjanah et al., 2022), (Kurniawan et al., 2021) and (Benyamin et al., 2021). Students who experience difficulties and getting low

grades is partly because their critical thinking skills are still lacking low (Nurjanah et al., 2022), (Kurniawan et al., 2021) and (Benyamin et al., 2021). Several possibilities critical thinking skills problems such as the education system and learning design which are still lacking optimal. Apart from that, students are not encouraged and are not directly involved in solving. The problem itself is that they tend to be less tenacious and thorough in solving problems, thus causing Students' critical thinking skills in solving the problems given are still low (Lase & Ndruru, 2022; Zagoto, 2022).

In Indonesia, there has been a lot of research on critical thinking skills, especially in field of Physics education. Some studies focus on identifying students' levels of critical thinking (Benyamin et al., 2021; Nurjanah et al., 2022; Putri et al., 2022; Sona et al., 2023; Wahyuningsih et al., 2021). Other research discusses the influence of specific designs on critical thinking skills (Akhir et al., 2023; Erlinawati, 2020; Febril et al., 2022; Hikmah & Agustin, 2020; Lestari & Muhajir, 2021; Novianto et al., 2018; Okta Fitriyani et al., 2018; Permadi & Setyaningsih, 2018; Rosyidah et al., 2021; Suryaningsih & Ainun Nisa, 2021b, 2021a; Widarti & Roshayanti, 2021). Apart from that, there are those who focus on skill relationships think critically with other variables (Alam et al., 2021; Rohani, 2013). However, among all of existing research, there has been no research that attempts to review the various results of research conducted the. Therefore, researchers want to conduct analysis from research that focuses on skills critical thinking that has been produced.

By using content analysis in several Physics education scientific journals published in Indonesia, starting from 2018 to 2023, this research aims to collect information about various studies that discuss critical thinking skills in Indonesia. In detail this research is intended to answer the following questions:

1. What is the trend in the number of critical thinking skills research from year to year? 2. How variations in research designs used to investigate critical thinking skills in Indonesia? 3. Topic What is most commonly used to investigate students' critical thinking skills? 4. Any treatment What do researchers apply to improve students' critical thinking skills? 5. What instruments are used researchers to measure critical thinking skills? 6. What data analysis techniques do researchers use? analyze critical thinking skills? 7. What is the description of the series of research that has been carried out? researchers in investigating critical thinking skills?

There are several things that differentiate this research from others, namely; First, research it focuses on all articles published from 2018 to 2023; Selected articles is accredited by the Science and Technology Index (SINTA) ranking one to three. Second, This research is devoted to investigating a number of articles with critical thinking skills as a focus main. Third, various parameters are used as a basis for content analysis.

Method

Research design

This study adheres to the principle of content analysis, namely focusing on findings from various studies has

been published in scientific journals in Indonesia. The research method used is similar to that used by Fauzi & Susetyarini (2019).

Data Source

The data source in this research comes from content analysis of physics education articles. The article selected from Physics education journals listed on the Science and Technology Index (SINTA) starting January 2018. SINTA (http://sinta2.ristekdikti.go.id/) is a platform for measuring progress science and technology designed and developed by the Ministry of Research, Technology and Indonesian Higher Education. The selected articles come from SINTA accredited journals ranked one to one These three are based on the keywords students' critical thinking skills. Articles analyzed in the research these were published online before July 2018. Of the hundreds of articles collected, there are articles that examine critical thinking. All these articles were analyzed in this study.

Research Instrument

The instrument used in this research is a content analysis guide that contains aspects related issues were observed (Table 1.). There are a total of seven main aspects reviewed for deep content analysis this research. These aspects include (1) number of publications per year; (2) type of research; (3) research subjects; (4) Physics topics selected for research; (5) Treatment; (6) data collection instruments; and (7) method data analysis. In particular, categories in aspects (1), (4), and (5) were not decided at the start because they did not yet exist previous research that might be a reference for determining what should be included within those categories and possibly overgeneralized categories. May appear when content analysis on several articles is carried out. Apart from that, categories in aspects (2), (3), (6), and (7) determined before data collection. These categories are shown in adapted from (Fauzi & Pradipta, 2018). Apart from that, aspect (2) is divided into two sub-aspects, including (2a) types of research general and (2b) quantitative research design.

Data Analysis

Each article is grouped into certain categories based on certain aspects that it meets specified category. The decision was based on information shared by the author on abstract, method, and discussion sections. Next, the data that has been collected is presented in the form bar chart.

Results
Number of Publications

The number of article publications shows how often research was conducted in a certain period. Referring to the graph in Figure 1, articles that review critical thinking skills can be discovered since 2018. There is no particular

shift pattern that occurs in the number of publications from year to year. However, if you refer to Figure 1, the number of publications since 2018 has increased a higher increase compared to previous years. Trend of increasing number of publications regarding critical thinking skills shows a significant increase in the number of researchers who passionate about researching higher order critical thinking skills.
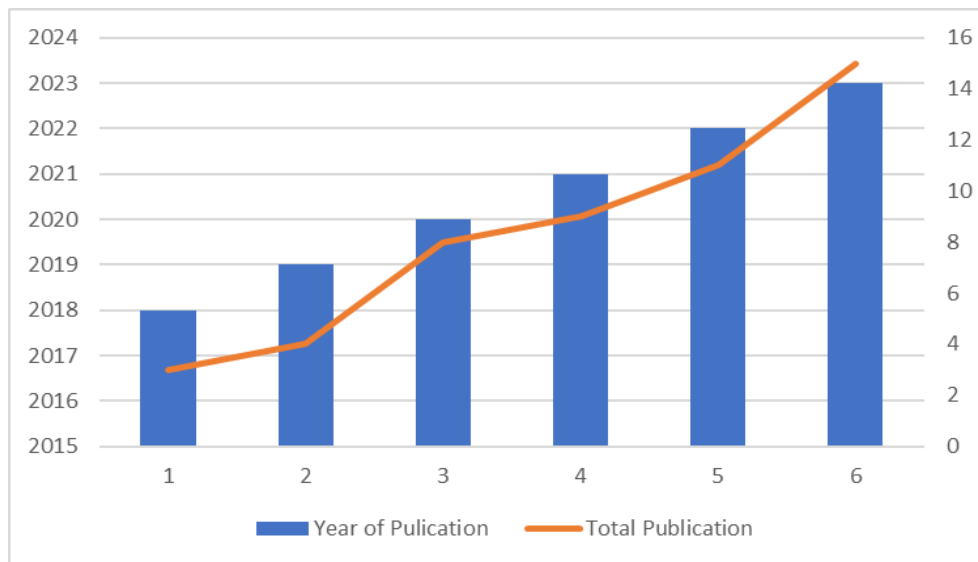
Figure 1. Distribution of Research with Critical Thinking Skills as the Main Concern Based on Number of Research

.

Most research results from the researcher's sensitivity to common, frequently occurring issues around them. One of the problems that is often encountered today is the level of thinking ability. Indonesian students' critical thinking is still relatively low. Therefore, conducting research is believed to be a way the most effective way to handle and overcome these problems. Through research, researchers can identify the most effective learning design or media that may be able to accommodate students' critical thinking skills optimally.

The more research that examines critical thinking skills, the greater it will be its positive influence on the development of Indonesian education. This premise is based on the idea that states that the ultimate goal of research is to improve educational practice (Coburn & Penuel, 2016). Furthermore, research will influence educational practice for various reasons, namely: (1) the findings can be used as credible information and can be applied by teachers; (2) can become a fundamental basis for educational decision making, whether at national, local or institutional institutions Specific; and (3) the findings can influence the way teachers think

Types of research

The type and design of research determines the focus of a study. The following is the distribution of research with Critical Thinking Skills as the main concern based on the type of research.
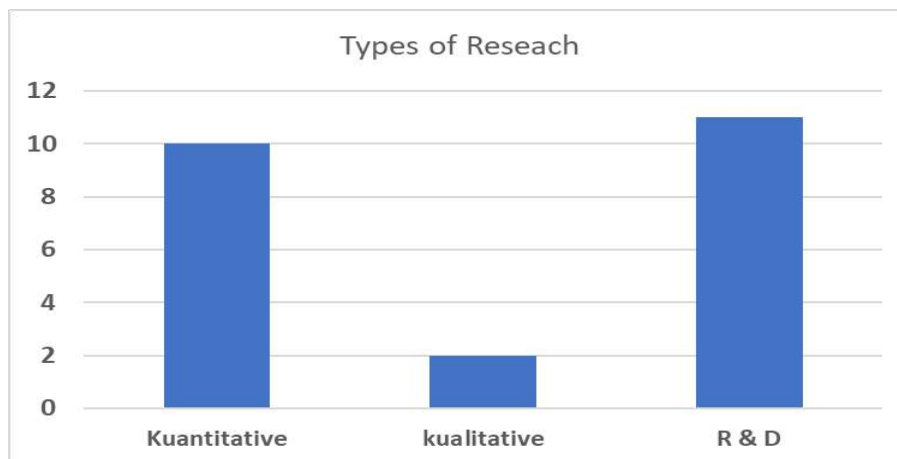
Figure 2. Distribution of Research with Critical Thinking Skills as the Main Concern by Type
Study.

Based on Figure 2 above, it appears that the type of research that is widely used is quantitative and research and development. Meanwhile, qualitative research is still rarely carried out. In kind Quantitative research found that many experimental studies were carried out by researchers. Experimental research is a part of quantitative research that is used to look for the effect of certain treatments against others in controlled conditions Arikunto (2006:3) Meanwhile, in R & D research, it is wrong One model that is widely used is R & D according to (Borg & Gall, 1983) this development model using a waterfall flow at the development stage. Borg and Gall's development model has relatively long stages because there are 10 implementation steps: (1) research and data collection (research and information colleting), (2) planning, (3) draft development product (develop preliminary form of product), (4) field trials (preliminary field testing), (5) initial product revision (main product revision), (6) field trials (main field testing), (7) perfecting the product resulting from field tests (operational product revision), (8) field implementation tests (operational field testing), (9) final product revision, and (10) dissemination and implementation (dissemination and implementation) (Hamdani, 2011). In addition, the R & D model according to (Thiagarajan, 1974) consists of four stages of development. The first stage, Define or often referred to as needs analysis stage, the second stage is Design, namely preparing a conceptual framework and model learning tools, then the third stage, Develop, namely the development stage involving validation tests or assessing the suitability of the media, and finally the Disseminate stage, namely implementation to the target actually the subject of research.

Research Subjects

Empowerment of critical thinking skills is aimed at students. Based on information regarding type of research, quasi-experimental design is the design most commonly used by researchers. This matter suggests that, in general, research seeks to compare several learning designs best in empowering students' critical thinking skills. In conducting research, researchers requires research subjects to test the hypothesis. Based on Figure 4, the research subjects are the most frequently chosen were high school students, followed by college and junior high

school students respectively. this finding in line with research conducted by (Fauzi & Pradipta, 2018).
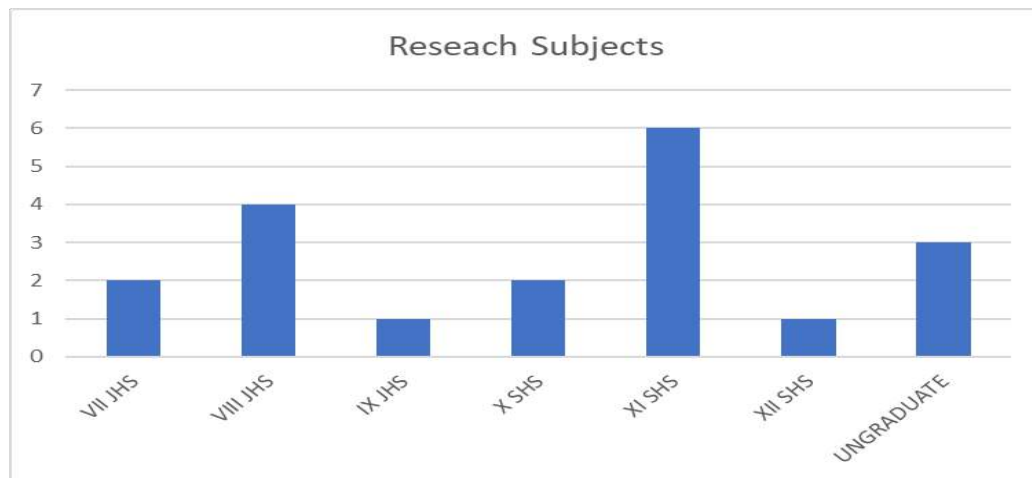
Figure 3. Distribution of Research with Critical Thinking Skills as the Main Concern Based on Research Subjects. The research subjects that are widely used are students in class VII of junior high schools and classes XII Senior High School. Meanwhile, class IX and Class XII classes are rarely held. This phenomenon occurs because of the tendency of most schools to be selective in granting permission to researchers conducting research in class IX SMP or XII SMA because of the busy national exam preparation schedule.

Physics Topics

Physics is a scientific subject with various topics.
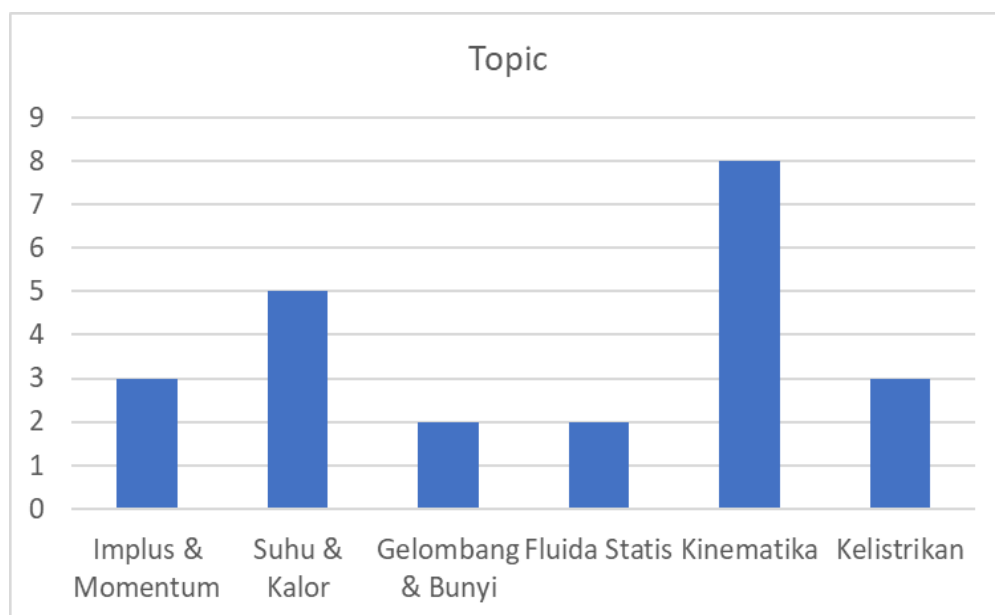
Figure 4. Distribution of Research with Critical Thinking Skills as the Main Concern Based on Topic Physics

g The Physics topic that is most frequently used is kinematics. Kinematics is divided into aspects related to quantities in straight motion, Uniform Straight Motion (GLB), and Motion Straight Changed Regularly (GLBB). Many examples of the application of kinematics are found in everyday life. days to make it easier for students to understand concepts in kinematics.

Treatment
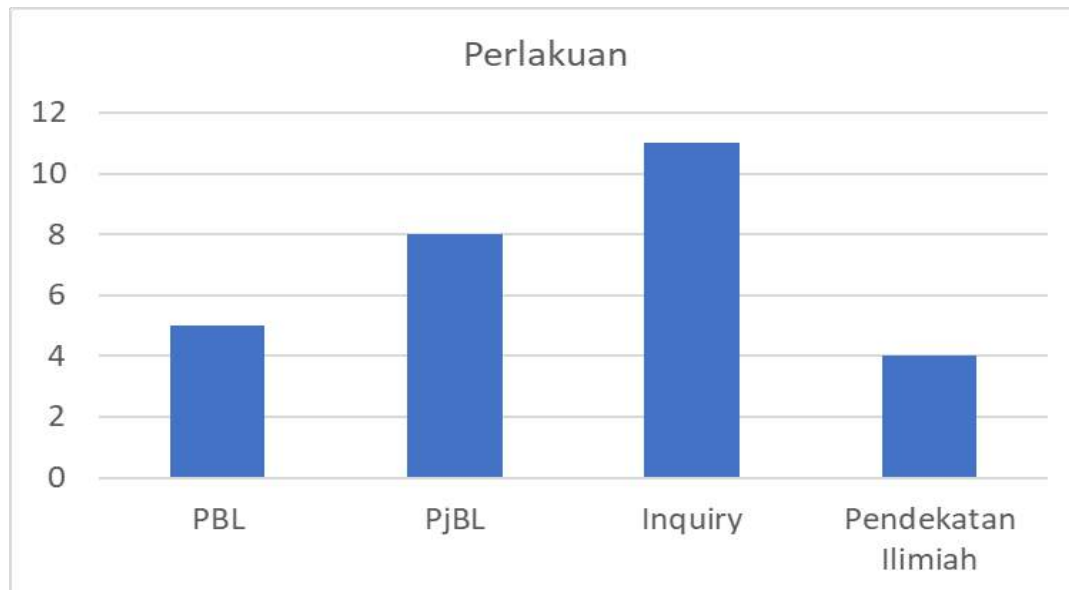
Figure 5. Distribution of Research with Critical Thinking Skills as the Main Concern Based on Research Subjects.

The aim of providing treatment is to test the researcher's hypothesis or identify significance a certain condition with respect to any parameter under investigation. Based on Figure 5, Learning Inquiry Based (IBL) and Project Based Learning (PjBL) are the most common treatments used in research on critical thinking skills. *Inquiry* and *PjBL* confront students with authentic problems that are similar to real work activities, and help develop soft skills, such as teamwork and collaboration, communication, critical thinking, and creativity. Involve students directly through Practical activities or involvement in projects is one strategy that can be applied for develop students' critical thinking abilities and science process skills (Putri et al., 2022).

Data analysis

The accuracy of selecting data analysis methods will determine the level of validity of a study. Referring In the graph in Figure 6, it appears that the N-Gain test is the most common data analysis method used in critical thinking research. Meanwhile, the ANCOVA test is very rarely used. Use ANCOVA is highly recommended especially when researchers try to choose a quasiexperimental design, where they cannot choose students one by one as research subjects (only students in that class specified which can be selected). By using ANCOVA in conditions like this, researchers can controlling for external variables that might influence the relationship

between the independent variables and dependent. Furthermore, by using ANCOVA you can identify differences that occur betweengroup to the corrected mean based on the characteristics of the research subjects shown in pre-test data (Warner, 2012). Thus, the use of ANCOVA is recommended for research quasi-experiment with pre-test and post-test data.
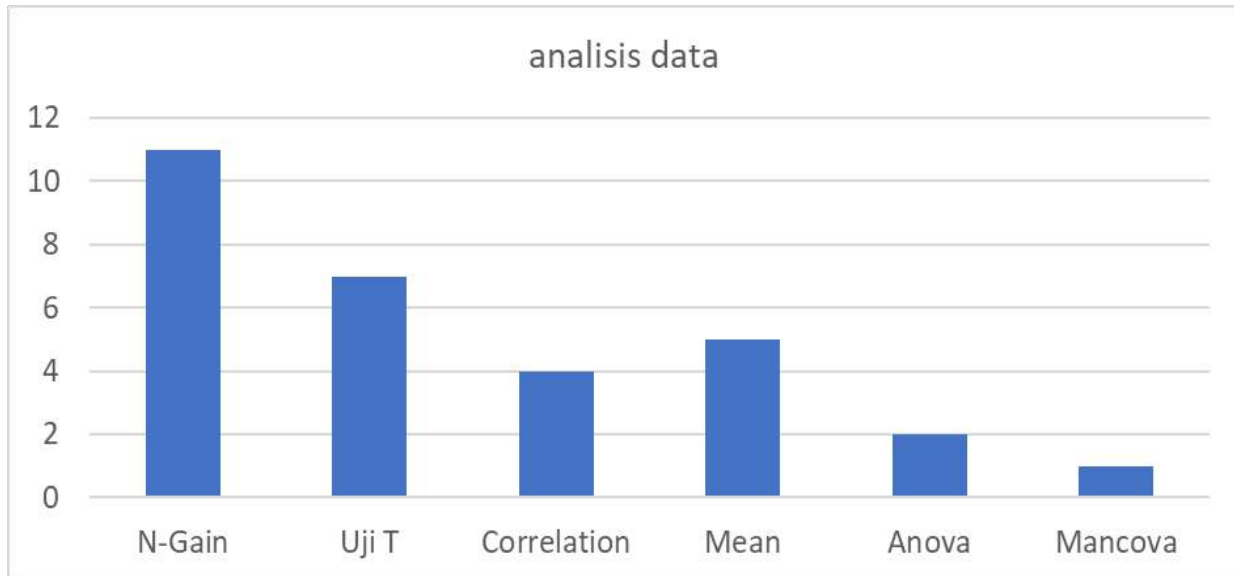
Figure 6. Distribution of Research with Critical Thinking Skills as the Main Concern Based on Research Subjects.

Conclusion

In this study, articles highlighted critical thinking skills and were published in Physics education journals throughout Indonesia from 2018 to 2023 have been reviewed. The trend is found there is an increase in the number of publications with critical thinking skills as the main concern in three last year. Among the publications, the most frequently found are quantitative research and R&D. In addition, students in class VII SMP and XI SMA were mostly chosen as research subjects; while material Kinematics or Motion is the most frequently chosen topic. PBL and PjBL indicate the treatment most widely applied; while the N-Gain test and T test are the most commonly used instruments for data collection and analysis.

Recommendations

Several recommendations have been prepared for further research. First, it's important to increase the frequency of conducting qualitative research to investigate the development of thinking skills critical. Second, research and development which aims to develop learning products provide clear information about the research instrument, as well as the validity and reliability of the instrument. Finally, it is recommended that researchers choose the most appropriate test for the hypothesis and research design in conducting any research.

Acknowledgements

References

Akhir, T., Studi, P., Fisika, P., Sains, F., Matematika, D. A. N., Kristen, U., & Wacana, S. (2023). *MENGAJARKAN BERPIKIR KRITIS SISWA SMA MELALUI GUIDED INQUIRY LEARNING TERINTEGRASI STEAM PADA Oleh :*

Alam, S. N., Hala, Y., & Palennari, M. (2021). Perbandingan Keterampilan Berpikir Kritis dan Keterampilan Proses Sains Biologi yang dibelajarkan Model Pembelajaran Inkuiri Terbimbing dengan Inkuiri Terstruktur. *Pinisi Journal Pendidikan Guru Sekolah Dasar*, *1*(1), 1–8.

Bao, L., & Koenig, K. (2019). Physics education research for 21st century learning. *Disciplinary and Interdisciplinary Science Education Research*, *1*(1), 1–12. https://doi.org/10.1186/s43031-019-0007-8

Benyamin, B., Qohar, A., & Sulandra, I. M. (2021). Analisis Kemampuan Berpikir Kritis Siswa SMA Kelas X Dalam Memecahkan Masalah SPLTV. *Jurnal Cendekia : Jurnal Pendidikan Matematika*, *5*(2), 909–922. https://doi.org/10.31004/cendekia.v5i2.574

Borg, & Gall. (1983). Educational research: An introduction. In: New York Longman. Dick, W., Carey, L., & Carey, J. O. (2005). The systematic design of instruction.

Erlinawati, C. E. (2020). Pengaruh Model Pembelajaran Project Based Learning (PjBL) Berbasis STEM Terhadap Keterampilan Proses Sains Dan Penguasaan Konsep Fisika Siswa Di SMA. *Repository.Unej.Ac.Id*.

Febril, A. N., Aradia, F. F., Oktavia, F., & Fitri, R. (2022). Pengaruh Pendekatan STEM Terhadap Kem ampuan Berpikir Kritis Peserta Didik : Literature Review The Effect of the STEM Approach on Students ' Critical Thinking : Literature Review. *Prosiding Seminar Nasional Biologi*, *2*(2), 974–986.

Graph, N. (2021). J urnal P endidikan F isika T adulako O nline TERHADAP GRAFIK NUMERIK GLB-GLBB Numerical Graph. *Jurnal Pendidikan Fisika Tadulako Online*, *9*(December), 108–112.

Hamdani. (2011). Strategi Belajar Mengajar. Bandung: CV Pustaka Setia.

Hikmah, L. N., & Agustin, R. D. (2020). Pengaruh Model Pembelajaran Project Based Learning terhadap Keterampilan Proses Sains. *Jurnal PRISMATIKA*, *1*(1), 1–9.

Kurniawan, N. A., Hidayah, N., & Rahman, D. H. (2021). Analisis Kemampuan Berpikir Kritis Siswa SMK. *Jurnal Pendidikan: Teori, Penelitian, Dan Pengembangan*, *6*(3), 334. https://doi.org/10.17977/jptpp.v6i3.14579

Lase, A., & Ndruru, F. I. (2022). Penerapan Model Pembelajaran Discovery Inquiry Dalam Meningkatkan Hasil Belajar Siswa. *Educativo: Jurnal Pendidikan*, *1*(1), 35–44. https://doi.org/10.56248/educativo.v1i1.6

Lestari, I. F., & Muhajir, S. N. (2021). Pendekatan STEM untuk Meningkatkan Keterampilan Berpikir Kritis Siswa pada Materi Fluida Statis. *Jurnal Pendidikan Dan Ilmu Fisika*, *1*(2), 62. https://doi.org/10.52434/jpif.v1i2.1483

Luvia Ranggi, N., Yokhebed, Ramli, M., & Yuliani, H. (2021). Meta-Analysis of the Effectiveness of Problem-Based Learning towards Critical Thinking Skills in Science Learning. *Journal of Physics: Conference Series*, *1842*(1). https://doi.org/10.1088/1742-6596/1842/1/012071

Novianto, N. K., Masykuri, M., & Sukarmin, S. (2018). Pengembangan Modul Pembelajaran Fisika Berbasis Proyek (Project Based Learning) Pada Materi Fluida Statis Untuk Meningkatkan Kreativitas Belajar Siswa Kelas X Sma/ Ma. *INKUIRI: Jurnal Pendidikan IPA*, *7*(1), 81. https://doi.org/10.20961/inkuiri.v7i1.19792

Nurjanah, S., Djudin, T., & Hamdani. (2022). Analisis Kemampuan Berpikir Kritis Peserta Didik pada Topik Fluida Dinamis. *Jurnal Education and Development*, *10*(3), 111–116.

Okta Fitriyani, L., Anggraini, W., Fisika, P., & UIN Raden Intan Lampung, F. (2018). Project Based Learning: The Effect On Student's Science Processes Skills In Tanggamus. *Indonesian Journal of Science and Mathematics Education*, *1*(3), 243–253. https://ejournal.radenintan.ac.id/index.php/IJSME/index

Permadi, D., & Setyaningsih, K. (2018). Pengembangan Modul Multi Representasi Berbasis Kontekstual Pada Materi Fluida Statis Untuk Meningkatkan Kemampuan Berpikir Kritis. *Jurnal Ilmu Fisika Dan Pembelajarannya (JIFP)*, *1*(2), 5–10. https://doi.org/10.19109/jifp.v1i2.1629

Putri, W. A., Astalini, A., & Darmaji, D. (2022). Analisis Kegiatan Praktikum untuk Dapat Meningkatkan Keterampilan Proses Sains dan Kemampuan Berpikir Kritis. *Edukatif : Jurnal Ilmu Pendidikan*, *4*(3), 3361–3368. https://doi.org/10.31004/edukatif.v4i3.2638

Rohani. (2013). Correlation Between Science Process Skill and Student Critical Thinking Through Inquiry Learning Strategy on Environment Pollution At Sma Negeri 3 Palangkaraya. *EduSains*, *1*(2), 1–10.

Rosyidah, N. D., Kusairi, S., & Taufiq, A. (2021). Kemampuan Berpikir Kritis Siswa melalui Model STEM PjBL disertai Penilaian Otentik pada Materi Fluida Statis. *Jurnal Pendidikan: Teori, Penelitian, Dan Pengembangan*, *5*(10), 1422. https://doi.org/10.17977/jptpp.v5i10.14107

Sona, T., Sahala Sitompul, S., & Oktavianty, E. (2023). Analisis Keterampilan Berpikir Kritis Peserta Didik Pada Materi Fluida Statis Di Sma Kristen Ekklesia Nanga Pinoh. *Jurnal Pendidikan : Riset Dan Konseptual*, *7*(1), 41. https://doi.org/10.28926/riset_konseptual.v7i1.531

Suryaningsih, S., & Ainun Nisa, F. (2021a). Kontribusi STEAM Project Based Learning dalam Mengukur Keterampilan Proses Sains dan Berpikir Kreatif Siswa. *Jurnal Pendidikan Indonesia*, *2*(6), 1097–1111. https://doi.org/10.36418/japendi.v2i6.198

Suryaningsih, S., & Ainun Nisa, F. (2021b). Kontribusi STEAM Project Based Learning dalam Mengukur Keterampilan Proses Sains dan Berpikir Kreatif Siswa. *Jurnal Pendidikan Indonesia*, *2*(6), 1097–1111. https://doi.org/10.36418/japendi.v2i6.198

Thiagarajan, S. (1974). Instructional development for training teachers of exceptional children: A sourcebook.

Wahyuningsih, D., Kurniawan, D. A., Maison, & Aziz, A. (2021). Analisis Kemampuan Berpikir Kritis Siswa Pada Materi Fluida Statis. *Seminar Nasional Matematika Dan Sains*, 400–406. https://prosiding.biounwir.ac.id/article/download/170/152

Widarti, R., & Roshayanti, F. (2021). Potensi Implementasi STEAM (Science, Technology, Engineering, Art and Mathematic) berorientasi ESD (Education for Sustainable Development) dalam Pembelajaran Fluida. *Unnes Physics Education Journal*, *10*(3), 291–295. http://journal.unnes.ac.id/sju/index.php/upej

Zagoto, M. M. (2022). Peningkatan Hasil Belajar Mahasiswa Pada Mata Kuliah Dasar-Dasar Akuntansi 1 Melalui Implementasi Model Pembelajaran Kooperatif Word Square. *Educativo: Jurnal Pendidikan*, *1*(1), 1–7. https://doi.org/10.56248/educativo.v1i1.1

Study of the Operating Parameters of Mining Machines

Mounia Taleb

Environmental Laboratory, Mining Institute, Echahid Cheikh Larbi Tebessi University,Tebessa 12000,Algeria https://orcid.org/0000-0003-2564-2141

Abdelkrim Rrechach

Mining Laboratory, Mining Institute, Echahid Cheikh Larbi Tebessi University, Tebessa 12000, Algeria https://orcid.org/0000-0001-9889-5735

Sihem Ghoudelbourk

Mining Laboratory, Mining Institute, Badji Mokhtar University, Annaba 23000, Algeria https://orcid.org/0000-0002-8536-4086

Abstract: Reliability-Based Maintenance (RBM) is one of the most efficient analysis methods that ensures the availability of production equipment at the best possible cost. It is for this purpose that we used this approach and we applied it to a fleet of mining machines, transport and loading machines on which we recorded several failures. Based on the feedback approach. Through the latter we can evaluate the operating parameters, predict, control failures and monitor the health of the machines. In this work, we carried out the study on mining machines (loaders, trucks and bulldozers). The results showed that mechanical failures are the most dominant in terms of downtime and number with a considerable failure rate. Subsequently we used the Ishikawa diagram which highlighted the major causes of the failures, finally the application of the Weibull model made it possible to determine the reliability of the three machines, the most reliable of which is the loader.

Keywords: Reliability, availability, mining machines, RBM, failure

Introduction

Maintenance plays a vital role in the management and performance of industrial equipment. Effective maintenance helps minimize unplanned downtime, optimize costs, and improve equipment reliability. However, maintenance based on traditional strategies can be costly and inefficient, as it does not fully take into account the actual reliability of equipment. It is a decisive factor of competitiveness and sustainability aimed at meeting industrial imperatives, namely improving the reliability of equipment and the quality of its products while reducing costs.

In this work, we address the importance of adopting a reliability-based approach for industrial maintenance management. The main objective is to propose a methodology and tools to optimize maintenance activities based on the reliability characteristics of equipment.

Maintenance is not just about repairing or troubleshooting at the lowest cost or restoring as quickly as possible. It is also not about keeping the installations running at all costs or ensuring high operational safety, at all costs, to achieve maximum but unprofitable availability. Maintenance begins with the design of the equipment: it must be able to be maintained (notion of maintainability), then to produce, its use must be easy and its safety maximum. Throughout its production life, maintenance monitors the equipment, follows its degradation and brings it up to standard with performance control, monitoring of costs and availability by looking for the simplest solutions. At the end of its life, maintenance first proposes a reduction in performance compatible with the possibilities of the equipment and finally its renewal

Method

Reliability Maintenance Optimization Method (OMF)

This method was first developed in the American civil and military aeronautics industry in the 1980s, under the name RCM (Reliability Centered Maintenance), with the aim of controlling aircraft operating costs. Developed from 1990, then generalized to nuclear power plants and then implemented on systems considered the most important in terms of safety, availability and operating costs. The method has been adapted for use on other types of installations (coal-fired thermal power plants, combustion turbines, power transmission lines, wind turbines, etc.). Companies providing maintenance services have transferred it to other industrial sectors (automotive, offshore, etc.). This approach makes it possible to choose a preventive maintenance strategy taking into account availability, safety and cost objectives, taking into account the potential consequences, namely the occurrence of failure modes and the effects on the operation of the system, as well as feedback data from equipment malfunctions.

The method used in this work is based on the determination of the different parameters of operational safety, namely reliability, maintainability and availability for each machine while relying on the study of their historical files, or even knowing how to decipher the needs and translate them into a research project. Therefore, the exploitation of the historical file constitutes a robust support for the method function, the brain of a maintenance service. This chronology allows us to determine the health status of each machine, target route and thus determine the priority actions that are required. Then using the Ishikawa diagram, find the appropriate solutions and finally draw up a maintenance plan for each machine.

This study will have the advantage of bringing together production, general resources and maintenance personnel on the one hand and increasing the probability of quickly recovering the real cause of an operating

anomaly on the other hand . The study is carried out for a period of five years (2018 to 2022), on 3 machines (truck, bulldozer and loader) located at the Ouenza mine, Tebessa East of Algeria.

Case study

The Ouenza deposit is located in the extreme north-east of Algeria near the Algerian-Tunisian border; 120 km south-east of the El-Hadjar steel complex (Annaba) to which it is connected by a railway line and 75 km from the capital of the Wilaya of Tébessa. (Fig.01).

Figure 1. geographical location of the Ouenza mine, city of Tébessa

Results

Study of the evolution of times and the number of breakdowns

Study of the loader
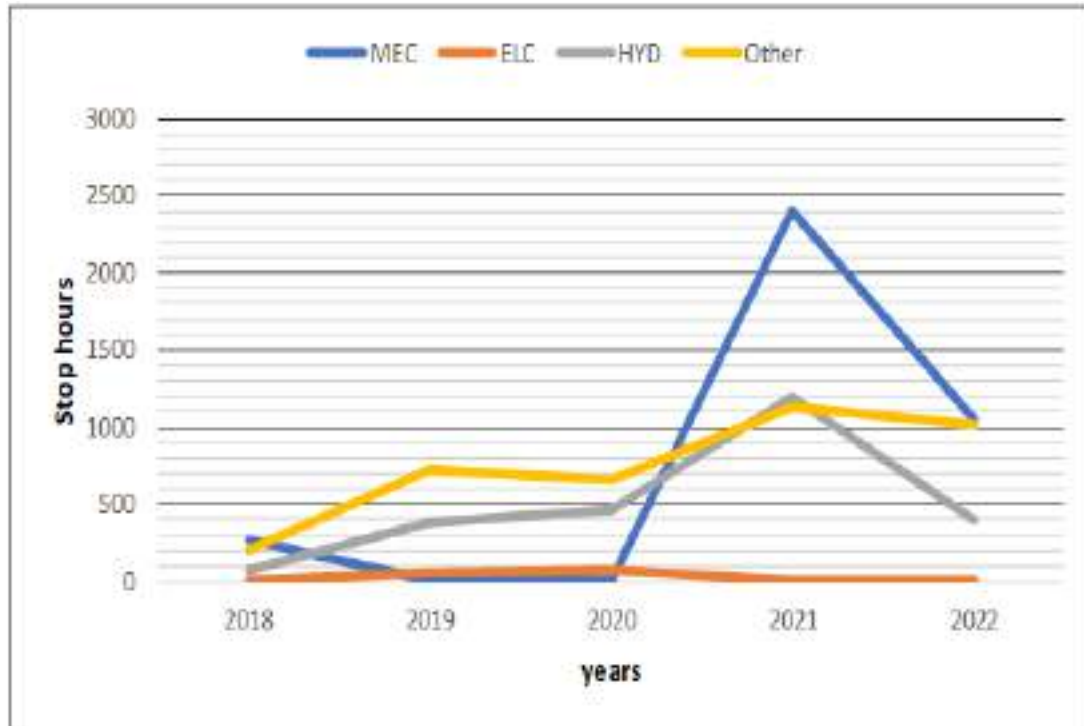
Figure 2. Evolution of loader down time
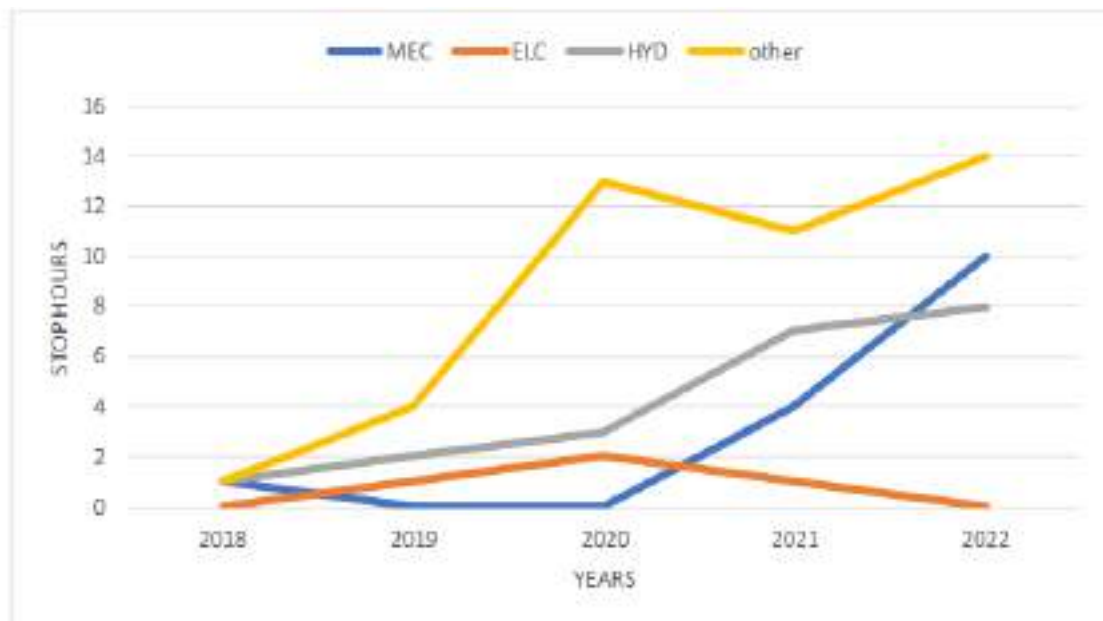
Figure 3. Evolution of the number of loader breakdown
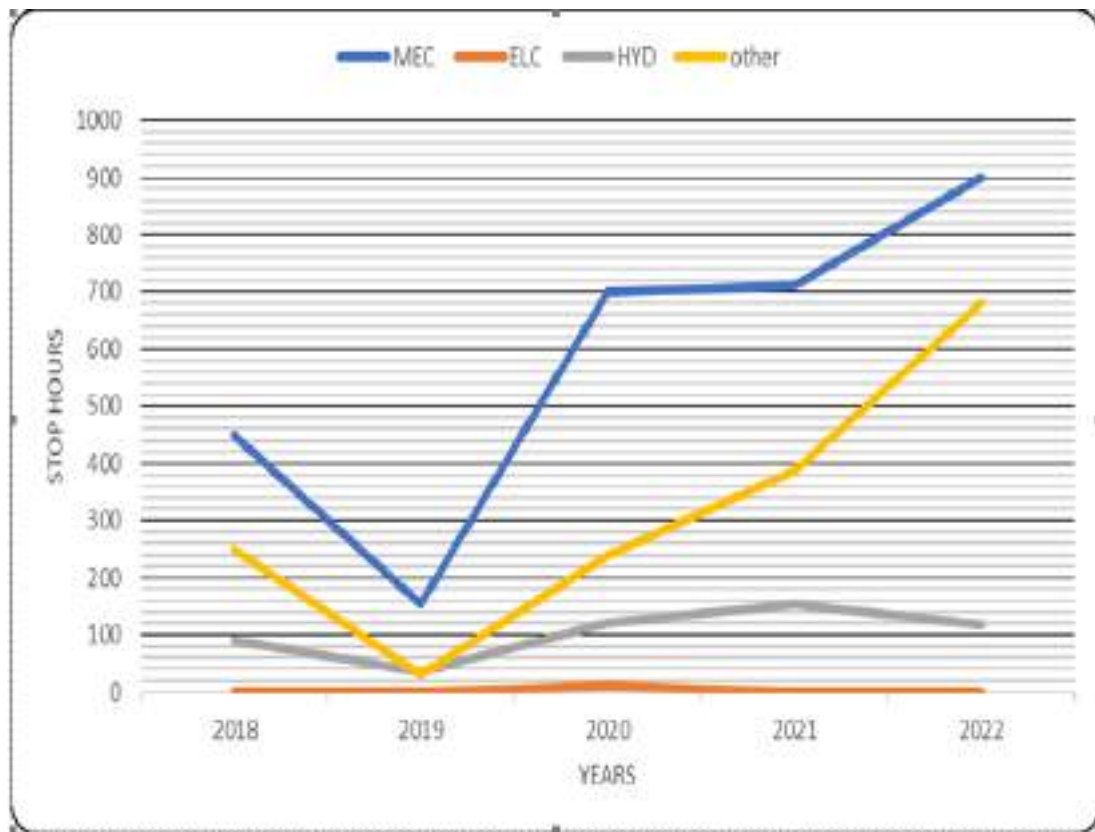
Figure 4. Evolution of Truck downtime

Figure 5. Evolution of the number of truck breakdowns
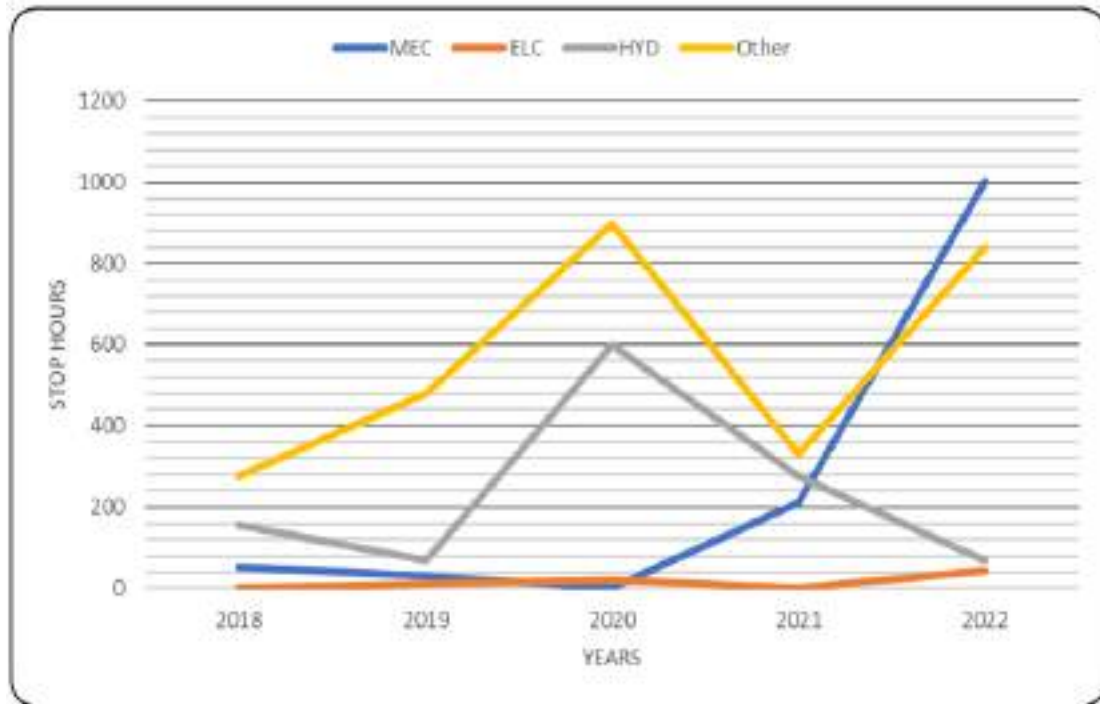
Figure 6. Evolution of Bulldozer Downtime
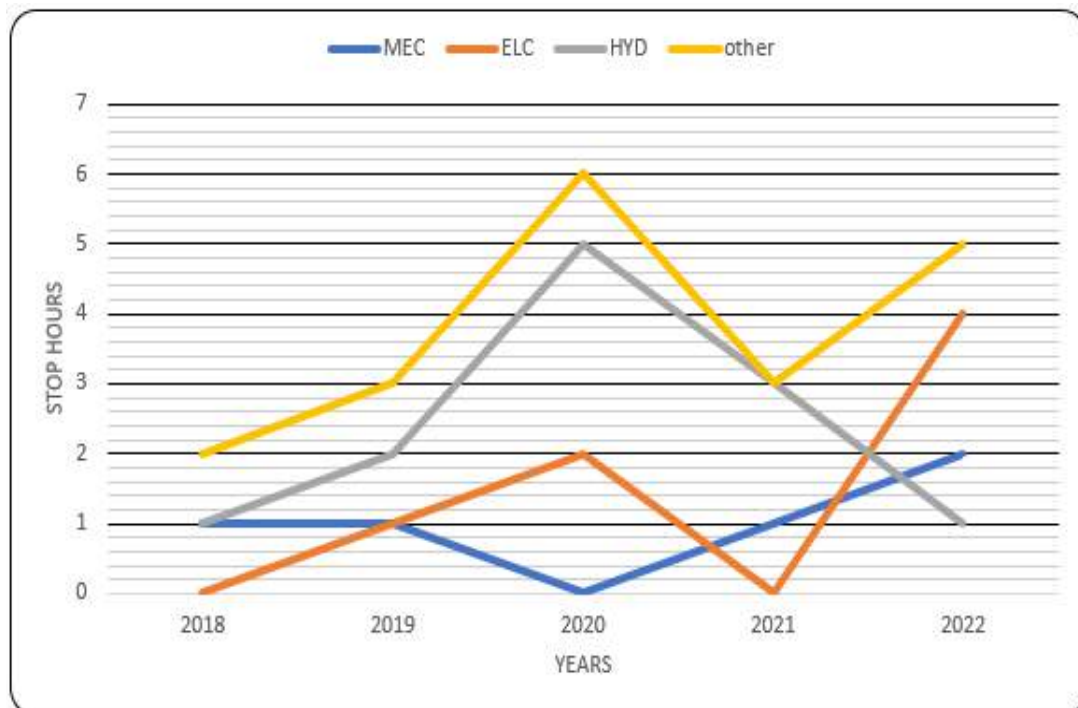
Figure 7. Evolution of the number of bulldozer breakdowns
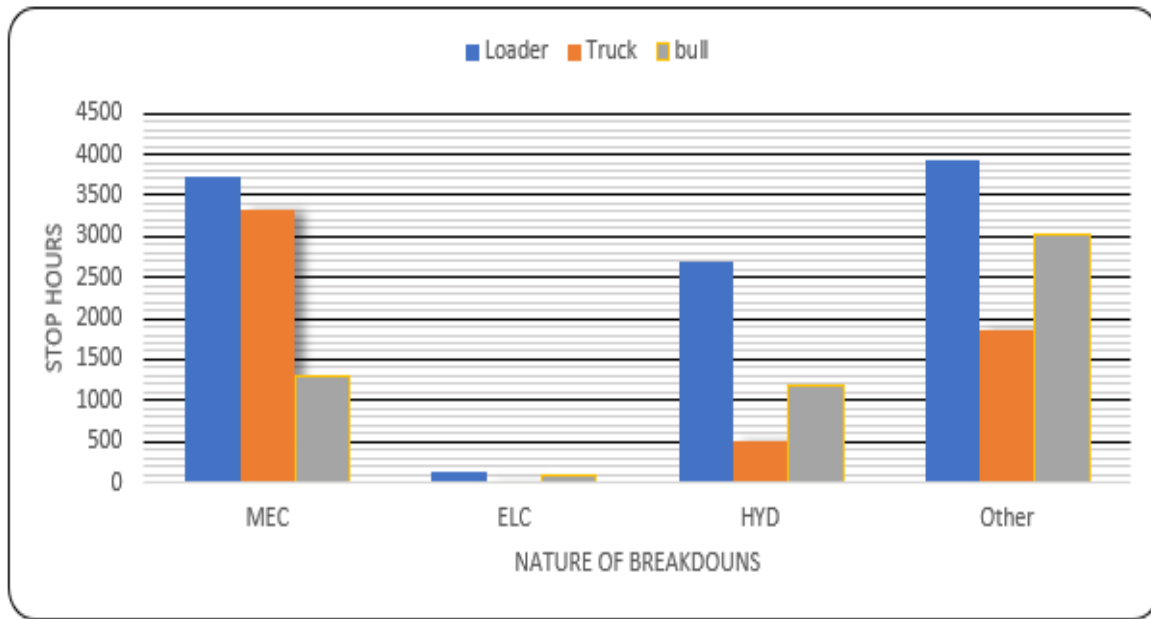
Figure 8. Downtime by type of the three machines together
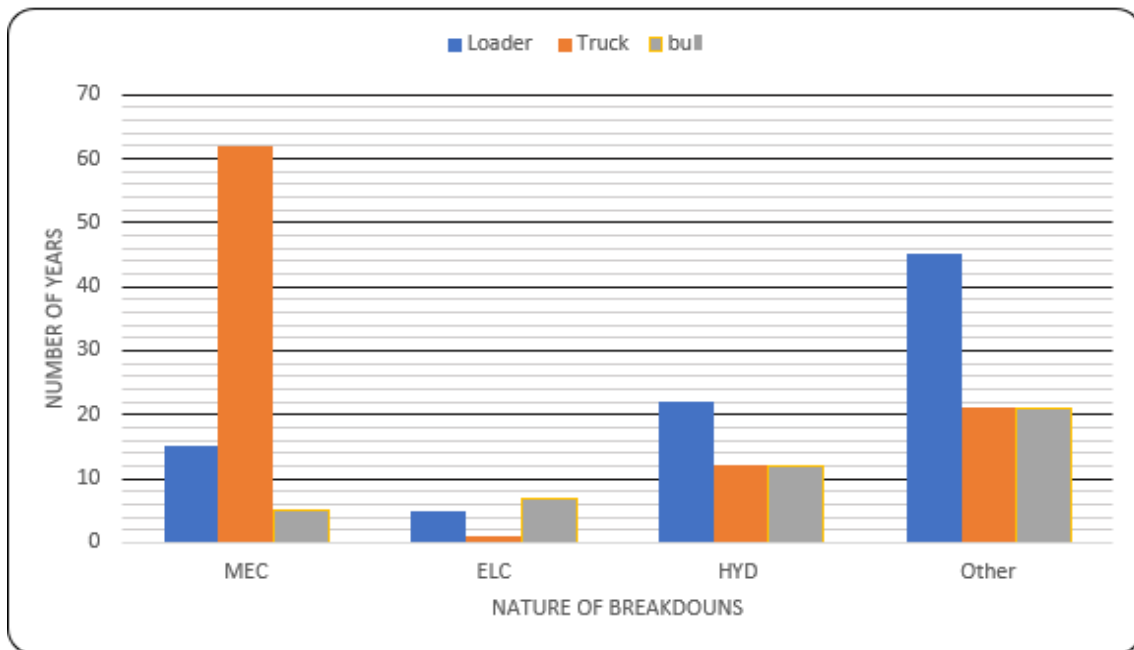
Figure 9. Number by type of breakdowns of three machines together

Application of Pareto's law (20-80 law)

Based on the downtime and the number of breakdowns of all production equipment over the last 5 years, the

following tables were produced (table1and 2)

Table 1. Statistics of downtime for all machines

Nature breakdouwn	Stop time	Ranking	Stop time	%	% Cumulative	Ranking ABC
MEC	7211	Other	8845,5	40,19%	40,19%	A
ELEC	231	MEC	7211	32,77%	72,96%	A
HYD	5717	HYD	5717	25,98%	98,94%	B
Other	8845,5	ELEC	231	1,04%	99,98%	C

Table 2. Statistics on the number of breakdowns of all machines

Nature of breakdouwns	Number of breakdouwns	Ranking	Number of breakdouwns	%	% Cumulative	Ranking ABC
MEC	82	Other	87	36,86%	36,86%	A
ELEC	13	MEC	82	34,75%	71,61%	A
HYD	54	HYD	54	22,88%	94,49%	B
Other	87	ELEC	13	5,51%	100,00%	C

Graphical representation

The graphical representation by the Pareto diagram for the three machines is respectively represented by figures 10 and 11.
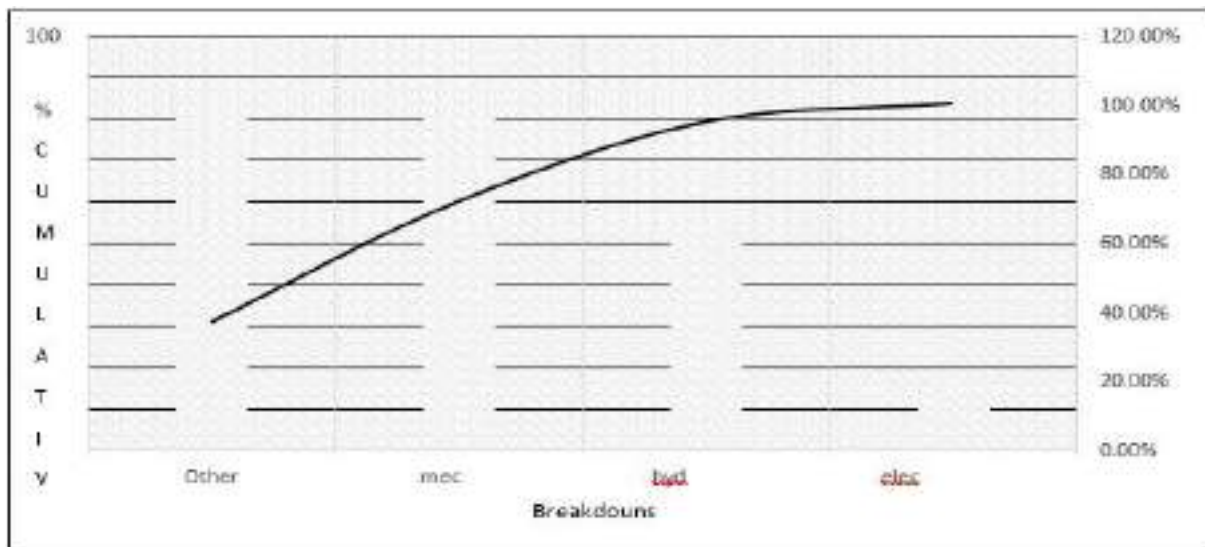
Figure 10. Pareto chart of machines (Breakdouns)
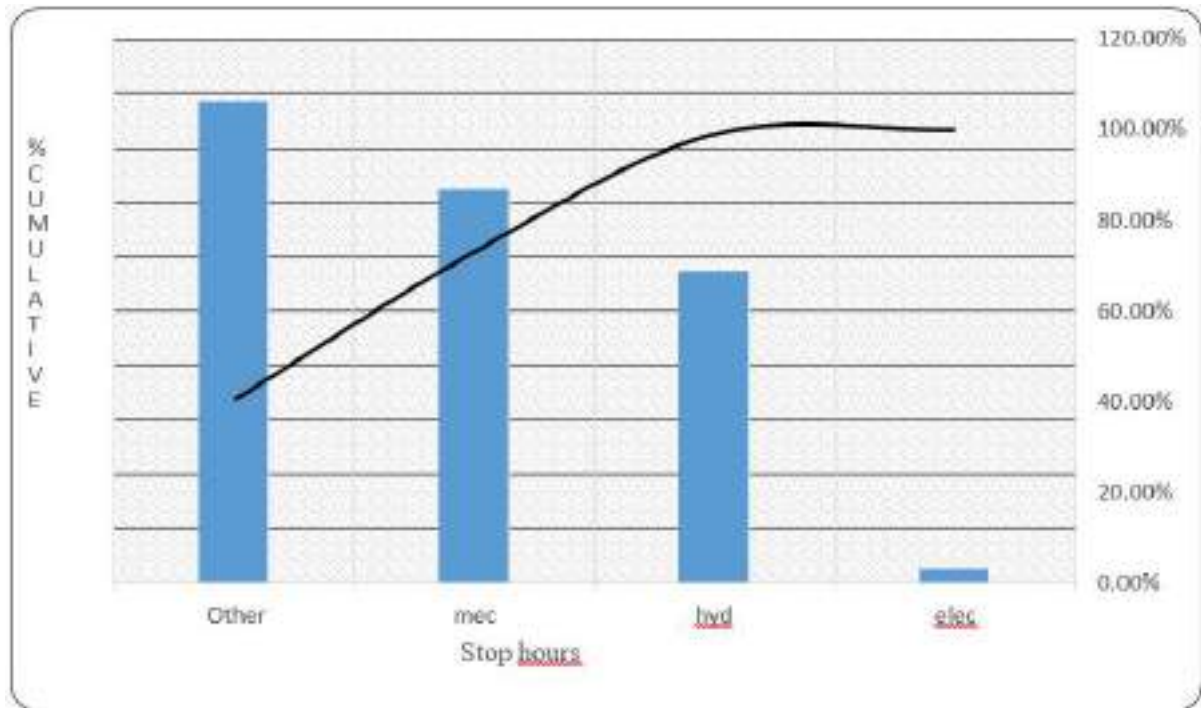
Figure 11. Pareto chart of machines (Stop hours)
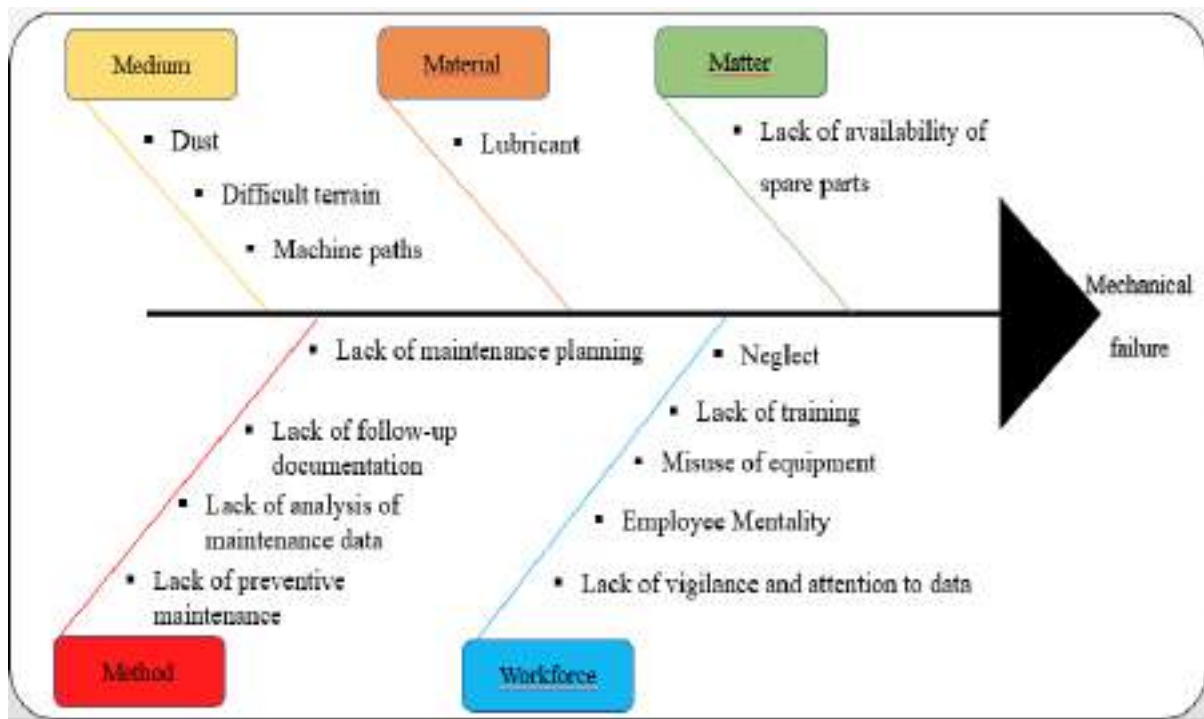
Figure 12. Ishikawa diagram

Application of Weibull law

Table 3. Weibull parameters of three engines over 5 years

	Year	β	η	γ	MTBF	Reliability
	2018	4.3	3400	0	3094.578	0.513
	2019				5309	1
Loader	2020				5222.5	1
	2021	2.6	660	0	586.21	0.479
	2022	1.8	620	0	551.359	0.445
	2018	1.4	1900	0	1731.698	0.415
	2019	1	850	0	850	0.367
Career	2020	1.1	170	0	164.0347	0.382
truck	2021	1	200	0	200	0.367
	2022	0.95	190	0	194.4479	0.359
	2018	1.5	3300	0	2979.075	0.424
	2019	3.55	3100	0	2791.335	0.502
Bull**dozer**	2020				4674	1
	2021	2	3100	0	2747.313	0.455
	2022	2.2	1550	0	1372.71	0.465

One of the main objectives of this study is the determination of the reliability of the three machines (loader, truck and bulldozer). The three-parameter Weibull law is used to model this reliability [8].

Weibull parameters

β: Shape parameter

η: Scale parameter

γ: Position parameter

Based on table 3 we apply the Weibull law (Figures 13,14 and 15). Then we calculate the reliability of the three machines studied (loader, truck and bulldozer) which is the objective of our study.
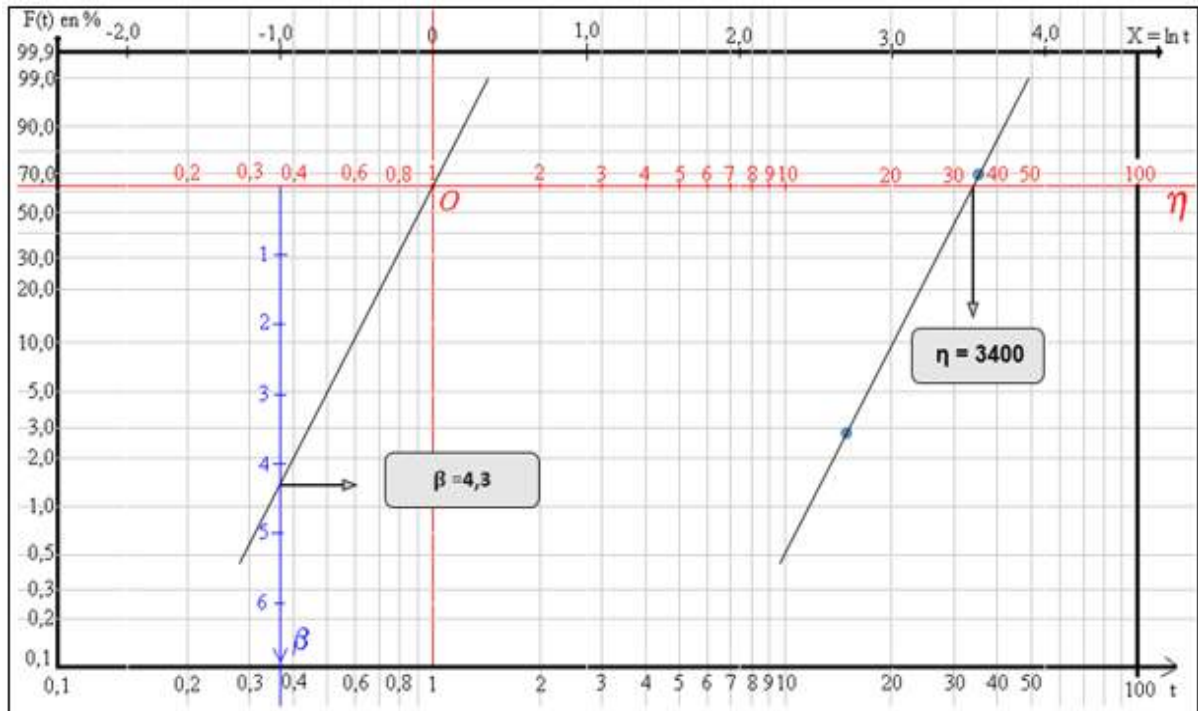
Figure 13. Application of the Weibull law the loader case
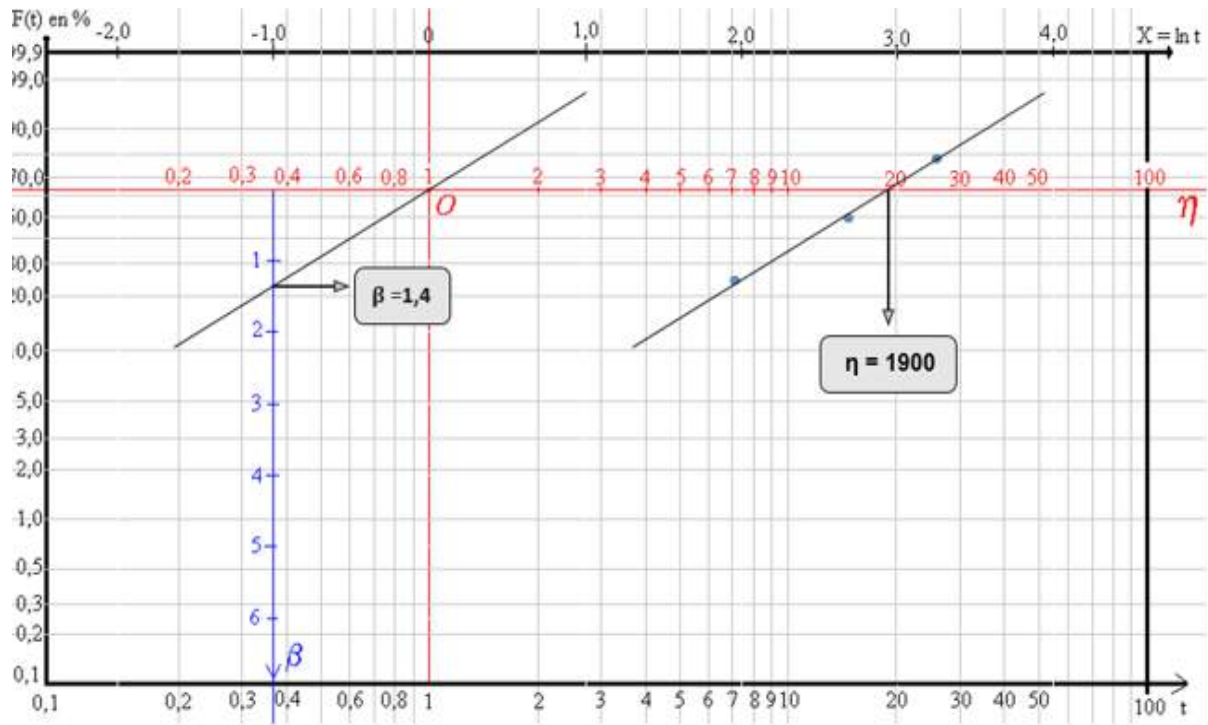
Figure 14. Application of Weibull law to the truck case
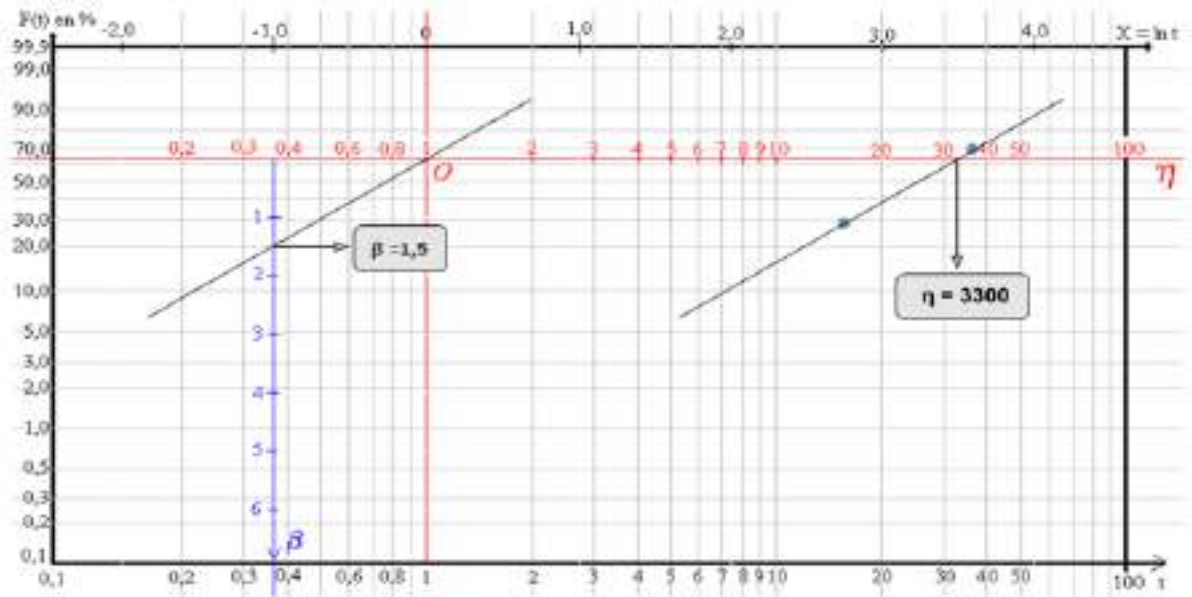
Figure 15. Application of Weibull law to the bulldozer case

Table 4. Reliability of three machines over 5 years

years	loader	Career truck	bull dozer
2018	51.3%	41.5%	**42.4%**
2019	100%	36.7%	**50.2%**
2020	100%	38.2%	**100%**
2021	47.9%	36.7%	**45.5%**
2022	44.5%	35.9%	**46.5%**
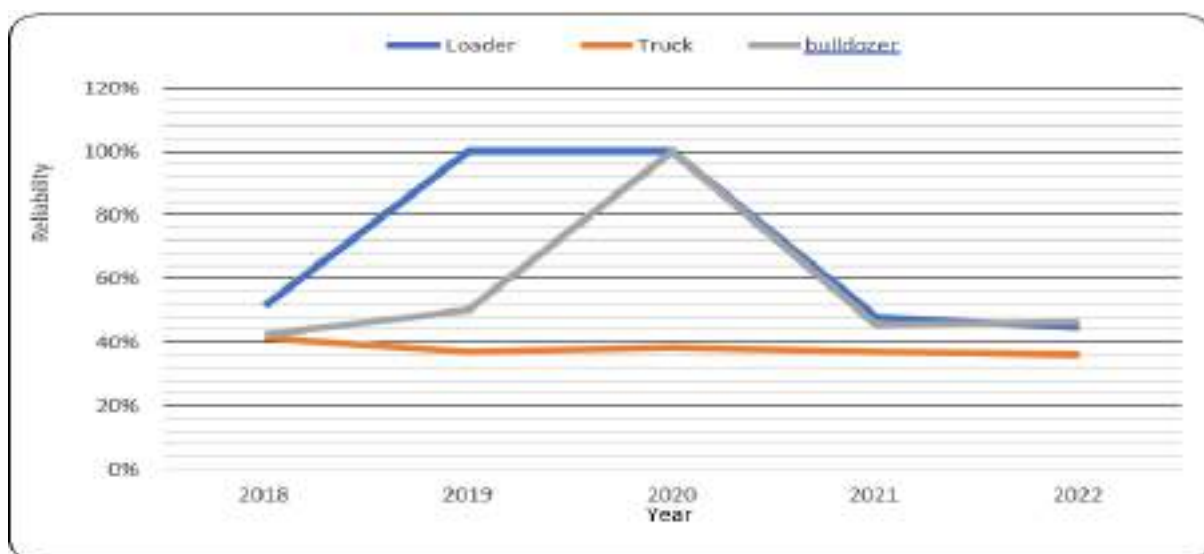
Figure 16. Reliability diagram of the three machines

Table 17. Preventive and corrective actions to be taken for the three machines

Mechanical breakdowns

Equipment	Causes	Solutions
	Difficulty in handling modern machines and poor use of equipment	**- Updating knowledge** **- Internal and external training** **- Collaboration with experts**
	Overuse or mishandling	**- Skills assessment** **- Workload planning** **- Driver training**
Career Truck	Priority of achieving production objectives to the detriment of maintenance	- Develop a maintenance plan in the company and impose it - Give enough time to maintenance personnel to prepare the machines
	Archaic repair and intervention techniques	- Adoption of modern technology - Evaluation of results - Documentation and monitoring of performance - Communication and sharing of knowledge - Encouragement of the culture of preventive maintenance - Adequate means of intervention
	Missing spare part	- Planning and management of spare parts stocks - Planning of intervention requests - Analysis of parts reliability
Loader	Degradation of lubrication and cooling systems	- Use of quality lubricants - Temperature monitoring - Cleaning and descaling - Visual inspection - Supervision and awareness
	Employee Negligence Fine dust	- Application of regulations - Watering - Cleaning
Bulldozer		

Discussion

Loader (Figure 2 and 3)

Mechanical failures were the main cause of shutdown in 2018, with 275 hours of shutdown. However, this category decreased significantly during the years (2019,2020) then the shutdown hours increase to 2400 hours for the year 2021 and 1055 hours for the year 2022 reaching an almost zero level after these years. On the other hand, electrical failures showed a steady increase until 2020, reaching a peak of 80 hours of shutdown. Hydraulic failures were relatively stable over the years, with a slight decrease from 2019 to 2020, then an increase until 2021. They then decreased in 2022. Other outages showed a general fluctuation with a significant increase in 2019 and a decrease in 2020. They reached a peak of 1128 hours of downtime in 2021 before decreasing again.

Based on the number and nature of failures of this production machine during the 05 years studied, we find that: Mechanical failures showed a gradual increase until 2022, reaching a peak of 10 failures this year. Electrical failures experienced fluctuations from one year to the next, with a slight increase from 2018 to 2020 (4 failures), then a decrease in 2021.Hydraulic failures also showed fluctuations, with a general increase until 2022, reaching a peak of 8 failures that year.Finally, other failures increased significantly from year to year, reaching a peak in 2022 with 14 failures.

Truck (figure 4and 5)

According to this graph (fig.4) we can see:

The downtime hours for mechanical breakdowns increased generally from 2018 to 2022, reaching a peak in 2022 with 900 downtime hours. On the other hand, electrical breakdowns showed relatively low and stable values in all years, with the exception of 10 downtime hours in 2020. As for the downtime hours for hydraulic breakdowns, they experienced fluctuations from one year to the next, reaching a maximum in 2021 with 155 downtime hours. The other breakdowns showed a significant increase from 2018 to 2022, reaching a peak in 2022 with 680 downtime hours.

For the number of outages by nature (figure 5) we see that: Mechanical breakdowns have shown a general upward trend, peaking in 2022 with 21 breakdowns, but electrical outages have been relatively stable with few to no breakdowns reported in all years except for one breakdown in 2020. Hydraulic breakdowns have shown some variability from year to year, with a slight increase in 2020 (4 breakdowns) and a gradual decrease. Other outages have also shown some variability from 1 to 6 breakdowns, with an increase in 2020, a decrease in 2021, and then an increase again in 2022.

Buldozer (Figure 6 and 7)

The graph (Figure 6) shows the following:

The downtime hours for mechanical breakdowns showed some variability from year to year, with relatively low values in most years. The machine peaked in 2022 but the downtime hours for electrical breakdowns showed an increase in the number of quantified hours to 12 hours in 2019, to 20 hours in 2020 and then reached 44 hours in 2022.As for the downtime hours for hydraulic breakdowns, they showed a significant increase in 2020 (600 hours) and then showed a decrease. The downtime hours for other breakdowns peaked in 2020 (899 hours) and then showed a decrease in 2021 (331 hours).

Based on the number and nature of breakdowns of this machine (figure 7) we note that mechanical breakdowns have shown some stability over the years, with relatively constant values, except for a slight increase in 2022 (2 breakdowns) as well as electrical breakdowns which have also shown overall stability, with some fluctuations from one year to the next. On the other hand, hydraulic breakdowns have increased progressively from 2018 to 2022 (5 breakdowns) and the other breakdowns have shown variability from one year to the next without a clear trend.

- The downtime due to mechanical failures is higher for the loader than the truck and the bulldozer. It is evident that the quarry truck is prone to mechanical problems that require careful attention.
- Regarding downtime due to electrical problems, the bulldozer records the highest number of downtime hours with 76 hours, while the loader and the truck only have 145 hours and 10 hours respectively. This indicates that the bulldozer is more likely to have electrical problems compared to the other machines.
- For downtime due to hydraulic problems, the loader records the highest figure with 2,696 hours, followed by the bulldozer with 1,172 hours and the truck with 519 hours. This shows that the loader and the bulldozer encounter more hydraulic problems than the truck.
- Regarding downtime attributed to other reasons, the loader records the highest figure with 3,941.5 hours, followed by the bulldozer with 3,037.5 hours and the truck with 1,866.5 hours. These figures indicate that there is a significant share of downtime due to unspecified reasons, which may require further analysis to identify the exact causes. - Overall, the total downtime for the three machines combined is highest for unspecified issues, followed by mechanical, hydraulic and electrical issues. This highlights the importance of monitoring and understanding the reasons for downtime for each machine type in order to implement appropriate corrective measures and improve operational availability.
- Mechanical failures are more common for the truck, with a total of 62 failures, followed by the loader with 15 failures and the bulldozer with 5 failures. This means that the truck is more prone to mechanical failures than the other machines.
- As for electrical failures, the bulldozer records the highest number with 7 failures, followed by the loader with 5 failures and the truck with only 1 failure. This indicates that the bulldozer is more likely to have electrical failures compared to the other machines.
- Hydraulic failures are more common for the loader, with a total of 22 failures, followed by the bulldozer with 12 failures and the truck with 12 failures. This shows that the loader encounters more hydraulic failures than the truck and the bulldozer.

- As for unspecified failures, the loader records the highest figure with 45 failures, followed by the truck with 21 failures and the bulldozer each. These figures indicate that there is a significant proportion of unspecified failures, requiring further analysis to identify the exact causes.

- Overall, the total failures for the three machines combined are highest for mechanical failures, followed by hydraulic and electrical failures.

By studying the chronology of breakdowns and their downtime, we see that the three machines are almost in the same operating condition except that each machine has its own characteristics. Thus, to determine the priority maintenance and servicing actions to be undertaken for each machine, a study of the Pareto diagram is required. The latter allows us to identify and classify the different malfunctions in order of importance, meeting the needs of real-time production, the primary objective of the maintenance department.

By consulting the Pareto diagram (fig.10) we can clearly see that mechanical failures dominate with a percentage of 32.77% which requires careful attention. Then come hydraulic failures with 25.98% and finally electrical failures with 1.04% are classified in zone C, requiring lesser interventions. The other failures cover several types of damage and are not subject to discussion.

The analysis of the Pareto diagram (fig.11) reveals a predominance of mechanical failures, representing 34.75% of the total, which requires special attention. Then come hydraulic failures with 22.28%. Electrical failures, for their part, represent only 5.51% of the total, which requires lesser interventions.

In the context of mechanical failures, the use of the Ishikawa diagram (fig 12) helps to break down the causes into different categories, namely labor, method, equipment, environment and matter. By identifying these causes (5M), organizations can take appropriate corrective measures to minimize failures, improve equipment performance and increase productivity.

The category of causes (Workforce) is the most considered with an estimated rate of 50% of effects.
- Employee mentality: attitude of professional conscience from the point of view and commitment to quality and safety.
- Lack of training: lack of necessary knowledge and skills.
- Misuse of equipment: incorrect handling, overloading, non-compliance with specifications.
- Neglect:: lack of attention or care when handling equipment.
- Lack of vigilance and attention to data: lack of regular monitoring of performance data, warning signals and preventive maintenance.

The method category acts with a rate of 40%
- Lack of maintenance planning: lack of maintenance schedule and procedures.
- Lack of follow-up documentation: lack of monitoring of equipment history and information on repairs carried

out.

- Lack of maintenance data analysis: failure to use data to identify recurring problems and opportunities for improvement.

- Lack of preventive maintenance: lack of regular preventive maintenance programs.

For the material, it was quantified at 2% effect, the main cause for this type is the lubricant due to lack of lubrication or inadequate use of the lubricant.

For the material cause it is the lack of availability of spare parts: When a defective part needs to be replaced, it is essential to have spare parts available. If they are not available in a timely manner, this can lead to prolonged downtime, and this has been quantified at 3%.

According to the graph (figure 16) we note that the reliability of the loader is estimated at 53.1% in 2018, then it increases to reach 1 ideal case of reliability in 2019 and 2020, this is explained by a zero number of mechanical failures for our machine and most of the failures in this case lie in the other categories of failure (electrical, hydraulic and others) then we see that it begins to decrease until reaching 47.9% in 2021, then 44.5% in 2022. for the 2nd machine (truck), we see that the reliability is equal to 41.5% in 2018, then it decreases to 36.7% and becomes almost constant over the remaining years. For the bulldozer, we note a reliability equal to 42.4% in

2018, then it rises to reach 50.2% during the year 2019, then it increases to a peak of 100% during the year 2020, then falls back to around 46% during the years 2021 and 2022.

Preventive and corrective actions to be taken

Maintaining industrial systems in operational condition at a lower cost has become a critical factor in business performance and traditional concepts of preventive and corrective maintenance are gradually being supplemented by a more reactive and proactive consideration of failures. Once critical failures have been identified, it is a question of determining their causes. The 5M approach is the best method adapted to this task (Figure 12).

At the end of this study, we recommend some preventive and corrective actions necessary to remedy the various problems affecting the three machines (Figure 17), thus we reduce as much as possible the failures that we can control which has a direct impact on maintenance costs. The final objective of this study is to optimize the maintenance of these machines through reliability.

Conclusion

This work allowed us to:

determine, using the historical file of the machines, the operating parameters of the loaders, trucks and bulldozers in the production section, which allows the maintenance department to develop a maintenance plan that meets the needs of production in real time, given that research in recent years shows that the probability of failure of a component is not as related to age or operating time as previously believed, but much more to the nature of the component and the conditions in which it operates[6],the use of advanced data analysis techniques, such as machine learning and predictive analysis, is essential to fully exploit the benefits of reliability maintenance. These techniques allow data to be collected, analyzed and interpreted proactively, facilitating early failure detection, effective planning of maintenance activities and optimization of resources.

Recommendations

At the end of this work, we recommend the following points:

- ✓ Develop a maintenance plan in line with the mine
- ✓ Put workers counting on the application of the maintenance plan
- ✓ The use of the necessary types of maintenance is in accordance with the appropriate condition
- ✓ Organize specialized training to international or national standards
- ✓ Organization of inventory management
- ✓ Integration of modern methods and provision of necessary tools
- ✓ Reconsider the company policy that emphasizes productivity to the detriment of maintenance
- ✓ Sensitize and motivate employees to make it profitable

References

El. Kihel. B., Zenati. R. (2005) Maintenance audit: a decisive step for any company progress, International Industrial Maintenance Days, Oujda, Maroc.

Riali, A., Talbi. A. (2012) Industrial maintenance engineering. Laboratory of production, energy and sustainable development, higher school of technology.

Zille, V. (2009) Modeling and evaluation of maintenance strategies on multi-component systems. Doctoral thesis, Troyes University, Charles Delaunay Institute.

Lorain, P. (2010) Adapting to new realities, prevention at work, *Hiver* (Pp21-23).

Baadech, A., Aoued R. *Contribution to the improvement of a maintenance plan in a company*, state engineer's thesis in mechanical engineering, Mentouri University Constantine.

Bouanaka, M.L., Chaib.R., Benidir, M., Bellaouar.A., &Verzea.I(2009) Optimization of the function maintenance, *word Journal of Engineering 6(4) Pp (49-54) Sun Light Publishing, Canada ISSN: 1708-5284.*

Chebbi, K., Mellouk.A., & Taleb.M *(2023) Optimization of maintenance through reliability (case of the Ouenza mine)*, Master's thesis in industrial maintenance, Institute of Mines, Echahid Cheikh Larbi Tebessi University, Tebessa.

Moungnutou, M.E. (2016) Estimation of the parameters of the WEIBULL model: application to the modeling of the reliability of the mechanical notching-drilling machine of railway ballasts of CAMRAIL, *Conference: IUT – Entreprises 2015At: Douala-Cameroon, Volume 17.*

Health And Nutritional Complications in Newborns of Hypertensive Mothers

Salima TALEB

Echahid Cheikh Larbi Tebessi University Tebessa, Algeria, 0000-0002-5152-9487

Feriel DJEMAI

Echahid Cheikh Larbi Tebessi University Tebessa, Algeria

Farah MECHAKRA

Echahid Cheikh Larbi Tebessi University Tebessa, Algeria

Abstract: The purpose of this study was to evaluate the fetal and neonatal immediate impact of pregnancy-induced hypertension, and the analysis of the influence of different types of this disease on   health and nutritional statut of the newborn.Case-control study conducted from February 1st to March 30, 2021 at Khaldi Abdelaziz maternity in Tébessa. Were included, newborns of mothers with gestational hypertension, each newborn of hypertensive mother was bet to a newborn of normotensive mother randomly selected on the same day of recruitment. Four developmental stages of pregnancy-induced hypertension has been specified: gestationnal hypertension without proteinuria, pre-eclampsia, chronic hypertension and added pre-eclampsia.Pregnancy hypertension was divided into 68 cases of gestationnal hypertension without proteinuria (61.82%), 36 cases of preeclampsia (32.72%), 4 cases of chronic gestationnal hypertension (3.63%) and 2 cases added preeclampsia (4.2%). The mean age of the hypertensive parturient was 32.67 ± 5.58 years. Primiparae constituted 39.09% in this group and delivery by cesarean section was (52.02%) vs (6.31%) ($p < 0.0001$). Pre-pregnancy body mass index (BMI) and pregnancy BMI were significantly correlated with newborn birth weight. Oligoamnios was significantly more common in mothers with hypertension (28.07%). Prematurity, hypotrophy, Intrauterine growth restriction (IUGR), Intrauterine malformation (IUMF), neonatal death, and respiratory distress syndrome are significantly more common in mothers with hypertension. Preeclampsia appears to be the type of hypertension that has the greatest impact on the health and nutritional status of the newborn with a statistically significant difference ($p < 0.05$). Fetal complications from the combination of high blood pressure and pregnancy are frequent and severe resulting in high neonatal mortality.

Keywords: Pregnant hypertension, newborn, IUGR, hypotrophy, prematurity

Introduction

Pregnancy is a particular physiological state where the maternal organism undergoes numerous metabolic adaptations allowing optimal development of the fetus, maintenance of maternal homeostasis and preparation for breastfeeding. (MARAIS, 2009). The 9 months of pregnancy are accompanied by significant changes in the maternal organism. Several pathologies can occur and some can have an impact on the development of the fetus. Regular monitoring and an adapted lifestyle are recommended for all pregnant women.

Among these conditions, hypertensive disorders of pregnancy are a major cause of severe morbidity, long-term disability, and maternal and neonatal mortality. In Africa and Asia, nearly one-tenth of maternal deaths are associated with hypertensive disorders during pregnancy, while in Latin America, one-quarter of these deaths are related to such complications. (WHO, 2014). Hypertensive disorders of pregnancy affect approximately one in ten pregnant women worldwide (DULEY, 2009, STEEGERS et al, 2010). These disorders include preeclampsia and eclampsia, pregnancy-induced hypertension, and chronic hypertension (STEEGERS et al, 2010).

In a normal pregnancy, fetal growth is a complex multifactorial phenomenon that depends on genetic and environmental factors. Schematically, fetal growth is controlled by placental, fetal and maternal factors. It is inseparable from placental growth and requires a continuous supply of nutrients adapted to each period of pregnancy (LEPERCQ and BOILEAU, 2005). However, the presence of maternal pathology during pregnancy can disrupt the normal evolution of this growth. In the case of this study, high blood pressure of any type can lead to several complications. It can impair the circulation of nutrients in the placenta, which can slow the baby's growth, lead to placental abruption and thus cause premature delivery. It therefore increases the risk of premature birth. Cesarean deliveries are also more common (OUELLET, 2020). HBP also exposes the fetus to the risks of IUGR (which is growth below the 10th percentile for gestational age), prematurity, hypotrophy (birth weight < 2500g), acute hypoxia and stillbirth or neonatal death.

For her part, the mother is exposed to various complications that can put her life at risk, including eclampsia, HELLP syndrome and retroplacental hematoma (AURÉLIA, 2009).

Our study is the first prospective study with an analytical aim in Tébessa, a city in eastern Algeria, which is interested in studying the impact of maternal arterial hypertension on the nutritional and health status of the newborn.

Methods

A case-control study was conducted from February 1st to March 30, 2021 at Khaldi Abdelaziz maternity in Tébessa. This is a retrospective descriptive and analytical study. Were included, newborns of mothers with

gestational hypertension, each newborn of hypertensive mother was bet to a newborn of normotensive mother randomly selected on the same day of recruitment. Four developmental stages of pregnancy-induced hypertension has been specified: HTAG without proteinuria, pre-eclampsia, chronic hypertension and added pre-eclampsia.

The descriptive study focused on 220 mother-newborn couples (110 hypertensive mothers and 110 mothers without pathologies), aged between 21 and 45 years old who had presented themselves to the high-risk pregnancy department and to the postpartum and post-operative department to give birth at the main maternity ward of the city of Tébessa at the KHALDI ABDELAZIZ hospital.

Each woman was interviewed for 15 to 20 minutes. Women who agreed to be interviewed had blood taken for the measurement of some biological parameters. Anthropometric measurements (weight and height) were taken for all mothers interviewed and (weight, height and head circumference) for all newborns of mothers interviewed.

In the section on the mother, we included age, education level, occupation, obstetric history, number of pregnancies and physical activity. We also sought to know whether the mother was hypertensive before or during her pregnancy.

To characterize households from a socioeconomic point of view, we retained the social levels of households and the levels of education.

Mothers was also asked about the follow-up and progress of her previous and current pregnancies. Some health data related to the current delivery were collected: Early rupture of the patient's water, threat of premature delivery, leukorrhea, mode of delivery by vaginal or cesarean section and forceps.

Anthropometric measurements of the mother and her newborn:

o The pregnant woman was weighed just before delivery to estimate the total weight gain (kg).

o The weight of the newborn was measured and recorded by the midwives. It is taken from the birth register.

o The measurement of the length of the newborn is carried out using the fixed part of the height rod placed on the midwife's work surface, according to international recommendations (COGILL, 2003; WHO, 1995).

o The measurement of the head circumference (in cm) is carried out using a 150 cm long extendable tape measure graduated to the mm.

o The Apgar score of the newborn was recorded by the midwives.

o Body mass index (BMI) was calculated using the formula: $BMI = weight/height^2$ (height in m, weight in kg: $kg/m2$)

o Weight gain during pregnancy allowed us to group mothers into three classes according to

recommended weight gain based on pre-pregnancy BMI according to the recommendations of the Institute of Medicine (IOM, 1990; IOM, 2009).

o Eating habits were assessed by 11 questions. This section concerns eating habits, number of meals, frequency of consumption of main meals and the composition of different meals.

o For newborns, we collected information on their birth weight, head circumference, Apgar score, fetal biometry and biological parameters that were available on their records.

Statistical processing:

Statistical tests were performed using Minitab software version 13, results are expressed as percentages and mean ± standard deviations. The significance threshold was set at 0.05

Results

Age

The mean age of the mothers studied is 31.72 ± 5.41 years, the age range is 21 to 45 years. (32.67 ± 5.58) in hypertensive mothers vs (30.78 ± 5.09) years in control mothers, $P = 0.009$). Table (1) shows the distribution of mothers according to their age group, The majority of pregnant hypertensive mothers (51.82%) belong to the age group 30 - 40 years, On the other hand, the majority of pregnant mothers without pathologies (56.36%) belong to the age group 20 - 30 years. The difference between the two groups is significant ($P = 0.010$).

Table 1. Distribution of parturients by age group (n=220)

Variables	Hypertensive mothers		Mothers whout pathologies	
Maternal age :	N	Mean ± SD	N	Mean ± SD
	(110)	$32,67 \pm 5,58$	(110)	$30,78 \pm 5,10$
Age group:	N	Percentage %	N	Percentage%
[20-30] years	41	(37,27%)	62	(56,36%)
] 30-40] years	57	(51,82%)	43	(39,09%)
>40 years	12	(10,91%)	5	(4,55%)

Obstetric history

According to the results of this study, we recorded 31 mothers (36.05%) who have obstetric history in hypertensive mothers vs. 2 mothers (2.35%) in controls ($P < 0.0001$). The most common obstetric history in

hypertensive mothers are: preeclampsia (27.91%) and abortion (5.88%) (Table 2).

Table 2. Distribution of parturients according to obstetric history (n=220)

Variables	Hypertensive mothers N (%)	Mothers without pathologies N (%)	P
Course of pregnancy:			
Normal	55 (63,95%)	83 (97,65%)	<0,0001
Complication :	31(36,05%)	2(2,35%)	
Preeclampsia :			
Yes	24(27,91%)	0 (0,00%)	
No	62(72,09%)	85 (100%)	<0,0001
Abortion:			
Yes	5(5,88%)	1(1,18 %)	
No	80(94,12%)	84 (98,82 %)	<0,0001

Mothers' anthropometric characteristics

In our study hypertensive mother's mean weight before pregnancy (78.6 ± 13.5 kg recorded an increase compared to the mean weight measured at the end of gestation 86.8 ± 13.8) and for mothers without pathologies the mean weight before pregnancy 70.7 ± 13.1 kg recorded an increase compared to the mean weight measured at the end of gestation (78.3 ± 12.6), The difference is significant (<0.0001) between the 2 categories of mothers.

Table 3. Comparison between hypertensive mothers and mothers without pathologies according to their anthropometric characteristics

Paramètre	Hypertensive mothers N (Mean ± SD)	Mothers without pathologies N (Mean ± SD)	P
Weight			
Before pregnancy	110 (78,6 ± 13,5)	110 (70,7 ± 13,1)	<0,0001
Current	110 (86,8 ± 13,8)	110 (78,3 ± 12,6)	<0.0001
Height	110 (1,63± 0,06)	110 (1,64 ± 0,05)	0,415
BMI :			
Before pregnancy	110 (29,34 ± 5,52)	110 (26,15 ± 4,89)	<0,0001
Pregnancy	110 (32,39 ± 5,74)	110 (28,93 ± 4,62)	<0.0001

Body size before pregnancy

The results of this study showed that the prevalence of overweight is higher in mothers without pathologies (40% vs 36.36%) than in hypertensive mothers on the other hand the prevalence of obesity is very high in hypertensive mothers than in mothers without pathologies (44.55% vs 17.27%). Thinness was found in 7 mothers. (P = <0.0001). (Table 4)

Table 4. Distribution of parturients according to BMI classes before pregnancy

BMI class before pregnancy	Hypertensive mothers N (%)	Mothers without pathologies N (%)	P
Thinness	1 (0.91 %)	6 (5.45 %)	<0.0001
Normal weight	20 (18.18 %)	41 (37.27 %)	
Overweight	40 (36.36 %)	44 (40.00 %)	
Obesity	49 (44.55 %)	19 (17.27 %)	

Type of hypertension

The most frequent type of hypertension in hypertensive mothers is gestational hypertension (pregnancy) 61.82% followed by pre-eclampsia 32.72%, chronic hypertension 3.64% and finally pre-eclampsia added 1.82%. (Figure 1).
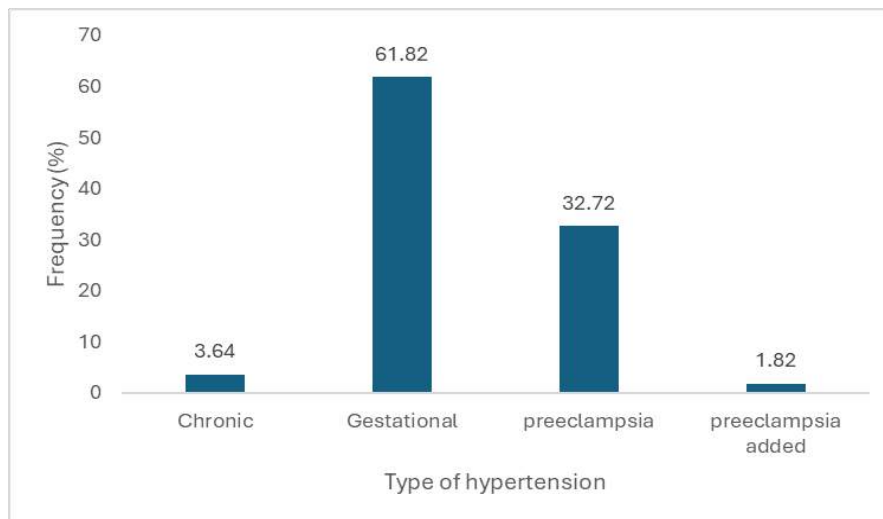
Figure 1. Distribution of hypertensive mothers according to the type of arterial hypertension (n=110)

Mode of delivery

Most hypertensive women (57.02%) gave birth by cesarean section vs. 6.31% of mothers without pathologies.

On the other hand, (90.99%) of mothers without pathologies gave birth vaginally vs. 41.23% of hypertensive mothers, (P < 0.0001). (Table 28) or (Figure 2).
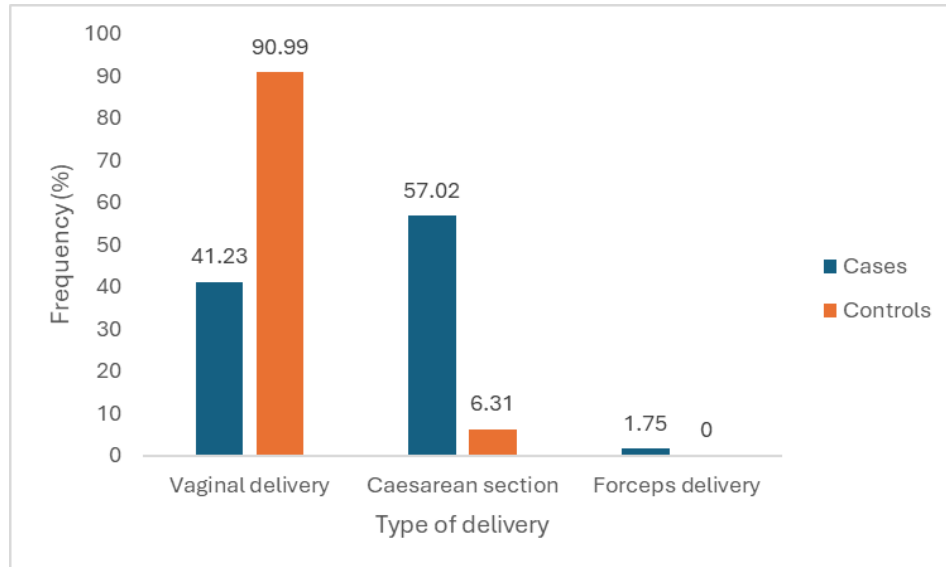
Figure 2. Type of delivery

Incidents during pregnancy

Our results showed that the threat of preterm delivery during pregnancy is significantly higher in hypertensive mothers than in mothers without pathologies (22.94% vs. 0.91%, P = < 0.0001). On the other hand, the incidence of early rupture of the membrane is significantly higher in mothers without pathologies than in hypertensive mothers (50% vs. 31.19%, P = 0.005). No significant difference was observed for the incidence of leukorrhea (Figure 3).
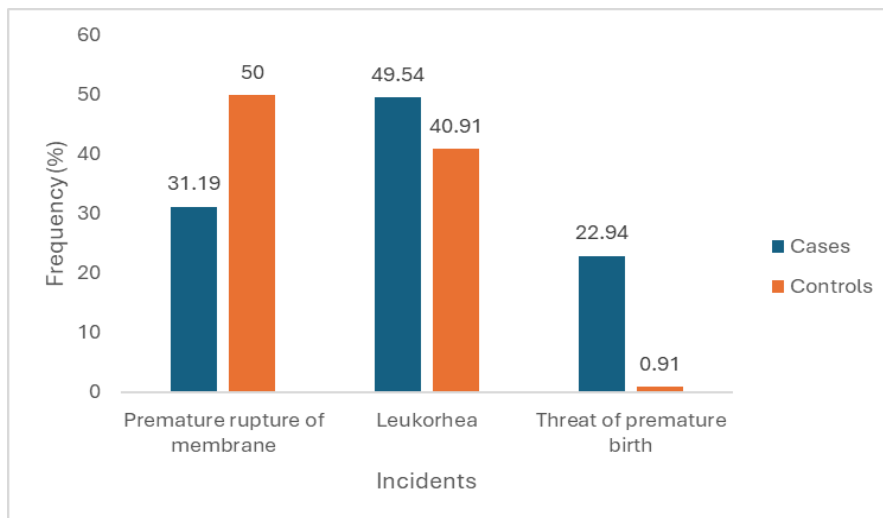
Figure 3. Incidents during pregnancy for hypertensive women and women without pathologies

Pre-pregnancy weight status and total weight gain

The frequency distribution of categories of total weight gain according to pre-pregnancy weight status is presented in figures (4,5,6). Excessive weight gain is more frequent in hypertensive women regardless of their pre-pregnancy weight status: normal weight, overweight or obese (28.57%, 35, 34) respectively, without the difference being significant. On the other hand, insufficient weight gain is more frequent in women without pathologies regardless of their pre-pregnancy weight status: normal weight, overweight or obese (57.45%, 45.45, 42.11) respectively, without the difference being significant between the two groups.
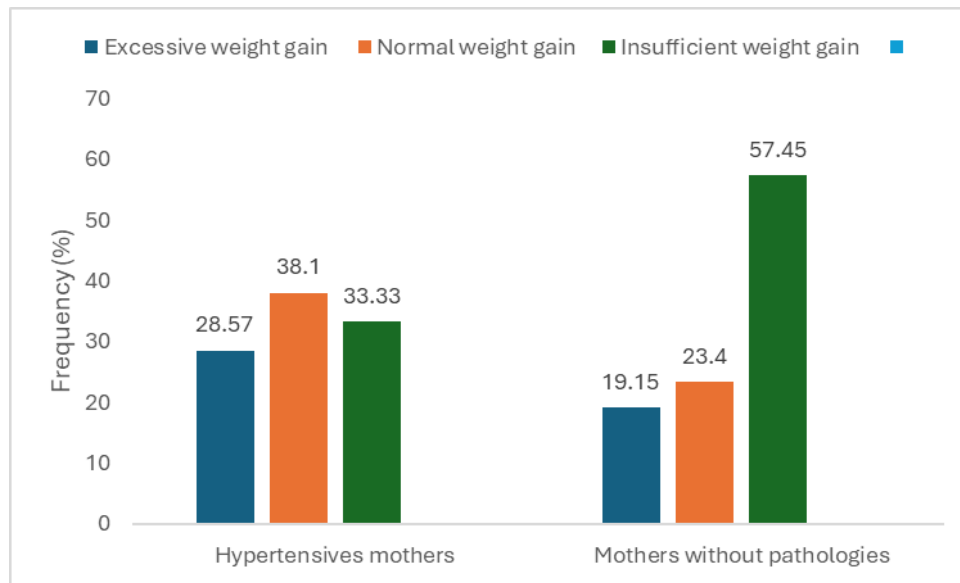
Figure 4. Total pre-pregnancy gestational weight gain in normal weight mothers
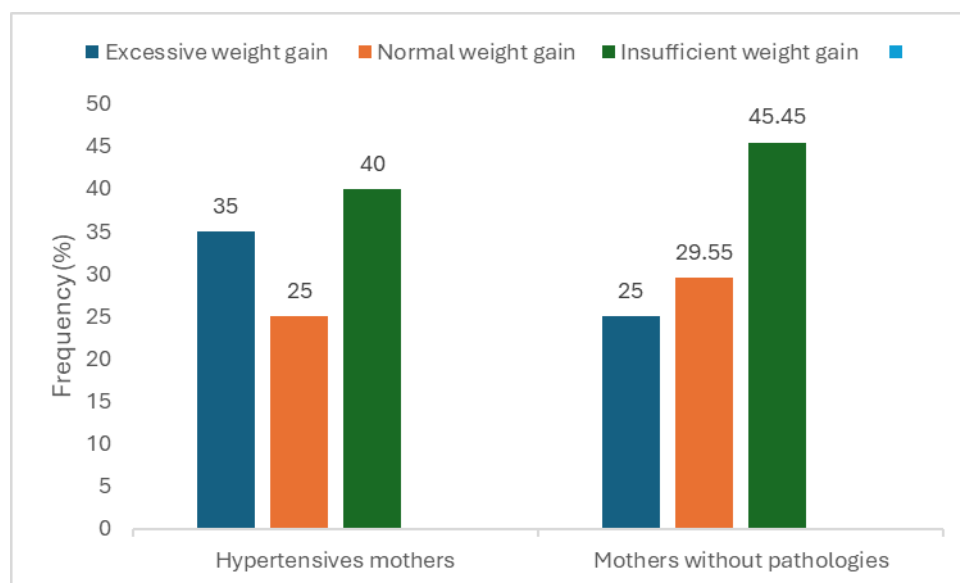
Figure 5. Total pre-pregnancy gestational weight gain in overweight mothers
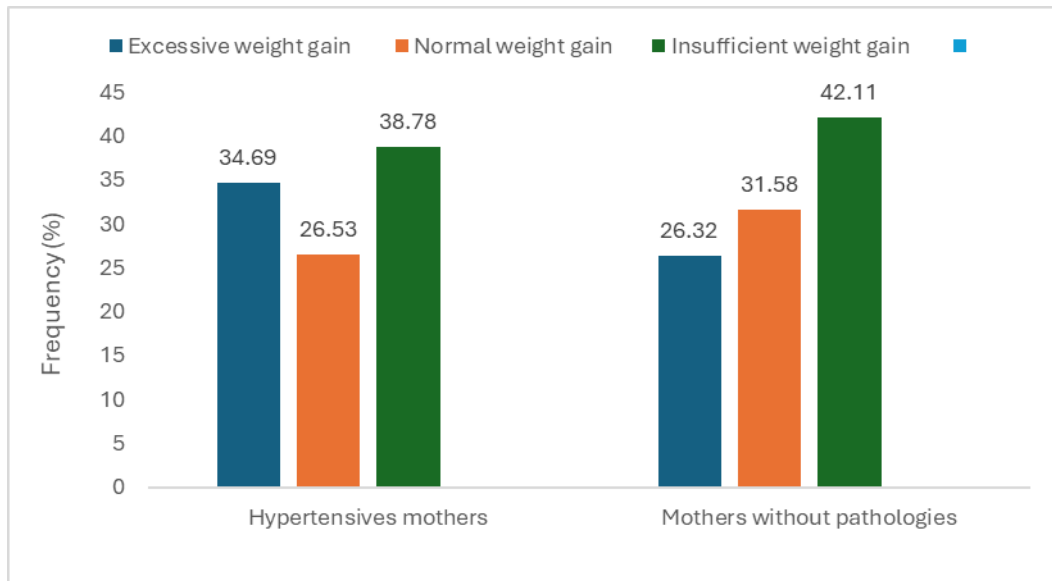
Figure 6. Total pre-pregnancy gestational weight gain in obese mothers

Anthropometry of newborns

Anthropometric measurements taken on newborns at birth are weight, height, and head circumference. The mean weight of newborns of mothers without pathologies is significantly higher than the mean weight of newborns of hypertensive mothers (3061 ± 4.79 vs. 3518 ± 4.10, P < 0.0001). The mean values of the head circumference of newborns of mothers without pathologies are higher than those of newborns of hypertensive mothers (P = 0.005), (Table 5).

Table 5. Anthropometry of newborns

Variables	Hypertensives mothers N (Mean ±SD)	Mothers without pathologies N (Mean ±ET)	P
Weight (g)	114 (3061 ± 4,79)	111 (3518 ± 4,10)	<0,0001
Height(cm)	90 (44,44 ± 4,79)	102 (45,38 ± 4,79)	0,150
Cranial perimeter (cm)	91 (34,16 ± 3,89)	102 (35,50 ± 2,25)	0,005

Health complications of newborns from hypertensive mothers and mothers without pathologies

Respiratory distress is significantly more frequent in newborns of hypertensive mothers 31.58% than in mothers without pathologies 6.31%, P < 0.0001. The same is true for prematurity 20.18% vs 0.91%, hypotrophy 20.18% vs 0%, P < 0.0001 and resuscitation in the delivery room 26.32% vs 6.31%, P < 0.0001. The main resuscitation used are: aspiration and oxygen therapy). In utero fetal mortality is higher in hypertensive parturients (3.51% vs

0%, P = 0.045, (Table 6).

Table 6. Health complications of newborns from hypertensive mothers and mothers without pathologies

Complication	Hypertensives mothers N (%)	Mothers without pathologies N (%)	P
Respiratory distress	36 (31.58 %)	7 (6.31 %)	<0,0001
Prematurity	23 (20,18 %)	1 (0,91 %)	<0,0001
Macrosomia	8 (7,02 %)	10 (9,01 %)	0,582
Hypotrophy	23 (20,18 %)	0 (0,00 %)	<0,0001
Perinatal asphyxia	2 (1,75 %)	1 (0,90 %)	0,577
Intrauterine fetal death	4 (3,51 %)	0 (0,00 %)	0,046
Intrauterine growth retardation (IUGR)	4 (3,51 %)	0 (0,00 %)	0,046
Resuscitation in the delivery room	30 (26,32 %)	7 (6,31 %)	<0,0001
Type of resuscitation:			
Suction	29 (25,44 %)	7 (6,31 %)	<0,0001
Oxygen therapy	24 (21,05 %)	7 (6,31 %)	0,001
Rewarming	2 (1,82 %)	0 (0,00 %)	0,155

Short-term evolution of newborns from hypertensive mothers without pathologies

After delivery, 100% of newborns from mothers without pathologies were breastfed compared to 80.70% of newborns from hypertensive mothers (P <0.0001). The number of hospitalized newborns is significantly higher among hypertensive mothers than among mothers without pathologies (28.07% vs. 6.31%, P <0.0001). Six (06) children were born with malformations (four children born to hypertensive mothers and two children born to mothers without pathologies (Table 7).

Table 7. Short-term evolution of newborns from hypertensive mothers without pathologies

Variables	Hypertensives mothers N (%)	Mothers without pathologies N (%)	P
Died	6 (5,26 %)	(0 (0,00 %)	0,014
Breastfeeding with good adaptation to outdoor life	92 (80,70 %)	111 (100 %)	<0.0001

Hospitalized	55 (48,24 %)	8 (12,61 %)	0,006
Malformation	4 (3,51 %)	2 (1,80 %)	0,427
Type of malformation :			
Facial	2 (1,75 %)		
greenish	1 (0,91 %)	1 (0,90 %)	0,557
		1 (0,91 %)	1,000
Hypertrophic cardiomyopathy	3 (2,63 %)	0 (0,00 %)	0,085
Fetal asphyxia	3 (2,63 %)	2 (1,80 %)	0,673

Biometry and fetal well-being of newborns from hypertensive mothers without Pathologies

The biparietal diameter was less than the 10th percentile for gestational age in 15 (6.81%) women (13 hypertensive women and 2 women without pathologies). 215 women (97.73%) carried a singleton pregnancy and 5 (2.27%) a twin pregnancy. Our results also showed that 29(26,36 %) of hypertensive mothers had oligohydramnios compared to 5 (4.55%) in mothers without pathologies. 10 (9.09%) among hypertensive mothers had hydramnios compared to 2 (1.82%), $P < 0.0001$. The fetal electrocardiogram was pathological in 2 (1.82%) newborns of hypertensive mothers (Table 8).

Table 8. Biometry and fetal well-being of newborns from hypertensive mothers without pathologies

Variables	Hypertensives mothers		Mothers without pathologies		
	N %		**N %**		**P**
Evolving pregnancy	104 (91,23 %)		110 (100 %)		0,001
Amniotic fluid					
Normal	71 (64,55 %)		103 (93,64 %)		
Oligohydramnios	29(26,36 %)		5 (4.55 %)		<0,0001
Hydramnios	10 (9,09 %)		2 (1,82 %)		
Biparietal diameter "BIP"	**N (Mean ± SD)**		**N (Mean ± SD)**		<0,0001
	93 (89,97 ± 5,38)		49 (93,58 ± 3,95)		
Fetal electrocardiogram					0,994
Normal	108 (98.18 %)		110 (100 %)		
Pathology	2 (1,82 %)		00 (0,00 %)		

Correlation of biological parameters with newborn birth weight

A positive correlation was found between BMI before pregnancy and BMI during pregnancy of hypertensive

mothers and newborn birth weight (r = 0.269, P = 0.004 and r = 0.261, P = 0.005) respectively (Table 9).

Table 9. Correlation of biological parameters with newborn birth weight

Variables	Hypertensives mothers		Mothers without pathologies	
	r	P	r	P
Hemoglobin vs NBW	- 0,14	0,136	-0,048	0,615
BMI berfore pregnancy vs NBW	0,269	**0,004**	0,141	0,141
BMI during pregnancy vs NBW	0, 261	**0,005**	0,168	0,078
Urea vs NBW	0,081	0, 392	-0,081	0,4
Creatinine vs NBW	-0,174	0,141	/	/
Proteinuria	-0,202	0,129	/	/

Impact of different types of hypertension on the health and nutritional status of newborns

Prematurity, hypotrophy, IUGR, IUMF, neonatal death and respiratory distress syndrome are significantly more frequent in hypertensive mothers. Preeclampsia seems to be the type of hypertension that has the greatest impact on the health and nutritional status of the newborn (Table 10).

Table 10. Impact of different types of hypertension on the health and nutritional status of newborns

Complications	Hypertensives mothers				Mothers without pathologies N = 110	P
	Pregnancy-high blood pressure N = 68	Preeclampsia N = 36	high blood pressure Chronic N = 4	Preeclampse added N = 2		
Prematurity	5 (23,8 %)	13(36,1 %)	1 (4,8 %)	1 (4,8 %)	1 (4,8 %)	< 0.0001
Hypotrophy	7 (33.3 %)	12 (57,1 %)	1 (4,8 %)	1 (4,1 %)	0 (0,00 %)	<0.0001
IUGR	1 (25 %)	2 (50 %)	1 (25.00 %)	0 (0.00 %)	0 (0.00 %)	0.012
Asphyxia P	1 (33.3 %)	1 (33.3 %)	0 (0,00 %)	0 (0,00 %)	1 (33.33 %)	0.772
MFIU	1 (25.00%)	3 (75.00 %)	0 (0,00 %)	0 (0,00 %)	0 (0,00 %)	0.032
Neonatal death	1 (16.67 %)	4 (66.67 %)	1 (16.71%)	0 (0,00 %)	0 (0,00 %)	0,002

Macrosomia	7 (35 %)	0 (0.00 %)	0 (0.00 %)	1 (5.56 %)	10 (55.56%)	0.113
Respiratory distress	20 (46.51 %)	11 (25.58 %)	5 (11.63 %)	0 (0,00 %)	7 (16.28 %)	<0.0001
Apgar at 1 min	**68 (7.02±1.22)**	**36 (6.55±2.41)**	**4 (6.80±1.78)**	**2 (7.33±0.57)**	**110(7.16±0.75)**	**0.202**
[0-2] at 1 min	6 (5,66 %)	0 (0.00 %)	0 (0.00 %)	0 (0.00 %)	0 (0,00 %)	0.001
[3-6] at 1 min	12 (11,32 %)	5 (12,8 %) 4 (10,26 %)	2 (25,00 %)	0 (0,00 %)	5 (4,50 %)	0.001
Apgar at 5 min	**70 (7.21±1.10)**	**36 (6.77±2.36)**	**5 (7.20±1.09)**	**3 (7.33±0.57)**	**111(7.40±0.66)**	**0.134**
[0-2] at 5 min	5 (4,72 %)	4 (10.26 %)	0 (0,00 %)	0 (0,00 %)	0 (0,00 %)	<0.0001
[3-6] at 5 min	10 (9,43 %)	4 (10.26 %)	2 (25,00 %)	0 (0,00 %)	2 (1,80 %)	<0.0001

Discussion

After the comparison between hypertensive mothers and mothers without pathologies according to age we found that there is a significant difference (32.67 ± 5.58) vs (30.78 ± 5.10) respectively with (P = 0.009). This difference shows that the oldest mothers [30-40 years] are the most affected by HTA. On the national level, results lower than those found in this study were observed in (MOUKADDIME, 2001) who showed that HTA was frequently encountered in the age group of 25 to 35 years with a rate of 43.94%. In the same sense (MANSOURI, 2005) noted 52.11% of patients aged between 25 and 35 years. Other authors, on the other hand, noted a high frequency of the disease in older parturients. Thus, (POONYTH, 2003) noted a rate of 48.9% of parturients over 40 years old. These disparities are mainly explained by the characteristics of the populations studied. However, the literature is almost unanimous on the fact that a maternal age that is too young or too advanced constitutes a risk factor for pregnancy-induced hypertension. (DUCKITT and HARRINGTON, 2005), in their remarkable literature review published in 2005, found a risk multiplied by two of developing pre-eclampsia in mothers whose age is greater than or equal to 40 years, whether they are primiparous or multiparous with a relative risk of 1.68 and 1.96 respectively.

Regarding obstetric history, the results of the literature confirm that patients with a history of gestational hypertension, pre-eclampsia, IUFD, abortion or other complications of HTAG represent a population at high risk of developing a second episode of the disease and especially its severe forms and can be identified from the beginning of pregnancy. Thus, the history of pre-eclampsia emerges as the most significant risk factor in many studies with a recurrence rate that varies between 20 and 55% depending on the publications [(DILDY et al, 2007, BROWN et al, 2007), for their part, found a risk multiplied by seven of developing pre-eclampsia in mothers who had a history of this condition, this same risk is multiplied by eight in Merviel et al (OR = 8.12) (MERVIEL et al, 2008). In our study, among women who had a history of pre-eclampsia (24 women), 9 women (37.5%) developed pre-eclampsia in current pregnancies.

Overweight and obesity appear to be very significant risk factors in the genesis of pregnancy-induced hypertension and in particular pre-eclampsia. This risk reaches an odds ratio of 2.50 for overweight and 2.61 for obesity in (MERVIEL et al, 2008). BOUDNAR et al, 2005 found a relative risk of developing the disease of 2 when the BMI before pregnancy is greater than 25 kg/m² and a relative risk of 2.9 when it is greater than 30 kg/m². According to (SIBAI et al, 1997), this same risk would be multiplied by three (OR of 3.22) when the BMI is greater than 35 kg/m². This same observation has been reported by other authors, in particular (BASSO et al, 2003). Being overweight is not only associated with an increased risk of developing pre-eclampsia but also correlated with the severity of the disease and the precocity of its onset (CATOV et al, 2007). Several hypotheses have been put forward to explain this fact: some postulate that hypertension occurs during pregnancy in obese patients due to an increase in cardiac output, while for others (and this is the hypothesis most often accepted) hyperlipidemia would promote the production of peroxides which would lead to an alteration of the maternal endothelium and vasoconstriction (MERVIEL et al, 2008). All these results are in agreement with our result and confirm that hypertension affects obese and overweight mothers much more.

The prevalence of each type of gestational hypertension varies from one study to another. In our study as in that of (TOURÉ et al, 1997), gestational hypertension predominates. The rate of chronic hypertension is less than 10%, except in the study of (ATTOLOU et al, 1998) where it is 41.51% without any explanation being provided. These classifications do not consider the term of pregnancy at the time of diagnosis of hypertension, whereas this is an element that has a great influence on the prognosis, in particular the fetal prognosis. Gestational hypertension discovered close to term does not pose the same problems of monitoring or management as gestational hypertension discovered before 34 weeks of amenorrhea.

In our sample, cesarean delivery was 57.02% in hypertensive mothers versus 6.31% in mothers without pathologies with a statistically significant difference (P = <0.0001). (CHAHID et al, 2014) in Morocco found 52.3% versus 20% cases of cesarean section. The data in the literature are thus consistent with the observation of early birth during preeclampsia and eclampsia, particularly due to premature fetal extraction by cesarean section justified by the frequent occurrence of suffering (GEYL et al, 2014). Other studies have shown variable results. In France (GEYL et al, 2014), and in Morocco (CHAHID et al, 2014), respectively 74.9% and 62.5% of women had given birth by cesarean section. On the other hand, in Congo Brazzaville (PAMBOU et al, 1999) and Benin (LOKOSSON, 2006), the cesarean rates were lower, respectively 57% and 44.7%. The major indications for cesarean section were dominated by severe preeclampsia, retro placental hematoma and acute fetal asphyxia. In our study, cesarean section was most often performed in an "emergency" context before the onset of labor.

According to our results, during the first 24 hours of life, only 80.70% of newborns from hypertensive mothers versus 100% of newborns from mothers without pathologies were immediately breastfed and 28.07% versus 6.31% respectively were referred to neonatology with a statistically significant difference (P = <0.0001). Neonatal death was 5.26%. NDIAYE et al in a descriptive study in Senegal found 36.5% of newborns

transferred to neonatology with 10.5% of deaths in the early neonatal period (NDIAYE et al, 2017).

The percentage of HBP is higher in hypertensive mothers with excessive weight gain regardless of their weight status before pregnancy: normopuncture, overweight or obese. These results are consistent with several studies that have confirmed that excessive gestational weight gain increases the risk of developing high blood pressure during pregnancy (TEBBANI et al. 2017; GAILLARD 2015; TANAKA et al. 2014; MCCLURE et al. 2013). In the study by BARTON et al, the rate of gestational hypertension increased with excessive weight gain (BARTON et al. 2015). Also, DERUELLE et al, (2004), highlighted that excessive weight gain during pregnancy increases the risk of vascular complications (5.2% versus 1.1%; p < 0.05). This is mainly an increase in the percentage of high blood pressure in mothers with excessive weight gain. Another study examined the impact of gestational weight gain above the IOM recommendations. The researchers found that the risk of being diagnosed with high blood pressure increased from 6.0% for pregnant mothers with normal weight gain to 9.0% in mothers with excessive weight gain (LANGFORD et al. 2011).

Other researchers suggest that there is a relationship between excessive weight gain during pregnancy and an increased risk of hypertension, independent of pre-pregnancy BMI (JOHNSON et al. 2013). Although the biological mechanisms surrounding gestational hypertension are not fully understood, the association between excess weight and increased risk of hypertensive diseases is well established. Adiposity leads to the production of more C-reactive protein and inflammatory cytokines, as well as contributing to increased levels of oxidative stress (ROBERTS et al. 2011). This may explain the association between excess body fat storage and the development of pregnancy-related diseases such as hypertension that may be mediated by these physiological changes. This mechanism may also explain the risk observed in mothers who experienced excessive weight gain. The study by (MASHO et al, 2016), showed a greater likelihood of HBP with increasing weight gain.

The perinatal prognosis is also poor. Indeed, we observed an excess risk of premature births 23.18%, respiratory distress 31.58% and hypotrophy 20.18%, in utero death, transfers to neonatology, and neonatal death. For other African authors [(BAH et al, 2001); (ADISSO et al, 2002)], only prematurity appeared as the most frequently encountered morbid factor. This could be explained by the underuse of diagnostic means of fetal distress, such as obstetric ultrasound and electronic recording of the fetal heart rate, means available in our department for several years. On the other hand, perinatal mortality in our series was lower than that published by (ADISSO et al, 2002) estimated at 20.8%. This author explained his high rate of perinatal deaths by the lack of rigorous monitoring of pregnant women hospitalized in his series, as well as the delay observed in the decision to terminate the pregnancy. Furthermore, RASOLONJATOVO et al, (2005) noted a rate significantly higher than ours (30%), without a valid explanation. On the other hand, lower rates of perinatal mortality (between 5.3 and 13.5%) have been observed by other African authors (YOMBISSI et al, 1987), thus approaching the rates published in Europe (MAMPUYA and SURCEL, 1997) without the strategies for better management of pregnant women by these African teams having been clearly described.

Only BMI before pregnancy and during pregnancy were associated with birth weight. This result confirms the

data already available in the literature. The same results show that the baby's weight varies little whether the mother gains 2 or 12 kg during pregnancy, but that it is when she gains more weight (more than 12 kg excluding the weight of the fetus and adnexa, or about 15 kg in total) that the impact of these kilos is evident on the baby's corpulence (EDEN, 2007).

Regarding the impact of maternal hypertension on the health and nutritional status of the newborn, we have observed highly significant differences between the different hypertensive disorders such as hypotrophy, prematurity, respiratory distress, neonatal death and the Apgar score) between newborns of hypertensive mothers and mothers without pathologies. Some studies have shown that high blood pressure during pregnancy is responsible for neonatal mortality and morbidity that vary considerably depending on the severity of the hypertensive pathology [(MEZIANI et al, 2007); BERKAN, 2010)]. The existence of a hepatic syndrome (HELLP syndrome) or other maternal complications (eclampsia or retroplacental hematoma) represents an additional major element of severity (NGOS et al, 2003). Ten to fifteen percent of pregnancies are complicated by high blood pressure. Among these, 10 to 20% have proteinuria, defining preeclampsia which represents a vital fetal or even maternal threat (ZUPAN-SIMUNEK, 2010). In our study, the type of hypertension that has the greatest impact on the health and nutritional status of the newborn is preeclampsia which represents (32.72%) of cases. Studies conducted in the United Kingdom, Germany, Italy and Saudi Arabia have also shown that hypertensive disorders during pregnancy were associated with prematurity, low birth weight and a depressed Apgar score (LOVE et al, 2012). Studies by DAO, 2005) and (ITOUA et al, 2013) report a morbid Apgar score in more than a third of newborns of hypertensive mothers (38.8% and 33% respectively).

Conclusion

Despite improved management, hypertensive syndromes of pregnancy remain common. They represent one of the main causes of maternal, fetal and neonatal morbidity and mortality. It is a complication of pregnancy of placental origin that is based on an abnormality of placental perfusion. Better pathophysiological knowledge would allow the development of therapeutic strategies contributing to feto-placental protection.

High blood pressure remains a real public health problem in our country due to its serious prognosis of a high mortality rate for the mother-child couple. Knowledge of its risk factors with a view to prevention would further reduce its frequency. The management of pregnant hypertensive women is a burden to be taken into consideration to protect the mother and the newborn.

Recommendations

At the end of this study, we recommend the management of pregnant women who suffer from high blood pressure to protect both the mother and the newborn.

Acknowledgements

References

Adısso S, Lokossou A, Komonguı D, Olowu-Salako Aa, Perrın R. 2002. Les syndromes vasculo-renaux sévères : aspects épidémiologiques et pronostiques. Journal de la SAGO ; 3 (2) : 1

Attolou V., Takpara I., Akvavıt J. 1998. Les différents types d'hypertension artérielle chez les femmes enceintes Béninoises admises au CNHU de Cotonou. *Cahiers d'études et de recherches francophones/ Santé. Octobre- Novembre : 8 (5) : 353-356.*

Aurélıa, R. D. M. 2009. Evaluation des facteurs de risque et du pronostic materno-foetal en cas d'association HTA et grossesse a la maternité du CENHOSOA. N : 166. P : 1.

Bah Ap, Dıallo Mh, Conde Am, Keıta N. 2001. Hypertension artérielle et grossesse : mortalité maternelle et périnatale Médecine d'Afrique Noire 2001; 48(11):461-4

Barton Jr, Joy Sd, Rhea Dj, Sıbaı Aj, Sıbaı Bm. 2015. The influence of gestational weight gain on the development of gestational hypertension in obese women. Am J Perinatol 2015;32(07):615–620.

Basso O, Weınberg Cr, Baırd Dd, Wılcox Aj, Olsen J. 2003. Subfecundity as a Correlate of Preeclampsia: A Study within the Danish National Birth Cohort Am J Epidemiol;157:195–202

Berkane N. 2010. Definitions et conséquences des hypertensions artérielles de la grossesse. Ann Fr Anesth Reanim;29:e1—6.

Boudnar Lm, Ness Rb, Markovıc N. 2005. The Risk of Preeclampsia Rises with Increasing Prepregnancy Body Mass Index. Ann Epidemiol;15(7): 475-82

Brown Ma , Mackenzıe C, Dunsmuır W, Roberts L, Ikın Et K . 2007. Can we predict recurrence of pre-eclampsia or gestational hypertension? BJOG;114:984–93.

Catov Jm, Ness Rb, Kıp Ke, Olsen J. 2007. Risk of early or severe preeclampsia related to pre-existing conditions Int J Epidemiol;36(2):412-419

Chahıd.N N, Boudana.S S, Kabırı M, Mrabet M, Knounı H, Karabach A. 2014. Retentissement foetal et néonatal de l'hypertension artérielle gravidique : données marocaines. Journal de pédiatrie et de puériculture. ; 27 (3) :111- 116.

Cogıll B.2003. Guide de mesure des indicateurs anthropométriques. Projet d'Assistance Technique pour l'Alimentation et la Nutrition, Académie pour le Développement de l'Education, Washington, D.C

Dao Zs. 2005. Hypertension artérielle et grossesse dans le Service de gynécologie obstétrique de l'hôpital Gabriel Toure à propos de 120 cas. Thèse de doctorat en Médecine. s.l. : Université de Bamako .

Deruelle P, Houffın-Debarge V, Vaast P, Delvılle N, Helou N, Subtıl D. 2004. Effets maternels et foetaux d'une prise de poids excessive au cours de la grossesse dans une population de patientes de poids normal avant la grossesse. Gynécologie Obstétrique et Fertilité; 32 : 398-403.

Dıldy Ga, Belfort Ma Et Smulıan Jc. 2007. Preeclampsia Recurrence and Prevention Seminars in Perinatology,;31:135-41

Duckıtt K, Harrıngton D. 2005. Risk factors for prééclampsia at antenatal booking: syste matie review ofcontrolled studies. BMJ. 330 :565 - 567.

Duley L. 2009. The global impact of pre-eclampsia and eclampsia. *Seminars in Perinatology*, Jun;33(3):130–137.

EDEN (2007), Etude des determinants pre et post natals précoces de la santé et de développement de l'enfant http://eden.vjf.inserm.fr/.

Gaıllard R 2015. Maternal obesity during pregnancy and cardiovascular development and disease in the offspring. Eur J Epidemiol. 2015 Sep 16.

IOM (Institute Of Medicine).1990 . Sub committee on nutritional status and weight gain during pregnancy. Nutrition during pregnancy. Washington DC. National Academy Press : 137-75.

IOM 2009. Weight Gain During Pregnancy: Reexamining the Guidelines; Committee to Reexamine IOM Pregnancy weight Guidelines; Sponsor Briefing May 27, 2009.

Itoua C.C. ; Ngounda Monıanga A.S. , Ellenga Mbolla B.F. , Mbemba Moutounou G.M. , Gombet Koulımaya C.E. , Gombet T.R. , Ilokı L.H. 2013. HYPERTENSION ARTÉRIELLE ET GROSSESSE : épidémiologie et pronostic maternofoetal au Centre Hospitalier Universitaire de Brazzaville (Congo). Médecine d'Afrique Noire , Vol.60, N°1.

Johnson J, Clıfton RG, Roberts JM, Myatt L, Hauth JC, Spong CY et al. 2013. Pregnancy Outcomes With Weight Gain Above or Below the 2009 Institute of Medicine Guidelines. Obstetrics and gynecology 121: 969–975.

Langford A, Joshu C, Chang JJ, Myles T, Leet T. 2011. Does gestational weight gain affect the risk of adverse maternal and infant outcomes in overweight women? Matern Child Health J. 7, 860-865.

Lepercq, J., & Boıleau, P. 2005. Physiologie de la croissance foetale. *EMC-Gynecologie Obstetrique*, *2*(3),p : 199-208.

Lokossou A, Avode DG, Komonguf DG, Takpara I, Sacca PC, Perrın RX. 2006. Prise en charge des manifestations de la prééclampsie sévères et de l'éclampsie par le sulfate de magnésium à Cotonou. AJNS ; 25 :41-45

Love ER, Crum J, Bhattacharya S. 2012. Independent effects of pregnancy induced hypertension on childhood development: a retrospective cohort study. Eur J Obstet Gynecol Reprod Biol 2012; 165: 219-224.

Mampuya A, Surcel IV. 1997. Importance de quelques paramètres dans l'évaluation de l'hypertension induite par la grossesse. Panorama Medical ; II (1) : 20-3.

Mansourı I. 2005. Hypertension artérielle gravidique: Expérience du service de maternité Souissi II (355 cas). Thèse de médecine de Rabat n° 167 .

Maraıs, J. 2009. *Besoins nutritionnels de la femme enceinte: point sur les recommandations en 2009* (Doctoral dissertation).

Masho SW, Urban P, Cha S, Ramus R. 2016. Body mass index, weight gain, and hypertensive disorders in pregnancy. Am J Hypertens 2016; 29:763–771.

Mcclure CK, Catov JM, Ness R, Bodnar LM. 2013. Associations between gestational weight gain and BMI, abdominal adiposity, and traditional measures of cardiometabolic risk in mothers 8 y postpartum. Am J Clin Nutr 2013, 98:1218–1225.

Merviel P, Touzart L, Deslandes V, Delmas M, Coicaud M, Gondry J. 2008. Facteurs de risque de la prééclampsie en cas de grossesse unique J Gynecol Obstet Biol Reprod;37:477-82

Meziani F, Tesse Ap, Asfar Schneide F, Andriantsitohaina R, Fournie A, Gairard A. 2007. De la toxémie gravidique à l'éclampsie. Physiopathol Reanim;16(5):380—5.

Moukkadime A. 2001. Pronostic foetal et maternel au cours de la toxémie gravidique à la maternité Lalla Meryem du CHU Ibn Rochd de Casablanca à propos de 330 cas. Thèse de médecine de Casablanca n° 306 année.

Ndiaye.O. 2017. Complications foetales et néonatales de la prééclampsie sévère et éclampsie Etude rétrospective à la maternité et au service de néonatologie au centre hospitalier abass ndao de Dakar (Sénégal). J Afr pediatr genet Med; 2 :10-14

OMS (Organisation Mondiale De La Sante). . 1995. Utilisation et interprétation de l'anthropométrie. Rapport d'un comité d'experts, OMS. Série de Rapports techniques N° 854. Genève. P : 498 .

OMS (Organisation Mondiale De La Sante°. 2014. Recommendations de l'OMS pour la prévention et le traitement de la prééclampsie et de l'éclampsie. Organisation mondiale de la Santé. https://apps.who.int/iris/handle/10665/138406.

Ouellet C. 2020. L'hypertension et la prééclampsie durant la grossesse. Naitre et grandir.

Pambou O, Ekoundzola JR, Malanda JP, Buambo S. 1999. Prise en charge et pronostic de l'éclampsie au CHU de Brazzaville (à propos d'une étude rétrospective de 100 cas) Med Afr Noire. ; 46 (11) :508-512.

Poonyth L, Sobhee R, Soomaree R. 2003. Epidemiology of preeclampsia in Mauritius island Journal of Reproductive Immunology ;59:101-9

Rasolonjatovo JDC, Raherizaka N, Rakotoarimanama S, Ravelomanana N, Andriamanantsara L, Rosolofondaibe A. 2005. Etude épidémiologique de l'hypertension artérielle gravidique à Antsirabe Madagascar. Med Afr Noire; 52: 121-5

Roberts JM, Bodnar LM, Patrick TE, Powers RW. 2011. The role of obesity in preeclampsia. Pregnancy Hypertens 2011; 1:6–16.

Sibai BM, Ewell M, Levine RJ, Klebanoff MA. 1997. Risk factors associated with preeclampsia in healthy nulliparous women Am J Obstet Gynecol ;177(5)

STEEGERS EA, VON DADELSZEN P, DUVEKOT JJ, PIJNENBORG R. PRE-ECLAMPSIA. LANCET, 2010. 21 ; 376(9741) :631–44

Tanaka T, Ashihara K, Nakamura M, Kanda T, Fujita D, Yamashita Y et al. 2014. Associations between the pre-pregnancy body mass index and gestational weight gain with pregnancy outcomes in Japanese women. J Obstet Gynaecol Res.2014; 40(5):1296– 1303.

Tebbani F, Oulamara H, Agli A. 2017. Pre-pregnancy body mass index and gestational weight gain as risk factors on maternal and birth outcomes. ejbps, 2017, Volume 4, Issue 7, 139-144.

Touré I.A., Brah F., Prual A. 1997. Hypertension artérielle et grossesse au Niger : Etude cas /témoins à propos de 70 cas. *Médecine d'Afrique Noire : 1997, 44 (4) :205-208.*

Yombıssı TJ, Kenmogne F, Fomulu N. 1987. Complications foetomatenelles liées aux maladies hypertensives de la grossesse chez la femme camerounaise. Med Afr Noire ; 34 (7) : 621-28.

Zupan-Sımunek V. 2010. Pronostic des nouveau-nés de mère prééclamptique. Ann Fr Anesth Reanim ;29(5):e135—9.

Material Analysis of Linear Inequalities with One Variable in Textbooks Based on Praxeological Theory

Iryana Muhammad

Universitas Pendidikan Indonesia, Indonesia, https://orcid.org/0009-0006-8941-8826

Al Jupri

Universitas Pendidikan Indonesia, Indonesia, https://orcid.org/0000-0002-0485-4332

Didi Suryadi

Universitas Pendidikan Indonesia, Indonesia, https://orcid.org/ 0000-0003-0871-8693

Abstract: This research aims to analyze the material on linear inequalities with one variable presented in the mathematics textbooks for Indonesia's Grade VIII, 2022 independence curriculum. The approach used in this research is the praxiological theory, focusing on the interconnection between task (T), Technique (τ), Technology (θ), and Theory (Θ). The research method involves observing the mathematics textbooks commonly used at the secondary education level. The analysis results in five tasks; T1, T2, T3, T4, and T5. These tasks can be solved using ($\tau1$) Perceptual, ($\tau2$) Logical, ($\tau3$) Memorial, ($\tau4$) Operational, ($\tau5$) Procedural, and ($\tau6$) Instrumental techniques. The technology used includes understanding basic concepts, algebraic approaches, graphical representations, real-world applications, and the theory involving the understanding of the concept of linear inequalities with one variable, mathematical sentences, and problem-solving for linear inequalities with one variable. These tasks can be solved using various techniques, such as using perceptual skills to understand basic concepts, logical reasoning to apply algebraic approaches, and memorization to recall graphical representations. Additionally, operational techniques can be used to solve real-world applications, while procedural techniques can be employed to tackle the theory behind linear inequalities with one variable. Finally, instrumental techniques can be utilized to solve mathematical sentences and problem-solving exercises related to linear inequalities with one variable.

Keywords: praxeological, textbook, linear inequalities with one variable

Introduction

Textbooks are considered one of the fundamental materials used by teachers for instruction and students for learning. Mathematics textbooks play a crucial role in the learning process at schools as they serve as the primary teaching material used in education. Textbooks are perceived to provide a structured and organized approach by presenting information logically and sequentially, making it easier for students to follow and comprehend complex mathematical concepts (Rozalia et al., 2022; Syutaridho, 2019). Additionally, textbooks are seen as serving the function of a reference guide with abundant information, including definitions, formulas, and examples. This wealth of information can be utilized by students when they encounter difficulties or need to review specific topics, allowing them to learn at their own pace and explore concepts more deeply, thereby promoting independent learning (Angelina et al., 2022).

In the effort to support classroom instruction, textbooks are considered to provide a common resource for both teachers and students, ensuring that everyone has a consistent understanding and facilitating discussions and explanations during lessons (Astria et al., 2022). Textbooks often include practical exercises and sample questions that help students prepare for exams, allowing them to assess their understanding of the material. This preparation for exams provides an opportunity for students to engage in tasks that require higher-level understanding, potentially resulting in higher scores for students using the textbook (Hadar, 2017).

However, it is important to note that not all textbooks are created equal. Some may be ineffective in engaging students or providing real-world applications of the taught concepts. Therefore, the quality of the textbooks used by students plays a crucial role in mathematics instruction, influencing learning opportunities, the quality of student learning, and overall student achievement. If the content of the textbook is not well-organized by established standards, learners may struggle to understand and gain knowledge from the textbook (Johar & Yusniarti, 2018; Rozalia et al., 2022). Hence, it is crucial for teachers to carefully select textbooks that align with their student's needs and complement them with teaching materials and methods to enhance the learning experience (Bittar, 2022; HastiYunianta et al., 2023a; Yang & Sianturi, 2017).

The tasks and examples listed in textbooks are the most essential and closely related elements. The recommended theory for analyzing textbooks is the praxiological theory. There has been no direct analysis previously regarding linear inequalities in one variable in textbooks based on praxiological theory. Praxiology consists of two components, praxis, and logos (Putra, 2019; Rizqi et al., 2021). This creates an opportunity for this research to differ from previous studies. This study focuses on the characteristics of the presentation in textbooks used by students and teachers, specifically the Electronic School Book (BSE) for Grade VIII of Junior High School, Semester 1, Curriculum Independence Year 2022, published by the Ministry of Education and Culture, based on the criteria set by the National Education Standards Body (BSNP). The analysis is centred on the material of linear inequalities in one variable, which is a fundamental and essential topic in mathematics.

In this research, the analysis goes beyond examining the four praxiological elements using the Didactic Situation Theory (TSD) method to assess whether the textbook facilitates students in constructing comprehensive and meaningful knowledge. The study also presents alternative presentations as references for teachers in delivering the material on linear inequalities in one variable to students. These alternative presentations are expected to facilitate meaningful knowledge construction according to the theory used in this research. Consequently, the results of this study aim to provide recommendations and insights to all stakeholders, emphasizing that textbook development is an ongoing process that evolves with the changing demands of education over time.

Method

This research employs a qualitative descriptive research design. The research methodology involves observation and documentation. The data collection technique utilized is content analysis. The data analysis technique is conducted in several steps. Firstly, collecting and reducing data, which involves gathering and selecting content to be analyzed using the ATD theory, specifically focusing on examples of questions and exercises presented in the textbook that are deemed necessary for in-depth study. The second step involves data presentation.

The object of this study is the student textbooks on the topic of Linear Inequalities in One Variable for Grade VIII in Junior High School, Curriculum Independence Year 2022, published by the Ministry of Education, Culture, Research, and Technology. Praxeological analysis comprises four components: type of task (T), technique (τ), technology (θ), and theory (Θ) (Chevallard, 2019; Chevallard & Bosch, 2020). The first two components form the "practice" (know-how) known as the praxis block, while the latter two reflect the "knowledge" (know-that) known as the logos block, providing logical explanations for why something is valid (Chevallard & Bosch, 2020).

In more detail, the type of task consists of a set of specific tasks (e.g., those solved with the same technique). There are mathematical methods that can be used to solve each type of task, and in this theory, they are referred to as techniques. Technology encompasses functions such as explaining, proving, and even designing techniques (Chevallard & Bosch, 2014). On the other hand, theory is a set of general models, concepts, and simple assumptions (axioms) that validate technology, enabling the organization of praxeological elements as a unity (Bosch, 2015). Here is a guide for analyzing the presentation of material in textbooks (see Table 1).

Table 1. Components of Praxeological Analysis

No	Elements of Praxeology	Indicator of Each Element
1	Task of Type (T)	a. The sequence is presented mathematically and coherently, capable of fostering conceptual understanding among students.
		b. The use of pictures or graphic illustrations and other

No	Elements of Praxeology	Indicator of Each Element
		modelling is adjusted to the cognitive development of students or is closely related to the student's environment.
		c. The tasks presented are assignments that contain problems related to linear inequalities in one variable that can be transformed into mathematical models.
		d. The tasks involve mathematical operations to solve problems related to linear inequalities in one variable.
2	Technique (τ)	Students have the space/opportunity to actively engage in the process of understanding the material, where students strive independently to solve problems and find their ways; there is an opportunity to determine the preferred method by the students.
3	Technology (θ)	Students have the space/opportunity to undergo the process of verification and justification regarding tasks and techniques.
4	Theory (Θ)	Students have the space/opportunity to engage in institutional situations, which is crucial to support them in applying the conclusions (theory) obtained in the validation of different contexts and previous problems.

The presentation of data is tailored to the analysis of practical theory in the form of tables, ensuring that the data is presented by specified criteria, and information is organized concisely and understandably. Lastly, there is the drawing of conclusions and verification of data, which involves assessing the alignment of the data findings obtained from the analysis.

Results

Praxis: Types of Tasks

Praxiology consists of four components: assignment types, techniques, technology, and theory. One of its components is the type of task, which is a part of the framework for understanding student behaviour (Wahyudi, 2022). In interpreted praxiology, the types of tasks found in the textbook are equivalent to exercises utilized during the learning of Linear Inequalities in One Variable material. There are five types of tasks outlined in the material on linear inequalities in one variable (see Table 2):

Table 2. Type and Number of Tasks

No	Type of Task	Amount
1	Discovering the concept of linear inequalities in one variable (T_1).	4
2	Creating a modelling of everyday problems related to linear inequalities in one variable into mathematical models (T_2)	4
3	Transforming problems related to linear inequalities in one variable into mathematical models (T_3)	2
4	Applying mathematical operations to solve problems involving linear inequalities in one variable (T_4)	5
5	Solving linear inequalities in one variable related to everyday context-based problems (T_5)	7
		22

The types of tasks are marked with the letter T. The order of task types is based on their first appearance in the textbook, which contains several questions presented as assignments for students to complete. Various task types were identified, labelled T_1 to T_5, with a total of 22 tasks, as seen in Table 2.

T_1 tasks are the primary assignments in the material on linear inequalities in one variable, designed to lead students to discover and master the concepts of linear inequalities with one variable effectively. T_5 tasks, which are the most frequently encountered in linear ınequalities with one variable material, involve solving linear inequalities in one variable related to everyday context-based problems. These tasks are also crucial in linear inequalities with one variable material to enable students to solve linear ınequalities with one variable problem relevant to daily life. Additionally, T_2, T_3, and T_4 tasks play significant roles in linear inequalities with one variable learning.

The types of tasks essentially accommodate students' knowledge towards two learning objectives of linear ınequalities with one variable material: how students understand the concept of linear inequalities in one variable and how students can solve problems related to linear inequalities with one variable. Therefore, the task types are divided into two categories (see Table 3).

Table 3. Learning Objectives of Linear Inequalities With One Variable Material

No	Learning objectives	Type of Task
1	Discovering the Concept of Linear Inequalities in One Variable	T_1, T_2, and T_3
2	Solving Problems Related to Linear Inequalities in One Variable	T_4 and T_5

Based on Table 3, the first category consists of tasks related to discovering concepts, where students are

provided opportunities to explore the concept of linear inequalities in one variable using relevant examples. The second category includes application tasks, where students must apply the linear ınequalities with one variable concept to solve real-life problems, such as determining the selling price of goods to make a profit or calculating the time needed to complete a task. With the presence of these two types of tasks, it is expected that students can master the linear ınequalities with one variable material effectively.

Praxis: Technique

Each type of task involves mathematical methods that can be employed to solve them. In theory, these methods are referred to as techniques (Chevallard, 2019; González-Martín et al., 2013). Several techniques can be applied to solve tasks (HastiYunianta et al., 2023a; Solis & Isoda, 2023). The specific techniques used in solving tasks related to linear inequalities with one variable material (see Table 4).

Table 4. Technical Description (τ)

No	Technique (τ)	Description
1	Perceptual	Utilizing visual abilities to identify information from images
2	Logical	Applying logical reasoning to connect solutions with the provided information
3	Memorial	Utilizing memory skills to recall information
4	Operational	Applying calculation algorithms
5	Procedural	Involving deeper understanding (integrating previous material)
6	Instrumental	Emphasizing the use of mathematical procedures

There are six techniques employed in solving tasks related to linear ınequalities with one variable material, namely Perceptual, Logical, Memorial, Operational, Procedural, and Instrumental. Each technique has its strengths and weaknesses. The perceptual technique is used to comprehend information by engaging visual, auditory, and sensory perception. Meanwhile, the Logical technique is utilized to organize information logically and systematically. The memorial technique proves useful in recalling information through note-taking or repetition.

Logos: Technology and Theory

Technology encompasses functions such as explaining, proving, and even designing techniques (Chevallard, 2019, 2022). On the other hand, theory is a collection of general models, concepts, and simple assumptions (axioms) that validate technology, enabling the organization of praxiological elements as a whole (Gok & Erdogan, 2023). Based on the results of the praxiological analysis of the student textbook on linear ınequalities with one variable material (see Table 5).

Table 5. Praxeology Results of Student Books

Task (T)	Technique (τ)	Technology (θ)	Theory (Θ)
Discovering the concept of linear inequalities in one variable (T_1)	(τ_1) *Perceptual* (τ_2) *Logical* (τ_3) *Memorial* (τ_4) *Operational*	Understanding Basic Concepts	Understanding the Concept of Linear Inequalities in One Variable
	(τ_2) *Logical* (τ_3) *Memorial* (τ_5) Procedural	Understanding Basic Concepts	Understanding the Concept of Linear Inequalities in One Variable
	τ_2) *Logical* (τ_3) *Memorial* (τ_4) *Operational* (τ_5) Procedural	Algebraic Approach	Understanding the Concept of Linear Inequalities in One Variable
	(τ_1) *Perceptual* (τ_2) *Logical* (τ_3) *Memorial*	Graphical Representation	Understanding the Concept of Linear Inequalities in One Variable
Creating a mathematical model from everyday problems related to linear inequalities in one variable (T_2)	(τ_1) *Perceptual* (τ_2) *Logical*	Algebraic Approach	Mathematical Sentence: Linear Inequality in One Variable
	(τ_2) *Logical* (τ_4) *Operational* (τ_5) Procedural τ_6) Instrumental	Application in Real-World Contexts	Solving Linear Inequality in One Variable.
	(τ_2) *Logical* (τ_5) Procedural	Application in Real-World Contexts	Mathematical Sentence: Linear Inequality in One Variable
	(τ_1) *Perceptual* (τ_4) *Operational* τ_6) Instrumental	Application in Real-World Contexts	Solving Linear Inequality in One Variable.
Transforming problems related to linear	(τ_1) *Perceptual* (τ_2) *Logical*	Graphical Representation	Solving Linear Inequality in One Variable.

Task (T)	Technique (τ)	Technology (θ)	Theory ($\varTheta$)
inequalities in one variable into mathematical models (T$_3$)			
	(τ_3) *Memorial*	Algebraic Approach	Solving Linear Inequality in One Variable.
Applying mathematical operations to solve problems involving linear inequalities in one variable (T$_4$)	(τ_2) *Logical* (τ_4) *Operational* (τ_5) Procedural	Application in Real-World Contexts	Solving Linear Inequality in One Variable.
	(τ_2) *Logical* (τ_4) *Operational* (τ_6) Instrumental	Application in Real-World Contexts	Solving Linear Inequality in One Variable.
	(τ_1) *Perceptual* (τ_4) *Operational* (τ_5) Procedural (τ_6) Instrumental	Algebraic Approach	Solving Linear Inequality in One Variable.
	(τ_2) *Logical* (τ_4) *Operational* (τ_6) Instrumental	Algebraic Approach	Solving Linear Inequality in One Variable.
	(τ_4) *Operational*	Algebraic Approach	Solving Linear Inequality in One Variable.
Solving linear inequalities in one variable related to everyday context-based problems (T$_5$)	(τ_2) *Logical* (τ_4) *Operational* (τ_5) Procedural	Application in Real-World Contexts	Solving Linear Inequality in One Variable.
	(τ_2) *Logical* (τ_4) *Operational* (τ_5) Procedural	Application in Real-World Contexts	Solving Linear Inequality in One Variable.
	(τ_2) *Logical*	Application in Real-World	Solving Linear Inequality in One Variable.

Task (T)	Technique (τ)	Technology (θ)	Theory (𝛩)
	(τ_4) *Operational*	Contexts	
	(τ_5) Procedural		
	(τ_2) *Logical*	Application in	Solving Linear Inequality in One
	(τ_4) *Operational*	Real-World	Variable.
	(τ_5) Procedural	Contexts	
	(τ_2) *Logical*	Application in	Solving Linear Inequality in One
	(τ_4) *Operational*	Real-World	Variable.
	(τ_5) Procedural	Contexts	
	(τ_2) *Logical*	Application in	Solving Linear Inequality in One
	(τ_4) *Operational*	Real-World	Variable.
	(τ_5) Procedural	Contexts	
	(τ_2) *Logical*	Application in	Solving Linear Inequality in One
	(τ_4) *Operational*	Real-World	Variable.
	(τ_5) Procedural	Contexts	

From Table 6, it is evident that there is a diversity of technologies used in solving T_1, with differences in the technologies (θ) employed, namely conceptual understanding, algebraic approach, and graphical representation, compared to the theory (Θ) of understandinglinear inequalities with one variable concepts. In T_2, there are two technologies (θ), namely the algebraic approach and real-world application, aligning with the theory of linear inequalities with one variable mathematical sentences and solutions. For T_3, T_4, and T_5, justification is found in the same theory of solving linear inequalities with one variable. However, T_3 is solved using θ graphical representation and algebraic approach. T_3 and T_4 both utilize θ real-world application, but T_3 is also solved using θ algebraic approach.

Discussion

The stages in presenting material related to the selection of learning designs can be one of the causes of didactic obstacles (Didi Suryadi, 2019). Based on the identification obtained, there are parts considered to be potential didactic obstacles, including aspects highlighted in the analysis of T_1 (see Table 6).

Task T_1 in Table 7 is an assignment that guides students in discovering the concept of linear inequalities in one variable. As previously identified, T_1 includes 4 (four) techniques, namely (τ_1) Perceptual, (τ_2) Logical, (τ_3) Memorial, and (τ_4) Operational. In τ_1, which is a technique that utilizes visual abilities to identify information from images, it has been recognized that this technique may not be universally applicable to all students. This is evident from the inadequacy of the perceptual aspect used. The errors associated with this τ_1 (see Figure 1).

Table 6. Description of Assignment 1 (T_1) in the Student Book

T_1	Description
Task on page 120 (Let's Explore)	Aktivitas kehidupan sehari-hari seringkali dijumpai beberapa aturan yang berupa visual atau pernyataan, baik tertulis dan tidak tertulis. Misalkan informasi pada tampilan *google maps* berikut. **Gambar 3.6** Rute Perjalanan dari Aceh Menuju Lampung *Sumber: https://bit.ly/RuteAcehkeLampung* Berdasarkan Gambar 3.6. Didapatkan informasi bahwa Rute perjalanan dari Aceh ke Lampung tidak lebih dari 44 jam dengan menggunakan mobil via jalur darat. Selain itu, juga didapatkan informasi bahwa jarak antara Aceh dan Lampung adalah kurang dari 2.047 *km*. Pada saat menempuh perjalanan melewati jalan tol juga terlihat tanda seperti gambar disamping. Tanda tersebut merupakan rambu-rambu yang dipasang di jalan tol yang berarti kecepatan maksimal adalah 100 km/jam dan kecepatan minimal adalah 60 *km*/jam. Perhatikan gambar dan informasi yang sudah kalian dapatkan sebelumnya. Jika terdapat beberapa pertanyaan, berapa waktu perjalanan minimal yang dibutuhkan untuk bepergian dari Aceh ke Lampung? Berapa jarak maksimal yang ditempuh dari Aceh ke Lampung? Berapakah kecepatan yang diperbolehkan sebuah mobil untuk melewati jalan tol yang terdapat tanda disamping? Kalian akan dapat menjawab pertanyaan tersebut setelah mempelajari materi pada bagian ini.

As shown in Figure 1, in this task, the perceptual technique (τ_1) is used to help students easily understand the concept of linear inequalities with one variable. However, the contextual scenario presented does not encompass all regions in Indonesia. For instance, students in Aceh already know that there is no toll road from Aceh connecting to Lampung. Therefore, perceptual errors may occur for students in Aceh, as there is currently no toll road connecting Aceh to the Trans-Sumatra toll road (up to Lampung). Hence, it is advisable to refine the contextual scenario presented to students to understand the concept of Linear Inequalities in One Variable with a more realistic context that covers all regions in Indonesia. Next, the Logical technique (τ_2) in solving T_1,

involves using logical reasoning to connect solutions with the provided information. Based on the analysis results, errors in the application of this technique are also observed (see Figure 2)

	Translate:
	Based on Figure 3.6. Obtained information that Route The journey from Aceh to Lampung takes no more than 44 hours by car via land route. Apart from that, information is also obtained that the distance between Aceh and Lampung is less than 2,047 km. When traveling along the toll road, you can also see signs like the picture beside. These signs are signs installed on toll roads which means the maximum speed is 100 km/hour and the minimum speed is 60 km/hour. Pay attention to the pictures and information provided To you got before. If there are several questions, what is the minimum travel time? needed to travel from Aceh to Lampung? What is the maximum distance traveled from Aceh to Lampung? What speed is allowed a car to pass through the existing toll road sign on the side?

Figure 1. Perceptual technique error part (τ_1)

	Translate:
	Based on Figure 3.6. Obtained information that Route The journey from Aceh to Lampung takes no more than 44 hours by car via land route. Apart from that, information is also obtained that the distance between Aceh and Lampung is less than 2,047 km. When traveling along the toll road, you can also see signs like the picture beside. These signs are signs installed on toll roads which means the maximum speed is 100 km/hour and the minimum speed is 60 km/hour. Pay attention to the pictures and information provided To you got before. If there are several questions, what is the minimum travel time? needed to travel from Aceh to Lampung? What is the maximum distance traveled from Aceh to Lampung? What speed is allowed a car to pass through the existing toll road sign on the side?

Figure 2. Description of the Logical technique (τ_2)

The questions used in technical logical (τ_2) are not appropriate because regardless of the speed used in travelling, the distance will remain the same; in this case, there is no maximum distance as in the question 'What is the maximum distance travelled from Aceh to Lampung?' Inappropriate questions like this are believed to cause obstacles for students in understanding the linear inequalities with one variable concept, so T_1 is not utilized effectively.

As for the Memorial technique (τ_3), which involves utilizing memory skills to remember, it is very suitable for

this T_1. The material on distance, time, and speed has already been learned in the fifth grade of elementary school, covering topics such as integers (number sequences). In the operational technique (τ_4), which uses algorithms, students can complete tasks by performing division operations to calculate the minimum travel time. With the τ_4 technique, by sorting numbers, students can provide a range of speeds from minimum (60 km/h) to maximum (100 km/h). Of the four techniques used to complete the task (T_1), all are justified for technology in the form of understanding the basic concept, and these activities lead to achieving the goal of the theory (Θ) of understanding the basic linear inequalities in one variable concept.

Conclusion

The analysis conducted on the student textbook regarding the material of linear inequalities with one variable involves the examination of four praxeological components. First, the types of tasks found in the textbook, such as understanding basic concepts, modelling, finding solutions, and solving linear inequalities with one variable related to real-life situations. Second, the techniques used in the textbook, include perceptual, logical, memorial, procedural, and instrumental techniques. Lastly, the theories applied in the textbook, such as basic theories about linear inequalities, rules of algebraic manipulation, and graphic concepts.

The overall analysis provides a comprehensive understanding of linear inequalities with one variable in the textbook. The material on linear inequalities with one variable in the textbook offers a comprehensive understanding through various analyses. However, in its development, some situations may pose challenges for students, especially in selecting the contexts presented in the textbook

Recommendations

The primary recommendation is to conduct a revision or further development of the analyzed mathematics textbook. Emphasis is needed on diversifying the types of tasks to encompass contexts that are more relevant to students' everyday lives. Adjusting teaching techniques in the textbook to accommodate variations in students' learning styles, thereby enhancing understanding and acceptance of the material on linear inequalities in one variable. Encouraging textbook developers to deepen the integration of basic theories on linear inequalities in an applicable context. This can provide a stronger understanding of the concept and relate it to real-life situations

Acknowledgments

presentation at the International Conference on Studies in Engineering, Science, and Technology (ICSEST) 2024 (www.2024.icsest.net) held in Istanbul/Turkey, November 7-10, 2024.

References

Angelina, W., Irsal, N. A., Siagian, T. A., & Lestary, R. (2022). Analisis Kelengkapan Materi Buku Teks Matematika SMP Kelas VII Kurikulum 2013 Terbitan Erlangga Revisi 2016 pada Pokok Bahasan Segiempat dan Segitiga. Jurnal Penelitian Pembelajaran Matematika Sekolah (JP2MS), 6(2), 167–176. https://doi.org/10.33369/jp2ms.6.2.167-176

Astria, R., Aliyyah Irsal, N., Alfra Siagian Analisis Materi Kegiatan Mengamati Pada Buku Teks Matematika SMP Kelas VII Semester, T., Pendekatan Saintifik, B., Alliyah Irsal, N., Alfra Siagian, T., & Studi Pendidikan Matematika, P. (2022). Analisis Materi Kegiatan Mengamati Pada Buku Teks Matematika SMP Kelas VII Semester 2 Berdasarkan Pendekatan Saintifik. Jurnal Penelitian Pembelajaran Matematika Sekolah, 6(JP2MS), 32–39. https://doi.org/10.33369/jp2ms.vi.i.32-39

Bittar, M. (2022). A Methodological Proposal For Textbook Analysis. The Mathematics Enthusiast. https://api.semanticscholar.org/CorpusID:245325340

Bosch, M. (2015). Doing Research Within the Anthropological Theory of the Didactic: The Case of School Algebra. In S. J. Cho (Ed.), Selected Regular Lectures from the 12th International Congress on Mathematical Education (pp. 51–69). Springer International Publishing. https://doi.org/10.1007/978-3-319-17187-6_4

Chevallard, Y. (2019). Introducing The Anthropological Theory Of The Didactic: An Attempt At A Principled Approach. In Hiroshima Journal Of Mathematics Education (Vol. 12).

Chevallard, Y. (2022). Challenges and Advances in Teacher Education Within the ATD. In Y. Chevallard, B. Barquero, M. Bosch, I. Florensa, J. Gascón, P. Nicolás, & N. Ruiz-Munzón (Eds.), Advances in the Anthropological Theory of the Didactic (pp. 81–89). Springer International Publishing. https://doi.org/10.1007/978-3-030-76791-4_7

Chevallard, Y., & Bosch, M. (2014). Didactic Transposition in Mathematics Education. In S. Lerman (Ed.), Encyclopedia of Mathematics Education (pp. 170–174). Springer Netherlands. https://doi.org/10.1007/978-94-007-4978-8_48

Chevallard, Y., & Bosch, M. (2020). Didactic Transposition in Mathematics Education. In S. Lerman (Ed.), Encyclopedia of Mathematics Education (pp. 214–218). Springer International Publishing. https://doi.org/10.1007/978-3-030-15789-0_48

Chevallard, Y., & Sensevy, G. (n.d.). Anthropological Approaches in Mathematics Education, French Perspectives. In J Res Math Educ (Vol. 22).

Gok, M., & Erdogan, A. (2023). Didactic Praxeologies Employed by Mathematics Teachers in Teaching the Inverse Function. Journal of Computer and Education Research, 11(22), 1089–1112. https://doi.org/10.18009/jcer.1361502

González-Martín, A. S., Giraldo, V., & Souto, A. M. (2013). The introduction of real numbers in secondary

education: an institutional analysis of textbooks. Research in Mathematics Education, 15(3), 230–248. https://doi.org/10.1080/14794802.2013.803778

Hadar, L. L. (2017). Opportunities to learn: Mathematics textbooks and students' achievements. Studies in Educational Evaluation, 55, 153–166. https://doi.org/10.1016/J.STUEDUC.2017.10.002

HastiYunianta, T. N., Suryadi, D., Dasari, D., & Herman, T. (2023a). Textbook praxeological-didactical analysis: Lessons learned from the Indonesian mathematics textbook. Journal on Mathematics Education, 14(3), 503–524. https://doi.org/10.22342/jme.v14i3.pp503-524

HastiYunianta, T. N., Suryadi, D., Dasari, D., & Herman, T. (2023b). Textbook praxeological-didactical analysis: Lessons learned from the Indonesian mathematics textbook. Journal on Mathematics Education, 14(3), 503–524. https://doi.org/10.22342/jme.v14i3.pp503-524

Johar, R., & Yusniarti, S. (2018). The Analysis Of Proportional Reasoning Problem In The Indonesian Mathematics Textbook For The Junior High School. Journal on Mathematics Education, 9(1), 55–68.

Putra, Z. H. (2019). Praxeological change and the density of rational numbers: The case of pre-service teachers in Denmark and Indonesia. Eurasia Journal of Mathematics, Science and Technology Education, 15(5). https://doi.org/10.29333/ejmste/105867

Rizqi, M. M., Wijayanti, D., & Basir, M. A. (2021). Analisis Buku Teks Matematika Materi Himpunan Menggunakan Model Prakseologi. Delta: Jurnal Ilmiah Pendidikan Matematika, 9(1), 57. https://doi.org/10.31941/delta.v9i1.1226

Rozalia, I., Hanifah, H., Susanto, E., & Lestary, R. (2022). Analisis Buku Teks Matematika Smp Kelas Vii Terbitan Kemendikbud Berdasarkan Kriteria BSNP. Jurnal Penelitian Pembelajaran Matematika Sekolah (JP2MS), 6(1), 86–96. https://doi.org/10.33369/jp2ms.6.1.86-96

Solis, D., & Isoda, M. (2023). Comparing elementary school textbooks of China, Japan, and Malaysia: a praxeological and developmental progression analysis regarding length measurement. Research in Mathematics Education, 25(3), 359–378. https://doi.org/10.1080/14794802.2022.2103022

Syutaridho, S. (2019). Pengembangan Bahan Ajar Bangun Datar dengan Pendekatan Contextual Teaching and Learning. Jurnal Pendidikan Matematika RAFA. https://api.semanticscholar.org/CorpusID:203359937

Wahyudi, B. (2022). Analisis Rencana Pelaksanaan Pembelajaran (RPP) dengan Praksiologi. Jurnal Indonesia Sosial Teknologi, 3(06), 764–771. https://doi.org/10.36418/jist.v3i6.452

Yang, D. C., & Sianturi, I. A. (2017). An Analysis of Singaporean versus Indonesian textbooks based on trigonometry content. Eurasia Journal of Mathematics, Science and Technology Education, 13(7), 3829–3848. https://doi.org/10.12973/eurasia.2017.00760a

Exploration of TPACK-based on Mathematics Learning

Roni Priyanda

Universitas Pendidikan Indonesia, Indonesia, https://orcid.org/0000-0002-5750-6390

Tatang Herman

Universitas Pendidikan Indonesia, Indonesia, https://orcid.org/0000-0002-4349- 4042

Abstract: Issues and trends in the development of TPACK in developed countries continue to develop and prepare educators to face future challenges in education, but in Indonesia it is still not optimized. Departing from this problem, the purpose of this study is to show the profile of TPACK- based mathematics learning and to show trends in the direction of TPACK-integrated research so that it can be a recommendation for researchers who are interested in conducting integrated research with TPACK. This study used a systematic literature review, using preferred reporting items for systematic reviews and meta analyzes (PRISMA) guidelines. The search strategy uses the Scopus database, the search terms used are: "TPACK", and Mathematical, the screening process goes through three stages: title, abstract, and full text screening. As a result, from the 693 articles and books collected, 8 articles were found that were suitable to be used as a TPACK-based mathematics learning profile. Furthermore, the trend towards research on TPACK and TPACK integrated with mathematics shows an increasing trend from 2013 to 2022, with the most researching countries on TPACK namely America, China and Taiwan, based on the number of citations that are the most reference sources, namely research by Mishar P and Koehler MJ based on co-occurrence trend of TPACK integration has a lot to do with ICT, education, TPACK model, online learning and digital learning.

Keywords: TPACK, PRISMA , Mathematic

Introduction

Technology Pedagogical Content Knowledge (TPACK) is a framework that describes the knowledge and skills that prospective teachers need to integrate technology effectively in teaching practice. The framework consists of three main components: technological knowledge, pedagogical knowledge, and content knowledge, which are integrated to create effective teaching with technology (Mishra, 2019). Technological knowledge is the

ability to use technology effectively in teaching (Akman & Güven, 2015; Feyerabend, 2021; Ozturk, 2023). Technology pedagogical content knowledge is the ability to integrate technology into classroom practice to improve student learning outcomes (Jang & Chen, 2010). This includes knowing how students learn best, including their cognitive style, such as visual learning and how students learn from certain types of technology, for example how to use math learning apps effectively in the classroom. Furthermore, technology pedagogical content knowledge is a form of subject knowledge that helps teachers understand how students learn best and how different types of technology can be used to enhance learning (Jang, 2010). Further knowledge of technological pedagogical content is a form of knowledge that helps teachers understand how students learn best and how different types of technology can be used to enhance learning (Oster-Levinz & Klieger, 2010).

There are many challenges impacting education systems around the world, including access to technology and quality teacher training (Chai et al., 2011). In the United States many schools and universities have adopted TPACK in their curricula. They realize the importance of continuous and effective learning in producing quality future generations. The advantages that can be obtained from adopting TPACK in the curriculum are: (1) improving learning outcomes; (2) strengthen student competence; and (3) increasing learning effectiveness (Culcasi et al., 2022). In the United States found that a curriculum that relies on TPACK provides better learning outcomes compared to other types of learning (Lin et al., 2013; Ozturk et al., 2023). Apart from that, TPACK also has a positive impact on students' competencies so as to make them more qualified. One example that shows government support is in the "Nationwide Math and Science Initiative" (NMSI) program launched by President Obama. (Santos-Trigo et al., 2019). NMSI is providing support to train teachers to implement TPACK and improve student learning outcomes across the country. In Europe TPACK has become a major focus in educational programs for educators. in the implementation of education several countries such as the UK, the Netherlands and Finland have adopted TPACK as part of their curriculum. In addition, several organizations such as the European Schoolnet and the European Commission have also promoted TPACK as an important tool in improving the quality of education across Europe.

Overall, the development of TPACK in developed countries continues to grow and plays an important role in preparing educators to face future challenges in education. In contrast to developed countries, TPACK in Indonesia is still not a major issue. This can be seen from the lack of attention from the government and the application of sufficient evidence to increase the effectiveness of the learning process in schools. Attention is focused on developing a more comprehensive and integrated TPACK model. This concept is a development that is expected to bring benefits to educators and education practitioners in Indonesia.Technology really supports and facilitates the learning process (Priyanda et al., 2021), (Mulyati & Evendi, 2020). in learning mathematics, especially with learning technology can be done more effectively and efficiently, teachers usually only use technology in training activities and practices that do not affect student learning. The research synthesis shows that TPACK in mathematics learning improves conceptual understanding, with technology enabling visualization, interactive exploration, and dynamic representation (Niess, 2005) , making abstract and complex mathematical ideas more accessible and real. (Keengwe, J., et al. 2008), with technology can also encourage engagement and motivation, support authentic problem solving (Schmidt et al., 2009) , facilitate

different instruction, and encourage collaboration and communication between students. This equips teachers with the necessary knowledge and skills to integrate technology effectively, leading to improved learning outcomes in mathematics education (Angeli & Valanides, 2009), (Niess, 2011) .

Methods

A systematic literature review was conducted using the Preferred Reporting Items for Systematic Review and Meta-Analyses (PRISMA) guidelines. The search strategy involved a comprehensive search of three electronic databases: Scopus, Web of Science, and Dimension. The search terms used are "TPACK", and "Mathematic". The criteria for articles are articles discussing TPACK-based mathematics learning and published between 2013 and 2022. The screening process includes three stages: screening of title, abstract, and full text, to be considered to be included, articles must meet the criteria of empirical and peer-reviewed studies.

The selected articles are summarized in tabular form containing 1. General information about the article author, year of publication and country, 2. Research model and design, 3. Profile of TPACK-based mathematics learning. to visualize the collected data, the VOSViewer application is used to analyze the existence of TPACK based on Co-Authorship, Co-Occurrence, citations, Bibliographic cupping and Co-citation with units of analysis Authors, Organizations and Countries

Results and Discussion

Preferred Reporting Items for Systematic Review and Meta-Analyses (PRISMA)

This study uses the Preferred Reporting Items for Systematic Review and Meta-Analyses (PRISMA) guidelines. PRISMA is a guide developed to assist systematic writers and readers in reporting and evaluating systematic reviews and meta-analyses in a transparent and thorough manner. PRISMA provides a clear and comprehensive framework for reporting on the process of tracing, selecting studies, collecting and analyzing data, and interpreting results in systematic reviews. (Utami & Jahar, 2021). The following steps are implemented using the PRISMA method.

Articles identified through a publish or perish search for the last 10 years from 2013 to 2022 recorded a total of 697 data, then based on the identified titles. So there were 6 articles that were deleted due to recording duplicates, and 556 articles that did not meet the requirements, the reasons for not fulfilling the requirements were due to the title does not only contain the word TPACK, there is no math word, then with 25 articles deleted because the complete document cannot be found, then the remaining 110 articles are analyzed through abstracts to see the profile of TPACK-based mathematics learning through research objectives, methods used and results found , then there were 78 articles that did not match the desired data, so that the remaining 32 articles were analyzed for their contents, and there was 1 document not reported for reasons unable to answer General information about the author's article, year of publication, 4 articles were also not included because

they could not answer Model and the research design used and 4 articles were not included because they could not answer the findings produced. Of the 13 remaining documents, 10 were reported because the other 3 documents had some similarities, such as the model used or the findings produced.
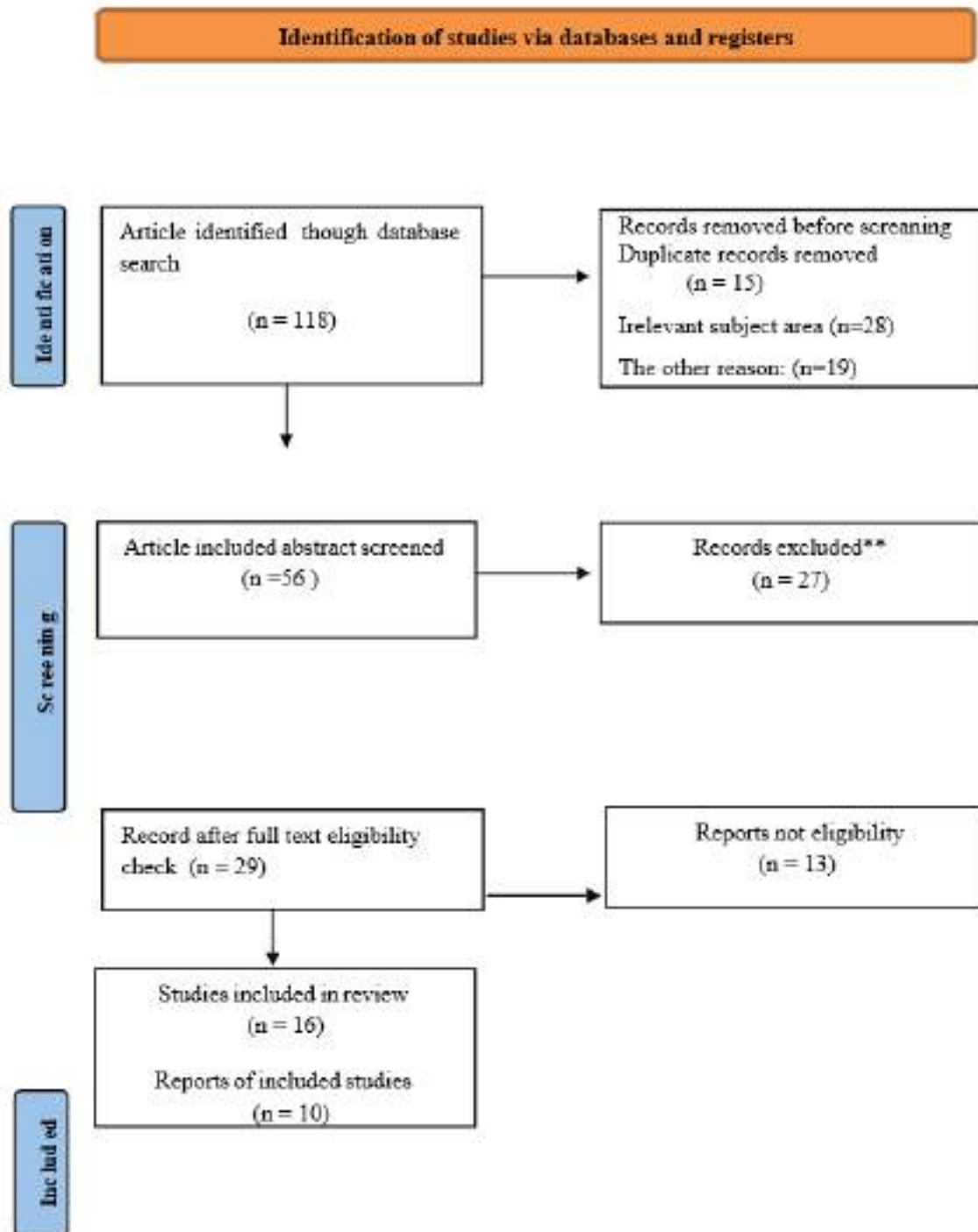

Figure 1. PRISMA Flow Diagram

The following summarizes the data analysis results using the Preferred Reporting Items for Systematic Review and Meta-Analyses (PRISMA) guidelines to see the profile of TPACK-based mathematics learning.

Table. 1 TPACK-based mathematics learning profile

Source	Purpose and Target Users	Research design	Results
(Yuniarwati, 2022)	designing a TPACK development learning model for prospective elementary school teachers in learning mathematics	Method: Literature Review	improve the independent learning and collaboration of prospective teachers and increase the TPACK of prospective teachers
(Gou, 2020)	to validate the TPACK measurement model which consists of 30 items	Quantitative method of cross- sectional survey Analysis of testing the TPACK measurement model using exploratory factor analysis (EFA) and confirmatory factor analysis (CFA) fit index test	The results showed that all of the fit index criteria had been met. It was concluded that the TPACK measurement model describes the TPACK level of senior mathematics teachers in the Indonesian scenario
(Koyuncuoğlu & An, 2021)	To find out and compare the perceptions of TPACK competency of postgraduate students studying at the Institute of Natural Sciences, Social Sciences and Education Sciences based on variables of gender, graduate program level and field	causal and correlational comparative research designs. with the help of a causal comparative design	technological knowledge and TPACK competency of postgraduate students is classified as moderate. It was also found that the technological knowledge and content knowledge of the male postgraduate students were high, whereas the female participants had a high level of perception of pedagogical knowledge. In addition, the perception of TPACK competence varies based on the field

			and level of graduate education
(Nugroho Yanuarto et al., 2021)	to understand the understanding of how the structure, representation, and adaptation of a topic, problem, and content are adapted according to the teacher's interests, technology,	a quantitative approach with a survey focus as a research design with the following procedures: 1) find a factor analysis of each construct; TPACK and ICT Literacy with Exploratory Factor Analysis; 2) arrange instruments with Confirmatory Factor Analysis to get a fit model; 3)	the TPACK construct consists of 7 valid sub-constructs and ICT literacy consists of 4 valid sub-constructs. Meanwhile, data analysis showed that there was a significant relationship between TPACK and ICT literacy with a strong significant contribution relationship b e t w e e n TPACK
	and abilities.	Structural Equation Model for the relationship between TPACK and ICT literacy.	and ICT literacy (β = 0.566).
(Sari et al., 2021a)	analyze the ability to think abstract mathematics and self-efficacy through TPACK learning.	This research is quantitative with a survey method and was conducted on class VII students. Data collection was carried out by interviews, questionnaires and tests of mathematical abstract thinking skills.	several indicators of the ability to think abstract mathematics, found indicators that have been achieved but some have not been achieved such as making generalizations. The results of the questionnaires and interviews concluded that most students still think that mathematics is difficult to learn and its abilities
(Mailizar et al., 2021)	to examine the TPACK of Indonesian mathematics teachers	quantitative method with a cross-sectional survey	there were significant differences in teacher TPACK levels by gender

	and investigate whether TPACK levels differ significantly in terms of gender, teaching experience, schooling level and teacher education level	used the ANOVA test to test for significant differences in TPACK levels according to the teacher's demographic background, namely gender, school level, educational level and teaching experience.	and educational level. However, it was found that there was no significant difference in the level of TPACK teachers according to their teaching experience and school level
(Rohati et al., 2021)	to see the effect of ethnomathematics integration with the TPACK framework (Technological, Pedagogical, Art, Content, And Knowledge) as a problem-based learning model, in junior high school on social arithmetic learning	Methodology: This study used a mixed methods, quasi-experimental research design with two experimental groups.	ethnomathematics learning with the TPACK intervention assisted by the PBL model is more effective than the simple ethnomathematics learning model
(Njiku, 2021)	to investigate the TPACK development of mathematics teachers through their participation in professional development activities	used the pre and post-test for the non-equivalent group quasi-experiment with three groups. Group 1 participates in a collaborative lesson design	Descriptive statistics show more improvement in group 1 followed by group 2. For example, when a comparison is made between the general TPACK mean scores at time 1 and survey data time 2, group
	particularly collaborative learning design activities.	team to integrate technology and implement the designed lesson in the classroom. Group 2 participates in the planning and	1's score changes from 3.71 to 4.07 with an increase of 0 .36 units, group 2 changed from 3.59 to 3.79 with an

		implementation of learning and group 3 operates conventionally.	increase of 0.20 units and group 3 changed from 3.75 to 3.86 with an increase of 0.11 units.
(Sari et al., 2021b)	To design a Technological Pedagogic Content Knowledge (TPACK) measuring instrument, particularly for prospective mathematics teachers	This study uses Design Research and Development (R n D) which refers to the ADDIE development model which includes Analysis, Design, Development and Evaluation. The TPACK assessment instrument developed was in the form of an observation sheet of learning activities and a survey (questionnaire) that refers to the operational definition of the seven aspects of TPACK	Based on the results of expert validation of the TPACK ability instrument, namely the TPACK ability questionnaire and teaching practice observation sheets based on TPACK aspects, they are included in the very valid category.
(Wijaya et al., 2020)	designing interactive mathematics learning media based on the TPACK framework using the Hawgentdynamicmathematics software to describe students' creativity in developing interactive learning media using the HAWGENT Dynamic Mathematics Software	Combined descriptive research and quasi-experiments using Hawgentdynamicmathematics software	students' creativity in designing mathematics learning media using the Hawgent dynamic mathematics software on various topics and different levels. Hawgent's dynamic math software has been proven to increase student creativity. using Hawgent's dynamic mathematics software with the TPACK

framework can assist teachers in explaining abstract mathematical concepts so that they are more easily understood by students.

Trends and Development Direction of TPACK

To see trends in the direction of TPACK research, researchers started by looking at the existence of TPACK and TPACK-based mathematics ranging from 2013 to 2022 in the Scopus dataset, which can be seen in Figure 1 below:
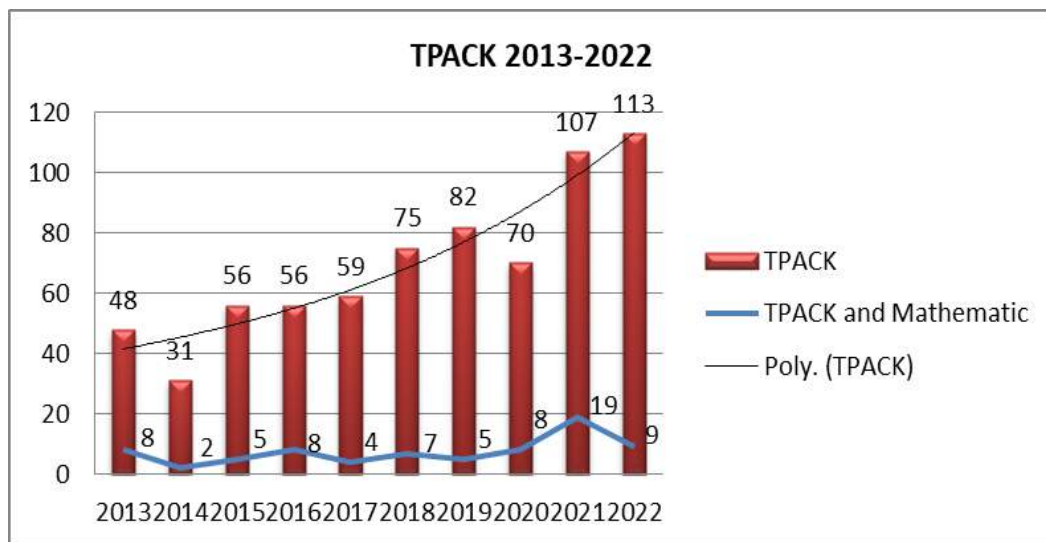
Figure 1. TPACK Trend Diagram

The data above uses Scopus data sources through publish or peris, by searching for the title word "TPACK" we get 697 documents with an increasing trend and the highest in 2022 are 113 documents. the most documents in 2021 amounted to 19 documents.

To see the development trend of countries where research is mostly integrated with TPACK, researchers use Scopus data and the results can be seen in Table 2.

Table 2 shows the most productive country in conducting research related to TPACK, namely the United States with a total of 523 documents, with 16,460 citations and spread across 106 journals, proceedings and the like which are indexed by Scopus. Furthermore, to see trends in research directions that are developing and integrated with TPACK based on Co-Occurrence can be seen in Figure 2.

Table 2. Research in countries using TPACK

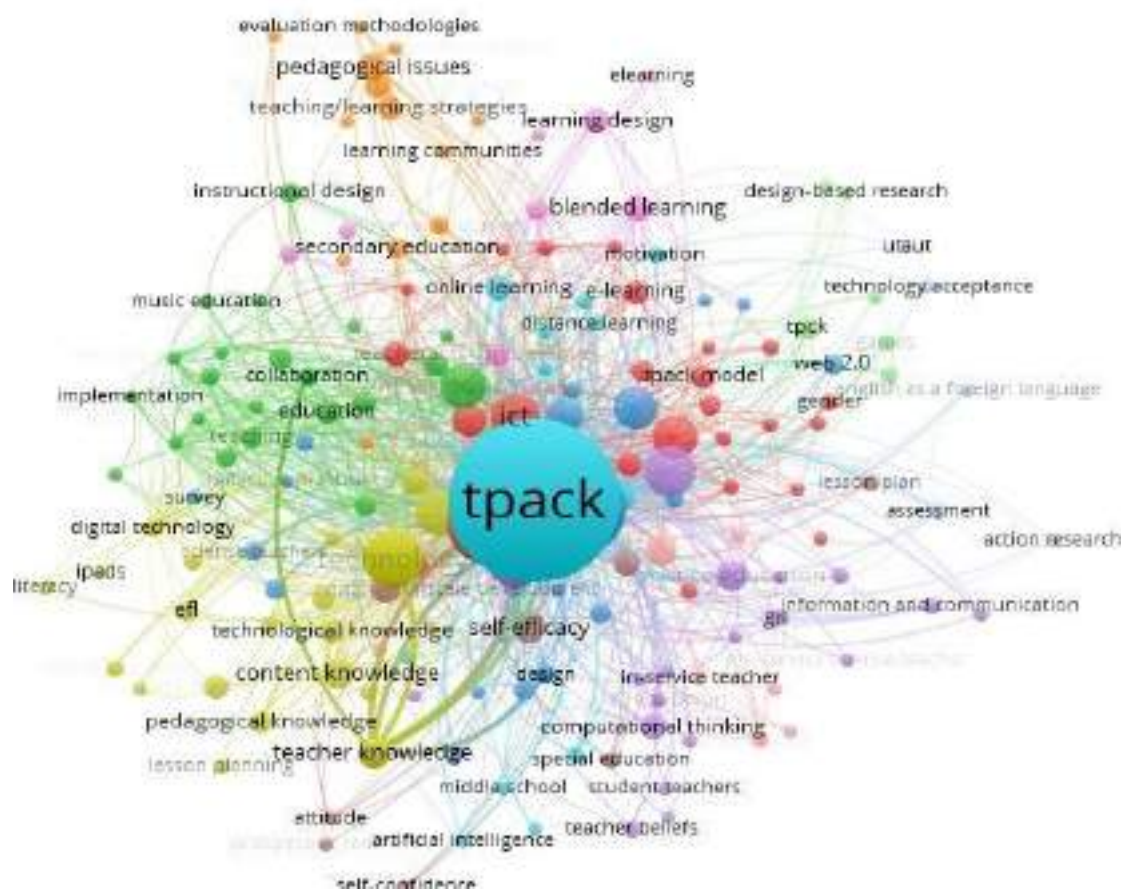| No	Country	Documents	Citations	Total Link Strength
1	United States	523	16460	106
2	China	162	1112	104
3	Taiwan	144	3886	72
4	Australia	130	1760	55
5	Singapore	70	3023	53
6	Hong Kong	54	637	50
7	Indonesia	203	683	44
8	Malaysia	77	434	43
9	United Kingdom	47	858	42
10	Netherlands	38	1612	26

.

Figure 2. TPACK Integration Visualization based on Co-Occurrence

Figure 2 shows the integration of research using TPACK which is also supported by ICT, technological knowledge, pedagogical knowledge, digital technology, education, distance learning and several other studies. Furthermore, to see researchers who are widely used as references related to research using TPACK or based on Co-citation and content analysis can be seen in table 3 below.

Table 3. Researchers who are widely referred to in the TPACK research

No	Author	Year	Citations
1	Mishra p; koehler mj	2006	4114
2	Schmidt da;baran e.; thomson ad;mishra p	2009	760
3	Angeli c.; valenindes	2009	645
4	Koehler mj;mishra p	2005	2005
5	robin br	2008	558
6	Harris j.; mishra p.; koehler mj	2009	476
7	Koehler mj; mishra p.; yahya k.	2007	459
8	Voogt j.; fisser p.; pareja robin n	2013	396
9	Graham cr	2011	321
10	Lee m. -h .; tsai c. -c.	2010	316

In table 3 it can be seen that researchers who have become a source of reference for other researchers in integrated TPACK research are Mishrar p; Koehler mj with a total of 4,114 citations

Conclusion

In this article the researcher uses the Preferred Reporting Items for Systematic Review and Meta-Analyses (PRISMA) guidelines which are useful in analyzing the profile of TPACK-based mathematics learning, then to see trends in the development issues of TPACK-based research the researcher uses the help of VOSViewer in analyzing the existence of TPACK based on Co-Authorship , Co-Occurrence, citation, Bibliographic cupping and Co-citation with the unit of analysis Authors, Organizations and Countries

Acknowledgements

The author expresses many thanks to Prof. Dr. H. Tatang Herman, M.Ed as the lecturer in the course on

cutting-edge developments and global issues . This research was funded by the Center for Educational Financing Services (Puslapdik), the Ministry of Education, Culture, Research and Technology (Kemendikbud) Republic of Indonesia, and the Educational Fund Management Institution (LPDP) through the Indonesian Education Scholarship (BPI). This article was presented as oral presentation at the International Conference on Studies in Education and Social Sciences, (www.icses.net) held in Istanbul/Turkey on November 07-10, 2024.

References

Angeli, C., & Valanides, N. (2009). Epistemological and methodological issues for the conceptualization, development, and assessment of ICT-TPCK: Advances in technological pedagogical content knowledge (TPCK). *Computers and Education, 52* (1), 154–168. https://doi.org/10.1016/j.compedu.2008.07.006

Akman, Ö., & Güven, C. (2015). TPACK Survey Development Study for Social Sciences Teachers and Teacher Candidates. *International Journal of Research in Education and Science, 1*(1), 1-10.

Chai, CS, Ling Koh, JH, Tsai, CC, & Lee Wee Tan, L. (2011). Modeling primary school pre-service teachers' Technological Pedagogical Content Knowledge (TPACK) for meaningful learning with information and communication technology (ICT). *Computers and Education, 57* (1), 1184–1193. https://doi.org/10.1016/j.compedu.2011.01.007

Culcasi, I., Russo, C., & Cinque, M. (2022). E-Service-Learning in Higher Education: Modelization of Technological Interactions and Measurement of Soft Skills Development. *Journal of Higher Education Outreach and Engagement, 26* (3), 39–56.

Feyerabend, P. (2021). *TPACK Newsletter, Issue # 44: March 2021. March* 1–118.

Gou, X. (2020). A measurement model of technological pedagogical content knowledge (TPACK) in Indonesian senior mathematics teachers' scenario A measurement model of technological pedagogical content knowledge (TPACK) in Indonesian senior mathematics teachers' scenario. *Journal of Physics: Conference Series, 1663.* https://doi.org/10.1088/1742-6596/1663/1/012018

Jang, SJ (2010). Integrating the interactive whiteboard and peer coaching to develop the TPACK of secondary science teachers. *Computers and Education, 55* (4), 1744–1751. https://doi.org/10.1016/j.compedu.2010.07.020

Jang, SJ, & Chen, KC (2010). From PCK to TPACK: Developing a Transformative Model for Pre-Service Science Teachers. *Journal of Science Education and Technology, 19* (6), 553–564. https://doi.org/10.1007/s10956-010-9222-y

Keengwe, J., Onchwari, G., & Wachira, P. (2008). Computer Technology Integration and Student Learning: Barriers and promises. Journal of Science and Technology Education, 17(6), 560-565

Koyuncuoğlu, Ö., & An, O. (2021). An Investigation of Graduate Students' Technological Pedagogical and Content Knowledge (TPACK) To cite this article: An Investigation of Graduate Students' Technological Pedagogical and Content Knowledge (TPACK). *International Journal of Education in Mathematics, Science, and Technology (IJEMST), 9* (2), 16.

Lin, TC, Tsai, CC, Chai, CS, & Lee, MH (2013). Identifying Science Teachers' Perceptions of Technological Pedagogical and Content Knowledge (TPACK). *Journal of Science Education and Technology, 22* (3), 325–336. https://doi.org/10.1007/s10956-012-9396-6

Mailizar, M., Mukhlis, H., & Abdulsalam, A. (2021). Examining the impact of mathematics teachers' TPACK on their acceptance of online professional development. *Journal of Digital Learning in Teacher Education*, *37* (3), 196–212. https://doi.org/10.1080/21532974.2021.1934613

Mishra, P. (2019). Considering Contextual Knowledge: The TPACK Diagram Gets an Upgrade. *Journal of Digital Learning in Teacher Education, 35* (2), 76–78. https://doi.org/10.1080/21532974.2019.1588611

Mulyati, S., & Evendi, H. (2020). Mathematics Learning Through Quizizz Game Media to Improve Mathematics Learning Outcomes at SMP 2 Bojonegara. *Journal of Mathematics Education, 03* (01), 64– 73.

Niess, ML (2005). Preparing teachers to teach science and mathematics with technology: Developing a technology pedagogical content knowledge. *Teaching and Teacher Education, 21* (5), 509–523. https://doi.org/10.1016/j.tate.2005.03.006

Niess, ML (2011). Investigating TPACK: Knowledge growth in teaching with technology. *Journal of Educational Computing Research, 44* (3), 299–317. https://doi.org/10.2190/EC.44.3.c

Njiku, J. (2021). Building Mathematics Teachers' TPACK Through Collaborative Lesson Design Activities. *CONTEMPORARY EDUCATIONAL TECHNOLOGY, 13* (2).

Nugroho Yanuarto, W., Mistima Maat, S., & Husnin, H. (2021). TPACK in mathematics teacher education: Are teachers ready to teach ICT literacy? *Journal of Physics: Conference Series, 1778* (1). https://doi.org/10.1088/1742-6596/1778/1/012012

Oster-Levinz, A., & Klieger, A. (2010). Online tasks as a tool to promote teachers' expertise within the Technological Pedagogical Content Knowledge (TPACK). *Procedia - Social and Behavioral Sciences*, *2* (2), 354–358. https://doi.org/10.1016/j.sbspro.2010.03.024

Ozturk, M.S., Kinik, M., & Ozturk, M.U. (2023). Investigation of Technological Pedagogical and Content Knowledge (TPACK) Competencies of University Students. *International Journal of Technology in Education (IJTE), 6*(3), 418-433. https://doi.org/10.46328/ijte.524

Ozturk, O.T. (2023). Examination of 21st Century Skills and Technological Competences of Students of Fine Arts Faculty. *International Journal of Education in Mathematics, Science, and Technology (IJEMST), 11*(1), 115-132. https://doi.org/10.46328/ijemst.2931

PRISMA_2020_flow_diagram_new_SRs_v1 . (n.d.).

Priyanda, R., Fadhelina, N., & Ihsan, IR (2021). *Google Forms as Worksheets to Foster Students' Learning Interest and Autonomy During Online Mathematics Learning. 576* (Icstms 2020), 73–77.

Rohati, R., Jambi, U., Kurniawan, DA, Jambi, U., Perdana, R., Jambi, U., Chen, D., & Jambi, U. (2021). Impact of the Integration of Ethno-mathematics with TPACK framework as a problem-based learning (PBL) model. *Journal of Physics: Conference Series, July 2022.* https://doi.org/10.14689/ejer.2021.96.14

Santos-Trigo, M., Aguilar-Magallón, D., & Reyes-Martínez, I. (2019). *A Mathematical Problem-Solving Approach Based on Digital Technology Affordances to Represent, Explore, and Solve problems via*

Geometric Reasoning. https://doi.org/10.1007/978-3-030-29215-7_8

Sari, IM, Yusibani, E., Mailizar, M., Hidayat, M., Artika, W., Yanuarto, WN, Maat, SM, & Husnin, H. (2021a). *Analysis The Ability of Thinking Abstractly of Mathematics And Self-Efficacy Through Tpack Analysis The Ability of Thinking Abstractly of Mathematics And Self-Efficacy Through TPACK.* https://doi.org/10.1088/1742-6596/1764/1/012122

Sari, IM, Yusibani, E., Mailizar, M., Hidayat, M., Artika, W., Yanuarto, WN, Maat, SM, & Husnin, H. (2021b). Design of instrument Technological Pedagogic Content Knowledge (T P A C K) for prospective mathematics teachers Design of instrument Technological Pedagogic Content Knowledge (TPACK) for prospective mathematics teachers. *Journal of Physics: Conference Series,* 8–12. https://doi.org/10.1088/1742-6596/1918/4/042097

Schmidt, DA, Baran, E., Ann, D., Mishra, P., & Koehler, MJ (2009). *Journal of Research on Technology in Education Technological Pedagogical Content Knowledge (TPACK). Nov. 2014,* 37–41. https://doi.org/10.1080/15391523.2009.10782544

Utami, C., & Jahar, AS (2021). REVIEW OF SCOPING REVIEWS AND CASE STUDY. *Journal of Civilization, Science, Engineering and Technology, 9* (2), 152–172.

Wijaya, TT, Tang, J., & Purnama, A. (2020). *Developing an Interactive Mathematical Learning Media Based on the TPACK Framework Using the Hawgent Dynamic Mathematics Software Developing an Interactive Mathematical Learning Media Based on the TPACK Framework Using the Hawgent Dynamic* (September Issue). Springer International Publishing. https://doi.org/10.1007/978-3-030-60036-5

Yuniarwati, EU (2022). The synthesis of qualitative evidence-based learning by design model to improve TPACK of prospective mathematics teacher The synthesis of qualitative evidence-based learning by design model to improve TPACK of prospective mathematics teacher. *Journal of Physics: Conference Series, 2157.* https://doi.org/10.1088/1742-6596/2157/1/012044

A New Option for Motorization and Control of Automobile Vehicles

Abdelkrim Rechach

Echahid Cheikh Larbi Tebessi University, Mining laboratory, Algeria, https://orcid.org/0000-0001-9889-5735

Sihem Ghoudelbourk

Badji Mokhtar University, Annaba, Algeria, https://orcid.org/0000-0002-8536-4086

Mounia Taleb

Echahid Cheikh Larbi Tebessi University, Envirment Laboratory Algeria, https://orcid.org/0000-0003-2564-2141

Abstract: The concept of an electric vehicle is based on three main elements: the electric drivetrain, the control system, and the batteries. The excessive price of the vehicle should be revised to make it affordable for the average citizen. To do that, we must move towards more economical technics while keeping at least the same vehicle performances. One of these solutions is the use of the switched reluctance motor. This latter has piqued the interest of modern automotive manufacturers; due to its many benefits, which include its robustness, simplicity of operation, lack of brushes, coils or permanent magnets; additionally, its ability to operate within a wide power range; its ease of use even in harsh environments, which ensures a longer lifespan and exceptional efficiency. However, because of the rotor's shape, the SRM is characterized by acoustic noise and vibrations. This latter problem can be resolved by the use of intelligent regulation techniques linked to direct torque control (DTC), to better use of the capabilities and performances of the SRM. These techniques appear to yield better results when compared to some recent control and command schemes mentioned in publications. A comparison using the Matlab/Simulink environment has confirmed the supremacy of the selected fractional order regulator.

Introduction

The greenhouse gas emissions from industrial activities and the worldwide inventory of combustion-powered vehicles cause the warm climate and ecosystem instability. The Earth is warming faster than ever before, and an environmental crisis is currently unfolding. The environmental impact and pollution of means transportation are significant. Currently, the global energy orientation is focused on machines that use the least amount of fuel to

produce the most in order to reduce the use of fossil fuel-derived fuel and fight against greenhouse gas emissions from intensive use of renewable or alternative energy sources. In Quebec, road transportation currently accounts for 34% of greenhouse gas emissions. The only practical solution is to electrify vehicles.

The contemporary interest of industrialists for SRM is essentially because they constitute a special class of electromagnetic machines compared to rotating machineries such as synchronous and asynchronous motors, induction and brushless permanent magnet machines. It's due for their following advantages: Simple rotor structure, robust, without coils or windings or permanent magnets, excellent performances in extreme environments, the high overload capacity, low manufacturing and maintenance costs, and operation in a wide power range. However, research is hampered by the high vibrations due to the peripheral discontinuities of its rotor, which are prohibitive to make it the motor of the first choice. SRMs have some disadvantages which are: torque ripple, vibrations and acoustic noises (Rechach, et al 2021., Ghoudelbourk et al., 2022], phase feeding in independent time sequences, low-speed operation requires a complex profile of the feeding wave and precise measurements of the position of the rotor.

The SRM's rotor conception is made with peripheral discontinuities and without conductors and permanent magnet. However, this motor is highly non-linear and works in saturation to maximize the value of the torque. Nevertheless, increasing the torque leads to the torque ripples and high acoustic noise. The structure of the SRM makes the controller design more difficult. Several researchers have focused on these problems to reduce their effects, improve the yield and perform the behavior of this machine and its control system. Full wave control is usually used to control SRM operating at high speed, where the torque undulations obtained with this command are significant. These undulations produce significant vibrations. The optimization of the control laws makes it possible to reduce these undulations and consequently these vibrations.

In addition to the torque's oscillations, phase-change feeding in independent temporal sequences requires a sophisticated dietary wave profile and precise rotor position measurements. This is where the need for an appropriate choice of control and regulation arises. The SRM's control cannot be compared to either a continuous-current motor or an alternator motor powered by sinusoidal waveforms. To achieve the simplest control, each stator phase must magnetize and demagnetize the pole corresponding to the optimal rotor position, in such a way that the current-wave square form can be employed. However, considering the fact that the motor is highly nonlinear, the electromagnetic torque depend not only on the instantaneous current value but also on a nonlinear inductance profile. This means that using only square forms of current wave would result in a torque with high undulations.

The tension, current, and torque controllers are chosen based on required performances and costs. The controllers with the lowest performance in impulsion control are the least expensive, while the controller with the highest performance in couple control is the most expensive.

Due to the non-linear nature of the SRM, non-linear control strategies to compensate for all or part of these irregularities can be used to control a high-speed (Boufadene, et al., 2018; Mathieu et al., 2013) The use of SRM systems is nowadays much replied. Despite this enormous expansion, they face limitations in their control. For these reasons, we were focused in this study for these systems control. Therefore, the use of the classic proportional integrator regulator (PI) to control the speed provoke practically a high level of torque ripples and noises.

In order to solve the issue of the acoustic noses and vibration in the SRM, better utilize its capabilities and performances, and make better use of it in severe conditions, we suggest using intelligent techniques like artificial neural network regulators ANN, fuzzy logic control and fractional order regulators (FOPI). These topologies linked to the direct couple control DTC yield better results after being compared to some control and command schemes mentioned in recent publications.

This article aims at the improvement of the strategy of the control of the torque (DTC) using FOPI, ANN and FLC. At last, a comparison between the ANN, FLC and the FOPI under Matlab/Simulink environment confirmed the superiority of the fractional order regulator FOPI.

Switched Reluctance motor model

While SRM are comparable in design and method of operation, we have taken into consideration, for simplicity's income the SRM whose features were published in (Srinivas, et al,. 2012). The first magnetization curve B=F(H) of the ferromagnetic material (Steel M19) is displayed in Figure 1. It is crucial to note that the magnetic unsaturation zone will be the focus of the simulation. The mentioned characteristics used here and shown at the table 1 are identical to those appearing in (Durmu, et al,. 2007). The selection of ferromagnetic material characterizes the magnetic properties capable of significantly increasing the motor's efficiency.

The main idea of the operation of the SRM is that windings housed in the stator teeth are fed alternately, while the rotor teeth, without coil or magnets, are attracted to the stator windings (David. Meeker., 2015). The entire structure of our SRM is shown in figure 2, which shows the whole machine with its different parts. The figure 3 shows the design topology of the prototype of the rotor object of our simulation with a four-phase power supply of the SRM 8/6. Figure 4 is a clear picture of the poles lamination of the stator without winding.

Table 1. The main characteristics of the SRM chosen, subject of this study

Designation	Notation	Dimension
Outside stator radius	R_s	143mm
Rotor radius	R_r	69mm
Air Gap	E	0.40 mm
Polar arc of the stator	B_s	0.416 rd

Polar arc of the rotor	B_r	0.492 rd
Stator tooth height	h_s	24,50mm
Rotor tooth height	h_r	12,50mm
Stator pole width	B_s	30mm
Rotor pole width	B_r	30mm
Stator yoke thickness	Y_s	12,10mm
Rotor yoke thickness	Y_r	9,00mm
Stack length	SL	143mm
Shaft Radius	R_a	13mm
Ferromagnetic material	M19	M19
Maximum Current	I	30A
Maximum Flux	ϕmax	0,30Wb
Stator poles	NP_s	8
Rotor poles	NP_r	6

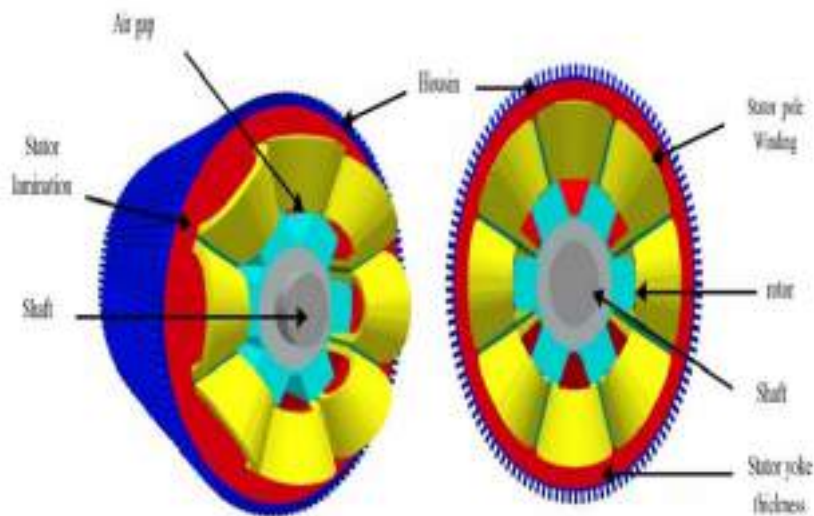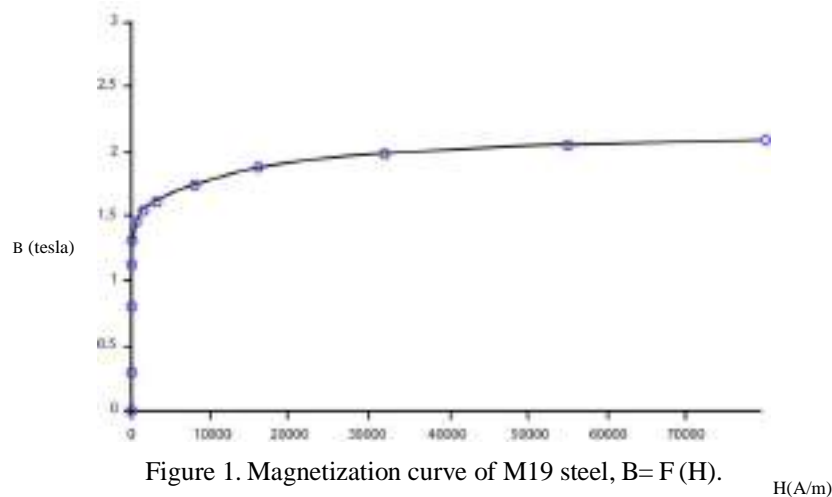Figure 1. Magnetization curve of M19 steel, B= F (H).

Figure 2. The entire structure of SRM 8/6poles with its different parts

The structure to which we are interested and which presents a four-phase machine, type 8/6. The operation of an SRM is comparable to an electromagnet. This article's SRM object's schematic structure and the way the four phases are coupled around the stator poles are depicted in Figure 5.

The SRM's basic working principle is determined by where the rotor and stator teeth are located. The rotor rotates to the location where the stator's generated flux is at its maximum when a phase is applied (Dong, et al., 2020). This latter position is called the conjunction position. Where the flux is minimum, we call it the opposition position. The torque is created by magnetic variation between the stator pole and the rotor pole, hence its name "Switched reluctance motor". During a cycle of variation of the magnetic permeability, four periods are observed (Kushwaha, et al., 2020):
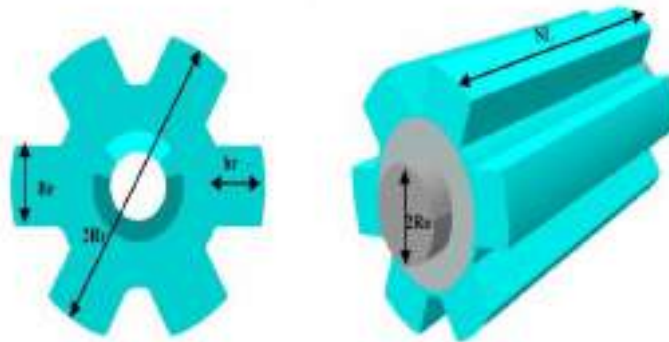

Figure 3. Rotor structure of the SRM 8/6 and its poles

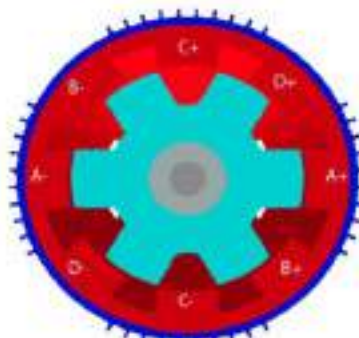Figure 4. The Stator lamination of the SRM 8/6

Figure 5. Connection of the 4 phases of the stator for SRM 8/6

The idealized form of the inductance of a phase as a function of the rotor position is expressed by the following equations system and shown in the figure 6.

$$
L(\theta) =
\begin{cases}
\bullet \quad L_{min} & 0 \le \theta < \theta_1 \\
\bullet \quad L_{min} + p\theta & \theta_1 \le \theta < \theta_2 \\
\bullet \quad L_{max} & \theta_2 \le \theta < \theta_3 \\
\bullet \quad L_{max} - p(\theta - \beta_r) & \theta_3 \le \theta < \theta_4 \\
\bullet \quad L_{min} & \theta_4 \le \theta < \theta_5
\end{cases}
\tag{1}
$$

Where $L(\theta)$: Inductance variation over one rotor pole pitch,

L_{min}: Unaligned inductance (H),

L_{max}: Aligned inductance (H),

β_s: Stator pole arc(rad),

β_r :Rotor pole arc(rad) $\beta_r > \beta_s$

$$
p = \frac{L_{max} - L_{min}}{\beta_s}
\tag{2}
$$
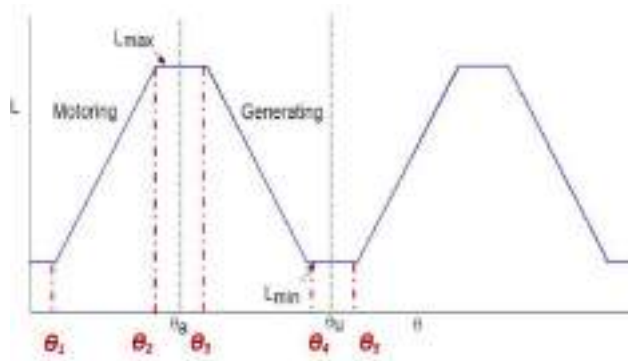
Figure 6. Inductance Profile for Switched Reluctance Motor

The variation of the magnetic permeability between a stator tooth and a rotor tooth is responsible for creating the torque [6]. The supply electric voltage of the stator coil of the SRM is given by:

$$
v = Ri + \frac{d\psi(\theta, i)}{dt}
\tag{3}
$$

where $d\psi(\theta, i)$ is the phase flux linkage, which depends on rotor position θ and stator current I.

$$
v = Ri + \frac{d\psi(\theta, i)}{di}\frac{di}{dt} + \frac{d\psi(\theta, i)}{d\theta}\frac{d\theta}{dt}
\tag{4}
$$

The differential mechanical energy obtained (Srinivas et al., 2011) is shown as:

$$
dW_m = i\frac{d\psi(\theta, i)}{d\theta}d\theta - \frac{dW_f}{d\theta}\frac{d\theta}{dt}
\tag{5}
$$

And the instantaneous torque are defined as :

$$T \approx i \frac{d\psi(\theta,i)}{d\theta} \tag{6}$$

Electric Supplying of SRM8/6 and DTC used for electric vehicle

The conception and the dimensioning of the variable resistance machine are inextricably linked to the converters. In fact, there are several converter schemes available for its feeding. In this part, we will go over the most common ones called "asymmetric half bridge converter".

This latter feature is explained according to equation (6), where the phase flux depends on the position of the rotor (θ) and the stator current (i). SRM supply can be explained as follows (Nagesh, et al., 2020; Nandhini et al., 2017): The asymmetric half bridge converter is often used for SRM drives (As shown in figure 7 and 8), where each powered phase has three possible distinct states. When both the switches are turned ON (see Figure 9.a), the current circulates into the coil through two switches and apply a positive voltage to the SRM phase. This mode is called commonly "Magnetizing state". When the switch is turned OFF like shown in Figure 9.b, the current flows through the diode and coil, and a no voltage loop occurs. It is the "freewheel state 0 ". Figure9.c illustrates the state when the two switches are deactivated, the current flows through the phase coil and the diodes, the voltage applied is negative and it is the state (-1), said demagnetization".
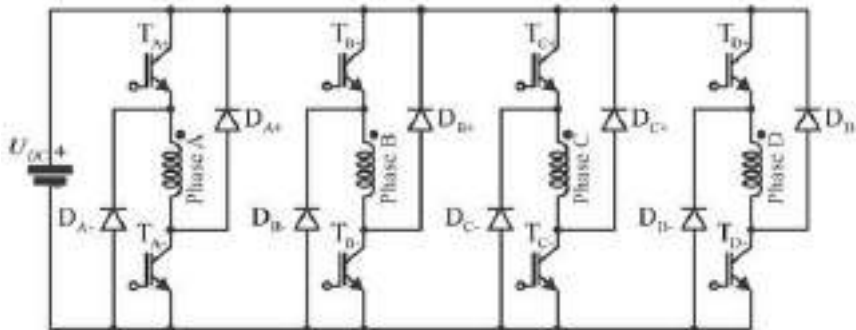

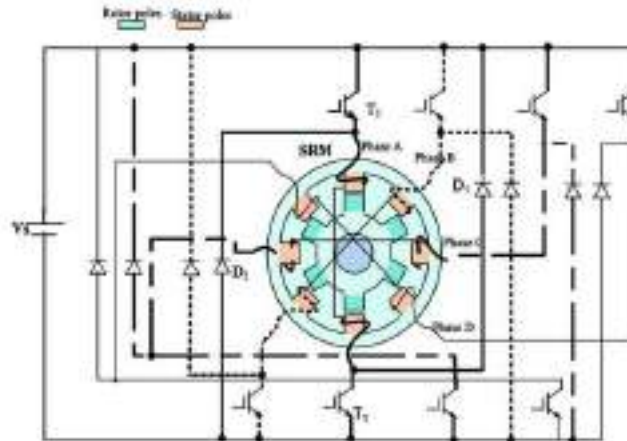Figure 7. Asymmetric half bridge converter

Figure 8. SRM 8/6 voltage supplying with asymmetric converter (Sanjib, et al., 2005)
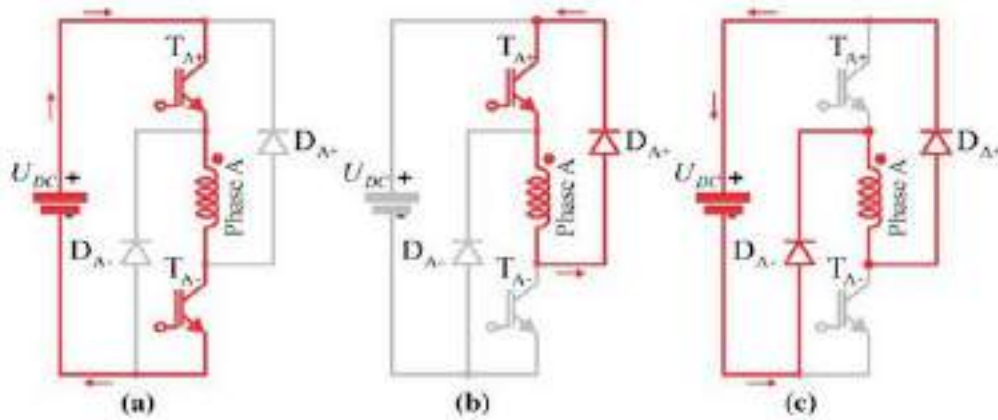
Figure 9. SRM voltage states: a- State (1);   b- State (0);   c- State (-1)

A methodology called "direct torque control" is utilized to lessen noise and vibrations that are brought on by torque ripples in the SRM's rotor shape. This article uses the SRM 8/6's DTC control performance and its effects on the torque ripple in both the steady and transient states in association with : on the first side, control by Artificial Neural Network and on the other side with the fuzzy logic control and on the third side the fractional-order control. A comparison between them is made under the Matlab/Simulink environment.

Direct Torque Control solely employs voltage and current measurements; it does not require position or speed sensors. When choosing the matching voltage vector, magnetic flux and torque are estimated and maintained. The 4-phase unbalanced converter (see Figure7) have up to 81 possible Space Voltage Vectors, but only eight spatial voltage vectors are sufficient for the DTC application to the SRM, as shown clearly in Figure 9. The DTC is therefore ideally suited for electric cars.

Figure 9. Space voltage vectors and eight sectors

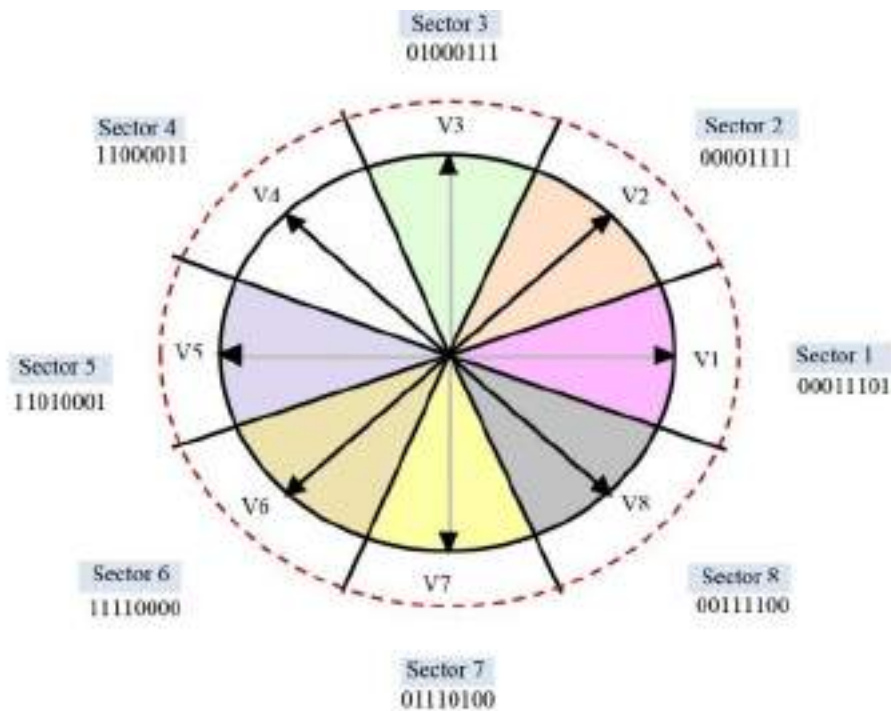The proposed technique based DTC for SRM 8/6 is a 4-phases spatial vector modulation (SVM) by choosing an appropriate set of eight spatial voltage vectors. Pulse Width Modulation (PWM) here is no more used. The inverter receives the commands successively and directly. If the kth sector is attributed to the stator flux link vectors, the spatial voltage vectors V_{k+1} and V_{k+2} are selected if the motor requires an increase in torque and if the decrease in torque is requested, the voltage vectors responsible of decelerate the vector of flux V_{k-1} and V_{K-2} are applied. The appropriate spatial voltage vectors are shown in the following Table 2 and 3, based on the output of the hysteresis blocks where torque and flux are estimated.

Table 2. DTC switching table for SVM

N	$\Psi Q = 1$		$\Psi Q = 0$	
	$T_Q=1$	$T_Q=0$	$T_Q=1$	$T_Q=0$
1	V_2	V_7	V_3	V_6
2	V_3	V_8	V_4	V_7
3	V_4	V_1	V_5	V_8
4	V_5	V_2	V_6	V_1
5	V_6	V_3	V_7	V_2
6	V_7	V_4	V_8	V_3
7	V_8	V_5	V_1	V_4
8	V_1	V_6	V_2	V_5

Table 3. Evolution of the flux vector according to the space voltage vector

Vector	V_{k+1}	V_{k-1}	V_{k+2}	V_{k-2}
Magnetic Flux Ψs	Increase	Decrease	Decrease	Decrease
Torque T	Increase	Decrease	Increase	Decrease

The fluxes vectors of the four phases are solved in the α-β axes (Korkmaz., 2017) using the transformation shown in Figure 10. So the magnetic fluxes equation α-β axes is:

$$\psi_\alpha = \psi_1 \cos 45° - \psi_2 \cos 45° - \psi_3 \cos 45° + \psi_4 \cos 45° \tag{7}$$

$$\psi_\beta = \psi_1 \sin 45° + \psi_2 \sin 45° - \psi_3 \sin 45° + \psi_4 \sin 45° \tag{8}$$

$$\psi_s = \sqrt{(\psi_\alpha^2 + \psi_\alpha^2)} \tag{9}$$

$$\delta = \arctan\left[\frac{\psi_\alpha}{\psi_\beta}\right] \tag{10}$$

ψ_1, ψ_2, ψ_3 and ψ_4: are flux phases

ψ_α, ψ_β: respectively the fluxes in α and β axes

δ: angle of flux vector

The DTC diagram for SRM 8/6 poles is displayed in Figure 11. The voltages and currents at the output of the inverter that powers the SRM are the measured values for each of the four phases. We first calculate the

magnetic flux of each phase, which is subsequently translated into two phases based on the α-β axes. The flux vector's amplitude (Ψs) and angle (δ) are automatically identified.
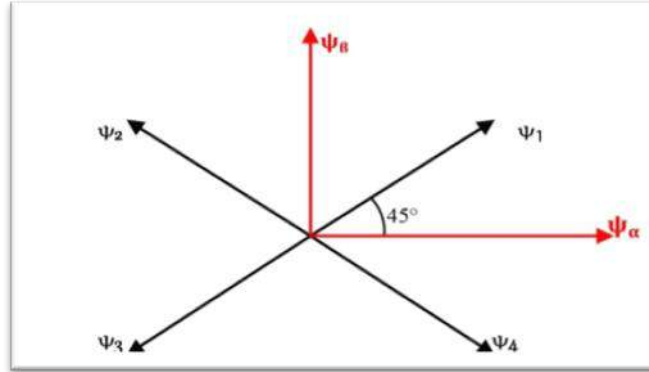
Figure 10. Fluxes Vectors of four phases in the α,β axes

Next, the motor torque (T) and the flux vector (Ψs) amplitude are introduced to the torque hysteresis and flux blocks, which leads to an increase or decrease in flux Ψ and torque T, as a result of comparing the reference flux and torque to the real ones. Utilizing switching tables and an asymmetric converter, voltage vectors appropriate for the SRM's four-phase windings are applied. Utilizing switching tables and an asymmetric converter, voltage vectors appropriate for the SRM's four-phase windings are applied. After comparing the reference values, the error is sent to the PI controller.

Figure 11. Diagram of DTC for SRM 4 phases 8/6 poles

Using calculated flux and torque values, the DTC directly controls the inverter's switches opening and closing. The goal of switching command is to provide the vector of the stator flux with the direction specified by the input values. Determining the control of the inverter's switches requires knowledge of the motor's electrical state.
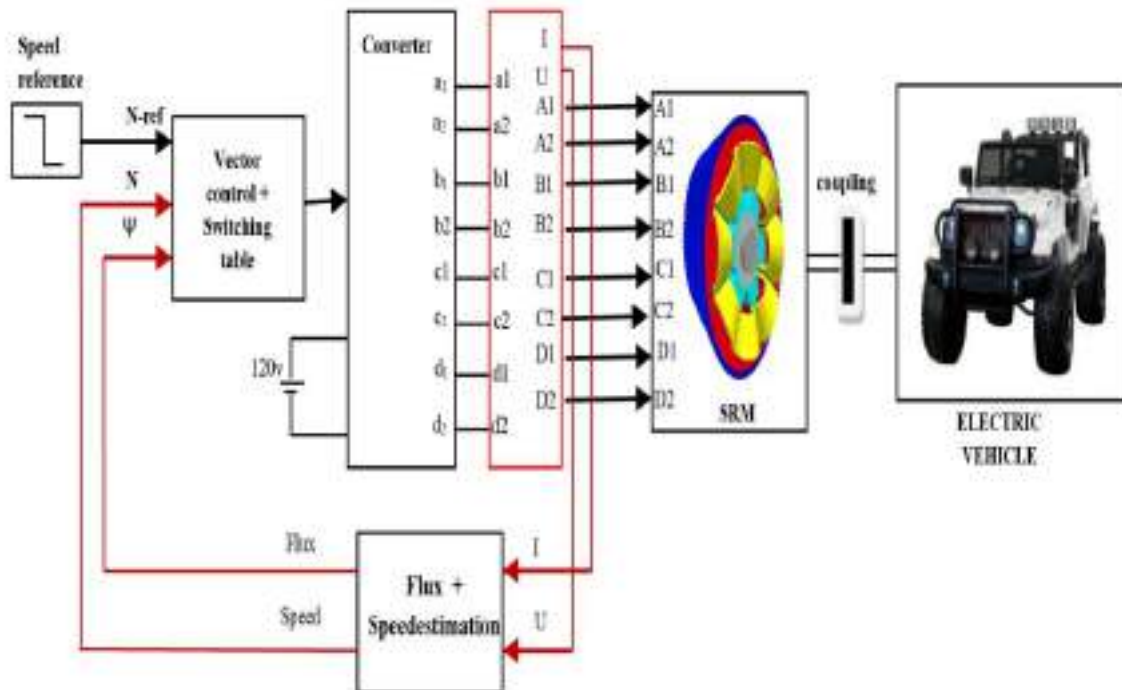
Based on continuous tension measurements at the inverter's input of statoric currents, the model provides, at each moment [99], the real stator magnetic flux, real developed couple and rotational speed.

One major benefit of using the DTC is that there is no requirement for speed measurement at the output shaft. To find the command times of the interrupters for at least holding constant the magnetic flux.

The PI-ANN controller of the SMR8/6

Artificial neural networks are structures based on a collection of neurons, which are connected by weighted and adjustable links in a specific architecture through a process known as learning (Korkmaz, 2017; Kumar, et al., 2013). Three fundamental components make up the formal neuron (as shown in Figure 12):

- A collection of links, each with a weight w_j (also known as the synaptic coefficient), that represents the connection's efficiency and a specific input x_0 that is always equal to 1, that allows the network to be more flexible by allowing the weight, also known as bias and denoted as b, to be adjusted when learning $w_0 = b$.
- An adder or summing unit for the weighted signals.
- An activation function to limit the output value.

An ANN's learning algorithm seeks to iteratively adjust the network's weights until the difference between the reference input and the measured or estimated value is less than the desired amount. The DTC control approach has been applied in this instance. As seen in Figure 13, an artificial neural network (ANN) was created using the error between the reference speed and the estimated speed as input values.

Because of its ability to learn and approximate, a neural network can mimic the behavior of an existing conventional controller (PI, PID, etc.). The following procedures (Milan, et al 2015; Kritarth Shrivastava., 2015) used with the suggested model to compute the reference torque T_{ref} from the error (e) and its derivative (Δ_e):

- Set the number of hidden layers between the input and output layers. The analyst must decide on the number of intermediate layers.
- Determine the total number of neurons in the hidden layers; each time a new neuron is added, certain input neuron profiles need to be considered.
- Define the activation function.

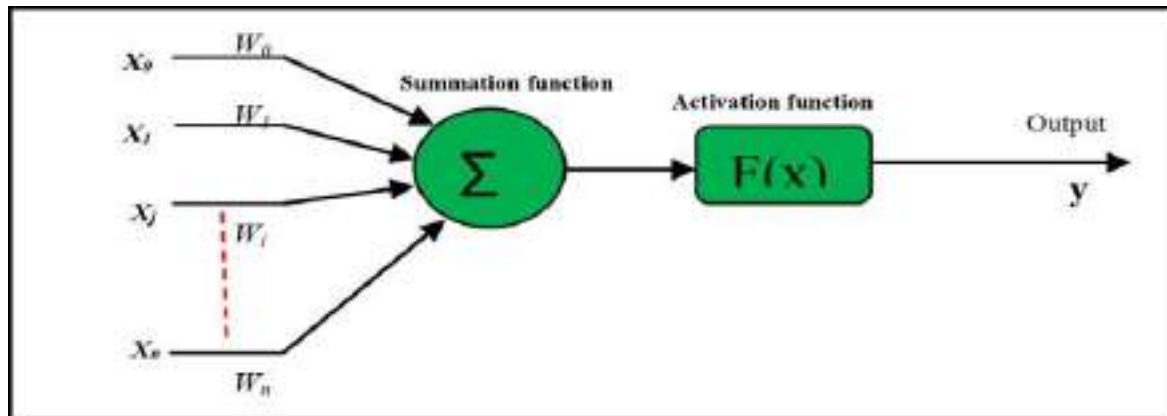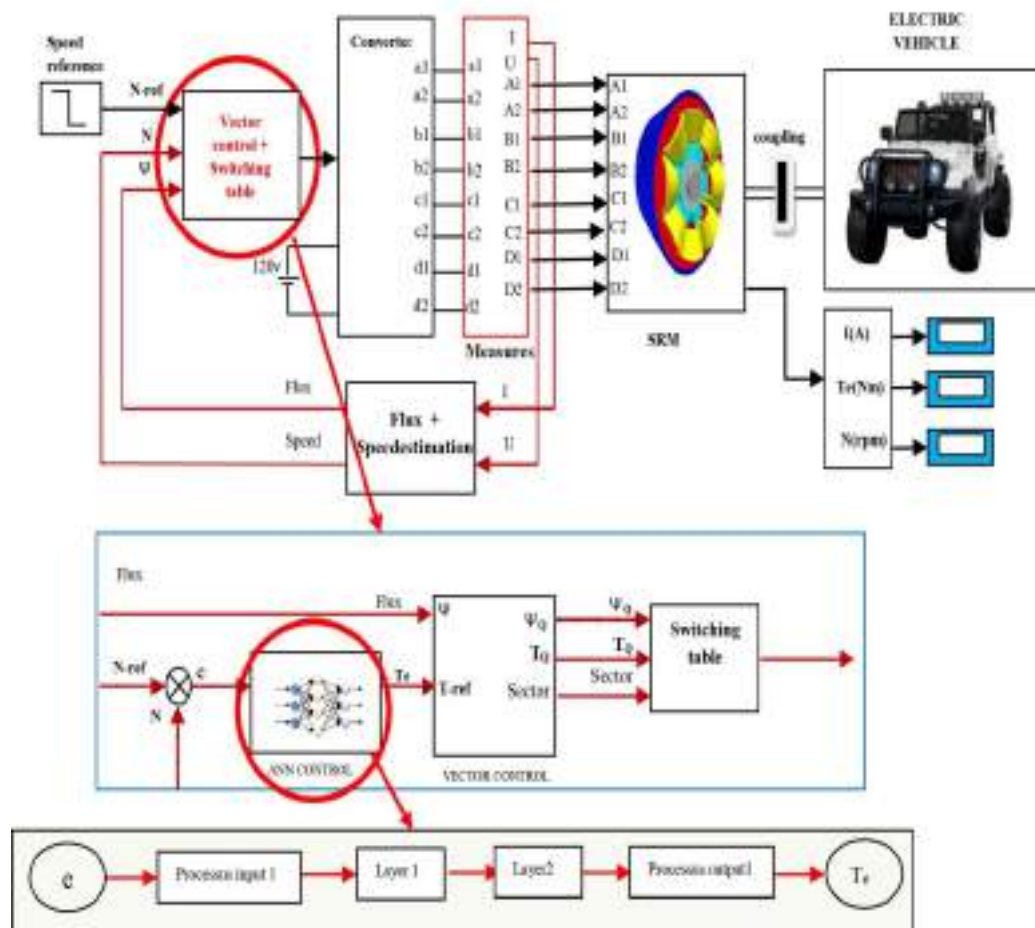Figure 12. Model of the formal neuron

Figure 13. Sensor-less block diagram for of SRM 8/6 using Artificial Neural Network with DTC

The FLC for switched reluctance motor 8/6 poles

SRM is employed at slow rates in the majority of applications. When SRM is working at a high speed, full wave control is typically utilized to manage it because this command produces noticeable torque undulations and

significant vibrations are produced by these undulations. Reducing these torque undulations and subsequently these vibrations is made achievable by the adjustment of the control rules. A high-speed can be controlled by using non-linear control strategies to partially or fully compensate for these anomalies because the SRM is a non-linear system (Kritarth Shrivastava., 2015; Khan, et al 2019).

In today's industry, switching reluctance systems are widely used. Even with this massive growth, they still have some control issues. These factors make the study of such systems a topical area in which we are engaged. The goal of this part of study is to enhance the Direct Torque Control (DTC) approach for SRM coupled with FLC. The figure bellow shows the sensor-less block diagram for of SRM 8/6 using fuzzy logic control with DTC.

In order to describe the inputs of error and the changes of error also the output of fuzzy controller we need to partition the universe of discourse of each variable into fuzzy membership function (Nandhini, and al., 2017). We will divide each to 7 linguistic fuzzy terms: big positive (PB), average positive (PM), small positive (SP), zero error (ZE), big negative (NB), small negative (NS) and average negative (NM), as shown in Figures .15.
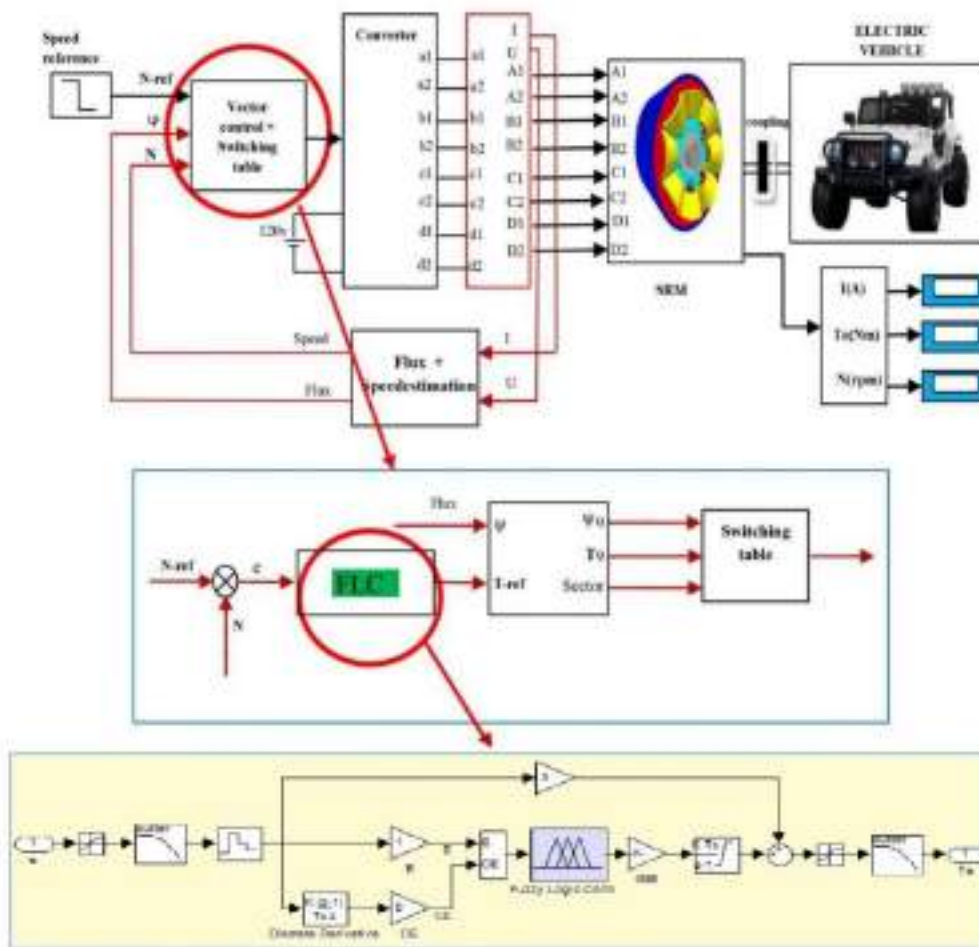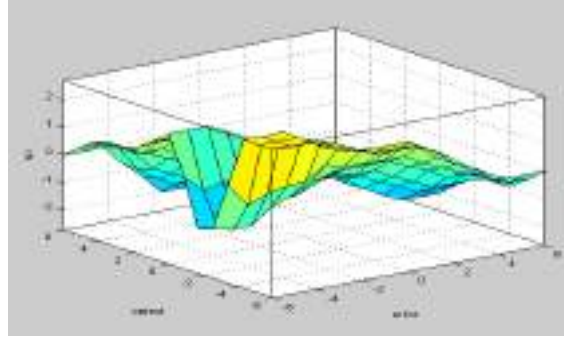

Figure 14. Sensor-less block diagram for of SRM 8/6 using fuzzy logic control with DTC

Figures 15. the input error; input the changes of error, output voltage
and Surface Viewer for SRM with FLC Simulation

A combination of direct torque control (DTC) and fuzzy logic control (FLC) has been proposed in which, based on the difference between the reference value and the real value of the flux and the torque, the voltage vectors are chosen with fuzzy logic with great precision. The results obtained under Matlab environment shows that the torque ripples are very low, the speed is stable and the response is fast with a high precision of control.

Fractional order controller of the SMR

Fractional applications calculus are very recent due to the fact that we are nowadays able to update processes whose study of their models needs the fractional-order derivative, which are expressed with the fractional power pole equation (PPF):

$$G(s) = \frac{1}{S^\alpha} = \frac{K}{(1+\frac{S}{W_f})^\alpha} \qquad (11)$$

α is a non-integer complex number; S express Laplace transform and W_f is the fractional pole. In SRM control the FOPI system was motivated by the good performances compared to PI order. The FOPI regulator has the following transfer function :

$$H(S) = K_p + K_i S^{-\alpha} + K_d S^{+\beta} \qquad (12)$$

K_p, K_i, and K_d are the proportional, integral, and derivative gain, both α and β are real numbers. The classic PID regulator is caracterised by $\alpha=1$ and $\beta=1$. The most important step In the implementation of the FOPI is the numerical evaluation of the discretization of the fractional-order derivations S^α. The fractional-order system is characterized by the following transfer function (Podlubny, 1999; Ghoudelbourk, et al., 2022):

$$G(S) = \frac{b_m S^{\beta_m} + b_{m-1} S^{\beta_{m-1}} + \cdots + b_0 S^{\beta_0}}{a_n S^{\alpha_n} + a_{n-1} S^{\alpha_{n-1}} + \cdots + a_0 S^{\alpha_0}} \qquad (13)$$

Hence the discrete transfer function of the fractional-order system is obtained as:

$$G(z) = \frac{b_m (w(z^{-1}))^{\beta_m} + b_{m-1}(w(z^{-1}))^{\beta_{m-1}} + \cdots + b_0 (w(z^{-1}))^{\beta_0}}{a_n (w(z^{-1}))^{\alpha_n} + a_{n-1}(w(z^{-1})^{\alpha_{n-1}} + \cdots + a_0 (w(z^{-1})^{\alpha_0}} \qquad (14)$$

$w(z^{-1})$ is the discrete equivalent of the Laplace operator S. To implement the fractional-order model in the control object, we use basically the singularity function method, developed by (Charef, et al., 1992; Bai, et al., 2015). In the fractional system of the 1st order, the targets of the approximation method is the slope of 20mdB/dec on the Bode plot of the PPF by the number of lines in zig-zag form, produced by an alternation of

20dB/dec and 0 dB/Dec:

$$p_0 < z_0 < p_1 < z_1 < . . . < z_{N-1} < p_N \qquad (15)$$

Which conduct us to the following expression:

$$G(s) = \frac{1}{s^\alpha} \cong \frac{K}{\left(1+\frac{S}{W_f}\right)}\alpha \cong K.\frac{\Pi_{i=0}^{N-1}\left(1+\frac{S}{Z_i}\right)}{\Pi_{i=0}^{N-1}\left(1+\frac{S}{p_i}\right)} \qquad (16)$$

Where N+1 is the determined total number of singularities by the frequency band. So the singularity function is obtained as:

$$p_i = (ab)^i p_0 \; ; \quad for \; i = 0,1,2,,3,\dots,N \qquad (17)$$

$$z_i = (ab)^i a p_0 \; for \; i = 1,2,,3,\dots,N-1 \qquad (18)$$

$$p_0 = W_f 10^{\frac{\epsilon p}{20\alpha}} \qquad (19)$$

$$a = 10^{\frac{\epsilon p}{10(1-\alpha)}} \; ; \; b = 10^{\frac{\epsilon p}{10\alpha}} \; and \; N = \left[Integer\left[\frac{\log\left(\frac{w_{max}}{p_0}\right)}{\log(ab)}\right]+1\right] \qquad (20)$$

Where ϵp is the tolerated error in dB. The simulation under Matlab environment for different values of α was carried out. The chosen transfer function for the present control system is α = 0,6. Figure 16. shows a sensorless block diagram vector control for SRM 8/6 poles using fractional controllers with DTC. A selected α for our simulation is equal to 0,6.
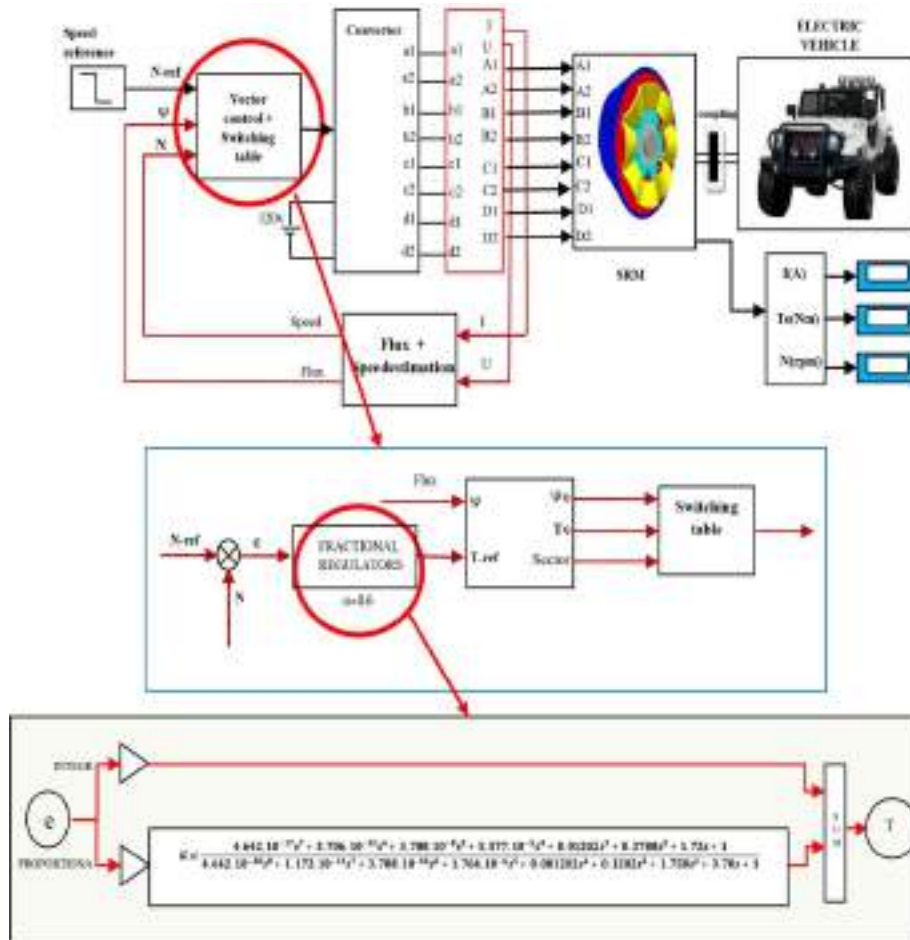

Figure 16. Senseless block diagram for vector control of SRM 8/6 using Fractional Regulators with DTC

Results and Discussion

The simulation under the Matlab/Simulink for the SRM8/6 with the same specifications indicated in Table 4 outcomes the results presented in Figure 18, 19 and 20. To better study the behaviour of SRM we provoked the test with a speed change from 1000 rpm to 1500 rpm/min under a load of 4N.m at the instant t=0.5s.

Figure 17 shows the currents obtained for the four phases at the output of the inverter according to the block diagrams proposed (see Figure 13, 14 and Figure 16). We compared the results of the systems with the ANN controller, FLC and the fractional-order controller under the same constraints of the motor whose specifications are already indicated, both associated to the DTC.

With FOPI system, the output signals attests a very good performances, a satisfactory speed trajectory, the torque undulations are considerably improved and seems much better than the other controls protocols and a better behaviour under unpredictable overload conditions. On the other hand, with ANN control and FLC cases, the overshoot is significant (see Figure 18 and 19). These results demonstrate the superiority of the fractional FOPI controller under unpredictable overload conditions.

TABLE 4. Specifications OF THE SRM

Designation	value
Phases	4
Stator pole number	8
Rotor pole number	6
Rated voltage	230V
Rated current	10A
Rated speed	4000 rpm
Rated load	0.75 kW
Moment of inertia (J_m)	0.005 Kg-m^3
Viscous friction	0.005Nm/(rad/s)
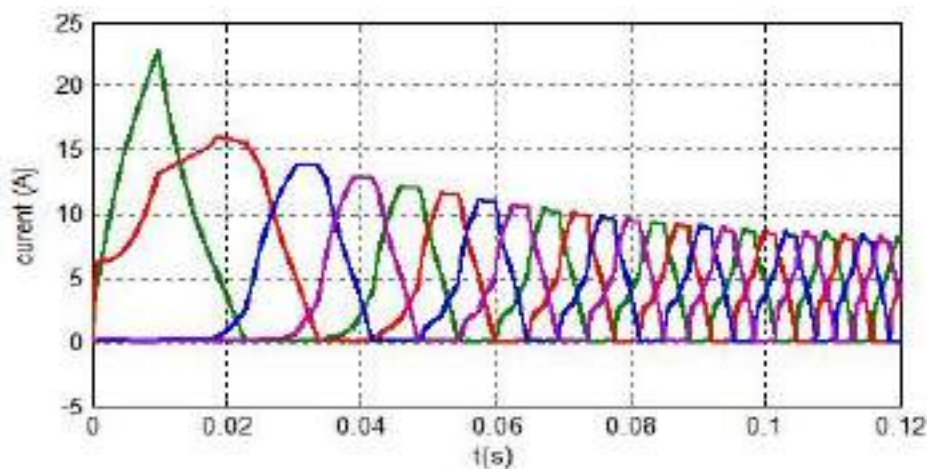
Figure 17. Output current waveform of SRM 8/6
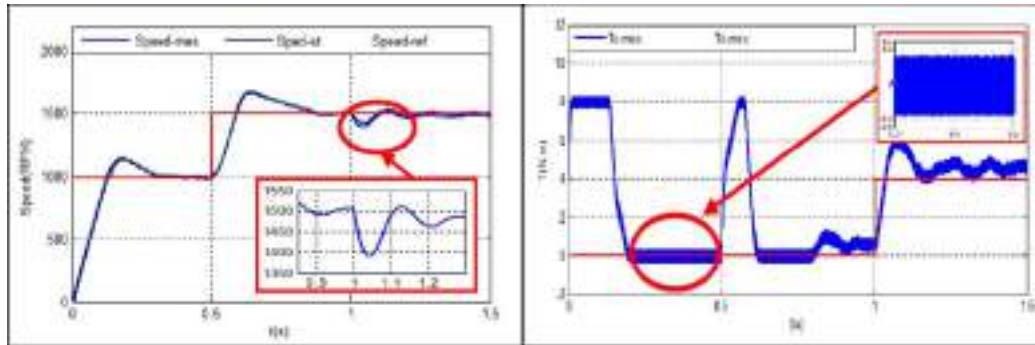
Figure 18. Results of SRM8/6 behaviour with ANN controller

On the left the waveform speed output, on the right waveform torque output
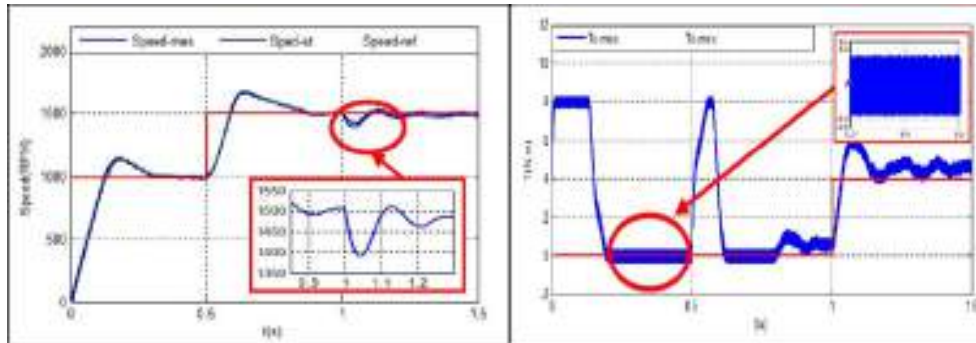
Figure 19. Results of SRM8/6 behaviour with FLC controller

On the left the waveform speed output, on the right waveform torque output
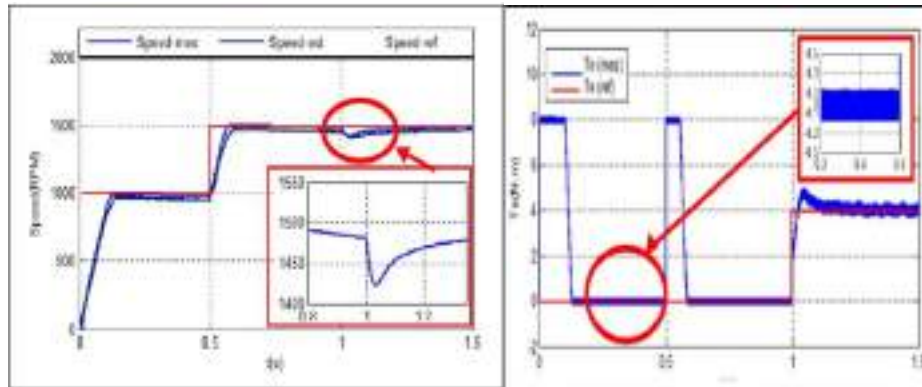
Figure 20. Results of SRM8/6 behaviour with FOPI controller

On the left the waveform speed output, on the right waveform torque output

The comparison with the other schemes of control found in the literature eulicidate that : without any controller, the torque ripples are excessively high which makes the use of SRM undesirable; With the use of the controllers, the torque characteristic is considerably improved as indicated in Table 5. By designing DTC and with different types of controllers, ranging from a simple PI to intelligent controllers such as FLC, ANN, and FOPI, the torque undulations are considerably reduced. At least the torque ripple rate obtained from each technique was

analyzed, and we concluded that the direct DTC torque control method associated with fractional-order control gives the best results and behaviour of the SRM .

Table 5. Comparative table of the results obtained with those found in recent reviews

Techniques used	$\pm \Delta C$ (N.m)
Without any controller (Pranil, et al., 2016)	13
PI controller (Nagesh, et al., 2020)	0,6
DTC with simple PI (Srinivas, et al., 2012)	0,45
DTC with FLC (Ab Ghani, et al., 2016)	0,3
DTC with ANN (Shrivastava, 2015)	0,3
DTC with Fractional-order in present work	0.1

Conclusion

The use of direct torque control improves considerably the behaviour of the SRM by reducing particularly and significantly, the torque ripples mainly due to the peripheral discontinuities of the shape of the rotor. The DTC seems to be well suitable to the SRM 8/6 in view of the fact that, it is sensor-less with better precision to overcome load constraints of the driven system. The response became even better in the case of using both the DTC and the fractional order controller. We had compared the latter topology and several precedent works using different protocols of control of SRM like simple PI, FLC, simple DTC and Artificial Neurone Network regulator ANN regulator. FOPI regulator shows the best stability in dynamic mode, speed without overshoot, better behaviour in irregular load and disturbances, and better lifetime and robustness compared to those obtained with the other regulators already evoked. These results are obtained by simulation under Matlab/Simulink environment.

References

Sihem Ghoudelbourk, Ahmad Taher Azar, Djalel Dib, and Abelkrim Rechach. "Fractional order control of switched reluctance motor", International Journal of Advanced Intelligence Paradigms Vol. 21, No. 3-4 Published Online: 7 Apr 2022.

Abdelkrim Rechach, Sihem Ghoudelbourk, Zoubir Aoulmi, Dib Djalel. "Smart Controls for Switched Reluctance Motor 8/6 Used for Electric Vehicles Underground Mining Security", European Journal of Electrical Engineering Vol. 23, No. 6, December, 2021, pp. 423-432. https://doi.org/10.18280/ejee.230601.

Boufadene, Mourad., Belkheiri, Mohammed., and Rabhi, Abdelhamid., (2018) 'Adaptive nonlinear observer augmented by radial basis neural network for a nonlinear sensorless control of an induction machine' International Journal of Automation and Control, International Journal of Automation and Control, Vol.12 No. 1, pp. 27 – 43.

Mathieu, O. P. J., Anthonis, J., Gyselinck, J., Li J., Song, Z. and S.Faid "Miniature-Shaker Spectral Tests of Switched Reluctance Motor Stators, Automotive Safety and Energy Journal, 4 (2), 189–197, (2013).

Srinivas Pratapgiri , Prasad PolakiVenkataNarsimha, " Direct torque control of 4 phase8/6 switched reluctance motor drive for constant torque load ",ISSN1 746-7233, England, UK World Journal of Modelling and Simulation Vol. 8 (2012) No. 3, pp. 185-195.

Durmu uygun*, Caner Akuner **, Mehmet Yumurtaci, "A New Construction of Switched Reluctance Motor Improving Magnetic Field Energy and Torque Production" Proceedings of the 6th WSEAS International Conference on Applications of Electrical Engineering, Istanbul, Turkey, May 27-29, 2007

David Meeker, Finite Element Method Magnetics Version 4.2 User's Manual October 25, 2015

Dong, F., Chen, H., Xu, S., and Cui, S., (2020) 'A fault-tolerant sensorless position estimation scheme for switched reluctance motor at low speed', COMPEL - The international journal for computation and mathematics in electrical and electronic engineering, Vol. 39, No. 4, pp. 823-837.

Kushwaha, A., and Kanagaraj, R., (2020) 'Peak-current estimation using a simplified current-rise model of switched reluctance generator operating in single-pulse mode', Int. J. Electr. Power Energy Sys, Vol.120, 105971.

P.Srinivas, P.V.N.Prasad. "Torque ripple minimization of 4 phases 8/6 switched reluctance motor drive with Instantaneous Torque Control", International Journal on Electrical Engineering & Informatics, (2011), 3(4):488-497. https://doi.org/10.15676/ijeei.2011.3.4.8.

Abdelkrim Rechach, "Modélisation et contrôle intelligent du moteur à réluctance variable en vue de son utilisation en énergie propre", (2022) Doctorate thesis, Cheikh Larbi Tebessi University, Tebessa, Algeria

K.Nagesh, D.Lenine, P. Sujatha. (2020). "Modelling and analysis of 8/6 Switched Reluctance Motor with PI controller", J. Mech. Cont. & Math. Sci., Special Issue, No.5, pp 357-370, https://doi.org/10.26782/jmcms.spl.5/2020.01.00029.

K.Nandhini, "Analysis and experimental investigation of mechanical vibration in switched reluctance motor", International Journal of Advanced Research Methodology in Engineering & Technology, Volume 1, Issue 2, March 2017, ISBN 978-1-63535-889-6.

Sanjib K Sahoo, Sanjib K Panda, and Jian-Xin Xu. "Indirect torque control of switched reluctance motors using iterative learning control", IEEE Transactions on Power Electronics, 20(1) :200–208, 2005.

Korkmaz, F., (2017) 'Speed And Torque Control Of An Induction Motor With ANN Based DTC', in International Journal Of Instrumentation And Control Systems (IJICS), vol.7, no.1, pp.15-24.

R.S.Kumar, J.A. Vasanth. (2013), "Intelligent neuro-controller based on speed and torque control of five phase switched reluctance motor. Information Communication and Embedded Systems", ICICES 2013 International Conference, 966-973. https://doi.org/10.1109/ICICES.2013.6508296.

Milan Diko, PavolRafajdus, PavolMakys, Peter Dubravka, LorandSzabo and MirceaRuba, "Concept of Short-Flux Path Switched Reluctance Motor for Electrical Vehicles Power engineering and electrical engineering volume", 13 Number: 3 -2015 .

Kritarth Shrivastava, "VECTOR CONTROL OF SWITCHED RELUCTANCE MOTOR 8/6 USING FUZZY LOGIC CONTROLLER" International Journal of Electrical Engineering & Technology (IJEET) Volume 6, Issue 8, Sep-Oct, 2015, pp.99-107.

Khan, Y.A., and Verma, V., (2019) 'Novel speed estimation technique for vector-controlled switched reluctance motor drive', IET Electric Power Applications, vol.13, Issue. 8, pp.1193-1203.

K.Nandhini . Analysis and experimental investigation of mechanical vibration in switched reluctance motor . International Journal of Advanced Research Methodology in Engineering & Technology, Volume 1, Issue 2, March 2017, ISBN 978-1-63535-889-6.

Podlubny, I., (1999) ' Fractional-Order Systems and PID-Controller', IEEE Transactions on Automatic Control, Vol. 44, n° 1, pp. 208-214.

Charef, A., Sun, H.H., Tsao, Y.Y., and Onaral, B., (1992) 'Fractal system as represented by singularity function', IEEE Trans. On Automatique   Control, Vol. 37, pp.1465-1470.

Bai, D. Y., Wang, Ch.Y., and Zou, J., (2015) 'Design and Simulation of Fractional Order Control Systems Based on Bode's Ideal Transfer Function', International Journal of Control and Automation, Vol.8, No.3, pp.1-8.

P.Viswanathan, M.Thathan. (2016), "Torque ripple minimization of direct torque controlled four-phases switched reluctance motor using artificial intelligent controller", World Journal of Modelling and Simulation, 12(3):163-174.

Ab Ghani, Mohd. Ruddin., Farah, Nabil., and Tamjis, M.R., (2016) 'Vector Control of Switched Reluctance Motor Using Fuzzy Logic and Artificial Neutral Network Controllers', International Conference on Electrical, Electronics, and Optimization Techniques (ICEEOT), pp. 4412-4417.

How Combinatorics Concepts Presented in Indonesian School Mathematics Textbook: A Praxeological Study

Herizal Herizal

Universitas Pendidikan Indonesia, Indonesia, , https://orcid.org/0000-0003-3360-0582

Nanang Priatna

Universitas Pendidikan Indonesia, Indonesia, https://orcid.org/0000-0003-2294-745X

Didi Suryadi

Universitas Pendidikan Indonesia, Indonesia, https://orcid.org/0000-0003-0871-8693

Ratri Isharyadi

Universitas Pendidikan Indonesia, Indonesia, https://orcid.org/0000-0002-5955-9699

Abstract: A textbook played an important role in the mathematics teaching and learning process, especially in presenting concepts to construct student knowledge. Due to the importance of the mathematics textbook, qualitative research with a phenomenology study was conducted to analyze how the concepts of combinatorics theory in senior high were presented. An Indonesian School Mathematics textbook for 12th grade was analyzed using praxeology, a part of the Anthropological Theory of Didactics (ATD), as a framework. The results showed that the combinatorics concepts introduced through several tasks contained contextual problems following the five steps of a scientific approach to learning approach. Each concept was presented starting with the task of completing examples up to the formula and its justification. Generally, the concepts were presented inductively. The tasks designed could involve students in constructing knowledge so that the learning could be meaningful for the students. For the material order, the tasks were begun with addition and multiplication rules, arrangement and selection, permutation, combination, permutation of things not all alike, and circular permutation. The order of the tasks, especially in topics of permutation does not present interrelationships among concepts and continuity of the thinking process. It is indicated that the order of the tasks can cause didactical obstacles.

Keywords: Anthropological Theory of Didactics (ATD), combinatorics, mathematics textbook, praxeology

Introduction

Combinatorics is a study about the arrangement of objects, enumeration, and calculation of objects with certain characteristics (Rosen, 2012). Harris et al. (2008) defined combinatorics as the study of arrangements: pairings and groupings, rankings and orderings, selections and allocations. Based on these two opinions, it can be interpreted that combinatorics is a study about techniques for determining the number of ways of arranging or selecting objects, with some certain requirements. In Indonesia, combinatorics formally has been taught in Senior High School. Based on the Indonesian mathematics curriculum document, the scope of combinatorics is addition rules, multiplication rules, permutations and combinations. Those topics included in counting techniques (Rosen, 2012). Studying combinatorics is very important for students. Kapur (1970) stated that the urgency of combinatorics for students was to train students to count, make estimates, generalize, and think systematically. If seen in the structure of the Indonesian curriculum, this topic is also important as a tool for solving problems on other topics in mathematics, namely the theory of probability, especially the probability of multiple events.

Even though it is important, the research showed that there were still problems for students, undergraduate students, and teachers related to the combinatorics material, such as combinatorics concepts that are difficult for students to learn and master (Melusova & Vidermanova, 2015). The results of the study also showed that there were still students' errors and difficulties in solving combinatorics problems (Lockwood et al., 2015; Meika et al., 2018; Sukoriyanto et al., 2016; Usry et al., 2016; Sulistiyorini, dkk, 2018; Annin & Lai, 2010). One of the difficulties faced by the students was that they were difficult to distinguish when to use permutations and when to use combination concepts in solving problems (Sukoriyanto et al., 2016). The same thing was acknowledged by students who the researchers had asked when teaching high school combinatorics material in the Capita Selecta School Mathematics (*Kapita Selekta Matematika Sekolah*) Course, they still had difficulty in distinguishing the use of permutations and combinations in solving combinatorics problems. Batanero (1997) found that there were several types of student errors in solving combinatorics problems, which were error in understanding the meaning of the problem, error in using the formulas, and error in operation proses. Meanwhile, Syahputra (2015) revealed that the students experienced related to combinatorics material were that they failed to understand the given combinatorics problem, they did not understand how to use the enumeration process in calculations, and they were obsessed with the fastest formula to solve problems without considering the mathematical model of the combinatorics problem. From the results of the studies that have been described, it can be seen that there are still many problems related to learning and mastering the concept of combinatorics.

Research on combinatorics that has been studied is dominated by the analysis of student errors and difficulties (Meika, dkk, 2020; Sulistiyorini, dkk, 2018; Sukoriyanto, dkk, 2016; Annin & Lai, 2010). In addition, there is also research on combinatorial thinking (Lockwood, 2013; Syahlan, 2019), experimental study of applying a learning model to improve mathematical abilities in combinatorics topic for both students and undergraduate students (Ammamiarihta, 2019; Irawandi et al., 2021; Suherman, 2017), anticipatory model and didactical

situation of combinatorics material based on indirect approach (Suryadi et al., 2010), as well as the didactical design of counting rules material (Jatmiko et al., 2021). From these studies, no research has been found showing how the quality of mathematics textbooks used by teachers and students, even though mathematics textbooks have an important role in the process of constructing students' knowledge through the process of sequencing material as well as presenting concepts and solving mathematical problems. (O'Halloran, 2017).

One of the ways to analyze textbooks is by using praxeology. Praxeology is a part of Anthropological Theory of Didactics (ATD) introduced by Chevallard. Praxeology in ATD is considered as the main object of analysis to approach "cognition", i.e. to describe examples of knowledge and know-how (Chevallard & Bosch, 2020). Praxeology consists of two interrelated components, namely praxis *(practice)* dan *logos (theory)*. This indicates that praxeology is a mixed model of several theories and practices in human daily life (Barbé et al., 2005).

Chevallard (2005) defined *Praxis* (practical block) as human activities, dan *logos* (theoretical block) refers to the human mind and reasoning. *Praxis* is formed by two subcomponents which are *type of task* (T) and *technique* (τ). *The type of task* shows the problem or situation given, while the *technique* states how to solve the problem that has been given or how to do the task from the given situation. The next component, *Logos* consists of *technology* (θ) and *theory* (Θ). *Technology* refers to the reasons for the techniques used and the *theory* used to justify or explain the technology (techniques used). Praxeology is very important to do. One of the purposes of analysis using praxeology is to see whether there are didactical problems from a task design, for example tasks contained in textbooks or learning steps planned by the teacher.

Several studies on textbook analysis using praxeology have been carried out, such as Wijayanti & Aufa (2020) studied textbook description about exponential concepts, Takeuchi & Shinno (2020) compared textbook in Japan and England on the topic of symmetry and transformations in geometry, Wijayanti & Winslow (2017) analyzed mathematical practice in the textbooks on ratio topic, Putra (2020) analyzed mathematics textbook on rational numbers topics, and Rizqi et al. (2021) analyzed mathematics textbook on set theory. From the research described above, the study of school mathematics textbooks on combinatorics had not been obtained. Starting from this and considering that students' understanding of combinatorics material still has many problems, the importance of mathematics textbooks in learning, and praxeology is an epistemic framework for analyzing textbooks, a study was conducted to study how combinatorics concepts are presented in high school mathematics textbooks in Indonesia. The objective of this research is to see whether the tasks given can facilitate students to construct an understanding of combinatorics concepts and whether the order of the material shows the interrelationships between concepts and the continuity of students' thinking processes to avoid didactical obstacle.

Method

To obtain the description about how the combinatorics concepts presented in Indonesian school mathematics

textbook, qualitative research with phenomenology study was used as the method in this study. The use of qualitative research because it is considered to provide an in-depth description of a particular program, practice, or setting (Mertens, 2010). Furthermore, the use of phenomenology because it is a design which the researcher describes the lived experiences of individuals about a phenomenon as described by participants (Giorgi, 2009; Moustakas, 1994).

In this study, the authors studied the tasks of how the combinatorics concepts presented using praxeological a part of Anthropological Theory of Didactics. Chevallard (2019) stated that praxeology means praxis and logos, to indicate that a praxeology is a model of some specific amalgam of human practice and knowledge. Concretely a praxeology is a 4-tuple (T, τ, θ, Θ) where the four letters denote different, but closely related, components of the praxeology. The interaction within these four components is in the following way: a task (T) is a problem of a given type, a technique (τ) is an action (way of performing) required to carry out the task, technologies (θ) are the explanations or argument related to the techniques, and a theory (Θ) is what explains or justifies a technology. To analyze how the combinatorics concepts presented in Indonesian school mathematics textbook, the authors just focused on practical block which were task (T) and technique (τ). Using this block, it can be concluded that whether the material presented is systemic or not. A senior high school mathematics textbook of 12th grade published by the ministry of education and culture at 2018 in chapter Probability especially in subchapter counting rules was analyzed for each component of the practical block.

Results

In Indonesia's curriculum, combinatorics theory has been taught in Senior High School level. The topic taught included counting techniques which were addition rules, multiplication rules, permutations and combinations. Refer to the details of the material, in other words it can be said that the combinatorics material taught in high school is the basic concept of combinatorics. To introduce these concepts, there are six activities presented in the book. The six activities are (1) Addition and multiplication rules, (2) Ordering and selecting, (3) Determine the permutation formula and its application, (4) Determine the combination formula and its application, (5) Determine the formula of the permutation of things not all alike and its application, and (6) Determine the circular permutation formula and its application. Using practical block praxeology, the type of task (T) for each activity and the techniques (τ) for each type of task have been identified. A description of each type of task (T) and techniques (τ) can be seen in the explanation below.

Type of Task (T)

The first analysis for practical blocks is to identify the type of task. For each activity, there are several types of tasks which are symbolized by T_1, T_2, and so on. In total, there are 15 types of tasks for all activities, as shown in the Table 1.

Table 1. Description Type of Task

Activity	Type of Task	Number of task (n)
Addition and Multiplication Rules	T_1: Taking one playing card from one type of card (e.g. Taking an Ace: List of Possible Draws)	4
	T_2: Taking one playing card from two types of cards (e.g. Taking an Ace or Queen: List of Possible Draws)	6
	T_3: Taking two cards one by one without replacement (e.g. Take one Ace card (without replacement) then one Queen card)	3
	T_4: Determining the Possible Relationship between Two Activities at T_1 (mutually exclusive or non-mutually exclusive events) and the same list of possible outcomes for two events (e.g. Relationship of Activities 1 and 2 and the same list of possible outcomes for two events)	6
	T_5: Determining the Possible Relationship between Two Activities at T_1 (mutually exclusive or non-mutually exclusive events) (e.g. Possible Relationships Activities take one Ace or Queen card and the number of ways to take)	6
	T_6: Determine the Relationship between Two Activities on T_3 (mutually exclusive or non-mutually exclusive events) (e.g. Possibility relationship of taking one Ace card activity (without replacement) then taking one Queen card and the number of ways to take)	3
Arrangement and Selecting	T_7: Arranging r cards from the available n cards (List of possible arrangements and the many ways to arrange them) (e.g. Arranging 2 Ace cards from 4 Ace cards)	4
	T_8: Taking r cards from the available n cards (The list of possibilities drawn and the number of ways to take) (e.g. Taking 3 Ace cards from 4 Ace cards)	4
Determining Permutation Formula and Its Application	T_9: Determining the factorial of some numbers (e.g. $3! + 4! = \dots$)	4
	T_{10}: Determining the number of ways of arranging a number of cards (e.g. In how many ways can 2 Ace cards be arranged from 4 Ace cards? (A-C, A-S, A-H, A-D)?)	3
	T_{11}: Determining the number of ways to distribute a number of different cards to several players with the condition that each	1

Activity	Type of Task	Number of task (n)
	player gets at most one card (e.g. Find the number of ways to distribute 3 different cards to 5 players with the condition that each player gets at most one card!)	
Determining Combination Formula and Its Application	T_{12}: Determining the number of ways to select a number of cards (e.g. In how many ways can 2 Ace cards be selected from 4 Ace cards? (A-C, A-S, A-H, A-D)?)	3
	T_{13}: Determining the number of ways to distribute a number of the same elements to a number of different places with the condition that each place is filled with at most 1 element (e.g. Determine the number of ways to distribute the same 3 elements to 5 different places with the condition that each place is filled with at most 1 element)	1
Determining Permutation of things not all alike Formula and Its Application	T_{14}: Determining the number of arrangements with the condition that there are several equal elements (e.g. In how many ways can words be arranged from words "SUSUNAN"?)	2
Determining Circular Permutation Formula and Its Application	T_{15}: Determining the number of cyclic permutations of a number of elements (e.g. Find the number of cyclic permutations of the 4 elements!)	3

From the table above it can be seen that the presentation of the concept of the counting rules starts with the addition and multiplication rules (T_1-T_6) including the identification of mutually exclusive events (T_4-T_6) which are the requirements for the multiplication rule. Next, to explain the concepts of permutations and combinations, the author of the book presents the concepts of arrangement and selection through T_7-T_8. The next activity is to determine the permutation formula and its application. However, previously the factorial concept (T_9) was also presented which will be used in the permutation formula. The discovery of the permutation formula begins with examples such as in T_{10}, how many ways can 2 Aces be arranged from 4 Aces (A-C, A-S, A-H, A-D)? In solving these examples, students are directed to the form of permutation formulas, after previously being solved manually. For example, in the example of how many ways to arrange 2 Ace cards from 4 Ace cards (A-C, A-S, A-H, A-D), the answer is 4.3 = 12. This form can be written as $\frac{4.3.2.1}{2.1} = \frac{4!}{(4-2)!}$. Starting from the example, the author of the book presents a solution in a general form, namely the arrangement of r elements from n different elements. From there, the permutation formula r of n elements is obtained, namely $\frac{n!}{(n-r)!}$. The same method is also used to find the combination formula (T_{12}-T_{13}), the formula of the permutation of things not all alike (T_{14}) and circular permutation (T_{15}).

Techniques (τ)

To identify the techniques for each type of task, the author first determines the solution for each task presented. From there, the authors make categories as a completion technique for each type of task. At least, there are four categories of techniques that are formed. To complete each task, there are one or more techniques. The four techniques formed are counting, analyzing, looking for patterns, and using formulas. Counting used to count manually each possibility of the events. Analyzing is using to identify the relationship among activities or concepts. Looking for pattern is performed when students asked to look at the pattern formed from the examples or specific activities. The last, using a formula is a technique when solving the problems mechanically, that is, directly using the formula. The distribution of techniques for each task as well as a description of each technique can be seen in the Table 2.

Table 2. Description of Techniques for each type of task

Task	Technique	Description of Technique
T_1	τ_1: Counting	Counting one by one for various possibilities
T_2	τ_1: Counting	Counting one by one for various possibilities
T_3	τ_1: Counting	Counting one by one for various possibilities
T_4	τ_2: Analyzing	Analyzing the relationship among activities
T_5	τ_2: Analyzing	Analyzing the relationship among activities
	τ_3: Looking for pattern	Looking at the pattern to determine how many ways
T_6	τ_2: Analyzing	Analyzing the relationship among activities
	τ_3: Looking for pattern	Looking at the pattern to determine how many ways
T_7	τ_1: Counting	Counting one by one for the various possible results of the arrangement
T_8	τ_1: Counting	Counting one by one for the various possible results of the selecting
T_9	τ_4: Using Formula	Using Factorial definition
T_{10}	τ_2: Analyzing	Analyzing the relationship of the problems with the multiplication rules
	τ_3: Looking for pattern	Looking at the pattern to determine how many ways
T_{11}	τ_2: Analyzing	Analyzing the relationship of the problems with the multiplication rules
	τ_3: Looking for pattern	Looking at the pattern to determine how many ways
T_{12}	τ_1: Counting	Counting one by one for various possibilities
	τ_2: Analyzing	Analyzing the relationship of the problems with the permutation concept and definition of combination
	τ_3: Looking for pattern	Looking at patterns to determine the number of ways of counting results

Task	Technique	Description of Technique
T_{13}	τ_2: Analyzing	Analyzing the relationship of the problems with the permutation concept and definition of combination
	τ_3: Looking for pattern	Looking at the pattern to determine how many ways
T_{14}	τ_2: Analyzing	Analyzing the relationship of the problems with the combination concepts
	τ_3: Looking for pattern	Looking at the pattern to determine how many ways
T_{15}	τ_1: Counting	Counting one by one for various possibilities
	τ_2: Analyzing	Analyzing the arrangement formed
	τ_3: Looking for pattern	Looking at patterns to determine the number of ways of counting results

From the four categories of techniques that have been grouped as shown in table 2 above, the most used technique is analyzing (n=9), followed by counting (n=7), looking for patterns (n=7), and using formulas (n=1). Analyzing is used in several conditions such as analyzing whether two events are mutually exclusive and analyzing the relationship of the problem given to the concept or rule that has been studied as in T10, the analysis is carried out to see the relationship between the problem of arrangement and the multiplication rule. Whereas counting is used as a first step to solve problems, such as in T10 determining the number of ways to arrange 2 Ace cards out of 4 Ace cards (A-C, A-S, A-H, A-D), the presentation of answers in the book was begun by enumerating the various possible arrangements that can be formed, then the looking for pattern technique is used to see the pattern of problem solving that exists in the example with the final form of the intended formula. From these patterns, the final formula for permutations or combinations and other formulas in general cases is derived. As for the technique of using the formula, namely the use of the formula directly only in factorial problems, as in T9, the task given is to determine the value of 3! +4!. To solve this problem, of course, the easiest way for the students is by using the formula or the definition of n! directly then replacing n=3 and n=4.

Discussion

In the previous section, it has been explained that the presentation of high school combinatorics concepts in Indonesian mathematics textbooks starts with addition rules and multiplication rules. (T_1-T_6), ordering and selecting (T_7-T_8), permutation (T_9-T_{11}), combination (T_{12}-T_{13}), permutation of things not all alike (T_{14}), and circular permutation (T_{15}). Seen from the way of presented, the concepts are introduced through tasks with specific examples which eventually lead to general concepts. Presentation of material like explained above followed learning with an inductive approach, namely presenting examples, observing, generalizing, and verifying (Atta et al., 2015; Singh & Yadaf, 2017). The activities can increase students' participation in the learning process. In addition, the existence of a task that directs students to be able at the level of obtaining a formula is an important step. This is part of constructing an epistemic knowledge. In the process of constructing

mathematical proofs, for example proofs for formulas, the concept of permutations and combinations will be clearly seen, so that students' understanding will also be formed there. This is in line with Hersh (1993) stated that one of the functions of mathematical proof is to help students understand mathematical concepts.

In terms of the order of presentation of the material, seen from the order of the type of task, there is a jump. The concepts of permutation begin with permutation of r objects of n distinct objects. As for the concept of permutation of n distinct objects, it explained just for certain condition when the number of r equals to number of n (n=r). If referring to Cohen (1978), the concept of permutation that was first introduced was a general permutation, namely the permutation of n distinct elements. Then proceed with more specific permutations, namely permutations of r elements from n different elements. The unsystematic sequence was also shown in circular permutation (T_{15}). The concept was introduced after combination (T_{12}-T_{13}) whereas the formula of circular permutation constructed using the concept of permutation of n distinct objects (T_9-T_{11}). In combinatorics books that are referred to as scholarly knowledge, they also place circular permutations after the explanation of linear permutations and before combination material. (Cohen, 1978; Rosen, 2012). The order of material as described above do not present interrelationship among concepts and continuity of thinking process. It can impact on students learning process and also caused didactical obstacle (Suryadi, 2019). Didactical obstacle, a kind of learning obstacles, defined as learning obstacle caused by sequence factors and stages of presentation of a material (Brousseau, 1997; Suryadi, 2019).

Conclusion

A textbook played an important role in the mathematics teaching and learning process, especially in both presenting concepts and constructing student knowledge. In the Indonesian textbook, the combinatorics concepts introduced through several tasks contained contextual problems and followed five steps of a scientific approach type of learning approach. Each concept was presented starting with the task of completing examples up to the formula and its justification. Generally, the concepts were presented inductively. The tasks designed can involve students in constructing knowledge so that the learning can be meaningful for them. For the material order, the tasks were begun with both addition and multiplication rules, arrangement and selection, permutation, combination, permutation of things not all alike, and circular permutation. The order of the tasks, especially in topics of permutation does not present interrelationships among concepts and continuity of the thinking process. It is indicated that the order of tasks can cause didactical obstacles.

Recommendations

Future research is needed to check the knowledge by the students as an effect of using the mathematics textbooks. It will get a comprehensive situation of the topics and their problems so that, at the end, an alternative learning design can be proposed to overcome the problems found.

Acknowledgements

References

Ammamiarihta, A. (2019). Upaya Meningkatkan Kemampuan Pemecahan Masalah Kombinatorik Siswa Dengan Menerapkan Model Pembelajaran Problem Based Learning Di Kelas Xi Sma Istiqlal Delitua. *AXIOM : Jurnal Pendidikan Dan Matematika*, *8*(1). https://doi.org/10.30821/axiom.v8i1.544

Atta, M. A., Ayaz, M., & Nawaz, Q. (2015). Comparative Study of Inductive & Deductive Methods of Teaching Mathematics at Elementary Level. *Gomal University Journal of Research (GUJR)*, *31*(1), 20–28.

Barbé, J., Bosch, M., Espinoza, L., & Gascón, J. (2005). Didactic restrictions on the teacher's practice: The case of limits of functions in Spanish high schools. In C. Laborde, M.-J. Perin-Glorian, & A. Sierpinska (Eds.), *Beyond the Apparent Banality of the Mathematics Classroom* (Vol. 59, pp. 235–268). Springer New York, NY. https://doi.org/10.1007/s10649-005-5889-z

Batanero, C. (1997). Combinatorial Reasoning and its Assessment. In I. Gal & J. B. Garfield (Eds.), *The Assessment Challenge in Statistics Education* (pp. 239–252). IOS Press.

Brousseau, G. (1997). *Theory of Didactical Situations in Mathematics*. Kluwer Academic Publishers.

Chevallard, Y. (2019). Introducing the Anthropological Theory of the Didactic: an Attempt At a Principled Approach. *Hiroshima Journal of Mathematics Education*, *12*, 71–114.

Chevallard, Y. (2005). Steps towards a new epistemology in mathematics education. In M. Bosch (Ed.), *Proceedings of the Fourth Congress of the European Society for Research in Mathematics Education* (pp. 21–44). FUNDEMI IQS – Universitat Ramon Llull.

Chevallard, Y., & Bosch, M. (2020). Didactic Transposition in Mathematics Education. In S. Lerman (Ed.), *Encyclopedia of Mathematics Education* (pp. 214–218). Springer. https://doi.org/10.4324/9780203825495

Cohen, D. I. . (1978). *Basic Techniques of Combinatorial Theory*. John Wiley & Sons Inc.

Giorgi, A. (2009). *The descriptive phenomenological method in psychology: A modified Husserlian approach*. Duquesne University Press.

Harris, J. M., Hirst, J. L., & Mossinghoff, M. J. (2008). *Combinatory and Graph Theory*. Springer.

Hersh, R. (1993). Proving Is Convincing and Explaining. *Educational Studies in Mathematics*, *24*(4), 389–399.

Irawandi, S. H., Syahputra, E., & Salayan, M. (2021). Pengaruh Model Pembelajaran Berbasis Masalah Terhadap Kemampuan Kombinatorik dan engaruh Model Pembelajaran Berbasis Masalah Terhadap Kemampuan Kombinatorik dan Disposisi Matematis Siswa. *Jurnal MathEducation Nusantara*, *4*(1), 52–59.

Jatmiko, M. A., Herman, T., & Dahlan, J. A. (2021). Desain Didaktis Materi Kaidah Pencacahan Untuk Siswa SMA Kelas XI. *Hipotenusa Journal of Research Mathematics Education (HJRME)*, *4*(1), 35–54. https://doi.org/10.36269/hjrme.v4i1.464

Kapur, J. N. (1970). Combinatorial analysis and school mathematics. *Educational Studies in Mathematics*, *3*(1), 111–127. https://doi.org/10.1007/BF00381598

Lockwood, E. (2013). A model of students' combinatorial thinking. *Journal of Mathematical Behavior*, *32*(2), 251–265. https://doi.org/10.1016/j.jmathb.2013.02.008

Lockwood, E., A. Swinyard, C., & S. Caughman, J. (2015). Patterns, Sets of Outcomes, and Combinatorial Justification: Two Students' Reinvention of Counting Formulas. In *International Journal of Research in Undergraduate Mathematics Education* (Vol. 1, Issue 1). https://doi.org/10.1007/s40753-015-0001-2

Meika, I., Suryadi, D., & Darhim, D. (2018). Students' errors in solving combinatorics problems observed from the characteristics of RME modeling. *Journal of Physics: Conference Series*, *948*(1). https://doi.org/10.1088/1742-6596/948/1/012060

Melusova, J., & Vidermanova, K. (2015). Upper-secondary Students' Strategies for Solving Combinatorial Problems. *Procedia - Social and Behavioral Sciences*, *197*(February), 1703–1709. https://doi.org/10.1016/j.sbspro.2015.07.223

Mertens, D. M. (2010). *Research and Evaluation in Education and Psychology*. SAGE Publications, Inc.

Moustakas, C. (1994). *Phenomenological research methods*. Sage.

Niven, I. (1965). Mathematics of Choice or How to Count without Counting. In *Biometrics* (Issue 1). Mathematical Association of America. https://doi.org/10.2307/2528475

O'Halloran, K. (2017). A multimodal approach for theorizing and analyzing mathematics textbooks. In G. Schubring, L. Fan, & V. Geraldo (Eds.), *Proceedings of the Second International Conference on Mathematics Textbook Research and Development* (pp. 25–48). Universidade Federal do Rio de Janeiro: Instituto de Matemática.

Putra, Z. H. (2020). Didactic transposition of rational numbers: A case from a textbook analysis and prospective elementary teachers' mathematical and didactic knowledge. *Journal of Elementary Education*, *13*(4), 365–394. https://doi.org/10.18690/rei.13.4.365-394.2020

Rizqi, M. M., Wijayanti, D., & Basir, M. A. (2021). Analisis Buku Teks Matematika Materi Himpunan Menggunakan Model Prakseologi. *Delta: Jurnal Ilmiah Pendidikan Matematika*, *9*(1), 57. https://doi.org/10.31941/delta.v9i1.1226

Rosen, K. H. (2012). *Discrete Mathematics and its Applications 7th edition*. Mc. Graw Hill, Inc.

Singh, N. K., & Yadaf, A. K. (2017). Inductive and Deductive Methods in Mathematics Teaching. *International Journal of Engineering Research and Application*, *7*(11), 19–22. https://doi.org/10.9790/9622-0711021922

Suherman. (2017). Pengaruh Penerapan Strategi Pembelajaran Contextual Theacing and Learning Terhadap Hasil Belajar Mahasiswa Pada Materi Kombinatorik di Semester 1 Jurusan Teknologi Informasi Dan Compter Politeknik Negeri Lhokseumawe. *Jurnal Pendidikan Almuslim*, *5*(1), 1–7.

Sukoriyanto, S., Nusantara, T., Subanji, S., & Chandra, T. D. (2016). Students' Errors in Solving the Permutation and Combination Problems Based on Problem Solving Steps of Polya. *International*

Education Studies, *9*(2), 11. https://doi.org/10.5539/ies.v9n2p11

Sulistyorini, Y., Argarini, D. F., & Yazidah, N. I. (2018). Analisis Kesalahan dalam Memecahkan Masalah Kombinatorika Ditinjau dari Gaya Kognitif. *AKSIOMA: Jurnal Program Studi Pendidikan Matematika*, *7*(1), 114. https://doi.org/10.24127/ajpm.v7i1.1360

Suryadi, D. (2019). *Philosophical Foundation of Didactical Design Research (DDR)*. Gapura Press.

Suryadi, D., Yulianti, K., & Junaeti, E. (2010). Model Antisipasi Dan Situasi Didaktis Dalam Pembelajaran Matematika Kombinatorik Berbasis Pendekatan Tidak Langsung. *Procedia - Social and Behavioral Sciences*, *12*(1), 665–670.

Syahlan, D. O. (2019). Kontribusi Kemampuan Berpikir Kombinatorik Dalam Pembelajaran Statistika Matematika. *δELTΔ Jurnal Ilmiah Pendidikan Matematika*, *9*(2), 201–210.

Takeuchi, H., & Shinno, Y. (2020). Comparing the Lower Secondary Textbooks of Japan and England: a Praxeological Analysis of Symmetry and Transformations in Geometry. *International Journal of Science and Mathematics Education*, *18*(4), 791–810. https://doi.org/10.1007/s10763-019-09982-3

Usry, R., Rosli, R., & Mistima Maat, S. (2016). An Error Analysis of Matriculation Students' Permutations and Combinations. *Indian Journal of Science and Technology*, *9*(4). https://doi.org/10.17485/ijst/2016/v9i4/81793

Wijayanti, D., & Aufa, D. N. (2020). *Picturing Textbook on Exponent Equations Based on Praxeology Organization*. *409*(SoRes 2019), 494–498. https://doi.org/10.2991/assehr.k.200225.107

Wijayanti, D., & Winslow, C. (2017). Mathematical practice in textbooks analysis: Praxeological reference models, the case of proportion. *Journal of Research in Mathematics Education*, *6*(3), 307–330. https://doi.org/10.17583/redimat.2017.2078

System of Linear Equations in Two Variables: A Praxeological Analysis of Indonesian Textbooks

Marhami Marhami

Universitas Pendidikan Indonesia, Indonesia, ⓘD https://orcid.org/ 0000-0002-0241-2944

Didi Suryadi

Universitas Pendidikan Indonesia, Indonesia, ⓘD https://orcid.org/ 0000-0003-0871-8693

Dadan Dasari

Universitas Pendidikan Indonesia, Indonesia, ⓘD https://orcid.org/ 0000-0003-2600-2170

Abstract: This research aims to analyze the characteristics of Indonesian mathematics textbooks used in the Merdeka Curriculum for Grade IX Junior High School, with a focus on praxeological analysis of the material on System of Linear Equations in Two Variables (SLETV). The research method employs a four-component praxeological approach are task types, techniques, technologies, and theories. The analysis results reveal the existence of 11 task types of SLETV and 5 techniques, namely perceptual, memorial, operational, logical, and analytical, which applied in solving SLETV tasks in the mathematics textbooks. Additionally, there are 11 technologies supporting the selection of techniques and 4 theories serving as the basis for justifying the use of these technologies. Furthermore, the analysis concludes that the mathematics textbooks contain some sections that may create epistemological and ontogenetic obstacles. All findings from this analysis are expected to be utilized for the development and improvement the quality of Indonesian mathematics textbooks.

Keywords: System of linear equations, Praxeological analysis, Indonesian textbooks

Introduction

The System of Linear Equations with Two Variables (SLETV) is one of the mandatory topics taught in Junior High School. This is in accordance with Regulation of the Minister of Education and Culture Number 22 of 2016, where one of the competency standards for junior high school students is to understand SLETV and apply it in problem-solving. The SLETV material is crucial as it directly relates to real-life situations (Wu, 2016). SLETV is a system or combination of several linear equations with two similar variables. At the secondary

school level, SLETV problems can be solved using four methods: graphical, substitution, elimination, and combination methods.

SLETV often confuses students because it is the first time they encounter the manipulation of two equations to solve two variables (Cai et al., 2010). The SLETV material poses a relatively high level of difficulty, leading to many students struggling with problem-solving (Kolo et al., 2021). Several studies address the difficulties students face in SLETV, such as the research by Rifadena & Hidayanto (2021), which found that students lack understanding of the problem's intent, making it challenging to represent information symbolically and visually. This is attributed to students struggling to build knowledge on how to comprehend and solve problems (Amelia et al., 2018; Nuraeniah et al., 2022; Putri & Manoy, 2013). Numerous factors contribute to this, including the use of mathematics textbooks as a learning source (Chinn, 2020).

Textbooks play an integral role in the teaching and learning process (Hendriyanto et al., 2023; Purnomo et al., 2019; Weinberg & Wiesner, 2011). As one of the primary learning resources, textbooks are not merely complementary to the role of teachers (Piper et al., 2018). Valverde et al. (2002) elaborate on the substantial influence textbooks exert on how teachers elucidate mathematical concepts and employ their understanding of learning paths within the classroom. (Remillard et al., 2018) said that the introduction of curriculum content can be conveyed to both teachers and students also through textbooks, serving as a guide to lead students toward learning objectives. The role of textbooks in education can be elucidated through three essential aspects: providing guidance in determining the topics to be taught, assisting teachers in organizing materials in a structured manner, and offering ideas related to teaching activities for educators (Erbaş et al., 2012).

In teaching mathematical concepts, the use of effective and relevant teaching materials is crucial (Fan, 2013). Previous research indicates that the quality of mathematics textbook significantly influences students' understanding (Azzumar et al., 2023; Sievert et al., 2019). However, there is limited research specifically analyzing textbook in SLETV teaching materials using a praxeological approach. Therefore, this study aims to fill this gap by analyzing existing SLETV teaching materials using a praxeological approach.

In the field of education, praxeology has been widely used in both research and the learning process. In research, praxeology is employed to analyze textbooks. According to Chevallard (2019), no human action is taken without underlying thought. An ideal human action fulfills four elements, known as components in praxeology, presented in two blocks/types: the practical block (praxis) consisting of the type of task and techniques, and the theoretical block (logos) consisting of technology (argumentation/justification for why a technique is used) and theory underlying the justification of technology.

According to Yunianta et al. (2023), the praxeological approach can serve as a useful theoretical framework for analyzing teaching materials. The praxeological approach involves understanding the practices that occur in the classroom and the learning context. Mathematical Praxeology pertains to how mathematics is presented in student textbooks or teacher manuals (Takeuchi & Shinno, 2020).
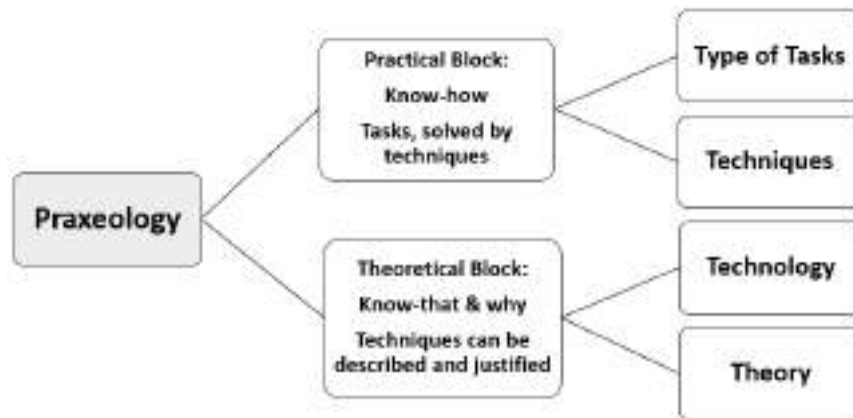
Figure 1. Praxeological Approach (Chevallard, 1998)

By employing the praxeological approach, the author can analyze how the teaching materials used facilitate students' understanding of the SLETV concept and how students interact with these teaching materials. In this study, the teaching materials to be analyzed are the student textbook and teacher's guidebook for Grade IX Junior High School, which follow the Merdeka curriculum and were published by the Ministry of Education, Culture, Research, and Technology (Kristanto et al., 2022). This is intended to analyze the content of the teaching materials and how they overall facilitate students' understanding of the SLETV concept, such as the assignment of tasks, activities, or other elements in the student book, while alternative discussions are provided in the teacher's guide. The results of this research are expected to provide insights for mathematics teachers in schools.

Method

The research method employed is qualitative research with content analysis. Content analysis of the textbook involves examining the content and activities presented within its pages. According to Zuchdi & Wiwiek (2021), content analysis always involves relating or comparing findings to various criteria or theories. The theory used for the textbook analysis process is the praxeological theory.

The research process for analyzing the SLETV material in textbooks using the praxeological theory involves several steps, which are modified from Azzumar et al. (2023): (1) Selection of the textbook sample, where the researcher chooses a mathematics textbook for Grade IX junior high school students (Kristanto et al., 2022) following the Merdeka curriculum, published by the Ministry of Education, Culture, Research, and Technology in 2022, with the material limitation being SLETV; (2) Praxeological analysis, where the researcher identifies and analyzes how the SLETV material in the textbook applies praxeological principles in presenting the content and activities; (3) Content analysis, where the researcher thoroughly reads the textbook content, noting relevant information about task types and concept representations; and (4) Alternative recommendations, based on the analysis results, the researcher attempts to provide recommendations for improving the textbook to support SLETV learning with a praxeological theory approach.

The initial step taken in the praxeological analysis involves documenting the types of tasks (T) from the given example problems. Subsequently, techniques (τ) are identified through the provided examples to solve the problems in the book. The technique (τ) used to solve the task types (T) in the book becomes the technique (τ) most likely used by students in completing the given practice problems. There is a basis or reason for choosing the technique (τ), referred to as Technology (θ). This Technology (θ) is used to justify the existence of the Technique (τ). Then, from this Technology (θ), there is a reference or basis for why that reason is taken, known as Theory (Θ).

Results

Practical Block: Task Types and Techniques

All task types listed in the mathematics textbook on SLETV are included in this analysis. The task types are represented by questions (problems) posed from the introductory part of the book to the exercise problems at the end of the material. The objective of analyzing all the task types is to examine how tasks are presented in the classroom, allowing the identification of any didactic obstacles within them. The selected textbook is the one used by students in accordance with the Merdeka curriculum. This choice is made with the aim of discovering didactic situations in the mathematics textbook.

Task types are denoted by the symbol T. Labeling and coding of task types are based on the data results in Table 1. All task types labeled with T are ordered based on their first appearance in the textbook. The book contains several questions described as tasks that students need to complete. The number of task types found is eleven, labeled T1 to T11, with a total of 58 task types, as shown in Table 1. Task types T1 and T10 are the most frequently encountered in the textbook and are also part of the main topics covered in the SLETV material. Task T1 is a fundamental concept highly emphasized for students to understand as the basis for learning SLETV. Similarly, task T10 involves the application of SLETV in everyday life, making it the most dominant task so that students are expected not only to comprehend the theory of SLETV but also to apply it to everyday life problems.

Table 1. Types and number of task in SLETV

Tipe Task	Number of Tasks
T_1 : Understanding the concept and modeling LETV from given cases.	7 (12.1%)
T_2 : Determining the solution of a LETV.	5 (8.6%)
T_3 : Understanding the concept of SLETV.	3 (5.2%)
T_4 : Modeling SLETV from given cases.	2 (3.4%)
T_5 : Solving SLETV using the graphical method.	4 (6.9%)
T_6 : Determining the type of SLETV solution using the slope of the line.	6 (10.3%)
T_7 : Solving SLETV using the substitution method	5 (8.6%)
T_8 : Solving SLETV using the elimination method.	4 (6.9%)
T_9 : Solving SLETV using the combination method.	5 (8.6%)

T_{10} : Modeling and solving real-life cases of SLETV from everyday problems.	11 (19%)
T_{11} : Modeling and solving SLETV cases that are connected with other mathematical topics.	6 (10.3%)
Total	58 (100%)

Each type of task is defined at various levels. Each type of task is categorized into 3 levels, namely level 1 for understanding concepts, level 2 for applying concepts, and level 3 for reasoning. The results are as follows.

Table 2. Textbook Task Levels

Tasks	Level of Tasks		
	Level 1	Level 2	Level 3
T_1	3 (42.9%)	4 (57.1%)	0 (0%)
T_2	4 (80%)	1 (20%)	0 (0%)
T_3	1 (33.3%)	1 (33.3%)	1 (33.3%)
T_4	2 (100%)	0 (0%)	0 (0%)
T_5	1 (25%)	2 (50%))	1 (25%)
T_6	2 (33.3%)	3 (50%)	1 (16.7%)
T_7	0 (0%)	4 (80%)	1 (20%)
T_8	1 (25%)	3 (75%)	0 (0%)
T_9	0 (0%)	5 (100%)	0 (0%)
T_{10}	0 (0%)	10 (90.9%)	1 (9.1%)
T_{11}	0 (0%)	5 (83.3%)	1 (16.7%)
Total	14 (24.2%)	38 (65.5%)	6 (10.3%)

In Table 2, the tasks most frequently given in the textbook are at level 2 (application of concepts), totaling 39 out of 58 questions. Additionally, there are 25.9% of questions related to understanding concepts. These questions are typically found at the beginning of the learning process before students engage in application or calculations. Questions at level 3, requiring high-level skills such as reasoning, are relatively few at 6.9%. This is somewhat concerning as students may be less accustomed to Higher Order Thinking Skills (HOTS) questions. Each type of task requires the appropriate technique as a solution, especially in algebraic material. Takeuchi & Shinno (2020) selected four techniques in problem-solving: perceptual, operational, algebraic, and physical. Solis & Isoda (2023) mentioned seven techniques used for solving tasks related to the topic of length measurement in textbook analysis using praxeological analysis, namely: physical, transitive, iterative, partitioning, operational, instrumental, and conservation.

Table 3. Techniques for Each Task

Tugas	Teknik	Deskripsi Teknik
T_1	$\tau 1$: Perceptual	$\tau 1$: Utilizing visual skills to identify information from images or given

	$\tau 2$: Memorial	problems.
		$\tau\mathbf{2}$: Utilizing memory skills to remember concepts and model of SLETV
T_2	$\tau 3$: Operasional	$\tau\mathbf{3}$: Using addition, subtraction, multiplication, and division operations or employing calculation algorithms.
T_3	$\tau 1$: Perceptual $\tau 2$: Memorial $\tau 3$: Operasional	$\tau\mathbf{1}$: Utilizing visual skills to identify information from images or given problems. $\tau\mathbf{2}$: Utilizing memory skills to remember concepts and model of SLETV $\tau\mathbf{3}$: Using addition, subtraction, multiplication, and division operations or employing calculation algorithms.
T_4	$\tau 1$: Perceptual $\tau 2$: Memorial	$\tau\mathbf{1}$: Utilizing visual skills to identify information from images or given problems. $\tau\mathbf{2}$: Utilizing memory skills to remember concepts and model of SLETV
T_5	$\tau 2$: Memorial $\tau 3$: Operasional $\tau 4$: Logical	$\tau\mathbf{2}$: Utilizing memory skills to remember concepts and model of SLETV $\tau\mathbf{3}$: Using addition, subtraction, multiplication, and division operations or employing calculation algorithms. $\tau\mathbf{4}$: Applying logical reasoning to connect solutions with the provided information.
T_6	$\tau 1$: Perceptual $\tau 2$: Memorial $\tau 3$: Operasional $\tau 4$: Logical $\tau 5$: Analytical	$\tau\mathbf{1}$: Utilizing visual skills to identify information from images or given problems. $\tau\mathbf{2}$: Utilizing memory skills to remember concepts and model of SLETV $\tau\mathbf{3}$: Using addition, subtraction, multiplication, and division operations or employing calculation algorithms. $\tau\mathbf{4}$: Applying logical reasoning to connect solutions with the provided information. $\tau\mathbf{5}$: Utilizing analytical skills to examine or break down a problem in detail with logical steps.
T_7	$\tau 2$: Memorial $\tau 3$: Operasional $\tau 4$: Logical	$\tau\mathbf{2}$: Utilizing memory skills to remember concepts and model of SLETV $\tau\mathbf{3}$: Using addition, subtraction, multiplication, and division operations or employing calculation algorithms. $\tau\mathbf{4}$: Applying logical reasoning to connect solutions with the provided information.
T_8	$\tau 2$: Memorial $\tau 3$: Operasional $\tau 4$: Logical	$\tau\mathbf{2}$: Utilizing memory skills to remember concepts and model of SLETV $\tau\mathbf{3}$: Using addition, subtraction, multiplication, and division operations or employing calculation algorithms. $\tau\mathbf{4}$: Applying logical reasoning to connect solutions with the provided information.
T_9	$\tau 3$: Operasional $\tau 4$: Logical	$\tau\mathbf{3}$: Using addition, subtraction, multiplication, and division operations or employing calculation algorithms.

		$\tau4$: Applying logical reasoning to connect solutions with the provided information.
T$_{10}$	$\tau2$: Memorial	$\tau2$: Utilizing memory skills to remember concepts and model of SLETV
	$\tau3$: Operasional	$\tau3$: Using addition, subtraction, multiplication, and division operations or employing calculation algorithms.
	$\tau4$: Logical	$\tau4$: Applying logical reasoning to connect solutions with the provided information.
	$\tau5$: Analytical	$\tau5$: Utilizing analytical skills to examine or break down a problem in detail with logical steps.
T$_{11}$	$\tau2$: Memorial	$\tau2$: Utilizing memory skills to remember concepts and model of SLETV
	$\tau3$: Operasional	$\tau3$: Using addition, subtraction, multiplication, and division operations or employing calculation algorithms.
	$\tau4$: Logical	$\tau4$: Applying logical reasoning to connect solutions with the provided information.
	$\tau5$: Analytical	$\tau5$: Utilizing analytical skills to examine or break down a problem in detail with logical steps.

The identification results are the outcome of categorization, some of which are adopted from existing references while choosing other techniques deemed suitable for solving tasks. When tasks can be solved using the senses, particularly visual ability to identify information from images or given problems, then perceptual technique is employed. Memory technique is used to recall stored memories in the mind, such as remembering concepts and modeling systems of linear equations with two variables.

The operational technique here refers to the use of arithmetic operations in solving problems operationally. Logical technique involves logically reasoning through the type of requested task. Analytical technique is used when the question type requires connecting at least two systematic and interconnected concepts. Thus, the techniques used to solve tasks related to SLETV include perceptual, memorial, operational, logical, and analytical as indicated by the information in Table 3.

Theoretical Block: Technology and Theory

Technology refers to the justification behind the selection of techniques for each type of task, while theory refers to the foundation or basis of these technologies. The technologies and theories used for each task are presented in Table 4.

Table 4. Praxeological Analysis Results

Task (T)	Technique (τ)	Technology (θ)	Theory (Θ)
T$_1$	$\tau1$, $\tau2$	θ_1 : Problems with two variables can be modeled into a system of two-variable	Θ_1 : General form of LETV is ax + by = c with a, b ≠ 0, and x, y

		linear equations	being variables.
T$_2$	τ3	θ_2 : The solution of LETV is obtained by finding replacements for variables x and y that make the SLETV true	Θ_2 : The solution set of LETV is the set of all ordered pairs (x,y) that satisfy the LETV.
T$_3$	τ1, τ2, τ3	θ_3 : Two LETV form a system of two-variable linear equations	Θ_3 : General form of a system of two-variable linear equations ax + by = c and px + qy = r with x and y as variables.
T$_4$	τ1, τ2	θ_4 : Problems are expressed in the form of two sets of two-variable linear equations	
T$_5$	τ2, τ3, τ4	θ_5 : Application of the graphical method to find solutions for SLETV	
T$_6$	τ1, τ2, τ3, τ4, τ5	θ_6 : Application of the graphical method and the concept of gradient, categorizing types of SLETV solutions into having exactly one solution, no solution, or infinitely many solutions	
T$_7$	τ2, τ3, τ4	θ_7 : Application of the substitution method to find solutions for SLETV	Θ_4 : Solution of SLETV using graphical method, substitution method, elimination method, or combination method.
T$_8$	τ2, τ3, τ4	θ_8 : Application of the elimination method to find solutions for SLETV	
T$_9$	τ3, τ4	θ_9 : Application of the combination method to find solutions for SLETV	
T$_{10}$	τ2, τ3, τ4, τ5	θ_{10} : Application of SLETV solution methods in contextual problems	
T$_{11}$	τ2, τ3, τ4, τ5	θ_{11} : Connection of concepts/formulas from other mathematical topics in solving SLETV.	

From the Table 4 above, the relationship between tasks, techniques, technology, and justified theories from the analyzed textbook can be observed. There are 11 task classifications, where each task has several techniques (τ) used in its completion. Additionally, each task (T) has one technology (θ) as justification for the chosen technique (τ), and there are 4 theories (Θ) that also serve as the basis for justifying these 11 technologies.

For example, to complete task T7 (solving SLETV graphically), three techniques are needed: technique τ2 by recalling concepts and modeling SLETV, then using technique τ3 by performing arithmetic operations (such as addition, subtraction, multiplication, or division) to determine the solution of SLETV, and finally, with technique τ4 using logical reasoning to connect the solution with information from the given SLETV case. Furthermore, the technology here justifies the chosen technique, which is θ5, and the justification for the chosen technology is Θ2. Based on this explanation, it is clear that through praxeology, the proof is epistemic.

Discussion

Praxeological analysis can be used to question how mathematics is taught in textbooks and how mathematics solves didactic problems (Bosch et al., 2017). Selection of level of order, level of tasks, or learning design can be one of the causes of didactic constraints discussed here.
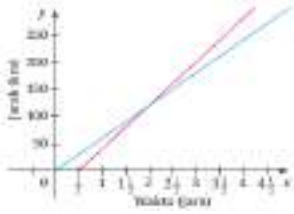

Through this exploration activity, you are invited to discover the concept of a system of linear equations in two variables. Consider the following problem. At 08:00, Putri begins her journey from Yogyakarta to Semarang at a speed of 60 km/h. Half an hour after Putri departs, Akbar sets off from the same location. Akbar travels at a speed of 80 km/h, following the same route and direction as Putri.

2. The case of Putri and Akbar is presented in figure below

c. Determine the intersection point of the two lines, then explain the meaning of the intersection point of two lines !

Figure 2. Initial tasks in understanding the concept of SLETV

Figure 2 represents the first task presented in the student handbook provided to guide students in understanding the concept of SLETV (T3). The task type T3 in this section uses solution techniques $\tau 1$, $\tau 2$, and $\tau 3$. The technology used is $\theta 3$, and the theory employed is $\Theta 3$. Didactic obstacles shown in Figure 4 are present in question 2c, where students are required to determine the intersection point of two lines. However, the concept of the intersection point of two lines is studied in the subsequent material, namely in solving SLETV graphically, making this task at 2c at level 2 (application of concepts in solving) and challenging for students.

In contrast, if this task is modified by providing instructions for the value of the intersection point of the two lines, this can be done by providing dashed lines or other methods so that students are not focused on finding the solution point by applying the concept (using techniques $\tau 2$ and $\tau 3$) but can be obtained only by using technique $\tau 1$. Thus, students can focus on understanding and finding the concept of SLETV as expected in the curriculum. Designating this task as a problem at the beginning of the material concept can result in ontogenetic obstacles that affect students' readiness to learn (Prabowo et al., 2022). According to Lutfi et al. (2021), students may become bored and disinterested due to the challenging sequence of material and tasks at the beginning, which can make them face difficulties These obstacles can reduce students' motivation and interest in learning (Suryadi, 2019).

Another obstacle can be seen in Figure 3, which is the task given in the student handbook. This task falls under

type T10, which involves modeling and solving cases of SLETV from everyday problems. The techniques used are techniques $\tau2$, $\tau3$, $\tau4$, $\tau5$ justified by technology $\theta10$ and its theory in $\Theta4$.

> Ampong is the older sibling of Mores. They go to the same school. Ampong leaves for school at 06:30 with a speed of 40 km/h. Mores departs 15 minutes after Ampong, taking the same route. What speed should Mores maintain to catch up with Ampong within 45 minutes?

Figure 3. Task of solving problems SLETV in textbook

The obstacle findings are depicted in Figure 4, which is the discussion of the answers to the task in Figure 3 as stated in the teacher's handbook.

> Let x represent time (in hours), y represent the distance traveled (in kilometers), and m represent the speed of Tata going to school. The system of linear equations is obtained as follows:
>
> $$\begin{cases} y = 40x \\ y = m\left(x - \frac{1}{4}\right) \end{cases}$$ Equation I
>
> Equation II
>
> Mores can catch up with Ampong in 45 minutes or $\frac{3}{4}$ hours, so it can be obtained $x = \frac{3}{4}$
>
> Substitute $x = \frac{3}{4}$ into Equation I:
>
> $$y = 40x$$
> $$y = 40\left(\frac{3}{4}\right)$$
> $$y = 30$$

Figure 4. The solution to SLETV in teacher's guidebook

There is an error in the discussion of the problem written in the teacher's guidebook. The first mistake lies in the name 'Tata' which suddenly appears, but this name is not mentioned in the problem. The next critical mistake is substituting the value $\frac{3}{4}$ into equation I. The value $\frac{3}{4}$ represents the time Mores can catch up with Ampong, so the correct substitution should be in equation II, so $x - \frac{1}{4} = \frac{3}{4}$, resulting in $x = 1$. This value is then substituted into equation I, obtaining $y = 40$. Substituting these values into equation II gives $m = 53.33$. So, Mores can catch up with Ampong in 45 minutes if traveling at a speed of 53.33 km/h.

These errors in the answer can lead to misconceptions for both students and even teachers, becoming an epistemological obstacle that hinders their ability to understand mathematical problems, concepts, and modeling (Yunianta et al., 2023). In this context, correcting the answers in this book is necessary. According to Brousseau (2002), this correction can prevent students from providing incorrect answers when solving problems. This is because students sometimes tend to mimic what has been demonstrated.

Conclusion

This research based on praxeology method provides a comprehensive analysis to enhance the quality of mathematics textbooks, particularly in the topic of System of Linear Equations with Two Variables (SLETV). The analysis results indicate the presence of 11 types of tasks and predict the use of 5 techniques in solving the given tasks in the mathematics textbook. These five techniques are perceptual, memorial, operational, logical, and analytical. There are 11 technologies used to justify the chosen techniques, as well as 4 theories underlying the justification of technology. Additionally, the results of didactic analysis show that both student textbooks and teacher guidebooks contain sections that can create epistemological and ontogenetic obstacles.

Recommendations

This article explores in-depth analysis of the SLETV material in the mathematics textbooks for Grade IX of Junior High School using a praxeological approach. The article may cover key findings such as types of tasks, techniques used, supporting technologies, theory and didactic obstacles identified through praxeological analysis. This article is expected to provide insights and concrete recommendations for the development of Indonesian mathematics textbooks that are more effective and supportive of students' understanding of SLETV.

Acknowledgements

References

Amelia, D., Putri, R. I. I., & Somakim. (2018). Learning material on the linear equation system with two variables (SPLDV) by using the context of train ticket receipts on VIII grade. *Sriwijaya University Learning and Education International Conference*, *3*(1), 562–568.

Azzumar, F., Suherman, T., & Turmudi, T. (2023). Characterıstıcs Of Mathematıc Books For Junıor Hıgh School Grade 7 Merdeka Currıculum : Praxeologıcal Analysıs Of Cuboids Volume. *Journal of Mathematics and Mathematics Education*, *13*(01), 76–84. https://doi.org/10.20961/jmme.v13i1.74319

Bosch, M., Gascón, J., & Trigueros, M. (2017). Dialogue between theories interpreted as research praxeologies: the case of APOS and the ATD. *Educational Studies in Mathematics*, *95*(1), 39–52. https://doi.org/10.1007/s10649-016-9734-3

Brousseau, G. (2002). *Theory of Didactical Situations in Mathematics*. Kluwer Academi Publisher.

Cai, J., Nie, B., & Moyer, J. C. (2010). The teaching of equation solving: Approaches in standards-based and traditional curricula in the United States. *Pedagogies*, *5*(3), 170–186.

https://doi.org/10.1080/1554480X.2010.485724

Chevallard, Y. (1998). *Analyse des pratiques enseignantes et didactique des mathématiques: l'approche anthropologique*. 91–118.

Chevallard, Yves. (2019). Introducing the Anthropological Theory of the Didactic: an Attempt At a Principled Approach. *Hiroshima Journal of Mathematics Education*, *12*, 71–114.

Chinn, S. (2020). *The Trouble with Maths: A Practical Guide to Helping Learners with Numeracy Difficulties (4th ed.)*. Routledge. https://doi.org/https://doi.org/10.4324/9781003017714

Erbaş, A. K., Alacaci, C., & Bulut, M. (2012). A comparison of mathematics textbooks from Turkey, Singapore, and the United States of America. *Educational Sciences: Theory and Practice*, *12*(3), 2324–2330.

Fan, L. (2013). Textbook research as scientific research: towards a common ground on issues and methods of research on mathematics textbooks. *ZDM*, *45*(5), 765–777. https://doi.org/10.1007/s11858-013-0530-6

HastiYunianta, T. N., Suryadi, D., Dasari, D., & Herman, T. (2023). Textbook praxeological-didactical analysis: Lessons learned from the Indonesian mathematics textbook. *Journal on Mathematics Education*, *14*(3), 503–524. https://doi.org/10.22342/jme.v14i3.pp503-524

Hendriyanto, A., Suryadi, D., Dahlan, J. A., & Juandi, D. (2023). Praxeology review: Comparing Singaporean and Indonesian textbooks in introducing the concept of sets. *Eurasia Journal of Mathematics, Science and Technology Education*, *19*(2), 1–13. https://doi.org/10.29333/ejmste/12953

Kolo, F., Nahak, S., & Fitriani, F. (2021). Analisis Kesulitan Siswa Dalam Menyelesaikan Soal Sistem Persamaan Linear Dua Variabel Pada Kelas VIII. *MATH-EDU: Jurnal Ilmu Pendidikan Matematika*, *6*(3), 100–114. https://doi.org/10.32938/jipm.6.3.2021.100-114

Kristanto, Y. D., Taqiyuddin, M., Yulfiana, E., & Rukmana, I. (2022). *Matematika Matematika SMP/MTs Kelas IX*. Kementerian Pendidikan, Kebudayaan, Riset, dan Teknologi. https://buku.kemdikbud.go.id

Lutfi, M. K., Juandi, D., & Jupri, A. (2021). Students' ontogenic obstacle on the topic of triangle and quadrilateral. *Journal of Physics: Conference Series*, *1806*(1). https://doi.org/10.1088/1742-6596/1806/1/012108

Nuraeniah, W., Fitriani, N., Amelia, R., Siliwangi, I., Terusan, J., Sudirman, J., Cimahi, J., & Barat, I. (2022). Analisis Kesulitan Pada Materi Sistem Persamaan Linear Dua Variabel Pada Pembelajaran Daring. *Jurnal Pembelajaran Matematika Inovatif*, *5*(1), 131–138. https://doi.org/10.22460/jpmi.v5i1.131-138

Piper, B., Simmons Zuilkowski, S., Dubeck, M., Jepkemei, E., & King, S. J. (2018). Identifying the essential ingredients to literacy and numeracy improvement: Teacher professional development and coaching, student textbooks, and structured teachers' guides. *World Development*, *106*, 324–336. https://doi.org/https://doi.org/10.1016/j.worlddev.2018.01.018

Prabowo, A., Suryadi, D., Dasari, D., Juandi, D., & Junaedi, I. (2022). Learning Obstacles in the Making of Lesson Plans by Prospective Mathematics Teacher Students. *Education Research International*, *2022*. https://doi.org/10.1155/2022/2896860

Purnomo, Y. W., Mastura, F. S., & Perbowo, K. S. (2019). Contextual Features of Geometrical Problems in Indonesian Mathematics Textbooks. *Journal of Physics: Conference Series*, *1315*(1). https://doi.org/10.1088/1742-6596/1315/1/012048

Putri, L. F., & Manoy, J. T. (2013). Identifikasi Kemampuan Matematika Siswa dalam Memecahkan Masalah

Aljabar di Kelas VIII Berdasarkan Taksonomi Solo. *MATHEdunesa*, *2*(1), 29–30. https://doi.org/10.26740/mathedunesa.v2n1.p%25p

Remillard, J., Reinke, L., & Kapoor, R. (2018). What is the point? Examining how curriculum materials articulate mathematical goals and how teachers steer instruction. *International Journal of Educational Research*, *93*. https://doi.org/10.1016/j.ijer.2018.09.010

Rifadena, S. R., & Hidayanto, E. (2021). Analisis Kesulitan Siswa SMP Kelas VIII dalam Penyelesaian Representasi Masalah Matematika Pada Materi Sistem Persamaan Linier Dua Variabel (SPLDV). *Prosiding Seminar Nasional Matematika dan Pembelajarannya*, 150–161.

Sievert, H., van den Ham, A.-K., Niedermeyer, I., & Heinze, A. (2019). Effects of mathematics textbooks on the development of primary school children's adaptive expertise in arithmetic. *Learning and Individual Differences*, *74*, 101716. https://doi.org/https://doi.org/10.1016/j.lindif.2019.02.006

Solis, D., & Isoda, M. (2023). Comparing elementary school textbooks of China, Japan, and Malaysia: a praxeological and developmental progression analysis regarding length measurement. *Research in Mathematics Education*, *25*(3), 359–378. https://doi.org/10.1080/14794802.2022.2103022

Suryadi, D. (2019). *Penelitian Desain Didaktis (DDR) dan Implementasinya*. Gapura Press.

Takeuchi, H., & Shinno, Y. (2020). Comparing the Lower Secondary Textbooks of Japan and England: a Praxeological Analysis of Symmetry and Transformations in Geometry. *International Journal of Science and Mathematics Education*, *18*(4), 791–810. https://doi.org/10.1007/s10763-019-09982-3

Valverde, G. A., Bianchi, L. J., Wolfe, R. G., Schmidt, W. H., & Houang, R. T. (2002). According to the Book. In *According to the Book* (Number January). https://doi.org/10.1007/978-94-007-0844-0

Weinberg, A., & Wiesner, E. (2011). Understanding mathematics textbooks through reader-oriented theory. *Educational Studies in Mathematics*, *76*(1), 49–63. https://doi.org/10.1007/s10649-010-9264-3

Wu, H.-H. (2016). Linear equations in two variables and their graphs. *Teaching School Mathematics: Algebra*, 53–84. https://doi.org/10.1090//mbk/099/04

Zuchdi, D., & Afifah, W. (2021). *Analisis Konten Etnografi & Grounded Theory, dan Hermeneutika Dalam Penelitian*. Bumi Aksara.

The Learning Machine based on BPSO Optimization Algorithm to Detect Rotor broken Bars Default in Asynchronous Machine

Noureddine Fares

Environment Laboratory, Institute of Mines, Echahid Larbi Tebessi University, Tebessa 12002, Algeria, 🆔
https://orcid.org/0000-0002-0811-4980

Chouaib Souaidia

LABGET Laboratory, Faculty of Science and Technology, Echahid Larbi Tebessi University, Tebessa 12002, Algeria, 🆔 https://orcid.org/0000-0002-4281-7671

Tawfik Thelaidjia

LABGET Laboratory, Faculty of Science and Technology, Echahid Larbi Tebessi University, Tebessa 12002, Algeria, 🆔 https://orcid.org/0000-0003-4222-323X

Abstract: Asynchronous machine health monitoring is considered a developing technology for the online detection of faults that occur even at the initial stage. The objective of this study is to present an artificial intelligence (AI) technique for the detection and localization of adjacent and distant broken bar faults in the asynchronous machine, through a multi-winding model for the simulation of these cases. In this work, it was found that the application of Artificial Neural Networks (ANN) based on Mean Squared Error (MSE) and Random Forest (decision tree) plays an important role in detecting and locating defaults. The stator current signal "Ias" of an asynchronous machine in the dynamic state was acquired from a healthy and faulty machine with a broken rotor bar fault. We extracted 9 statistical features and 8 wavelet packet parameters from the stator current signal. These features were employed as an input vector to train and test the ANN and Random Forest and determine whether the motor was running under normal conditions or defective. For optimizing the rotor bar defect classification procedure, we adopted feature selection algorithm, such as BPSO. The results showed that the Random Forest classifier based on statistical parameters and wavelet packet parameters followed by BPSO can detect the defective with high accuracy (**95%**) compared to without optimization method.

Citation: Fares, N., Souaidia, C. & Thelaidjia, T. (2024). The Learning Machine based on BPSO Optimization Algorithm to Detect Rotor broken Bars Default in Asynchronous Machine. In A. A. Khan, M. Demirbilek, & M. L. Ciddi (Eds.), *Proceedings of ICSEST 2024-- International Conference on Studies in Engineering, Science, and Technology* (pp. 125-134), Istanbul, Turkiye. ISTES.

Introduction

Fault diagnostic asynchronous machines are a component of many industrial process applications, due to their robustness, cost and performance. They are used in various applications as a means of energy conversion, pumps, electric vehicles, and asynchronous generators.

In this context, over the past two decades, the diagnosis of asynchronous machines failures has aroused great interest on the part of researchers. Major research has been carried out for the development of various techniques and methods for detecting and diagnosing defects. He proposed an algorithm for the online detection of rotor bar rupture in induction machines based on the use of wavelet packet decomposition and Neural Networks [2]. A new set of characteristic coefficients is obtained by the WPD of the stator current, to build a Neural Network for defect detection, thus accurately differentiating healthy and defective conditions. The algorithm analyzes rotor bar defects by WPD of the stator current of the induction motor. This diagnostic method is carried out using the MCSA method. The sideband components of the current spectrum are extracted and analyzed to prove rotor defects.

In this work, we presented a multi-winding model to simulate the behavior of the machine is healthy and defective cases when the rotor bar is broken, defect diagnosis is based on an Intelligent Artificial Technique (AIT) very important for the detection of a rotor defect in the asynchronous machine. The identification process shows a sequence of simulation configuration, data acquisition, data processing, classification algorithm, model evaluation, and last prediction. In the fourth section, the application of the ANN and RF configuration based on the learning machine is proposed to take the data set for machine training purposes.

The training dataset is taken for five failure conditions and one health condition. The defect condition is adjacent and distant broken rotor bars. This drive dataset is used to train the machine using BPSO algorithm, and without optimization.

Each algorithm shows a different accuracy for the defect identification method proposed in the fifth section (Table 3). The highest test accuracy classification of healthy or broken rotor bars of the induction machine is obtained by random forest (RF) with the hybrid parameter used by BPSO (statistical and wavelet packet parameters) is (**95**%).

Equivalent reduced model of the asynchronous machine

To do this, we use the generalized Clarke matrix extended to the rotor system. This makes it possible to move from " *n-phases* " modeling to equivalent two-phase modeling written as the reduced-size model (5X5) of the asynchronous machine with rotor bar breakage defects becomes:

$$\begin{bmatrix} L_{sc} & 0 & -\frac{N_r}{2}M_{sr} & 0 & 0 \\ 0 & L_{sc} & 0 & -\frac{N_r}{2}M_{sr} & 0 \\ -\frac{3}{2}M_{sr} & 0 & L_{rc} & 0 & 0 \\ 0 & -\frac{3}{2}M_{sr} & 0 & L_{rc} & 0 \\ 0 & 0 & 0 & 0 & L_e \end{bmatrix} \cdot \frac{d}{dt}\begin{bmatrix} I_{ds} \\ I_{qs} \\ I_{dr} \\ I_{qr} \\ I_e \end{bmatrix} = \begin{bmatrix} V_{ds} \\ V_{qs} \\ V_{dr} \\ V_{qr} \\ V_e \end{bmatrix} - \begin{bmatrix} R_s & -L_{sc}\omega & 0 & \frac{N_r}{2}M_{sr}\omega & 0 \\ L_{sc}\omega & R_s & -\frac{N_r}{2}M_{sr}\omega & 0 & 0 \\ 0 & 0 & R_{rdd} & R_{rdq} & 0 \\ 0 & 0 & R_{rqd} & R_{rqq} & 0 \\ 0 & 0 & 0 & 0 & R_e \end{bmatrix} \cdot \begin{bmatrix} I_{ds} \\ I_{qs} \\ I_{dr} \\ I_{qr} \\ I_e \end{bmatrix}$$

(01)

With:

$$R_{rdd} = 2.R_b(1 - \cos(\alpha)) + \frac{R_e}{N_r} + \frac{2}{N_r}(1 - \cos(\alpha)).\sum_k R_{bfk}(1 - \cos(2k-1).\alpha)$$

$$R_{rdq} = -\frac{2}{N_r}(1 - \cos(\alpha))\sum_k R_{bfk}\sin(2k-1).\alpha$$

(02)

$$R_{rqd} = -\frac{2}{N_r}(1 - \cos(\alpha))\sum_k R_{bfk}\sin(2k-1).\alpha$$

$$R_{rqq} = 2.R_b(1 - \cos(\alpha)) + 2.\frac{R_e}{N_r} + \frac{2}{N_r}(1 - \cos\alpha).\sum_k R_{bfk}(1 + \cos(2k-1).\alpha)$$

The index "k" indicates the broken bar.

For the mechanical part, we have the expression of the electromechanical torque:

$$C_{em} = \frac{3}{2}.p.\frac{N_r}{2}.M_{sr}.\left(I_{ds}.I_{qr} - I_{qs}.I_{dr}\right)$$

(03)

Table 1. Asynchronous machine parameters

Parameter	Meaning parameter	Value
P	Nominal power	1.1 KW
V	Rated line voltage	220 V
f_s	Feeding frequency	50 Hz
p	Number of pole pairs	1
R	average rotor diameter	35.76 mm
N_s	Number of turns per stator phase	160
l	Rotor active length	65 mm
R_e	Resistance of a portion of a short-circuit ring	150 μΩ
R_b	Resistance of a rotor bar	150 μΩ
L_e	Short circuit ring leakage inductance	0.1 μH
L_b	Rotor bar leakage inductance	0.1 μH
e	Air gap thickness	0.2 mm
R_s	Resistance of a stator phase	7.58 Ω
N_r	Number of rotor bars	16
L_{sf}	Stator leakage inductance	26.5 mH

f	Coefficient of friction	0
J	Moment of inertia	0.00541 Kgm2

Simulation results and discussion

Once the model of the asynchronous machine is established. The simulation aspect can be addressed in the MATLAB/Simulink environment, which provides the ability to observe and interpret visualized phenomena and quantities in real-time. We will represent the asynchronous machine in different states, healthy and defective. The results of the simulation in these cases are as follows:
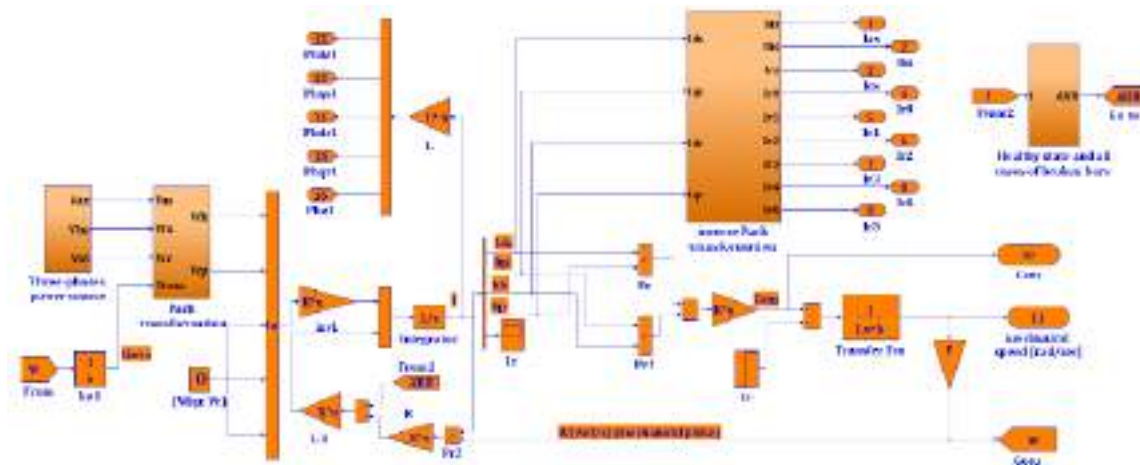

Figure 1. Simulation model of an asynchronous machine with healthy and all cases of broken Rotor bars state
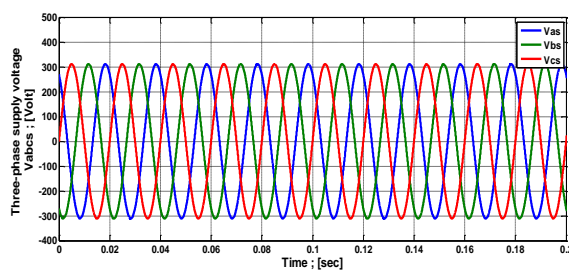
Figure 2. Three-phase supply voltage *Vabcs*
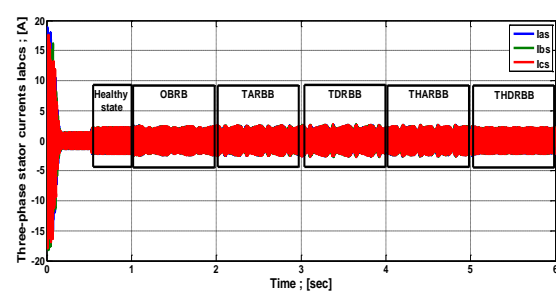
Figure 3. Three-phase stator currents *Iabcs* of an asynchronous machine with the healthy and all cases of broken rotor bars state

Observe and simulate the multi-winding model of the induction machine. At the time 0.5 s, apply a load torque of 3.5; [Nm]. Before 1 s the dynamic regime of the asynchronous machine in the healthy state, the time t = 1 s, simulates the rupture of the first bar, the time t = 2 s, breaking two adjacent bars, and the time t = 3 s, breaking two distant bars, and at time t = 4 s, breaking three adjacent bars, and at time t = 5 s, by breaking three distant bars, it is observed in Figure.4 that the mechanical speed decreases during the break of the bar and creates oscillations of rupture. Figure.5 electromagnetic torque increases in amplitude after the rupture of two bars, and

(Figure.3) is illustrated the modulation of the envelope of the stator currents "Iabcs" increases in amplitude with the number of broken bars.
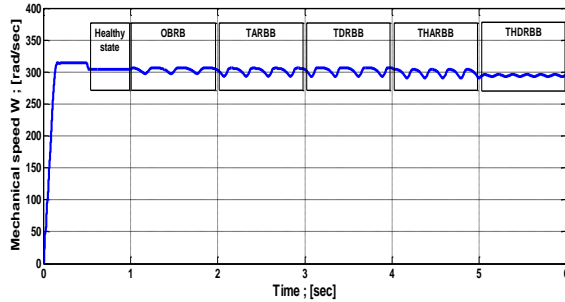
Figure 4. Mechanical speed of asynchronous machine with healthy and all cases of broken rotor bars state
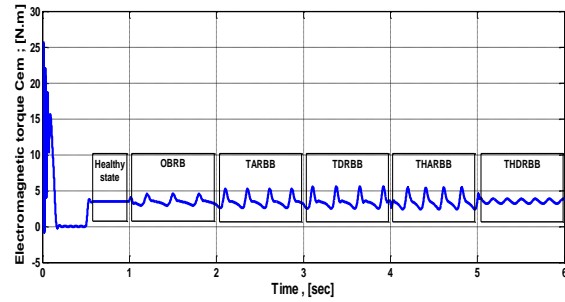
Figure 5. Electromagnetic torque of asynchronous machine with healthy an all cases of broken rotor bars state

Application of learning machine-based ANN and RF

In this work, a feed-forward neural network (ANN) is applied with a hidden layer of 10 neurons and a random forest (RF) with 20 trees to perform the four training and testing cases (without optimization and with BPSO optimization algorithm). The results obtained are shown in Table 3. But the best results of hybrid parameters (statistical and wavelet packet decomposition) with BPSO are inserted in part (4).

The first step is to acquire samples of "I_{as}" current from healthy motors and fault motors with rotor broken bars. This current data is used as input into the signal processing stage. The healthy and faulty motor current samples used in this study were obtained from the simulation results of the multi-wind model of the broken rotor bars.

The size of the input data set used is 600-by-17 matrix and target output data is 600-by-6 matrix whose outputs are binary in nature where a vector output of [1; 0; 0; 0; 0; 0] healthy motor condition, [0; 1; 0; 0; 0; 0] presence of one broken rotor bar until [0; 0; 0; 0; 0; 1] presence of Three distant rotor broken bars. 70% of the data set is used for ANN training and the rest for testing.

Table 2. Classification of several faults

Fault type	Symbol	Code					
		S1	S2	S3	S4	S5	S6
Healthy state	HS	1	0	0	0	0	0
One broken rotor bar	OBRB	0	1	0	0	0	0
Two adjacent rotor broken bars	TARBB	0	0	1	0	0	0
Two distant rotor broken bars	TDRBB	0	0	0	1	0	0
Three adjacent rotor broken bars	THARBB	0	0	0	0	1	0
Three distant rotor broken bars	THDRBB	0	0	0	0	0	1

BPSO algorithm

PSO is a population-based algorithm that mimics the social behaviors of flocks of birds and fish swarms. This algorithm was first introduced by Kennedy and Eberhart [**4**]. PSO is beneficial for performing feature selection because of its ease of implementation, speed of convergence and low compute cost [**5**, **6**]. In the PSO algorithm [**4**, **7**], a swarm consists of a set of particles (Population). Each particle "*i*" represents a candidate solution and has the speed "v_i" and position "x_i". The problem is optimized by improving each candidate solution by the motion of the corresponding particle in the research space. The motion of a particle is influenced by the best local position "*pbest*" of the particle as well as the best overall solution for the swarm "*gbest*", which corresponds to the particle with the best *pbest*. The evaluation of *pbest* and *gbest* depends on an objective function (fitness function), which measures the degree of effectiveness of the solution of each particle. During motion, each particle in the swarm updates its "v_i" speed and "x_i" position using:

$$v_i(t+1) = w * v_i(t) + c_1 * r_1\left(pbest_i - x_i(t)\right) + c_2 * r_2\left(gbest - x_i(t)\right) \tag{4}$$

$$x_i(t+1) = x_i(t) + v_i(t+1) \tag{5}$$

where, $v_i(t+1)$ represents the new speed of the particle, c_1 and c_2 are the acceleration coefficients, "*w*" is an inertial weight, "r_1" and "r_2" are random numbers, $v_i(t)$ is the velocity of particle "*i*" at time "*t*", $x_i(t)$ is the velocity of particle "*i*" at time "*t*", $pbest_i$ is the best position occupied by particle *"i"* at time *"t"*, *gbest* is the best position discovered by the swarm at time "*t*", and $x_i(t+1)$ is the new position of the particle. Algorithm 1 presents the pseudocode of the PSO algorithm, where Random Position and Random Velocity are used to initialize each particle with a random initial position and a random initial velocity, respectively; Best solution returns the best solution among all the particles in the swarm; Update Velocity returns the new velocity value of a particle using Eq. 4; Updating Position returns the new position of a particle using Eq. 5, and calculates the fitness value of a solution.

In the abovementioned explanation of the PSO algorithm, a continuous space is assumed; however, in this article, we use a version of PSO known as BPSO [8], which was developed to solve discrete problems. In addition, BPSO is one of the most effective methods of selecting packaging characteristics [5, 6]. In BPSO, the speed "v_i" represents the probability that "x_i" will take a value of 1 or 0. To restrict all real position values to "0 or 1", the sigmoid function is applied using:

$$x_i = \begin{cases} 1 & if \quad rand(0,1) < S(v_i) \\ 0 & else \end{cases} \tag{6}$$

$$S(v_i) = \frac{1}{1 + e^{-v_i}} \tag{7}$$

where, rand (x_i) is a random uniform number in the interval [0, 1]. The updated position is normalized using $S(v_i)$, where "v_i" denotes the updated speed of the particle. When $S(v_i)$ is greater than the random number generated, the position value of the particle (x_i) is 1; otherwise, "x_i" is 0.

The BPSO parameters and the problem of interest, which consist of the feature set, are passed to the PSO algorithm (Algorithm 1). The velocities and positions of the particles are updated according to Eq. (4) and Eq. (6), respectively. The main objective of this study is to improve the performance of the classifier. The Evaluate evaluation function is defined based on the accuracy results of the classifier, and the output is determined as Evaluate (y)=Accuracy (y). Precision (y) refers to the accuracy of the classifier for the model formed and tested using the subset of characteristics selected there by the particle evaluated in the PSO swarm. Subsequently, the Best Solution function returns the solution (a subset of characteristics (y)) with the best accuracy value obtained among the population.

Results and Discussion

Initially, all statistical (minimum, maximum, Standard deviation, Root mean square, Kurtosis, peak to peak, Mean, Skewness, and Crest factor) and wavelet packet features were evaluated without performing feature screening; the results are shown in Table 3. ANN and RF using hybrid features (statistical and wavelet packet parameters) for detection of healthy and broken rotor bar faults states produced higher accuracy than the other combinations. The RF classifier with BPSO achieved the highest accuracy (**95%**) compared to without optimization method.

Classification using a Hybrid Parameter with BPSO

Classification using Artificial Neural Network (ANN).

A histogram of an error after training ANN with BPSO optimization algorithm is shown in Figure 7. Moreover, validation performance is shown in Figure 8. The mean squared error of 2000 epochs show the best validation

performance at epoch 1542 is 0.032059 (Figure 9).
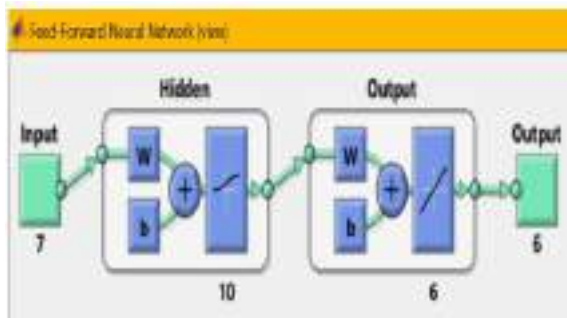

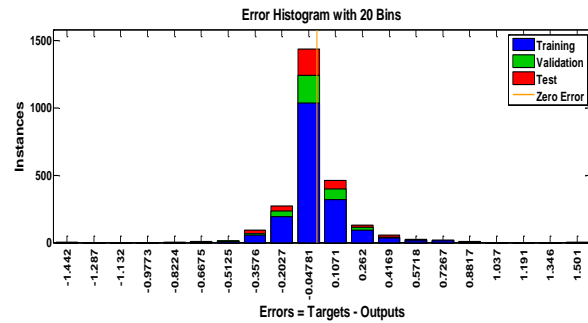Figure 6. Feed-forward neural network with BPSO

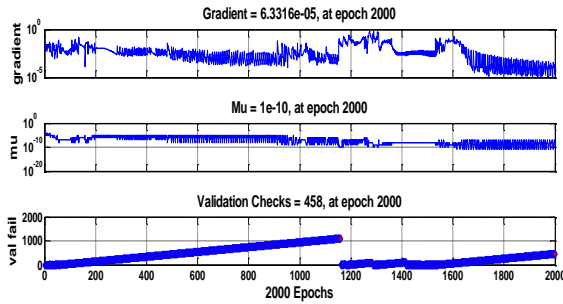Figure 7. Error histogram between target values and predicted values of ANN with BPSO
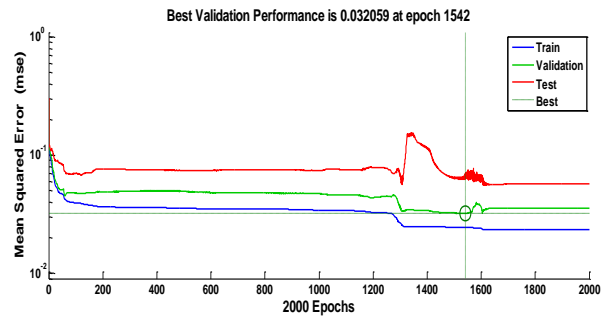

Figure 8. Training state of ANN with BPSO

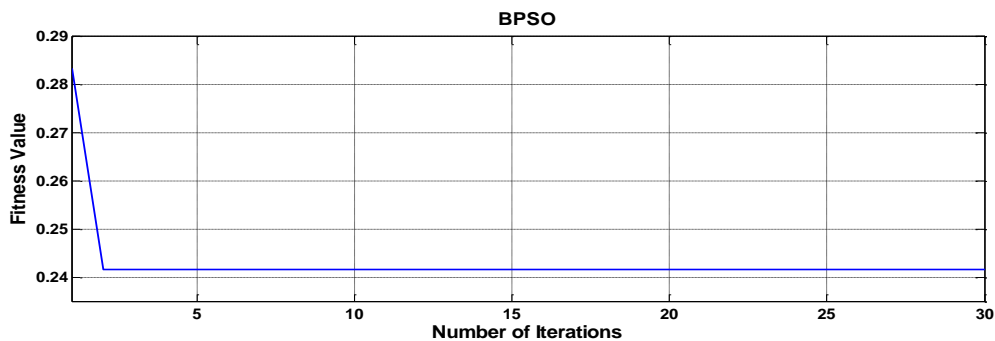Figure 9. Mean square error of 2000 Epochs for the ANN with BPSO

Figure 10 : Fitness results for BPSO algorithm with ANN

Classification using Random Forest

Several tests of classification using Random Forest -by increasing the number of trees- have been done. From the result illustrated in Figure 11. we can conclude that the balanced error rate of RF decreases when the number of trees increases. It can be seen also that the best-balanced error rate is obtained using 20 trees, for this reason the value (0.2) it will be considered as the best Random Forest classifier with 0.35 Fitness value (Figure 12).
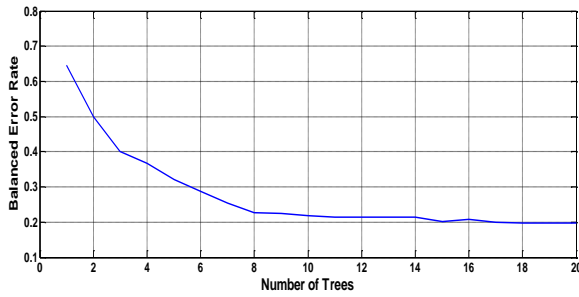
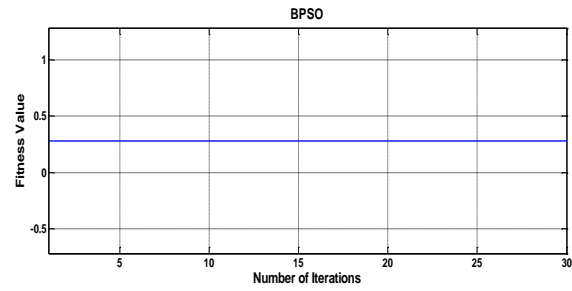Figure 11. The balanced error rate of RF with BPSO

Figure 12: Fitness results for BPSO algorithm with RF

Classification of the healthy and defective state of the rotor bars of the asynchronous machine with Artificial Intelligence Techniques like ANN and Random Forest assisted by the BPSO algorithm of features selection, from the statistical parameters and wavelet packet decomposition parameters are all shown on tables 3.

Table 3. Results of ANN and RF classifiers without and with BPSO optimization algorithm

			Without optimization		BPSO	
			Accuracy %	Time (s)	Accuracy %	Time (s)
Statistical parameters	Training	ANN	81.1905	109.8219	84.0476	50.7143
		RF	100	13.5052	99.7619	11.8571
	Testing	ANN	76.1111	2.7616	83.8889	2.5342
		RF	87.2222	8.1943	88.3333	4.9335
Wavelet Packet Decomposition parameters	Training	ANN	86.1905	63.207	82.8571	46.0295
		RF	98.8095	12.0571	99.7619	11.8125
	Testing	ANN	78.8889	2.6618	78.3333	2.6083
		RF	79.4444	4.9598	78.8889	4.8937
Hybrid (statistical and Wavelet Packet	Training	ANN	95.4762	127.3953	94.7619	88.9211
		RF	100	12.0414	99.7619	11.6481
	Testing	ANN	87.7778	6.3246	93.8889	2.5552
		RF	90	4.6141	**95**	4.8687

Conclusion

The detection and early diagnosis allow for reducing damage and maintaining other components of asynchronous machine, through the study of defects influence and the behavior of the machine in case of operation fault. In this paper, we presented the asynchronous machine fault by using a multi-winding model for the simulation of broken bars. The proposed diagnosis method could be applied by artificial intelligence represented by neural networks (ANN) and Random Forest (decision tree) with BPSO optimization algorithm on asynchronous machine during several parametric studies (selection of the type of network, choice of inputs,

and choice of outputs, number of trees in the random forest, ...). The data acquisition operation, to establish the learning machine base. To be reliable indicators for detection and location of fault broken bars. These results indicate clearly that the proposed RF with optimization algorithm BPSO used hybrid parameters (statistical and wavelet packet decomposition parameters) gave high accuracy (**95%),** it has great importance for fault identification, and it is capable to reduce the failure severity. Furthermore, it has been manifested that this approach is accurate and simple in the process implement diagnosis.

References

Bhasme, D.A., Chavhan, V.S. (2020). Induction motor condition monitoring system based on machine learning. International Research Journal of Engineering and Technology (IRJET), 7(5): 6590-6593.

Chouidira, I., Eddine, K.D., Benguesmia, H. (2019). Detection and diagnosis faults in machine asynchronous based on single processing. International Journal of Energetica (IJECA), 4(1): 11-16. http://dx.doi.org/10.47238/ijeca.v4i1.89

Sadeghian, A., Ye, Z., Wu, B. (2009). Online detection of broken rotor bars in induction motors by wavelet packet decomposition and artificial neural networks. IEEE Transactions on Instrumentation and Measurement, 58(7): 2253-2263. https://doi.org/10.1109/TIM.2009.2013743

Kennedy, J., Eberhart, R. (1995). Particle swarm optimization. In Proceedings of ICNN'95-international conference on neural networks, pp. 1942-1948. https://doi.org/10.1109/ICNN.1995.488968

Brezočnik, L., Fister Jr, I., Podgorelec, V. (2018). Swarm intelligence algorithms for feature selection: A review. Applied Sciences, 8(9): 1521. https://doi.org/10.3390/app8091521

Nguyen, B.H., Xue, B., Zhang, M. (2020). A survey on swarm intelligence approaches to feature selection in data mining. Swarm and Evolutionary Computation, 54: 100663. https://doi.org/10.1016/j.swevo.2020.100663

Eberhart, R.C., Shi, Y., Kennedy, J. (2001). Swarm intelligence. Elsevier. Book ISBN: 9780080518268. Hardcover ISBN: 9781558605954

Kennedy, J., Eberhart, R.C. (1997). A discrete binary version of the particle swarm algorithm. In 1997 IEEE International Conference on Systems, Man, and Cybernetics. Computational Cybernetics and Simulation, pp. 4104-4108. https://doi.org/10.1109/ICSMC.1997.637339

Modelling and Simulating the Electrical Hybrid System

Sihem Ghoudelbourk

Badji Mokhtar University, Annaba, Algeria, https://orcid.org/0000-0002-8536-4086

Mounia Taleb

Echahid Cheikh Larbi Tebessi University, Envirment Laboratory Algeria, https://orcid.org/0000-0003-2564-2141

Abdelkrim Rechach

Mining Institute, Mining Laboratory, Cheikh Larbi Tebessi University, Algeria, https://orcid.org/0000-0001-9889-5735

Abstract: The proposed system consists of solar PV and Doubly Fed Induction Generator (DFIG) based wind turbine. These two energy source are complimentary in nature .The quality of the energy supplied to the network by for hybrid PV–Wind system using DFIG Wind Turbines could be improved by the use of multilevel inverters. The need of several sources on the DC side of the converter makes multilevel technology attractive for photovoltaic applications. Of the same for the wind turbine systems and by increasing the level of the inverter we can get an improved system responses by reducing the harmonics of the stator current delivered to the grid and reduces the ripples of the couple. The results under environment Matlab /Simulink. Will be presented and analyzed. The connection of several PVs to the power grid through multi-level inverters reduces the total harmonic distortion (THD), thus improving the quality of electrical energy.

Keywords: Doubly Fed Induction Generator, hybrid PV–Wind system, Multi-level inverters; Photovoltaic system

Introduction

Energy consumption is significantly high in industries and educational institutions across the world, highlighting the need for sustainable and independent energy solutions. Conventional energy sources, such as fossil fuels, pose major environmental risks and are increasingly costly to operate. In response to these challenges, global interest is turning to renewable energy systems (RES), which offer viable and cost-effective solutions to meet growing energy demands. Solar and wind energy, although available in abundance, cannot on their own ensure a continuous supply of electricity, thus requiring the integration of hybrid systems with storage facilities. Hybrid

systems, combining photovoltaic (PV) and wind power, represent a promising solution. In addition to reducing CO2 emissions, these systems offer local production of clean energy, a better balance of resources and increased security of supply.

In view of the environmental problems caused by the emission of greenhouse gases, the use of renewable energy resources has become an interesting alternative offering the possibility of producing clean electricity. The proposed system consists of solar PV and Doubly Fed Induction Generator (DFIG) based wind turbine. These two energy source are complimentary in nature (Ka. Rajeshet et al.2015). (see figure 1).
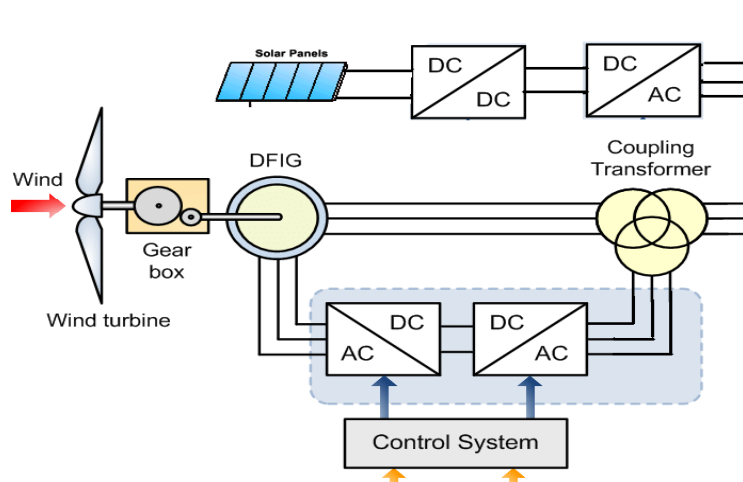
Figure 1. Hybrid PV–Wind Turbin System
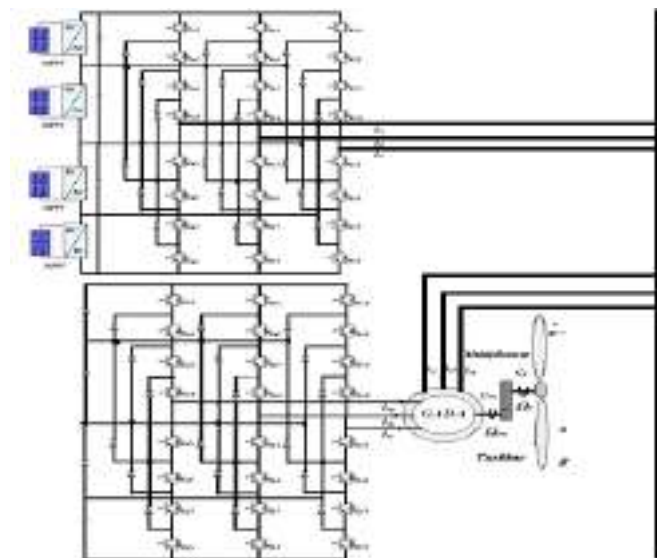
Figure 2. Hybrid PV–Wind   turbin system by the used of multilevel inverters

The quality of the energy supplied to the network by for hybrid PV–Wind system using DFIG Wind Turbines could be improved by the use of multilevel inverters (show in figure 2). Indeed the connection of several PVs to the power grid through multi-level inverters reduces the total harmonic distortion (THD), thus improving the quality of electrical energy, make it possible to increase the power delivered by the photovoltaic generator. And

for the wind turbine systems we can get an improved system responses by reducing the harmonics of the stator current delivered to the grid and reduces the ripples of the couple.

II. PV-Systems

Figure 3 shows the block diagram of the PV system. Figure 4 shows the electric model of a solar cell which consists of an ideal current source, connected with a series resistor R_s and a shunt resistor R_{sh} in parallel (D.Dib et al., 2015; Rechach.A et al., 2022) .Diode D describes the semiconductor properties of the cell. This model with an empirical diode) is currently the most used because of its simplicity.

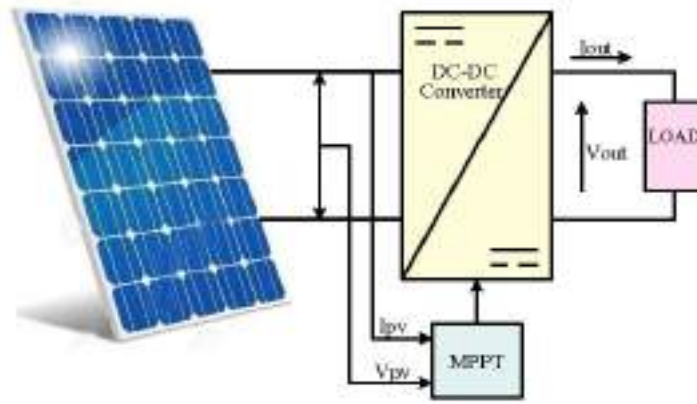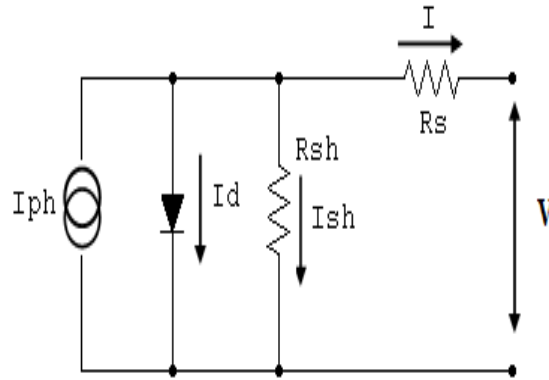Figure 3. Synoptic diagram of a system Photovoltaic controlled by MPPT

Figure 4. Equivalent circuit of a PV cell

The total current delivered by the photovoltaic generator is given by the following equation parallel (Adjei-Saforo.EK et al.2022 and Hassan.B et al 2013) :

$$I = I_{Ph} - I_d - I_0 \left(e^{\frac{q\,(V+IR_S)}{KT\gamma}} - 1 \right) - \left(V + I\,R_s\right) \Big/ \left(R_{Sh}\right)$$

(1)

With

R_{sh}: represents the leaks around the p-n junction due to impurities and the corners of cell.

R_s: the internal resistance of the cell;

I_{ph}: Current photo created by the cell [A].

I_d: Current called current of total darkness [A].

I_{sh}: Current flowing in $R_{\_sh}$ [A].

K_I : Temperature coefficient of the short-circuit current.

V: The voltage imposed at the terminals of the cell [V].

I: The current delivered by the cell [A].

I_o: Saturation current of the diode [A].

K: Constant of Boltzmann

q : The charge of the electron

Under the conditions of constant temperature and illumination example: (G = 1000w / m², T = 25C °). Figure 3 shows the current / voltage characteristic of a cell. On this curve, the empty operating point is identified: V_{co} for I = 0A and the short-circuiting operating point: I_{sc} for U = 0V. Figure 5 shows the power characteristic as a function of the voltage. This curve passes through a maximum power (P_{max}) at this corresponding power, a voltage V_{pm} and a current I_{pm} which can be seen on the curve (I = f (V)).
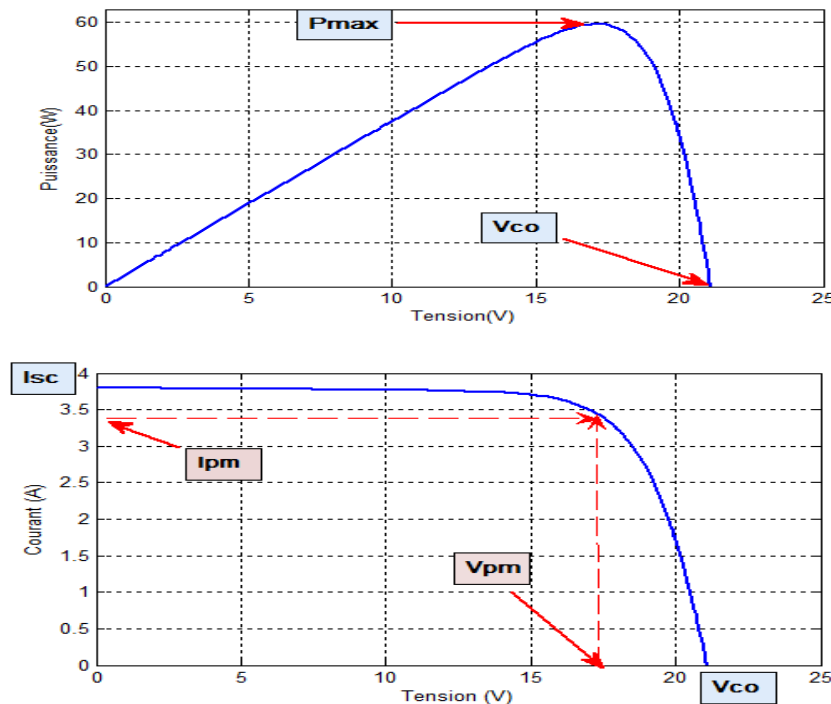
Figure 5. Caracteristique I=f(V) and P=f(V).

Photovoltaic generators have a random electrical production directly dependent on weather conditions. Thus, the optimal dimensioning and utilization of the energy produced by these generators requires the use of appropriate management methods. The MPPT control makes it possible to find the optimum operating point of the photovoltaic module this is based on the automatic variation of the duty cycle α of the signal controlling the

energy converter to an appropriate value so as to maximize the output power of the module (Park.H et al.2016 and Ghoudelbourk.S et al 2021). In order to extract the maximum power of a solar panel, one can rely on the disturbance and observation (P & O) method which is a widely used approach in MPPTs because it is simple and requires only the measurement of V_PV and I_PV. Figure 6 shows the flow chart of the P & O algorithm. We have tested the performance of the algorithm by simulation.
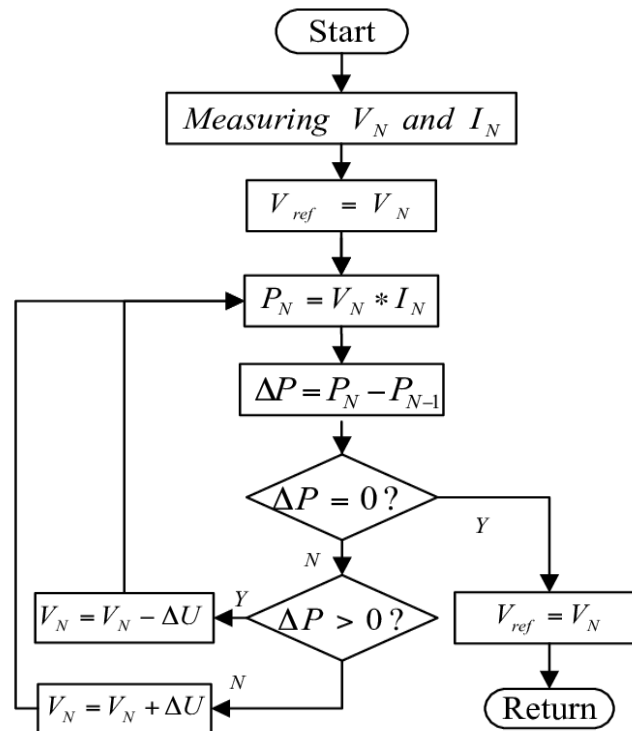
Figure 6. Algorithm of the disturbance and observation

The results are shown in Figure 7 and 8. It represents respectively the variation of the illumination and the power delivered by the PV system. During this simulation, the system is subjected to a change in brightness of [1000, 800, 1000] W / m^2 at times [0, 4, 8] under the effect of a constant temperature, MPPT technique follows the variation of the irradiation with a rather remarkable rapidity.
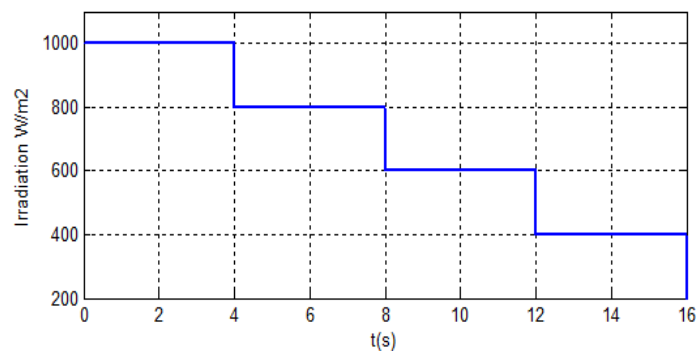
Figure 7. Variation of the irradiance in function of time(at T=25°C)
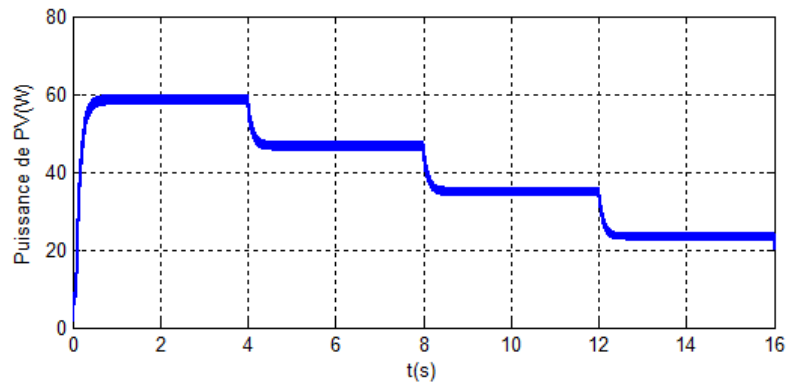
Figure 8. Variation of the Power of PV in function of time (at T=25°C)

Each phase of the NPC three-phase inverter with five voltage levels is composed of eight controlled switches that are unidirectional in voltage and bidirectional in current. These are conventional combinations of a transistor and an antiparallel diode and six holding diodes connected along the DC bus (Wu.YT. et al 2007). The inverter is powered by a continuous source E, it has four capacitors of equal values to give four distinct sources of E / 4 voltage. The three-phase structure of the NPC inverter with five voltage levels is shown in figure 9.

Figure 9. Structure of a five-level NPC inverter.

With the symmetry of the structure of the three-phase inverter using the control strategy triangular four-sinusoidal carrier the algorithm is defined by the following expressions in table 1 and Fig. 10 shows the control signals of three references and the signals of the five bipolar carriers.
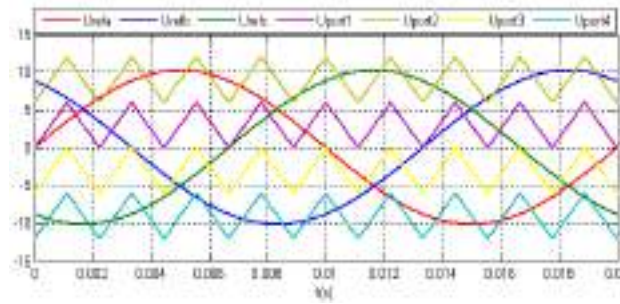
Figure 10. Control signals of switches

Table 1. Five Inverter Algorithm Control

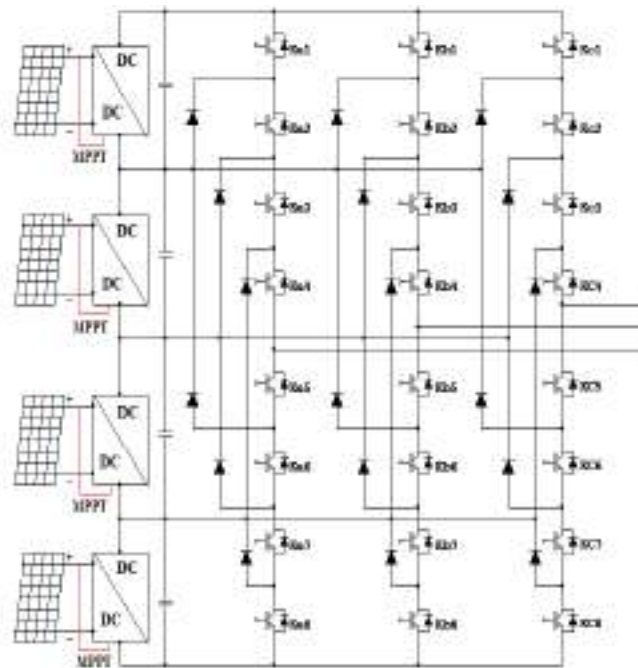| *Test*	U_{KM}
$U_r \geq U_{p1}$	E/2
$U_r < U_{p1}$	0
$U_r \geq U_{p2}$	E/4
$U_r < U_{p2}$	0
$U_r \geq U_{p3}$	0
$U_r < U_{p3}$	0
$U_r \geq U_{p4}$	-E/4
$U_r < U_{p1}$	-E/2

Figures 11.a and 11.b show respectively the single voltage between phase A and the origin point O U_{ao} and the compound voltage between phase A and phase B (U_{AB}) obtained at the output of the inverter. We note that the results give the following voltage levels: E / 2, E / 4, 0, -E / 4, -E / 2. Figures 11.a and 11.b show respectively the harmonic distortions obtained on these single and compound voltages.
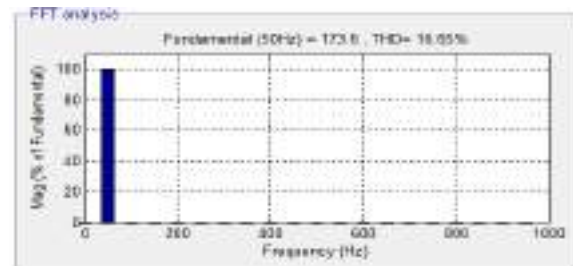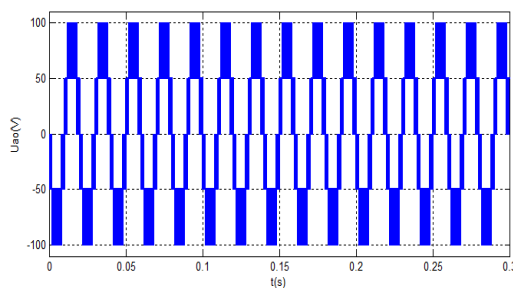
Figure 11. Result of the simulation of the 5 level inverter (NPC)

a - Spectral analysis U_{ab}; b- U_{ab} .

III. DFIG Fed by Multilevel Inverters

The Fig.12 illustrates the line diagram of the string conversion wind turbine that we considered in our study. Where the stator is directly connected to the distribution grid,   while the rotor windings are connected via slip

rings to a three-phase voltage source converter. In this section, we will present the modeling of the DFIG by developing the principle of separate control of active and reactive power. The vector control strategy and the control algorithm for five a level inverter will also be presented. We will consider the operation of the machine powered by two and five level inverters under constraint conditions imposed on the powers references. The performance of these structures are analyzed and compared.
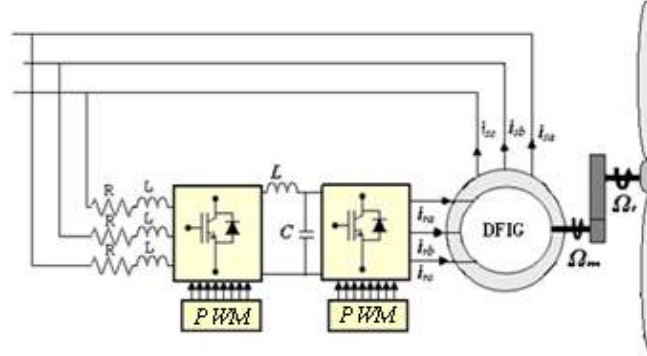

Figure 12.   Wind Turbin System

Constant air gap, effect of notches neglected, sinusoidal spatial distribution of magneto motive forces in the gap, the influences of skin effect and the heating are taken into account, the magnetic circuit is unsaturated and the permeability is constant and the neutral is not connected therefore no zero-sequence system.Thus, the equations of the stator voltages and rotor are:

$$\begin{cases} V_{sd} = R_s.I_{sd} + \dfrac{d\phi_{sd}}{dt} - \dot{\theta}_s.\phi_{sq} \\[2mm] V_{sq} = R_s.I_{sq} + \dfrac{d\phi_{sq}}{dt} + \dot{\theta}_s.\phi_{sd} \\[2mm] V_{rd} = R_r.I_{rd} + \dfrac{d\phi_{rd}}{dt} - \dot{\theta}_r.\phi_{rq} \\[2mm] V_{rq} = R_r.I_{rq} + \dfrac{d\phi_{rq}}{dt} + \dot{\theta}_r.\phi_{rd} \end{cases} \tag{2}$$

$$\begin{cases} \phi_{sd} = L_s.I_{sd} + M.I_{rd} \\ \phi_{sq} = L_s.I_{sq} + M.I_{rq} \\ \phi_{rd} = L_r.I_{rd} + M.I_{sd} \\ \phi_{rq} = L_r.I_{rq} + M.I_{sq} \end{cases} \tag{3}$$

The dynamic equation is:

$$J\frac{d\Omega}{dt} = T_{em} - T_r - K_f\Omega \tag{4}$$

Where the electromagnetic torque (T_{em}) is defined by:

$$T_{em} = p\frac{M}{L_s}(I_{rd}.\phi_{sq} - I_{rq}.\phi_{sd}) \tag{5}$$

Orienting the stator flux along the axis d:

$$\phi_{sd} = \phi_s \quad \text{and} \quad \phi_{sq} = 0$$

T_{em} will be expressed by the following equation:

$$T_{em} = -p\frac{M}{L_s}I_{rq}\phi_{sd}$$

(6)

Knowing that the active power and reactive power of stator will be written as (Rechech.A et al.2022) :

$$\begin{cases} P_s = V_{sd}I_{sd} + V_{sq}I_{sq} \\ Q_s = V_{sd}I_{sq} - V_{sq}I_{sd} \end{cases}$$

(7)

However, considering that the flux is constant and that the resistance of the stator windings is negligible (Ghoudelbourk.S et al.2022 and Praveen kumar.S .2017) , the equations of the components of the voltages across the stator can be written as follows:

$$\begin{cases} V_{sd} = 0 \\ V_{sq} = w_s\phi_s = V_s \end{cases}$$

(8)

From expression (2), we deduce the expressions of currents:

$$\begin{cases} I_{sd} = \frac{M}{L_s}.I_{rd} + \frac{\phi_s}{L_s} \\ I_{sq} = -\frac{M}{L_s}I_{rq} \end{cases}$$

(9)

So, after some arrangements of mathematical expressions of active and reactive powers, we obtain:

$$\begin{cases} P_s = -V_s.\frac{M}{L_s}I_{rq} \\ Q_s = -V_s.\frac{M}{L_s}I_{rd} + .\frac{V_s^2}{L_s.\omega_s} \end{cases}$$

(10)

$$\begin{cases} V_{rd} = R_r.I_{rd} + \sigma.L_r\frac{dI_{rd}}{dt}V_{rd} + S\omega_s(L_r - \frac{M^2}{L_s})I_{rq} \\ V_{rq} = R_r.I_{rq} + \sigma.L_r\frac{dI_{rq}}{dt} - S\omega_s(L_r - \frac{M^2}{L_s})I_{rd} - S\frac{MV}{L_s} \end{cases}$$

(11)

Where S is slip motor and the distribution coefficient is:

$$\sigma = 1 - \frac{M^2}{L_s.L_r}$$

(12)

So, after some arrangements of mathematical expressions of active and reactive powers, we obtain:

$$\begin{cases} V_{rd} + e_{rd} = R_r.I_{rd} + \sigma.L_r\frac{dI_{rd}}{dt} \\ V_{rq} - e_{rq} - e_\phi = R_{rq}.I_{rq} + \sigma.L_r\frac{dI_{rq}}{dt} \end{cases}$$

(13)

With:

$$\begin{cases} e_{rd} = Sw_s(L_r - \frac{M^2}{L_s})I_{rq} \\ e_{rq} = Sw_s(L_r - \frac{M^2}{L_s})I_{rd} \\ e_\phi = S\frac{MV}{L_s} \end{cases}$$

(14)

The analysis of these relations and their presentations by the expression (13) and (14) allows presenting the internal structure of the machine in figure 13.
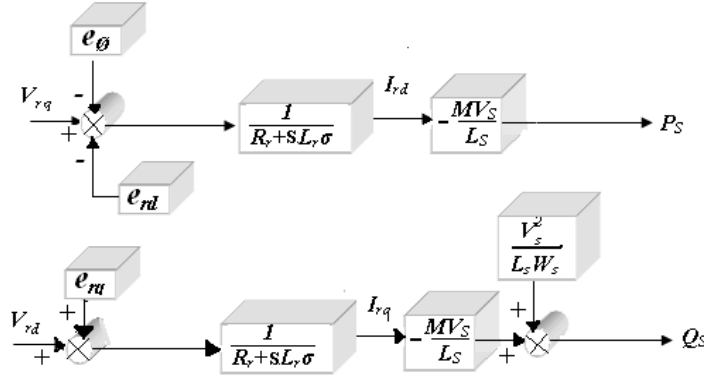
Figure 13.   Internal structure of DFIG

Thus, these powers can be controlled independently. We note that the powers and voltages are bound by a transfer function of the first order. In addition, due to the low value of the slip, it will be possible to establish a vector control without difficulty because the influences of the couplings remain weak, axis parameters d and q can be ordered separately with their own regulators. Fig. 14 shows the control system; we introduced two control loops so that each axis control contains two PI controllers, one for controlling the power and the other for the rotor current (Ayrir.W.2018 et al.2018 and Rezaiguia.D .2023).

This method takes into account the coupling terms and to compensate them. It consists to synthesize the control algorithm from reversing the transfer function of the control system to develop the rotor reference voltages according to the active and reactive power at the stator. The DFIG is fed by a three-phase inverter NPC five-level structure as shown in fig. 15.
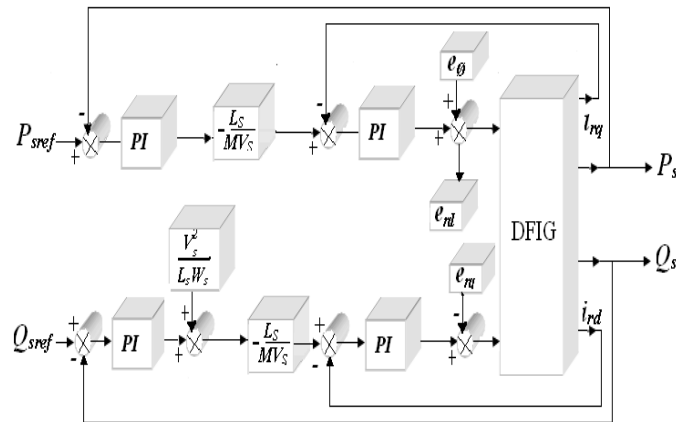
Figure 14. Block diagram of indirect control loop

Fig. 16.a and 17.a shows respectively active and reactive powers references as well as the power available to the stator of the machine. It is noticed that the powers follow their references perfectly. The fig. 17.b and 17.b represent the torque. We clearly see from Fig. 10.c, 11.c, 12.c and 13.c representing the couples zooms as we increase more the level of the inverter over the oscillation and ΔT_e torque decreased and this is a considerable reduction. From Table 4, we conclude that there are fewer harmonics in the current injected into the network and less oscillations in the torque when the level is higher. Fig. 16.a and 17.a shows respectively active and reactive powers references as well as the power available to the stator of the machine. It is noticed that the powers follow their references perfectly. The fig. 17.a and 17.b represent the torque. We clearly see from Fig. 16.a and 17.c representing the couples as we increase more the level of the inverter over the oscillation and ΔT_e torque decreased and this is a considerable reduction. From Table 2, we conclude that there are fewer harmonics in the current injected into the network and less oscillations in the torque when the level inverters is higher.
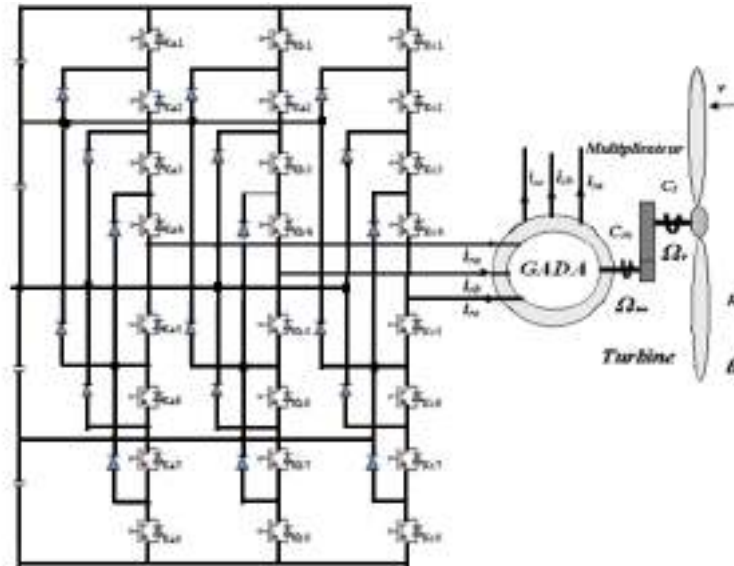
Figure 15. DFIG fed by a five levels inverter
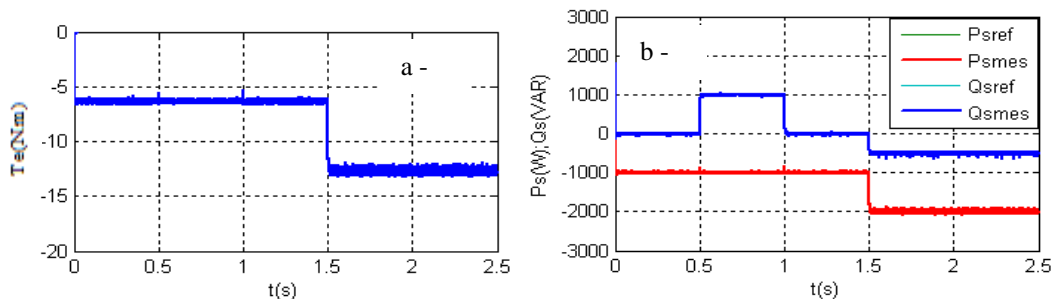
Figure 16. DFIG Power by two levels inverter

a- active powers; b- reactive powers
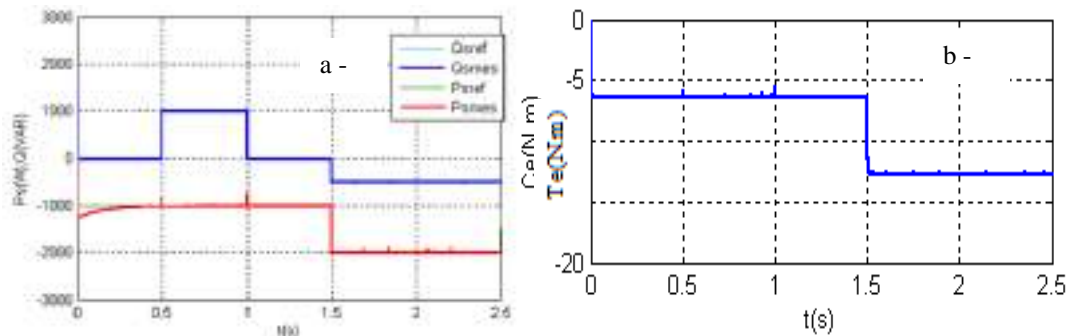
Figure 17. DFIG Power by five levels inverter

a-   active powers; b- reactive powers

Table 2. Comparison Of The Stator Current THD%

And ΔTe

Inverter	2 Level	5 Level
THD%	1.93	0 .9 8
ΔT_e(N.m)	0.6	0.25

IV. Simulation the Electrical Hybrid System by HOMER

HOMER (Hybrid Optimization Model for Electric Renewable) software plays a crucial role in optimizing these hybrid systems. Used to simulate and optimize energy configurations, HOMER helps create autonomous solutions by evaluating the performance and life cycle costs of energy systems. It performs hundreds of hourly simulations to determine the best match between supply and demand, taking into account parameters such as energy cost and investment costs. The sensitivity analyzes carried out by HOMER also make it possible to assess the impact of variables such as solar radiation and wind speed on the system configuration.

This article aims to demonstrate the robustness of HOMER in the evaluation of technical, economic, and environmental criteria of hybrid systems. By showcasing the benefits of renewable energy systems, such as local clean energy production and reduced battery storage requirements, this study highlights the reliability and economic viability of hybrid systems, while contributing to the fight against global warming. To maximize the efficiency of renewable hybrid energy systems (RHES), it is essential to focus on resource availability, sunlight duration, climate conditions and site location.

VI.1 Site location

The Badji Mokhtar University Residence is located in Annaba, a coastal town in northeastern Algeria. Annaba, known for its Mediterranean climate, offers variable weather conditions. The university residence, integrated into the campus, offers modern facilities for students, including comfortable accommodation, study spaces,

computer rooms, and leisure facilities. For the development of the hybrid system, the latitude and longitude coordinates of this site are specified in the figure below.

Figure 18. Site location selected for optimization purpose

VI.2 Load profile

Energy consumption is evaluated according to the seasons. In winter, radiators are used, while air conditioners are turned off. In summer, although the university is on vacation, consumption for air conditioning increases due to the presence of international students. In fall and spring, energy requirements are reduced, and outdoor lighting remains constant all year round. Consumption data is simulated in HOMER, showing daily, seasonal and annual variations. The average daily consumption is 756.25 kWh, with a peak load of 279.88 kW, taking into account random variations. Figure 19 illustrates the seasonal variation of the load profil.
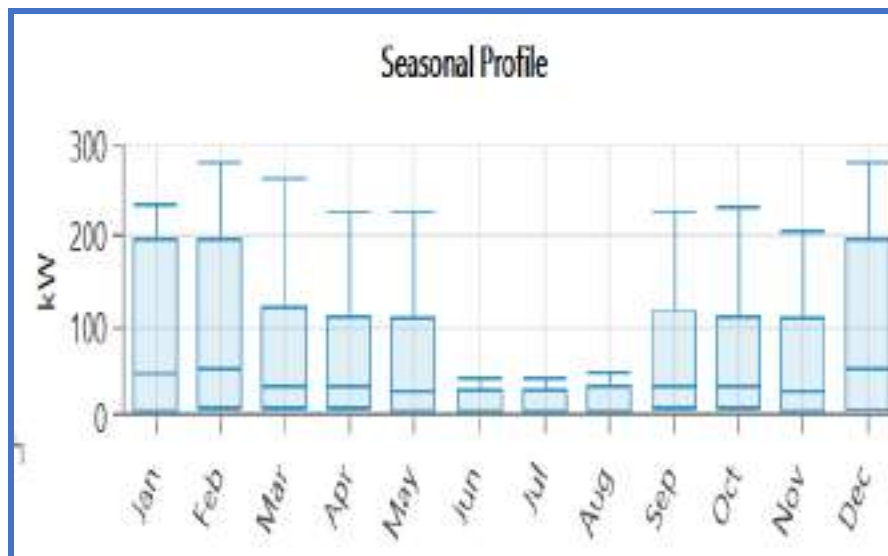
Figure 19. Seasonal load curve (HOMER) see

VI.3 Resources data

Solar and wind resource data, obtained via HOMER from NASA's Global Energy Resources Forecast, shows that the annual average solar radiation in Sidi Amar is 4.53 kWh/m²/day. From March to October, solar radiation is sufficient for optimal exploitation of solar energy, while it is low from November to January. Regarding wind resources, the wind speed measured at a height of 50 m above the surface shows an annual average of 5.02 m/s. The lowest wind speed of 3.18 m/s is recorded in August, and the highest of 6.09 m/s is observed in December. These data, presented in Figures 20 and 21, make it possible to determine the optimal periods for the exploitation of solar and wind energy in Sidi Amar.
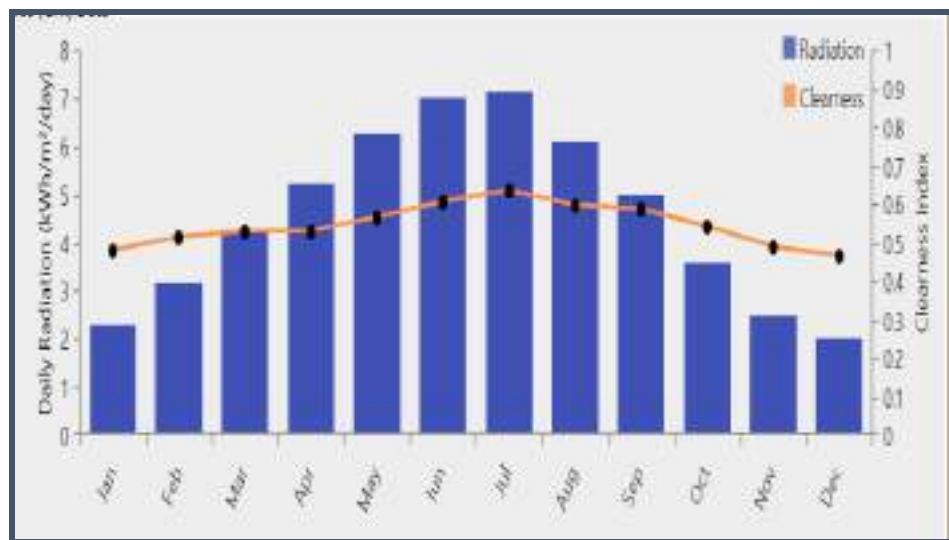
Figure 20. Sidi Amar. Monthly daily solar radiation and clearness-index

Figure 21. Average Wind speed data for Sidi Amar

VI.3 System design

In this work, a combination of technologies was considered, including wind turbines, photovoltaic systems, batteries, converters, and a backup biodiesel generator, or figure 22 presents the schematic diagram of the system configuration. The HOMER software evaluates various factors such as technical feasibility, climate, load consumption, diesel prices, as well as development and energy costs. Depending on these parameters, HOMER tests several configurations to determine the most suitable solution.
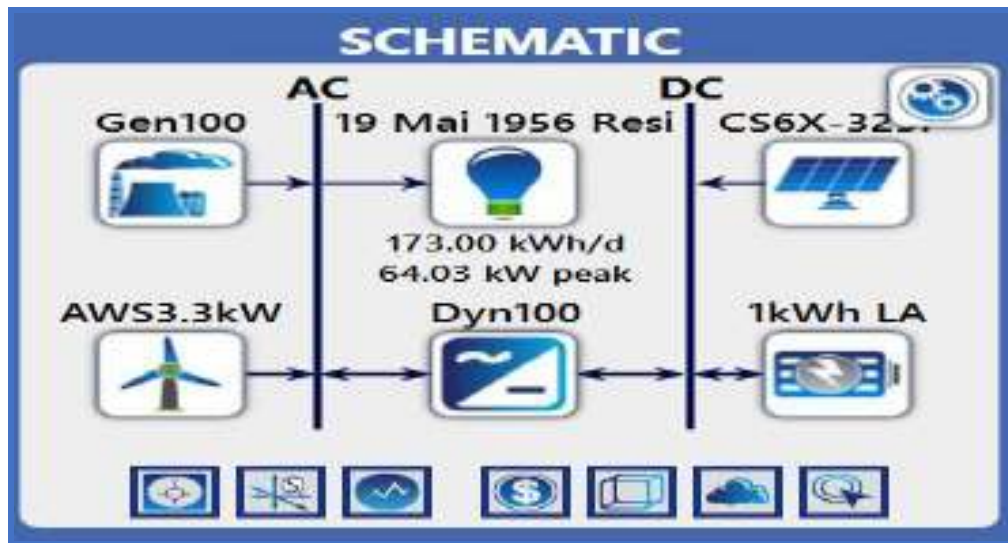
Figure 22. Design of the proposed configuration

VI.4 Properties of Components

The components used in this study were chosen straight from the HOMER library, and each has its own set of costs, capacity, lifespan, and other properties.

a. Solar PV properties

The Canadian-Solar Maxpower CS6X-325P PV modules was selected to arrive at the most optimal solution. Due to conditions such as ambient temperature influence, dust, shading, wiring losses, and PV degradation, the PV panels are bound to suffer losses. This PV's derating factor is 88%, and its temperature coefficient is -0.41% per degree Celsius. The efficiency of this PV system in standard conditions is 16.94%. There are 72 polycrystalline cells in this PV module with a capacity of 325 watts. The PV system is set at $600 per kW, with an O&M fee of $10 per year.

b. Wind Turbine properties

For the simulations in this study, an AWS HC 3.3kW rated capacity WT is used, and the capital cost is set at $

7000 per kW, replacement cost at $ 7000 and O&M at $20 per year for economic analysis, with an O&M cost of $ 100 per year. Hub height of this turbine is 12 m and life span of 20 years.

c. Generator properties

The generator considered for this simulation is the Generic 100kW Fixed Capacity Genset. The capacity of this generator is 100kW and cost about $40 000. The minimum load ratio considered is 25% for an operating life time of 15,000 hours. The O&M cost as $2 per hour. Fuel cost of $1 per liter.

d. Battery Storage Properties

For this simulation, a generic 1kWh lead acid battery with a nominal voltage of 12V, a maximum capacity of 83.4 Ah, an efficiency of 80%, a maximum charge current of 16.7A, and a lifetime of 10 years was used. As both the PV and the battery are connected to the DC bus in one configuration, their output voltages should be the same, thus the battery's 12V is connected in three strings to provide a 36V voltage, just like the PV system voltage. The cost of this battery is defined at $ 500, and its initial state of charge is 100%, with a minimum state of charge of 40%.

c. Converter

A bi-directional converter allows power to flow in both directions, making it easier to convert AC to DC for battery charging and supply AC to supply AC loads by converting DC to AC. A Dynapower SPS-100 with a capacity of 100 kW and an efficiency of 96.5% with a relative capacity of 100% was investigated. The converter has a 15-year life expectancy, with a considered capital cost of $ 600, a replacement cost of $ 500, and an annual O&M expense of $ 30. The capacity of this converter is slightly higher (approximately 19%) than the peak load.

VI.5 Economics Analysis

Net Present Cost (NPC) and the Levelized Cost of Energy or Cost of Energy (COE) are the two key economic factors utilized in the HOMER tool for economic analysis and optimal configurations. NPC is the most cost-effective metric in the HOMER tool for optimization

NPC is the total cost and revenue of a project across its whole life cycle, and it is represented by the expression;

$$NPC = \frac{CT-ann}{CRF(i,t)} \qquad (15)$$

Where; $CT-ann$ is the annualized total cost of the system, CRF the capital recovery factor, i the annual interest rate or discount rate, t the project life time. The annual effective interest rate is a percentage of the balance at the

end of the year in which interest is paid or earned and it is represented as;

$$i = \frac{i\prime - f}{1 + f} \qquad (16)$$

Where; $i\prime$ is the nominal interest rate, f is the annual inflation rate.

The capital recovery factor is the yearly payments required at a discount rate to achieve present value after several years. It is provided by;

$$CRF(i,n) = \frac{i(1+n)n}{(1+n)\,n - 1} \qquad (17)$$

Where; n = number of years.

The simulation is performed by comparing the optimal configuration from available AC and DC hybrid systems i.e., WT, Diesel Gen-set, PV system, and Battery storage system. The simulation was performed for a project lifetime of 25 years. HOMER software simulated 6234 solutions in about 15 min and found 4428 feasible solutions based on geographic location, technical feasibility, and Economics. It took into consideration various constraints considered while modeling each system. The HOMER results in show cases for Optimized results and sensitivity analysis. The cases are as shown below:

Table 3. The simulation results using the HOMER simulator

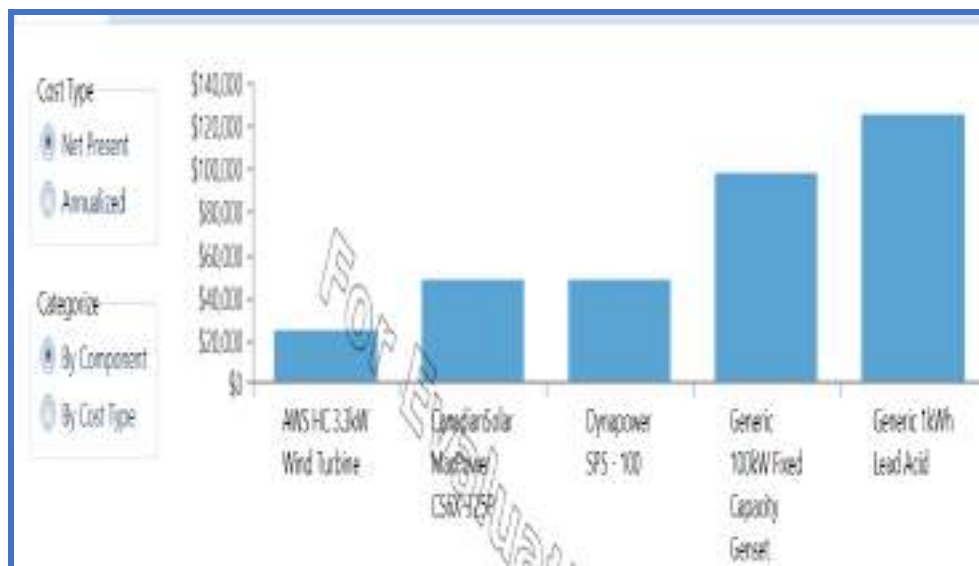| Component	PV (kW)	Wind turbine (kW)	Diesel generator (kW)	Battery storage (KW)	Converter (kW)	NPC ($)	COE ($/kWh)	Operating Costs ($/year)	Initial Capital ($)
Value	66.2	3	100	134	41.5	344,541	0.42	11,752	192,611

Figure 23. Cost summary standalone hybrid system

From Table III, the simulation findings also show a $ 334,540.70 NPC, a $ 0.4221 LCOE, and a $ 11,752.43 annual operating cost. Since not only renewable energy sources were used in the scenario, the renewable energy fraction is 82.5%. Fig III.8 summarizes the total cost of the standalone hybrid system, indicating details of the economic variables of each component that adds up to the NPC value. Compared to the other components in this design, the overall cost of a generic lead-acid battery is the highest.

Conclusion

In this work, our attention was focused on modeling, simulating and analyzing a optimization of energy for hybrid PV–Wind turbine System by the Used of five levels Inverters. The connection of several PVs to the power grid through multi-level inverters reduces the total harmonic distortion (THD), thus improving the quality of electrical energy. Their use proves to be an optimal solution for the connection of the photovoltaic system. To the electrical networks and they make it possible to increase the power delivered by the photovoltaic generator. The use of the latter in the areas of Photovoltaic high voltage and strong power allows you to solving simultaneously the difficulties relating to congestion and to the command of groupings of inverters at two levels generally used in this type of applications.   Separate control of powers for the DFIG are used was made for power two and five levels. Performance analysis and power comparison for these levels shows that the DFIG powered by the inverter with five-level offers more opportunities and improves system responses by reducing the harmonics of the stator current delivered to the grid and reduces the ripples of the couple. And the HOMER simulation provides the necessary flexibility in carrying simulations with efficient tools. This helps in understanding the system and constructing different models. The hybrid system can reduce the dependency on fossil fuels to great extent and supply individual power to AC or DC systems as required. The hybrid optimized systems are capable of providing the energy efficiently between their respective busses. The HOMER simulation carried out for this project takes into account the technical feasibility of the system and economic analysis of the system.

References

Adjei-Saforo.EK , Frimpong.EA, Effah.FB,. Adam.M, Ebrahimpanah.S et Hongsheng,S . (2022). Méthode de contrôle prédictif du courant par modèle avec performances améliorées pour un onduleur à pont en H en cascade triphasé à cinq niveaux connecté au réseau, 2022 *IEEE PES/IAS PowerAfrica , Kigali, Rwanda*, pp. 1-5.

Ayrir.W., Ourahou.M, and Haddi.A .(2018) ., DFIG stator reactive and active power control based fuzzy logic *International journal of circuits, systems and signal* processing Volume 12.

Dib.D ; Mordjaoui.M ., & S.Ghoudelbourk.S (2015). Contribution to the Performance of GPV Systems by an Efficient MPPT Control. Conference: *3rd International Renewable and Sustainable Energy Conference – IRSEC'15*, At Merrakech & Ouarzazet, Morroco.

Ghoudelbourk.S., Azar.AT., D Dib.D.(2021) .Three-level (NPC) shunt active power filter based on fuzzy logic and fractional-order PI controller. *International Journal of Automation and Control* 15 (2), 149-169.

Ghoudelbourk.S, Ben Si Ali.N & Rechach.A .(2022) . Hybrid Energy Storage System (HESS) for Standalone PV Microgrid. *WESC-2022 The 2nd World Energy Storage Conference December 18-21, 2022 Istanbul, Turkiye*.

Rechach, A., Ghoudelbourk, S., Larbi, M.M.: Impact of choice of neutralpoint clamped and h-bridge multilevel inverters for PV systems. Eur. J.Electr. Eng. 24(14), (2022)

Hasan. B.; Nabin. S.; Keith. C.H.; Tapas.K.M ,(2013). Numerical modeling and experimental validation of a low concentrating photovoltaic system,. Sol. *Energy Mater*. Sol. Cells , 113, 201–219.

Park.H., Yong-Jung .K and Hyosung.K, (2016), PV Cell Model by Single-diode Electrical Equivalent Circuit, *J.Electr Eng Technol* ; 11: 1921-718.

Praveen kumar.S ,. Ramprasad.R .(2017) . A Five Level Diode Clamped Multilevel Inverter System for Improving Dynamic Stability of a Grid Connected Wind Power System, , *International Journal of Scientific Engineering and Technology Research* Volume.06, IssueNo.26, Pages: 5147-5152.

Rajesh. Ka,A.D Kulkarnib.Ka ., & al (2015). Modeling and Simulation of Solar PV and DFIG Based Wind Hybrid System, SMART GRID Technologies, August 6-8, 2015 *Procedia Technology* 21 667 – 675.

Rechach.A, Ghoudelbourk.S and Louafi.L. .(2022) . Contribution to the improvement of the wind turbine energy quality; *1st International conference on applied chemistry and renewable energie ACREIC 2022;26:28 Nov; 2022 TEBESSA*.

Rezaiguia .D; S Ghoudelbourk.(2023) .Study and Simulation of the Hybrid System Composed of Solar Panels and Fuel Cell; *First International Conference on Advancec in Electrical and Computer Engineering(ICAECE'2023)*. Tebessa.

Wu.Y.T and Porte-Agel.F (2011). .,Large-Eddy Simulation of Wind-Turbine Wakes,: *Evaluation of Turbine Parametrisations, Bound-Lay. Meteorol.* 138, 345.

Transforming PV Power Systems: Cascaded NPC Multilevel Inverter Topology for Grid Interactivity without Transformers

Noureddine Ould cherchali

Research Laboratory in Electrical Engineering and Automatic (LREA) University of Medea, Medea, Algeria

Ibrahim Bentchikou

Department of Electrical Engineering, Djilali Bounaama Khemis Miliana University, Ain Defla, Algeria

Mohamed Redha Skender

Department of Electrical Engineering, Faculty of Technology Medea, Algeria, https://orcid.org/0000-0002-6572-8102

Abstract: In this paper, we showcase a simulation model that demonstrates the operation of a photovoltaic power system seamlessly integrated with the grid, utilizing a sophisticated three-phase multilevel voltage source inverter. The system proposed in this study consists of a boost converter and a grid, with the photovoltaic power source connected through a five-level NPC voltage source inverter. To track the maximum power points (MPPs) of the photovoltaic source, a fuzzy logic controller (FLC) is employed. The electrical energy generated by the photovoltaic source is converted from DC to AC and injected into the grid through the multilevel inverter. To maintain a constant voltage on the DC bus and generate the necessary switching commands for the multilevel inverter, PI controllers are utilized to control the current. Inductif auxiliary circuit is used to resolve the DC bus balancing problem. Additionally, an LC filter is incorporated at the output of the multilevel inverter to mitigate switching noise. MATLAB/Simulink is used for the simulation studies. The results demonstrate that the maximum power point tracking algorithm suggested in this study demonstrates a quick transient response. Additionally, the output currents generated by the multilevel inverter display a sinusoidal pattern and remain in sync with the line voltages.

Keywords: DC bus balancing, fuzzy logic control, grid, inductif auxiliary circuit, MPPTs, multilevel

Introduction

Sustainable energy sources will become the only reliable energy supply in the next years for their low influence

on the environment and independence from fossil and nuclear fuels. In the present day, Photovoltaic systems, characterized by their maintenance-free nature, lack of pollution emissions, modular design, and global availability, are widely employed in various applications. They are considered among the foremost and most important sources of sustainable energy [1][2].

Grid-connected photovoltaic (PV) systems convert irradiation into electricity energy and supply the energy into the grid directly by grid inverter, without storing energy by battery. The progress in the performance and dependability of these systems is crucial for Photovoltaic energy to maintain the further spread, as increasingly more scientists have focused on the topologies and control of the inverters in Photovoltaic systems [3]-[7].

The power demand has significantly increased in recent years until it reaches around some megawatts (about 10 MW), for low and medium tension. The use of conventional converters in two levels, high switching frequencies, is limited to the power level due to significant losses caused by the switching of the switches. Because of that multilevel inverter has been set up and used since 1975 [8].

The multilevel inverter has several advantages, including exceptional waveform quality. Multilevel converters have the capability to produce output voltages with minimal total harmonic distortion (THD) and mitigate the dV/dt stresses, thereby contributing to the reduction of electromagnetic compatibility (EMC) issues. [9].

It is in this order of ideas, in this paper, we want to analyze a cascade consisting of a photovoltaic source and a five-levels NPC topology inverter applied to connect this photovoltaic power system to the grid.

We start with a modelling of photovoltaic source with the application of a Fuzzy Logic Control (FLC) based MPPT technique. The inverter is then modelled and driven by a SPWM strategy. The problem of this type of multilevel inverter is the unbalance of the input DC bus voltages of the inverter. for that, we will study the use of an inductive balancing circuit to solve the stability problem. And we will simulate the all system with Matlab/Similink (SimPower toolbox).

Photovoltaic System

The tsudy of Photovoltaic System will be done in this part

Modeling of solar cell

The solar cell model falls into the category of a p-n semiconductor junction, similar to a diode. When illuminated by light, it produces a direct current (DC). Essentially, a solar cell functions as a specialized diode with a larger junction area than a standard diode. It's well-established that the current generated by the solar cell is contingent on factors such as solar irradiance, temperature, and load current. Figure 1 illustrates the standard equivalent electrical circuit of a solar cell [10].

The model of PV pannel and output current I_{PV} is described by:

$$I_{PV} = N_p.I_{ph} - N_p.I_0 \left[e^{\left(q. \frac{V_{PV} + I_{PV}.R_S}{N_S AKT} \right)} - 1 \right] \tag{1}$$

For the PV saturation current I_0,

$$I_0 = I_{rs}.\left[\frac{T}{T_r} \right]^3 e^{\left(q. \frac{E_g}{AK\left(\frac{1}{T_r} - \frac{1}{T} \right)} \right)} \tag{2}$$

The PV reverse saturation current, Irs, is described by

$$I_{rs} = \frac{I_{scr}}{e^{\left(q. \frac{V_{OC}}{N_S AKT} \right)} - 1} \tag{3}$$

For the PV photocurrent, Iph, one has

$$I_{ph} = [I_{scr} + K_i(T - T_r)] \frac{S}{1000} \tag{4}$$

Where:

Tr: The reference temperature = 298K

T: The module operating temperature (K)

I_{ph} Light generated current (A).

I_{PV} : the cell current (A).

I_{SC} : the light generated current (A).

R_S : the cell series resistance (ohms).

R_{sh} : the cell shunt resistance (ohms).

V_{PV} : Cell voltage (V).

q : Electron charge = -1.6 $\times 10^{-19}$ C

I_{scr} : Short Circuit Current

K_i: Temperature Coefficient of Isc

E_g: Band gap for silicon = 1.1 eV

I_{scr} Short Circuit Current

K_i: Temperature Coefficient of Isc

E_g: Band gap for silicon = 1.1 eV

K_V: Temperature Coefficient of Voc
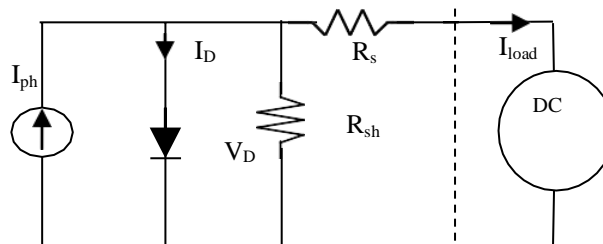
Figure 1. Typical circuit of PV solar cell

Figure 2 depicts the performance of a simulated photovoltaic panel as it responds to changes in irradiation while maintaining a consistent temperature. In reality, a photovoltaic generator connected to a load can function within a wide spectrum of voltage and current levels, contingent upon the prevailing environmental conditions.

So, whenever there is a change in irradiation or temperature, the MPPT controller needs to adapt and follow the updated maximum power point (MPP) on its corresponding curve.
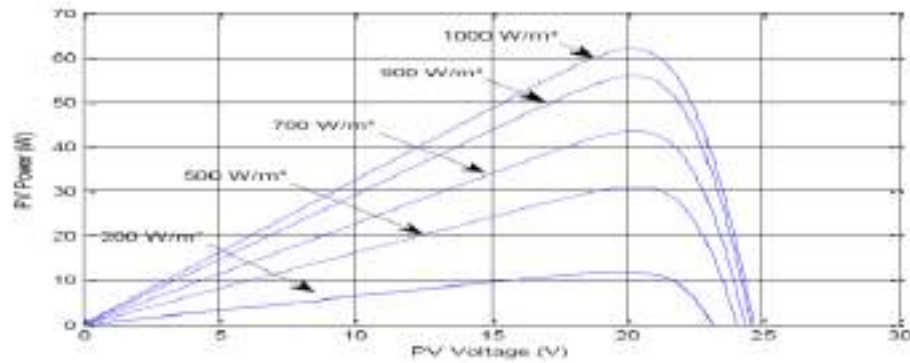
MPPT using Fuzzy Logic Control (Fuzzy MPPT)

In general, MPPT is employed to seek and lock onto the PV system's maximum power point, ensuring the generation of the highest available power output. The effectiveness of MPPT relies on both the MPPT control algorithm and the MPPT circuit.

Fuzzy logic controllers have been incorporated for tracking the maximum power point (MPP) in PV systems, as outlined in references [10]-[11]. Fuzzy Logic Control (FLC) offers various advantages, including improved performance, robustness, and a straightforward design approach. The FLC-based MPPT method doesn't require precise model knowledge, although it does necessitate a comprehensive understanding of the Photovoltaic system's operation by the designer.

The depicted Fuzzy Logic MPPT Controller, as presented in Figure 3, comprises two input parameters and one output parameter. These two FLC input variables are defined as the error E and the rate of error change CE, both evaluated at discrete time instances denoted as k.

$$E(k) = \frac{P_{ph}(k) - P_{ph}(k-1)}{V_{ph}(k) - V_{ph}(k-1)} \tag{5}$$

$$CE(k) = E(k) - E(k-1) \tag{6}$$

Here, $P_{ph}(k)$ represents the instantaneous power output of the photovoltaic generator. The input variable E(k) indicates whether the operating point of the load at time k is positioned to the right or left of the Maximum Power Point (MPP) on the P-V characteristic curve, while the input variable CE(k) signifies the direction of movement

of the load operating point.
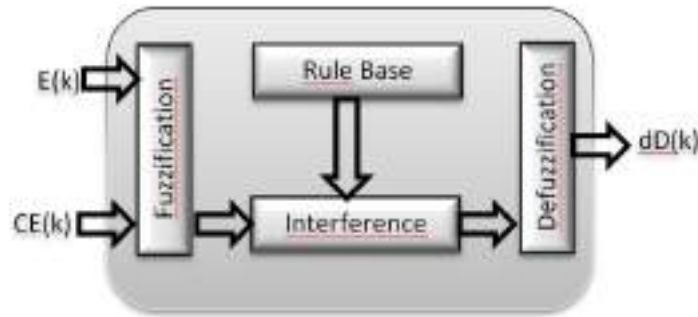
Figure 3. Structure of a FLC

Figure 3. presents the membership functions for both the antecedent and consequent aspects.

The universe of discourse for the first and the second input variables (the error E and change of error CE) are same. They are divided into five Fuzzy sets: NB (Negative Big), NS (Negative Small), ZE (Zero), PS (Positive Small), and PB (Positive Big).

The duty cycle, referred to as dD, is categorized into five fuzzy sets within its universe of discourse: NB, NS, ZE, PS, and PB.

(a)

(b)

(c)
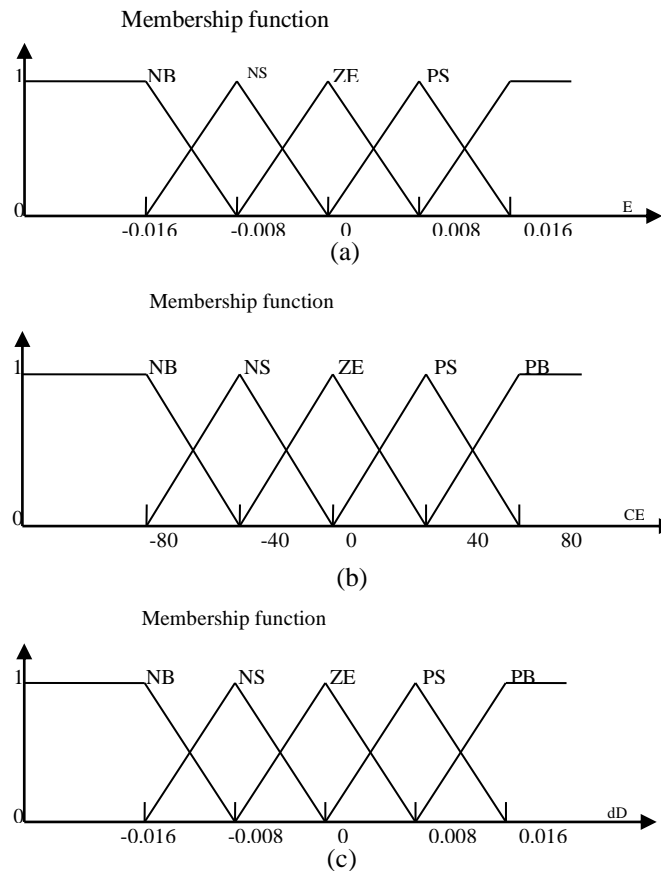
Figure 4. Membership function of (a) error € change error CB (c) duty ratio D.

The fuzzy inference process is implemented through Mamdani's method, and the calculation of the output,

specifically the duty cycle denoted as dD, is calculated using the Defuzzifier block (8).

The Defuzzifier block employs the centroid method to determine the output of this FLC, which corresponds to the duty cycle. This duty cycle output is generated based on the rules defined in TABLE I and is subsequently transmitted to the DC-DC converter.

$$dD_0 = \frac{\sum_{j=1}^{n} \mu(D_j) - D_j}{\sum_{j=1}^{n} \mu(D_j)} \tag{7}$$

Table 1. Fuzzy rule table

CE E	NB	NS	ZE	PS	PB
NB	ZE	ZE	PB	PB	PB
NS	ZE	ZE	PS	PS	PS
ZE	PS	ZE	ZE	ZE	NS
PS	NS	NS	NS	ZE	ZE
PB	NB	NB	NB	ZE	ZE

NPC Five Levels Inverter

Now the NPC study of five-level three-phase inverter will presented in this part.

Modelling of NPC Five Levels Inverter

Figure 5 illustrates the NPC topology of a five-level three-phase inverter, as detailed in references [12]-[14]. The structure's symmetry permits modeling by leg. Consequently, the initial step involves establishing a comprehensive model for a single leg without making any assumptions about the control.

In order to prevent voltage sources from creating short-circuits through the conduction of multiple switches, and to ensure full control over the converter, a complementary control strategy is employed. The optimal control strategy is defined as follows:

$$\begin{cases} Fk4 = 1 - F_{k2} \\ Fk5 = 1 - F_{k1} \\ Fk6 = 1 - F_{k3} \end{cases} \tag{8}$$

For a given leg, denoted as "k," the interconnections of the half-legs are expressed in terms of switch connections, as shown below, with "k" taking on values of 1, 2, and 3:

$$\begin{cases} F^b_{k1} = F_{k1}.F_{k2}.F_{k3} \\ F^b_{k0} = F_{k4}.F_{k5}.F_{k6} \end{cases} \tag{9}$$
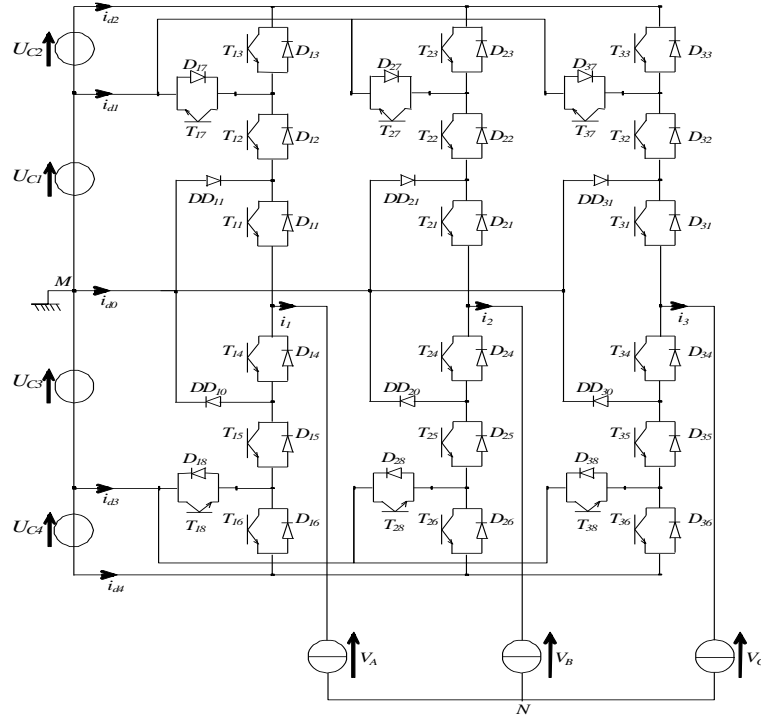
Figure 5. NPC five-levels three-phase inverter topology.

The connection configurations of the switches arranged in parallel are specified as follows:

$$\begin{cases} F_{k7} = F_{k1}F_{k2}(1-F_{k3}) \\ F_{k8} = F_{k4}F_{k5}(1-F_{k6}) \end{cases} \tag{10}$$

The potentials at nodes A, B, and C with respect to the central point M, assuming $U_{C1} = U_{C2} = U_{C3} = U_{C4} = U_C$, are described by the following system:

$$\begin{bmatrix} V_{AM} \\ V_{BM} \\ V_{CM} \end{bmatrix} = \begin{bmatrix} F_{17} + 2F^b_{11} - F_{18} - 2F^b_{10} \\ F_{27} + 2F^b_{21} - F_{28} - 2F^b_{20} \\ F_{37} + 2F^b_{31} - F_{38} - 2F^b_{30} \end{bmatrix} U_c \tag{11}$$

The simple voltages at the boundaries of the load are given by the following system:

The voltage values (V_A, V_B and V_C) at the edges of the load are defined by the following system:

$$\begin{bmatrix} V_A \\ V_B \\ V_C \end{bmatrix} = \frac{1}{3} \begin{bmatrix} 2 & -1 & -1 \\ -1 & 2 & -1 \\ -1 & -1 & 2 \end{bmatrix} \left\{ \begin{bmatrix} F_{17} + 2F^b_{11} - F_{18} - 2F^b_{10} \\ F_{27} + 2F^b_{21} - F_{28} - 2F^b_{20} \\ F_{37} + 2F^b_{31} - F_{38} - 2F^b_{30} \end{bmatrix} U_c \right\} \tag{12}$$

SPWM strategy of the five level NPC VSI

In this section, we will introduce the sinusoidal pulse width modulation (SPWM) strategy employing four triangular bipolar carriers, as depicted in Figure 6 [12]. This strategy need four bipolar triangular carriers (Up1, Up2, Up3, Up4) that are phase-shifted by one quarter of the period (Tp/4) relative to each other. This strategy is distinguished by two parameters the first is called the modulation index denoted as *m* and the second is the modulation index *r*:

$$m = \frac{f_p}{f} \quad\quad (13)$$

$$r = \frac{V_m}{U_{pm}} \quad\quad (14)$$
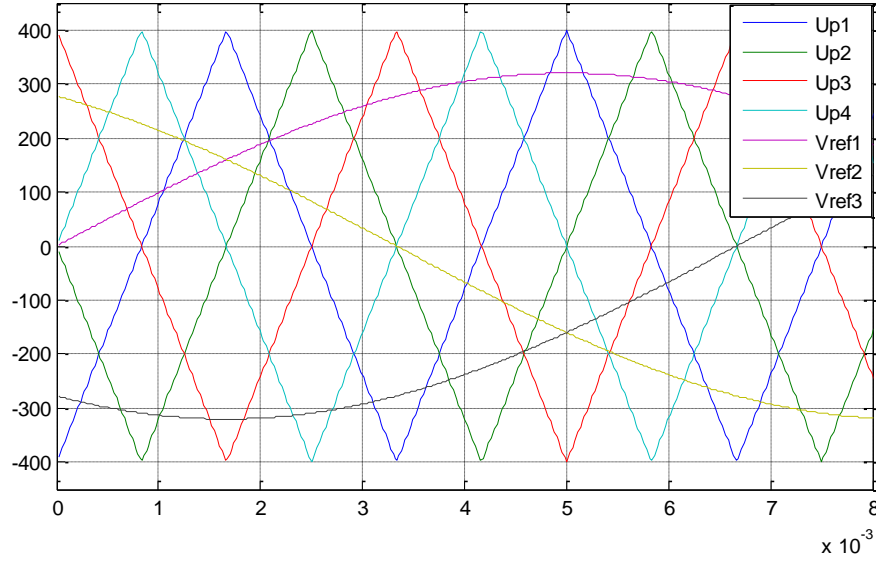
Figure 6. Different signals for four carriers SPWM strategy (m = 2, r = 0.8).

Clamping inductive bridge to stabilize the DC LinkCapacitor

Balancing the tension between U_{C1} to U_{C4} is a necessity for the correct functioning of the multilevel NPC inverter. For that auxiliary balancing circuits are employed, with the most widely recognized one being resistance-based [5],[13]. Its fundamental concept revolves around dissipating energy in resistors through Joule heating [14]. However, when dealing with photovoltaic sources, the objective is to optimize the performance of the cascade, as the energy generated carries a high economic value. To achieve this, we will implement an inductive balancing circuit, as illustrated in Figure 7 [14]. Its underlying principle revolves around transferring energy from the capacitor with the higher charge to the discharged capacitor through the utilization of a coil.
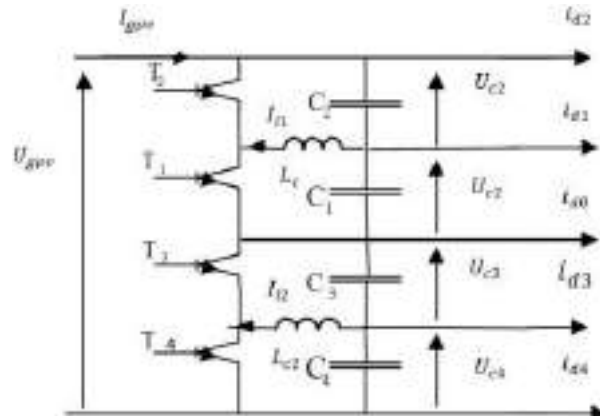
The description of the inductive circuit's modeling is presented below:

$$\begin{cases} L_{C1} \frac{di_{L1}}{dt} = S_1 U_{C1} - S_2 U_{C2} \\ L_{C2} \frac{di_{L2}}{dt} = S_4 U_{C4} - S_3 U_{C3} \end{cases} \tag{15}$$

The voltage levels across the capacitors can be described using the following set of equations:

$$\begin{cases} C_2 \frac{dU_{c2}}{dt} = I_{gpv} - i_{d2} - S_2 i_{L2} \\ C_1 \frac{dU_{c1}}{dt} = I_{gpv} - i_{d1} - i_{d2} - S_1 i_{c1} \\ C_3 \frac{dU_{c3}}{dt} = I_{gpv} + i_{d3} + i_{d4} - S_3 i_{c2} \\ C_4 \frac{dU_{c4}}{dt} = I_{gpv} + i_{d4} + S_4 i_{c2} \end{cases} \tag{16}$$

Such as S_i (i = 1,2,3,4) orders for the transistors T_i, (i = 1,2,3,4) of The algorithm for the balancing circuit is outlined as follows:

$$\begin{cases} U_{c2} > U_{c1} \Rightarrow S_1 = 0 \ and \ S_2 = 1 \\ U_{c2} < U_{c1} \Rightarrow S_1 = 1 \ and \ S_2 = 0 \\ U_{c3} > U_{c4} \Rightarrow S_3 = 1 \ and \ S_4 = 0 \\ U_{c3} < U_{c4} \Rightarrow S_3 = 0 \ and \ S_4 = 1 \end{cases} \tag{17}$$

Simulation Results and Discussion

The detailed scheme of the system layout can be observed in Figure 8. It comprises a solar array, a Boost DC-DC converter with FFC-MPPT control, a DC-link, a five-level three-phase NPC topology inverter, an Inductive Clamping circuit, RLs filter, and all are connectet to the grid. To achieve the necessary solar voltage and power rating, the solar cells are arranged in a series-parallel configuration (6X6). The Inductive Clamping bridge serves to stabilize the DC bus voltage. The multilevel three-phase inverter, along with the filter inductor, transforms a DC input voltage into an AC sinusoidal voltage through precise switch control signals, ensuring that the output current is in sync with the grid voltage, thereby achieving a unity power factor.
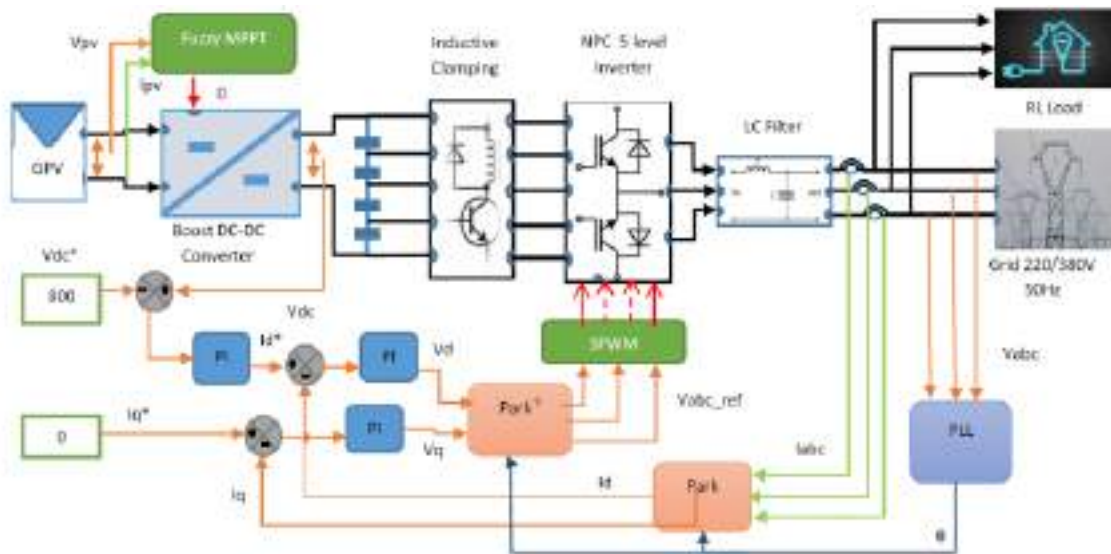
Figure 8. The principle scheme of system. (three-phase grid-connected photovoltaic system)

An MPPT technique based on Fuzzy Logic Control (FLC) is employed for tracking the Maximum Power Point (MPP) of the PV system, as outlined in reference [15]-[17]. Furthermore, the DC bus voltage is regulated using this voltage controller to fine-tune the inverter's output power. To ensure that the inverter's output current aligns with the grid's frequency and phase, a Phase-Locked Loop (PLL) algorithm is implemented. The PLL circuit is also utilized in the generation of reference currents. Additionally, a conventional Proportional-Integral (PI) current controller is employed to shape the inverter's output current.

To evaluate the effectiveness of the system and the performance of the MPPT controller, various parameters including solar irradiation levels, total output power of PV modules, DC bus voltage (Vdc), input DC-bus voltages (U_{C1}, U_{C2}, U_{C3}, and U_{C4}), grid voltage, and inverter output current are illustrated in Figure 9.

As seen from Figure 9.a, irradiation level is changed 1000 W/m^2 to 700 W/m^2 slowly. The used MPPT technique track very well the MPP as shown in Figure .9.b.

DC bus reference voltage is Vdc_ref=800V. For reactive power equals to zero, we chose Iq_ref = 0 (Figure 9). The used voltage and currents controllers (type PI) keep the voltage constant and equal to its reference (Figure 9.c), the Iq equal to zero and the Id follows quietly its reference (Id_ref) as shown in Figure 9.e. When the irradiation decreases, the Id decrease too.

The application of the inductive clamping circuit shows parfect balancing between U_{C1} to U_{C4} (Figure 9.d). With less ripple, and we don't have a power lose compared to resistive balancing circuit [13].

The inverter output current, denoted as Ia, exhibits a sinusoidal waveform and maintains synchronization with the inverter output voltage. Its Total Harmonic Distortion (THD) level is quantified at 1.81%, as depicted in Figure 9.f and Figure 9.g (where the current I_a is multiplied by a factor of 20).
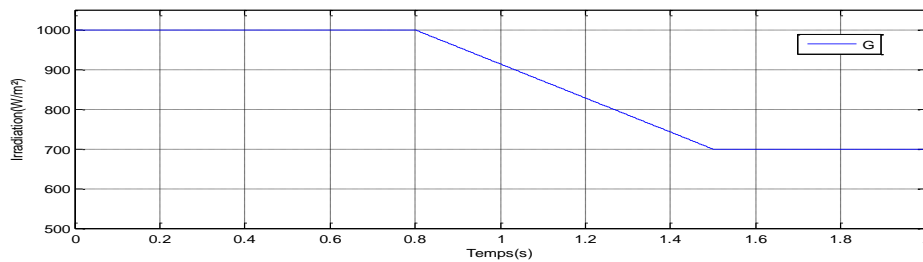
(a) Irradiation (G)
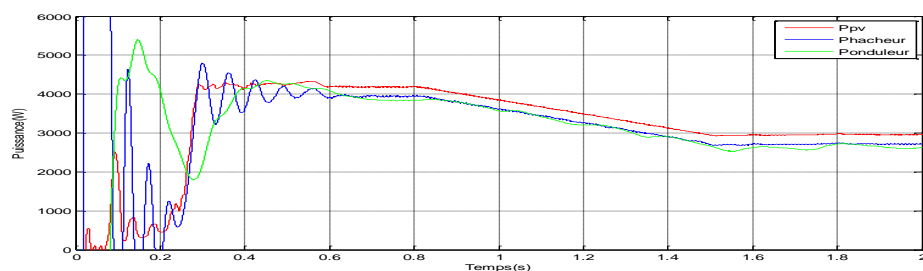
(b) Panel Power (P_{pv})
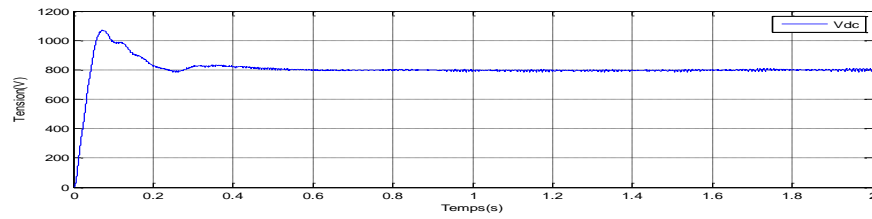
(c) DC-bus voltage Vdc
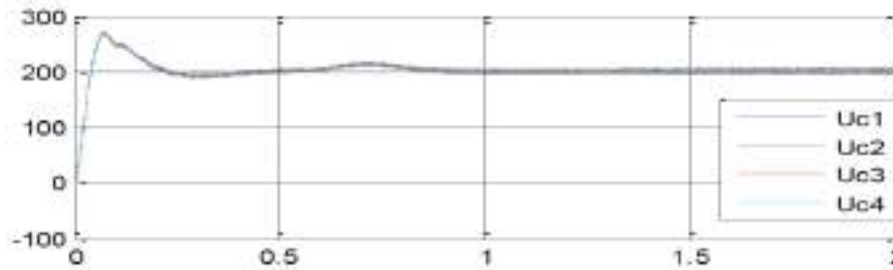
(d) The input DC-bus voltages UC1, UC2 , UC3 and UC4
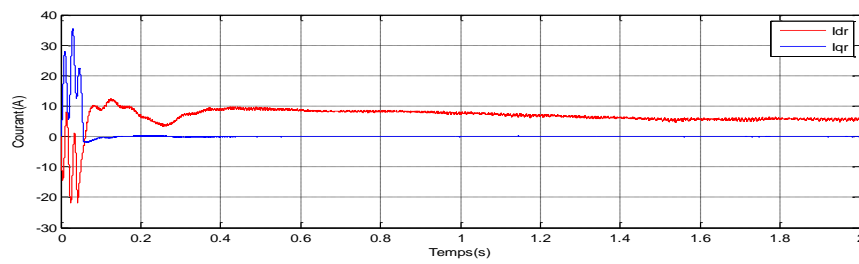
(e) Id and Iq courant and they Zoom
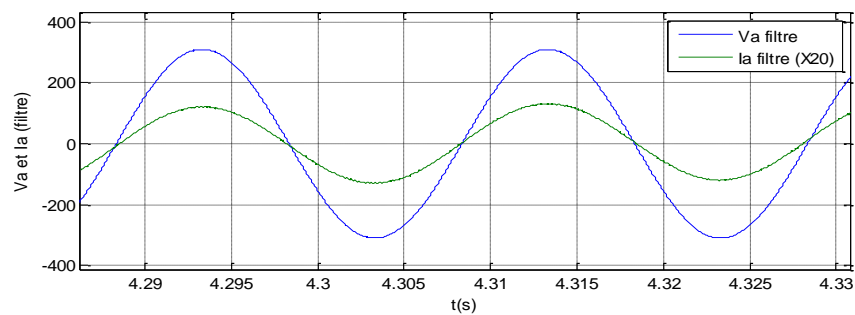
(f) Inverter output voltage after filter (Va) and Inverter line courant (20xIa) and
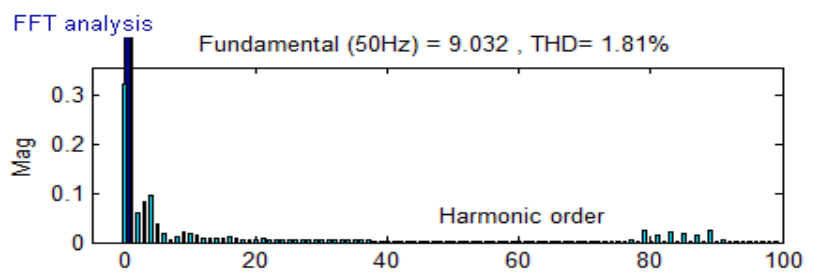
(g)FFT Courant I_a

Figure 9. The three-phase grid-connected photovoltaic system performances

Conclusion

In this paper, three-phase grid connected PV system is modeled and simulated. Proposed system consists of MPPT boost converter, five-level NPC topology inverter balanced by an inductive circuit, LC filter. FLC is used as MPPT algorithm.

Simulation results show that proposed FLC based MPPT controller has fast transient response. The application of the clamping bridge shows parfait following of the input DC and his reference and the stability of the input voltage of five-level NPC inverter. The results obtained with this solution confirm the good performances of the proposed solution. This study shows the effect of the stability of the DC voltages. The output current of the multilevel inverter is synchronized with the grid voltage phase and frequency therefor the power factor is one. The incorporation of the inductive balancing circuit enhances the stability of the input DC-bus voltages while allowing for an economical and straightforward electronic implementation.

The integration of the multilevel inverter NPC as an adaptive interface between the photovoltaic production system and the electrical grid is a highly prudent decision.

References

C. Shah et al., "Review of Dynamic and Transient Modeling of Power Electronic Converters for Converter Dominated Power Systems," in IEEE Access, vol. 9, pp. 82094-82117, 2021,

N. Altin, I. Sefa, "dSPACE based adaptive neuro-fuzzy controller of grid interactive inverter", Energy Conversion and Management Volume 56, pp. 130–139, April 2012.

D. Casadei, et al., "Multilevel Operation and Input Power Balancing for a Dual Two-Level Inverter with Insulated DC Sources," IEEE Transactions on Industry Applications, vol. 44, pp. 1815-1824, Nov-Dec 2008.

S. B. Kjaer, et al., "A review of single-phase grid-connected inverters for photovoltaic modules," IEEE Transactions on Industry Applications, vol. 41, pp. 1292-1306, Sep-Oct 2005.

F. Bouchafaa , A. Chouder and S. Boukhalfa "Stability of input voltages of a three-level inverter NPC fed by photovoltaic sources" Revue des Energies Renouvelables Vol. 15 N°3 pp.501 -512 , 2012.

Sulong, D., & Jeraputra, C. "A Grid Connected Flyback Inverter with a DC Active Filter for Photovoltaic Cells.", In Applied Mechanics and Materials, Trans Tech Publications. Vol 781, pp. 406-409. 2015.

Giacomini, J. C., Michels, L., Schuch, L., Pinheiro, H., & Rech, C.. "Design of a LCL filter for leakage current reduction in transformerless PV grid-connected three-level inverter." In Applied Power Electronics Conference and Exposition (APEC), IEEE, pp. 239-245. IEEE. 2015, March.

Bhagwat, P. M., & Stefanović, V. R. "Generalized structure of a multilevel PWM inverter. Industry Applications", IEEE Transactions on, (6), pp.1057-1069, 1983.

P. R. Bana, K. P. Panda, R. T. Naayagi, P. Siano and G. Panda, "Recently Developed Reduced Switch

Multilevel Inverter for Renewable Energy Integration and Drives Application: Topologies, Comprehensive Analysis and Comparative Evaluation," in IEEE Access, vol. 7, pp. 54888-54909, 2019

N. Ould Cherchali, M.S. Boucherit, A. Morsli, L. Barazane, "Robust Controller to Extract the Maximum Power of a Photovoltaic System," Journal of Electrical and Electronics Engineering, VOL7, N01, pp. 117-122, 2014

LIU, Chun-Liang, CHEN, Jing-Hsiao, LIU, Yi-Hua, et al. "An Asymmetrical Fuzzy-Logic-Control-Based MPPT Algorithm for Photovoltaic Systems.", Energies, vol. 7, no 4, pp. 2177-2193,2014.

N. Ould Cherchali, A. Tlemçani , M.S.Boucherit, L.Barazane "Comparative study between different modulation strategies for five levels NPC topology inverter," Energy and Power Engineering, Vol 3, N°3, pp. 276-284. 2011,

Abdelkrim, T., Berkouk, E., Benslimane, T., & Benamrane, K. "Feedback control of three-Level PWM rectifier: Application to the stabilization of DC Voltages of five-level NPC active power filter". Archives of Control Sciences, Vol 20, N.3, pp. 317-339, 2010.

Chibani, R., Berkouk, E. Boucherit, S.M, "Inductive Clamping Circuit for DC Link Voltage Balancing of Five–Level NPC–VSI." Journal of Electrical Engineering, Vol. 60, no 4, pp. 185-191. 2009,

N. Ould Cherchali, A. Morsli, M. S. Boucherit, L. Barazane and A. Tlemçani, "Comparison of two maximum power point trackers for photovoltaic systems using robust controllers," 3rd International Symposium on Environmental Friendly Energies and Applications (EFEA), Paris, France, 2014, pp. 1-5, doi: 10.1109/EFEA.2014.7059989.

N. Ould Cherchali, M. R. Skender, B. Bentchikou, A. Tlemçani and A. Morsli, "Parametric identification of a photovoltaic panel by the Firefly algorithm," 2022 13th International Renewable Energy Congress (IREC), Hammamet, Tunisia, 2022, pp. 1-5, doi: 10.1109/IREC56325.2022.10001922.

N. Ould Cherchali, A. Tlemçani, A. Morsli, M. S. Boucherit and L. Barazane, "Application of Firefly Algorithm on the SHEPWM strategy for the multilevel inverters," 2014 International Conference on Electrical Sciences and Technologies in Maghreb (CISTEM), Tunis, Tunisia, 2014, pp. 1-6, doi: 10.1109/CISTEM.2014.7076975.

Electroless Synthesis of Cobalt Nanowires in Magnetic Field and Their Characterization by the Resonant Magnetometry Method

Tsisana Gavasheli

Ivane Javakhishvili Tbilisi State University, Georgia, https://orcid.org/https://orcid.org/0000-0002-8915-0982

Grigor Mamniashvili

Ivane Javakhishvili Tbilisi State University, Georgia, https://orcid.org/0000-0001-8344-0885

Tatiana Gegechkori

Ivane Javakhishvili Tbilisi State University, Georgia, https://orcid.org/0009-0005-0811-7080

Tinatin Zedginidze

Ivane Javakhishvili Tbilisi State University, Georgia, https://orcid.org/0009-0006-1358-4123

Abstract: A simple and effective low-temperature electroless chemical method that provides the synthesis of cobalt micro- and nanowires due to the processes of self-organization of magnetic cobalt nanoparticles under the influence of a magnetic field, using the technology of chemical synthesis of magnetic nanoparticles and nanowires was proposed. Cobalt nanoparticles have magnetic dipole moments. The presence of an external magnetic field forces them to be oriented parallel to the field. Dipole-dipole interactions between magnetic nanoparticles lead to attraction between cobalt nanoparticles leading to their self-organization into nanowires, reducing their total energy. The resulting smaller nanoparticles fill the gaps between the ordered nanoparticles, leading to the formation of smooth cobalt nanowires. The magnetic and structural properties of the synthesized nanowires were studied by magnetometry and electron microscopy methods. This method is of interest for optimizing the coercive force of cobalt nanowires with a view to their possible use to create permanent magnets that do not use rare earth elements, as well as in information processing devices and sensors.

Keywords: Nanomagnetizm, Chemical synthesis, Cobalt nanowires, Magnetometry

Introduction

The formation of one-dimensional nanostructures such as nanowires has attracted considerable attention due to their large anisotropic surface magnetism for excellent applications (Scholzen et. al., 2022). Owning the high magnetization cobalt should become an ideal hard magnetic material if it can be prepared in the form with a large shape anisotropy. The use of template electrodeposition for the production of oriented magnetic nanowires of controlled diameter and length (Karim & Maaz, 2011) is complicated by the preparation of templates and the subsequent removal of nanowires from them. The use of magnetic fields in the recovery of solutions, i.e. hydrothermal and solvothermal synthesis, used for the production of one-dimensional Co nanostructures (Wang et. Al., 2008) requires high temperature, high pressure, and long reaction times.

We present a simple and effective low-temperature chemical method that provides the synthesis of nanowires due to the processes of self-organization of magnetic cobalt nanoparticles under the influence of a magnetic field, using the technology of electroless synthesis of magnetic nanoparticles and nanowires used in works (Khoperia et. al., 2011; Japaridze et. al., 2019; Mamniashvili et. al., 2024; Gavasheli et. al., 2020).

Cobalt nanoparticles have magnetic dipole moments. The presence of an external magnetic field forces them to orient themselves parallel to the magnetic field. Dipole-dipole interactions between magnetic nanoparticles lead to the attraction between cobalt nanoparticles leading to their self-organization into nanowires, reducing their total energy. The resulting smaller nanoparticles fill the gaps between the ordered nanoparticles, leading to the formation of smooth cobalt nanowires.

The magnetic and structural properties of the synthesized nanowires will be studied by the resonant magnetometry and electron microscopy methods.

Since the direct observation of magnetization reversal processes in nanostructures the magnetic nanopowders systems is hard to achieve, the magnetoresistance measurements as an indirect sensing tool were applied (Hausmanns et. al., 2002).

In this work, the individual Co nanowires were prepared by the electron beam lithography. Nonmagnetic gold contacts were attached to the Co nanowires to exclude an influence of the contact structures on the magnetization reversal process. Depending on the direction of the applied field three different magnetoresistance measurements were distinguished: in plane parallel and antiparallel to the wire axis, which called the longitudinal direction, and in plane perpendicular to the wire axis, the so-called transversal direction. The clear correspondence of the magnetoresistance, to the magnetization reversal was demonstrated. The magnetoresistance shows a hysteretic behavior with pronounced minima marking switching fields, which are identical to the coercive fields.

In the present work, the processes of magnetization reversal of cobalt nanowires are studied using a non-contact method of resonant magnetometry, similar to that used in (Figueroa et. al., 2012; Mamniashvili et. al., 2014). In this case, an LC-resonant generator was used, assembled according to a standard circuit using field-effect transistors to measure the resonant frequency of LC-generator changes at the magnetization direction change of cobalt nanowires.

The change in the resonant frequency of the LC-generator depending on the applied external magnetic field characterizes the magnetic susceptibility change of a sample related to the DWs displacement under the influence of the external magnetic field. Typical dependences of susceptibility on the external magnetic field show characteristic peaks associated with the process of a sample magnetization reversal. The susceptibility peaks of correspond to the minima in the resonant frequency changes of the LC generator (Mamniashvili et. al., 2014).

Method

An improved version of the electroless chemical method is developed (Mamniashvili et. al., 2024; Gavasheli et. al., 2020) for the synthesis of Co nanowires. The method consists in separating cobalt metal from a chemical solution Figures 1(a-e), when placed between the poles of a permanent magnet, Figure 1(f). This is a simple and inexpensive method that does not use expensive catalysts.

Figure 2 shows electron diffraction patterns of synthesized and commercial samples of cobalt nanowires obtained using a SEM TESCAN VEGAS XMU scanning microscope. A cobalt nanowire from PlasmaChemGmbH with an average diameter of 200-300 nm and a length of up to 200 μm was used. The average diameters of both types of nanowires are close, but the average length of the synthesized nanowires is approximately 5 times shorter.
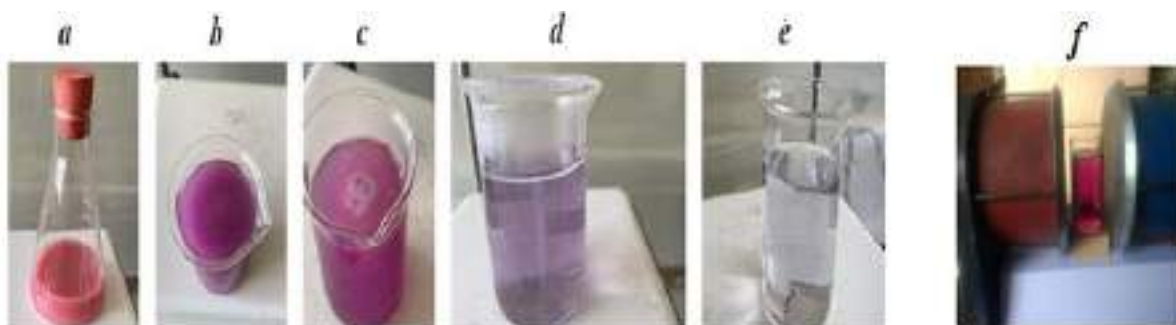
Figure 1. Chemical synthesis dynamics (a-e) and experimental set-up (f) for of cobalt nanowire

The method for synthesizing cobalt nanowires used in this work is based on their formation from a chemical solution when placed between the poles of a permanent magnet. This is a simple and inexpensive method that does not use expensive catalysts. The reagents used in the experiment are of analytical grade.

In particular, we prepare a solution of the following composition: $CoSO_4 \cdot 7H_2O$ -10 g/l; $KNaC_4H_4O_6$ $4H_2O$ – 40 g/l; N_2H_4 H_2O -50 ml/l; NaOH ≈ pH 13, where the main source of cobalt ions is its salt, and sodium potassium tartrate $KNaC_4H_4O_6$ $4H_4O$ acts as a complexing agent, which determines the stability of the solution. Hydrazine hydrate N_2H_4 H_2O is a reducing agent. It determines the process of releasing cobalt ions in metallic form. The participation of a surfactant in this process is also important. Toluene was used, which helps to separate the cobalt ions reduced in solution, preventing their agglomeration. To obtain cobalt nanopowder, a complexing agent is first added to a cobalt salt solution, and then hydrazine hydrate, as a result of which the color of the solution becomes pale pink and cloudy (Figure 1a). At this moment, the measured pH of the solution is 11, then add NaOH solution until the solution is completely transparent (pH = 13) and begin to heat the solution to 75-80°C. It is necessary to add a surfactant to the solution (Figure 1b) to prevent agglomeration of the released particles of metallic cobalt. At 75°C, the first particles of metallic cobalt are released from the solution (Figure 1c). The intensity increases at 80°C. In this case, the solution is placed on an electric furnace outside the magnet. With the help of toluene, cobalt particles rising to the surface of the chemical solution are periodically removed from the solution with a magnet and the solution is returned to the furnace. NaOH is periodically added to the depleted solution (Figure 1d) (up to pH-13), which ensures complete depletion of the solution in Co particles. The solution becomes colorless and transparent (Figure 1e). The total amount of NaOH used in this solution is ≈ 10 g/L
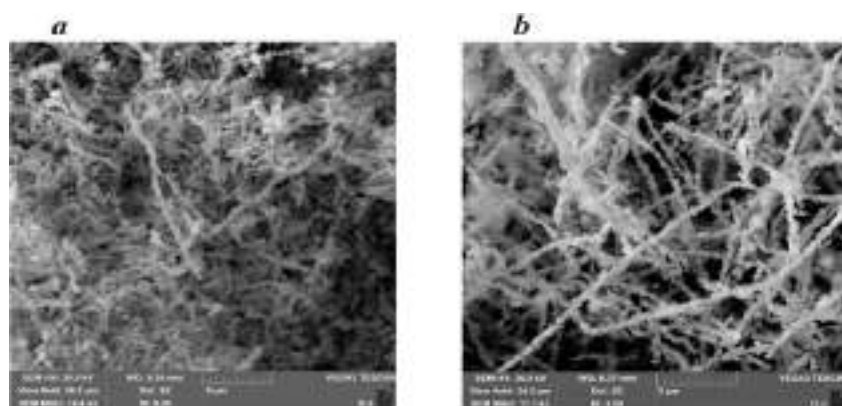
Figure 2. The electron diffraction patterns of the synthesized (a) and commercial (b) cobalt nanowires.

In the next step, to obtain cobalt nanowires, the same solution (heated to 80°C) is placed between the poles of a magnet, Figure 1f, where cobalt nanowires begin to form. It is advisable to apply a surfactant (surfactant) to the surface of the solution so that the separated cobalt nanowires do not agglomerate.

After the formation of cobalt nanowires begins, the resulting nanowire is removed on average once every 2 minutes, and the cobalt solution is returned to its original position between the poles of the magnet. As the pH of the solution decreased, the rate of formation of cobalt nanowires correspondingly decreased; therefore, the addition of NaOH maintained a high pH until the solution was completely decolorized. The duration of the process determines the size of the resulting nanowires. Nanowires are separated from the solution using a magnet. Then they are washed with alcohol using an ultrasonic device. In addition to the long-term synthesis

reaction, the thickness and length of cobalt nanowires are affected by the concentration of the reducing agent and the magnitude of the external magnetic field.

Cobalt nanopowders are synthesized under the same conditions as their nanowires, except for the presence of an external magnetic field.

Next, epoxy capsules with cobalt nanowires and micropowders are produced. The nanowires and micropowders obtained as a result of the experiment are placed in a polyethylene tube with epoxy resin. In particular, a transparent polyethylene tube with a length of 3 cm and an internal diameter of 6 mm is used. The tube is closed on one side with a silicone plug (5 mm long), then the required amount of cobalt nanowire is placed in it (in our case 0.4 g) and epoxy resin is added to form a capsule 2 cm long. Then the liquid epoxy resin is mixed in the capsule using a small wooden stick until a homogeneous suspension of cobalt nanowires is obtained. Finally, the capsule is closed with a silicone plug and placed between the poles of the magnet for 1 day until the epoxy resin completely hardens. Next, the direction of the magnetic field on the resulting capsule is noted and it is examined. After hardening, the polyethylene shell can be removed from the sample and further research can be carried out.

To characterize the magnetic properties of the received the homemade radio-frequency (RF) resonant magnetometer (RF RM) was used allowing one to carry out more easily and quickly assessment of the magnetic state (ferromagnetic, superparamagnetic) of the tested sample compared to the comparatively long-term measurements by the VSM magnetometry (Mamniashvili et. al., 2014).

The circuit based on the LC resonant generator, Figure 3, is used for the measurements of the transverse susceptibility of magnetic samples.
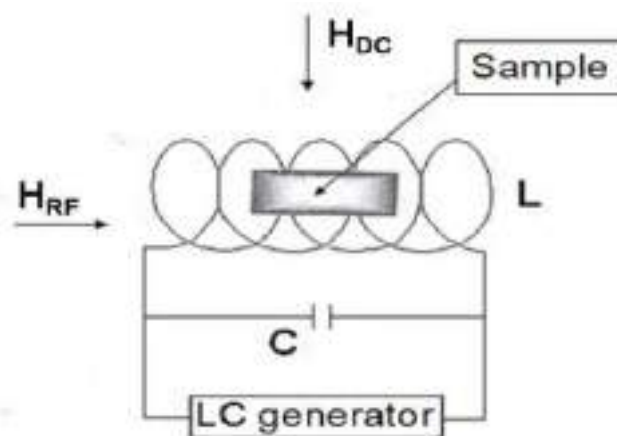
Figure 3. LC generator circuit scheme.

The sample was placed into the induction coil of the LC generator. The variations of its resonance frequency

were measured at the variations in the external magnetic field H_{DC}, which was perpendicular to the coil field H_{RF}.

The standard representation of the frequency of the LC generator oscillations is

$$f = \frac{1}{2\pi\sqrt{LC}}$$

where L is the coil inductance and C is its capacity

The introduction of the sample into the induction coil changed the inductance value by ΔL. If $\Delta L/L << 1$, by differentiating this equation, we get:

$$\frac{\Delta f}{f} = -\frac{\Delta L}{2L}$$

The inductance variations are connected with the changes in the magnetic susceptibility of studied magnetic nanopowders.

Results and Discussion

The work (Gavasheli et. al., 2020) a possibility of measuring the degree of pinning (pinning) of domain boundaries (DWs) in cobalt nanowires using the NMR method under the influence of an additional magnetic video pulse was shown.

The DW pinning force in nanowires turned out to be on the order of 100 Oe and higher. Therefore, it should be expected that the magnitude of the external magnetic field required for the reversal (flip) of the nanowire magnetization pre-polarized in a magnetic field is close to the DW pinning force in these nanowires. Since the residual magnetic field of the iron cores of the electromagnet turned out to be about 200 Oe, the Helmholtz coils were used to measure in the required range of the external magnetic field from 0 to 200 Oe. The process of magnetization reversal of nanowires was studied for three cases: in the case of an increase in the magnetic field along the magnetization of the nanowire and the opposite direction, as well as in the case of the direction transverse to nanowires.

In Figures 4 and 5, these dependences of the resonance frequency change $\Delta f(H)$ under the influence of magnetic field (the resonant frequency $f_0 = 10$ MHz in the absence of magnetic field) are presented for samples using commercial and synthesized nanowires.
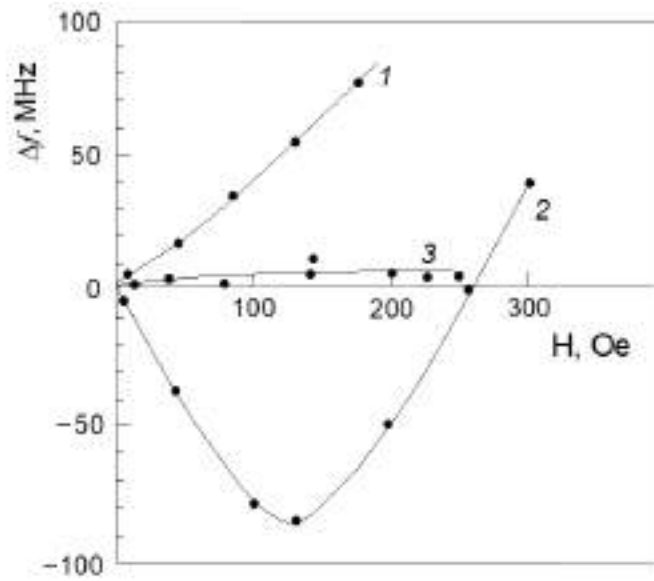
Figure. 4. Resonant frequency change on the commercial Co nanowire: *1* – magnetic field increases along its magnetization direction, *2* - magnetic field increases in the opposite direction, *3* - magnetic field increases in the perpendicular direction to the nanowire.

Figure 6 shows a typical hysteresis dependence of the change in the resonant frequency of an LC-generator Δf(H) at the longitudinal external magnetic field. It can be seen that the dependence Δf(H) passes through a negative minimum at a value of H close to the magnetization reversal field H_c

In this case, it coincides with the coercivity of the cobalt nanowire.
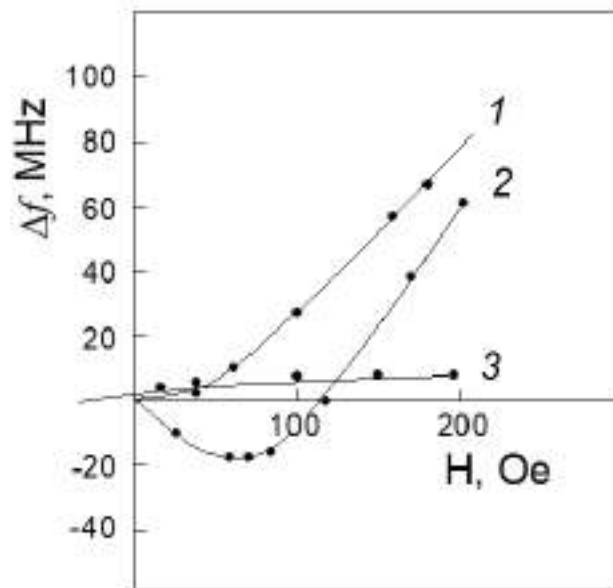
Figure 5. The Δf(H) dependence for the synthesized nanowires for three directions: *1*- along and *2* - in opposite direction to the magnetization of the Co nanowire, and *3* - magnetic field directed in perpendicular to the synthesized nanowire.

It is interesting to compare the obtained hysteresis dependence Δf(H) of cobalt nanowires in Figure. 6. with similar data on the effect of magnetization reversal of thin Co nanowires obtained by electron beam lithography on their longitudinal magnetoresistance, Figure 7 (Hausmanns, et. al., 2002).
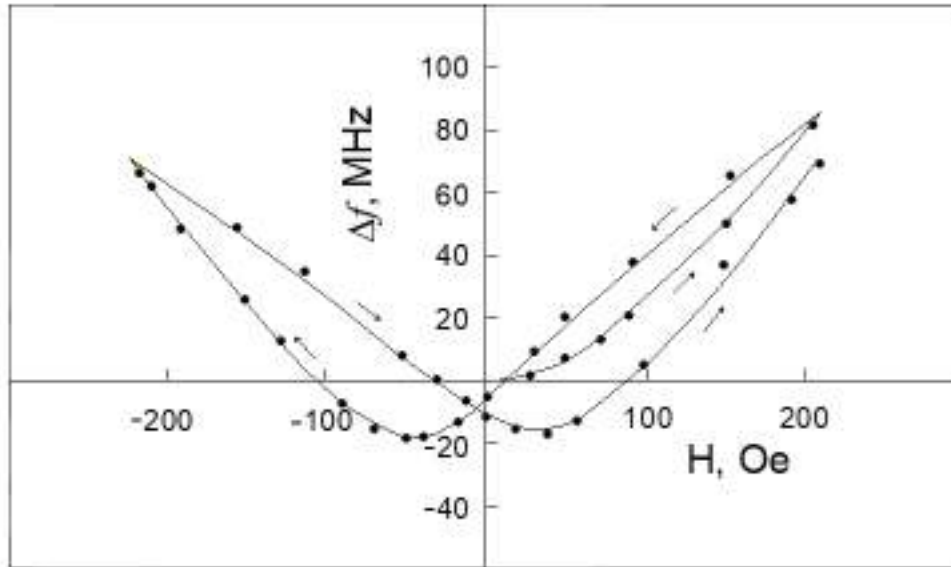
Figure 6. The Δf(H) hysteresis curves for synthesized nanowires. A magnetic field was directed along nanowires.

It can be seen that the resistance passes through a clearly defined minima at values of the longitudinal magnetic field close to the coercive field H.
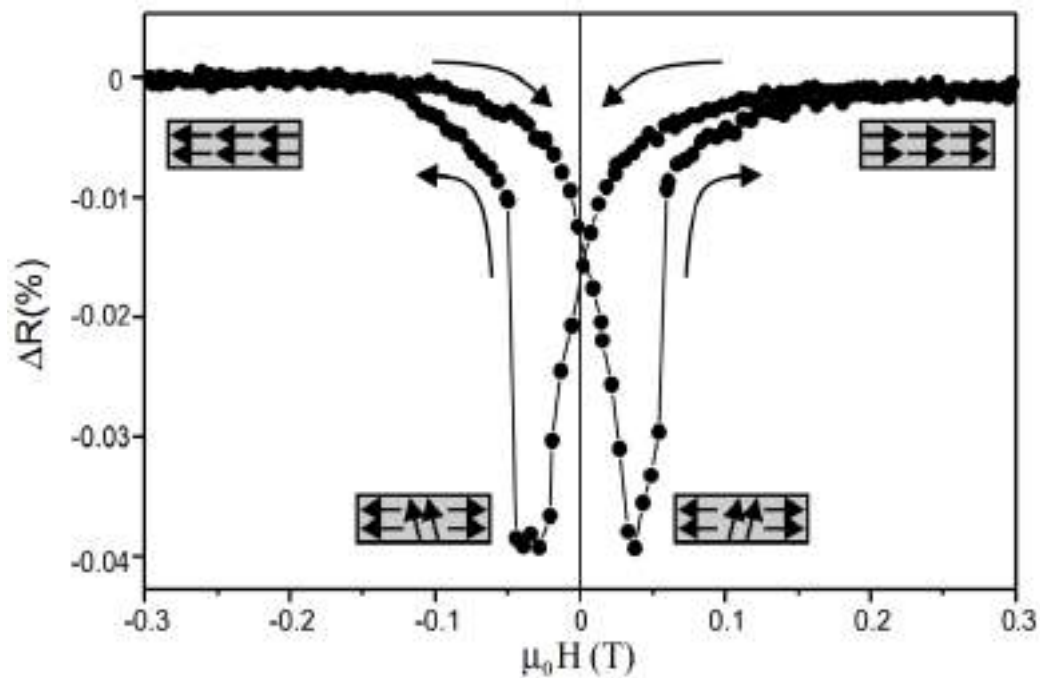
Figure 7. Longitudinal magnetoresistance of a Co nanowire (width = 529 nm T = 4.2 K). It is shown the relative resistance value referring to the saturation value (Hausmanns et. al., 2022).

Conclusion

The contactless resonant magnetometry method was developed for the assessment of the coercive forces of cobalt nanowires. The precise assessment of the coercive forces in cobalt nanowires, combined with an improvement in the method of their synthesis, makes their use promising for the manufacture of permanent magnets without rare earth elements, memory devices, etc.

Acknowledgements

References

Figueroa, A. I., Bartolomé, J., García del Pozo, J. M., Arauzo, A., Guerrero, E., Téllez, P., Bartolomé, F., & García, L. M. (2012). Low temperature radio-frequency transverse susceptibility measurements using a CMOS oscillator circuit. *Journal of Magnetism and Magnetic Materials, 324*(17), 2669-2675.

Gavasheli, T. A., Mamniashvili, G. I., Shermadini, Z. G., Zedginidze, T. I., Petriashvili, T. G., Gegechkori, T. O., & Janjalia, M. V. (2020). Investigation of the pinning and mobility of domain walls in cobalt micro-and nanowires by the nuclear spin echo method under the additional influence of a magnetic video pulse. *Journal of Magnetism and Magnetic Materials, 500*, 1555310.

Hausmanns, B., Krome, T. P., Dumpich, G., Wassermann, E. F., Hinzke, D., Nowak, U., & Usadel, K. D. (2002). Magnetization reversal process in thin Co nanowires. *Journal of Magnetism and Magnetic Materials, 240*(1-3), 297-300.

Japaridze, D., Daraselia, E., Chikvaidze, E., Gogoladze, T., Nadareishvili, M., Gegechkori, T., Zedginidze, T., Petriashvili, T., Mamniashvili, G., & Shengelaya, A. (2019). Magnetic properties and photocatalytic activity of the TiO_2 micropowders and nanopowders coated by Ni nanoclusters. *Journal of Superconductivity and Novel Magnetism, 32*(10), 3211-3216.

Karim, S., & Maaz. K. (2011). Magnetic behavior of arrays of nickel nanowires: Effect of microstructure and aspect ratio. *Materials Chemistry and Physics, 130*(3), 1103-1108.

Khoperia, T., Mamniashvili, G., Nadareishvili, M., & Zedginidze, T. (2011). Competitive nanotechnology for deposition of films and fabrication of powder-like particles. *ECS Transactions*, *35*(17), 17-30.

Mamniashvili, G. I., Gegechkori, T. O., Zedginidze, T. I., Petriashvili, T. G., Janjalia, M. V., Gavasheli, T. A., & Kezerashvili, R. Y. (2024). Chemical synthesis of cobalt nanowires in an external magnetic field and their characterization by NMR. *Journal of Applied Spectroscopy, 91*(1), 1-4.

Mamniashvili, G. I., Mikeladze, S. V., Gegechkori, T. O., Surguladze, B. V., Pichkhaia, G. N., Akhalkatsi, A. M., Daraselia, D. M., & Japaridze, D. L. (2014). Magnetometry and hyperthermia study of magnetic fluid preparation UNIMAG. *World Journal of Condensed Matter Physics 4*(1), 6-12.

Scholzen, P., Lang, G., Andreev, A. S., Quintana, A., Malloy, J., Jensen, C. J., Liu, K., & Lacaillerie, J. B.

(2022). Magnetic structure and internal field nuclear magnetic resonance of cobalt nanowires. *Physical Chemistry Chemical Physics, 24*(19), 11898-11909.

Wang, J., Yao, M., Xu, C., Zhu, Y., Xu, G., & Cui, P. (2008). Magnetic chains of Co spheres synthesized by hydrothermal process under magnetic field. *Materials Letters, 62*(19), 3431-3433.

Self-Powering of An Electrical Grid by Fuel Cells Controlled by Series Multicell Converter Using Osprey Optimization Algorithm and FOPID

Mohamed Redha Skender

Medea University, Algeria, https://orcid.org/0000-0002-6572-8102

Noureddine Ould Cherchali

Medea University, Algeria

Ahmed Medjber

Medea University, Algeria

Amel Abbadi

Medea University, Algeria, https://orcid.org/0000-0002-2039-062X

Tlemcani Abdelhalim

Medea University, Algeria, https://orcid.org/0000-0002-4385-671X

Fethia Hamidia

Medea University, Algeria, https://orcid.org/0000-0002-2212-0922

Abstract: This paper presents a comprehensive investigation into the concept of self-powering an electrical grid by integrating fuel cells under the control of a series multicell converter. The integration of fuel cells into the grid infrastructure is a complex process that requires careful consideration of stability, efficiency, and control strategies. To address these challenges, we propose the utilization of the Osprey Optimization Algorithm (OOA) in conjunction with Fractional Order Proportional Integral Derivative (FOPID) control techniques. The OOA offers a novel approach to optimizing system parameters, while FOPID control provides a robust framework for regulating the multicell converter operation. Through extensive simulation studies, we assess the efficacy of our proposed approach in optimizing grid integration, enhancing system stability, and improving energy conversion efficiency. Furthermore, this research explores the intricate dynamics of the fuel cell-grid interface, considering factors such as load variations, grid disturbances, and fuel cell performance characteristics. We investigate the impact of different control parameters on system performance and evaluate the trade-offs between stability, efficiency, and grid compatibility. Additionally, we analyze the scalability and reliability of the proposed self-powering system, considering potential deployment scenarios and real-world constraints. The findings of this study contribute to advancing the understanding of renewable energy integration in grid systems, offering valuable insights for policymakers, energy planners, and researchers in the

field.

Citation: Skender, MR., Ould Cherchali, N., Medjber, A., Abbadi, A., Abdelhalim, T., & Hamidia, F. (2024). Self-Powering of An Electrical Grid by Fuel Cells Controlled by Series Multicell Converter Using Osprey Optimization Algorithm and FOPID. In A. A. Khan, M. Demirbilek, & M. L. Ciddi (Eds.), *Proceedings of ICSEST 2024-- International Conference on Studies in Engineering, Science, and Technology* (pp. 177-190), Istanbul, Turkiye. ISTES.

Introduction

Our earth is going through a deep energy crisis. The consumption of electrical energy is increasing every day around the world, and major delays in generating capacity upgrades are seen in all countries. This situation is aggravated by the low availability in the execution or expansion of works for the generation of conventional electric energy, using long implementation times for large hydroelectric and nuclear plants, political reasons, and environmental enhancements. Such reasons have provided a change in the generation capacity expansion policy, with the emergence of small generating plants in various countries, bringing with it the problem of the imbalance of the power distribution network in the ruling countries. The benefits from the use of distributed generation units are widely known, such as reduced losses considering the transmission and distribution lines, reduced expenditures for expansion of the distribution system, reduced voltage drop, improved voltage regulation, reduced costs in the expansion of systems, increased reliability and security of the energy supply against natural disasters, and the diversification of the energy matrix and the consequent reduction of the environmental impacts.

Moreover, people or entities can install small generating units for their own use, transferring any excess generation to the electricity distribution network, thus encouraging the use of photovoltaic or wind generation units. Fuel cell energy systems are considered a new possibility for fuel use in the future. Their high efficiency and relatively good environmental behavior make them very attractive from the energetic perspective. In combination with renewable energies, such as wind or solar energy converters, an advanced concept for the future generation of power is formed. However, the main drawbacks of energy generation systems with fuel cells are the voltage and frequency fluctuations they generate, originating from their coupling with renewable energy converters. The proposed use of fixed-point charging loops to use their control properties in the coordination of power fuel cells, the reactive compensation stage, and voltage regulation of the fuel cells in the case of the fuel cells with renewable energy converters.

Alqahtani et al. (2024) introduced the Osprey optimization algorithm, which outperforms traditional methods in computational efficiency and accuracy(Alqahtani et al., 2024), Yuan et al. (2024) Attack-defense strategy

assisted osprey optimization algorithm for PEMFC parameters identification(Yuan et al., 2024), Hasanien et al. (2024) demonstrated the effectiveness of a hybrid Osprey-PSO method in optimizing power flow (OPF) with electric vehicles and wave energy systems (Hasanien et al., 2024).

This paper's main objective is to apply and implement a Fractional Order PID- Osprey Optimization Algorithm (OOA) to the grid-connected multicellular converter connected to the Fuel Cells system. This control scheme is well suited to this type of converter and constitutes an effective solution for stabilizing the load in the face of variations.

PEM Fuel Cell Modeling

Figure 1 depicts the components of a PEMFC, which include two electrodes, two plates, and two thin layers of platinum-based catalysts separated by a membrane. Upon injection of hydrogen fuel, an electrochemical reaction occurs, generating electricity (Schmid et al., 2024). The hydrogen and oxygen are supplied through channels in the plates, with the hydrogen flowing on one side of the membrane and the oxygen on the other (Mo et al., 2023). Through the catalyst, the hydrogen molecule is split into protons and electrons, allowing the protons to pass through the membrane while the electrons must pass through an external circuit, thereby producing useful electricity. On the oxygen side of the membrane, the protons and electrons react with oxygen, in the presence of a second catalyst layer, to produce water, heat, and electrical energy. Equations (1)–(3) provide the relevant reactions occurring within the PEMFC (Tellez-Cruz et al., 2021):

$$\text{Anode: } 2H_2 \Rightarrow 4H^+ + 4e^- \tag{1}$$

$$\text{Cathode: } 4H^+ + O_2 + 4e^- \Rightarrow 2H_2O \tag{2}$$

$$\text{Cell: } 2H_2 + O_2 \Rightarrow 2H_2O + EE \tag{3}$$
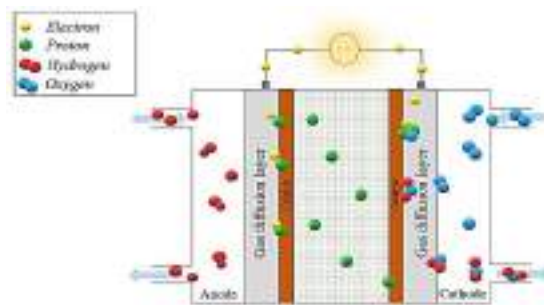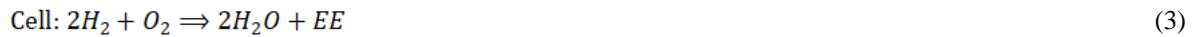
Figure 1. A cross-section of a PEMFC.

PEMFC Static Model

According to (Benchouia et al., 2013), the Nernst (E_{Nern}) equation describes the cell's electrochemical thermodynamic potential and gives the relationship between the open-circuit voltage of electrochemical cells under standard conditions and non-standard condition (E_{Nop}).

The equation is as follows :

$$E_{Nop} = 1.299 - 0.85.10^{-3}.(T - T_r) + 4.3085.10^{-5}T\left[\ln\left(P_{H_2}\right) + \frac{1}{2}.\ln\left(P_{O_2}\right)\right] \tag{4}$$

where T is the cell operating temperature, T_r represents the reference temperature in Kelvin, which is equal to 298.15 K at 25 °C, and P_{O_2} and P_{H_2} represent the inlet oxygen and hydrogen gas pressures, respectively .

The following expression can define the output voltage of a single PEMFC (Benchouia et al., 2013).

$$V_{Sfc} = E_{Nop} - E_{Act} - E_{Ohm} - E_{Con} \tag{5}$$

where E_{Act}, EOhm, and ECon represent the polarization potentials or the voltage losses that are generated by the reversibility of the system.

The activation polarization EAct is due to the kinetics of the reactions taking place at the electrode/membrane reaction interface. This loss can be calculated using Equation (6) :

$$E_{act} = \gamma 1 + \gamma 2.T + \gamma 3.T.\ln(CO_2) + \gamma 4.T.\ln(I_{fc}) \tag{6}$$

where the parameters $g1$, $g2$, $g3$, and $g4$ are the parametric coefficients for each PEMFC model; CO2 is the oxygen concentration in the catalysts (mol/cm3).

The E_{Ohm} polarization is caused by the electrical resistance of the different elements of the cell. This loss has two origins: the equivalent resistance of the membrane to proton conduction R_{mem} and the contact resistance Rcon between the bipolar plates and the electrodes.

The EOhm voltage can be calculated using Equation (7) :

$$E_{Ohm} = I_{fc}.(R_{mem} + R_{con}) \tag{7}$$

Where

$$R_{mem} = \frac{\Gamma_{mem}.l}{A} \tag{8}$$

where l is the membrane thickness (m), A is the cell active area (cm^2), and Gmem is the specific resistance of the membrane, which is obtained by the following :

$$\Gamma_{mem} = \frac{181.6\left[1 + 0.03\left(\frac{I_{fc}}{A}\right) + 0.062\left(\frac{T}{303}\right)^2\left(\frac{I_{fc}}{A}\right)^{2.5}\right]}{\left[\psi - 0.634 - 3\left(\frac{I_{fc}}{A}\right)\right].\exp\left[\frac{4.18(T - 303)}{T}\right]} \tag{9}$$

where y is the water content in the membrane, assuming a minimum and maximum value of 0 and 24, respectively.

The concentration polarization ECon is caused by the variation in the concentration of reagents on the electrode. This loss can be calculated using Equation (10) :

$$E_{Con} = \delta.\ln\left(1 - \frac{j}{j_{max}}\right) \tag{10}$$

where d, J, and Jmax are the constant parameters, the current density, and the maximum

current density, respectively.

A single PEMFC output voltage under standard conditions does not exceed 1.29 V.

In order to produce the required amount of power, it is necessary to have cells in series,which finally forms a

stack. Thereafter, the power generated by the PEMFC stack is given in Equation (11) :

$$P_{stack} = V_{Sfc}.I_{fc}.N_{Cell} \qquad (11)$$

where I_{fc} represents the single cell current and N_{Cell} represents the number of stack layers.

The PEMFC static model is represented in Figure 2.
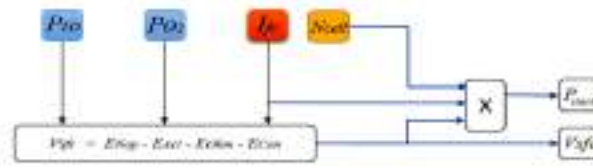
Figure 2. PEMFC static model.

PEMFC Dynamic Model

In a Proton Exchange Membrane Fuel Cell (PEMFC), a solid membrane separates the two electrodes. This

membrane allows the protons to pass through but restricts the flow of electrons. Electrons move from the anode,

pass through the external circuit, and reach the cathode surface where they combine with attracted hydrogen

protons. The result is the formation of two oppositely charged layers across the porous boundary between the

cathode and the membrane. These layers are referred to as "double electrochemical layers" and can function as a

super capacitor by storing electrical energy . Figure 3 depicts the PEMFC equivalent circuit that demonstrates

this phenomenon.
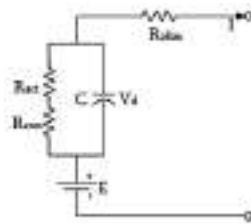
Figure 3. PEMFC equivalent circuit.

The electrodes of a PEMFC are porous. The capacitance is very large and can be of the order of several farads.

Ract and Rconc are the activation equivalent resistance and the concentration equivalent resistance, respectively.

By using Kirchhoff's law,

the dynamical equation of the model is represented by :

$$\frac{dV_d}{dt} = (\frac{I}{C} - \frac{V_d}{\tau}) \qquad (12)$$

where Vd is the dynamical voltage across the capacitor, C is the equivalent capacitor, and *t* is the PEMFC time

constant, which is given by the following equation :

$$\tau = C.(R_{act} + R_{conc}) = C.(\frac{E_{Act} + E_{Con}}{I}) \tag{13}$$

Therefore, the PEMFC voltage is given by the equation below :

$$V_{Sfc} = E_{Nern} - V_d - IR_{ohm} \tag{14}$$

where Rohm,act,conc represent the ohmic, activation, and concentration resistances, respectively.

Using Equations (12) and (13) and the Laplace transformations in Equation (14),

the PEMFC voltage is given as follows :

$$V_{Sfc} = E_{Nern} - \left(\frac{E_{Act} + E_{Con}}{sC(E_{Act} + E_{Con}) + 1} + R_{ohm} \right).I \tag{15}$$

According to (Maleki Bagherabadi et al., 2022), PEMFC inlet gas pressures are variable in different conditions. In order to calculate the dynamic partial pressures, each individual gas is considered separately and the ideal gas equation is applied for each one . The partial gas pressures are given as follows :

$$P_{H_2} = \frac{\frac{1}{K_{H_2}}}{\left(1 + \tau_{H_2}\right)}.(q_{H_2} - 2.I.K_r) \tag{16}$$

$$P_{O_2} = \frac{\frac{1}{K_{O_2}}}{\left(1 + \tau_{O_2}\right)}.(q_{O_2} - 2.I.K_r) \tag{17}$$

where

$$\begin{cases} \tau_{H_2} = \frac{V_{an}}{R.T.K_{H_2}} \\ \tau_{O_2} = \frac{V_{an}}{R.T.K_{O_2}} \end{cases} \tag{18}$$

By using the previous equations, the PEMFC dynamic model can be represented, as in Figure 4.
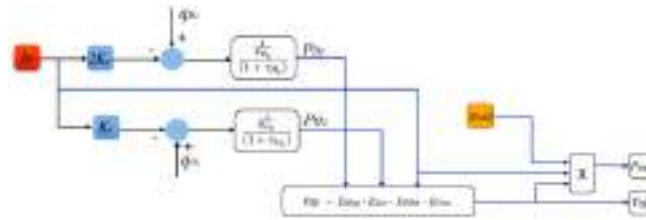
Figure 4. PEMFC dynamic model.

The meanings of the variables used in Equations (16)–(18) are listed in Table 2.

Table 2. PEMFC nomenclature.

Variable	Meaning
K_{H_2}	Hydrogen valve molar constant(kmol/atm.s)
K_{O_2}	Oxygen valve molar constant(kmol/atm.s)
τ_{H_2}	Hydrogen time constant(s)

τ_{O_2}	Oxygen time constant(s)
q_{H_2}	Molar flow rate of Hydrogen(kmol/s)
q_{O_2}	Molar flow rate of Oxygen (kmol/s)
K_r	Modeling constant(kmol/s.A)
R	Universal gas constant(I.atm/kmol.K)
V_{an}	Volume of the anode(cm^3)

Osprey Optimization Algorithm

The osprey is a piscivorous bird, about 99% of its diet is fish. It usually catches alive fish weighing from 150 to 300 g and 25–35 cm in length. However, it can catch any fish from 50 g to 2 kg. Ospreys have the high vision to detect underwater objects. When the osprey is flying at a height of 10–40 m above the water's surface, it detects the position of the fish underwater. Then it moves toward the fish, dips its feet into the water, and dives under the water to catch the fish. After the osprey catches its prey, it carries it to a nearby rock and begins to eat it (Dehghani & Trojovsky, 2023).

The osprey's strategy in hunting fish and carrying fish to a suitable position to eat it are intelligent natural behaviors that can be the basis of designing a new optimization algorithm (Dehghani & Trojovsky, 2023). Therefore, the mathematical modeling of these intelligent osprey behaviors is employed in the design of the proposed OOA approach, which is discussed in the following part.

Figure 5. Photo of osprey

OOA is a population-based intelligent optimization algorithm inspired by the hunting behavior of osprey in nature (Wen et al., 2024). Similar to other intelligent optimization algorithms, it performs a random initialization population operation in the search space with the population initialization formula (19):

$x_{i,j} = lb_j + r \cdot \left(ub_j - lb_j \right),$	(19)

where $x_{i,j}$ is the individual, lb_j is the lower bound of the search, ub_j is the upper bound of the search, and r is a random number between [0, 1]. The first phase of the OOA is an exploratory phase, which is modeled by simulating the behavior of osprey locating and catching fish in nature. During the design process of the OOA

algorithm, each individual in the population will consider other individuals with better positions as a school of fish, and the mathematical model of the target school of fish for each individual is as follows (20):

$$FP_i = \{X_k \mid k \in \{1, 2, \ldots, N\} \wedge F_k < F_i\} \cup \{X_{\text{best}}\}$$

(20)

where *FPi* is the set of fish for the *ith* eagle and *Xbest* is the location of the best eagle. Ospreys prey based on a stochastic detection mechanism, and by modeling the behavior of ospreys attacking fish (predation) (Wen et al., 2024), the algorithm individual position update formula is as follows (21) :

$$x_{i,j}^{NEW} = x_{i,j} + r_{i,j} \cdot \left(SF_{i,j} - I_{i,j} \cdot x_{i,j}\right)$$

(21)

where *SF* is the target fish selected by the individual, *r* is a random number between [0, 1], and the value of *I* is one of {1, 2}.

Boundary checking is performed for individuals with completed positional updating with the following equation (22):

$$x_{i,j}^{NEW} = \begin{cases} x_{i,j}^{NEW}, & lb_j \leq x_{i,j}^{NEW} \leq ub_j \\ lb_j, & x_{i,j}^{NEW} < lb_j \\ ub_j, & x_{i,j}^{NEW} > ub_j. \end{cases}$$

(22)

If the updated individual position is better than the previous position, the previous position is replaced by the new position. The equation is as follows:

$$X_i = \begin{cases} X_i^{NEW}, & F_i^{NEW} < F_i \\ X_i, & \text{else} . \end{cases}$$

(23)

Here X_i^{NEW} is the updated position, and F_i^{NEW} is the updated fitness value.

After catching a fish in nature, the osprey takes the fish to a safe location to feed and the development phase of the algorithm is modeled based on the above behavior. Each individual in the population calculates a new random location as a feeding area and the mathematical model of this behavior is as follows:

$$x_{i,j}^{NEW_2} = x_{i,j} + \frac{lb_j + r \cdot \left(ub_j - lb_j\right)}{t},$$

(24)

Boundary checking for all individuals using the position update phase of the following equation:

$$x_{i,j}^{NEW_2} = \begin{cases} x_{i,j}^{NEW_2}, & lb_j \leq x_{i,j}^{NEW_2} \leq ub_j \\ lb_j, & x_{i,j}^{NEW_2} < lb_j \\ ub_j, & x_{i,j}^{NEW_2} > ub_j. \end{cases}$$

(25)

Compare the quality of the updated individual with that of the original individual, and if the new position is superior, the new position is used to replace the original position.

$$X_i = \begin{cases} X_i^{NEW_2}, & F_i^{NEW_2} < F_i \\ X_i, & \text{else} . \end{cases}$$

(26)

Here, X_i^{NEW2}, *i* is the new position of the *ith* individual, and FX_i^{NEW2} *i* is the updated individual fitness value.

The flowchart of the OOA algorithm is shown in Figure 6. After analyzing the mathematical model of the OOA

algorithm, it has been found that it possesses a simple structure and a reasonable mechanism, offering certain advantages. However, the actual testing process revealed that during the iterative process, the OOA algorithm updates individual positions randomly, which can lead to the detection of sub-optimal targets and result in invalid searches, impacting the algorithm's convergence speed. In the later stages of iteration, although individuals adopt a random perturbation strategy to enhance the algorithm's ability to escape local optima, this approach can result in less precise local searches and reduce the accuracy of finding the optimum. Based on the above analysis, the OOA algorithm's optimization performance has significant room for improvement. Implementing a multi-strategy fusion approach to enhance the OOA algorithm can greatly improve its optimization performance, which has considerable research significance.

The first iteration of the planned OOA was finished by revising all of the ospreys' positions according to the first and second stages. The best candidate solution was then modified based on a comparison of the values of the objective function. The algorithm then moved on to the following iteration with the revised osprey placements, and so forth until the last iteration based on Equations (22)–(26). The best candidate solution saved during the iterations is finally presented as a solution to the problem after the algorithm was fully implemented. The chart in Figure 6 [52] show the OOA implementation processes.
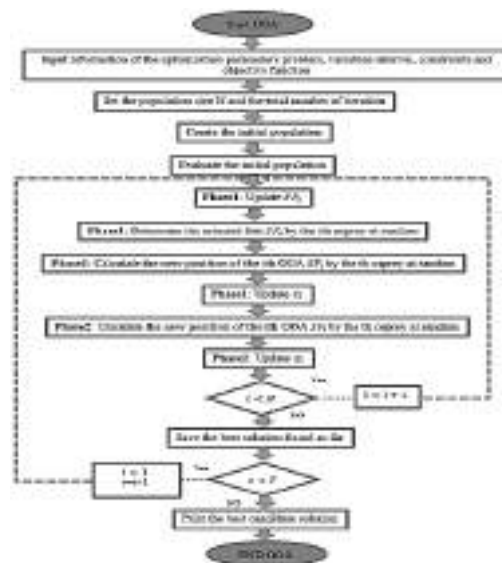
Figure 6. The flowchart of the OOA algorithm

In this simulation, the population size equals 50 search agents, and the number of iterations equal 100. The implementation of OOA is intended to minimize the fitness function ITAE [53], while the adaptive gains $\mu_{p,i,d}$, are taken as decision variables. The variation ranges of the decision variables used in the simulation are given in Table 4.

Table 4. OOA upper and lower bounds.

algorithm	range	μ_p	μ_i	μ_d
OOA	Min	0	0	0
	Max	1	1	1

Fractional-Order Pid Controller

The FOPID controller control loop feedback mechanism and reduce the error between a measured variable and the desired set point of a process (Skender & others, 2023). The generalized transfer function is given by

$$C(s) = \frac{U(s)}{E(s)} = K_P + \frac{K_I}{s^\lambda} K_D s^\mu \quad (\lambda, \mu \geq 0) \tag{27}$$

where $C(s)$ represents the controller output; $U(s)$ and $E(s)$ are the control signal and the error signal, respectively; The FOPID equation has five unknown parameters, KP, KI, and Kd are the proportional, integral, and derivative constant gains, respectively; λ is the order of integration; and μ is the order of differentiator .If λ = 1 and μ = 1, a classical PID controller is recovered (Skender & others, 2023).

The block diagram of control system employing soft computing FOPID control action is shown in Figure 7.
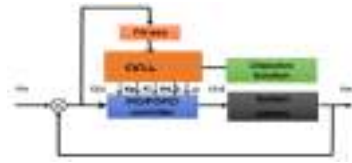
were

$V_{in}(s)$: Input Signal

$E(s)$: Error Signal

$V_{out}(s)$: Output Signal

$U(s)$: Control Signal

Figure 7. A block diagram of Intelligent FOPID controller

cost function

To evaluate the qualities of the regulator, there are different types of control such as the Integral of Squared Error (ISE), Integral of Absolute Error (IAE), Integral of Time Squared Error (ITSE) , and Integral of Time Absolute Error (ITAE) (Skender & others, 2023).

A drawback of the IAE and ISE categories which influence all errors equally and independent of time) is that they may train in a response with a long settling time and relatively small overshoot. To surmount this disadvantage, an ITAE is used as fitness function.

Therefore, the controller can be evaluated using the following performance index:

$$j(K_p, K_i, K_d, \mu, \lambda) = \int_0^\infty t|e(t)|dt \tag{28}$$

j is called as ITAE. It means that the controlled object is close to the set point model. Where t is the time and $e(t)$ is the error between reference and controlled variable.

Modellıng And Control Strategy of The Grıd-Connected Fuel Cells System

The inverter is responsible for the following tasks (Skender & others, 2023).
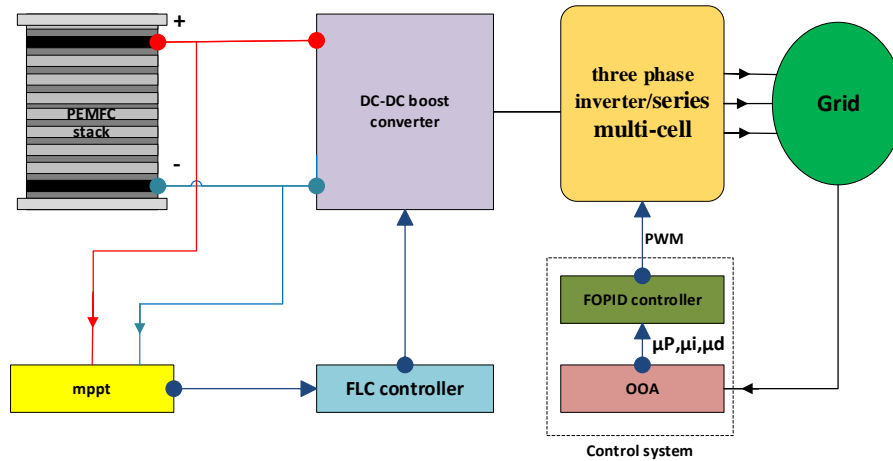
Figure 8. Proposed control structure of three phase grid-connected Fuel cell system.

1. Control of active power supplied to the grid

2. Control of DC link voltage

3. Ensure high quality of injected power

4. Grid synchronization.

PID and FOPID controller using OOA optimizations

From the comparison between (PID) controller and (FOPID-OOA) controller in figures 9, their performance is almost similar, little difference between them.
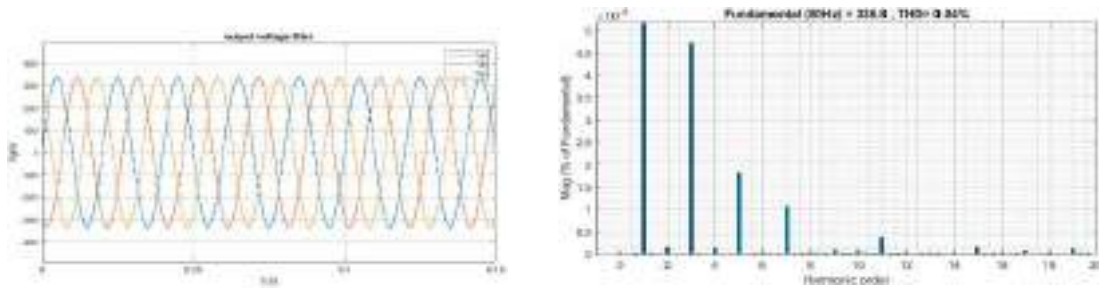
Figure 9. a – Output voltage filter of PID methods .
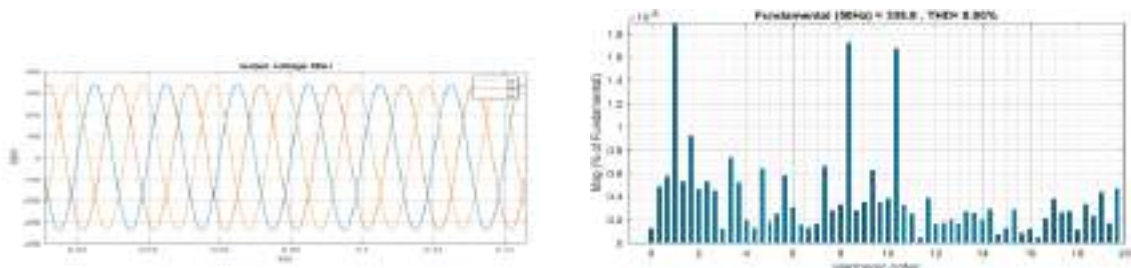
Figure 9. b – Output voltage filter of (FOPID-OOA) methods.
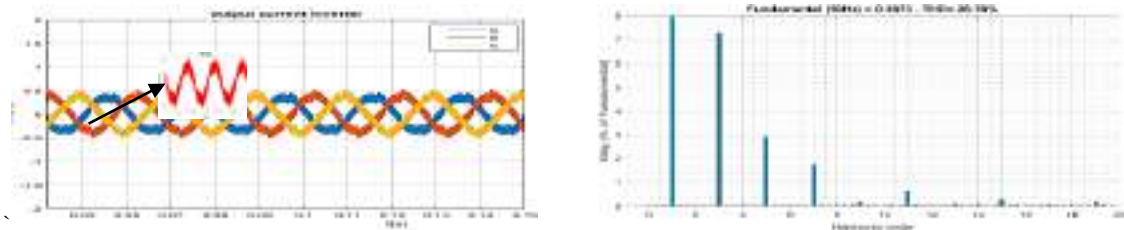
Figure 9. c – Output current filter of PID methods.
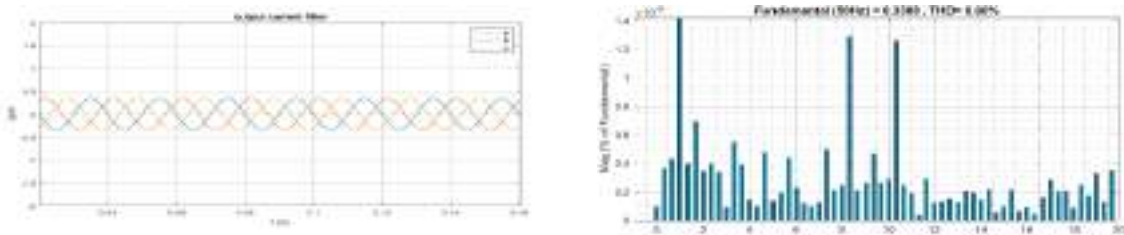
Figure 9. d – Output current filter of (FOPID-OOA) methods.

Figure 9. simulation results present a comparison of PID and (FOPID-OOA) methods

For (PID-OOA) methods the THD is 26,76% as it can be seen on Figure 9.c. The load output current from LCL filter is smooth and harmonic analysis show the effectiveness of the designed (FOPID-OOA), the attenuation has been specified for 0% THD on Figure 9.d.

On the other hand, the output voltage shown in Figure 9a, b is very sinusoidal in both cases with better performance in Figure 9.b.

Moreover, the search for the optimal parameters of the FOPID controller here shows that the results are obtained faster and more efficiently by the OOA algorithm than by the PID algorithm.

Conclusion

This paper presents a detailed study of a three-phase grid-connected Fuel Cells system. The paper explains the state space modeling of inverter current control and DC link voltage control, and designs the corresponding controllers using PID and Fractional Order PID- Osprey Optimization Algorithm (FOPID-OOA) methods. The performance of both methods is evaluated through simulation studies of a grid-connected Fuel Cells system that uses a three-phase series multi-cells converter (inverter) to connect the Fuel Cells to the grid. The simulation results show that the proposed system is capable of extracting maximum power from the Fuel Cells system. A 100 kW grid-connected Fuel Cells system is used to verify the developed control strategies through simulation studies. The FOPID-OOA control method exhibits a better transient response and settling time, resulting in a stable closed-loop system response.

The paper also presents the design of an LCL filter and the calculation of current harmonics using FFT analysis.

The simulation results show that the proposed FOPID controller outperforms a conventional PID controller by minimizing trajectory tracking error and reducing control efforts. The effectiveness of the proposed FOPID controllers is verified through different trajectories in MATLAB-Simulink software package. The developed control strategy for the FOPID-OOA control makes the Fuel Cells system stable under different conditions.

References

Alqahtani, A. H., Fahmy, H. M., Hasanien, H. M., Tostado-Véliz, M., Alkuhayli, A., & Jurado, F. (2024). Parameters estimation and sensitivity analysis of lithium-ion battery model uncertainty based on osprey optimization algorithm. *Energy*, *304*, 132204. https://doi.org/10.1016/J.ENERGY.2024.132204

Benchouia, N., Hadjadj, A. E., Derghal, A., Khochemane, L., & Mahmah, B. (2013). Modeling and Validation of Fuel Cell PEMFC. *Revue Des Energies Renouvelables*, *16*(2), 365–377.

Dehghani, M., & Trojovsky, P. (2023). Osprey Optimization Algorithm: A New Bioinspired Metaheuristic Algorithm for Solving Engineering Optimization Problems. *Frontiers in Mechanical Engineering*, *8*, 1126450. https://doi.org/10.3389/fmech.2022.1126450

Hasanien, H. M., Alsaleh, I., & Alassaf, A. (2024). Impact of electric vehicles and wave energy systems on OPF of power networks using hybrid Osprey-PSO approach. *Energy*, *308*, 132818. https://doi.org/10.1016/J.ENERGY.2024.132818

Maleki Bagherabadi, K., Skjong, S., & Pedersen, E. (2022). Dynamic modelling of PEM fuel cell system for simulation and sizing of marine power systems. *International Journal of Hydrogen Energy*, *47*(40), 17699–17712. https://doi.org/10.1016/J.IJHYDENE.2022.03.247

Mo, S., Du, L., Huang, Z., Chen, J., Zhou, Y., Wu, P., Meng, L., Wang, N., Xing, L., Zhao, M., Yang, Y., Tang, J., Zou, Y., & Ye, S. (2023). Recent Advances on PEM Fuel Cells: From Key Materials to Membrane Electrode Assembly. *Electrochemical Energy Reviews*, *6*(1), 28. https://doi.org/10.1007/s41918-023-00190-w

Schmid, M. A., Kaczerowski, J., Wilhelm, F., Scholta, J., Muller, B., & Holzle, M. (2024). Aging Effects Observed in Automotive Fuel Cell Stacks by Applying a New Realistic Test Protocol and Humidity Control. *Fuel Cells*. https://doi.org/10.1002/fuce.202300227

Skender, M. R., & others. (2023). A Series Multi-Cells Converter Controlled by Dspace 1103 Using PID and FOPID Controller Tuning with GWO and PSO Algorithms: Experimental on Grid-Connected Solar PV System. *Tob Regul Sci*, *9*(1), 1475–1495. https://doi.org/10.18001/TRS.9.1.100

Tellez-Cruz, M. M., Escorihuela, J., Solorza-Feria, O., & Compay, V. (2021). Proton Exchange Membrane Fuel Cells (PEMFCs): Advances and Challenges. *Polymers (Basel)*, *13*(18), 3064. https://doi.org/10.3390/polym13183064

Wen, X., Liu, X., Yu, C., Gao, H., Wang, J., Liang, Y., Yu, J., & Bai, Y. (2024). IOOA: A Multi-Strategy Fusion Improved Osprey Optimization Algorithm for Global Optimization. *Electronic Research Archive*. https://doi.org/10.3934/era.2024093

Yuan, Y., Yang, Q., Ren, J., Mu, X., Wang, Z., Shen, Q., & Zhao, W. (2024). Attack-defense strategy assisted

osprey optimization algorithm for PEMFC parameters identification. *Renewable Energy*, *225*, 120211. https://doi.org/10.1016/J.RENENE.2024.120211

A Brief Review of Molecular Techniques to Study Medicinal Plants

Qemal Shehu

Albanian University, Albania, https://orcid.org/0009-0002-2929-7824

Dhimitër Peçi

University of Tirana, Albania, https://orcid.org/0009-0002-2664-0527

Ani Bajrami

University of Tirana, Albania, https://orcid.org/0000-0001-5349-2510

Aida Dervishi

University of Tirana, Albania, https://orcid.org/0000-0002-2173-632X

Abstract: Since ancient times, many plant species have been utilized by humans of different cultures for various purposes, including health and food, highlighting the pivotal role of these plants in traditional medicinal practices. Many plants have been studied regarding their medical characteristics and properties. Nowadays, the development of molecular techniques such as Next Generation Sequencing (NGS), which are no longer applicable only for studies on the human genome but also in plant research, has shown notable advancements. The evolution of sequencing instruments, by enhancing their sensitivity and lowering their operative costs is helping scientists to have a better focus on plants by characterizing, identifying, and defying their linkage in hereditary. Due to the biological activity of medicinal plants' chemical compounds, known as secondary metabolites, interest in studying them has increased dramatically, resulting in several groundbreaking studies. Molecular techniques have accelerated the discovery and purifying of bioactive compounds, another vital aspect of what pharmaceutical companies are interested in. Additionally, the combination of these techniques with bioinformatics does significantly contribute to results interpretations in terms of gene relationship, gene sequencing, genome transcript, proteomics as well as metabolomics. In the present article, we provide a brief review of molecular techniques that can be employed to facilitate medicinal plant studies, enhance research efficiency, and prompt the advancement of the studies and future promising projects regarding medicinal plants.

Keywords: Humans, Health, Medicinal Plants, Molecular Techniques

Introduction

Medicinal plants are defined as plants that can be used for medicinal purposes. They have a crucial role in the traditional medicine practices employed worldwide. Humans have widely utilized them for centuries to treat various diseases and improve physical and mental health, which vary significantly across cultures (Marrelli, 2021). The importance of medicinal plants extends beyond their medicinal properties as their use embodies a cultural heritage passed through generations. Several paleontological studies provided evidence of the use of medicinal plants around 60,000 years ago, traces of *Ephedra altissima* and *Centaurea solstitialis* were found in a tomb of prehistoric Neanderthal; Sumerian clay slab discovered in Nagpur (India) showed herbal drug preparation provided an additional proof on the use of medicinal plants around 5000 years ago; furthermore such evidence was provided from scripts such as "Chinese book on roots and grasses" (2500 BC), "Indian holy books Vedas", "Eberes Papyrus" (1550 BC), and the Bible (Petrovska, 2012). In over 300,000 extant seed plants, about 60% have been used for medicinal purposes, in the post-Neolithic human history. According to IUCN 50, 000 to 80, 000 flowering plant species serve as a source of pharmaceutical compounds (Jamshidi-Kia et al., 2018). The demand for plant-derived products has increased worldwide due to the extended use of herbal medicine as primary health care. It was estimated, that around one-third of clinical drugs have been derived from plant extracts and their derivatives (Hao & Xiao, 2015), increasing the importance of scientific studies on identifying plant compounds and their therapeutic effects. Most medicinal plants are collected in the wild; therefore, the accuracy of their identification is critical for ensuring the quality and safety of plant-derived products. To ensure accurate identification of medicinal plants, several methodologies have been used over the years and researchers have attempted to solve this problem by performing morphological, microscopic, physical, chemical, and DNA-based identification. However, the application of each of the techniques is associated with advantages and disadvantages (Chen et al., 2023) making accurate plant identification a challenge. This review provides an overview of techniques employed in medicinal plant identification, whose development and integration will potentially change the perspective of medicinal plant utilization worldwide.

Macroscopic and Microscopic identification

Macroscopic identification

Botanical identification is performed via examination of the intact, whole plant, mostly during the collection or harvest time, while macroscopic identification is performed through evaluation of relevant morphological or organoleptic (sensory) characteristics of particular parts of the plant (e.g. whole roots, fruits, or parts of the plant). Macroscopic methods of identification have traditionally been used throughout history as a method for medicinal plant authentication, due to several advantages. Firstly, macroscopic evaluation is based on morphological features of the plant such as color, size, and shape of the whole plant or its parts of interest and does not require high costs. These techniques can be applied to both wild and cultivated plants and might provide a physical reference sample to be referred to by researchers in the identification of the same plant species in the future. In macroscopic identification, an assessment of plant material quality can be

simultaneously carried out by examining the organoleptic characteristics and assessing the presence/absence of contaminants, such as sand, gravel (Techen et al., 2004), or plant diseases/infected plant material. However, macroscopic identification relies on the personal experiences of the evaluator, requiring a high level of expertise and training of the individual performing the macroscopic evaluation. In addition, access to herbaria that serves as a reference database, to voucher specimens, or a photo reference library is necessary to perform an accurate identification of plant species, increasing considerably the time, effort, and costs of this analysis, especially in cases when these databases do not previously exist and should be constructed or effectively maintained and stored (Techen et al., 2004). Another major disadvantage of macroscopic evaluation is the lack of effectiveness in distinguishing closely related species that might have very similar characteristics (Zhao et al., 2011) or differentiate species chemotypes and ecotypes (Techen et al., 2004) as different growing ecological conditions can greatly influence macroscopic characteristics and a particular phenotype used as a marker in macroscopic identification is influenced by the habitat and vegetative phase of the plant. Therefore, the macroscopic evaluation should be continuously carried on in combination with other identification techniques.

Microscopic identification

Microscopic identification of medicinal plants involves detailed examination of plant material through microscopic techniques. It has long been used in the identification of medicinal plants as it requires a small amount of sample, is simple, and has low cost, moreover, histochemical techniques allow the identification of the different tissue and cellular structures that can be used as markers for species identification (Au et al., 2009). Microscopic techniques enable the evaluation of several characteristics such as foliar epidermal traits, pollen features, glandular and non-glandular trichomes, and stomata index, enabling the identification of a plant species (Ayaz et al., 2020) and may apply also to the quality control of medicinal plants (de Oliviera et al., 2012). The microscopic evaluation of the above-mentioned plant traits allows the discrimination of closely related species and ecotypes (Ayaz et al., 2020). In addition, histochemical analysis enables the identification of the biologically active substances present in tissues and provides data on the distribution of secondary compounds (Matias et al., 2016), which is relevant in the analysis of medicinal plants. Microscopic analysis is used on a large scale in fresh plant tissue and has limited applicability in processed or dried plant material. Like macroscopic techniques, microscopic techniques have disadvantages related to sample collection and long-term storage requirements, as before the analysis plant material must be stored and transferred to the laboratory under specific conditions moreover the technique application requires moderate to high level trained researcher and expertise.

Macroscopic and microscopic examination can be used as a rapid, low-cost identification and evaluation of medicinal plants before or following the harvesting process of plant material. Used alongside molecular techniques (DNA-based techniques) and DNA barcoding, macroscopic and microscopy techniques can provide a more comprehensive characterization and identification of medicinal plants.

Molecular DNA Methods

The molecular DNA-based methods complement conventional techniques used in medicinal plant identification, overcoming their limitations. These approaches are less affected by tissue type, development stage of the plant, and environmental conditions. Molecular-based identification of medicinal plants requires a low amount of plant material, it is fast, reliable, and with high discriminatory power, enabling the analysis and identification of closely related species (Lo and Shaw, 2019). These techniques can provide an efficient, accurate, and low-cost means of testing the authenticity of a high number of samples simultaneously as these can be amenable to automation (Ganie et al., 2015). The innovation of PCR (Polymerase Chain Reaction) made the application of molecular markers a useful tool for the correct identification of plant species, which is crucial for medicinal plants because some species having similar morphological characteristics may contain toxic substances (Hyder et al., 2024), as well as to assess and monitor the quality of herbal pharmaceutical products (Ganie et al., 2015).

The majority of DNA-based technologies employ PCR, which was used for direct amplification of random or targeted specific regions of genomic DNA using arbitrary or specific primers, respectively. Using arbitrary primers, PCR yields amplicons of various sizes that can be differentiated by electrophoresis, evidencing polymorphism within species. This method offers more rapid sample identification, but it lacks the reproducibility of fingerprinting patterns (Sucer and Carles, 2008) and does not distinguish homozygotes from heterozygotes. Vast numbers of nonspecific dominant molecular markers are available, the most commonly used in medicinal plant identification are RAPDs, AFLPs, and ISSRs. Random Amplification of Polymorphic DNA (RAPDs) technology uses a single arbitrary primer to amplify several polymorphic fragments. It is employed in medicinal plant identification due to low cost and simplicity of the technique, foremost it can be employed in analyzing any species since it is not specific. Despite its advantages, its limitations in reproducing the results classify this technique as less efficient in the studies aiming identification of medicinal plants. Amplified Fragment Length Polymorphism (AFLP), introduced by Vos et al. (1995), is based on the selective PCR amplification of restriction fragments from a digest of genomic DNA. This technique is a useful tool in evolution and genetic diversity studies in germplasm, because it has proven to be highly reliable and reproducible, generated a high multiplex ratio, and does not require prior knowledge of the DNA sequence (Danaeipour et al., 2019). AFLPs have higher discriminative power and can discriminate even among clones. One of their main disadvantages is the high cost of the technique. Inter Simple Sequence Repeat (ISSR) is more polymorphic and is imperative in biodiversity, genome mapping, and developmental hereditary studies. This PCR-based approach is utilized in totally different plant types and can resolve certain shortcomings of other marker approaches, such as the high costs of AFLP and the lack of the reproducibility of RAPD (Alotaibi & Abd-Elgawad, 2022).

Several other methods of fingerprinting such as SSRs and SNPs were developed and used in identifying medicinal plants, however, there is no ideal methodology as each of them has its own advantages and limitations. A combination of this category of markers technology with the HRM and barcoding methodologies

enabled accurate identification with lower costs, compared to whole genome sequencing.

HRM-High Resolution Melting

High Resolution Melting (HRM) technique was first developed by Jaakola et al., (2010), it detects small differences between PCR amplified fragments via differences in their melting curves. In this technique, initially genomic DNA is extracted from both the authentic medicinal plant and the adulterant(s). The SSR-HRM amplification is performed using specific primers as a template gDNA from both authentic, known plant as well as their adulterants. A preliminary test is carried out to detect adulterants in commercial products by performing SSR-HRM using the selected primers, where the melting curves should overlap to confirm the identity of the unknown sample, otherwise, if the amplicon melting curve differs from the known standard plant, the DNA barcoding can be used as an additional step to assist with the unknown species identification (Li et al., 2018). HRM has notable advantages due to its simplicity, rapidity, sensitivity, and accuracy combined with barcodes. The HRM techniques can be combined with universal primers barcoding, to reduce the analysis cost (Chen et al., 2023).

DNA Barcoding

The development of next-generation sequencing (NGS), a high throughput technique, performs rapid sequencing of millions of DNA fragments simultaneously, providing a vast number of sequences enriched the database of sequences for a huge number of medicinal plant species, facilitating their identification (Satam et al., 2023). Because of the limitations related to the high cost of whole genomic sequencing, in studies aiming for the identification of medicinal plants, this technique was used in combination with barcoding. Furthermore, standard and high-species coverage DNA barcode reference libraries have been constructed to provide reference sequences for species identification, which increases the accuracy and credibility of species discrimination based on DNA barcodes. Therefore, DNA barcoding is a promising tool that plays a key role in the quality control of traditional herbal medicine and the international herb trade (Chen et al., 2023). The principle of barcoding is based on the identification of minor changes that have occurred in high coding or non-coding DNA-conserved regions through the years and evolution. These sequences that might be in the mitochondrial, chloroplast DNA, or segments of nuclear DNA make suitable candidates for barcoding. The data provided by the comparison of these sequences enables the differentiation of species and facilitates the identification of unknown species using as a reference the sequences of DNA barcodes in the available databases (Letsiou et al., 2024). According to the Consortium for the Barcode of Life (CBOL) two regions the *matk* and the *rbcL* could be used as consensus ones in the barcoding of plant species, while *internal transcribed spacer 2* (ITS2) might be used for species identification as supplement marker in species identification. However, the ITS2 marker proved to discriminate among nine different plant species in a multiplex HRM analysis (Xanthopoulou et al., 2016), it remains the most used single locus barcode in herb identification, due to high variability that enables the distinguishing closely related species (Chen et al., 2023). Several other studies applied successfully in medicinal plant identification of different single locus barcoding markers such as *rpoB*, *trnH-psbA*, *atB-rbcL*, *rbcL*, *trnL*,

trnF, *pbsA-trnH*, *mat K*, etc. To increase the information and ensure accurate identification of species the single locus markers were combined and their resolution was tested in different medicinal species (Yu et al., 2021). Conventional DNA barcodes have been widely used for their versatility in the identification of fresh or well-preserved samples, while super-barcodes which were based on plastid genomes have rapidly developed and have shown efficiency in the identification of species at low taxonomic levels. The mini barcodes perform better in the degraded DNA of herbal material. Future studies and applications of DNA barcoding may shift from inter-species to germplasm and interregional identification with the accomplishment of genome fine mapping, especially for entries in the Medicinal Plant Genome Database, which will make it an efficient tool for geo-herbalism research in the field of herbal medicine. On the other side, to avoid herbal misidentification, and artificial adulteration and promote sustainable development of the herbal industry DNA barcoding should be focused on updating the DNA barcoding database and developing novel markers derived from whole sequencing of medicinal plants assisting breeding practice and phylogenetic analysis (Chen et al., 2023).

Conclusions and Perspective

The comparative analysis of approaches used in medicinal plant identification, based on the literature demonstrated that molecular techniques, particularly DNA barcoding, showed higher accuracy in the identification and differentiation of closely related species, even in dried and mixed samples, overcoming the drawbacks of conventional macroscopic, morphological trait-based and microscopic approaches. However, these techniques require certain expertise, capacities, and funds, making them less accessible in some laboratories. The integration of DNA barcoding with other techniques such as morphological/cytological ones, besides their limitations, provides a valuable tool for medicinal plant authentication and identification, essential to advanced studies and quality monitoring of herbal medicine and the herbal industry.

The development of whole genomic sequence databases, especially those of medicinal plants, will serve as an important base to comprehensively understand species' genetic relationships and evolution. Since the pioneering sequencing of *Arabidopsis thaliana*, many other species have been sequenced or are in process, providing a reference database that not only will facilitate plant identification but will reshape human perspectives in diversity, conservation efforts, and sustainable utilization of medicinal plants in the future, ultimately leading to innovative ethnopharmacology studies and novel herbal therapeutic findings.

References

Alotaibi, M. O., & Abd-Elgawad, M. E. (2022). *ISSR and SCoT for evaluation of hereditary differences of 29 wild plants in Al Jubail Saudi Arabian*. Saudi Journal of Biological Sciences, 29 (5), 3223–3231.https://doi.org/10.1016/j.sjbs.2022.01.053

Au, D.T., Chen, H., Jiang, Z., Zhao, Z. (2009). *A novel method to identify the Chinese herbal medicine Wuzhimaoto by quantification of laticifers*. Microscopy research Teqniques, 72: 293-298. Doi.

10.1002/jemt.20650.

Ayaz, A., Zaman, W. Ullah, F., Saqib, S., Jamshed, S., Bahadur, S., Shakoor, A., Arshad, B. (2020). *Systematics study through scanning electron microscopy; a tool for the authentication of herbal drug Mentha suaveolens Ehrh*. Microsopy Research and Technique, 83 (1); 81-87

Chen, S., Yin, X., Han, J., Sun, W., Yao, H., Song, J., & Li, X. (2023). *DNA barcoding in herbal medicine: Retrospective and prospective.* Journal of Pharmaceutical Analysis, 13(5), 431–441. https://doi.org/10.1016/j.jpha.2023.03.008

Danaeipour, Z., Fotokian, M. H., Talei, D., & Mohammad Naji, A. (2019). *Genetic structure and relationships among Melissa officinalis accessions using AFLP markers.* Biocatalysis and Agricultural Biotechnology, 22, 101416. https://doi.org/10.1016/j.bcab.2019.101416

de Oliviera, A.B., de Mendoca, M. S., Azevedo A.A., Meira, R.M.S.A. (2012). *Anatomi and histochemistry of the vegetative organs of Cissus verticillata-a native medicinal plant of Brasilian Amazon*. Brasilian Journal of Pharmacognosy, 22 (6); 1201-1211.

Ganie, S.H., Upadhay, P., Das, S., Sharma, M.P. (2015). *Authentication of medicinal plants by DNA markers.* Plant Gene, 4: 83-89.

Hao, D.-C., & Xiao, P.-G. (2015). *Genomics and Evolution in Traditional Medicinal Plants: Road to a Healthier Life.* Evolutionary Bioinformatics, 11, EBO.S31326. https://doi.org/10.4137/EBO.S31326

Hyder, Z., Rizwani G.H., Shareef, H., Azhar, I., Zehra, M. (2024). *Authentication of important medicinal herbal species through DNA-based molecular characterization.* Saudi Journal of Biological sciences, 31(6): 103985.

Jaakola, L., Suokas, M., and Häggman, H. (2010). *Novel approaches based on DNA barcoding and high-resolution melting of amplicons for authenticity analyses of berry species.* Food Chem.123 (2), 494–500. doi:10.1016/j.foodchem.2010.04.069

Jamshidi-Kia, F., Lorigooini, Z., Amini-Khoei, A. (2018). *Medicinal plants: Past history and future perspective.* Journal of herbmed pharmacology, 7 (1): 1-7. doi: 10.15171/jhp.2018.01

Jedrzejczyk, I., & Rewers, M. (2020). *Identification and Genetic Diversity Analysis of Edible and Medicinal Malva Species Using Flow Cytometry and ISSR Molecular Markers.* Agronomy, 10(5), 650. https://doi.org/10.3390/agronomy10050650

Letsiou, S., Madesis, P., Vasdekis, E., Monemurro, C., Grigoriou M.E., Skavdis, G., Moussis, V., Koutelidakis, A.E., Tzakos, A.G. (2024). *DNA barcoding as a plant identification method.* Applied Sciences, 4, 1415. https://doi.org/10.3390/app14041415.

Li, J., Xiong, C., He, X., Lu, Z., Zhang, X., Chen, X., & Sun, W. (2018). *Using SSR-HRM to Identify Closely Related Species in Herbal Medicine Products: A Case Study on Licorice.* Frontiers in Pharmacology, 9, 407. https://doi.org/10.3389/fphar.2018.00407

Lo, T., Shaw, P.C. (2019). *Application of next-generation sequencing for the identification of herbal products.* Biotechnology Advances, 37 (8), 107450. https://doi.org/10.1016/j.biotechadv.2019.10745

Marrelli, M. (2021). *Medicinal Plants.* Plants, 10(7), 1355. https://doi.org/10.3390/plants10071355

Matias, L.J., Mercandante-Simoes, M.O., Royo, V.A., Ribeiro, L.M., Santos, A.C., Fonseca J.M.S. (2016). *Structure and histochemistry of medicinal species of solanum.* Brasilian Journal of Pharmacognosy, 26

(2): 147-160. https://doi.org/10.1016/j.bjp.2015.11.002

Petrovska, B. (2012). *Historical review of medicinal plants' usage.* Pharmacognosy Reviews, 6(11), 1. https://doi.org/10.4103/0973-7847.95849

Sarin, B., Clemente, J. P. M., & Mohanty, A. (2013). *PCR–RFLP to distinguish three Phyllanthus sp., commonly used in herbal medicines.* South African Journal of Botany, 88, 455–458. https://doi.org/10.1016/j.sajb.2013.09.011

Satam, H., Joshi, K., Mangrolia, U., Waghoo, S., Zaidi, G., Rawool, S., Thakare, R.P., Banday, S., Mishra, A.K, Das, G., Malonia, S.K. (2023). *Next-Generation Sequencing Technology: Current Trends and Advancements.* Biology (Basel).;12(7):997. doi: 10.3390/biology12070997

Su, X.-Z., & Miller, L. H. (2015). *The discovery of artemisinin and the Nobel Prize in Physiology or Medicine.* Science China Life Sciences, 58(11), 1175–1179. https://doi.org/10.1007/s11427-015-4948-7

Sucer, N.J., Carles M.C. (2008). *Genome based Approaches to the authentification of medicinal plants.* Planta Med, 78:603-623.

Techen, N., Crockett, S. L., Khan, I. A., & Scheffler, B. E. (2004). *Authentication of medicinal plants using molecular biology techniques to compliment conventional methods.* Current medicinal chemistry, 11(11), 1391–1401. https://doi.org/10.2174/0929867043365206

Techen, N., Parveen, I., Pan, Z., & Khan, I. A. (2014). *DNA barcoding of medicinal plant material for identification.* Current Opinion in Biotechnology, 25, 103–110. https://doi.org/10.1016/j.copbio.2013.09.010

Wu, K., Liu, Y., Yang, B., Kung, Y., Chang, K., & Lee, M. (2022). *Rapid discrimination of the native medicinal plant Adenostemma lavenia from its adulterants using PCR-RFLP.* PeerJ, 10, e13924. https://doi.org/10.7717/peerj.13924

Xanthopoulou, A., Ganopoulos, I., Kalivas, A., Osathnunkul, M., Hatzopoulou P.C., Tsafataris, A., Madesis P. (2016). *Multiplex HRM analysis as a took for rapid molecular authentification of nine herbal teas.* Food control, 60:113-116.

Yu, J., Wu, X., Liu, Ch., Newmaster, S., Ragupathy, S., Kress, J. (2021). *Progress in the use of DNA barcodes in the identification and classification of medicinal plants.* Ecotoxicology and Environmental Safety. 111691. https://doi.org/10.1016/j.ecoenv.2020.111691.

Zhao, Zh., Liang, Zh., Guo, P. (2011). *Macroscopic identification of Chinese medicinal materials: Traditional experiences and modern understanding.* Journal of Ethnopharmacology, 134 (3), 556-564. https://doi.org/10.1016/j.jep.2011.01.018.

Assessing R&D Project Complexity: A Bayesian Belief Network Approach

Zülfiye Derin Uslu

Istanbul Technical University, Turkiye, https://orcid.org/0000-0001-7222-743X

Assoc. Prof. Ayberk Soyer

Istanbul Technical University, Turkiye, https://orcid.org/0000-0002-4429-3525

Abstract: Complexity is referred to as one of the significant causes of project failures. Especially in the R&D environment, defining the complexity and managing the uncertainty has become more critical for the projects' success. Several studies have been conducted to assess project complexity. However, existing literature underscores the necessity to focus on causal relationships of complexity factors and consider uncertainty for R&D projects. This research develops a novel measurement model to assess R&D projects' complexity using the Bayesian Belief Network (BBN) approach, which offers a practical probabilistic modeling technique to mitigate uncertainty, one of the significant drivers of complexity. The study consists of four main phases: (i) identifying complexity factors and data collection, (ii) designing BBN structure and network optimization, (iii) model validation, and (iv) model reasoning. The significant findings of this research reveal that the R&D projects' complexity is highly sensitive, particularly to the novelty of the technology, the strategic importance of the project, variability and uncertainty in customer demands, and uncertainty in project objectives. This study's main contribution is applying the BBN approach to measuring R&D projects' complexity, thus considering the interrelationships among project complexity factors and its potential to guide project managers in managing the complexity.

Keywords: Project complexity measurement, Bayesian belief network, Explanation reasoning, R&D projects, Project success

Introduction

Today, projects form the basis of many organizations, whether public or private (Geraldi et al., 2011). Projects are carried out for an organization to achieve its strategic goals. They are designed to produce unique outputs with a new product or service that cannot be obtained in the operational dimension. In project management methodology, unlike operations, time and repetitive processes are limited. At the same time, the goal of producing a unique output at the end of the project involves high risk and uncertainty. Therefore, the management of projects requires a methodology different from that of operational aktivitesi. *Project*

management can generally be defined as planning, managing, monitoring, and controlling the activities targeted to meet the project requirements within a given time and budget using some techniques and tools. Although different methods, such as traditional, agile, and hybrid, are used in project management, the main goal of all methods is the successful completion of the project. Although many factors affect project success, *complexity management* is one of the most important criteria affecting project success (Luo et al., 2017). Baccarini (1996) emphasized in his study that project-based management is generally related to complexity management.

Project complexity is challenging to define and measure (Luo et al., 2017). Baccarini (1996) defined a *wide variety* of interrelated parts as a dimension of complexity. *Project complexity* is a project characteristic that makes it difficult to understand, predict, and control the overall behavior of a project, even with sufficient knowledge of the project system (Vidal & Marle, 2008). It is emphasized that project complexity is an inherent feature of the project (PMI, 2021). This complexity, which introduces non-linear and dynamic variability (Geraldi et al., 2011), brings additional managerial challenges in achieving project objectives. Consequently, the broad meaning of complexity and its intuitive management pose a challenge to the study of this topic (Dao et al., 2022). However, in the project management process, the lack of attention to project complexity is cited as a reason for project failures (Luo et al., 2017). Therefore, understanding project complexity, identifying the factors that cause complexity, and managing this complexity efficiently have become critical issues for researchers and industry experts (Bakhshi et al., 2016). Especially in the volatile environment created by developing technology and increasing competitiveness in recent years, it has become necessary to keep the value obtained from projects at the highest levels, and understanding and managing complexity, which is an obstacle to success, has become an inevitable need.

According to Smith, high competition forces organizations to be more productive, and this is an essential driver for innovation that can help reduce the competitiveness gap between competitors (as cited in OECD, 2023). R&D activities, which are at the heart of innovative projects (Namazi et al., 2023), play an important role in this environment. R&D is systematic research to discover new knowledge and skills to develop new products, processes, or services or improve existing products, processes, or services (KPMG, 2021). R&D projects involve uncertainty about the planned cost or time to achieve the expected results and whether their objectives can be achieved to any extent (OECD, 2015). Therefore, the ability to initiate and complete R&D projects successfully has become a critical differentiator for organizations in this highly competitive and rapidly evolving technological environment.

A study published by McKinsey stated that R&D investments help companies develop new products, services, or business models and enable them to outperform their competitors by offering differentiated outputs to the market (Brennan et al., 2020). R&D activities are of strategic importance not only for companies but also for the economic and sustainable growth of countries. Innovation, which is a fundamental tool for increasing productivity, is strengthened by R&D expenditures. As a result, developed economies such as South Korea, Japan, the US, Germany, and the Nordic countries are leaders in R&D investments (Deloitte, 2022). Target 9.5 of the United Nations' Sustainable Development Goals encourages countries to innovate and calls for increased

R&D spending in the public and private sectors. One of the indicators of this goal is the ratio of R&D expenditures to gross domestic product (United Nations, 2016). A report published by the US Congressional Research Center in 2022 stated that global R&D expenditures tripled from $675 million in 2000 to $2.4 trillion in 2020 (Congressional Research Services, 2022). Companies are also optimistic about R&D investments. A research survey conducted by Deloitte (2022) revealed that 39% of companies plan to invest more in R&D in the next 3-5 years compared to previous years.

In an environment where the performance gap between successful innovators and non-innovators is widening, getting the best out of R&D investments is challenging. This is because the revenue from R&D projects is uncertain. R&D projects are characterized as highly uncertain, interdependent processes, sensitivity to changes in the research environment, and expertise (Nath & Mrinalini, 2000). The McKinsey study found that most companies tend to undertake short-term, more secure projects that protect their existing markets and are driven by customer demands (Brennan et al., 2020). One of the reasons for this is that R&D projects are long-term and complex, and the activities still need to be fully understood within the company. Although R&D projects are strategically important for both companies and countries, they are challenging to manage due to unclear objectives, the need for specialized multidisciplinary teams, and extended project duration. Therefore, R&D projects are considered complex due to these characteristics (Molepo et al., 2019).

This study aims to develop a model to assess the complexity of R&D projects using the Bayesian Belief Network (BBN) method, which offers a practical probabilistic modeling technique to manage uncertainty, one of the critical complexity factors. In this context, the model development studies were carried out in four main phases: (i) identification of complexity factors and data collection, (ii) Bayesian network model building and optimization, (iii) model validation, and (iv) model analysis and inferences. First, based on the literature review and expert knowledge, 28 complexity factors were identified under four categories: macro environment, task environment, organizational factors, and project characteristics. Then, data is collected through a survey with a 5-point Likert scale (1: very low; 5: very high) to define the complexity levels of the factors. From 157 data, 137 consistent data were converted from a 5-point Likert scale to a 3-point Likert scale (low, medium, high) to facilitate the solution of the model. In the second phase, structural learning was performed in the GeNIe software using expert knowledge and the collected data, and a Bayesian network structure was created. To avoid unreasonable causality in the model, the network structure was evaluated by four experts with more than ten years of experience. Then, the conditional probability table of each factor was obtained by parameter learning to calculate the relationships between the factors. In the third phase, k-fold cross-validation was performed to check the accuracy. The model's accuracy was above 80%, indicating that the network structure can be effectively used for modeling complexity. In the fourth phase, sensitivity, influence chain, and scenario analysis were conducted on the developed model. As a result of this research, it was found that the complexity of R&D projects is highly sensitive to the novelty of technology, strategic importance of the project, variability and uncertainty in customer demands, and uncertainty in project objectives. Therefore, changes in the complexity levels of these factors significantly affect the overall project complexity.

Moreover, one of the highest causal relationships between factors in the model is between "cooperation between individuals and departments in the project organization" and "project team structure" factors emphasize the importance of organizational climate for project success. When the complexity level of the factors in the macro environment, task environment, organization, and project characteristic categories are specified as "High" respectively by scenario analysis, it is determined that the project characteristic is the category that causes the probability of project complexity to have "High" complexity with 97%. The main contribution of this study to the literature is the application of the BBN approach to measure the complexity of R&D projects, including the interrelationships among factors. Another contribution of the study is its potential to guide project management professionals in managing project complexity and increasing project success.

The rest of the paper is organized into four sections: *The Literature Review* section summarizes studies on defining project complexity, identifying complexity factors, and measuring project complexity. *The Methodology* section describes the BBN methodology used in the study. *The Application* section describes in detail the application of the Bayesian Belief Network model developed for assessing the complexity of R&D projects. In addition, the analysis results (sensitivity analysis, influence chain analysis, scenario analysis) are explained. Finally, *the Conclusions and Future Work* section provides conclusions, recommendations, and suggestions for future work and discusses the practical and theoretical implications of the results.

Literature Review

An examination of the historical development of project management reveals that numerous large-scale projects have been carried out in environments with varying degrees of uncertainty and variability, emphasizing the crucial role of managing this uncertainty for project success (Morris, 1994). In the current VUCA (Volatility, Uncertainty, Complexity, and Ambiguity) climate, the importance of this issue has become undeniably significant. This era is characterized by accelerated technological advancements, rapid globalization driven by economic and social interdependencies, political and economic instabilities, and heightened competition, all of which have made project management and successful completion more challenging. Consequently, it has become essential to identify the factors leading to project failures and to implement appropriate corrective measures. Luo et al. (2017) identified neglecting project complexity as a cause of project failure in their study. Managing project complexity is a success factor in modern project management (Jaber et al., 2021). As a result, project complexity has become an increasingly significant focus within project management literature.

Complexity is defined as a characteristic that makes it difficult to understand and control the overall behavior of a project system, even when a certain level of information exists within the system (Vidal & Marle, 2008), and it introduces additional managerial challenges (Dao et al., 2022). Therefore, project complexity affects the selection of the project's organizational structure, the choice of project inputs, and the objectives related to time, cost, and quality (Jaber et al., 2021). However, project professionals or teams have an intuitive perception of project complexity, which can depend on many factors, such as the experience of the project team, resource

availability, and stakeholders (Dao et al., 2022). Thus, understanding and defining project complexity is critical for managing it effectively.

Complexity is an inherent characteristic of a project (Baccarini, 1996; Mamédio & Meyer, 2020; PMI, 2021). However, defining this complexity is challenging (Luo et al., 2017). Baccarini (1996) defined *project complexity* as a characteristic comprising many varied (differentiation) and interrelated (interdependency) parts and stated that this complexity arises from organizational and technological factors. In a study by T. M. Williams (1999), it was emphasized that complexity arises from the number of interdependent components (structural complexity) and uncertainty in goals and means (uncertainty). In research conducted by Ribbers & Schoo (2002), diversity, integration, and variability (dynamism) were used to measure the complexity of software projects. In another study by T. Williams (2005), speed resulting from time constraints was included among the complexity factors, in addition to structural complexity and uncertainty. Geraldi et al. (2011) included socio-political complexity alongside structural complexity, uncertainty, dynamism, and speed factors in their study. Bosch-Rekveldt et al. (2011) developed a new framework for project complexity consisting of Technological, Organizational, and Environmental (TOE) factors. In a study conducted by Luo et al. (2017), who have performed extensive research on the complexity of construction projects, a definition of complexity was formulated by incorporating goal, task, and information complexity factors in addition to TOE.

In the reviewed literature, it is observed that project complexity emerges within the framework of uncertainty, variability, diversity, and size, manifesting in areas such as organizational structure, technological maturity, human resource composition in the project, environmental factors, stakeholders, project scope, goals and objectives, and project characteristics. Therefore, the factors contributing to complexity consist of macro-environmental elements, which refer to external conditions that influence the project; task environment factors indicate the external factors directly affect the project's success; organizational factors define the internal factors and project dynamics refer to inherent to project and come from its nature (G. Gönen & Soyer, 2020). The project complexity factors influenced by the ecosystem are summarized in *Figure 1*.

Figure 1. Complexity factors in the project ecosystem

The complexity of projects has been increasing in recent years (Jaber et al., 2021). When this complexity is not effectively managed, it can combine with other factors and negatively impact project outcomes (Dao et al., 2022). In order to manage complexity, it is essential to identify the factors that contribute to it. However, not every identified factor has the same level of impact on project success (Luo et al., 2017). Therefore, measuring the extent to which complexity factors influence project complexity supports project managers in the decision-making process for managing such complexity. Consequently, studies have been conducted in this area. Various methods used to measure project complexity are illustrated in *Figure 2*.

Figure 2. Project complexity measurement methods

Based on the methods presented, it is observed that the Analytic Hierarchy Process (AHP) simplifies the decision-making process by determining the significance of project complexity factors and converting subjective evaluations into numerical values ((Vidal et al., 2011). The Fuzzy Analytic Hierarchy Process (FAHP) utilizes the mathematical structure of AHP and integrates fuzzy logic into the method, enabling a flexible model that better handles uncertainty (Nguyen et al., 2015). However, FAHP requires more expert knowledge than AHP. The Fuzzy Analytic Network Process (FANP) model allows for managing uncertainty by incorporating the interdependencies among project complexity factors into the model (He et al., 2015). It is noted that FANP has a more extended data collection and analysis process and is more complex than FAHP.

Structural Equation Modeling (SEM) can be used to evaluate the relationship between project complexity and project success. This method models the relationships between dependent and independent variables within the model (Luo et al., 2017). However, SEM is used when it is necessary to confirm causal relationships and conduct confirmatory factor analysis. Nonetheless, it cannot dynamically analyze the impact of changes in project complexity on project success, and it possesses dynamic characteristics. Studies have employed a combination of SEM and Fuzzy Cognitive Mapping (FCM) to address this need. FCM is used to model complex systems and infer causal relationships, allowing for scenario-based analysis. However, due to the lengthy process of weighting the factors used in the model and the lack of factor verification, the system might not entirely reflect its characteristics. Therefore, hybrid models that combine the strengths of SEM and FCM can be developed (Luo et al., 2020).

The Bayesian Belief Network (BBN) is a graphical probabilistic model that can model causal relationships between complexity factors, providing a flexible approach to managing uncertainty. The primary distinction

between BBN and FANP is that BBN enables the measurement of the degree of complexity under different uncertainty scenarios (Luo, Zhang, & Wu, 2020). In this model, based on conditional probabilities, conditional independence is assumed between variables. Additionally, a directed acyclic network structure represents the relationships among factors, meaning no feedback system exists. Moreover, BBN is a static model, whereas project complexity has a dynamic structure that can change throughout the project lifecycle. The Dynamic Bayesian Network (DBN) method, developed to address this need, models the dynamic systems using time series (Luo et al., 2022). However, the design and calculations of the model are more complex, requiring a higher level of information.

Methodology

This study aims to develop a new measurement model for assessing the complexity of R&D projects using the Bayesian Belief Network (BBN) method, which offers a practical probabilistic modeling approach to reduce uncertainty, one of the critical factors contributing to complexity. This research aims to address the following questions:

- What are the factors contributing to the complexity of R&D projects?
- How do these factors interact with each other?
- How can project complexity be measured, and to which factors is it sensitive?
- How does project complexity change under different scenarios?

The methodology followed in this study consists of four phases: (i) identification of complexity factors and data collection, (ii) development of the Bayesian Belief Network model, (iii) model validation, and (iv) model analysis and inferences (see *Figure 3*).
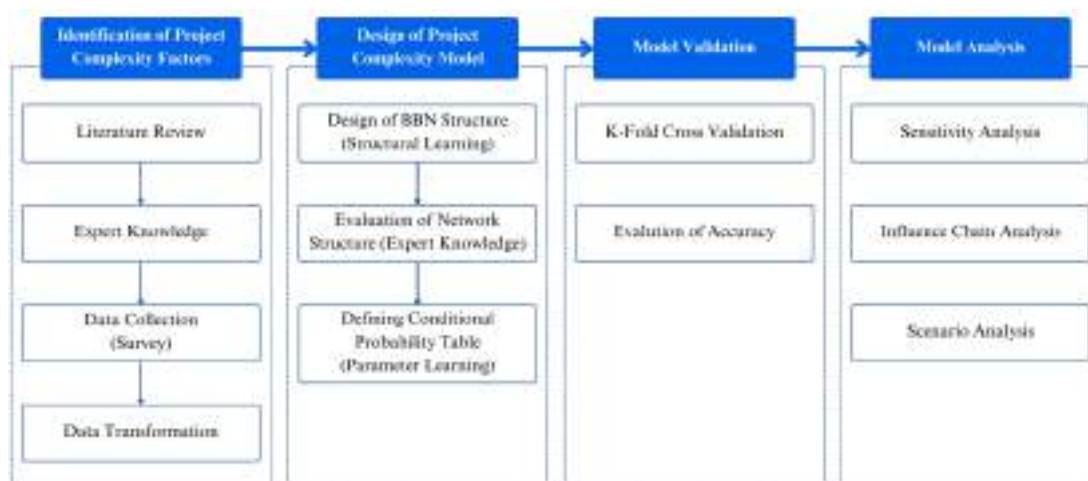

Figure 3. Research framework

First, the complexity factors of R&D projects were identified. The BBN structure was developed in the second

phase using GeNIe Bayesian Network Modeling Software. In the third phase, the validity of the developed model was verified using the k-fold cross-validation method. Finally, predictive analysis, sensitivity analysis, and influence chain analysis were conducted.

Theoretical Background

The Bayesian approach is considered one of the most reliable theorems for managing uncertainty. Several methods, such as Bayesian Hierarchical Models and Bayesian Decision Trees, have been developed using the Bayesian approach. The Bayesian Belief Network (BBN), or Bayesian Network, is a network structure that allows for modeling the dependencies among variables within a domain or system using probabilities, thereby enabling inferences about the future (Akçaoğlu, 2012; Ekici & Ekici, 2016). BBN is recognized as one of the most commonly used probabilistic models for uncertainty modeling (Ekici & Ekici, 2016). Graph theory, which analyzes relationships between variables, is combined with Bayesian theory in this approach. Thus, it enables monitoring system changes through scenario analysis. It provides a model that visually explains heuristic findings and supports decision-makers with analysis, allowing for flexible inferences based on observations (Ekici & Ekici, 2016).

BBN is a method in which variables are connected through conditional probabilities, and the probabilities of various states are calculated using Bayes' Theorem, represented by Directed Acyclic Graphs (Marcot & Penman, 2019). In BBN, nodes represent variables, while directed acyclic arcs depict the relationships between variables. Each variable has discrete states, meaning each variable has its probability table. In BBN, variables are interrelated, so joint probability distributions of these variables are required (Ekici & Ekici, 2016). One of the essential features of BBN is that the directed acyclic arcs indicate that each variable is conditionally independent of all other variables, given its parent variables (Ekici & Önsel Ekici, 2021). The product of the conditional probability distributions of the variables forms the joint probability distribution. This principle is the chain rule, which is the fundamental principle of BBN. The joint probability distribution of a model with *n* variables is given in Equation 1 (Çinicioğlu et. al., 2015; Ekici & Önsel Ekici, 2021).

$$P(X_1, \ldots, X_n) = \prod_{i=1}^{n} P(X_i \mid Parent\ (X_i)) \qquad (1)$$

The relationship between child variables and all of their parent variables in a Bayesian network is defined as a conditional probability table. If a variable has no parent, its marginal probability is used in the model (Pollino & Henderson, 2010). Data is required to calculate the marginal probabilities of variables. The data for a variable can be categorical (e.g., high, medium, low), discrete (e.g., 1, 2, 3), or continuous. However, in BBN, the data must be discrete. Converting continuous data into discrete forms may result in information loss, which is considered a disadvantage of BBN. Thus, it is recommended that models be constructed using discrete data instead of continuous data (Lee et al., 2009).

BBN consists of two components: qualitative and quantitative. The first component, the qualitative section, involves *Structural Learning*, where the graphical representation of relationships among variables is created. The second component, the quantitative section, is *Parameter Learning*, which calculates the conditional probabilities of the interrelated variables (Lee et al., 2009). Modeling BBN is a challenging process. As the number of variables in the model increases, the complexity of the conditional probability table also increases, making mathematical calculations more difficult and time-consuming. Therefore, several software programs have been developed for use in this area.

Research Framework

As stated in the previous section, BBN consists of nodes representing variables and directed acyclic arcs that illustrate the connections between these variables. To construct a BBN model:

- **Step 1:** First, a problem domain should be identified, and the related variables (factors) should be determined. The probabilities of these identified factors are required for model development. Therefore, a data collection process is necessary to calculate these probabilities.
- **Step 2:** A network structure must be established to define the relationship between variables (Structural Learning). Subsequently, a conditional probability table for each factor must be obtained to quantify the relationships between the factors (Parameter Learning).
- **Step 3:** The validity of the constructed model should be evaluated to determine whether it accurately represents reality.
- **Step 4:** Specific inferences related to the identified problem domain can be made through sensitivity or scenario analysis (Ekici & Önsel Ekici, 2021; Luo, Zhang, & Wu, 2020).

Accordingly, this research has been conducted using a methodology consisting of four phases.

Application
Identification of R&D Project Complexity Factors

A problem domain must first be identified to design a Bayesian network structure. This problem could relate to topics such as risk management in large-scale engineering projects (Lee et al., 2009), the management of project complexity (Luo, Zhang, & Wu, 2020), or evaluating production bottlenecks using scenario analysis (Akçaoğlu, 2012). For instance, when project complexity is identified as a problem domain, defining the factors (variables) contributing to project complexity is essential. This definition can be obtained through expert knowledge or literature reviews focusing on the problem area (Luo et al., 2022; Luo, Zhang, & Wu, 2020). After identifying the variables, it is necessary to determine their states and collect data to calculate their probabilities. In the example of project complexity, data on how much technological innovation contributes to project complexity can be collected using a 5-point Likert scale (1: very low contribution to 5: very high contribution). Similarly,

probability distributions for all variables used in the model are required. Thus, data should be collected through expert knowledge, focus groups, or surveys.

In the first stage of this study, a literature review was conducted to identify complexity factors related to R&D projects. Through the literature review, project complexity factors and their categories were obtained. As a result of the literature review, a scope analysis was carried out, and the factors were classified into four categories: macro environment, task environment, organizational factors, and project characteristics, based on the perspective used in the study of G. Gönen & Soyer (2020). Following this classification, the factors that cause the complexity of R&D projects were evaluated, and the complexity factors that could be used in the model were listed. The listed factors were evaluated by six experts with 3-5 years of experience as R&D project managers and four experts with 15 years of experience or more, and the necessary revisions were made. For example, the experts suggested a new complexity factor related to project duration and time pressure, which was subsequently included in the model. The importance of expert knowledge in determining factors and their impact on model results was also emphasized in the study by Nguyen et al. (2015). After the evaluations, it was decided to incorporate 28 complexity factors categorized under four groups specifically for R&D projects into the model shown in *Table 1*.

Next, an online survey was prepared to determine the contribution of each factor to project complexity. Data were collected using a 5-point Likert scale (1: very low to 5: very high) between September 2023 and April 2024 from project managers, team members, and industry experts with R&D project experience. The data collected using the 5-point Likert scale were converted into a 3-point scale to develop the BBN model (1: low; 2: medium; 3: high). In this conversion, values 1 and 2 on the 5-point Likert scale were categorized as low, 3 as medium, and 4 and 5 as high. A similar methodology was followed in the study by Luo, Zhang, and Wu (2020). The reason for this approach is that as the complexity of the network increases in a multi-factor model, the model development process becomes more challenging and time-consuming (Ekici & Ekici, 2016).

A total of 157 responses were collected between September 2023 and April 2024. After excluding responses that were inconsistent or unrelated to R&D projects, 137 valid responses were obtained for use in the model design process. Of the survey participants, 70% were male, 34% were in the 20-30 age group, and 43% held a master's degree. Additionally, 23% of the participants work in the defense industry, and 58% are employed as project managers. Half of the participants have more than ten years of total work experience, and 37% have over ten years of project management experience. For 58% of the participants, the budget of the most recent R&D project they managed or were involved in was TRY 10 million or less, and for 41% of them, the duration of the last R&D project they managed or were involved in was between 12 and 24 months.

According to the survey results, 62% of the participants indicated that the complexity (PC) of the most recent R&D project they managed, led, or participated in as a team member was highly complex. This result supports the identification of the complexity of R&D projects as a problem domain within the scope of this study. Additionally, the levels of factors such as economic factors (ME2), political/legal factors (ME3), interaction and

dependency with external stakeholders (TE1), uncertainty and variability in customer demands and expectations (TE3), competence and sufficiency of human resources (P8), project duration (P12), and the strategic importance of the project (P13) were reported as 50% or higher. Defined R&D project complexity factors and their probabilities are shown in **Error! Reference source not found.**.

Table 1. Defined R&D project complexity factors and survey results for complexity levels

Categories	R&D Project Complexity Factors	Low Complexity	Medium Complexity	High Complexity
Macro Environment (ME; 5)	Environmental Factors (MC1)	53%	23%	23%
	Economic Factors (MC2)	16%	17%	67%
	Political/Legal Factors (MC3)	29%	17%	54%
	Technological Factors (MC4)	34%	23%	43%
	Social Factors (MC5)	50%	24%	26%
Task Environment (TE; 5)	Dependence and Interaction with External Stakeholders (TE1)	23%	23%	54%
	Number and Diversity of External Stakeholders (TE2)	33%	26%	41%
	Uncertainty and Variability in Customer Demands (TE3)	22%	22%	55%
	Dependence and Interaction with Suppliers (TE4)	25%	20%	55%
	Competitive Environment and Competitors (TE5)	20%	30%	50%
Organizational Factors (O; 5)	Organizational Climate/Interaction and Collaboration (O1)	24%	32%	44%
	Cultural Structure and Diversity (O2)	48%	29%	23%
	Financial Risks (O3)	45%	23%	32%
	Operational Risks (O4)	26%	38%	36%
	Organizational Structure (O5)	41%	24%	35%
Project Characteristics (P; 13)	Uncertainty in Goals/Objectives (P1)	47%	21%	32%
	Number, Diversity and Dependency of Goals/Objectives (P2)	47%	23%	29%
	Budget Constraints (P3)	28%	27%	45%
	Uncertainty and Variation in Project Outcome (P4)	23%	28%	49%
	Uncertainty in Scope/Activities (P5)	31%	29%	40%
	The Breadth of Scope/ Number and Diversity of Activities (P6)	31%	27%	42%
	Availability of Resources (P7)	36%	34%	29%
	Competence and Adequacy of Project Team (P8)	19%	25%	56%
	Interaction and Collaboration in Project Team (P9)	29%	32%	39%
	Managerial Competence in Project Management (P10)	47%	24%	29%
	Project Management Methods and Tools (P11)	47%	24%	29%
	Project Duration (P12)	16%	39%	45%
	Strategic Importance of the Project (P13)	29%	25%	46%
Project complexity (PC)	Overall Project Complexity	5%	33%	62%

Design of BBN Model

After determining the project complexity factors and their prior probabilities, the model design phase of the Bayesian network was initiated. To establish the Bayesian network structure, it is necessary first to design a network structure, derive the causal relationships between factors (structural learning), and then obtain the conditional probability table of each factor to quantify the causal relationships (parameter learning). Two

different methods are used to construct a Bayesian network structure: a data-driven and expert knowledge-based network structure. This study uses expert knowledge and data to establish a network structure, including causal relationships, and thereby build a model that better represents real-world conditions. The GeNIe Bayesian Network Modeling program was used for these processes. This section explains the causal relationships obtained through expert knowledge, structural learning, and parameter learning.

Determination of Causal Relationships

While determining the relationships among factors required for constructing the BBN structure, support was received from four experts: a faculty member, two senior researchers working at a research institute, and one expert researcher (PMP). All experts have more than ten years of experience in project management. During this process, the experts were asked to specify the causal relationships (parent-child relationships) among the factors. Before this evaluation, the experts were informed about the necessity for Bayesian networks to have a directed acyclic structure, and they were also asked to ensure that each factor has no more than eight parents. Although the maximum number of parents can be increased, this limitation was applied to prevent the conditional probability table from becoming overly complex due to increased causal relationships. Additionally, it is explained that project complexity, as a factor, is the target variable and, therefore, cannot be a parent of any other factor. Based on the inputs obtained from the four experts, causal relationships were identified for the constructing of the Bayesian network.

Construction of the BBN Network Structure (Structural Learning)

Following determining causal relationships between factors through expert knowledge and the data collected via the survey, structural learning was performed using the GeNIe software, and the initial network structure was obtained. In establishing the network structure, the 28 complexity factors and project complexity were defined as "nodes." The causal relationships obtained through expert knowledge were represented by "arcs" and used as background knowledge. Bayesian Search is used for the learning algorithm. Then, the first network structure is obtained. In the initial network structure obtained through expert knowledge and data, the relationships generated by the algorithm, which differed from the expert knowledge, were examined. As a result of structural learning, three new directed relationships emerged. Experts evaluated the algorithm-generated relationships to determine their relevance and significance. Following the evaluation, it was concluded that these relationships should remain in the model, and consequently, the final network structure could be used for parameter learning.

Determination of Conditional Probabilities (Parameter Learning)

After determining the relationships between factors through structural learning, parameter learning is required to quantify these relationships and obtain probability distributions. The randomized initialization method for parameter learning is used due to its better predictive performance (GeNIe User's Manual, 2024). The EM algorithm was used for parameter learning, which means that the parameters iteratively maximize the log-

likelihood of the observed data. The log-likelihood value represents how well the estimated parameters explain the observed data. The log (p) value ranges between negative infinity and zero (0), indicating the model's fit to the data. As a result of parameter learning, the log (p) value was found to be -3345.630. With the completion of parameter learning, the conditional probability tables of the factors were obtained.

The probabilities obtained for each factor due to the conditional probability tables were presented in a single graphical representation in *Figure 4*. The graph shows that the probability of the project complexity (PC) factor being high is 51%. This result is consistent with the results obtained from the prior probability distributions of project complexity. The determination of these probabilities established a foundation for model analysis. However, before proceeding to the analysis phase, testing the model's validity and determining how accurately it explains the actual data is necessary.
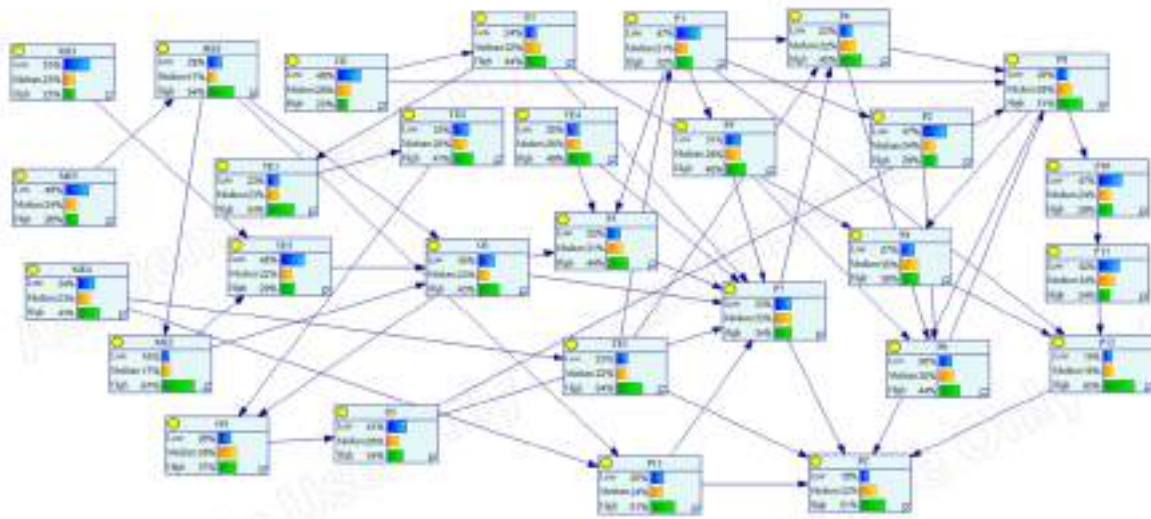
Figure 4. Probability distributions obtained as a result of the BBN model

Model Validation

The model's validity needs to be checked after designing the BBN structure and determining conditional probabilities. The model's validity is obtained by comparing the prediction power of the model with the actual values. Different algorithms are used for this purpose. One of the most potent methods is the k-fold cross-validation. In k-fold cross-validation, the dataset is divided into *k* equal parts, and the model is trained on *k-1* parts and tested with the final dataset in *k*. As a result, validation data is generated for each *k* data set, and the process is repeated *k* times. *k* is usually chosen between 5 and 10 times. The final accuracy value is obtained by averaging the accuracy value in each iteration. Models with an accuracy of 80% and above are described as efficient models (Cooper & Herskovits, 1992).

In this study, validation was carried out using the k-fold cross-validation method to determine to what extent the designed model reflects real life. First, the data of all factors used in the model were included in the validation

process. Considering the size of the dataset, the k value is set as "5" for this study. The dataset is divided into five equal parts, trained on 4 (5-1) parts, and tested on the last dataset within k. As a result, validation data is generated for 5 data sets, and the process is repeated five times. In addition to determining the value of k, the parameter initialization method must also be determined. The randomized initialization method was used as parameter learning in the validation process. Also, the variable (factor) to be tested in the validation process needs to be selected. Since the primary purpose of this study is to evaluate the project complexity, the project complexity factor (PC) is chosen as the class node. The validation process was initiated once the necessary information was defined and model accuracy was obtained. It was concluded that the model correctly predicted 111 out of 137 data and worked with 81% accuracy.

Model Analysis

With the model accuracy being determined as 81%, it has been identified that the model can effectively evaluate the complexity of R&D projects. Consequently, the model analysis phase was initiated. The Bayesian Belief Networks analysis is based on the probability computation process. Two main analysis types are commonly employed in BBNs (Luo, Zhang, & Wu, 2020).

i. Forward Reasoning – Predictive Analysis: *Predictive analysis* is a forward reasoning analysis that estimates the future value of a variable when the state of another variable is hypothetically changed. When a variable's state is altered hypothetically in a BBN model, the probabilities are recalculated (Luo, Zhang, & Wu, 2020), providing insights for future predictions. For example, if a project complexity factor, such as technological novelty, is high, the overall project complexity level will also change. Consequently, predictive analysis enables inferences regarding project complexity levels under different scenarios.

ii. Explanation Reasoning – Sensitivity Analysis and Influence Chain Analysis: Sensitivity analysis, one of the explanatory analyses, examines how sensitive a variable is to other variables (Luo, Zhang, & Wu, 2020). To observe sensitivity, a target node must be selected within the model. Sensitivity analysis determines which variables can cause a significant change in the probability of the target node. For instance, if *project complexity* is defined as the target node and it shows high sensitivity to the factor of technological novelty, it can be inferred that possible changes highly influence project complexity in this variable. At this point, sensitivity analysis is a crucial tool in the decision-making process. Another type of explanatory analysis is influence chain analysis, which demonstrates the degree of mutual influence among variables, i.e., the dependency levels of conditional probabilities between variables (Luo, Zhang, & Wu, 2020).

In this study, sensitivity analysis, influence chain analysis, and scenario analysis were conducted to analyze the developed BBN model.

Sensitivity Analysis

Sensitivity analysis was conducted to determine which factors the project complexity is most sensitive to, meaning which factors significantly influence the probability of project complexity when they change. In this context, the project complexity (PC) factor was defined as the target node in the GeNIe software. The result is shown in *Figure 5*. The sensitivity analysis highlights the factors that project complexity is sensitive to in red. A lighter shade of red indicates a lower sensitivity level. Accordingly, the factors to which R&D projects are most sensitive are as follows:

- P13: Challenging conditions arising from the strategic importance and criticality level of the project
- TE3: Challenging conditions arising from variability and uncertainty related to customer demands and expectations
- ME4: Challenging conditions arising from variability, uncertainty, and dependence related to the technological environment
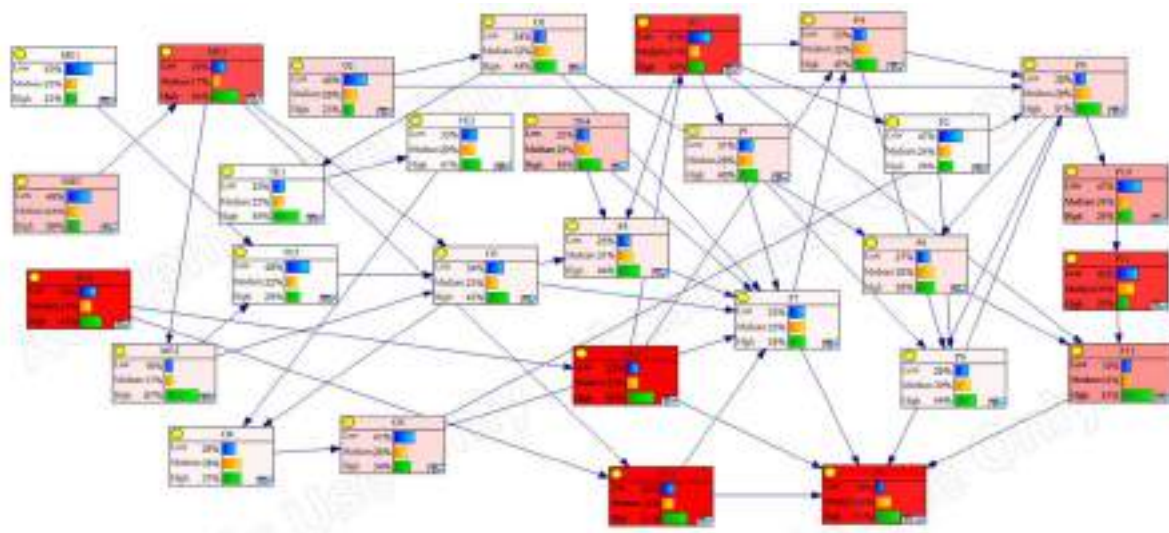
Figure 5. Sensitivity analysis results

The most sensitive factor for R&D projects is the project's strategic importance (P13). R&D projects aiming to develop innovative products, services, or processes are critically important in enhancing national and international competitiveness. These projects are also included among the United Nations' Sustainable Development Goals as the foundation of technological innovation. Moreover, R&D expenditures are associated with the development levels of countries. Therefore, the fact that the strategic importance and criticality of R&D projects emerged as the most sensitive factor influencing project complexity further underscores the significance of these projects.

The second most sensitive factor for R&D projects is the uncertainty and variability in customer demands and expectations (TE3). Uncertainties and changes in customer demands can lead to ambiguities in project goals and objectives, causing uncertainties in defining requirements. At the same time, the need for flexible management,

ensuring accurate information flow, and managing resources can result in various managerial challenges. Additionally, constant changes in the design or development processes can lead to prolonged design periods, the need for additional resources, and deviations from the planned budget and project schedule. Therefore, it is considered an expected outcome that project complexity is sensitive to this factor.

Technological uncertainties, changes, and dependencies in the macro environment (ME4) are also among the factors to which project complexity is most sensitive. Since R&D projects are designed to produce innovative outcomes, they are one of the project types with the highest degree of technology utilization. For instance, if the technology planned for the project needs to be sufficiently mature in the country or the relevant organization, it poses a significant risk to the R&D process. Moreover, the continuous change of sufficiently mature technologies can frequently require testing in developed designs or prototypes, resulting in challenges in adapting to these changes. Therefore, the fact that the MC4 factor emerged as a factor that creates a significant difference in the complexity level of R&D projects supports the validity of this study.

Influence Chain Analysis

The degree of dependency between conditional probabilities is represented using influence chain analysis (Luo, Zhang, & Wu, 2020). *Figure 6* illustrates the dependency relationships between nodes in a Bayesian network and shows the graphical representation of the influence analysis conducted for this study. In this graph, it is evident that the arcs between factors have varying thicknesses. The thickness of these arcs indicates the intensity of the effect between factors. This intensity was calculated based on the mean value of Euclidean distance (for low, medium, and high complexity situations).

When examining the results of the influence chain analysis, the highest dependency is found between the "complexity of objectives and goals" factor (P1) and the "number, diversity, and dependencies of objectives and goals" factor (P2). Unclear objectives and goals imply that these goals need to be more well-defined. Ambiguous goals can lead to the emergence of more diverse and numerous objectives. This study's high intensity of the effect between these two factors supports this relationship.

Unclear objectives and goals significantly impact the diversity of these goals, and this diversity and a large number of objectives can cause several challenges in the project management process, including planning. At this point, developing strategies to clarify the objectives and goals as much as possible through detailed planning to reduce this ambiguity is recommended. The factors "financial risks of the organization" (O3) and the "project budget constraints" factor (P3) are the factors that have the most strong influence after P1 and P2. This situation indicates that the organization's financial strength significantly influences the financial management of the projects conducted within that organization. Financial risks can lead to financial uncertainties in projects. Therefore, it has been concluded that the organization's financial risks should also be considered in the project budget management.
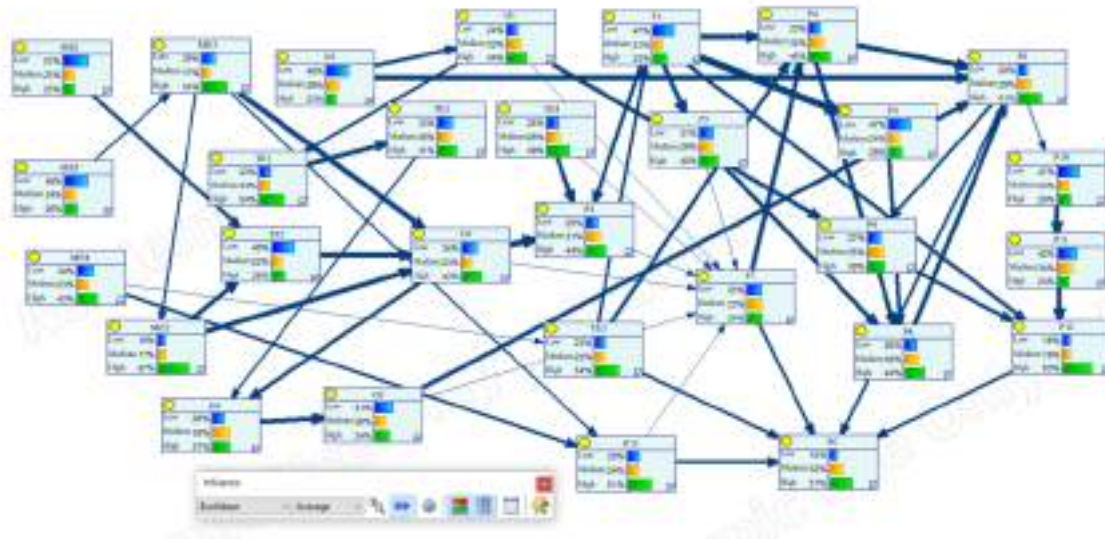
Figure 6. Influence chain analysis results

Two causal chains have been obtained from the parent nodes with the highest dependency. The first chain is as follows: "Uncertainty in the project's objectives and goals (P1)" → "Number, diversity, and dependencies of the project's objectives and goals (P2)" → "Structure of the project's human resources (P8)" → "Interaction and collaboration among project team members (P9)" → "Project complexity (PC)." As previously mentioned, uncertainty in project objectives and goals leads to increased number and diversity of goals. For diverse goals, human resources with different competencies may be required. Depending on the diversity of the project team members, managing interaction and collaboration may become challenging, which in turn contributes to project complexity. As observed, this entire chain belongs to "project characteristic" factors. The factors in this chain have also been used in scenario analysis.

The second causal chain is as follows: "Difficulties in the economic environment (MC2) → Challenges arising from the competitive environment (GC5) → Financial risks of the organization (O3) → Structure of the planned project budget (P3) → Availability and management of the planned project resources (P7) → Project complexity (PC)." Economic difficulties or instability in the macro environment can influence the competitive environment. The competitive environment, in turn, may lead to financial risks within the organization, thereby creating constraints on the project budget. Challenges may arise in accessing planned project resources in such cases, ultimately contributing to project complexity. In this causal chain, it can be observed that the macro environment affects the task environment, the task environment affects organizational factors, and organizational factors impact project characteristics, thus forming a causal chain. The factors in this chain have also been utilized in scenario analysis.

Scenario Analysis

In scenario analysis, one of the forward validation techniques, future outcomes are estimated under different

scenarios. For this purpose, *factors* under macro environment, task environment, organization, and project characteristics were defined as "high" level groups in the GeNIe software, and the probabilities of project complexity levels were obtained for four scenarios. Additionally, scenario analysis were conducted separately and collectively for the factors to which project complexity is most sensitive. Furthermore, scenario analysis was performed for the factors in the two causal chains derived from the influence chain analysis. The results are presented in *Table 2.*

Table 2. Scenario analysis results on project complexity

Scenario	Complexity Category/ Factors	Complexity Level	Project Complexity		
			Low	Medium	High
1	Macro Environment (5)	High	17%	31%	52%
2	Task Environment (5)	High	14%	30%	56%
3	Organization (5)	High	16%	33%	51%
4	Project Characteristics (13)	High	1,5%	1,5%	97%
5	P13	High	13%	25%	62%
6	TE3	High	13%	31%	56%
7	ME4	High	16%	30%	54%
8	P1	High	12%	33%	55%
	P2	High			
	P8	High			
	P9	High			
9	ME2	High	16%	26%	58%
	TE5	High			
	O3	High			
	P3	High			
	P7	High			

Scenario analysis began with project complexity categories. For this purpose, the probability of project complexity was observed, assuming that the macro environment, task environment, organizational factors, and project characteristic factors are defined as "high" (Scenarios 1-4). The project complexity is 97% likely to be highly complex while defining the 13 factors of the project characteristics category as highly complex. This result indicates that project dynamics is the most critical complexity category among the four categories.

In the following scenario analysis (Scenarios 5-7), the three factors to which project complexity is most sensitive were defined separately as highly complex, and their impact on project complexity was observed. When the level of the most sensitive factor, the strategic importance of the project (P13), was defined as high, project complexity resulted in a 62% probability of being highly complex. Although there are probabilistic differences among the sensitive factors, when these factors are defined as high, project complexity has a probability of over 50% being high.

The complexity factors in the two causal chains from the influence chain analysis were examined in the last two scenario analyses. First, when all the factors (P1, P2, P8, and P9) in the most intensive causal chain were

defined as high, project complexity was observed to have a 55% probability of being high. All these factors also belong to the project characteristic factors. Finally, when all the factors (ME2, TE5, O3, P3, and P7) in the other causal chain were defined as high, project complexity resulted in a 58% probability of being highly complex. This scenario analysis included at least one factor from each category: macro environment, task environment, organization, and project characteristics.

Through the scenario analysis, the effects of factors influencing project complexity were probabilistically analyzed. As a result, project characteristic factors were found to have the highest impact on project complexity. Moreover, it was observed that in all nine scenario analyses, project complexity resulted in a probability of over 50% of being highly complex. These findings indicate the need for continuous monitoring of specific factors to reduce complexity in project management. It is also recommended that these factors be focused on through strategic planning.

Conclusion and Future Work

This study was conducted using the BBN method to facilitate the understanding and quantitative assessment of complexity within the scope of R&D projects. In this study, 28 factors creating complexity in R&D projects were identified. Expert knowledge was incorporated into the process to establish a more realistic foundation in determining the relationships among these factors. Structural learning was performed using data collected through surveys and expert knowledge. Then, the Bayesian network structure was established, and conditional probability tables for the factors were obtained through parameter learning. As a result of the established model predicting the project complexity level with 81% accuracy, it aimed to present this study's theoretical and practical contributions through analysis and inferences.

The BBN method was chosen in this study because it allows the quantitative assessment of project complexity and the analysis under different uncertainty scenarios. BBN is a practical method for understanding and managing uncertainty in complex systems. Managing project complexity can offer strong inferences to decision-makers by identifying the factors causing complexity and modeling the relationships among these factors to manage the uncertainty within the system. Expert knowledge was sought on several aspects necessary to conduct this study, such as determining complexity factors, defining causal relationships between factors, and evaluating meaningless relationships that might arise from structural learning to improve the model. The aim was to evaluate project complexity, often managed more intuitively, with a more realistic modeling approach. The model's accuracy of 81% is considered a result of these efforts.

In the model established based on causal relationships specific to R&D projects and proven for its accuracy, sensitivity analysis was performed, and three factors to which the complexity of R&D projects is most sensitive were identified. Scenario analysis was conducted with the same factors, and future inferences were made by observing the extent to which project complexity was affected by these factors. It is recommended that project

management professionals consider the effects of these three identified factors and develop effective strategies to manage complexity. Four different scenario analyses were conducted, including factors from the macro environment, task environment, organization, and project characteristics. The results indicate that each category significantly affects project complexity; however, the project characteristics category has a substantial impact with a 97% likelihood. Therefore, this result is considered a critical contribution to the literature and practical applications. During the project's planning and implementation phases, a significant need for monitoring and control emerges for the 13 complexity factors under this category.

This study provides a new measurement model to evaluate the complexity of R&D projects using the BBN approach, which offers practical probabilistic modeling based on causal relationships. The scope of this study is centered on R&D projects due to their significant role in enhancing companies' competitiveness and decisive influence in global competition. By nature, R&D projects are characterized by numerous uncertainties, high technological dependency, the requirement for multidisciplinary teams, and long-term durations. Therefore, R&D projects are more complex than other project types and require flexible management approaches. Therefore, this study aims to contribute to theoretical and practical applications in managing R&D project complexity for the literature and project management professionals.

However, some areas for improvement that can be applied in future studies have been identified in the developed model. First, the dataset used in the model can be expanded, thus improving the model's accuracy. Additionally, R&D projects involve dynamic processes that can change over time. Therefore, there may be a need for updates in this static Bayesian model, and in response to this need, a Dynamic Bayesian Network model can be designed. Moreover, just as R&D projects have a dynamic structure, project management phases are also dynamic and flexible. The project's initiation phase may not involve the same levels of complexity as the planning or implementation phases. This study can be conducted as multiple studies representing different project management phases. Complexity management can be carried out more effectively with the specified phases for improvement.

References

Akçaoğlu, Ö. (2012). Değer Akış Haritalarında Belirlenen Darboğazların Çözümü İçin Bayes Ağları İle Senaryo Üretimi: Çamaşır Makinası Fabrikasında Bir Uygulama. İstanbul Teknik Üniversitesi, Fen Bilimleri Enstitüsü, Yüksek Lisans Tezi, 66.

Baccarini, D. (1996). The concept of project complexity - A review. *International Journal of Project Management*, *14*(4). https://doi.org/10.1016/0263-7863(95)00093-3

Bakhshi, J., Ireland, V., & Gorod, A. (2016). Clarifying the project complexity construct: Past, present and future. *International Journal of Project Management*, *34*(7). https://doi.org/10.1016/j.ijproman.2016.06.002

Bosch-Rekveldt, M., Jongkind, Y., Mooi, H., Bakker, H., & Verbraeck, A. (2011). Grasping project complexity

in large engineering projects: The TOE (Technical, Organizational and Environmental) framework. *International Journal of Project Management*, *29*(6). https://doi.org/10.1016/j.ijproman.2010.07.008

Brennan, T., Ernst, P., Katz, J., & Roth, E. (2020). Building an R&D strategy for modern times. *McKinsey Insights*, *November*, 1–15. https://www.mckinsey.com/business-functions/strategy-and-corporate-finance/our-insights/building-an-r-and-d-strategy-for-modern-times

Çinicioğlu, Esma Nur; Öncel Ekici, Şule; Ülengin, F. (2015). *Bayes Ağ Yapısının Oluşturulmasında Farklı Yaklaşımlar: Nedensel Bayes Ağları Ve Veriden Ağ Öğrenme*. *November*, 265–284.

Congressional Research Services. (2022). Global Research and Development Expenditures: Fact Sheet. *Congressional Research Services*, 1–5. https://crsreports.congress.gov

Cooper, G. F., & Herskovits, E. (1992). A Bayesian method for the induction of probabilistic networks from data. *Machine Learning*, *9*(4). https://doi.org/10.1007/bf00994110

Dao, B., Kermanshachi, S., Shane, J., Anderson, S., & Damnjanovic, I. (2022). Developing a logistic regression model to measure project complexity. *Architectural Engineering and Design Management*, *18*(3). https://doi.org/10.1080/17452007.2020.1851166

Deloitte. (2022). *Central European Corporate R & D Report 2022*.

Ekici, A., & Önsel Ekici, Ş. (2016). A Bayesian Network Analysis of Ethical Behavior. *Journal of Macromarketing*, *36*(1). https://doi.org/10.1177/0276146715607620

Ekici, A., & Önsel Ekici, Ş. (2021). Understanding and managing complexity through Bayesian network approach: The case of bribery in business transactions. *Journal of Business Research*, *129*. https://doi.org/10.1016/j.jbusres.2019.10.024

G. Gönen, E., & Soyer, A. (2020). Proje Karmaşıklığının Ölçümlenmesine Yönelik Bir Model Önerisi. *International Journal of Advances in Engineering and Pure Sciences*, *32*(4). https://doi.org/10.7240/jeps.690962

GeNIe User's Manual. (2024). *GeNIe Modeler User Manual*.

Geraldi, J., Maylor, H., & Williams, T. (2011). Now, let's make it really complex (complicated): A systematic review of the complexities of projects. İçinde *International Journal of Operations and Production Management* https://doi.org/10.1108/01443571111165848

He, Q., Luo, L., Hu, Y., & Chan, A. P. C. (2015). Measuring the complexity of mega construction projects in China-A fuzzy analytic network process analysis. *International Journal of Project Management*, *33*(3). https://doi.org/10.1016/j.ijproman.2014.07.009

Jaber, H., Marle, F., Vidal, L. A., Sarigol, I., & Didiez, L. (2021). A framework to evaluate project complexity using the fuzzy topsis method. *Sustainability (Switzerland)*, *13*(6). https://doi.org/10.3390/su13063020

KPMG. (2021). *Global R&D Incentives Guide Report*.

Lee, E., Park, Y., & Shin, J. G. (2009). Large engineering project risk management using a Bayesian belief network. *Expert Systems with Applications*, *36*(3 PART 2). https://doi.org/10.1016/j.eswa.2008.07.057

Luo, L., He, Q., Xie, J., Yang, D., & Wu, G. (2017). Investigating the Relationship between Project Complexity and Success in Complex Construction Projects. *Journal of Management in Engineering*, *33*(2). https://doi.org/10.1061/(asce)me.1943-5479.0000471

Luo, L., Zhang, L., & He, Q. (2020). Linking project complexity to project success: a hybrid SEM–FCM

method. *Engineering, Construction and Architectural Management*, *27*(9). https://doi.org/10.1108/ECAM-05-2019-0241

Luo, L., Zhang, L., & Wu, G. (2020). Bayesian belief network-based project complexity measurement considering causal relationships. *Journal of Civil Engineering and Management*, *26*(2). https://doi.org/10.3846/jcem.2020.11930

Luo, L., Zhang, L., Yang, D., & He, Q. (2022). A probabilistic approach to assessing project complexity dynamics under uncertainty. *Soft Computing*, *26*(8). https://doi.org/10.1007/s00500-021-06491-w

Mamédio, D. F., & Meyer, V. (2020). Managing project complexity: how to cope with multiple dimensions of complex systems. *International Journal of Managing Projects in Business*, *13*(4). https://doi.org/10.1108/IJMPB-06-2019-0147

Marcot, B. G., & Penman, T. D. (2019). Advances in Bayesian network modelling: Integration of modelling technologies. Içinde *Environmental Modelling and Software* (C. 111). https://doi.org/10.1016/j.envsoft.2018.09.016

Molepo, P. M., Marnewick, A., & Joseph, N. (2019). Complexity factors affecting research and development projects duration. *2019 IEEE Technology and Engineering Management Conference, TEMSCON 2019*. https://doi.org/10.1109/TEMSCON.2019.8813667

Morris, P. W. G. (1994). *4. The Management of Projects*. Thomas Telford, 1994.

Namazi, M., Tavana, M., Mohammadi, E., & Bonyadi Naeini, A. (2023). A new strategic approach for R&D project portfolio selection using efficiency-uncertainty maps. *Benchmarking*, *30*(10). https://doi.org/10.1108/BIJ-02-2022-0129

Nath, P., & Mrinalini, N. (2000). Benchmarking the best practices of non-corporate R&D organizations. *Benchmarking: An International Journal*, *7*(2). https://doi.org/10.1108/14635770010322315

Nguyen, A. T., Nguyen, L. D., Le-Hoai, L., & Dang, C. N. (2015). Quantifying the complexity of transportation projects using the fuzzy analytic hierarchy process. *International Journal of Project Management*, *33*(6). https://doi.org/10.1016/j.ijproman.2015.02.007

OECD. (2015). Frascati Manual 2015 | OECD READ edition. Içinde *Frascati Manual 2015: Guidelines for Collecting and Reporting Data on Research and Experimental Development, The Measurement of Scientific, Technological and Innovation Activities*.

OECD. (2023). Competition and Innovation a Theoretical Perspective. *Organisation for Economic Cooperation and Development*, *18*(5).

PMI. (2021). *Project Management Body of Knowledge (PMBOK®) 7th Edition* (Sayı July).

Pollino, C. A., & Henderson, C. (2010). Bayesian networks: A guide for their application in natural resource management and policy. *A Technical Report No. 14. Integrated Catchment Assessment and Management Centre, Fenner School of Environment and Society, Australian National University, Canberra*, *14*.

Ribbers, P. M. A., & Schoo, K. C. (2002). Program management and complexity of erp implementations. *EMJ - Engineering Management Journal*, *14*(2). https://doi.org/10.1080/10429247.2002.11415162

United Nations. (2016). The Sustainable Development Goals Report 2016. *United Nations publication issued by the Department of Economic and Social Affairs*, 64. https://unstats.un.org/sdgs/report/2021/#

Vidal, L. A., & Marle, F. (2008). Understanding project complexity: Implications on project management. *Kybernetes*, *37*(8). https://doi.org/10.1108/03684920810884928

Vidal, L. A., Marle, F., & Bocquet, J. C. (2011). Measuring project complexity using the Analytic Hierarchy Process. *International Journal of Project Management*, *29*(6). https://doi.org/10.1016/j.ijproman.2010.07.005

Williams, T. (2005). Assessing and moving on from the dominant project management discourse in the light of project overruns. Içinde *IEEE Transactions on Engineering Management* (C. 52, Sayı 4). https://doi.org/10.1109/TEM.2005.856572

Williams, T. M. (1999). The need for new paradigms for complex projects. *International Journal of Project Management*, *17*(5). https://doi.org/10.1016/S0263-7863(98)00047-7

Examining The Impact of Green Logistics Practices on Sustainability Performance: Logistics Sector Application

İmge Benay Sivuk

Istanbul Technical University, Türkiye, https://orcid.org/ 0000-0002-3859-2000

Ayberk Soyer

Istanbul Technical University, Türkiye, https://orcid.org/ 0000-0002-4429-3525

Abstract: The recognition of global warming as a significant threat reveals the necessity of various actors taking sustainable actions. One of the most important application areas of these actions is the supply chain. Given the observed rise in energy consumption and emissions levels in recent times, it is critical for logistics companies to adopt green logistics management practices to mitigate the associated environmental impacts. This is particularly important due to the escalating sustainability worries among governments and society regarding logistics operations, which play a vital role in the supply chain. Logistics companies will be able to contribute to environmental, economic, and social sustainability by increasing their sustainability performance with green logistics practices. Based on this view, this study aims to evaluate the contributions of green logistics practices to the sustainability performance of a logistics company that adopts green logistics management and to prioritize these practices. To achieve this, 36 green logistics practices impacting sustainability were identified through a literature review and grouped into seven categories. Subsequently, based on the opinions of experts working in a Turkey-based logistics company, the identified green logistics practices were ranked in terms of their contribution to sustainability performance using the Full Consistency Method.

Keywords: Sustainability, Sustainability performance, Green logistics practices, Full consistency method

Introduction

The reality of global warming as a significant threat underscores the vital necessity for various actors to engage in sustainable actions. In recent years, there has been a notable increase in the factors that contribute to global warming. For example, the global spread of the SARS-CoV-2 virus has resulted in a significant increase in the generation of healthcare-related waste, thereby intensifying the environmental impact of solid waste (World Health Organization, 2022). Such negative environmental impacts have resulted in climate change, which has

led to the emergence of global environmental problems at levels that threaten the survival of humanity on a daily basis. It can be reasonably argued that several processes are collectively contributing to a range of global environmental issues. These include pollution, global warming, ozone depletion, acid rain, the depletion of natural resources, overpopulation, waste disposal, deforestation, and loss of biodiversity (Singh & Singh, 2017). It is thus evident that, in order to mitigate the potential adverse consequences, it is of great importance for individuals, governments, and corporations to implement the necessary measures to protect against such risks.

As posited by Groves (2019), the concept of sustainability is predicated on the notion that the future is a significant concern, particularly in light of the necessity to re-examine the relationship between humanity and the natural world. Over time, this feeling has evolved into a concern focused on the legacy that will be left to future generations. In response to these concerns, there is a growing awareness of the need to act in accordance with sustainable principles. Therefore, the concept of sustainability has emerged as a key priority in recent years, driven by environmental concerns and the intensifying competition between companies. The integration of sustainability practices into operational procedures has been enabled by several factors, including the emergence of consumer demand for environmentally friendly products and the pursuit of cost savings through the utilization of economically recycled materials. The pursuit of sustainable value creation has emerged as a core strategic objective for companies aiming to achieve superior performance while upholding environmental responsibility (Hristov & Chirico, 2019). Sustainability can be considered from the perspectives of the environment, economy, and society. In this context, companies are striving to assess and enhance their sustainability performance by taking into account the relevant sustainability dimensions in a manner that aligns with their specific business models (Vivas et al., 2019). A company's sustainability performance is associated with a number of factors, including the protection of natural resources, emission levels, environmental activities and initiatives, employment, occupational health and safety, community relations, stakeholder engagement, and economic impacts (Adams et al., 2014).

In a globalized world, the creation of sustainable value depends to a great extent on the activities of those involved in the supply chain. It is evident that each activity within the supply chain has the potential to influence the ecosystem in a multitude of ways, both positively and negatively. The implementation of green practices within companies operating in the supply chain will contribute significantly to the reduction of potential adverse effects. As a component of the broader supply chain, the activities undertaken by the logistics sector are responsible for a range of detrimental effects on the natural environment. These effects include increased greenhouse gas emissions, noise pollution, and excessive consumption of resources. As indicated by Doherty & Hoyle (2009), approximately 2,800 of humanity's 50,000 mega-tones of annual CO_2e greenhouse gas emissions can be attributed to logistics and transportation activities. Furthermore, the excessive utilization of resources has an adverse impact on economic growth, which, in turn, poses a threat to public health. In light of the detrimental effects of the aforementioned damages, it is essential for logistics companies to prioritize the improvement of their sustainability performance. The implementation of green logistics practices (GLPs) within the scope of green management represents a viable strategy for logistics companies seeking to enhance their sustainability performance. This approach offers a means of contributing to environmental, economic, and social

sustainability, thereby aligning the interests of logistics companies with the broader objectives of sustainable development.

In line with the above-mentioned explanations, the objective of this study is twofold: firstly, to evaluate the contributions of GLPs to sustainability performance; and secondly, to prioritize these practices. In order to achieve this objective, a comprehensive literature review was conducted to gain insight into the primary factors influencing sustainability performance and GLPs. Subsequently, the GLPs identified within the scope of the study were ranked in terms of their contribution to sustainability performance by taking the opinions of experts working in the operations and sustainability departments of a logistics company based in Turkey that adopts green logistics management.

Literature Review

Logistics operations are concerned with the efficient transportation of goods and services from their point of origin to their destination. This encompasses a range of activities, including the management of transportation, storage, and materials. In accordance with the prevailing trends of globalization in recent years, the operations of the logistics industry have undergone a notable expansion on a global scale. This growth is projected to persist over the foreseeable future. Consequently, in conjunction with this expansion, the environmental, economic, and social consequences of transportation operations are also intensifying. In order to mitigate these adverse effects, companies in the logistics industry have commenced a shift towards green logistics management, prioritizing the implementation of environmentally conscious strategies. Green logistics management is defined as the strategic planning, implementation, control, and management of logistics activities through the use of advanced logistics technologies and environmental management systems, with the objective of reducing pollutant emissions (Chang & Qin, 2008). GLPs encompass an array of activities. These activities are classified in various ways in the literature (Colicchia et al., 2013; Evangelista et al., 2017; Zhang et al., 2014). According to Sureeyatanapas et al. (2018), green logistics activities include practices such as alternative energy and vehicle technology, modal transition, eco-driving, reverse logistics, green packaging, vehicle routing, and green management. A summary of GLPs as presented in the literature and the categories under which these practices are grouped are provided in Table 1.

Table 1. GLPs and GLP Categories (GLPCs)

GLPCs	Sources	GLPs	Sources
Vehicle and Fuel Practices	(Rakhmangulov et al., 2018; Sureeyatanapas et al., 2018)	Using alternative energy/fuel sources and vehicles that cause less emissions (biofuel, electric, hybrid, etc.)	(Colicchia et al., 2013; Dioha & Kumar, 2020; Sureeyatanapas et al., 2018; Vienažindienė et al., 2021; Zhang et al., 2014)
		Reducing vehicle speeds to save fuel and reduce emissions	(Colicchia et al., 2013; Rakhmangulov et al., 2018)
		Monitoring pollutants (emissions) from vehicles	(Vienažindienė et al., 2021; Zhang et al., 2014)

GLPCs	Sources	GLPs	Sources
		Tracking the useful life of vehicles	(Zhang et al., 2014)
		Monitoring vehicle fuel consumption	(Zhang et al., 2014)
		Use of vehicles with larger carrying capacity	(Rakhmangulov et al., 2018)
		Reducing the number of second-hand vehicles	(Vienažindienė et al., 2021; Zhang et al., 2014)
Transportation Practices	(Colicchia et al., 2013; Evangelista et al., 2017; Rakhmangulov et al., 2018; Vienažindienė et al., 2021; Zhang et al., 2014)	Use of lower energy transportation modes (intermodal, multimodal, and combined transportation)	(Colicchia et al., 2013; Evangelista et al., 2017; Rakhmangulov et al., 2018; Sureeyatanapas et al., 2018; Vienažindienė et al., 2021)
		Optimizing transport load distribution	(Colicchia et al., 2013; Sureeyatanapas et al., 2018; Zhang et al., 2014)
		Using guidance systems to minimize travel distances (vehicle routing applications)	(Colicchia et al., 2013; Sureeyatanapas et al., 2018)
		Turning off the vehicle engine during loading and unloading operations	(Rakhmangulov et al., 2018)
		Mechanization and automation of loading, unloading, and storage operations	(Rakhmangulov et al., 2018)
		Using eco-driving (safe driving and fuel-saving) systems	(Rakhmangulov et al., 2018; Sureeyatanapas et al., 2018)
		Reducing turns with empty load	(Rakhmangulov et al., 2018)
Packaging Practices	(Colicchia et al., 2013; Evangelista et al., 2017; Rakhmangulov et al., 2018; Sureeyatanapas et al., 2018; Vienažindienė et al., 2021; Zhang et al., 2014)	Reducing the use of packaging	(Colicchia et al., 2013; Evangelista et al., 2017; Sureeyatanapas et al., 2018; Vienažindienė et al., 2021; Zhang et al., 2014)
		Using ecological materials for packaging	(Colicchia et al., 2013; Rakhmangulov et al., 2018; Sureeyatanapas et al., 2018; Vienažindienė et al., 2021)
		Using recyclable or reusable packaging and containers	(Colicchia et al., 2013; Rakhmangulov et al., 2018; Sureeyatanapas et al., 2018; Vienažindienė et al., 2021; Zhang et al., 2014)
		Using the eco-labelling system	(Rakhmangulov et al., 2018)
Waste Management Practices	(Rakhmangulov et al., 2018; Vienažindienė et al., 2021)	Implementing sustainable waste separation practices	(Colicchia et al., 2013; Evangelista et al., 2017; Sureeyatanapas et al., 2018; Zhang et al., 2014)
		Implementation of reverse logistics practices	(Rakhmangulov et al., 2018; Sureeyatanapas et al., 2018)
		Improving disposal and waste monitoring technologies	(Rakhmangulov et al., 2018; Vienažindienė et al., 2021; Zhang

GLPCs	Sources	GLPs	Sources
			et al., 2014)
Storage Practices	(Colicchia et al., 2013; Evangelista et al., 2017; Rakhmangulov et al., 2018; Vienažindienė et al., 2021)	Optimizing storage space	(Rakhmangulov et al., 2018; Vienažindienė et al., 2021; Zhang et al., 2014)
		Using storage methods suitable for the product	(Rakhmangulov et al., 2018; Vienažindienė et al., 2021; Zhang et al., 2014)
		Using alternative energy sources for storage	(Colicchia et al., 2013; Evangelista et al., 2017; Rakhmangulov et al., 2018)
		Eco-friendly warehouse design	(Colicchia et al., 2013; Evangelista et al., 2017; Rakhmangulov et al., 2018)
		Using energy-efficient material handling equipments	(Colicchia et al., 2013; Evangelista et al., 2017; Rakhmangulov et al., 2018; Vienažindienė et al., 2021)
Internal Practices	(Colicchia et al., 2013)	Providing training to employees about green logistics practices and sustainability and increasing employee awareness (adoption of Green Human Resources Management)	(Colicchia et al., 2013; Evangelista et al., 2017; Rakhmangulov et al., 2018; Sureeyatanapas et al., 2018; Vienažindienė et al., 2021; Zhang et al., 2014)
		Carrying out energy-saving practices and audits within the company	(Colicchia et al., 2013; Evangelista et al., 2017; Rakhmangulov et al., 2018; Sureeyatanapas et al., 2018; Vienažindienė et al., 2021; Zhang et al., 2014)
		Using Green Information Technologies (e.g., reducing the number of servers, using green software, etc.) and using Information Management Systems to support sustainable logistics practices (Decision Support Systems, Electronic Data Interchange, etc.).	(Colicchia et al., 2013; Rakhmangulov et al., 2018; Vienažindienė et al., 2021; Zhang et al., 2014)
		Establishing environmental management strategies (Implementation of emission offset programs, publishing carbon emission reports)	(Evangelista et al., 2017; Sureeyatanapas et al., 2018; Zhang et al., 2014)
		Measuring and monitoring the company's environmental performance	
			(Colicchia et al., 2013; George et al., 2016; Sureeyatanapas et al., 2018)
External	(Colicchia et al., 2013;	Providing training on green logistics	(Colicchia et al., 2013;

GLPCs	Sources	GLPs	Sources
Practices	Evangelista et al., 2017)	practices and sustainability to customers, suppliers, subcontractors, and third-party logistics service providers	Evangelista et al., 2017)
		Cooperating with customers, suppliers, subcontractors, and third-party logistics service providers on environmental management	(Ahmed et al., 2018; Colicchia et al., 2013; Vienažindienė et al., 2021; Zhang et al., 2014; Zhu et al., 2007)
		Selecting suppliers, subcontractors, and third-party logistics service providers based on their environmental performance; measuring and monitoring the environmental performance of these stakeholders	(Fan & Kang, 2023; Rakhmangulov et al., 2018; Sureeyatanapas et al., 2018; Vienažindienė et al., 2021; Zhang et al., 2014)
		Membership in environmental management programs	(Colicchia et al., 2013)
		Obtaining environmental management certification (ISO14000, etc.)	(Evangelista et al., 2017; Vienažindienė et al., 2021; Zhang et al., 2014)

The concept of sustainability is typically delineated in academic literature based on three interrelated sub-dimensions: economic prosperity, social equality, and environmental quality. According to Elkington (2006), these three sub-dimensions express the fact that organizations create value in multiple dimensions (i.e., economic, social, and environmental values). In recent years, there has been a growing body of evidence indicating that corporate sustainability is a prominent area of research, with a particular focus on understanding the factors that drive sustainable innovation (Nicolăescu et al., 2015). Wartick & Cochran (1985) argue that the corporate sustainability performance model is a reflection of the interaction between three key concepts: the interaction between social responsibility principles, the process of social sensitivity, and the policies developed to address social problems. Organizations that demonstrate a high level of corporate sustainability performance integrate sustainability principles into all aspects of their operations. In other words, green strategies are implemented across all departments within these organizations.

Considering the environmental impact of logistics activities, it is evident that these operations contribute to several detrimental effects, including noise pollution, poor air quality, rising emission rates, and traffic congestion. Furthermore, the growing awareness of the climate crisis has led to a rise in societal concern about the future. In this context, the role of GLPs in improving the sustainability performance of companies is becoming increasingly crucial. The implementation of GLPs not only enhances a company's environmental performance but also facilitates the optimization of its operational efficiency from an economic and social perspective. According to Maji et al. (2023), a business's green logistics practices enhance its reputation as an environmentally responsible brand, which subsequently increases customer loyalty, brand trust, and profits.

Similarly, as postulated by Sai (2018), in contrast to conventional logistics, green logistics integrates sustainable, economic, and social development.

The implementation of distinct GLPs within a logistics company can significantly contribute to enhancing the company's sustainability performance. According to Vienažindienė et al. (2021), the environmental dimension of sustainability encompasses the utilization of renewable energy sources, the preservation of energy derived from fossil fuels, the minimization of atmospheric emissions, and the deployment of environmentally friendly vehicles. By employing these strategies, organizations can concurrently diminish their environmental footprint and realize economic advantages, including reduced expenditures on fuel and enhanced efficiency in the use of energy resources. In a study conducted by Pautasso et al. (2019), the environmental, economic, and social impacts of the widespread adoption of electric vehicles were evaluated. The researchers tested the model they developed in eight different scenarios and they concluded that the increase in the number of electric vehicles contributes to a reduction in air pollutants (environmental impact), a reduction in the cost of public health (economic impact), and, as a result, an improvement in quality of life (social impact).

Transportation, as one of the logistics activities, has a significant impact on the sustainability performance of organizations, both in terms of its environmental impact and its economic importance. In the study conducted by Sureeyatanapas et al. (2018), a significant number of the interviewed managers asserted that eco-driving behavior is a major contributor to cost savings. This is due to reduction in fuel consumption and maintenance costs, as well as an increase in vehicle efficiency. Furthermore, the same study highlighted that railway transportation is less energy-intensive and emits fewer CO_2 emissions per unit of product than road transportation. Additionally, concerning the environmental dimension, vehicle routing practices have been directly associated with reductions in fuel consumption and air emissions.

On the other hand, green packaging practices have been shown to significantly reduce the consumption of natural resources. Moreover, packaging made with recycled materials also has a positive economic impact on businesses. In their 2013 study, Copeland et al. examined the environmental benefits of reusing the Eco-Clamshell, a reusable packaging container made from polypropylene. The researchers found that reusing an Eco-Clamshell over 29 times resulted in significant environmental savings, with a reduction in energy use and a reduction in greenhouse gas emissions after just 15 uses. The environmental impact of waste generated as a result of logistics activities is undeniable. According to Ali et al. (2023), scrap handling operations can enable environmental protection through waste reduction, waste control measures, and waste monitoring.

Reverse logistics is another GLP that contributes to the sustainability performance of companies. In their 2007 study, Presley et al. demonstrated that reverse logistics contributes to economic, environmental, and social sustainability. Their findings indicate that reverse logistics applications provide direct economic benefits to companies, including reduced costs and the transformation of material use into intangible and competitive benefits. These benefits are associated with the organization's provision of return services to consumers and its improvement in image. Furthermore, from an environmental standpoint, it has been posited that reverse logistics

enhances environmental performance, as it encompasses environmentally friendly practices such as recycling, remanufacturing, and reclamation.

Storage of transported products is of great importance in logistics. Therefore, it is very important to include green solutions in warehousing operations. For organizations seeking to enhance their supply chain sustainability and economic performance, the implementation of appropriate warehouse management systems represents a promising strategy (Harris et al., 2014). It is thus recommended that logistics companies seeking to enhance their sustainability performance integrate green principles into their internal and external policies, as well as their transportation operations.

A further area of concern for logistics companies seeking to enhance their sustainability performance is the implementation of environmentally conscious practices within the company. One such practice is Green Human Resources Management (GHRM), which has been demonstrated to have a significant impact on organizational performance. Green training, an application of GHRM, encompasses training provided to employees both during work hours and on an ongoing basis to achieve the company's ecological goals. According to the study conducted by Pham et al. (2018), green training has been shown to contribute considerably to the environmental performance of a company and also serves to enhance its competitive advantage.

The nature of logistics companies' operations entails the establishment of relationships with numerous entities within the supply chain. Therefore, to enhance their sustainability performance, companies must also develop GLPs that take into account the actions of other actors in the chain (i.e., external practices). For example, external green collaboration by an organization has been demonstrated to significantly enhance its green performance (Ahmed et al., 2018). According to Fan & Kang (2023), the sustainability performance of a company is influenced by the selection of sustainable suppliers and the subsequent implementation of sustainable supplier development practices. Furthermore, organizations that seek to mitigate environmental impact throughout their operations seek to integrate various standards into their management strategies, with a particular emphasis on environmental management systems. One of these standards is ISO14001, developed by the International Organization for Standardization in 1996, which results in substantial enhancements in both environmental and business performance for organizations (Ferrón-Vílchez, 2016). In light of the aforementioned points, this study seeks to assess the influence of GLPs on sustainability performance. The subsequent methodology section elucidates the steps undertaken to attain this objective.

Methodology

The purpose of this study is to assess the contribution of GLPs to sustainability performance and to prioritize these practices. The general framework with the steps followed in the study for this prioritization is given in Figure 1.
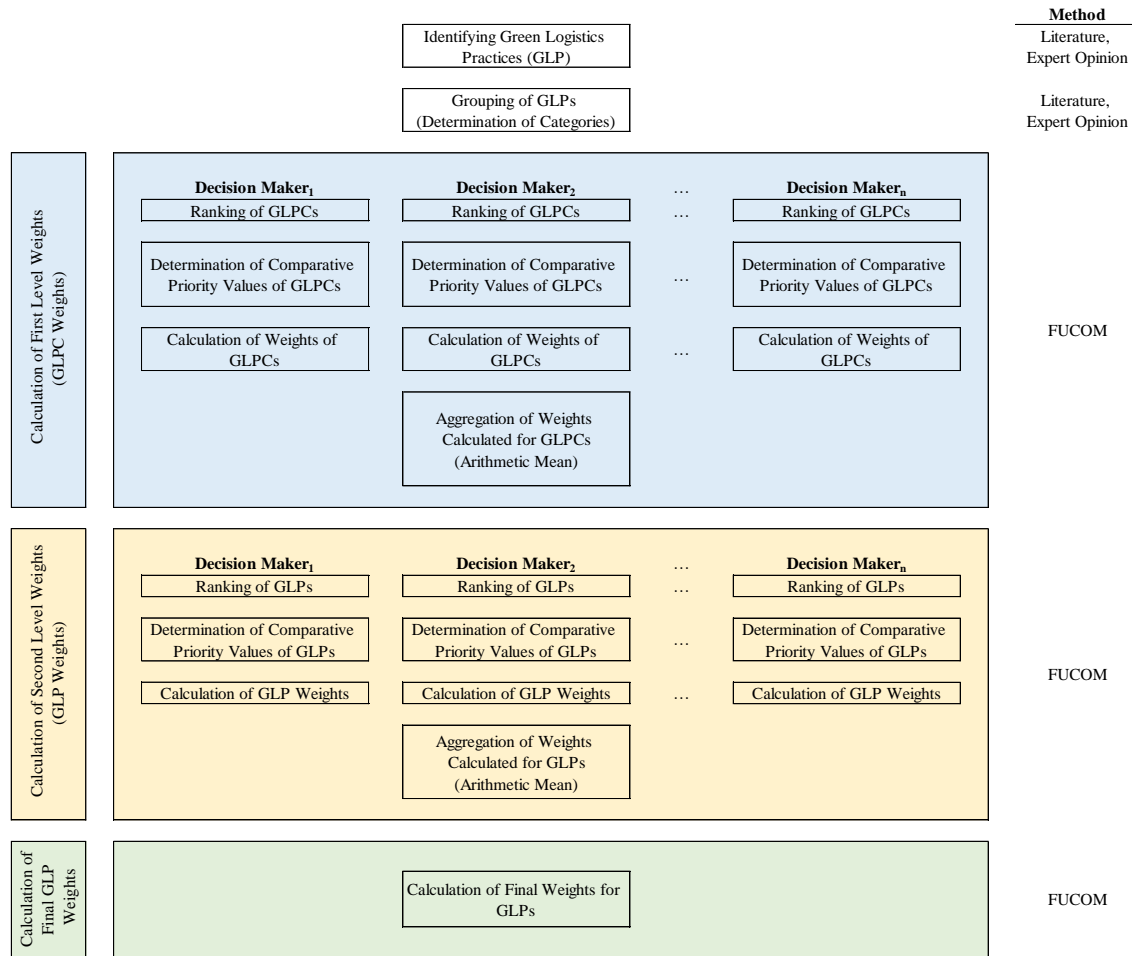
Figure 1. Steps of the Methodology

Step 1: Identifying Green Logistics Practices

In order to identify the GLPs that are the subject of this research and examine their impact on sustainability performance, a review of the relevant literature and consultation with experts in the field were undertaken. The listed GLPs were grouped by consulting expert opinions, and finally, 36 GLPs were identified to be examined in this study (See Figure 2).

Step 2: Grouping of Green Logistics Practices

In the second step, the 36 GLPs identified in the previous step were grouped. Firstly, the research examined whether the practices in question were grouped in the studies included in the literature review. Additionally, expert opinions were sought and the relevant categories were clarified and finalized. Subsequently, the 36 GLPs identified through the literature review were classified into seven categories (See Figure 2).

Step 3: Creating a Hierarchical Structure

In the third step, considering the purpose of the research, a hierarchical structure was created for the GLPs

identified in the previous step. The GLPs and GLPCs whose effects on sustainability performance are analyzed are shown in this hierarchy (See Figure 2).
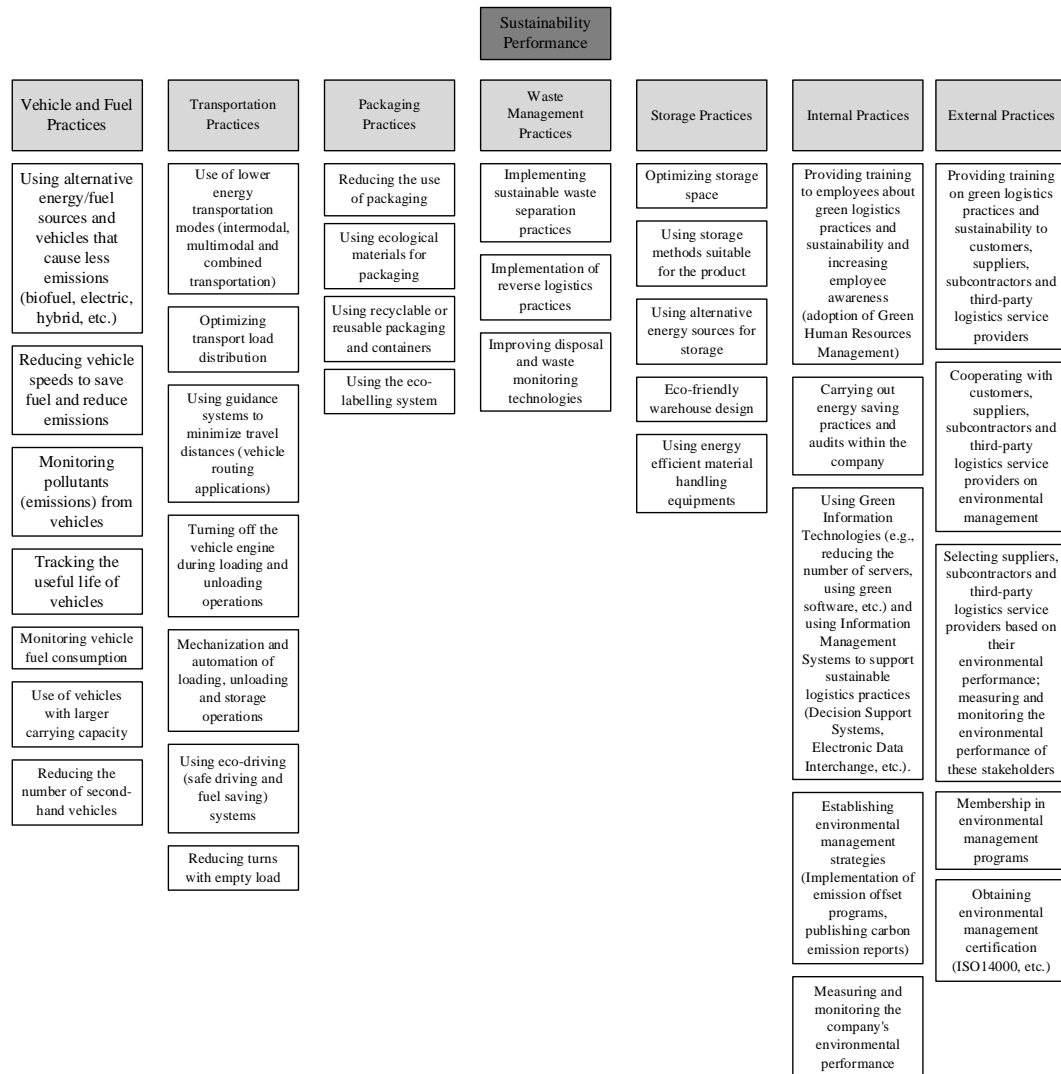

Figure 2. Hierarchical Structure for GLPs

Step 4: Determining the Method to be Used

In the fourth step, the method to be used in this study was determined based on the results of expert opinion and literature research. For this study, Multi-Criteria Decision Making (MCDM) methods, which require experts to choose among multiple alternatives, were investigated. For example, the Analytic Hierarchy Process (AHP) (Saaty, 1980), Best-Worst Method (BWM) (Rezaei, 2015), and Decision Making Trial and Evaluation Laboratory (DEMATEL) (Fontela & Gabus, 1974) are among these methods. If there are 'n' criteria in the decision problem, 'n(n-1)/2' pairwise comparisons are required in AHP, '(2n-3)' in BWM, and 'n(n-1)' in DEMATEL (Ecer, 2020).

A large number of comparisons makes the application of the model more complex, especially when there are a

large number of criteria (Žižović & Pamucar, 2019). On the other hand, in the Full Consistency Method (FUCOM) (Pamučar et al., 2018), only 'n-1' comparisons are sufficient for the solution. FUCOM is very advantageous in terms of reaching a consistent solution with a much smaller number of comparisons. As a result, it was decided to use the FUCOM method for this study.

Step 5: Applying the FUCOM Method

Since the study examines the effects of both GLPCs and GLPs in these categories on sustainability performance, the FUCOM method was applied separately for two levels in the hierarchical structure, and the weight values of GLPCs were calculated at the first level and the weight values of GLPs at the second level. Then, using these weights, the final weights of GLPS were calculated.

FUCOM is one of the MCDM methods developed by Pamučar et al. (2018). In this method, the weight coefficients of the criteria are compared in accordance with the method and consistently. FUCOM consists of the following steps:

Step 5.1: Ranking of Criteria/Options

The ranking is done within a predefined set of criteria/options $C = \{C_1, C_2, \ldots, C_n\}$. The ranking is done according to the importance of the criteria, i.e., starting from the criterion that is expected to have the highest weight coefficient to the criterion with the least importance. This results in a ranking.

$$C = C_{j(1)} > C_{j(2)} > \cdots > C_{j(k)} \tag{1}$$

k: number of observed criteria

If there are two or more criteria of the same importance, a "=" sign is placed between the criteria in question instead of a ">" sign in the expression in Equation (1).

Step 5.2: Determining the Importance of the Criteria/Options

In this step, a pairwise comparison is made between the ranked criteria/options, and the comparative priority of these criteria/options ($\varphi_{k/(k+1)}$, for k = 1, 2, …, n, where k represents the ranking of the criteria/options) is determined. Here, $\varphi_{k/(k+1)}$ is the superiority value of the kth ranked criterion/option over the $(k+1)^{th}$ ranked criterion/option. Thus, the comparative priorities of the evaluated criteria/options are obtained as shown in Equation (2).

$$\Phi = \left(\varphi_{1/2}, \varphi_{2/3}, \ldots, \varphi_{k/(k+1)}\right) \tag{2}$$

Step 5.3: Finding the Final Values of the Weight Coefficients

In this step, the final values of the weight coefficients of the evaluated criteria/options $(w_1, w_2, \ldots, w_n)^T$ are calculated. The calculated weight coefficients must satisfy the following two conditions.

Condition 1: The ratio of the weight coefficients is equal to the comparative priority $(\varphi_{k/(k+1)})$ between the criteria/options considered, defined in step 5.2. Therefore, the condition given in Equation 3 is satisfied.

$$\frac{w_k}{w_{(k+1)}} = \varphi_{k/(k+1)} \tag{3}$$

Condition 2: The final values of the weight coefficients must satisfy the mathematical transitivity condition as shown below.

$$\varphi_{k/(k+1)} \otimes \varphi_{(k+1)/(k+2)} = \varphi_{k/(k+2)} \tag{4}$$

Accordingly,

$$\varphi_{k/(k+1)} = \frac{w_k}{w_{(k+1)}} \tag{5}$$

and

$$\varphi_{(k+1)/(k+2)} = \frac{w_{(k+1)}}{w_{(k+2)}} \tag{6}$$

$$\frac{w_k}{w_{(k+1)}} \otimes \frac{w_{(k+1)}}{w_{(k+2)}} = \frac{w_k}{w_{(k+2)}} \tag{7}$$

Thus, the second condition stated in Equation 8 is obtained, which the final values of the weight coefficients of the criteria/options under consideration must satisfy.

$$\frac{w_k}{w_{(k+2)}} = \varphi_{k/(k+1)} \otimes \varphi_{(k+1)/(k+2)} \tag{8}$$

When the conditions specified in Equation 3 and Equation 8 are met, maximum consistency is achieved and the value of the Deviation from Maximum Consistency (DMC) (χ) coefficient is minimal. Based on these definitions, the ultimate model for determining the final values of the weight coefficients of the criteria under consideration is defined as follows.

$$\min \chi$$
$$s.t.$$

$$\left| \frac{w_{j(k)}}{w_{j(k+1)}} - \varphi_{k/(k+1)} \right| = \chi \,, \forall_j$$

$$\left| \frac{w_{j(k)}}{w_{j(k+2)}} - \varphi_{k/(k+1)} \otimes \varphi_{(k+1)/(k+2)} \right| = \chi \,, \forall_j$$

$$\sum_{j=1}^{n} w_j = 1 \,, \forall_j$$

$$w_j \geq 0 \,, \forall_j \tag{9}$$

Application and Results

Details on the application of the methodology described in the previous section to assess the contribution of GLPs to sustainability performance and prioritize these practices will be explained in this section.

Data Collection

Expert opinions are needed to apply the FUCOM method to calculate the weights of GLPs. Accordingly, a logistics company operating in Turkey is considered. The company was established in 1990, based in Turkey, and carries out its operations in 11 countries, primarily in Turkey, and provides services using land, sea, air, rail, intermodal, and national distribution transportation models. It also carries out warehousing activities, and customs clearance operations and offers technological solutions to logistics applications with its first R&D center in the sector. Furthermore, the company has strategically positioned sustainability as a core value and goal and has adopted green logistics and sustainability principles in its operations. Within the scope of this study, the operational and sustainability-related departments in the company were contacted and four experts were identified to be consulted. These experts work in the company's 'Sustainability Strategies', 'Climate Change Adaptation - Corporate Sustainability', and 'Land Transportation' departments. Their experience in the sector ranges from 8 to 14 years. The data required for the calculation of the importance weights of GLPCs and GLPs using the FUCOM method were obtained by consulting the opinions of these four experts.

The expert interviews were conducted separately with each expert online and lasted approximately one hour. Firstly, the purpose of the study was explained to the experts, information about sustainability performance was given, and GLPs and GLPCs were explained. Since a two-level FUCOM will be applied for the weight calculations of the GLPCs and GLPs whose impact on sustainability performance is measured, the interviews with the experts were conducted at two levels accordingly and the following questions were asked to the experts.

- **Level 1:**
  - Rank the GLPCs in order of importance in terms of contribution to sustainability performance.
  - In your ranking, how important is the first (most important) GLPC compared to the second, third, fourth, ... ranked GLPC?

- **- Level 2:**
  - Rank the GLPs in order of importance in terms of contribution to sustainability performance.
  - According to your ranking, how important is the first (most important) GLP compared to the second, third, fourth, ... ranked GLP?

While determining the comparative priority values of GLPCs and GLPs, the experts used the relative importance scale given in Table 2. In addition, GLPCs and GLPs that experts will rank and determine

comparative priority values are given in Table 3.

Table 2. Relative Importance Scale Used for Comparisons

Intensity of Importance	Explanation
1	Equally important
2	Equally important to Moderately Important
3	Moderately important
4	Moderately important to Strongly important
5	Strongly important
6	Strongly important to Very strongly Important
7	Very strongly important
8	Very strongly Important to Extremely Important
9	Extremely Important

Application of FUCOM: Calculation of First Level GLPC Weights

Details on the calculation of the weights of GLPCs are explained in detail in the following sections.

Ranking GLPCs

First, decision-makers (DMs) ranked the GLPCs given in Table 3 according to their importance (from most important to least important) in terms of contribution to sustainability performance. Accordingly, the importance rankings of each DM for the GLPCs are given in Table 4. The ">" sign in Table 4 indicates that one category is more important than the other, while the "=" sign indicates that one category is of equal importance with the other.

Table 3. GLPCs and GLPs Used in the Study

GLPCs	Definition	GLPs	Definition
$GLPC_1$	Vehicle and Fuel Practices	GLP_{11}	Using alternative energy/fuel sources and vehicles that cause less emissions (biofuel, electric, hybrid, etc.)
		GLP_{12}	Reducing vehicle speeds to save fuel and reduce emissions
		GLP_{13}	Monitoring pollutants (emissions) from vehicles
		GLP_{14}	Tracking the useful life of vehicles
		GLP_{15}	Monitoring vehicle fuel consumption
		GLP_{16}	Use of vehicles with larger carrying capacity
		GLP_{17}	Reducing the number of second-hand vehicles
$GLPC_2$	Transportation Practices	GLP_{21}	Use of lower energy transportation modes (intermodal, multimodal, and combined transportation)

		GLP$_{22}$	Optimizing transport load distribution
		GLP$_{23}$	Using guidance systems to minimize travel distances (vehicle routing applications)
		GLP$_{24}$	Turning off the vehicle engine during loading and unloading operations
		GLP$_{25}$	Mechanization and automation of loading, unloading, and storage operations
		GLP$_{26}$	Using eco-driving (safe driving and fuel-saving) systems
		GLP$_{27}$	Reducing turns with empty load
GLPC$_3$	Packaging Practices	GLP$_{31}$	Reducing the use of packaging
		GLP$_{32}$	Using ecological materials for packaging
		GLP$_{33}$	Using recyclable or reusable packaging and containers
		GLP$_{34}$	Using the eco-labelling system
GLPC$_4$	Waste Management Practices	GLP$_{41}$	Implementing sustainable waste separation practices
		GLP$_{42}$	Implementation of reverse logistics practices
		GLP$_{43}$	Improving disposal and waste monitoring technologies
GLPC$_5$	Storage Practices	GLP$_{51}$	Optimizing storage space
		GLP$_{52}$	Using storage methods suitable for the product
		GLP$_{53}$	Using alternative energy sources for storage
		GLP$_{54}$	Eco-friendly warehouse design
		GLP$_{55}$	Using energy-efficient material handling equipment
GLPC$_6$	Internal Practices	GLP$_{61}$	Providing training to employees about green logistics practices and sustainability and increasing employee awareness (adoption of Green Human Resources Management)
		GLP$_{62}$	Carrying out energy-saving practices and audits within the company
		GLP$_{63}$	Using Green Information Technologies (e.g., reducing the number of servers, using green software, etc.) and using Information Management Systems to support sustainable logistics practices (Decision Support Systems, Electronic Data Interchange, etc.).
		GLP$_{64}$	Establishing environmental management strategies (Implementation of emission offset programs, publishing carbon emission reports)
		GLP$_{65}$	Measuring and monitoring the company's environmental performance
GLPC$_7$	External Practices	GLP$_{71}$	Providing training on green logistics practices and sustainability to customers, suppliers, subcontractors, and third-party logistics service providers
		GLP$_{72}$	Cooperating with customers, suppliers, subcontractors, and third-party logistics service providers on environmental management

GLP$_{73}$	Selecting suppliers, subcontractors, and third-party logistics service providers based on their environmental performance; measuring and monitoring the environmental performance of these stakeholders	
GLP$_{74}$	Membership in environmental management programs	
GLP$_{75}$	Obtaining environmental management certification (ISO14000, etc.)	

Determination of Comparative Priority Values of GLPCs

After ranking the GLPCs described in the previous section, the DMs determined the comparative priority values of these categories. In order to determine the priority values, the most important category was compared with the other categories and the relative importance scale previously mentioned in Table 2 was used to make these comparisons. The determined comparative priority values are presented in Table 5 for each DM separately.

Table 4. Ranking of GLPCs

Decision Makers	Ranking of GLPCs
DM$_1$	GLPC$_2$ > GLPC$_1$ > GLPC$_5$ > GLPC$_3$ > GLPC$_4$ > GLPC$_6$ > GLPC$_7$
DM$_2$	GLPC$_2$ > GLPC$_1$ > GLPC$_4$ > GLPC$_6$ > GLPC$_3$ > GLPC$_5$ > GLPC$_7$
DM$_3$	GLPC$_2$ > GLPC$_1$ > GLPC$_3$ = GLPC$_4$ > GLPC$_5$ > GLPC$_6$ = GLPC$_7$
DM$_4$	GLPC$_2$ > GLPC$_1$ > GLPC$_3$ > GLPC$_6$ > GLPC$_5$ > GLPC$_4$ > GLPC$_7$

Table 5. Comparative Priority Values of GLPCs

DM$_1$						
Order of Importance	GLPC$_2$	GLPC$_1$	GLPC$_5$	GLPC$_3$	GLPC$_4$	GLPC$_6$	GLPC$_7$
Comparative Priority Value	1	3	5	6	7	8	9
DM$_2$						
Order of Importance	GLPC$_2$	GLPC$_1$	GLPC$_4$	GLPC$_6$	GLPC$_3$	GLPC$_5$	GLPC$_7$
Comparative Priority Value	1	2	3	4	5	7	8
DM$_3$						
Order of Importance	GLPC$_2$	GLPC$_1$	GLPC$_3$	GLPC$_4$	GLPC$_5$	GLPC$_6$	GLPC$_7$
Comparative Priority Value	1	2	3	3	5	7	7
DM$_4$						
Order of Importance	GLPC$_2$	GLPC$_1$	GLPC$_3$	GLPC$_6$	GLPC$_5$	GLPC$_4$	GLPC$_7$
Comparative Priority Value	1	3	4	5	7	8	9

Calculating the Weights of GLPCs

After determining the comparative priority values of the GLPCs, the weights of these GLPCs were calculated. For this purpose, a linear programming model was constructed for each DM using the rankings and comparative priority values determined by them. Below the calculations for the construction of the linear programming model of DM$_1$ are given. The comparative priority values of GLPCs:

$$\varphi_{GLPC_2/GLPC_1} = \frac{3}{1} = 3; \varphi_{GLPC_1/GLPC_5} = \frac{5}{3} = 1.67; \varphi_{GLPC_5/GLPC_3} = \frac{6}{5} = 1.2; \varphi_{GLPC_3/GLPC_4} = \frac{7}{6} = 1.17;$$

$$\varphi_{GLPC_4/GLPC_6} = \frac{8}{7} = 1.14; \varphi_{GLPC_6/GLPC_7} = \frac{9}{8} = 1.12$$

$$\Phi = (3; \ 1.67; \ 1.2; \ 1.17; \ 1.14; \ 1.12)$$

Referring to Equation 3

$$\frac{W_{GLPC_2}}{W_{GLPC_1}} = 3; \frac{W_{GLPC_1}}{W_{GLPC_5}} = 1.67; \frac{W_{GLPC_5}}{W_{GLPC_3}} = 1.2; \frac{W_{GLPC_3}}{W_{GLPC_4}} = 1.17; \frac{W_{GLPC_4}}{W_{GLPC_6}} = 1.14; \frac{W_{GLPC_6}}{W_{GLPC_7}} = 1.12$$

and referring to Equation 8

$$\frac{W_{GLPC_2}}{W_{GLPC_5}} = 3 \times 1.67 = 5; \frac{W_{GLPC_1}}{W_{GLPC_3}} = 1.67 \times 1.2 = 2; \frac{W_{GLPC_5}}{W_{GLPC_4}} = 1.2 \times 1.17 = 1.4; \frac{W_{GLPC_3}}{W_{GLPC_6}} = 1.17 \times 1.14 = 1.33;$$

$$\frac{W_{GLPC_4}}{W_{GLPC_7}} = 1.14 \times 1.12 = 1.28$$

Therefore, the linear programming model for DM_1 to calculate the weights of GLPCs is given below. Linear programming models for the other DMs were created in a similar way.

$$\min \chi$$

$$s.t.$$

$$\left| \frac{W_{GLPC_2}}{W_{GLPC_1}} - 3 \right| = \chi$$

$$\left| \frac{W_{GLPC_1}}{W_{GLPC_5}} - 1.67 \right| = \chi$$

$$\left| \frac{W_{GLPC_5}}{W_{GLPC_3}} - 1.2 \right| = \chi$$

$$\left| \frac{W_{GLPC_3}}{W_{GLPC_4}} - 1.17 \right| = \chi$$

$$\left| \frac{W_{GLPC_4}}{W_{GLPC_6}} - 1.14 \right| = \chi$$

$$\left| \frac{W_{GLPC_6}}{W_{GLPC_7}} - 1.12 \right| = \chi$$

$$\left| \frac{W_{GLPC_2}}{W_{GLPC_5}} - 5 \right| = \chi$$

$$\left| \frac{W_{GLPC_1}}{W_{GLPC_3}} - 2 \right| = \chi$$

$$\left| \frac{W_{GLPC_5}}{W_{GLPC_4}} - 1.4 \right| = \chi$$

$$\left| \frac{W_{GLPC_3}}{W_{GLPC_6}} - 1.33 \right| = \chi$$

$$\left| \frac{W_{GLPC_4}}{W_{GLPC_7}} - 1.28 \right| = \chi$$

$$\sum_{j=1}^{7} w_j = 1 \, , \forall_j$$

$$w_j \geq 0 \, , \forall_j$$

The models for all DMs were solved using the Excel Solver add-in and the weight values of the GLPCs calculated for each DM are given in Table 6.

Aggregation of Weights Calculated for GLPCs

The final weights were calculated by taking the arithmetic mean of the GLPC weights calculated for each DM in the previous step (See Table 6). Based on these weight values calculated for GLPCs, when the effects of GLPCs on sustainability performance are considered, the most important category is the transportation practices category (i.e., $GLPC_2$), which has the highest weight value of 0.428.

Table 6. Weights of GLPCs

GLPCs	DM_1	DM_2	DM_3	DM_4	Final Weights
$GLPC_1$	0.160	0.196	0.188	0.154	0.174
$GLPC_2$	0.481	0.392	0.377	0.462	0.428
$GLPC_3$	0.080	0.078	0.126	0.116	0.100
$GLPC_4$	0.069	0.132	0.126	0.058	0.096
$GLPC_5$	0.096	0.056	0.075	0.067	0.074
$GLPC_6$	0.061	0.098	0.054	0.092	0.076
$GLPC_7$	0.053	0.048	0.054	0.051	0.052

Application of FUCOM: Calculation of Second Level GLP Weights

Details on the calculation of the weights of GLPs are explained in detail in the following sections.

Ranking GLPs

First, DMs ranked the GLPs given in Table 3 according to their importance (from most important to least important) in terms of contribution to sustainability performance. Accordingly, the importance rankings of each DM for the GLPs are given in Table 8.

Determination of Comparative Priority Values of GLPs

After making the category rankings described in the previous section, the DMs determined the comparative priority values of the GLPs. In order to determine these values, the most important GLP was compared with

other GLPs, and the relative importance scale given in Table 2 was used to make these comparisons. The determined comparative priority values are presented in Table 9 for each DM separately.

Calculating the Weights of GLPs

After determining the comparative priority values of the GLPs, the weights of these GLPs were calculated. For this purpose, a linear programming model was constructed for each DM using the rankings and comparative priority values determined by them, similar to that described for the GLPCs (See Table 10).

Table 8. GLP Rankings for Each DM

DMs	GLP Rankings
	$GLP_{11} > GLP_{12} > GLP_{17} > GLP_{16} > GLP_{15} = GLP_{13} > GLP_{14}$
	$GLP_{21} > GLP_{23} > GLP_{26} > GLP_{22} > GLP_{27} > GLP_{25} > GLP_{24}$
	$GLP_{31} > GLP_{32} = GLP_{33} > GLP_{34}$
DM_1	$GLP_{41} > GLP_{42} > GLP_{43}$
	$GLP_{53} = GLP_{55} > GLP_{54} > GLP_{51} = GLP_{52}$
	$GLP_{64} > GLP_{65} > GLP_{63} > GLP_{62} > GLP_{61}$
	$GLP_{75} > GLP_{73} > GLP_{74} > GLP_{71} = GLP_{72}$
	$GLP_{11} > GLP_{16} = GLP_{17} > GLP_{15} > GLP_{12} > GLP_{14} > GLP_{13}$
	$GLP_{21} > GLP_{23} > GLP_{27} = GLP_{22} > GLP_{25} > GLP_{26} > GLP_{24}$
	$GLP_{33} > GLP_{31} > GLP_{32} > GLP_{34}$
DM_2	$GLP_{41} > GLP_{42} > GLP_{43}$
	$GLP_{53} > GLP_{55} > GLP_{52} > GLP_{54} > GLP_{51}$
	$GLP_{62} = GLP_{63} = GLP_{64} > GLP_{65} > GLP_{61}$
	$GLP_{75} > GLP_{74} > GLP_{73} > GLP_{72} > GLP_{71}$
	$GLP_{11} > GLP_{12} > GLP_{13} = GLP_{15} > GLP_{17} > GLP_{14} > GLP_{16}$
	$GLP_{21} = GLP_{23} > GLP_{22} > GLP_{27} > GLP_{26} > GLP_{24} = GLP_{25}$
	$GLP_{31} > GLP_{33} > GLP_{32} > GLP_{34}$
DM_3	$GLP_{41} > GLP_{42} > GLP_{43}$
	$GLP_{53} > GLP_{55} > GLP_{54} > GLP_{51} > GLP_{52}$
	$GLP_{64} > GLP_{62} > GLP_{65} > GLP_{63} > GLP_{61}$
	$GLP_{75} > GLP_{73} > GLP_{71} > GLP_{72} > GLP_{74}$
	$GLP_{11} = GLP_{12} > GLP_{16} > GLP_{13} > GLP_{14} > GLP_{15} > GLP_{17}$
	$GLP_{23} > GLP_{21} > GLP_{26} > GLP_{27} > GLP_{25} > GLP_{22} > GLP_{24}$
	$GLP_{31} > GLP_{33} > GLP_{32} > GLP_{34}$
DM_4	$GLP_{42} > GLP_{41} > GLP_{43}$
	$GLP_{53} = GLP_{55} > GLP_{51} > GLP_{54} > GLP_{52}$
	$GLP_{64} > GLP_{62} > GLP_{63} > GLP_{61} = GLP_{65}$
	$GLP_{75} > GLP_{74} > GLP_{73} > GLP_{72} > GLP_{72}$

Aggregation of Weights Calculated for GLPs

The final weights were calculated by taking the arithmetic mean of the GLP weights calculated for each DM in the previous step (See Table 10).

Based on these weight values calculated for GLPs, when the effects of GLPs on sustainability performance are considered, the most important GLP in the vehicle and fuel practices category is the use of alternative energy/fuel sources and vehicles (biofuel, electric, hybrid, etc.) that cause less emissions, which has the highest weight value of 0.416.

Application of FUCOM: Calculation of the Final Weights for GLPs

As a final step, the final GLP weights were calculated by multiplying the weights of each GLP by the weight values of the GLPCs in which they are located. Afterwards, these final weights were ranked from largest to smallest to obtain the impact ranks. These final weights and rankings are given in Table 11.

Table 9. Comparative Priority Values of GLPs

DM₁							
Order of Importance	GLP_{11}	GLP_{12}	GLP_{17}	GLP_{16}	GLP_{15}	GLP_{13}	GLP_{14}
Comparative Priority Value	1	3	4	6	7	7	9
Order of Importance	GLP_{21}	GLP_{23}	GLP_{26}	GLP_{22}	GLP_{27}	GLP_{25}	GLP_{24}
Comparative Priority Value	1	3	4	6	7	8	9
Order of Importance	GLP_{31}	GLP_{32}	GLP_{33}	GLP_{34}			
Comparative Priority Value	1	6	6	7			
Order of Importance	GLP_{41}	GLP_{42}	GLP_{43}				
Comparative Priority Value	1	5	6				
Order of Importance	GLP_{53}	GLP_{55}	GLP_{54}	GLP_{51}	GLP_{52}		
Comparative Priority Value	1	1	2	3	3		
Order of Importance	GLP_{64}	GLP_{65}	GLP_{63}	GLP_{62}	GLP_{61}		
Comparative Priority Value	1	3	4	5	6		
Order of Importance	GLP_{75}	GLP_{73}	GLP_{74}	GLP_{71}	GLP_{72}		
Comparative Priority Value	1	2	4	5	5		
DM₂							
Order of Importance	GLP_{11}	GLP_{16}	GLP_{17}	GLP_{15}	GLP_{12}	GLP_{14}	GLP_{13}
Comparative Priority Value	1	3	3	5	6	8	9
Order of Importance	GLP_{21}	GLP_{23}	GLP_{27}	GLP_{22}	GLP_{25}	GLP_{26}	GLP_{24}
Comparative Priority Value	1	2	3	3	5	7	9
Order of Importance	GLP_{33}	GLP_{31}	GLP_{32}	GLP_{34}			
Comparative Priority Value	1	2	5	8			
Order of Importance	GLP_{41}	GLP_{42}	GLP_{43}				
Comparative Priority Value	1	3	7				
Order of Importance	GLP_{53}	GLP_{55}	GLP_{52}	GLP_{54}	GLP_{51}		
Comparative Priority Value	1	3	4	6	9		
Order of Importance	GLP_{62}	GLP_{63}	GLP_{64}	GLP_{65}	GLP_{61}		
Comparative Priority Value	1	1	1	8	9		
Order of Importance	GLP_{75}	GLP_{74}	GLP_{73}	GLP_{72}	GLP_{71}		
Comparative Priority Value	1	3	5	7	9		
DM₃							
Order of Importance	GLP_{11}	GLP_{12}	GLP_{13}	GLP_{15}	GLP_{17}	GLP_{14}	GLP_{16}
Comparative Priority Value	1	2	4	4	5	7	8

Order of Importance	GLP$_{21}$	GLP$_{23}$	GLP$_{22}$	GLP$_{27}$	GLP$_{26}$	GLP$_{24}$	GLP$_{25}$
Comparative Priority Value	1	1	3	4	5	7	7
Order of Importance	GLP$_{31}$	GLP$_{33}$	GLP$_{32}$	GLP$_{34}$			
Comparative Priority Value	1	2	3	5			
Order of Importance	GLP$_{41}$	GLP$_{42}$	GLP$_{43}$				
Comparative Priority Value	1	2	5				
Order of Importance	GLP$_{53}$	GLP$_{55}$	GLP$_{54}$	GLP$_{51}$	GLP$_{52}$		
Comparative Priority Value	1	2	5	7	9		
Order of Importance	GLP$_{64}$	GLP$_{62}$	GLP$_{65}$	GLP$_{63}$	GLP$_{61}$		
Comparative Priority Value	1	2	3	4	5		
Order of Importance	GLP$_{75}$	GLP$_{73}$	GLP$_{71}$	GLP$_{72}$	GLP$_{74}$		
Comparative Priority Value	1	3	7	8	9		
DM$_4$							
Order of Importance	GLP$_{11}$	GLP$_{12}$	GLP$_{16}$	GLP$_{13}$	GLP$_{14}$	GLP$_{15}$	GLP$_{17}$
Comparative Priority Value	1	1	4	5	7	8	9
Order of Importance	GLP$_{23}$	GLP$_{21}$	GLP$_{26}$	GLP$_{27}$	GLP$_{25}$	GLP$_{22}$	GLP$_{24}$
Comparative Priority Value	1	3	4	5	6	7	9
Order of Importance	GLP$_{31}$	GLP$_{33}$	GLP$_{32}$	GLP$_{34}$			
Comparative Priority Value	1	5	6	9			
Order of Importance	GLP$_{41}$	GLP$_{42}$	GLP$_{43}$				
Comparative Priority Value	1	3	5				
Order of Importance	GLP$_{53}$	GLP$_{55}$	GLP$_{51}$	GLP$_{54}$	GLP$_{52}$		
Comparative Priority Value	1	1	5	6	8		
Order of Importance	GLP$_{64}$	GLP$_{62}$	GLP$_{63}$	GLP$_{61}$	GLP$_{65}$		
Comparative Priority Value	1	3	4	5	5		
Order of Importance	GLP$_{75}$	GLP$_{74}$	GLP$_{73}$	GLP$_{72}$	GLP$_{75}$		
Comparative Priority Value	1	3	5	7	8		

Based on Table 11, the GLP that contributes the most to sustainability performance is the application of "Use of lower energy transportation modes (intermodal, multimodal and combined transportation)", which ranks first with the highest final weight value of 0.1421. This practice is followed by the application of "Using guidance systems to minimize travel distances (vehicle routing applications)", which ranks second with a final weight value of 0.12027. The third GLP that contributes the most to sustainability performance is the "Using alternative energy/fuel sources and vehicles that cause less emissions (biofuel, electric, hybrid, etc.)", which has a final weight value of 0.07238. As can be seen in Table 11, the GLP that contributes the least to sustainability performance is "Providing training on green logistics practices and sustainability to customers, suppliers, subcontractors and third-party logistics service providers". This practice is of minimal importance, as indicated by its lowest importance value and final weight value of 0.004, which places it 36th rank in terms of importance.

Table 10. Weight Values of GLPs

	GLPs	**DM$_1$**	**DM$_2$**	**DM$_3$**	**DM$_4$**	**Weight Values**
GLPC$_1$ Vehicle and Fuel Practices	GLP$_{11}$	0.465	0.441	0.405	0.353	0.416
	GLP$_{12}$	0.155	0.073	0.203	0.353	0.196
	GLP$_{13}$	0.067	0.049	0.101	0.071	0.072
	GLP$_{14}$	0.052	0.055	0.058	0.050	0.054

	GLP$_{15}$	0.067	0.088	0.101	0.044	0.075
	GLP$_{16}$	0.078	0.147	0.051	0.088	0.091
	GLP$_{17}$	0.116	0.147	0.081	0.039	0.096
	GLP$_{21}$	0.470	0.382	0.326	0.151	0.332
	GLP$_{22}$	0.078	0.127	0.109	0.065	0.095
GLPC$_2$	GLP$_{23}$	0.153	0.191	0.326	0.454	0.281
Transportation	GLP$_{24}$	0.052	0.042	0.047	0.050	0.048
Practices	GLP$_{25}$	0.059	0.076	0.047	0.076	0.065
	GLP$_{26}$	0.117	0.055	0.065	0.113	0.088
	GLP$_{27}$	0.067	0.127	0.081	0.091	0.091
GLPC$_3$	GLP$_{31}$	0.677	0.274	0.492	0.677	0.530
Packaging	GLP$_{32}$	0.113	0.110	0.164	0.113	0.125
Practices	GLP$_{33}$	0.113	0.548	0.246	0.135	0.261
	GLP$_{34}$	0.097	0.068	0.098	0.075	0.084
GLPC$_4$ Waste	GLP$_{41}$	0.732	0.745	0.588	0.652	0.679
Management	GLP$_{42}$	0.146	0.149	0.294	0.217	0.202
Practices	GLP$_{43}$	0.122	0.106	0.118	0.130	0.119
	GLP$_{51}$	0.105	0.060	0.073	0.080	0.080
	GLP$_{52}$	0.105	0.134	0.057	0.050	0.087
GLPC$_5$ Storage	GLP$_{53}$	0.316	0.537	0.512	0.401	0.441
Practices	GLP$_{54}$	0.158	0.090	0.102	0.067	0.104
	GLP$_{55}$	0.316	0.179	0.256	0.401	0.288
	GLP$_{61}$	0.085	0.034	0.088	0.101	0.077
	GLP$_{62}$	0.103	0.309	0.219	0.168	0.200
GLPC$_6$ Internal	GLP$_{63}$	0.128	0.309	0.109	0.126	0.168
Practices	GLP$_{64}$	0.513	0.309	0.438	0.504	0.441
	GLP$_{65}$	0.171	0.039	0.146	0.101	0.114
	GLP$_{71}$	0.093	0.062	0.083	0.069	0.077
	GLP$_{72}$	0.093	0.080	0.073	0.079	0.081
GLPC$_7$ External	GLP$_{73}$	0.233	0.112	0.195	0.111	0.163
Practices	GLP$_{74}$	0.116	0.187	0.065	0.185	0.138
	GLP$_{75}$	0.465	0.560	0.584	0.555	0.541

Table 11. Final Weights and Rankings Calculated for GLPs

GLPCs	GLPs	Final Weights	Rankings
	GLP$_{11}$ (0.416)	0.07238	3
	GLP$_{12}$ (0.196)	0.0341	9
	GLP$_{13}$ (0.072)	0.01253	23
GLPC$_1$ (0.174)	GLP$_{14}$ (0.054)	0.0094	26
	GLP$_{15}$ (0.075)	0.01305	21
	GLP$_{16}$ (0.091)	0.01584	19
	GLP$_{17}$ (0.096)	0.0167	18
	GLP$_{21}$ (0.332)	0.1421	1
	GLP$_{22}$ (0.095)	0.04066	6
GLPC$_2$ (0.428)	GLP$_{23}$ (0.281)	0.12027	2
	GLP$_{21}$ (0.048)	0.02054	16

	GLP$_{25}$ (0.065)	0.02782	13
	GLP$_{26}$ (0.088)	0.03766	8
	GLP$_{27}$ (0.091)	0.03896	7
GLPC$_3$ (0.1)	GLP$_{31}$ (0.53)	0.053	5
	GLP$_{32}$ (0.125)	0.0125	24
	GLP$_{33}$ (0.261)	0.0261	14
	GLP$_{34}$ (0.084)	0.0084	29
GLPC$_4$ (0.096)	GLP$_{41}$ (0.679)	0.06518	4
	GLP$_{42}$ (0.202)	0.01939	17
	GLP$_{43}$ (0.119)	0.01142	25
GLPC$_5$ (0.074)	GLP$_{51}$ (0.08)	0.00592	33
	GLP$_{52}$ (0.087)	0.00644	32
	GLP$_{53}$ (0.441)	0.03263	11
	GLP$_{54}$ (0.104)	0.0077	30
	GLP$_{55}$ (0.288)	0.02131	15
GLPC$_6$ (0.076)	GLP$_{61}$ (0.077)	0.00585	34
	GLP$_{62}$ (0.2)	0.0152	20
	GLP$_{63}$ (0.168)	0.01277	22
	GLP$_{64}$ (0.441)	0.03352	10
	GLP$_{65}$ (0.114)	0.00866	27
GLPC$_7$ (0.052)	GLP$_{71}$ (0.077)	0.004	36
	GLP$_{72}$ (0.081)	0.00421	35
	GLP$_{73}$ (0.163)	0.00848	28
	GLP$_{74}$ (0.138)	0.00718	31
	GLP$_{75}$ (0.541)	0.02813	12

Conclusions and Discussions

The intensifying climate crisis and growing societal concern about environmental issues have led to an increased emphasis on the concept of sustainability in a multitude of contexts, including social, governmental, and corporate realms. Considering the impact of the supply chain on the environment, economy, and social life, it is evident that all actors within this chain have initiated sustainable practices and aspire to enhance their sustainability performance. When one considers the emission and economic impacts of logistics activities within a supply chain, the sustainability performance of the logistics companies concerned becomes a matter of great importance. It is, therefore, essential for these companies to adopt GLPs in order to make sustainable progress.

This study aimed to evaluate the impact of GLPs on sustainability performance. To this end, seven GLPCs and 36 GLPs within these categories were identified through a review of the literature and input from experts. The influence of these GLPs on sustainability performance was then assessed using the FUCOM method, which involved consulting expert opinions. This process yielded the final weights for the GLPs, allowing for their ranking in terms of their contribution to sustainability performance.

The study yielded two key findings: 'transportation applications' and 2vehicle and fuel applications' emerged as

the most significant GLPCs. Furthermore, the final importance values calculated for GLPs indicate that the most significant applications are the use of lower energy transportation modes (intermodal, multimodal, and combined transportation), the use of guidance systems that minimize travel distances (vehicle routing applications), and the use of alternative energy and fuel sources and vehicles that reduce emissions (biofuel, electric, hybrid, etc.).

Of the GLPs, the one that has the most significant impact on sustainability performance is the use of lower-energy transportation modes, including intermodal, multimodal, and combined transportation. Mode change in transportation has a multitude of effects on sustainability. As an illustration, a shift in transportation modes from road to rail will diminish traffic congestion on the road and the potential for accidents. Similarly, the physical stress experienced by the drivers will be reduced. These effects will contribute to an increase in societal welfare and a positive impact on social sustainability, which is a dimension of sustainability performance. In this regard, Chen et al. (2020) asserts that, among the various transportation modes, road transportation is the most polluting one, whereas railway transportation is the mode with the least carbon emissions. Therefore, the transition from road to railway transportation will result in a reduction in emissions and an enhancement in environmental sustainability. Furthermore, the overloading of road vehicles will be reduced with the implementation of this new mode of transportation, and the fuel consumption of vehicles carrying less load will also decrease. In consequence, costs will decline and economic sustainability will improve. When all these aforementioned issues are taken into consideration, it becomes evident that mode shift in transportation has a considerable impact on sustainability performance.

The second most impactful GLP is the use of guidance systems to minimize travel distances, specifically vehicle routing applications. The implementation of vehicle routing activities offers a multitude of advantages. When a vehicle is assigned a road route that is optimized for distance, the vehicle will deliver its loads over a shorter distance, thus using less fuel. It can be reasonably assumed that reduced fuel consumption will also result in reduced costs, thereby conferring an economic advantage upon logistics companies and simultaneously enhancing their sustainability performance. Furthermore, the reduction in fuel consumption resulting from the shorter distances traveled has a positive impact on the environment, contributing to greater sustainability. The same is true of road vehicles traveling on the optimum route, which prevents accidents by reducing travel distances and times, and also contributes to reducing noise, thereby indirectly having a positive impact on the social dimension of sustainability. For these reasons, vehicle routing practices have a significant role to play in contributing to sustainability performance.

The third GLP that contributes the most to sustainability performance is the utilization of alternative energy and fuel sources, as well as vehicles that emit fewer emissions (biofuel, electric, hybrid, etc.). The utilization of alternative energy sources in transportation vehicles has a significant impact on sustainability. The environmental impact of gasoline and diesel-powered vehicles is considerable, with increased carbon emissions, air pollution, and noise being particularly noteworthy. In contrast, the environmental impact of vehicles utilizing alternative energy sources is significantly reduced. In light of these environmental contributions, it can be

posited that the overall welfare level of societies will increase and that the disease rate of people living in cleaner airspace will concomitantly decrease. This has the effect of indirectly contributing to the social dimension of sustainability. Moreover, these vehicles, which utilize a renewable energy source, markedly diminish the consumption of resources on a global scale. In light of these environmental benefits, it can be reasonably assumed that logistics companies with alternative energy vehicles in their fleets will experience a notable enhancement in their sustainability performance. While the initial cost may be higher than that of gasoline or diesel-powered vehicles, alternative energy vehicles indirectly contribute to economic sustainability, as they will offset the purchase cost in a relatively short time frame when considering their expected lifespan and low malfunction rates. This GLP, which has a positive impact on all three dimensions of sustainability, subsequently makes a significant contribution to sustainability performance.

The GLPs that have the least impact on sustainability performance are as follows: (i) Providing training to customers, suppliers, subcontractors, and third-party logistics service providers about GLPs and sustainability; and (ii) Cooperating with customers, suppliers, subcontractors, and third-party logistics service providers on environmental management. Both of these applications are classified as "external applications". Accordingly, the practices that contribute the least to sustainability performance are the relevant logistics company's relationships with other actors in the supply chain and the policies it carries out. It may be reasonably assumed that, given the environmental impact of logistics companies' operations, other GLPs, such as those related to transportation, vehicle fuel, and packaging, will exert more significant influence on a company's overall sustainability performance. As these operations have a direct impact on the environment, the economy, and consequently, social life, companies are primarily focused on enhancing their sustainability performance in these operations. Improvements and investments in these applications will automatically increase sustainability performance and contribute to sustainability by preventing the climate crisis that threatens the world.

Future Research Directions

The objective of this study was to assess the impact of GLPs on sustainability performance, with a particular focus on a logistics company. Given the environmental damage caused by logistics operations, it is crucial to consider the role of logistics in addressing the climate crisis. To this end, this study identifies and presents the most effective GLPs as a recommendation for logistics companies seeking to enhance their sustainability performance. As there is a lack of studies on this subject in the national literature, this study is expected to contribute to the existing body of knowledge. In future studies, the number of companies and experts can be increased by considering more than one logistics company in Turkey, and the relationship between GLPs and sustainability performance in Turkey can be discussed in a more comprehensive manner. Additionally, for comparison purposes, prioritization can be done using more than one MCDM method. Furthermore, the relationship between GLPs and sustainability performance can be analyzed through statistical models.

References

Adams, C. A., Muir, S., & Hoque, Z. (2014). Measurement of sustainability performance in the public sector. *Sustainability Accounting, Management and Policy Journal*, *5*(1), 46–67.

Ahmed, W., Ahmed, W., & Najmi, A. (2018). Developing and analyzing framework for understanding the effects of GSCM on green and economic performance: Perspective of a developing country. *Management of Environmental Quality: An International Journal*, *29*(4), 740–758.

Ali, K., Kausar, N., & Amir, M. (2023). Impact of pollution prevention strategies on environment sustainability: role of environmental management accounting and environmental proactivity. *Environmental Science and Pollution Research*, *30*(38), 88891–88904. https://doi.org/10.1007/s11356-023-28724-1

Chang, Q., & Qin, R. (2008). Analysis on development path of Tianjin green logistics. *International Journal of Business and Management*, *3*(9), 96–98.

Chen, S., Wu, J., & Zong, Y. (2020). The impact of the freight transport modal shift policy on China's carbon emissions reduction. *Sustainability (Switzerland)*, *12*(2). https://doi.org/10.3390/su12020583

Colicchia, C., Marchet, G., Melacini, M., & Perotti, S. (2013). Building environmental sustainability: Empirical evidence from Logistics Service Providers. *Journal of Cleaner Production*, *59*, 197–209.

Copeland, A. M., Ormsby, A. A., & Willingham, A. M. (2013). Assessment and comparative analysis of a reusable versus disposable to-go system. *Sustainability*, *6*(6), 353–358. https://doi.org/10.1089/SUS.2013.9832

Dioha, M. O., & Kumar, A. (2020). Sustainable energy pathways for land transport in Nigeria. *Utilities Policy*, *64*. https://doi.org/10.1016/j.jup.2020.101034

Doherty, S., & Hoyle, S. (2009). *Supply Chain Decarbonization: The Role of Logistics and Transport In Reducing Supply Chain Carbon Emissions*.

Ecer, F. (2020). Çok kriterli karar verme geçmişten günümüze kapsamlı bir yaklaşım. *Ankara: Seçkin Yayınevi*.

Elkington, J. (2006). Governance for sustainability. *Corporate Governance: An International Review*, *14*(6), 522–529.

Evangelista, P., Colicchia, C., & Creazza, A. (2017). Is environmental sustainability a strategic priority for logistics service providers? *Journal of Environmental Management*, *198*, 353–362. https://doi.org/10.1016/j.jenvman.2017.04.096

Fan, Z., & Kang, T.-W. (2023). Linking Sustainable Supplier Selection to Firm's Sustainable Performance: The Moderated Mediating Role of Supplier Development and Leadership for Functional Integration. *Sustainability*, *15*(12). https://doi.org/10.3390/su15129757

Ferrón-Vílchez, V. (2016). Does symbolism benefit environmental and business performance in the adoption of ISO 14001? *Journal of Environmental Management*, *183*, 882–894. https://doi.org/10.1016/j.jenvman.2016.09.047

Fontela, E., & Gabus, A. (1974). DEMATEL, innovative methods, rep. no. 2, structural analysis of the world problematique (methods). *Battelle Institute, Geneva Research Center, Geneva*.

George, R. A., Siti-Nabiha, A. K., Jalaludin, D., & Abdalla, Y. A. (2016). Barriers to and enablers of sustainability integration in the performance management systems of an oil and gas company. *Journal of Cleaner Production*, *136*, 197–212.

Groves, C. (2019). Sustainability and the future: reflections on the ethical and political significance of sustainability. *Sustainability Science*, *14*(4), 915–924. https://doi.org/10.1007/s11625-019-00700-0

Harris, I., Mumford, C. L., & Naim, M. M. (2014). A hybrid multi-objective approach to capacitated facility location with flexible store allocation for green logistics modeling. *Transportation Research Part E: Logistics and Transportation Review*, *66*, 1–22. https://doi.org/https://doi.org/10.1016/j.tre.2014.01.010

Hristov, I., & Chirico, A. (2019). The Role of Sustainability Key Performance Indicators (KPIs) in Implementing Sustainable Strategies. *Sustainability*, *11*(20). https://doi.org/10.3390/su11205742

Maji, I. K., Mohd Saudi, N. S., & Yusuf, M. (2023). An assessment of green logistics and environmental sustainability: Evidence from Bauchi. *Cleaner Logistics and Supply Chain*, *6*, 100097. https://doi.org/https://doi.org/10.1016/j.clscn.2023.100097

Nicolăescu, E., Alpopi, C., & Zaharia, C. (2015). Measuring Corporate Sustainability Performance. *Sustainability*, *7*(1), 851–865. https://doi.org/10.3390/su7010851

Pamučar, D., Stević, Ž., & Sremac, S. (2018). A New Model for Determining Weight Coefficients of Criteria in MCDM Models: Full Consistency Method (FUCOM). *Symmetry*, *10*(9). https://doi.org/10.3390/sym10090393

Pautasso, E., Osella, M., & Caroleo, B. (2019). Addressing the sustainability issue in smart cities: A comprehensive model for evaluating the impacts of electric vehicle diffusion. *Systems*, *7*(2). https://doi.org/10.3390/systems7020029

Pham, N. T., Phan, Q. P. T., Tučková, Z., Vo, N., & Nguyen, L. H. L. (2018). Enhancing the organizational citizenship behavior for the environment: the roles of green training and organizational culture. *Management & Marketing*, *13*(4), 1174–1189. https://doi.org/doi:10.2478/mmcks-2018-0030

Presley, A., Meade, L., & Sarkis, J. (2007). A strategic sustainability justification methodology for organizational decisions: A reverse logistics illustration. *International Journal of Production Research*, *45*(18–19), 4595–4620. https://doi.org/10.1080/00207540701440220

Rakhmangulov, A., Sladkowski, A., Osintsev, N., & Muravev, D. (2018). Green Logistics: A System of Methods and Instruments-Part 2. *Nase More*, *65*(1), 49–55. https://doi.org/10.17818/NM/2018/1.7

Rezaei, J. (2015). Best-worst multi-criteria decision-making method. *Omega*, *53*, 49–57. https://doi.org/https://doi.org/10.1016/j.omega.2014.11.009

Saaty, T. L. (1980). *The Analytic Hierarchy Process*. McGraw-Hill, Inc.

Sai, F. (2018). Study on Green Logistics Initiatives through Text Mining. *2018 Conference on Technologies and Applications of Artificial Intelligence (TAAI)*, 110–115. https://doi.org/10.1109/TAAI.2018.00033

Singh, R. L., & Singh, P. K. (2017). Global Environmental Problems. In R. L. Singh (Ed.), *Principles and Applications of Environmental Biotechnology for a Sustainable Future* (pp. 13–41). Springer Singapore. https://doi.org/10.1007/978-981-10-1866-4_2

Sureeyatanapas, P., Poophiukhok, P., & Pathumnakul, S. (2018). Green initiatives for logistics service providers: An investigation of antecedent factors and the contributions to corporate goals. *Journal of Cleaner Production*, *191*, 1–14. https://doi.org/10.1016/j.jclepro.2018.04.206

Vienažindienė, M., Tamulienė, V., & Zaleckienė, J. (2021). Green logistics practices seeking development of sustainability: Evidence from lithuanian transportation and logistics companies. *Energies*, *14*(22). https://doi.org/10.3390/en14227500

Vivas, R., Sant'anna, Â., Esquerre, K., & Freires, F. (2019). Measuring Sustainability Performance with Multi Criteria Model: A Case Study. *Sustainability*, *11*(21). https://doi.org/10.3390/su11216113

Wartick, S. L., & Cochran, P. L. (1985). The Evolution of the Corporate Social Performance Model. *The Academy of Management Review*, *10*(4), 758–769. https://doi.org/10.2307/258044

World Health Organization. (2022). *Global analysis of healthcare waste in the context of COVID-19: status, impacts and recommendations*.

Zhang, Y., Thompson, R. G., Bao, X., & Jiang, Y. (2014). Analyzing the Promoting Factors for Adopting Green Logistics Practices: A Case Study of Road Freight Industry in Nanjing, China. *Procedia - Social and Behavioral Sciences*, *125*, 432–444. https://doi.org/10.1016/j.sbspro.2014.01.1486

Zhu, Q., Sarkis, J., & Lai, K. (2007). Initiatives and outcomes of green supply chain management implementation by Chinese manufacturers. *Journal of Environmental Management*, *85*(1), 179–189. https://doi.org/https://doi.org/10.1016/j.jenvman.2006.09.003

Žižović, M., & Pamucar, D. (2019). New model for determining criteria weights: Level Based Weight Assessment (LBWA) model. *Decision Making: Applications in Management and Engineering*, *2*(2), 126–137. https://doi.org/10.31181/dmame1902102z

Obstetrıc Antiphospholipid Syndrome in the Optic of New Classification Criteria

Ina Toska

University of Tirana, Albania, https://orcid.org/0009-0004-4184-9497

Rexhep Shkurti

University of Tirana, Albania, https://orcid.org/0000-0003-3158-7222

Anila Mitre

University of Tirana, Albania, https://orcid.org/0000-0001-7361-7106

Abstract: Antiphospholipid syndrome is a systemic autoimmune disorder characterized by clinical symptoms of venous or arterial thrombosis, morbidity in pregnancy, or non-thrombotic experiences and persistence of specific auto antibodies, including anticardiolipin, anti β-2 glycoprotein antibodies and lupus anticoagulant. These autoantibodies lead to the generation of thrombotic events and obstetric complication. APS's obstetric complications are classified in those that occur in the first trimester or those that occur in the second or third trimester. Sapporo criteria for APS classification initially published in 1999, then revised in 2006 as Sydney criteria require at least one clinical symptoms (thrombosis or pregnancy loss) and one laboratory test positive (LAC and/or anti-CL and/or aβ-2GPI antibodies IgM/IgG in moderate or high titers). New classification criteria for APS are published in 2023 from American College of Rheumatology and Alliance of Associations for Rheumatology, in attempt to develop classification criteria with high specificity and sensitivity. The recent criteria divided clinical symptoms and laboratory test in domains weighed with a specific score - points. The purpose of this review is to show how early or late complications of obstetric antiphospholipid syndrome are classified according new criteria ACR/EULAR and how can apply it in practice.

Keywords: antiphospholipid syndrome, Sapporo criteria, ACR/EULAR criteria, obstetric complications, anticardiolipin, anti β-2 glycoprotein antibodies, lupus anticoagulant

Introduction

Antiphospholipid Syndrome (APS) is a systemic autoimmune disorder characterized by trombotic or obstetrical

events and the persistent presence of antiphospholipid antibodies, known as lupus anticoagulant, anticardiolipin antibody and anti-β2GPI, in the patient's plasma (Musial, 2023). Despite the etiology of APS is poorly understood, is very important to describe laboratory and clinical features, in order to develop classification criteria for research purposes.

The APS classification for research purposes is based on the Sapporo criteria, first published in 1999 and revised in 2006. The revised Sapporo criteria or Sydney criteria, require at least one clinical and one laboratory criterion to classify as APS (Miyakis et al., 2006). Lack of strict definition and limitations of Sapporo criteria, initiated a multidisciplinary effort from American college and Rheumatology and European Alliance of Associations for Rheumatology (EULAR), to develop new APS classification criteria, with high specificity and sensitivity (Erkan, 2024 & Barbhaiya et al., 2023).

New criteria ACR/EULAR differ from the Sapporo criteria in several aspects. The "entry" criteria, was first introduced and had to be fulfilled for the patient to be classified as APS. Clinical symptoms and laboratory criteria are hierarchically clustered in domains and each of them is weighted with score-points. A patient is classified as APS if he meets the entry criteria and accumulates at least 3 points from clinical domain and 3 points from laboratory domain (Barbhaiya et al., 2023; Erkan, 2024; Musial, 2023).

APS may be seen in healthy individuals and in this case is named primary APS, or in patients with other autoimmune diseases such as systemic lupus erythematosus, known as secondary APS (Keleşoğlu & Erkan 2023; Branch 2019). Catastrophic antiphospholipid syndrome (CAPS) is a rare and life-threatening condition, characterized by thromboses with the development of multiple organ failure (Knight et al., 2023).

Obstetric Antiphospholipid Syndrome (OAPS) is an autoimmune disorder associated with various pathological pregnancies, such as recurrent miscarriage, stillbirth, severe pre-eclampsia and severe placental insufficiency. The persistence of antiphospholipid antibodies is the most important laboratory characteristic of OAPS (Gao & Qin, 2024).

Standard classification

Sydney Clinical criteria

According Sydney standard, clinical criteria involve:

- One or more unexplained deaths of a morphologically normal fetus at or beyond the 10th week of gestation, with normal fetal morphology documented by ultrasound or by direct examination of the fetus.
- One or more premature births of a morphologically normal neonate before the 34th week of gestation because of 1) eclampsia or severe pre-eclampsia, 2) recognized features of placental insufficiency.
- Three or more unexplained consecutive spontaneous abortions before the 10th week of gestation, with

maternal anatomic or hormonal abnormalities and paternal and maternal chromosomal causes excluded (Antovic et al., 2018; Peng et al., 2023; Gao & Qin, 2024).

Sydney Laboratory criteria

Laboratory criteria according Sydney Classification includes:

- Lupus Anticoagulant (LAC) present in plasma, on two or more occasions at least 12 weeks apart;
- aCL-IgG/IgM in serum or plasma, present in medium or high titer, on two or more occasions, at least 12 weeks apart, measured by a standardized ELISA;
- aβ2GPI-IgG/IgM in serum or plasma (in titer >99th percentile), present on two or more occasions, at least 12 weeks apart, measured by a standardized ELISA (Antovic et al., 2018; Peng et al., 2023; Gao & Qin, 2024).

Obstetric antiphospholipid syndrome requires the combination of at least on clinical and one laboratory criterion.

OAPS is an autoimmune disorder characterized by pregnancy morbidity associated with persistent antiphospholipid antibody positivity. Cases fulfilling the Sydney criteria for obstetric morbidity with no previous thrombosis, are known as obstetric antiphospholipid syndrome (OAPS). Accros literature, there are also prescribed cases where women can fulfill the clinical, but not the laboratory criteria for OAPS and vice versa. Cases when patients fail to completely meet the clinical Sydney criteria are classified as aPL-related Obstetric Morbidity (OMAPS) (Alijotas-Reig et al., 2022; Gao & Qin, 2024).

OMAPS clinical criteria includes:

1. Two consecutive unexplained miscarriages of well – formed embryos.
2. Three or more non-consecutive miscarriages of well-formed embryos.
3. PE/eclampsia after 34th week of gestation or at puerperium.
4. Placental abruption.
5. Late premature birth.
6. Premature rupture membranes.
7. Unexplained recurrent implantation failure in IVF fertilization.

OMAPS laboratory criteria includes:

Fulfilling the laboratory criteria for OAPS, including the detection of lupus anticoagulant, IgM/IgG anticardiolipin antibodies or anti-β2GPI IgG/IgM in medium or high titers.
We also can mention cases that fulfill clinical criteria, but fail to reach the laboratory values for OAPS, with low titers of aPL or with only one positive test that are not in agreement of Sydney recommendations and are

classified as **Non – Criteria OAPS** (Alijotas-Reig et al., 2022; Peng et al., 2023).

Clinical criteria NC-OAPS involves:

Fulfilling the clinical criteria described for OAPS, as mentioned above.

Laboratory criteria for NC-OAPS includes:

1. Positivity for lupus anticoagulant, aCL or aβ2GPI positivity only detected once
2. Low positive IgG/IgM aCL or aβ2GPI titers
3. Persistent positivity for non-criteria aPL, including IgA -aCL and aβ2GPI
4. Resistance to Annexin A5 anticoagulant activity
5. Thrombocytopenia

New classification criteria.

New antiphospholipid syndrome classification criteria are published in 2023, according the standardized EULAR methodology. New set of criteria was developed by a group of experts of the American College of Rheumatology (ACR) and EULAR. They differ from revised Sapporo in several aspects. Firstly, "the entry criteria" was presented and require the presence at least one clinical criterion and one laboratory criterion within 3 years. The clinical and laboratory criteria are differentially weighted and organized in hierarchical domains. The goal of this new classification is to classify patients having APS, with high specificity and sensitivity for research purposes (Musial, 2023; Barbhaiya et al., 2023; Erkan 2024).

Obstetric domain-clinical criteria.	**Weight**
≥3 consecutive pre-fetal (<10 weeks) and/or early (10-16 weeks) fetal deaths, or ≥1 fetal death (16-34 weeks) alone.	1
Fetal death (16-33 weeks) in the absence of pre-eclampsia with sever features or placental insufficiency with severe features.	1
Preeclampsia with severe features or placental insufficiency with severe features (<34 weeks) with or without fetal death	3
Preeclampsia with severe features and placental insufficiency with severe features (<34 weeks) with or without fetal death	4
Laboratory domain	**Weight**
Lupus anticoagulant test:	
Positive LA (single - one time)	1
Positive LA (persistent)	5
aPL testing by solid phase assays: aCL IgG/IgM and aβ2GPI IgG/IgM (persistent)	
Moderate or high positive (IgM alone) aCL and/or aβ2GPI	1

Moderate positive (IgG) aCL and/or aβ2GPI	4
High positive (IgG) aCL or aβ2GPI	5
High positive (IgG) aCL and aβ2GPI	7

(Musial, 2023; Barbhaiya et al., 2023; Erkan 2024; Gao & Qin, 2024).

Conclusions and Perspective

In this short article we want to realize a comparison of two classification criteria standards for obstetric antiphospholipid syndrome. Firstly, it is important to mention that these criteria represent only a standard research classification and not a diagnostic tool for APS (Erkan, 2024; Musial, 2023; Barbhaiya et al., 2023). According Sydney standard, to be classified as an OAPS, it is required to fulfill one clinical and one laboratory criteria.

New classification criteria as well as Sydney standard, use two positive test for LAC, aCL or aβ2GPI at an interval of more than 12 weeks. In the new ACR/EULAR criteria, in contrary of Sydney standard, where the continuously positivity of one of three aPL mentioned above meets the classification requirements, LAC, aCL-IgG, aβ2GPI IgG have a higher proportion and meet the requirement for APS, while aCL-IgM and aβ2GPI IgM positivity alone, do not meet the laboratory standards for APS (Gao & Qin, 2024).

Considering the evaluation of the points in the new criterion, more emphasis is placed on eclampsia, pre-eclampsia and placental insufficiency and recurrent miscarriage could not be classified as OAPS. According several studies, aPL can directly act on trophoblast or decidual tissues, causing fetal loss (Garcia & Erkan, 2018). Recurrent pregnacy loss has been considered a hallmark of APS, since reporting association between repeated spontaneous abortions and LAC in 1975 and aCL and miscarriages in 1984 (Antovic & Sennström 2018). Furthermore, epidemiological studies suggest that recurrent miscarriage is the most common manifestation of OAPS. Evaluation of recurrent miscarrige with only one point, excluding it from clinical criteria, may lead in inadequate diagnosis and treatment.

With the new ACR/Eular criteria, classification as OMAPS or NC APS could not be applicable, and there is no proposed method yet. This is an important topic that must be reviwed by experts, for the future.

References

Alijotas-Reig, J., Esteve-Valverde, E., Anunciación-Llunell, A., Marques-Soares, J., Pardos-Gea, J., & Miró-Mur, F. (2022). Pathogenesis, Diagnosis and Management of Obstetric Antiphospholipid Syndrome: A Comprehensive Review. *Journal of clinical medicine*, *11*(3), 675. https://doi.org/10.3390/jcm11030675

Antovic, A., Sennström, M., Bremme, K., & Svenungsson, E. (2018). Obstetric antiphospholipid syndrome. *Lupus science & medicine*, *5*(1), e000197. https://doi.org/10.1136/lupus-2016-000197

Bahar Keleşoğlu Dinçer, A., & Erkan, D. (2023). The ABCs of antiphospholipid syndrome. *Archives of rheumatology*, *38*(2), 163–173. https://doi.org/10.46497/ArchRheumatol.2023.41875

Barbhaiya, M., Zuily, S., Naden, R., Hendry, A., Manneville, F., Amigo, M. C., Amoura, Z., Andrade, D., Andreoli, L., Artim-Esen, B., Atsumi, T., Avcin, T., Belmont, H. M., Bertolaccini, M. L., Branch, D. W., Carvalheiras, G., Casini, A., Cervera, R., Cohen, H., Costedoat-Chalumeau, N., … ACR/EULAR APS Classification Criteria Collaborators (2023). The 2023 ACR/EULAR Antiphospholipid Syndrome Classification Criteria. *Arthritis & rheumatology (Hoboken, N.J.)*, *75*(10), 1687–1702. https://doi.org/10.1002/art.42624

Branch D. W. (2019). What's new in obstetric antiphospholipid syndrome. *Hematology. American Society of Hematology. Education Program*, *2019*(1), 421–425. https://doi.org/10.1182/hematology.2019000043

Erkan D. (2024). Antiphospholipid Syndrome: To Classify or Not to Classify?. *Turkish journal of haematology : official journal of Turkish Society of Haematology*, *41*(1), 37–40. https://doi.org/10.4274/tjh.galenos.2024.2024.0003

Gao, R., & Qin, L. (2024). Obstetric Antiphospholipid Syndrome: Insights on the Diagnosis, Treatment, and Hot Issues]. *Sichuan da xue xue bao. Yi xue ban = Journal of Sichuan University. Medical science edition*, *55*(3), 513–520. https://doi.org/10.12182/20240560104

Garcia, D., & Erkan, D. (2018). Diagnosis and Management of the Antiphospholipid Syndrome. *The New England journal of medicine*, *378*(21), 2010–2021. https://doi.org/10.1056/NEJMra1705454

Knight, J. S., Branch, D. W., & Ortel, T. L. (2023). Antiphospholipid syndrome: advances in diagnosis, pathogenesis, and management. *BMJ (Clinical research ed.)*, *380*, e069717. https://doi.org/10.1136/bmj-2021-069717

Miyakis, S., Lockshin, M. D., Atsumi, T., Branch, D. W., Brey, R. L., Cervera, R., Derksen, R. H., DE Groot, P. G., Koike, T., Meroni, P. L., Reber, G., Shoenfeld, Y., Tincani, A., Vlachoyiannopoulos, P. G., & Krilis, S. A. (2006). International consensus statement on an update of the classification criteria for definite antiphospholipid syndrome (APS). *Journal of thrombosis and haemostasis : JTH*, *4*(2), 295–306. https://doi.org/10.1111/j.1538-7836.2006.01753.x Calfee, R. C., & Valencia, R. R. (1991).

Musiał J. (2023). New classification criteria for antiphospholipid syndrome. — *Journal of transfusion medicine*, 16(3): 103-109.https://doi.org/10.5603/jtm.97795

Peng, X., Tan, X., & Xing, A. (2023). An advanced understanding of the heterogeneous clinical features of "non-criteria" obstetric antiphospholipid syndrome: Two case reports and a literature review. *Frontiers in immunology*, *14*, 1122127. https://doi.org/10.3389/fimmu.2023.1122127

Wilson, W. A., Gharavi, A. E., Koike, T., Lockshin, M. D., Branch, D. W., Piette, J. C., Brey, R., Derksen, R., Harris, E. N., Hughes, G. R., Triplett, D. A., & Khamashta, M. A. (1999). International consensus statement on preliminary classification criteria for definite antiphospholipid syndrome: report of an international workshop. *Arthritis and rheumatism*, *42*(7), 1309–1311. https://doi.org/10.1002/1529-0131(199907)42:7<1309::AID-ANR1>3.0.CO;2-F

Acetylcholinesterase Levels in Non-Target Fish *Gambusia Affinis* in The Annaba-El Tarf Region: Relationship with Pollutionhip with Pollution

Salima Chouahda

Laboratory of Applied Animal Biology, Department of Biology, Faculty of Science Badji Mokhtar University
23000 Annaba, Algeria, https://orcid.org/0000-0003-4699-1615

Abir Denna

Laboratory of Applied Animal Biology, Department of Biology, Faculty of Science Badji Mokhtar University
23000 Annaba, Algeria

Hinda Berghiche

Laboratory of Applied Animal Biology, Department of Biology, Faculty of Science Badji Mokhtar University
23000 Annaba, Algeria

Abstract: Many organisms are used as indicators of freshwater quality, and *Gambusia affinis* was chosen as the biological model because of its position in aquatic ecosystems, its abundance in the region studied and its relevance for toxicity tests. Introduced to Algeria in 1928 to control Anopheles larvae, *G. affinis* is the subject of our study, which aims to assess the impact of pollution on its growth and the response of a neurotoxicity biomarker, acetylcholinesterase (AChE). Individuals were collected during the breeding season at three sites with different pollution levels: Sidi Brahim, El Karma and Messida River. The biometric study revealed that the weight and linear growth of individuals from Messida River and El Karma were higher than those from Sidi Brahim, where a significant inhibition of AChE activity was observed, especially in males. The analyses show a significant effect of site and an interaction between sex and site, indicating that Sidi Brahim is particularly affected by pollution, with males being more sensitive to environmental stress than females.

Keywords: Pollution, *Gambusia affinis*, growth, Acetylcholinesterase, Reproduction.

Introduction

Pollution is a major problem, particularly in developing countries, with adverse effects on the environment and human resources. Generated by human activities, it can cause direct and visible damage, as well as long-term

disruption to ecosystems **(Patra *et al*., 2022)**. This highlights the scale of the environmental crimes perpetrated by humanity against itself **(Al Naggar *et al*., 2014 ; 2018)**. Freshwater ecosystems, which account for just 2.5% of the world's water, are highly vulnerable to pollution from human activities **(Palmate *et al*., 2017)**. Domestic waste and agricultural and industrial effluents are seriously damaging these habitats **(Peyrelasse *et al*., 2022)**. In addition, environmental factors such as temperature and oxygen levels exacerbate the effects of chemical contaminants **(Blazer *et al*., 2018)**.

Pesticides and trace metals pose major problems due to their persistence and toxicity for aquatic organisms and humans. Pesticides, designed to protect crops, also harm non-target species, particularly fish, because of their accumulation **(Hara & Singh, 2021)**. Trace metals, which do not degrade and accumulate, have acute and chronic effects on the growth and reproduction of aquatic organisms **(Jekayinfa & Bawa-Allah, 2022)**.

Awareness of pollution problems has led to the emergence of biomonitoring as an effective method for assessing and managing pollution **(Quiroz-Jara *et al*.,2021)**. Biomarkers are essential for understanding the toxic effects of pollutants on different biological levels **(Tang *et al*., 2022)**. However, their ecological relevance is limited, as various non-polluting factors, such as health and environmental conditions, can influence their responses **(Dalzochio *et al*., 2016)**.

Acetylcholinesterase (AChE) is a crucial biomarker of neurotoxicity, playing a key role in neurotransmission by breaking down acetylcholine **(Afsa *et al*., 2022)**. This enzyme is highly sensitive to chemical contaminants, particularly insecticides, and its inhibition can lead to an accumulation of acetylcholine **(Chang *et al*., 2020)**. This can cause neuromuscular paralysis and potentially lead to the death of the organism, underlining its importance in environmental risk assessment **(Olasehinde & Olaniran, 2022)**.

Fish are excellent bioindicators of environmental health because of their sensitivity to contaminants. *Gambusia affinis*, in particular, is a useful model for assessing pollution and studying the effects of endocrine disruption thanks to its resistance to pollutants **(Sellaoui & Bounaceur, 2020)**.

The aim of this study was to assess the impact of pollution on the morphometric and weight parameters of *G. affinis*, as well as on the activity of acetylcholinesterase (AChE), a neurotoxicity biomarker. The fish were collected during the spawning period at three sites in north-eastern Algeria, close to sources of pollution : Messida River, El Karma and Sidi Brahim.

Method
Presentation of study sites

Messida River, the site is located in the El Kala National Park, in the far north-east of Algeria **(36°54'0.01 N and 8°31'0.01 E)**. It's a relatively healthy site.

El Karma, the site is located in an agricultural area of El Hadjar, south of the town of Annaba **(36°44.8080' N and 7°40.2960' E)**. It is known for its significant contribution to agricultural production, particularly in the areas of cereals and industrial crops such as tomatoes, soya, sugar beet, alfalfa and cotton. **Sidi Brahim,** the site **(36°53.098044'N and 7°44.6970' E)** is located near a hotel in Sidi Brahim, Annaba, and is exposed to urban waste. It is also close to the Fertial complex, an Algerian-Spanish facility specialising in the production of ammonia and fertilisers.

Collection of samples

Individuals of *Gambusia affinis* were collected using a 0.40 mm mesh net during the breeding season at three study sites. The samples were transported in plastic containers containing water from the sites and analysed the same day, before being stored at -20°C. Water temperature, salinity and pH were measured using a multiparameter analyser.

Mesures morphométriques

One hundred (100) individuals of *G. affinis* were collected at random from each site, with a distribution of 84 females and 16 males at Messida River, 57 females and 43 males at El Karma, and 55 females and 45 males at Sidi Brahim. The fish were anaesthetised with MS-222 before their standard length and body weight were measured.

Biomarker analysis

Biomarker assays were carried out on 4 individuals of similar average size at each site. Acetylcholinesterase (AChE) activity was assessed in the head using specific protocols. Biomarker activity was normalised to the measured protein concentration.

Statistical analysis

Results are presented as arithmetic mean ± standard error of the mean (m ± SEM). Statistical analyses were performed using Prism version 7, and morphometric and enzymatic data were subjected to the non-parametric Kruskal-Wallis test, followed by Dunn's test to compare sites. A Mann-Whitney test was performed to examine gender differences, with significance retained at $p<0.05$.

Results
Growth parameters

The results obtained for the biometric parameters (total weight and total size) of adult female and male *G. affinis*

collected at three study sites show a maximum total weight for females at the Messida River site with a mean value of 677.8 ± 23.27 mg, and a minimum total weight for males at the Sidi Brahim site with a mean value of 193.6 ± 5.91 mg (Table 1). Similar observations were made for total size, with a mean maximum for females at the Messida River site of 39.70 ± 0.20 mm and a minimum for males at the Sidi Brahim site of 27.63 ± 0.30 mm at the start of reproduction (Table 2).

Statistical analysis using the Kruskal-Wallis test followed by the Dunn's test for comparison of the means of the biometric parameters (total weight and total size) measured in *G. affinis* between the three sites reveals significantly higher total weights in individuals from the Messida River and El Karma sites compared with those from the Sidi Brahim site ($p < 0.0001$) (Table1). Significant differences were also revealed for total size ($p < 0.0001$) with higher values for individuals at the Oued Messida and El Karma sites compared with those at the Sidi Brahim site shown in (Table 2).

Comparison of means between sexes within the same site, using the Mann-Whitney test, revealed significant differences between females and males at the same site (Oued Messida, El Karma and Sidi Brahim) for total weight ($p < 0.0001$) (Table 1) and total size ($p < 0.0001$) (Table 2).

Specific acetylcholinesterase activity

The results obtained show maximum AChE activity in males at the Sidi Brahim site with an average value of 0.148 ± 0.013 μM/mn/mg protein, and minimum activity in females at the Messida River site with an average value of 0.482 ± 0.013 μM/mn/mg protein (Table 3),

Statistical analysis using the Kruskal-Wallis test followed by the Dunn's test for the comparison of activities between the three sites presented in (Table 3), reveals a significant inhibition at the Sidi Brahim site (p = 0.0099 for females and p = 0.0012 for males) compared to the Messida River and El Karma sites. Comparison of the means between the sexes at the same site, using the Mann-Whitney test, revealed a significant difference between females and males (p = 0.0286) at the same site (Messida River, El Karma and Sidi Brah

Table 1. Total weight (mg) of adult females and males of *G. affinis* collected at three sites (Messida River, El Karma and Sidi Brahim) during the breeding period (mean ±SEM; n=100).

Sex	Messida River	El Karma	Sidi Brahim
Females	677,8 ± 23,27 **a**	661,4 ± 12,27 **a**	453,1 ± 14,36 **b**
	A	**A**	**A**
Males	249,6 ± 7,29 **a**	245,3 ± 3,57 **a**	193,6 ± 5,91 **b**
	B	**B**	**B**

The means followed by the same lower case letter are not significantly different ($p > 0.05$) between sites while

the means followed by the same upper case letter are not significantly different (p> 0.05) between the sexes.

Table 2. Total size (mm) of adult females and males of *G. affinis* collected at three sites (Messida River, El Karma and Sidi Brahim) during the breeding period (mean ±SEM; n=100).

Sex	Messida River	El Karma	Sidi Brahim
Females	39,70 ± 0,20 **a**	38,93 ± 0,22 **a**	34,86 ± 0,36 **b**
	A	**A**	**A**
Males	31,56 ± 0,32 **a**	30,63 ± 0,26 **a**	27,63 ± 0,30 **b**
	B	**B**	**B**

The means followed by the same lower case letter are not significantly different (p> 0.05) between sites while the means followed by the same upper case letter are not significantly different (p> 0.05) between the sexes.

Table 3. Variation in the specific activity of acetylcholinesterase (μM/mn/mg protein) in the heads of adult females and males of *G. affinis* collected at three sites (Messida River, EL Karma and Sidi Brahim) during the breeding period (sexual activity) (mean ±SEM; n=4).

Sex	Messida River	El Karma	Sidi Brahim
Females	0,482 ± 0,013 **a**	0,468 ± 0,016 **a**	0,258 ± 0,001 **b**
	A	**A**	**A**
Males	0,385 ± 0,009 **a**	0,360 ± 0,005 **a**	0,148 ± 0,013 **b**
	B	**B**	**B**

The means followed by the same lower case letter are not significantly different (p> 0.05) between sites while the means followed by the same upper case letter are not significantly different (p> 0.05) between the sexes.

Discussion

Growth is a key indicator of fish health and reflects the impact of stress on individuals and populations. It is essential for studying fish stocks and their dynamics in their environment **(Vidhya et *al*., 2019)**. Various factors **(Poletto *et al*., 2018)**, such as season **(Aliko *et al*., 2010)**, age, physiological condition and habitat quality, influence growth **(Kapute *et al*., 2016)**.

The study of biometric parameters (total height and weight) at three study sites revealed that individuals at the Messida River site, followed by the El Karma site, grew faster than those at the Sidi Brahim site. This difference suggests that the Sidi Brahim site has a relatively higher level of pollution due to various urban, industrial and domestic discharges, thus causing a delay in growth.

A reduction in growth was observed in the freshwater fish Tilapia du Nile (*Oreochromis niloticus*) following exposure to the insecticide deltamethrin **(Dawood *et al*., 2020)**. The study by **Vidhya *et al*. (2019)** demonstrated a progressive decrease in growth measured by weight in *Etroplus suratensis* (freshwater fish) with increasing concentrations of lambda-cyhalothrin (insecticide, pyrethrinoiide).

Acetylcholinesterase (AChE) is an essential enzyme present in the cell membranes of vertebrates and invertebrates **(Jebali *et al*., 2013)**, responsible for hydrolysing the neurotransmitter acetylcholine at cholinergic synapses **(Marinho *et al*., 2021)**. Its inhibition by neurotoxins leads to an accumulation of acetylcholine, causing continuous nerve transmission, which can lead to muscle contractions, paralysis and even death **(Atamanalp *et al*., 2021)**. AChE activity is therefore used as a key biomarker for assessing the exposure of aquatic organisms to various neurotoxic contaminants such as pesticides and metals **(Ajima *et al*., 2021)**.

Analysis of the results of specific AChE activity in *G. affinis* sampled at the three sites revealed a more marked inhibition of AChE activity in individuals from Sidi Brahim compared to those from Messida River and El Karma. This inhibition could be attributed to the presence of contaminants in the environment. The levels of organic pollutants such as pesticides and metals in the Sidi Brahim site are undetermined, but it is thought that this site is heavily contaminated by urban and industrial residues, and the inhibition of AChE activity observed in *G. affinis* from this site will be a response to the presence of such contaminants.

Mijošek *et al.* (2019) noted an inhibition of AChE activity in brown trout *Salmo trutta* (freshwater fish) collected from a site contaminated with technological and municipal wastewater compared to a reference site in the Krka karst river in Croatia. The study by **Gerber *et al*. (2018)** also reported inhibition of AChE activity in *Hydrocynus vittatus* (freshwater fish) in the Olifants River in South Africa after exposure to pesticides, antibiotics and heavy metals.

Conclusion

The study of growth (weight and total size) confirmed better growth at the Messida River and El Karma sites than at the Sidi Brahim site. Biomarker analysis revealed a more marked inhibition of specific AChE activity in individuals sampled from the Sidi Brahim site compared with those from the Messida River and El Karma sites. This difference is linked to the qualitative and quantitative abundance of pollutants, as well as to the physico-chemical parameters of the water, which have an effect on their availability.

Taken together, the results enabled the study sites to be classified in descending order of pollution : the Sidi Brahim site (a polluted site, characterised by its proximity to urban, industrial and domestic pollution), followed by El Karma and Messida River (relatively less polluted sites). A comparison of the population suggests that males are more sensitive to environmental stress than females.

References

Afsa, S., Vieira, M., Nogueira, A. F., ben Mansour, H., & Nunes, B. (2022). A multi-biomarker approach for the early assessment of the toxicity of hospital wastewater using the freshwater organism Daphnia magna. *Environmental Science and Pollution Research, 29* : 19132–19147. https://doi.org/10.1007/s11356-021-16977-7

Ajima, M. N. O., Kumar, K., Poojary, N., & Pandey, P. K. (2021). Sublethal diclofenac induced oxidative stress, neurotoxicity, molecular responses and alters energy metabolism proteinsin Nile tilapia, *Oreochromis niloticus*. *Environmental Science and Pollution Research, 28* : 44494–44504. https://doi.org/10.1007/s11356-021-13899-2

Al Naggar, Y., Khalil, M. S., & Ghorab, M. A. (2018). Environmental Pollution by Heavy Metals in the Aquatic Ecosystems of Egypt. *Journal of Toxicology*, *3 (1)* : 555603. DOI : 10.19080/OAJT.2018.03.555603.

Al Naggar, Y., Naiem, E., Mona, M., Giesy, J., & Seif., A. (2014). Metals in agricultural soils and plants in Egypt. *Toxicological & Environmental Chemistry*, *96 (5)* : 730-742. https://doi.org/10.1080/02772248.2014.984496

Aliko, N. G., Da Costa, K. S., Konan, K. F., Ouattara, A., & Gourène, G. (2010). Fish diversity along the longitudinal gradient in a man-made lake of West Africa, Taabo hydroelectric reservoir, Ivory Coast.Ribarstvo, *68* (2) : 47-60.

Atamanalp, M., Parlak, V., Özgeriş, F. B., Yeltekin, A. Ç., Ucar, A., Keleş, M. S., & Ala, G. (2021).Treatment of oxidative stress, apoptosis, and DNA in jury with N-acetylcysteine at simulative pesticide toxicity in fish. *Toxicology Mechanisms and Methods, 1* (3) : 224-234. https://doi.org/10.1080/15376516.2021.1871794

Blazer, V. S., Walsh, H. L., Braham, R. P., & Smith, C. (2018). Necropsy-based Wild Fish Health Assessment. *Journal of Visualized Experiments, 139* : e57946. doi:10.3791/57946.

Chang, T., Wei, B., Wang, Q., He, Y., & Wang, C. (2020). Toxicity assessment of municipal sewage treatment plant effluent by an integrated biomarker response in the liver of crucian carp (*Carassius auratus*). *Environmental Science and Pollution Research, 27* : 7280–7288. https://doi.org/10.1007/s11356-019-07463-2

Dalzochio, T., Rodrigues, G. Z. P., Petry, I. E., Gehlen, G., & da Silva, L. B. (2016). The use of biomarkers to assess the health of aquatic ecosystems in Brazil : a review. *International Aquatic Research, 8* (4) : 283–298. https://doi.org/10.1007/s40071-016-0147-9

Dawood, M. A. O., AbdEl-kader, M. F., Moustafa, E. M., Gewaily, M. S., & Abdo, S. E., 2020. Growth performance and hemato-immunological responses of Nile tilapia (*Oreochromis niloticus*) exposed to deltamethrin and fed immunobiotics. *Environmental Science and Pollution Research*, *27* : 11608–11617.

Gerber, R., Smit, N. J., van Vuren, J. H. J., Ikenaka, Y., & Wepener, V. (2018). Biomarkers in tigerfish (*Hydrocynus vittatus*) as indicators of metaland organic pollution in ecologically sensitive subtropical rivers. *Ecotoxicology and Environmental Safety, 157* (15) : 307–317.

https://doi.org/10.1016/j.ecoenv.2018.03.091

Hara, T. O., & Singh, B. (2021). Electrochemical Biosensors for Detection of Pesticides and Heavy Metal Toxicants in Water : Recent Trends and Progress. *ACS EST Water, 1* : 462−478. https://dx.doi.org/10.1021/acsestwater.0c00125

Jebali, J., Khedher, S. B., Sabbagh, M., Kamel, N., Banni, M., & Boussetta, H. (2013). Cholinesterase activity as biomarker of neurotoxicity: Utility in the assessment of aquatic environment contamination. Revista de Gestão Costeira Integrada. *Journal of Integrated Coastal Zone Management, 13* (4) : 525–537. https://doi.org/10.5894/rgci430

Jekayinfa, O., & Bawa-Allah, K. (2022). Assessing the potential toxicity of paint industry effluents to aquatic organisms using the whole effluent testing (WET) approach. *Environmental Monitoring and Assessment, 194* (3) : 172. https://doi.org/10.1007/s10661-022-09832-w

Kapute, F., Valeta, J., Likongwe, J., Kang, J., Nagoli, J., & Mbamba, D. (2016). Growth performance of three tilapia fish species raised at varied pond sizes and water depths. *International Journal of Fisheries and Aquaculture, 8* (8) : 81-86. https://doi:10.5897/IJFA2016.0566

Marinho,C. S., Matias,M. V. F., Toledo, E. K. M., Smaniotto, S., da-Silva,A. X., Tonholo, J., Santos, E. L., Machado, S. S., & Zanta,C. L. P. S.. (2021). Toxicity of silver nanoparticles on different tissues in adult *Danio rerio*. *Fish Physiology and Biochemistry, 47* :239–249. https://doi.org/10.1007/s10695-020-00909-2

Mijošek, T., Marijić, V. F., Dragun, Z., Krasnići, N., Ivanković, D., & Erk, M. (2019). Evaluation of multi-biomarker response in fish intestine as an initial indication of anthropogenic impact in the aquatic karst environment. *Science of the Total Environment,660* : 1079–1090. https://doi.org/10.1016/j.scitotenv.2019.01.045

Olasehinde, T. A., & Olaniran, A. O. (2022). Neurotoxicity of anthracene and benz[a]anthracene involves oxidative stress-induced neuronal damage, cholinergic dysfunction and disruption of monoaminergic and purinergic enzymes. *Toxicological Research, 38* : 365–377. https://doi.org/10.1007/s43188-021-00115-z

Palmate, S. S., Pandey, A., Kumar, D., Pandey, R. P., & Mishra, S. K. (2017). Climate change impact on forest cover and vegetation in Betwa Basin, India. *Applied Water Science,7* : 103–114.

Patra, B. C., Shit, P. K., Bhunia, G. S., & Bhattacharya, M. (2022). River Health and Ecology: Perspective View and Approa. *River Health and Ecology in South Asia*, 1-7. https://doi.org/10.1007/978-3-030-83553-8_1

Peyrelasse, C., Jacob, M., & Lallement, A. (2022). Multicriteria Comparison of Ozonation, Membrane Filtration, and Activated Carbon for the Treatment of Recalcitrant Organics in Industrial Effluent : A Conceptual Study. *Environmental Processes, 9*. https://doi.org/10.1007/s40710-022-00563-1

Poletto, J. B., Martin, B., Danner, E., Baird, S. E., Cocherell, D. E., Hamda, N., Cech, J., Joseph, J., & Fangue, N. A. (2018). Assessment of multiple stressors on the growth of larval green sturgeon *Acipenser medirostris*: implications for recruitment of early life-history stages. *Journal of Fish Biology, 93* :952–960. https://doi.org/10.1111/jfb.13805

Quiroz-Jara, M., Casini, S., Fossi, M. C., Orrego, R., Gavilán, J. F. & Barra, R. (2021). Integrated Physiological

Biomarkers Responses in Wild Fish Exposed to the Anthropogenic Gradient in the Biobío River, South-Central Chile. *Environmental Management, 67* (6) : 1145-1157. https://doi.org/10.1007/s00267-021-01465-y

Sellaoui, N., & Bounaceur, F. (2020). Growth and length-weight relationships of *Gambusia affinis* (Baird et Girard, 1853) population in Algeria (Cyprinodontiformes Poeciliidae). *Biodiversity Journal, 11* (4) : 951–959. https://doi.org/10.31396/biodiv.jour.2020.11.4.951.959

Tang, M., Chen, Y., Xian, H., Tan, S., Lian, Z., Peng, X., & Hu, D. (2022). Circulating exosome level of indigenous fish may be a novel biomarker for the integrated ecotoxicity effect of water environment. *Ecotoxicology and Environmental Safety*, *229* : 113084. https://doi.org/10.1016/j.ecoenv.2021.113084

Vidhya, V., Sreeja, S. J., Nair, C. R., & Nair, S. G. (2019). Induction of Nuclear Abnormalities (Na) In Erythrocytes of Fish, *Etroplus Suratensis* Following the Exposure of Pyrethroid Insecticide, Lambda-Cyhalothrin. *Think India Journal, 22* (14) : 13467-13479.

Effect of *Thymus Munbyanus* Essential Oil on the Activity of a Neurotoxicity Biomarker Ache in a Stored Food Pest *Ephestia Kuehniella*

Yezli-Touiker Samira

University Badji Mokhtar Annaba, Faculty of sciences, Applied Animal biology laboratory, Algeria, [ID]
https://orcid.org/: 0000-0002-1156-2100

Bendjedid Hadjira

University Badji Mokhtar Annaba, Faculty of sciences, Applied Animal biology laboratory, Algeria [ID]
https://orcid.org/0000-0002-6199-6214

Yezli Amina

University Badji Mokhtar Annaba, Faculty of sciences, Applied Animal biology laboratory, Algeria [ID]
https://orcid.org/0000-0003-2624-4743

Abstract: Insect pests, considered one of the major problems in agriculture, can also be vectors of pathogens and pose a threat to animals including humans. Thus, in the context of sustainable development, non-polluting pesticides have been marketed by pharmaceutical and phytosanitary companies. These molecules, alternatives to conventional pesticides, are represented by synthetic pesticides of the 3rd generation (growth regulators) or by pesticides of natural origin (biopesticides). EO was diluted in acetone and administered by topical application, on newly exuviated pupae at two doses (ID25: 15.38 μl/mL and ID50: 25.22 μl/mL) and the effects were observed on two successive generations, the parental generation (P) which was exposed to the treatment and the first generation (F1) not exposed. The EO of *T. munbyanus* was evaluated on a neurotoxicity biomarker acetylcholinesterase (AChE) on the 2nd generation of adults. The comparison between the control and treated series shows that HE induces a highly significant reduction in the specific activity of acetylcholinesterase (AChE) in the adults of *E. kuehniella*. Indeed, the EO of *T. munbyanus* acts with a dose- response relationship. The values obtained show that HE causes neurotoxicity which results in a reduction in the activity of acetylcholinesterase (AChE).

Keywords: Essential oil, Biopesticides, Neurotoxicity, Pest control, Sustainable development

Introduction

Each year, insects ruin one-fifth of the world's food production; they are the most diverse collection of animals on Earth, with just 0.5% of them classified as pests (Bendjedid *et al.*, 2024). The pyralid Mediterranean flour moth, *Ephestia kuehniella* Zeller, is a major pest of stored grain products as well as flour and other milled products (Yezli-touiker *et al.,* 2018; Taffar *et al.,* 2022), and considered as a significant model to study interactions between pesticides and insects (Shahriari *et al.,* 2018). Many storage systems rely on the use of synthetic insecticides and fumigants to control stored-product pests (Campos *et al.,* 2016).

However, in recent decades, the development of insect resistance and adverse effects on non-target organisms, soil, water, and air have increased significantly (Johnson *et al.,* 2023) and became a real health and environmental problems. Scientists are looking forwards to develop and to propose new alternatives, instead of the used conventional pesticides, such as a natural plant extracts, called botanical insecticides or bioinsecticides (Bendjedid *et al.,* 2021; Yezli *et al.,* 2024a). Many bioassays using plant extracts and essential oils (EOs), from different plant parts are tested against different insect orders (Yang et al., 2020). According to these positive results, insecticides of botanical origin are increasingly being used as safe alternatives to the conventional chemical and synthetic insecticides for pest control, in both agriculture and public health sector, a sustainable and ecologically friendly manner (Ma *et al.,* 2023).

The *Thymus* sp. (Thyme) is small permanent therapeutic botanical herbs native to the Mediterranean region. They belong to the Lamiaceae family, which is one of the largest families among flowering plants, practically, with almost a range of 220 genera and 4000 species in the world. Among them, the species *Thymus munbyanus* shows different biological activities like anti-microbial, anti-bacterial, (Javad *et al.,* 2013) and anti-proliferative activity on human cells antioxidant activity (Sadou *et al.,* 2020). *T. munbyanus* essential oil presents various families of compounds such as monoterpenes, sesquiterpenes, diterpenes, oxygenated derivatives also aromatic hydrocarbons, aldehydes, and ketones (Dukiˊ *et al.,* 2023).

The current study was aimed to give additional information of mode action of EO, the activities of the biomarker of neurotoxicity (AChE) was measured and interpreted.

Method

Insect

Ephestia kuehniella Zeller (Lepidoptera: Pyralidae) is a major pest of stored food all over the world. In Algeria, it is particularly abundant in grains stores and wheat flour (Yezli-Touiker *et al.,* 2019). The insect was reared in the laboratory at a temperature of 27°C and a humidity of 80% in almost continuous darkness as previously described (Bendjedid *et al.,* 2021). Pupae were staged according to their age in days from pupal ecdysis.

Plant collection

The plant material consists of aerial parts samples subspecies of Algerian *T. munbyanus* subsp. *coloratus* (Boiss & Reut) Greuter & Burdet. harvest was carried out in June 2020 when the plant was fluorescent (the flowering stage), with an amount of 8.7 kg in the municipality of Chetaibi (Northeast Algeria, Annaba; 36°56'47.4"N 7°23'43.9"E), then dried at room temperature ($27 \pm 2°C$) for 15 days, to obtain 2.7kg of the shade-dried plant. Dr. Hamel Tarek based on Algerian flora   identified the plant and the voucher specimen (N°145394) was deposited in the herbarium of the Department of Botany (Faculty of Science, University of Badji Mokhtar Annaba, Algeria).

Isolation of essential oil

The Isolation was done by hydrodistillation and it consists of immersing the cut aerial part of *T. Munbyanus* (100 g) directly in a 4-liter flask filled with distilled water (1 L) using a Clevenger type apparatus Clevenger, 1928) . The whole is then brought to a boil for 3 hours, then the oil is separated from the aqueous phase in the presence of anhydrous sodium [2] sulfate to remove all traces of water and the essential oil was stored in a little opaque bottle at 4°C in the dark. The hydrodistillation was performed six times. The yield is calculated following the (AFNOR, 2000) formula: oil % (w / w) = weight of essential oil (g) / weight of plant material (g) $\times$ 100.

Biomarkers activities

AChE activity was assessed in accordance with the method of Ellman et al. (1961), using acetylthiocholine as a substrate, The samples were homogenized in 1 ml of detergent solution (1 mM EGTA / 1% triton X / 1 M NaCl / 0.01 M Tris, pH7).

After centrifugation (5,000 rpm for 5 min), the activity of AChE was measured on an aliquot of 100 μl of supernatant to which 100 μl of 5,5'-dithiobisnitrobenzene (DTNB) acid and 1 ml of Tris buffer (0.1 M, pH 7) were added. After 5 min of reaction, 100 μl of substrate (acetylthiocholine) was added. Optical density was measured at a wavelength of 412 nm every 4 min for 20 min. The specific activity of AChE is expressed in μM/min/mg of protein.

The samples were homogenized individually in 1 ml of phosphate buffer (0.1 M, pH 6). After centrifugation (14.000 rpm for 30 min), an aliquot of 200 μl of the supernatant was added to 1.2 ml of a mixture of CDNB (1mM)/GSH (5 mM) substrate in phosphate buffer (0.1 M, Ph 6). The absorbance readings were taken, every minute, for 5 min at a wavelength of 340 nm.

EO was diluted in acetone and administered by topical application, on newly exuviated pupae at two doses (ID25: 15.38 μl/mL and ID50: 25.22 μl/mL) and the effects were observed on two successive generations, the

parental generation (P) which was exposed to the treatment and the first generation (F1) not exposed. The EO of *T. munbyanus* was evaluated on a neurotoxicity biomarker acetylcholinesterase (AChE) on the 2nd generation of adults.

Data analysis

Statistical analyses were performed using Prism version 6 for Windows (Graph Pad Software, La Jolla, CA, USA, www Graphpad.com), and $p < 0.05$ was considered to be a statistically significant difference. Data have been expressed by the mean ± standard deviation (mean ± SD). All data were verified by the Brown-Forsythe test and analyzed by one-way ANOVA and two-way analysis treatment series. The oil induced a significant AChE inhibition from 24 h of treatment. The one-way ANOVA indicated of variance (ANOVA). A Tukey post-hoc analysis HSD test was used to evaluate differences between the control and treated series.

Results

For AChE, the activity was determined in the control and a significant effect of treatment ($F_{(2, 6)} = 25.93$; $p < 0.0011$). Different lowercase letters above the same exposure time indicated a significant difference and different uppercase letters above the same exposure treatment indicated a significant difference ($p < 0.05$). It can be observed that, the *T. munbyanus* essential oil caused a significant increase in AChE enzyme activity compared to the control series (Fig. 1). A decrease has been observed in second-generation adults (Fig.2) . The *T. munbyanus* hour thus affects the activity of the AChE in adult females during the two successive generations of *E. kuehniella* following the treatment.
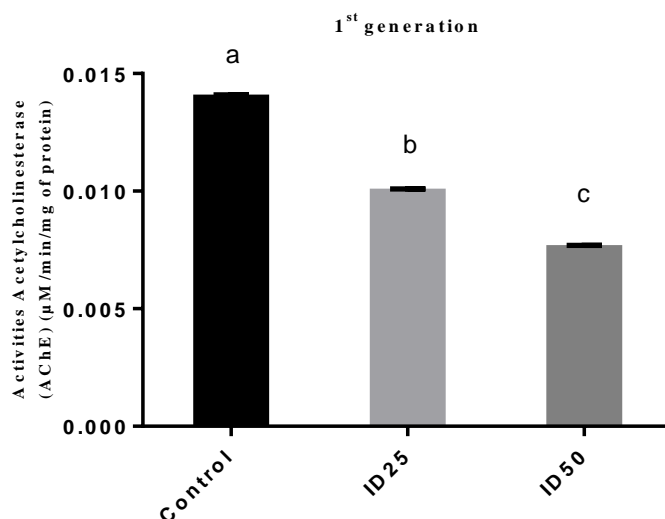
Figure 1. Effect of *Thymus munbyanus* essential oil (ID25 and ID_{50}) topically applied to newly molted pupae of *E. kuehniella* (mean ± SD, n= 6) on the AChE activity (M / min/mg of protein) during 1st generation adult stage. (Different lowercase letters above the same exposure time indicate a significant difference (p<0.05)
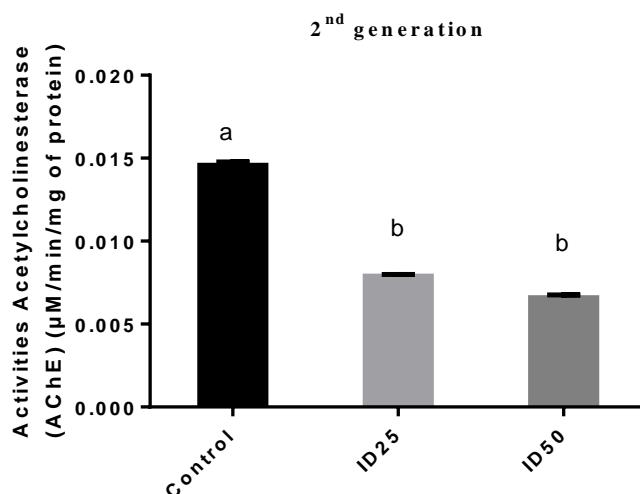
Figure 2. Effect of *Thymus munbyanus* essential oil (ID25 and ID_{50}) topically applied to newly molted pupae of *E. kuehniella* (mean $\pm$ SD, n= 6) on the AChE activity (μM / min/mg of protein) during 2nd generation adult stage. (Different lowercase letters above the same exposure time indicate a significant difference (p<0.05)

Discussion

Acetylcholine esterase (AChE) is one of the most important hydrolytic enzymes in insect nervous system that equilibrate neural signal transduction by rapid hydrolyzing of acetylcholine signal in the synaptic cleft (Jacob and Mason, 2005). The monoterpenes abundantly present in essential oils (EOs) are lipophilic in nature and can interfere with the metabolic, biochemical, physiological and behavioral functions of insects (Mann and Kaufman, 2012). Due to their bioactive chemical constituents, aromatic plant Eos act on the nervous system of insects (Abdullah *et al.,* 2015). The high level of esterases in various insect species, including mosquitoes, has been primarily associated with the phenomenon of resistance against insecticide compounds (Polson *et al.,* 2011).

The results demonstrate that *T. munbyanus* EO significantly reduced the activity of AChE in the treated series compared to the control ones of *E. kuehniella*. This decrease in activity is likely due to the essential oil's inhibition of the enzyme. Similar results reported inhibition of the AChE activity which was observed in *E. kuehniella* after treatment by α-pinene, transanethole, and thymol oil Shahriari *et al .,* 2018. More recently, *E .kuehniella* larvae treated by EOs of *Allium sativum* and *Eucalyptus globulus*, significantly decreased the activity of acetylcholine esterase. The decrease in the specific activity of AChE tends to confirm the neurotoxicity effects of *T. munbyanus* EO in both stages compared to the control series. This could be explained by an inhibition of AChE which Dandlen et al.(2011) already reported that different essential oils isolated from various Portuguese spices of Thymus presented AChE inhibition capacity pointing out the strong AChE inhibition potential of *T. zygis* subsp. Zygis essential oil, marked with a relatively high amount of carvacrol (43.6 %). From this research, it is noteworthy that carvacrol is a very active inhibitor against AChE.

Furthermore, López et al. (2018) reported that *Origanum syriacum* and carvacrol inhibited the activity of AChE in *Anisakis simplex*). The results obtained with *Cx. pipiens* after treatment with *M. communis* EO showed a very significant increase in enzyme levels in the treated series compared to the control series at 24, 48, 72 and 96 h, respectively (Yezli *et al.,* 2024b)

Conclusion

Our research showed that *T. munbyanus* subsp *coloratus* EO topically applied to newly molted pupae caused significant mortality of *E. kuehniella* with low concentrations. The obtained results have showed of EO of *T. munbyanus* subsp *coloratus* exhibited toxic effects against adult of *E. kuehniella.*
The overall results suggested that *T. munbyanus* could be used in integrated pest management programs as an alternative to synthetic chemical insecticides.

Acknowledgements

References

Abdullah, F., Subramanian, P., Ibrahim, H., Abdul Malek, S. N., Lee, G. S. & Hong, S. L. (2015). Chemical composition, antifeedant, repellent, and toxicity activities of the rhizomes of galangal, *Alpinia galanga* against Asian subterranean termites, *Coptotermes gestroi* and *Coptotermes curvignathus* (Isoptera: Rhinotermitidae). *Journal of Insect Science,* https://doi.org/10.1093/jisesa/ieu175.

Abdullah, F., Subramanian, P., Ibrahim, H., Abdul Malek, S. N., Lee, G. S. & Hong, S. L. (2015): Chemical composition, antifeedant, repellent, and toxicity activities of the rhizomes of galangal, *Alpinia galanga* against Asian subterranean termites, *Coptotermes gestroi* and *Coptotermes curvignathus* (Isoptera: Rhinotermitidae). *Journal of Insect Science*, https://doi.org/10.1093/jisesa/ieu175.

AFNOR. (2000). « Recueil de normes Francaise : Les huiles essentielles ». Tome 2.

Bendjedid, H., Yezli-Touiker, S., Taffar, A. & Soltani, N. (2021). Phytochemical composition and insecticidal activities of essential oil of *Thymus munbyanus* (Lamiales: Lamiaceae) aerial parts and its properties against biomarkers of Ephestia kuehniella Zeller (Lepidoptera: Pyralidae). *J. Essent. Oil-Bear. Plants*, 24(4), 792-807.

Bendjedid, H., Yezli-Touiker, S., Taffar, A., Yezli, A., & Souileh, N. (2024). Impact of Infestation of Flour by *Bioresource Management*, 11 (1), 2309-3854

Campos, E.V., & Proença, P. (2019). Use of botanical insecticides for sustainable agriculture: Future perspectives. *EcoIndic*, 105, 483-495.

Campos, E.V., Proença, P.L., Oliveira, J.L., Bakshi, M., Abhilash, P.C. & Fraceto, L.F. (2019). Use of botanical insecticides for sustainable agriculture: Future perspectives. *Ecol. Indic.*105, 483-495.

Clevenger, J.F. (1928). Apparatus for the determination of volatile oil. *J. Am. Pharm. Assoc*, 17, 345-349.

Dandlen, A.S, Lima, A.S., Mendes, M.D., Miguel, M.G., Faleiro, M.L., Sousa, M.J., Pedro, L.G., Barroso, J.G. & Figueiredo, A.C. (2010). Antioxidant activity of six Portuguese thyme species essential oils. *Flavour Fragr J* , 25, 150-155.

Dandlen, S.A., Miguel, M.G., Duarte, J., Faleiro, M.L., Sousa, M.J., Lima, A.S., Figueiredo, A.C., Barroso, J.G. & Pedro, L.G. (2011). Acetylcholinesterase Inhibition Activity of Portuguese *Thymus* Species Essential Oils. *J. Essent. Oil-Bear. Plants*, 14(2), 140-150.

Đuki´, N., Markovi´, T., Miki´, S., ˇCutovi´, N. (2023). Repellent activity of basil, clary sage and celery essential oils on *Tribolium castaneum* (Herbst*). Journal of Stored Products Research*, 103, 102150.

Ellman, G. L., Courtney, K. D., Andres, V. & Featherstone, R. M. (1961). A new and rapid colorimetric determination of acetylcholinesterase activity. *Biochemical Pharmacology*, 7, 88-95.

Jacob, R.F. & Mason, R.P. (2005). Lipid peroxidation induces cholesterol domain formation in model membranes. *J. Biol. Chem*, 280, 39380-39387.

Jacob, R.F., & Mason, R.P.(2005). Lipid peroxidation induces cholesterol domain formation in model membranes. *Journal of Biological Chemistry*, 280, 39380-39387.

Javed, H., Erum, S., Tabassum, S. & Ameen, F. (2013). An overview on medicinal importance of *Thymus vulgaris. J. Asian Sci. Res*, 3(10), 974-982.

Johnson, E. J., McComic, S. E., Rault, L. C., Swale, D. R. & Anderson, T. D. (2023). Bioinsecticidal activity of cajeput oil to pyrethroid-susceptible and-resistant mosquitoes. *Pesticide Biochemistry and Physiology*, 193, 105458. https://doi.org/10.1016/j.pestbp.2023.105458.

López, V., Cascella, M., Benelli, G., Maggi, F. & Gómez-Rincón, C. (2018). Green drugs in the fight against *Anisakis simplex* larvicidal activity and acetylcholinesterase inhibition of *Origanum compactum* essential oil. *Parasitol. Res*, 117, 861-867.

Ma, X., Hu, J., Ding, C., Portieles, R., Xu, H., Gao, J., Du, L., Gao, X., Yue, Q., Zhao, L. & Borrás-Hidalgo, O. (2023). New native Bacillus thuringiensis strains induce high insecticidal action against *Culex pipiens* pallens larvae and adults. *BMC Microbiology*, 23, 100. https://doi.org/10.1186/s12866-023-02842-9.

Mann, R. S., & Kaufman, P. E. (2012). Natural product pesticides: their development, delivery and use against insect vectors. Mini-Reviews in Organic Chemistry, 9(2), 185-202.

Polson, K. A., Brogdon, W. G., Rawlins, S. C. & Chadee, D. D. (2011). Characterization of insecticide resistance in Trinidadian strains of *Aedes aegypti* mosquitoes. *Acta Tropica*, 117(1), 31-38.

Sadou, N., Boughendjioua, H., Seridi, R. & Hamel, T. (2020). Effect of solvent extraction and growth stages on the content phenolics and antioxidant activity of *Thymus munbyanus* subsp*. coloratus* (Boiss. & Reut.). *PhytoChem & BioSub Journal*, 14(3), 2170-1768.

Shahriari, M., Zibaee, A., Sahebzadeh, N. & Shamakhi, L. (2018). Effects of a-pinene, trans anethole, and thymol as the essential oil constituents on antioxidant system and acetylcholine esterase of *Ephestia kuehniella* Zeller (Lepidoptera: Pyralidae). *Journal of Pest Science*, 150, 40-47.

Stored Food Pest Insects Ephestia Kuehniella on Quality Flour: Physico-Chemical Analyses*, Journal of*

Yang, Y., Isman, M. B. & Tak, J. H. (2020): Insecticidal activity of 28 essential oils and a commercial product containing *Cinnamomum cassia* bark essential oil against. *Insect*, 11, 474-498.

Yezli, A., Arroussi, D.E.R., Boudjelida, H. & Bensouici, C (2024a). Repellency and activity evaluation of *Myrtus communis* essential oil on physiology and reproduction of mosquito species *Culex pipiens. Fresen. Environ. Bull*, 33(5), 407-417.

Yezli, A., Boudjelida, H., & Arroussi, D. (2024b). Components and toxicological effects *of Myrtus communis* L. (myrtales: myrtaceae) essential oil against mosquito *Culex pipiens* L. (diptera: culicidae). *Applied ecology & environmental research*, 22(3), 2164.

Yezli-Touiker S., Taffar A., Meskache R. Soltani N. (2018). Impact of captopril on *Ephestia kuehniella*: Ovarian Nucleic Acid Amounts and Protein Analysis. Tunis. *J. Plant Prot*, 13,77-85.

Yezli-Touiker, S., Kirane-Amrani, L., Meskache, R. and Soltani, N.(2019). Effect of captopril on growth development and cuticular secretion in pupae of the mediterranean flour moth, *Ephestia kuehniella Zeller. Fresenius Environ Bull*, 28 (2), 526-531.

Optimizing Photovoltaic System Performance with Type-2 Fuzzy Logic Controller-Based Maximum Power Point Tracking

Noureddine Ould cherchali

Research Laboratory in Electrical Engineering and Automatic (LREA) University of Medea, Medea, Algeria

Mohamed Redha Skender

Department of Electrical Engineering, Faculty of Technology Medea, Algeria, https://orcid.org/0000-0002-6572-8102

Ibrahim Bentchikou

Department of Electrical Engineering, Djilali Bounaama Khemis Miliana University, Ain Defla, Algeria

Abstract: This paper presents a robust approach for maximizing power point tracking (MPPT) in photovoltaic (PV) systems, utilizing a Type-2 fuzzy logic controller. The controller uses solar irradiation and PV cell temperature as its input parameters and produces the optimal duty cycle to achieve maximum power output. This novel method is designed to ensure efficient maximum power operation across various photovoltaic arrays, even when subjected to fluctuations in solar irradiation and PV cell temperature. The Type-2 fuzzy logic controller stands out due to its advanced handling of uncertainties and non-linearities inherent in solar power generation. By incorporating solar irradiation and temperature data, the controller dynamically adjusts to varying environmental conditions, maintaining optimal performance. This adaptability is crucial for PV systems, which often experience significant changes in weather and operational conditions. Simulation results presented in the paper highlight the effectiveness of the Type-2 fuzzy logic controller. Compared to traditional methods, the controller consistently delivers higher power output, showcasing its superior performance. The study compares the Type-2 fuzzy logic controller with other existing MPPT techniques, demonstrating its ability to extract more power from the PV systems under different scenarios. Moreover, the paper discusses the implementation details of the Type-2 fuzzy logic controller, providing insights into its algorithmic structure and operational principles. The controller's design enables it to manage the variability and unpredictability of solar energy, making it a reliable and efficient solution for enhancing the performance of PV systems.

Keywords: MPPT, Type-2 fuzzy logic, photovolaic system, optimization

Introduction

Photovoltaic power is widely recognized as a promising energy source in many regions characterized by high solar power density. Over the past few decades, the adoption of both independent and grid-connected solar energy systems has seen significant growth. These applications encompass a wide range of uses, including PV power plants, electric vehicles, air conditioning, illumination, water pumping, refrigeration, vaccine storage, hybrid systems, as well as military and space applications.

Regrettably, PV systems come with a substantial manufacturing cost and exhibit relatively low energy conversion efficiency. Moreover, they feature V-I (voltage-current) characteristics that are nonlinear and influenced by insolation and temperature. The operational point, which corresponds to maximum power output, undergoes nonlinear changes in response to various environmental conditions, such as irradiation, temperature fluctuations, and degradation levels.

The primary factors contributing to the reduced electrical efficiency of photovoltaic systems include the nonlinear variation of output voltage and current in response to changes in solar radiation levels, operating temperature, aging, and load current. To address these issues, efforts are made to track the maximum power point of the PV system, specific to given conditions, using either online or offline algorithms. These algorithms aim to guide the system's operating point towards this optimal condition.

In the literature, many techniques for Maximum Power Point Tracking (MPPT) have been proposed and put into practice. These methods encompass approaches such as perturbation and observation (P&O) methods [1][2] and computational strategies [3]-[5]. Among these computational methods, one that has exhibited exceptional performance across various environmental operating conditions is the fuzzy MPPT technique [6]-[10].

This paper introduces the application of Type-2 Fuzzy Logic Control (T2FLC) to MPPT control. The simulation study in this paper is conducted using MATLAB and Simulink.

The Photovoltaic System

The solar cell model falls into the category of a p-n semiconductor junction. When it's exposed to light, it generates DC current. As established by numerous researchers, the magnitude of the generated current is contingent upon factors such as solar irradiance, temperature, and load current.

Figure 1 illustrates the customary equivalent circuit for a PV cell [09][11].
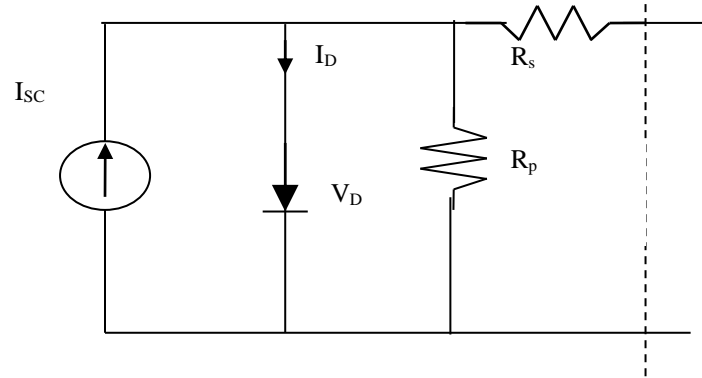
Figure 1. Typical circuit of PV solar cell

The basic equations describing the I-V characteristic of the PV model are given in the following equations:

$$0 = I_{SC} - I_D - \frac{V_D}{R_P} - I_{PV}$$

(1)

$$I_D = I_0(e^{V_D/V_T} - 1)$$

(2)

$$V_{PV} = V_D - R_S I_{PV}$$

(3)

Where:

I_{PV} is the cell current (A).

I_{SC} is the light generated current (A).

I_D is the diode saturation current (A).

R_S is the cell series resistance (ohms).

R_P is the cell shunt resistance (ohms).

V_D is the diode voltage (V).

V_T is the temperature voltage (V).

V_{PV} is the cell voltage (V).

Method Maximum Power Point Tracking Techniques MPPT

In PV systems, it's common practice to employ Maximum Power Point Tracking (MPPT) to trace the optimal power point. The effectiveness of MPPT hinges on two key elements: the MPPT control algorithm and the MPPT circuit. Typically, the MPPT control algorithm is implemented within the DC-DC converter, which serves as the conventional choice for the MPPT circuit. A typical illustration of how MPPT is integrated into a PV system is depicted in Figure 2.
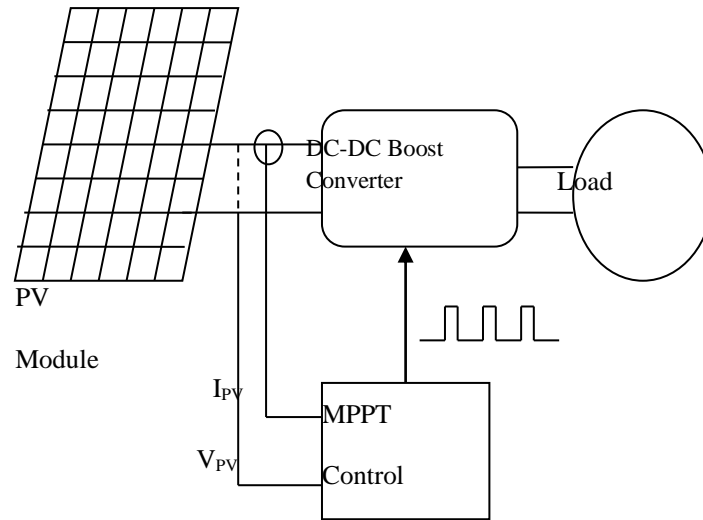
Figure 2. Typical diagram of MPPT in PV System

Figure 3 and Figure 4 depict the response of a photovoltaic panel simulation to fluctuations in irradiation and temperature, under conditions where either temperature or irradiation remains constant. It's important to note that a PV generator linked to a load can function across a wide range of current and voltage values, contingent upon prevailing weather conditions.

Consequently, the MPPT controller needs to adapt and follow the updated maximum power point along its corresponding curve whenever changes in temperature and/or insolation levels occur.
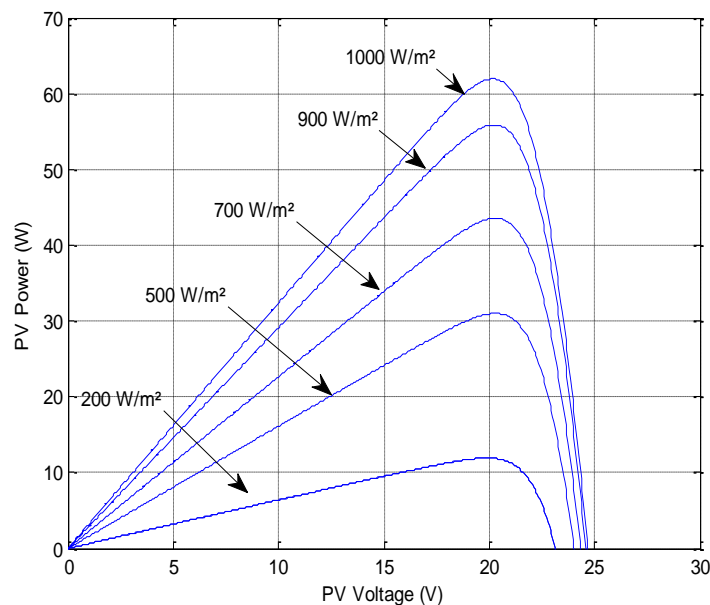
Figure 3. Influence of the solar radiation for constant temperature 25 °C
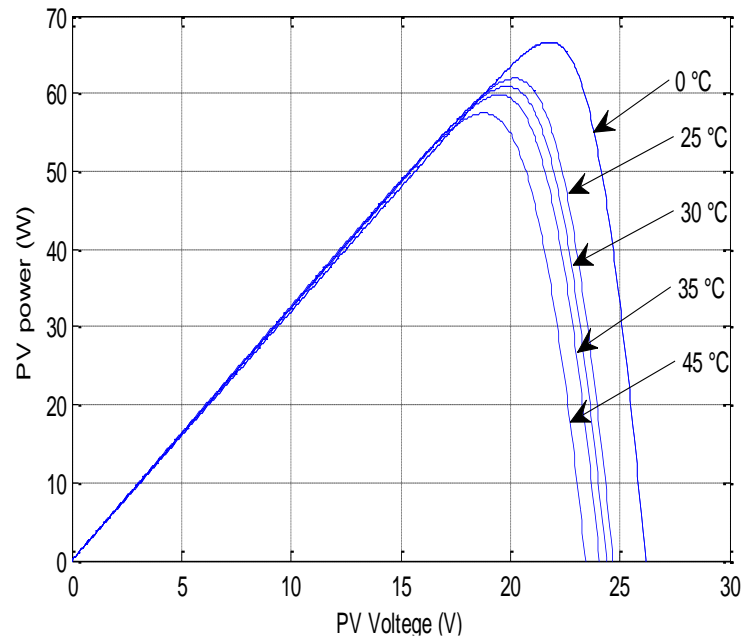
Figure 4. Influence of the temperature of junction for constant irradiation =1000 W/m²

MPPT using Fuzzy Logic Control (Fuzzy T2FLC MPPT)

Figure 5 illustrates the configuration of a Type-2 Fuzzy Logic Controller (FLC), which closely resembles a Type-1 Fuzzy Logic System (FLS) [12][14]. The key distinction lies in the fact that at least one of the Fuzzy sets is of Type-2, and a Type-reducer is essential to convert the output from the Fuzzy inference engine into a Type-1 Fuzzy set known as the Type-reduced set. This Type-reduced set is subsequently defuzzified to yield the precise output, denoted as "dD"[14].
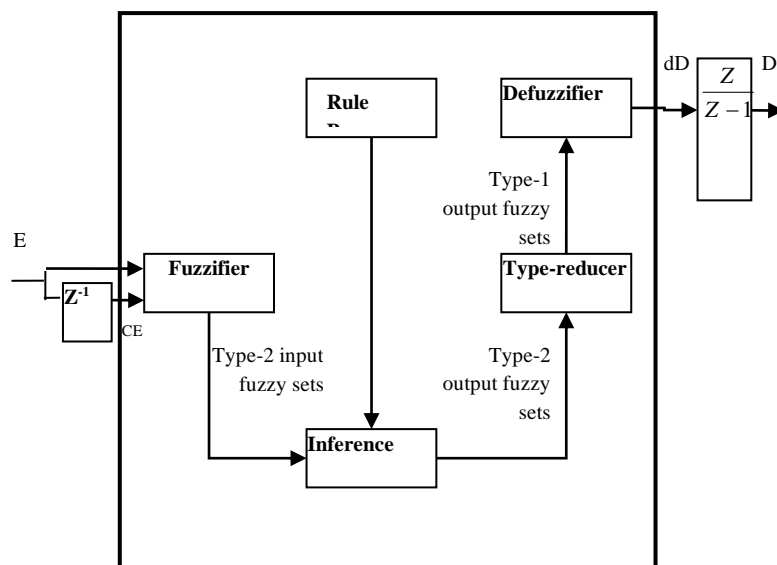
Figure 5. Structure of a T2FLC

The T2FL MPPT Controller, as depicted in Figure 6, is designed with two input variables and one output. These two input variables in the T2FLC are defined as the error (E) and the rate of change of error (CE) at discrete time points denoted as 'k'. E and CE are defined by:

$$E(k) = \frac{P_{ph}(k) - P_{ph}(k-1)}{V_{ph}(k) - V_{ph}(k-1)}$$

(4)

$$CE(k) = E(k) - E(k-1)$$

(5)

Where "$P_{ph}(K)$" represents the instantaneous power output of the photovoltaic generator at the time instant 'k'. The input 'E(K)' indicates whether the operating point of the load at time instant 'K' is situated to the left or right of the maximum power point on the PV characteristic, while the input 'CE(K)' conveys the direction in which this point is shifting.

The value of 'dD' is calculated by using the T2FLC depicted in Fig. 8, which employs the rule base detailed in Table I.

Assume that there are M rules in the Type-2 Fuzzy system, where the ith rule has the following form:

$$R^i: \quad if \quad E \quad is \quad \tilde{F}_E^i \quad and \quad CE \quad is \quad \tilde{F}_{CE}^i \quad THEN \quad dD \quad is \quad \tilde{G}^i = \begin{bmatrix} U_l^i & U_r^i \end{bmatrix}$$

(6)

with i= 1,..,M

Where $\tilde{F}_E^i$ and $\tilde{F}_{CE}^i$ are antecedent linguistic terms modelled by the interval Type-2 triangular Fuzzy sets, dD is the output and the consequent term G^i is an interval Type-1 set called Type-reduced Fuzzy set represented by the weighting interval set $\begin{bmatrix} U_l^i & U_r^i \end{bmatrix}$. U_l^i and U_r^i are the singleton lower and upper control actions of the consequent part. The antecedent and consequent Type-2 membership functions are shown in Figure 6. The Fuzzy labels are negative big (NB), negative small (NS), zero (ZE), positive medium (PM) and positive big (PB).

Table 1. Fuzzy rule table

CE E	NB	NS	ZE	PS	PB
NB	ZE	ZE	PB	PB	PB
NS	ZE	ZE	PS	PS	PS
ZE	PS	ZE	ZE	ZE	NS
PS	NS	NS	NS	ZE	ZE
PB	NB	NB	NB	ZE	ZE

The firing interval $f^i = \begin{bmatrix} \underline{f}^i, \overline{f}^i \end{bmatrix}$ of the ith rule is an interval Type-1 set, which is determined by its left-most

and right-most points   and   such that, see Figure 7.

$$\underline{f}^{i} = \min(\underline{\mu}_{\tilde{F}^i_E}(E), \underline{\mu}_{\tilde{F}^i_{CE}}(CE)) \tag{7}$$

$$\overline{f}^{i} = \min(\overline{\mu}_{\tilde{F}^i_E}(E), \overline{\mu}_{\tilde{F}^i_{CE}}(CE)) \tag{8}$$

Where $\underline{\mu}_{\tilde{F}^i_x}(x)$ and $\overline{\mu}_{\tilde{F}^i_x}(x),$ represent the grade of membership for the lower and upper membership functions of the crisp input 'x' within the Type-2 Fuzzy set in the 'i-th' rule.

The first stage of the calculation of the Type-reduced sets is the computation of the interval set $\begin{bmatrix} U^i_l & U^i_r \end{bmatrix}$ i = 1,...,M. The output is an interval Type-1 set; therefore, we only need to compute its two endpoints dD$_l$ and dD$_r$ as follows (eq.9 and eq.10):

Membership function

(a)

Membership function

(b)

Membership function

(c)
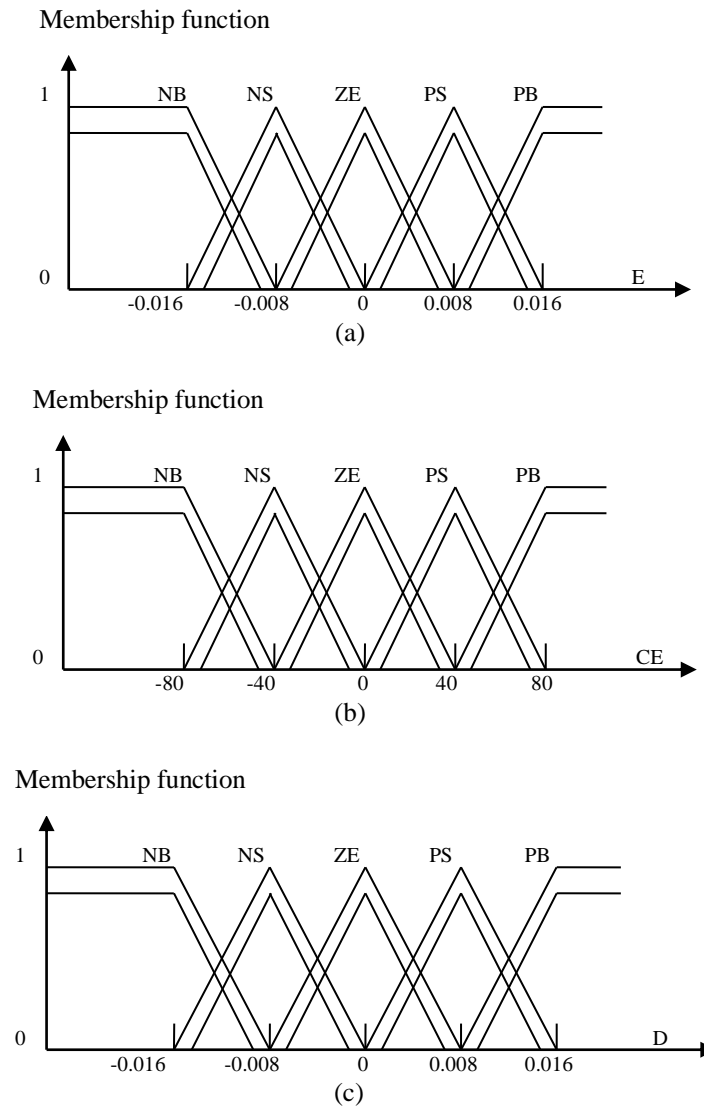
Figure 6. membership function of (a) error E   (b) change error CE   (c) duty ratio D

$$dD_l = \frac{\sum_{i=1}^{M} f_l^i u_l^i}{\sum_{i=1}^{M} f_l^i}$$

(9)

$$dD_r = \frac{\sum_{i=1}^{M} f_r^i u_r^i}{\sum_{i=1}^{M} f_r^i}$$

(10)

In order to calculate dD, dD_l and dD_r are computed. This can be done using the iterative procedure given in [10-11]. Initially, we compute the right-most point dD_r.

0) Arrange U_r^i in ascending order, i.e

$$U_r^1 \le U_r^2 \le \cdots \le U_r^M$$

(11)

1) Compute dD_r in (eq.10) by initially setting $f^i = \lfloor \underline{f}^i, \overline{f}^i \rfloor / 2$, for i = 1,2,...,M where $\underline{f}^i$ and $\overline{f}^i$ have been computed using (eq.7) and (eq.8) respectively, and let $dD_r' = dD_r$

2) Find k (1≤k≤ -1) such that $U_r^k \le dD_r' \le U_r^{k+1}$

3) Compute dD_r in (10) with $f_r^i = \underline{f}^i$ for I ≤ k and $f_r^i = \overline{f}^i$ for i>k , then set $dD_r'' = dD_r$

4) If $dD_r'' \ne dD_r'$, then go to step 5). If $dD_r'' = dD_r'$ then $dD_r = dD_r''$ and stop

5) Set $dD_r' = dD_r''$ and return to step 2).

The procedure for computing dD_r is very similar, only two changes need to be made: In step 2), we finding 1 ≤k' ≤M-1) such that $U_l^{k'} \le dD_l' \le u_l^{k'+1}$. In step 3), let $f_r^i = \underline{f}^i$ for i ≤k' and $f_r^i = \overline{f}^i$ for i>k' .

Following the Type-reduction stage, we obtain a Type-reduced set for each output. The precise output of the controller corresponds to the midpoint of this Type-reduced set.

$$dD = \frac{dD_l + dD_r}{2}$$

(12)
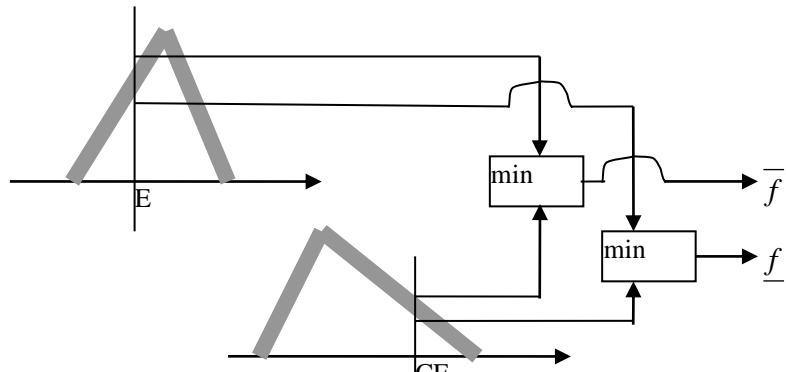
Figure 7. Fuzzification with minimum t-norm

P&O techniques

In order to evaluate and contrast the effectiveness of MPPT employing T2FLC with alternative MPPT techniques, one of the most straightforward and widely used methods is the Perturbation and Observation (P&O) technique. . The main concept behind this approach is to steer the system towards operation in a direction where the PV system's output power increases. The following equation outlines the power change, which underpins the strategy of the P&O technique.

$$\Delta P = P(k) - P(k-1)$$

(13)
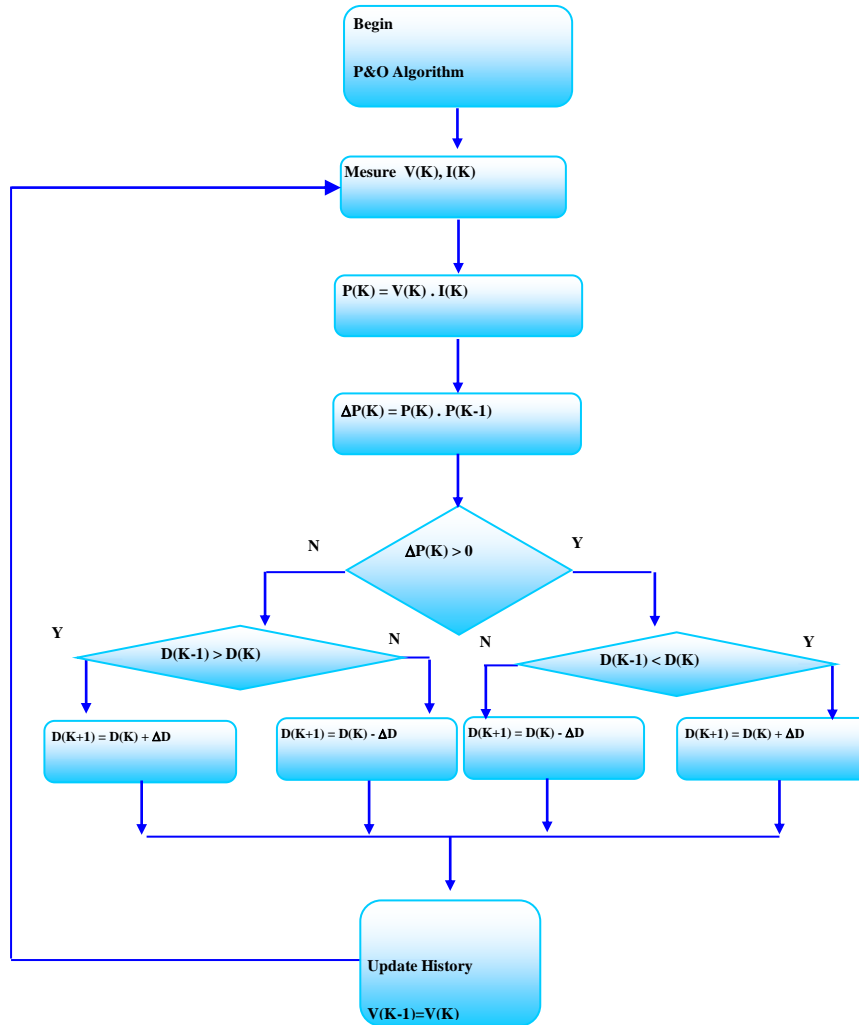
Figure 8. Flow Chart of the P&O Method

If the change in power, as defined by equation (eq.12), is positive, the system will maintain the same direction for the incremental current (whether increasing or decreasing the PV current). Conversely, when the change is negative, the system will alter the direction of the incremental current command to the opposite direction. This technique performs effectively under steady-state conditions where radiation and temperature changes occur

gradually. However, the P&O method struggles to track the Maximum Power Point (MPP) when atmospheric conditions change rapidly. You can find the flow chart illustrating the P&O method in Figure 8.

Results

Figure 2 shows the functional diagram of the simulated photovoltaic system. The boost chopper serves as the DC-DC converter. The T2FL and P&O MPPT controllers were subjected to testing scenarios as detailed below:

- Test Scenario 1 involved maintaining constant temperature and irradiation conditions, specifically adhering to standard values: the temperature set at 25°C and the irradiation held at 1000W/m².
- Test Scenario 2 was characterized by rapidly changing irradiation levels while maintaining a constant temperature of 25°C.
- Test Scenario 3 entailed rapid fluctuations in temperature while keeping the irradiation constant at 1000W/m².

For a sampling frequency equal to 100Hz Figure 9 shows the variation of the panel power, battery power and the duty ratio D. Figures 10 and 11 show the result of tests.
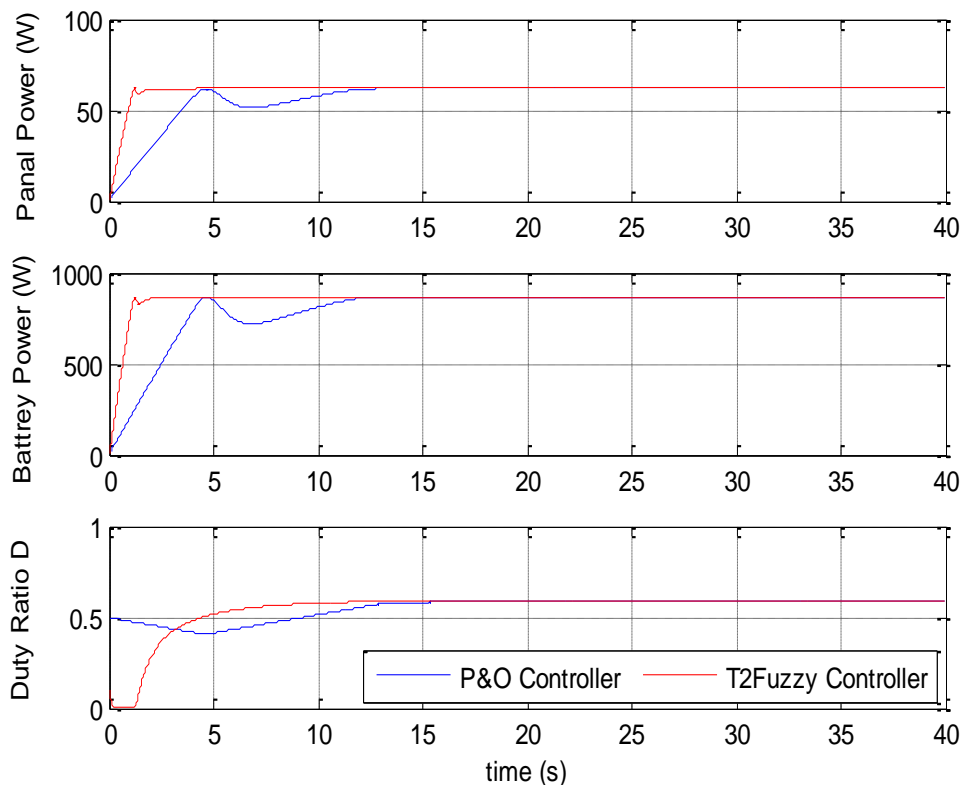
Figure 9. Variation of the panel power, battery power and the duty ratio D, under standard conditions: temperature (25 °C) and solar irradiation (1000 W/m2)

Figure 10 displays the performance of the PV system employing the T2FLC and P&O algorithms during rapid changes in irradiance. Meanwhile, Figure 11 showcases the performance of the PV system utilizing the T2FLC

and P&O algorithms when subjected to rapid temperature fluctuations.
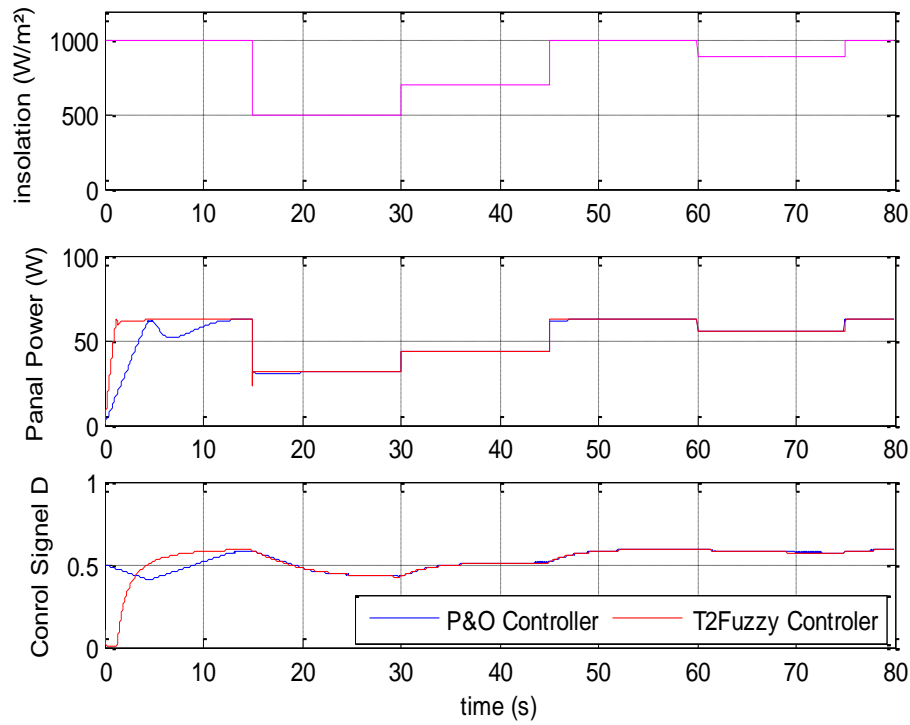
Figure 10. The performance of the PV system using T2FLC and P&O algorithms under fast changing of irradiation
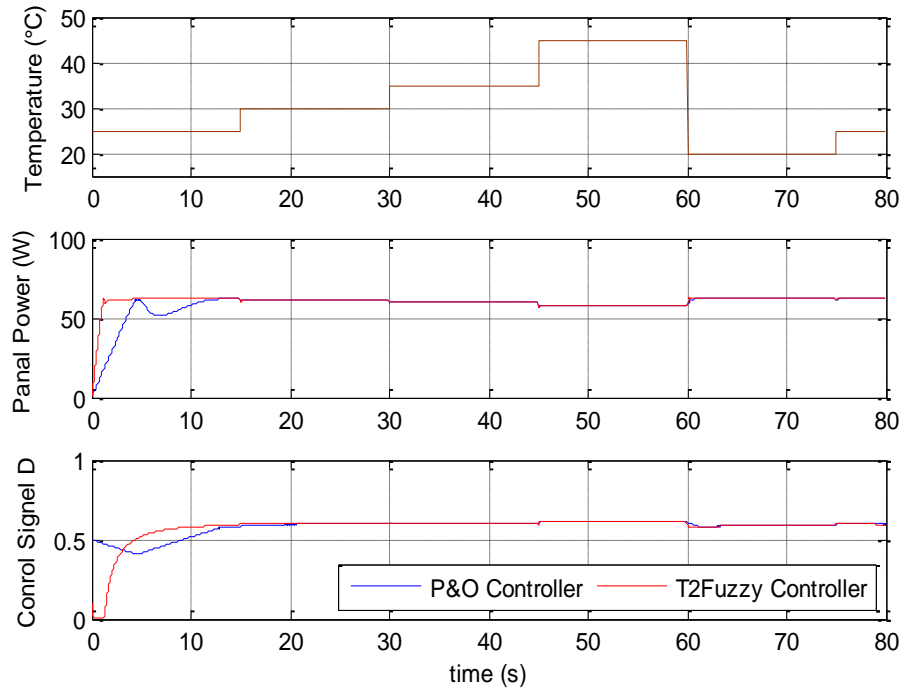
Figure 11. The performance of the PV system using T2FLC and P&O algorithms under fast changing of Temperature

Discussion

The MPPT approach employing T2FLC outperforms the P&O method in various segments of the tracking curve. Notably, the Type-2 fuzzy controller demonstrates superior speed and performance compared to the P&O controller during transitional phases, as illustrated in Figure 9, Figure 10, and Figure 11.

T2FLC offers enhanced accuracy in locating the MPP thanks to its fuzzy sets, minimizing energy losses. It often proves to be faster than conventional techniques like the Perturbation and Observation (P&O) method, which may take longer to converge to the MPP.

T2FLC can adapt more effectively to rapid variations in environmental conditions, such as sudden changes in irradiance or temperature. Other methods, like P&O, may struggle to keep up with these changes.

Fuzzy control systems can provide better stability by maintaining MPP tracking even in the presence of noise or minor fluctuations, ensuring stable energy production.

Conclusion

In summary, our study has presented a robust and intelligent MPPT control strategy, leveraging Type-2 Fuzzy Logic Control (T2FLC), for photovoltaic systems. Through comprehensive simulations, we have demonstrated that our novel MPPT method achieves a faster and more efficient tracking of the Maximum Power Point (MPP) when contrasted with the conventional Perturbation and Observation (P&O) technique.

These results underscore the potential of T2FLC-based MPPT as a valuable enhancement for photovoltaic systems. By harnessing the adaptability and precision of fuzzy logic control, our approach can significantly enhance the overall performance of these systems, particularly in situations involving rapidly changing environmental conditions. This advancement holds promise for optimizing energy generation and promoting the widespread adoption of photovoltaic technology in diverse applications, ultimately contributing to more efficient and sustainable energy solutions.

T2FLC can be more complex to implement compared to some simpler MPPT techniques, which can impact implementation costs and hardware/software requirements.

References

J.H.R. Enslin, D.B. Snyman, "Combined Low-cost, High-Efficient Inverter, Peak Power Tracker and Regulator for PV Applications", IEEE Trans. on Power Electronics, Vol.6, No.1, January 1998.

J.H.R. Enslin, M.S. Wolf, D.B. Snyman, W. Swiegrs, "Integrated Photovoltaic Maximum Power Point Tracking

Converter", IEEE Trans. on Energy Conversion, Vol.44, No.6, Dec. 1997.

S.M. Alghuwainem, "Speed Control of a PV Powered DC Motor Driving a Self-Excited Three-Phase Induction Generator for Maximum Utilization Efficiency", IEEE Trans. on Energy Conversion, Vol.11, No.4, Dec. 1998.

M.A.S. Masoum, H. Dehbonei, E.F. Fuchs, "Theoretical and Experimental Analyses of Photovoltaic Systems with Voltage and Current–Based Maximum Power Point Tracking", Accepted for publication in IEEE Trans. on Energy Conversion.

Kececioglu, O.F.; Gani, A.; Sekkeli, M. Design and Hardware Implementation Based on Hybrid Structure for MPPT of PV System Using an Interval Type-2 TSK Fuzzy Logic Controller. Energies 2020, 13, 1842. https://doi.org/10.3390/en13071842.

M.G. Simoes, N.N. Franceschetti, "Fuzzy Optimization Based Control of a Solar Array", IEE Proc. Electr. Power Appl., Vol.146, No.5, pp.552-558, September 1999.

M. S. Aït Cheikh, C. Larbes, G. F. Tchoketch Kebir and A. Zerguerras. "Maximum power point tracking using a fuzzy logic control scheme". Revue des Energies Renouvelables Vol. 10 N°3 (2007).

Titri, Sabrina, Karim Kaced, and Cherif Larbes. "Maximum power point tracking based on the bio inspired BAT algorithm." Smart Energy Empowerment in Smart and Resilient Cities: Renewable Energy for Smart and Sustainable Cities. Springer International Publishing, 2020..

Ould cherchali, N., Boucherit, M. S., Barazane, L., et al. Study of two MPPTs for photovoltaic systems using controllers based in fuzzy logic and sliding mode. International Journal of Electrical and Computer Engineering, 2015, vol. 9, no 5, p. 1253-1258.

N. Ould Cherchali, M. R. Skender, B. Bentchikou, A. Tlemçani and A. Morsli, "Parametric identification of a photovoltaic panel by the Firefly algorithm," 2022 13th International Renewable Energy Congress (IREC), Hammamet, Tunisia, 2022, pp. 1-5, doi: 10.1109/IREC56325.2022.10001922..

N. Ould Cherchali, A. Morsli, M. S. Boucherit, L. Barazane and A. Tlemçani, "Comparison of two maximum power point trackers for photovoltaic systems using robust controllers," 3rd International Symposium on Environmental Friendly Energies and Applications (EFEA), Paris, France, 2014, pp. 1-5, doi: 10.1109/EFEA.2014.7059989.

N. N. Karnik, J. M. Mendel, and Q. Liang, "Type-2 Fuzzy logic systems", IEEE Trans. Fuzzy Syst., Vol. 7, No. 6, 1999, pp. 643-658.

VERMA, Pallavi, GARG, Rachana, et MAHAJAN, Priya. Asymmetrical interval type-2 fuzzy logic control based MPPT tuning for PV system under partial shading condition. ISA transactions, 2020, vol. 100, p. 251-263.

Q. Liang, J. M. Mendel, "Interval Type-2 Fuzzy logic systems: Theory and design", IEEE Trans. Fuzzy Syst., Vol. 8, No. 5, 2000, pp. 535-550.

Enhanced Speed Estimation of Dual-Star Induction Motors Using a Reduced-Order Observer

Mohamed Redha Skender

Medea University, Algeria, https://orcid.org/0000-0002-6572-8102

Noureddine Ould Cherchali

Medea University, Algeria

Ahmed Medjber

Medea University, Algeria

Amel Abbadi

Medea University, Algeria, https://orcid.org/0000-0002-2039-062X

Fethia Hamidia

Medea University, Algeria, https://orcid.org/0000-0002-2212-0922

Tlemcani Abdelhalim

Medea University, Algeria, https://orcid.org/0000-0002-4385-671X

Abstract: This paper introduces a novel reduced-order observer designed for the precise and efficient estimation of the speed of dual-star induction motors. Dual-star induction motors, known for their enhanced reliability and performance in industrial applications, pose specific challenges in control and estimation due to their complex dynamics. The proposed observer leverages the unique electrical and mechanical characteristics of these motors to minimize the computational complexity typically associated with traditional estimation methods. By effectively reducing the order of the system, the observer simplifies the control algorithm, making it more streamlined and responsive. This reduction is achieved without compromising the accuracy of the speed estimation, ensuring that the motor operates optimally under various conditions. The observer's performance is rigorously validated through comprehensive simulations, which demonstrate its robustness and precision across a wide range of operating scenarios. The results from these validations indicate that the reduced-order observer can significantly improve the dynamic performance of motor control systems. It provides a more efficient and reliable solution compared to conventional methods, particularly in scenarios where computational resources are limited. This approach not only enhances the overall performance of the motor but also contributes to the development of more advanced and dependable industrial applications.

Keywords: reduced-order observer, dual-star induction motor, speed estimation, robustness, efficiency

Introduction

The Double-Star Induction Machine (DSIM) is an advanced motor configuration commonly used in applications that require high performance, such as electric vehicles, aerospace technology, and industrial drives. This machine features two sets of stator windings, which are electrically shifted by a specific angle, usually 30° or 60°. This design helps improve the distribution of electromagnetic forces, reduces torque ripple, and enhances fault tolerance.

Controlling a DSIM is more challenging than managing a standard single-star induction machine because of the additional complexity introduced by the dual stator windings. Conventional control methods like scalar control (V/f control) are often insufficient for fully harnessing the potential of a dual-star system, particularly when precise control over torque and magnetic flux is critical. To overcome these challenges, more sophisticated control strategies, such as vector control (Field-Oriented Control, FOC) and direct torque control (DTC), are employed to optimize the machine's performance.

Vector control is particularly advantageous for DSIM because it enables separate control of torque and flux by transforming the three-phase stator currents into a two-axis reference frame (d-q frame). However, the dual-star configuration adds layers of complexity to the control process, requiring careful coordination between the two stator windings to maintain synchronization and prevent issues such as circulating currents and unbalanced magnetic forces.

The electromagnetic model of a double-star induction machine consists of a system of ten differential equations with coefficients that vary periodically over time. Solving this system directly is challenging. However, by applying the PARK transformation—a suitable change of variables—this complexity can be bypassed, resulting in a more manageable and usable.

Lan et al. (Lan et al., 2018) proposed a novel stator current observer designed to ensure fault-tolerant control of stator current sensors in Doubly-Fed Induction Generators (DFIG). Skender, et al. (Skender et al., 2017) presented a novel observer algorithm for estimating the voltages across capacitors in multi-cells converters. Oumar et al. (Oumar, Chakib, & Cherkaoui, 2020) addressed the challenge of current sensor faults in Double Star Induction Machines (DSIM). Boukhalfa et al. (Boukhalfa et al., 2023) introduced a novel PID controller for DSIMs, employing a Grey Wolf Optimization (GWO) strategy to optimize the controller's parameters. Lazreg (Lazreg & Bentaallah, 2018) proposed a sensorless control approach using a fuzzy sliding-mode control

technique for DSIMs. Oumar et al. (Oumar, Chakib, Labbadi, et al., 2020) developed a robust nonlinear speed controller for DSIMs that remains effective even in the presence of sensor faults. Chaabane et al. (Chaabane et al., 2021) explored a speed sensorless vector control strategy for DSIMs, employing a sliding mode observer based on Lyapunov stability theory.

In this paper, we explore the use of a reduced-order Luenberger observer for speed estimation in Double-Star Induction Machines (DSIM). The method offers a sensorless approach, eliminating the need for mechanical sensors, which reduces both the complexity and cost of the system. By focusing on essential state variables like stator currents and rotor flux, the observer ensures robust and accurate speed estimation, even under varying operating conditions. This approach is particularly advantageous for applications requiring precise control and enhanced system reliability.

DSIM Mathematic Model

The Double-Star Induction Machine (DSIM) features a stator with two identical three-phase windings that are electrically displaced by an angle α (in this model, α = γ = 30˚). The rotor can be either wound or squirrel-cage. For simplification, the rotor circuits are considered equivalent to a three-phase winding in short-circuit (Saad et al., 2019).

(Figure 1) illustrates the arrangement of the winding axes for the nine phases of the machine, including six phases for the stator and three phases for the rotor.
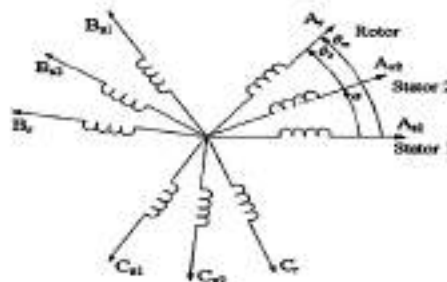
Figure 1. Schematic Representation of the DSIM Windings

The rotating reference frame is used for the modeling and control of the Double-Star Induction Machine (DSIM). In this reference frame, the model of the DSIM is simplified and can be expressed as (Zerzeri & Khedher, 2021).

Voltages equations

For star 1:

$$v_{ds1} = R_s i_{ds1} + \frac{d}{dt}\psi_{ds1} - \omega_s\psi_{qs1}$$

(1)

$$v_{qs1} = R_s i_{qs1} + \frac{d}{dt}\psi_{qs1} + \omega_s\psi_{ds1}$$

For star 2:

$$v_{ds2} = R_s i_{ds2} + \frac{d}{dt}\psi_{ds2} - \omega_s\psi_{qs2}$$

(2)

$$v_{qs2} = R_s i_{qs2} + \frac{d}{dt}\psi_{qs2} + \omega_s\psi_{ds2}$$

For the rotor:

$$v_{dr} = R_r i_{dr} + \frac{d}{dt}\psi_{dr} - (\omega_s - \omega_r)\psi_{qr} = 0$$

(3)

$$v_{qr} = R_r i_{qr} + \frac{d}{dt}\psi_{qr} + (\omega_s - \omega_r)\psi_{dr} = 0$$

Mechanical equation

$$C_{em} = P\big(\psi_{ds1}i_{qs1} - \psi_{qs1}i_{ds1} + \psi_{ds2}i_{qs2} - \psi_{qs2}i_{ds2}\big)$$ (4)

Flux equations

$$\begin{cases}
\psi_{ds1} = L_{s1}i_{ds1} + L_m(i_{ds1} + i_{ds2} + i_{dr}) \\
\psi_{qs1} = L_{s1}i_{qs1} + L_m\big(i_{qs1} + i_{qs2} + i_{qr}\big) \\
\psi_{ds2} = L_{s2}i_{ds2} + L_m(i_{ds1} + i_{ds2} + i_{dr}) \\
\psi_{qs2} = L_{s2}i_{qs2} + L_m\big(i_{qs1} + i_{qs2} + i_{qr}\big) \\
\psi_{dr} = L_r i_{dr} + L_m(i_{ds1} + i_{ds2} + i_{dr}) \\
\psi_{qr} = L_r i_{qr} + L_m\big(i_{qs1} + i_{qs2} + i_{qr}\big)
\end{cases}$$ (5)

Vector Control of the Double-Star Induction Machine

Vector control enables the separation of current components into two distinct axes: one for flux (d-axis) and one for torque (q-axis). This separation allows for independent control of magnetic flux and torque, providing superior regulation precision compared to other methods. The main challenge in implementing vector control for the double-star induction machine lies in determining the position and magnitude of the rotor flux, as these parameters are not easily measurable. Accurate knowledge of these parameters is crucial for effective dynamic control of the machine (Bodson, 2020). To address this, the Indirect Field-Oriented Control (IFOC) method is selected.

The equations (6) for the stator voltages in the rotating reference frame are described in the system of equations for stator voltages (Kumar et al., 2019).

$$v_{ds1}^* = R_{s1}i_{ds1} + L_{s1}\frac{di_{ds1}}{dt} - w\left(L_{s1}i_{qs1} + T_r\psi_r^*\omega_{gl}^*\right)$$

$$v_{qs1}^* = R_{s1}i_{qs1} + L_{s1}\frac{di_{qs1}}{dt} + w_s^*(L_{s1}i_{ds1} + \psi_r^*)$$

$$v_{ds2}^* = R_{s2}i_{ds2} + L_{s2}\frac{di_{ds2}}{dt} - w\left(L_{s2}i_{qs2} + T_r\psi_r^*\omega_{gl}^*\right)$$ (6)

$$v_{qs2}^* = R_{s2}i_{qs2} + L_{s2}\frac{di_{qs2}}{dt} + w_s^*(L_{s2}i_{ds2} + \psi_r^*)$$

Où : $T_r = \frac{L_r}{R_r}$ Constante de temps rotorique.

By applying this principle ($\psi_{qr} = 0$ and $\psi_{dr} = \psi_r$) to equations (3) and (4), we will have the expression of the electromagnetic torque and slip speed:

$$w_{gl} = \frac{R_r L_m}{(L_m + L_r)}\frac{\left(i_{qs1} + i_{qs2}\right)}{\psi_r}$$ (7)

$$C_{em} = p\frac{L_m}{(L_m + L_r)}\psi_r\left(i_{qs1} + i_{qs2}\right)$$ (8)

$$C_{em} = p\frac{L_m}{(L_m + L_r)}\psi_r\left(i_{qs1} + i_{qs2}\right)$$ (9)

The system of electrical equations (7) demonstrates that the voltages $\left(v_{ds1}^*, v_{qs1}^*, v_{ds2}^*, v_{qs2}^*\right)$ simultaneously affect the direct and quadrature current components $\left(i_{ds1}, i_{qs1}, i_{ds2}, i_{qs2}\right)$, thus impacting both flux and torque. Consequently, it is essential to implement a decoupling strategy. This involves defining new variables $v_{ds1r}, v_{qs1r}, v_{ds2r}$ et v_{qs2r} that specifically influence the corresponding current components $i_{ds1}, i_{qs1}, i_{ds2}$ et i_{qs2}, separately, as detailed in (Zerzeri et al., 2019).

$$v_{ds1r} = R_{s1}i_{ds1} + L_{s1}\frac{di_{ds1}}{dt}$$

$$v_{qs1r} = R_{s1}i_{qs1} + L_{s1}\frac{di_{qs1}}{dt}$$

$$v_{ds2r} = R_{s2}i_{ds2} + L_{s2}\frac{di_{ds2}}{dt}$$ (10)

$$v_{qs2r} = R_{s2}i_{qs2} + L_{s2}\frac{di_{qs2}}{dt}$$

To compensate for the error introduced during the decoupling process, the reference stator voltages for constant flux are expressed as follows:

$$v_{ds1}^* = v_{ds1r} - v_{ds1c}$$
$$v_{qs1}^* = v_{qs1r} + v_{qs1c}$$
$$v_{ds2}^* = v_{ds2r} - v_{ds2c} \tag{11}$$
$$v_{qs2}^* = v_{qs2r} + v_{qs2c}$$

Or

$$v_{ds1c} = \omega_s^*\left(L_{s1}i_{qs1} + T_r\psi_r^*\omega_{gl}^*\right)$$
$$v_{qs1c} = \omega_s^*(L_{s1}i_{ds1} + \psi_r^*)$$
$$v_{ds2c} = \omega_s^*\left(L_{s2}i_{qs2} + T_r\psi_r^*\omega_{gl}^*\right) \tag{12}$$
$$v_{qs2c} = \omega_s^*(L_{s2}i_{ds2} + \psi_r^*)$$

The control scheme for the Double-Star Induction Machine (DSIM) is illustrated in the following (figure 2):
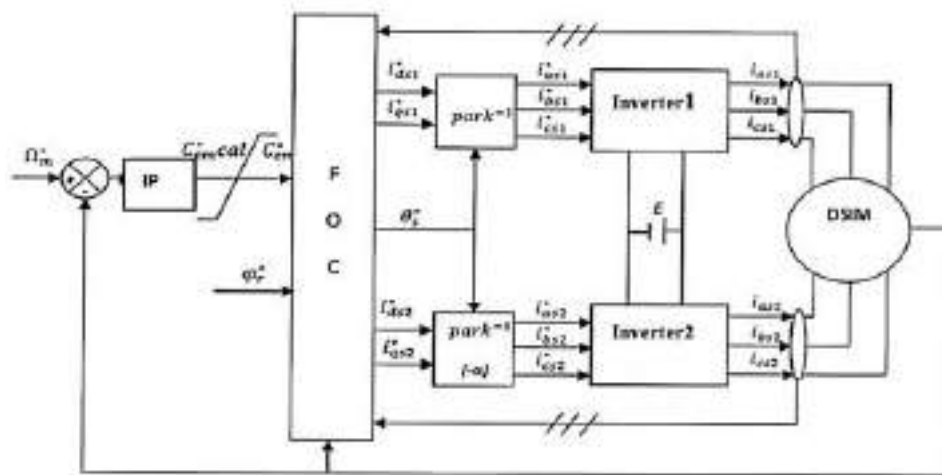
Figure 2. Indirect Vector Control of the DSIM.

Simulation Results

The simulation results illustrate the behavior of the Double-Star Induction Machine (DSIM) under speed regulation using the indirect control method. The scenarios include the application of a resistive load Cr=15N.m at t = 1 while maintaining a reference speed of $\omega_{ref} = 314\ rad/s$.

- First Test: A load of Cr=15N.m is applied starting at t = 2, with the reference speed set to 314 rad/s.

- Second Test: The direction of rotation is reversed, changing the speed from 314rad/s to -314rad/s during the time interval t= [2s, 6s] while the machine operates under no load.

- Third Test: At t = 8s, the machine is restarted, beginning with a low speed of 10rad/s.
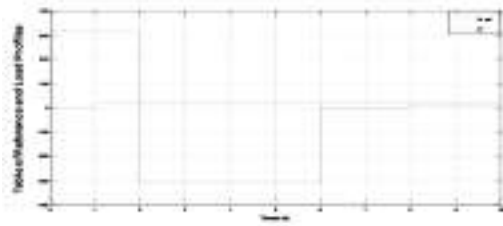
Figure 3. Table of Reference and Load Profiles.
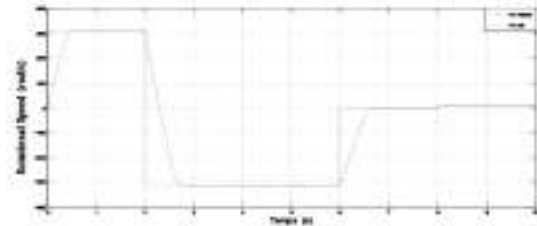
Figure 4. Rotational Speed (rad/s)
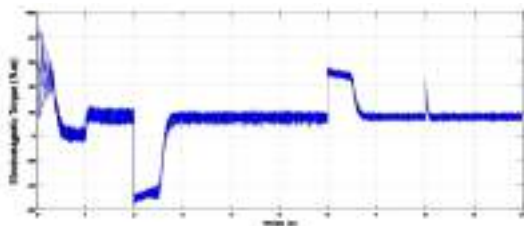
Figure 5. Electromagnetic Torque (N.m)
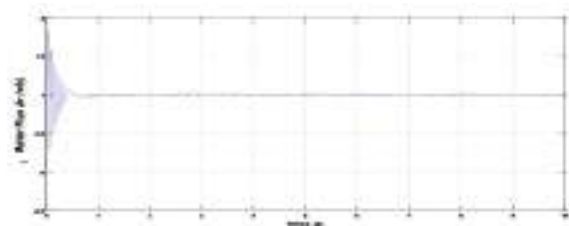
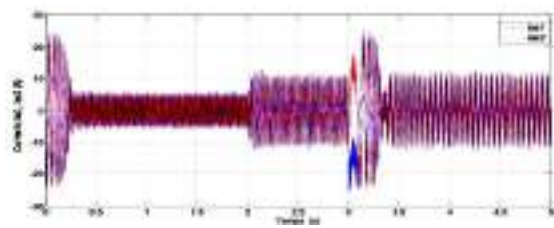Figure 6. Rotor Flux dr (wb)
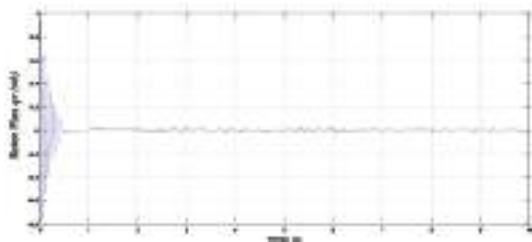
Figure 7. Rotor Flux qr (wb)
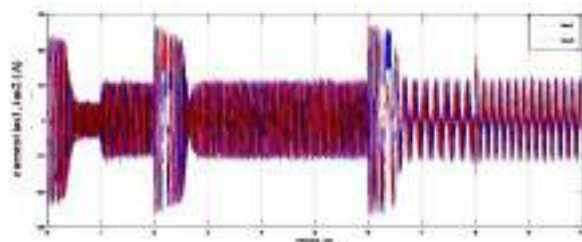
Figure 8. current ias1, ias2 (A)

Discussion

(Figure 3) shows the performance characteristics of the Double-Star Induction Machine (DSIM) without speed regulation using the indirect control method.

- Startup and No-Load Operation: At startup, the speed reaches the reference value of 314 rad/s within approximately 0.79 seconds. When a load torque of 15 N.m is applied at t = 1s, there is a noticeable drop in speed. However, due to the action of the inverter and PI controller, the speed quickly returns to the reference value.

- Reversing Rotation: At t = 2s, the direction of rotation is reversed to -314 rad/s, taking about 0.93 seconds for the speed to stabilize. At t = 6s, the speed reaches zero for approximately 0.83 seconds.
- Restarting the Machine: At t = 8s, the machine is restarted with a low speed of 10 rad/s under load, and this speed is achieved within 0.054 seconds.

-Electromagnetic Torque: (Figure 5) shows that the electromagnetic torque reaches a peak of 90.74 N.m at startup and then oscillates around zero. The torque exhibits spikes when the load is applied.

- Stator Currents: The stator currents i_as1 and i_as2 (Figure 8) initially have sinusoidal waveforms with the same amplitude. At startup, the currents peak at more than seven times their stabilized value, reaching 23.73 A before stabilizing at 5.26 A. When the load is applied, the amplitude increases to i_as1} = i_as2 = 11.95 A, with noticeable spikes during the reversal of the rotation direction.

- Rotor Flux Components: The rotor flux ψ_{qr} peaks at 0.93 Wb (Figure 6) before approaching nearly zero, while ψ_{dr} peaks at 1.84 Wb and then stabilizes at its setpoint of 1 Wb(Figure 7).

Speed Estimation Using a Reduced-Order Luenberger Observer

When using an estimator, controlling the error dynamics is challenging because it is influenced by the physical system. To improve accuracy, it is preferable for the estimation process to have a much faster dynamic response than the system itself, which is why observers are advantageous.

For the electrical equations, which are linear in the state variables but depend on the mechanical speed Ωr, a Luenberger observer can be constructed as follows :

$$\frac{d\hat{x}}{dt} A(\widehat{\Omega})\hat{x} + Bu + G(y - C\hat{x}) \tag{13}$$

The challenge with this type of observer lies in selecting the gain G, which generally depends on the mechanical speed and affects the rate at which estimation errors decrease. The mathematical model of the Double-Star Induction Machine (DSIM) presents a nonlinear, time-varying system. To address this nonlinearity, a linear observer is employed, with the mechanical speed Ωr included as an additional variable. This approach results in a reduced-order Luenberger observer.

The system of equations can be rewritten as two subsystems as follows:

$$\begin{cases} \dfrac{di_{sd1}}{dt} = \dfrac{1}{L_{s1}} v_{sd1} - \dfrac{r_{s1}}{L_{s1}} i_{sd1} - w_s \left(\dfrac{L_r}{rr} \phi_r w_{gl} + L_{s1} i_{sq1} \right) \\[2mm] \dfrac{di_{sd2}}{dt} = \dfrac{1}{L_{s1}} v_{sd2} - \dfrac{r_{s2}}{L_{s2}} i_{sd2} - w_s \left(\dfrac{L_r}{rr} \phi_r w_{gl} + L_{s2} i_{sq} \right) \\[2mm] \dfrac{d\phi_r}{dt} = -\dfrac{1}{T_r} \phi_r + \dfrac{L_m}{T_r} (i_{ds1} + i_{ds2}) \end{cases} \tag{14}$$

$$\begin{cases} \dfrac{di_{qs1}}{dt} = \dfrac{1}{L_{s1}} v_{qs1} - \dfrac{r_{s1}}{L_{s1}} i_{ds1} - w_s(\phi_r + L_{s1} i_{ds1}) \\[2mm] \dfrac{di_{qs2}}{dt} = \dfrac{1}{L_{s1}} v_{qs2} - \dfrac{r_{s2}}{L_{s2}} i_{qs2} - w_s(\phi_r + L_{s2} i_{qs2}) \\[2mm] \dfrac{d\Omega_r}{dt} = \dfrac{P}{J} \dfrac{L_m}{L_m + L_r} \phi_r(i_{qs1} + i_{qs2}) - \dfrac{K_f}{J} \Omega_r - \dfrac{1}{J} C_r \end{cases} \tag{15}$$

To estimate the speed, only the subsystem (14) is used (Kiani-Nezhad et al., 2005). It is evident that estimating

the speed from the model described by subsystem (15) requires the estimation of the load torque and rotor flux.

If one also wishes to estimate the constant resistive torque Cr , it is assumed that this torque changes slowly, allowing the use of the following model for the load torque:

$$\frac{dC_r}{dt} = 0 \tag{16}$$

This assumption holds true in most applications(Kiani-Nezhad et al., 2005). By adding equation (16) to the system (15), the complete estimation model is obtained:

$$\begin{cases}
\dfrac{di_{qs1}}{dt} = \dfrac{1}{L_{s1}} v_{qs1} - \dfrac{r_{s1}}{L_{s1}} i_{ds1} - w_s(\phi_r + L_{s1} i_{ds1}) \\[2mm]
\dfrac{di_{qs2}}{dt} = \dfrac{1}{L_{s1}} v_{qs2} - \dfrac{r_{s2}}{L_{s2}} i_{qs2} - w_s(\phi_r + L_{s2} i_{qs2}) \\[2mm]
\dfrac{d\Omega_r}{dt} = \dfrac{P}{J} \dfrac{L_m}{L_m + L_r} \phi_r(i_{qs1} + i_{qs2}) - \dfrac{K_f}{J} \Omega_r - \dfrac{1}{J} C_r
\end{cases} \tag{17}$$

Based on the system of equations (17), and assuming that the rotor flux ϕ_r remains constant, we can construct our reduced-order linear observer as follows:

$$\begin{cases}
\dfrac{d\hat{\imath}_{qs1}}{dt} = \dfrac{1}{L_{s1}} v_{qs1} - \dfrac{R_{s1}}{L_{s1}} \hat{\imath}_{qs1} - w_s\left(i_{ds1} + \dfrac{1}{L_{s1}} \hat{\phi}_r\right) + G_1 \tilde{\imath}_{qs} \\[2mm]
\dfrac{d\hat{\imath}_{qs2}}{dt} = \dfrac{1}{L_{s2}} v_{qs2} - \dfrac{R_{s2}}{L_{s2}} \hat{\imath}_{qs2} - w_s\left(i_{ds2} + \dfrac{1}{L_{s2}} \hat{\phi}_r\right) + G_1 \tilde{\imath}_{qs} \\[2mm]
\dfrac{d\hat{\Omega}_m}{dt} = \dfrac{P}{J} \dfrac{L_m}{L_m + L_r} \hat{\phi}_r(i_{qs1} + i_{qs2}) - \dfrac{P}{J} \hat{C}_r - \dfrac{K_f}{J} \hat{\Omega}_m + G_2 \tilde{\imath}_{qs} \\[2mm]
\dfrac{d}{dt} \hat{C}_r = G_3 \tilde{\imath}_{qs} \\[2mm]
\dfrac{d\hat{\phi}_r}{dt} = \dfrac{L_m}{T_r} (i_{ds1} + i_{ds2}) - \dfrac{1}{T_r} \hat{\phi}_r
\end{cases} \tag{18}$$

Where : $\tilde{\imath}_{qs} = (i_{qs1} + i_{qs2}) - (\hat{\imath}_{qs1} + \hat{\imath}_{qs2})$, G1, G2 and G3 are the gains of the reduced-order Luenberger observer.

With a specific selection of G1, G2 and G3 which depend on the mechanical speed, stability is ensured by choosing observer gains that place the poles in the left half-plane, assuming constant speed. To achieve optimal performance, the observer gains are selected to ensure a faster response than that of the system. However, choosing gains that are too fast can lead to increased sensitivity to parameter variations.

The following functional diagram(figure 9) represents the sensorless vector control of a Double-Star Induction Machine (DSIM) equipped with a reduced-order Luenberger observer:
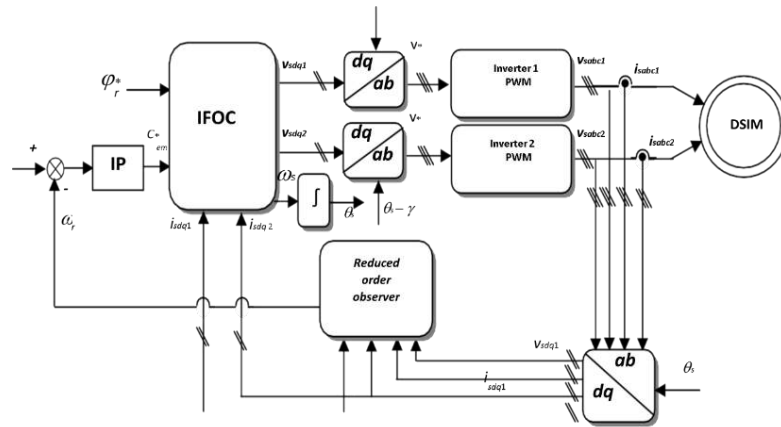
Figure 9. Indirect Vector Control Without Speed Sensor of a DSIM Equipped with a Reduced-Order Linear Observer

Results

Figure 10 illustrates the speed profile and load torque used in the simulation study. It can be observed that the speed reaches its target value of 157 rad/s during no-load startup. At t=2s, a load torque of 15 N.m is introduced, followed by a reversal in the direction of rotation to −157 rad/s from t=3 s to t=6 s. Finally, at t=7s, the machine resumes the reference speed of 157 rad/s.
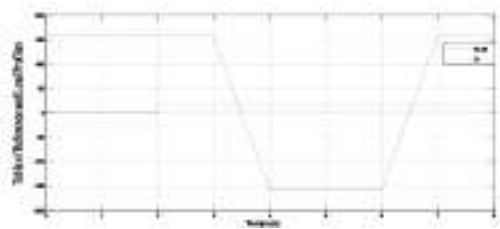
Figure 10. Table of Reference and Load Profiles.
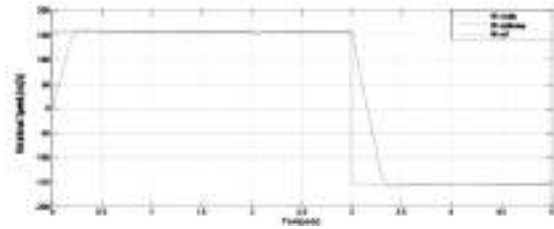
Figure 11. Rotational Speed (rad/s)
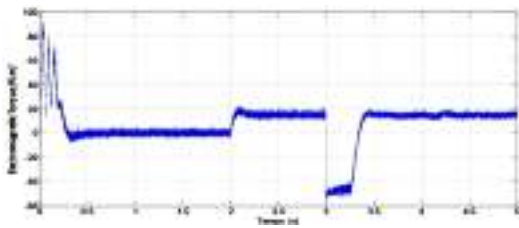
Figure 12. Electromagnetic Torque (N.m)

Figure 13. Currents Ias1, Ias2 (A)
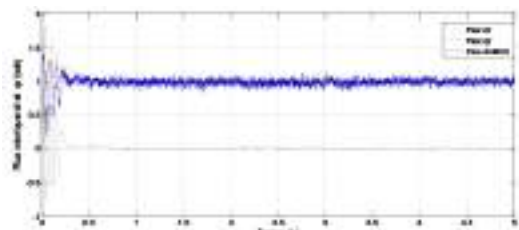
Figure 14. Rotor Flux dr et qr (Wb)
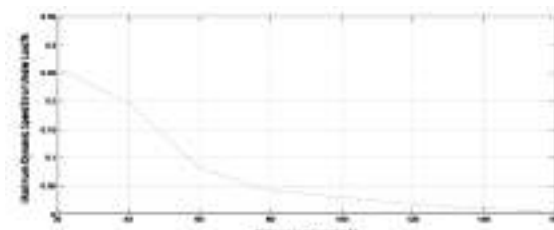
Figure 15. Maximum Dynamic Speed Error Under Load as a Function of Reference Speed

To highlight the performance and robustness of speed and flux estimation for the Double-Star Induction Machine (DSIM) using a reduced-order Luenberger observer, we conducted a simulation study that provided the following results. For each speed step, a load disturbance (Cr = 15 N.m) was applied at t=2s, followed by a reversal of the rotation direction at t=3s. The observer gains used in all simulations were selected after multiple adjustment tests: (G1 = 180, G2 = -6, G3 = 0).

The results include the corresponding torque, stator current, actual and estimated speed, and actual and estimated flux for a sensorless DSIM with a reduced-order Luenberger observer, operating at a nominal speed setpoint of ±157 rad/s:

Discussion

(Figures 11,12,13 and 14) depict the electromagnetic torque, stator currents, actual and estimated speed, and actual and estimated flux for a sensorless speed control system using a reduced-order Luenberger observer applied to a Double-Star Induction Machine (DSIM) with a speed setpoint of 157 rad/s. The results indicate an excellent match between the estimated and actual speed.

(Figure 15) illustrates the maximum dynamic speed error for various reference speed values. It is observed that the maximum dynamic error decreases as the reference speed increases. The maximum dynamic error does not exceed 26% at low speeds (20 rad/s).

The observer demonstrates good speed tracking performance, with a minimal dynamic error and an almost negligible static error.

Conclusion

The simulation results obtained in this study allow us to conclude that the sensorless speed control of the Double-Star Induction Machine (DSIM) equipped with a reduced-order Luenberger observer is both fast and robust, even in the face of load disturbances and changes in the speed setpoint. Additionally, this control method is characterized by its simplicity in design and robustness, making it particularly advantageous by eliminating the need for a mechanical speed or position sensor, which is both costly and prone to failure.

References

Bodson, M. (2020). Speed Control for Doubly Fed Induction Motors with and without Current Feedback. *IEEE Transactions on Control Systems Technology*, *28*(3), 898–907. https://doi.org/10.1109/TCST.2019.2898372

Boukhalfa, G., Chikhi, A., Belkacem, S., Mazouz, F., & Boubir, M. (2023). PID controller using new GWO

strategy to drive dual star induction motor. *2023 International Conference on Electrical Engineering and Advanced Technology (ICEEAT)*, *1*, 1–7. https://api.semanticscholar.org/CorpusID:267660798

Chaabane, H., Eddine, K. D., Salim, C., & Djamel, H. (2021). Speed Sensorless Vector Control of Double Star Induction Machine Using Sliding Mode Observer Based Lyapunov Stability. *Modelling, Measurement and Control A*. https://api.semanticscholar.org/CorpusID:247123779

Kiani-Nezhad, R., Nahid-Mobarakeh, B., Betin, F., & Capolino, G.-A. (2005). Sensorless Field-Oriented Control for Six-Phase Induction Machines. *IAS'05*, 999–1006.

Kumar, R., Das, S., & Bhaumik, A. (2019). Speed sensorless model predictive current control of doubly-fed induction machine drive using model reference adaptive system. *ISA Transactions*, *86*, 215–226. https://doi.org/10.1016/j.isatra.2018.10.025

Lan, Z., Li, L., Deng, C., Zhang, Y., Yu, W., & Wong, P. (2018). A Novel Stator Current Observer for Fault Tolerant Control of Stator Current Sensor in DFIG. *2018 IEEE Energy Conversion Congress and Exposition (ECCE)*, 790–797. https://api.semanticscholar.org/CorpusID:54456330

Lazreg, M. H., & Bentaallah, A. (2018). *Sensorless fuzzy sliding-mode control of the double-star induction motor using a sliding-mode observer*. https://api.semanticscholar.org/CorpusID:202709731

Oumar, A., Chakib, R., & Cherkaoui, M. (2020). Current Sensor Fault-Tolerant Control of DSIM Controlled by ADRC. *Mathematical Problems in Engineering*. https://api.semanticscholar.org/CorpusID:221712782

Oumar, A., Chakib, R., Labbadi, M., & Cherkaoui, M. (2020). Robust Nonlinear Controller of the Speed for Double Star Induction Machine in the Presence of a Sensor Fault. *International Journal of Intelligent Engineering and Systems*, *13*, 124–133. https://api.semanticscholar.org/CorpusID:218964796

Saad, K., Abdellah, K., Ahmed, H., & Iqbal, A. (2019). Investigation on SVM-Backstepping sensorless control of five-phase open-end winding induction motor based on model reference adaptive system and parameter estimation. *Engineering Science and Technology, an International Journal*, *22*(4), 1013–1026. https://doi.org/10.1016/J.JESTCH.2019.02.008

Skender, M. R., Tlemçani, A., & Nouri, H. (2017). A novel observer algorithm of voltages across capacitors based on the higher sliding mode control: Application to multi-cells converter. *International Journal of Modelling, Identification and Control*, *27*(2), 136–145. https://doi.org/10.1504/IJMIC.2017.082944

Zerzeri, M., Jallali, F., & Khedher, A. (2019). A Robust Nonlinear Control Based on SMC Approach for Doubly-Fed Induction Motor Drives Used in Electric Vehicles. *2019 International Conference on Signal, Control and Communication, SCC 2019*, 138–144. https://doi.org/10.1109/SCC47175.2019.9116183

Zerzeri, M., & Khedher, A. (2021). Optimal speed–torque control of doubly-fed induction motors: Analytical and graphical analysis. *Computers & Electrical Engineering*, *93*, 107258. https://doi.org/10.1016/J.COMPELECENG.2021.107258

Hybrid Methods and Technology Interventions for Transforming Post-Covid Teaching and Learning

Hussain T.

Military Technological College Muscat Oman

Khan A. A

Military Technological College Muscat Oman

Pillai J.R

Military Technological College Muscat Oman

Masud S.

Lahore University of Management Sciences Pakistan

Tashtoush T.H.

Texas A&M International University USA

Hussain S.

Texas A&M International University USA

Abstract: The use of educational technology has surpassed its effective application, leading to a digital divide in higher education. The expected increase in blended/hybrid learning after COVID-19, while holding promise for enhancement of learning, presents challenges because of its complex and multidimensional nature. During the pandemic, the world has lived decades in years. This fast-forwarding of living and experiences in other spheres of life has forced the learning of new technologies at a pace much faster than most of us could cope with. Lack of prior exposure to technology-based methods caused unexpected outcomes, preventing effective engagement in hybrid learning. However, it is believed that hybrid learning, supported by advanced technologies and innovative learning and teaching methodologies is the way forward. This paper delves into the transformative potential of hybrid teaching and learning, analyzing models at MTC (Oman), LUMS (Pakistan), and TAMIU (USA). Each institution's unique approaches provide valuable lessons for effective hybrid learning implementation.

Keywords: Hybrid learning, digital learning, higher education, instructional design, case studies, technological interventions

Citation: Hussain T., Khan A. A., Pillai J.R., Masud S., Tashtoush T.H. & Hussain S. (2024). Hybrid Methods and Technology Interventions for Transforming Post-Covid Teaching and Learning. In A. A. Khan, M.

Demirbilek, & M. L. Ciddi (Eds.), *Proceedings of ICSEST 2024-- International Conference on Studies in Engineering, Science, and Technology* (pp. 298-305), Istanbul, Turkiye. ISTES.

Introduction

The COVID-19 pandemic forced higher education institutions to undergo a major shift, compelling them to rapidly adopt online education initially and hybrid learning models later. This sudden and unprecedented transformation disrupted traditional educational practices worldwide, fundamentally shaking the bricks-and-mortar foundation of conventional learning (Dhawan, 2020). The impact was particularly intense in engineering and science programs, where hands-on laboratory work, practical demonstrations, and interactive, in-person teaching are crucial components of the curriculum (Bao, 2020). Faced with strict lockdowns and social distancing measures, institutions were challenged to maintain academic standards while ensuring the safety of students and faculty.

Figure 1 illustrates the impact of the sudden shift not only in academia but it also highlighting how the abrupt transition to online and hybrid learning affected various component of educational practices such as digital divide, social divide and economic divide. It visually represents the challenges faced by both institutions and individuals, such as the need for rapid technological adaptation, disruptions and how widening digital divide among students. Additionally, it demonstrates the positive outcomes, including accelerated innovation and the increased adoption of digital tools in teaching and learning. The shift identified gaps in technology infrastructure, faculty training, and student access to resources, leading to inconsistent and, in some cases, suboptimal educational outcomes (Hodges et al., 2020). However, this crisis also became an opportunity for innovation, driving educators to explore new teaching methodologies and rapidly adopt advanced technological tools, often previously overlooked except on a need basis (Bozkurt et al., 2020). This paper contributes to the existing literature by examining the experiences of three diverse institutions—Military Technological College (MTC) in Oman, Lahore University of Management Sciences (LUMS) in Pakistan, and Texas A&M International University (TAMIU) in the USA. Each of these institutions had to develop unique strategies to navigate the challenges posed by the pandemic, and their efforts provide valuable lessons for the future of education (Ali, 2020).

By focusing on a variety of case studies, this research identifies the specific approaches used by these institutions to integrate hybrid learning models, highlights the technological interventions they implemented, and evaluates the impact on student engagement and learning outcomes. The analysis presented in this paper reveals how MTC adopted a hybrid approach that blended virtual simulations with in-person sessions to ensure practical training for engineering students, while adhering to strict safety protocols (Al Siyabi, 2024). All institutions invested significantly in upgrading their Learning Management Systems (LMS) and integrated platforms like Teams or Zoom to deliver secure, interactive online education (Crawford et al., 2020). Meanwhile, MTC and TAMIU took measures to address the digital divide among their students by providing essential hardware; however, TAMIU went a step further by ensuring reliable internet access, making remote

learning more inclusive and effective (Murphy, 2020). Despite the successes, each institution also faced challenges, such as issues with academic integrity in online assessments, technical difficulties, and the challenge of keeping students engaged without the traditional classroom environment (Alturki, 2021).
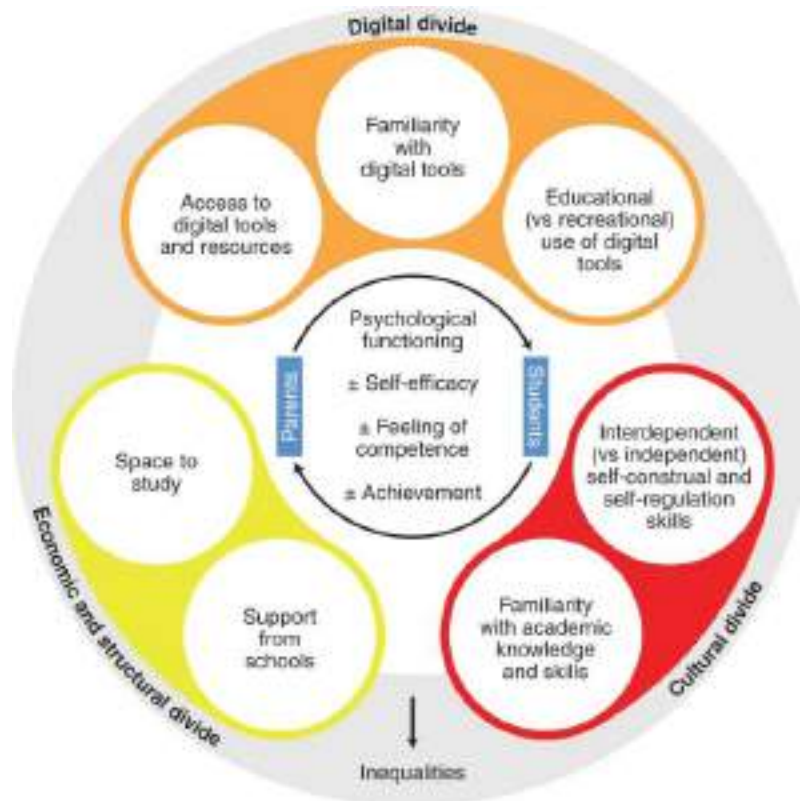
Figure 7. The impact of sudden shift to the technology-based learning

By analysing the experiences of MTC, LUMS, and TAMIU, this study explores the challenges and opportunities presented by hybrid learning, offering valuable insights for future educational practices. It investigates the role of advanced digital tools and evaluates their effectiveness in maintaining the quality of education during a global crisis (Selwyn, 2020). Furthermore, this research outlines the long-term implications of these adaptations, emphasizing the importance of robust technological infrastructure, comprehensive faculty training, and flexible, student-centered pedagogical approaches (Zhou, 2024). As higher education continues to evolve, the lessons learned from these institutions can guide efforts to create a more resilient, equitable, and innovative learning environment (Moore et al., 2021).

Methodology

This research employs a comparative case study design to investigate the experiences of MTC, LUMS, and TAMIU. Data was collected either based on personal experience or through a combination of document analysis, semi-structured interviews, and surveys. Document analysis involved examining institutional policies, course materials, and student feedback (Yin, 2018). Semi-structured interviews were conducted with key

stakeholders, including faculty, administrators, and students (Creswell & Poth, 2017). Surveys were administered to a sample of students to gather quantitative data on their perceptions of the hybrid learning experience (Bryman, 2016).

How COVID-19 Transformed Education

The impact of COVID-19 on higher education was swift and far-reaching, fundamentally altering teaching and learning methods. When campuses closed in early 2020, institutions had to quickly adapt to remote learning, investing heavily in digital infrastructure and rethinking traditional approaches to instruction (Crawford et al., 2020). This abrupt transition exposed disparities in technology access and highlighted the need for faculty to rapidly learn and implement new tools. However, it also created opportunities for innovation and growth, pushing institutions to adopt more flexible and resilient educational practices (Bao, 2020).

Institutional Responses

Each institution tailored its response to address unique challenges:

Military Technological College (MTC): Faced with significant challenges in delivering lab-based engineering education, MTC implemented hybrid strategies that adhered to strict safety protocols. They developed virtual simulations and resumed limited in-person labs as conditions allowed (Al Siyabi, 2024).

Lahore University of Management Sciences (LUMS): LUMS responded by establishing open-air classrooms to accommodate in-person sessions while adhering to social distancing measures. They also invested in upgrading their Learning Management System (LMS) to facilitate secure, effective remote learning (Ali, 2020).

Texas A&M International University (TAMIU): Recognizing the digital divide among students, TAMIU provided essential hardware, such as loaner laptops, and ensured internet access for those from underserved backgrounds, making remote learning more equitable (Murphy, 2020).

Table 1 summarises the overview of the support students received from their institutions.

Table 1. Summary of Technical Interventions for Covid Support

Video Presentation Tools	MS Teams
	Zoom
	Google Meet
Course Management System	Sakai
	Moodle
	MS Teams
	Google Docs

Scheduling and Repository for Video Lectures	Sakai LMS
	MS Teams
Online Exams	Sakai module
	Moodle module
Grading System	Oracle based course registration and grading system
	Sakai LMS Gradebook
Hardware Support	IPAD
	Laptop with / without touch screen
	Cameras for blackboard recording

Modifications Needed in Classroom Teaching
Instructor Capacity Building

The sudden shift to online education required instructors to transition from traditional blackboard methods to digital platforms. Comprehensive training sessions were conducted to familiarize faculty with video conferencing tools like Zoom and Microsoft Teams (Alturki, 2021). LUMS and TAMIU provided ongoing support to help instructors develop engaging digital resources and enhance interaction through platforms like WhatsApp (Bozkurt et al., 2020).

Infrastructure Upgrades

The pandemic necessitated significant upgrades to existing LMS platforms, such as Sakai and Moodle, to better support remote teaching (Selwyn, 2020). LUMS integrated Zoom with their LMS and developed advanced assessment modules, while MTC invested in virtual lab technology to ensure that practical training continued effectively (Crawford et al., 2020).

Impact on Exams and Evaluation

Conducting assessments during the pandemic was challenging, particularly in terms of maintaining academic integrity. Institutions had to devise new strategies to address these challenges:

LMS Tools: Systems like Sakai were enhanced with features such as randomized question banks to minimize cheating (Moore et al., 2021).

Proctoring and Viva Voce: TAMIU implemented proctoring software to secure online exams, while MTC opted for in-person examinations as restrictions eased (Zhou, 2024).

Challenges and Solutions

Academic Integrity: Online exams raised concerns about dishonesty, prompting faculty to design open-book assessments and employ higher-order thinking questions that were more difficult to cheat on (Hodges et al., 2020).

Technology Glitches: Inadequate internet access created connectivity issues for students. Institutions addressed these problems by offering recorded lectures and providing alternative ways for students to submit assignments (Bao, 2020).

Laboratories and Practicum

Hands-on lab work is a critical component of STEM education, and the pandemic presented significant challenges in this area. Institutions adopted creative solutions to ensure students continued to receive practical training (Bozkurt et al., 2020):

Lab Kits: LUMS sent lab kits to students' homes, enabling them to complete experiments remotely with online guidance from instructors (Ali, 2020).

Virtual Labs: MTC developed virtual labs that utilized simulation software, offering an immersive experience that closely replicated physical lab environments (Al Siyabi, 2024).

Case Examples

Digital Logic Circuits at LUMS: Students were mailed lab kits and completed experiments at home, followed by online viva assessments to verify their understanding (Selwyn, 2020).

Metaverse Lab at MTC: This virtual lab provided engineering students with a realistic simulation of physical experiments, enhancing their practical skills despite the restrictions (Crawford et al., 2020).

Technological Interventions

The pandemic accelerated the adoption of video conferencing and other digital tools to support hybrid learning (Murphy, 2020). Institutions implemented a range of technological interventions to ensure the continuity of education:

Video Conferencing Tools: Platforms like Zoom, Microsoft Teams, and Google Meet became essential for conducting live classes and facilitating collaboration (Alturki, 2021).

LMS Enhancements: Learning Management Systems were upgraded to streamline course delivery, support

automated grading, and enable secure exam administration (Zhou, 2024).

Hardware and Software Enhancements

Hardware: To support remote learning, laptops, iPads, and cameras were distributed to faculty and students (Bozkurt et al., 2020).
Software: New LMS modules were introduced for grading and secure assessments, while existing systems were optimized for better performance (Hodges et al., 2020).

Lessons Learned

The pandemic revealed critical areas for improvement in higher education and underscored the benefits of hybrid learning models (Moore et al., 2021):

Flexibility and Engagement: Hybrid learning provides adaptable solutions, but maintaining student engagement remains an ongoing challenge. Interactive tools and active learning strategies are crucial for success (Bao, 2020).

Infrastructure Investment: Continuous investment in digital infrastructure is essential to future-proof education and ensure institutions are prepared for any disruptions (Zhou, 2024)

Conclusion

The COVID-19 pandemic catalyzed significant innovation in education, with hybrid and digital learning models proving essential for continuity. The experiences of MTC, LUMS, and TAMIU demonstrate the potential for technology-enhanced education to improve accessibility and resilience. By refining pedagogical approaches and investing in robust infrastructure, higher education can be better prepared for future challenges, creating a more inclusive and innovative learning environment.

References

Ali, W. (2020). Online and Remote Learning in Higher Education Institutes: A Necessity in Light of COVID-19 Pandemic. *Higher Education Studies*, 10(3), pp. 16-25.

Zhou, Yujie, Huiping Wu, and Ge Cao. "Does community of inquiry really matter in understanding online learning? A confirmed perspective using mixed method." *British Journal of Educational Technology* (2024)..

Bao, W. (2020). COVID-19 and Online Teaching in Higher Education: A Case Study of Peking University. *Human Behavior and Emerging Technologies*, 2(2), pp. 113-115.

Bozkurt, A., et al. (2020). A Global Outlook to the Interruption of Education Due to COVID-19 Pandemic: Navigating in a Time of Uncertainty and Crisis. *Asian Journal of Distance Education*, 15(1), pp. 1-126.

Bryman, A. (2016). *Social Research Methods*. 5th ed. Oxford: Oxford University Press.

Crawford, J., et al. (2020). COVID-19: 20 Countries' Higher Education Intra-Period Digital Pedagogy Responses. *Journal of Applied Learning & Teaching*, 3(1), pp. 1-20.

Creswell, J.W., & Poth, C.N. (2017). *Qualitative Inquiry and Research Design: Choosing Among Five Approaches*. 4th ed. Thousand Oaks: SAGE Publications.

Dhawan, S. (2020). Online Learning: A Panacea in the Time of COVID-19 Crisis. *Journal of Educational Technology Systems*, 49(1), pp. 5-22.

Hodges, C., et al. (2020). The Difference Between Emergency Remote Teaching and Online Learning. *Educause Review*, 27 March.

Goudeau, S., Sanrey, C., Stanczak, A. *et al.* Why lockdown and distance learning during the COVID-19 pandemic are likely to increase the social class achievement gap. *Nat Hum Behav* 5, 1273–1281 (2021). https://doi.org/10.1038/s41562-021-01212-7

Al Siyabi, M., et al. "Evaluating the Impact of E-Learning and Online Assessment on Engineering Education in Oman HEIs during COVID-19: A Mixed-Method Study." *Journal of Educational Research and Reviews* 12.1 (2024): 1-11.

Alturki, U. and Aldraiweesh, A., 2021. Application of learning management system (Lms) during the covid-19 pandemic: A sustainable acceptance model of the expansion technology approach. *Sustainability*, *13*(19), p.10991.

Moore, J.L., Dickson-Deane, C., & Galyen, K. (2021). e-Learning, Online Learning, and Distance Learning Environments: Are They the Same? *Internet and Higher Education*, 14(2), pp. 129-135.

Murphy, M.P.A. (2020). COVID-19 and Emergency eLearning: Consequences of the Securitization of Higher Education for Post-Pandemic Pedagogy. *Contemporary Security Policy*, 41(3), pp. 492-505.

Numerical Study of Forced Convection Heat Transfer in A Convergent-Divergent Channel Using a Nanofluid

Rahima Benchabi

University of Freres Mentouri, Constantine 1, 25000, Algeria

Ahsene Lanani

University of Freres Mentouri, Constantine 1, 25000, Algeria

Abstract The present work concerns the two-dimensional numerical study of laminar forced convection in a triangular corrugated channel using the SiO_2-Water nanofluid. The top and bottom walls of the channel are heated at a constant temperature. Continuity, momentum and energy equations are discretized by the finite volume method. The effects of $\frac{l}{p}$ ratio and volume fraction on flow, heat transfer and entropy generation are presented and analysed. Numerical simulations were carried out for different Reynolds numbers in the range 50 to 400 and volume fractions of nanoparticles, which vary from 0 to 5%; using the ANSYS-Fluent software. We have noted that increasing the Reynolds number has an effect on the size of the recirculation zone. Also, an increase in the Reynolds number leads to an increase in the Nusselt number and the pressure drop. When the l/P ratio increases, the Nusselt number decreases. An increase in the volume fraction of the nanoparticle leads to an increase in the Nusselt number and also in the pressure drop. The SiO2-water nanofluid with a 5% volume fraction gives the best improvement in heat transfer. In addition, the results obtained by the present study are in good agreement with those existing in the literature.

Keywords: Numerical simulation, Forced convection, Entropy generation, SiO_2-Water nanofluid.

Introduction

In recent years, forced convection in corrugated channels has received a great deal of research attention, as it is used in various thermal machines such as heat exchangers. When the fluid flows through these tubes, the rate of heat transfer improves due to the secondary flows that appear near the corrugated walls. Furthermore, the production of entropy is increased. This phenomenon leads to a reduction in the energy efficiency of the system under consideration. On the other hand, due to the

increasing demand from many technical applications for a more compact design of heat exchangers and higher performance, the search for additional passive techniques has become very important. To this end, the addition of nanoparticles to the base fluid; an operation that gives rise to nanofluids, has attracted a great deal of interest from many researchers. This technique consists of improving the thermal conductivity of conventional liquids such as water, oil, etc., thereby increasing the rate of heat transfer. Furthermore, the effect of corrugated channels on thermo-hydraulic performance using nanofluids is still a field of study to be explored. Many researchers have been interested numerically and/or experimentally in forced convection in corrugated channels filled with nanofluids in order to obtain the best technique for improved heat transfer.

In a numerical study, Bahaidarah (2016) analyzed the rate of volumetric entropy generation in sharp-edged corrugated channels. Air is considered as the working fluid in this analysis. Two parameters, namely the Reynolds number and the ratio between the horizontal pitch and the corrugation length, are considered as variables. The effect of these variables on the generation of volumetric entropy is analyzed numerically using the finite volume method. The results show that the total entropy generation increases with increasing Reynolds number and that the pitch size affects the distribution of this entropy generation. Alawi et al. (2022) presented an experimental and numerical study of turbulent flow and heat transfer in a corrugated surface in triangular shape using MWCNTs-TiO$_2$ nano-hybrids for different concentrations 0.025, 0.05, 0.075 and 0.1%. A significant improvement in heat transfer is observed with increasing concentration. Turbulent kinetic energy, pressure, velocity, turbulence intensity contours, as well as velocity vectors of water flow and MWCNTs-TiO$_2$ nanohybrids were presented. Also, correlations were established from the results to predict the mean Nusselt number for water and MWCNTs-TiO$_2$ nano-hybrids as a function of nanoparticle concentrations. A numerical study of the laminar flow and heat transfer characteristics of the CuO-water nanofluid in channels with four different geometries (straight, triangular, trapezoidal and sinusoidal channel) was reported by Ahmed et al. (2014). The effects of nanoparticle volume fractions and Reynolds number on velocity, temperature and mean Nusselt number were studied. Also, the velocity and temperature contours, the non-dimensional pressure drop, the mean Nusselt number and the thermal-hydraulic performance factor are presented and analyzed. The results show that the mean Nusselt number and the thermal-hydraulic performance factor increase with the nanoparticle volume fraction and the Reynolds number for all channel shapes. In addition, the non-dimensional pressure drop increases with increasing nanoparticle volume fraction, while it decreases with increasing Reynolds number for all considered geometries. In addition, the trapezoidal channel has the highest Nusselt number, followed by the sinusoidal, then the triangular and finally the straight channel. Dormohammadi et al. (2018) numerically investigated the entropy generation rate in a sinusoidal channel with corrugated walls with copper-water (Cu-water) nanofluid flow. The effects of geometrical and flow parameters, including nanoparticle volume fraction ($0.01 < \phi < 0.05$), Richardson number ($0.1 < Ri < 10$), wave amplitude ($0.1 < \alpha < 0.3$) and wavelength ratio ($1 < \lambda < 3$) were investigated. The results reveal that increasing the nanoparticle volume fraction for the studied Richardson number increases the Nusselt number. In addition, the maximum entropy generation rate decreases as the Richardson number increases. The optimal wave amplitude ratio (corresponding

to the lowest entropy generation) for wavelength ratios of $\lambda = 1$ and $\lambda = 2$, turns out to be $\alpha = 0.2$. Similarly, for the wavelength ratio of $\lambda = 3$, the minimum entropy generation occurs approximately at $\alpha = 0.1$. Ahmed et al. (2015) presented an experimental and numerical study of the flow of SiO_2 - water nanofluid in channels with different shapes (trapezoidal, sinusoidal and straight channels). The studies were carried out for Reynolds numbers ranging from 400 to 4000 and volume fractions from 0 to 1%. The results showed that heat transfer and Nusselt number increase with increasing particle volume fraction at the expense of a pressure drop. In addition, the trapezoidal channel had the highest Nusselt number compared with the other channels (sinusoidal and straight).

A numerical study devoted to the entropy generation of turbulent heat transfer in corrugated helical tubes with Reynolds numbers ranging from 10020 to 40060 and a constant temperature imposed on the wall, was reported by Wang et al. (2018). The effects of corrugation pitch and height on flow and entropy generation due to transfer and friction are presented and analyzed. The results indicate that the local entropy of heat transfer is improved with increasing secondary flow. Also, the mean friction entropy generation shows an exponential growth; while the transfer entropy and the total entropy show a linear growth with increasing Reynolds number. The analysis carried out by Han et al. (2021), concerned a numerical study of the effects of the trapezoidal rib of the micro channel with the addition of particles in water on heat transfer and entropy generation with an imposed magnetic field. The Reynolds and Hartmann number values vary in the ranges 50-400 and 0-20, respectively. The obtained results confirm that the addition of trapezoidal ribs both increases the heat transfer zone and intensifies the possibility of vortex formation. As the Reynolds number increases, the likelihood of vortex formation intensifies, which in turn reduces the positive effects of using trapezoidal ribs. The authors also found that increasing the Hartmann number weakens the strength of the vortex and, as a result, transfer is improved. In addition entropy generation is intensified with the increase of both Reynolds and Hartmann numbers.

The objective of the present work is to numerically study the thermal and hydraulic behavior of laminar, two-dimensional forced convection flow in corrugated, triangular and trapezoidal channels filled with SiO_2 silicon oxide particles dispersed in a base fluid which is water, using the commercial code Fluent-ANSYS.

Mathematical modeling

Physical model

The studied geometries are shown in Figure 1. Corrugated channels are considered with a triangular and symmetrical trapezoidal base and characterized by a minimum (H_{min}) and a maximum height (H_{max}) such that $\frac{H_{max}}{H_{min}} = 3$; a corrugation pitch $P = 28\ mm$ and horizontal pitch l with (A, $\frac{l}{P} = 0$) (B, $\frac{l}{P} = 0.1$) (C, $\frac{l}{P} = 0.25$) (D, $\frac{l}{P} = 0.5$).

The upstream and downstream lengths of the corrugations are $150\ mm$ and 24 mm, respectively.
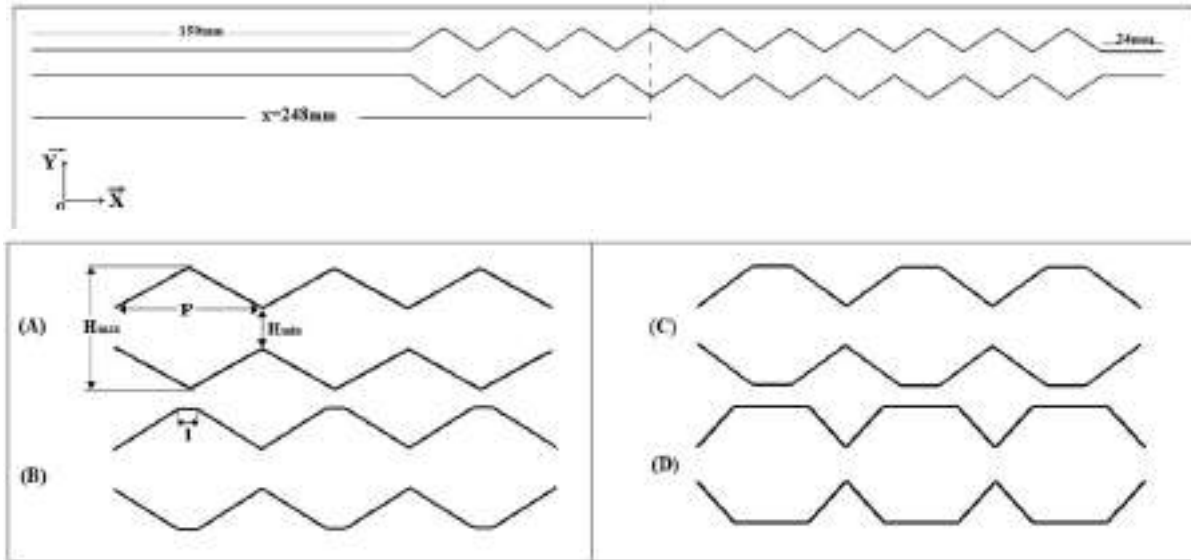
Governing equations

Continuity equation

$$\frac{\partial u}{\partial x} + \frac{\partial v}{\partial y} = 0 \tag{1}$$

 x - Momentum equation

$$\left(u\frac{\partial u}{\partial x} + v\frac{\partial u}{\partial y}\right) = \frac{1}{\rho_{nf}}\left[-\frac{\partial P}{\partial x} + \mu_{nf}\left(\frac{\partial^2 u}{\partial x^2} + \frac{\partial^2 u}{\partial y^2}\right)\right] \tag{2}$$

 y - Momentum equation

$$\left(u\frac{\partial v}{\partial x} + v\frac{\partial v}{\partial y}\right) = \frac{1}{\rho_{nf}}\left[-\frac{\partial P}{\partial y} + \mu_{nf}\left(\frac{\partial^2 v}{\partial x^2} + \frac{\partial^2 v}{\partial y^2}\right)\right] \tag{3}$$

Energy equation

$$u\frac{\partial T}{\partial x} + v\frac{\partial T}{\partial y} = \alpha_{nf}\left(\frac{\partial^2 T}{\partial x^2} + \frac{\partial^2 T}{\partial x^2}\right) \tag{4}$$

With α_{nf} is the thermal diffusivity of the nanofluid.

Boundary conditions

Channel inlet

A velocity U_{in} is imposed at the inlet, deduced from the Reynolds number and the characteristics of the nanofluid. It is calculated as follows:

$$U_{in} = \frac{Re\ x\ \mu}{H_{moy}\ x\ \rho} \tag{5a}$$

A fluid temperature at the channel inlet is imposed, $T_{in} = 300K$

Channel outlet

The outlet is sufficiently far from the inlet, so the flow can be assumed to be fully developed. This results in a zero normal gradient for all the physical quantities governed by a differential transport equation.

$$\frac{\partial u}{\partial x} = 0, \quad \frac{\partial v}{\partial x} = 0, \qquad \frac{\partial T}{\partial x} = 0 \tag{5b}$$

Treatment near the walls

The solid walls are assumed to be adiabatic before and after the corrugations. Due to viscosity, velocities are zero at the walls $(u = v = 0)$. A constant temperature of $310K$ is imposed at the corrugated walls.

Nanofluid property

i. Density:

$$\rho_{nf} = (1 - \varphi)\, \rho_f \, + \varphi \rho_P \tag{6}$$

ii. Heat capacity: *T*he model given by Xuan & Roetzel (2000) is:

$$(\rho\, Cp)_{nf} = (1 - \varphi)\, (\rho\, Cp)_f + \varphi(\rho\, Cp)p \tag{7}$$

iii. Effective dynamic viscosity: The model is evaluated by the following correlation (Corcione (2010)):

$$\frac{\mu_{nf}}{\mu_f} = \frac{1}{1 - 34.87(\frac{dp}{df})^{-0.3}\varphi^{1.03}} \tag{8}$$

Where: dp is the diameter of the SiO$_2$ particle and df that of the base liquid.

iv. Effective thermal conductivity: The effective thermal conductivity is given by (Choi & Eastman (1995); Eastman at al. (1996); Frouillat et al. (2011); Maxwell (1881). In this section, the used conductivity is that introduced by Maxwell [13].

$$K_{nf} \; = \frac{(k_p + 2k_f) - 2\varphi(k_f - k_p)}{(k_p + 2k_f) + \varphi(k_f - k_p)} . K_f \tag{9}$$

Where: K_{nf} is the thermal conductivity of the nanofluid; k_f that of the base fluid; k_p that of solid particles and φ the volume fraction.

Table 1. Thermo-physical properties of the water base fluid and the SiO$_2$ nanoparticle

	ρ $[kg/m^3]$	C_p $[J/kg.\,k]$	K $[W/m.\,K]$	μ $[kg/m.\,s]$
Water	998.2	4182	0.6	0.001003
SiO$_2$	2220	745	1.4	-

The thermo-physical properties of the base fluid (water) and the nanoparticles taken at 300K are summarized in Table 1.

Numerical method

The flow equations and heat exchange are solved by the finite volume method. In order to simulate and calculate the fluid flow properties of the studied problem, the CFD calculation code ANSYS FLUENT was used. This code offers extensive solutions for the most complicated geometries. The precision and stability of the results of our simulation depends on the quality of the mesh, so a mesh independence test has been carried out for different numbers of nodes. The SIMPLE algorithm is adopted to solve the velocity - pressure coupling problem. Also, the upwind second order scheme is used to discretize the momentum and energy equation.

Mesh effect and validation

Mesh effect

To demonstrate the influence of the mesh size on the solution, four mesh sizes were examined 22806; 30400; 40571 and 55114 for $Re = 100$ and $\phi = 0\%$. The effect of the nodes number on the solution is expressed by the profile of the axial velocity and the variation in the local Nusselt number.
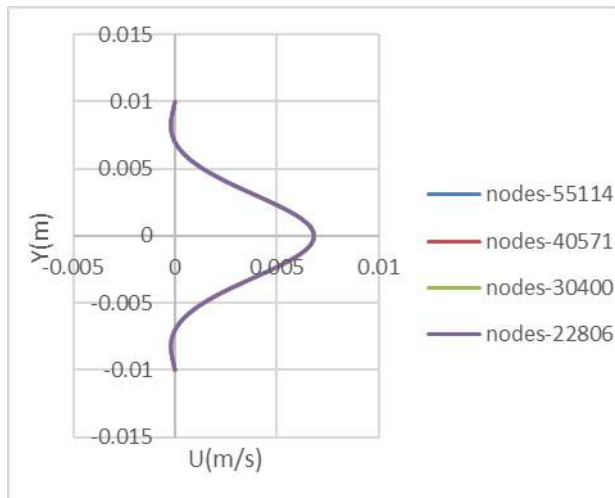
Figure 2: Axial velocity profiles with $Re = 100$ for different mesh sizes at the station $x = 0.248m$.
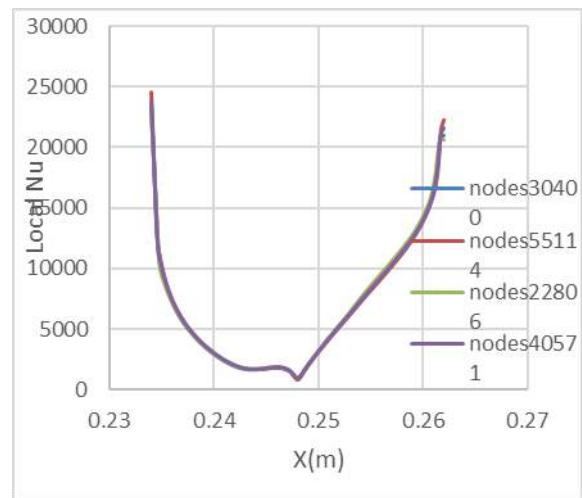
Figure 3: Variation of the local Nusselt number with $Re = 100$ for different mesh sizes

Figures 2 show the variation of the axial velocity; while figure 3 illustrates the variation of the local Nusselt number. It can be seen that the curve corresponding to mesh 22806 has always an effect on the solution compared with the curves for meshes (30400, 40571, 55114), which are identical. The considered mesh in this study is 40571.

Validation of the results

Validation of the numerical simulation is necessary in order to verify the accuracy of the numerical results obtained by the Ansys-Fluent code. A comparison of our results was made with the study carried out by the authors Incropera and DeWitt (1996), where they considered fluid flow and heat transfer in a parallel-plate channel with a constant temperature imposed on the walls. The average Nusselt number obtained numerically in the smooth channel is equal to 7.58, which agrees favorably with the Nusselt number of 7.54 mentioned by the authors Incropera and DeWitt (1996).

Results and Discussions

This section is devoted to showing the findings obtained by numerical simulation using the Ansys-Fluent calculation code, based on the finite volume method, where the effect of the l/p ratio, which varies between 0 and 0.5 and that of the volume fraction between 1% and 5%, will be studied.

Reynolds number effect

In this subsection, the effect of Reynolds numbers ranging from 50 to 400 on the forced convection flow of water in a corrugated channel with the ratio $l/P = 0$ will be studied.

a- Dynamic field

Figure 4 (a, b and c) shows the contours of the mean velocity for different Reynolds numbers. The velocity is highest at the center of the channel and increases with increasing Reynolds number. Also, there is a decrease to zero near the wall, satisfying the no-slip condition.

(a)   (b)
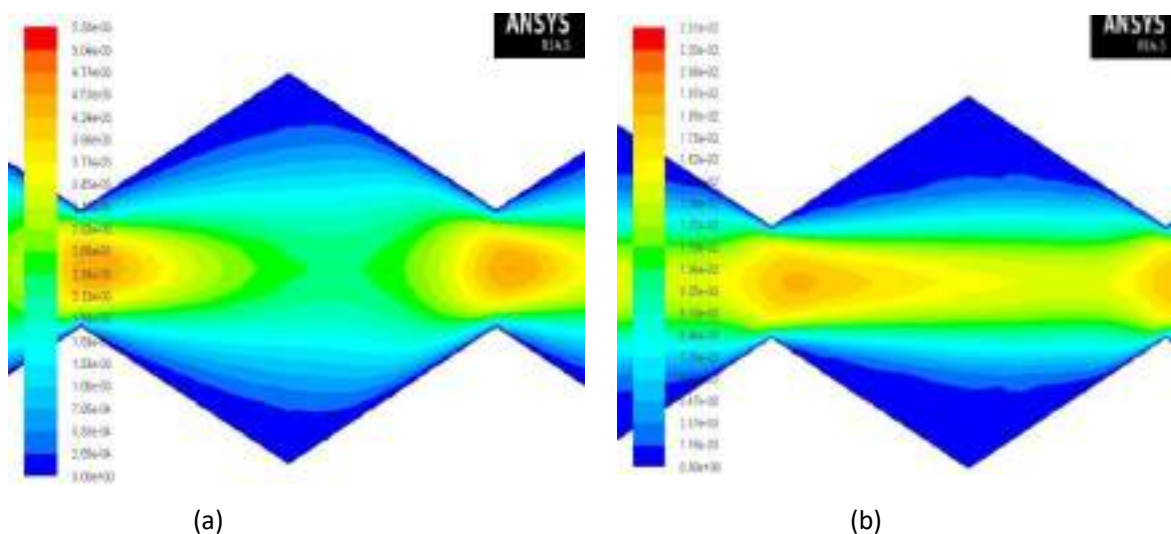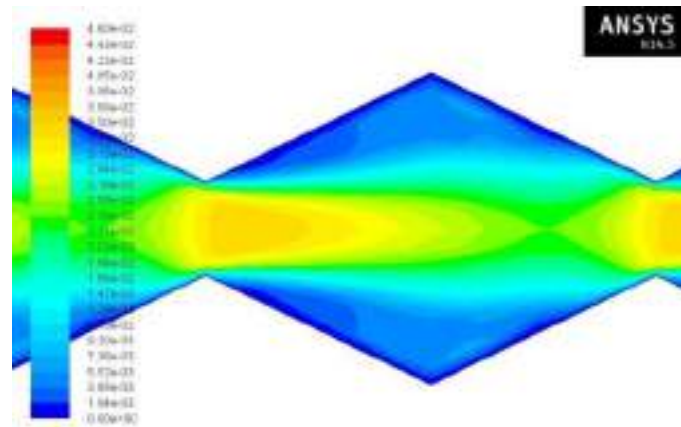
(c)

Figure 4. Average velocity contours for different Reynolds numbers.

Figure 5 shows the axial velocity profiles at station $x = 0.248\,m$ for different Reynolds numbers. It can be seen that the velocity values increase with increasing Reynolds number, and that the maximum velocity is located on the axis of the corrugated channel and we also note that with increasing Reynolds number there is an appearance of negative velocity values which clearly show the return of the fluid which characterises the appearance of recirculation zones.
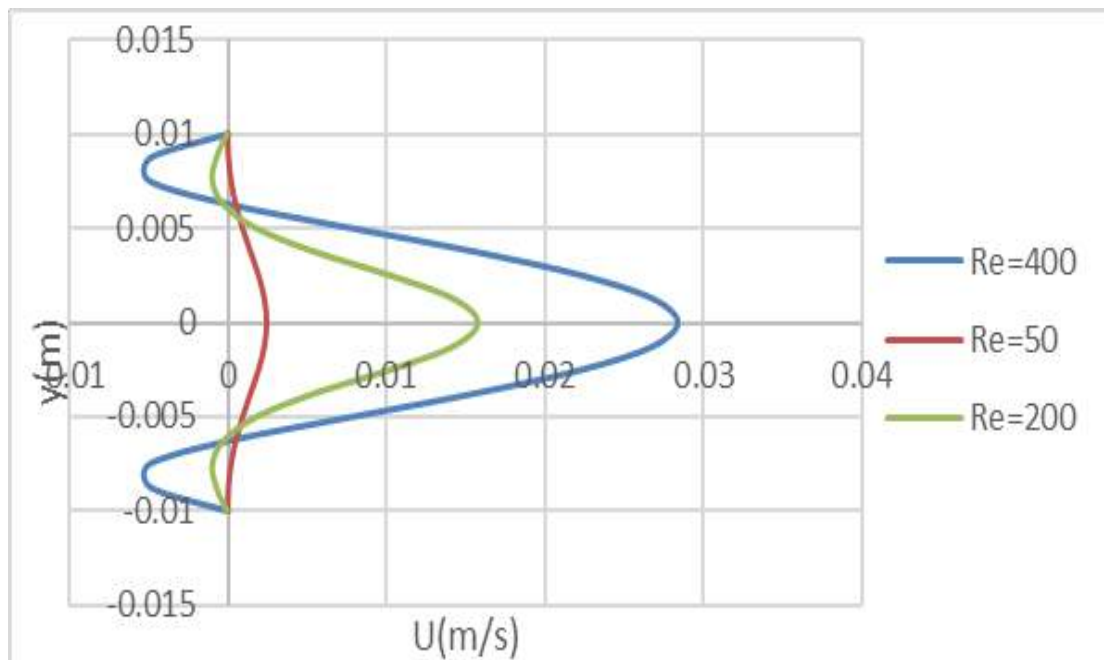
Figure 5. Variation of axial velocity profiles for different Reynolds numbers

The average coefficient of friction as a function of the Reynolds number is shown in Figure 6. It can be seen that the coefficient of friction is influenced by the Reynolds number and that a decrease is caused by an increase in the Reynolds number.
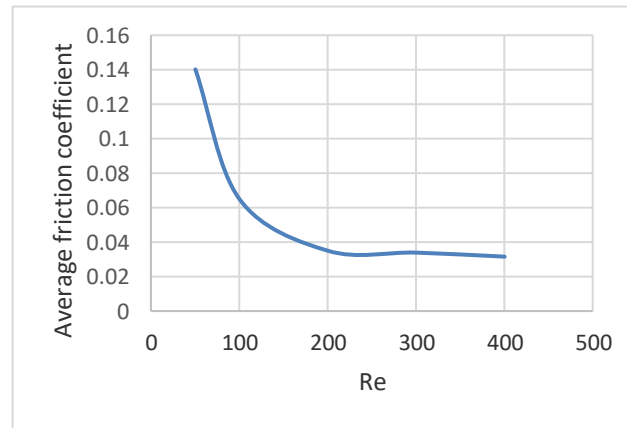
Figure 6. Variation of the average coefficient of friction as a function of Reynolds

b- Thermal field

The variation of the local Nusselt number for different Reynolds numbers is shown in figure 7. Maximum values are reached by the Nusselt number located in the corners where the velocities are high and which decrease immediately downstream of the point of detachment and upstream of the point of attachment of the fluid to the corrugated wall, due to the appearance of recirculation zones. This figure clearly confirms the effect of Reynolds number on energy exchange. We can clearly see that an increase in Reynolds number leads to an increase in the local Nusselt number.
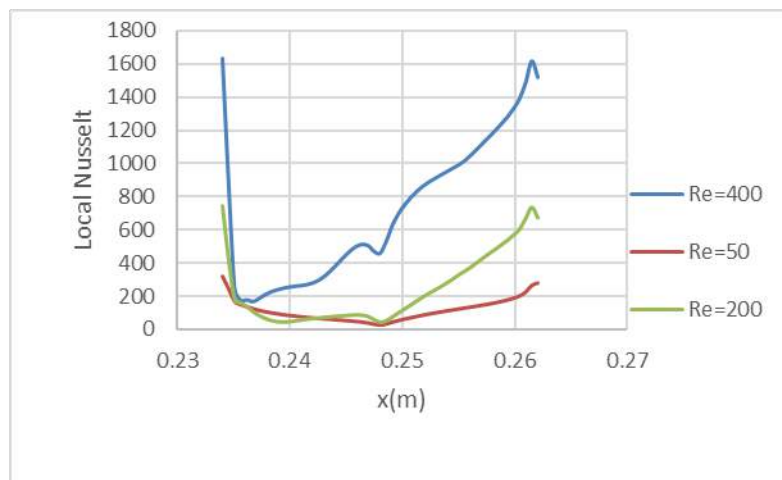
Figure 7. Variation of the local Nusselt number for different Reynolds

Figure 8 shows the variation of the mean Nusselt number as a function of the Reynolds number. It can be seen that the mean Nusselt number increases as the Reynolds number increases.
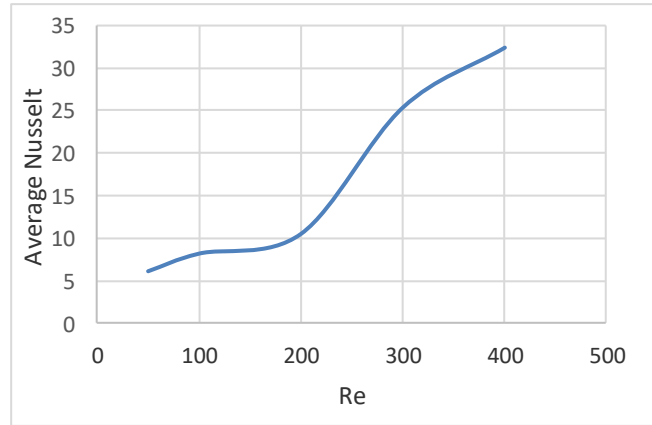
Figure 8. Variation of the average Nusselt number for different Reynolds

Figure 9 shows the variation in entropy due to heat transfer as a function of the Reynolds number. It can be seen that an increase in entropy is caused by an increase in Reynolds number.
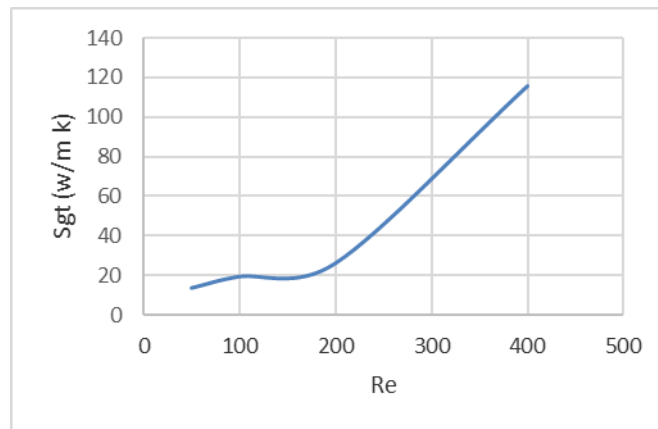
Figure 9. Variation of entropy generation due to heat transfer as a function of the Reynolds number

The variation in entropy generation due to friction as a function of the Reynolds number is illustrated in Figure 10. It can be seen that increasing the Reynolds number leads to an increase in entropy.

Figure 11 illustres the variation in total entropy generation as a function of the Reynolds number. It expresses the sum of entropies generated by transfer and friction, so it can be seen that it increases as the Reynolds number increases.
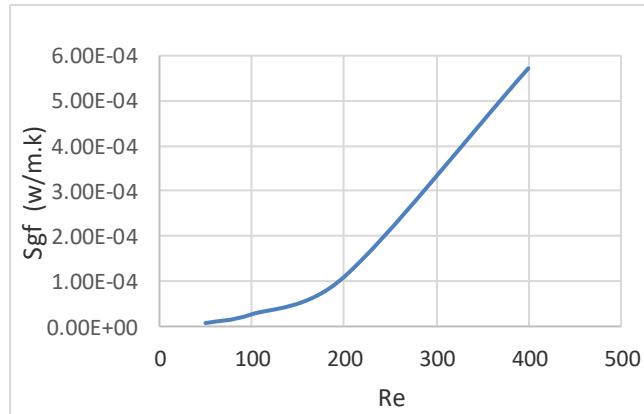
Figure 10. Variation of entropy generation due to friction as a function of Reynolds number
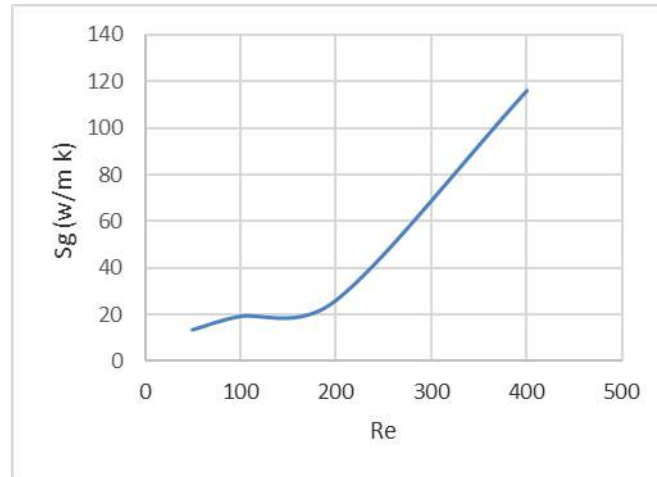
Figure 11. Variation of total entropy as a function of Reynolds number

Effect of the l/p ratio

In this subsection, we will study the effect of the l/P ratio (0; 0.1; 0.25; 0.5) on the flow of water in forced convection, for $Re = 200$. Figure 12 (a, b, c and d) shows the contours of the streamlines for different ratios with $Re = 200$. It can be seen that the ratio has an effect on the flow, with the appearance of recirculation zones in the triangular and trapezoidal channels. The size of these zones increases as the l/p ratio increases.

Figure 13 depicts the average coefficient of friction for different ratios as a function of Reynolds number. It can be seen that the average coefficient of friction decreases with increasing velocity and l/p ratio.

(a)

(b)

(c)

(d)
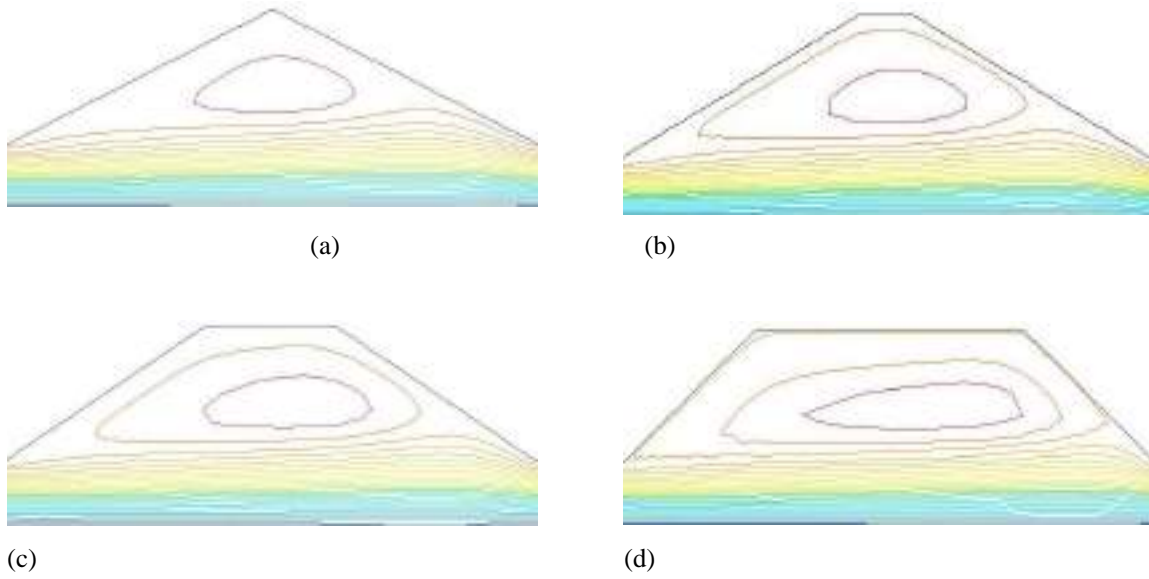
Figure 12. Contours of current lines for different ratios: (a) $l/p = 0$, (b) $l/p = 0.1$, (c) $l/p = 0.25$, (d)
$$l/p = 0.5$$
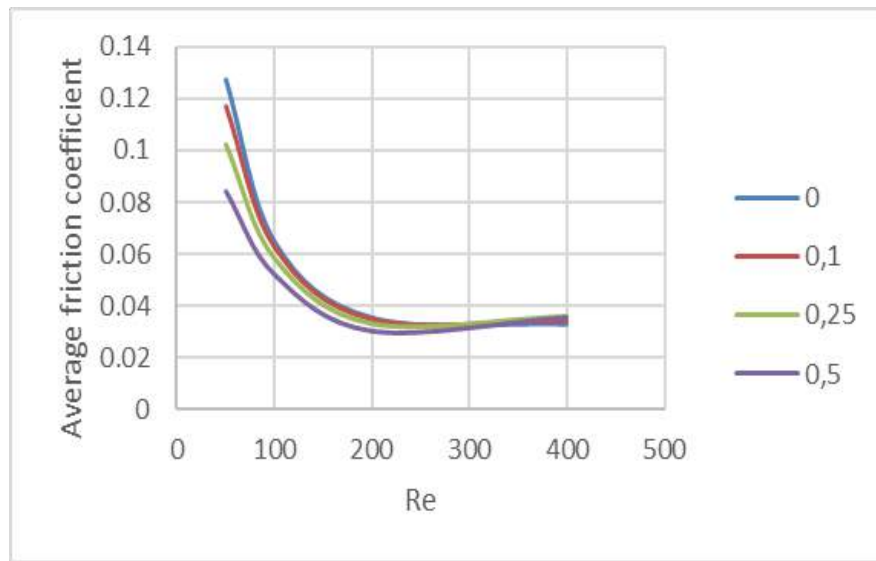
Figure 13. Variation in the average coefficient of friction for different ratios

Thermal field

Figure 14 shows the variation of the average Nusselt number as a function of Reynolds for different ratios. It can be seen that the Nusselt number is influenced by the Reynolds number, where an increase in the latter leads to an increase in the mean Nusselt number, the values of which are larger and larger. It can also be seen that the $\frac{l}{P} = 0$ ratio gives better heat transfer than the other ratios.
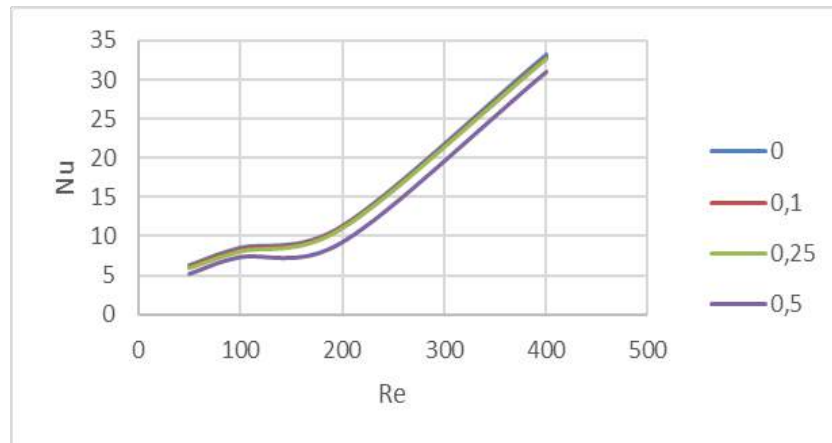
Figure 14. Variation of the average Nusselt number versus the Reynolds number for different ratios

Effect of volume fraction

This last subsection will be devoted to the study of the effect of the volume fraction of the SiO_2-water nanofluid on heat transfer and flow in a triangular channel.
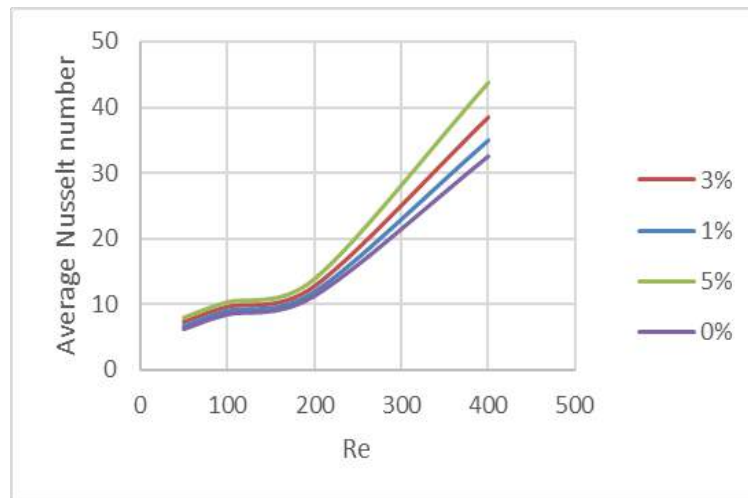
Figure 15. Variation of average Nusselt number as a function of Reynolds number for different volume fractions

Figure 15 shows the variation of the mean Nusselt number as a function of the Reynolds number for pure water $\varphi = 0\%$ and the SiO2-water nanofluid with different volume fractions ranging from 1% to 5%. This figure clearly shows the effect of the flow velocity on the heat transfer and it is also observed that the values of the average Nusselt number obtained by the SiO_2-water nanofluid for a volume fraction $\varphi = 5\%$ are the highest in comparison with those of the other fractions. The nanofluid therefore gives better thermal performance.

Figure 16 shows the pressure drops for different volume fractions of the SiO_2-water nanofluid as a function of Reynolds number. It can be seen that these pressure losses increase with increasing Reynolds number and

volume fraction. It can also be clearly seen that the pressure losses of the nanofluid for a volume fraction $\varphi = 5\%$ are the highest compared with those of the other fractions. This increase is linked to the high viscosity of the nano fluid, which is proportional to the volume fraction.
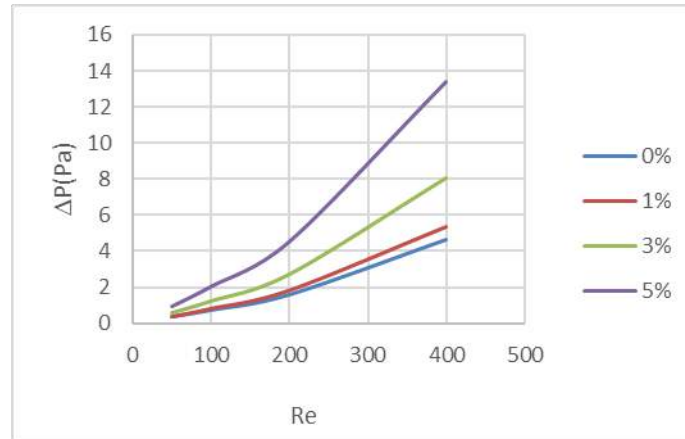
Figure 16. Variation of pressure losses for different fractions as a function of the Reynolds number.

Reynolds number

Figure 17 shows the thermal enhancement factor as a function of Reynolds number for different volume fractions of the SiO_2-water nanofluid. It can be clearly seen that the values of the thermal performance coefficient increase with increasing volume fraction. It can also be seen that the nanofluid with a fraction of 5% has the highest values of the thermal improvement factor, followed by 3% and 1%.
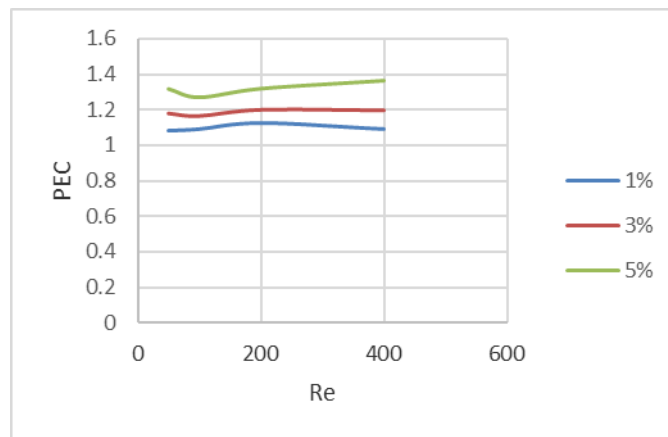
Figure 17. Variation of the thermal enhancement factor (PEC) as a function of Reynolds for different volume fractions of the SiO_2-water nanofluid.

Conclusion

In this work, we have numerically studied the two-dimensional heat transfer by forced convection for water and the SiO2-water nanofluid inside a corrugated channel with a triangular and trapezoidal base in which the upper

and lower walls are subjected to a constant temperature. The study of the effect of the Reynolds number, the l/P ratio and the volume fractions of the SiO_2 oxide particle on the thermal-hydraulic behavior in the corrugated channel yielded the following results:

- Increasing the Reynolds number leads to an increase in the Nusselt number.
- When the l/P ratio increases, the Nusselt number decreases.
- An increase in the volume fraction of the nanoparticle leads to an increase in the Nusselt number and also in the pressure drop.
- The SiO_2-water nanofluid with a 5% volume fraction gives the best improvement in heat transfer compared with the other fractions.

References

Bahaidarah, H. M. S. (2016). Entropy generation during fluid flow in sharp edge wavy channels with horizontal pitch, *Advances in Mechanical Engineering*, 8(8), 1–10.

Alawi, O. A., Kamar, H. M. & Hussein, O. A. (2022). Effects of binary hybrid nanofluid on heat transfer and fluid flow in a triangular-corrugated channel: An experimental and numerical study, *Powder Technology,* 395, 267–279.

Ahmed, M. A., Yusoff, M. Z., Ng, K. C. & Shuaib, N. H. (2014). Effect of corrugation profile on the thermal - hydraulic performance of corrugated channels using CuO–water nanofluid, *Case Studies in Thermal Engineering*, 4, 65–75.

Dormohammadi, R., Farzaneh-Gord, M., Moghadam, A. E. & Ahmadi, M. H. (2018). Heat transfer and entropy generation of the nanofluid flow inside sinusoidal wavy channels, *Journal of Molecular Liquids*, 269, 229–240.

Ahmed, M. A., Yusoff, M. Z. & Shuaib, N. H. (2015). Numerical and experimental investigations on the heat transfer enhancement in corrugated channels using SiO_2–water nanofluid, *Case Studies in Thermal Engineering,* 6, 77–92.

Wang, W., Zhang, Y., Liu, J., Wu, Z., Li, B. & Sunden, B. (2018). Entropy generation analysis of fully-developed turbulent heat transfer flow in inward helically corrugated tubes, *Numerical Heat Transfer*, Part A, 73(11), 788–805.

Han, L., Lu, C., Yumashev, A., Bahrami, D., Kalbasi, R., Jahangiri, M., Karimipour, A., Band, S. S., Chau, K. W. & Mosavi, A. (2021). Numerical investigation of magnetic field on forced convection heat transfer and entropy generation in a micro channel with trapezoidal ribs, *Engineering Applications of Computational Fluid Mechanics*, 15(1), 1746–1760.

Xuan,Y. & Roetzel, W. (2000). Conceptions for heat transfer correlation of nanofluids, *International Journal of Heat Mass Transfer*, 43, 3701–3707.

Corcione, M. (2010). Heat transfer features of buoyancy-driven nanofluids inside rectangular enclosures differentially heated at the sidewalls, *International Journal. Therm. Sci*, 45, 1536-1546.

Choi, S. & Eastman, J. A. (1995). *Enhancing thermal conductivity of fluids with nanoparticles*. Argonne National Laboratory, Lemont..

Eastman, J. A., Choi, S. U. S., Li, S., Thompson, L. J. & Lee, S. (1996). *Enhanced thermal conductivity through the development of nanofluids*, in MRS Proceeding, 457, 3.

Frouillat, S., Bontemps, A., Ribeiro, J. P., Gruss, J. A., & Soriano, O. (2011). Hydraulic and heat transfer study of SiO_2 /Water nanofluids in horizontal tubes with imposed wall temperature boundary conditions, *Int. J. Heat Fluid Flow*, 32, 424-439.

Maxwell, J. A. (1881). *A treatise on electricity and magnetism*, Oxford: Clarendon Press, second edition.1.

Incropera, F. P. & Dewitt, D. P. (1996). *Fundamentals of Heat and Mass Transfer*, John Wiley and Sons, New York, USA.

Improvement of Dynamic Characteristic Behavior of Composite Beams Reinforced with Functionally Graded Graphene Nano-Platelet

Bensaid Ismail

University of Abou Beckr Belkaid (UABT), IS2M Laboratory, Tlemcen, Algeria, https://orcid.org/0000-0003-4316-0648

Saimi Ahmed

University of Abou Beckr Belkaid (UABT), IS2M Laboratory, Tlemcen, Algeria, https://orcid.org/0000-0002-3722-2526

Guenifed Abdelhalim Farouk

University of Abou Beckr Belkaid (UABT), IS2M Laboratory, Tlemcen, Algeria

Abstract: In this study, the free vibration response of multilayer functionally graded graphene platelets reinforced composite (FG GPLRC) beams is presented. The distribution of graphene platelets (GPLs) in the polymer matrix either uniformly or non-uniformly including diverse arrangements are considered. The Young's modulus and density of the nanocomposites are predicted by the modified Halpin–Tsai micromechanics model. The governing equations of motion are extracted by minimizing Hamiltonian's principle Depending on the generalized coordinates based on Euler Bernoulli beam theory. After that, a two-noded C1 beam element with three degree-of-freedom per node is used to solve the problem. Impacts played by GPLs weight fraction, GPLs distribution patterns, number of layers, thickness-to-length ratio are all explored.

Keywords: Composite beams; Graphene based nanoplatelet; free vibration; Finite element analysis (FEM)

Introduction

Please Graphene nanoplatelets (GPLs) Noveselov et al. (2004), which are novel two-dimensional carbon materials, can be considered as brilliant candidates for the polymer matrix reinforcement to enhance their mechanical properties. To prove that, Rafiee et al. (2009)carried out some pioneering experiments and demonstrated that by adding 0.1% weight fraction of GPLs, the mechanical stiffness and strength of the reinforced polymer composites are similar to the same degree achieved by adding 1.0 wt.% of carbon nanotubes

(CNTs) and elastic modulus increases around 31%. This stimulates the scientific researchers for the development of advanced lightweight structures made of graphene-based polymer nanocomposites. Therefore, GPLs reinforced polymer matrices have become an interesting and promising research topic. Song et al. (2017) developed the functionally graded multilayer graphene nanocomposite in which the graphene reinforcements are nonuniformly distributed in a layer-wise manner in the thickness direction of polymer nanocomposite plates. Shen et al. (2017) used the two-step perturbation technique to analyze the thermal postbuckling of GRC beams resting on two parameters elastic foundation by means of the third order shear deformation beam theory. The Ritz method was used by Kiani & Mirzaei (2018) to investigate the buckling and postbuckling of functionally graded graphene reinforced composite (FG-GRC) beams resting on two parameter elastic foundation. It is shown by the works of Yang and his coworkers (Yang, Wu et al., 2007), that by adding a small amount of GPLs into epoxy can considerably increase the buckling and postbuckling strength and reduce the principle unstable region of (GPLRC) composite beams. Feng et al (2017) estimated the nonlinear bending and free vibration of functionally graded polymer composite beams reinforced with GPLs. Kitipornchai and his coauthors (Kitipornchai, Chen, et al., 2017) proved also that, by ading of a small amount of GPLs can remarkably reinforce the stiffness of functionally graded porous beams. Arefi et al. (2019) analyzed the bending behavior of Functionally Graded (FG) polymer composite curved beams reinforced by graphene nanoplatelets resting on a Pasternak foundation.

In this study, the free vibration analysis of the multilayer FG GPLRC composite beams based on Euler Bernoulli beam model and finite element procedure is presented for the first time. The Young's modulus, Poisson's ratio and density of the nanocomposites are defined by the Halpin–Tsai model and the rule of mixtures, respectively. Governing equations of motion are derived by Hamilton's principle and the finite element formulation based on a two-noded C1 beam element with three degree-of-freedom (DOF) per node is employed to obtain natural frequencies of the multilayer FG GPLRC beams. extensive numerical results are presented to show the effects of the physical and geometrical parameters of GPLs on the maximum values of natural frequencies.

Mathematical formulations

Multilayer GPLs beam

A multilayer functionally graded graphene nanoplatelet/polymer nanocomposite beam with the thickness h and length L is considered. The beam includes NL layers with the same thickness of each layer *h/NL* as shown in Figure 1.

The GPL volume fraction VGPL for the three symmetrical distribution patterns in Fig. 1(b) are governed by (Yang, Wu et al., 2017)

$$U - GPLRC : V_{GPL}^{(k)} = V_{GPL}^{*} \tag{1}$$

$$X - GPLRC : V_{GPL}^{(k)} = 2V_{GPL}^{*} \left| 2k - N_L - 1 \right| / N_L \tag{2}$$

$$O - GPLRC : V_{GPL}^{(K)} = 2V_{GPL}^{*}\left(1 - |2k - N_L - 1| / N_L\right) \tag{3}$$

$$A - GPLRC : V_{GPL}^{(k)} = V_{GPL}^{*}\left(2k - 1\right) / N_L \tag{4}$$

where NL is the total number of layers of the plate, and $V_{GPL}^{(k)}$ is the value of VGPL in the kth layer (k = 1, 2, …, NL). V∗GPL is total GPL volume fraction in the whole beam.

The modified Halpin-Tsai model that takes into account the effects of GPL geometry and dimension is used to estimate the effective Young's modulus E of GPLRC (Wu et al., 2017):

$$E = \frac{3}{8}\frac{1 + \xi_L \eta_L V_{GPL}}{1 - \eta_L V_{GPL}} \times E_m + \frac{5}{8}\frac{1 + \xi_T \eta_T V_{GPL}}{1 - \eta_T V_{GPL}} \tag{5}$$

According to the rule of mixture, mass density, the Poisson's ratio ν and thermal expansion coefficient α of GPLRCs are expressed as.
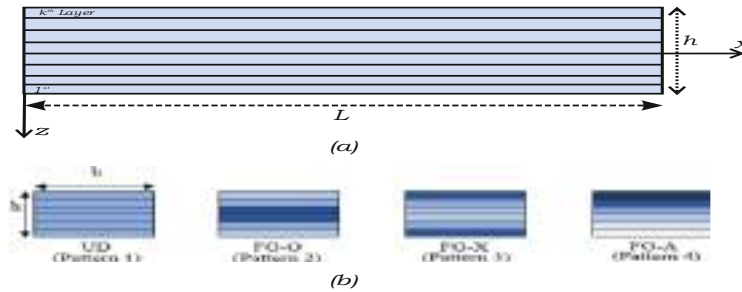
Figure 1. Example of an image

$$\rho = \rho_m V_m + \rho_{GPL} V_{GPL} \tag{6}$$

$$\nu = \nu_m V_m + \nu_{GPL} V_{GPL} \tag{7}$$

where ρ_m and ρ_{GPL} are mass densities, ν_{GPL} and ν_m are the Poisson's ratios with the subscripts "*GPL*" and "*m*" referring to the GPL and matrix, respectively. $V_m = 1 - V_{GPL}$ is the matrix volume fraction.

Kinematics

In the present investigation, based on the Euler Bernoulli beam theory EBT, the displacement field at any arbitrary point of the beam are supposed to be written as follows (Bensaid & Saimi 2022):

$$u(x, z) = u_0(x) - z\frac{\partial w_0}{\partial x} \tag{8}$$

$$w(x, z) = w(x) \tag{9}$$

In which *u* is the displacement of the mid-surface and *w* is the bending displacement. The associated nonzero strains of the current beam model are expressed as

$$\varepsilon_{xx} = \varepsilon_{xx}^0 - zk_x^0, \quad \varepsilon_{xx}^0 = \frac{\partial u_0(x)}{\partial x}, \quad k_x^0 = \frac{\partial^2 w_0(x)}{\partial x^2} \tag{10}$$

Variational statement

In order to derive the equations of motion, he Hamiltonian of a dynamic system as:

$$H = U - K \tag{11}$$

where U is the variation of the strain energy and the variation of the kinetic energy is given by K.

By substituting the expressions of U, and K, in equation (11) and minimizing it to field coefficients U_i and W_i, and assembling the coefficients, the equations of motion regarding the vibration of the functionally GPLs beam will be obtained.

Governing equations of motion

After some mathematical manipulations, the explicit form of the governing equations of motion can be expressed with respect to the laminate stiffnesses (A_{ij}, B_{ij}, D_{ij})

$$A_{xx}\frac{\partial^2 u_0}{\partial x^2} - B_{xx}\frac{\partial^3 w_0}{\partial x^3} - I_0\frac{\partial^2 u}{\partial t^2} + I_1\frac{\partial^3 w}{\partial t^2 \partial x} = 0 \tag{12a}$$

$$B_{xx}\frac{\partial^3 u_0}{\partial x^3} - D_{xx}\frac{\partial^4 w_0}{\partial x^4} - I_0\frac{\partial^2 w}{\partial t^2} -$$
$$I_1\frac{\partial^3 u}{\partial t^2 \partial x} + I_2\frac{\partial^4 w}{\partial t^2 \partial x^2} = 0 \tag{12b}$$

Finite element solution

A two-noded beam element with three degrees of freedom (DOF) per node is used herein to solve the above governing equations. Since the bending components of transverse displacement w must be twice differentiable, a C^1-continuous procedure is used, whereas the axial displacement u must be only once differentiable and C^0-continuous required. The generalized displacements are expressed over each element as a combination of the linear interpolation function Ψ_j for u and Hermite-cubic interpolation function ψ_j for w corresponding with node j and the nodal values:

$$u = \sum_{j=1}^{2} u_j \Psi_j \tag{13a}$$

$$w = \sum_{j=1}^{4} w_j \psi_j \tag{13b}$$

Substituting these expressions in Eq. (13) into the corresponding weak statement in Eq. (12), the finite element model of a typical element can be expressed as the standard eigenvalue problem

$$\left(\left[K \right] - \omega^2 \left[M \right] \right) \{ \Delta \} = \{ 0 \} \tag{14}$$

where $[K]$ and $[M]$ are the element stiffness matrix, and the element mass matrix, respectively.

The explicit forms of $[K]$ and $[M]$ can be found in Ref. (Vo & Thai 2012)

Numerical examples

The convergences and verifications of proposed approach have been respectively done; the vibrational frequencies are converged via selecting fifteen elements for S-S GPLs beams and thirty elements for C-C beams.

In this part, a number of numerical examples are presented and analyzed for verification the accuracy of the present model and investigation the natural frequencies, for this purpose the multilayer GPLRC host of thickness **h** is made from a mixture of epoxy and GPLs with a length of a_{GPL} = 2.5 μm, width of bGPL = 1.5 μm and thickness of tGPL = 1.5 nm (Rafiee et al., 2009).

Table 1. Comparison of Nondimensional fundamental frequency of simply supported FGM beam

L/h	Model	0	0.2	0.5	1	5
5	Ebrahimi et al. (2016)	5.3953	5.0219	4.5936	4.1483	3.7793
	Simsek (2010)	5.3953	5.0206	4.5931	4.1483	3.7793
	FEM (Present)	5.3953	5.0542	4.7328	4.4520	3.9659
20	Ebrahimi et al. (2016)	5.4777	5.0980	4.6645	4.2163	3.8471
	Simsek (2010)	5.4777	5.0967	4.6641	4.2163	3.8471
	FEM (Present)	5.4777	5.1303	4.8038	4.5194	4.2026

Comparison Studies

Thus, to check the accuracy of the proposed model based FEM solution, an example including FGMs beams is performed in the following, since there is no available results concerning free vibration analyses of FG GPLRC beam. Then, some new results are analyzed and considered as benchmark problems for further studies of the FG GPLRC beams.

Consider a simply supported FG beam with the length $L=1$, E_c= 380 GPa, E_m=70 GPa, ρ_c= 3800 kg/m³, ρ_m= 2707 kg/m³, length-to-thickness ratio L/h=5 and 20. For verification of the proposed methodology, the analytical solutions [15,16], using the EBT are considered. The maximum natural frequencies of the FGM beams are summarized in Table 1. It can be observed that the present results are in good agreement with those of the reference solutions for all patterns.
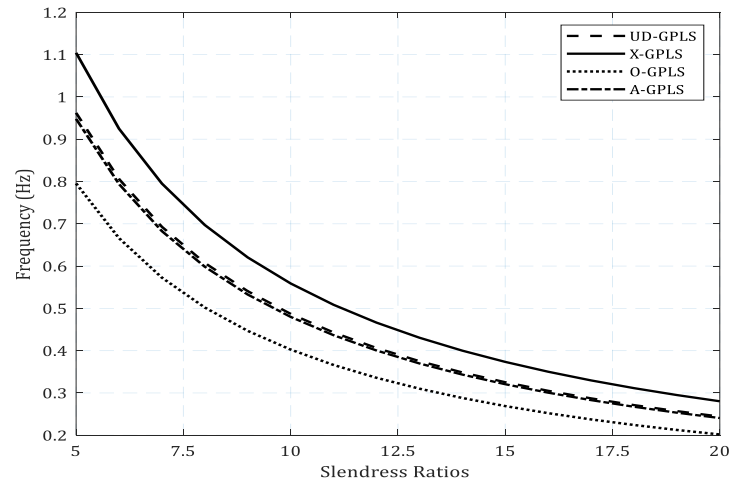
Figure 2. Variation of dimensionless frequency of GPLRC beam versus slenderness ratio for GPL distribution pattern.
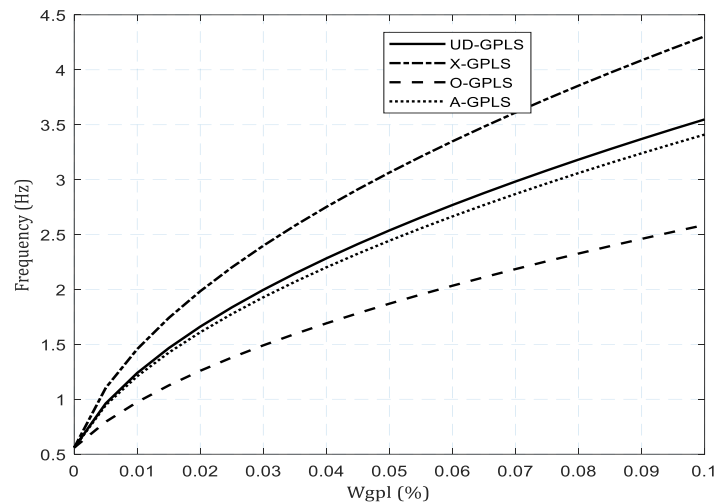
Figure 3. Effect of GPL distribution pattern and weight fraction on the dimensionless frequency of GPLRC beams.

The effects of GPL distribution pattern and length to thickness ratio on the natural frequency of functionally graded multilayer GPLRC beams is shown in Fig .2 with a weight fraction $W_{gpl} = 0.5\%$. One can see that an increase into slenderness ratio (L/h) leads to decrement into nondimensional frequency, also FGPL-X beams have higher natural frequency at, followed by the beams with U-, A- and O-GPLRC distributions.

Fig. 3 exhibits the effect induced by the GPL distribution pattern and the weight fraction on the nondimensional natural frequency of GPLRC composite beams. It is demonstrated that the nondimensional frequency of the GPLRC composite beam is remarkably increased as the GPL weight fraction is raised with just of small amount. The X-GPLRC beam is also for this case capable of vibrating with high rate, since pattern X makes the better use of GPL reinforcements and gives the higher bending stiffness.
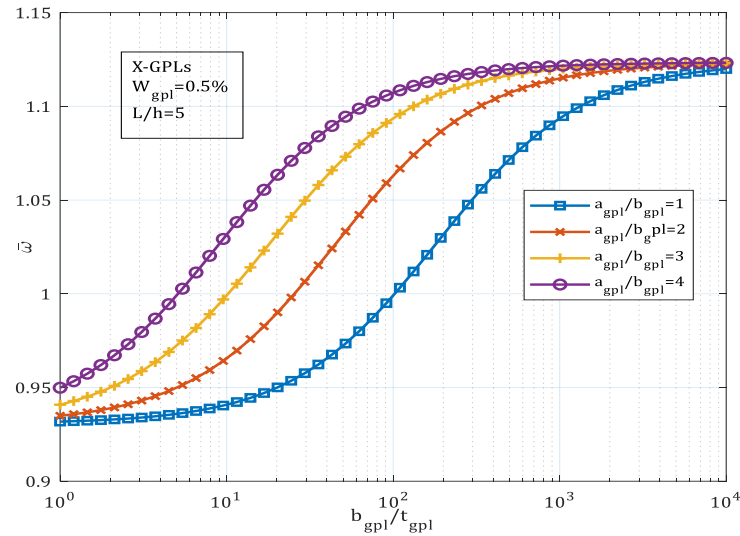
Figure 4. Impacts of GPL geometry and dimension on the dimensionless frequency of X-GPLRC beams.

Figure 4 demonstrates the effect of GPL geometry and dimension on the fundamental frequency parameter of composite X-GPLRC beams, in which a higher value of aGPL/bGPL represents a lager GPL surface area and a greater magnitude of bGPL/tGPL signifies that each individual GPL contains fewer monolayer graphene sheets. It can be seen from this figure that an increase in both aGPL/bGPL and bGPL/tGPL gives rise to an increment in the natural frequency.

The impact of the total number of layers NL on the dimensionless frequency   in terms of for various patterns of GPL distributions at Wgpl=0.5%, and L/h=5 is presented in Figure. 5. It is concluded that the increase in the number of layers and with a number that exceeds ten, the natural frequency seems to remain almost unaffected by the numbers of layers, for a reinforcement distribution of type U, whereas it increases for Patterns X and A and tend to an asymptotic value. In addition, the numerical results related to shape O decrease monotonically up to a threshold value.
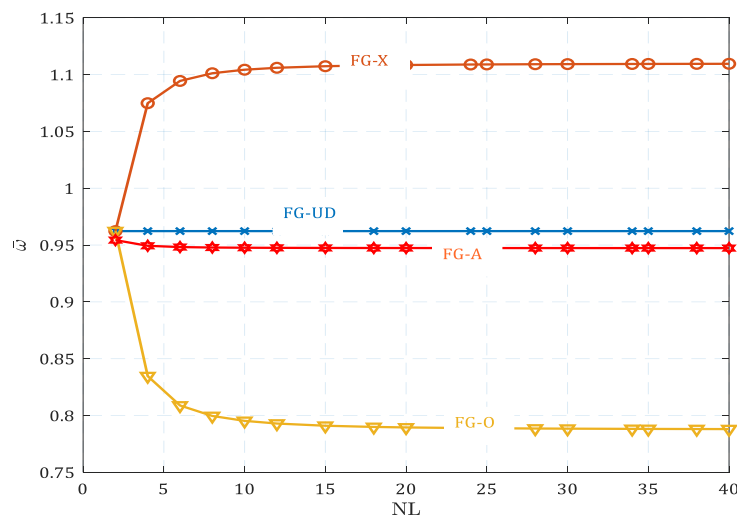
Figure 5. Nondimensional frequency in terms of total number of layers NL for various GPLs shapes.

In Fig.6 the free vibration curve for graphene layered composite beam has been depicted based on FG-X shape of graphene dispersion under different boundary conditions, namely S-S, C-C, C-S at L/h=5.
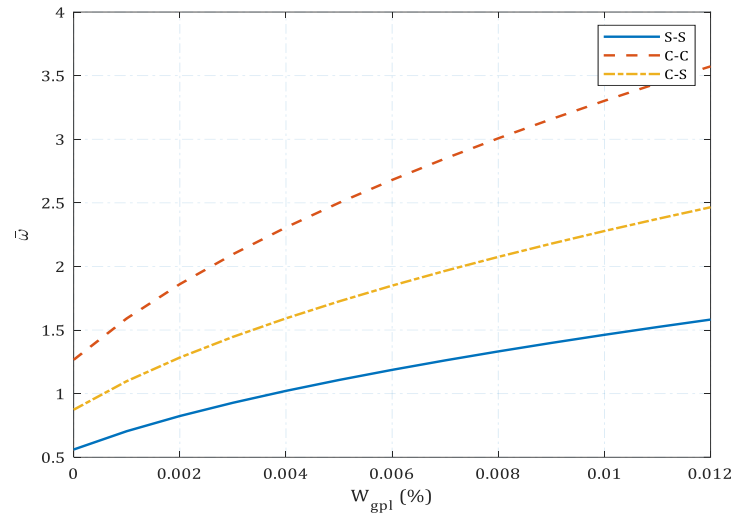
Figure 6. Effect of various boundary conditions on Nondimensional frequency of X-GPLRC beams.

It can be seen that, enforcing more constraints at the edges leads to a rise in the flexural rigidity of GRLC beam and gives a larger natural frequency. Hence, the C-C GPLs beam provides greater natural frequency folowed by C-S and S-S.

Conclusion

In the present manuscript, free vibration exploration of multilayer functionally graded graphene platelets reinforced composite (FG GPLRC) Euler-Bernoulli beams model was provided based on finite element approach. Several dispersions have been considered and investigated for the through-the-thickness distribution of graphene nanoplatelets. The effective Young's modulus, mass density and Poisson's ratio have been computed by means of the Halpin-Tsai model and the rule of mixture, respectively. The following remarks can be deduced:

- The growth slenderness ratios yields to a decrement in the non-dimensional frequency.
- It is shown that, pattern *X* reinforcement with more GPLs distributed near the surface layers gives the higher values of natural frequencies compared to others dipersions.
- Increase of graphene weight fractions leads to a dramatic enhacment in structural rigidity which leads to higher frequecies.
- The effects of GPL content and geometry have a signficant impact on vibration characteristic.
- The total number of plies does not affects the results with a number of layers N_L more than 15 for all FG-GPLs dipersions.

References

Novoselov, K.S., Geim, A.K., Morozov,S.V., Jiang, D., Zhang, Y., Dubonos, S.V., Grigorieva, I.V., Firsov, A.A. (2004). Electric field effect in atomically thin carbon films, *Science*., vol. 306 (5696), (pp. 666–669).

Rafiee, M.A., Rafiee, J., Wang, Z., Song, H., Yu, Z and Koratkar, N. (2009). Enhanced mechanical properties of nanocomposites at low graphene content, *ACS Nano*, vol. 3, (pp. 3884-3990).

Song, M., Yang, J., Kitipornchai, S., and Zhu, W. (2017). Buckling and postbuckling of biaxially compressed functionally graded multilayer graphene nanoplatelet-reinforced polymer composite plates, *Int. J. Mech. Sci*.,vol. 131, (pp. 345-355).

Shen, H.S., Xiang, Y., and Lin, F. (2017). Nonlinear bending and thermal postbuckling of functionally graded graphene-reinforced composite laminated beams resting on elastic foundations, *Eng. Struct*., vol. 140, (pp. 89-97).

Kiani, Y., and Mirzaei, M. (2018). Enhancement of Non-linear Thermal Stability of Temperature Dependent Laminated Beams with Graphene Reinforcements, Compos. Struct, vol. 186, (pp. 821-832).

Yang, J., Wu, H., and Kitipornchai, S. (2017) Buckling and postbuckling of functionally graded multilayer graphene plateletreinforced composite beams, Compos. Struct, vol. 161, (pp.111-118).

Wu, H., Kitipornchai, S., and Yang, J. (2017) Thermal buckling and postbuckling of functionally graded graphene nanocomposite plates, Mater. Des., vol. 132, (pp. 430-441).

Feng,C., Kitipornchai, K., Yang,   J. (2017). Nonlinear bending of polymer nanocomposite beams reinforced with non-uniformly distributed graphene platelets (GPLs), Compos. Part B Eng, vol. 110, (pp.132–140).

Kitipornchai, K., Chen, D., and J. Yang,J. (2017). Free vibration and elastic buckling of functionally graded porous beams reinforced by graphene platelets, Mater. Des., vol. 116,(pp. 656 665).

Chen, D., Yang, J., Kitipornchai, K. (2017). Nonlinear vibration and postbuckling of functionally graded graphene reinforced porous nanocomposite beams, Compos. Sci. Technol. vol. 142, (pp.235–245).

Arefi, M., Bidgoli, E.M.R., Dimitri, R., Biocciocchi, M., Tornabene, F. (2019) Nonlocal bending analysis of curved nanobeams reinforced by graphene nanoplatelets, Compos. Part B: Eng., vol. 166, (pp. 1-12).

Wu, H., Yang, J., and Kitipornchai, S. (2017). Dynamic instability of functionally graded multilayer graphene nanocomposite beams in thermal environment, Comp. Struc., vol. 162, (pp.244-254).

Bensaid, I., and Saimi, A. (2022). Dynamic investigation of functionally graded porous beams resting on viscoelastic foundation using Generalised differential quadrature method, Aus. J. Mech. Eng. (pp.1-21).

Vo, T.P., and Thai, H.T. (2012) Static behaviour of composite beams using various refined shear deformation theories, Composite Structures,vol. 94 (8), (pp. 2513–2522).

Ebrahimi, F., Ghasemi, F. and Salari, E. (2016), Investigating thermal effects on vibration behavior of temperature-dependent compositionally graded Euler beams with porosities, Meccanica, 51, (pp.223-249).

Simsek, M. (2010), Fundamental frequency analysis of functionally graded beams by using different higherorder beam theories, Nucl. Eng. Des, 240(4), (pp.697-705).

Study Through Molecular Techniques of Viral Respiratory Infections of SARS Cov-2, RSV, Influenza A And Influenza B During Jan. 2023 – Jan. 2024 In A Group Population of Albania

Migena Nezha

University of Tirana, Albania, https://orcid.org/0009-0005-1730-2958

Anila Mitre

University of Tirana, Albania, https://orcid.org/0000-0001-7361-7106

Abstract: Respiratory viruses commonly cause illness such as flu, COVID-19, and respiratory syncytial virus (RSV), especially in the fall and winter. The COVID-19 (also known as the coronavirus pandemic), caused by Severe Acute Respiratory Syndrome Coronavirus 2 (SARS-CoV-2), began with an outbreak in Wuhan, China, in December 2019 and caused million deaths. On the other hand, presence of other viruses such influenza (flu) and respiratory syncytial virus (RSV) manifest similar illness and may include fever, cough, and shortness of breath. Because of symptoms similarity, it can be difficult to distinguish between illnesses caused by respiratory viruses. To diagnose a potential case, healthcare professionals are using several diagnostic tests which they differ from their detection method such antigenic, serologic up to molecular diagnostics. In this review we will discuss about this situation describing and analyzing the viral respiratory tract viruses through different molecular techniques.

Keywords: COVID19, RSV, Influenza A, Influenza B, detection methods

Introduction

Respiratory infections are the most widespread cases of infections. The disease is mainly limited to the upper respiratory tract, but a small percentage can also progress to the lower respiratory tract (Moriyama et al .,2020). Children and the elderly are the most risk ages. According to Centers for Disease Control and Prevention (CDC) website (www.cdc.gov), every child up to two years of age has an average of 4 to 6 episodes of upper respiratory tract infection. A group of viruses that can cause respiratory tract infections are families ortho and paramyxoviridae, picornoviridae, coronavirus and adenoviruses. Respiratory diseases are important causes of

morbidity and mortality throughout the world. Every year, according to the World Health Organization (www.who.int), they are accompanied by more than 7.6 million deaths.

Severe Acute Respiratory Syndrome, Coronavirus 2 (SARS-CoV-2) named before 2019-nCoV, belong to the family coronavirus and SARS-CoV is classified in the sort of Beta coronavirus. It has emerged as the most consequential global health crisis since the era of the influenza pandemic of 1918 (Cascella et., 2023). At the end of 2019, SARS -CoV -19 was identified as the causative pathogen of accumulated cases of pneumonia of unclear origin. The virus caused a wave of infection that spread rapidly throughout the world and was declared a pandemic by the WHO at the beginning of 2020. In February 2020, the disease caused by SARS -CoV-2 was named COVID-19 by the WHO. Like other RNA viruses, SARS-CoV-2 adapts with genetic evolution and developing mutations. This results in mutant variants that may have different characteristics than their ancestral strains. Several variants of SARS-CoV-2 have been described during the course of this pandemic, among which only a few are considered variants of concern (VOCs).

Influenza A and B cause respiratory tract infections (seasonal viruses) which circulate throughout the world. The annual influenza epidemic differs in the level of symptoms according to the country depending on the climate, as a result, the number of affected is different, in different countries (Krammer et al., 2018).

In the early disease stage, COVID-19 and influenza cannot be distinguished based on clinical symptoms. In the same way, infections with influenza viruses A and B cannot be clinically delimited. In the following table, the clinical characteristics of infections with SARS-CoV-2 and influenza viruses A and B are summarized:

Table 3. Summarised comparison between SARS CoV-2, Influenza A and Influenza B virus infection (Cit. EUROIMMUN, Instructions of Use).

	SARS-CoV-2	**Seasonal influenza viruses**
Transmission through	Droplets, also aerosols and smear infection.	
Highest infectiousness	Usually shortly before onset of symptoms	After onset of symptoms
Incubation period	2 – 14 days	1 – 4 days
Risk factors for a severe course	Risk increases with increasing age Adiposis, high blood pressure, chronic diseases	Younger than two years and older than 65 years of age Immunosuppression, pregnancy, adiposis, chronic disease
Most frequent disease symptoms	Fever, chills, headache, muscle pain, dry cough, shortness of breath, fatigue, olfactory loss.	Fever, chills, headache, muscle pain, cough, sputum, stuffed nose, sore throat, fatigue.
Peak of the disease	2nd or 3rd week	Within 3 to 7 days

Materials and Methods

1500 swab samples have been collected during January 2023-January 2024 into four different areas around Albanian state. For each sample we have filled a questionnaire about their symptoms and clinical anamnesis prescribed from medical doctor of healthcare center. Every patient has been notified about the study and the aim and once they accept to use their data, we have continued with sampling.

After samples collection, RNA purifying procedure was performed from Qiagen Viral RNA Mini Kit with instructions followed as described on instructions of usage (IFU). Testing of these viral stains is performed EURORealTime SARS CoV-2 and Influenza A / B (EUROIMMUN, Lubeck, Germany) and steps performed as described on the IFU. Regarding IFU the test is based on a one-tube reaction comprising reverse transcription (RT) to convert viral RNA into complementary DNA (cDNA) followed by PCR amplification and fluorescence-based real-time detection of two defined sections within the ORF1ab- and N-genes of the SARS-CoV-2 genome as well as one defined section each in the genomes of influenza virus types A and B.

Reverse transcription, amplification and detection of cDNA of SARS-CoV-2 and influenza virus types A and B are carried out by means of SARS-CoV-2-specific primers and probes. The test contains an internal amplification control which serves as an inhibition control and can additionally be used as an extraction control. The test kit includes a SARS-CoV-2/influenza A/B positive control that is used as an external control in every test run. Other data have been exported into excel for further analysis that will be discussed next.

Results and Discussion

The year 2023 began with a significant wave of cases of respiratory tract infections, including a combination of viruses such as Influenza A and B, COVID-19, and respiratory syncytial virus (RSV). As mentioned by National Foundation for Infectious Diseases (www.nfid.org), respiratory infections, including those classified as SARS-CoV-2 and influenza, have shown similar symptoms, including fever, fatigue, and cough, making differential diagnosis essential in the proper management of patients. Clinical symptoms of COVID-19 and Influenza are often difficult to distinguish based on clinical presentations, therefore testing advanced methods such as PCR has taken a central role (Farfour et al., 2022).

To cope with the spread of these viral infections and to help in the treatment of infection, the Polymerase Chain Reaction (PCR) testing has taken on great importance. According to Cobo (2012), this method is sensitive and specific compared to other diagnostic tests, being a key tool to correctly identify the type of virus and guide therapy. Through this method, testing can not only distinguish between viral infections but can also identify the exact subtypes of specific virus variants, which have implications for disease prevention and treatment.

Out of 1500 tampons tested, 292 turned out to be positive cases with COVID 19, which were then grouped

based on age and gender. The division by gender resulted in 117 men and 175 women positive with COVID 19, while by age in an irregular distribution of cases (Fig. 1).
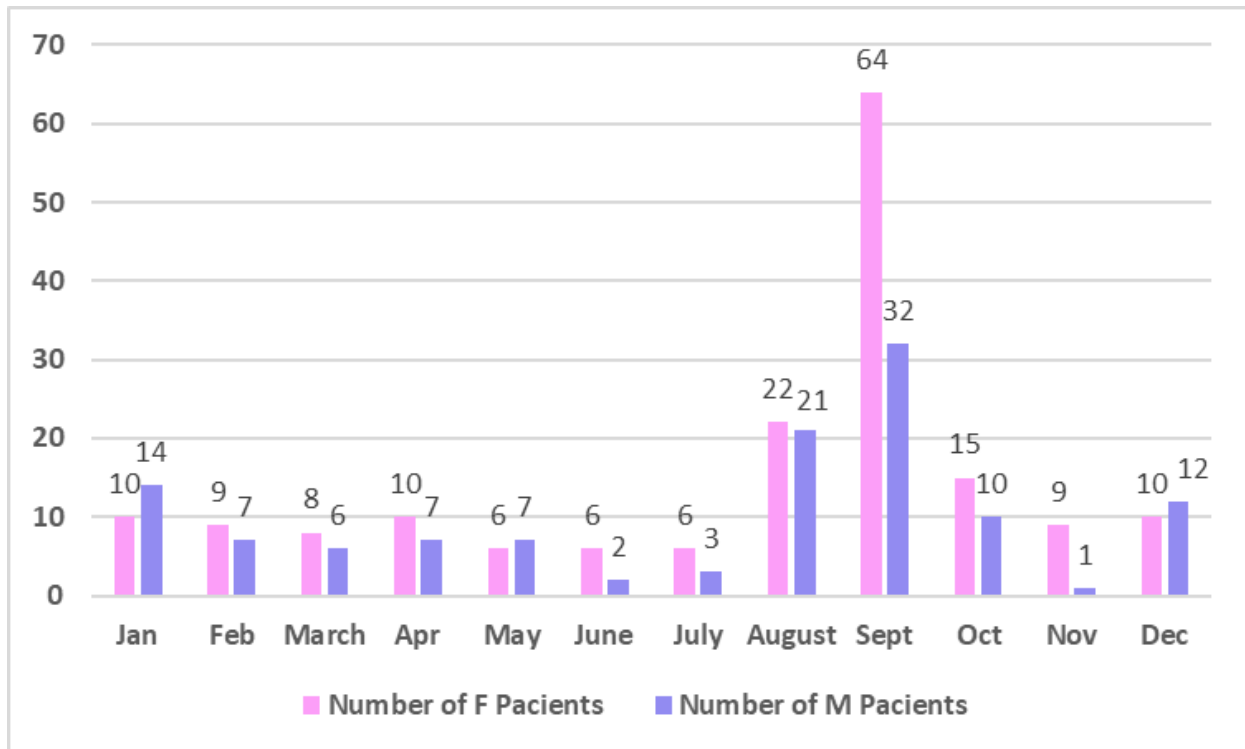
Figure 8. Number of COVID19 positive cases during 2023 separated by gender.

The tests performed to confirm the presence of the SARS-CoV-2 virus were carried out during the months of January 2023-January 2024. During these months, has been a change in the number of tests performed, compared to the number of tests with positive results, confirming the presence of the virus. The month of September marks the highest number of positive SARS-CoV-2 tests and we have a predominance of the female sex (Fig1).

The viability of the virus in the environment is influenced by several factors, including climatic parameters such as humidity and temperature. Temperature has been proposed as a factor that affects SARS-CoV-2 transmission. Previous studies found that the temperature affected the transmission of the SARS-CoV-2 in which high environmental temperature reduced the number of COVID-19 cases. This is the reason why June and July are the months with the lowest number of cases.

The relationship between COVID-19 and atmospheric temperature has been extensively researched worldwide. During these years, understanding the impact of seasonal temperature changes on virus transmission was an important factor in reducing the spread of the virus.
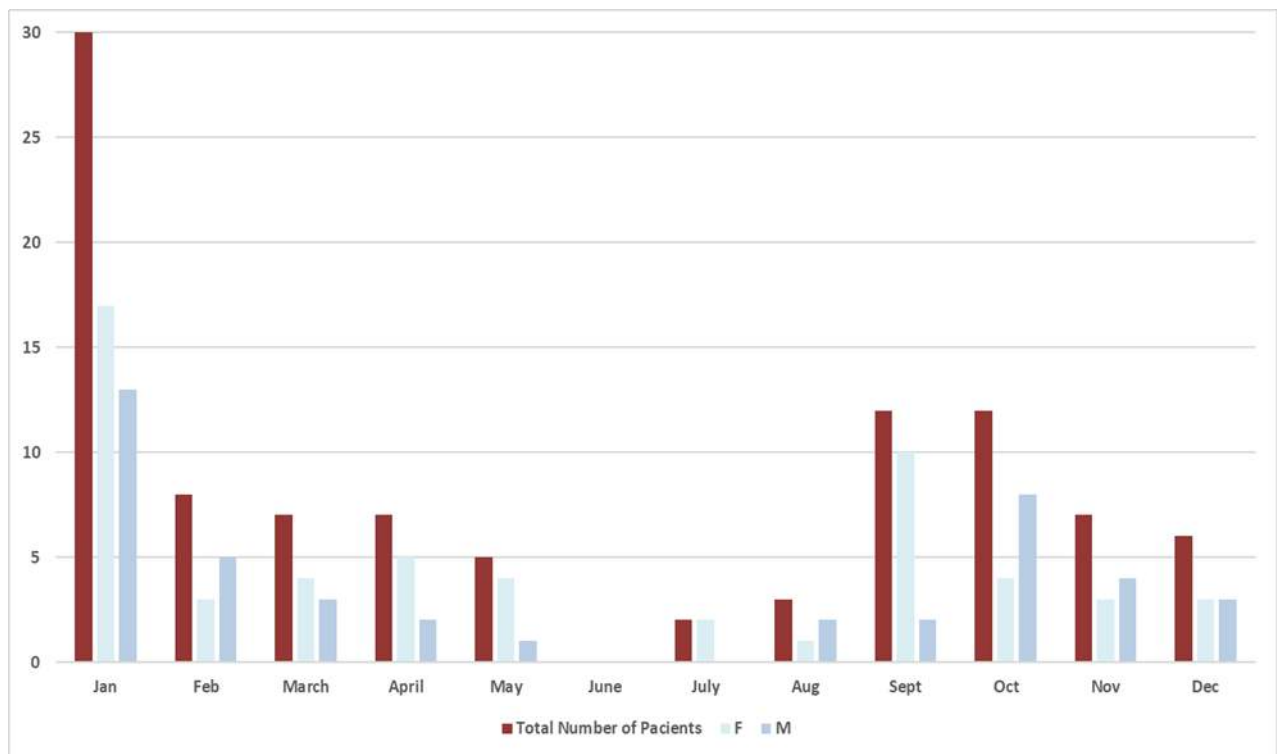
Figure 9. Graph illustration of total positive Influenza A patients during 2023.

Both type A and B influenza viruses regularly spread among people and are responsible for seasonal flu each year. The disease occurs throughout the year with a greater frequency during the winter due to the lower resistance of the mucous membranes of the respiratory organs and the greater presence of people in narrow spaces and close to each other due to the cold weather (Uyeki et al.,2022). From 100 positive cases with Influenza A, the division by gender resulted in 43 men and 57 women positive with Influenza A (Fig. 2). Even in the case of Influenza A, we have a predominance of the female sex, as in cases with Covid 19. During June, no case of Influenza A was identified, while in July and in August, the number of cases were low. The largest number of cases appears in January and is dominated by the female sex.

Influenza B virus, which also causes acute respiratory infections, has increased in prevalence in recent years. Influenza viruses can spread to others before and after a person shows signs and symptoms of being sick. In the case of Influenza B, we have a predominance of the male sex, in contrast to Covid 19 and Influenza A. From the data analysis, there were 39 positive cases with Influenza B, which were then grouped based on age and gender.

The division by gender resulted in 22 men and 17 women positive with Influenza B (Fig 3). The largest number of cases appears in January and is dominated by the male sex. But a larger number of people affected by this virus appears from January to April. Then a decrease is noticed and during the three months of summer (with the increase of temperatures) no cases of Influenza B have been identified.

Respiratory Syncytial Virus is the most common virus that causes lower respiratory tract infection in infants and

young children worldwide (Jain et al., 2023). RSV is mainly transmitted by droplet or direct contact and the population is generally susceptible. People of all ages are susceptible to RSV, but symptoms vary. Infants (especially infants aged 2 - 6 months) are very sensitive to RSV, which often causes serious respiratory diseases such as bronchiolitis and pneumonia. It is the most common cause of bronchiolitis and pneumonia in children younger than 1 year of age.
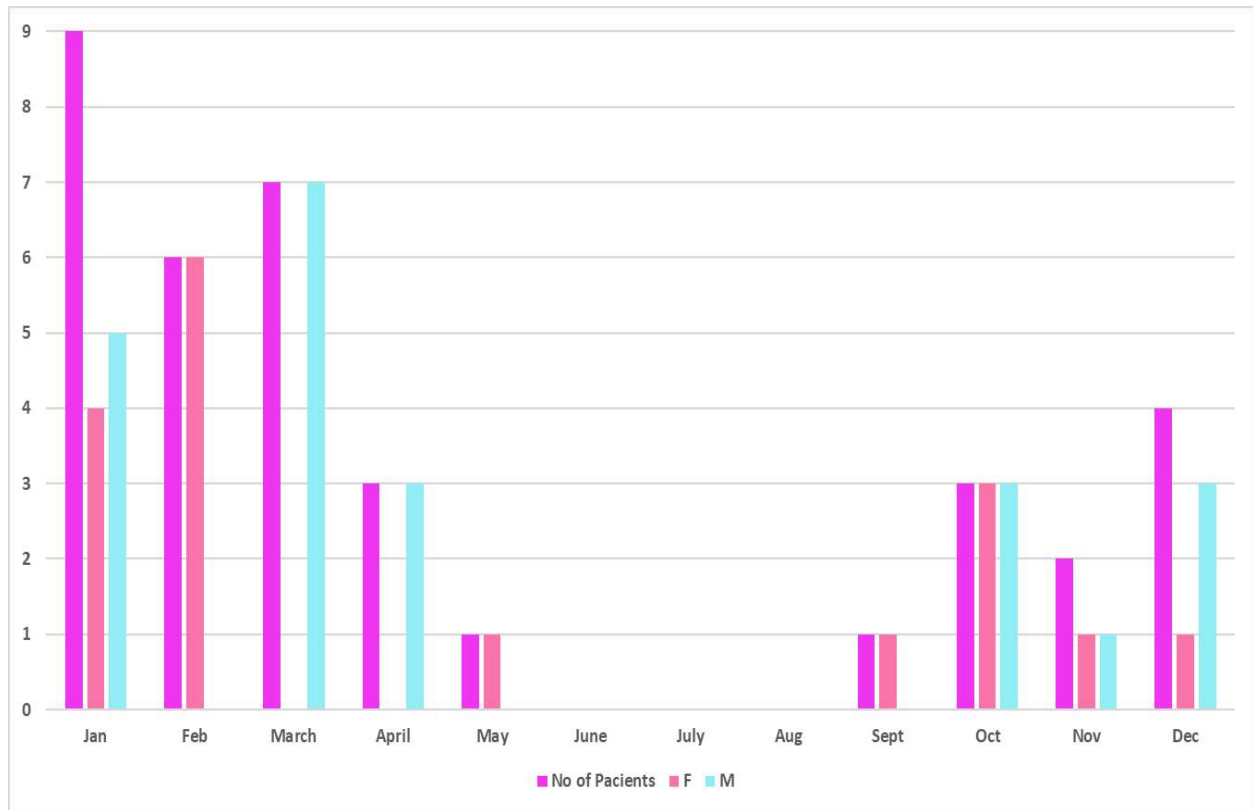
Figure 10. Illustration of Influenza B positive cases during 2023.

Virtually all children will have been infected with RSV by the age of two, and reinfections are common throughout life (Shi et al., 2019) . Since antigenic variation, which is frequently observed among other respiratory viruses such as SARS-CoV-2 or influenza viruses, can only be observed for RSV to a limited extent, reinfections may result from short-term or incomplete immunity.

After decades of research, two RSV vaccines were approved to prevent lower respiratory tract infections in older adults. Recently, the FDA approved a vaccine for active vaccination of pregnant women to prevent severe RSV disease in infants during their first RSV season.

RSV appear with the smallest number of cases, there is not a difference between the sexes and the peak season is from November to April (Fig. 4).
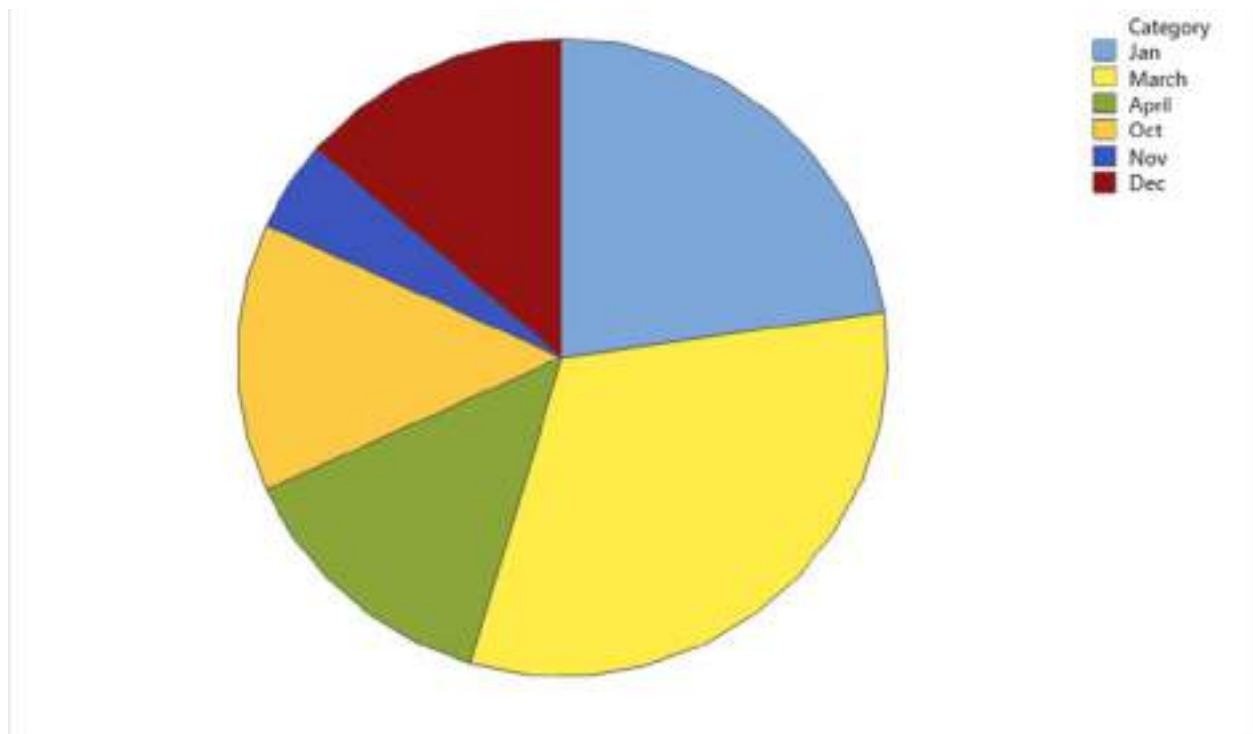
Figure 11. Pie Chart that shows total positive cases of RSV positive patients.

Conclusion

The emergence of different variants of SARS-CoV-2 has further challenged the world's health systems, including the need for repeated vaccinations and the development of new treatments to combat the new variants. While advances in PCR testing have improved diagnostic capabilities, accuracy in the proper treatment of respiratory tract infections requires a deep understanding of the differences between these viruses, to ensure patient recovery and to prevent potential complications.

References

Cascella, M., Rajnik, M., Aleem, A., Dulebohn, S. C., & Di Napoli, R. (2023). Features, Evaluation, and Treatment of Coronavirus (COVID-19). In StatPearls. StatPearls Publishing.

Cobo, F. (2012). Application of Molecular Diagnostic Techniques for Viral Testing. The Open Virology Journal, 6, 104–114. https://doi.org/10.2174/1874357901206010104

Duncan, Krammer, F., Smith, G. J. D., Fouchier, R. A. M., Peiris, M., Kedzierska, K., Doherty, P. C., Palese, P., Shaw, M. L., Treanor, J., Webster, R. G., & García-Sastre, A. (2018). Influenza. Nature reviews. Disease primers, 4(1), 3. https://doi.org/10.1038/s41572-018-0002-y

Farfour, E., Yung, T., Baudoin, R., & Vasse, M. (2022). Evaluation of Four Fully Integrated Molecular Assays for the Detection of Respiratory Viruses during the Co-Circulation of SARS-CoV-2, Influenza and RSV. Journal of Clinical Medicine, 11(14), 3942–3942. https://doi.org/10.3390/jcm11143942

Jain, H., Schweitzer, J. W., & Justice, N. A. (2023). Respiratory Syncytial Virus Infection in Children. In StatPearls. StatPearls Publishing.

Moriyama, M., Hugentobler, W. J., & Iwasaki, A. (2020). Seasonality of Respiratory Viral Infections. Annual Review of Virology, 7(1). https://doi.org/10.1146/annurev-virology-012420-022445

Nam, H. H., & Ison, M. G. (2021). Respiratory Syncytial Virus. Seminars in respiratory and critical care medicine, 42(6), 788–799. https://doi.org/10.1055/s-0041-1736182

Prasad, S., Lownik, E., & Ricco, J. A. (2016). Viral Infections of the Respiratory Tract. Springer EBooks, 507–517. https://doi.org/10.1007/978-3-319-04414-9_41

Shi, T., Ooi, Y., Zaw, E. M., Utjesanovic, N., Campbell, H., Cunningham, S., Bont, L., Nair, H., Nair, H., Campbell, H., Shi, T., Zhang, S., Li, Y., Openshaw, P., Wedzicha, J., Falsey, A., Miller, M., Beutels, P., Bont, L., & Pollard, A. (2019). Association Between Respiratory Syncytial Virus-Associated Acute Lower Respiratory Infection in Early Life and Recurrent Wheeze and Asthma in Later Childhood. The Journal of Infectious Diseases, 222(Supplement_7), S628–S633. https://doi.org/10.1093/infdis/jiz311

Uyeki, T. M., Hui, D. S., Zambon, M., Wentworth, D. E., & Monto, A. S. (2022). Influenza. The Lancet, 400(10353), 693–706. https://doi.org/10.1016/s0140-6736(22)00982-5

Effect of Partial Shading on Photovoltaic Systems and Strategies for Power Maximization

Ben Si Ali Nadia

LEA Laboratory, Badji Mokhtar Annaba university, Annaba, Algeria, https://orcid.org/0000-0001-7248-4823

Benalia Nadia

LEA Laboratory, Badji Mokhtar Annaba university, Annaba, Algeria, https://orcid.org/0000-0003-4819-5313

Zerzouri Nora

LEA Laboratory, Badji Mokhtar Annaba university, Annaba, Algeria, https://orcid.org/0000-0003-1209-4617

Abstract: Traditional energy sources, involving coal, petrochemicals, natural gas, fossil fuels, and others, run out and break down quickly. They additionally cause negative impacts on the environment, which is why sustainable energy sources (SES) are required. Photovoltaic (PV) systems, increasingly used as sustainable energy sources, can face significant efficiency challenges due to partial shading. Integrating bypass diodes allows current to bypass shaded cells, mitigating the effects of partial shading and reducing hot spot formation. Arranging panels and Utilizing micro inverters can improve performance in shaded conditions, as each panel operates independently, reducing mismatch losses. Mathematical models and simulation tools are used to assess the impact of shading on PV systems. The use of PV system simulation software allows for detailed analysis of different shading scenarios and their effects on energy yield. This paper investigates the effects of partial shading on PV system performance and discusses strategies for power maximization, with a focus on optimization techniques. The performance of the proposed techniques used in this work, was rigorously evaluated by comparing their efficiency, tracking error, using Matlab/Simulink software. The article is structured as follows: Section 1 describes the proposed system; Sections 2 and 3 present modeling and simulation of the PV system and step up converter, respectively; and Section 4 presents the proposed PSO-Based MPPT Algorithm, as well as its MATLAB/Simulink Simulation results and discussion. Section 6 conclusion.

Keywords: Sustainable energy, Solar energy, Partial shading, MPPT.

Introduction

Solar energy is a powerful resource, and photovoltaic technology allows us to harness this energy and convert it into electrical power using semiconductor materials. Solar arrays' output characteristics are nonlinear. They also fluctuate based on sunlight irradiation and temperature. To solve these issues, many traditional MPPT approaches were applied. Various control methods exist, including perturb and observe (P&O) (Aghaei, S., et al 2022), (Ben Si Ali, N et al, 2018), incremental conduction (INC) (Alshahrani, M., & Raza, A. 2023), (Mitchell et al, 2017). hill climbing (Ben Si Ali, N., et al,2023), (Jately, V., Azzopardi et al, 2021), fuzzy logic control search (Wang, L., et al, 2023), (Yilmaz, et al, 2018) and sliding management (Bjaoui, et al, 2019). To maximize energy production, it is crucial to ensure the efficiency of these systems. However, partial shading caused by objects like trees, buildings, or dirt on panels can lead to a significant decrease in energy output. By understanding the shading dynamics and implementing effective mitigation strategies, we can optimize the performance of photovoltaic systems and significantly increase energy production.

Basic Components and Operation

The equivalent circuit of a photovoltaic cell is shown on figure 1. A PV cell can be represented generically by a current source that is paralleled with a diode and two resistors, one of which is shunt and the other is connected in series (Chaibi, Y., et al, 2018) Olayiwola, O. I., et al, 2019).
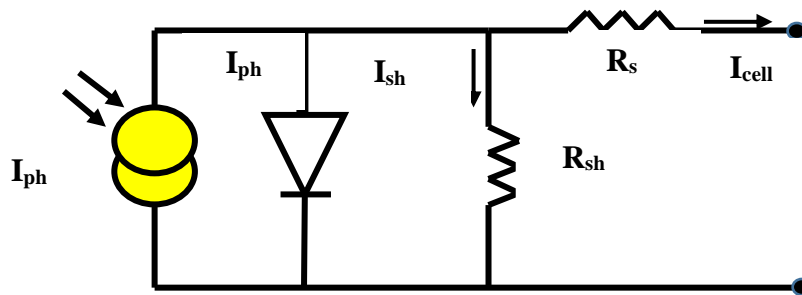
Figure 1. Solar PV cell model
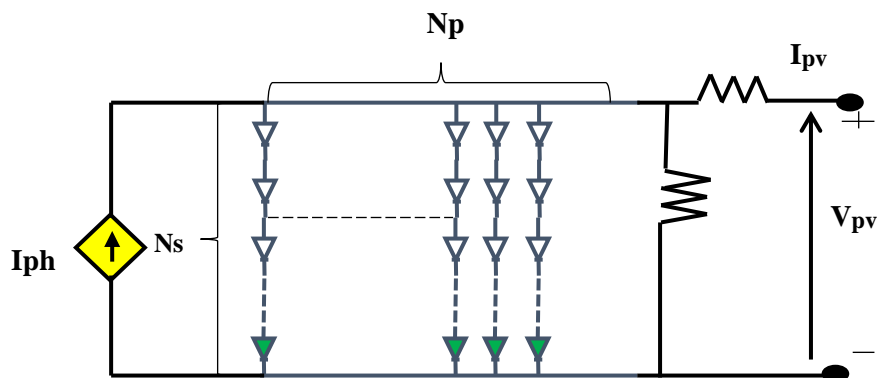
Figure 2 . Solar PV array model

A PV array is a group of several PV cells which are electrically connected in series and parallel circuits to generate the required current and voltage. Fig. 2 illustrates a basic solar photovoltaic array model.

The photovoltaic module's I-V characteristic can be defined by the following general equations:
The output current Ipv of the PV panel is given by equation (3).
Photonic generated current basically depends on irradiance and temperature.

$$I_{ph} = I_{sc} + k_i(T - T_{ref})(\frac{G}{1000}) \tag{1}$$

The short-circuit current Isc is defined by:

$$I_{sc=}I_{s=}I_{ph}$$

The module-reverse saturation current Irs and I_0 which varies with cell temperature are given by:

$$I_{rs} = I_{sc}/[\exp\left(\frac{qV_{oc}}{N_s knT}\right) - 1] \tag{2}$$

$$I = I_{ph} - I_s\left(e^{\frac{q(V+IR_s)}{nKT_c}} - 1\right) - \frac{V + IR_s}{R_{sh}} \tag{3}$$

Maximum Power Point Tracking (MPPT) is a technique used in photovoltaic (PV) systems to optimize the energy output of solar panels. PV systems rely on converting sunlight into electrical energy, and the amount of energy produced depends on various factors such as the angle of incidence of the sunlight, irradiation, and temperature. The MPPT technology, a dynamic process, maximizes the power output of solar panels by continuously tracking and adjusting the operating point of the PV system to extract the maximum power available from the panels at any given time. Usually, an adaptation stage DC-DC converter is used to extract the maximum power available at the terminals of the photovoltaic module and transfer it to the load at all times. The proposed model incorporates a PV array and a step-up converter, used as an interface device connecting the PV panel to the load (Bayrak, G., et al, 2019). et al, 2019),(Prathibha, M. R., et al, 2017).

Figure 3 shows electrical characteristics of one module for atmospheric condition variations. It is clear that increased solar radiation increases the short-circuit current and maximum output power of PV cells. As temperature rises, the PV cell's open circuit voltage decreases, while the short-circuit current increases slightly. This results in an overall reduction in the maximum output power level.

.
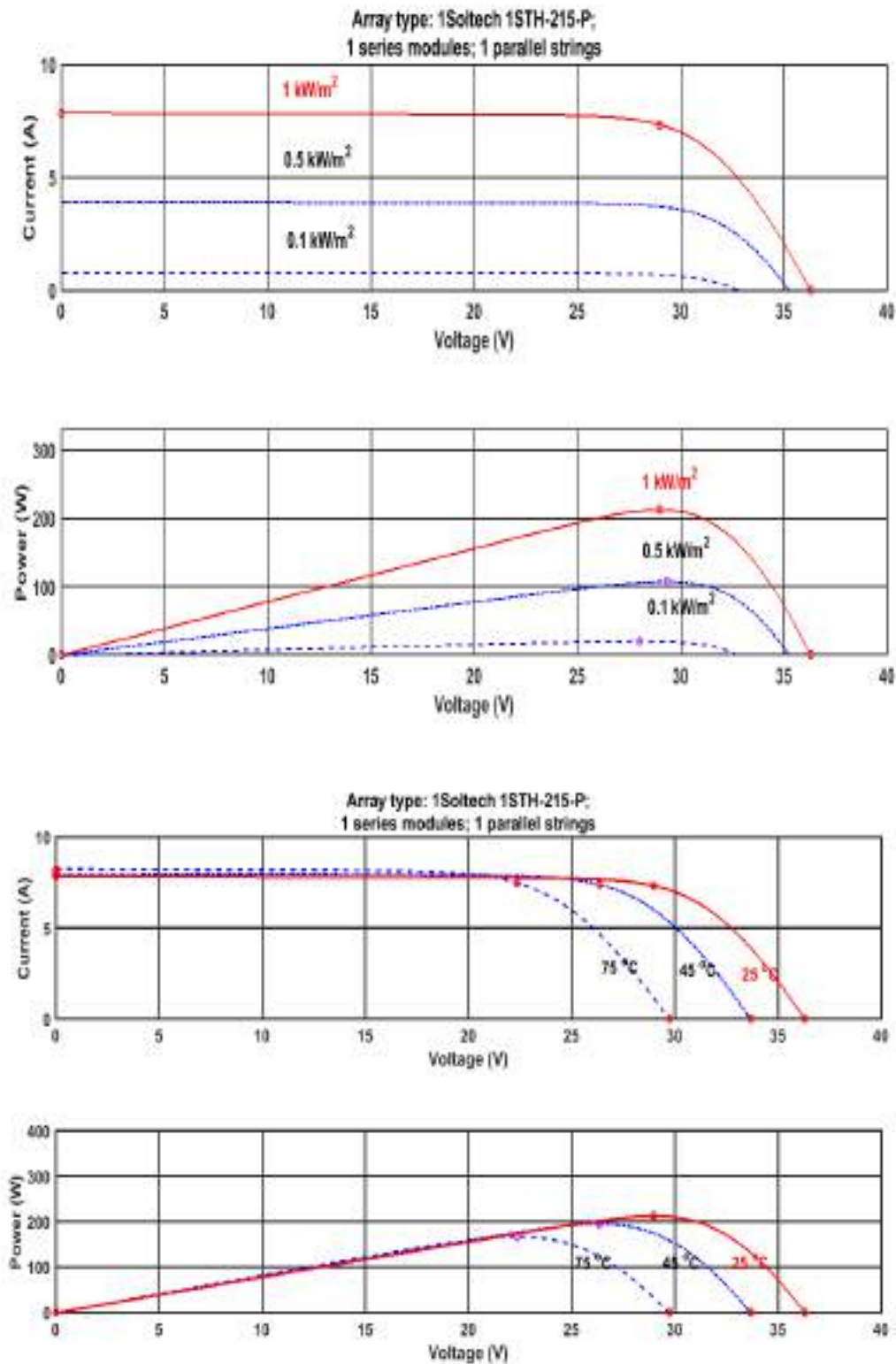
Figure 3 . P-V and I-V characteristics for irradiation and temperature variation

The PV array type simulated in Matlab/Simulink software is: **1Soltech 1STH-215-P** with one series modules and

one parallel strings. Each module is composed by 60 series cells. The various parameters of PV module are listed in Table-1.

Table 1. Parameters of The Solar Module

Parameters	Label	Value
Short circuit current	I_{SC}	7.84(A)
Open circuit voltage	V_{oc}	36.3 (V)
Current at Pmax	I_{MPP}	7.35 (A)
Voltage at Pmax	V_{MPP}	29 (V)
Maximum power	P_{MPP}	213.15 (w)

DC-DC Converter

The DC-DC converter's role is to transfer the maximum power from the module to the load. There are many topologies of DC-DC converters that are used in PV systems, like buck, boost, and buck-boost. In this paper, the boost converter is implemented. The output voltage in this case is greater than the input voltage. The boost structure parameters are given in Table 2. Relationships between input and output voltage and current are given by equation 4.

$$\frac{V_{out}}{V_{in}} = \frac{I_{in}}{I_{out}} = \frac{1}{1 - D} \tag{4}$$

Table 1 DC-DC converter parameters

Parameter	Value
Resistor R	50 Ω
Inductor L	1.147 mH
Capacitor C	460 μF

Mppt Techniques Design and Considerations

Various approaches can be used to mitigate the negative consequences of partial shading. Using optimal panel layout or integrating bypass diodes can significantly improve performances. Advanced technologies such as MPPT algorithms can optimize the output PV power by continuously adjusting the load or the duty cycle of the DC-DC converter to find the maximum power point, even under varying shading conditions. Traditional optimization methods may fall short in dynamically changing environments. Particle Swarm Optimization (PSO), inspired by social behavior in nature, offers a robust solution to navigate the complex search space of PV system parameters for optimal performance (Naseem, M., et al, 2021), (Amiri, M., et al, 2021).

Perturb and Observe P&O Technique

The Perturb and Observe (P&O) algorithm is regarded as the most popular because of its ease of use and effectiveness (Rezaei, M. M., et al, 2019), (Alik, R., et al, 2017). Each iteration involves perturbing (increasing or decreasing) the array terminal voltage and observing the impact on the PV output power, then comparing it with the previous iteration's value (Ahmad, M., et al, 2022). If the power is increased, the perturbation will continue in its current direction; otherwise, it will reverse. The operating point begins to oscillate around the maximum power point (MPP) after it is achieved. This technique presents some limitations, such as an increase in power losses as a result of the steady state condition oscillation around the MPP, particularly in the case of big steps. The (P&O) algorithm is sluggish during a quick change of atmospheric conditions. The flow chart in Figure 4, which is a summary of the P&O algorithm
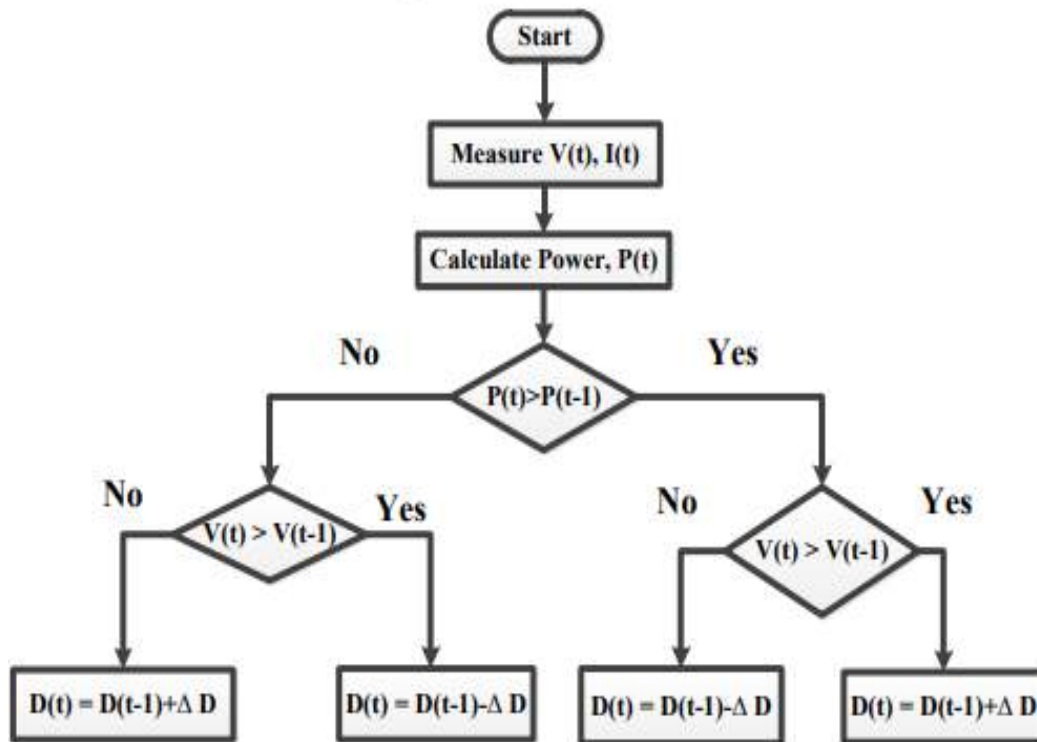
Figure 4. Flowchart of P&O algorithm

Incremental conductance (INC) technique

As shown in Figure 5, the incremental conductance approach is based on tracking the MPP based on the slope of the solar panel's output power. In this technique, the incremental conductance ($\Delta I/\Delta V$) and the instantaneous conductance (I/V) are compared. The terminal voltage of the PV array decreases if the slope of the P-V curve ($\Delta P/\Delta V$) is negative, indicating that the operating point is to the right of the MPP. If the slope is positive, the

operating point is to the left of the MPP and the terminal voltage of the PV array is raised; if the slope is zero, the MPP is attained and the instantaneous and incremental conductance are equal (Zakzouk, N. E., et al, 2016), (Rupesh, M., et al, 2018).
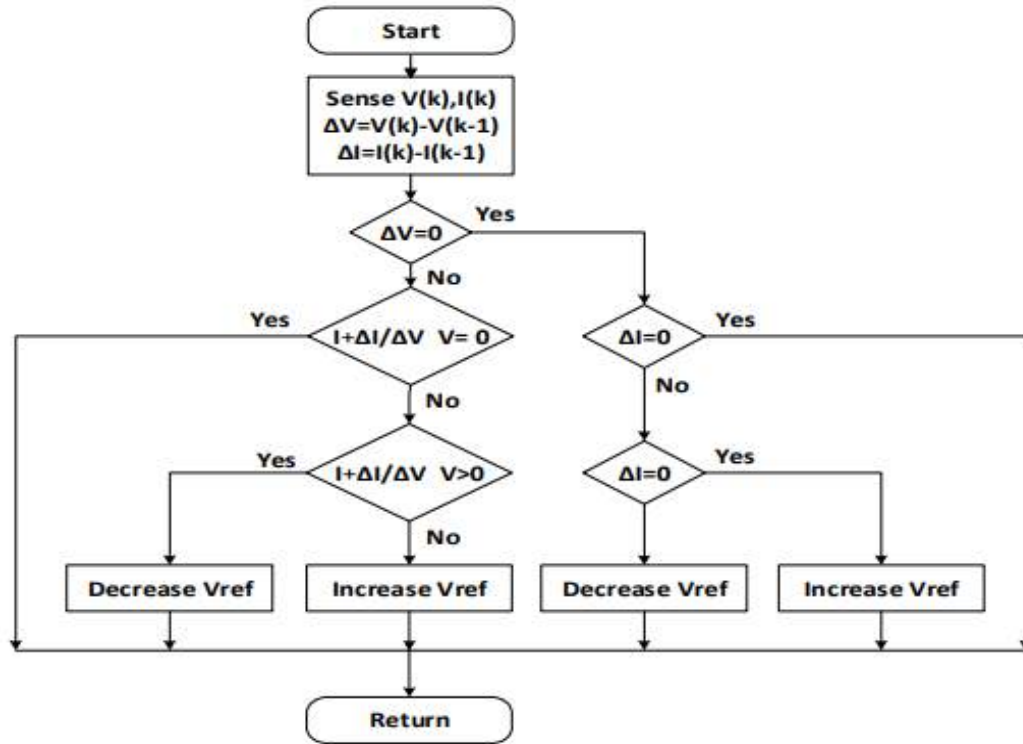
Figure 5. Incremental Conductance Algorithm Flowchart

Overview of PSO Nature Inspired Algorithm

Particle Swarm Optimization is an algorithm proposed by Kennedy and Eberhart in 1995 (Ghasemi, A., et al, 2023). It is inspired by the social behavior of swarming animals. In fact, we can observe in these animals relatively complex movement dynamics, whereas each individual has a limited "intelligence" and has only local knowledge of their situation. The particle swarm corresponds to a population of simple agents, called particles. Each particle is considered as a solution to the problem, where it has a position x_i and a velocity p_i (displacement). In addition, each particle has a memory allowing it to remember its best performance (in position and speed) and the best performance achieved by the particles of the swarm. The displacement of a particle is influenced by the following three components (Hassan, M., et al, 2023), (Ramakrishnan, V., et al, 2023).

1. A component of inertia: the particle tends to move in the same direction as it is now.
2. A cognitive component: the particle tends to move towards the best site through which it has already passed.
3. A social component: the particle tends to rely on the experience of its congeners and, thus, to take the best site already reached by the other particles.

The particle displacement strategy is illustrated on Figure 6.
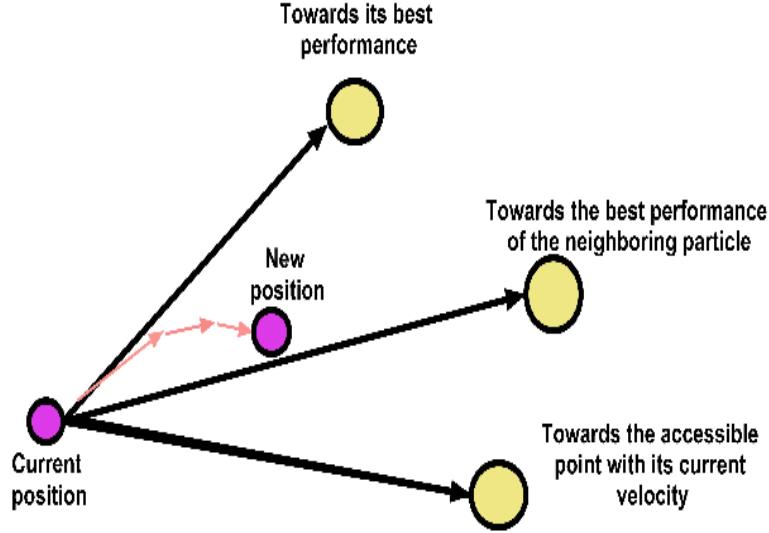
Figure 6. Particle displacement strategy

Inspired by the social and cooperative behavior of many kinds of animals in the search space, particle swarm optimization (PSO) emerged. The method uses the present search space. Equations (2) and (3) define the conventional PSO technique.

$$x_i(k+1) = x_i(k) + v_i(k+1) \tag{2}$$

$$v_i(k+1) = \omega v_i(k) + c_1 r_1 \cdot (p_{best} - x_i(k)) + c_2 r_2 \cdot (g_{best} - x_i(k)) \tag{3}$$

v_i and x_i are the velocity and position of particle i, respectively; k is the iteration number; ω is the inertia weight; r1 and r2 are random variables with values that are uniformly distributed between [0,1]; and c1, c2 are the cognitive and social coefficients. p_{besti} is the best individual position of particle i, while g_{best} is the best swarm position of all particles. If the initialization condition (4) is met, the method is adjusted as follows:

$$f(x_{ik}) > f(p_{besti}) \tag{4}$$

$$P_{besti} = x_{ik} \tag{5}$$

where f is the objective function that should be maximized (Hayder, W., et al, 2020). Figure 7 shows the flowchart of the PSO algorithm.
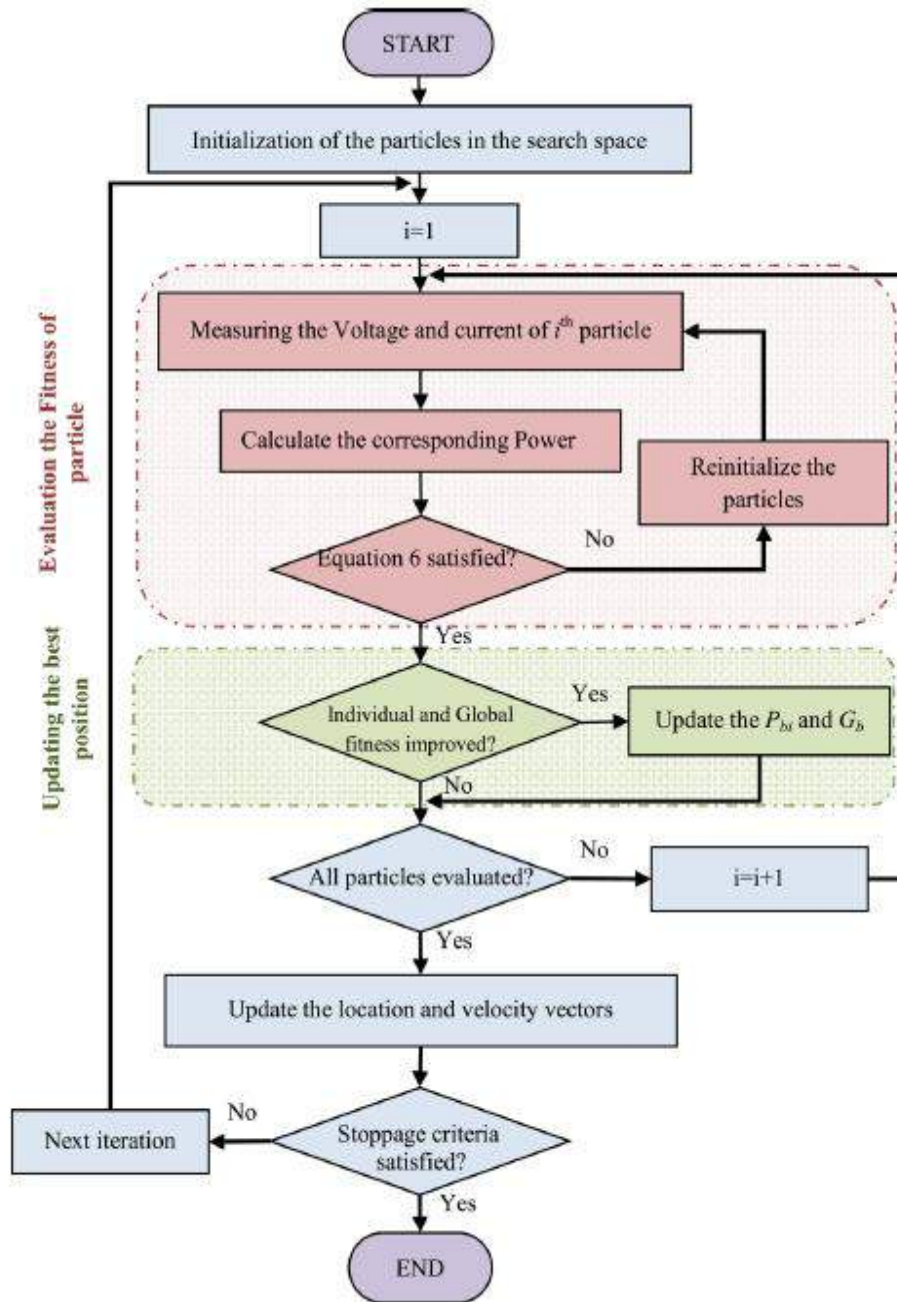
Figure 7. Flowchart of PSO algorithm

Impact of Partial Shading on PV Systems

Partial shading (PS) can have several negative effects on PV performance. In order to assess the impact of uneven shading on system efficiency, a PV system consisting of three PV modules connected in series, a DC/DC step-up converter, a resistive load, and an MPPT controller is simulated using MATLAB/Simulink software. Three different shading patterns are examined, as detailed in Table 2. Figure 8 illustrates the PV system operating under uniform irradiation and various PS patterns.

Table 2. uneven shading patterns

Irradiation (w/m^2)	Pattern 1	Pattern 2	Pattern 3
Module 1	1000	1000	800
Module2	1000	500	400
Module 3	1000	200	100

Uniform irradiation   **Partial shading Pattern1**   **Partial shading Pattern2**
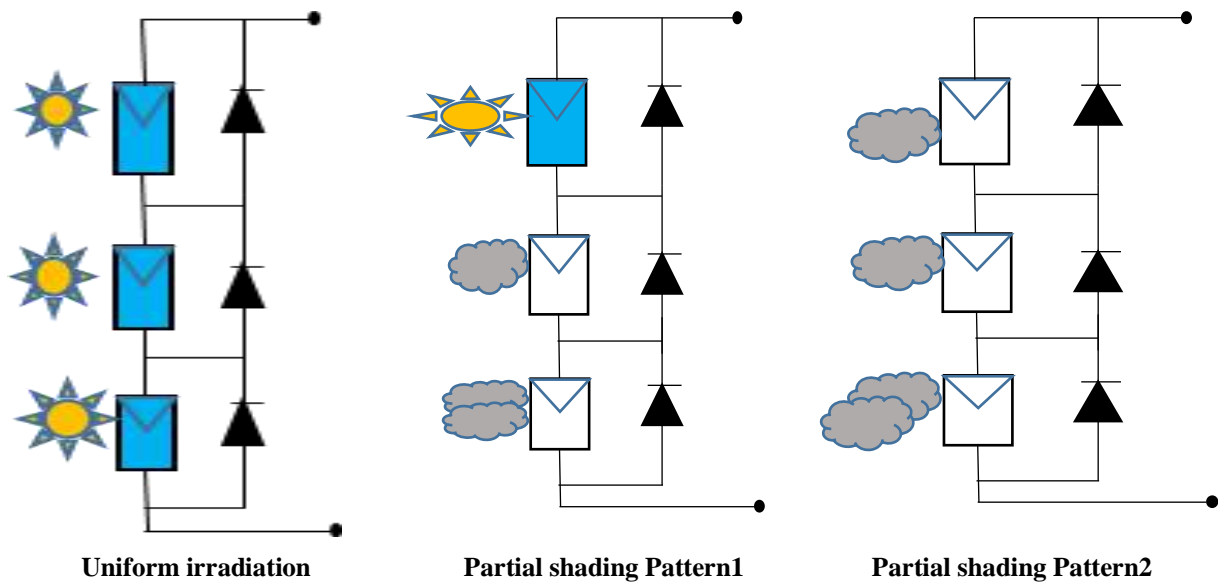
Figure 8 . PV system under uniform irradiation and different PS patterns

Simulink software is used to simulate a PV system composed of three modules, a DC/DC step up converter, a resistive load, and a controller in order to test the suggested approach's accuracy and performance. The simulation model is shown on Figure 9. Three different shading patterns are examined, as detailed in Table 2. Figure 10 illustrates the PV system operating under uniform irradiation and various PS patterns.

Table 2. uneven shading patterns

Irradiation (w/m^2)	Pattern 1	Pattern 2	Pattern 3
Module 1	1000	1000	800
Module2	1000	500	400
Module 3	1000	200	100

Electrical **P-V** and **I-V** curves for both partial shading and standard test circumstances are shown in Figure 10. It is apparent that for STC, the **P-V** curve has a single maximum point and for PSCs, there are two local maximum (**LMPP**) and one global maximum point (**GMPP**).
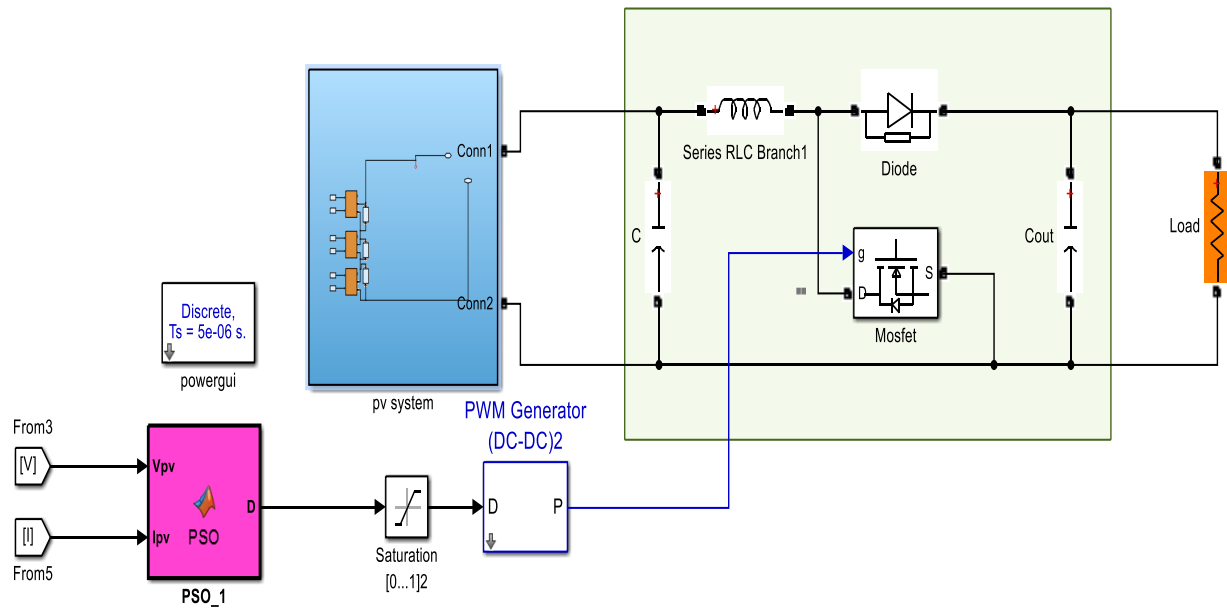
Figure 9 . Simulink model of PV system connected to the Boost converter
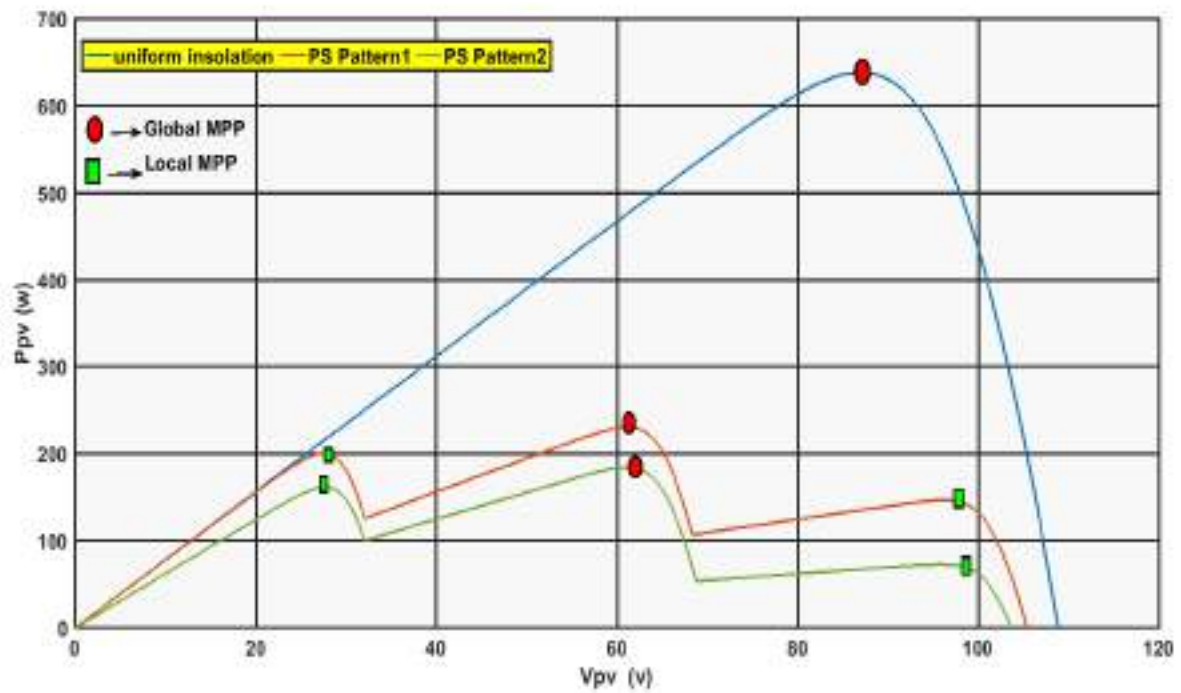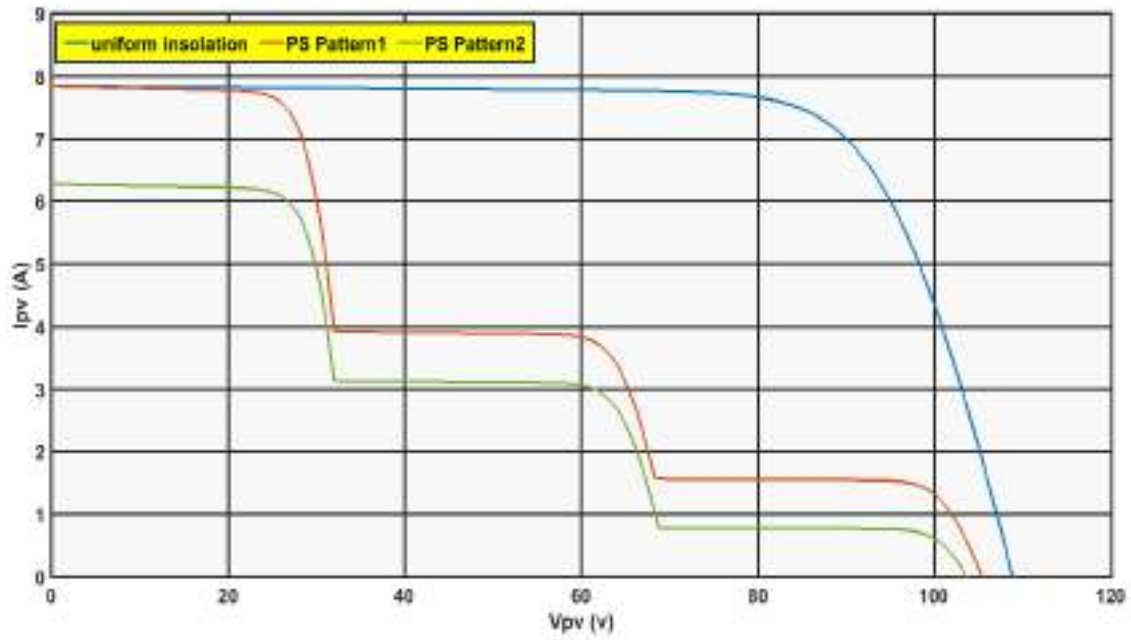
Figure 10 . P–V and I-V curves under partial shading patterns
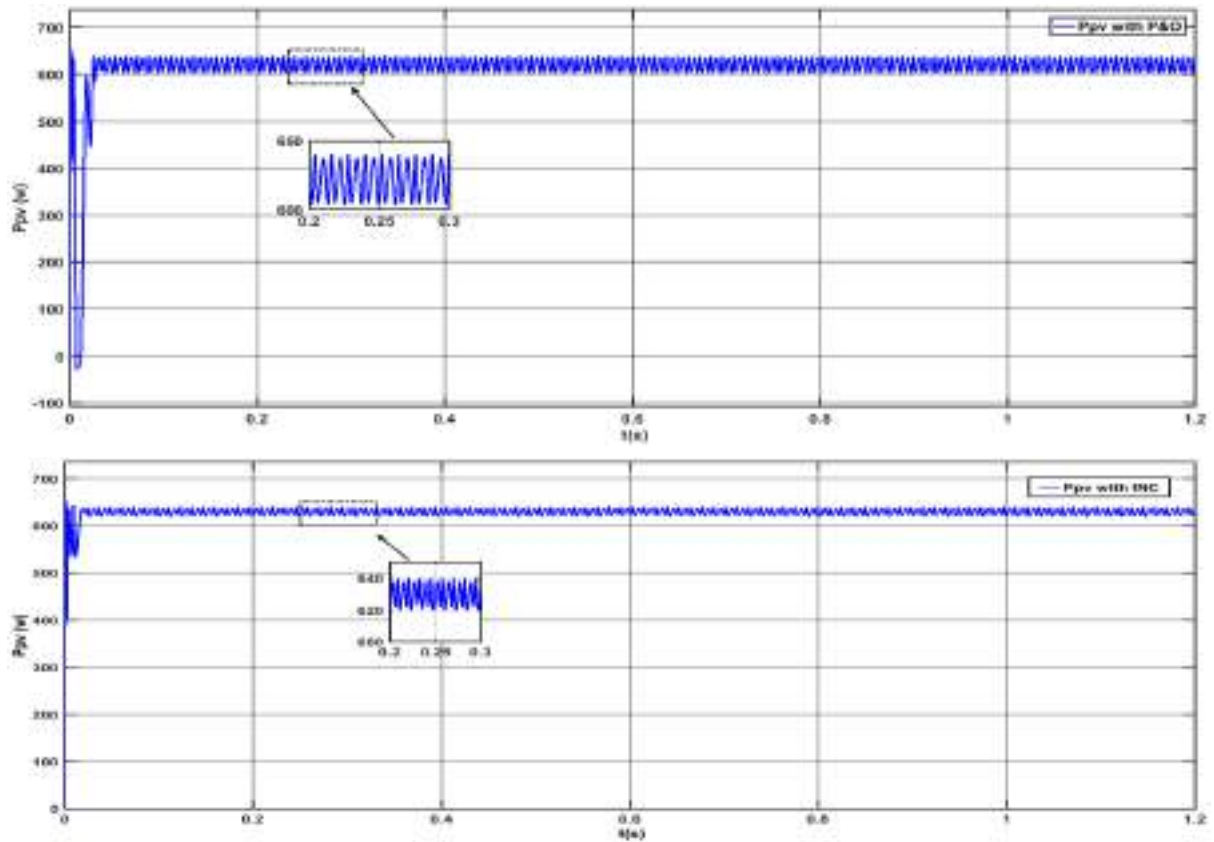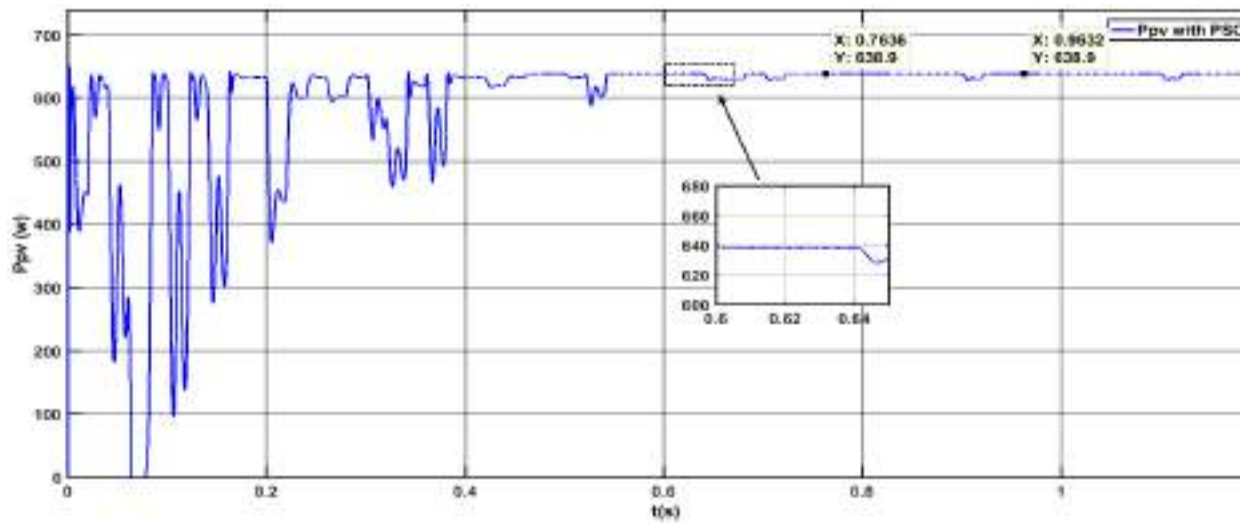
Figure 11 . PV power for standard test conditions
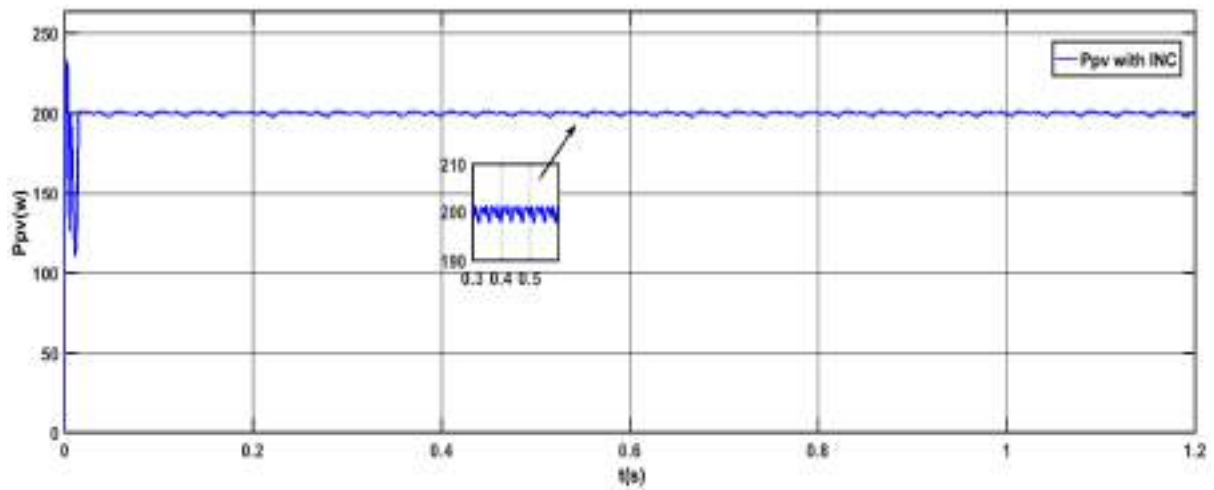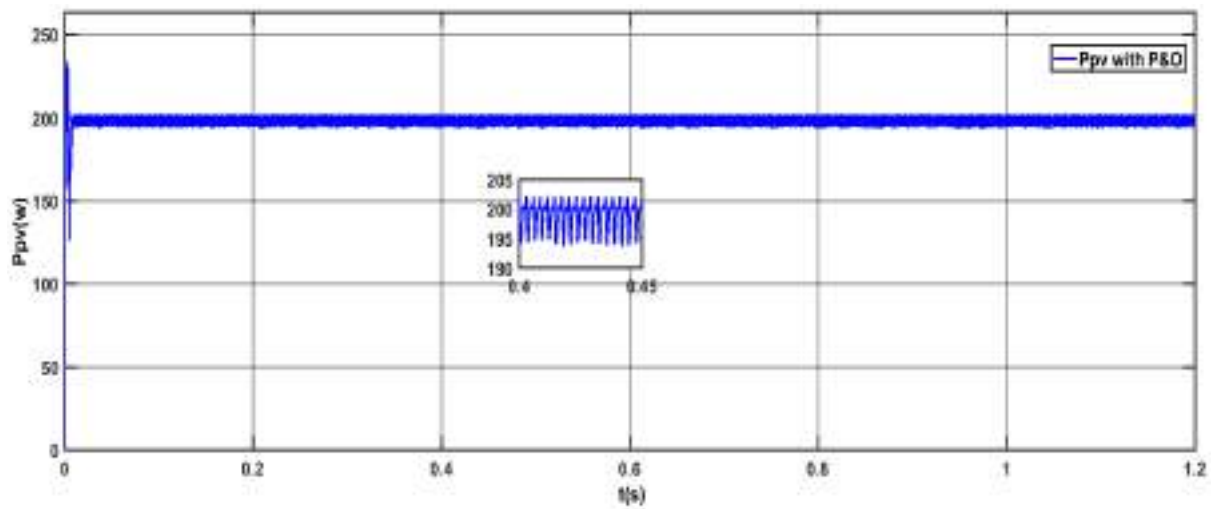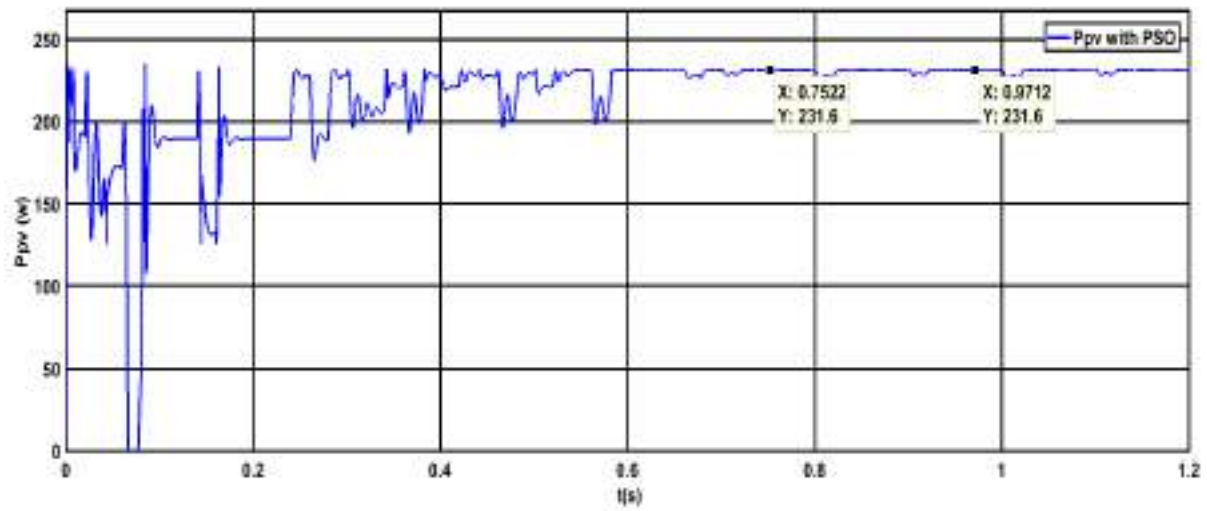
Figure 12. PV power for partial shading pattern2 [1000 500 200]
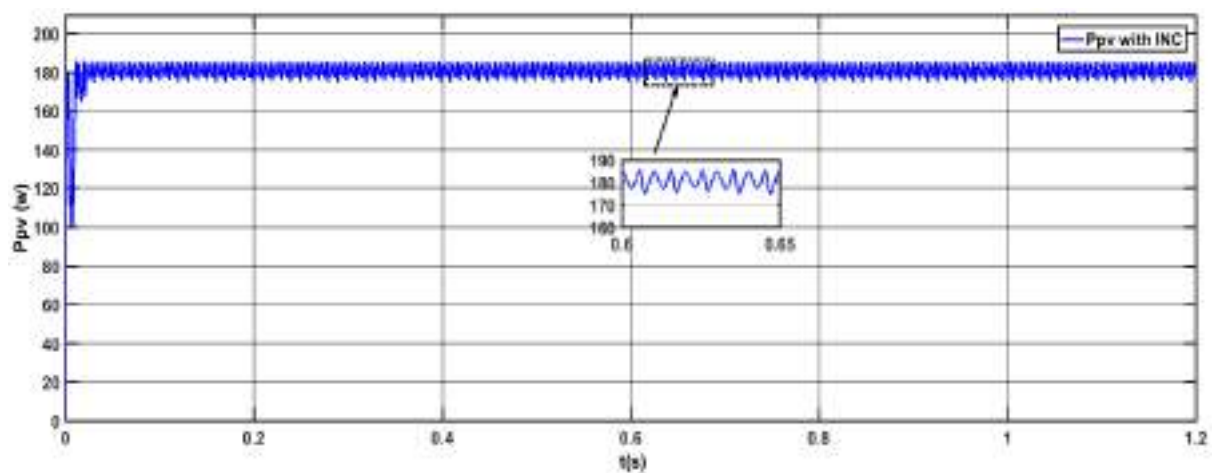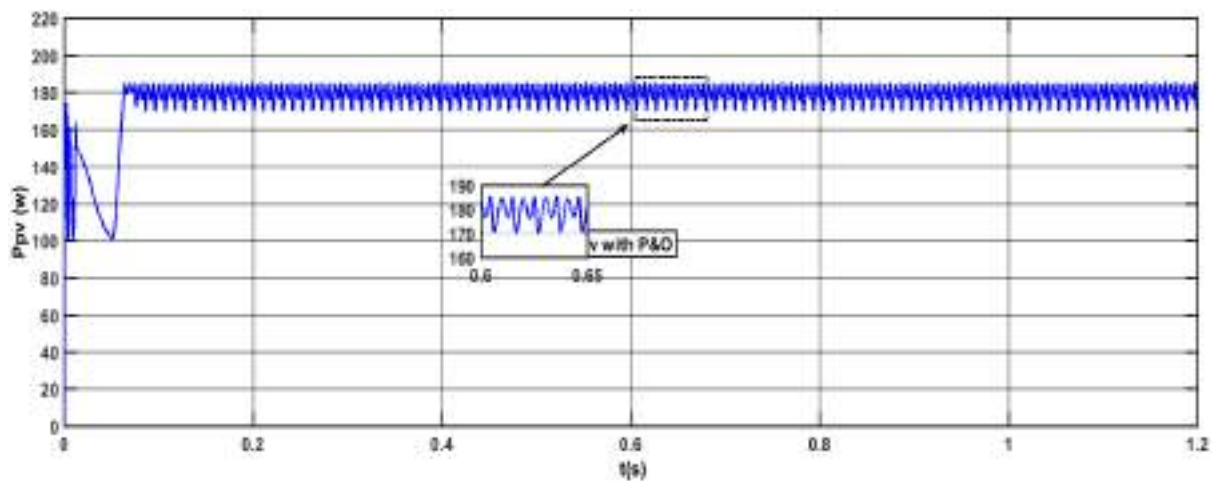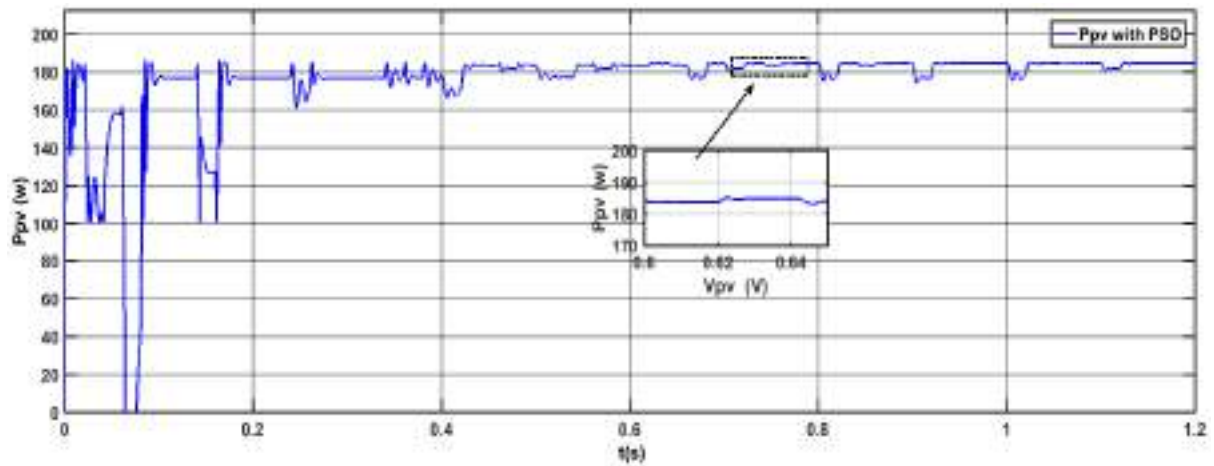
Figure 13. PV power for partial shading pattern 3 [800 400 100]

-a-

-b-

-c-
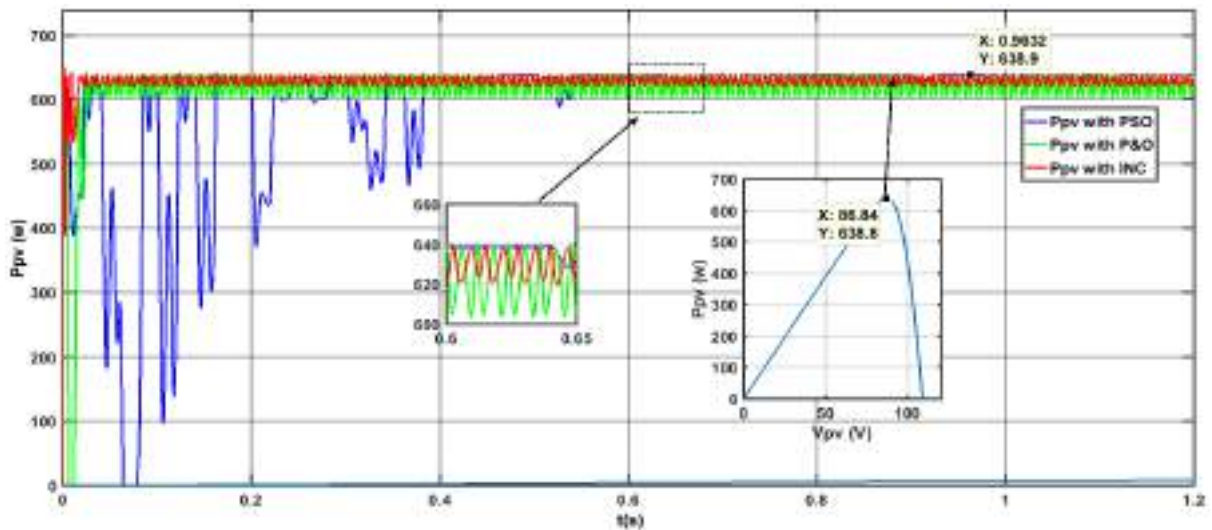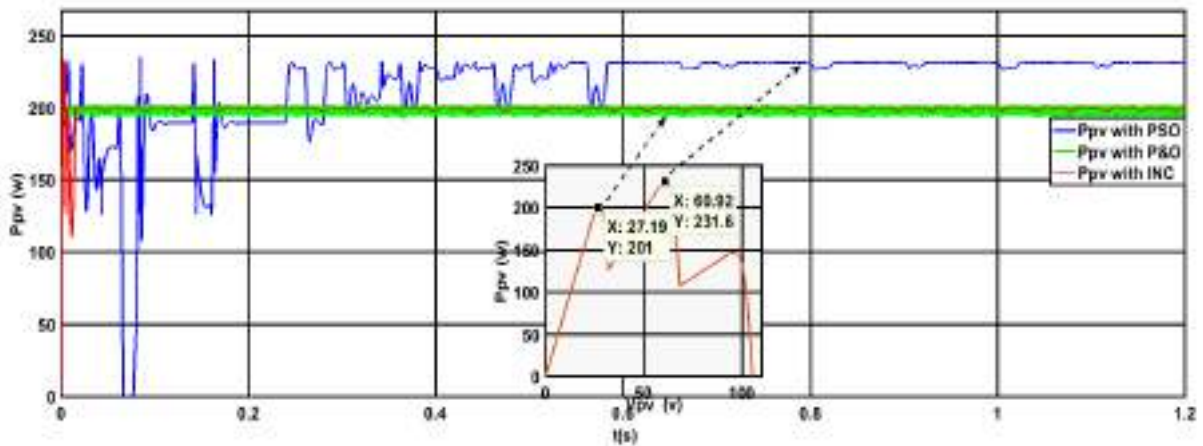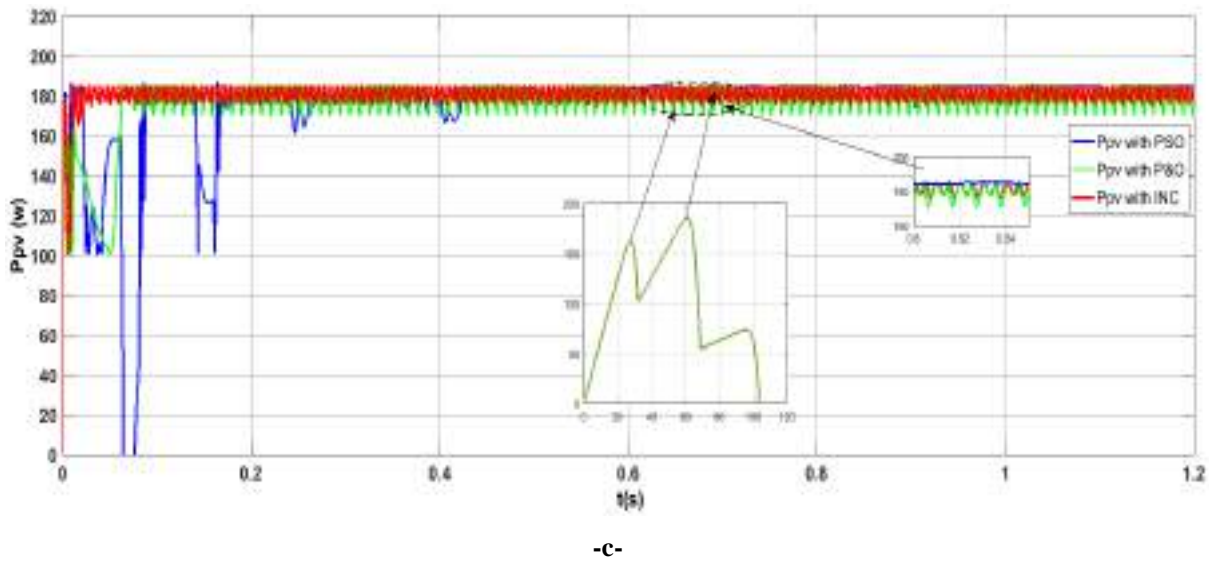
Figure 14. PV power with MPPT techniques for : a) pattern1 STC, b) pattern2, c) pattern3

Results and Discussion

Robustness of the suggested controllers is tested and evaluated by varying the temperature and sun irradiation. The simulation results for maximum power point tracking for atmospheric condition fluctuation for three distinct patterns using the P&O, INC, and PSO algorithms are displayed in Figures 11 to 14. It is evident that the efficiency and accuracy of MPP tracking varies among PSO, P&O, and INC. A PV panel operates at 25 °C and 1000 w/m2 of irradiation under standard test scenarios. The PV panel takes advantage of the three approaches to obtain its maximum value, which equals 639 w, as seen in Figure 11.

Tracking trajectories with partial shading are shown on Figures 12 and 13. PV modules in PSCs are not exposed to the same radiation. It is apparent that in terms of speed, the P&O and INC outperform the PSO, although the maximum power produced is less. It is evident that MPP may be monitored in various types of environmental circumstances using the PSO technique. Power with P&O and INC converges to the first LP, as Table II illustrates; this power is approximately 75.5% of the GP power, which is closely tracked using the PSO algorithm.

The performance of each MPPT technique was analyzed based on the following metrics:

1. **Tracking Efficiency**:
   - **P&O** showed moderate efficiency but struggled with rapid fluctuations in power due to oscillations.
   - **IncCond** demonstrated higher efficiency in tracking the MPP, effectively handling varying irradiance conditions.

- **PSO** outperformed both P&O and IncCond, particularly under significant shading, maintaining a consistent tracking efficiency.

2. **Response Time**:

- **P&O** exhibited the quickest initial response but was slower to stabilize at the MPP due to oscillations.
- **IncCond** had a moderate response time, providing a good balance between speed and accuracy.
- **PSO** had a longer initial response time due to its complex algorithm but achieved stability faster in shaded conditions.

3. **Robustness to Shading**:

- Under partial shading scenarios, **P&O** struggled, often locking onto local maxima rather than the global MPP.
- **IncCond** effectively adapted to changing conditions, maintaining good performance.
- **PSO** was notably robust, successfully navigating multiple local maxima to find the global MPP in most scenarios.

Table 3**.** PV System Accuracy with P&O INC and PSO Algorithms

Technique	Perturb and Observe (P&O)	Incremental Conductance (IncCond)	Particle Swarm Optimization (PSO)
Methodology	Perturbs the operating point to find MPP	Calculates derivatives to find MPP	Uses a swarm of particles to explore solutions
Convergence Speed	Moderate	Faster under varying conditions	Potentially faster with many particles
Complexity	Simple implementation	More complex than P&O	Complex due to swarm dynamics
Oscillation Around MPP	Yes, especially under rapidly changing conditions	Reduced oscillation	Can oscillate but often converges well
Adaptability	Limited	More adaptable to changes in conditions	Highly adaptable with dynamic strategies
Application	Common in solar applications	Used in solar and other energy systems	Versatile applications in optimization tasks

Conclusion

The highest power is indicated by the global maximum point, while smaller powers are indicated by the other points. In this case conventional methods cannot distinguish between the overall maximum power point and multiple maximums. In this paper a nature-inspired metaheuristic optimization algorithm (PSO) is used to track the global maximum power point GMPP under partial shading conditions. Comparison with other conventional techniques is done using Simulink/Matlab software.This comparative analysis highlights the importance of selecting the appropriate MPPT technique for PV systems operating under partial shading conditions. PSO emerges as the most effective method, but the choice may ultimately depend on specific system requirements, including response time, efficiency, and available computational power. Future work should explore hybrid approaches that combine the strengths of these techniques to further enhance performance under variable environmental conditions.

References

Aghaei, S., & Arefi, H. (2022). A novel approach for maximizing PV output under partial shading using a dynamic optimization algorithm. *Renewable Energy*, 185, 197207. https://doi.org/10.1016/j.renene.2021.12.015

Ben Si Ali, N., Benalia, N., & Zerzouri, N. (2018). Modelling and power control of grid connected wind energy system. Global Journal of Computer Sciences: Theory and Research, 8(1), 14–23. http://dx.doi.org/10.18844/gjcs.v8i1.3286

Alshahrani, M., & Raza, A. (2023). Review on the strategies for enhancing solar PV performance under partial shading. *Journal of Renewable and Sustainable Energy*, 15(3), 045001. https://doi.org/10.1063/5.0084796

Ben Si Ali, N., Ghoudelbourk, S., Benalia, N., & Zerzouri, N. (2023, December). Maximum Power Harvest from Shadowed PV Panels Using PSO Algorithm. In *2023 IEEE 11th International Conference on Systems and Control (ICSC)* (pp. 562-566). IEEE.

Jately, V., Azzopardi, B., Joshi, J., Sharma, A., & Arora, S. (2021). Experimental Analysis of hill-climbing MPPT algorithms under low irradiance levels. *Renewable and Sustainable Energy Reviews*, *150*, 111467.

Wang, L., & Zhang, Y. (2023). Intelligent control methods for PV systems in partial shading environments. *Renewable and Sustainable Energy Reviews*, 172, 112934. https://doi.org/10.1016/j.rser.2022.112934

Yilmaz, U., Kircay, A., & Borekci, S. (2018). PV system fuzzy logic MPPT method and PI control as a charge controller. *Renewable and Sustainable Energy Reviews*, *81*, 994-1001.

Bjaoui, M., Khiari, B., Benadli, R., Memni, M., & Sellami, A. (2019). Practical implementation of the backstepping sliding mode controller MPPT for a PV-storage application. *Energies*, *12*(18), 3539.

Chaibi, Y., Salhi, M., El-Jouni, A., & Essadki, A. (2018). A new method to extract the equivalent circuit

parameters of a photovoltaic panel. *Solar Energy*, *163*, 376-386.

Olayiwola, O. I., & Barendse, P. S. (2019). Photovoltaic cell/module equivalent electric circuit modeling using impedance spectroscopy. *IEEE Transactions on Industry Applications*, *56*(2), 1690-1701.

Bayrak, G., & Ghaderi, D. (2019). An improved step-up converter with a developed real-time fuzzy-based MPPT controller for PV-based residential applications. *International Transactions on Electrical Energy Systems*, *29*(12), e12140.

Prathibha, M. R., & Sridhar, H. S. (2017, March). High step-up high frequency push pull DC-DC converter using MPPT with DC motor load. In *2017 International Conference on Computation of Power, Energy Information and Commuincation (ICCPEIC)* (pp. 677-680). IEEE.

Naseem, M., Husain, M. A., Kumar, J. D., Ahmad, M. W., Minai, A. F., & Khan, A. A. (2021, December). Particle swarm optimization based maximum power point tracking technique for solar PV system under partially shaded conditions. In *2021 International Conference on Control, Automation, Power and Signal Processing (CAPS)* (pp. 1-6). IEEE.

Amiri, M., & Khosravi, A. (2022). Optimized MPPT techniques for PV systems under non-uniform shading conditions. *Energy Reports*, 8, 568-579. https://doi.org/10.1016/j.egyr.2022.11.001

Alik, R., & Jusoh, A. (2017). Modified Perturb and Observe (P&O) with checking algorithm under various solar irradiation. *Solar Energy*, *148*, 128-139.

Ahmad, M., Numan, A., & Mahmood, D. (2022). A comparative study of perturb and observe (P&O) and incremental conductance (INC) PV MPPT techniques at different radiation and temperature conditions. *Eng. Technol. J*, *40*(2), 376-385.

Rezaei, M. M., & Asadi, H. (2019). A modified perturb-and-observe-based maximum power point tracking technique for photovoltaic energy conversion systems. *Journal of Control, Automation and Electrical Systems*, *30*, 822-831.

Zakzouk, N. E., Elsaharty, M. A., Abdelsalam, A. K., Helal, A. A., & Williams, B. W. (2016). Improved performance low-cost incremental conductance PV MPPT technique. *IET Renewable Power Generation*, *10*(4), 561-574.

Rupesh, M., & Shivalingappa, D. V. (2018). Comparative analysis of P&O and incremental conductance method for PV system. *International Journal of Engineering & Technology*, *7*(3.29), 519-523.

Ghasemi, A., & Zare, M. (2023). Enhancing energy extraction from PV panels using a modified PSO algorithm under shaded conditions. *Energy*, 260, 124835. https://doi.org/10.1016/j.energy.2022.124835

Hassan, M., & Marzuki, A. (2023). Multi-criteria decision-making for optimal PV system design under shading effects. *Renewable Energy*, 205, 553-564. https://doi.org/10.1016/j.renene.2022.12.027

Ramakrishnan, V., & Mohan, K. (2023). Optimization techniques for photovoltaic systems under varying shading conditions. *Journal of Solar Energy Engineering*, 145(2), 021007. https://doi.org/10.1115/1.4054827

Hayder, W., Ogliari, E., Dolara, A., Abid, A., Ben Hamed, M., & Sbita, L. (2020). Improved PSO: a comparative study in MPPT algorithm for PV system control under partial shading conditions. *Energies*, *13*(8), 2035.

Analysis of the Effect of Natural Pozzolan Algerian from Beni Saf on the Mechanical Strength of Binary Mortars

Boumaiza Malika

University of Bouira- faculty of sciences and applied sciences, Algeria, ⓘ https://orcid.org/0009-0006-6581-0612

Mohamadi Saddika

University of Bouira- faculty of sciences and applied sciences, Algeria ⓘ https://orcid.org/0009-0001-0644-031X

Arbaoui Ahcene

University of Bouira- faculty of sciences and applied sciences, Algeria

Daou Sohaib

University of Bouira- faculty of sciences and applied sciences, Algeria

Abstract: The use of cementitious additives in cement production is one of the most recent developments in cement production, as they improve the mechanical properties of cementitious materials and reduce clinker consumption, which leads to reducing problems associated with environment. The main objective of this work is to study the possibilities of obtaining other cements elaborated with natural Algerian pozzolan, which is found in large quantities in the Beni Saf deposit in the west of the country. Our experimental work analyses the possibility and the influence of substituting part of the cement by natural pozzolan in the mortar, in the following percentages: 0%, 10%, 20% and 30%. The characteristics of the cement and the behaviour of the pozzolan mortar were also analyzed.The results of this research confirm that the use of 10% and 20% of pozzolan contribute to improve the mortar's compressive and flexural strength. Substitution of the pozzolan additive and the chemical composition of the cement resulted in conservation of the mechanical performance of the mortars tested. The substitution, which is of economic interest, reduces the quantity of cement and results in an increase in strength.

Keywords: natural pozzolan, mechanical strength, binary mortars, cement.

Introduction

The construction materials sector is consuming more and more energy and has therefore sought to review its energy expenditure and reduce CO_2 emissions by adapting new strategies. The international Energy Agency and the World Business Council for Sustainable Development, their approaches were based on the use of alternative fuels and the replacement of clinker by supplementary cementitious materials represented by natural mineral additives and alternative industrial wastes or by-products that obtain physical and mechanical properties similar to cement but at a low cost (Khelafi, H. & al , 2000).

Additives are one of the latest developments in the production of cementitious materials (mortars and concrete), since their use improves their physicochemical and mechanical properties on the one hand, and on the other, their use aims to reduce clinker consumption and solve environmental problems in a simple and economical way (Goufi, N ,2019).

The aim of our work is to study the effect of incorporating natural pozzolans on the cement characteristics and mechanical properties of binary mortars, such as compressive strength and flexural strength. The substitution rate varied between 0% and 30%. The results of this research work confirm that the 10% and 20% pozzolanic content makes a positive contribution to improving the durability of construction. It was found that the quantity of pozzolanic additives and the chemical composition of the cement used were the main parameters influencing variations in the mechanical strength (flexion and compression) of the mortars tested.

Experimental methods

Materials and properties

Pozzolan

The natural pozzolan used throughout this study as the base material of aluminosilicates was scoria type. It is obtained from the Algerian company of pozzolan and building materials (SPMC spa Beni-Saf) located in the northwest of Algeria located in the northwest of Algeria. The raw pozzolan has the form of a dark basaltic tuff. This latter was kept in a 50 ∘C oven for 24 h to make it more easily grindable by removing any moisture, which leads to a particle clogging phenomenon. Afterward, it was grounded in a ball mill over 75 min and screened to obtain particles with a maximum size of less than 60 μm. Their chemical compositions after grinding see Table 1. The Blaine's specific areas, main physical properties of Beni Saf Pozzolan (see Table 2).

Table 1. Oxide composition of Beni Saff Pozzolan by XRF analyses

Oxides	Values (%)	Oxides	Values %	Oxides	Values%	Oxides	Values%
SiO_2	47.8	Al_2O_3	15.89	CaO	10.49	SO_3	0.05
Na_2O	2.21	FeO_3	10.21	MgO	8.5	K_2O	16.3

Table 2. Physical properties of the natural pozzolan

Physical properties	Unit	Values
The Blain specific area	m^2 /kg	477,6
Absolute density	g /cm^3	2,76
Apparent density	g /cm^3	0,96
Porosity	%	40,46

Cement

The cement used to prepare the mix is a CEM-I 42.5, with a guaranteed minimum strength of 40 MPa at 28 days. From the Sour El Ghozlane cement works, it has a fineness of 3675cm^2/g and an absolute density of 3.13 g/cm^3. Their chemical compositions see Table 3.

Table 3. Chemical composition of CEM-I 42

Oxide	Value (%)	Oxide	Value (%)	Oxide	Value (%)	Oxide	Value (%)	Oxide	Value (%)
SiO_2	47.8	Al_2O_3	15.89	CaO	10.49	SO_3	0.05	P_2O_3	0.163
Na_2O	2.21	FeO_3	10.21	MgO	8.5	K_2O	16.3	TiO_2	0.235

Natural sand and mixing water

The sand used is natural sand of a siliceous nature (70%). The characteristics of the sand are given in table 4. The mixing water used to prepare the mortars is laboratory tap water.

Table 4. Sand properties

Apparent density kg/m^3	Specific density kg/m^3	Water content %	Sand equivalent (piston) %	Sand Equivalent (visual) %	Methylene Blue	Absorption	Porosity
1812.05	2514	0.4	67.3	69.7	0.77	0.48	27.9

Mixture proportion and experimental methods

The mortars were prepared following the European norm NF 15 403, the moulds are prismatic (40x40x160 mm). The mortars were placed in the moulds in two layers, which underwent 60 movements per layer for 60 seconds on a shock table. Prisms were covered with plastic film and cured in air at a temperature of 20°C± 1 ^{0}C and relative humidity of 50^{0}C. Specimens were demolded at 24 hours. See figure 1. The fresh state properties (workability and setting) and hardened state properties (strength) were studied on cement pastes and mortars. The various mixture proportions are given in Table 5. The reference mortar without pozzolan was composed of three parts of sand and one part of cement (by mass). All mixtures containing the pozzolan were prepared with

the same proportions of sand and binder (cement + pozzolan). The replacement rates of cement by the pozzolan were 10, 20 and 30% by mass. A constant water/binder (cement + pozzolan) ratio of 0.52 was chosen. it was decided to keep the workability of the mortars constant.

Figure 1. Preparation and conservation of specimens

Table 5. The various mixture proportions

Designation	CEMI	PZN 10	PZN 20	PZN 30
Cement (kg/m^3)	450	405	360	315
Pozzolan (kg)	0	45	90	135
Water (l/m^3)	234			
Sand (kg)	1350			
W/b	0.52			

The different properties of the mortars were studied in the fresh and hardened states. The workability tests were performed by studying the spreading of mortars on a shock table, in accordance with Standard NF EN 12350-5 (AFNOR, 1999). The setting times were measured using Vicat apparatus (EN 196-3 (AFNOR, 2006)). Finally, the strength tests (flexure and compression) were performed following European Standard NF EN 196-1 (AFNOR, 2006). Each result was the average of three measurements for flexural strength and six for compressive strength. The mechanical strengths are measured at 2, 7 and 28 days. Figure 2.

(a) Flexural   (b) Compression

Figure 2. Mechanical testing machines

Results and analysis

Effect of Beni Saff pozzolan on pastes and mortars

Density of the mixture

Analysis of the results (figure 3) shows that for 7 days and 28 days the density is reduced by 2.9% and 4.8% respectively for the control mortar. For substitution rates equal to 10%, 20% and 30%, the reduction for 7 and 28 days is 4.2% and 5.4%, 3.1% and 5.1%, 6.7% and 5.1% respectively. This is explained by the replacement of cement by pozzolan, which has a lower density (2.76 g/cm^3) than cement (3.13 g/cm^3). These results are common for Algerian natural pozzolans (O.Chaib & al, 2016).
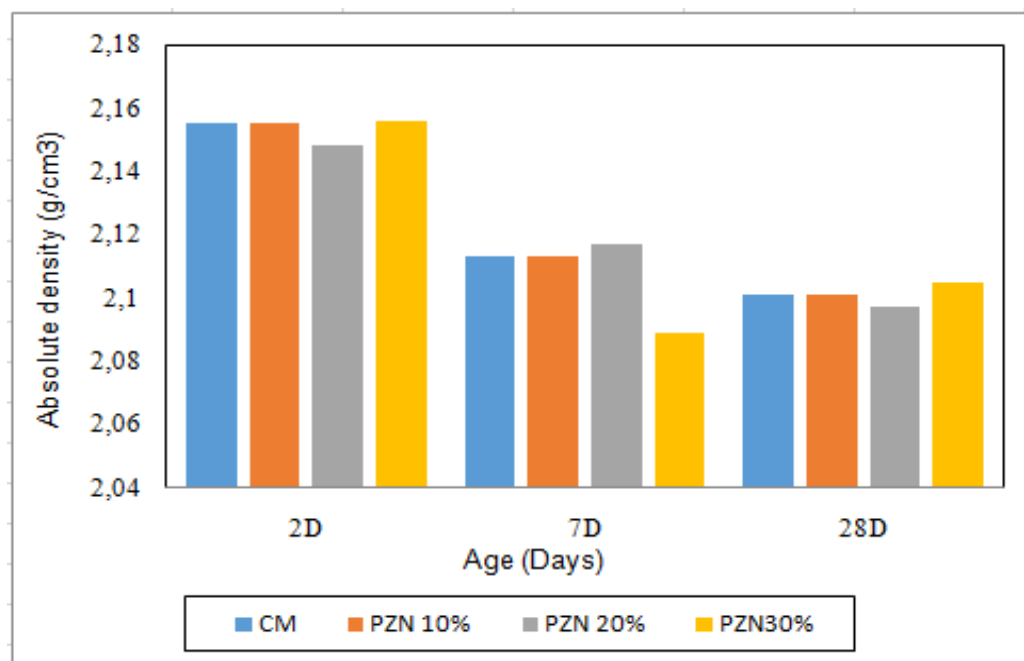
Figure 3. Variation of absolute density

Water demand and setting time

The water demand related to the use of the pozzolan was evaluated on mortars using a shock table. The figures 4, 5 present the effect of pozzolan natural on the normal consistency of hydrated cement and the start and end of mortar

The results show that the W/B ratio is proportionally related to the pozzolan content of the cement, increasing by 2.5% at 10%, 4.5% at 20% and 5% at 30% to obtain a normal paste compared with the control paste. This is explained by the large specific surface area of the pozzolan (477.6 m^2/g), compared with that of the cement (367.5 m^2/g), as well as the percentages of substitution of cement by pozzolan. In conclusion, in order to keep the workability of the different mixes constant, the quantity of mixing water must be increased.
setting.
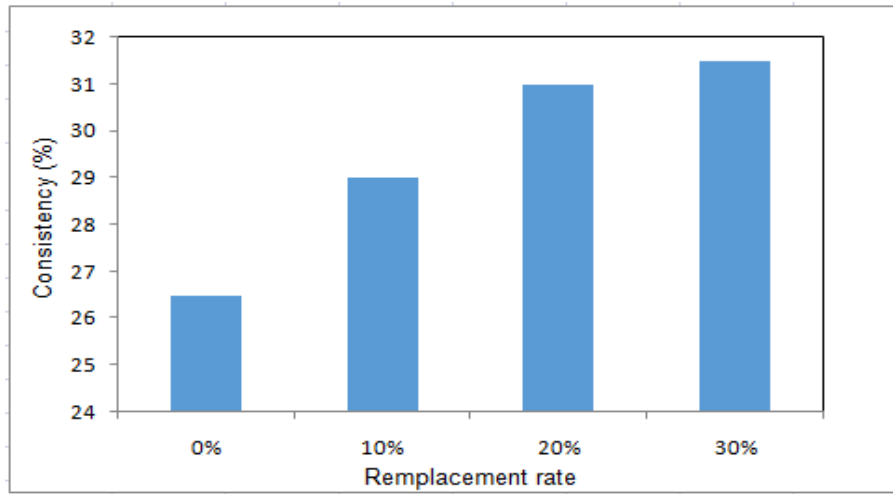
Figure 4. Variation of consistency when increasing proportioned of pozzolan are used to replace cement
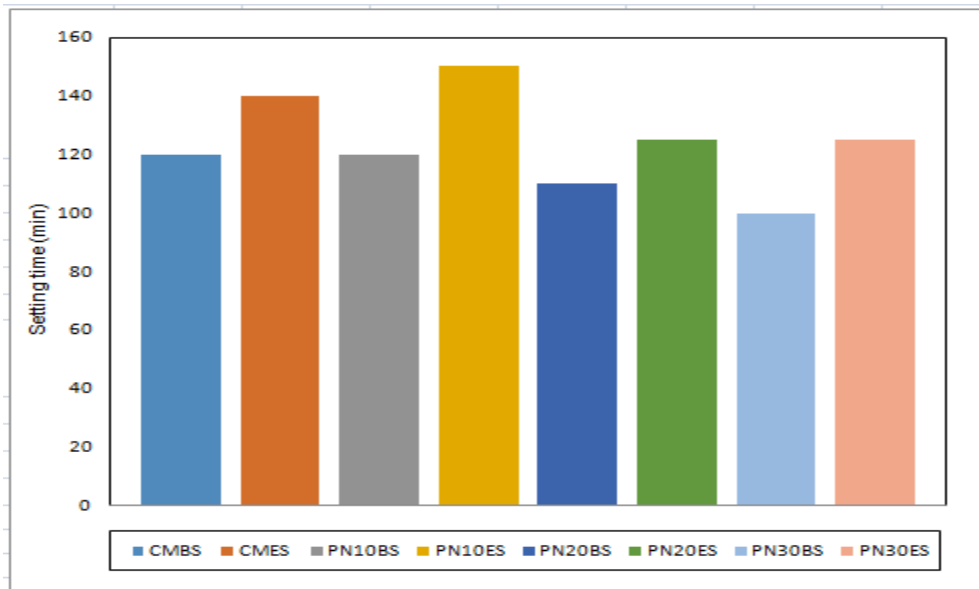
Figure 5. Setting times of cement pozzolan pastes

The beginning and end times of setting performed on cement pastes having a constant water binder ratio are given in figure 4, were measured for the different pastes prepared, in accordance with NF 196-3 standards.

The mixture containing 10% pozzolan showed an increase of 7% in the setting end time, while the pastes with 20% and 30% pozzolan showed a decrease of 11%. For the setting start time, the paste with 10% pozzolan showed the same value as the control paste, while the other pastes with 20% and 30% pozzolan showed a decrease of 10% and 17% respectively compared with the control paste. It can therefore be seen that at a young age, setting is faster for the control paste and for the paste with 10% pozzolan, whereas for the others pastes, the opposite is observed, as the pozzolan delayed the hydration of the cement by almost two hours. As already stated by Chaib &al, Mebrouki & al (Chaib, 2016; Mebrouki, 2014). The increase in setting time means that the

hydration of cements with mineral additions takes place at different kinetics. This hydration is slightly more complex than that of Portland cement, due to the slow pozzolan reaction of natural pozzolan.

Compressive and flexural strengths

Figures 6, 7 shows the effect of replacement rate on compressive and flexural strength for the mortars containing 0 %, 10%, 20% and 30% of pozzolan, measured at three different ages.

Compressive strength
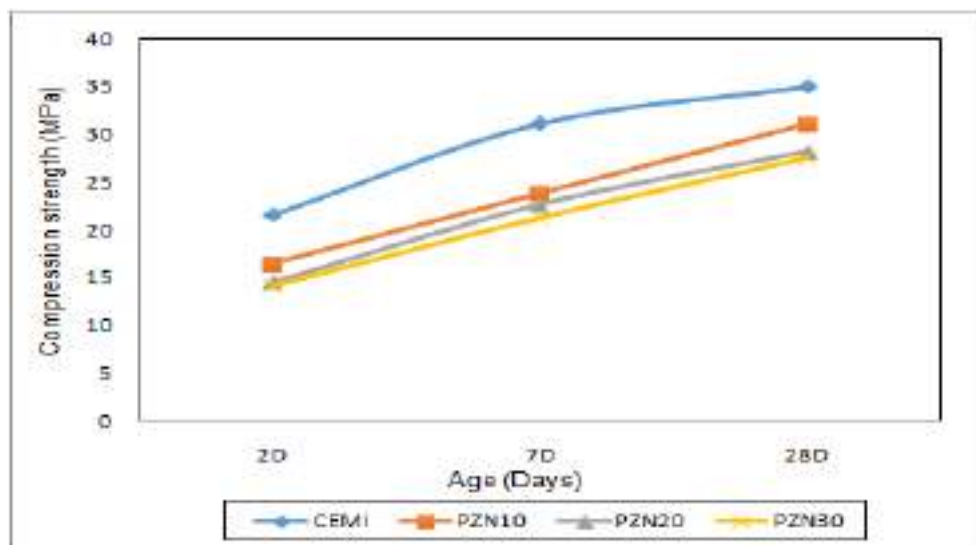
Figure 6. Compressive strength for pozzolanic mortars as a function of replacement rate

The compressive strengths of mortars made with different pozzolan substitution rates are always lower than those of the control mortar, for all the different ages. In terms of compressive strength, at a young age, increasing the dosage rate of pozzolan led to a reduction in compressive strength from 23% to 34% at 2 days and from 24% to 32% at 7 days, but this reduction tended to decrease at 28 days, from 11% to 21%, highlighting the positive effect of the pozzolan rate in the long term. The mortar with 10% natural pozzolan was found to give strength very close to that of the control mortar.

Chaib et al, in his study found a 15% reduction in the compressive strength at age 28 days of a mortar containing 20% pozzolan compared to the control mortar, with the same working conditions. However, in our work, we note that this reduction is well appreciated for a pozzolan content equal to 10% .
This is essentially due to the very fine grinding of the pozzolan (particles passing through a 60μm sieve), which makes it more active.

The strength is low at a young age, which can also be attributed to the pozzolan activity which is slow at a young age and develops in the long term by fixing the Portlandite $Ca(OH)_2$ released by the hydration of the

Portland cement, giving rise to additional second-generation C-S-H occupying a large space in the cement matrix and thus contributing to the development of strength (Ghrici, 2007; Bessenouci, 2011; Mansour, 2010; Siad, 2010, Goufi, 2019)

Flexural strength

The results show a reduction in mortar strength at ages 2 and 7 days as the pozzolan content increases. This reduction is 19%, 19% and 41% at age 2 days compared with the control mortar, and at age 7 days is 22.5%, 19.25% and 11.75% respectively. At the age of 28 days, the rates were 15.71%, 2.65% and 13.67% respectively. It can be seen that the strength of mortars with pozzolanic substitution compared with the control mortar tends to decrease in the long term. This can be explained by the value of the fineness of the pozzolan (477.6 m^2/kg), which generates greater reactivity.
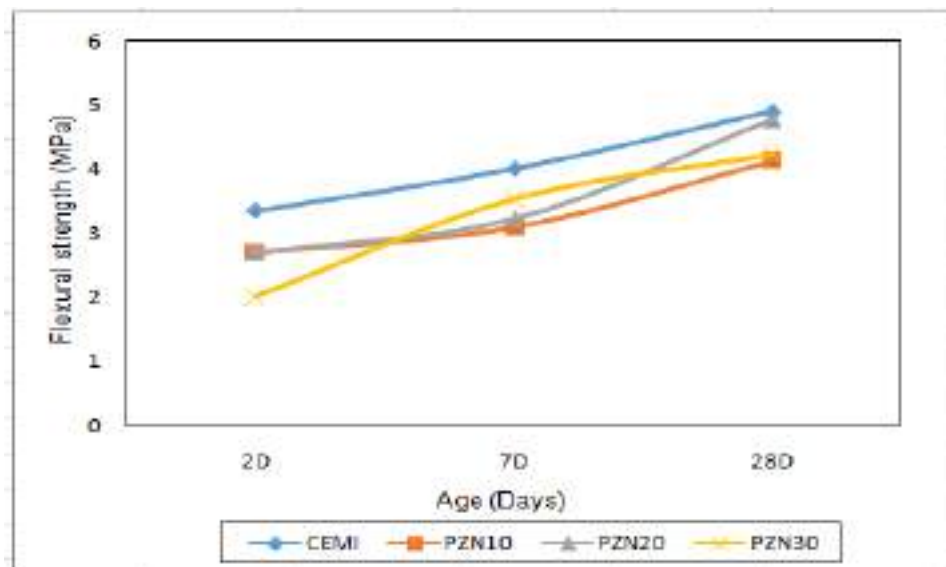
Figure 7**.** Flexural strength for pozzolanic mortars as a function of replacement rate

Conclusion

This study was performed to evaluate the influence of replacing cement with naturally Algerian pozzolan from Beni-Saf on changes in the characteristics of cement and the mechanical strength of mortars.

Consistency is proportional to the rate of addition, and the higher the rate, the greater the increase in consistency. The results show a decrease in density, which explains the good contribution of the addition to compactness, and implies good durability.

The increase in setting time means that the hydration of cements with mineral additions takes place at different kinetics. This hydration is slightly more complex than that of Portland cement, due to the slow pozzolanic

reaction of natural pozzolans.

The incorporation of pozzolan leads to low mechanical strength at young ages. This reduction is explained by the pozzolanic reaction which is slowed down at the beginning of the cement hydration reaction. In the medium term, these strengths begin to develop quite significantly due to the delayed onset of the pozzolanic reaction. At a pozzolan content of 10%, the compressive strength approaches the reference strength. At a young age, increasing the addition rate has a negative effect on compressive strength and flexural strength, but as the age increases the strength increases. The setting test carried out on pure paste and on binder paste confirmed a delay in setting as a result of grain flocculation. At very young ages, this effect is essentially limited to a deceleration of the hydration process.

We have found that substituting this addition (pozzolan) results in the preservation of mechanical performance. This substitution, which is of economic interest, reduces the quantity of cement and increases strength.

Acknowledgements

References

ACI, American Concrete Institute. (2000). *Use of raw or processed natural pozzolans in concrete. ACI Committee 232*, Manual of concrete Practice ACI IR-00

AFNOR, Association francaise de normalisation. (1965). *Concrete-Pozzolans*, French Standard NF P18-308.

AFNOR, Association francaise de normalisation. (1990). *Determination of the cleanliness of sands-sand equivalent* , French Standard NFP18-597.

AFNOR, Association francaise de normalisation. (1999). *Testing fresh concrete-Part 5: Flow table test, European Standard* NFEN 12350-5

AFNOR, Association francaise de normalisation. (2006). *Methods of testing cement, Part1; determination of strength, European Standard* NFEN 196-1

AFNOR, Association francaise de normalisation. (2006). *Methods of testing cement, Part3*; *determination of setting time and soudnes*s, European Standard NFEN 196-3

ASTM, American Society for Testing and Materials. (2005). *Standard specification for coal fly ash c alcined natural pozzolan for use in concrete,* American Standard C618-05

Bessenouci, (2011) 12. Bessenouci M Z., Bibi Triki N E., Khelladi S., Draoui B., Abene A., *Physics Procedia.* 21 (2011) 59 –66

Chaib, O. & al. (2016). *Etude de l'influence de la pouzzolane naturelle sur la résistance mécanique des mortiers à base des ciments composés.* J. Mater. Environ. Sci. 7 (2), 422-428

Goufi, N (2019), *Activation chimique de produits pouzzolanique et l'élaboration d'un nouveau ciment,* (Unpublished doctoral dissertation). Oran University, Algeria.

Goufi, N (2019)*, Potential use of activated Algerian natural pozzolan powder as a cement replacement material*, European journal of environmental and civil engineering. DOI: 10.1080/19648189.2018.1559241

Ghrici, M (2007) 13.Ghrici M., Kenai S., Said Mansour M., *Cem. Concr. Compos.* 29 (2007) 542-549.

Khelafi, H. & al. (2000). *Influence chimique et physique de la pouzzolanes sur la résistance en compression des mortiers .* Washington, DC: American Psychological Association

Mansour (2010) 13.Ghrici M., Kenai S., Said Mansour M., *Cem. Concr. Compos.* 29 (2007) 542-549.

Mebrouki, A. & al. (2014). *Enhancing value of local materials in developing countries Case of an Algerian pozzolan .* EJECE. Volume 13 – No. 10/2009, pages 1263 to 1278

Siad (2010) Siad H., Mesbah H.A., Khelafi H., Kamali S., Mouli M., *Arab. J. Sci. Eng.,* 35 (2010) 183-195

General Data of the Specimens from Libohovë, Dropull and Gjirokastër Municipalities Preserved in the National Herbarium of Albania

Ajola Mesiti

University of Tirana, Research Center of Flora and Fauna, Albania, ⏺ https://orcid.org/0000-0001-6167-1666

Marjol Meço

University of Tirana, Department of Biology, Albania, ⏺ https://orcid.org/0000-0002-9893-907X

Oresta Saliaj

University of Tirana, Research Center of Flora and Fauna, Albania, ⏺ https://orcid.org/0000-0002-0312-6528

Ermelinda Mahmutaj

University of Tirana, Research Center of Flora and Fauna, Albania

Skerdilajd Xhulaj

University of Tirana, Research Center of Flora and Fauna, Albania

Petrit Hoda

University of Tirana, Research Center of Flora and Fauna, Albania

Ani Bajrami

University of Tirana, Research Center of Flora and Fauna, Albania, ⏺ https://orcid.org/0000-0001-5349-2510

Julian Shehu

University of Tirana, Research Center of Flora and Fauna, Albania

Abstract: The National Herbarium is an esteemed institution, part of the Research Center of Flora and Fauna, located in Tirana, Albania. A general analysis was carried out for the wild plants in Gjirokastër, Libohovë, and Dropull Municipalities based on detailed research of the NH plant collection, plant localities, and their collecting date. These areas are affluent in biodiversity values, due to the favorable relief conditions, climatic, soil, lithological conditions, inclinations, etc. It resulted in a total of 380 plant species preserved in the National Herbarium. Most of the collected species come from Gjirokastër Municipality (80%), followed by the Dropull Municipality (12%) and Libohovë Municipality (8%). The reason why there is a small number of species preserved for Libohovë Municipality is due to the lack of botanical studies in this area. The flora of this area is distinguished by its Balkan and Mediterranean character. The most representative family is the Asteraceae (40 species), to be followed by the Fabaceae (34 species) and Rosaceae (29 species), Lamiaceae (26 species). Also,

10% of the preserved specimens have medicinal values, which are used by the local community. Analyzing the specimens collected date resulted in the first botanical expeditions dating back to the 1800s. Meanwhile, most of the plant specimens were collected after the 1950s, with the creation of Botanical Institutions, such as the University of Tirana, the Department of Biology, the Botanical Garden, etc. Such a review will be helpful to analyze the actual data and to plan further botanical investigations in the area.

Keywords: Botanical studies, historical review, National Herbarium, vascular plants, Gjirokastër, Albania

Citation: Mesiti A., Meço M., Saliaj O., Mahmutaj E., Xhulaj S., Hoda P., Bajrami A., Shehu J., (2024). General Data of the Specimens from Libohovë, Dropull and Gjirokastër Municipalities Preserved in the National Herbarium of Albania. In A. A. Khan, M. Demirbilek, & M. L. Ciddi (Eds.), *Proceedings of ICSEST 2024-- International Conference on Studies in Engineering, Science, and Technology* (pp. 369-385), Istanbul, Turkiye. ISTES.

Introduction

The National Herbarium of Albania was established in 1947 and contains more than 3000 species and 150.000 specimens of mostly vascular plants (Saçdanaku et al., 2018). The National Herbarium of Albania is part of the Research Center of Flora and Fauna since 2010. Its main contribution involves two major tasks: the enrichment of the herbaria collection and the taxonomic identification of plants. Several scientific publications have been made possible and considered a direct output of the scientists associated with the National Herbarium of Albania such as the four published volumes of the "Flora of Albania" from 1988 until the 2000s (Saçdanaku et al., 2018). Besides published works showing the Albanian flora, digitizing plant specimens in the Herbarium is critically important; some of the specimens found in the Herbarium date from the 1890s. Plants were gathered by Franciscan priests working in Albania and are still well maintained in the National Herbarium although specimens may be susceptible to water damage or other factors involved. Even though storage conditions have improved considerably in the last few years, it is important to mention the recent technological improvement in the conservation, management, and promotion of herbaria specimens in terms of digitization and digitalization. Although the two terms are used interchangeably there is an important difference. With digitalization, we refer to technological means implemented to make specimens more accessible and virtually construct them. On the other hand, digitization refers to transforming the specimens into their digital equivalents or in a digit format. Through the process of digitization and digitalization novel research could be enabled (Soltis 2017), converting the physical specimen into flexible data formats and mirroring into a virtual herbarium as practice shows (Roma-Marzio et al, 2023); commercialization of scientific knowledge (Niedzielski and Markiewicz 2023), facilitate large-scale of plant data (Smedt et al., 2024) and other services could be provided for science education purposes.

This article will show the wild plants in Gjirokastër, Libohovë, and Dropull Municipalities based on detailed

research of the National Herbarium plant specimens. The three municipalities are part of the Gjirokastra County. Gjirokastra is a city in southern Albania situated on the valley of the Drino River and Mali i Gjerë; Libohovë is a town situated at the foot of Bureto Mountain and found in the south-eastern of Gjirokastër city; the municipality of Dropull is situated in the south of the city of Gjirokastër.

From the literature, it is noticed that according to the method of Brawn - Blanquet, the area is dominated by dry stony pastures, usually in hilly areas, belonging mainly to the class *Ononido-Rosmarinetea* (syn. Cisto-Micromerietea julianae (Oberd. 1954).

The first botanical expedition in the area was conducted by Heldreich in 1878 and later on, by the Italian botanist A. Baldacci at the beginning of the 1900s (Baldacci, 1896; 1898; 1899). Between the two, Baldacci made the longest itinerary in the area and reported 18 species. In the 1930s to 1940s other foreign botanists such (Rechinger, Alston, and Sandwith) identified important plants such as the endemic plant of *Athamanta macedonica* subsp. albanica and Minuartia stellata. During the communist regime in Albania, in the 1950s, Albanian and foreign botanists like F.K. Meyer (1951-1960), I. Mitrushi (1955-1966), Penzes (1960), Horvat (1974), Vangjeli (1984), Mersinllari (1987), Malo (2010), S. Malo & L. Shuka (2008; 2009), Z. Barina and D. Pifko (2011) and Dring et al., (2022).

Methods

This study was carried out during 2023-2024, by a careful revision of authentic specimens from Libohovë, Dropull, and Gjirokastër Municipalities which are preserved in the National Herbarium. During this process, the plant species with its historical data, such as collection date, place, and collector. To have a complete view of the species presented in the areas, it was used Albanian literature such as Flora of Albania (Paparisto et al., 1988; Qosja et al., 1992; Qosja et al., 1996; Vangjeli et al., 2000). By doing such work the intention was to create a floristic list with some indicators, such as life forms based on the Raunkiaer system (Ellenberg & Mueller-Dombois, 1967), the chorological form (Vangjeli et al. 2003, 2015); the species medicinal values, and their conservation status according to the National List of Flora (Group Author 2013) and IUCN global database (www.iucn.org). The specimens' names were updated according to the international database of Euro + Med Plant Database (http://ww2.bgbm.org/euroPlusMed/query.as).

Results

From the floristic investigation of the National Herbarium of Albania, are preserved a total of 380 species, located in the Libohovë, Dropull, Gjirokastër Municipalities, which contain 78 families and 260 genera. The most representative plant family is the Asteraceae (40 species), followed by the Fabaceae (34 species), Orchidaceae (32 species), Rosaceae (29 species), Lamiaceae (24 species), Poaceae (22 species), etc. (Table 1.). It is well noticed that most families are represented by only one species, which is a very good indicator for the

flora richness in the areas.

Table 1. Presence of total plant families preserved in National Herbarium, from Libohovë, Dropull and Gjirokastër

Family	N
Asteraceae	40
Fabaceae	34
Orchidaceae	32
Rosaceae	29
Lamiacea	24
Poaceae	22
Brassicaceae	18
Geraniaceae	13
Boraginaceae	11
Ranunculaceae	9
Scrophulariaceae	9
Apiaceae	8
Liliaceae	8
Fagaceae	8
Rubiaceae	7
Caryophyllaceae	7
Corylaceae	4
Dipsacaceae	4
Polygonaceae	4
Anacardiaceae	4
Aspidiaceae	4
Oleaceae	4
Cistaceae	3
Primulaceae	3
Linaceae	3
Plantaginaceae	3
Tiliaceae	3
Crassulaceae	3
Caprifoliaceae	3
Sapindaceae	2
Aceraceae	2
Violaceae	2
Campanulaceae	2

Family	N
Cyperaceae	2
Euphorbiaceae	2
Saxifragaceae	2
Loranthaceae	2
Solanaceae	2
Rhamnaceae	2
Cupressaceae	2
Cornaceae	2
Heliotropiaceae	2
Ulmaceae	1
Convolvulaceae	1
Araceae	1
Aristolochiaceae	1
Hippocastanaceae	1
Buxaceae	1
Zygophyllaceae	1
Asclepiadaceae	1
Gentianaceae	1
Moraceae	1
Acanthaceae	1
Cannabaceae	1
Thymelaceae	1
Dennstaedtiaceae	1
Juncaceae	1
Paeoniaceae	1
Resedaceae	1
Papaveraceae	1
Colchicaceae	1
Pinaceae	1
Salicaceae	1
Dioscoreaceae	1
Gesneriaceae	1
Plumbaginaceae	1
Selaginellaceae	1
Asparagaceae	1
Taxaceae	1
Ephedraceae	1

Family	N
Hypericacea	1
Polypodiaceae	1
Valerianaceae	1
Potamogetonaceae	1
Vitaceae	1
Ericaceae	1
Araliaceae	1
Aquifoliaceae	1
Total	386

As well the genera's analysis shows the richness of the study areas, since 193 genera are represented by only 1 species, 84 genera are represented with two species, and 39 genera are represented with 3 species. The most representative genera are *Geranium* sp. (12 species), followed by *Ophrys* (8 species), *Rosa* and *Orchis* (7 species), *Quercus* sp. (6 species), etc.

In the floristic list derived by the above analysis, is shown that 113 species have medicinal values (Table 2).

Table 2. Aromatic and Medicinal Plants in National Herbarium

Gender	Species	Author	Albanian Name	Family	Life Form	Chorology cal type
Acanthus	spinosus	L.	Dashtër gjembore	Acanthaceae	H	Steno-Med
Agrimonia	eupatoria	L.	Rodhëz, kallar, podigë e egër	Rosaceae	H	Med
Lysimachia	arvensis	(L.) U.Manns & Anderb.	Barcapoj i arave, rruthë e fushave, barmorth, baruri	Primulaceae	T	EuMed
Anthemis	cotula	L.	Maraq	Asteraceae	Ch	EuAz
Arum	italicum	Miller	Këlkaze e Italisë, misërgjarpni, këlnazë, këlmajë	Araceae	G	Steno-Med
Bellis	perennis	L.	Luleshqerrë shumëvjecare, lule baka, lule kacidhe	Asteraceae	T	Med
Buxus	sempervirens	L.	Bush, shimshir	Buxaceae	NPh	Med
Campanula	pyramidalis	L.	Lulekambanë piramidore	Campanulaceae	H	EuJ
Capsella	bursa-pastoris	(L.) Medicus	Shtrapër, lule kacimacë, qurkaz, kam-s'kam	Brassicaceae	T	Kozmop
Carlina	acaulis	L.	Ushonjëz e pakërcelltë, ushojzë,	Asteraceae	H	EuQ

Gender	Species	Author	Albanian Name	Family	Life Form	Chorological type
Carpinus	orientalis	Miller	shotorr, cicëlope Shkozëzezë, shkerre, shkozë e egër	Corylaceae	Ph	Pontik
Castanea	sativa	Miller	Gështenjë, gishtajë, kshtajë	Fagaceae	Ph	
Centaurea	solstitialis	L.	Gjemb i bardhë, tëmballëz, kokorkë	Asteraceae	H	Kozmop
Cercis	siliquastrum	L.	Lofatë, lajthatë, filetë e egër, ftue i egër	Fabaceae	Ph	EuJ-Pontik
Chaerophyllum	temulum	L.	Stërpujë marramendësh	Apiaceae	T	EuAz
Glebionis	segetum	(L.) Fourr.	Krizantemë e të lashtave	Asteraceae	T	EuMed
Cichorium	intybus	L.	Cikore, kore, parkalidhë, bar'çairje, tamëlçak	Asteraceae	H	Kozmop
Cistus	incanus	L.	Mënishte, ndroçkëz, lule breshke, rrushe	Cistaceae	H	StenoMed
Colchicum	autumnale	L.	Xhërokull vjeshtor, luleshlline, lulepreshi	Colchicaceae	G	EuKaukaz
Cornus	mas	L.	Thanë, thanë e kuqe, sharrëkuqe	Cornaceae	Ph	EuJL
Crataegus	heldreichii	Boiss.	Murriz i Heldraihit	Rosaceae	Ph	Balk
Crataegus	monogyna	Jacq.	Murriz njëbërthamësh	Rosaceae	Ph	EuAz
Cruciata	laevipes	Opiz.	Kruciatë levipe	Rubiaceae	H	EuAz
Daphne	oleoides	Schreber	Xërxelë, bar thëllëze, qershi e egër	Thymelaceae	Ch/NPh	AzQ
Digitalis	grandiflora	Miller	Luletogëzi lulemadhe	Scrophulariaceae	H	EuSiber
Echium	italicum	L.	Ushqerrëz e Italisë	Boraginaceae	H	EuMed
Erica	arborea	L.	Shqopë, mrece, kokoriqe, rrameçë, vrikë	Ericaceae	Ph	StenoMed
Eryngium	campestre	L.	Gjembardhë fushash, gjëmë dybeke, therrëiriçi	Apiaceae	H	EuMed
Erysimum	sylvestre	(Crantz) Scop.	Erisimë	Brassicaceae	H	Med
Filago	pygmaea	L.	Evaks xhuxh	Asteraceae	T	StenoMed
Fragaria	vesca	L.	Luleshtrydhe, marëz, ortytë, plyshkë	Rosaceae	H	EuSiber
Fraxinus	ornus	L.	Frashër i bardhë	Oleaceae	Ph	EuMed
Galium	odoratum	(L.) Scop.	Ngjitëse erëmirë	Rubiaceae	G	EuAz
Galium	verum	L.	Ngjitëse e vertetë	Rubiaceae	H	EuAz
Geranium	rotundifolium	L.	Kamaroshe gjetherumbullakët	Geraniaceae	T	Paleotemp
Geranium	tuberosum	L.	Kamaroshe zhardhokore	Geraniaceae	G	EuJ

Gender	Species	Author	Albanian Name	Family	Life Form	Chorological type
Geranium	columbinum	L.	Kamroshe e pëllumbave	Geraniaceae	T	Kozmop
Hedera	helix	L.	Urth, bërshlen, shermashek, qisar, lerth	Araliaceae	Lian	Med
Humulus	lupulus	L.	Sumbullar, luvër, kampatë	Cannabaceae	G	EuKaukaz
Hypericum	perforatum	L.	Lulebasani, balc, lulegjaku, bar i të premit	Hypericacea	H	Kozmop
Hypochaeris	urens	L.	Hipoker i Kretës	Asteraceae	H	Med
Scorzoneroides	cichoriacea	(Ten.) Greuter	Dhëmbëluan cikorengjashëm	Asteraceae	H	Med
Ligustrum	vulgare	L.	Voshtër, gjipës, puqlore	Oleaceae	Ph	AzP
Lonicera	etrusca	G. Santi	Laverdhë etruskë, mustrakë guri	Caprifoliaceae	Ph	EuMed
Loranthus	europaeus	Jacq.	Evull, kripth, name, mell, veshk, veshkull qarri	Loranthaceae	Ph	EuKaukaz
Malus	sylvestris	Miller	Mollë e egër, mollçinë, viaqkë, thaqkë	Rosaceae	Ph	EuKaukaz
Marrubium	incanum	Desf.	Marubë e thinjur	Lamiacea	H	Med
Medicago	sativa	L.	Jonxhë e kultivuar	Fabaceae	H	EuAz
Melittis	melissophyllum	L.	Melit gjethemilcë	Lamiacea	H	StenoBalk
Onobrychis	viciifolia	Scop.	Esparcetë gjethegrashinë	Fabaceae	H	Med
Orchis	mascula	(L.) L.	Salep mashkull	Orchidaceae	G	Eu
Orchis	coriophora	L.	Salep koriofor	Orchidaceae	G	Eu
Phillyrea	latifolia	L.	Mretë, krifshë, gjethimë, mëreshtë, rrundëz	Oleaceae	Ph	StenoMed
Pistacia	lentiscus	L.	Xinë, sqinde, shqinde, gushtericë, përcëllashmë	Anacardiaceae	Ph	StenoMed
Pistacia	terebinthus	L.	Bafër, qelbës, rucë, rrunjë, rruç	Anacardiaceae	NPh	EuMed
Platanthera	bifolia	(L.) L.C.M. Richard	Platanterë dygjethëse, koçeturrec, veshkali	Orchidaceae	G	EuAz
Polygonatum	multiflorum	(L.) All.	Poligonatë shumëlulëshe	Asparagaceae	G	EuAz
Populus	tremula	L.	Plep i egër, plep dridhës, plep mali	Salicaceae	Ph	EuSiber
Pteridium	aqulinum	(L.) Kuhn	Fiershqipe, vralo	Dennstaedtiaceae	G	Kozmop

Gender	Species	Author	Albanian Name	Family	Life Form	Chorology cal type
Pulicaria	dysenterica	)L.) Bernh.	Plenër dizanterike, brëngëçë	Asteraceae	H	EuMed
Pulicaria	vulgaris	Gaertner	Plenër e rëndomtë	Asteraceae	T	Paleotemp
Putoria	calabrica	(L.fil.) DC.	Bar I qelbur, rrojbë, marrologë, fendëse	Rubiaceae	Ch	Med
Quercus	frainetto	Ten.	Shparth, ballgum, bungëkeqe, bungël	Fagaceae	Ph	Steno-Med
Quercus	ilex	L.	Ilqe, hilqe, lëqeshtë, ylnjë, ylqer	Fagaceae	Ph	Steno-Med
Quercus	pubescens	Willd.	Bungëbutë, lis i butë, gogrek, bungëleshe	Fagaceae	Ph	Med
Quercus	cerris	L.	Qarr, lis i bardhë, qarr i bardhë	Fagaceae	Ph	Steno-Med
Ramonda	serbica	Pancic	Ramondë e Serbisë	Gesneriaceae	H	Balk
Ranunculus	velutinus	Ten.	Zhabinë e velustë	Ranunculaceae	H	Med
Ranunculus	sardous	Crantz	Zhabinë e Sardenjës	Ranunculaceae	T	EuMed
Rhus	coriaria	L.	Shqemë, tumak, barru, rrungël	Anacardiaceae	Ph	Steno-Med
Rosa	agrestis	Savi.	Trëndafil fusharak	Rosaceae	NPh	EuMed
Rosa	canina	L.	Trëndafil qeni, krocë, kromë, kaçibardh	Rosaceae	NPh	EuKaukaz
Rubus	canescens	DC.	Manaferrë e përhimtë	Rosaceae	NPh	EuMed
Rubus	ulmifolius	Schott	Manaferrë, manxë, manëbollicë	Rosaceae	Ch	EuMed
Rumex	acetosa L. subsp. acetosa	L.	Lëpjetë, lëpjetë e thartë	Polygonaceae	H	Circumbor
Rumex	alpinus	L.	Lëpjetë alpine	Polygonaceae	H	EuKaukaz
Rumex	pulcher	L.	Lëpjetë e bukur	Polygonaceae	H	EuMed
Ruscus	aculaetus	L.	Rrushkull gjembor, herëpelë, përce, ruspë, gargafec	Liliaceae	Ch	EuMed
Salvia	officinalis	L.	Sherbelë mjeksore, gjumënesh, dunicë mali	Lamiacea	Ch	Steno-Med
Salvia	verbenaca	L.	Sherbelë shporizë	Lamiacea	H	EuMed
Salvia	verticillata	L.	Sherbelë qerthullake, mendëkrejçe, mendër krejcë	Lamiacea	H	EuKaukaz
Sambucus	nigra	L.	Shtog i zi	Caprifoliaceae	Ch	EuKaukaz
Satureja	montana	L.	Trumzë, shtërmen	Lamiacea	Ch	Med
Securigera	securidaca	(L.) Degen & Doerfler	Sekurigerë sekuridakë	Fabaceae	T	EuMed
Phedimus stellatus (L.) Raf.		L.	Rrushqyqe yllore	Crassulaceae	T	StenoMed
Jacobaea	aquatica	(Hill) G.Gaertn.,	Pulith ujor	Asteraceae	H	EuQ

Gender	Species	Author	Albanian Name	Family	Life Form	Chorological type
		B.Mey. & Scherb.				
Senecio	doronicum	(L.) L.	Pulith doronikë	Asteraceae	H	EuJ
Sesleria	coerulans	Friv.	Pirë e kaltërt	Poaceae	H	SubBalk
Sideritis	montana	L.	Siderit malesh	Lamiacea	T	MedTuran
Silene.	latifolia	Poir	Klokëz e bardhë	Caryophyllaceae	T	StenoMed
Solanum	villosum	Miller	Solanë e verdhë	Solanaceae	T	EuMed
Sorbus	aucuparia	L.	Vadhe e egër, allxhuran, burkijë, rruç	Rosaceae	Ph	Eu
Sorbus	domestica	L.	Vadhe, brreki, vojsë, survë, voesë	Rosaceae	Ph	EuMed
Spartium	junceum	L.	Xanë, gjineshtër, sallaftogë	Fabaceae	Ph	EuMed
Taxus	baccata	L.	Tis, tam, dysne, urenjë, vejnë	Taxaceae	Ph	Temp
Teucrium	chamedrys	L.	Arrs si dushk i vogël	Lamiacea	Ch	EuMed
Teucrium	polium	L.	Bar i majasëllit, lule zoje	Lamiacea	Ch	StenoMed
Thymus	capitatus	(L.) Hoffmans. & Link.	Thrumë	Lamiacea	Ch	StenoMed
Tilia	tomentosa	Moench.	Bli shajakor	Tiliaceae	Ph	EuJ
Tilia	platyphylos	Scop.	Bli gjethegjerë, bli llapush, llukë, lipë	Tiliaceae	Ph	EuKaukaz
Tribulus	terrestris	L.	Tribulë toksore	Zygophyllaceae	T	Kozmop
Trifolium	campestre	Schreber	Trifil fushash, tetelinë e egër, tërfojë e saritë	Fabaceae	T	Paleotemp
Tulipa	sylvestris	L.	Tulipan pyjesh	Liliaceae	G	EuMed
Ulmus	minor	Miller	Vidh	Ulmaceae	Ph	EuKaukaz
Valerianella	coronata	(L.) DC. In Lam. & DC.	Haraqinëz e kurorëzuar	Valerianaceae	H	Eu
Verbascum	blattaria	L.	Netull e furrtares	Scrophulariaceae	H	Kozmop
Verbascum	phlomoides	L.	Netull bezgëngjashme	Scrophulariaceae	H	EuAz
Vicia	sativa	L.	Grashinë e kultivuar, groshilë, buxhak, mozgë	Fabaceae	T	MedTuran
Vicia	villosa	Roth	Grashinë leshtore	Fabaceae	H	StenoMed
Viola	odorata	L.	Manushaqe, vjollcë	Violaceae	H	EuMed
Viola	tricolor	L.	Manushaqe tringjyrëshe, surratkë	Violaceae	T/H	EuAz
Viscum	album	L.	Veshtull, dishël, name, evull	Loranthaceae	NPh	EuAz
Vitis	vinifera	L.	Hardhi	Vitaceae	Lian	EuAz

Among the medicinal species, the most representative family is the Asteraceae (13 species), followed by the

Rosaceae (11 species), Lamiaceae (10 species), and Fabaceae 8 species, (figure 1).
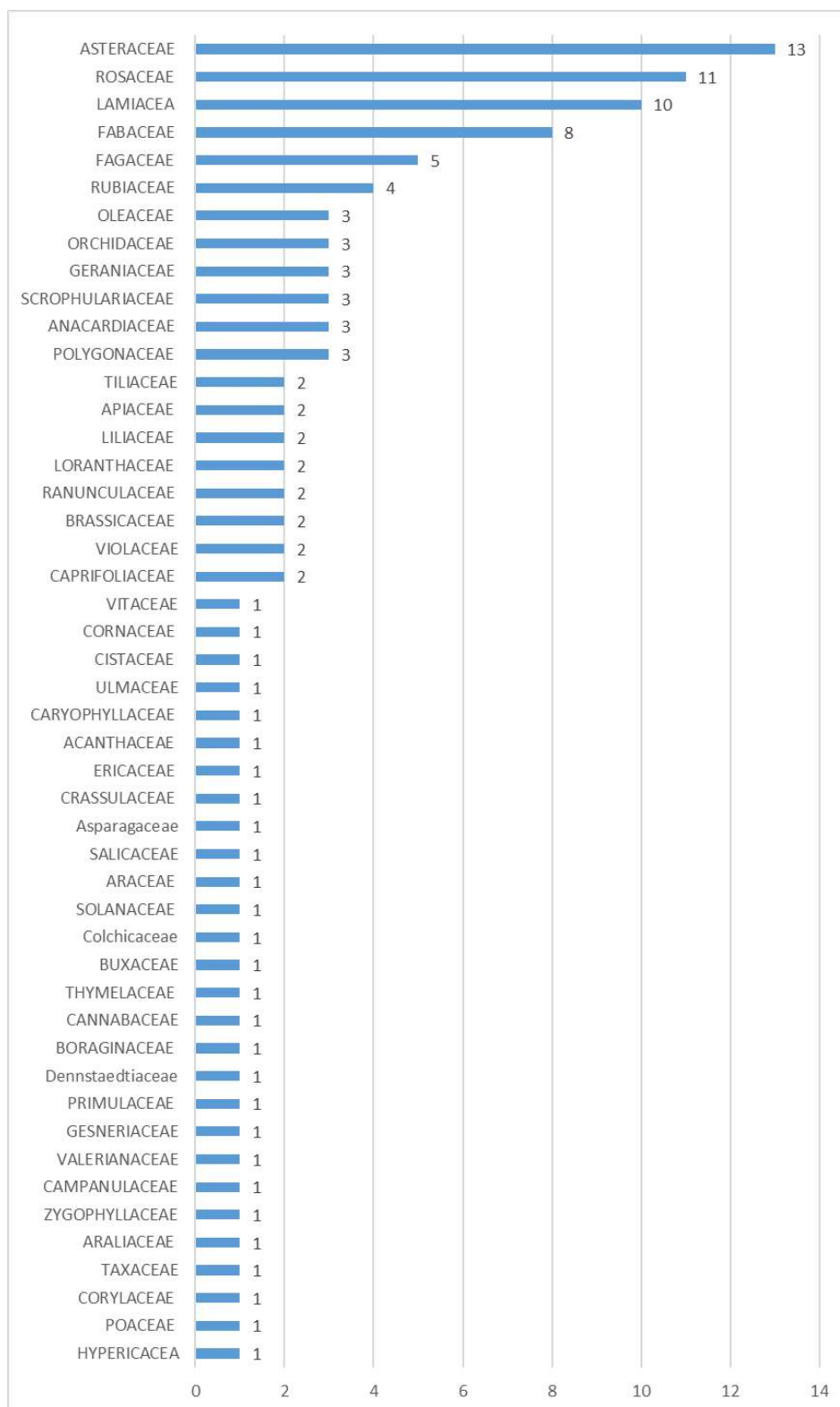
Figure 1. Representative plant families of Medicinal Plants for species preserved in NH, from Libohove, Dropull, Gjirokastër

In general, the herbaceous species are dominant compared to the shrubs and trees, since the dry calcareous pastures are the predominant vegetation communities. Among the total list of species, the most represented biological form is the hemichryptophyta (H), to be followed by the therophyte (T) and Geophyta (G), (figure 2).
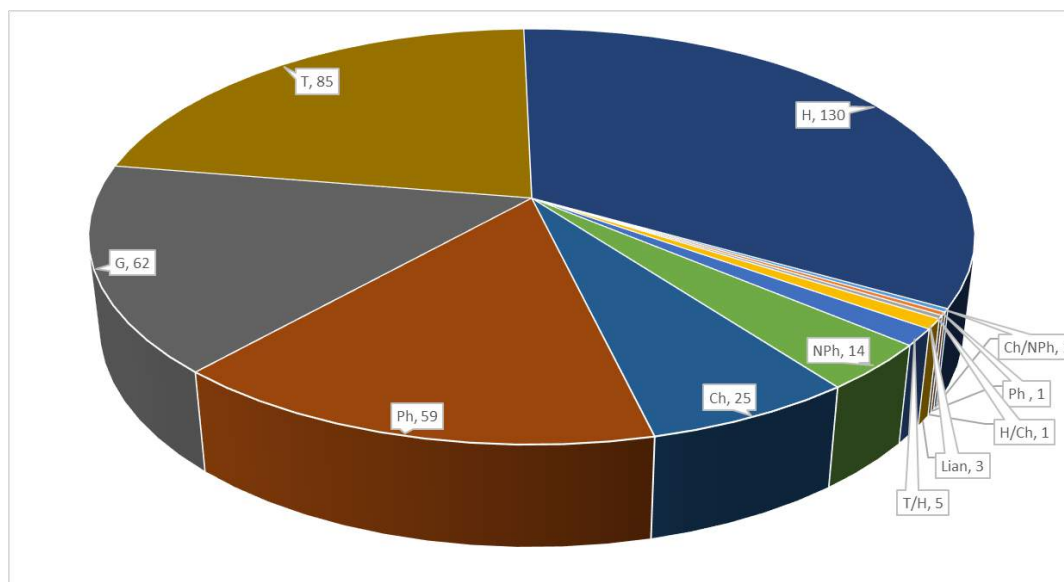
Figure 2. Total life form of the species preserved in NH

Even for medicinal plants, the most representative life form is the Hemichryptophita (37 species MAP), which is in line with the national statistics. Then it is followed by the Phanerophyta (26 species), Therophyta (18 species).
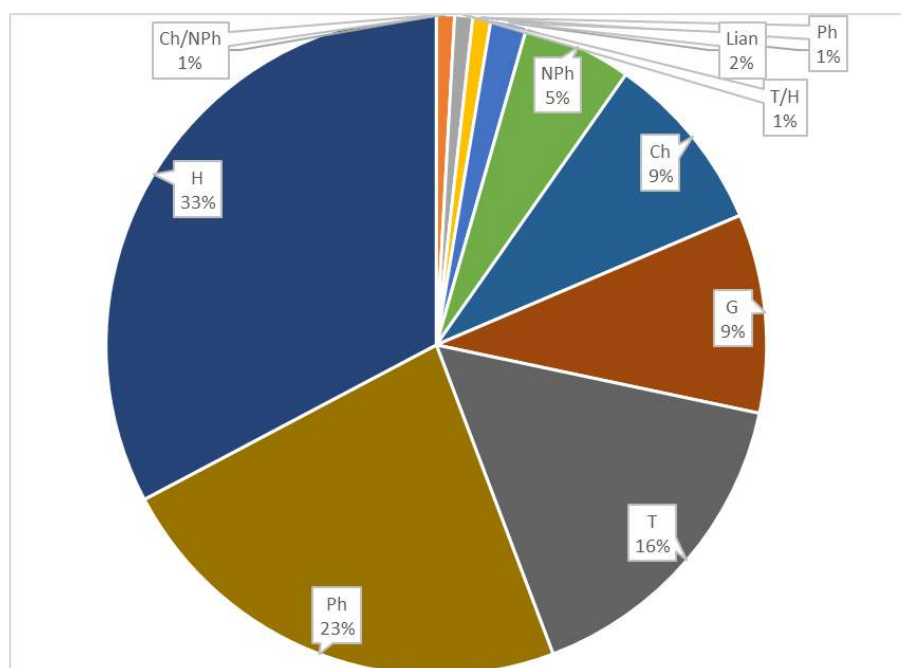
Figure 3. Medicinal plant life forms for plant species preserved in NH for the study areas

The species preserved in the National Herbarium for the study areas are part of 44 chorological types, where the most representative are the European-Mediterranean group (66 species), and European Asiatic group (37 species). Such results come due to the geographical position of Albania, which is part of a biogeographic region: The Mediterranean and the Alpine ones. What is well noticed is the high number of species that are strictly limited in the Mediterranean area (StenoMed, 30 species), and the Balkan species (20 species). The medicinal plants belong to 25 chorological groups, where most of them are from the European Mediterranean group (22 species), followed by the Steno Mediterranean group (10 species), etc., (Figure 4).
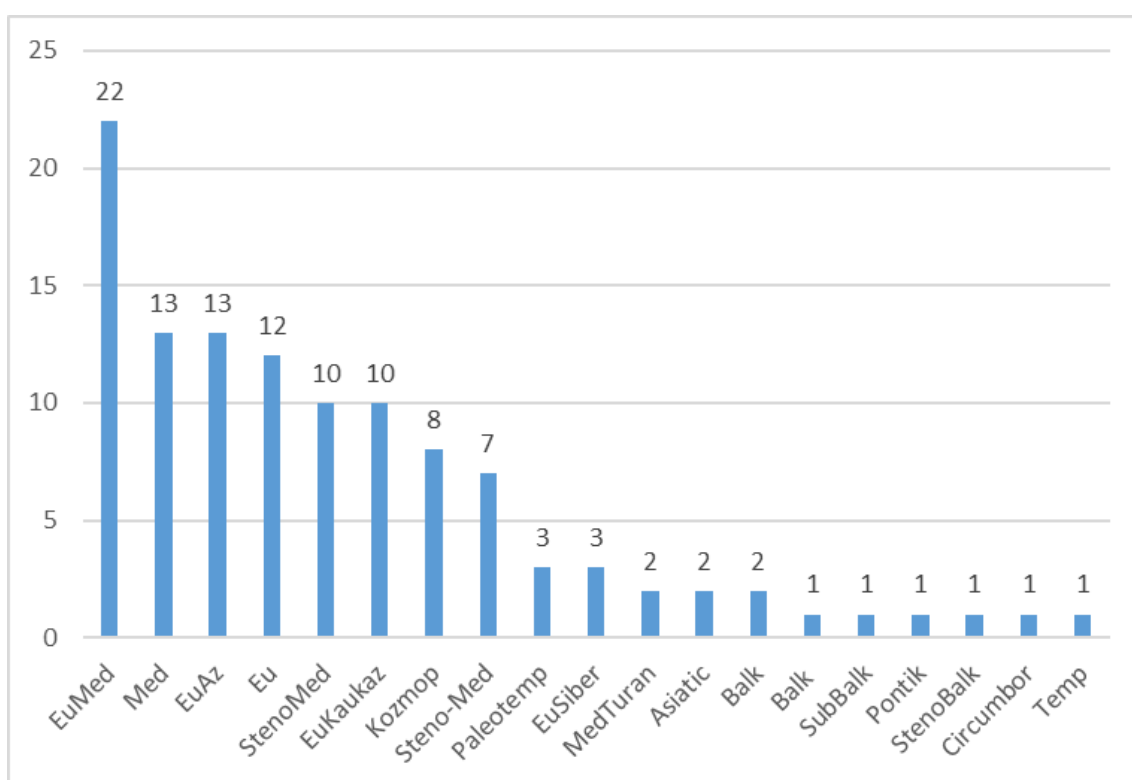
Figure 4. Chorological groups that belong to the aromatic plants preserved in the NH, for the study areas

Of the species listed, a subset holds a conservation status at national and international levels, where 8 species of these are medicinal plants (table 3). Such species are*: Ramonda serbica* Pancic (VU A1b), *Salvia officinalis* L. (VU A1b), *Satureja montana* L. (VU A1C), *Sideritis raeseri* Boiss. & Heldr. (EN A1c), *Viscum album* L. (VU A1c) Many medicinal plants are overharvested with unsustainable practices, due to their therapeutic properties, leading to a decline in their populations or their habitat loss. This over-exploitation often places them at risk, warranting conservation efforts. In Albania the trade of medicinal plants is one of the main economic income, for local inhabitants.

While some medicinal plants can be cultivated, many are still sourced from the wild. The difficulty or cost of cultivation contributes to their overcollection in natural habitats, increasing the risk of extinction. As well dangerous as unsustainable harvesting, climate change has a very high impact.

Table 3. Total List of Species with conservation status according to Albanian Red List of Flora (Group of Authors, 2013)

Genera	Species	Author	Family	Albanian Status	Medicinal Values
Achillea	frasii	Schultz Bip.	ASTERACEAE	CR B3c	
Anacamptis	pyramidalis	(L.) C.M. Richard	ORCHIDACEAE	VU A1b	
Colchicum	autumnale	L.	Colchicaceae	EN A1b	Medicinal
Hypericum	perforatum	L.	HYPERICACEA	EN A1b	Medicinal
Juniperus	foetidissima	Willd.	CUPRESSACEAE	EN A1b	
Juniperus	oxycedrus	L.	CUPRESSACEAE	VU A1b	
Ophrys	bombyliflora	Link in Schrader	ORCHIDACEAE	VU A1b	
Ophrys	ferrum-equinum	Desf.	ORCHIDACEAE	VU A1b	
Ophrys	insectifera	L.	ORCHIDACEAE	VU A1b	
Ophrys	lutea	(Govan) Cav.	ORCHIDACEAE	VU A1b	
Ophrys	reinholdii	Spruner ex Fleischm.	ORCHIDACEAE	VU A1b	
Ophrys	scolopax	Cav.	ORCHIDACEAE	VU A1b	
Ophrys	sphegodes	Miller	ORCHIDACEAE	VU A1b	
Ophrys	tenthredinifera	Willd.	ORCHIDACEAE	VU A1b	
Orchis	quadripunctata	Cyr. ex Ten.	ORCHIDACEAE	VU A1b	
Orchis	simia	Lam.	ORCHIDACEAE	VU A1b	
Orchis	purpurea	Hudson	ORCHIDACEAE	VU A1b	
Orchis	provincialis	Balbis	ORCHIDACEAE	LR cd	
Anacamptis	papilionacea	(L.) R.M.Bateman, Pridgeon & M.W.Chase	ORCHIDACEAE	VU A1b	
Anacamptis	morio	(L.) R.M.Bateman, Pridgeon & M.W.Chase	ORCHIDACEAE	VU A1b	
Orchis	mascula	(L.) L.	ORCHIDACEAE	VU A1b	Medicinal

Genera	Species	Author	Family	Albanian Status	Medicinal Values
Anacamptis	laxiflora	(Lam.) R.M.Bateman, Pridgeon & M.W.Chase	ORCHIDACEAE	VU A1b	
Orchis	coriophora	L.	ORCHIDACEAE	VU A1b	Medicinal
Orchis	spitzelli	Sauter ex Koch	ORCHIDACEAE	VU A1b	
Origanum	vulgare	L.	LAMIACEA	EN A1b	
Prunus	avium	L.	ROSACEAE	VU A1b	
Ramonda	serbica	Pancic	GESNERIACEAE	VU A1b	Medicinal
Salvia	officinalis	L.	LAMIACEA	VU A1b	Medicinal
Satureja	montana	L.	LAMIACEA	VU A1c	Medicinal
Sideritis	raeseri	Boiss. & Heldr.	LAMIACEA	EN A1c	
Viscum	album	L.	LORANTHACEAE	VU A1c	Medicinal

According to the IUCN global, most of the species has the status Least Concern (60 species), to be followed by two species with the status Near threatened, which are *Orchis spitzelli* Sauter ex Koch and *Sideritis raeseri* Boiss. & Heldr. Both these species have aromatic values and their unsustainable harvesting, as well as the climate change has led to their global habitat loss. Also, according to IUCN global, the European species of *Sorbus aucuparia* L. has the status of Vulnerable, due mostly to the forest loss, by cutting, fires and floods.

By the historical analysis of the flora found in the National Herbarium for the study areas, it is revealed that the first specimens were collected by Albanian botanists in 1948, by Ilia Mitrushi (*Quercus pubescens* Wild.). But most of the specimens were collected after the 50s up to the 90s, by the creation of the Biological Research Institution and the Albanian National Herbarium. After the 9s due to the political changes in Albania, there is lack specimen's collection, to be recovered after the 2000s, where the newest entry is dated in2024, by local botanists.

The National Herbarium is constantly enriched by different botanists, local or international. Most of the specimens were collected in Gjirokaster Municipality (380 species), to be followed by Dropull Municipality (55 species) and Libohovë Municipality (18 species) shown in figure 5. As it is mentioned before most of the collections date during communism period and the low incomes from Dropull and Libohovë are due to the time restrictions for border areas.
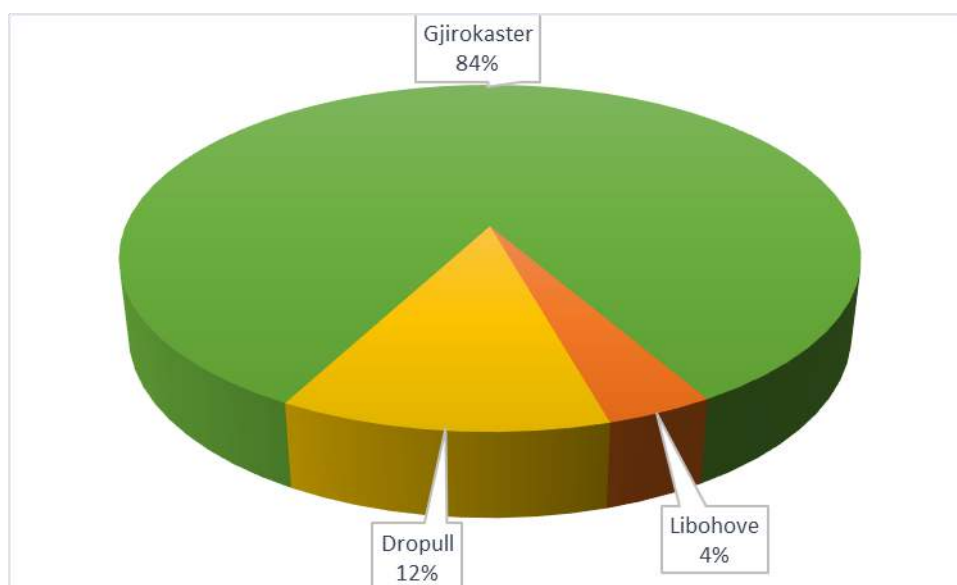
Figure 5. Percentages of specimen locations found in NH for the study areas

Discussion

In the National Herbarium are preserved several considerable specimens of Albanian Flora from the Municipalities Libohovë, Dropull, and Gjirokastër. It resulted in a total list of 380 species where 113 of which have medicinal values. The area is mostly dry stony pastures therefore most of the species dominated are the hemicryptophyte and the therophyte. Due to the presence of the Mediterranean biogeographic region and Alpine biogeographic region, the Euro – Mediterranean chorological group is dominant. The species were first collected, in 1948, to be followed in the 50s up to 90s. The newest data entry collection is 2024 which perfectly shows the crucial role of NH in botanical studies. Most of the collected species are from Gjirokaster Municipality, and fewer are from Dropull and Libohovë, due to their position as border areas and the restrictions before the 90s.

Due to the high inclinations of the study area is favorable for a rich plant collection, with important species which have a conservation status at national and international levels. Therefore, according to the Albanian Red List of flora, 33 species from the total list are under protection. Most of the species has the status Vulnerable (60%), to be followed by Endangered (15%) , Critically Endangered (1%), Least Concern (1%). Notably, 8 of these species are identified as medicinal plants, which are: *Ramonda serbica* Pancic (VU A1b), *Salvia officinalis* L. (VU A1b), *Satureja montana* L. (VU A1C), *Sideritis raeseri* Boiss. & Heldr. (EN A1c), *Viscum album* L. (VU A1c)

The National Herbarium of Albania is very important in strengthening botanical research and sustainable resource management. By updating and curating the collections, including digitalization and digitization, researchers will provide the next step for further research in the study areas, in various scientific fields such as ecology, ethnobotany, taxonomy, and habitats studies.

Acknowledgements

References

Barina, Z., Pifko, D. (2011). Contributions to the flora of Albania. *Willdenowia*, 41, 139-149.

Ellenberg, H., Mueller-Dombois, D. 1967: A key to Raunkiaer plant life forms with reviesed subdivision. *Berichte des Geobotanischen Instituts der ETH*, Stift., Rübel, Zürich, 37: 56-73.

Malo, S. & Shuka, L. (2008). New records on the Flora of Gjirokastra region (South Albania). – Natura Montenegrina 7(3), 369–373

Malo, S. & Shuka, L. (2009). Ekologjia, përhapja dhe statusi aktual i bimëve të rralla dhe të rrezikuara të rrethi Gjorokastër. (Ecology, distribution and present status of rare and endangered plants of the Gjirokastra district) – *Buletini Shkencor, Seria e Shkencave Natyrore* (Skhodër) 59, 125–139.

Niedzielski, P., Markiewicz, J. (2023). Digitalization of herbarium collections as a tool for the commercialization of scientific knowledge. *Proceedia Computer Science*, 225, 2194-2203.

Paparisto K., Demiri M., Mitrushi I., Qosja Xh., Vangjeli J., Ruci B., Mullaj A. 1988-2000: Flora e Shqipërisë, 1-4. *Instituti i Kërkimeve Biologjike*. Tiranë.

Roma-Marzio, F., Maccioni, S., Dolci, D., Astuti, G. (2023). Digitization of the historical herbarium Michele Guadagno at Pisa (PI-GUAD). *PhytoKeys* 234, 107-125.

Saçdanaku, E., Bajrami, A., Saliaj, O., Mullaj, A. (2018). Museum of Natural Sciences "Sabiha Kasimati": past and present. *Museologia Scientifica* 12, 130-137.

Smedt, S., Bogaerts, A., Meeter, N., Dillen, M. (2024). Ten lessons learned from the mass digitization of a herbarium collection. *PhytoKeys*, 244, 23-37.

Soltis, P.S. (2017). Digitization of Herbaria enables novel research. *American Journal of Botany*, https://doi.org/10.3732/ajb.1700281

Vangjeli J., Ruci B., Mullaj A., Paparisto K., Qosja Xh. (2000). Flora e Shqipërisë. Vol. 4, *Akademia e Shkencave e Republikes të Shqipërisë, Qendra e Kërkimeve Biologjike*.

Vangjeli, J. 2003: Udhëheqës fushor i florës së Shqipërisë. Tiranë, 602 p.

Vangjeli, J. 2015: Excursion Flora of Albania. *Koeltz Scientific Books*. 662 p.

An Ethnobotanical Investigation among Albanians and Greek Minority in the Libohovë and Dropull Areas in South Albania: Preliminary Data

Ajola Mesiti

University of Tirana, Research Center of Flora and Fauna, Albania, ⓘ https://orcid.org/0000-0001-6167-1666

Ermelinda Mahmutaj

University of Tirana, Research Center of Flora and Fauna, Albania

Marjol Meço

University of Tirana, Department of Biology, Albania, ⓘ https://orcid.org/0000-0002-9893-907X

Ani Bajrami

University of Tirana, Research Center of Flora and Fauna, Albania, ⓘ https://orcid.org/0000-0001-5349-2510

Julian Shehu

University of Tirana, Research Center of Flora and Fauna, Albania

Abstract: Ethnobotanical research in the Balkan region is important for documenting local ecological knowledge and practices of the people who inhabited this area and promoting biocultural diversity. An ethnobotanical investigation of medicinal and aromatic plants was carried out for the first time among Albanians and Greek minorities living in the Libohovë and Dropull areas, in South Albania. The survey was conducted by interviewing 12 respondents from seven villages, regarding the traditional uses of medicinal and aromatic plants. Thirty-three plant taxa were found to comprise folk medicinal knowledge and practices. The decoction is the dominant preparation practice in both areas and the most quoted botanical families were Lamiaceae (7), Asteraceae (5), Rosaceae (3), and Apiaceae (2). The uncommon medicinal use of the leaves of *Origanum majorana* L. or manxuranë as shërbet (thick and sweet liquid) for body and mind relaxation was reported for the first time in Albania. Additionally, the different naming of plants by the Greek minority as an essential aspect of ethnobotanical research is important to be recorded as soon as possible, due to the high migration rate in the Dropull area. The preliminary data recorded provide an important basis for further research in medicinal plant knowledge and uses in Southern Albania, focusing on folk plant names, knowledge, and uses by the Greek minority. In the future, the rate of cultural divergence and convergence of Albanians and the Greek minority needs to be addressed to investigate the patterns of cultural diffusion between them due to geographical proximity, living environments, and their shared history.

Keywords: Ethnobotany, Traditional knowledge, Albanians, Greek minority, Balkans

Introduction

Ethnobotany is a distinct field of research concerned with understanding the interrelationship between people and the plants of their environment (Nolan & Turner 2011; Albuquerque & Alves 2016; Schultes 2016). Since its historical foundation, ethnobotany has been regarded as an important field of ethnobiology, or botanical and zoological knowledge present and past (Clement 1998; Hunn 2007). Our deep relationship with plants, or our plant heritage is embodied in culture and traditionally constituted the components mostly concerned with solving specific problems of survival such as fighting diseases (Bajrami, Miri & Rexhepi 2023). In this context, medicinal plants have constituted valuable resources for healing around the world for thousands of years and remain an important healthcare mode for people around the world, with significant economic and health benefits (Srivastava 2018; Fitzgerald, Heinrich & Booker 2019; Asigbaase et al., 2023).

Additionally, the folk classification of plants and their role in each culture combined with the relevance of plants for a group of people, is an important theoretical and methodological approach in ethnobotany (Bajrami & Rexhepi 2018). Ethnobotany strongly contributes to drug development (Heinrich 2000; Domingo-Fernandez et al., 2023), the conservation of biological diversity and sustainable development (Bussman 2002; Pei et al., 2020), conservation and preservation of biocultural diversity (Carlson & Maffi 2004; Bridgewater & Rotherham 2019; Wall et al., 2023; Soukand et al., 2024), food security (Hussain et al., 2023) documenting traditional knowledge (Luczaj 2023) and comparative study of plant names (Nebel & Heinrich 2009). Furthermore, the resilience of social-ecological systems and local ecological knowledge, and properties associated with them such as innovations and adaptations over time, is an important facet of the biocultural system as a whole and ethnobiology as a discipline (Folke et al., 2016; Zank et al., 2022).

Several ethnobotanical studies and extensive fieldwork in the Balkan region have been conducted to assess traditional environmental knowledge about potential applications in the future, including Albania (Pieroni et al., 2005; Pieroni & Quave 2014). In Albania, the first ethnobiological studies were conducted by travelers, explorers, missionaries, naturalists, anthropologists, and botanists, from the late 18th century (1796) to the early decades of the 20th century (1940) (Saraçi & Damo 2021,). They collected traditional knowledge on plant uses related to various purposes (Saraçi & Damo 2021).

Additionally, during communist times, data and sources on the traditional use of plants can be found in the works of several Albanian botanists and ethnobotanists with some of them working at the Institute of Folk Medicine in Tirana (Bajrami 2023). After the turmoil caused by the fall of the communist regime in the 1990s,

an exciting new era for ethnobotanical field studies after the 2000s launched into north, north-eastern, east, south, and south-eastern Albania but is absent in the major cities and the deep south of Albania especially, for minorities such as Roma, Greek minorities and Çam population (Bajrami 2023; Bajrami et al., 2023). In this context, we will try to glimpse into the relationship between people and plants in Gjirokastër county for the first time. Gjirokastër county is one of the 12 counties of Albania, and it is in southern Albania with a population of 58.031 in an area that spans 2884 km2. It consists of seven municipalities, including Libohovë and Dropull.

Libohovë is a town and a municipality situated in the south-eastern of Gjirokastër city, with a total population of 3,667 people yielding a population density of 28.83 individuals per km2 in an area of 248.42 km2. Nestled in Zagori Valley and Pogon, it has a captivating landscape with various habitats, rich flora, and fauna. Three of its most important villages which constitute the municipality of Libohovë are Labovë e Sipërme, Labovë e Poshtme, and Nepravishtë. Additionally, the municipality of Dropull which stretches from south of the city of Gjirokastër and lies on both sides of Drinos river, has a population of 3,503 living in an area of 448.45 km2. The seat of the municipality of Dropull is the village of Sofratikë. Other important villages situated in Dropull are Dervician, Goranxi, and Sotirë.

It is important to mention, that in both municipalities Albania's ethnic Greek minority lives in so-called "minority zones" and constitutes a linguistic, cultural, and religiously distinct minority, with a particular concentration in Drino Valley; the villages of the minority areas are eerily deserted because up to two-thirds of the minority population, have gone to live in Greece, except for the older generation (Vickers 2006). This study aimed to identify and document knowledge and ethnomedical practices in the villages of Libohovë and Dropulli municipalities.

Materials and Methods

The study was conducted in seven villages within the Libohovë and Dropull municipality, located in Gjirokastër County, South Albania on the Balkan Peninsula in Europe (Fig. 1).

Covering an expanse of 2884 km2, the county boasts a current population of 58.031. Interviews were conducted in Labovë e Sipërme, Labovë e Poshtme, Nepravishtë, Dervician, Goranxi, Sofratikë, Sotirë in April and May of 2024, more precisely, from 22.04.2024 until 27.04.2024 and from 27.05.2024 until 29.05.2024. All individuals who participated in this research consented to be included in the study through verbal agreement, aligning with the guidelines set forth by the International Society of Ethnobiology (ISE, 2024) (http://www.ethnobiology.net/). The demography of the respondents is highlighted in Table 2.

A total of 12 respondents were interviewed of which seven were women (n=7) and five men (n=5) and age distribution indicates a prevalence of individuals in the 41-60 age range. Educational attainment does not have a high variability, with individuals holding mostly high school diplomas and bachelor's degrees. Locals

interviewed in the seven villages were housewives, traders/ working in ecotourism, and retired. Additionally, religious affiliation highlights most Orthodox followers (Albanians and Greek minority) and only 3 respondents living in the villages of Libohovë were Bektashi followers (Albanians). The plant specimens were identified with the help of a plant taxonomist and confirmed using Flora of Albania (Demiri 1983).
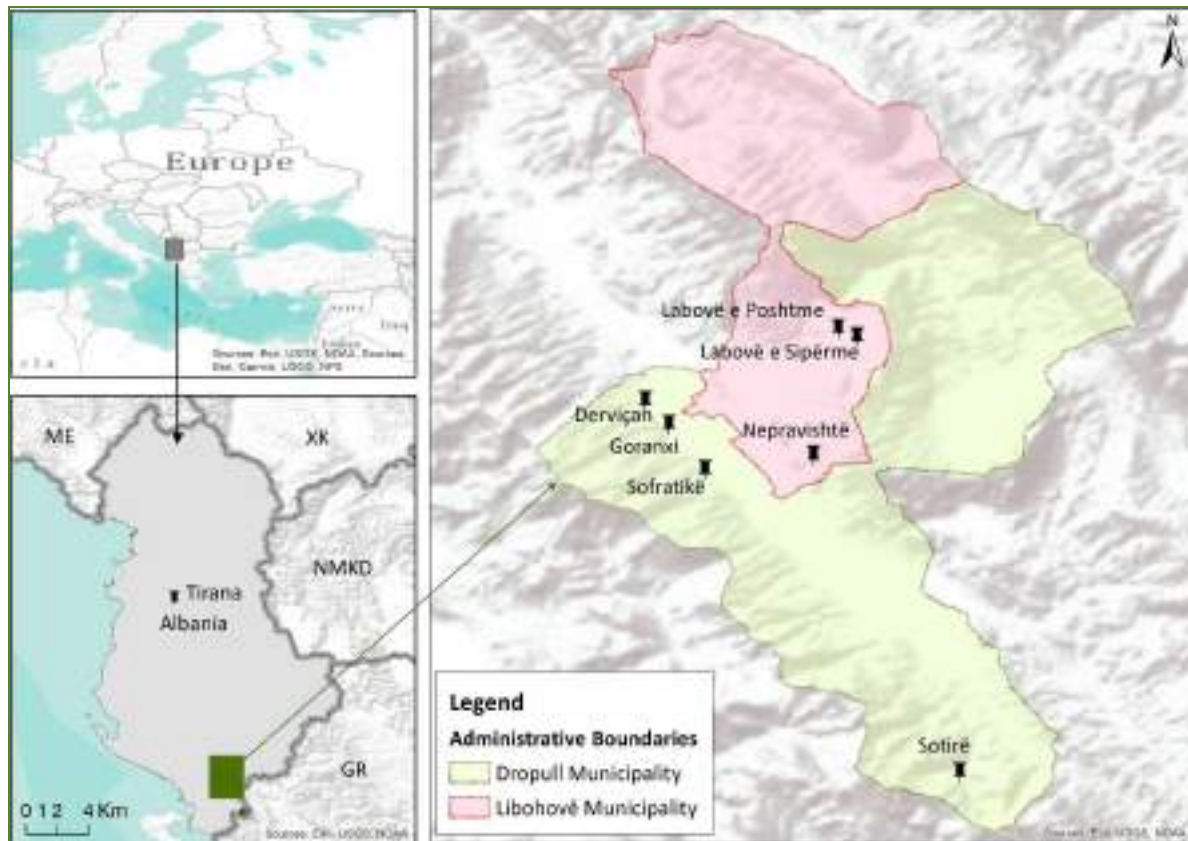
Figure 1. Map of the study area

Table 1. The demography of the interviewers in seven villages (N=12)

Locality		Labovë S	Labovë P	Nepravishtë	Dervician	Goranxi	Sofratikë	Sotirë
Sex ratio	F	1	1	2	1	1	1	1
	M	1	1	1	1	-	-	-
	41-60	2	2	-	1	1	1	1
	61 -	-	-	-	1	-	-	-
Education	High school	2	2	3	1	-	-	1
	Bsc.	1	-	-	1	1	1	-
Occupation	Trader	1	1	1	-	1	1	1
	Housewife	-	-	-	1	-	-	-
	Ecotourism	1	1	2	-	-	-	-

Locality		Labovë S	Labovë P	Nepravishtë	Dervician	Goranxi	Sofratikë	Sotirë
	worker							
	Retired	-	-	-	1	1	-	-
Religion	Muslim (Bektashi)	-	-	3	-	-	-	-
	Orthodox	2	2	-	2	1	1	1

Results

The ethnobotanical data was collected in the seven villages in Libohovë and Dropull. A total of 33 plants belonging to 19 families and 33 genera were reported by our respondents (Table 3). 18 plant species were wild, 11 were cultivated, 3 were both wild and cultivated, and 1 was semi-domesticated.

Table 3. Ethnobotanical uses of the reported taxa

Scientific name	Local name	Origin of availability	Plant parts used	Uses
Allium cepa L.	Qepa	cultivated	Bulb	Antimicrobial/ Used as juice/ *External applications*: skin infections
Anethum graveolens L.	Kopër	wild	Aerial parts	*Decoction*: Antimicrobial properties
Cannabis sativa	Kërpi	cultivated (illegally)	Aerial parts	*Decoction*: For sleep (used in small children/ very small doses)
Cynara cardunculus var. scolymus L.	Angjinarja	cultivated	Flower	*Decoction*: Anti-cholesterol
Dianthus carophylus	Karafili	cultivated	Bulb/ Flower	*Decoction*: Relaxation
Ephedra phoemina	Politriqi	Wild	Stem	*Decoction*: Urinary and kidney problems
Ficus carica L.	Fiku	wild, cultivated	Fruit	*External application*: Ear pain relief
Helichrysym arenarium	Lule akulli; Akja	wild	Aerial parts	*Decoction*: Kidney problems/ for kidney stones
Hypericum perforatum L.	Lule basami	wild	Aerial parts	*External applications:* To cure wounds
Juniperus oxycedrus L.	Dëllinja	wild	Fruit	*Decoction*: Urinary problems

Scientific name	Local name	Origin of availability	Plant parts used	Uses
Laurus nobilis L.	Dafina	semi-domesticated	Plant Specimens/fruit	*Decoction*: Respiratory illnesses (Cold, flu).
Malva sylvestris L.	Mollohe (mëllaga)	wild	Flower/ Leaves	*External applications*: To cure wounds
Matricaria chamomilla L.	Kamomili	wild/ cultivated	Aerial parts	*Decoction*: Relaxation and respiratory illnesses (Cold, flu).
Melissa officinalis	Bar blete	wild	Leaves	*Decoction*: Used for psychoactive effects/sleep and relaxation/ to stabilize blood pressure
Mentha x piperita L.	Dhjozëm	cultivated	Aerial parts	*Decoction*: Digestive issues
Nicotiana tabacum	Duhani	cultivated	Leaves	*External application*: Hemostatic agent to stop bleeding
Ocimum basilicum	Vasiliko (borzilok)	cultivated	Leaves	*Decoction*: For relaxation/ headache
Olea europaea L.	Ulliri	cultivated	Fruit	*External application*: Skin infections
Origanum majorana L	Manxuranë/ rigoni i bardhë	cultivated	Leaves	Used as *shërbet* (thick sweet liquid): For relaxation. *Decoction*: digestive issues
Origanum vulgaris L.	Rigoni	wild	Leaves	*Decoction*: Digestive issues
Papaver rhoeas L.	Paparuna (lulëkuqja)	wild	Seeds	*Decoction:* Used for psychoactive effects/sleep
Petroselinum crispum (Mill.) Fuss	Majdanoz	cultivated	Aerial parts	*Decoction*: Boost immune system; Anti-inflammatory; Digestive health; Wound healing.
Prunus avium L.	Qershia	cultivated	Stem	*Decoction*: Kidney and bladder problems
Prunus spinosa	Kulumbri; kumri	wild	Fruit/ flowers	*Decoction*: Kidney and bladder problems
Rosa canina	Trëndafili	wild	Fruit, petals	*Decoction:* Boost immune system
Salvia officinalis L.	Hamosfaka/ Sherebelë	wild	Leaves	*Decoction*: Respiratory illnesses (Cold, flu); Infections and inflammatory

Scientific name	Local name	Origin of availability	Plant parts used	Uses
				conditions (fever).
Sambucus nigra L.	Lule shtogu	wild	Fruits and flower/ Leaves	*Decoction*: Cold, flu
Sideritis raeseri Boiss & Heldr	Caj mali	wild	Leaves	*Decoction*: Respiratory illnesses (Cold, flu).
Silybum marianum (L.) Gaertn.	Gomarangatho (gjembi i gomarit)	wild	Seeds	Liver issues
Taraxacum officinale L.	Përkalidhe (rradhiqe/ çikore)	wild	Leaves	*Decoction*: Blood purification/ Diabetes
Tilia platyphyllos Scop.	Bliri	wild	Leaves/	*Decoction*: Respiratory illnesses (Cold, flu).
Urtica dioica L.	Cukunidha (hithra)	wild	Leaves	*Decoction*: Blood purification/ Hair health
Zea mays	Mistri	cultivated	Mustaqet e misrit	*Decoction*: Kidney problems

Lamiaceae (7 species), Asteraceae (5 species), Rosaceae (3 species), and Apiaceae (2 species) were the dominant families, followed by other families with one species each (Figure 2).
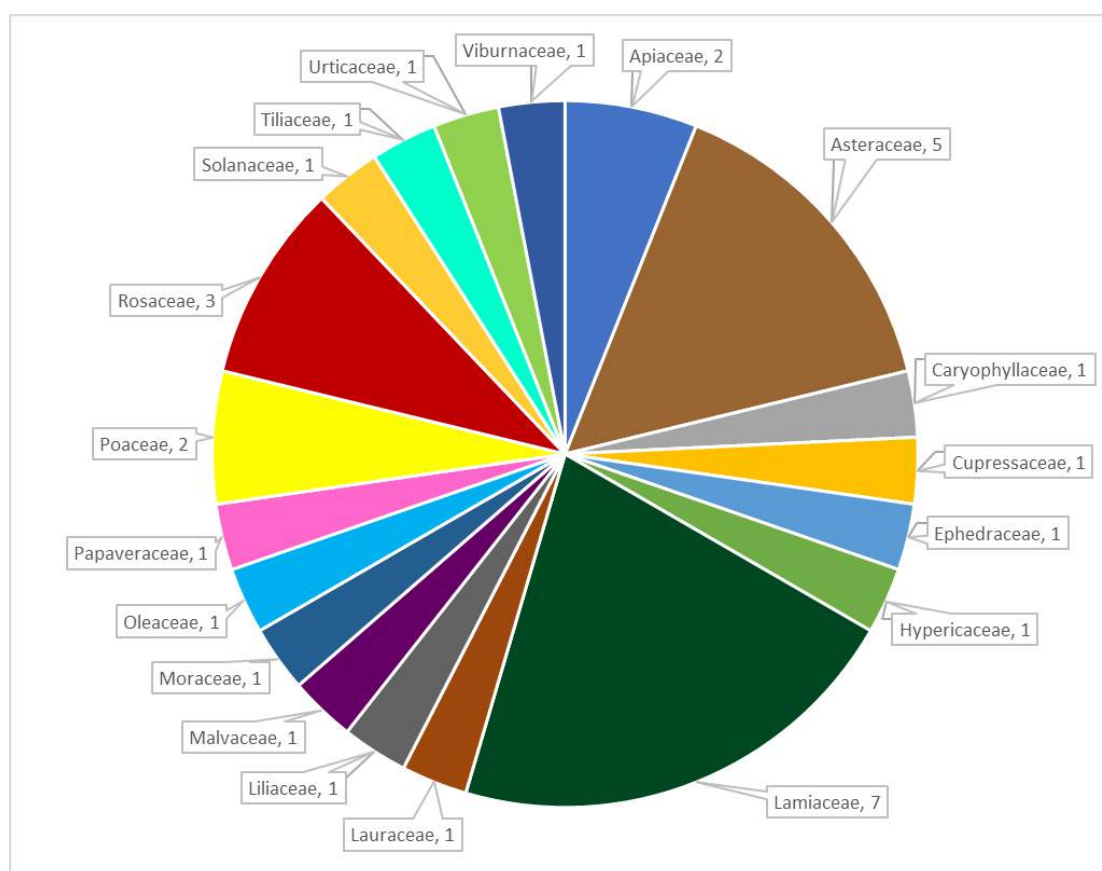
Figure 2. Plant families of reported species

The prevalence of certain plant families in the seven villages as reported by our respondents implies that there is considerable knowledge and practices associated with these families and their plant species; earlier studies have shown that dominant families mentioned in our research are well-established among the Balkan countries (Rexhepi et al., 2013). Additionally, the most frequently cited medicinal uses referred to psychological problems (21%), urological problems (19%), dermatological problems (14%), respiratory problems (14%), gastrointestinal problems (10%), etc. (Figure 3).
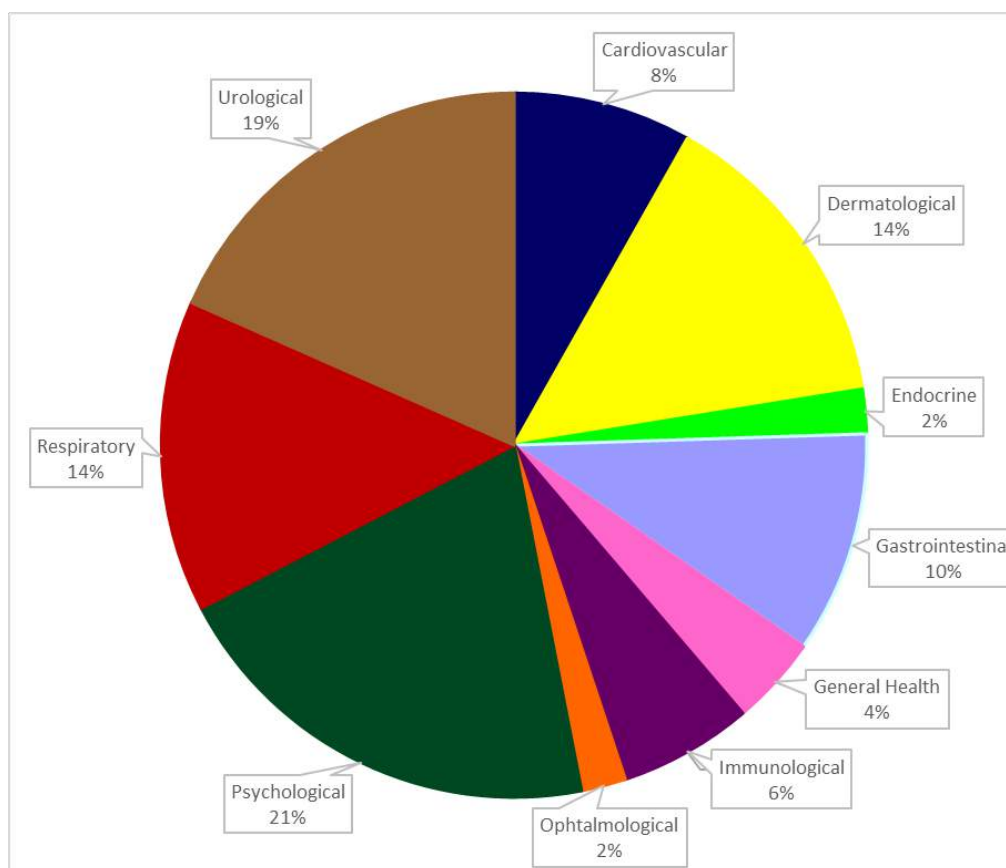
Figure 3. Ethnomedicinal uses of reported plants

The most frequently quoted manner of preparation of plants reported by our respondents was presented by decoction (84%) (Figure 4). External application constituted 12 % of plants reported, mostly for skin infection (*Allium cepa* L. and *Olea europea* L.), to cure wounds *(Hypericum perforatum* L. and *Malva sylvestris* L.), ear pain relief (*Ficus carica* L.) and as a hemostatic agent to stop bleeding (*Nicotiana tabacum*).

An uncommon manner of preparation was shërbet, a thick sweet liquid made from *Origanum majorana* L. leaves, boiled with sugar, and used mainly for relaxation. *Origanum majorana* L. commonly known as sweet marjoram is a medicinal and aromatic plant that belongs to the large Lamiaceae family of plants distributed in the Mediterranean region and it is used in traditional medicine for the treatment of many diseases (Bouyahya et al., 2021). Additionally, the medicinal properties of the parts of the plants used were mostly leaves (33%), aerial parts (18%), flowers (16%), fruit (15%) etc. (Figure 5).
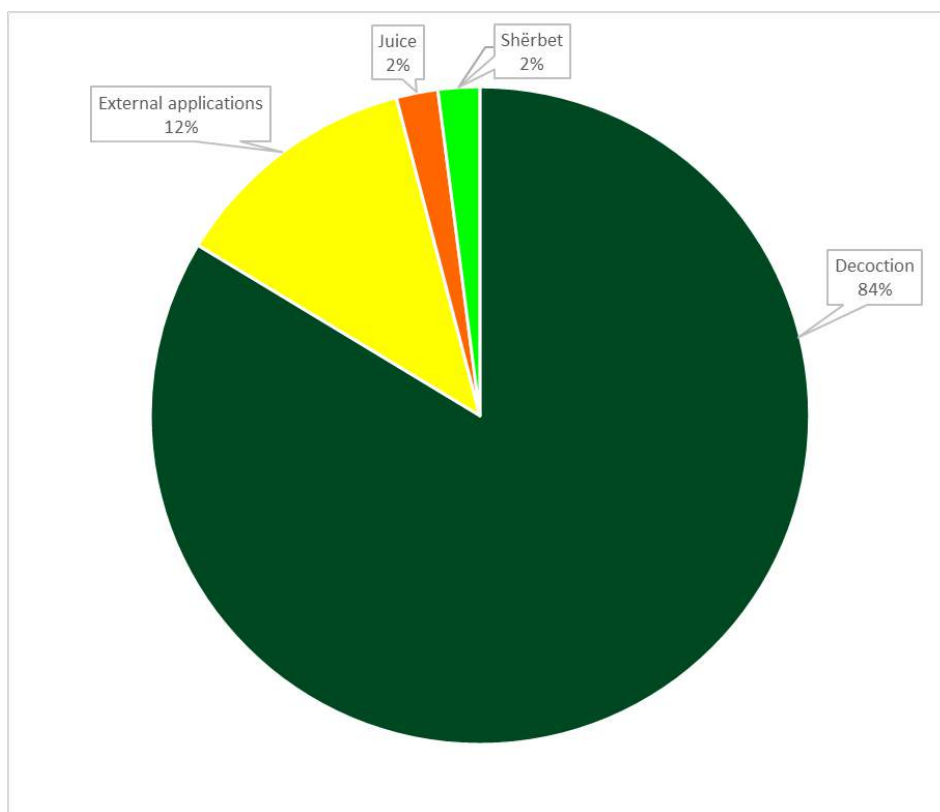
Figure 4. Manner of preparations and administration of the reported medicinal plants.
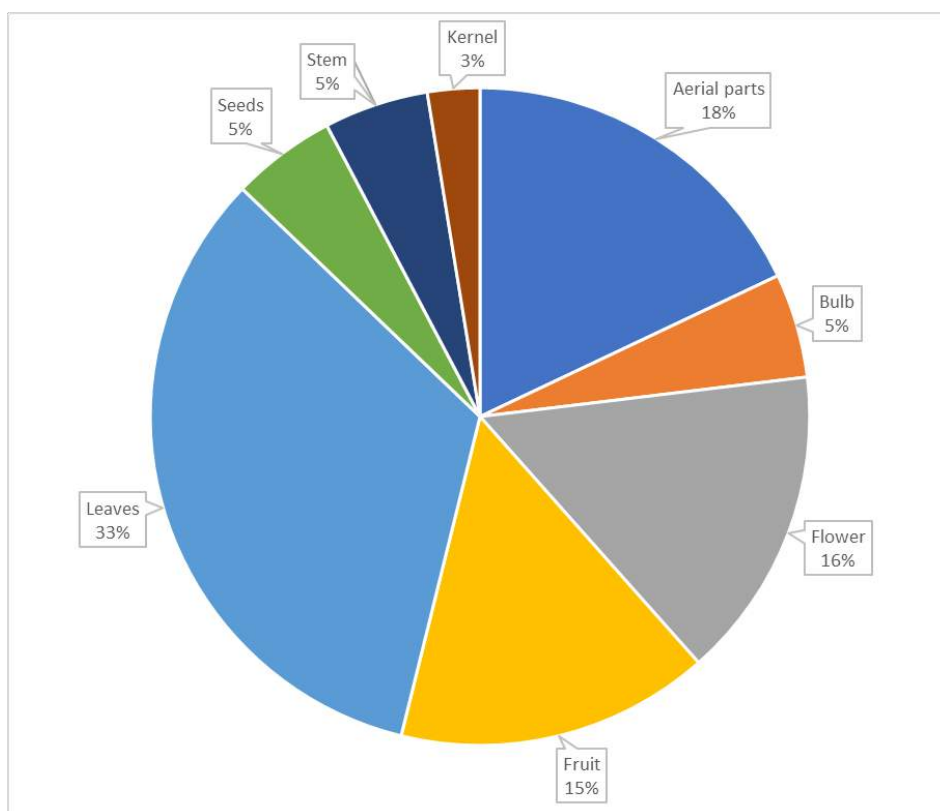
Figure 5. Part of the plants used

Conclusions

The traditional knowledge recorded in the Libohovë and Dropull areas of Southern Albania, despite the limitations of this study in terms of respondents, demonstrates the continuous and rich cultural heritage presented in both areas. The most important finding was the reported medicinal use of the leaves of *Origanum majorana* L, which is commonly known as manxuranë in the local language as a thick and sweet liquid for body and mind relaxation called shërbet; it is an important drink treat (made from fruits or herbs, sugar, and water) still in use today in the Muslim world and a reminder of the Ottoman cultural tradition in Albania. Our study is the first assessment of the Greek minority medicinal plant knowledge and practices in Southern Albania. Local plant names serve as a repository of traditional knowledge (Saraçi, Damo & Bajrami 2023) and along with their medicinal uses serve as a clear indication of their different cultural pathways, mostly due to different religious affiliation and their lack of intermarriage. Further studies should investigate in more detail the patterns of cultural diffusion of the Albanian and Greek minorities in Southern Albania, and document the rich local plant name repository, periled by the area's high emigration rate.

Acknowledgements

References

Albuquerque UP, Alves AGC. (2016). What Is Ethnobiology? In: Albuquerque, U., Nóbrega Alves, R. (eds) Introduction to Ethnobiology. Springer, Cham. https://doi.org/10.1007/978-3-319-28155-1_1

Asigbaase M, Adusu D, Anaba L, Abugre S et al., (2023). Conservation and economic benefits of medicinal plants: Insights from forest-fringe communities of southwestern Ghana. Trees, Forests, People 14, 100462

Bajrami A, Mesiti A, Mahmutaj E & Hoda P. (2023). "The New Normal": Ethnobiology of cities and urban ecological knowledge. Journal of Natural Sciences 34: 139-147.

Bajrami A. (2023). Current status of ethnobotany in Albania. European Journal of Medicine and Natural Sciences 6 (1): 9-17.

Bajrami A, Miri F, Rexhepi B. (2022). Problemet e mbijetesës: Paleoetnobotanika e paraardhësve tanë. Buletini i Shkencave të Natyrës 32: 137-147.

Bajrami A & Rexhepi B. (2018). Antropologjia: Një perspektivë biokulturore. Shtëpia Botuese Morava, Tiranë, Shqipëri.

Bouyahya A, Chamkhi I, Benali T, Guaouguaou FE et al., (2021). Traditional use, phytochemistry, toxicology, and pharmacology of Origanum majorana L. Journal of Ethnopharmacology 265, 113318. https://doi.org/10.1016/j.jep.2020.113318

Bridgewater P & Rotherham ID. (2019). A critical perspective on the concept of biocultural diversity and its emerging role in nature and heritage conservation. People and Nature https://doi.org/10.1002/pan3.10040

Bussmann RW. (2002). Ethnobotany and Biodiversity Conservation. In: Ambasht, R.S., Ambasht, N.K. (eds) Modern Trends in Applied Terrestrial Ecology. Springer, Boston, MA. https://doi.org/10.1007/978-1-4615-0223-4_18

Carlson TJS & Maffi L. (2004). Introduction: Ethnobotany and conservation of biocultural diversity. Advances in Economic Botany. 15: 1-6. http://www.jstor.org/stable/43927638.

Demiri M. (1983). Flora ekskursioniste e Shqipërisë. Tiranë: Shtëpia Botuese e Librit Shkollor.

Domingo-Fernandez D, Gadiya Y, Mubeen S, Bollerman TJ et al., (2023). Modern drug discovery using ethnobotany: A large-scale-cross-cultural analysis of traditional medicine reveals common therapeutic uses. Science 26 (9): 107729. doi: 10.1016/j.isci.2023.107729

Fitzgerald M, Heinrich M & Booker A. (2019). Medicinal plant analysis: A historical and regional discussion of emergent complex techniques. Frontiers in Ethnopharmacology https://doi.org/10.3389/fphar.2019.01480

Folke C, Biggs R, Norstrom AV, Reyers B & Rockstrom J. (2016). Social-ecological resilience and biosphere-based sustainability science. Ecology and Society 21 (3): 41.

Heinrich M. (2000). Ethnobotany and its role in drug development. Phytotherapy Research 14 (7): 479-488.

Hunn E. (2007). Ethnobiology in four phases. Journal of Ethnobiology 27(1): 1–10.

Hussain ST, Muhammad S, Khan S, Hussain W & Pieroni A. (2023). Ethnobotany for food security and ecological transition: wild food plant gathering and consumption among four cultural groups in Kurram District, NW Pakistan. Journal of Ethnobiology and Ethnomedicine 19(1):35. DOI: 10.1186/s13002-023-00607-2.

Ismailati B, Çobani B, Beqari E. (2022). Libohova: Përshkrim gjeografiko-administrativ. Botimet Barleti, Tiranë, Shqipëri.

Łuczaj Ł. (2023). Descriptive ethnobotanical studies are needed for the rescue operation of documenting traditional knowledge. Journal of Ethnobiology and Ethnomedicine 19, 37. https://doi.org/10.1186/s13002-023-00604-5

Nebel S & Heinrich M. (2009). Ta Chorta: A comparative ethnobotanical- linguistic study of wild food plants in a Graeceanic area in Calabria, Southern Italy. Economic Botany 63, 1: 78-92.

Nolan J & Turner NJ. (2011). Ethnobotany: The study of people-plant relationships. Ethnobiology.

Pieroni A & Quave, C. (2014). Ethnobotany in the Balkans: Quo Vadis? In: Pieroni, A., Quave, C. (eds) Ethnobotany and Biocultural Diversities in the Balkans. Springer, New York, NY. https://doi.org/10.1007/978-1-4939-1492-0_1

Pieroni A, Dibra B, Grishaj Gj, Grishaj I, Maçai S. (2005). Traditional phytotherapy of the Albanians of Lepushe, Northern Albanian Alps. Fitoterapia 76: 379– 399.

Pei S, Alan H & Wang Y. (2020). Vital roles for ethnobotany in conservation and sustainable development. Plant Diversity 25: 42(6):399-400. DOI: 10.1016/j.pld.2020.12.001.

Rexhepi B, Mustafa B, Hajdari A, Rushidi-Rexhepi H , Quave CL & Pieroni A. (2013). Traditional medicinal plant knowledge among Albanians, Macedonians and Gorani in the Sharr Mountains (Republic of

Macedonia). Genetic Resources and Crop Evolution 60(7), 2055-2080.

Saraçi A, Damo R & Bajrami A (2023). Plants and religion- Religious motivation in naming of plants in Albania. Collegium Antropologicum 47, 2: 163-169. doi:10.5671/ca.47.2.8

Saraçi A, & Damo R. (2021). A historical overview of ethnobotanical data in Albania (1800s-1940s). Ethnobiology and Conservation 10:08. doi:10.15451/ec2020-10-10.08-1-2.

Schultes RE (2016). Ethnobotany. In: Selin, H. (eds) Encyclopedia of the History of Science, Technology, and Medicine in Non-Western Cultures. Springer, Dordrecht. https://doi.org/10.1007/978-94-007-7747-7_9566

Soukand R, Kalle R, Prakofjewa J, Sartori M & Pieroni A. (2024). The importance of practicity and practice: ethnobotany of Kihnu Island (Estonia) from 1937 to 2021. Plants People Planet 6 (1): 186-196.

Vickers M. The Greek minority in Albania-Current tensions. Balkan Series: Research and Assessment Branch.

Wall J, Lukawiecki J, Young R, Powell L, McAlvay A, Moola F. (2023). Operationalizing the biocultural perspective part II: A review of biocultural action principle since the Declaration of Belem. Environmental Science & Policy https://doi.org/10.1016/j.envsci.2023.103573

Zank S, Ferreira Júnior WS, Hanazaki N, Kujawska M, Ladio AH et al., (2022). Local ecological knowledge and resilience of ethnomedical systems in a changing world – South American perspectives. Environmental Science & Policy 135: 117-127. ISSN 1462-9011.

Implementation of a Perturb and Observe (P&O) Algorithm-Based Technique for Maximum Power Point Tracking (MPPT) in Solar Photovoltaic Systems

Tayoub Hadjira

Research Center in Industrial Technologies CRTI, P.O.BOX: 64, Cheraga 16014, Algiers-Algeria.

Laboratoire d'Analyse des Signaux et Systèmes, Department of Electronics, University of M'Sila BP.166, Route Ichebilia, M'Sila, 28000, Algeria

Bedoud Khouloud

Research Center in Industrial Technologies CRTI, P.O.BOX: 64, Cheraga 16014, Algiers-Algeria,

Merabet Hichem

Research Center in Industrial Technologies CRTI, P.O.BOX: 64, Cheraga 16014, Algiers-Algeria,

Drici Djalel

Research Center in Industrial Technologies CRTI, P.O.BOX: 64, Cheraga 16014, Algiers-Algeria,

Ouajani Brahim

Research Center in Industrial Technologies CRTI, P.O.BOX: 64, Cheraga 16014, Algiers-Algeria,

Abstract: Photovoltaic (PV) systems, serving as sustainable alternatives to conventional energy sources, harness solar energy to generate electricity. PV systems function by converting sunlight into electricity via photovoltaic cells. These cells, typically made of semiconductor materials like silicon, generate a direct current (DC) when exposed to sunlight. However, the output power of a PV system is highly dependent on environmental factors such as solar irradiance, temperature, and shading. MPPT techniques are crucial for optimizing the power output of PV systems by continuously adjusting the operating point to track the Maximum Power Point (MPP). The MPP represents the voltage and current combination at which the PV system delivers its maximum power output for a given set of environmental conditions. By dynamically tracking the MPP, MPPT techniques ensure that the system operates efficiently and extracts the maximum available power from solar irradiance. Among MPPT techniques, the Perturb and Observe (P&O) method is notable for its simplicity and effectiveness. P&O operates by perturbing the operating point of the PV system, typically by varying the system voltage and observing the resulting change in power output. Based on the direction of the power change, the operating point is adjusted accordingly, either increasing or decreasing the voltage. This iterative process continues until the MPP is reached or approximated. Despite its limitations, the P&O technique remains widely used in PV systems, particularly in small to medium-scale installations where simplicity and cost-effectiveness are paramount. Continuous research efforts aim to mitigate the shortcomings of P&O and improve its

performance under challenging operating conditions. In this context, the performance of solar modules under various environmental conditions, such as solar temperature and solar irradiance, is analyzed. The main contribution of this paper is the implementation of the P&O algorithm using MATLAB/Simulink program.

Keywords: PV system, MPPT techniques, P&O algorithm, MATLAB/Simulink

Citation: Hadjira, T., Khouloud, B., Hichem, M., Djalel, D. & Ouajani B. (2024). Implementation of a Perturb and Observe (P&O) Algorithm-Based Technique for Maximum Power Point Tracking (MPPT) in Solar Photovoltaic Systems. In A. A. Khan, M. Demirbilek, & M. L. Ciddi (Eds.), Proceedings of ICSEST 2024-- International Conference on Studies in Engineering, Science, and Technology (pp. 398-409), Istanbul, Turkiye. ISTES.

Introduction

Solar energy stands as a critical renewable energy resource due to its inexhaustible nature and environmentally friendly attributes [1]. Unlike finite fossil fuels, solar power relies on abundant and freely available sunlight, making it a sustainable option for meeting global energy demands while minimizing environmental impact. Unfortunately, the dynamic movement of the sun across the sky, from east to west, introduces variations in solar radiation received by solar panels, consequently impacting their performance [2].

A Maximum Power Point Tracking (MPPT) algorithm is a crucial tool employed to optimize the power output from photovoltaic (PV) modules, especially under fluctuating weather conditions [3]. This algorithm continuously adjusts the operating point of the PV system to ensure that it operates at its maximum power point (MPP), thereby maximizing energy extraction from the solar panels. By dynamically adapting to changing environmental factors such as solar irradiance and temperature, MPPT algorithms enhance the efficiency and performance of PV systems, resulting in increased energy harvest and improved overall system reliability. Research in this field focuses on developing advanced MPPT techniques, such as perturb and observe (P&O), incremental conductance (INC), and fuzzy logic control, to further optimize energy extraction and mitigate the impact of varying weather conditions on solar power generation.

Given the nonlinear characteristics of photovoltaic (PV) modules, modeling and simulation are essential for effective Maximum Power Point Tracking (MPPT) in PV system applications [4]. These models capture the complex behavior of PV modules under varying environmental conditions, such as solar irradiance and temperature, allowing for accurate prediction of the module's power output at different operating points. By simulating MPPT algorithms within these models, we can evaluate the performance of different tracking techniques and optimize their implementation for maximum energy extraction from the PV system. Through advanced modeling and simulation, the design and control of PV systems can be refined to enhance efficiency, reliability, and overall performance, contributing to the widespread adoption of solar energy technologies.

In practice, the Perturb and Observe (P&O) method stands out as the most commonly used technique for Maximum Power Point Tracking (MPPT) in photovoltaic systems [3]. This method operates by perturbing the operating point of the PV system and observing the resulting change in power output to determine the direction of maximum power. Despite its simplicity, the P&O method offers fast response times and robust performance under various operating conditions, making it a popular choice for MPPT implementation in solar energy systems.

In this study, modeling and simulation analysis were conducted to simulate the performance of the photovoltaic (PV) module. Through rigorous simulation procedures, the electrical characteristics of the PV module, including its current-voltage (I-V) and power-voltage (P-V) curves, were systematically evaluated under various operating conditions, such as different levels of solar irradiance and temperature. These analyses provided valuable insights into the nonlinear behavior of the PV module and its response to changing environmental factors. By obtaining a comprehensive understanding of the module's characteristics through simulation, we gained valuable insights into its performance and efficiency, which are essential for the design and optimization of PV systems for maximum energy extraction.

Modeling of Photovoltaic Cell

Photovoltaic Cell Equivalent Circuit

The equivalent circuit model of a photovoltaic (PV) cell is commonly represented by a combination of current sources, diodes, resistors, and shunt resistance. One of the most widely used equivalent circuit models is the single-diode model, which provides a simplified representation of the complex behavior of a PV cell [5].

In the single-diode model, the PV cell is represented by the following elements:

1. Photovoltaic current source (Iph): represents the current generated by the absorption of photons and the creation of electron-hole pairs within the semiconductor material of the PV cell.
2. Diode: represents the junction between the semiconductor materials in the PV cell. It accounts for the nonlinear behavior of the cell, allowing current to flow in one direction (under illumination) and blocking it in the reverse direction.
3. Series resistance (Rs): represents the internal resistance of the PV cell, including the resistance of the semiconductor material and the metal contacts.
4. Shunt resistance (Rsh): represents the leakage current paths in parallel with the diode, typically resulting from defects or imperfections in the semiconductor material.
5. Parallel current source: in some models, a parallel current source is included to account for additional leakage currents.

This equivalent circuit model can be represented mathematically by a set of nonlinear equations that describe the voltage-current relationship of the PV cell under varying operating conditions, such as changes in irradiance and temperature. It serves as a valuable tool for analyzing and predicting the performance of PV systems and

optimizing their design for maximum energy output.
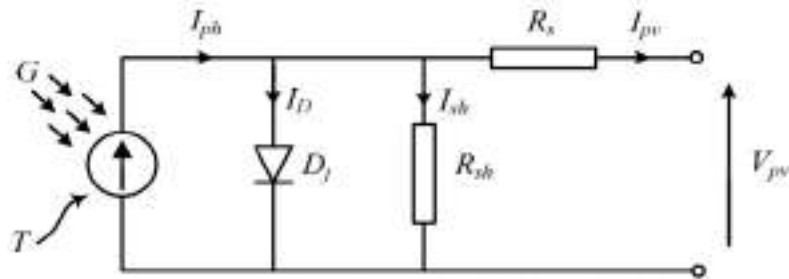
Figure.1. The electric equivalent circuit of a solar cell.

Effect of Irradiation

Simulated I-V (current-voltage) and P-V (power-voltage) characteristics of a photovoltaic (PV) module under varying solar irradiances are essential for understanding the performance of the module under different lighting conditions, they illustrate how the module's performance changes with different levels of sunlight intensity. Figure 2 shows the I-V and P-V characteristics of the solar PV matrix (SunPower SPR-315E-WHT-D) modules at constant temperature (25°C) and variable solar irradiances of 0.1KW/m^2, 1 KW/m^2, and 5 KW/m^2, respectively. Both sets of curves are crucial for understanding the performance of a PV module under real-world conditions and for optimizing its operation to maximize energy production.

As illustrated in Figure 2. a, as solar irradiance increases, both the current and voltage output of the PV module typically increase, leading to a shift in the I-V curve towards higher current values. The change in solar irradiance also has a clear effect on the shape and position of the P-V curve, as well as the location of the MPP, affecting the overall power output of the module (Figure 2.b).

In general, the increment in the irradiation level leads to a theoretical increment in the maximum power voltage when there is no change in the cell temperature. On the other hand, the short circuit current I_{SC} depends totally and linearly on the irradiance level; therefore, the maximum power current is changed as shown in Figure 2 [6].
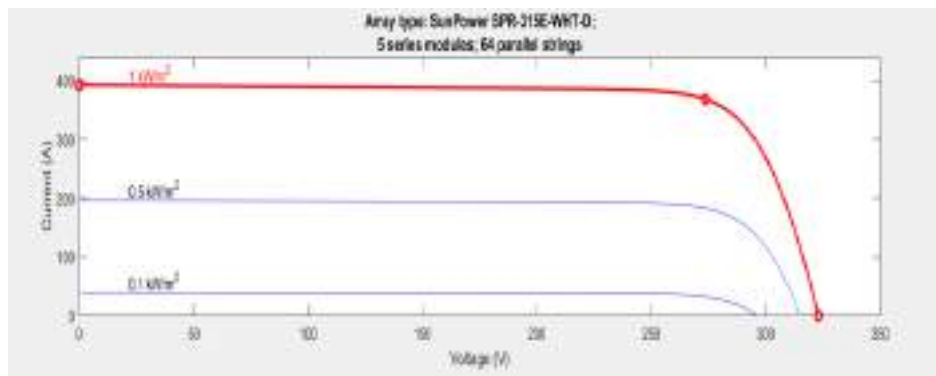
(a)
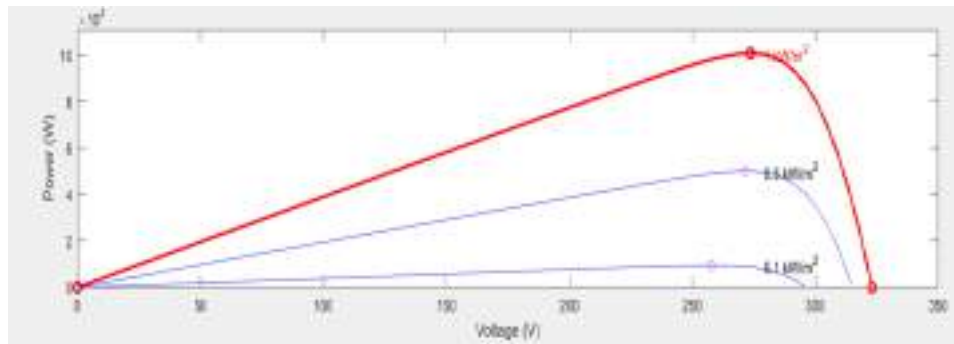
(b)

Figure. 2. Simulated I-V (a) and P-V (b) characteristics of a PV module under varying solar irradiances.

Effect of Temperature

The panel temperature is considered one of the most important parameters due to its effect on the output power of a photovoltaic panel [6]. Figure 3 shows the I-V and P-V characteristics of the solar PV matrix (SunPower SPR-315E-WHT-D) modules at a fixed irradiation level of 1 KW/m^2 and variable temperatures of 5°C, 15°C, 25°C, 35°C and 45 °C, respectively. As shown in Figure 3, the open circuit voltage V_{OC} is highly influenced by the increase of the temperature. Besides, as the temperature increases, it results in a slight increase in the short circuit current I_{SC}, because the band gap energy decreases and more photons have enough energy to create electron-hole pairs.

On the other hand, the increase in temperature has an obvious reduction in the PV panel output power due to the drop in the open circuit voltage V_{OC} and the fill factor; therefore, the module efficiency is reduced [6]. Simulating I-V and P-V characteristics under varying temperatures helps in optimizing the design and performance of PV systems for different climatic conditions, allowing for better prediction of energy output and system efficiency.
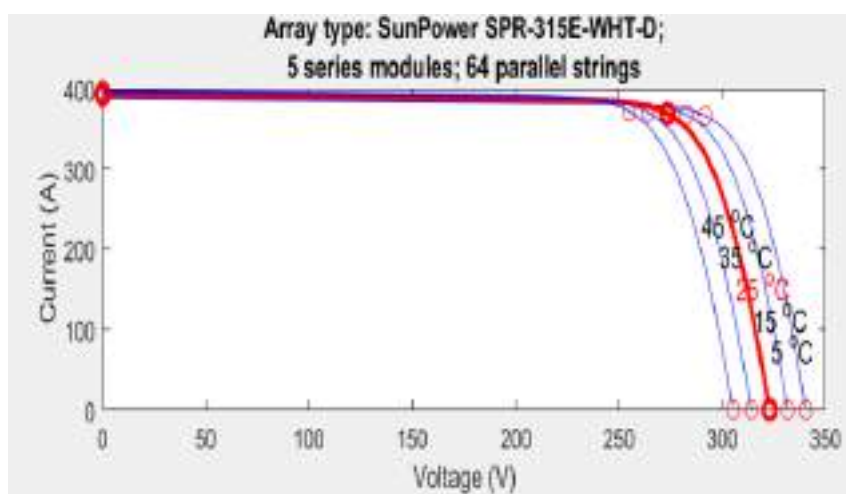
(a)
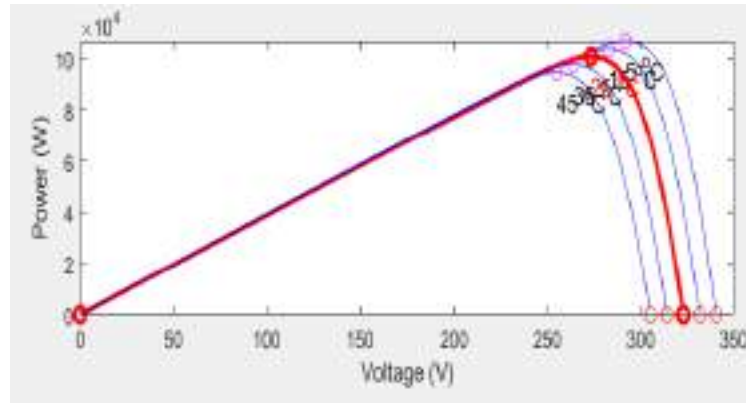
(b)

Figure. 3. Simulated I-V (a) and P-V (b) characteristics of a PV module under varying temperatures.

The design of the photovoltaic panel matrix is started by selecting the PV panel module SunPower SPR-315E-WHT-D. The specifications of the PV matrix and the selected PV panel parameters used in all of the simulations are given in Table 1.

Table 1. Specification of the solar module: SunPower SPR-315E-WHT-D.

Characteristic	Value
Number of series panels	5
Number of parallel PV lines	64
Maximum Power (W)	315.072 W
Voltage Maximum Power (V_{max})	54.7 V
Current at Maximum power (I_{max})	5.76 A
Voltage at Open circuit (V_{OC})	64.6 V
Photo Current (I_{SC})	6.14 A
Temperature coefficient of Voc	-0.2727 %/°C
Temperature coefficient of Isc	0.061743 %/°C

Perturb and Observe Algorithm (P&O)

Photovoltaic (PV) systems employ the Perturb and Observe (P&O) approach for Maximum Power Point Tracking (MPPT). Its main objective is to guarantee that the PV system works at or close to its maximum power point (MPP) under varying environmental factors, such as variations in solar irradiance, temperature, and shading. To determine whether the power is increased or decreased, adjustments are made to the voltage of the PV module. When an increase in voltage results in a corresponding increase in power, it indicates that the operating point of the PV module is on the left of the MPP [26]. Hence, further perturbation is required towards the right to reach MPP. On the contrary, if an increase in voltage leads to a decrease in power, it indicates that the operating point of the PV module is on the right of the MPP. Therefore, additional perturbations towards the

left are necessary to reach the MPP [7]. By continuously perturbing the operating point of the PV system and observing the resulting change in power output, the P&O algorithm can dynamically adjust the system's operating conditions to maintain operation at the MPP. This helps maximize the energy harvest from the PV array, thereby improving overall system efficiency and performance.

In a standard photovoltaic (PV) system, the maximum power point tracking (MPPT) function block regulates the duty cycle of a converter, such as a boost or buck-boost converter, to align the impedance of the PV array with that of the impedance of the load or output side. This matching allows the maximum power transfer to occur between the PV array and the load, maximizing the efficiency of the system. Therefore, while direct connection is simpler and may be suitable for certain applications, using a DC-DC converter with MPPT capability is often preferred in PV power conversion systems to maximize energy harvest and system efficiency, especially in variable environmental conditions. A schematic of the complete model can be seen in Figure 4.
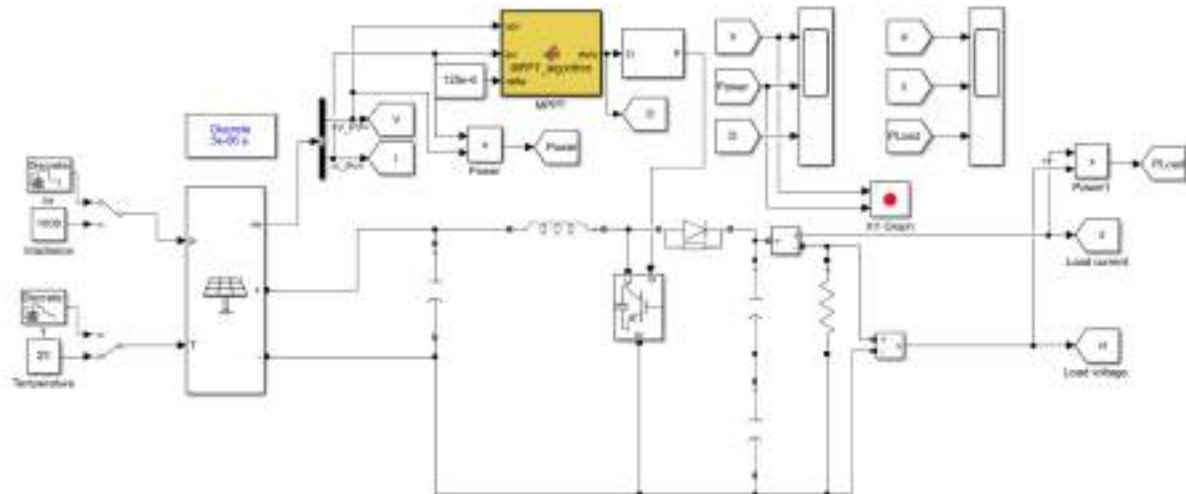
Figure.4. The model of PV array in Simulink.

Methodology Adopted

The Perturb and Observe (P&O) algorithm represents a simple Maximum Power Point Tracking (MPPT) technique employed in PV systems. Essentially, it continuously perturbs the operating point of the photovoltaic system and observes the consequent variation in power output to determine the direction toward the maximum power point (MPP). Here's a concise explanation of the P&O algorithm:

1. Start at an initial operating point.

2. Perturb the operating point by a small amount.

3. Measure the change in power output (dP_{PV}).

4. If the power output increases, continue perturbing in the same direction.

5. If the power output decreases, reverse the perturbation direction.

6. Repeat steps 2-5 until the maximum power point is found or convergence criteria are met.

In summary, if following a voltage disturbance, the PV power increases, the disturbance direction is maintained. If not, it is reversed to resume convergence to the new MPP [8]. The methodology of the P&O algorithms is presented in Table 2.

Table 2. Methodology of the P&O algorithms.

Conditions	Actions
(i) $DP_{PV} < 0$ and $DV_{PV} < 0$	Duty decrease
(ii) $DP_{PV} > 0$ and $DV_{PV} > 0$	Duty decrease
(iii) $DP_{PV} > 0$ and $DV_{PV} < 0$	Duty increase
(iv) $DP_{PV} < 0$ and $DV_{PV} > 0$	Duty increase
(v) $DP_{PV} = 0$ and $DV_{PV} = 0$	No action

Simulation Results

Effect of Temperature and solar Irradiation on Output Voltage, Power and Duty Cycle

At a Constant Temperature of 25°C and Sun Irradiation of 500W/m²

Figure. 5 shows the variation of the output voltage, power, and duty cycle with respect to time at a temperature of 25°C and a sun irradiance of 500 W/m². It can be observed that the output voltage may remain relatively stable if other factors, such as shading or aging effects, are negligible. At a constant temperature and solar irradiance, the duty cycle may remain relatively stable too if the system is operating near its maximum power point (MPP). However, variations in solar irradiance or changes in load conditions may require adjustments to the duty cycle to maintain operation at or near the MPP.
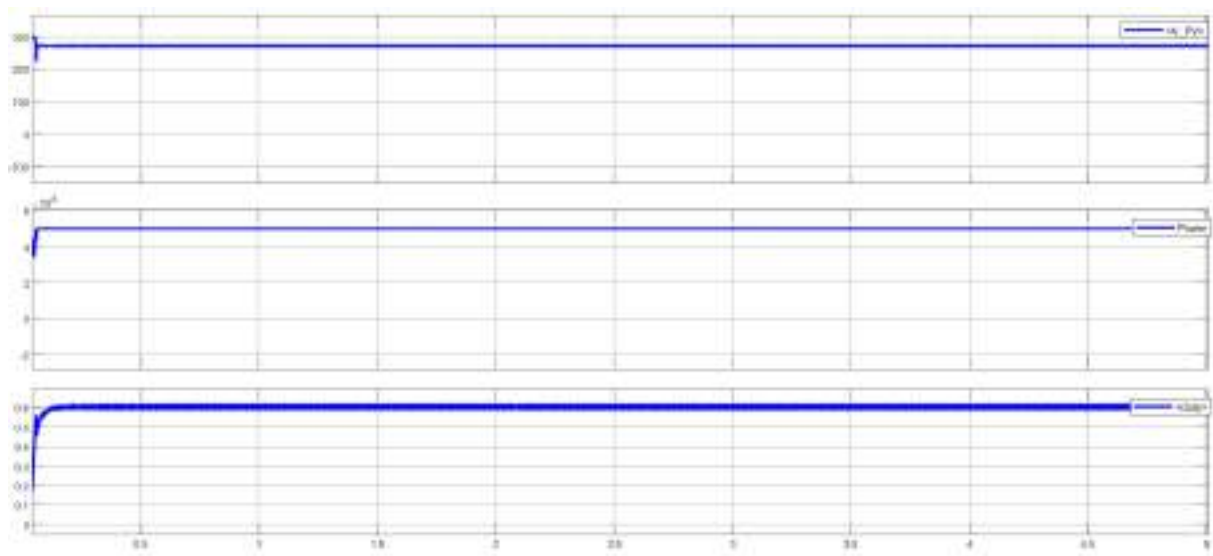
Figure.5. The output voltage, power and, duty with respect to time at temperature of 25°C and irradiance of 500 W/m².

Overall, at a constant temperature of 25°C and solar irradiance of 500 W/m², the output voltage, power, and duty cycle of a PV system may exhibit some stability but can still be influenced by changes in environmental conditions and load characteristics. Effective control and optimization methods, like MPPT algorithms, are crucial for enhancing the efficiency and performance of the photovoltaic system under diverse operating conditions.

At a Constant Temperature of 25°C and Sun Irradiation of 1000W/m²

Figure.6 depicts the variation of the output voltage, power, and duty cycle with respect to time when the temperature is taken to be 25°C and the sun irradiance is 1000 W/m². At a higher solar irradiance of 1000 W/m², the output voltage typically increases compared to lower irradiance levels. This is because higher irradiance levels lead to increased electron-hole pair generation in the PV cells, resulting in higher voltage output. The output power of the PV system also generally increases compared to lower irradiance levels. This is because higher irradiance levels lead to greater power generation in the PV cells.

Overall, at a temperature of 25°C and solar irradiance of 1000 W/m², the output voltage, power, and duty cycle of a PV system may exhibit trends of increased values compared to lower irradiance levels. Besides, the duty cycle rises from 0.6 at lower irradiations (500W/m²) to 0.7 at higher irradiations (1000 W/m²).
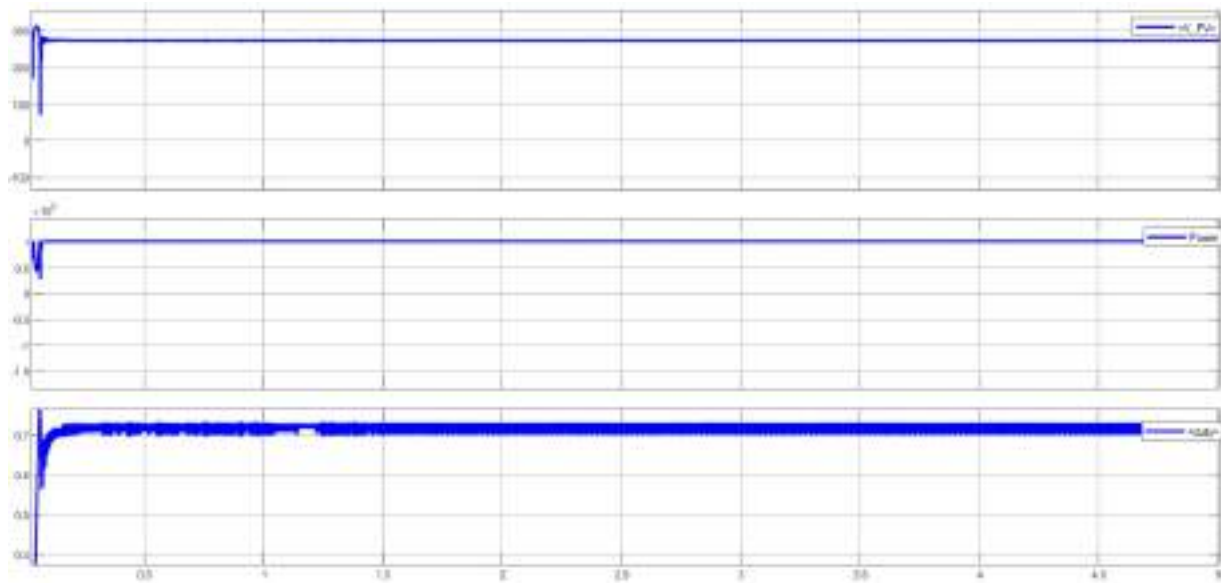
Figure.6. The output voltage, power, and duty with respect to time at a temperature of 25°C and irradiance of 1000 W/m².

P(V) Characteristics under Constant Uniform Temperature and Irradiance

The effect of constant uniform temperature and constant sun irradiance on the P(V) characteristics is shown in

Figure.7. From the curve, we can notice that the P-V curve has a characteristic shape, with power increasing initially as voltage increases, reaching a unique peak at the MPP, where the array operates with maximum efficiency and produces maximum output power., and then decreasing as voltage continues to increase beyond the MPP.
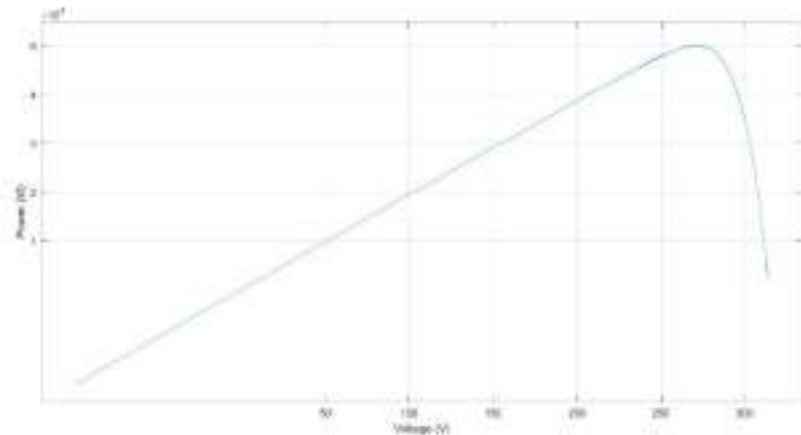
Figure.7. P(V) characteristics for constant temperature of 25°C and constant sun irradiation condition of 1000 W/m².

P(V) Characteristics under Constant Temperature and for Three Levels of Sun Irradiation Condition

Due to the dynamic nature of environmental conditions, the MPP of a PV system can shift continuously throughout the day and across seasons. This is the reason why PV systems utilize Maximum Power Point Tracking (MPPT) algorithms. MPPT algorithms continuously monitor the system's operating conditions and adjust the voltage and current to ensure that the system operates at or near its MPP under varying environmental conditions. This helps maximize the power output and overall efficiency of the PV system, even as environmental conditions fluctuate.

For three different levels of solar irradiation conditions (100 W/m², 500 W/m², and 1000 W/m²), the P-V characteristics would differ due to the varying intensity of sunlight (Figure.8). As previously described, the MPP of a PV system is directly influenced by the intensity of sunlight, represented by solar irradiance. Higher irradiance levels lead to higher power output, and thus, the MPP shifts to accommodate this change. As solar irradiance increases, the MPP tends to move towards higher voltages and currents to maximize power output [9]. Furthermore, we can clearly notice that:

- At lower irradiance levels, the power output of the PV system would be lower compared to higher irradiance levels;
- The P-V curve for 500 W/m² irradiance would show higher power output across the entire range of voltages compared to 100 W/m² irradiance;
- At 1000 W/m² irradiance, the curve would exhibit the highest MPP voltage and current compared to the lower irradiance conditions.
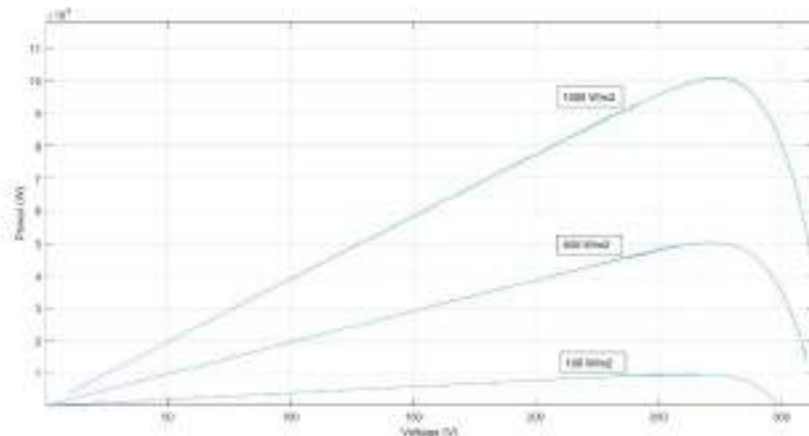
Figure.8: P(V) characteristics for three levels of sun irradiation condition (at constant temperature (25°C)) of 100 W/m^2, 500 W/m^2 and 1000 W/m^2.

Conclusion

The development and implementation of efficient Maximum Power Point Tracking (MPPT) methods are indeed crucial for optimizing the performance of PV systems, particularly under rapidly changing atmospheric conditions. The method used in this work is the Perturb and Observe (P&O) MPPT method, which is known for its simplicity and ease of implementation compared to other techniques. The design and results of the P&O MPPT technique were presented and explained. The simulation results demonstrated the effectiveness of the P&O MPPT technique in improving MPP tracking performance and overall system efficiency. Efforts to optimize MPPT techniques contribute not only to maximizing the energy yield of PV systems but also to enhancing their economic viability and environmental sustainability.

References

Maka, A. O. M. and Alabid, J. M. (2022). Solar energy technology and its roles in sustainable development. *Clean Energy*, 6, 476–483.

M. S. I. Md Sadequl Azam, A. Bhattacharjee, M. Hassan, M. Rahaman, S. Aziz, Md. A. A. Shaikh (2024), Performance enhancement of solar PV system introducing semi-continuous tracking algorithm based solar tracker, *Energy*, 289.

A. B. M. S. O. Z. Musong, L. Katche and M. S. Adaramola, (2023) A Comprehensive Review of Maximum Power Point Tracking (MPPT) Techniques Used in Solar PV Systems, *Energies*, 16.

E. Moshksar and T. Ghanbari (2018), A model-based algorithm for maximum power point tracking of PV systems using exact analytical solution of single-diode equivalent model *Sol. Energy*, 162,117–131.

S. Silvestre (2018), Strategies for Fault Detection and Diagnosis of PV Systems, *Adv. Renew. energies power Technol*, 231–255.

S. Gupta, O. Singh, and M. A. Ansari (2019), Maximum power point tracking techniques for photovoltaic

system: A review," *Lect. Notes Electr. Eng*, 526, 455–465.

V. Dabra, K. K. Paliwal, P. Sharma, and N. Kumar (2017), Optimization of photovoltaic power system : a comparative study.

B. Djamel Eddine Tourqui, Achour, S. Atallah, and A. Tayeb, (2016), Improved Performance of a Photovoltaic Panel by MPPT Algorithms, *IntechOpen*, 11, 13.

M. A. Yildirim. (2020), Maximum Power Point Tracking Techniques for Solar Photovoltaic Applications, (Doctoral dissertation).

Growing Plant Literacy: Science Communication for Plant Conservation

Ermelinda Mahmutaj

University of Tirana, Albania,   https://orcid.org/0009-0001-4966-433X

Ani Bajrami

University of Tirana, Albania,   https://orcid.org/0000-0001-5349-2510

Abstract: Plants have been traditionally considered static life forms. Beyond the anthropocentric tendencies that continue to exist about human cognitive abilities for language, recent studies have pointed out plant cognition and communicative processes. Different authors state that two interesting or unique features characterize plants' communication: they can discriminate between self and non-self and recognize kin from strangers. The idea that plants communicate with each other, and their environment coupled with their amazing complexity may seem strange to the public. How can biologists be more proactive in increasing plant literacy through effective communication and outreach? Because climate changes are causing widespread ecological degradation and species extinctions at alarming rates, there is a growing need to be proactive and provocative in increasing plant literacy. In this context, understanding audience bias can lead to more effective science communication; it is important to educate and involve the public, policymakers, and key stakeholders, on environmental issues and research, with a special focus on plants to make an impact on today's problems because of climate change.

Keywords: plant literacy, plant conservation, climate change, science communication, environmental education.

Introduction

In his magnum opus, *On the Origin of Species*, Charles Darwin proposed that all life forms are related. In this context, plants deserve attention because we descend from a common ancestor and to understand evolution better, it is important to shed light on plants' origin and evolution (Niklas 2024).

The evolution of plants suited to living on land constitutes an important landmark of life on Earth (Kenrick and Crane 1998; de Vries &Archibald 2018). Plant evolution transformed the Earth, with possibly two major episodes of horizontal gene transfer: the evolution of streptophytes and the origin of land plants; the later event took place approximately 450 Ma in mid-Paleozoic (Ordovician- Devonian) and led to the colonization of land

by plants and plant biodiversity due to an increased level of structural and physiological complexity (Ma et al., 2022; Kumar et al., 2022). Furthermore, these newly evolved terrestrial creatures served as geobiological agents by altering Earth's climate and increasing Earth's O_2 levels (Dahl & Arens 2020).

Additionally, although there is debate regarding the definition of plant intelligence and plant behavior (Hendlin 2022), their behavior is described as active, purposeful, and intentional (Trewavas 2009), as rapid morphological or physiological responses to events (Karban 2008), plants possess intelligence even though they do not have a nervous system (Castiello 2023) and they demonstrate agency and learning (Novoplansky et al., 2024). In recent years, the study of adaptive behavior in plants and how they communicate with each other via volatile chemicals has been of intense scientific interest (Blande & Glinwood 2016).

It is important to mention that the increased level of structural and physiological complexity during plant evolution cannot be viewed purely in mechanical terms; from the semiotic approach and computational perspective, plants acquire, store, process, and evaluate information from the environment relevant to their fitness and modify their behavior accordingly (Witzany 2006; Duran-Nobreda 2019). Therefore, semiotics of plants or *phytosemiotics* gained attraction in academic circles; during the last decades, the semiotic approach to describing living systems has also been growing as an important tool for understanding living systems (Krampen 1981; Kull 2000).

Furthermore, plants are central to people's well-being and have constituted a key aspect of people's system of knowledge and practices for millennia (Raven 20220; Davis and Choisy 2024). They are rooted in an evolutionary and complex relationship with humans and could be considered key components of our cultures, arts, religions, and medicines (Schaal 2019). The scientific development regarding plants' origin, and evolution, and the recent findings on plants' behavior, intelligence, and modes of communication coupled with plants' cultural interests have set the stage for a deeper understanding and the need for botanical literacy, particularly considering the contemporary climate crisis and to achieve the UN Sustainable Goals.

Botanical Literacy

Botanical literacy is usually associated with scientific literacy and is often related to biological literacy. One of the most used definitions of botanical literacy is "the ability to know, and understand plant terminology, explain natural phenomena about plants, engage in conversation, and make personal decisions about sociocentric issues related to plants" (Uno 2009).

Additionally, other definitions of botanical literacy in contemporary literature notice it is a subset of biological literacy (Uno 2009), consider it a crucial component of science education in fostering an awareness of plants and strengthening science-literate citizens' understanding and appreciating the interconnections between plants and humans and helps understand the role plants play in ecosystem service (Hemingway et al., 2011; Beasley et

al., 2022; Pedrera et al., 2023; Dunser et al., 2023).

In a broader sense, scientific literacy or science literacy encompasses not only the science process understanding but also refers to the level of people's engagement in science in terms of knowledge and creation (Dibner 2016). Additionally, in terms of enhancing scientific literacy through the lens of appreciation of the nature of science itself and in analogy with the broad term of literacy, it becomes clear that there are many facets and components related to science literacy not limited to knowledge about science but also society usefulness (Holbrook & Rannikmae 2009).

Therefore, social participation and emancipation are considered key components of science literacy that can enhance the role of science as a tool for social change (Valladares 2021).

Science Communication and Socio-scientific Issues

Socio-scientific issues and challenges of the twenty-first century such as the climate crisis or biodiversity loss are sometimes misunderstood or not accepted at all due to excessive circulation of misinformation in social media. Nowadays social media is considered one of the key tools to get information in most of the world's countries and is an important facilitator in creating and disseminating content, albeit unscientific and unverified, rapidly spreading to a wide audience.

There is widespread concern among scientists and the public about rampant misinformation circulating on social media. Numerous studies have been conducted on how it influences people's perceptions, beliefs, and attitudes regarding socio-scientific issues (Högström et al., 2024). Besides nearly a unanimous consensus among scientists on climate change, misinformation has confused the public for decades and the consequential misperceptions are seen in the reduced levels of policy support (Oreskes 2004; Ding et al., 2011). Conversely, when scientific consensus on climate change is communicated, there is an increase in beliefs, worry, and support across different audiences (Veckalov et al., 2024).

On the other hand, influencers have become important figures in today's realm of socio-scientific issues in the media ecosystem. Climate influencers focus on their perspective and this individual narrative on the personal level and obvious authenticity and credibility are at the base of a new social media influence although it remains unclear their role and influence concerning climate change discourse and potentially leading to behavioral changes (Haastrup & Marshall 2024; Vilkaite- Vaitone 2024; Cheng 2024).

Conclusions

Plants have played a crucial role throughout human history, and they show interesting characteristics in terms of their evolution, behavior, and communication. Additionally, climate change has brought major societal

challenges and plant science can play an important role in mitigating the worst impacts of the climate crisis by crop development to enhance their resilience to the newly harsh conditions (Eckardt et al., 2022). In this context, botanical literacy is of the uttermost importance to foster plant awareness; engaging the public in plant knowledge by the efficient use of media to respond to societal challenges and transforming public perception of the various benefits of plants to humans and the biosphere is important and can be helpful in the future. Science communication tools such as traditional media, videos, and podcasts along with the use of influencers to propagate information on plants by thus avoiding misinformation are useful in nowadays digital age and can foster botanical literacy by creating and disseminating scientific content about plants. In addition, botanists should be engaged and have an active role in creating and disseminating scientific content to foster public awareness of plants and their many benefits by being innovative and inclusive with the audiences.

References

Beasley, K., Hesterman, S., Lee-Hammond, L. (2022). Reviving botany in the curriculum: the botanical journey of two western Australian early childhood teachers. *Australian Journal of Environmental Education*, 39 (2), 166-180.

Blande, J.D., Glinwood, R. (2016). *Deciphering chemicals language of plant communication*. Springer Cham. https://doi.org/10.1007/978-3-319-33498-1

Castiello, U. (2023). Plant intelligence from a comparative psychology perspective. *Biology*, 12 (6), 819. doi: 10.3390/biology12060819

Cheng, D. (2024). Climate influencers on social media. *Nature Climate Change*, 14 (309), https://doi.org/10.1038/s41558-024-01988-2

De Vries, J., Archibald J.M. (2018). Plant evolution: landmarks on the path to terrestrial life. *New Phytologist* https://doi.org/10.1111/nph.14975

Dahl, T.W., Arens, SKM. (2022). The impacts of land plant evolution on Earth's climate and oxygenation state – An interdisciplinary review. *Chemical Geology,* 547, 119665.

Davis, C.C., Choisy, P. (2024). Medicinal plants meet modern biodiversity science. *Current Biology* https://doi.org/10.1016/j.cub.2023.12.038

Duran-Nobreda, S., Bassel, G.W. (2019). Plant behavior in response to the environment: information processing in the solid state. 374 (1774), *Philosophical Transaction of the Royal Society B* https://doi.org/10.1098/rstb.2018.0370

Dunser, B., Moller, A., Fondriest, V., Boeckle M., Lampert, P., Pany, P. (2023). Attitudes towards plants-exploring the role of plants' ecosystem service. *Journal of Biological Education*, https://doi.org/10.1080/00219266.2024.2308293

Eckardt, N.A., Ainsworth, E.A., Bahuguna, R.N., Broadley, M.R. et al., (2022). Climate change challenges, plant science solutions. *Plant Cell*, 35 (1), 24-66. doi: 10.1093/plcell/koac303

Haastrup, H.K., Marshall, P.D. (2024). The influencer in the age of climate change: the authentic role model for sustainability. *Celebrity Studies*, 15, 160-176. https://doi.org/10.1080/19392397.2024.2341596

Hemingway, C., Dahl, W., Hauffler, C., Stuessy, C. (2011). Building plant literacy. *Science*, 331 (6024), 1535-1536.

Hendlin, Y.H. (2022). Plant philosophy and interpretation: Making sense of contemporary plant intelligence debate. *Environmental Values*, 31, 253-276.

Holbrook, J., Rannikmae, M. (2009). The meaning of scientific literacy. *International Journal of Environment and Science Education*, 4 (3), 275-288.

Högström, P., Gericke, N., Wallin, J. et al., (2024). Teaching Socioscientific Issues: A Systematic Review. *Science & Education*. https://doi.org/10.1007/s11191-024-00542-y

Kenrick, P., Crane, P. (1997). The origin and early evolution of plants on land. *Nature*, 389, 33–39 https://doi.org/10.1038/37918

Krampen, M. (1981). Phytosemiotics. *Semiotica* 36 (3/4), 187-209.

Kull, K. (2000). An introduction to phytosemiotics: Semiotic botany and vegetative sign systems. *Sign System Studies*, 28.

Kumar, P., Kumar, P., Verma, V., Irfan, M. (2022). How plants conquered land: evolution of terrestrial adaptation. *Journal of Evolutionary Biology*, 35 (5), 5–14, https://doi.org/10.1111/jeb.14062

Ma, Jianchao., Wang, Sh., Zhu, X., Sun, G. et al., (2022). Major episodes of horizontal gene transfer drove the evolution of land plants. *Molecular Plant*, 15 (5), 857 – 871.

Morris, J.L., Puttick, M.N., Clark, J.W., Edwards, D. et al., (2018). The timescale of early plant evolution. *Proceedings of the National Academy of Sciences of the United States of America*, 115, 2274-2283.

Niklas, K.J. (2024). *Plant evolution: An introduction to the history of life.* The University of Chicago Press, MA.

Novoplansky, A., Souza, G.M., Brenner, E.D., Bhatla, S.C., Van Volkenburgh, E. (2024). Exploring the complex information processes underlying plant behavior. *Plant Signaling and Behavior*, 19 (1). https://doi.org/10.1080/15592324.2024.2411913

Oreskes, N. (2004). The scientific consensus on climate change. *Science*, 306 (5702), 1686. DOI: 10.1126/science.110361

Pedrera, O., Barrutia, O., Diez, J.R. (2023). Do textbooks provide opportunities to develop meaningful botanical literacy? A case study of the scientific model of plant nutrition. *Journal of Biological Education*, https://doi.org/10.1080/00219266.2024.2365679

Schaal, B. (2019). Plants and people: Our shared history and future. *Plants, People, Planet*, 1 (1), 14-19. https://doi.org/10.1002/ppp3.12

Raven, P.H. (2021). Plants make our existence possible. Plant, People, Planet, 3 (1), 2-6.

Trewavas, A. (2009). What is plant behavior? *Plant, Cell and Environment*, 32 (6), 606-616.

Uno, G.E. (2009). Botanical literacy: What and how should students learn about plants? *American Journal of Botany*, 96 (10), 1753-1759.

Valladares, L. (2021). Scientific literacy and social transformation. *Science and Education*, 50, 557-587. https://doi.org/10.1007/s11191-021-00205-2

Veckalov, B., Geiger, S. J., Bartos, F., White, M.P., Rutjens, B.T. et al., (2024). A 27- country test of communicating the scientific consensus on climate change. Nature Human Behavior, 8, 1892-1905.

https://doi.org/10.1038/s41562-024-01928-2

Vilkaite-Vaitone, N. (2024). From likes to sustainability: How social media influencers are changing the way we consume. *Sustainability*, 16 (4). 10.3390/su16041393

The Evolutionary Leitmotif in Ethnobiology: Historical Roots and Theoretical Perspectives

Ermelinda Mahmutaj

University of Tirana, Albania, https://orcid.org/0009-0001-4966-433X

Anyla Saraçi

University "Fan Noli", Albania, https://orcid.org/0000-0002-2394-3875

Ani Bajrami

University of Tirana, Albania, https://orcid.org/0000-0001-5349-2510

Abstract: Ethnobiology is a scientific discipline aiming to understand and analyze the relationships and intricacies between human societies and biota. Due to its interdisciplinary nature, ethnobiology communicates with different fields of knowledge and embraces different approaches. In this context, the emergence of evolutionary ethnobiology aids new understanding of people and biota, in various human societies and environmental contexts. First, evolutionary ethnobiology studies how people perceive and understand the environment following their evolutionary and cultural heritage. Secondly, understanding how to preserve and transmit environmental knowledge across and between generations is crucial. This micro-level evolutionary process enables us to generate hypotheses to understand changes at the macro level, expressed in the evolving relationships and interactions of human societies with the environment, particularly in the context of the contemporary climate crisis. This article will outline the historical foundation of Extended Evolutionary Synthesis (EES), Cultural Evolution (CE), and the emergence of evolutionary psychology. Additionally, we will outline the basic concepts and some examples of recent research in evolutionary ethnobiology.

Keywords: ethnobiology, Cultural Evolution (CE), social-ecological systems, traditional ecological knowledge, evolutionary psychology

Introduction

Ethnobiology is a scientific discipline aiming to understand the interactions between people and the environment (Albuquerque and Albes, 2016; Ferreira Júnior et al., 2022). Today's ethnobiology encompasses

such scientific disciplines as botany, zoology, ecology, evolutionary biology, etc., and consists of the subdisciplines of ethnobotany and ethnozoology (Clement 1998; Hunn 2007; Alves and Souto 2015; Alves et al., 2018).

According to Clement (1998) the history of ethnobiology comprises three phases: pre-classic, classic, and post-classic, spanning a period from 1860 to 1992; each phase encompasses the birth of ethnobotany and ethnozoology as distinctive disciplines, the adoption of the emic approach and the importance of conservation, in the face of climate crisis. Additionally, Hunn (2007), proposed four phases of ethnobiology history, related to both theoretical and methodological interactions with other disciplines, emphasizing in the IV phase (1990 to the present day) the exploitation of Indigenous communities and the importance of ethnobiological studies in preserving and promoting indigenous traditional ecological knowledge, in a proactive manner. That is clearly shown in the components of ethnobiological research such as the principles of Prior Informed Consent (PIC), Intellectual Property Rights (IPR), and the Code of conduct.

Both last phases proposed by Clement and Hunn set the stage for another Phase (Phase V) or what is known as "conservation ethnobiology" matching the contemporary environmental and cultural profound changes; conservation is related to the interaction between biological, social, and cultural aspects or what is referred to as "biocultural conservation" including the application of the ethnobiology principles to the study of cities and urban settings (Wolverton 2013; Hidayati et al., 2015; Albuquerque and Sousa 2016; Emery and Hurley 2016; Wolverton et al., 2023; Bajrami et al., 2023).

On the other hand, evolutionary ethnobiology recently formally conceptualized, whose main aim is to understand the relationship between humans and nature from a broader perspective, uses or adopts ecological and evolutionary hypotheses, and constitutes the sixth phase in the history of ethnobiology or Phase VI (Albuquerque and Ferreira Júnior 2017). In an article by Santoro et al., 2018 it is stated that evolutionary ethnobiology examines the cognitive and behavioral characteristics within ecological and evolutionary frameworks (Santoro et al., 2018). In this article, we will briefly outline the historical foundation of the Extended Evolutionary Synthesis (EES), Cultural Evolution (CE), and the emergence of evolutionary psychology as a relatively new discipline. But first, let us delve into the history of evolutionary thought and how it permeated other scientific fields.

Historical Foundations of Extended Evolutionary Synthesis (EES): Cultural Evolution and the Emergence of Evolutionary Psychology

The evolutionary aspects of human behavior and the evolutionary concept of culture began to take shape in the 1980s. They owe their development to the formulation of the Extended Evolutionary Synthesis (EES), Cultural Evolution (CE), and the emergence of evolutionary psychology. The theory of evolution helps scientists create an explanatory framework for the origin, evolution, and diversity of features and behaviors of living organisms

(Bajrami & Rexhepi 2018). The core concepts are natural selection and adaptation. Natural selection favors only inheritable variations of organisms with higher reproductive success than other organisms (Gregory 2009). Simply put, the features and behaviors favored by natural selection have beneficial characteristics for organisms. Additionally, according to this theory, only those organisms that have been selected due to their ability to adapt will evolve. In this context, natural selection is responsible for shaping adaptations of physiological, morphological, and behavioral nature (Lenski 2017).

In the early 20th century, classical ethology used Darwinian principles to study animal behaviors. Simultaneously, evolutionary biologists formulated the Modern Evolutionary Synthesis (MES). Theoretical developments in ethology and evolutionary biology, together with the rise of behavioral ecology, paved the way for the study of mental processes in humans (Bajrami 2018). The study of mental processes in ethnobotanical "language" means understanding how people perceive, and gain knowledge and meaning about the environment they live in.

In the 1980s, a new discipline called evolutionary psychology was developed, and its main claim is that the human mind is composed of mental adaptations for solving various adaptive problems due to different selection mechanisms (Barkow et al., 1992; Bolhuis et al., 2011) These mechanisms are inherited because they have solved and continue to solve specific adaptive survival problems "activating" only in response to specific environmental information (Moura et al., 2017; 2018). The evolutionary echo of the human mind can explain, for example, preferences regarding the use or non-use of certain plant species over others (Texeira et al., 2022). The theories proposed by Darwin influenced the study of culture in the 1980s and onward. Cultural features are considered differently: the repertoire of human behavior cannot be understood without considering variations among individuals. Additionally, this repertoire is closely linked to how these variations are transmitted across generations. In cultural evolution, randomly generated cultural mutations or variations are the primary material for the actions of various selection mechanisms that either help or hinder the adaptation of their bearers (Cavalli-Sforza & Feldman 1981).

On the other hand, the niche concept, along with the niche construction, as an integral part of the Extended Evolutionary Synthesis, was used to understand culture. The niche construction perspective put forward by Harvard biologist R. Lewontin in the 1980s maintains that human activities direct human evolution as demonstrated by the agricultural practices during the Neolithic Revolution (O'Brien and Laland 2012; Bajrami 2022; Odling-Smee 2024). These two notions are closely related to Cultural Evolution (CE), both a process and scientific discipline based on Darwinian concepts. In this context, the cultural niche is linked to the ongoing modification of the environment by members of society (Boyd et al. 2011).

Recent Research in Evolutionary Ethnobiology

In a recent study (Dantas et al., 2020), it was found that the exchange and modification of cultural information among individuals regarding medicinal plants can lead to mutations in this learned information. In other words,

when considering the medical system of a society, the occurrence of mutations in information about medicinal plants is attributed to the cultural transmission of this information from generation to generation. Consequently, these "errors" in information can impact the adaptive capacity of this society to the environment.

In addition to cultural mutations, cultural drift, analogous to genetic drift, causes the frequency of a cultural trait to increase or decrease to extinction because of the small number of individuals within a society. For example, in small societies with limited cultural contact with other societies, knowledge about plants among their members may be preserved or completely lost entirely by chance. Therefore, chance and the small number of individuals can become determining factors in the preservation and flow of ethnobotanical knowledge and practices in a society.

The factor that acts on units of cultural transmission is cultural selection, analogous to natural selection. As transmission units change and are enriched with continuous information, the action of selection becomes stronger, resulting in changes occurring within a generation. This type of evolution is closely related to the learning and transmission of information from generation to generation. For instance, there are studies on how this knowledge is transmitted, highlighting the fact that society members learn from the elderly, mothers, or traditional healers (Geissler et al., 2002; Lozada et al. 2006; Reyes-Garcia et al. 2009; Ouma 2022). Those manners in which knowledge and practices of ethnobotany evolve due to evolutionary mechanisms cannot be understood independently of the environment. Like any other cultural traits, these knowledge and practices are passed down from generation to generation or within a generation.

Research Avenues and Opportunities

For all the authors who have delved into the history of ethnobiology, the developmental phases and the formulation of theories and methodologies give ethnobiology a holistic character. Research conducted using an evolutionary approach provides a new theoretical framework for interpreting ethnobiological data, which goes beyond mere documentation or cataloging. The evolutionary approach serves as complementary to conservation ethnobiology; it guides contemporary ethnobiological research with a deeper understanding on how the human mind gather information about the environment and categorizes the natural world and how this information shapes the components of mind and behavior, even at a societal level. Additionally, an evolutionary approach sheds light on the rate of change at the micro and macro levels and the mechanisms involved in giving rise to new ecological knowledge and practices in a certain society, including cultural maladaptation's.

References

Albuquerque, U.P., Alves, A.G.C. (2016). What Is Ethnobiology? In: Albuquerque, U., Nóbrega Alves, R. (eds) *Introduction to Ethnobiology*. Springer, Cham. https://doi.org/10.1007/978-3-319-28155-1_1

Albuquerque, U.P., de Sousa, D.C.P. (2016). Ethnobiology and Biodiversity Conservation. In: Albuquerque, U.,

Nóbrega Alves, R. (eds) *Introduction to Ethnobiology*. Springer, Cham. https://doi.org/10.1007/978-3-319-28155-1_33

Albuquerque, U.P., Ferreira Júnior, W.S. (2017). What Do We Study in Evolutionary Ethnobiology? Defining the Theoretical Basis for a Research Program. *Evolutionary Biology* 44, 206–215https://doi.org/10.1007/s11692-016-9398-z

Alves, R.R.N., Souto, W.M.S. (2015). Ethnozoology: A brief introduction. *Ethnobiology and Conservation* 4: 1. https://doi.org/10.15451/ec2015-1-4.1-1-13

Alves, R.R.N., Souto, W.M.S., Albuquerque, U.P. (2018). Ethnozoology: Conceptual and historical aspects. *Ethnozoology* https://doi.org/10.1016/B978-0-12-809913-1.00002-8

Bajrami, A., Rexhepi, B. (2018). *Antropologjia: Një perspektivë biokulturore*. Shtëpia Botuese Morava, Tiranë, Shqipëri.

Bajrami, A., Sokoli, E., Qirjo, M. (2019). Që prej Darvinit: Nga mendja te kuptimi evolucionar i kulturës. *Buletini i Shkencave të Natyrës* 27,83-93.

Bajrami, A., Qirjo, M. (2019). Roli i të mësuarit në konstruksionin e nishit dhe dijeve tradicionale ekologjike. *Buletini i Shkencave të Natyrës* 27, 94-102.

Bajrami, A. (2022). From nature to man: Environmental anthropology in the Anthropocene. *Journal of Biological Research.* https://doi.org/10.4081/jbr.2022.10377

Bajrami, A., Mesiti, A., Mahmutaj, E., Hoda, P. (2023). The New Normal: Ethnobiology of cities and urban ecological knowledge. *Journal of Natural Sciences* 34, 139-148.

Barkow, J., Cosmides, L., Tooby, J. (1992). *The adapted mind: Evolutionary psychology and the generation of culture*. Oxford University Press, UK.

Bolhuis, J.J., Brown, G.R., Richardson, R.C., Laland, K.N. (2011). Darwin in mind: New opportunities for evolutionary psychology. *PLoS Biol* 9(7): e1001109. https://doi.org/10.1371/journal.pbio.1001109

Boyd, R., Richerson, P.J., Henrich, J. (2011). The cultural niche: Why social learning is essential for human adaptation. [Colloquium Paper]. *Proceedings of the National Academy of Sciences USA*. doi: 10.1073/pnas.1100290108.

Cavalli-Sforza, L., & Feldman, M.W. (1981). *Cultural transmission and evolution: A quantitative approach*. Princeton University Press, USA.

Clement, D. (1998). The historical foundations of ethnobiology. *Journal of Ethnobiology* 18: 161-187.

Dantas, J.I.M., Nascimento, A.L.B., Silva, T.C., Albuquerque, U.P. (2020). Mutation of cultural information on the use of plant complexes in local medical systems. *Evidence-Based Complementary and Alternative Medicine*. https://doi.org/10.1155/2020/7630434

Emery, M.R., Hurley, P.T. (2016). Ethnobiology in the city: Embracing the urban ecological moment. *Journal of Ethnobiology* 36 (4), 807-819.

Hidayati, S., Franco, FM., Bussman, R. (2016). Ready for phase 5- current status of ethnobiology in Southeast Asia. Journal of Ethnobiology and Ethnomedicine. *Journal of Ethnobiology and Ethnomedicine* 11, 17. https://doi.org/10.1186/s13002-015-0005-7

Hunn, E. (2007). Ethnobiology in four phases. *Journal of Ethnobiology* 27(1), 1–10.

Geissler, PW., Harris, SA., Prince, RJ., Olsen, A., Achieng'Ochiambo, R et al. (2002). Medicinal plants used by

Luo mothers in Bondo district, Kenya. *Journal of Pharmacology* 83, 39-54.

Gregory, T.R. (2009). Understanding Natural Selection: Essential Concepts and Common Misconceptions. *Evolution Education and Outreach* 2, 156–175. https://doi.org/10.1007/s12052-009-0128-1

Ferreira Júnior, W.S., Medeiros, P.M., & Albuquerque, U.P. (2022). Evolutionary ethnobiology. *Ethnobiology and Conservation*, 11. https://doi.org/10.15451/ec2022-04-11.10-1-8

Lozada, M., Ladio, A.H., Weigandt, M. (2006). Cultural transmission of ethnobotanical knowledge in a rural community of Northwestern Patagonia, Argentina. *Economic Botany* 60, 374-385.

Lenski, R.E. (2017). What is adaptation by natural selection? Perspectives of an experimental microbiologist. *PLoS Genetics*,13 (4): e1006668.

O'Brien, M.J., Laland, K. (2012). Genes, culture and agriculture: An example of human niche construction. *Current Anthropology* 53, 434-70.35.

Odling-Smee, J. (2024). The niche construction: How life contributes to its own evolution. The MIT Pres. Cambridge, USA.

Moura, J.M.B., Ferreira Junior, W.S., Silva, T.C, Albuqueruqe, U.P. (2017). Landscapes preferences in the human species: Insights into ethnobiology from evolutionary psychology. *Ethnobiology and Conservation* 6.

Moura, J.M.B., Ferreira Júnior, W.S., Silva, T.C., Albuquerque, U.P. (2018). The Influence of the Evolutionary Past on the Mind: An Analysis of the Preference for Landscapes in the Human Species. *Frontiers in Psychology* 9, 2485. doi:10.3389/fpsyg.2018.02485.

Ouma, A. (2022). Intergenerational learning processes of traditional medicinal knowledge and socio-spatial transformations dynamics. *Frontiers in Sociology*, PMCID: PMC9301457 PMID: 35874449

Reyes- Garcia, V., Broesch, J., Calvet-Mir, L., Fuentes Pelaez, N. (2009). Cultural transmission of ethnobiological knowledge: An empirical analysis from an Amerindian society. *Evolution and Human Behavior* 30 (4), 274- 285.

Santoro F.R., Nascimento, A.L.B., Soldati, G.T., Ferrera Junior, W.S., Albuquerque, U.P. (2018). Evolutionary ethnobiology and cultural evolution: opportunities for research and dialogue. *Journal of Ethnobiology and Ethnomedicine* 14: 1. doi: 10.1186/s13002-017-0199-y.

Teixeira, CP., Fernandes, CO., Ryan, R., Ahern J. (2022). Attitudes and preferences towards urban green spaces: Implications for the design and management of Novel Urban Ecosystems. *Journal Environmental Management*, [E-book] Available: DOI:10.1016/j.jenvman.2022.115103.

Wolverton, S (2013). Ethnobiology 5: Interdisciplinarity in an Era of Rapid Environmental Change. *Ethnobiology Letters* 4, 21-25.

Wolverton, S., Nolan, JM., Ahmed, W. (2023). Ethnobiology, Political Ecology and Conservation. *Journal of Ethnobiology*, 34, 2. https://doi.org/10.2993/0278-0771-34.2.125

Study of the Performance of an Eco-Mortar Based on Perlite

Mohamadi Saddika

University of Bouira, Algeria https://orcid.org/ 0009-0001-0644-031X

Boumaiza Malika

University of Bouira, Algeria, https://orcid.org/0009-0006-6581-0612

Arbaoui Ahcène

University of Bouira, Algeria, https://orcid.org/0009-0006-1714-9225

Kahlal Sofiane

University of Bouira, Algeria, https://orcid.org/0009-0004-6310-8913

Yagoub Ayoub

University of Bouira, Algeria, https://orcid.org/0009-0007-2438-2401

Abstract: In the cement industry, the quest for more cost-effective binders using waste and natural resources has become essential to address the shortage of Portland cement while being environmentally responsible. Algeria is rich in natural resources like perlite, a volcanic rock that can be finely ground and used as an active mineral additive in cement production to reduce CO_2 emissions. This study explores the advantages and feasibility of using perlite as a partial replacement for cement in mortar production, with substitution rates of 5%, 10%, 15%, 20%, and 25%. Various tests were conducted to assess physical, mechanical, and thermal properties, including consistency, setting time, workability, capillary absorption, mechanical strength, and thermal conductivity. The results show that perlite increases water demand, accelerates the setting time in the fresh state, and enhances capillary absorption in the hardened state. Over time, mortar containing perlite exhibits higher mechanical strength than the reference mortar (0% perlite), with strength improvements proportional to the perlite content. Additionally, perlite-based mortar demonstrates favorable thermal and physical properties, underscoring its potential as an effective thermal insulator and reinforcing the ecological benefits of this addition.

Keywords: Eco-mortar, Perlite, Fresh state, Mechanical Strength, Thermal behavior.

Introduction

The search for an economical and ecological binder using natural and industrial resources in the cement industry has become a crucial concern for the development of sustainable construction. (Hamidi., 2014; Huedo and al., 2016; Achour and al., 2024).

Ordinary Portland cement plays an important role in the construction industry, as it not only consumes natural resources, but also leads to a significant increase in CO_2 gas emissions (Hadj Sadok and al., 2021; Huntzinger and al., 2009; Erdem and al., 2007).

As the cement industry is responsible for a massive 8% of global CO_2, however, it is possible to reduce CO_2 emissions by substituting some cement with specific pozzolanic materials (Safer and al., 2021; Safer and al., 2017; Hadj Sadok and al., 2024).

Supplementary cementing materials (SCMs) such as fly ash, blast furnace slag and silica fume are increasingly used to improve cement performance while reducing its environmental footprint.

Algeria has large deposits of pozzolanic volcanic rocks, such as the natural pozzolan of Béni Saf and the perlite of Hammam Boughrara-Maghnia, which can be used as additional minerals in the production of local cements. (Hadj Sadok and al., 2021; Meral and al., 2004; Erdogan and al., 2013; Chihaoui., 2018).

A great deal of research has recently been carried out on the use of perlite as a pozzolanic supplementary cementing material (Chikouche and al., 2016; Chaib and al., 2018) based on physicochemical, mechanical (Guenanou and al., 2019; Hamadache et al., 2016; Ayed and al., 2022) and durability characterization (Chihaoui and al., 2022; El Mir., 2020).

Other research has investigated the possibility of partial substitution of cement by pozzolanic additives in the production of pozzolanic pastes, mortars and concretes (Guemidi and al., 2024; Belaribi and al., 2014).

Due to their characteristics, the study of perlite-based mortars is an area of research with strong development potential. The physical and mechanical properties of these mortars are interesting in both fresh and hardened states. It is therefore crucial that they are used in the construction industry (Bouzidi et al., 2022; Zhang et al., 2024, Belaribi and al., 2024).

The aim of this work is to investigate the possibility of using perlite as a partial cement substitute in mortars, focusing on its effects on workability, mechanical strength and thermal conductivity.

Materials and Properties

Perlite

The natural perlite used comes from the deposit located in Hammam Boughrara in Maghnia, in the northwest of Algeria, and was supplied by the national non-ferrous mining products company ENOF Maghnia. After its extraction in the form of gray rocks (Figure 1), the perlite is dried in the oven for 24 hours at a temperature of 80°C to eliminate any possible humidity and facilitate its grinding then it is crushed and sieved through an 80 µm sieve.

Figure 1. (a) Natural perlite in rock form before the grinding process, (b) Natural perlite reduced to powder after grinding and sieving.

The perlite powder used has a a specific gravity of 2.42 g/cm^3 and a Blaine fineness of 3675 g/cm^2 according to standard NF EN 196-6. Its chemical composition is presented in Table 1.

Table 1. Chemical composition of perlite.

Oxides	CaO	SiO_2	Al_2O_3	Fe_2O_3	SO_3	K_2O	Na_2O	MgO	TiO_2	LOI
(%)	0.42	74.37	14.38	1.15	0.02	4.12	3.89	0.24	0.01	2

Cement

The cement used in our mortars is type CEM I 42.5, supplied by Société des Ciments de Sour El Ghozlane (SC.SEG), a subsidiary of Groupe Industriel des Ciments d'Algérie "GICA". Its specific gravity is 3.13 g/cm3, with a Blaine fineness of 3219 g/cm2 according to NF EN 196-6. Tables 2 and 3 show the chemical composition of cement and the mineralogical composition of clinker respectively.

Table 2. Chemical composition of cement CEM I 42.5

Oxides	SiO_2	Al_2O_3	Fe_2O_3	CaO	MgO	K_2O	Na_2O	SO_3	Cl	TiO_2	LOI
(%)	20.96	5.14	3.68	63.82	2.69	0.79	0.176	1.96	0	0.235	0.163

Table 3. Mineralogical composition of clinker

C_3S (%)	C_3A (%)	C_2S (%)	C_4AF (%)
61,04	7,23	11,69	11,16

Sand

The sand used is silica sand from Biskra. The grain size curve of this sand, shown in figure 2, falls within the control range for mortar sand specified in standard EN 196-1. The chemical and physical characteristics of the sand used are shown in Tables 4 and 5.
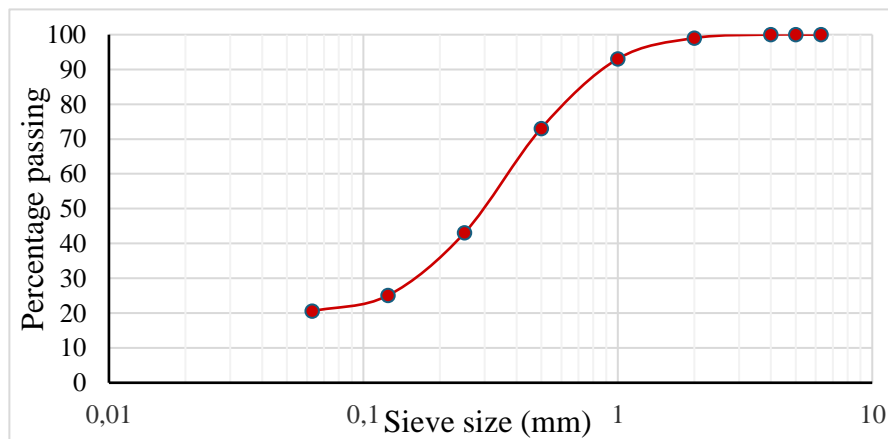
Figure 2. Grain size analysis of the sand of Biska.

Table 4. Chemical composition of the sand of Biskra

Oxides	SiO_2	Al_2O_3	Fe_2O_3	CaO	MgO	K_2O	Na_2O	SO_3	Cl	TiO_2	LOI
(%)	88.32	2.96	0.42	4.19	0.04	1.40	0.11	0.17	0.018	0.04	2.40

Table 5. Physical properties of Biskra sand

Properties	Value
Bulk density (g/cm^3)	1.58
Specific gravity (g/cm^3)	2.54
Water absorption (%)	1
Sand equivalent (%)	72
Fineness modulus	2.45

Mixing water

The water used is tap water from the building materials laboratory at the University of Bouira, at a temperature of between 18 and 20°C. We assume that it meets all the requirements of the concrete standard EN 1008.

Experimental methods

Cement paste tests

Consistency and setting time tests were carried out in accordance with standard EN-196-3 on pastes based on 0, 5, 10, 15, 20 and 25% perlite partially substituted for cement, using the Vicat apparatus to determine the quantity of water required to bring each paste to a normal consistency.

Then, pastes with different percentages of perlite addition were used to determine initial and final setting times, as shown in figure 3.
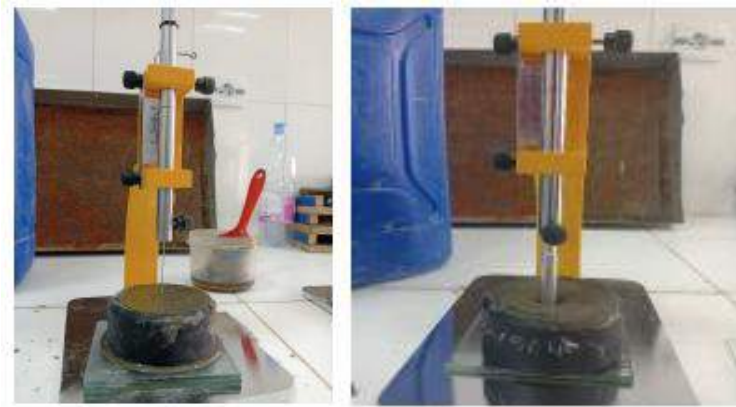
Figure 3. Consistency and setting time tests on cement paste.

Mortar tests

In order to evaluate the effect of perlite on the thermo-physical properties and mechanical strengths of mortars, $40 \times 40 \times 160$ mm^3 test specimens were prepared in accordance with EN196-1, using the compositions given in Table 6.

Table 6. Mix proportions of mortars

Mix. ID	Remplacement percentage (%)	Cement (g)	Sand (g)	Perlite (g)	Water (g) W/C=0.55
PR-0	0	450	1350	0	250
PR-5	5	427.5	1350	22.5	250
PR-10	10	405	1350	45	250
PR-15	15	382.5	1350	67.5	250
PR-20	20	360	1350	90	250
PR-25	25	337.5	1350	112.5	250

Workability tests

The workability test is the measurement of the time taken for the mortar to flow under the effect of vibration, as

shown in Figure 4, and is determined in accordance with the procedure in standard NF P 18-452.

The time taken for the mortar to flow is an indicator of its fluidity. If the mortar is more fluid or more workable, which corresponds to the name of the device, this time will be reduced.
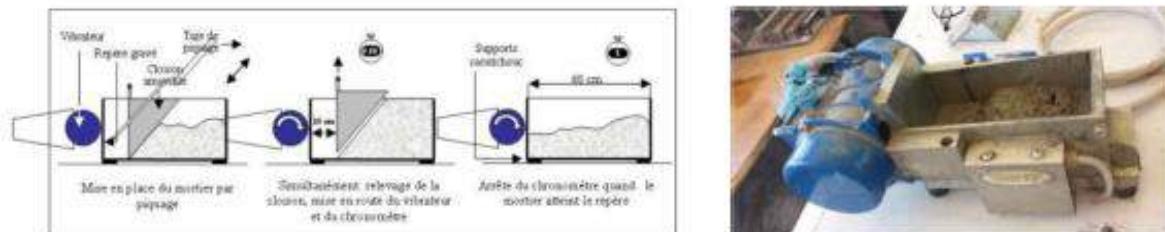
Figure 4. Workability test.

Capillary absorption test

The capillary absorption test is carried out in accordance with standard EN 480-5, and measures the rate of water absorption by capillary suction of unsaturated mortar specimens placed in contact with water without hydraulic pressure.

Test specimens measuring 40x40x160 mm3 are kept at a temperature equal to (20 ± 2) °C and (65 ± 5) % relative humidity, weighed, then placed vertically in a container filled with water at a constant level (3±1) mm above their base (figure5).

Figure 5. Essai d'absorption d'eau capillaire.

Mechanical strength tests

Compressive strength and three-point bending tests were carried out in accordance with EN 196-1 and EN 1015-11 on specimens (40×40×160) mm3 at ages of 7 and 28 days in the building materials laboratory of the Civil Engineering Department at the University of Bouira. The following figure shows the three-point bending and

compression tests carried out on the various mortars.

<div align="center">(a)   (b)</div>
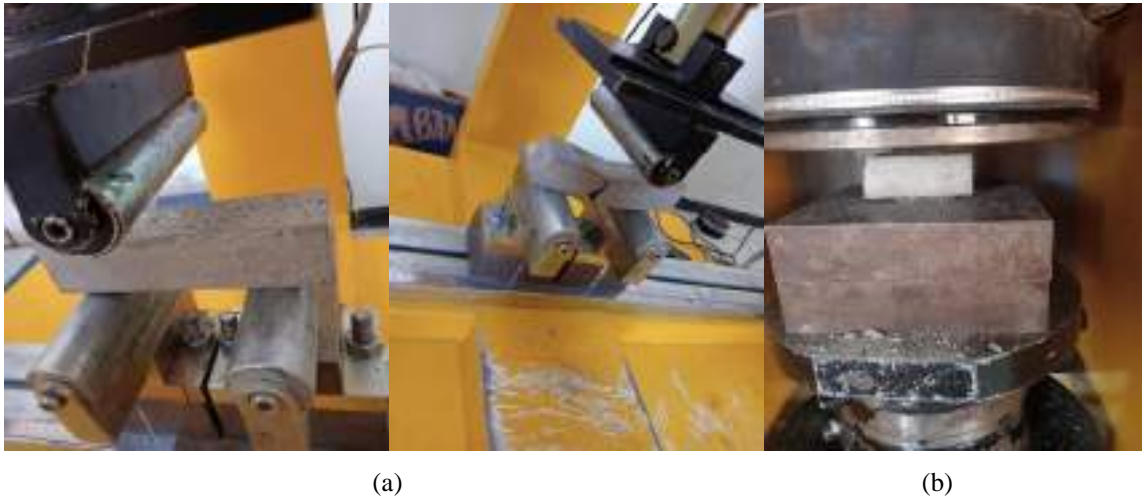
Figure 6. (a)Three-point bending tests, (b) Compressive Strength test.

Thermal test

The mortars are used to create precisely sized specimens (30x50x100 mm3). To analyze the thermal characteristics of these mortars and evaluate the effect of substituting Hammam Boughrara perlite for cement, we measured their thermal conductivity using the portable "Isomet 2104" instrument. Using surface probes and syringe exchanges, this instrument enables direct measurement of the thermal conductivity coefficient, specific volumetric capacity and temperature, in accordance with ISO 8302.

Figure 7. Conductivity meter of the mechanical engineering laboratory at the University of Bouira.

Results and analysis

Paste consistency and setting

The addition of perlite, as shown in figure 8, increases the water requirement of pastes to reach a normal consistency.
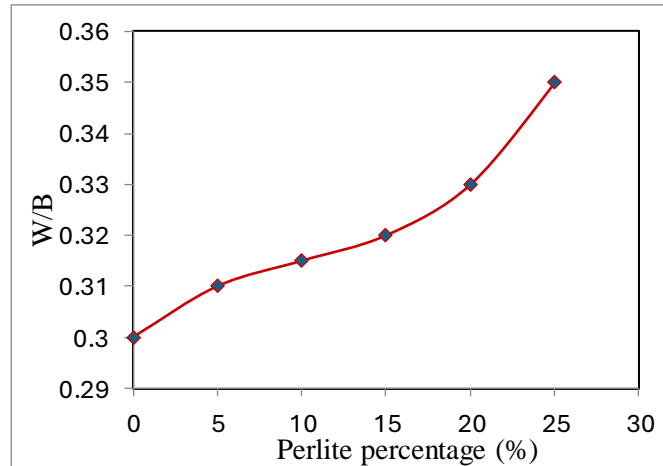
Figure 8. Variation in Water/Binder ratios as a function of perlite dosage

This observation stems from perlite's ability to absorb a non-negligible proportion of the mixing water, thus reducing the quantity available for cement hydration, which is in line with studies carried out by some researchers (Belaribi & al., 2024., Chaib & al., 2024; Ghrici & al., 2006).

Setting time.

Analysis of initial setting time, final setting time and setting time for pastes with different proportions of perlite to cement shows significant trends (figure.9).
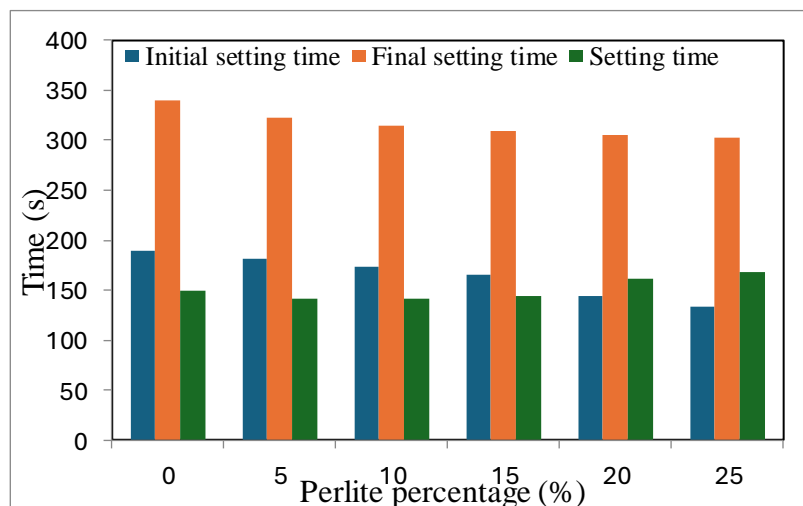
Figure 9. Setting times for perlite-based pastes.

The addition of perlite accelerates the intitial and final setting times: for 0% perlite, the intitial time is 190 minutes and the final time 340 minutes, while for 25% perlite, these times increase to 143 and 302 minutes respectively. This acceleration is due to perlite's ability to absorb mixing water, reducing the water available for

cement hydration. Several authors have reported the same findings (Belaribi & al., 2024., Achour & al., 2024; Chaib & al., 2018). Setting time varies, decreasing slightly up to 15% perlite and then increasing for 20% and 25%, suggesting complex interactions between perlite and cement. Overall, the addition of perlite affects slightly the setting time.

Workability time

Figure 10 shows the evolution of workability times for perlite-based mortars. To compare the workability of the different mortars with that of a control mortar, we maintained a constant W/C ratio of 0.55.
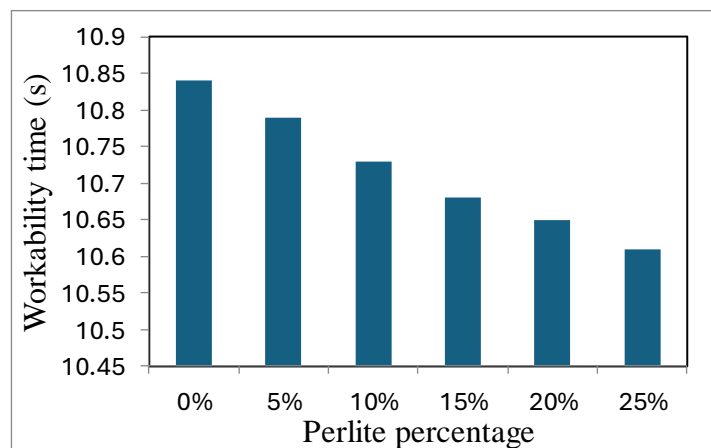
Figure 10. Evolution of workability times for perlite-based mortars.

The flow times of perlite-based mortars are slightly lower than those of the control mortar, but the times satisfy the conditions. To maintain a more or less constant workability, an admixture must be used to obtain a workable and manageable mix (Chihaoui., 2018; Hamadache., 2018).

Several authors (Guenanou., 2018; Senhadji., 2013) have also demonstrated the same finding. The workability of pozzolanic mortars decreases as the rate of cement substitution by perlite increases. This proves that increasing the perlite rate increases significantly water demand (Chaib et al., 2024; Hamadache., 2018).

Capillary absorption

Mortars containing various percentages of natural perlite, including a control mortar, were evaluated for their ability to absorb water by capillary action after one day's storage on a thin layer of water.

Figure 11 shows the results of the capillary absorption test, which clearly highlight a trend: as the percentage of perlite in the mortar increases, the absorption coefficient decreases. Furthermore, these results underline that mortar without perlite has the highest absorption coefficient, demonstrating the significant impact of adding

perlite on the mortar's capillary absorption properties. In conclusion, the incorporation of perlite seals the capillaries resulting from the interaction of cement, water and sand, in line with the results of (Belaribi & al., 2024., Ayed & al., 2022).
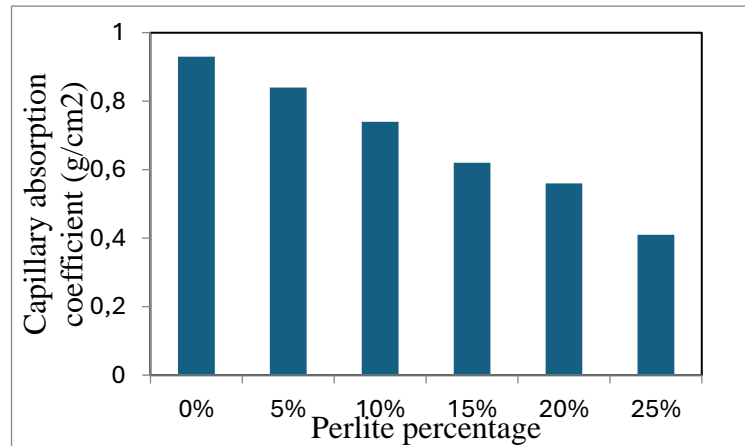
Figure 11. Capillary absorption coefficient at 1 day for various perlite-based mortars.

Flexural strength

Tensile strength measurements were carried out by subjecting specimens (size $4 \times 4 \times 16$ cm³) made with mixes containing 5%, 10%, 15%, 20% and 25% perlite respectively, as well as control specimens, to three-point flexure. Figure 12 illustrates the evolution of flexural strength as a function of age for mixes containing different percentages of perlite. It should be noted that all the strengths of the mixes increase steadily with time.
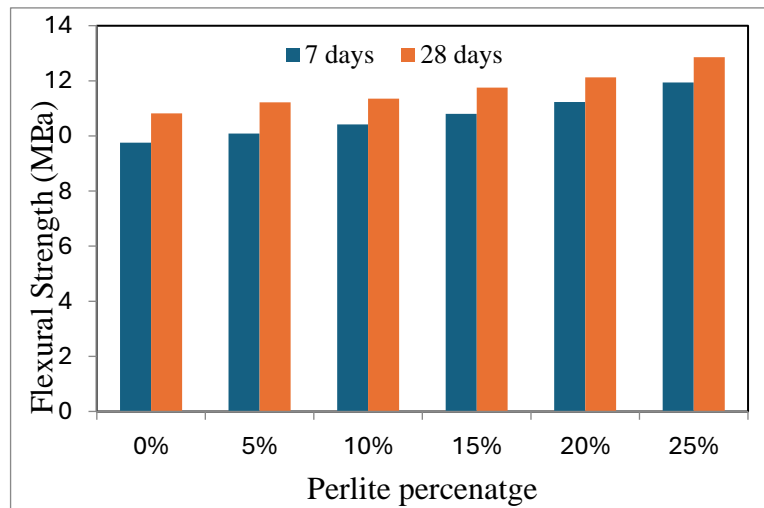
Figure 12. Evolution of flexural tensile strength at 7 and 28 days.

The results of flexural tensile strength measurements demonstrate the significant impact of perlite incorporation

on the mortar's mechanical properties. Overall, an increase in flexural strength was observed as the percentage of perlite in mortar increased, both at 7 and 28 days. This linear increase in tensile strength is consistent with the reinforcing nature of perlite, which acts as a pozzolanic addition offering higher mechanical performance. Control mortars, without perlite, show lower strength values than mixes with perlite (Yu et al., 2003; Achour et al., 2024). Furthermore, the difference in strength between the 7-day and 28-day samples indicates a progressive improvement in mechanical properties with mortar curing time, which coincides with the results of (Belaribi & al.,2024; Chaib and al., 2024; Chaib & al., 2018).

Compressive strength

Figure 13 shows the evolution of the compressive strength of perlite-based mortars as a function of mortar age.
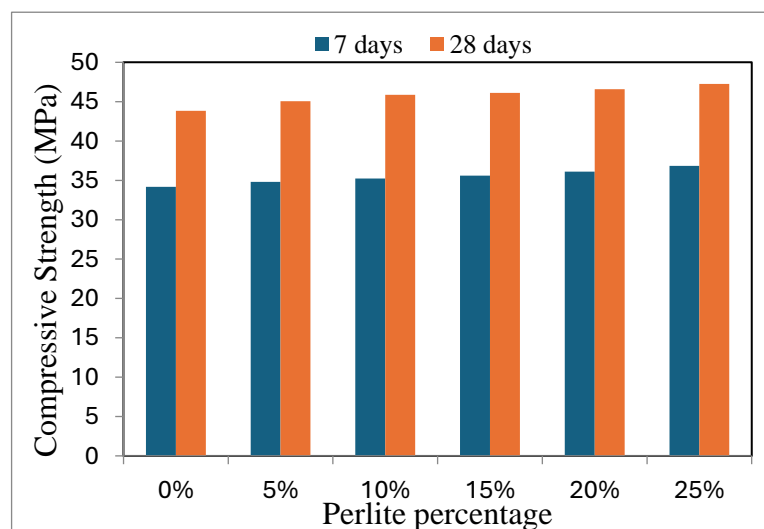
Figure 13. Evolution of compressive strength at 7 and 28 days.

The strengths of all mortars increase proportionally with age, reflecting a continuous improvement in mechanical performance. More specifically, samples containing higher percentages of perlite generally showed higher strength values, suggesting a beneficial effect of perlite addition on mortar compressive strength. These results highlight the potential of perlite as an effective pozzolanic additive for improving the mechanical properties of mortar (Yu & al., 2003; Chaib & al., 2024; Achour & al., 2024).

Thermal conductivity measurement

Figure 14 shows the variation in conductivity of mortar containing 25% perlite at 28 days versus the control mortar. A decrease in the thermal conductivity of the perlite-based mortar compared with that of the control was observed at 28 days of age, which explains the latter's good thermal insulation. This generally confirms the results obtained by (Hamadache., 2018) who deduced a better thermal insulation of perlite mortars. These mortars can therefore be recommended as materials with better thermal insulation than the control mortar.
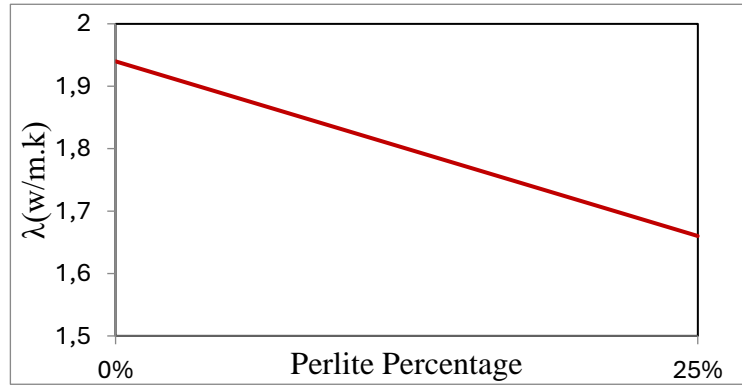
Figure 14. Variation in thermal conductivity at 28 days.

Conclusion

This work has enabled us to confirm the possibility of introducing the perlite of Maghnia, as a finely ground powder, into mortars at percentages ranging from 0 to 25%, by substituting cement quantities.

The aim of this work was to characterize the physicochemical, mechanical and thermal properties of these mortars. The main conclusions are as follows:

The incorporation of perlite affects significantly the setting time and accelerates the initial and final setting times compared with pastes without additions.

A study of normalized consistency shows a proportional variation with the rate of perlite addition. The water required to achieve normalized consistency also increases with the rate of cement substitution.

The workability of mortars decreases as the rate of substitution of cement by perlite increases. Hence the need to use superplasticizer-type admixtures to ensure more or less constant workability equivalent to that of the control mortar.

Increasing the perlite dosage helps to reduce capillary absorption. The 25% substitution rate remains the most interesting, as perlite improves mortar durability by sealing capillaries that interact with cement, water and sand. Thermal insulation is considerably improved at a substitution rate of 25%, due to the reduction in thermal conductivity compared with the control mortar.

The addition of natural perlite to cement improves compressive and flexural strength in proportion to the percentage of cement substitution, from 0% to 25%.

The mechanical behavior of mortar containing 25% perlite is the most advantageous, with high strengths noted

at 7 and 28 days compared with the control mortar. This explains why adding natural perlite to the cement improves the mortar's mechanical strength by triggering the pozzolanic reaction.

References

Achour, M., Belas, N., Hadj Sadok, R. (2024). Effect of incorporation of calcined sediments and perlite as partial cement replacement on mortars behavior. The Journal of Engineering and Exact Sciences – jCEC, 10 (02). https://doi:10.18540/jcecvl10iss2pp17398

Ayed, K., Midoune, N., Mechebek, S. (2022). Formulation d'un mortier à base de perlite avec étude thermique et Acoustique. Communication Science et Technologie, 11, 01, 34–46, enpo– maurice audin asjp/essn

ASTM C187. (1998). Standard test method for normal consistency of hydraulic cement. West Conshohocken, PA: American Society for Testing and Materials: (ASTM) International.

ASTM C191. (2004). Standard test method for time of setting of hydraulic cement by vicat needle. West Conshohocken, PA: American Society for Testing and Materials: (ASTM) International.

Belaribi, O., Belas, N., Aggoun, S., Bendani, K., Bouhamou, N., Mebrouki, A. (2014). Enhancing the value of dam dredged sediments as a component of a self compacting concrete, Cement Wapno Beton, (6), 370–375.

Belaribi, O. (2015). Durabilité des bétons autoplaçants à base de vase et de pouzzolane. Thèse de doctorat à l'Université de Cergy-Pontoise, France et de l'Université de Mostaganem, Algérie.

Belaribi, O & Safer, O & Belas, N & Belguesmia, K & Hadj Sadok, R (2024). Influence de la perlite sur le comportement mécanique, l'absorption capillaire et la conductivité thermique des mortiers. The Journal of Engineering and Exact Sciences. 10. 18800. 10.18540/jcecvl10iss3pp18800.

Belas, N., Besseghier, N., Mebrouki, A., Bouhamou, N. (2009). Vers une protection de l'environnement en valorisant la vase draguée du barrage comme composant du béton. Matériaux & Techniques, 97,4, 231–240. https://doi.org/10.1051/mattech/2009039

Belguesmia, K., Belas Belaribi, N., Amiri, O., Leklou, N., Belaribi, O. (2018). Influence of treated sediment substitution percentage on workability, strength and porosity of SCC', Journal of Materials and Engineering Structures, 5,1, 47–55.

Bouzidi, C., Boutadjine, Z. (2022). Etude du comportement physico-mécanique des mortiers à base de 10 et 20% de perlite naturelle de Maghnia, Mémoire de Master académique.

Chaib, O., Mouli, M., Benosman, A. S., Hamadache, M. (2018). Study of the effects of shrinkage on concretes based on pozzolana and perlite, Asian Journal of Civil Engineering, 19, (3), 287–294.

Chaib, O.; Safer, O.; Dif, F. (2024). Mechanical Behavior and Durability of Perlite Based Mortar Exposed to Sodium Sulfate Attack, Materials Science (MEDŽIAGOTYRA). http://doi.org/10.5755/j02.ms.34760

Chihaoui, R. (2018). Etude de durabilité des matériaux cimentaire exposés aux attaque, Thèse de Doctorat en Sciences, USTOMB.

Chihaoui, R., Siad, H., Senhadji Y., Mouli, M., Nefoussi, A. M., Lachemi, M., (2022). Efficiency of natural pozzolan and natural perlite in controlling the alkali-silica reaction of cementitious materials, Case

Studies in Construction Materials, 17, https://doi.org/10.1016/j.cscm.2022.e01246

Chikouche, M. A., Ghorbel, E., & Bibi, M. (2016). The possibility of using dredging sludge in manufacturing cements: Optimization of heat treatment cycle and ratio replacement. Construction and Building Materials, 106, 330–341. https://doi.org/10.1016/j.conbuildmat.2015.12.128

El Mir A. (2020). Durability of self-consolidating concrete containing natural waste perlite powder, Heliyon, 6, (1). https://doi.org/10.1016/j.heliyon.2020.e03165

Erdem, T.K., Meral, Ç., Tokyay, M., Erdoğan, T.Y. (2007). L'utilisation de la perlite comme une addition pouzzolanique dans la production de ciments, Moyen Science Direct Scopus Applications, 29, (1),13–21. https://doi.org/10.1016/j.cemconcomp.2006.07.018

Erdogan, S.T., Saglik, A.Ü. (2013). Early-age activation of cement pastes and mortar, Cement and Concrete Composites, 38, 29–39.

Ghrici, M. (2006). Etude des propriétés physico Mécaniques et de la durabilité des ciments à base de pouzzolane naturelle, Thèse de doctorat, Université de sciences et de la technologie d'Oran MB, Algérie.

Guenanou, F. (2018). Durabilité des mortiers contenant la perlite vis-à-vis de la corrosion des armatures, Thèse de Doctorat en Sciences, Université d'Oran, Algérie.

Guenanou, F., Khelafi, H., Aattache, A. (2019). Behavior of perlite-based mortars on physicochemical characteristics, mechanical and carbonation, Case of perlite of Hammam Boughrara, Journal of Building Engineering, 24, 100734. https://doi.org/10.1016/j.jobe.2019.100734

Guemidi, I., Taleb, H. A., Abdelaziz, Y. (2024). Effect of W/C ratio on the rheological and physico-mechanical behavior of high-performance concrete formulated with natural pozzolana, The Journal of Engineering and Exact Sciences, 10, (2), 17490. https://doi.org/10.18540/jcecvl10iss2pp17490

Hadj Sadok, R., Belas Belaribi, N., Hadj Sadok, F. (2024). Performance assessment and cost-benefit analysis of low-carbon binders containing calcined sediments from Chorfa II dam as new building materials. Construction and Building Materials, 415, 135039. https://doi.org/10.1016/j.conbuildmat.2024.135039

Hadj Sadok, R., Belas Belaribi, N., Mazouzi, R., Hadj Sadok, F. (2022). Life cycle assessment of cementitious materials based on calcined sediments from Chorfa II dam for low carbon binders as sustainable building materials. Science of Total Environment, 826, 154077. https://doi.org/10.1016/j.scitotenv.2022.154077

Hadj Sadok, R., Belas, N., Tahlaiti, M., Mazouzi, R. (2021). Reusing calcined sediments from Chorfa II dam as partial replacement of cement for sustainable mortar production, Journal of Building Engineering, 40, 102273, https://doi.org/10.1016/j.jobe.2021.102273

Hadj Sadok, R., Maherzi, W., Benzerzour, M., Lord, R., Torrance, K., Zambon, A., Abriak, N. E. (2021). Mechanical properties and microstructure of low carbon binders manufactured from calcined canal sediments and ground granulated blast furnace slag (GGBS). Sustainability, 13, 9057. https://doi.org/10.3390/su13169057

Hadj Sadok, R,. Tahlaiti, M,. Belas Belaribi, N,. Mazouzi, R. (2019). Environmental life cycle assessment of industrialization process of calcined dredged sediments, Journal of Materials and Engineering Structures, 6,1, 25–37.

Hamadache, M., Mouli, M., Bouhamou, N., Benosman, A.S., Chaib, O., Dif, F. (2016). Caractérisation des

ajouts pouzzolaniques dans le mortier pour l'efficacité énergétique des bâtiments, Journal of materials and Environmental Sciences, 7, (2), 416–421.

Hamadache, M., (2018). Résistances mécaniques, conductivité et résistance à la corrosion des. Pouzzolaniques, Thèse doctorat en science, Ecole Nationale Polytechnique Mauris Audin, Oran, Algérie.

Hamidi, M. (2014). Elaboration d'un éco-ciment composé à base d'un ajout andésitique brut et activé, Thèse de doctorat En Sciences, Université des Sciences et de la Technologie d'Oran Mohamed Boudiaf, Faculté de Chimie Département de Génie des Matériaux, Algérie.

Huedo, P., Mulet, E., López-Mesa, B. (2016). A model for the sustainable selection of building envelope assemblies, Environmental Impact Assessment Review, 57, 63–77. https://doi.org/10.1016/j.eiar.2015.11.005

Huntzinger, D., Eatmon, T. D. (2009). A life-cycle assessment of Portland cement manufacturing : Comparing the traditional process with alternative technologies. Journal of Cleaner Production, 17, (7), 668–675. https://doi.org/10.1016/j.jclepro.2008.04.007

ISO8302-91. (1991). Isolation thermique, détermination de la résistance thermique et des propriétés connexes en régime stationnaire, méthode de la plaque chaude gardée, Model ISOMET 2104, Heat Transfer Analyzer.

Meral, Ç. (2004). Use of perlite as a pozzolanic addition in blended cement production, Turkey, Middle East Technical University.

NF P18-452 et NF P18-437. (1996). Maniabilité (ouvrabilité), AFNOR – Paris.

Norme EN ISO 6946 SIA 180.071-96. (1996). Composants et parois de bâtiments-Résistance thermique et coefficient de transmission thermique-Méthode de calcul, Catalogue d'éléments de construction avec calcul de la valeur de coefficient de transmission thermique.

Norme EN 480-5. (2006). Adjuvants pour béton, mortier et coulis Méthodes d'essai Partie 5 : Détermination de l'absorption capillaire.

Norme EN 196-1. (2007). Méthodes d'essais des ciments - Détermination des résistances mécaniques.

Norme NF 15 403. (2011). Préparation des éprouvettes, réalisations, malaxages.

Norme SIA 180-99. (1999). Isolation thermique et protection contre l'humidité dans les bâtiments, Catalogue d'éléments de construction avec calcul de la valeur de coefficient de transmission thermique.

Norme NA442., Equiv EN 197-1. (2001). Ciment- composition, spécification et critères de conformité des ciments courants, P15–101–1, comité 37 N°20.

Prénorme SIA 279-00. (2000). Isolants thermiques, Catalogue d'éléments de construction avec calcul de la valeur de coefficient de transmission thermique.

Safer, O., Belas, N., Belaribi, O., Belguesmia, K., Bouhamou, N., Mebrouki, A. (2018). Valorization of dredged sediments as a component of vibrated concrete: Durability of these concretes against sulfuric acid attack. International Journal of Concrete Structures and Materials, 12, 44. https://doi.org/10.1186/s40069-018-0270-7

Safer, O., Belas Belaribi, N., Belaribi, O., Belguesmia, K., Taieb, F., Hamadache, M. (2021). Resistance of concrete based on treated mud to sea water attack, Journal of Materials and Engineering Structures, 8, 111–121. https://revue.ummto.dz/index.php/JMES/article/view/2497/0

Safer, O., Belas, N., Belaribi, O., Belguesmia, K., Mebrouki, A., Hamadache, M. (2017). Study of the behavior in the fresh and hardened state of an eco-concrete based on dredged sediments. Journal of Materials and Environmental Sciences, 8 (6), 2026–2033. http://www.jmaterenvironsci.com

Sengul, O., Azizi, S., Karaosmanoğlu, F., Tasdemir, M. A. (2011). Effect of expanded perlite on the mechanical properties and thermal conductivity of lightweight concrete, Energy and Buildings ,43, (2–3), 671–676. https://doi.org/10.1016/j.enbuild.2010.11.008

Senhadji, Y. (2013). L'influence de la nature du ciment sur le comportement des mortiers vis à- vis des attaques chimiques (acides et sulfates), Thèse de doctorat, Université de sciences et de la technologie d'Oran MB, Algérie.

Skibsted, J., Snellings, R. (2019). Reactivity of supplementary cementitious materials (SCMs) incement blends. Cement and Concrete Research, 124, 105799. https://doi.org/10.1016/j.cemconres.2019.105799

Stefanidou, M., Pachta, V., Konstantinidis, G. (2023). Exploitation of waste perlite products in lime-based mortars and grouts. Sustainable Chemistry and Pharmacy, 32, 101024. https://doi.org/10.1016/j.scp.2023.101024

Taieb, F., Belas, N., Belaribi, O., Belguesmia, K., Hadj Sadok, R. (2018). Influence of calcined mud on the mechanical properties and shrinkage of self-compacting concrete, Matec Web of Conferences, 149, 01026, https://doi.org/10.1051/matecconf/ 201814901026

Yu, L. H., Ou, H., Lee, L. L. (2003). Investigation on Pozzolanic Effect of Perlite Powder in Concrete, Cement and Concrete Research, 33, (1), 73–76. https://doi.org/10.1016/S0008-8846(02)00924-9

Zhang, H., Cao, M., Xing, Z. (2024). Early-age properties of cement paste with mechanically ground Yellow River sediment. Construction and Building Materials, 411, 134635. https://doi.org/10.1016/j.conbuildmat.2023.134635

Study of the Influence of The Earthquake's Direction on The Dynamic Response of Irregular Buildings

Mohamadi Saddika

University of Bouira, Algeria, ⓘD https://orcid.org/ 0009-0001-0644-031X

Boumaiza Malika

University of Bouira, Algeria, ⓘD https://orcid.org/0009-0006-6581-0612

Bouraine Karim

University of Bouira, Algeria, ⓘD https://orcid.org/0009-0006-1714-9225

Boumekouaz Mahdi

University of Bouira, Algeria, ⓘD https://orcid.org/0009-0001-9324-384X

Abstract: This research consists to study the effect of the angle of incidence of the earthquake on the dynamic response of irregular buildings. For this we are examining a building of irregular shape braced by shear walls composed of five levels (R+4) located in the commune of Bouira which is, according to Algerian seismic regulations RPA99/V2003, considered as a medium seismic zone (zone IIa). The structure is used for the critical analysis of the dynamic response by varying the direction of the earthquake from 0° to 90° in steps of 10°. Spectral modal analysis was carried out using the structural analysis software "ETABS19.1.0". The variations in the dynamic response of the structure as a function of the angle of incidence of the earthquake are expressed in terms of the reaction at the base, the maximum displacement and the stresses in the different load-bearing elements (normal force, shear force and bending moment) in columns, beams and shear walls. The results obtained showed that the dynamic response of the structure varies according to the angle of incidence of the earthquake but the maximum responses always coincide with the main axes X and Y for the structure with shear walls. The analysis of the response of the building without shear walls (with only frames) as a function of the angle of incidence also showed that the existence of shear walls has no impact on the reaction at the base and the maximum responses always correspond to angles 0° and 90° but affects the maximum horizontal displacement which corresponds to an angle of 70° and the maximum normal stress which corresponds to an angle of 45°.

Keywords: Dynamic response, Angle of incidence, Irregular building, Shear walls, RPA 99/2003.

Introduction

Today, the main objective of structural engineers is to create structures that can support not only permanent and live loads, but also accidental loads such as earthquakes. Earthquakes, one of the most destructive natural disasters, occur unintentionally, causing massive destruction and significant human losses. In countries such as Algeria, where thousands of people lost their lives and were injured in the 2003 BOUMERDES earthquake, it is essential that earthquake engineering experts and civil engineers develop structures capable of withstanding these destructive forces.

One approach to reducing the risk of earthquakes is to strengthen the resistance of structures, but the crucial question is: how do you strengthen the resistance of structures under variations in the direction of the earthquake?
When designing the structure of a building, seismic action is generally considered following the planes or main axes of the structure. The Algerian seismic code RPA99/2003 [1] defines the two orthogonal axes of the horizontal plane as the main axes of the structure.

However, in recent years, research has obtained significant insights into the impact of the angle of incidence of earthquakes on the dynamic behavior of structures [2-5]. With this in mind, and in the context of our work, our main objective is to evaluate the impact of earthquake direction on the seismic response of an irregular reinforced concrete building braced by frames and shear walls. This will be achieved by applying it to a building consisting of a ground floor and four storey (R+4) located in the wilaya of Bouira, which is considered to be a medium seismicity zone according to RPA99/V2003 [1].

The building was used to analyze the critical incidence, with a variation in the direction of the earthquake from 0° to 90° degrees with a step of 10° degrees. The impact of this variation on the seismic response of our structure is examined using software based on the finite element method, ETABS 2019. The variation in the seismic response is studied as a function of the reaction at the base of the structure, its maximum horizontal displacement and stresses (axial force, shear force, bending moment) in the columns, beams and shear walls.

Description of the Structure

The structure under study is an irregular, five-storey residential building braced by frames and shear walls. It is located in the wilaya of Bouira, which is classified as a medium seismicity zone (zone IIa) according to the Algerian seismic code RPA 99 /2003.

The building is classified as a standard structure of medium importance (use group 2), as its height does not exceed 48m. The site is considered a soft site (S3).
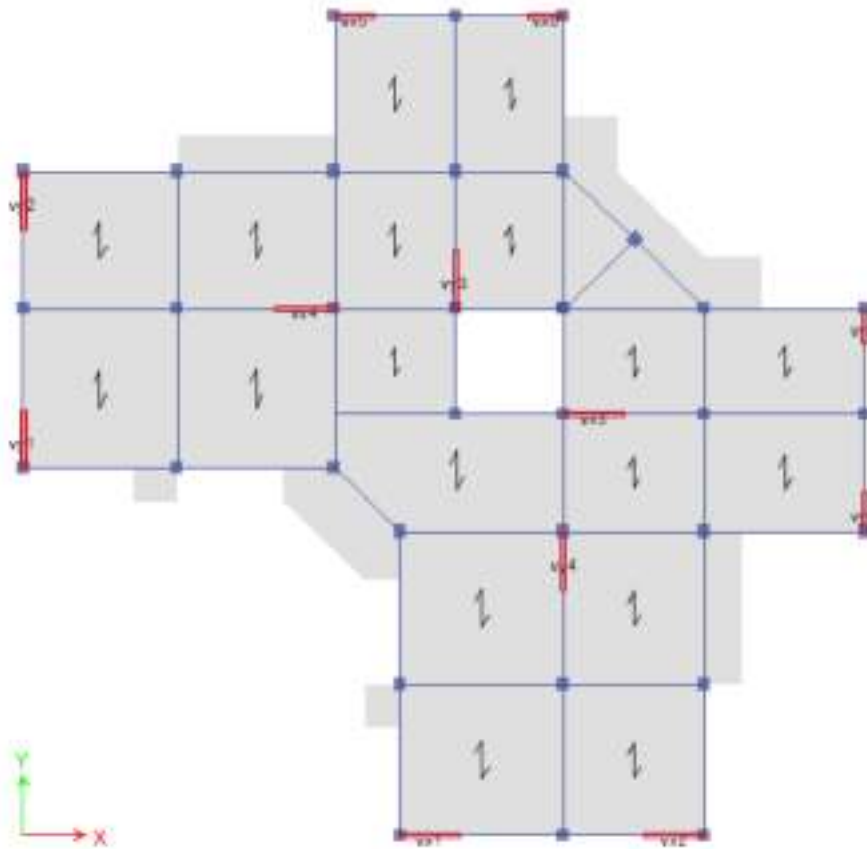
Figure 1. Plan view of the structure

The geometric characteristics of the structure are given in Table 1.

Table 1. Geometric characteristics of the structure studied.

	Designation	Value (m)
Total length	L	26
Total width	l	26
Total height	H	15,30
Ground floor height	h_{Gf}	3,06
Current story height	h_{cs}	3,06

The dimensions and cross-sections of the building's structural elements (columns, beams, shear walls, slabs) are shown in Table 2. The columns, beams, shear walls and slabs (balcony) of the structure were considered to be made of reinforced concrete with linear elastic behavior. The material proprieties are summarized in Table 3 [6], the behavior of the structural elements was considered as linear elastic. A structural Rayleigh damping ratio of

8.5% [1], was assigned for all the elements in the concrete frame-shear wall building.

Table 2. Structural sections considered in the building

Section	Notation	Sections (cm^2)	Thickness (cm)
Columns story 1-3	C$_1$	40x40	
Columns story 4-5	C$_2$	35x40	
	SW1	15x110	
Shear wall	SW2	15x 125	
	SW3	15x185	
	PB	30x40	
Beam	SB	30x40	
Balcony slab	BS		20
Slab (Hollow body)	HBS		21(16+5)

Table 3. Material properties considered for the structural elements in the building

Parameter	Notation	Columns, beams and shear walls
Young modulus (GPa)	E	32
Shear modulus (GPa)	G	12,5
Volumic weight (kg/m^3)	ρ	2500
Poisson Ratio	ν	0,2
Damping Ratio	ξ	0,085

Analysis of the Effect of the Earthquake's Angle of Incidence on the Dynamic Response of the Structure

To study the effect of the earthquake direction on the dynamic response of the structure, the seismic action is defined by two horizontal components along x and y as follows [6] [7], as shown in Figure 2. The seismic action is introduced using a design response spectrum.

The dynamic characteristics of the structure according to RPA 99/2003 are shown in table 4.
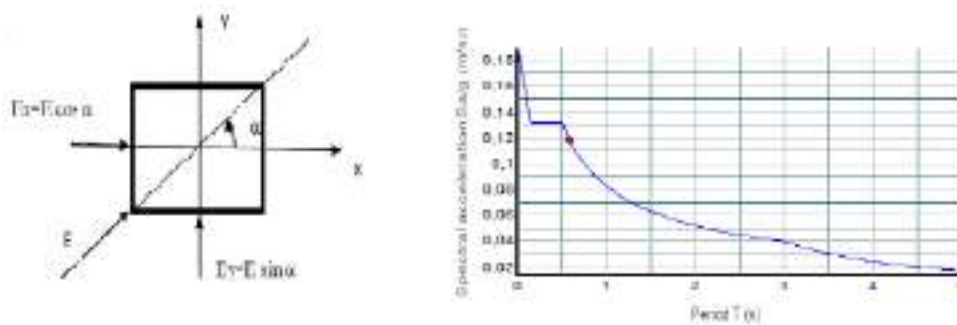
Figure2. Components of the seismic load and design response spectrum

Table 4. Dynamic properties of the building

Behavior coefficient	Acceleration coefficient zone	Dynamic amplification factor D	Quality factor Q
3,5	0,15	$D_x=D_y=2,041$	$Q_x=Q_y=1,2$

Numerical Analysis of Dynamic Response of the Structure

To study the influence of the direction of the earthquake on the dynamic response of the structure, we carried out a spectral modal analysis [7] using ETABS 2019 software based on the finite element method (FEM), varying the angle of incidence of the earthquake from 0° to 90° with a step of 10°. The columns and beams were modeled with frame elements. The slab floors were modeled with deck elements. The shear walls and balcony slabs were modeled by shell elements [6]. Beam structural elements were two-noded, straight, finite elements with six degrees of freedom per node, including three translational components and three rotational components. The shell structural elements were four-noded, flat finite elements with 20 degrees of freedom. Soil-structure interaction is not considered in the model and base are restraints in all three X, Y and Z directions. For the Response Spectrum Analysis RSA, SSRS (square root of the sum of square) and CQC (Complete quadratic Combination) are considered [8]. A sufficient number of modes (16 modes) are considered in the analysis such that to get the sum of mass for all modes assumed 90% of the total seismic mass, according to the RPA 99/2003 [1]. The mesh size used is the default mesh size in the ETABS software.

The arrangement of the braced walls was made in such a way that the first and second modes of vibrations are translations along X and Y and the third mode is a rotation around Z. The eccentricity between the center of mass and the center of rigidity at each floor (ex=0.009m and ey=0.019m). The first vibration mode is translation along X with a period T1= 0.492s, the second vibration mode is translation along Y with a period T2= 0.46s, while the third mode is rotation around Z with a period T3= 0.367s. The response of the structure is calculated in both directions for the most unfavorable load combination:

G+Q+E

G: Dead load

Q: Live load

E: Seismic load

The values of G and Q for the various elements are given in the following table:

Table 5. Dead and live loads

Element	Terrace floor	Current floor	Balcony
G (KN/m^2)	6,14	5,60	5,35
Q (KN/m^2)	1	1,5	3,5

The variation in response studies the following parameters: reaction at the base of the structure, maximum

displacement and maximum solicitations in columns, beams and shear walls.

Slab Floor
thikness 21 cm

C2 35x40 cm²

C1 40x40

SW2 15x 125

SW1 15x 110
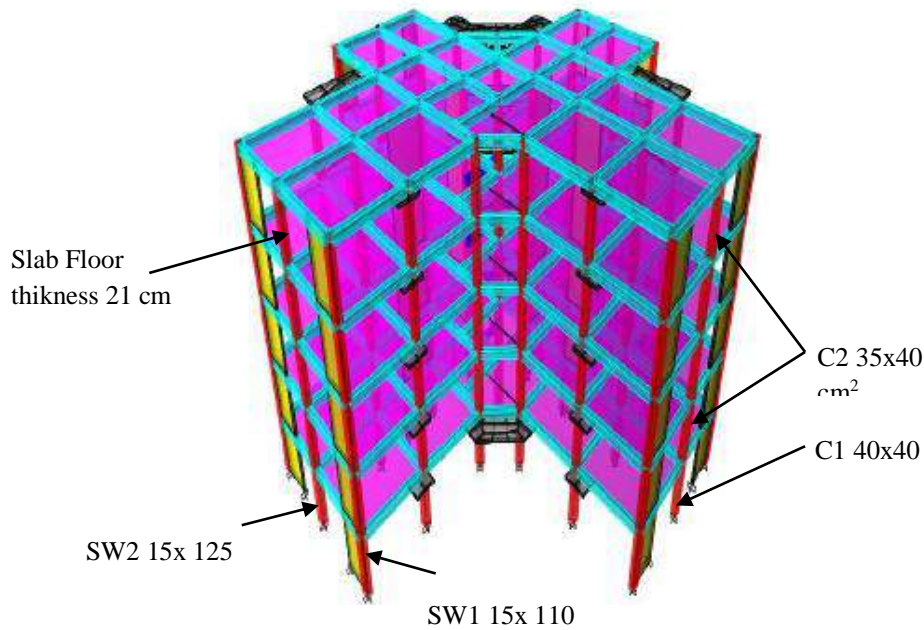
Figure 3. Numerical simulation of the structure by ETABS 2019

Results and Discussion

Effect of the Earthquake Direction on the Seismic Reaction at the Base of the Structure

The results of the dynamic analysis of the structure in terms of reaction at the base in both directions X and Y as a function of the earthquake incidence angle are shown in Figure 4.
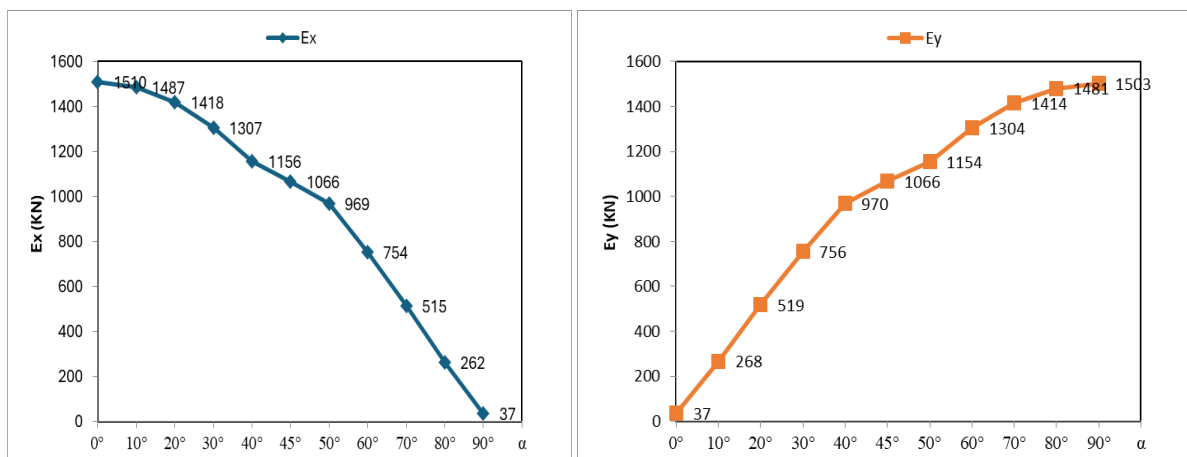
Figure 4. Seismic reaction at the base as a function of the earthquake incidence angle.

The seismic reaction at the base in the x direction has a maximum value of Ex=1519.89 KN at angle α=0°, then decreases to reach a value of Ex= 37.46 KN at angle α=90°. On the other hand, the seismic reaction at the base in the y direction varies from Ey=37.47 KN at angle α=0° to reach a maximum value of Ey=1503 KN at α=90°.

Effect of the Earthquake Direction on the Horizontal Displacement of the Structure

The results of the dynamic analysis of the structure in terms of horizontal displacement in both directions as a function of the earthquake incidence angle are shown in Figure 5.
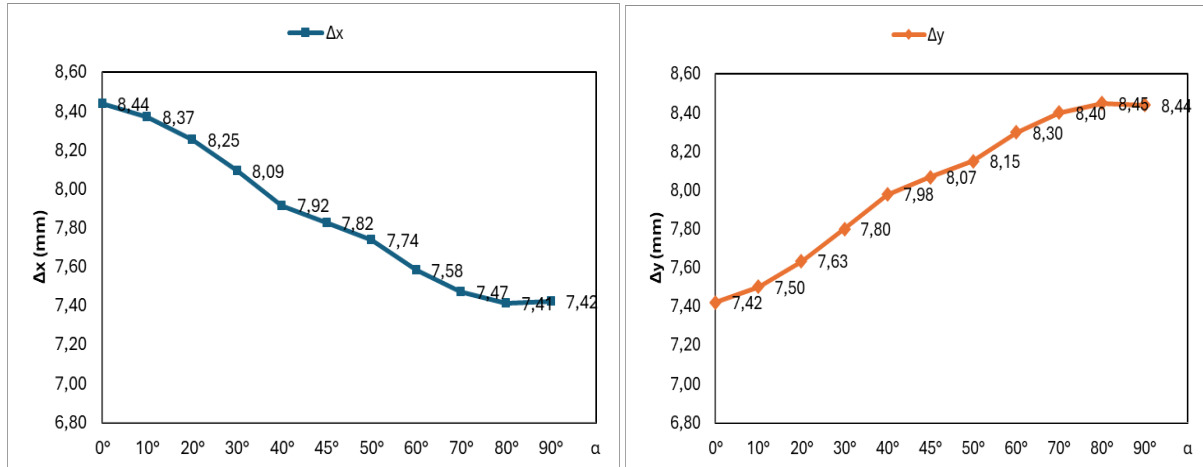
Figure 5. Horizontal displacement of the structure as a function of the earthquake incidence angle.

It can be seen that the maximum displacement in the x direction is Δx =8.44mm at angle α= 0°, then it decreases until reaching a value of Δx =7.41mm at angle α=90°. On the other hand, the displacement following the direction y varies from Δy = 7.42mm at the angle α=0° until reaching a maximum value Δy = 8.45mm at α=90°.

Effect of the Earthquake Direction on the Stresses in the Columns

The objective of this analysis is to study the dynamic behaviour of columns under the effect of variation in the earthquake incidence angle. The results obtained for the most stressed column are shown in figures 6,7 and 8.
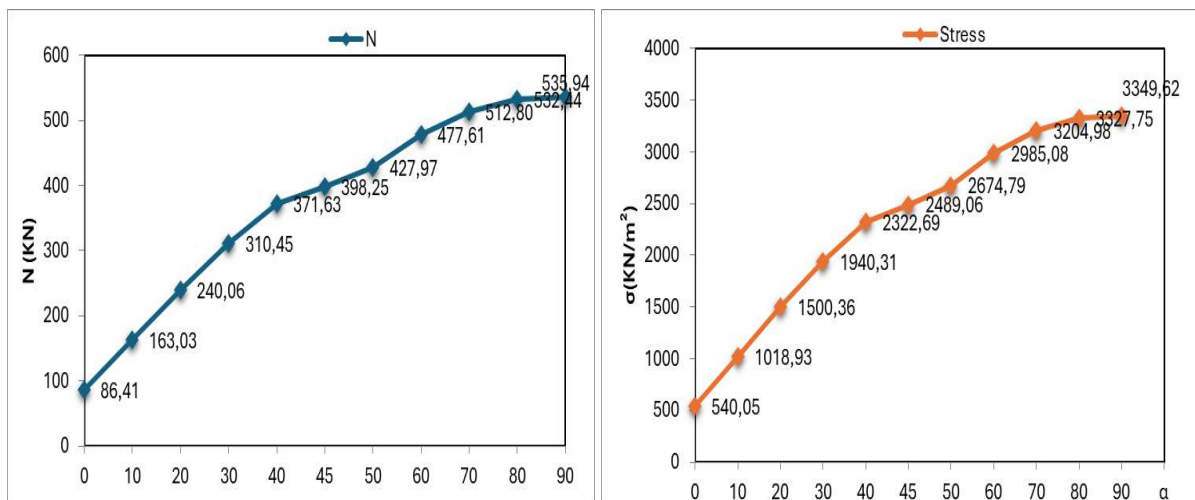
Figure 6. Axial force and normal stress in the most stressed column as a function of the earthquake incidence angle.
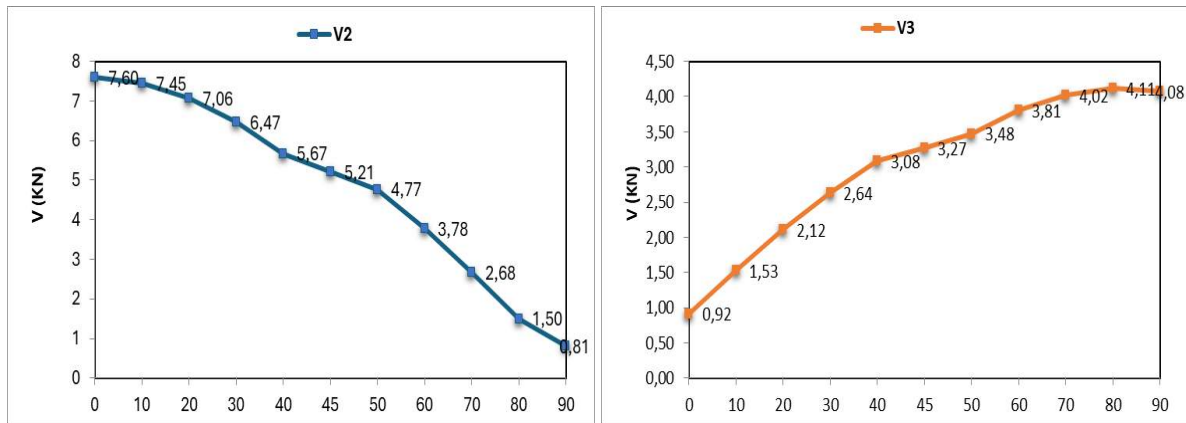
Figure 7. Shear force in the most stressed column as a function the earthquake incidence angle.
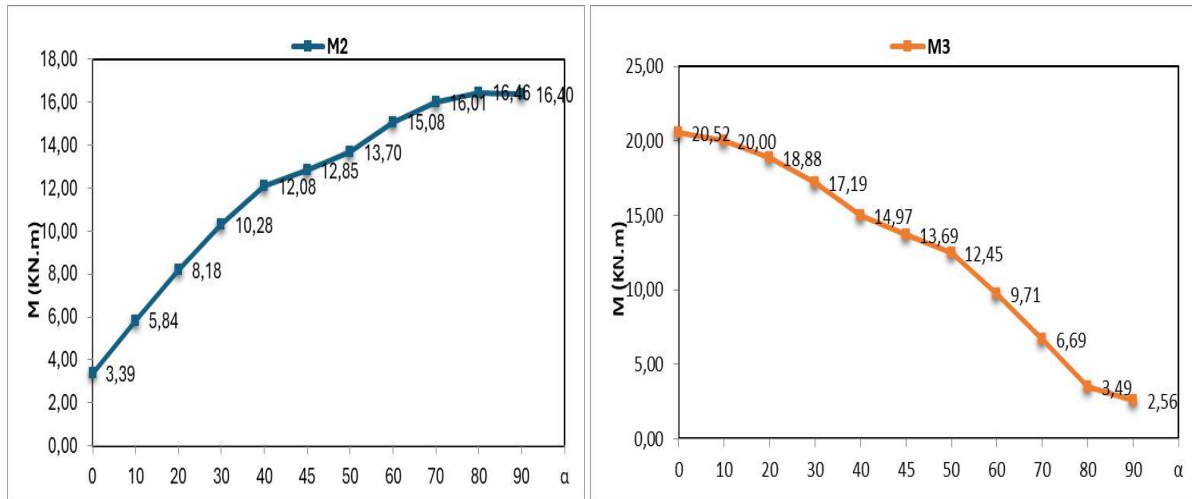
Figure 8. Bending moment in the most stressed column as a function the earthquake incidence angle.

Discussion

We not that the axial force in the most stressed column varies from N=86.41KN at angle α=0° to a maximum force of N=535.94 KN at angle α= 90°. The normal stress varies from σ =540.05 KN/m2 at an angle of incidence of 0° until reaching the maximum value σ =3349.62 KN/m2 at the angle 90°.

As for the shear force, the maximum value along axis 2.2 V2=7.60 KN is obtained at angle α=0° and decreases until reaching a value of V2=0.81 KN at angle α=90°. The shear force along axis 3.3 varies from V3=0.92 KN at angle α=0° and increases until reaching a maximum value of V3=4.08 KN at angle α=90°.

We note that the bending moment along axis 2.2 varies from M2=3.39 KN.m at an angle of incidence of 0° until reaching the maximum M2=16.40 KN.m at the angle 90°. the most unfavourable value of M3=20.52 KN.m is obtained at angle α=0° then it decreases until reaching a minimum value of M3=2.56 KN.m at angle α=90°.

Effect of the Earthquake Direction on the Stresses in Beams

The variation of bending moment and shear force as a function of the earthquake direction in the most stressed principal and secondary beams are shown in figures 9 and 10.
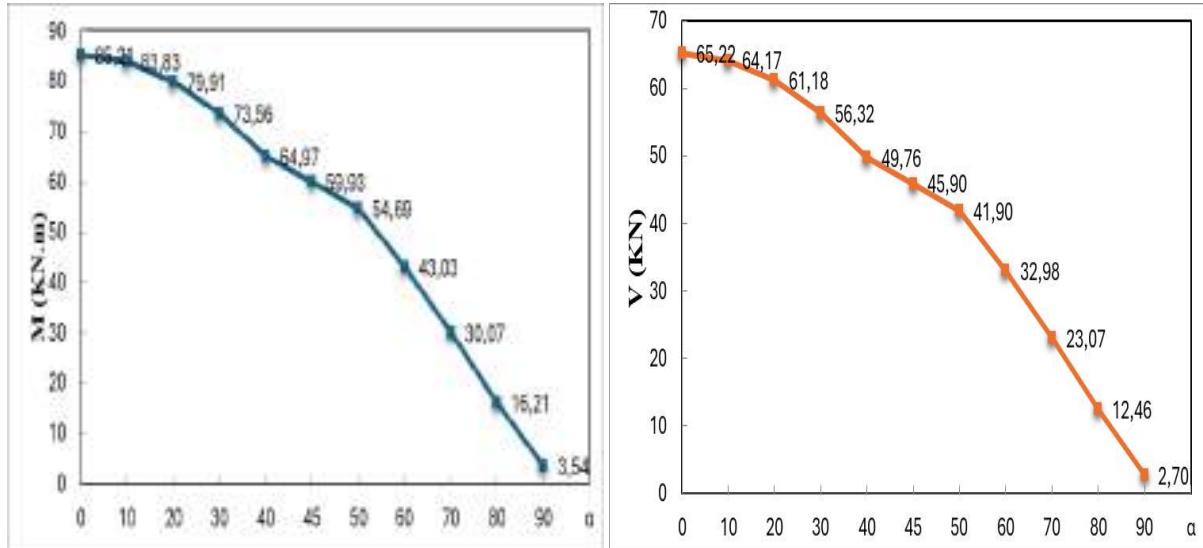
Figure 9. Stresses in the most stressed principal beam as a function of the earthquake incidence angle.
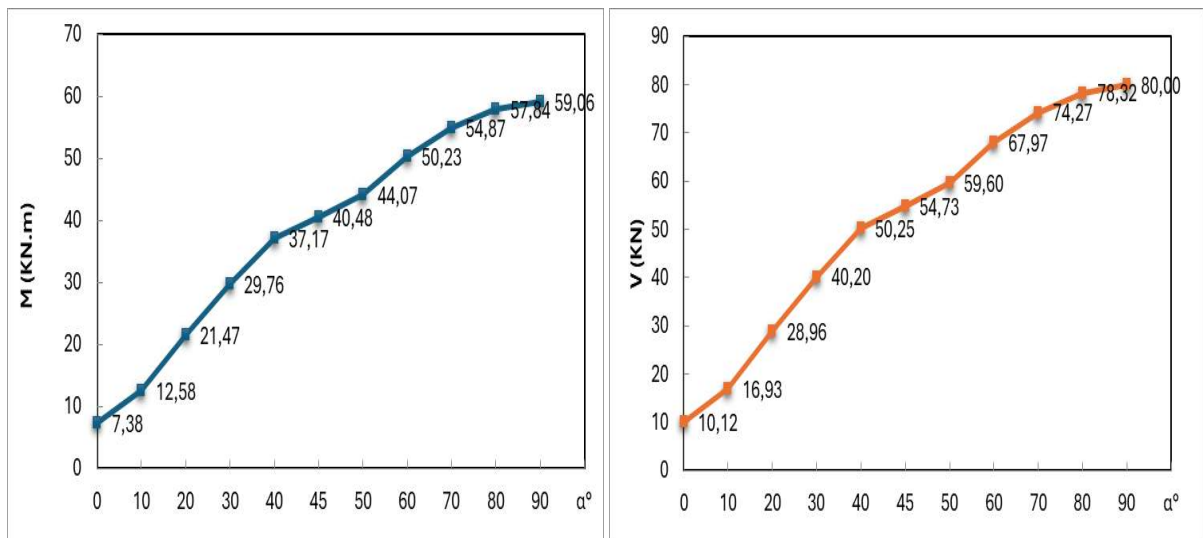
Figure 10. Stresses in the most stressed secondary beam as a function of the earthquake incidence angle.

For the principal beam, it can be seen that the maximum bending moment M=85.21 KN.m is obtained at angle α=0°, then it decreases until reaching a value M=3.54 KN.m at angle α=90°. As for the shear force, itself decreases from V=65.22 KN at angle α=0° to reach a minimum value of V=2.70 KN at angle α=90°.

For the secondary beam, we note that the most unfavorable earthquake direction is at angle α= 90° where we obtain a maximum moment M=59.06 KN.m and maximum shear force V = 79.99 KN. The minimum values of bending moments M=7.38 KN.m and shear force V = 10.12 KN are obtained at angle α= 0°.

Effect of the Earthquake Direction on the Stresses in Shear Walls

In reinforced concrete frame structures braced by shear walls, the walls take up no more than 20% of the stresses due to vertical loads and all the stresses due to horizontal loads [1]. To this end, we studied the effect of varying the earthquake direction on the stresses in shear walls. The results obtained for the most stressed wall are shown in Figure 11.
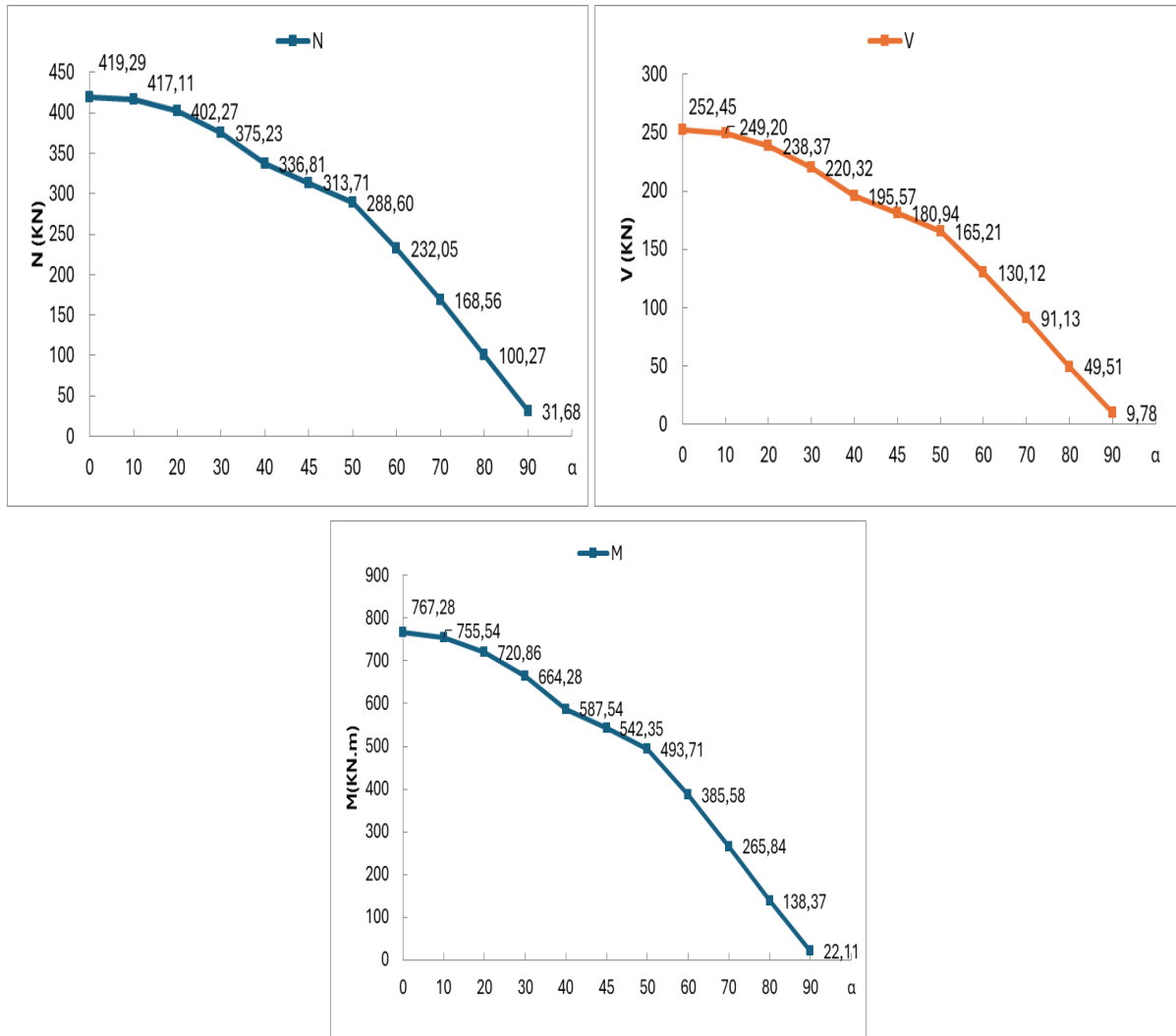
Figure 11. Axial force, shear force and bending moment in the shear wall as a function of the the earthquake incidence angle.

It can be seen that the axial force has a maximum value N=419.29 KN at angle α=0°, which decreases as the incidence angle varies, reaching a minimum value of N=31.68KN at angle α=90°.With regard to shear force along axis 2.2, seismic action develops the most unfavorable value V2= 252.45 KN at angle α=0°, which then decreases to reach a minimum value V2= 9.78 KN at angle α=90°. For the bending moment along axis 3.3, the most unfavorable value M=767.28 KN.m is obtained at angle α=0° which decreases until reaching a minimum

value M=22.11 KN.m at angle α=90°. The obtained results show that the maximum responses always coincide with one of the main axes of the structure (0° or 90°) and this can be due to the existence of shear walls which are arranged along these axes and which increase the rigidity of the structure in the 0° and 90° directions.In order to study the influence of the existence of shear walls on the dynamic response of the structure as a function of the variation in the earthquake direction, the same building without shear walls was used for the analysis, varying the incidence angle of the earthquake from 0° to 90° in steps of 10°.

Effect of the Earthquake Direction on the Seismic Reaction at the Base of the Structure without Shear Walls

The results of the dynamic analysis of the structure braced only by frame in terms of reaction at the base in both directions as a function of the earthquake incidence angle are shown in Figure 12.
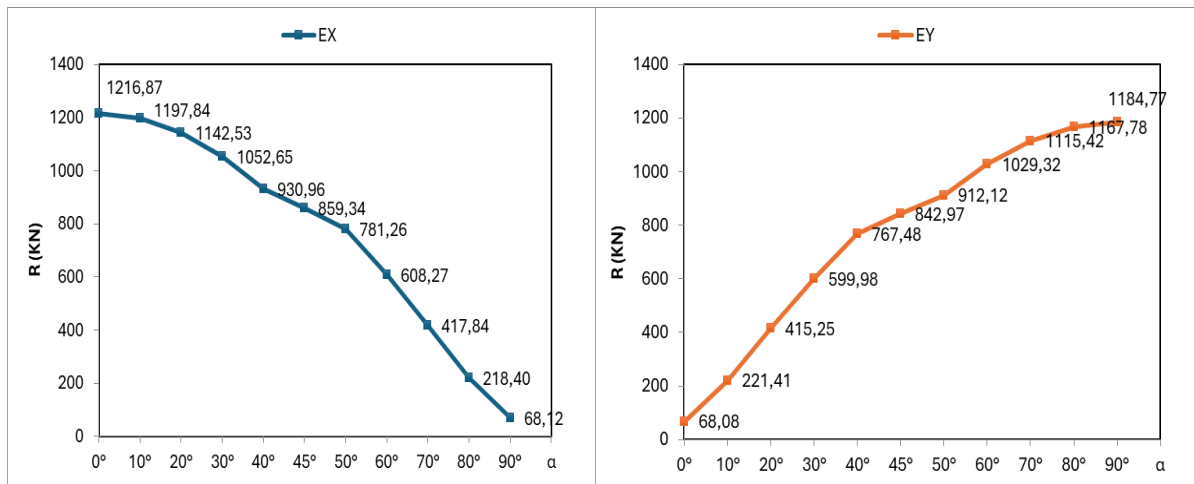
Figure 12. Seismic reaction at the base of the structure without shear walls as a function of earthquake direction.

The seismic reaction at the base in the x direction has a maximum value of Ex=1216.87 KN at angle α=0°, then decreases until it reaches a value of Ex= 68.12 KN at angle α=90°. On the other hand, the seismic reaction at the base in the y direction varies from Ey=68.08 KN at angle α=0° to reach a maximum value of Ey=1184,77 KN at α=90°.

Effect of the Earthquake Direction on the Horizontal Displacement of the Structure without Shear Walls

The results of the dynamic analysis of the structure without shear walls in terms of horizontal displacement in both directions as a function of the earthquake incidence angle are shown in Figure 13. It can be seen that the maximum displacement in the x direction Δx =14.12 mm is at angle α= 0°, then it decreases until reaching a value of Δx =13.26 mm at angle α=70°. On the other hand, the displacement following the direction y varies from Δy = 13.38 mm at the angle α=0° until reaching a maximum value Δy = 14.28mm at α=70°.
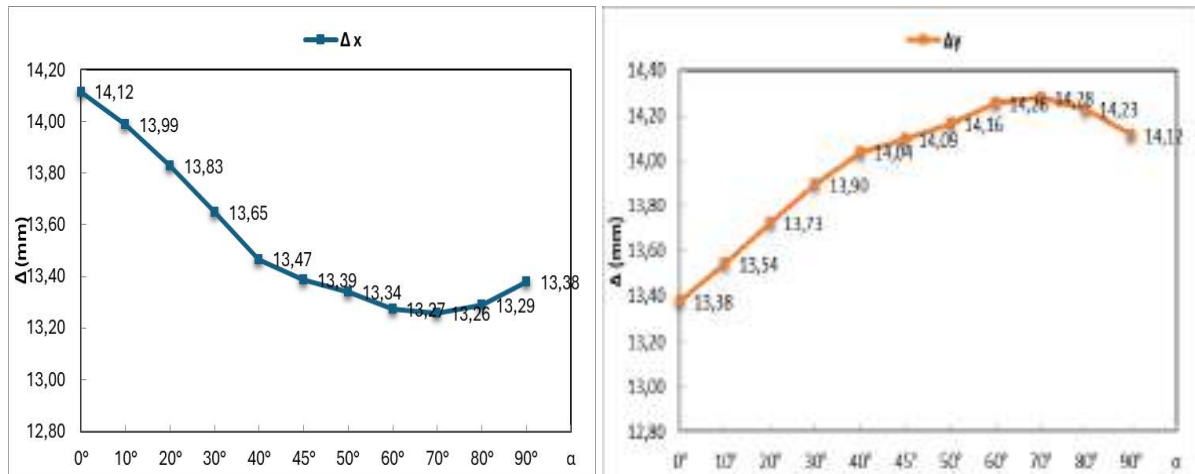
Figure 13. Horizontal displacement of the structure without shear walls as a function of earthquake direction.

Effect of the Earthquake Direction on the Stresses in the Columns of the Structure without Shear Walls

For structures braced only by frames, all horizontal and vertical loads are supported by columns and beams. The results obtained for the most stressed column are shown in next figures.
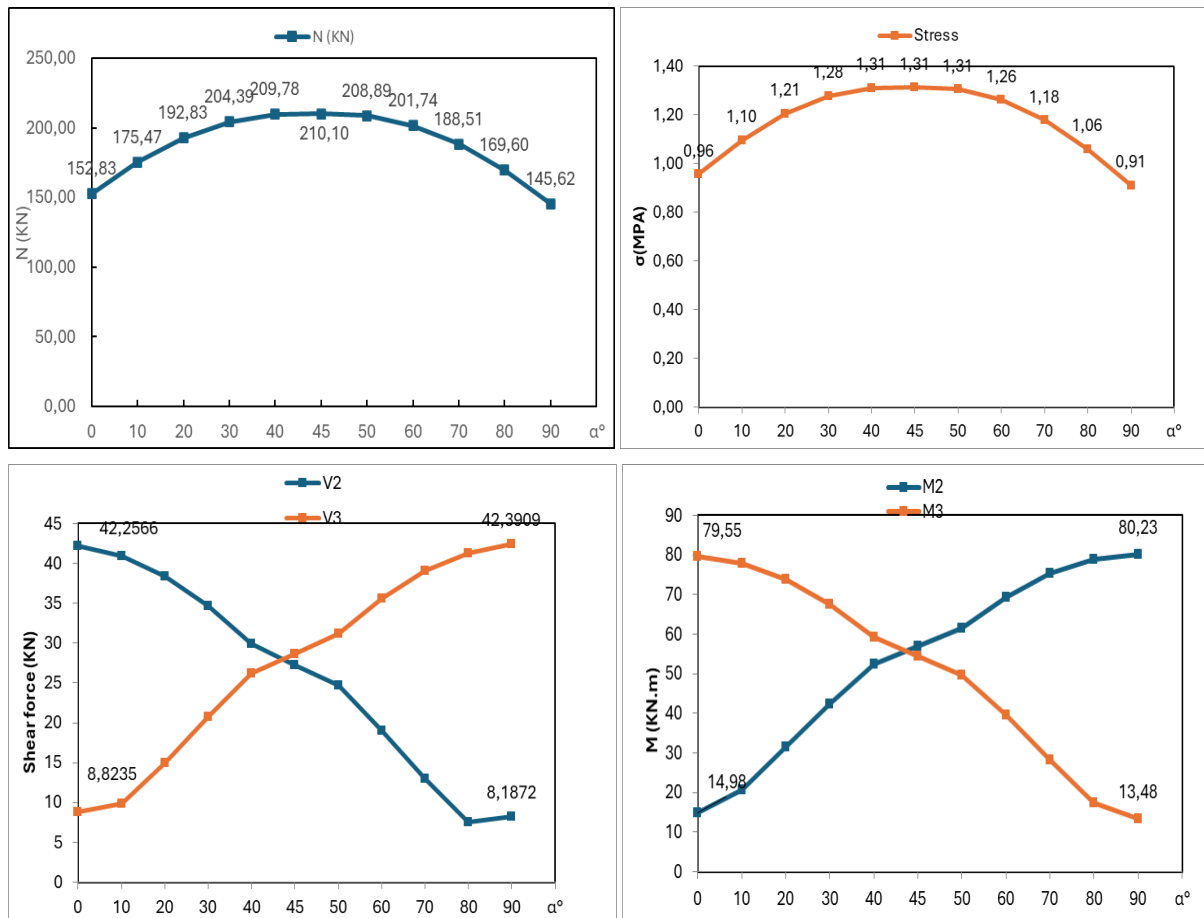
Figure 14. Axial force, normal stress, shear force and bending moment in the most stressed column as a function of earthquake direction (structure without shear walls).

It can be seen that the most unfavorable earthquake direction for axial force and normal stress occurs at an angle α= 45°, where the maximum axial force is N=210.10 KN and the maximum stress is σ = 1.31 MPa.

We note that the moment along axis 2.2 varies from M2=14.98 KN.m at an angle of incidence of 0° until reaching the maximum M2=80.23 KN.m at the angle 90°. the most unfavourable value of M3=79.55 KN.m is obtained at angle α=0° then it decreases until reaching a minimum value of M3=13.48 KN.m at angle α=90°.

As for the shear, the most unfavorable earthquake direction is 0° et 90° for V2 and V3 respectively.

Effect of the Earthquake Direction on the Stresses in the Beams of the Structure without Shear Walls

The variations of bending moments and shear forces in the most stressed principal and secondary beams as a function of the earthquake incidence angle are presented in the figures below.
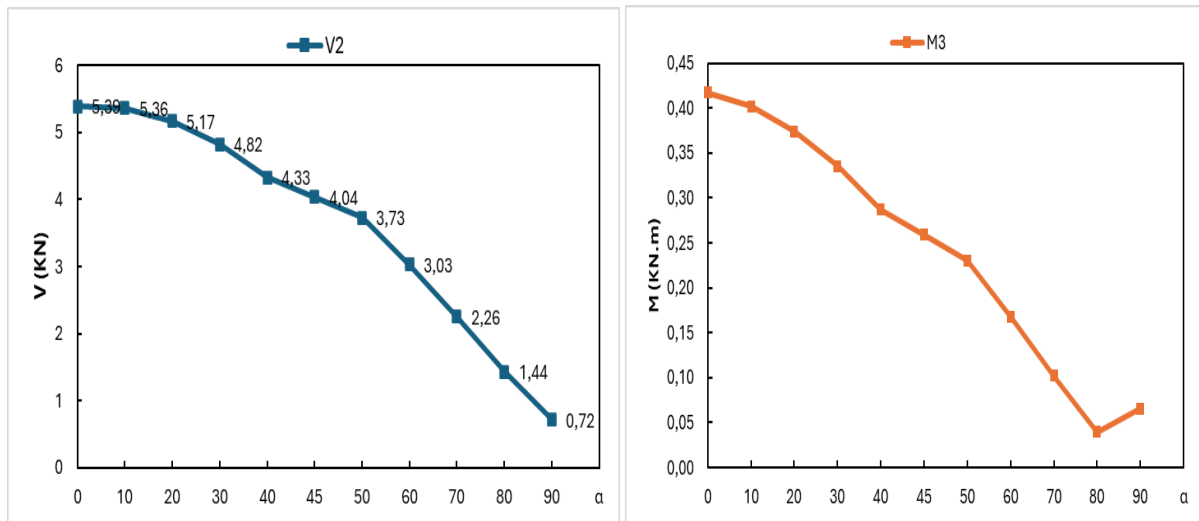
Figure 15. Shear force and bending moment in the most stressed principal beam as a function of earthquake direction (structure without shear walls).
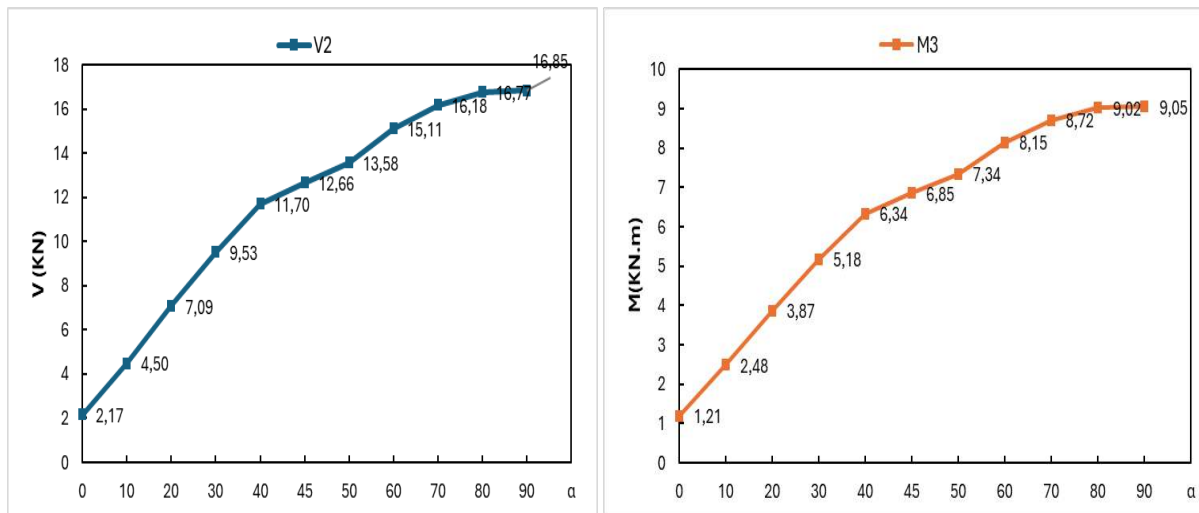
Figure 16. Shear force and bending moment in the most stressed secondary beam as a function of earthquake direction (structure without shear walls).

It can be seen that the most unfavorable earthquake direction for principal beams is at angle α=0°. The maximum values of shear force and bending moment are V2= 16.85 KN and M3=9.05 KN.m respectively.

For secondary beams, we note that the most unfavorable earthquake direction is at angle α=90°. The maximum values of shear force and bending moment are V2= 5.39 KN and M3=0.42 KN.m respectively.

Conclusion

This analysis shows that the seismic reactions at the base (Ex and Ey) for the two cases of structures (with and without shear walls) are maximum along one of the main directions of the building 0° or 90° and this is due to the fact that the load-bearing elements that resist to the seismic action (Shear walls and frames) are arranged along the two orthogonal directions X and Y.

For the horizontal displacement (Δx and Δy), the maximum values for the structure with shear walls correspond to 0° and 90°, while for the structure without shear walls they correspond to 0° and 70°. This is due to the effect of eccentricity, which decreases with the introduction of shear walls in the structure.

The bending moments and shear forces in columns, beams and shear walls are also extreme for α=0° a or α=90° for the two structural variants (with and without shear walls) depending arrangement elements. The most unfavorable earthquake direction of normal stress in columns is 90° for the structure with shear walls, since the shear walls support all the vertical forces each in its own direction, whereas the maximum normal stress coincides with the 45° angle in the structure without walls, since the columns support the vertical forces in both directions simultaneously and since the building and the columns are symmetrical about the 45° axis, interaction is greatest along this angle.

Finally, we deduce that the earthquake incidence angle has no influence on the dynamic response of irregular structures with shear walls arranged along the main axes (X and Y), so the most unfavorable direction of the earthquake coincides with the principal axes of the building but it has an influence on the dynamic response of irregular structures braced only by frames particularly the maximum horizontal displacement which corresponds to an angle of 70° and the maximum normal stress which corresponds to an angle of 45°.

On the basis of this limited study, we propose to carry out further studies or work on all structural typologies (V shape, L shape with inclined shear walls, without shear walls), taking into account the vertical component of the earthquake, and to see whether the seismic response of the structure can be different for angles of incidence of the earthquake different from the principal axes of the building.

References

Ministère de l'Habitat et de l'Urbanisme, Règles Parasismiques Algériennes RPA 99/Version 2003, Edition

CGS,2003.

M. Athanatopoulou, A. Tsourekas & G. Papamanolis, (2005) Variation of response with incident angle under two horizontal correlated seismic components, Earthquake Resistant Engineering Structures, vol 81.

C. Cantagallo, G. Camata & E. Spacone, The Effect of the Earthquake Incidence Angle on Seismic Demand of Reinforced Concrete Structures, 15th WCEE, Lisboa, 2012.

P. Gonzalèz, *Considering earthquake direction on seismic analysis*, Earthquake Engineering, Tenth world conference, Balkema, Rotterdam, 1992.

M. Sri Kanya, B D V Chandra Mohan Rao, Effect of earthquake incidence angle on seismic performance of RC buildings, IJRET: International Journal of Research in Engineering and Technology, Dec-2015. Volume : 04 Special Issues : 13, ICISE-2015

Anastassiadis, K., Directions sismiques défavorables et combinaisons défavorables des efforts. Annales de l'I.T.B.T.P. 512 (Mars/Avril), pp. 83-99, 1993.

Lopez, O.A., and Torres R., The critical angle of seismic incidence and the maximum structural response. Earthquake Eng. Struct. Dyn. 26, pp. 881-894, 1997.

G. A. L. Jiménez et D. Dias, « Dynamic Soil–Structure Interaction Effects in Buildings Founded on Vertical Reinforcement Elements », CivilEng, vol. 3, no 3, p. 573-593, juin 2022, doi: 10.3390/civileng3030034.

A. K. Chopra, *Dynamics of Structures: International Edition*. Pearson Education Limited, 2015.

B. K. Bohara, K. H. Ganaie, M.Tech in Structural Engineering Sharda University, P. Saha, et Department of Civil Engineering, Sharda University, India, « Effect of position of steel bracing in L-shape reinforced concrete buildings under lateral loading », Res. Eng. Struct. Mater., 2021, doi: 10.17515/resm2021.295st0519.

S. E. Abdel Raheem, M. M. M. Ahmed, M. M. Ahmed, et A. G. A. Abdel-Shafy, « Seismic performance of L-shaped multi-storey buildings with moment-resisting frames », *Proc. Inst. Civ. Eng. - Struct. Build.*, vol. 171, no 5, p. 395-408, mai 2018, doi: 10.1680/jstbu.16.00122.

Investigation on the Duration of Strong Earthquake Motion in Turkey

Issam Aouari

University Akli Mohand Oulhadj of Bouira, Algeria, https://orcid.org/0000-0001-6920-4608

Aicha Rouabeh

University Akli Mohand Oulhadj of Bouira, Algeria

Baizid Benahmed

University Ziane Achour of Djelfa, Algeria, https://orcid.org/0000-0003-4924-0059

Mehmet Palanci

Istanbul Arel University, Turkey, https://orcid.org/0000-0002-9223-5629

Abstract: The duration of earthquake shaking at a specific location is quantified by the ground motion duration (GMD) of the strong-motion segment in the earthquake signal. In structural design, extended earthquake durations amplify stresses on structures, increasing the risk of cumulative damage, material fatigue, and failure of energy dissipation systems. While numerous GMD prediction equations exist for many active tectonic regions, there is a lack of such predictive models for the Turquoise region. This study addresses that gap by proposing a new GMD predictive relationship for Turkey, using data from the Engineering Strong Motion Database (ESM). A total of 1 579 earthquake records from various tectonic regions within Turkey were selected, focusing on events with magnitudes greater than 4. The resulting GMD model incorporates the influence of target and soil type on GMD. Comparisons with existing models reveal that the duration of ground motions from subduction earthquakes tends to be shorter than those of Turkish earthquakes with similar magnitudes and distances.

Keywords: Significant Duration, Earthquake, ESM database, Ground motion, Turkey.

Introduction

In civil engineering, one of the important factors to reduce the damage caused by earthquakes is to properly estimate the parameters incorporated in the design of structures. The duration of strong ground motion plays a

crucial role in evaluating the seismic performance and resilience of structures during earthquakes. According to recent seismic records, the duration of the earthquake is longer in some areas, which leads to more structural damage.

The influence of ground motion duration on structures damage has been presented by a number of studies in the last decades (Hancock & Bommer, 2006). More recently, studies show the influence of ground motion duration on the dynamic deformation capacity of reinforced concrete frame structures (Bhanu et al., 2021). The seismic collapse capacity assessment of SDOF systems incorporating duration parameter shows the instability effects (Bravo-Haro et al., 2020) on the SDOF systems. Also, coupling ground motion duration and pulse effects in the collapse of ductile systems (Liapopoulou et al., 2020). In the other hand, the influence of ground motion duration on the dynamic deformation capacity of steel frame buildings is presented by Bhanu et al. (2019) (V. Bhanu et al., 2019).

The effects of ground motion duration on seismic performance have been widely studied in various structural contexts. For instance, research has shown that ground motion duration can significantly increase the collapse rate of light-frame wood houses, as explored in (Pan et al., 2018). Similarly, the dynamic deformation capacity of reinforced concrete frame structures is notably impacted by the duration of seismic events, as examined by Bhanu et al. (Bhanu et al., 2020). In the case of long-duration earthquakes, there is a significant impact on the fragility of reinforced concrete structures subjected to successive earthquake-tsunami sequences (Harati & van de Lindt, 2024). Predictive models for ground motion duration, particularly on soft soils, have been developed to better understand these effects, such as the empirical model given by Aouari et al. (Aouari et al., 2024).

Additionally, the importance of incorporating ground motion duration in building-portfolio loss assessments has been emphasized to improve risk analysis and mitigation strategies, as demonstrated in (Otárola et al., 2023). The development of prediction models for significant ground motion duration in specific regions, like India, has further contributed to these efforts, as seen in (Bhargav et al., 2022). Moreover, studies have investigated the influence of significant earthquake duration on the seismic performance of adjacent steel structures in near-source regions (Manesh et al., 2021), and the inclusion of strong motion duration in incremental-based seismic assessments has been proposed to enhance the accuracy of structural evaluations, as shown in (Mashayekhi et al., 2020). These studies collectively highlight the crucial role of ground motion duration in understanding and predicting structural vulnerabilities during seismic events.

More than 40 definitions (J. Bommer & Martinez-Pereira, 2000) are used in the literature to measure the duration of ground motion. However, earthquake duration starts at low shaking levels, is followed by strong movement and ends up with low shaking until the disappearance of all shaking movement. Therefore, many researchers tried to find out the significant time interval of this movement. The definitions in the literature identified the duration as a part of the earthquake record based on high acceleration amplitude, energy content, intensity or other seismic parameters that significantly affect the structural response. These definitions can be grouped into three main categories: Bracketed duration is estimated as the time between the first and last

instance when the accelerogram exceeds the fixed level of acceleration a_0. This definition is used by Bolt (Bolt, 1973), Bommer (J. J. Bommer et al., 2009), Lee (Lee & Green, 2012), Anbazhagan (Anbazhagan et al., 2017). Uniform duration: estimated for a given upper and lower boundary of acceleration level (a_0), it is calculated by the sum of the time intervals which the acceleration values are outside of this boundary. This definition was used by Rezaee and Saffari (Rezaee Manesh & Saffari, 2020). Significant duration: based on the energy accumulation of accelerograms represented by the square integral of the ground acceleration, velocity or displacement. This definition widely used by researchers (Bahrampouri et al., 2021; Bhargav et al., 2022; Lee, 2014; Trifunac & Brady, 1976).

A number of definitions for the ground motion duration measure have been proposed in the past. Approximately thirty definitions of earthquake duration formulas were evaluated by Bommer and Martines (1999) (J. J. Bommer & Martínez-Pereira, 1999). The most generally used are bracketed, uniform and significant durations, both absolute and relative duration. They need to be calculated with user-specified limits, which make direct comparison between the derived results often difficult.

On the other hand, various GMD prediction equations are provided for many regions (J. J. Bommer & Martinez-Pereira, 1996; Yaghmaei-Sabegh, 2018; Yaghmaei-Sabegh et al., 2022; Zhila & Neaz, 2014). As a result, the amount of ground motion in the international database is limited to the Turkish region. In other words, special attention is not paid, especially for Turky. For this reason and with the availability of records in the European strong motion database (ESM), a new empirical prediction equation for GMD is proposed in this study based on seismic indicators such as magnitude, distance, and site condition.

Strong Motion Database

Earthquake records data are essential for developing empirical prediction models of significant duration, as they provide the foundational information needed to understand how ground motion behaves during seismic events. By analyzing extensive earthquake records, engineers and researchers can identify patterns in how ground motion duration varies with factors like earthquake magnitude, distance from the epicenter, soil conditions, and fault mechanisms. This data allows the development of empirical models that can predict the likely duration of ground shaking for a given set of conditions. Such models are crucial for regions with limited historical seismic data, as they can help estimate the potential impact of future earthquakes.

Recent studies on GMD prediction have indicated differences in seismic parameter selection. In general, moment magnitude (M_w), epicentral distance (Epi), and the average shear wave velocity over the uppermost 30 m at the site ($V_{s,30}$) are used for the GMD prediction.

The collection data for the present study are provided from the Engineering Strong-Motion Database (ESM) (Luzi et al., 2020). This data source is openly accessible for strong-motion data from seismic events, primarily focused on Europe and the Mediterranean region, and managed by the European Mediterranean Seismological

Centre (EMSC) and various research institutions. The ESM database provides high-quality ground-motion recordings from earthquakes. The data includes detailed information such as ground-motion time histories (acceleration, velocity, displacement, location, magnitude, depth, site conditions, station location, and epicentral distance).

This study covered 348 earthquake events from several Tukey regions (for earthquake localization, see Figure 1). Note that the database processes and fixes the acceleration records that ESM provides. The total of 1369 accelerograms (two horizontal and one vertical) representing earthquake records were accumulated for the present study. The moment magnitudes (M_w) are in the range of 4.0 to 7.6. The epicentral distance (Epi) range was set at 0.5–428.6 km to represent different regions of Italy. The shear wave velocity uppermost 30 m soil layers ($V_{s,30}$) ranges from 176 to 1024 m/s.

Figure 1. Location of recorded station for study region (Luzi et al., 2020).

The database distribution for the different seismic parameters (M_w, Epi, $V_{s,30}$, and fault stilling, respectively) distributions is plotted in Figure 2. The figures show that the distribution of data is not equal in each bin. The average of the moment magnitude is around 4.84. For the epicentral distance the average is equal to 127.15 km, and the average shear wave in the first 30 meters is equal to 387.14 m/sec.

It is noted that the majority of the recordings are located on sites of class Z2 and Z3 according to the classification of the seismic code of Turkey with an interval of $V_{s,30}$ between 200 and 700 m/sec. The numbers of events in a tectonic setting can be presented as 480, 46, 480, and 391 events, which correspond to 34.36%, 3.3%, 34.36, and 27.98% of the database for normal, reverse, strike slip, and undefined fault stilling, respectively.
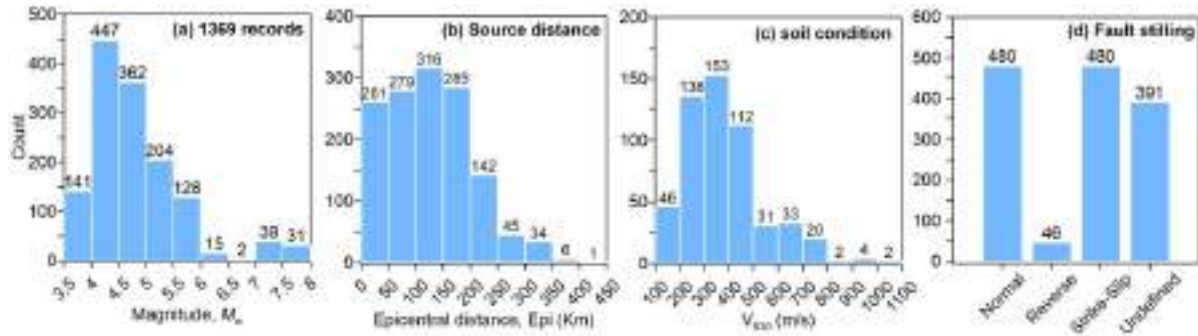
Figure 2. Histograms of data distribution: (a) magnitude, (b) epicentral distance, (c) soil conditions, and (d) fault stilling.
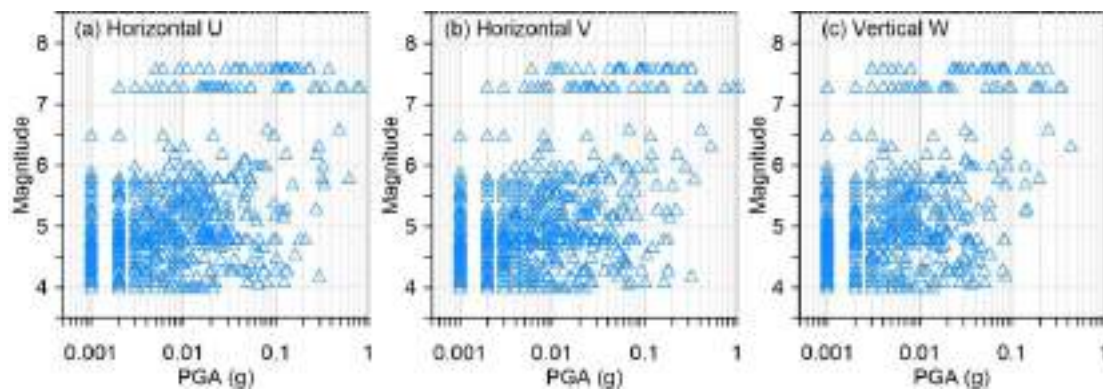
Figure 3. Scatter plots of moment magnitude distribution with PGA: (a)-(b) for horizontal U and V components, and (c) for vertical W component.

Table 1. Site soil classification according to Turkish Seismic Code

Site class	Description	Vs (m/s)
Z1	Firm to hard rocks (e.g., rock, very stiff clay, very dense sands)	> 700
Z2	Gravelly soils and soft to firm rocks (e.g., tuffs, agglomerate, stiff clays, dense sands)	400 - 700
Z3	Stiff clays and sandy soils (e.g., soft deposits, medium dense sand, stiff clay and silt)	200 - 400
Z4	Soft soils (e.g., high water table + alluvial deposits loose and soft clay and silt)	< 200
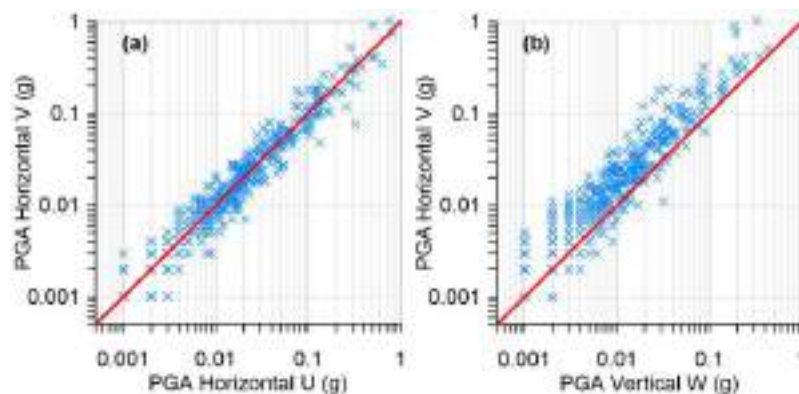
Figure 4. Scatter plots of moment magnitude distribution with: (a) horizontal U with V components and (b) Vertical W with Horizontal V. Red line is the linear adjustment

The Figure 3 shows the distribution of the acceleration peak for the three acceleration components, two horizontal (U,V) and vertical (W), respectively. the comparison between these values (Figure 4) shows a similarity of the acceleration peak values for the two horizontal components, on the other hand, the PGA of the vertical component is slightly small.

Significant Duration Estimation

The significant duration in seismology, often referred to as the duration between 5% and 95% of Arias intensity, corresponds to the period during which the most important seismic energy is released. This duration is calculated based on the cumulative intensity of Arias over time. The Arias intensity (I_A) is a measure used in seismology to quantify the energy contained in a seismic recording(Arias, 1970). It is defined as the integral of the acceleration squared over time. The formula to calculate the intensity of Arias is given by:

$$I_A = \frac{\pi}{2g} \int_0^T a(t)^2 \, dt \tag{1}$$

where: $a(t)$ is the acceleration as a function of time, T is the duration of the recording, and g is the acceleration due to gravity (9.81 m/s²).

After integrating the acceleration squared at each incremental time to obtain the curve of the cumulative intensity of Arias, we identify the time when the cumulative intensity reaches 5% and 95% of the total Arias intensity. The significant duration is the difference between the times associated with these intensity levels.

(a)   (b)
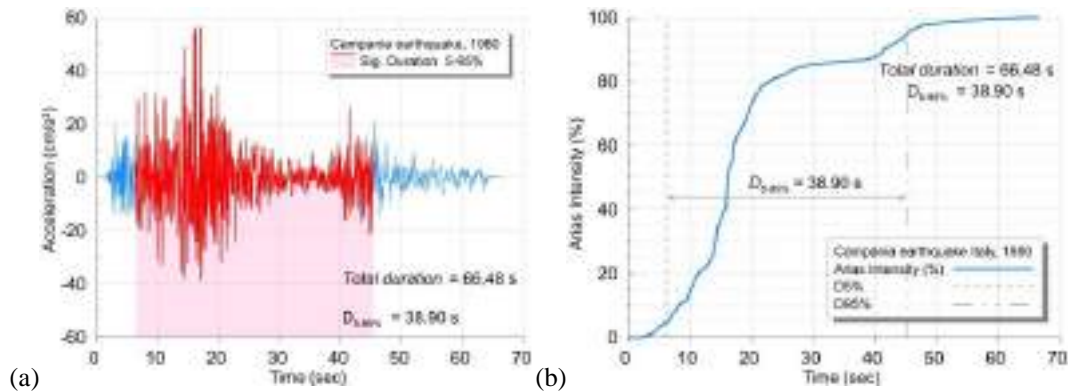
Figure 5. (a) Acceleration, (b) area intensity of the Campania Italy earthquake, 23/11/1980 (ESM ID: IT-1980-0012). M_w = 6.9, Epi = 23.4 km and $V_{s,30}$ = 1018 m/s. The red region represents the significant ground motion duration with a level of 5-95%.

Figure 5a and 5b presents the acceleration and the energy accumulation from 0 to 100% of the Arias intensity (I_A), respectively, of the Campania Italy earthquake. We can see that the 95% threshold of I_A covers the strong motion part of the full seismic signal. This methodology was adopted to calculate all significant durations ($D_{s5-95\%}$) for all selected data collected for the Turkey region.
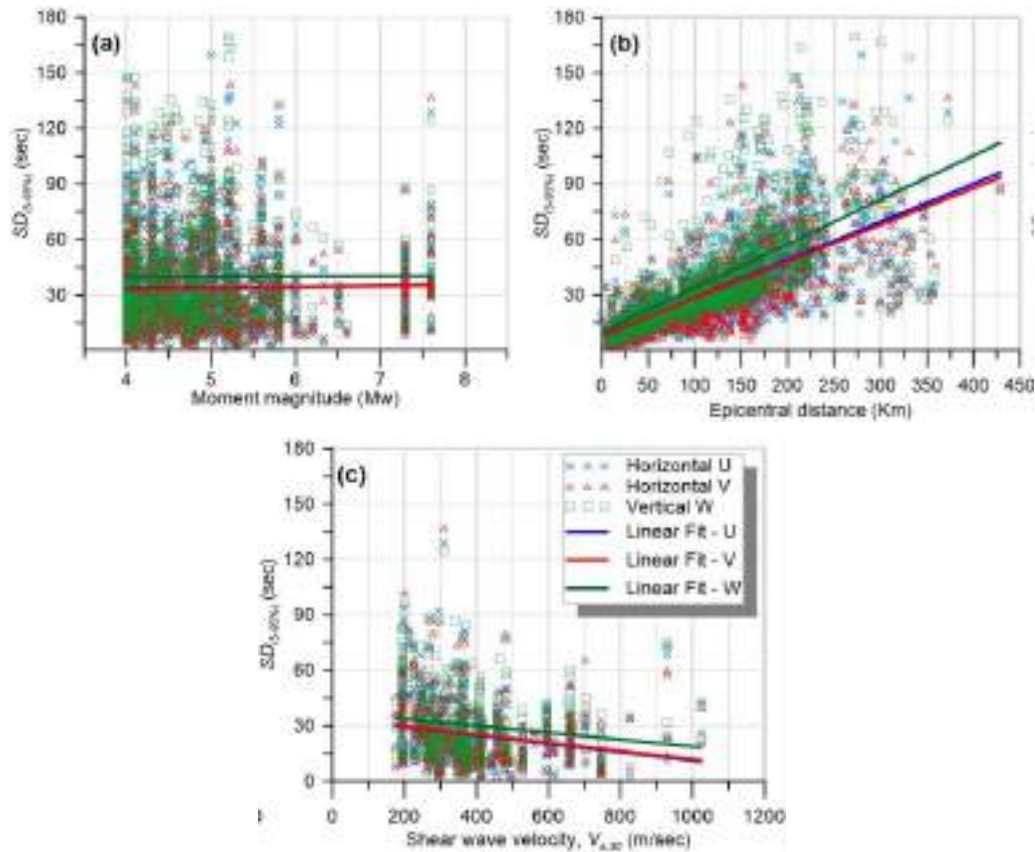
Figure 6. Distribution of $SD_{(5-95\%)}$ values for different ground motion parameters and events in the database: (a) moment magnitude, (b) epicentral distance, and (c) shear wave velocity.

Figure 6 illustrates the obtained results presented as a function of magnitude moment M_w (Figure 6a), epicentral distance, *Epi* (see Figure 6b), and shear wave velocity, $V_{s,30}$ (Figure 6c). It can be seen that the increasing correlation between $D_{s5-95\%}$ and *EpiD* was observed. However, there is a non-significant correlation identified between M_w and $V_{s,30}$.

Also, we note that the significant duration for the three components decreases with the increase in $V_{s,30}$ (hard and rock soil). We can observe from Figure 6a that the ground motion duration is not affected by earthquake magnitude (intensity of earthquake).

Proposed Model and Discussion

The functional form of the predictive relationship was obtained by using the model developed by (Snaebjörnsson & Sigbjornsson, 2008). In this study, nonlinear relationships were found to be the best functional form for site-to-source distance dependence, local site effects, and magnitude coupled with local site effects. The resulting model form of the predictive relationship for significant durations of horizontal and vertical ground motions proposed for the application in the Turkey region takes the following form:

$$\log_{10}(SD_{(5-95\%)}) = a_1 + a_2 M_w + a_3 \log_{10}\left(\sqrt{Epi^2 + a_4{}^2}\right) \pm \sigma \tag{2}$$

M_w and *Epi* are the moment magnitude and epicentral distance, respectively. The a_1, a_2, a_3, and a_4 are the regression coefficients. These parameters refer to distance (km) and duration (s). The last coefficient, σ, represents the residual error. The results of the regression coefficients are listed in Table 2 for the three predicted significant durations (SD_U, SD_V, and SD_W).

Table 2. Regression analysis of the proposed model.

	a_1	a_2	a_3	a_4	σ
SD_U	-0.4002	-0.005823	0.9054	35.97	0.1835
SD_V	-0.2966	-0.0006036	0.8461	32.08	0.1787
SD_W	-0.2834	0.001133	0.8752	30.49	0.1593

The results of the regression analysis are displayed in Figure 7 using linear scales and normalized duration. As can be seen, there is considerable scatter in the displayed results; however, the data fits within the error bounds of ± one standard deviation, and the model seems to display the general trend of the data fairly well. The observed scatter is linked to the fact that ground motions are affected by the three main factors, such as source, path, and local site effects.
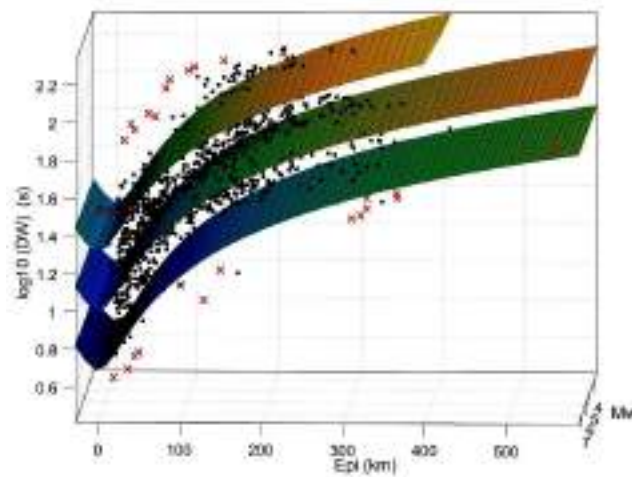
Figure 7. 3D presentation of GMD prediction model and its 95% confidence bounds for $SD_{(5-95\%)}$ of vertical component

The lower and upper surfaces indicated ± one standard error as obtained from the total dataset applied. Visually, the fit of the model to these data appears fare for longer distances (Epi > 200 km), even though the model tends

to give a longer duration for distances shorter than 200 km than the duration reflected by the data points.

The distributions of the predicted and real GMD values are presented in Figure 7 for all records component (U, V, W) of the study database. The results indicate that the trend can be accepted as linear and overlaps the y = x function for both N&R and SS events. It can also be assumed that the obtained correlation coefficients are quite acceptable. Therefore, it can be noted that there is a good correlation between the real and predicted values.
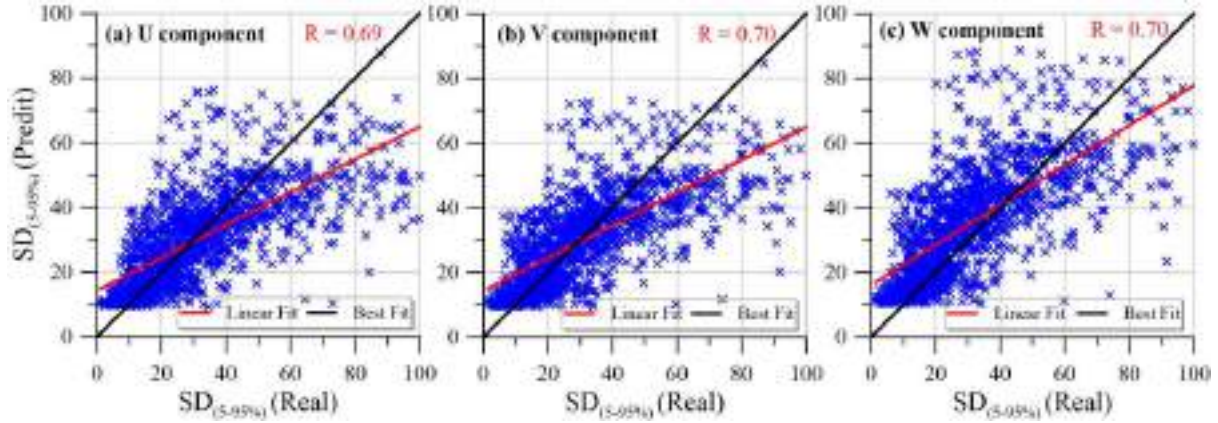
Figure 8. Scatter plot of predicted GMD using proposed model versus real values for the three components of the used database.

In Figure 8, we give the relative significant duration $SD_{(5-95\%)}$ as a function of epicentral distance (*Epi*) for different earthquake magnitude values: 5, 6, and 7, respectively. It is seen that the significant duration in the near fault area is not expected to exceed 10 s on average for all magnitude values. It can clearly see the difference between the values predicted by the proposed model for the region of Turkey with those given by the model of Snaebjörnsson and Sigbjornsson (2008). This difference is obvious for lower magnitude $M_w < 5$. On the other hand, this trend is reversed for large magnitudes >7, where the Snaebjörnsson and Sigbjornsson (2008) model underestimates the value of $SD_{(5-95\%)}$.
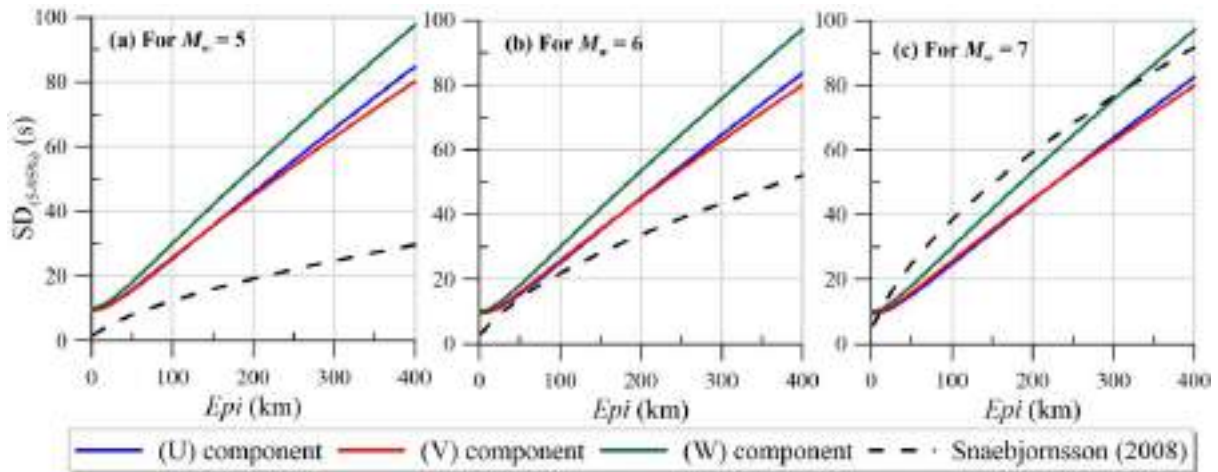
Figure 9. Comparison of proposed models with the model given by Snaebjörnsson and Sigbjornsson (2008) for

three magnitude values (5, 6, and 7, respectively)

Conclusion

In engineering design and the construction of structures resistant to earthquakes, one of the measures required to define the length of seismic loading is the duration of strong shaking. It also has a significant impact on the operational reliability of equipment during earthquakes. Duration is defined in a number of ways. In our assessment of duration, we have used the significant duration, which is the interval of time between two distinct fixed threshold values of the normalized Arias intensity being exceeded.

A model to predict the GMD is presented for the Turkish region using regression analysis based on an appropriate data set of moment magnitude and epicentral distance. The data set applied is taken from the ESM database and contains earthquakes from different active regions of Turkey.

The significant duration is going to increase with increasing magnitude and epicentral distance. The regression model appears to have an adequate correlation with the observed data set. According to the observed dataset versus predicted values, the regression model has an acceptable correlation.

References

Anbazhagan, P., Neaz Sheikh, M., Bajaj, K., Mariya Dayana, P. J., Madhura, H., & Reddy, G. R. (2017). Empirical models for the prediction of ground motion duration for intraplate earthquakes. *Journal of Seismology*, *21*(4), 1001–1021. https://doi.org/10.1007/s10950-017-9648-2

Aouari, I., Benahmed, B., Palanci, M., & Aidaoui, L. (2024). Empirical Model for the Prediction of Ground Motion Duration on Soft Soils. *Indian Geotechnical Journal*, *54*(2), 421–440. https://doi.org/10.1007/s40098-023-00778-5

Arias, A. (1970). A measure of earthquake intensity. In Hansen (Ed.), *Seismic Design for Nuclear Power Plants* (MIT Press, pp. 438–483).

Bahrampouri, M., Rodriguez-Marek, A., & Green, R. A. (2021). Ground motion prediction equations for significant duration using the KiK-net database. *Earthquake Spectra*, *37*(2), 903–920. https://doi.org/10.1177/8755293020970971

Bhanu, V., Chandramohan, R., & Sullivan, T. J. (2020). Investigating the influence of ground motion duration on the dynamic deformation capacity of reinforced concrete framed structures. *Pacific Congress on Earthquake Engineering*, 189.

Bhanu, V., Eeri, R. C. M., & Sullivan, T. J. (2021). Influence of ground motion duration on the dynamic deformation capacity of reinforced concrete frame structures. *Earthquake Spectra*, *37*(4), 2622–2637. https://doi.org/10.1177/87552930211033879

Bhargav, N. C., Challagulla, S. P., & Farsangi, E. N. (2022). Prediction Model for Significant Duration of

Strong Motion in India. *Journal of Applied Science and Engineering*, *26*(2), 279–292. https://doi.org/10.6180/jase.202302_26(2).0014

Bolt, B. A. (1973). Duration of strong ground motion. *5th World Conference on Earthquake Engineering*, *1*, 1304–1313.

Bommer, J. J., & Martinez-Pereira, A. (1996). The prediction of strong-motion duration for engineering design. *11th World Conference on Earthquake Engineering*, Paper No. 84.

Bommer, J. J., & Martínez-Pereira, A. (1999). THE EFFECTIVE DURATION OF EARTHQUAKE STRONG MOTION. *Journal of Earthquake Engineering*, *3*(2), 127–172. https://doi.org/10.1080/13632469909350343

Bommer, J. J., Stafford, P. J., & Alarcón, J. E. (2009). Empirical equations for the prediction of the significant, bracketed, and uniform duration of earthquake ground motion. *Bulletin of the Seismological Society of America*, *99*(6), 3217–3233. https://doi.org/10.1785/0120080298

Bommer, J., & Martinez-Pereira, A. (2000). Strong-motion parameters: definition, usefulness and predictability. *12th World Conference on Earthquake*, 1–8.

Bravo-Haro, M. A., Liapopoulou, M., & Elghazouli, A. Y. (2020). Seismic collapse capacity assessment of SDOF systems incorporating duration and instability effects. *Bulletin of Earthquake Engineering*, *18*(7), 3025–3056. https://doi.org/10.1007/s10518-020-00829-9

Hancock, J., & Bommer, J. J. (2006). A state-of-knowledge review of the influence of strong-motion duration on structural damage. *Earthquake Spectra*, *22*(3), 827–845. https://doi.org/10.1193/1.2220576

Harati, M., & van de Lindt, J. W. (2024). Impact of Long-Duration Earthquakes on Successive Earthquake-Tsunami Fragilities for Reinforced Concrete Frame Archetypes. *Journal of Structural Engineering*, *150*(10). https://doi.org/10.1061/JSENDH.STENG-13018

Lee, J. (2014). Directionality of strong ground motion durations. *NCEE 2014 - 10th U.S. National Conference on Earthquake Engineering: Frontiers of Earthquake Engineering*. https://doi.org/10.4231/D3445HC94

Lee, J., & Green, R. A. (2012). An empirical bracketed duration relation for stable continental regions of North America. *Earthquakes and Structures*, *3*(1), 1–15. https://doi.org/10.12989/eas.2012.3.1.001

Liapopoulou, M., Bravo-Haro, M. A., & Elghazouli, A. Y. (2020). The role of ground motion duration and pulse effects in the collapse of ductile systems. *Earthquake Engineering & Structural Dynamics*, *49*(11), 1051–1071. https://doi.org/10.1002/eqe.3278

Luzi, L., Lanzano, G., Felicetta, C., D'Amico, M. C., Russo, E., Sgobba, S., Pacor, F., & ORFEUS Working Group 5. (2020). *Engineering Strong Motion Database (ESM), version 2.0*. https://doi.org/10.13127/ESM.2

Manesh, M. R., Fattahi, S. H. F., & Saffari, H. (2021). Investigation of Earthquake Significant Duration on the Seismic Performance of Adjacent Steel Structures in Near-Source. *Journal of Rehabilitation in Civil Engineering*, *9*, 84–101. https://api.semanticscholar.org/CorpusID:231774290

Mashayekhi, M., Harati, M., Darzi, A., & Estekanchi, H. E. (2020). Incorporation of strong motion duration in incremental-based seismic assessments. *Engineering Structures*, *223*(November 2019), 111144. https://doi.org/10.1016/j.engstruct.2020.111144

Otárola, K., Gentile, R., Sousa, L., & Galasso, C. (2023). Accounting for earthquake-induced ground-motion duration in building-portfolio loss assessment. *Earthquake Engineering & Structural Dynamics*, *52*(4), 887–909. https://doi.org/10.1002/eqe.3791

Pan, Y., Ventura, C. E., & Liam Finn, W. D. (2018). Effects of Ground Motion Duration on the Seismic Performance and Collapse Rate of Light-Frame Wood Houses. *Journal of Structural Engineering*, *144*(8). https://doi.org/10.1061/(ASCE)ST.1943-541X.0002104

Rezaee Manesh, M., & Saffari, H. (2020). Empirical equations for the prediction of the bracketed and uniform duration of earthquake ground motion using the Iran database. *Soil Dynamics and Earthquake Engineering*, *137*(July), 106306. https://doi.org/10.1016/j.soildyn.2020.106306

Snaebjörnsson, J. T., & Sigbjornsson, R. (2008). The duration characteristics of earthquake ground motions. *14th World Conference on Earthquake Engineering*, 12–17.

Trifunac, M. D., & Brady, A. G. (1976). A study on the duration of strong earthquake ground motion. 14F, 1T, Refs. *International Journal of Rock Mechanics and Mining Sciences & Geomechanics Abstracts*, *13*(3), 28. https://doi.org/10.1016/0148-9062(76)90487-3

V. Bhanu, R. Chandramohan, & T.J. Sullivan. (2019). Influence of ground motion duration on the dynamic deformation capacity of steel frame buildings. *17th World Conference on Earthquake Engineering*, 2751.

Yaghmaei-Sabegh, S. (2018). Earthquake ground-motion duration estimation using general regression neural network. *Scientia Iranica*, *25*(5A), 2425–2439. https://doi.org/10.24200/sci.2017.4217

Yaghmaei-Sabegh, S., Karimzadeh, S., Ebrahimi, M., Ozsarac, V., & Du, W. (2022). A new region-specific empirical model for prediction of ground motion significant duration in Turkey. *Bulletin of Earthquake Engineering*, *20*(10), 4919–4936. https://doi.org/10.1007/s10518-022-01417-9

Zhila, S. Y., & Neaz, S. M. (2014). *A new model for the prediction of earthquake ground- motion duration in Iran*. 69–92. https://doi.org/10.1007/s11069-011-9990-6

Proposed Damping Reduction Factor of the Vertical Acceleration Response Spectrum for the Turkey Building Earthquake Code

Aicha Rouabeh

University Akli Mohand Oulhadj of Bouira, Algeria

Issam Aouari

University Akli Mohand Oulhadj of Bouira, Algeria, https://orcid.org/0000-0001-6920-4608

Baizid Benahmed

University Ziane Achour of Djelfa, Algeria, https://orcid.org/0000-0003-4924-0059

Mehmet Palanci

Istanbul Arel University, Turkey, https://orcid.org/0000-0002-9223-5629

Abstract: The damping reduction factor is used in structural design, especially in dynamic analysis, to account for how the level of damping in a structure effects its response to dynamic loads, such as earthquakes, wind, or vibrations. Hence, the role of DRF is to adjust the response of a structure based on its damping characteristics. Structures with higher damping can reduce the forces applied during dynamic events because they dissipate more energy. Most building codes, such as the International Building Code, Turkish Building Earthquake Code, or Eurocode, provide response spectra for a standard level of damping, often 5% of critical damping. If the structure has a different level of damping, the damping reduction factor is applied to adjust the seismic demands accordingly. The goal of this study is to provide DRF prediction models for the vertical response acceleration spectra specifically for the Turkey region. In general, building codes give the formula of the DRF for the horizontal acceleration spectra. Given the importance of the vertical seismic component, empirical models of the DRF for acceleration is proposed in this study for the Turkish region. A 70 real vertical accelerometric records from the strong motion database of the Pacific Earthquake Engineering Research Center is used. The vertical DRFs for damping ratio ζ = 1%, 3%, 7%, 10%, 15%, 20%, and 30% are computed using the 5%-damped vertical response spectra as targets. Furthermore, a comparison is made between the proposed DRF and the equations given in the literature and design codes.

Keywords: Duration, Earthquake, ESM database, Ground motion.

Introduction

For many years, the impact of an earthquake's vertical component on structural response was overlooked. Researchers, engineers, and even seismic codes viewed this component as less significant than the horizontal one. Recently, some researchers have highlighted the importance of the vertical component, showing that it can have a substantial effect on buildings and infrastructure. Vertical ground motions, for instance, may cause a significant increase in the axial forces on columns, the vertical displacement of beams (Abdollahiparsa et al., 2016), the vertical acceleration demands on the columns (Moschen et al., 2016) in frames, and several important seismic demand parameters in highway bridges (Gulerce et al., 2012; Gülerce & Abrahamson, 2010). In addition, vertical components recorded far from faults can cause significant damage to buildings, as detailed by numerous study (Kim et al., 2018; Mwafy et al., 2006; Mylonas, 1997). Thus, an appropriate vertical design spectrum at various damping levels is essential to evaluate the effects of vertical ground motions on structures and establish a suitable structural design. Considerable progress has been made in this area over recent decades. According to studies conducted by multiple researchers (Ambraseys & Douglas, 2003; Bozorgnia et al., 1995; Campbell & Bozorgnia, 2003; Li et al., 2007) on the characteristics of the vertical response spectra using recorded ground motions, the vertical-to-horizontal response spectral ratio may surpass 2/3 for short periods. Currently, the vertical response spectra provided by many seismic design codes (ASCE/SEI 41-13, 2014; Eurocode-8, 2004; GB, 2010; TBEC, 2018) and research publications (Bozorgnia & Campbell, 2004) mainly consider a 5% damping ratio.

A significant number of structures with damping ratios other than 5% are vulnerable to the effects of vertical ground motion. For example, long cantilevered trusses (Setareh, 2012), large-span spatial trusses (Ye et al., 2010), cold-formed steel floors (Davis et al., 2008), and composite floor decks (Varela & Battista, 2011) have damping ratios below 5%. Conversely, structures equipped with additional damping devices (Kitayama et al., 2017; Zhou et al., 2016)and certain types of steel structures with vertical hysteretic behavior (Xiang et al., 2017, 2018) may have damping ratios exceeding 5%.

To seismically design these structures to withstand vertical seismic actions at different damping ratios, the damping reduction factor (DRF) of the vertical response spectrum is required. In recent decades, Various researchers have analyzed vertical response spectra and damping reduction factors (DRF) using earthquake ground motion data. Studies by Mohraz (Mohraz, 1976), Trifunac and Lee (Trifunac & Lee, 1989), and Berge-Thierry (Berge-Thierry et al., 2003) examined vertical response spectra with different damping ratios across California and European events, while Malhotra (Malhotra, 2006) and Rezaeian (Rezaeian et al., 2014) developed DRF models based on parameters like damping, period, and magnitude. Site-related DRF models were proposed by Liu et al. (Liu et al., 2021), Zhang, and Chao (Zhang & Zhao, 2020), who found magnitude and distance significantly influence DRFs, while Elhout (Elhout, 2022) noted earthquake magnitude as impactful but minimal effects from soil type and distance. Çelik and Merter (Çelik & Merter, 2023) studied DRF variations with damping ratios and ground motion periods, showing stability at longer periods, and

Sriwastav and Basu recommended simplified period-based DRF calculations with minor influence from magnitude and soil type.

According to previous literature, existing studies have relied on local earthquakes, limited databases, or specific response spectra to calculate DRFs. As a result, there is still a need to develop a DRF model for the vertical component specific to the Turkish region.

Strong Motion Database

The primary earthquakes analyzed in this study were obtained from the PEER strong motion database and include the following events: Caldiran (1976), Izmir (1977), Dursunbey (1979), Erzincan (1992), Dinar (1995), Duzce (1999), and Kocaeli (1999). A total of 70 vertical records was selected, encompassing sites with diverse soil conditions. According to the Turkish Building Earthquake Code 2018 (TBEK 2018), site classifications are based on soil properties, using parameters such as shear wave velocity (Vs30), standard penetration test values (SPT-N), and undrained shear strength (cu). The Vs30 parameter represents the average shear wave velocity in the upper 30 meters of soil. For sites with mixed soil layers, weighted average properties are applied. Table 1 provides a summary of the site classifications outlined in the Turkish Building Earthquake Code.

Table 1. Site Classes according to TBEK (2018).

Site	Soil type	Vs30 range (m/s)	Characteristic
Z1	Rock Site	> 1500 m/s	Generally hard rock formations
Z2	Firm Rock Site	$760 < V_{s30} \leq 1500$	Corresponds to moderately strong rock formations
Z3	Very Dense or Stiff Soil	$360 < V_{s30} \leq 760$	Dense sands, gravels, and stiff clays.
Z4	Soft Soil	$180 < V_{s30} \leq 360$	Medium-dense sands and gravels, medium-stiff clays.
Z5	Very Soft Soil	$V_{s30} \leq 180$	Loose sands, gravels, and very soft clays

Figure 1a illustrates that the event magnitudes range from 6.0–6.5 to 7.0–7.5, highlighting the occurrence of the strongest earthquakes in the study region. Most events (39 records) were recorded at distances of less than 100 km, indicating that the earthquake sources are located very close to the surface (see Figure 1b). Additionally, the majority of the data (65 records) were recorded at sites classified as Z3 and Z4 (see Figure 1c-d).
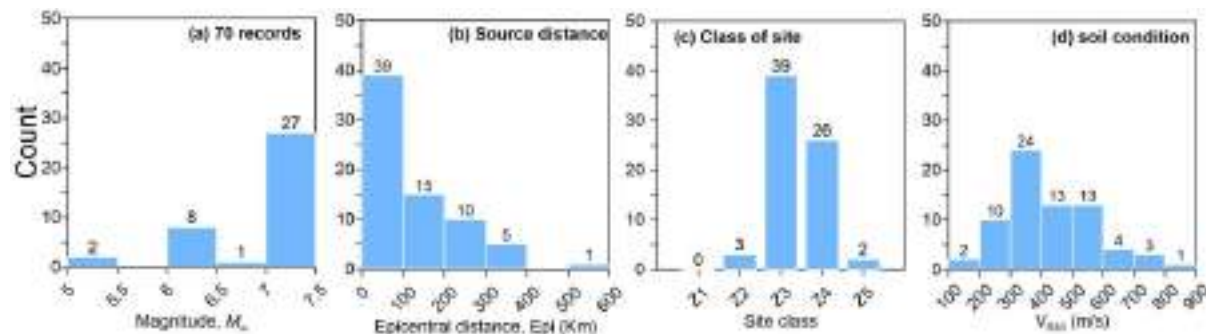
Figure 1. (a)-(d) database distribution according to selected parameters; Magnitude, M_w, epicentral distance, Epi, site classes, and shear wave velocity upper 30 m, V_{s30})

The scatter plots in Figure 2 depict the distribution of moment magnitude as a function of epicentral distance, shear wave velocity, and peak ground acceleration (PGA). It is observed that the PGA reaches a maximum value of 0.35g, with most values clustering around 0.1g and 0.2g.
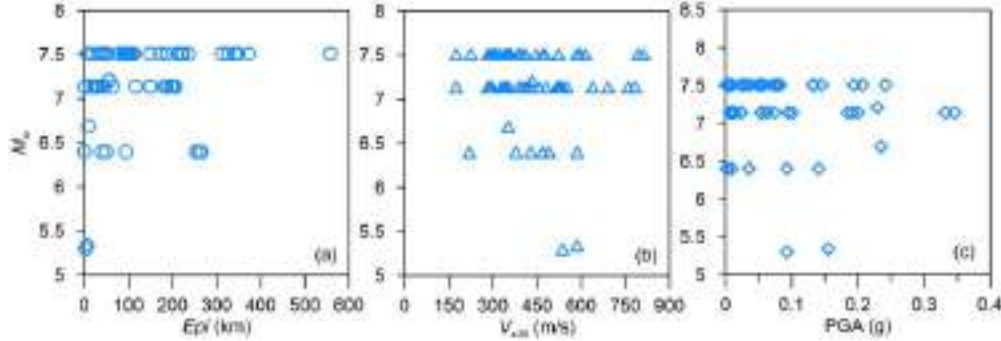
Figure 2. distribution of moment magnitude M_w versus; (a) epicentral distance Epi, (b) shear wave velocity V_{s30}, and (c) peak ground acceleration PGA.

Vertical Response Spectra Computation

The spectra are determined by time-integrating the equation of motion for a series of single-degree-of-freedom systems. From this, the peak acceleration response values are obtained and plotted against the period, resulting in what is known as the response spectra. Detailed explanations of these procedures can be found in structural dynamics textbooks, such as Clough and Penzien (Clough R.W. & Penzien J., 1994) and Chopra (Chopra, 2012). The response spectra are plotted for a range of periods (0 – 5.0s) and damping ratios (ξ = 1%, 3%, 5%, and 7%), as shown in the plots of Figure 3.
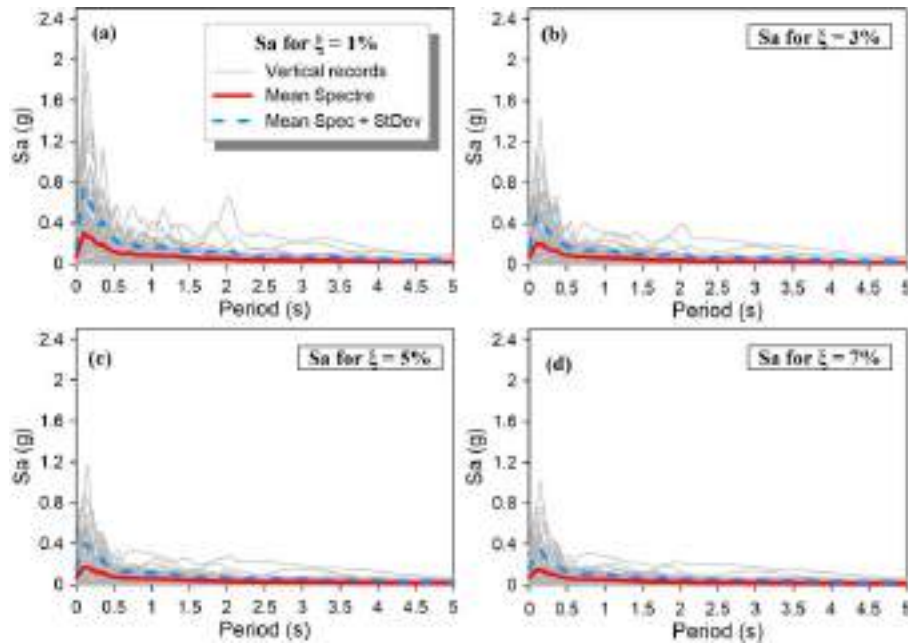
Figure 3. (a–d) Spectral acceleration spectra of selected earthquakes calculated for different damping ratios ξ = 1, ξ = 3, ξ = 5, ξ = 7, respectively.

The spectra are determined by time-integrating the equation of motion for a series of single-degree-of-freedom systems. From this, the peak acceleration response values are obtained and plotted against the period, producing what is known as the response spectra. Detailed explanations of these procedures can be found in structural dynamics textbooks, such as Clough and Penzien (1994) and (Chopra, 2012). The response spectra is plotted for a range of periods (0 – 5.0s) and damping ratios (ξ = 1%, 3%, 5, and 7%) us representing in plots of figure 3.

The same procudure is applied to plot the mean response spectra for all dumping ration. The results are shon in curves of figure 4.
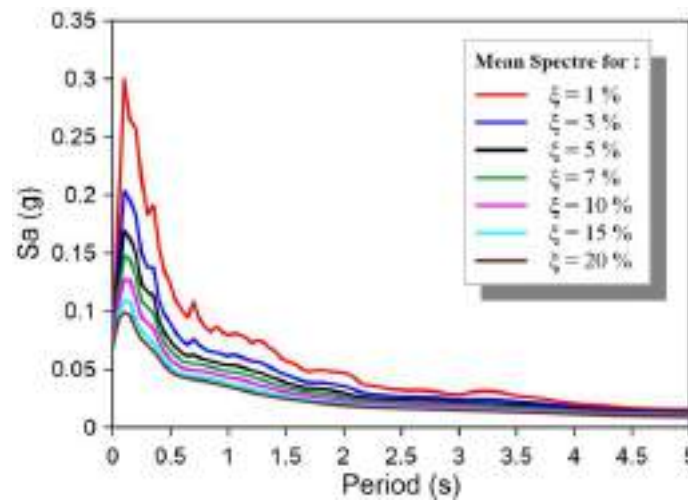
Figure 4. Mean acceleration spectra calculated for all damping ratios (ξ = 1, 3, 5, 7, 10, 15, 20).

Damping reduction factors (DRFs) are essential in seismic design and structural evaluation. They are used to adjust the elastic response spectra with a 5% damping ratio to account for other damping levels, whether higher or lower (Baizid & Cardone, 2021). This factor is defined by the following relationship (Hatzigeorgiou, 2010):

$$DRF_a = \frac{Sa(\xi,T)}{Sa(5\%,T)} \tag{1}$$

Here, $Sa(\xi, T)$ represents the spectral accelerations for a given damping level. The notation Sa (5%, T) refers to the spectral accelerations corresponding to a 5% damping ratio.

The first research to identify DRFs was carried out by Newmark and Hall (Newmark & Hall, 1972), and this groundbreaking work highlighted that these factors rely upon the natural vibration period (Dávalos et al., 2022). This study inspired scientists in this field, and afterward, DRFs were adopted in many seismic design codes. Table 1 shows the different DRF relationships for different design codes. In Figure 1, the code-based DRF relations determined using the equations given in Table 1 are presented based on different viscous damping ratios. The figure shows significant differences among the code-based period-independent DRF definitions. The lowest values for the DRFs have been suggested in the Japanese seismic design code. The great differences between the design codes imply the importance of studies on DRFs.

Table 1. Expressions for period-independent DRFs based on displacement response spectra defined in various design codes.

	Equation	Code name	Reference
(1)	$DRF = \sqrt{10/(5+\xi)}$	Eurocode 8 (2004)	(Eurocode-8, 2004)
(2)	$DRF = 150/(100+10\xi)$	Japan JPN (2001)	(Japanese code (JPN), 2001)
(3)	$DRF = 1 + (5-\xi)/(6+1.4\xi)$	China (2010)	(GB, 2010)
(4)	$DRF = (5.6 - \ln(\xi))/4$	ASCE/SEI (2014)	(ASCE/SEI 41-13, 2014)
(5)	$DRF = (5/\xi)^{0.3}$	AASHTO (2010)	(AASHTO, 2010)
(6)	$DRF = \sqrt{7/(2+\xi)}$	Algerian RPA99 (2003)	(RPA99, 2003)
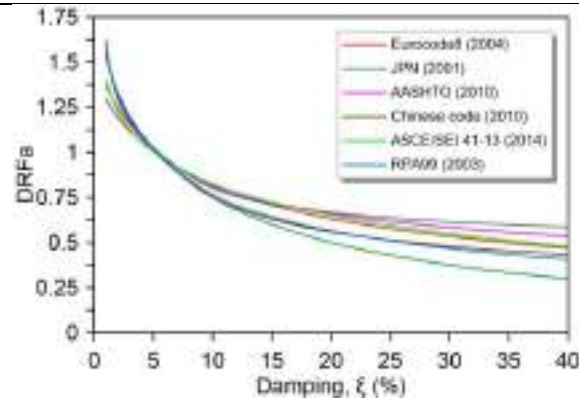
Figure 5. Damping reduction factors (DRFs) according to formulas proposed in seismic design codes.
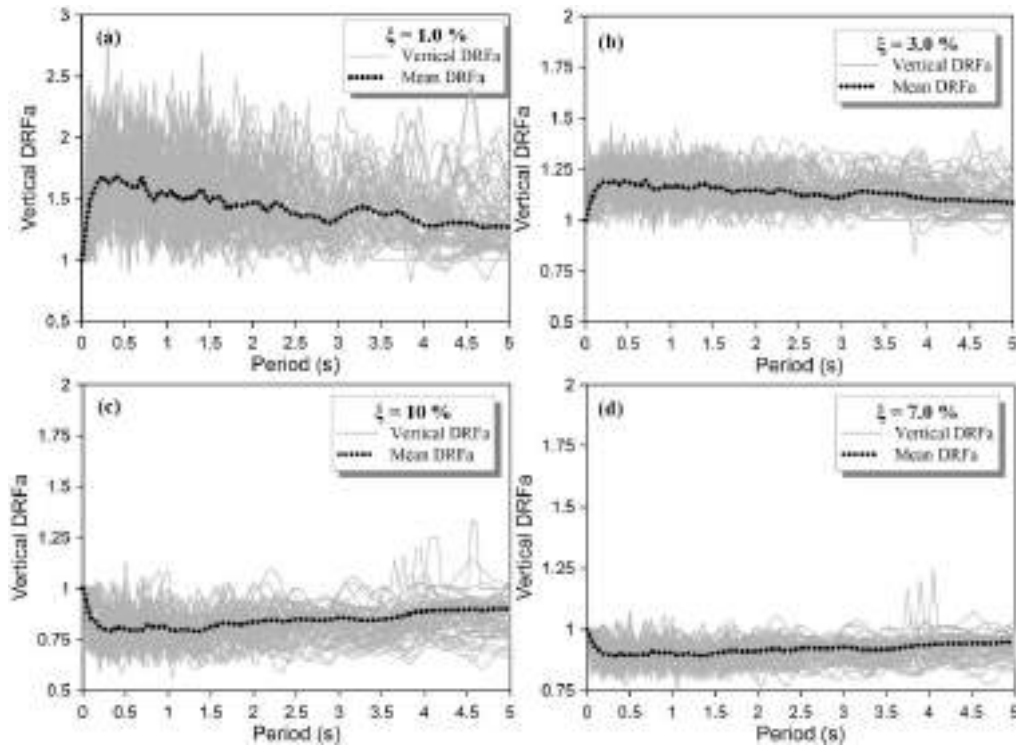
Figure 6. DRFa for all records computed for damping values: (a) 1%, (b) 3%, (c) 10%, and (d) 7%. The black dashed line represents the mean DRFa.

Figure 7 compares the differences between the DRF curves at various damping ratios. The figure shows that DRFa values are generally greater than 1 for damping ratios of 1% and 3% across the entire period range (1.0 s – 5.0 s), while they are less than 1 for damping ratios greater than 5% (7%, 10%, 15%, and 20%). Additionally, it is observed that DRFa values exhibit less sensitivity for longer periods greater than 2.0 s. Beyond these periods, the differences become more pronounced at higher damping ratios and for shorter periods.
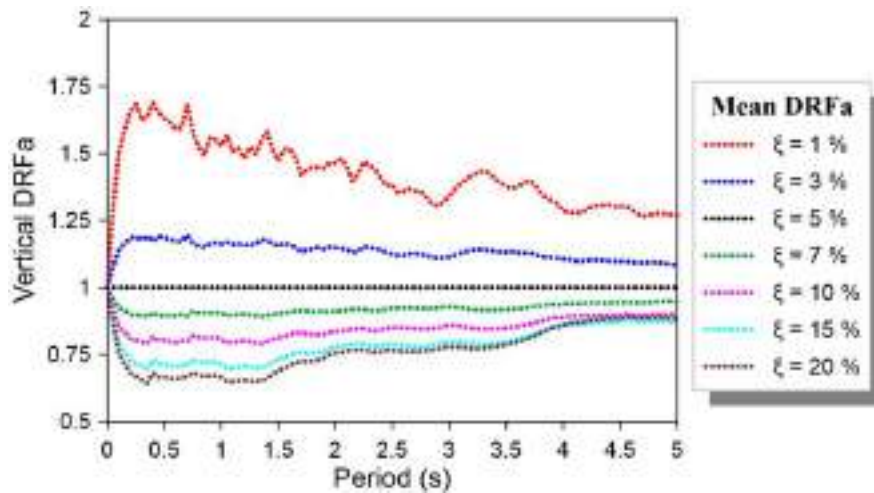
Figure 7. Variation of the median DRFa for different damping ratios (ξ = 1%, 3%, %5, 7%, 10%, 15%, and 20%).

Proposed Model

As shown in Figure 7, for short periods of less than 0.5 s, the DRFa values are highly dependent on the period T, reaching a value of 1 at a zero period. On the other hand, the DRFa trend becomes less sensitive to changes in period values for periods ranging from 0.5 s to 5.0 s. When compared to the DRFa curve for damping ratios greater than 5%, the same functional form can be applied to develop the DRFa relationship for Turkey. Based on these findings, it can be concluded that different mathematical equations should be proposed to provide the most accurate predictions for DRFa values across various damping ratios.

In the next step, new period-dependent equations are developed to describe the average damping reduction factors for the selected earthquakes. The matching of predicted and computed DRF values serves as the evaluation criterion, and the correlation between them is assessed. Additionally, the coefficient of determination (R^2), Sum of Squares for Error (SSE), and Root Mean Square Error (RMSE) are used to assess the effectiveness of the proposed equations. Nonlinear regression is employed to analyze the complex relationships between the dependent and independent variables, with the Levenberg–Marquardt algorithm being applied as the standard method for solving nonlinear least-squares problems to achieve the best fit.

After several attempts, Equations (2) are proposed to approximate the DRFa. It is observed that the resulting equations show a strong correlation with the real DRFa values.

$$DRF_a = \begin{cases} 1, & \text{for } T = 0 \\ a_1 \times T^{a_2} + a_3, & \text{for } 0 < T \leq 0.5s \\ a_4 \times e^{a_5 T}, & \text{for } 0.5s < T \leq 5s \end{cases} \qquad (2)$$

Where: T is the period and $a_1, a_2, a_3, a_4,$ and a_5 are the regression coefficient.

Table 2 presents the values of the fitting coefficients used to predict the mean DRFs. The R^2 value, indicating the correlation between the calculated and predicted mean DRFs across the database, is approximately 0.9. The RMSE is generally below 0.01, reaching a maximum of 0.03, which reflects both strong correlation and minimal error. Additionally, the SSE values are included in the tables for each model comparison. Based on calculations, the SSE varies between approximately 0.0002–0.00 for $T \leq 0.5$ s and 0.002–0.13 for $T > 0.5$ s. This slight increase in SSE for $T \geq 0.5$ s may be attributed to the simplified equation used. However, the R^2 remains above 0.95, and the RMSE is consistently low, around 0.01, indicating the model's accuracy. These statistical outcomes suggest that the proposed DRF models effectively capture the key characteristics of DRFs as a function of both vibration period and damping ratio.

Table 2. Coefficients and quality regression of the mean DRFa constructed from acceleration spectra using equations 2.

		1%	3%	7%	10%	15%	20%
For T ≤ 0.5 s	a_1	-0.00604	-0.002507	0.001961	0.003411	0.00633	0.008139
	a_2	-1.39200	-1.28600	-1.18200	-1.21900	-1.14600	-1.11800
	a_3	1.67900	1.19400	0.89040	0.790500	0.69340	0.63810
	SSE	0.006739	0.0004808	0.0002448	0.0007613	0.001296	0.001584
	R^2	0.94690	0.95680	0.93290	0.94480	0.95610	0.96120
	RMSE	0.03103	0.008287	0.005914	0.01043	0.01361	0.01504
For T > 0.50 s	a_4	1.61400	1.18400	0.88890	0.78170	0.67990	0.62380
	a_5	-0.05045	-0.01645	0.01259	0.02931	0.05344	0.07505
	SSE	0.1300	0.008742	0.002569	0.008195	0.01921	0.03108
	R^2	0.85360	0.85750	0.88810	0.91970	0.93370	0.94250
	RMSE	0.03843	0.009967	0.005403	0.00965	0.01478	0.01879

Comparison of the proposed model with existing literature

Numerous DRF prediction models have been proposed in the literature, as discussed in the introduction. However, the accuracy of these models depends on several factors, including the chosen database, limitations in the analysis models, and variations in the vertical spectra used. To demonstrate the accuracy of the proposed model, comparisons are made with several published models. The vertical DRF models proposed in this study specifically target acceleration.

The predictive models listed in Table 3, developed for different vertical response spectra, are used for

comparison.

Table 3. The considered DRFs proposed in the literature for comparison.

Equation	Reference
(1) $\text{DRFa} = \begin{cases} 1, & T \leq 0.02\ s \\ c_1 + c_2 e^{c_3 T}, & 0.02s < T \leq 0.2\ s \\ c_1 + c_4 T, & T > 0.2\ s \end{cases}$	(R. K. Sriwastav & D. Basu, 2023)
(2) $\text{DRFa}(T, \xi) = 0.342 \xi^{-0.354} + (0.0186 + 0.368\xi - \dfrac{1}{10.644\xi^2})T$	(Lin & Chang, 2004)
(3) $\text{DRFa}(T, \xi) = \begin{cases} 1 - \dfrac{aT^b}{(T+1)^c}, & \xi < 0.05 \\ (d + eT), & \xi > 0.05 \end{cases}$	(Piscal A & López-Almansa, 2018)
(4) $\text{DRFa} = a_0 + a_1 \cos(T \times w) + b_1 \sin(T \times w) + a_2 \cos(2 \times T \times w) + b_2 \sin(2 \times T \times w)$	(Rouabeh et al., 2024)
(5) $\text{DRFa} = \begin{cases} a_1 \log(T)^2 + b_1 \log(T) + c_1 & 0.03 \leq T \leq 0.12\ s \\ a_2 + b_2 \cos(f_2 \log(T)) + c_2 \sin(f_2 \log(T)) & 0.12 \leq T \leq 10.0\ s \\ + d_2 \cos(2f_2 \log(T)) + e_2 \sin(2f_2 \log(T)) \end{cases}$	(Xiang & Huang, 2019)
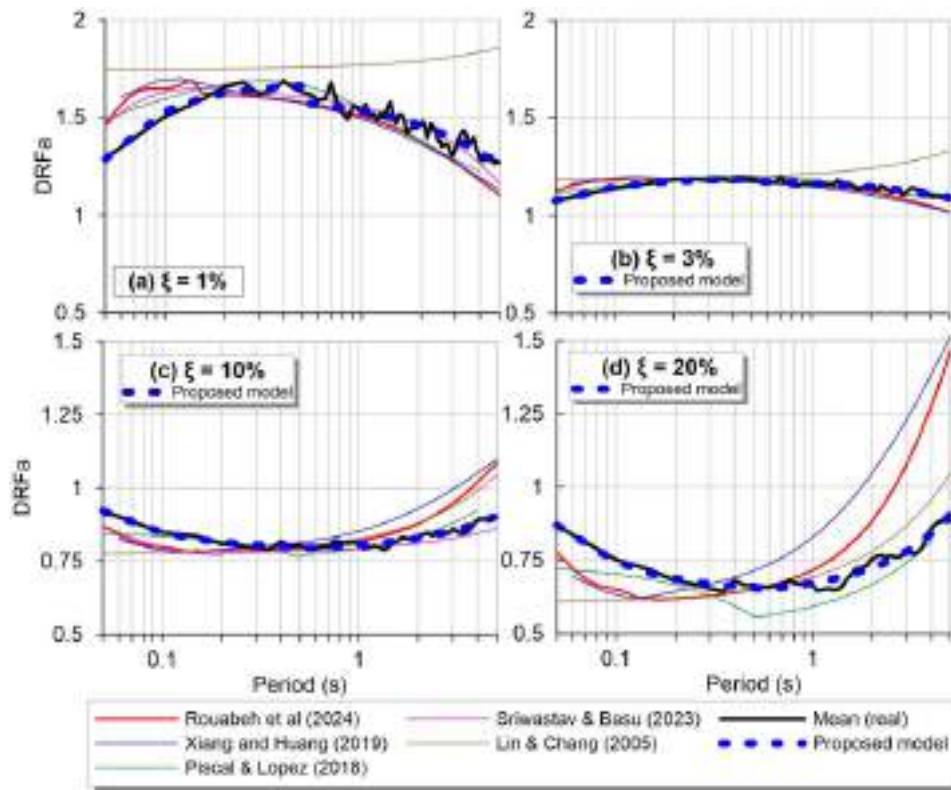
Figure 8. Comparison of proposed DRFa with equations given in Table 3 for different damping values.

Figure 8 presents a comparison of the mean DRFa values predicted by the proposed model and those from existing models in the literature at damping ratios of 2%, 3%, 7%, 10%, and 20%. The figure reveals variations in DRFa predictions across the models at different damping ratios. Notably, the Lin and Chang model exhibits a distinct behavior, with nearly identical DRF values at a damping ratio of 3% across all periods, except for its own predictions. This divergence makes Lin and Chang's model significantly different from others when the damping ratio is less than 10%.

For damping ratios of ξ ≤ 10% and longer periods (T > 1.0 s), the proposed model aligns closely with existing models, showing only minor differences. However, for damping ratios exceeding 10%, the models begin to diverge, and the differences between their predictions become more pronounced. Despite this, the proposed model demonstrates the highest accuracy across all damping ratios and period ranges, outperforming the other models in capturing the DRFa behavior.

Conclusion

This study calculates the maximum absolute acceleration response to determine the damping reduction factor (DRFa) values for different types of response spectra. A total of 70 real vertical ground motions, selected from the PEER database and recorded in the Turkish region, were analyzed. Response spectra were computed for damping ratios (ξ) of 1%, 3%, 5%, 7%, 10%, 15%, and 20%. The DRF values were then calculated for damping ratios other than the 5% reference spectrum. Based on these analyses, new nonlinear prediction equations were developed for each response spectrum, with the damping ratio and natural vibration period as variables. The proposed equations demonstrated strong compatibility with real DRFs and exhibited high robustness when compared to existing DRF models.

References

AASHTO. (2010). LFRD Bridge design specifications. In *American Association of State Highway and Transportation Officials* (3rd ed.). American Association of State Highway and Transportation Officials.

Abdollahiparsa, H., Homami, P., & Khoshnoudian, F. (2016). Effect of vertical component of an earthquake on steel frames considering soil-structure interaction. *KSCE Journal of Civil Engineering*, *20*(7), 2790–2801. https://doi.org/10.1007/s12205-016-0687-y

Ambraseys, N. ., & Douglas, J. (2003). Near-field horizontal and vertical earthquake ground motions. *Soil Dynamics and Earthquake Engineering*, *23*(1), 1–18. https://doi.org/10.1016/S0267-7261(02)00153-7

ASCE/SEI 41-13. (2014). *Seismic evaluation and retrofit of existing buildings*. *American Society of Civil Engineers (ASCE)*.

Baizid, B., & Cardone, D. (2021). Estimation of stochastic damping reduction factor using monte carlo simulation and artificial neural network method. *Ingegneria Sismica*, *38*(4), 37–53.

Berge-Thierry, C., Cotton, F., Scotti, O., Griot Pommera, D.-A., & Fukushima, Y. (2003). New empirical response spectral attenuation laws for moderate European earthquakes. *Journal of Earthquake Engineering*, *7*(2), 193–222. https://doi.org/10.1080/13632460309350446

Bozorgnia, Y., & Campbell, K. W. (2004). The vertical-to-horizontal response spectral ratio and tentative procedures for developing simplified v/h and vertical design spectra. *Journal of Earthquake Engineering*, *8*(2), 175–207. https://doi.org/10.1080/13632460409350486

Bozorgnia, Y., Niazi, M., & Campbell, K. W. (1995). Characteristics of Free-Field Vertical Ground Motion

during the Northridge Earthquake. *Earthquake Spectra*, *11*(4), 515–525. https://doi.org/10.1193/1.1585825

Campbell, K. W., & Bozorgnia, Y. (2003). Updated near-source ground-motion (attenuation) relations for the horizontal and vertical components of peak ground acceleration and acceleration response spectra. *Bulletin of the Seismological Society of America*, *93*(1), 314–331. https://doi.org/10.1785/0120020029

Çelik, E. Ç., & Merter, O. (2023). An investigation of damping modification factors corresponding to different damping ratios for sdof systems. *Stavební Obzor - Civil Engineering Journal*, *32*(1), 42–53. https://doi.org/10.14311/CEJ.2023.01.0004

Chopra, A. K. (2012). *Dynamics of structures : theory and applications to earthquake engineering*. https://www.pearson.com/us/higher-education/product/Chopra-Dynamics-of-Structures-4th-Edition/9780132858038.html

Clough R.W., & Penzien J. (1994). *Dynamics Of Structures* (McGraw Hill (ed.); 2nd Editio). https://api.semanticscholar.org/CorpusID:121098648

Dávalos, H., Miranda, E., Bantis, J., & Cruz, C. (2022). Response spectral damping modification factors for structures built on soft soils. *Soil Dynamics and Earthquake Engineering*, *154*, 107153. https://doi.org/10.1016/j.soildyn.2022.107153

Davis, B. W., Parnell, R., & Xu, L. (2008). Vibration performance of lightweight floor systems supported by cold-formed steel joists. *19th International Specialty Conference on Recent Research and Developments in Cold-Formed Steel Design and Construction*, 325–339.

Elhout, E. A. (2022). Damping modification factor of the vertical response spectrum. *Asian Journal of Civil Engineering*, *23*(6), 929–942. https://doi.org/10.1007/s42107-022-00465-5

Eurocode-8. (2004). Eurocode 8: Design of structures for earthquake resistance - Part 1 : General rules, seismic actions and rules for buildings. In *European Committee for Standardization*. European Committee for Standardization.

GB. (2010). *Code for seismic design of buildings*. China Architecture and Building Press.

Gülerce, Z., & Abrahamson, N. A. (2010). Vector-Valued Probabilistic Seismic Hazard Assessment for the Effects of Vertical Ground Motions on the Seismic Response of Highway Bridges. *Earthquake Spectra*, *26*(4), 999–1016. https://doi.org/10.1193/1.3464548

Gulerce, Z., Erduran, E., & Kunnath, S. K. (2012). *Seismic demand models for probabilistic risk analysis of near fault vertical ground motion effects on ordinary highway bridges*. *June 2011*, 159–175. https://doi.org/10.1002/eqe

Hatzigeorgiou, G. D. (2010). Damping modification factors for SDOF systems subjected to near-fault, far-fault and artificial earthquakes. *Earthquake Engineering and Structural Dynamics*, *39*(11), 1239–1258. https://doi.org/10.1002/eqe.991

Japanese code (JPN). (2001). Guidelines for Calculation Procedure and Technical Standard on Seismically Isolated Structures (In Japanese), Building Center of Japan. *Ministry of Vehicle, Infrastructure and Transport*.

Kim, S., Kim, S. J., & Chang, C. (2018). Analytical Assessment of the Effect of Vertical Ground Motion on RC Frames Designed for Gravity Loads with Various Geometric Configurations. *Advances in Civil*

Engineering, *2018*, 1–11. https://doi.org/10.1155/2018/4029142

Kitayama, S., Lee, D., Constantinou, M. C., & Kempner, L. (2017). Probabilistic seismic assessment of seismically isolated electrical transformers considering vertical isolation and vertical ground motion. *Engineering Structures*, *152*, 888–900. https://doi.org/10.1016/j.engstruct.2017.10.009

Li, X., Dou, H., & Zhu, X. (2007). Engineering characteristics of near-fault vertical ground motions and their effect on the seismic response of bridges. *Earthquake Engineering and Engineering Vibration*, *6*(4), 345–350. https://doi.org/10.1007/s11803-007-0723-5

Lin, Y., & Chang, K. (2004). Effects of Site Classes on Damping Reduction Factors. *Journal of Structural Engineering*, *130*(11), 1667–1675. https://doi.org/10.1061/(asce)0733-9445(2004)130:11(1667)

Liu, T., Wang, W., Wang, H., & Su, B. (2021). Improved damping reduction factor models for different response spectra. *Engineering Structures*, *246*(January), 113012. https://doi.org/10.1016/j.engstruct.2021.113012

Malhotra, P. K. (2006). Smooth Spectra of Horizontal and Vertical Ground Motions. *Bulletin of the Seismological Society of America*, *96*(2), 506–518. https://doi.org/10.1785/0120050062

Mohraz, B. (1976). A study of earthquake response spectra for different geological conditions. *Bull Seismol Soc Am*, *66(3)*, 915–35.

Moschen, L., Medina, R. A., & Adam, C. (2016). Vertical acceleration demands on column lines of steel moment-resisting frames. *Earthquake Engineering & Structural Dynamics*, *45*(12), 2039–2060. https://doi.org/10.1002/eqe.2751

Mwafy, A., Salah, A., & Elnashai, E. (2006). Vulnerability of code-compliant RC buildings under multi-axial earthquake loading. *Proceedings of the 4th International Conference on Earthquake Engineering*, *February 2014*.

Mylonas. (1997). Vertical Response of Instrumented Structures. *Engineering Seismology and Earthquake Engineering Section, Imperial College, London.*, *MSc dissertation*, 102pp.

Newmark, N. M., & Hall, W. J. (1972). Procedures and criteria for earthquake resistant design. *Building Practices for Disaster Mitigation, National Bureau of Standards, Building Science Series 46,* 209–236.

Piscal A, C. M., & López-Almansa, F. (2018). Generating damping modification factors after artificial inputs in scenarios of local records scarcity. *Bulletin of Earthquake Engineering*, *16*(11), 5371–5396. https://doi.org/10.1007/s10518-018-0406-9

R. K. Sriwastav, & D. Basu. (2023). Simplified Damping Modification Factor for Vertical Response Spectra. In M. Shrikhande, P. Agarwal, & P. C. A. Kumar (Eds.), *Proceedings of 17th Symposium on Earthquake Engineering* (Vol. 4, Issue 2023, pp. 655–667). Springer Nature Singapore. https://doi.org/10.1007/978-981-99-1459-3_52

Rezaeian, S., Bozorgnia, Y., Idriss, I. M., Abrahamson, N. A., Campbell, K. W., & Silva, W. J. (2014). Damping Scaling Factors for Vertical Elastic Response Spectra for Shallow Crustal Earthquakes in Active Tectonic Regions. *Earthquake Spectra*, *30*(3), 1335–1358. https://doi.org/10.1193/100512EQS299M

Rouabeh, A., Benahmed, B., Palanci, M., & Aouari, I. (2024). The Derivation of Vertical Damping Reduction Factors for the Design and Analysis of Structures Using Acceleration, Velocity, and Displacement

Spectra. *Applied Sciences*, *14*(11), 4348. https://doi.org/10.3390/app14114348

RPA99. (2003). *Algerian earthquake resistant regulations*. National center of applied research in earthquake engineering.

Setareh, M. (2012). Vibrations due to Walking in a Long-Cantilevered Office Building Structure. *Journal of Performance of Constructed Facilities*, *26*(3), 255–270. https://doi.org/10.1061/(asce)cf.1943-5509.0000188

TBEC. (2018). Turkish building earthquake code. In *Disaster and Emergency Management Presidency*. Disaster and Emergency Management Presidency.

Trifunac, M. D., & Lee, V. W. (1989). Empirical models for scaling pseudo relative velocity spectra of strong earthquake accelerations in terms of magnitude, distance, site intensity and recording site conditions. *Soil Dynamics and Earthquake Engineering*, *8*(3), 126–144. https://doi.org/10.1016/S0267-7261(89)80008-9

Varela, W. D., & Battista, R. C. (2011). Control of vibrations induced by people walking on large span composite floor decks. *Engineering Structures*, *33*(9), 2485–2494. https://doi.org/10.1016/j.engstruct.2011.04.021

Xiang, Y., & Huang, Q. (2019). Damping modification factor for the vertical seismic response spectrum: A study based on Japanese earthquake records. *Engineering Structures*, *179*(June 2018), 493–511. https://doi.org/10.1016/j.engstruct.2018.11.021

Xiang, Y., Luo, Y., Huang, Q., & Shen, Z. (2018). Vertical ductility demand and residual displacement of roof-type steel structures subjected to vertical earthquake ground motions. *Soil Dynamics and Earthquake Engineering*, *104*, 259–275. https://doi.org/10.1016/j.soildyn.2017.10.019

Xiang, Y., Luo, Y., Zhu, Z., & Shen, Z. (2017). Estimating the response of steel structures subjected to vertical seismic excitation: Idealized model and inelastic displacement ratio. *Engineering Structures*, *148*, 225–238. https://doi.org/10.1016/j.engstruct.2017.06.043

Ye, J.-H., Ding, Y.-L., Liu, X.-M., & Huang, Z. (2010). Vibration Test and Analysis of An Aircraft Maintenance Hangar under Multi-Support Excitations. *Advances in Structural Engineering*, *13*(4), 695–706. https://doi.org/10.1260/1369-4332.13.4.695

Zhang, H., & Zhao, Y. (2020). Damping modification factor based on random vibration theory using a source-based ground-motion model. *Soil Dynamics and Earthquake Engineering*, *136*(May), 106225. https://doi.org/10.1016/j.soildyn.2020.106225

Zhou, Z., Wong, J., & Mahin, S. (2016). Potentiality of Using Vertical and Three-Dimensional Isolation Systems in Nuclear Structures. *Nuclear Engineering and Technology*, *48*(5), 1237–1251. https://doi.org/10.1016/j.net.2016.03.005

Development of a Prototype for Green Hydrogen Production from Natural Sources

Sari Hassoun Zakaria

MECACOMP, Mechanical Engineering Department, Abou-Bekr Belkaid University, P.O. Box 119 13000 Tlemcen, Algeria.

Berrezoug Hiba Imane

Theoretical Physics Laboratory, Abou-Bekr Belkaïd University, P.O. Box 119, 13000, Tlemcen, Algeria.

Aliane Khaled

MECACOMP, Mechanical Engineering Department, Abou-Bekr Belkaid University, P.O. Box 119 13000 Tlemcen, Algeria.

Abstract: The photovoltaic conversion of solar radiation into electricity is one of the ways to harness solar resources. This is achieved through solar cells. A system that combines a photovoltaic array with an electrolyzer allows for the storage of electricity in the form of gas (hydrogen). It is true that hydrogen (H) is one of the most abundant elements on Earth, but it is not available in its pure form in nature. The emerging world needs energy to grow and support its development. This translates into a greater need for electricity production capacity and an increased demand for gas, as economic growth cannot occur without an expansion in energy supply. Ultimately, 90% of new energy needs will be in these regions, and it is our role to support this growth. Due to the acceleration of population growth, energy from fossil resources (oil, coal, natural gas or nuclear) is insufficient to meet the growing energy needs of the planet and has a significant impact on the environment. Moreover, these energies are not renewable. A workable solution must therefore be found. Producing electricity from renewable energies is a solution for the future. For example, Algeria is considered as one of the important countries that have enormous environmental capacities to exploit these energies. This is what prompted us to carry out this work which relates to the study of the system for the improvement and production of green hydrogen by electrolysis from solar energy and sea water, hydrogen being a source of electrical energy in order to use it as fuel because of its distinctive chemical and physical properties and does not cause any polluting emissions. [2]

Keywords: green hydrogen, water electrolysis, solar energy, sea water

Introduction

Algeria initiates a green energy dynamic by launching an ambitious program for the development of renewable energies and energy efficiency. This vision of the Algerian government is based on a strategy focused on harnessing inexhaustible resources like solar energy and using them to diversify energy sources and prepare Algeria for the future. Through the combination of initiatives and expertise, Algeria is committing to a new sustainable energy future. To this end, a national renewable energy development program has been mapped out for the period 2011-2030, aiming, in the long term, to produce 40% of the country's electricity consumption from solar energy sources.

This program plans to install nearly 22,000 MW of capacity, with 12,000 MW intended for domestic demand and 10,000 MW for export [1]. Emerging markets need energy to grow and support their growth. This notably translates into more electricity production capacities and an increased need for gas, as without growth in energy supply, there can be no economic growth. This is where 90% of the new demand will eventually be, and this is where our role is to support that growth [3].

Thus, the needs of the emerging world are both quantitative and qualitative, and they must be met through appropriate production methods. The photovoltaic conversion of solar radiation into electricity is one of the ways to harness solar energy. This is achieved through solar cells. A system combining a photovoltaic field with an electrolyzer allows for electricity storage in the form of gas (hydrogen).

It is true that hydrogen (H) is one of the most abundant elements on Earth, but it is not available in its pure state in nature. It is only found in a combined form. Green hydrogen is a renewable energy source produced by splitting water molecules into hydrogen and oxygen using renewable electricity. This process, known as electrolysis, generates hydrogen without any emissions. Additionally, the byproducts of its combustion are non-polluting, which, combined with economic and ecological reasons, makes hydrogen's time as an energy carrier appear to have come.

In fact, almost all the hydrogen available today comes from natural gas reforming. Thermochemistry is still in the laboratory stage, and electrolysis accounts for less than 1% of the total hydrogen production capacity. The latter is only used if the electricity is either surplus (as in the case of renewables like wind or solar) or cheap and/or if a high purity of the produced hydrogen is required.

Currently, the increasing reliance on renewable sources is leading to the development of electrolysis, a process well-suited for the valorization of these new energies. In addition to physical solutions, such as compressed or liquefied gas—which are still largely unsatisfactory at this stage—original chemical solutions are being explored, including hydrometallurgy and porous solid materials.

I could conclude by saying that the study of this subject is one of humanity's great scientific adventures, which is equally exciting. Our objective is to contribute to a better understanding of a new technology for the production and storage of clean energy. [4]

Material and Methods

Experimental Devices and Equipment

This study will allow us to design and produce a production prototype (PV-Thermal) composed of an electrolysis of seawater supplied by two PV-thermal panels (hybrid). It is a new technology for the production of green hydrogen from natural sources.

Selection of photovoltaic modules

A photovoltaic cell produces electrical energy by converting light from solar radiation into direct electricity through the use of semiconductors that exhibit the photovoltaic effect. The process of photovoltaic conversion relies on three key mechanisms: the absorption of photons by the material of the cell, the transformation of photon energy into electrical energy (which involves the generation of electron-hole pairs in the semiconductor), and the collection of these generated particles. For photovoltaic cells to function effectively, the materials used must possess two distinct energy levels and demonstrate adequate conductivity to facilitate the flow of current. This underscores the critical role that semiconductors play in the photovoltaic industry. [3]

After conducting research to determine the appropriate type of photovoltaic modules and consulting with specialists in photovoltaic electricity, three type photovoltaic modules were selected. The first one is The Solar Pro 50W solar panels shown in figure 1.a , made with monocrystalline technology, provide a power output of 50 watts each, allowing for a total production of 100 watts when installed in parallel. Each panel operates a current at maximum power $Imp = 2.70$ A, a voltage at maximum power $Vmp = 18.24$ V, a short-circuit current $Isc = 2.97$ A and an open-circuit voltage $Voc = 21.8$ V. The standard dimensions of the panels are approximately 670 mm x 550 mm x 30 mm, and they typically weigh between 5 and 6 kg. With an efficiency of around 15 to 20%, these panels are designed to maximize space utilization. Additionally, they feature a temperature coefficient of about -0.4%/°C, meaning they lose less efficiency as the temperature increases.

The seconde one, The LAGUA Solar Panel 80W (figure 1.b) is a high-performance polycrystalline solar panel designed to provide efficient energy conversion. With a power output of 80 watts, this panel operates a current at maximum power $Imp = 4.44$ A, a voltage at maximum power $Vmp = 18$ V, a short-circuit current $Isc = 4.80$ A and an open-circuit voltage $Voc = 22.32$ V. The panel features durable construction, ensuring resistance to weather elements, and is designed for easy installation on rooftops or ground-mounted systems. With a size of around 1,640 mm x 670 mm x 35 mm, the LAGUA Solar Panel 80W strikes a balance between compactness and efficiency, making it an excellent choice for off-grid applications, battery charging, and enhancing energy

independence. The third one is a hybrid solar panel figure 1.c, also known as a mixed solar collector, is a system that uses both thermal and photovoltaic sensors to operate. An 8-meter coiled copper tube is used at the back of the LAGUA Solar panel, forming a closed circuit to heat seawater with the aim of increasing green hydrogen production and cooling the solar cells to improve the efficiency of the panel. From this, we can say that the innovative idea is to use a hybrid (PV-Thermal) panel.
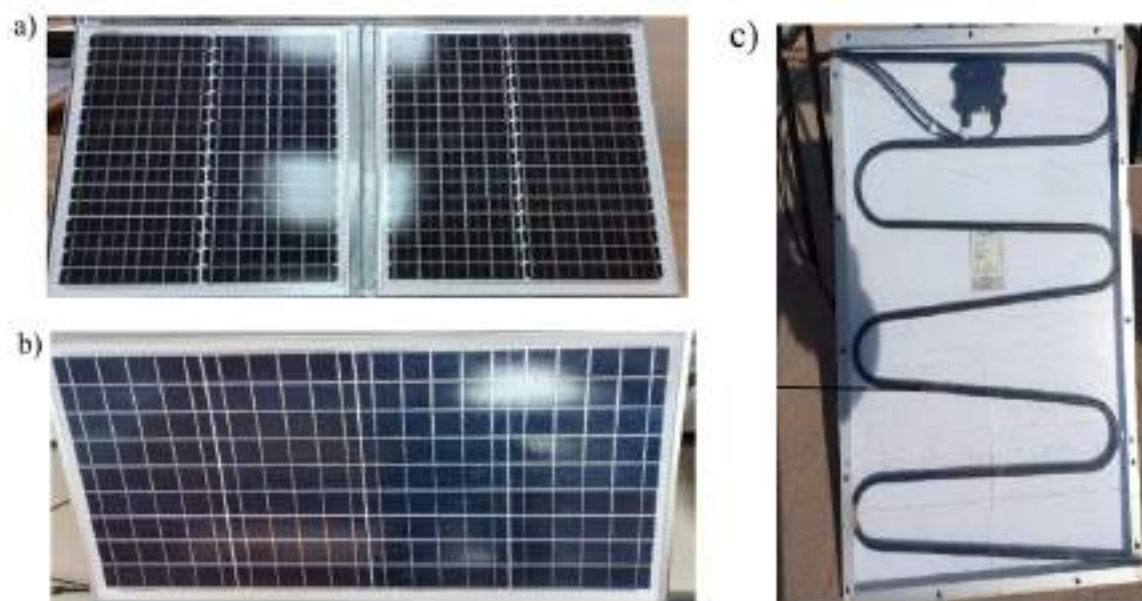
Figure 1. a) Two panels in parallel (Solar Pro), **b)** LAGUA Solar Panel, **c)** hybrid solar panel.

Alkaline Electrolysis
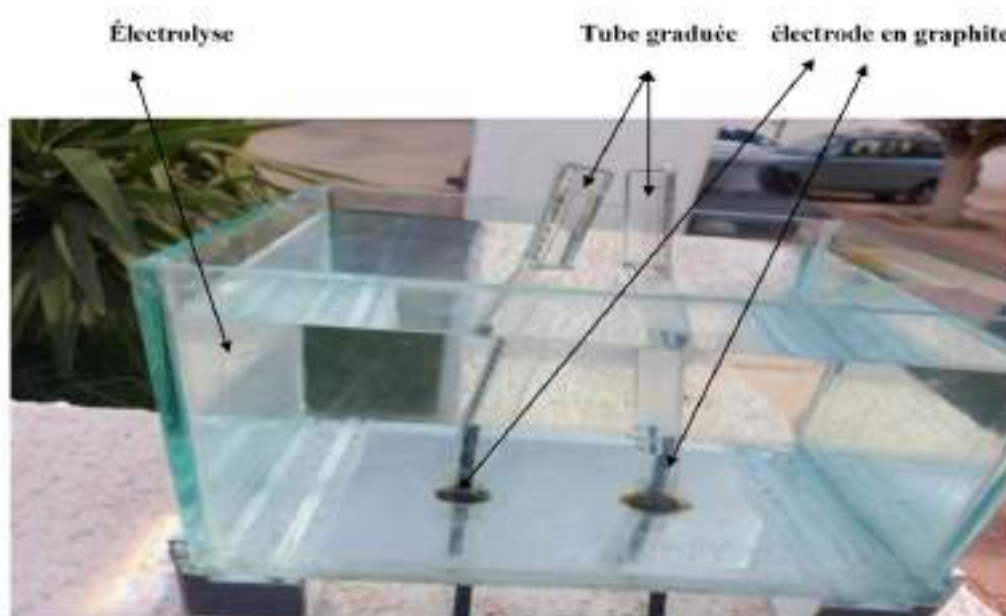
Figure 2. Elements of Water Electrolysis

Alkaline electrolysis, is a hydrogen production method that involves the separation of oxygen and hydrogen from water through the application of an electric current in an alkaline solution. In this process, an electrolyte, typically potassium hydroxide (KOH) or sodium hydroxide (NaOH), is used to enhance the conductivity of water. When an electric current is applied, water molecules are split at the electrodes: hydrogen is produced at the cathode, while oxygen is generated at the anode. This method is well-established in the industry and is known for its efficiency and cost-effectiveness, making it a vital technology for the sustainable production of hydrogen.

The catalyst used, as illustrated in Figure 2, comprises several essential components for our experiment. The graduated cylinder, a laboratory instrument for accurately measuring volumes, was used to measure the hydrogen produced in cubic centimeters (cm³), with each of the two cylinders having a volume of 35 cm³. The glass tank was designed with two 6 mm holes in the center to accommodate the anode and cathode, both made of carbon, with each electrode measuring 6 mm in thickness and 5.5 cm in length. The surface area of these carbon electrodes is 10.36 cm², and the total volume of the glass tank is 11.178 L. The cathode functions as the electrode where the reduction reaction occurs, known as cathodic reduction, and corresponds to the positive terminal (+) in a battery. Seawater was chosen for this experiment due to its rich ionic content, characterized by a salinity of 35 g/L.

Experimental scenarios on 50W and 80W Solar Panel:

In this work, the Algerian region of Tlemcen, its latitude is 34.27° so we used a metal support inclined at 34° to have the maximum solar radiation on the panels, was selected as the study area. This section outlines the steps taken to prepare for the various experimental tasks, beginning with the purchase of technically photovoltaic modules (PV 50W) and (PV 80W), followed by the manufacture of water electrolysis, and the acquisition of various measuring instruments. The experiment was conducted on February 13, 2023, from 10:00 AM to 12:00 PM, and involved alkaline electrolysis powered by two 50 W photovoltaic panels connected in parallel, providing a total power of 100 W figure 3. The same day, from 12:00 PM to 2:00 PM, the two 50 W panels were replaced with two 80 W panels, also connected in parallel, yielding a total power of 160 W figure 4. And on May 29, 2023, from 10:00 AM to 1:00 PM this experiment was conducted, involving alkaline electrolysis powered by two 80 W photovoltaic hybrid panels connected in parallel, with a total power output of 160 W figure 5.

All climatic parameters, including solar radiation, wind speed, and ambient air temperature, were measured experimentally using the equipment to measure the electric current, voltage, and electrical resistance of the system, along with their quantities, characteristics, accuracy, and uncertainty.
Measuring equipment used in experimental work are:

- The multimeter, often referred to as a voltmeter, is a tool used to measure voltage, current, resistance, and temperature. To use it, place the wire leads into the appropriate terminals: the black lead into COM

and the red lead into VΩ. Select AC voltage (VAC) or DC voltage (VDC), depending on the measurement needed.Be cautious, as measuring voltage with the lead set to mA or 10A can destroy the device's fuse. Place the test probes in parallel with the terminals of the device to be measured.

- A luxmeter is a sensor used to measure illuminance within the visible spectrum. The measurement is absolute, not relative. The unit of measurement is lux.

- A thermocouple is a sensor used to measure temperature. It consists of two different types of metals joined at one end. When the junction of the metals is heated or cooled, a variable voltage is produced, which can then be converted into a temperature reading.

- A stopwatch is a time-measuring instrument. We use it to calculate the time taken to fill the tube with hydrogen gas.

- A Convertisseur est un appareil électronique qui produit du courant alternatif à partir du courant continu. Il est directement connecté aux batteries.

- Batteries are optional components in a photovoltaic system and are used to store electricity for the regulator and the inverter.

- Le régulateur est une unité électronique dont le rôle est de gérer les flux de courant.

Figure 3. Experience using 50 W panels.

Figure 4. Experience using 80 W panels.

Figure 5. Experience using 80 W hybrid panels.

Results and Discussion

The experimental work was conducted on the 13 of February and 29 of May of the year 2023 in Tlemcen area (latitude is 34.27°, metal support inclined at 34° to have the maximum solar radiation on the panels) at northwest Algeria. Measurements were taken for three experiments using 50 W panels, 80 W panels, and 80 W hybrid panels. the parameters determined in this experiment are: water temperature (Te), ambient temperature (Ta), panel temperature (Tp), illuminance E, voltage U, current I, volume of hydrogen VH2, and volume filled each minute ΔV.

Using 50 W panels and analyzing the curve representing the variation of H_2 volume as a function of time figure 6.a, it is observed that it takes 18 minutes to produce 32.5 cm³ of hydrogen. This indicates a relatively consistent production rate within this timeframe, allowing for an evaluation of the efficiency of the electrolysis process under the specific conditions of the experiment. Upon examining the curve representing the variation of illuminance as a function of ΔV_1 figure 6.b, it can be concluded that illuminance and the change in volume ΔV_1 occur simultaneously. This correlation suggests that as the illuminance increases, there is a corresponding change in the volume of hydrogen produced, indicating a direct relationship between light intensity and the efficiency of the electrolysis process.

According to the curve representing the variation of current I_1 as a function of illuminance E figure 6.c , it is observed that the current I_1 varies proportionally with the illuminance, reaching a maximum value of 593.51 W/m². This indicates a strong relationship between the intensity of the light and the current produced, suggesting that as the illuminance increases, the current also increases, enhancing the overall efficiency of the electrolysis process. It is observed that both illuminance and current are parameters that influence the production of H_2 figure 6.d. The relationship between these factors suggests that higher light intensity and current levels contribute positively to the efficiency of hydrogen production during the electrolysis process. Understanding how these parameters interact can help optimize the conditions for generating hydrogen, making the system more effective.
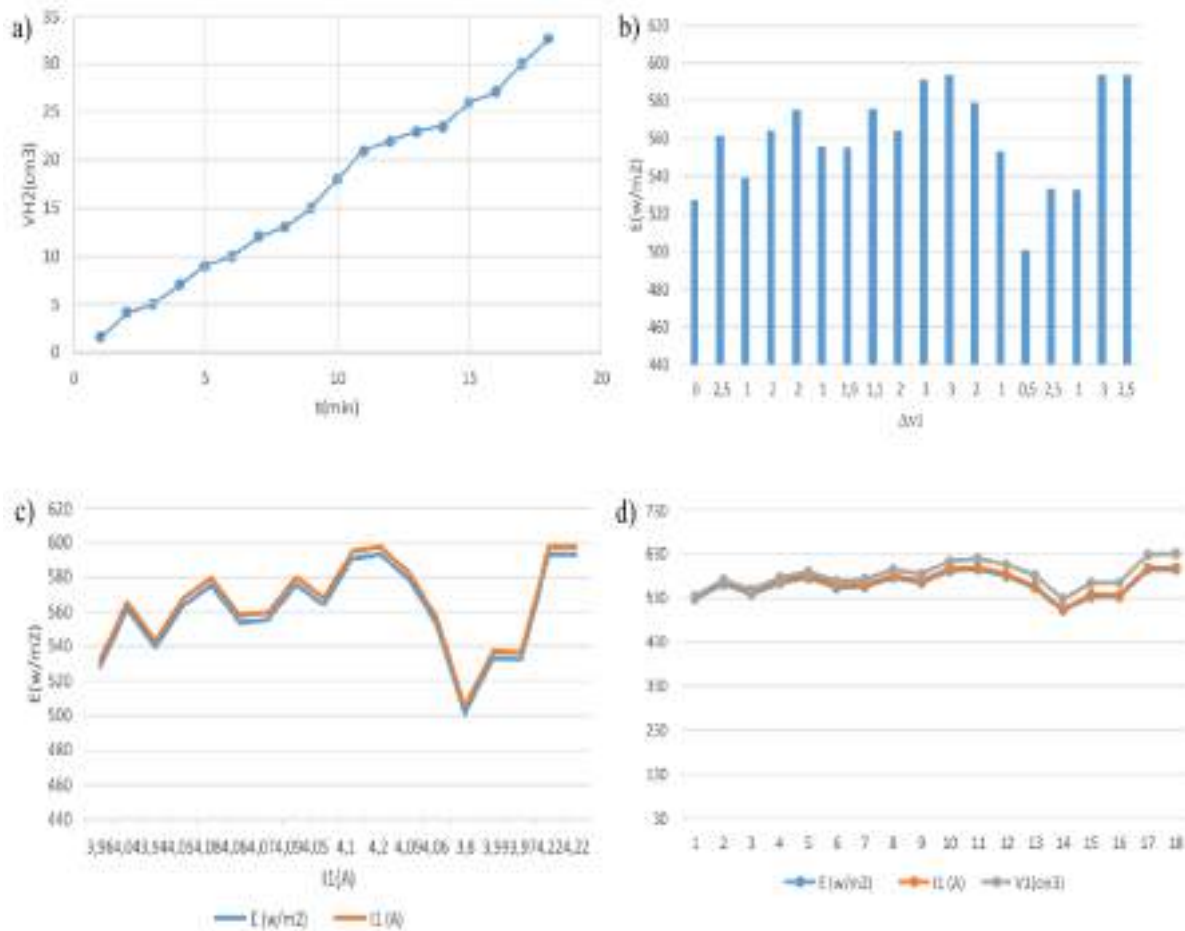
Figure 6. The Variations Using 50 W panels a) of H₂ Volume as a Function of Time, b) of H₂ Volume as a Function of Time, c) of Current as a Function of Illuminance and d) of H₂, I₁, and Illuminance.

Switching to 80 W panels and analyzing the curve of H_2 volume as a function of time (Figure 7.a), it is observed that hydrogen production increases, taking only 13 minutes to produce 33.8 cm³. The curve of H_2 variation as a function of illuminance (Figure 7.b) reinforces the simultaneous nature of illuminance and hydrogen production, suggesting that higher light intensity results in more hydrogen being produced, thus improving electrolysis efficiency. The curve illustrating ΔV and current I (Figure 7.c) shows that the volume of ΔV_2 increases as amperage rises, indicating a direct link between the current and hydrogen production.

Finally, there is an inverse relationship between voltage and temperature (Figure 7.d), where higher temperatures lead to decreased voltage, potentially impacting the system's efficiency. Higher temperatures can negatively affect voltage output, reducing the overall effectiveness of the electrolysis process.

Based on Experiment 2 (80 W panels), we can conclude that the panel temperature negatively affects the system's performance, leading to a decrease in total power output. This is primarily due to the reduction in voltage, which subsequently lowers the overall efficiency of the system. In the 80W panel, the production time is shorter compared to the 50W panel. The volume of hydrogen collected in the tube with the 80W panel is

greater than that of the 50W panel. Additionally, the volume filled per minute with the 50W panel is lower than that with the 80W panel. Furthermore, the maximum voltage of the 80W panel is higher than that of the 50W panel. A comparison between the 50W PV panel and the 80W PV panel is presented in Table 1.
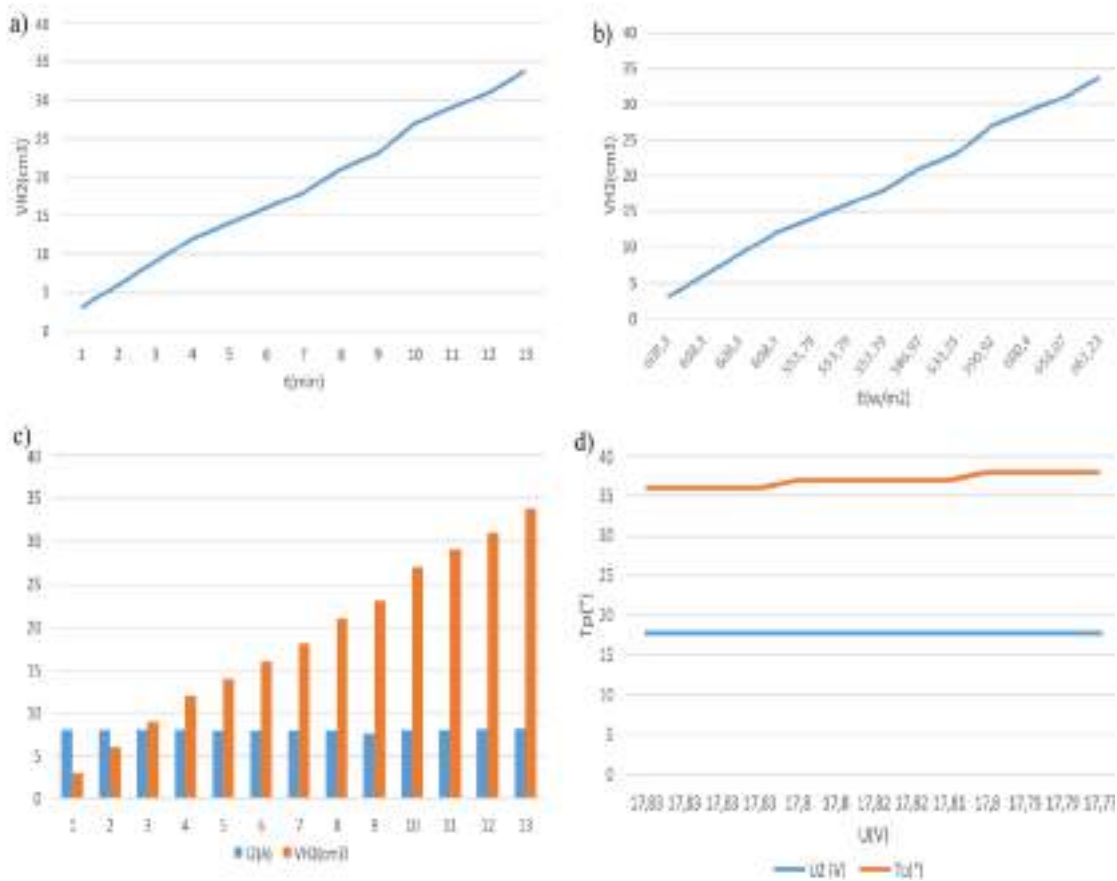
Figure 7. The Variations Using 80 W panels a) of H_2 Volume as a Function of Time, b) of H_2 Volume as a Function of Illuminance, c) of ΔV as a Function of Current I and d) of tension U and temperature.

Table 1. Comparison of parameters between 50W PV and 80W PV.

Parametrs	PV (50W)	PV (80W)
Production Time (min)	18	13
Volume of hydrogen (cm^3)	32.5	33.8
Amperage I_{max}	4.22	8.2
$\Delta_V m$ (cm^3)	1.77	2.36
Voltage (V)	17.83	17.99

Using 80 W hybrid panels, and according to the curve showing the variation of H_2 volume over time in (Figure 8.a), it takes 10 minutes to produce 34 cm³ of hydrogen. This observation highlights a relatively fast production, which may be linked to the efficiency of this electrolysis system. The curve of the variation of water

temperature Te as a function of Δv (Figure 8.b) is linear, indicating that the volume of Δv increases with the rise in water temperature.

This linear relationship suggests that as the water heats up, the volume of gas produced, particularly hydrogen in the context of electrolysis, increases. This can be attributed to the acceleration of electrochemical reactions at higher temperatures. Noting also that the relationship between voltage and temperature is inverse; as the temperature increases, the voltage decreases (Figure 8.c).

This inverse correlation indicates that higher temperatures can negatively affect the voltage output, potentially reducing the overall efficiency of the system. It is evident that both illuminance and amperage play crucial roles in influencing hydrogen production (H_2) (Figure 8.d). Higher levels of illuminance correlate with increased amperage, which enhances the electrolysis process. This relationship underscores the importance of optimizing light exposure and current levels to maximize hydrogen generation efficiency. Understanding how these parameters interact can significantly contribute to improving the overall performance of the electrolysis system and the effective production of hydrogen.
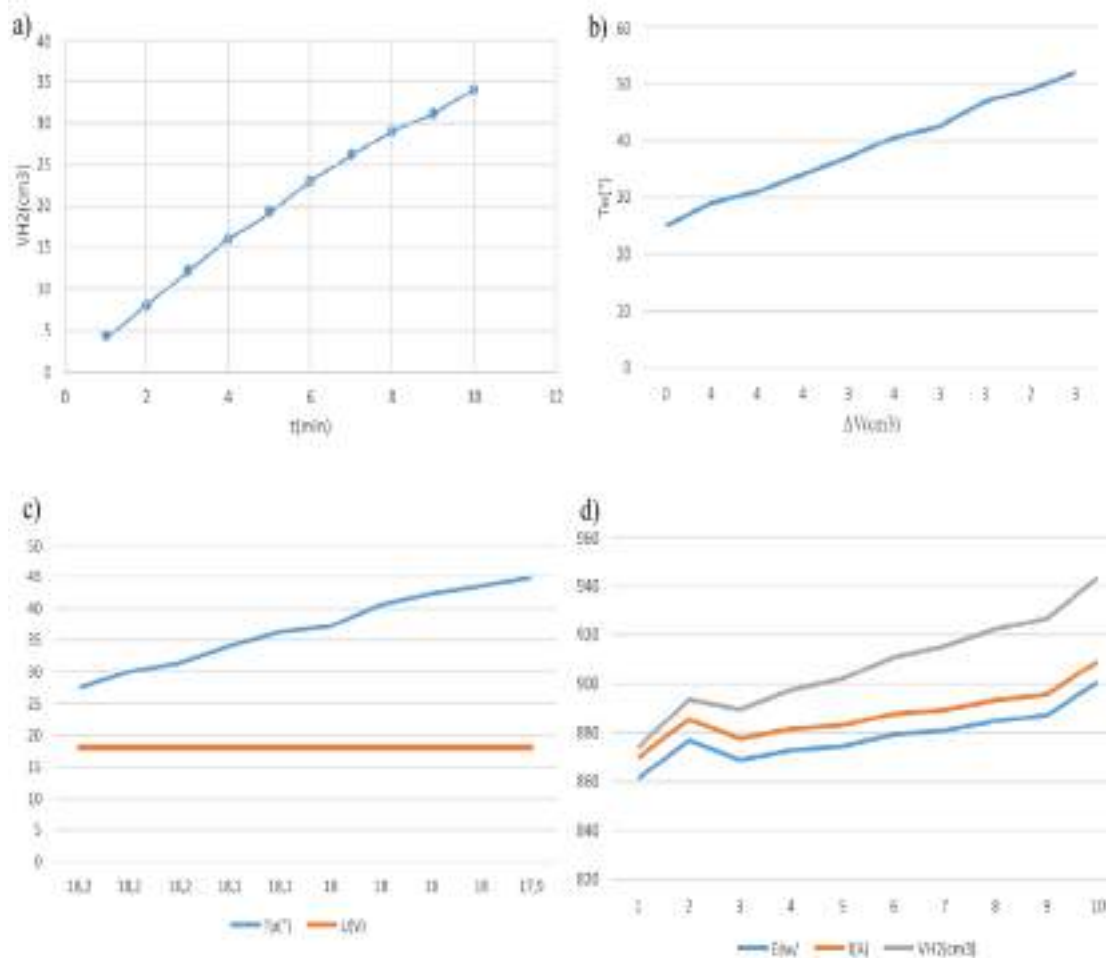
Figure 7. The Variations Using 80 W hybrid panels a) of H_2 Volume as a Function of Time, b) of Te as a Function of ΔV , c) of tension U and temperature, and d) of Illuminance, H_2 Volume and amperage.

From this last experiment (Using 80 W hybrid panels) , we can conclude that the volume of hydrogen (H_2) increases with the rise in water temperature, illuminance, and amperage. This observation suggests that optimizing these factors can enhance the hydrogen production efficiency during the electrolysis process. As the water temperature rises, along with increased light exposure and current levels, the electrolysis system performs better, leading to greater hydrogen generation. Understanding this relationship is essential to improving the overall efficiency of hydrogen production methods.

Conclusion

Based on our experiment, we can conclude that three main parameters influence the production of green hydrogen from photovoltaic energy: water temperature, illuminance, and current. Increased illuminance leads to a corresponding increase in current, enhancing the electrolysis process. The electric current is directly proportional to the volume of hydrogen produced, demonstrating the importance of optimizing current levels for efficient electrolysis. Additionally, closed circuit parameters affect seawater temperature, with warmer water significantly influencing hydrogen production, indicating that maintaining an optimal temperature is crucial for efficiency. Utilizing natural photovoltaic and solar thermal sources for green hydrogen production ensures non-polluting options. Furthermore, renewable energy sources, particularly solar energy, have been harnessed as the primary source of electrical current for water analysis, ensuring the operation of a circulation pump and employing solar thermal energy for heating water, which is a major factor in increasing green hydrogen production. Understanding these parameters and their interactions can help optimize conditions for more effective hydrogen production, contributing to sustainable energy solutions.

References

M. Beckert and E. Brun, "Changements climatiques 2014 : Rapport de synthèse Résumé à l'intention des décideurs," GIEC, vol. 3, 2014.

Club du CO2, "Captage, Stockage et Valorisation du CO2 : Une solution pour demain." 2016.[Online]. Available: http://www.captage-stockage-valorisation-co2.fr/. [Accessed: 28-Nov-2016].

The Center for Climate and Energy Solutions, "Carbon capture use and storage," 2016. [Online].Available: http://www.c2es.org/technology/factsheet/CCS. [Accessed: 27-Nov-2016].

"Great point energy." 2016. [Online].Available : https://www.greatpointenergy.com/leadingcarbonsolution.php. [Accessed: 20-Apr-2016].

SoCalCarb, "Storage Saline aquifers," 2010. [Online]. Available: http://socalcarb.org/. [Accessed:27-Nov-2016].

S. Benson et al., "Underground geological storage," Ipcc, pp. 195–276, 2005.

J. Howard, "What water taught me," Creation Science., 2012. [Online]. Available:https://alreadyanswered.org/page/201/. [Accessed: 01-Dec-2016].

M. R. Wright, "An Introduction to electrolyte solutions," Wiley 2007.

C. Wells, Solubility of DDT and 2,4-D in Supercritical Carbon Dioxide and Supercritical CarbonDioxide Saturated with Water" Ind. Eng. Chem. Res., vol. 33, pp. 2757-2763, 2014.

D. Koschel, J. Y. Coxam, L. Rodier, and V. Majer, "Enthalpy and solubility data of CO2 in water andNaCl(aq) at conditions of interest for geological sequestration," Fluid Phase Equilib., vol. 247, pp.107–120, 2006.

R. L. Berg and C. E. Vanderzee, "Thermodynamics of carbon dioxide and carbonic acid: (a) thestandard enthalpies of solution of Na2CO3(s), NaHCO3(s), and CO2(g) in water at 298.15 K; (b) thestandard enthalpies of formation " J. Chem. Thermodyn., vol. 10, pp. 1113–1136, 1978.

S. Gill and I. Wadsö, "Flow-microcalorimetric techniques for solution of slightly soluble gases.Enthalpy of solution of oxygen in water at 298.15 K," J. Chem. Thermodyn., vol. 14, pp. 905–919,1982.

J. M. S. Fonseca, R. Dohrn, and S. Peper, "High-pressure fluid-phase equilibria: Experimentalmethods and systems investigated (2005-2008)," Fluid Phase Equilib., vol. 300, pp. 1–69, 2011.

S. Wroblewski, "The solubility of carbon dioxide in water," Ann. Phys. Chem., vol. 18, pp. 290–308,1883.

W. Sander, "The solubility of carbon dioxide in water.," Z. Phys. Chem., Stochiom. Verwandtsch.,vol. 78, pp. 513 – 549, 1912.

O. Haehnel, "Uber die Loslichkeit des Magnesiumcarbonats in kohlensiiurehaltigem Wasser nnterhoheren Kohlen-," vol. 165, pp. 61–74, 1924.

https://www.asjp.cerist.dz/en/downArticle/649/5/2/211260

https://www.cairn.info/revue-responsabilite-et-environnement-2015-2-page-24.htm

124.

Development of a Dynamic Fault Simulator for Gear Box Faults Diagnosis

Chorfi Sidi Mohammed

Department of Mechanical Engineering, Faculty of Technology, University of Tlemcen, Algeria,
https://orcid.org/0000-0003-4590-9157

Benaissa Mohammed

Department of Electrical Engineering, Faculty of Technology, University of Tlemcen, Algeria,
https://orcid.org/0000-0001-6638-6864

Belalia Sid Ahmed

Department of Mechanical Engineering, Faculty of Technology, University of Tlemcen, Algeria, ,
https://orcid.org/0000-0001-8395-4165

Beldjelili Youcef

Department of Civil Engineering, Faculty of Technology, University of Sidi Belabbas, Algeria,
https://orcid.org/0000-0003-3877-9665

Amine Hadj-Abdelkader

Department of Electrical Engineering, Faculty of Technology, University of Tlemcen, Algeria,
https://orcid.org/0000-0001-9829-434X

Sidi Mohammed Meliani

Department of Electrical Engineering, Faculty of Technology, University of Tlemcen, Algeria,
https://orcid.org/0000-0001-5107-3830

Melih Asma

Master student, Department of Electrical Engineering, Faculty of Technology, University of Tlemcen, Algeria

Mesaoudene Fethi

Master student, Department of Electrical Engineering, Faculty of Technology, University of Tlemcen, Algeria

Abstract: Vibration problems related to increasingly complex and sensitive structures, faster and more sophisticated machines, and networked production processes have become more prevalent in recent years. Likewise, effective vibration signal extraction techniques play a vital role in the diagnosis of a rotating machine. This work enabled the development of a machine fault simulator, which is a complete laboratory-scale machine for performing experiments on gearbox dynamic faults diagnosis. Additionally, it facilitates the controlled

acquisition of vibration signatures associated with typical machine faults without sacrificing production quality or profitability. The simulator's modular architecture provides resilience and versatility. A variety of faults can be detected in many applications including bearing faults, gear faults, shaft and motor faults. With the ability to control the input speed using the Seimens control unit.

Keywords: vibration analysis, fault diagnosis, rotating elements, fault simulator, Bearing

Citation: Sidi Mohammed, C., Mohammed, B., Sid Ahmed, B., Beldjelili, Y., Hadj-Abdelkader, A., Sidi Mohammed, M., Asma, M. & Mesaoudene, F. (2024). Development of a Dynamic Fault Simulator for Gear Box Faults Diagnosis. In A. A. Khan, M. Demirbilek, & M. L. Ciddi (Eds.), *Proceedings of ICSEST 2024-- International Conference on Studies in Engineering, Science, and Technology* (pp. 490-502), Istanbul, Turkiye. ISTES.

Introduction

Detecting a particular problem or failure that a system produces is known as machinery fault diagnosis. The cost of routine maintenance can be seriously reduced using condition-based maintenance. Equipment condition monitoring includes specialized fields including mechanical and electrical measures., tribology and process measurement and performance. Two major categories can be used to classify fault detection and diagnosis: vibration analysers and fault generators [1].
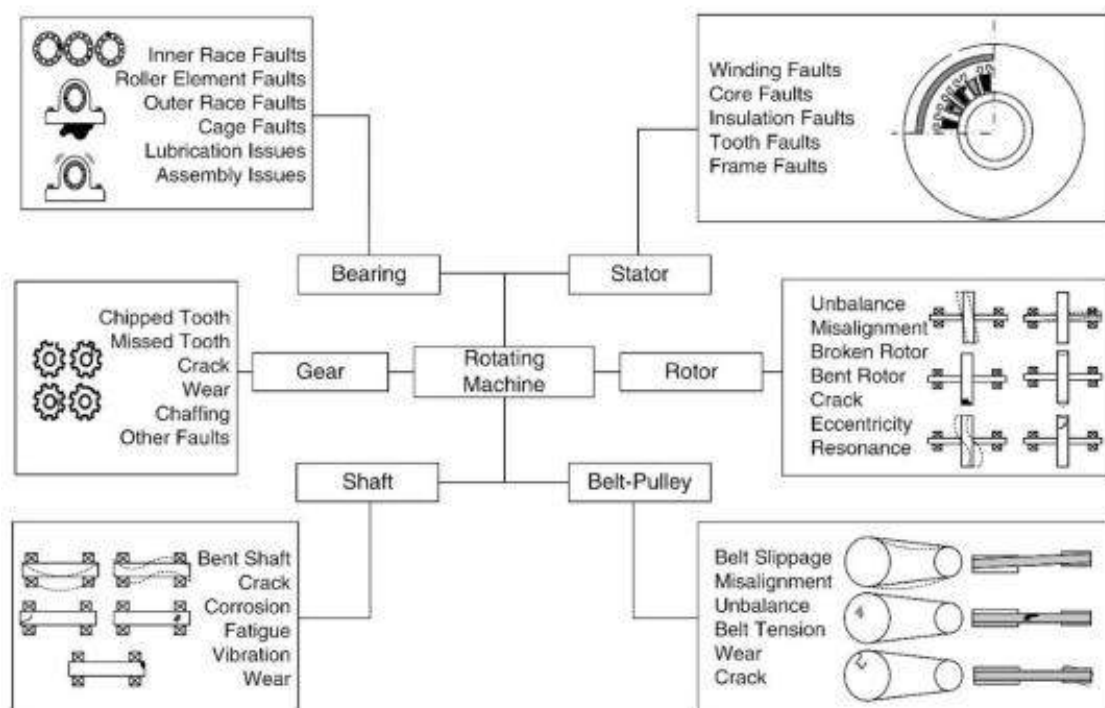
Figure 1. Components and faults in the rotating machine [1]

The Machine Fault Simulator (MFS) unit is a fault generator. An AC motor powers the shaft rotor assembly that makes up MFS. A rotating machine refers to a system where the components rotate around an axis to generate mechanical energy for numerous purposes. Such machines are utilized in pumping fluids, turbines, generators, fans, compressors robots and vehicles.

The fault diagnosis and prognosis procedures regarding a rotating machine are generally conducted on its components. Fig. 1 shows the parts of the rotating machinery including the fault types that may occur. It is seen in Fig. 1 that the common faults in rotating machinery are considered including shaft faults [3,4,5], bearing faults [3–6], gear faults [7,8], rotor faults [13–17], stator [18-19], and other component faults [20-23].

A transmission (also called a gearbox) is a mechanical device which uses a gear set—two or more gears working together to change the torque, direction of rotation, or speed multiplication/reduction in a machine [24-25]. Transmissions can have a single fixed-gear ratio, multiple distinct gear ratios, or continuously variable ratios. Variable-ratio transmissions are used in all sorts of machinery.

The objective of this work is to produce a laboratory-scale machine able to include the majority of the faults in gearbox rotating machinery including gear, bearing, shaft failures and lubrification issues. It must be designed, so that it is both easy to operate and versatile.
.

Method

Kinematic scheme and component assembly

The Machine fault simulator developed, must be a low-cost set-up and simple in manipulation. Additionally, fault diagnosis can be performed for the majority of gearbox rotating elements. Therefore, one needs to correctly choose the components. Furthermore, the components can be intentionally damaged removed and/or changed for specific sorts of tests.

The outcomes of the design process are given by figure 2 of the kinematic scheme and the figure 3-4 of the final motor gearbox assembly. In fact, after traying to manufacturing some components where the cost is relatively excessive, we decide to use one manufactured low-cost gearbox (1:24) disponible in the local market. The coupling system is also integrated with the gearbox supports and the actuator.

The feature of the simulator consists of a three-shaft with a gear on the first and the third one. The second shaft has two gears, all shafts are supported on six bearings. The AC electrical motor is the source of the rotating motion, which make it easy to control the speed by using SEIMENS control-unit. The mechanical components can be intentionally damaged removed and/or changed for specific sorts of tests.

The simulator is also able to output several signals from different sensor positions adjacent to the three rotating shafts and easy to operate(see figure.4).

Gear **Z4** : 64 tooths

OUTPUT   shaft 3

Gear **Z1** : 11 tooths   **INPUT**

shaft 1   Motor

Bearing R5   Bearing R4   Bearing R2
9 rollers   Bearing R1
11 rollers   Coupling system

shaft 2   Control Unit

Bearing R3
7 rollers   Gear **Z3** : 14 tooths   Bearing R3 : 7 rollers

Gear **Z2** : 58 tooths
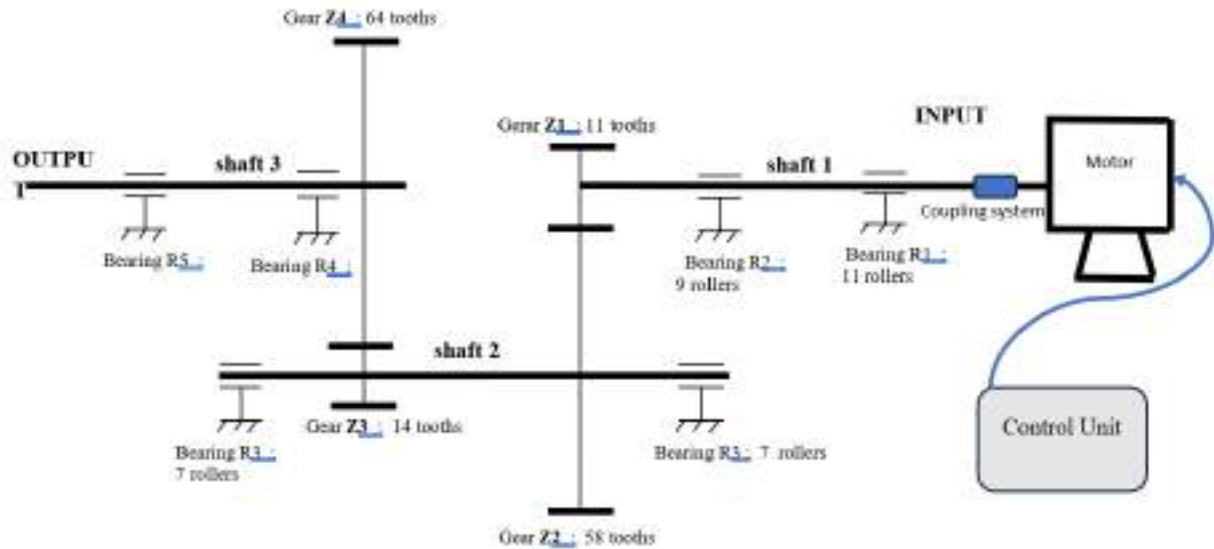
Figure 2. Kinematic scheme and the simulator components

Infrared Tachometer

Seimens CU

Motor JM74A4

Gearbox reducer : 1/24

Vibration Sensor
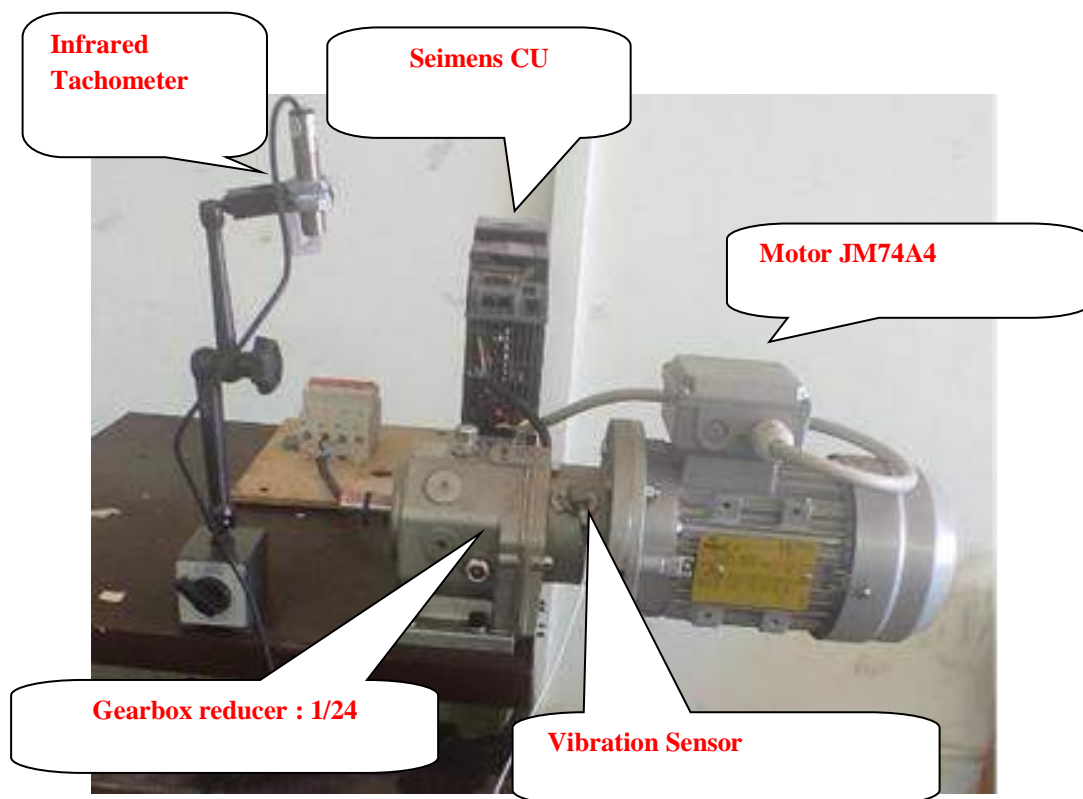
Figure 3. Machine fault simulator assembled in laboratory

Figure 4. Sensors positions in the fault simulator

Motor and speed variator

The fault simulator is driven by a three-phase asynchronous AC motor, the technical characteristics are: Shaft: Ø = 9 mm, l=20mm , P = 0.25kW , Nmax = 1330rpm Frequency = 50 Hz , voltage = 220-240/380-420V, Weight = 6 Kg. The three-phase Seipee induction motor properties are given by figure 5 and some inner components are given by figure 6.

The speed variation are electronic devices that allow speed and torque of motor to be varied. The speed variator developed by SIEMENS, is a voltage and frequency converter that generates a nearly constant rotational magnetic flow in the air gap of the induction motor. As its name suggests, SIEMENS controller is used to control the rotating frequency of the motor. It is programmed to varies between 500 and 1000 rpm

Figure 5. Motor used type SEIPEE JM71A4

Fig. 6 Iner components: rotating shaft, bearing and helicoidal gears

Results

Characteristic frequencies

In a vibration analysis, bearings and gears can manifest themselves in the vibration spectrum as peaks at specific frequencies. The system's INPUT rotational speed, expressed in rpm, is a crucial factor in determining the characteristic frequencies associated with bearings and gears.

- Bearing frequeny

The rolling element passing frequency, often called the bearing rotation frequency (f_{rb}), can be calculated

based on the motor rotation speed (RPM) and the number of rolling elements (N) using the formula:

$$f_{rb} = \frac{N \times RPM}{60} \ [Hz]$$

This frequency will usually appear as a peak in the vibration spectrum.

- Gear frequency

The rotation frequency of the gears (f_g) depends on the rotation speed of the motor (RPM) and the number of teeth of the gear (Z) according to the formula:

$$f_g = \frac{Z \times RPM}{60} \ [Hz]$$

In addition, the gears can generate harmonics of this rotation frequency depending on the characteristics of the gear and the operating conditions.

- Shaft frequency

For shafts, their contribution to the vibration spectrum can be more complex and will depend on several factors including the motor rotational speed, the shaft dimensions, the load characteristics, and any imbalance or misalignment.

These vibrations can manifest themselves in the vibration spectrum at different harmonic frequencies of the motor rotational speed with amplitudes greater than the rotational frequency [26-27].

Experimentation

Detection of rotational speed

We used a tachometer to measure the output rotation speed in revolutions per minute (N output= 46.15 RPM rpm) at the output of the gearbox reducer (1:24). That means that the input reducer speed witch is the motor speed is (N input =46.15x24=1107.6rpm). In order to ensure this speed, we applied a fast Fourier transform (FFT) on the data collected by using OROS 35 Analyzer and accelerometer sensor. Figure 7.

Table 1. Rotating shaft speed

Rotating shaft		Output shaft	Input shaft
speed N (rpm)		46.15	1107.6 (=46.15x24)
frequency (Hz)	Tachometer value	0.77 (=46.15/60)	18.46 (=1107.6/60)
	Spectrum value	0.8	18.5

This FFT analysis made it possible to detect the rotational frequency, materialized by the appearance of a

distinct peak at 18.46 Hz in the frequency spectrum. This peak corresponds to the input rotation frequency, thus confirming the accuracy of our measurements obtained by the tachometer. In addition, the input frequency (INPUT), set by the control unit (CU), is 24 times higher than the input speed, and this INPUT frequency also appears as a peak at 0.76 Hz in the frequency spectrum, thus validating our control of the system.

Table 1 illustrates the frequency values obtained with a slight shift between the tachometer value and that of the spectrum. This is mainly due to two essential parameters:

- Place a regulator to fix the speed at the CU output
- Increase the resolution of the spectrum, which generates more calculation.
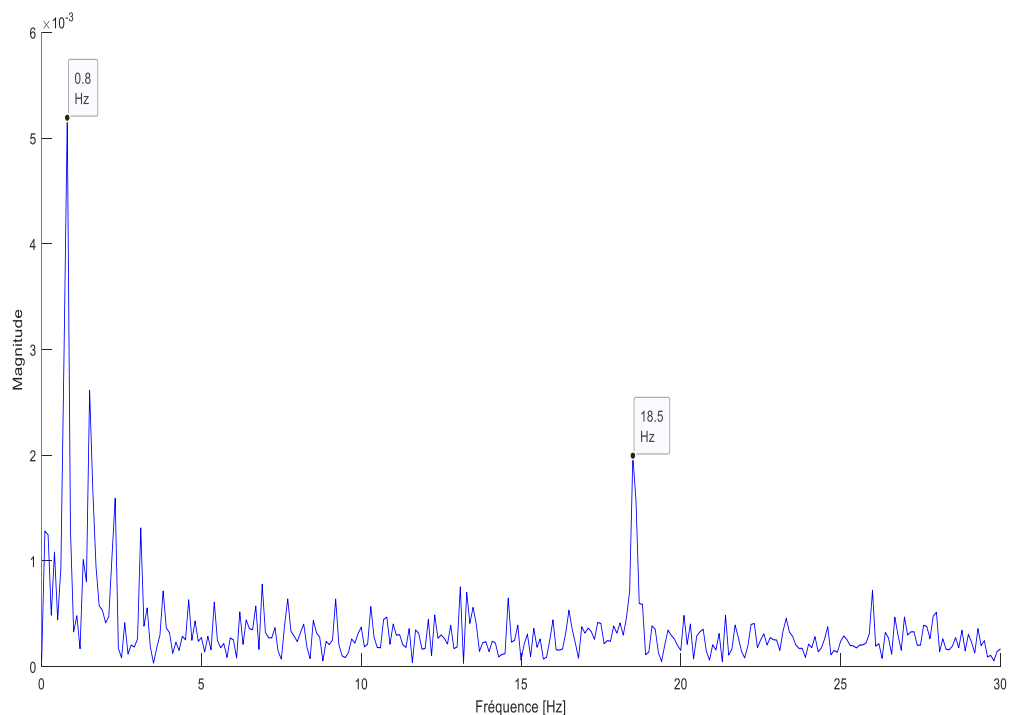
Figure 7. Detection of INPUT and OUTPUT speed peaks

Misalignment Detection

Figure 8 shows the spectrum of the data collected by the vibration sensor positioned on our test bench. A distinct peak is observed at 0.8 Hz, corresponding to the output rotation frequency (N = 46.15 rpm). Harmonics also appear at 1.5 Hz and 2.3 Hz, probably due to a small misalignment of this shaft.

Another peak is noted at 18.5 Hz, corresponding to the input rotation frequency. In addition, a significant harmonic at 37.8 Hz, of higher amplitude, is present. This high harmonic could be attributed to a considerable imbalance of the input shaft 1 .
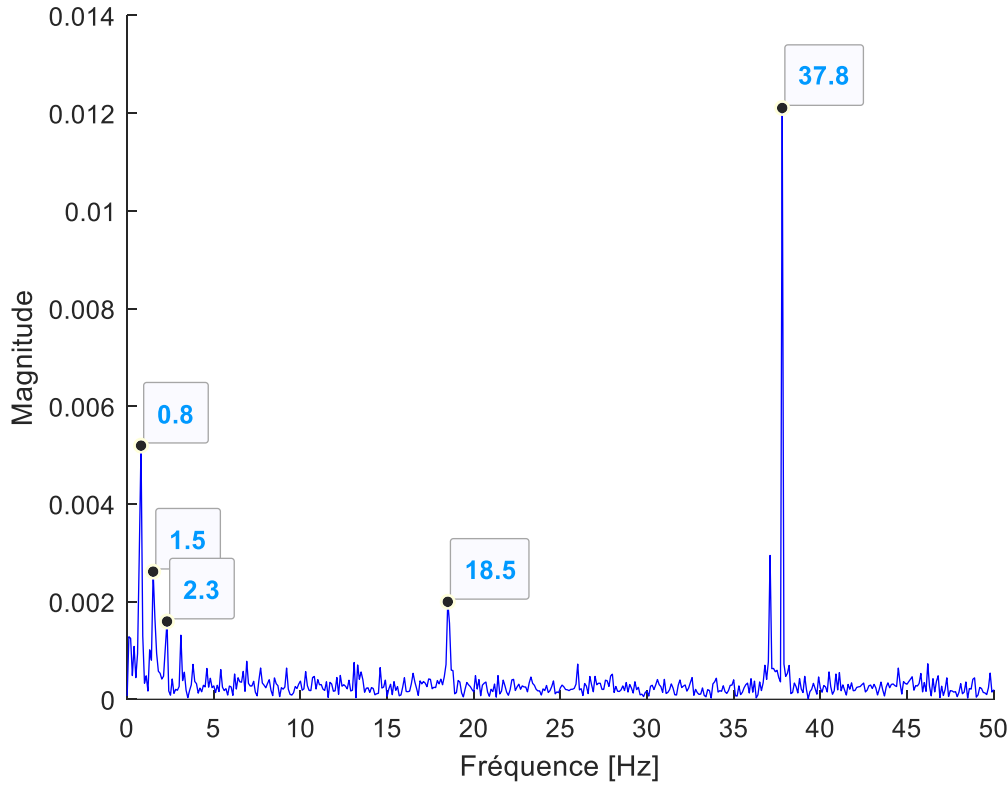
Figure 8. Detection of peaks due to alignment defects

Bearing frequency detection

Our test bench contains bearings with 7, 9, and 11 roller elements . Using the input rotation frequency (INPUT), which is 46.15 RPM multiplied by 24, or 1107.6 RPM, we calculated the rolling frequencies for these bearings:

- For 7-rolling element bearings

$$f_{rb} = \frac{N \times RPM}{60} = \frac{7 \times 1107.6}{60} = 129.22 \; [Hz]$$

- For 9-rolling element bearings

$$f_{rb} = \frac{9 \times 1107.6}{60} = 166.14 \; [Hz]$$

- For 11-rolling element bearings

$$f_{rb} = \frac{11 \times 1107.6}{60} = 203.06 \; [Hz]$$

Thus, the rolling frequencies for the 7-, 9-, and 11-element bearings are approximately 129.22 Hz, 166.14 Hz, and 203.06 Hz, respectively. These frequencies appear as peaks in the vibration spectrum shown in Figure 9.
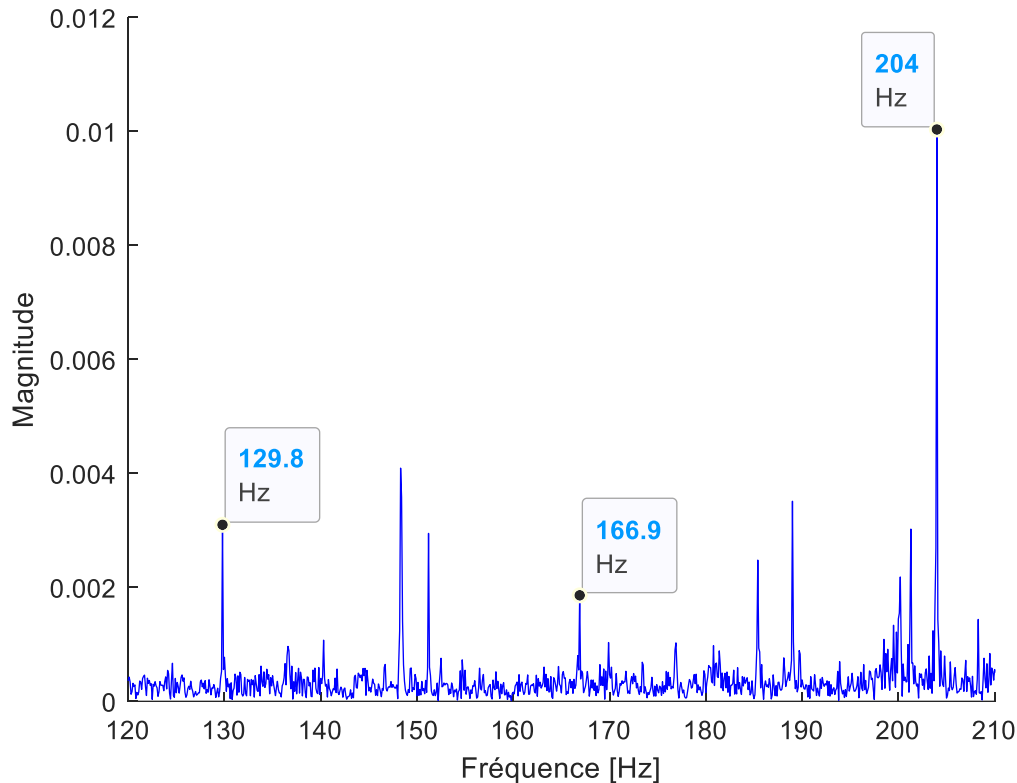
Figure 9. Detection of rolling frequency peaks

Conclusion

The dynamic Fault simulator is an essential tool for vibration analysis in machine monitoring. It was carried out with the aim of allowing to understand and to analyze the various defects of gearbox affected by lubrication, wears, noise, vibration, moisture, and dust. The simulator in question will allow both students and researchers to simulate and intentionally create the following vibration defects:

- Bearing defects.
- Gear faults
- misalignment
- Lubrification defects

The vibration analysis for machine monitoring and diagnosis typically consists of three main steps, which are data acquisition, signal processing, and fault recognition.

By reviewing the motor specifications and performing vibration analysis tests using Fast Fourier Transform (FFT) on the resulting signals, we were able to identify characteristic frequencies associated with the bearings, gears and shafts in the system. The results revealed the importance of carefully monitoring components and detecting any potential imbalances or defects, highlighting the crucial impact of vibration analysis on failure prevention.

While we have successfully detected the frequencies associated with the system components with precision, challenges remain in interpreting the vibration spectra, particularly for higher frequencies. This highlights the need to develop more sophisticated analysis methods and continue research in this area. The first prototype of gearbox fault simulator of this work can be upgraded and improved in the future prototypes including other faults simulation.

Acknowledgements

References

Chitresh Nayak, Vimal Kumar Pathak, Sagar Kumar, Prashant Athnekar.Design And Development Of Machine Fault Simulator (Mfs) For Fault Diagnosis, International Journal of Recent advances in Mechanical Engineering (IJMECH) Vol.4, No.4, November 2015.

Oguzhan Das, Duygu Bagci Das , Derya Birant, Machine learning for fault analysis in rotating machinery: A comprehensive review, Heliyon 9 (2023) e17584.

J. Xiong, Q. Zhang, Z. Peng, G. Sun, W. Xu, Q. Wang, A diagnosis method for rotation machinery faults based on dimensionless indexes combined K-nearest neighbor algorithm, Math. Probl Eng. (2015), https://doi.org/10.1155/2015/563954 (2015) 1–9.

M. Kang, J.-M. Kim, Reliable Fault diagnosis of multiple induction motor defects using a 2-D representation of Shannon wavelets, IEEE Trans. Magn. 50 (2014)1–13,

 https://doi.org/10.1109/tmag.2014.2316474.

M.A. Hassan, M.R. Habib, R.A. Abul Seoud, A.M. Bayoumi, Wavelet-based multiresolution bispectral analysis for detection and classification of helicopter drive-shaft problems, J. Dyn. Syst. Meas. Control 140 (2017), https://doi.org/10.1115/1.4038243.

H. Cao, H. Shao, B. Liu, B. Cai, J. Cheng, Clustering-Guided novel unsupervised domain adversarial network for partial transfer Fault Diagnosis of rotating machinery, IEEE Sensor. J. 22 (2022) 14387–14396, https://doi.org/10.1109/jsen.2022.3182727.

 R.A. Patel, B.R. Bhalja, Condition monitoring and Fault Diagnosis of induction motor using support vector machine, Elec. Power Compon. Syst. 44 (2016) 683–692, https://doi.org/10.1080/15325008.2015.1131762.

D. Cabrera, F. Sancho, R.-V. S´ anchez, G. Zurita, M. Cerrada, C. Li, R.E. Vasquez, ´ Fault diagnosis of spur gearbox based on random forest and wavelet packet decomposition, Front. Mech. Eng. 10 (2015) 277–286, https://doi.org/10.1007/s11465-015-0348-8.

B. Merainani, C. Rahmoune, D. Benazzouz, B. Ould-Bouamama, A novel gearbox fault feature extraction and classification using Hilbert empirical wavelet transform, singular value decomposition, and SOM

neural network, J. Vib. Control 24 (2017) 2512–2531, https://doi.org/10.1177/1077546316688991.

A. Yin, Y. Yan, Z. Zhang, C. Li, R.-V. Sanchez, ´ Fault diagnosis of wind turbine gearbox based on the optimized LSTM neural network with cosine loss, Sensors 20 (2020) 2339, https://doi.org/10.3390/s20082339.

G. Krishna Durbhaka, B. Selvaraj, M. Mittal, T. Saba, A. Rehman, L. Mohan Goyal, Swarm-LSTM: condition monitoring of gearbox Fault Diagnosis based on hybrid LSTM deep neural network optimized by swarm intelligence algorithms, Comput. Mater. Continua (CMC) 66 (2021) 2041–2059, https://doi.org/10.32604/cmc.2020.013131

J. Shi, D. Peng, Z. Peng, Z. Zhang, K. Goebel, D. Wu, Planetary gearbox fault diagnosis using bidirectional-convolutional LSTM networks, Mech. Syst. Signal Process. 162 (2022), https://doi.org/10.1016/j.ymssp.2021.107996.

N. Lu, Z. Xiao, O.P. Malik, Feature extraction using adaptive multiwavelets and synthetic detection index for rotor fault diagnosis of rotating machinery, Mech. Syst. Signal Process. 52–53 (2015) 393–415, https://doi.org/10.1016/j.ymssp.2014.07.024.

S. Altaf, M.W. Soomro, M.S. Mehmood, Fault Diagnosis and Detection in Industrial Motor Network Environment Using Knowledge-Level Modelling Technique, Modelling and Simulation in Engineering, 2017, pp. 1–10, https://doi.org/10.1155/2017/1292190, 2017.

S. Zgarni, H. Keskes, A. Braham, Nested SVDD in DAG SVM for induction motor condition monitoring, Eng. Appl. Artif. Intell. 71 (2018) 210–215, https://doi.org/10.1016/j.engappai.2018.02.019.

B. Wu, S. Feng, G. Sun, L. Xu, C. Ai, Fine-grained fault recognition method for shaft orbit of rotary machine based on convolutional neural network, Journal of Vibroengineering 21 (2019) 2106–2120, https://doi.org/10.21595/jve.2019.20359.

V. Biot-Monterde, A. Navarro-Navarro, I. Zamudio-Ramirez, J.A. Antonino-Daviu, R.A. Osornio-Rios, Automatic classification of rotor faults in soft-started induction motors, based on persistence spectrum and convolutional neural network applied to stray-flux signals, Sensors 23 (2022) 316, https://doi.org/10.3390/s23010316.

M. Seera, C.P. Lim, D. Ishak, H. Singh, Application of the fuzzy min–max neural network to fault detection and diagnosis of induction motors, Neural Comput. Appl. 23 (2013) 191–200, https://doi.org/10.1007/s00521-012-1310-x

W. Sun, S. Shao, R. Zhao, R. Yan, X. Zhang, X. Chen, A sparse auto-encoder-based deep neural network approach for induction motor faults classification, Measurement 89 (2016) 171–178, https://doi.org/10.1016/j.measurement.2016.04.007.

H. Sun, K. Li, P. Chen, H. Wang, X. Ping, Y. Cao, A sequential fuzzy diagnosis method for rotating machinery using ant colony optimization and possibility theory, J. Mech. Sci. Technol. 28 (2014) 1189–1201, https://doi.org/10.1007/s12206-014-0112-8.

X. Jin, J. Feng, S. Du, G. Li, Y. Zhao, Rotor fault classification technique and precision analysis with kernel principal component analysis and multi-support vector machines, Journal of Vibroengineering 16 (2014).

R. Chen, S. Chen, L. Yang, J. Wang, X. Xu, T. Luo, Looseness diagnosis method for connecting bolt of fan

foundation based on sensitive mixed-domain features of excitation-response and manifold learning, Neurocomputing 219 (2017) 376–388, https://doi.org/10.1016/j.neucom.2016.09.041.

J. Liu, G. Yang, X. Li, S. Hao, Y. Guan, Y. Li, A deep generative model based on CNN-CVAE for wind turbine condition monitoring, Meas. Sci. Technol. 34 (2023), 035902, https://doi.org/10.1088/1361-6501/aca496.

J. J. Uicker; G. R. Pennock; J. E. Shigley (2003). Theory of Machines and Mechanisms (3rd ed.). New York: Oxford University Press. ISBN 9780195155983.

B. Paul (1979). Kinematics and Dynamics of Planar Machinery. Prentice Hall.

Boulenger, A., & Pachaud, C. (2009). Surveillance des machines par analyse des vibrations.

Melih Asma , Mesaoudene Fethi, Localisation des Défauts Mécaniques par l'Analyse Spectral, Mémoire inédit présenté en vue de l'obtention d'un master en Génie Electrique option Instrumentation, , Université Abou Bekr Belkaid, Faculté de Technologie, Tlemcen, Algerie,2024

Initial Principal Study of Electronic and Optical Behavior in Ga-Doped Zno Across Varying Concentrations

Berrezoug Hiba Imane

Theoretical Physics Laboratory, Abou-Bekr Belkaïd University, P.O. Box 119, 13000, Tlemcen, Algeria

Sari Hassoun Zakaria

MECACOMP, Mechanical Engineering Department, Abou-Bekr Belkaid University, P.O. Box 119 13000 Tlemcen, Algeria

Benramdane Mohammed

ETAP Laboratory, Abou-Bekr Belkaïd University, P.O. Box 119 13000 Tlemcen, Algeria

Abstract: The structural, electronic, and optical properties of pure and Ga-doped ZnO (GZO) with varying Ga concentrations (6.25%, 12.5%, and 25%) were studied using the ab initio full-potential linearized augmented plane wave (FP-LAPW) method. This study employed the generalized gradient approximation (GGA) and the modified Becke–Johnson (mBJ) exchange potential to explore the effects of Ga doping on various material properties. Electronic properties such as the band structure and density of states, along with optical properties including the dielectric function $\varepsilon(\omega)$, refractive index $n(\omega)$, reflectivity $R(\omega)$, and electron energy-loss spectrum $L(\omega)$, were analyzed. The lattice constants and optical band gap of pure ZnO (3.27 eV) were consistent with experimental data. Ga doping introduced shallow donor states (Ga-4s) near the Fermi level, leading to an increase in both the optical band gap and electrical conductivity. Furthermore, the absorption edge and other optical parameters shifted to higher energies with increasing Ga concentration. The reflectivity and refractive index of GZO also increased with higher Ga content. The $L(\omega)$ spectrum revealed enhanced metallic character in GZO, with two peaks: one near 2 eV due to Ga doping, and another at higher energies, indicating that Ga incorporation enhances the metallic nature of ZnO.

Keywords: FP-LAPW method, Ga-doped ZnO, mBJ potential, electronic structures, optical properties

Introduction

Transparent conducting oxides (TCOs) have been extensively studied for their use in optoelectronic devices due

to their unique combination of low absorption and reflectivity, along with high electrical conductivity and optical transparency in the visible spectrum [1]. Among potential TCO materials, ZnO is emerging as a promising alternative to indium tin oxide (ITO), which is widely used in commercial applications but is associated with issues of high toxicity, scarcity, and cost of indium [2,3]. Therefore, there is an increasing need to develop high-performance, cost-effective TCO materials, particularly from the ZnO family, while enhancing their electronic and optical properties through doping strategies.

To address this challenge, Lalanne et al. [4], Phan et al. [5], and others [6- 8] have proposed doping ZnO with gallium (Ga) atoms, offering a promising solution for TCO applications. Ga, acting as an n-type dopant, can enhance the carrier concentration in ZnO, thereby improving its conductivity. Moreover, Yamamoto and Katayama-Yoshida demonstrated through first-principles calculations that co-doping with Ga (as donor) and nitrogen (N, as acceptor) is highly effective for producing low-resistivity p-type ZnO [9, 10]. This approach was successfully realized, achieving a resistivity of 2 $\Omega \cdot$cm and a hole concentration of 4×10^{19} cm^{-3} at room temperature [11].

In the new compound, known as GZO (gallium-doped ZnO), Ga^{3+} ions substitute Zn^{2+} ions in the lattice, and due to the similar ionic radii of Ga^{3+} (0.06 nm) and Zn^{2+} (0.062 nm), this substitution occurs with minimal distortion to the host lattice [12, 13]. The covalent bond lengths of Ga–O (0.192 nm) and Zn–O (0.197 nm) are also quite similar [14], further facilitating this substitution. With their low cost, high transmittance (up to 90%) in the visible spectrum, low resistivity (down to 10^{-4} $\Omega \cdot$cm), and wide optical band gap, GZO films are considered a compelling alternative to Sn-doped In_2O_3 (ITO) films for TCO applications [15, 16].

Previous studies on Ga-doped ZnO (GZO) have focused on a limited range of gallium concentrations, with a maximum of 10.81% [4–8]. However, these publications do not thoroughly explain how the properties of GZO vary with increasing Ga incorporation in the ZnO lattice, despite the importance of optimizing Ga concentration for the design of optoelectronic devices. In this contribution, we investigate the structural, electronic, and optical properties of Ga-doped ZnO ($Zn_{1-x}Ga_xO$) for different Ga concentrations (x = 6.25%, 12.5%, and 25%). The results are obtained using the full potential linearized augmented plane-wave plus local orbital (FP-(L)APW + lo) method, within the framework of density functional theory (DFT), utilizing the modified Becke–Johnson (mBJ) exchange potential.

This paper is structured as follows: In the second section, a brief overview of the calculation method is presented. The third section analyzes the obtained results in relation to dopant concentration, comparing them with findings from existing literature. Finally, the conclusion is provided in the last section.

Calculation Method

The structural, electronic, and optical properties of both pure ZnO and Ga-doped ZnO were examined. Total

energies and all derived quantities were calculated using the full-potential linearized augmented plane wave (FP-LAPW) method, as implemented in the WIEN2K package [17]. This method relies on first-principles calculations based on density functional theory (DFT), specifically through the self-consistent solution of the Kohn–Sham (KS) equations [18] in two regions: the muffin-tin sphere and the interstitial space. It has become one of the most widely used and accurate methods for calculating the band structure of solids.

In our computations, the structural properties were determined using the Generalized Gradient Approximation (GGA) as parameterized by Perdew et al.[19] This potential is known to accurately reproduce the band structure of complex metallic systems, but it can underestimate the band gap of semiconductors by up to 50% compared to experimental values. To address this limitation, we employed the modified Becke–Johnson (mBJ) exchange-correlation potential for our calculations of electronic and optical properties, as introduced by Tran and Blaha.[20] This potential has been shown to reliably reproduce the experimental band gaps for a wide range of semiconductors and insulators. Convergence tests revealed that using 100 k-points and 75 k-points in the irreducible part of the Brillouin zone is adequate for achieving good accuracy in total energy minimization for ZnO and Ga-doped ZnO (GZO), respectively.

The energy cut-off for the plane wave expansions in the interstitial region, defined by $R_{MT}K_{max}$, was set to 8.5 for ZnO and 7 for GZO. Here, R_{MT} represents the smallest radius of the muffin-tin spheres, while K_{max} denotes the maximum value of the reciprocal lattice vectors used in the plane wave expansion. The muffin-tin atomic sphere radii (R_{MT}) were set to 1.84 nm for Zn, 1.77 nm for Ga, and 1.5 nm for O atoms. The Fourier charge density parameter G_{max} was set to 12 (Ry). For the wave expansion within the atomic spheres, the maximum quantum number l_{max} was chosen to be 10. This study focused on investigating the effects of varying concentrations of Ga in ZnO, where Zn atoms are substituted with Ga atoms. This study investigated the impact of varying concentrations of Ga in ZnO, where Zn atoms are substituted by Ga atoms. The supercell models considered for Ga concentrations of 6.25%, 12.5%, and 25% consist of 32 atoms with dimensions of $(2 \times 2 \times 2)$, 16 atoms with dimensions of $(1 \times 2 \times 2)$, and 8 atoms with dimensions of $(1 \times 1 \times 2)$, respectively.

Results and Discussion

Structural Optimization and Properties

In this section, we discuss the structural optimization and properties of both pure ZnO and Ga-doped ZnO. Structural optimization involves minimizing the total energy of the system to determine the most stable arrangement of atoms. The calculations were performed for different concentrations of Ga (6.25%, 12.5%, and 25%), allowing us to analyze how Ga substitution affects the lattice parameters and overall structure of ZnO. Hexagonal wurtzite structure ZnO, characterized by a space group symmetry of P63-mc. The experimentally determined lattice parameters for pure ZnO are a=b=3.25 Å, c=5.2066 Å, with angles α=β=90 and γ=120 [21]. To optimize the lattice parameters, we calculated the total energy as a function of the unit cell volume around the equilibrium cell volume V_0, and the ratio c/a for both pure and Ga-doped ZnO using different supercell

models. The optimized lattice parameters for pure ZnO were determined to be a=b=3.294 Å and c=5.252 Å, which align well with various theoretical and experimental results [21–23].

Table 1 presents the lattice parameters, bulk modulus, and pressure derivative for Ga-doped ZnO ($Zn_{1-x}Ga_xO$) at different Ga concentrations (x = 6.25%, 12.5%, and 25%). It was observed that the lattice parameters increase proportionally with Ga concentration, consistent with findings from other studies [24]. Additionally, the calculated bulk modulus indicates that $Zn_{0.75}Ga_{0.25}O$ exhibits greater rigidity compared to pure ZnO, as it corresponds to the lowest volume among the samples with 6.25% and 12.5% Ga concentrations.

Table 1. Calculated Results of Lattice Parameters, Bulk Modulus And Its Pressure Derivate For $Zn_{1-x}Ga_xO$ At Different Ga Concentrations.

X (%)	a (Å)		c (Å)		B_0 (GPa)		B'	
	Our cal.	Others	Our Cal.	Others	Our cal.	Others	Our cal.	Others
0	3.294	3.25 [24], 3.258 [25]	5.252	5.232 [24], 5.221 [25]	129.135	—	4.424	—
6.25	3.298	3.254 [24], 3.2641 [25]	5.255	5.255 [24], 5.243 [25]	127.463	—	4.583	—
12.5	3.299	3.256 [24]	5.377	5.283 [24]	124.934	—	4.598	—
25	3.311	3.261 [24]	5.379	5.318 [24]	120.868	—	4.607	—

Band Structures and Density of States:

The calculated band structures and density of states (DOS) for pure ZnO and Ga-doped ZnO ($Zn_{1-x}Ga_xO$) at concentrations of x = 0%, 6.25%, 12.5%, and 25% were analyzed, as these properties are closely linked to the optical characteristics of the materials. Figure 1 presents the band structures obtained using the modified Becke–Johnson (mBJ) exchange potential. The Fermi level was set to 0 eV for reference. As depicted in Figure 1(a), the minimum of the conduction band and the maximum of the valence band for pure ZnO are located at the same K-point (Γ), confirming that ZnO is a direct-gap semiconductor, with an estimated band gap of approximately 3.27 eV. This value aligns well with other theoretical calculations [26, 27] and is consistent with experimental findings [28–30].

Upon doping ZnO with Ga, new occupied states appear at the bottom of the conduction band due to the higher valence of Ga compared to Zn. This results in an upward shift of the Fermi level into the conduction band, as illustrated in Figures 1(b)–(d), indicating the characteristics of a degenerate n-type semiconductor. The calculated optical band gaps for $Zn_{1-x}Ga_xO$ at concentrations of x=25%, 12.5%, and 6.25% were found to be 4.33 eV, 4.05 eV, and 3.78 eV, respectively. Furthermore, these band gap values are greater than that of pure ZnO, indicating that the substitution of Zn with Ga in the different supercells leads to an increase in the band gap.
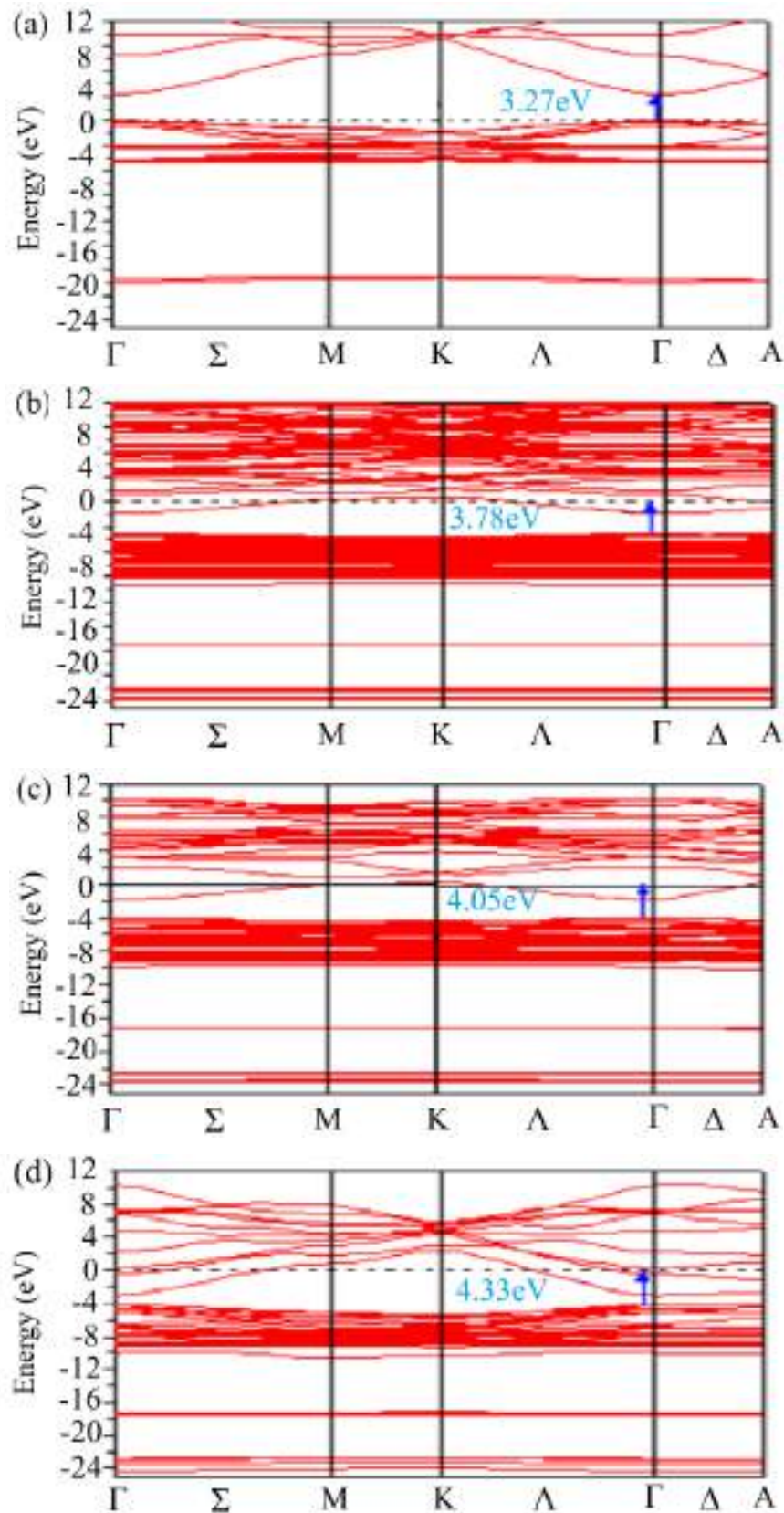
Figure 1. Calculated Band Structure Of: (a) Pure ZnO; (b) Zn0.9375 Ga0.0625O; (c) Zn0.875 Ga0.125O; (d)Zn0.75 Ga0.25O.

Figure 2 illustrates the total and partial densities of states (TDOS and PDOS) for both pure and Ga-doped ZnO at various concentrations. In the case of undoped ZnO, depicted in Figure 2 (a), the lower portion of the valence band (around -20 eV) is primarily attributed to the O-2s orbitals. In contrast, the upper part of the valence band (between -5 eV and 0 eV) is predominantly composed of Zn-3d and O-2p orbitals, which contribute to the p-d coupling. The lower part of the conduction band is mainly formed by Zn-4s and O-2p orbitals. As shown in Figures 2 (b)–(d), when one Zn atom is substituted by one Ga atom at varying concentrations, a localized Ga-3d orbital emerges in the lower region of the valence band. This Ga-3d orbital shifts to higher energy levels with increasing Ga concentration. The energies observed for the Ga-doped ZnO (GZO) compounds are approximately ~ -24 eV, ~ -17.5 eV, and ~ -17 eV for dopant concentrations of 6.25%, 12.5%, and 25%, respectively. This trend highlights how Ga doping influences the electronic structure of ZnO by modifying the distribution of electronic states within the band structure. The O-2s orbitals shift to lower energy levels (approximately -22.66 eV) and maintain this position across all Ga concentrations. The Ga-4s and Ga-4p orbitals contribute to the formation of the lower part of the conduction band. Notably, the Fermi level resides within the conduction band and rises towards the top of this band as the Ga concentration increases. This behavior indicates that the number of electrons in the conduction band is not constant. Furthermore, the occupied states of electrons near the Fermi level in the conduction band are influenced by the concentrations of donor species. The width of occupied states are 1.19 1.57 2.92 for 6.25%, 12.5%, and 25%, respectively, these occupied states, increases with Ga concentration, leading to enhanced conductivity. Our findings align well with those presented by Wu et al. in [31], which were obtained using the CASTEP code. These occupied states create an additional energy barrier that must be overcome for electron excitation from the valence band to the conduction band.
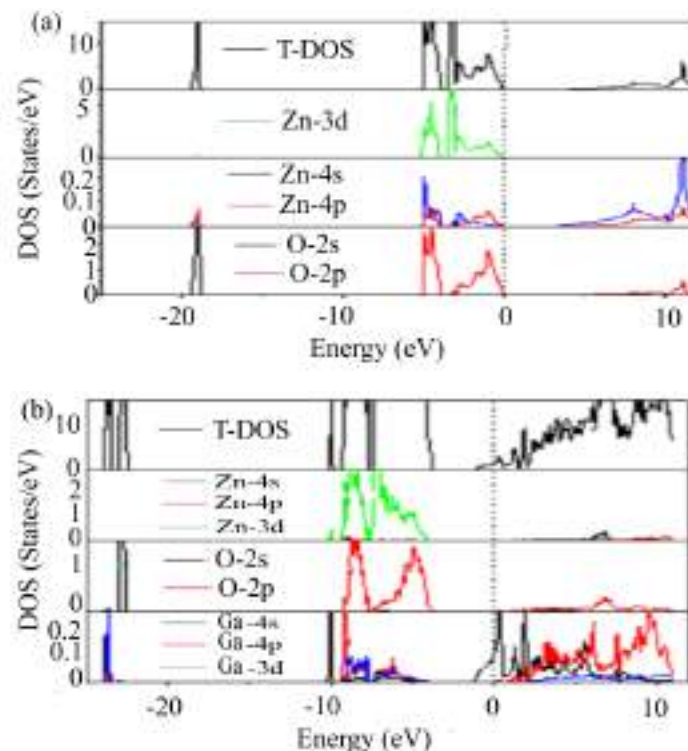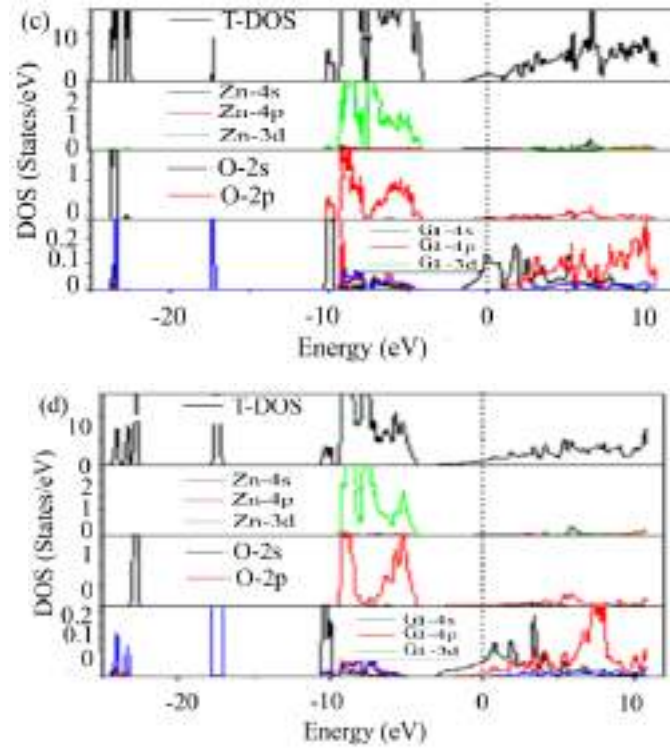
Figure 2. Total And Partial Density Of States For: (a) Pure ZnO; Ga doped ZnO (b) 6.25%; (c) 12.5% (d) 25%.

Optical Properties

The optical properties of pure and Ga-doped ZnO are described through the dielectric function $\varepsilon(\omega)$, which is expressed as the sum of its real and imaginary components: $\varepsilon(\omega)=\varepsilon_1(\omega)+i\varepsilon_2(\omega)$.

The imaginary part, $\varepsilon_2(\omega)$, is directly related to the electronic band structure and can be calculated from the momentum matrix elements between the occupied and unoccupied electronic states [32]. The real part, $\varepsilon_1(\omega)$, can be derived using the Kramers–Kronig transformation, which connects the real and imaginary parts of the dielectric function [33]. Furthermore, both $\varepsilon_1(\omega)$ and $\varepsilon_2(\omega)$ can be used to determine several key optical properties, including the refractive index $n(\omega)$, the reflectivity $R(\omega)$, and the electron energy loss function $L(\omega)$, using the following relationships:

$$n(\omega) = \sqrt{\varepsilon_1(\omega) + i\varepsilon_2(\omega)} \qquad (1)$$

$$R(\omega) = \left| \frac{1 - n(\omega)}{1 + n(\omega)} \right|^2 \qquad (2)$$

$$L(\omega) = \mathrm{Im}\left(-\frac{1}{\varepsilon_1(\omega) + i\varepsilon_2(\omega)} \right) \qquad (3)$$

Figure 3 (a) presents the imaginary part of the dielectric function, $\varepsilon_2(\omega)$, for ZnO and Ga-doped ZnO (GZO) at various Ga concentrations. For pure ZnO, three main peaks, labeled 'a', 'b', and 'c', are observed at 4.15 eV, 9.18 eV, and 14.84 eV, respectively. These peaks correspond to transitions between the following states:

- **Peak 'a'**: Transition between Zn-4s and O-2p states

- **Peak 'b'**: Transition between Zn-3d and O-2s states
- **Peak 'c'**: Transition between Zn-3d and O-2p states

For Ga-doped ZnO, additional occupied states appear, resulting in a new peak labeled 'o', which occurs at 1.05 eV, 1.2 eV, and 1.6 eV for Ga concentrations of 6.25%, 12.5%, and 25%, respectively. This peak increases in intensity with higher Ga concentrations. Additionally, a second peak appears at 2.96 eV for the 25% Ga concentration, likely due to the larger width of the occupied states at this concentration.

Figure 3 (b) shows the real part of the dielectric function, $\varepsilon_1(\omega)$, for both pure and Ga-doped ZnO. For pure ZnO, three peaks appear at 3.65 eV, 8.59 eV, and 13.62 eV, which correspond to the same electronic transitions observed in $\varepsilon_2(\omega)$. After the third peak, $\varepsilon_1(\omega)$ decreases, approaching zero and becoming negative, before reaching a minimum value. At higher energies, it increases again towards 0 and eventually stabilizes near 1. For the Ga-doped ZnO (GZO) system, a sharp decline in the real part of the dielectric function, $\varepsilon_1(\omega)$ is observed around 0.65 eV, 0.90 eV, and 1.06 eV for Ga concentrations of 6.25%, 12.5%, and 25%, respectively. After this steep drop, $\varepsilon_1(\omega)$ approaches zero, becomes negative, and reaches a minimum value. Finally, it begins to rise again as the energy increases.
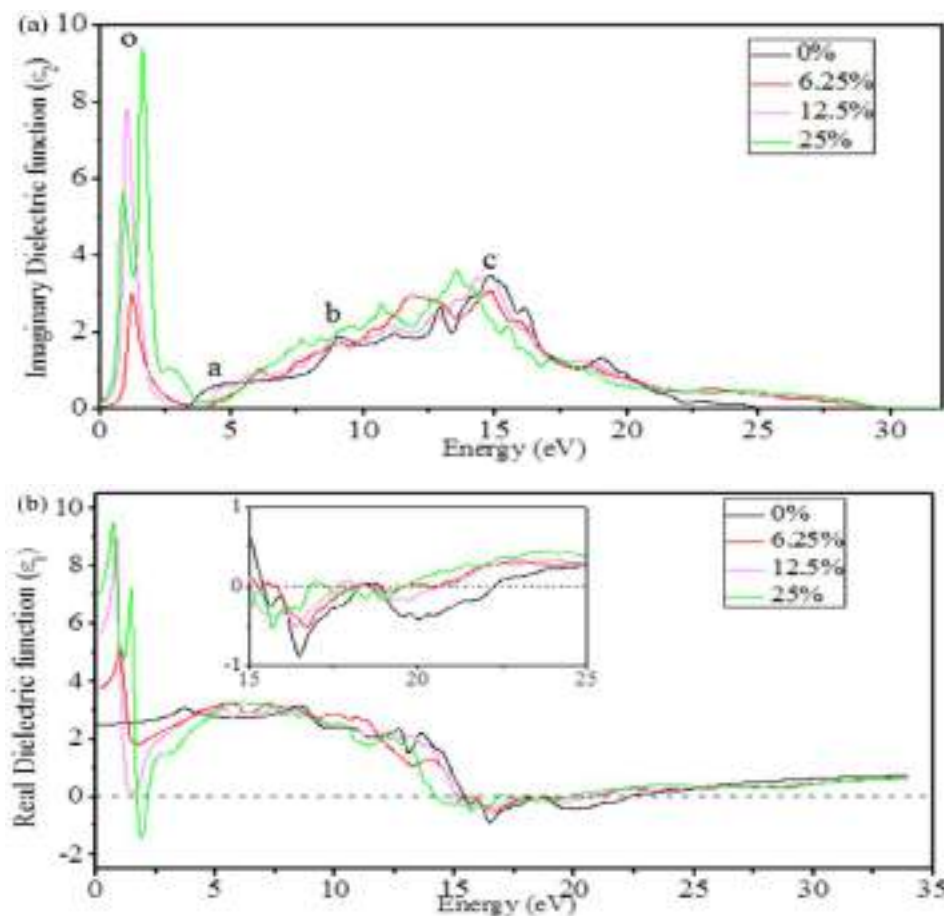
Figure 3**.** (a) The Imaginary, (b) The Real Part Of The Dielectric Functions For Various Ga Concentrations.

To emphasize the changes in the optical properties of Ga-doped ZnO compared to pure ZnO, we calculated the refractive index $n(\omega)$, reflectivity $R(\omega)$, and energy loss spectrum $L(\omega)$ using the relevant equations. The variations in the transition states observed in the imaginary dielectric function $\varepsilon_2(\omega)$ are also evident in both the refractive index $n(\omega)$ and reflectivity $R(\omega)$, as shown in Figures 4 and 5, respectively. Between 13 eV and 27 eV, the reflectivity of Ga-doped ZnO decreases when compared to pure ZnO, with only slight differences based on the Ga concentration. The static dielectric constant $\varepsilon_1(0)$, refractive index $n(0)$, and reflectivity $R(0)$ at zero energy for different Ga concentrations are presented in Table 2. The energy loss function $L(\omega)$ (figure 6) describes the energy lost by a fast electron traveling through the material. Its main peak is associated with the bulk plasma frequency ωp, which occurs when $\varepsilon_2(\omega)<1$ and $\varepsilon_1(\omega)$ equals zero . For pure ZnO, the peak of $L(\omega)$ is located at 22.30 eV. This peak diminishes in magnitude as Ga doping increases, and the corresponding energy rises from 25 eV to 31 eV, indicating that the metallic properties are maintained up to 31 eV. This reveals the significance of n-type doping. We deduce that the metallic nature of pure ZnO, characterized by a pronounced peak in $L(\omega)$ is stronger than in Ga-doped ZnO. We attribute this difference to the more homogeneous distribution of Zn ions in pure ZnO, leading to a higher degree of structural order. In contrast, Ga-doped ZnO, which contains both Zn and Ga ions, shows greater disorder due to the variation in the electronic and physical properties of these ions, leading to increased energy losses. The peaks in the energy loss curves represent transitions from positive to negative values of $\varepsilon_1(\omega)$, signifying a shift from metallic to dielectric behavior. The occupied states in Ga-doped ZnO are further identified by the second peak at around 2.6 eV.

Table 2. Calculated Optical Parameters for $Zn_{1-x}Ga_xO$ At Different Ga Concentrations.

Concentrations x(%)	Static dielectric constant $\varepsilon_1(0)$	Refractive index n(0)	Reflectivity R(0)
0	2.50	1.59	0.05
6.25	3.78	1.94	0.10
12.5	5.62	2.36	0.16
25	6.98	2.65	0.20
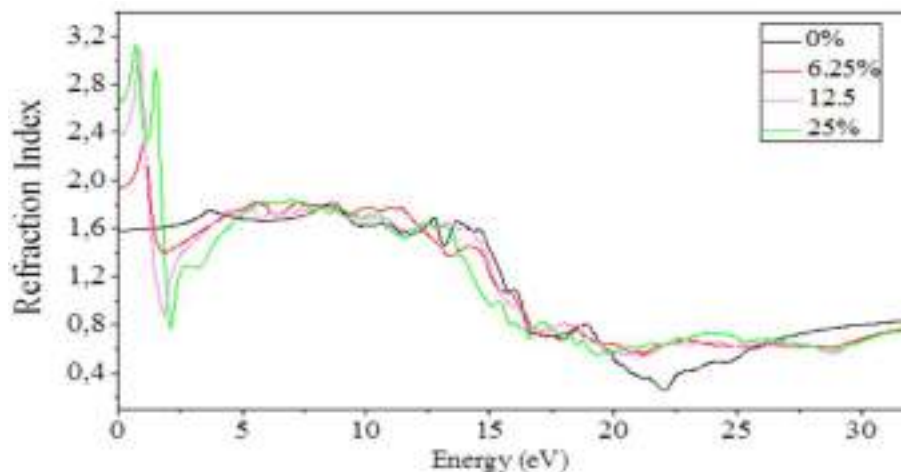
Figure 4. The Variation of The Refraction Index For Various Ga Concentrations.
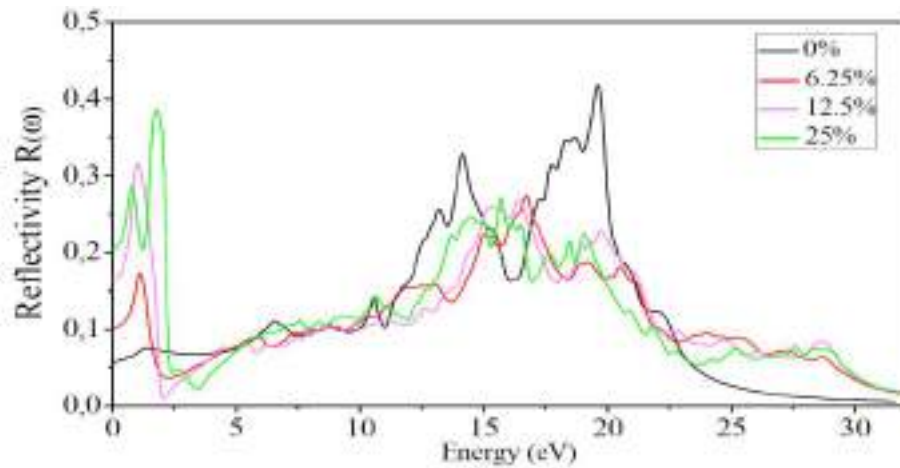
Figure 5. The Variation of The Reflectivity For Various Ga Concentrations.
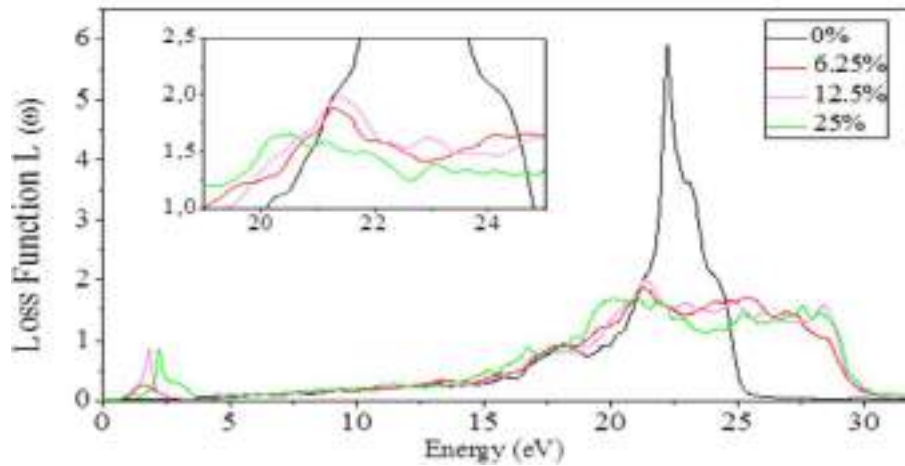
Figure 6. The Variation of The Energy Loss for Various Ga Concentrations.

Conclusion

This paper presents an analysis of the structural, electronic, and optical properties of Ga-doped ZnO ($Zn_{1-x}Ga_xO$) at varying Ga concentrations, utilizing density functional theory (DFT) with the modified Becke–Johnson (mBJ) exchange potential. The results show that the calculated band gap and lattice parameters for pure ZnO align well with both experimental and theoretical data. Incorporating Ga into ZnO increases the optical band gap and donor concentration as the Ga content rises, leading to enhanced conductivity. This Ga incorporation introduces shallow donor states, specifically Ga-4s, at the lower part of the conduction band near the Fermi level.

The study also examines the optical properties such as the dielectric function, refractive index, reflectivity, and electron energy-loss function. The absorption edge in the imaginary part of the dielectric function shifts to higher energies with increasing Ga concentrations. In the energy-loss spectrum, a significant peak at 22.30 eV for pure ZnO corresponds to its metallic characteristics. For Ga-doped ZnO (GZO), two peaks emerge: one around 2 eV due to Ga doping, and another shifting toward higher energies, indicating an enhanced metallic

character in doped samples compared to pure ZnO. Additionally, the static refractive index and reflectivity of GZO increase as Ga concentrations rise. These findings suggest that Ga doping of ZnO is a promising approach for creating transparent conducting oxides (TCOs), potentially serving as a replacement for indium tin oxide (ITO) in applications such as solar photovoltaics, offering desirable structural, electronic, and optical properties without the reliance on indium-based compounds.

References

Ginley D S and Bright C 2000 Transparent conducting oxides *MRS Bull.* 25 15.

M.V. Ganduglia-Pirovano, A. Hofmann, J. Sauer, Surf. Sci. Rep. 62 (2007) 219.

V.I. Anisimov, J. Zaanen, O.K. Andersen, Phys. Rev. B 44 (1991) 943.

D. Koller, F. Tran, P. Blaha, Phys. Rev. B 83 (2011) 195134.

L.J. Sham, M. Schluter, Phys. Rev. Lett. 51 (1983) 1888.

Z. Charifi, H. Baaziz, A.H. Reshak, Phys. Stat. Solidi b 244 (2007) 3154.

P. Dufek, P. Blaha, K. Schwarz, Phys. Rev. B 50 (1994) 7279.

E. Engel, S.H. Vosko, Phys. Rev. B 47 (1993) 13164.

A. Segura, J.A. Sans, F.J. Manjon, A. Munoz, M.J. Herrera-Cabrera, Appl. Phys. Lett. 83 (2003) 278.

A. Ashrzafi, C. Jagadish J. Appl. Phys. 102 (2007) 071101.

J.A. Sans, A. Segura, F.J. Manjon, B. Mari, A. Munoz, M.J. Herrera- Cabrera, Microelectron. J. 36 (2005) 928.

Kim K, Song Y-W, Chang S, Kim I-H, Kim S and Lee S Y 2009 Fabrication and characterization of Ga-doped ZnO nanowire gas sensor for the detection of CO Thin Solid Films 518 1190.

Han N, Tian Y, Wu X and Chen Y 2009 Improving humidity selectivity in formaldehyde gas sensing by a two-sensor array made of Ga-doped ZnO Sensors Actuators B 138 228.

Ko H J, Chen Y F, Hong S K, Wenisch H, Yao T and Look D C 2000 Appl. Phys. Lett. 77 3761.

Kuprenaite S, Murauskas T, Abrutis A, Kubilius V, Saltyte Z and Plausinaitiene V 2015 Properties of In-, Ga-, and Al-doped ZnO films grown by aerosol-assisted MOCVD: influence of deposition temperature, doping level and annealing Surf. Coat. Technol. 271 156.

Kim J H and Yer I H 2015 Ga-doped ZnO films grown on GaN templates by plasma-assisted molecular-beam epitaxy Ceram. Int.41 10227.

Madsen G K H, Blaha P, Schwarz K, Sjöstedt E and Nordström L 2001 Efficient linearization of the augmented plane-wave method Phys. Rev. B 64 195134.

Khon W and Sham L J 1965 Self-consistent equations including exchange and correlation effects Phys. Rev. 140 A1133.

Perdew J P, Burke K and Ernzerhof M 1996 Generalized gradient approximation made simple Phys. Rev. Lett. 77 3865.

Tran F and Blaha P 2009 Accurate band gaps of semiconductors and insulators with a semilocal exchange-correlation potential Phys. Rev. Lett. 102 226401.

Desgreniers S 1998 High-density phases of ZnO: structural and compressive parameters Phys. Rev. B 58 14102.

Erhart P, Albe K and Klein A 2006 First-principles study of intrinsic point defects in ZnO: Role of band structure, volume relaxation, and finite-size effects Phys. Rev. B 73 205203.

Schleife A, Fuchs F, Furthmüller J and Bechstedt F 2006 First-principles study of ground-and excited-state properties of MgO, ZnO, and CdO polymorphs Phys. Rev. B 73 245212.

Wu H C, Peng Y C and Chen C C 2013 Effects of Ga concentration on electronic and optical properties of Ga-doped ZnO from first principles calculations Opt. Mater. 35 509.

Sorokin A V, Zhukovskii Y F, Purans J and Kotomin E A 2012 The effect of Zn vacancies and Ga on the electronic structure of ZnO: ab initio simulations Mater. Sci. Eng. 38 012015.

Khan I, Ahmad I, Rahnamaye Aliabad H A and Maqbool M 2015 DFT-mBJ studies of the band of the II–VI semiconductors Mater. Today Proc. 2 5122.

Slassi A, Naji S, Benyoussef A and El Kenz A 2014 On the transparent conducting oxide Al doped ZnO: first principles and Boltzmann equations study J. Alloys Compd. 605 118.

Ozgür -, Alivov Ya I, Liu C, Teke A, Reshchikov M A, Dogan S, Avrutin V, Cho S-J and Morkoç H 2005 A comprehensive review of ZnO materials and devices J. Appl. Phys. 98 041301.

Bedia A, Bedia F Z, Aillerie M, Maloufi N, Ould Saad Hamady S, Perroud O and Benyoucef B 2014 Optical, electrical and structural properties of nano-pyramidal ZnO films grown on glass substrate by spray pyrolysis technique Opt. Mater. 36–7 1123.

Chang S H, Cheng H-M, Tien C-L, Lin S C and Chuang K P 2014 Optical, electrical and mechanical properties of Ga-doped ZnO thin films under different sputtering powers Opt. Mater. 38 87.

Wu H C, Peng Y C and Chen C C 2013 Effects of Ga concentration on electronic and optical properties of Ga-doped ZnO from first principles calculations *Opt. Mater.* **35** 509.

Zhang Y G, Zhang G B and Wang Y X 2011 First-principles study of the electronic structure and optical properties of Ce-doped ZnO J. Appl. Phys. 109 063510.

Kuzmenko A B 2005 Kramers–Kronig constrained variational analysis of optical spectra Rev. Sci. Instrum. 76 083108.

Linear Hybrid Analytical Modeling of Magnetic Fields Applied to Permanent Magnet Synchronous Machine

Brahim Ladghem-Chikouche

University of M'sila, Algeria, https://orcid.org/ 0000-0002-8473-0523

Haddi Bakhti

University of M'sila, Algeria, https://orcid.org/ 0000-0003-2888-8454

Miloud Bentoumi

University of M'sila, Algeria, https://orcid.org/ 0009-0004-5272-5078

Abstract: This work introduces an innovative two-dimensional (2-D) hybrid analytical model (HAM) applied for dual-rotor permanent-magnet (PM) synchronous machines. The proposed HAM seamlessly combines the semi-analytical Maxwell-Fourier formulations with finite-element method (FEM) across all machine subdomains, offering a comprehensive and efficient approach to electromagnetic analysis. The semi-analytical component employs a rigorous formulation derived from Maxwell's equations, specifically tailored for regions with unitary relative permeability, enabling high-precision electromagnetic field computations in non-ferromagnetic domains while maintaining computational efficiency. For regions of high magnetic permeability, such as the ferromagnetic teeth and yoke structures, the model employs a finite-element method (FEM) approach, leveraging its superior capability to accurately represent complex geometries and nonlinear magnetic properties. The analytical model (AM) and finite-element method are connected in both directions of the periodicity and non-periodicity direction. It is found that whatever the iron core relative permeability, the developed hybrid analytical model (HAM) give accurate results for no-load and on-load conditions. Finite-element analysis (FEA) shows very good results of the advanced technique.

Keywords: Hybrid magnetic model, exact subdomain technique, magnetic equivalent circuit, finite-element analysis.

Introduction

Due to advancements in electrical actuator technology, linear permanent magnet (PM) synchronous actuators

have gained significant popularity in industrial applications. Their widespread adoption can be attributed to key advantages including compact design, high torque-to-size ratio, excellent efficiency, precise controllability, and minimal heat generation.

Throughout the engineering design phase, scientists have utilized an array of modeling techniques to achieve an ideal trade-off between computational accuracy and processing speed. These analyses need to incorporate multiple physical considerations, encompassing electrical, magnetic, mechanical, and thermal variables.

In recent years, hybrid analytical approaches have emerged as an effective alternative for modeling electrical actuators, offering a balance between accuracy and computational efficiency. In the field of electrical machines, hybrid analytical methods refer to the combination of two or more analytical methods into one. These methods are used in electrical machine calculations to achieve high-speed solutions while maintaining acceptable accuracy. The purpose of proposing these methods in electrical machine calculations is to offer powerful hybrid computational tools, considering the rapid growth of computer capabilities and the simultaneous need for high-speed and less resource-intensive programs compared to existing methods.

The hybrid analytical approach has been utilized to develop various reliable solutions in the field of electrical engineering, including applications such as Maxwell-Fourier method which can be coupled with:

1) Finite-difference method (Yan et al., 2021; Carpi et al., 2018);
2) Finite element method (FEM) (Shen et al., 2021);
3) Magnetic equivalent circuit (MEC) (Barakat and Amara, 2014; Ladghem-Chikouche et al., 2021; Pluk et al., 2015; Taqavi and Taghavi, 2021; Verbeek et al., 2021; Zhu et al., 2022).

This research aims to introduce an innovative hybrid analytical technique that integrates the Maxwell-Fourier analytical method with finite element analysis. A significant advantage of this methodology is its capacity to explicitly couple all regions along both x- and y-axes, eliminating the need to assume infinite permeability for the iron core. The coupling process is specifically implemented at the interface between adjacent regions with distinct magnetic properties. Furthermore, this approach offers the advantage of eliminating the need for approximations typically used when representing the slot region, such as employing an equivalent magnetomotive force (MMF) or similar simplifying assumptions.

Assumptions of the Model

The electromagnetic model employs the following simplifications:

1) A quasi-static approach is adopted.
2) Both longitudinal end-effects and transverse edge-effects are omitted from consideration.
3) Stator tooth-tips are excluded from the model, though they could be incorporated if necessary.
4) All geometric regions are assumed to have radial sides.
5) The magnetic vector potential is constrained to a single component along the z-axis in all regions.

6) Current density in the stator slots is limited to a single component along the z-axis.

7) Electrical conductivity is assumed to be zero in all regions, eliminating eddy-current losses in both permanent magnets (PMs) and armature windings.

8) All regions are treated as isotropic.

9) The PMs are modeled with a linear second quadrant characteristic, with their absolute permeability equated to that of vacuum.

10)

Figure 1 depicts a cross-sectional of the proposed machine. The fixed armature region includes a simplified representation of the slot geometry, while both movable armatures are equipped with radially magnetized surface-mounted permanent magnets (PMs). Table I outlines the key geometric and physical parameters of the proposed linear PM machine.
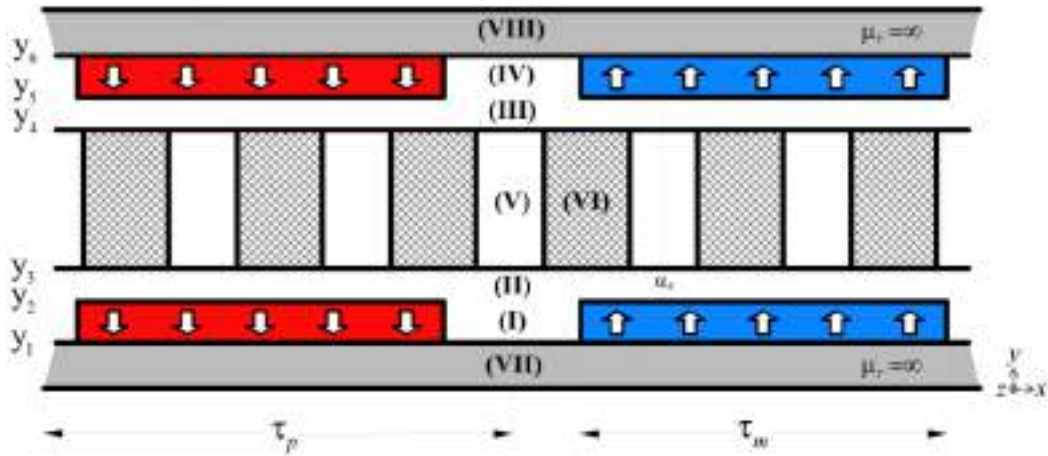
Figure 1. The proposed linear PM electrical machine

Table 1. Machine's parameters

Symbol	Parameter (unit)	Value	Symbol	Parameter (unit)	Value
B_{rem}	Remanent of flux density of PMs (T)	1.25	w	Opening of slot (mm)	6
Q	Slots number	24	τ_p	Pole pitch (mm)	60
y_1	Inner magnet height (mm)	7	β	PM pole-width to pole-pitch ratio (%)	80
y_2	External magnet height (mm)	10.0	J_m	Current density (A/m²)	$15 \cdot 10^3$
y_3	Inner slot height (mm)	10.5	L_z	Axial length (mm)	50
y_4	External slot height (mm)	22.5	V	Average speed (m/s)	1
y_5	External magnet height (mm)	23.0	nh	Number of harmonics	130
y_6	Inner magnet height (mm)	26.0	-	Magnetization type	Radial

Description of HAM

Introduction

The study categorizes the PM linear electrical machine into two sets of areas. The initial group consists of areas with an absolute permeability equal to unity, including permanent airgap (II and III), magnets (I and IV), and slots (V). Areas with absolute permeability values other than one are included in the second set, such as mobile armature yoke (VII and VIII) and teeth (VI). The subdomain method is applied to model the first set, while a numerical approach utilizing finite elements is employed for the second set.

To differentiate between effects caused by the relative magnetic permeability of the movable armature core and those of the stationary armature teeth, this analysis omits Regions (VII) and (VIII). As a result, the relative magnetic permeability values for these two regions are treated as theoretically infinite.

2-D Exact subdomain technique

The vector magnetic potential distributions across the five distinct regions are characterized by their respective general solutions, which are expressed as follows:

1) in Region (I) and (IV):

$$A_z^{I,IV} = \sum_n \left(C_{3n}^{I,IV} e^{K_n y} + C_{4n}^{I,IV} e^{-K_n y} + \Gamma_s \right) \sin(K_n x) + \sum_n \left(C_{5n}^{I,IV} e^{K_n y} + C_{6n}^{I,IV} e^{-K_n y} + \Gamma_c \right) \cos(K_n x) \quad (1a)$$

with

$$\Gamma_s = -\mu_0 \frac{Mr_{ycn}}{K_n} \quad \text{and} \quad \Gamma_c = \mu_0 \frac{Mr_{ysn}}{K_n} \quad (1b)$$

where τ_p and $K_n = n\pi/\tau_p$, are respectively the pole-pitch and the spatial harmonic order and, μ_0 is the vacuum permeability, Mr_{ysn} and Mr_{ycn} are spatial harmonic of the magnetisation.

2) Region (II) and (III):

$$A_z^{II,III} = \sum_n \left(C_{3n}^{II,III} e^{K_n y} + C_{4n}^{II,III} e^{-K_n y} \right) \sin(K_n x) + \sum_n \left(C_{5n}^{II,III} e^{K_n y} + C_{6n}^{II,III} e^{-K_n y} \right) \cos(K_n x) \quad (2)$$

3) Region (V):

$$A_{zs}^V = C_{s1}^V + C_{s2}^V y - \frac{1}{2} \mu_0 J_{zs} y^2 + \sum_m \left(C_{s3m}^{IV} e^{\beta_m^V y} + C_{s4m}^V e^{-\beta_m^V y} \right) \cos\left[\beta_m^V \left(x - \alpha_s + \frac{w}{2} \right) \right] +$$

$$\sum_v \left(C^V_{s5v} \sinh\left[\lambda^V_v\left(x - \alpha_s + \frac{w}{2}\right)\right] + C^V_{s6v} \sinh\left[\lambda^V_v\left(x - \alpha_s - \frac{w}{2}\right)\right]\right) \sin[\lambda^V_v(y - y_3)] \quad (3a)$$

where J_{zs} is the current density in the slot s, α_s is the position of sth slot and w is the slot-opening. β^V_m and λ^V_v can be written as

$$\beta^V_m = \frac{m\pi}{w} \quad \text{and} \quad \lambda^V_v = \frac{v\pi}{y_4 - y_3} \quad\quad\quad (3b)$$

where m and v represent respectively the spatial harmonic orders in the x- and y-axis.

The magnetic field elements can be derived using a 2-D Cartesian coordinate system as follows

$$\mathbf{B} = \nabla \times \mathbf{A} = \frac{\partial A_z}{\partial y}\mathbf{u_x} - \frac{\partial A_z}{\partial x}\mathbf{u_y} \quad\quad\quad (4)$$

where $\mathbf{u}$ is the unit vector in the x- and y-axis

2-D FEM

The tooth region (VI), as shown in Figure 2a, is divided into a grid of uniform finite elements (Figure 2b). This discretization enables the precise determination of the magnetic vector potential distribution within the teeth regions through the solution of Laplace's equation. The solution is obtained using variational methods, which are grounded in the principle of energy minimization, ensuring an optimal and physically accurate representation of the magnetic field.
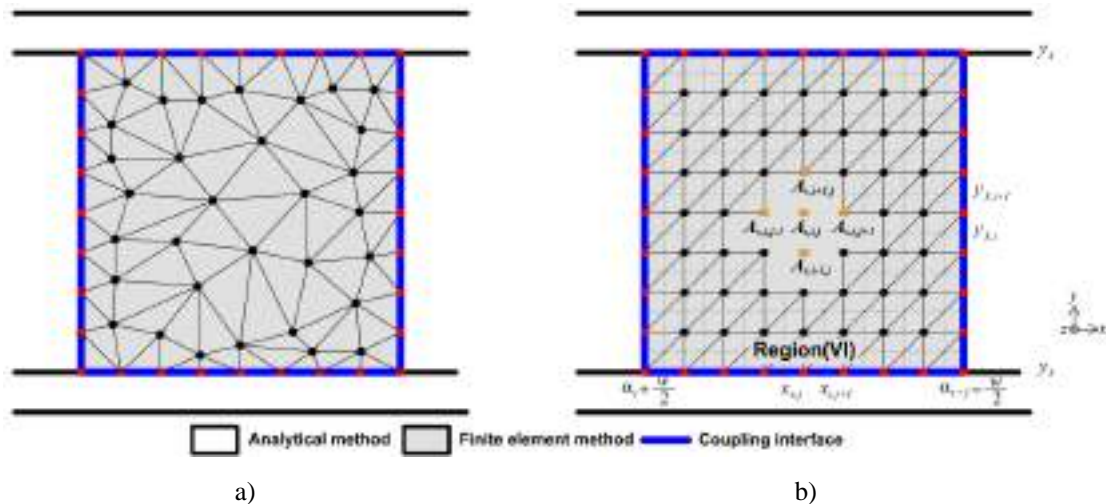
Figure 2. a) Random and b) regular discretization of the Region (VI) using finite regular elements

Laplace's equation governing $\mathbf{A}$ in an isotropic and continuous region can be obtained by solving

$$\mathbf{rot}\left(\frac{1}{\mu_0 \mu_r} \cdot \mathbf{rot}(\mathbf{A})\right) = 0 \qquad (5)$$

where μ_0, μ_r represent the permeability of vacuum and the relative permeability of the iron core respectively.

Definition of BCs

The normal component of **B** must be continuous across the interface. In contrast, the tangential component of **H** can be discontinuous across the interface. This discontinuity is related to the surface current density at the interface. These boundary conditions are fundamental in electromagnetic theory and are crucial for solving problems involving magnetic fields in different regions.

Results and Validation

The approach proposed in this study is evaluated using the electrical machine shown in Figure 1. All results obtained in this work are compared with predictions from Finite Element Analysis (FEA) (Meeker; 2019).

Fig.1   (a)   (b)
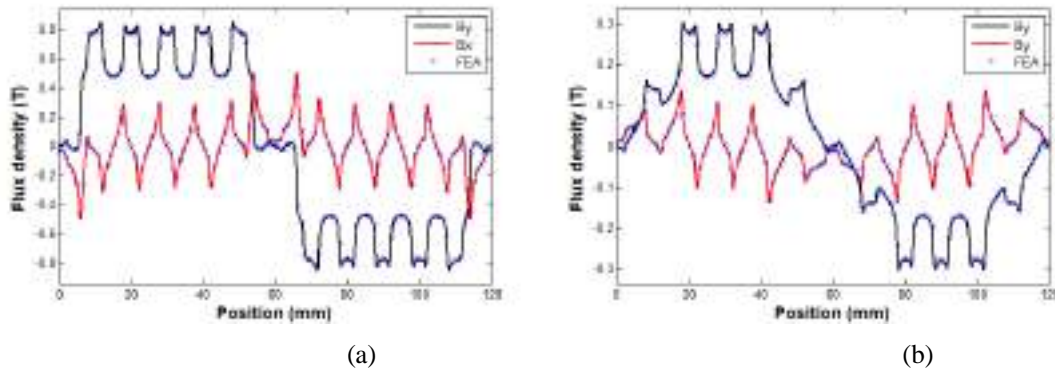
Fig.2   Figure 3. Normal and circumferential component of **B** calculated in the Region (II) under a) no-load and b) armature reaction condition considering $\mu_r = 5$
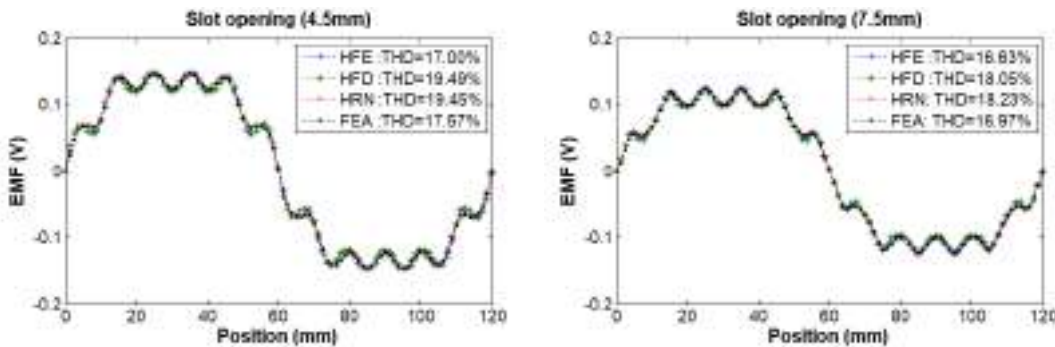
Fig.3   Figure 4. Back-EMF representation calculated by HAM and validated by FEA for $\mu_r = 5$

The normal and tangential components of a magnetic flux density, calculated under no-load and armature reaction current conditions, are shown in Figure 3. Figure 4 demonstrates the distribution of back-EMF waveform per turn calculated under $\mu_r = 5$. The mover's average speed is 1 m/s, while its incremental displacement is 0.25 mm. All results from various Analysis Methods (HAMs) align closely with Finite Element Analysis (FEA) findings.

Conclusion

This paper proposes a two-dimensional hybrid analytical-finite element (HFE) method for permanent magnet linear electrical actuators. The innovative approach combines an exact analytical model with finite element analysis, taking into account the global magnetic saturation of the iron core by incorporating its relative permeability. The study also shows that slot regions are represented using current density instead of magnetomotive force (MMF). This novel HFE approach yields accurate results regardless of the machine's complex geometry, the magnetic core's relative permeability value, or the operating conditions.

The study demonstrates that the predicted performance closely aligns with results obtained from Finite Element Analysis (FEA). Furthermore, the Hybrid Finite Element (HFE) method shows a favorable balance between computational accuracy and efficiency when compared to similar approaches like Hybrid Reluctance Network (HRN) and Hybrid Finite Difference (HFD).

References

Barakat, G. and Amara, Y., (2014) "A simple and effective way to couple analytical formal solution of magnetic potential and reluctance network models," 9th IET Int. Conference on Computation in Electromagnetics (CEM 2014), London, DOI: 10.1049/cp.2014.0199.

Ladghem-Chikouche, B. Boughrara, K. Dubas, F. and Ibtiouen, R. (2021) "Analytical magnetic field calculation for flat permanent-magnet linear machines with dual-rotor by using improved two-dimensional hybrid analytical method," COMPEL – Int. J. Comput. Math. Electr. Electron. Eng. vol. 40, no. 3, https://doi.org/10.1108/COMPEL-02-2021-0039.

Meeker, D.C., (2019) "Finite Element Method Magnetics", Version 4.2, 2019, Build, http://www.femm.info.

Pluk, K. J. W., Jansen, J. W. and Lomonova, E. A., (2015) "Hybrid analytical modeling: Fourier modeling combined with mesh-based magnetic equivalent circuits," IEEE Trans. Magn., vol. 51, no. 8, DOI: 10.1109/TMAG.2015.2419197.

Shen, M. Pfister, P-D. Tang, C. and Fang, Y., (2021) "A hybrid model permanent-magnet machines combining Fourier analytical model with finite element method, taking magnetic saturation into account," IEEE Trans. Magn, vol. 57, no. 2, DOI: 10.1109/TMAG.2020.3005802.

Taqavi, O. and Taghavi, N., (2021) "Development of a mixed solution of Maxwell's equations and magnetic equivalent circuit for double-sided axial-flux permanent magnet machines," IEEE Trans. Magn., vol.

57, no. 4, DOI: 10.1109/TMAG.2021.3060538.

Verbeek, N. Baudart, F. and Dehez, B., (2021) "Loop formulation in hybrid analytical modeling for solving 2-d nonlinear magnetostatic problems," IEEE Trans. Magn, vol. 57, no. 8, DOI: 10.1109/TMAG.2021.3083418.

Yan, B. Yang Y. and Wang, X., (2021) "A semi-numerical method to assess start and synchronization performance of a line-start permanent magnet synchronous motor equipped with hybrid rotor," IET Elect. Power Appl., vol. 15, no. 4, DOI: 10.1049/elp2.12043.

Zhu, Y. Liu, G. Xu, L. Zhao, W. and Cao, D., (2022) "A hybrid analytical model for permanent magnet vernier machines considering saturation effect," IEEE Trans. Ind. Electron., vol. 69, no. 2, DOI: 10.1109/TIE.2021.3060656.

Empirical Modal Decomposition Applied to Leak Detection in a Water Distribution Pipeline

Haddi Bakhti

University Mohamed BOUDIAF-Msila, Algeria, https://orcid.org/0000-0003-2888-8454

Miloud Bentoumi

University Mohamed BOUDIAF-Msila, Algeria, https://orcid.org/ 0009-0004-5272-5078

Brahim Ladghemchikouche

University Mohamed BOUDIAF-Msila, Algeria, https://orcid.org/0000-0002-8473-0523

Abstract: This paper deals with the problem of water leak detection in the pipeline based on the empirical mode decomposition (EMD) method. At low frequencies, leaks produce acoustic and vibration signals propagating along the pipeline, which have nonlinear and non-stationary characteristics. The hydraulic pressure, pipe diameter, the pipe's nature, and the leak's size can also be considered as other sources of the received signals, with unknown frequencies.rnThe analysis of such leakage signals using conventional methods like the FFT, the correlation, and the cepstrum is limited by the choice of the narrow periods and causes, therefore, the loss of useful information. By accommodating the EMD non-stationary time domain decomposition method, the received signals can be treated separately via several stationary components (IMFs). For some leak positions in the pipeline, the EMD analysis is applied and compared with the existing leak methods. Working in the time domain analysis, our experimental results demonstrate that the EMD method provides better leak detection performances.

Keywords: Leak, Detection, Vibration sensor, FFT, EMD

Introduction

One discipline that is a part of the non-destructive testing method is leak detection. Since the fluid we are attempting to safeguard is scarce and has the potential to inflict harm at its vanishing point, numerous detection and localization approaches have been developed. Communities are becoming quite concerned about their drinking water [1]. To act when it was most suitable, the network operators therefore started looking at ways to

identify breaches as soon as feasible. One of the most important things to accomplish optimal system performance is to shorten the time interval between the occurrence of a leak and its exact location [2]. A pipe break can contaminate water when there is less pressure and result in large financial losses [3]. To put it another way, finding a leak involves employing tools and methods. Considerable water is lost as a result of these leaks [4]. Various techniques are used [5-7], usually in phases, to find leaks accurately. We attempt to locate the fugitive section (pre-location) from a sector that is deemed degraded, and then we pinpoint the exact place of the leak (localization). The sensitivity of conventional techniques (FFT, correlation) based on the Fourier transform, which is extensively employed in the leak detection field, is unpredictable and dependent on a variety of variables (fluid nature, fault geometry, background noise, etc.).

Although the wavelet transform gets over these problems, it is still challenging to adequately classify signals using its interpretation. For many applications, the Hilbert-Huang transform offers a revolutionary method of signal decomposition. The latter can handle non-stationary and non-linear data with effectiveness. It has been demonstrated that this method works well for finding bearing flaws. A pressurized pipeline vibrates at the water departure point and spreads throughout the pipe if there is a breach. Localized variations in the pressure field brought on by different fluid processes are what are responsible for the vibrations. Numerous hydraulic changes in terms of time and fluid volume happen arbitrarily and incoherently when a leak happens. Under at least these circumstances, the resultant signal appears to be quasi-stationary noise [8].

Empirical mode decomposition (EMD) will be used in this work to identify water leaks in distribution networks that use HDPE pipes. This method will be applied to analyze the efficiency and validity of the experimentally measured data. An acquisition system linked to a sensor installed on canalizations constructed in the laboratory gathers the data. The findings acquired by this methodology are compared with those obtained by the application of another detection method. The outcomes are used to evaluate the selected approach.

Experimental Procedure

To implement the methods mentioned in 2, we created and implemented a suitable system consisting of a closed-circuit pumping system connected to a canal via a hydraulic circuit and an acquisition system using a piezoelectric sensor connected to a PC through an acquisition card.

Acquisition System

Correct signal acquisition translates into accurate or proper analysis. We developed a system that fully satisfies the measurement specifications for this. Low-frequency impulses are produced by the leak and cause vibrations. A piezoelectric sensor (KB12) that is specifically designed for low-frequency vibration measurements is installed in the canal. It is a 6500 ±20 pc/g sensitivity sensor that was bought from Metra Meβ. Figure 1 shows how the sensor may be adjusted to cover our canal prototype at predefined distances based on the location of the leak created by drilling a 2 mm hole in the PEHD pipe. Additionally, a signal conditioning experiment using an

electronic card was conducted in the lab. A digital oscilloscope GDS1000 with a 2M bandwidth receives the output signal. The latter can use the RS232 serial port to connect directly to a PC or store the signals in an external memory. The requirements are satisfied by the realized measurement system. Signals were gathered within 500 ms time intervals with a 2 KHz sample frequency.
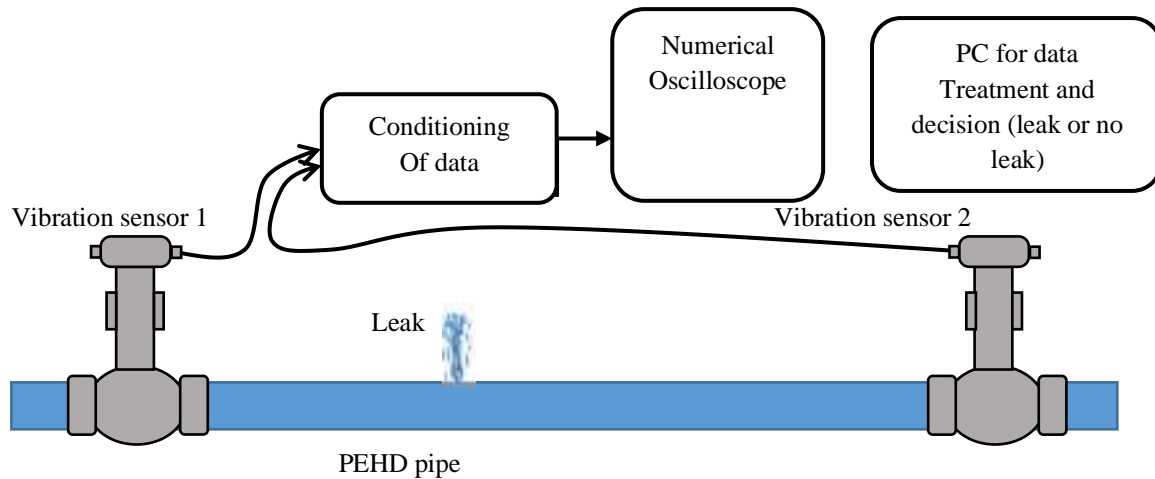
Figure 1. Acquisition system

Hydraulic Circuit

Pipeline in PEHD   pump

Vibration sensor (KB12)   PC for data Treatment and decision (leak or no leak)

Figure 2. Hydraulic circuit

In this work, we used a high-density polyethylene (HDPE) pipe with a diameter of $\emptyset = 4$ cm and length of $L = 100$ m. To simulate a leak, we drilled holes with a diameter of $\emptyset=12$ mm at different locations on the pipe. On this pipeline, we installed pressure transducers. The first is installed at a fixed position before the leak and concerning the pumping system and the second transducer can be installed at different distances from the leak on the pipeline. High-quality pressure and very precise transducers are used in this study.

Treatment procedure

Programs are developed for the treatment of acquired signals. These last are based on conventional signal processing algorithms such as FFT, Welch power spectral density estimate (WPSDE), and the empirical mode decomposition EMD.
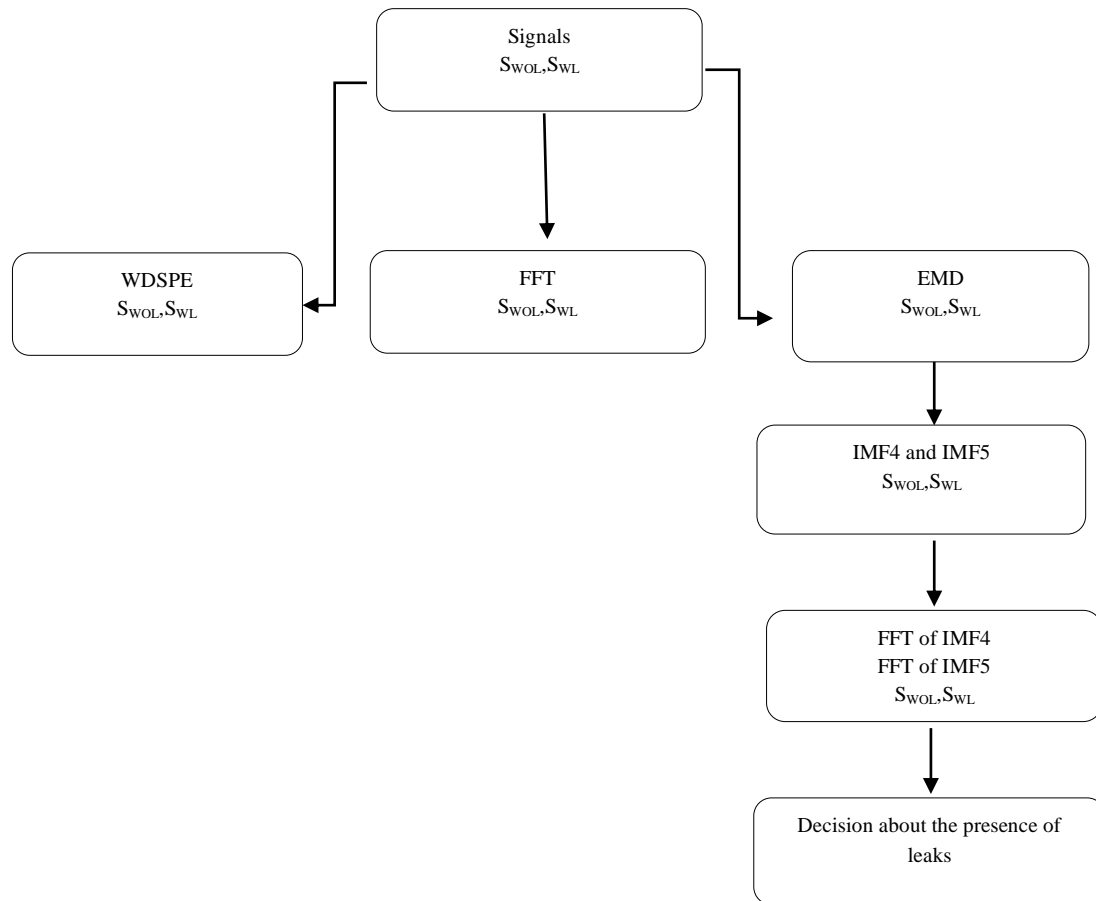
Figure 3. Processing protocol

Results and Discussion

For our study, we made acquisitions along the pipe at distances ranging from 10 cm to 4m concerning the position of the leak and with a step of 10 m. The analysis was done on all distances but we present the signal of 40 cm analysis as an example.
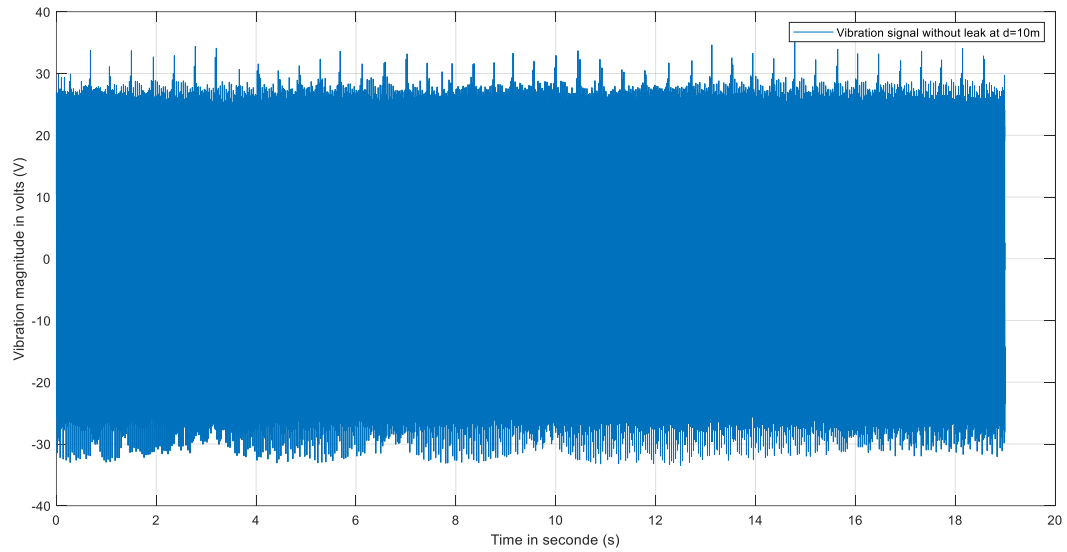
Figure 5. Signal without leak (S_{WOL}) for d=10m.
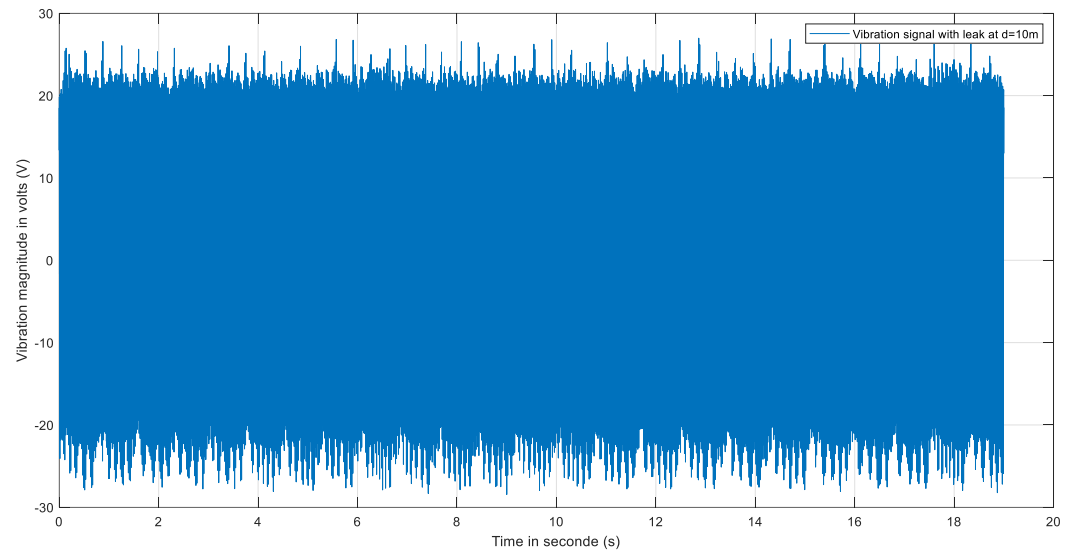
Figure 6. Signal with a leak (S_{WL}) for d=10m.

The observation of the temporal signals with and without leak (S_{WL} and S_{WOL}) at any position of the sensor on the pipe shows fluctuations in the amplitude of these signals. Although, some singular fluctuations exist in the S_{WL} compared to the S_{WOL} Fig.5. However, some singular fluctuations exist in the leakage signal compared to the signal without leakage. Nevertheless, it does not confirm the presence of a leak in the channel due to interference from external vibration sources that may affect the signal.

To affirm the detection of a leak, we will proceed to the transformation from the time domain to the frequency domain signals. Knowing approximately the channel vibration frequencies under the effect of leaks.

Detection by application of the WDSPE

The power spectral density allows us to have an idea about the presence of a leak by comparing the S_{WL} with and S_{WIL}. The power spectral density allows us to have an idea about the presence of a leak by comparing the signals with and without leakage. For an accurate decision of a leak, the knowledge of the frequency of vibration generated by the latter is primordial. However, the power spectral density can reduce the frequency band or leakage peaks appear. For this, we used an algorithm to estimate the DSP Welch (WPSDE). The latter Estimates the power spectral density PSD of the input signal vector using Welch's method. Welch's method splits the data into overlapping segments, computes modified periodograms of the overlapping segments, and averages the resulting periodograms to produce the power spectral density estimate. The power spectral density is calculated in units of power per radians per sample. The corresponding vector of frequencies f is computed in radians per sample and has the same length as WPSDE.

Fig. 7 shows a superposition of the two signals S_{WL} and S_{WIL} into the upper to 400 Hz frequency range. For against, the frequency range from zero to 400 Hz has a clear difference between the density of the two signals with and without leakage or leakage can be detected.
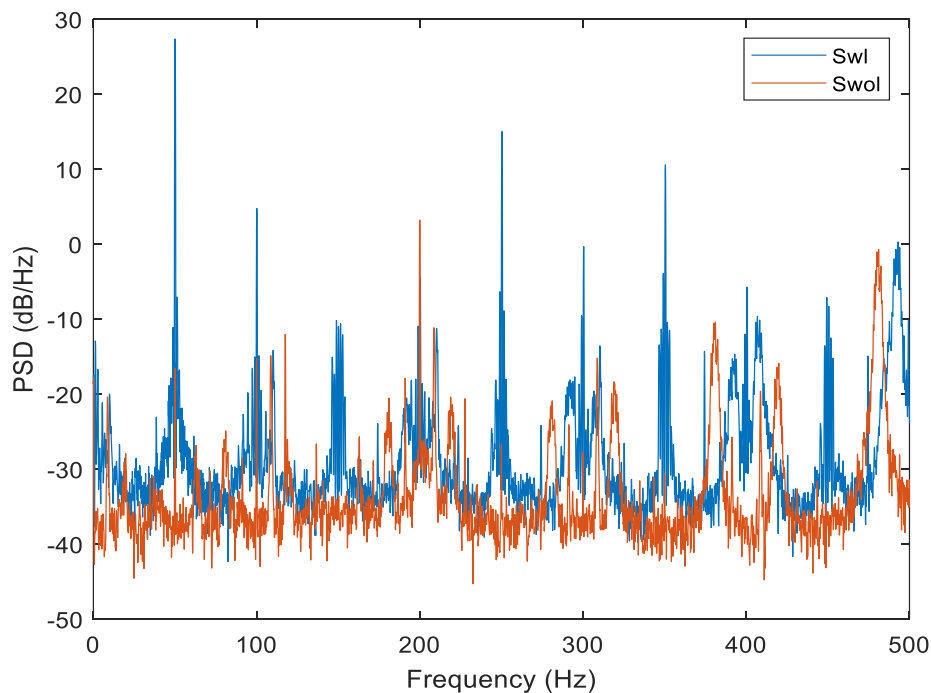
Figure 7. WPDSE of the S_{WL} and S_{WOL}.

Detection by the application of the FFT

In this section, the spectra of the two signals (S_{WL} and S_{WIL}) obtained by applying the FFT are shown in Figures 8. and 9
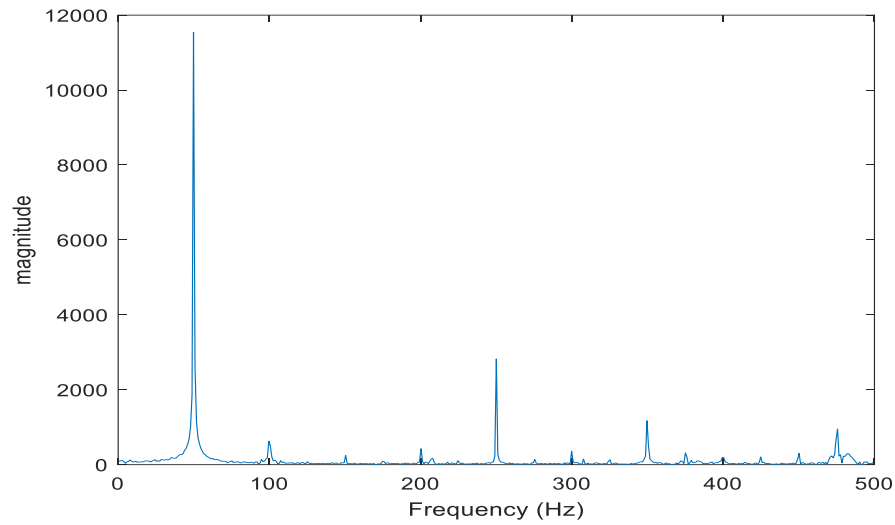
Figure 8. The FFT of S_{WOL}.
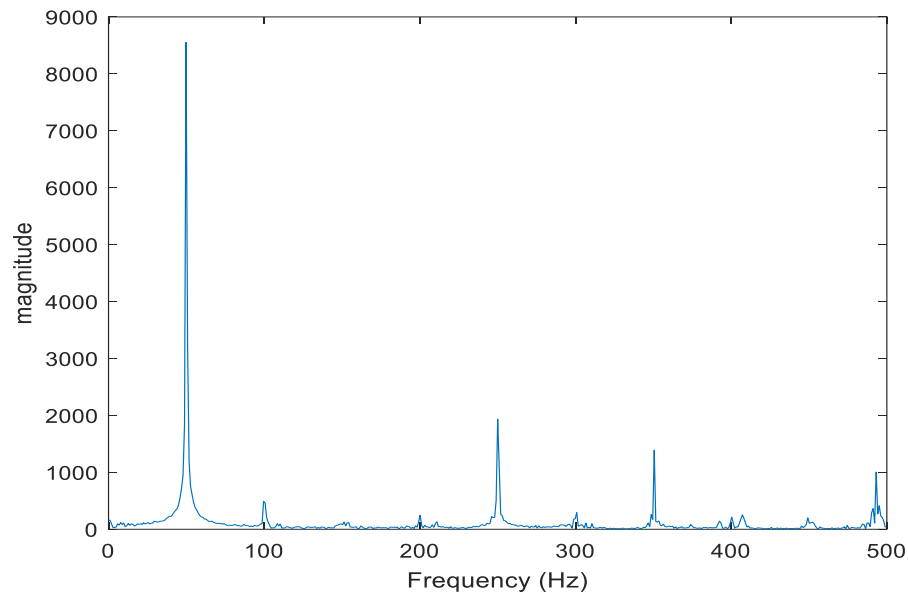
Figure 9. The FFT of S_{WL}.

Analysis of the spectra of the two signals S_{WL} and S_{WIL} shows that the difference between them appears in the frequency bands 150 and 300Hz for all distances.

Detection by the use of the EMD

We applied the empirical modal decomposition algorithm to the two signals S_{WOL} and S_{WL}. After a certain number of tests, we concluded that the empirical mode decomposition could be stopped in the seventh IMFs. The latter can be considered as a noise devoid of useful information that can help us to detect leaks. Fig. 10 shows the IMFs for a S_{WL} and S_{WOL} signals to a distance of 10 m after the application of the EMD program.
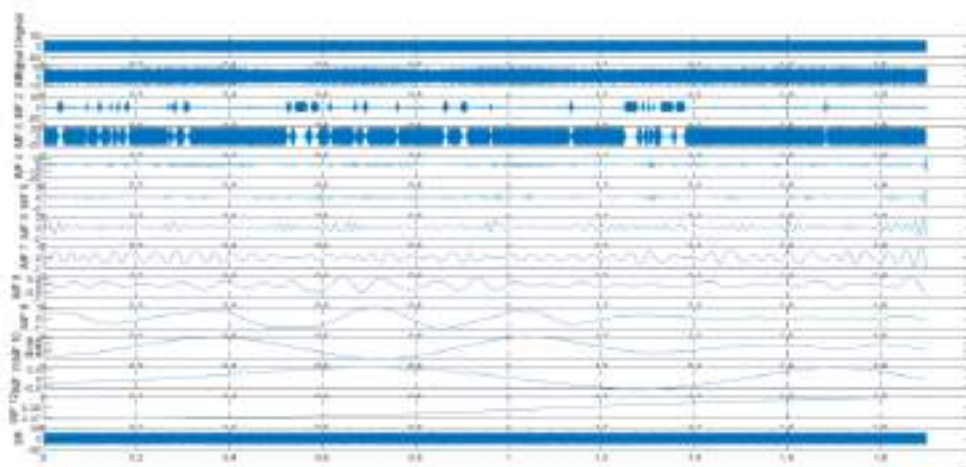
(a)
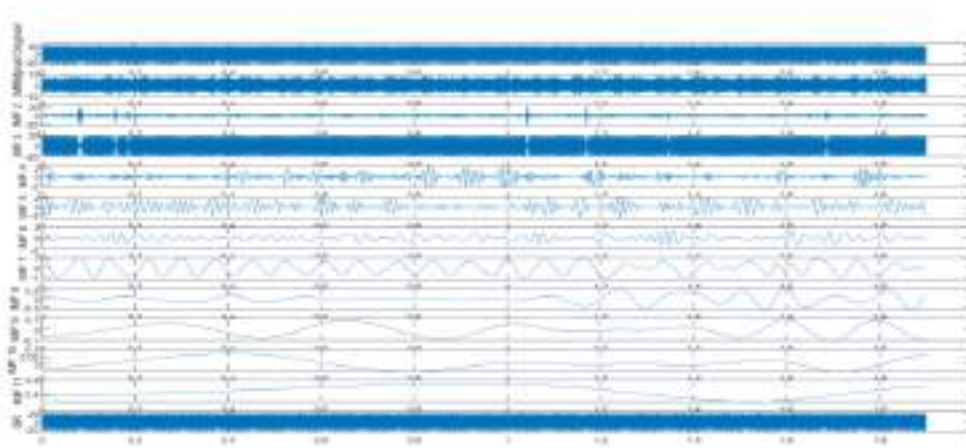
(b)

Figure 10. The EMD (a) S_{WOL} (b) S_{WL}
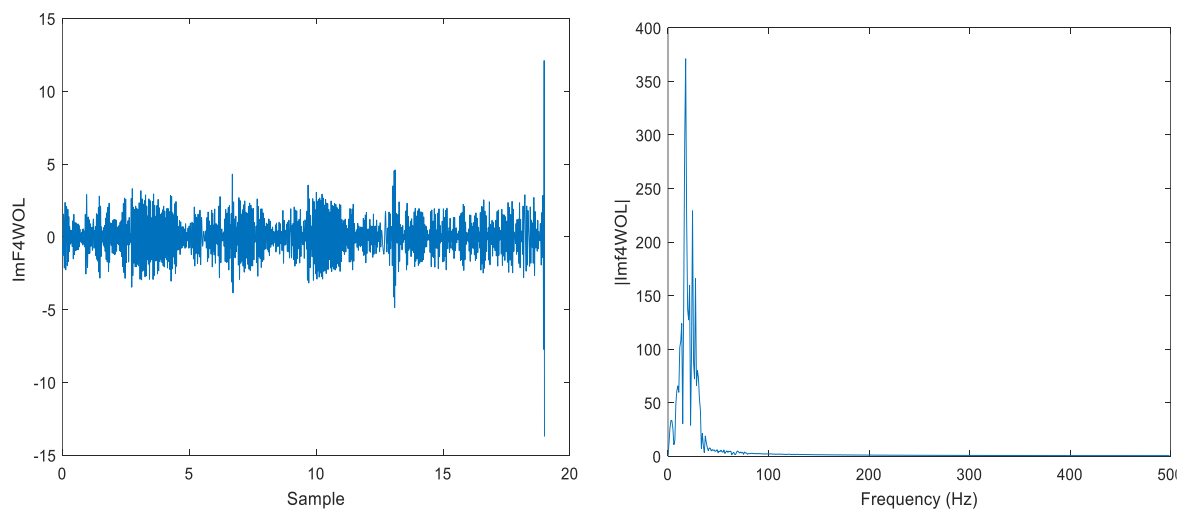
(a)

(b)

Figure 11. (a) IMF4 S_{WOL} ,(b) The FFT of IMF4 S_{WOL}

(a)   (b)
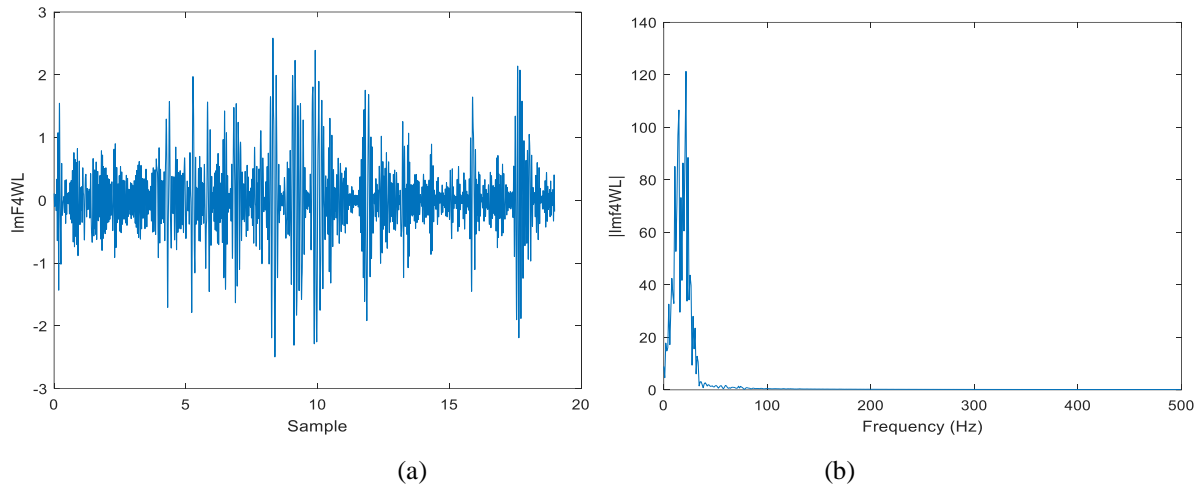
Figure 12. (a) IMF5 S_{WL} ,(b) The FFT of IMF5 S_{WL}

(a)   (b)
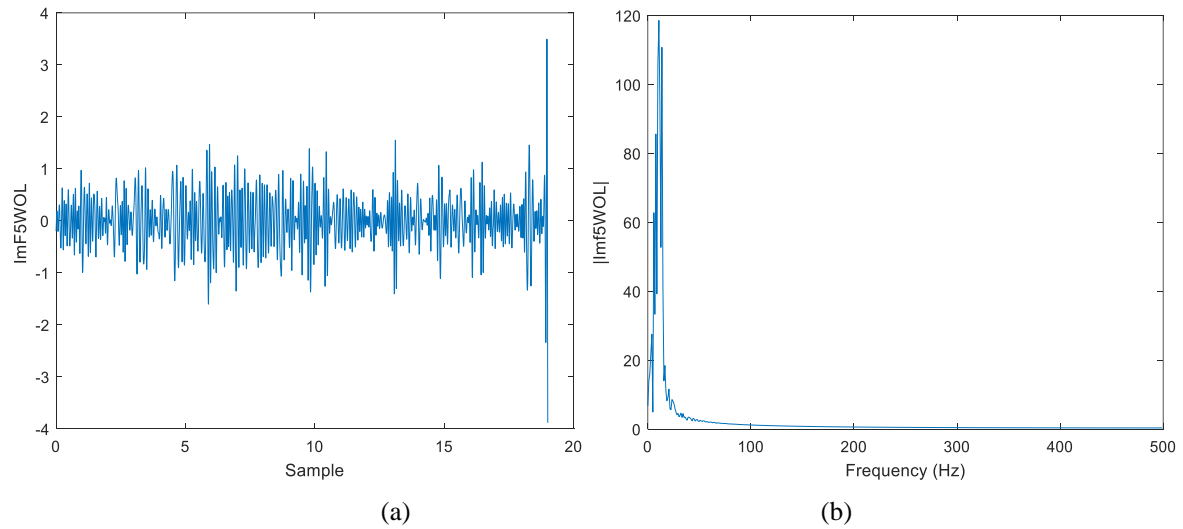
Figure 13. (a) IMF5 S_{WOL} ,(b) The FFT of IMF5 S_{WOL}

(a)   (b)
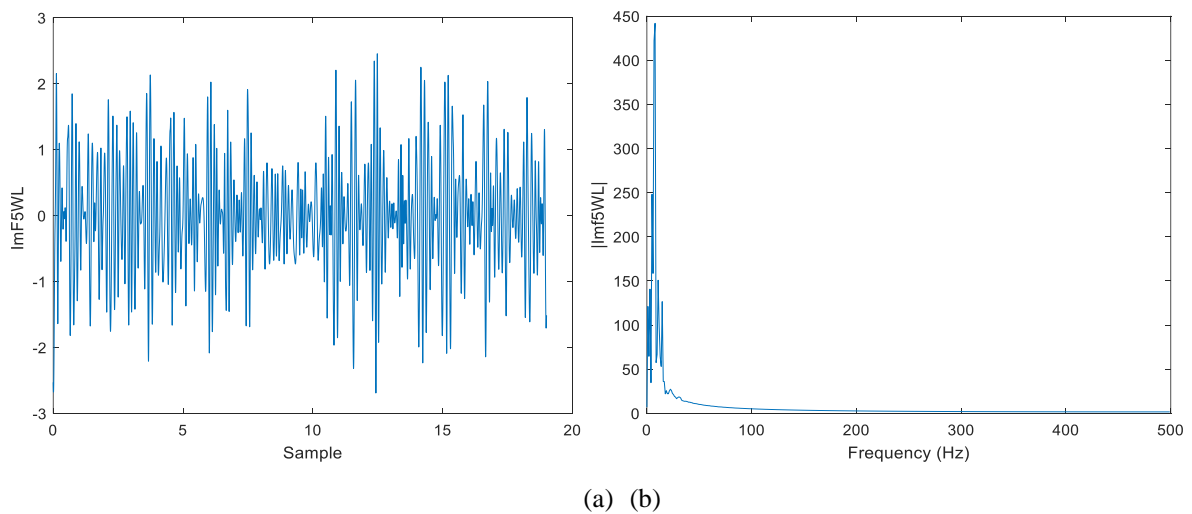
(b) Figure 14. (a) IMF5 S_{WL} ,(b) The FFT of IMF5 S_{WL}

(c)

Empirical Mode Decomposition to show its effectiveness for this kind of signal. By doing a little comparison with the FFT we found for distances used for example for d = 10 m difference between the signal with and without leakage is evident on the IMFs. 4 and 5 It was also found that the difference in area is in the vicinity of 200Hz like that found by applying the FFT.

Conclusion

The empirical mode decomposition is a very recent technique specialized for analyzing nonlinear and non-stationary signals. Early in its appearance, it was applied to the sonar signals, then it found other applications such as the detection of premature bearing defects and analyzing ECG signals. In our work, this technique was applied to the distribution networks to analyze the defects that occur on these. Analysis has shown the efficacy of the chosen technique. Unfortunately, the application was made in OFFLINE which gives prospects for future work.

References

R. IONEL, S. IONEL, P.BAUER, F.QUINT. "Water Leakage Monitoring Education: Cross-Correlation Study via Spectral Whitening".

M. Taghvaei, S. B. M. Beck and W. J. Staszewski, "Leak detection in pipelines using cepstrum analysis". Journal of Measurement Science and Technology IOP sciences, Vol 17, N°. 2. 2006, pp.367-372.

A.L. Ekuakille, G. Vendramin, A. Trotta. "Robust spectral leak detection of complex pipelines using filter diagonalization method". IEEE Sensors Journal.VOL.9.N°.11, 2009, pp: 1605 - 1614

A. Nasirian, M.F. Maghrebi, S. Yazdani. "Leakage detection in water distribution network based on a new heuristic genetic algorithm model. Journal of Water resource and protection".Vol.5, N° 3, 2013.pp:294-303.

A. Martini, M.Troncossi, and A.Rivola, "Automatic Leak Detection in Buried Plastic Pipes of Water Supply Networks by Means of Vibration Measurements," Shock and Vibration, vol. 2015, Article ID 165304, 13 pages, 2015. doi:10.1155/2015/165304

E.A. Claudia Deniss, C .Garza, L. Eduardo and V-M. Adriana, "Multi-leak detection with Wavelet analysis in water distribution networks", IEEE Mediterranean conference on control& Automation, Barcelona, 3-6 July 2012, Spain, pp.1155-1160.

A. Cataldo, G. Cannazza, E.D. Benedetto. "A new method for detecting leaks in underground water pipelines". IEEE Sensors Journal, Vol 12, N°.6.2012, pp.1660-1667.

Application of Cepstral Analysis to The Leaks Detection in Water Distribution Networks

Bentoumi Miloud

University of M'sila , Algeria, https://orcid.org/ 0009-0004-5272-5078

Bakhti Haddi

University of M'sila, Algeria, https://orcid.org/0000-0003-2888-8454

Ladghem Chikouche Brahim

University of M'sila, Algeria, https://orcid.org/0000-0002-8473-0523

Abstract: Leakage detection in water distribution systems is an important issue in water resource-saving and management. Inspired by speech and speaker signal processing. In this paper, we apply the cepstrum analysis to identify the leak of the pipeline when this latter occurred. To detect a leak in WDN we consider water flow in pipes similar to the sounds flowing through the vocal tract. The leak can be likened to an opening of the vocal tract, such as the mouth or the nose. A prototype pipeline was made at the laboratory level. The pipeline in our case is made of steel. Experimentally obtained results of the proposed cepstrum methods have been compared to those obtained using three conventional methods: autocorrelation, FFT, and log of FFT. Comparative results prove the effectiveness of the proposed method to track the leaks in different considering cases with very clear peaks and almost in the same frequency (same moment) compared to the three considered methods.

Keywords: Detection, Leak, Cepstrum, WDN, Vibration sensor

Introduction

Freshwater scarcity will be the defining global crisis of the 21st century. A decade ago, analysts warned of future water wars, even a world war. Water was labeled "the next oil" because of its importance to economic growth, and its use in everything from agriculture to industry, energy, and manufacturing. We have alternative energy sources, but nothing can ever replace water [1]. Pipelines are fixed systems that transport fluid commodities from one location to another systems include all physical devices, components, computer systems, telecommunication systems, and the pipe itself, which is required to move the water product between various

locations.

In this spirit, leakage detection in water distribution systems is an important issue in water resource-saving and management. According to an international survey, 20–50% of the produced quantities are lost due to leakage [2]. As a consequence, water leak detection has become an important issue in the signal processing field.

In the last decades, a vast number of leak detection methods have been proposed: Fast Fourier transform [3], the Short Time Fourier transform [4], cross-correlation [5], Extended Kalman Filter [6], Statistical Process Control [7], Time Series Modeling [8], Empirical Mode Decomposition [9], wavelet DT [10], etc. From the literature, the FFT and STFT are the most used methods in leak detection in water supply networks. Despite the disadvantage of FFT, which is only applicable to stationary signals. The problem is circumvented by dividing the acquisition time into intervals where the FFT can be considered stationary. Other methods subsequently appeared such as wavelets, EMD (empirical mode decomposition), and EEMD (enhanced mode decomposition). These new methods are effective for non-stationary signals.

A leakage in a pressurized pipe is known to generate vibration waves that travel along the pipe. These waves are caused by local fluctuations of the turbulent fluid and other phenomena. The pipe's geometrical properties, including its configuration, hydraulic components, and flow characteristics, influence wave propagation[. The effectiveness of leak detection and location algorithms relies on the availability of accurate measurements, including desired leakage signals with noise, within the network. In this paper, inspired by speech and speaker signal processing, we apply the cepstral analysis to identify pipe leak detection by considering water flow in pipes similar to the sounds flowing through the vocal tract. They are considered to be an opening of the vocal tract, such as the mouth or the nose. Simulation and experimental results show the effectiveness of the method.

Method

Cepstrum: The cepstrum of a signal x[n] is a transformation of this signal from the time domain to another time domain, that of Qufrency. The idea is to consider a given periodic signal as the convolution of a pulse train by a damped filter. In the frequency domain, the spectra are multiplied. If we take the logarithm of the result, we obtain the sum of the independent results. Thus, a convolution in the space of times corresponds to an addition in the domain of the cepstrum: If the two spectra have different characteristics, it becomes possible to separate them.

The cepstrum (1) is obtained by calculating the logarithm of the modulus of the Fourier transform of the signal, and taking the inverse Fourier transform of the result.

$$C(n) = FFT^{-1}(\log |FFT(x_n)|) = \frac{1}{2\pi} \int_{-\pi}^{\pi} \log(|X(e^{jw})|) e^{jwn} dn \tag{1}$$

Experimental Procedure

This work was done on a hybrid channel prototype composed of two parts: a steel part of 10m and plastic part of 20m. The leak is located on the first part (steel), so the leak is fixed. A vibration sensor is placed on the channel and will be moved along the steel pipe to collect signals at different positions of prototype channel (see Figure. 1).

Figure. 1. Experimental hybrid channel prototype.

Results

To evaluate the prposed cepstral method in leak detection at different distance. Tests are done at 22 positions by moving the vibrtion sensor along the steel part of the experimental hybrid channel prototype. In each position, 9 tests were conducted 1 without leak and 8 with leaks, so we have 198 tests. Below, we present the results for few positions to prove the effectiveness of the proposed cepstral method for leak detection (**Table 1**).

Table 1. Quantitative analysis result of sample.

Test\Leak	30 (cm)	60 (cm)	100(cm)	200(cm)
Test 1	x			
Test 2		x		
Test 3			x	
Test 4				x

Discussion

Figure 2 to 5 show the results using the proposed methods for the 4 cited tests. Experimental obtained results of the proposed cepstral methods have been compared to those obtained using three conventional methods: autocorrelation, FFT and log of FFT. Comparative results prove the effectiveness of the proposed method to track the leaks in different considering cases with very clear peaks and almost in the same frequency (same

moment) compared to the other three considered methods.
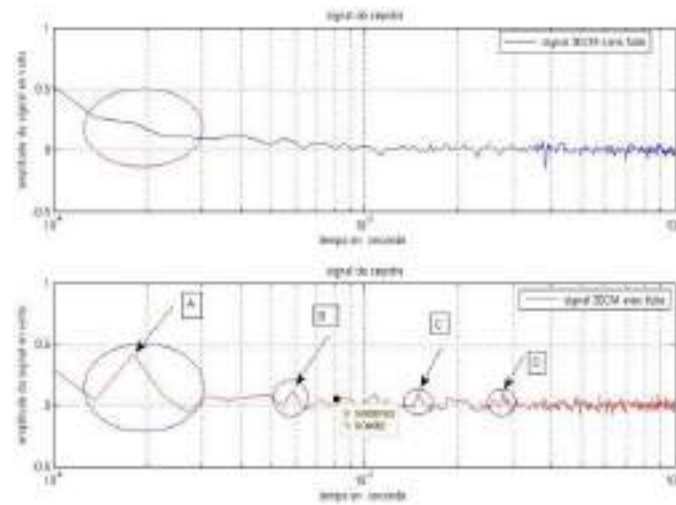
Figure 2. Test 1: top) without leak, bottom) with leak.
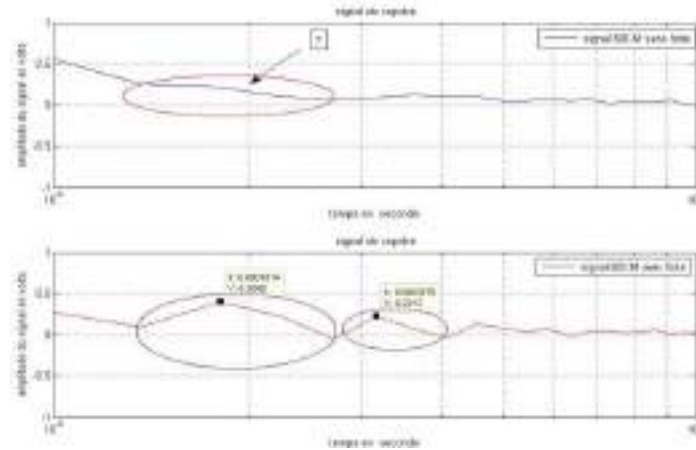
Figure 3. Test 2: top) without leak, bottom) with leak.
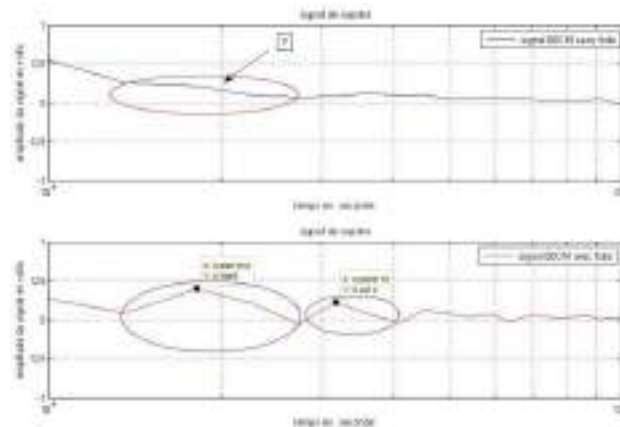
Figure 4. Test 3: top) without leak, bottom) with leak.
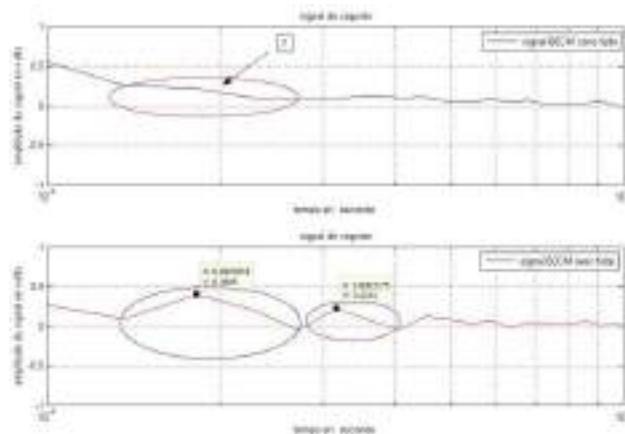
Figure 5. Test 4: top) without leak, bottom) with leak.

Conclusion

In this paper we apply the cepstral analysis to identify the pipe leak detection by considering water flow in pipes similar to the sounds flowing throw the vocal tract and where the leak can considered as an opening of the vocal tract, such as the mouth or the nose. The proposed method has been evaluated considering different distance on the experimental hybrid channel prototype composed of two parts: a steel part of 10m and plastic part of 20m. Tests are done at 22 positions by moving the vibration sensor along the steel part of the experimental hybrid channel prototype. In each position, 9 tests were conducted 1 without leak and 8 with leaks, so we have 198 tests. Below, we present the results for few positions to prove the effectiveness of the proposed cepstral method for leak detection. Experimental obtained results of the proposed cepstral methods have been compared to those obtained using three conventional methods: autocorrelation, FFT and log of FFT.Comparative results prove the effectiveness of the proposed method to track the leaks in different considering cases with very clear peaks and almost in the same frequency (same moment) compared to the other three considered methods.

References

Sabir, M., Miloud, B., Dirman. Hanafi, B., Haddi, B., Chaima, C. 'Novel Leak Detector Based on DWT an Experimental Study'. IJRCS, Vol. 4, No. 3, 2024, pp. 1109-1134. https://doi.org/10.31763/ijrcs.v4i3.1458

Miloud, B., Ahmed, B., and Haddi, B., "Welsh DSP Estimate and EMD Applied to Leak Detection in a Water Distribution Pipeline," Instrumentation Mesure Métrologie, vol. 19, no. 1, pp. 35-41, 2020, https://doi.org/10.18280/i2m.190105.

H. Bakhti, M. Bentoumi, A. Harrag, and K. El-Hadi, "Experimental Validation of Hybrid EMDCorrelation Acoustic Digital Leaks Detector in Water Distribution Network System," Instrumentation

Mesure Métrologie, vol. 18, no. 6, pp. 535-545, 2019, https://doi.org/10.18280/i2m.180604.

Miloud Bentoumi, Djamel Chikouche, Amar Mezache, Haddi Bakhti 'Wavelet DT method for water leak-

detection using a vibration sensor: an experimental analysis', IET Signal Processing ,Volume 11, Issue 4 , June 2017, pp: 349-493 DOI:10.1049/iet-spr.2016.0113

CHAIMACHABIRA , Haddi BAKHTI , Miloud BENTOUMI , Sabir MEFTAH , 'RNL used for the verification of the efficiency of a localization model in a real WDNs' The 2022 International Conference of Advanced Technology in Electronic and Electrical Engineering (ICATEEE) M'sila (Algeria) Year:2023 IEEE Xplore: 17 April 2023 DOI: 10.1109/ICATEEE57445.2022.10093092

Sabir Meftah;Miloud Bentoumi;Haddi Bakhti;Chaima Chabira 'Parameterization and Validation of the Physical Coefficients of a WDNs by BBO' The 2022 International Conference of Advanced Technology in Electronic and Electrical Engineering (ICATEEE) M'sila (Algeria) Year:2023 IEEE Xplore: 17 April 2023 DOI: 10.1109/ICATEEE57445.2022.10093730

Miloud Bentoumi;Haddi Bakhti;Chaima Chabira;Sabir Meftah 'S.G Filter And Speed of Pressure Wave Applied to locate leak in water pipe networks'The 2022 International Conference of Advanced Technology in Electronic and Electrical Engineering (ICATEEE) M'sila (Algeria) Year:2023 IEEE Xplore: 17 April 2023 DOI: 10.1109/ICATEEE57445.2022.10093689

Ahadi, M., Bakhtiar, M.S. (2010). Leak detection in water filled plastic pipes through the application of tuned wavelet transforms to acoustic emission signals. Applied acoustics journal Elsevier, 71(7): 634-639. https://doi.org/10.1016/j.apacoust.2010.02.006

Taghvaei, M., Beck, S.B.M., Staszewski, W.J. (2006). Leak detection in pipelines using cepstrum analysis. Journal of Measurement Science and Technology IOP Sciences, 17(2): 367-372, https://doi.org/10.1088/0957-0233/17/2/018

Martini, A., Troncossi, M., Rivola, A. (2015). Automatic leak detection in buried plastic pipes of water supply networks by means of vibration measurements. Shock and Vibration, 2015: 165304. https://doi.org/10.1155/2015/16530440

Gao, Y., Brennan, M.J., Joseph, P.F. (2006). A comparison of time delay estimators for the detection of leak noise signals in plastic water distribution pipes. Journal of Sound and Vibration Elsevier, 292: 552-570. https://doi:10.1016/j.jsv.2005.08.014

Influence of Tire Rubber Aggregates on The Sound and Thermal Insulation Properties of Cement Mortars

Si Bachir Djaffar

University of Sciences and Technology Houari Boumediene (USTHB)

Sadoudi Lyassaa

University of Sciences and Technology Houari Boumediene (USTHB)

Bakiri Abdeldjalil1

University of Sciences and Technology Houari Boumediene (USTHB)

Aoudjane Kheireddine

University of Sciences and Technology Houari Boumediene (USTHB)

Abstract: The present study explores the influence of tire rubber aggregates on the insulating properties of Portland cement mortars. Rubber aggregates were obtained by mechanical grinding of waste automobile tires, and introduced in the mixtures as partial replacement of sand at four different levels by volume. Ultrasonic pulse velocity and thermal conductivity tests were conducted on all rubber modified mortars, and the results obtained were compared to those of a non-modified control mortar. Test results showed that the incorporation of rubber aggregates in cement mortars notably improved their insulating properties, and that this improvement was much more marked on the thermal conductivity than on the sound conductivity. The most promising rubber modified mortar mixture showed very interesting results, as its thermal and sound conductivities were reduced by 40% and 17% respectively. These results could open very interesting application possibilities for these mortars, particularly as a coating material for residential buildings. This application would have two major environmental benefits: participating in solving the waste tires issue, but also enabling better insulated/less energy consuming residential buildings.

Keywords: Tire rubber, Thermal insulation, Sound insulation, Cement mortars.

Introduction

The accumulation of waste tires has become a major health, safety and environmental issue nowadays. The stockpiling of waste tires in landfills causes a variety of issues including fire hazards, water, soil and air pollution... In Algeria, H. Trouzine [1] estimated that 25918,5 tons of used tires were generated each year up until 2010, a number that has much likely widely increased, making this issue not only a global one, but very much an Algerian issue. Many solutions are used worldwide to deal with waste tires (reuse in plastic and rubber products, incineration with energy recovery...).

However, one of the most popular applications is the use of waste tire aggregates as a replacement aggregate in construction materials (concrete, cement mortars and bituminous materials). In this study, the influence of tire rubber aggregates on the sound and thermal insulation properties of cement mortars was investigated. Four different mixtures of rubber modified mortars were prepared, and the tests results obtained were then compared to those of a non-modified control mortar.

Experimental program

Materials and Mortars Preparation

Our mortars were prepared according to standard EN 196-1. Rubber aggregates were introduced in the mixture as partial replacement of sand by volume at four levels: 5, 10, 15 and 20 %. The mixture proportions were determined on a double basis: the recommendations of standard EN 196-1, and an optimum workability target defined by a slump flow ranging between 3 and 4 cm on the Abrams mini cone. This means that the water/cement ratio has been varied to ensure the same workability for all mortar mixtures. Sand/cement ratio was kept constant. No plasticizer has been used in this study.

Mixture proportions are recapitulated in Table [1]. The rubber aggregates used in this study were obtained by mechanical grinding of used tires from the automobile industry. They are very homogenous in size as more than 80% have dimensions included between 1.25 and 2.5 mm. Apparent density is 540 kg/m. Cement used was Matine from manufacturer Lafarge, it is a CEM II/B-L 42,5 N. Sand is a regular river sand with apparent density of 1720 kg/m, and fineness modulus 2.11.

Table 1. Mixture proportions

Cement [g]	450	427.5	405	382.5	360
	1350	1282.5	1215	1147.5	1080
Rubber aggregates [g]	0	21.2	42.4	63.6	84.8
	234	222.3	214.7	210.4	201.6
W/C	0.52	0.52	0.53	0.55	0.56
	3.3	3.4	3.6	3.5	3.7

Test Procedures

The sound insulation properties of the rubber modified mortars were studied by applying longitudinal ultrasonic vibrations in accordance with standard EN 12504-4. The vibrations frequency was 53 kHz. The device used was a TICO seen in Figure [1]. Thermal conductivity was determined using a specially designed device called the CT meter. It is a device that is used for the determination of the thermal properties of materials. Figure [2] shows the CT meter used for this study. The specimens used for both tests, prepared in accordance with standard EN 196-1 have dimensions of $(4 \times 4 \times 16)$ cm and are shown in figures [1] and [2].

Figure.1. TICO device used for the determination of the ultrasonic pulse velocity.

Figure.2. CT meter used for the determination of the thermal conductivity

Results and Discussions

Ultrasonic pulse velocity

Test results indicate that the ultrasonic pulse velocity decreases with the increase of rubber proportions in mortars. This decrease is proportional to the amount of rubber aggregates added in the mixtures, meaning that each time the proportion of rubber aggregates in the mixtures was increased, the ultrasonic pulse velocity decreased. Ultrasonic pulse velocity was measured at 3.63 km/s, 3.53 km/s, 3.43 km/s, 3.27 km/s and 3.00 km/s for mortars M0, M5, M10, M15 and M20 respectively, which corresponds to decreases of 2.76 %, 5.51 %, 9.92 % and 17.36 %. Figure [3] shows the variations in ultrasonic pulse velocity according to the proportion of rubber aggregates.
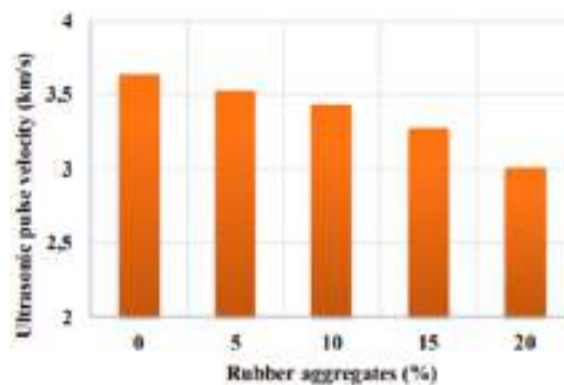
Figure.3. Influence of tire rubber aggregates on the ultrasonic pulse velocity of cement mortars

The decrease in ultrasonic pulse velocity is attributed to 2 reasons: 1) the higher porosity in rubber modified mortars [2]. Because ultrasonic pulses are better transmitted through dense materials, ultrasonic pulse velocity is closely linked to porosity, it decreases when porosity is increased as it is in the rubber modified mortars 2) the insulating properties of the rubber aggregates, which influence negatively the propagation of ultrasonic pulses. Considering the link between ultrasonic pulse velocity and sound insulation, these results indicate that the introduction of rubber aggregates in mortars improves their sound insulation properties.

Thermal conductivity

Test results show that the introduction of rubber aggregates in the mortars induced a progressive reduction in their thermal conductivity. Thermal conductivity was at a maximum of 1.698 W/mK for mortar M0, then progressively decreased as the proportion of rubber aggregates increased, reaching 1.486 W/mK for M5, 1.410 W/mK for M10, 1.195 W/mK for M15 and 1.016 W/mK for M20. We note that the introduction of rubber aggregates massively decreased the thermal conductivity of our mortars, as the mixture containing 20 % of rubber aggregates saw its thermal conductivity decreased by as much as 40.14 %. Thermal conductivity tests results are represented in figure [4].
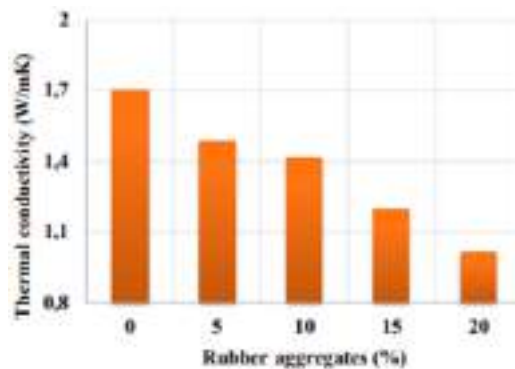
Fig.4. Influence of tire rubber aggregates on the thermal conductivity of cement mortars

Regarding the decrease in the thermal conductivity of rubber modified mortars, it can be explained by 2 main reasons. First, the intrinsic properties of the rubber aggregates, which are an insulating material with low thermal conductivity. A. Benazzouk [3] measured the thermal conductivity of rubber aggregates originated from waste automobile tires at 0.19 W/mK, which is roughly 1/9 of the thermal conductivity of our control mortar M0. Second, the increase in porosity caused by the rubber aggregates means that the rubber modified mortars contain more air, which participates in this decrease because of its own very low thermal conductivity (0.026 W/mK).

Conclusion

The work presented here focuses on the influence of tire rubber aggregates on the sound and thermal insulation properties of cement mortars. Results obtained showed that the rubber modified mortars' insulation properties were notably improved, with the mortar M20 showing the most interesting results, as its thermal and sound conductivities were reduced by 40% and 17% respectively. These results could open multiple application possibilities for this material, the most evident one being as a coating material or brick binder for residential buildings. Besides the technical advantages of this application, it would also present several advantages from the environmental point of view: providing a partial solution to the waste tires issue, and simultaneously reducing the consumption of sand reserves, but also enabling better insulated/less energy consuming residential buildings.

References

H. Trouzine et al. "*Problématique des pneumatiques usagés en Algérie"*, Nature & Technologie. 05. 2011.

A. Bakiri et D. Si bachir. "*Influence of tire rubber aggregates on the physico-mechanical properties of cement mortars"*, International Journal of Sustainable Building Technology and Urban Development. 10. 2019

A. Benazzouk et al. "*Thermal Conductivity of Cement Composites Containing Rubber Waste Particles"*, Construction and Building Materials. 22. 2008

PI Controls Power Generated by PV Solar Inverter Injected into The Electrical Grid

Nora Zerzouri

University Badji Mokhtar Annaba, Algeria, https://orcid.org/0000-0003-1209-4617

Nadia Benalia

University Badji Mokhtar Annaba, Algeria, https://orcid.org/0000-0003-4819-5313

Nadia BenSiAli

University Badji Mokhtar Annaba, Algeria, https://orcid.org/0000-0001-7248-4823

Abstract: The production of electrical energy by photovoltaic solar energy has experienced strong growth and remarkable developments in recent years because this energy source is clean, and non-polluting. However, connecting the photovoltaic system to the electrical grid can cause numerous harmful impacts on network operation. Among these, the most significant effect is injecting harmonics into the grid. The main objective of this study is to control a photovoltaic system connected to the grid to improve energy quality and minimize the harmful effects of this connection. In this paper, we presented the generalities of a photovoltaic system study and simulation, and then we inserted the DC-DC converter to raise the voltage level and improve the operation of the PV panel by pursuing the operating point at maximum power, the technique used is the Incremental Conductance INC. Connection to the network is done by inserting a three-phase voltage inverter allowing synchronization with the network and operation at unity power factor. Finally, the controller performance is examined using a numerical simulation.

Introduction

The increasing demand for sustainable energy solutions has propelled the adoption of photovoltaic (PV) solar energy systems worldwide. As a clean and renewable power source, solar energy reduces greenhouse gas emissions and promotes energy independence. However, integrating PV systems into the electrical grid presents several challenges, particularly in maintaining power quality and stability. One of the key factors influencing the

effective operation of grid-connected PV inverters is the control strategy employed to manage the power output. Proportional-integral (PI) control is a widely used method in power electronics for regulating the production of PV inverters. This control strategy offers a robust solution for managing the system's dynamic behavior, ensuring that the generated power is efficiently injected into the grid while adhering to regulatory standards (**Guerrero, Loh, Lee, & Chandorkar,** 2013).

By continuously adjusting the inverter's output based on voltage and current feedback, PI controllers can effectively minimize deviations from the desired set points, thereby enhancing the overall stability of the grid. The primary objective of this introduction is to outline the significance of PI control in optimizing the power generated by PV solar inverters. We will discuss the operational principles of PI control, its advantages in the context of solar energy systems, and its role in mitigating issues such as harmonics and power factor discrepancies. Furthermore, we will highlight the importance of synchronizing the inverter with the grid to ensure seamless integration and reliable performance. As the demand for clean energy continues to rise, the development and implementation of effective control strategies like PI control will be paramount in maximizing the benefits of PV solar systems while ensuring grid stability and reliability.

Proposed System Overview

The proposed system is illustrated in Figure. 1, comprises a three-phase symmetrical grid integrated with a two-level inverter. This inverter is connected in parallel with a nonlinear load through an output filter composed of inductance (L_f) and resistance (R_f). A DC-link capacitor and a photovoltaic (PV) array regulate the output voltage injected into the grid.
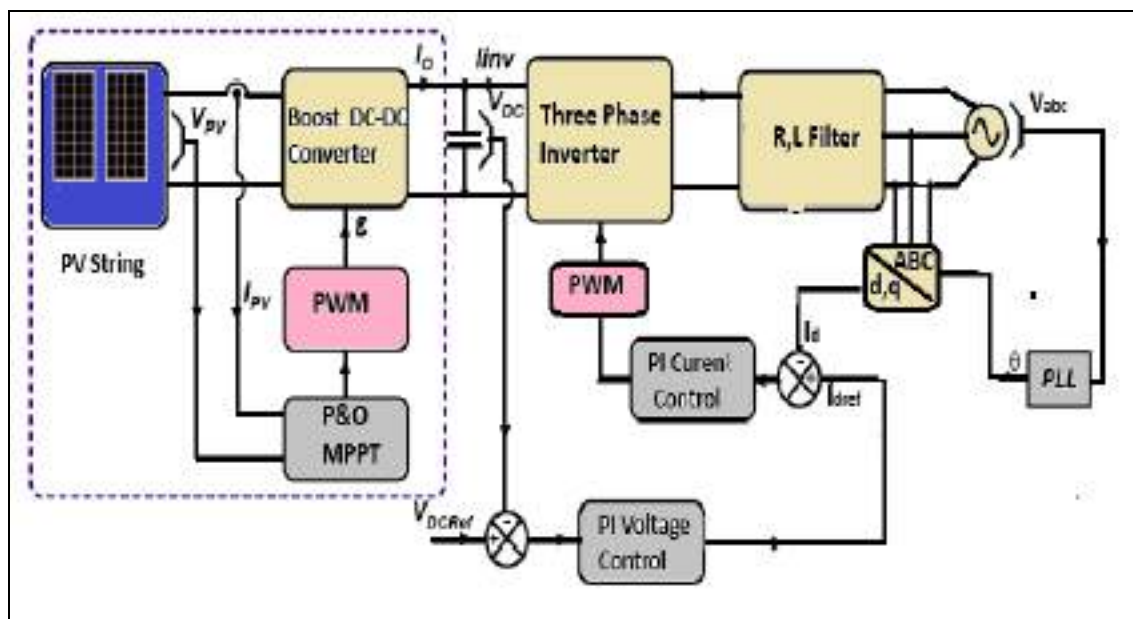
Figure 1. Block Diagram of PV Energy Generation System.

The inverter utilizes bidirectional switching devices, specifically Insulated Gate Bipolar Transistors (IGBTs), with a clamped diode on each bridge arm. This configuration facilitates a stable connection to the reference point, ensuring reliable operation under varying load conditions. On the DC side, the DC-link capacitor is connected to the PV system to smooth out voltage fluctuations and maintain a consistent output voltage. Through this configuration, the system is designed to optimize the performance of the PV array, ensuring maximum energy harvesting while minimizing potential disturbances to the grid.

PV Mathematical Modelling

The different equivalent circuits of PV cells have been proposed in the literature (Munish, Obulesu, Shivi, Sairaj, Rambabu, Satyanarayana**, 2023**), for example, single-diode, two-diode, and three-diode equivalent circuits of PV cells. The single diode-based PV cell circuit is widely used for power systems studied because of its simplicity and accuracy (Saleem, Farhan, Raza, Awan, Butt, & Safdar, 2023).

The equivalent circuit of a single-diode PV cell is shown in Figure 1. It consists of a diode connected in parallel with the current source, parallel resistance R_{sh} representing the leakage resistance of the *pn* junction, and series resistance R_s representing the PV cell's internal resistance.
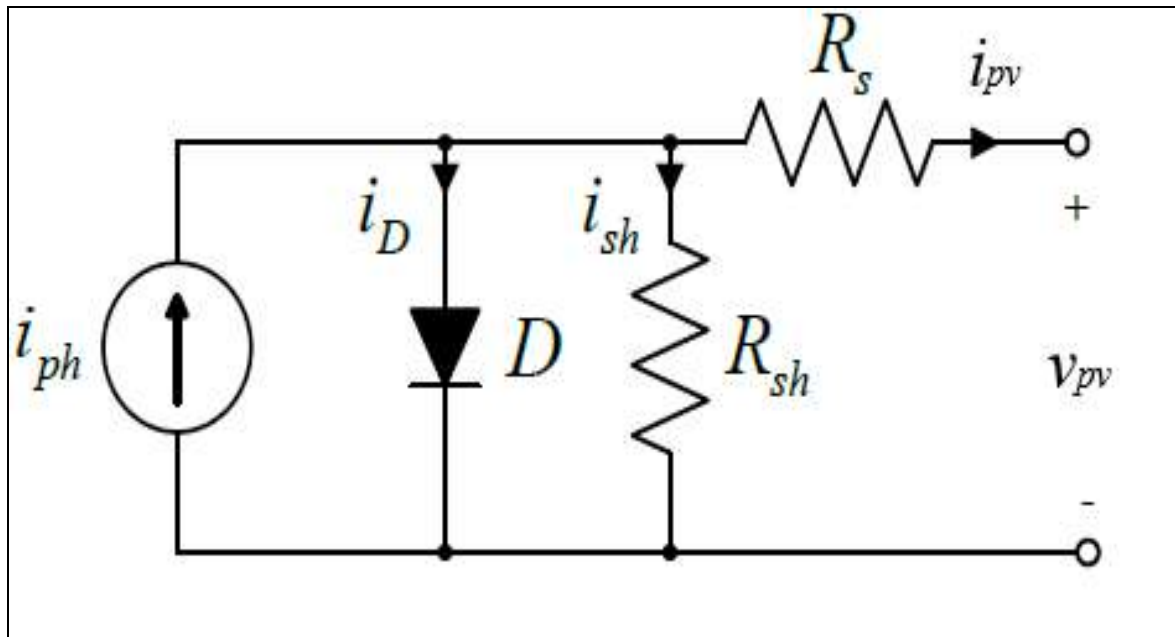
Figure 2. Electrical PV module equivalent circuit

According to the Shockley equation, the current is as follows (Zerzouri, Ben Si Ali, & Benalia, 2023):

$$I_D = I_0 \left(\exp\left[\frac{qV_C}{aT_C K}\right] - 1 \right) \tag{1}$$

In general, the cell current is obtained from the current difference between the current generated by solar radiation and the diode current (Ben Si Ali, Benalia, & Zerzouri, 2023):

$$I_{pv} = I_{SC} - I_D - I_{sh} \tag{2}$$

The saturation current of the cell diode is as follows:

$$I_0 = I_{rs} \left(\frac{T}{T_{ref}}\right)^3 \left(\exp\left[\frac{qE_g}{aK}\left(\frac{1}{T_{ref}} - \frac{1}{T}\right)\right]\right) \tag{3}$$

The equation of the I-V characteristic PV module is given by (**Boubakir, Touil, Labiod, & Boudjerda, 2023**):

$$I_{pv} = I_{ph} - I_0\left[e^{\left(\frac{V_{pv}+R_SI_{pv}}{\alpha V_t}\right)} - 1\right] - \frac{V_{pv}+R_SI_{pv}}{R_{sh}} \tag{4}$$

Where I_{pv} is the output current of PV cell (A), I_{ph} is the photo-generated current (A), I_D is the diode current (A), I_{sh} is the shunt current (A). I_{sc} is the short-circuit cell current, the Charge of an electron (q) is 1.602×10^{-19} C, Boltzmann's constant (k) is 1.380×10^{-23} J/K, a is the ideality factor of a diode, Temperature in ($\circ C$), ($V_t = NskT/q$) is the thermal voltage of the array with Ns cells connected in series, R_s is the equivalent series resistance, R_{sh} is the equivalent shunt resistance.

Table 1 shows the main characteristics of the PV array, designed using Advanced Renewable Energy AREi-215-M6-G modules connected in a proper series-parallel, making up a peak installed power of 25.8 kW.

Table 1. Nameplate of reference solar module

Parameter	Value
Rated power/voltage/current of PV module	215 W, 29.52V, 7.28A
Number of series-connected PV modules	12
Number of parallel connected PV strings	10
Rated power/voltage/current of PV array	25.8KW,354.2V,72.8A

Figures 3 and 4 display the simulation results of the Power-Voltage and Current-Voltage characteristic curves for the 25.8 kW PV module.

Many factors impact a PV system's output characteristics. Ambient temperature and solar irradiance influence PV panels' output voltage (Livinti, 2021). Higher irradiance increases the maximum power and efficiency of the solar cell, but temperature reduces them.
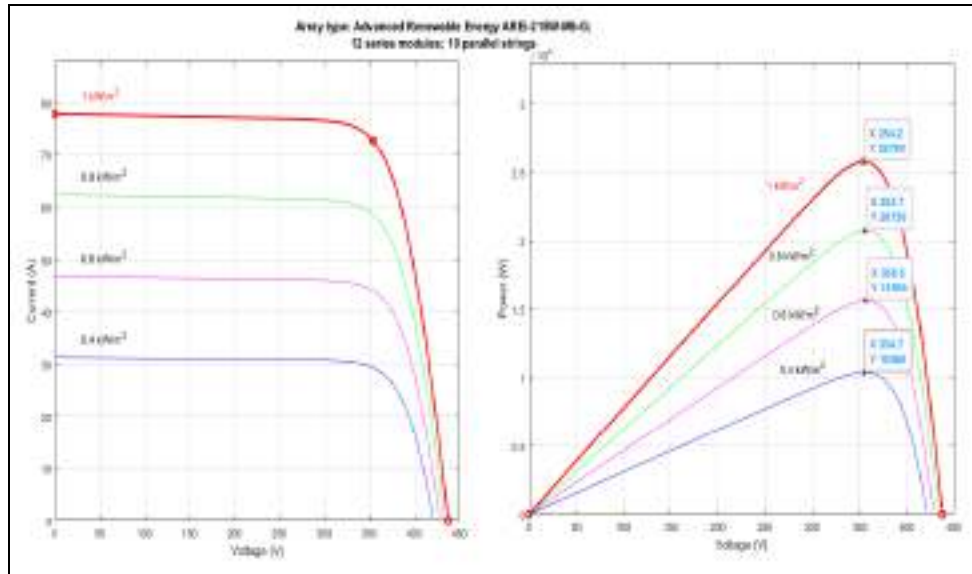
Figure 3. I-V and P–V characteristics of the PV Array at different insolation levels.
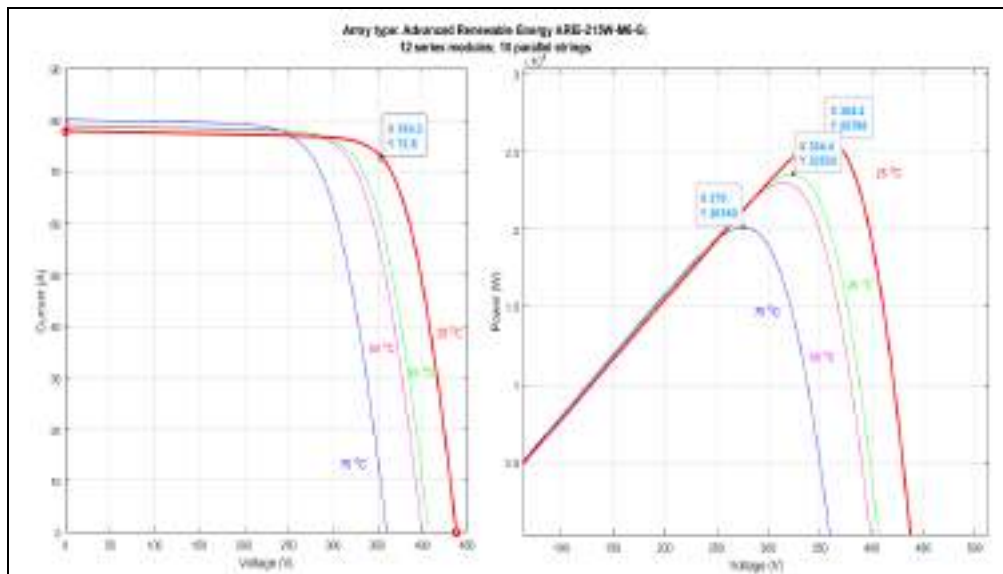
Figure 4. I-V and P–V characteristics of the PV Array at different Temperatures.

Modeling of the boost converter and the incremental conductance MPPT technique

DC-DC Boost Converter

A cascade boost converter DC-DC is a powerful electronic device that is commonly utilized to boost the voltage of a PV solar panel. Solar PV systems produce electricity with different voltages based on sunlight intensity, temperature, and load demand. By increasing the voltage to a more usable level, a cascade boost converter enables the system to handle these variations, which can be used for either direct use or storage. This configuration aims to obtain a higher output voltage than a single-stage converter by connecting multiple boost converter stages in series. The voltage increases at each stage as the input from the PV solar panel is processed

sequentially. The DC-DC converter design also typically includes Maximum Power Point Tracking (MPPT) algorithms, which optimize the operating point of the solar panels to ensure the most efficient energy harvest For applications that necessitate high-voltage DC, like electric vehicles, grid-tied inverters, or battery energy storage systems, this converter is particularly advantageous. The DC-DC boost converter contains an inductor, capacitor, diode, and an IGBT as it is a high-frequency switch. It produces higher voltage during power supply to the load. Based on the switch duty cycle the output voltage may change. Generally transformer can step up the voltage, but there may be losses in the transformer. So to overcome this loss DC-DC Boost converter is used to get the desired output voltage.

Based on the DC-DC converter circuit shown in Figure 5, the mathematical model can be written with the following equation (Khan, Khan, Khan, Ullah, & Latif, 2024):

$$\begin{cases} \frac{dv_{pv}}{dt} = \frac{1}{C_{pv}} i_{pv} - \frac{1}{C_{pv}} i_L \\ \frac{di_L}{dt} = \frac{1}{L}(1-D)v_{pv} - \frac{1}{L} v_{dc} \end{cases} \tag{5}$$

where, v_{pv} and i_{pv} are the *PV* panel output voltage and current, i_L is the DC-DC converter inductor current, v_{dc} is the DC-link voltage, C_{pv} and L are the DC-DC converter electrical parameters.

The pulse width or duty cycle D is the ratio between the times that the pulse lasts at a high level.
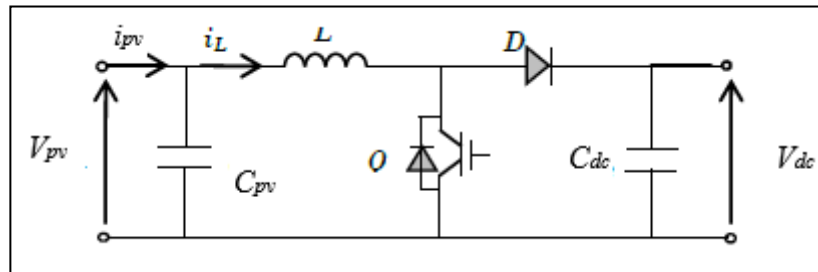
Figure 5. DC-DC Boost converter

The boost converter output voltage and current are given as (Mai, Zhang, & Hu2024):

$$\begin{cases} V_{dc} = \frac{V_{pv}}{1-D} \\ I_{out} = (1-D)I_{pv} \end{cases} \tag{6}$$

The inductor and capacitor are chosen so that the ripple current and ripple voltage are within the limits as follows (Singh, Hussain, & Singh, 2018, Mai, Zhang, & Hu, 2024; Rujas, Landaburu, Lopez-Martin, & Barambones, 2023, Zeb, Islam, S., Uddin, Khan, Ishfaq, Busarello, & Kim, 2021):

$$L = \frac{V_{dc} - V_{pv}(1-D)}{\Delta I_{dc} f_s} \tag{7}$$

$$C_{pv} = \frac{I_{dc}D}{\Delta V_{dc}f_s} \tag{8}$$

In this context, ΔI_{dc} link represents the ripple current, and ΔV_{dc} denotes the ripple voltage. The switching frequency of the DC-DC converter is denoted as fs. Based on equations (7) and (8), the critical values of the inductor and capacitor are calculated to be 4.8 mH and 2600 μF, respectively, for Vpv = 354.2 V, Vdc = 620 V, duty cycle D = 0.42, and fs = 1 kHz. To ensure the converter operates in continuous conduction mode, the chosen inductor and capacitor values must exceed these critical values.

Incremental Conductance MPPT Technique

Due to the continuous variation of maximum power in photovoltaic (PV) installations caused by changing atmospheric conditions, implementing a robust Maximum Power Point Tracking (MPPT) controller is crucial. The primary objective of MPPT techniques is to ensure that the PV system operates at its maximum power point (MPP), thereby optimizing energy collection from available resources. Various approaches to MPPT have been discussed in the literature, as referenced in (Haro-Larrode, & Bayod-Rújula, 2023, Prajapati, Garg, & Mahajan, 2024).
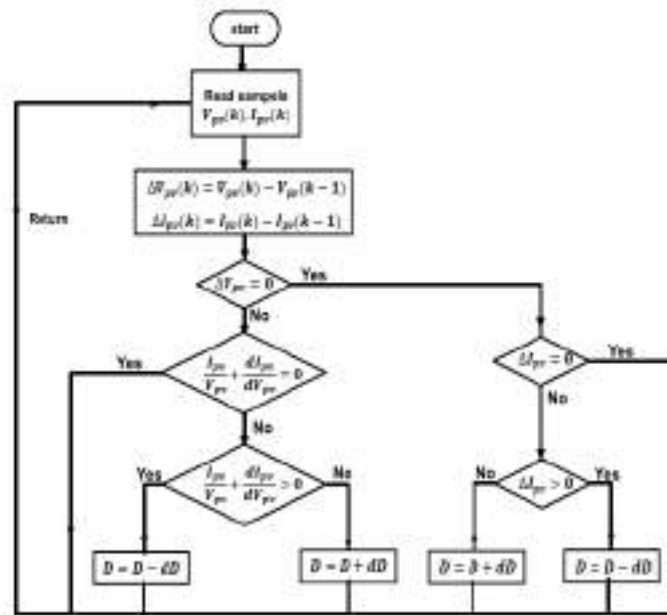
Figure 6. Flowchart of Incremental Inductance

One effective method for MPPT is Incremental Conductance, which analyzes a PV panel's Power-Voltage (P-V) curve. This curve represents the relationship between the power output and the voltage across the panel. The incremental conductance method evaluates the slope of the P-V curve to determine the optimal operating point. Mathematically, the slope of the P-V function can be characterized as follows:

$$\frac{dP}{dV} = 0 \qquad \text{On V}_{MMP}$$

$$\frac{dP}{dV} < 0 \qquad \text{On the right V}_{MMP}$$

$$\frac{dP}{dV} > 0 \qquad \text{On the left V}_{MMP}$$

The flowchart in Figure 6 illustrates the algorithm of this technique.

Control of Three-Phase Currents in Electrical Networks

The goal of controlling the PV system using a voltage inverter is to achieve balanced sinusoidal currents in phase with the voltage, ensuring that the generated reactive power remains zero. The general control structure of a grid-connected PV system includes two nested control loops: an outer loop for regulating the DC bus voltage and an inner loop for managing the direct and quadrature currents.

The power generated is injected into the grid through a voltage inverter, which facilitates energy transfer by performing the following two tasks:

- Maintain a constant DC bus voltage by controlling the power transferred to the grid through the voltage inverter.
- Control the static switches to inject the reference power into the grid, which is the power generated by the photovoltaic panel minus the power stored in the capacitor
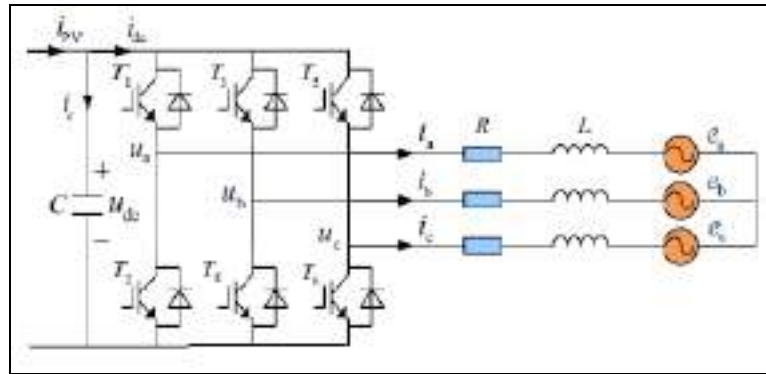
Figure 7. Voltage source Inverter

The proposed system, illustrated in Figure 7, comprises a three-phase symmetrical grid, based on a two-level inverter connected in parallel with a nonlinear load through an output filter (L_f R_f), a PV array, and a DC-link capacitor. The General relationship of the grid-tied inverter voltages and line currents can be expressed as:

$$\begin{cases} u_a = R_f i_a + L_f \frac{di_a}{dt} + e_a \\ u_b = R_f i_b + L_f \frac{di_b}{dt} + e_b \\ u_c = R_f i_c + L_f \frac{di_c}{dt} + e_c \end{cases} \tag{9}$$

Where e_a, e_b, e_c are the three-phase grid voltages, u_a, u_b, u_c are the inverter output voltages, and i_a, i_b, i_c are the three-phase line currents.

Given the need for voltage-oriented vector control to manage current control for the inverter module's injection, it is essential to model the system in the synchronous coordinate domain. From Equation (9), the grid-tied inverter model in the rotating frame (d-q) can be expressed as (Singh, Hussain, & Singh, 2018; Boopathi, & Indragandhi, 2024):

$$\begin{cases} u_d = R_f i_d + L_f \frac{di_d}{dt} + \omega i_q + e_d \\ u_d = R_f i_q + L_f \frac{di_q}{dt} - \omega i_d + e_q \end{cases} \tag{10}$$

Where u_d, and u_q are the d-axis and q-axis inverter-voltage components, e_d, and e_q are the grid d-axis and q-axis voltage components, i_d and i_q are the d-axis and q-axis injected grid currents and ω is the grid angular frequency.

To simplify the control of active and reactive powers in a grid-tied inverter, we can utilize the voltage orientation technique by aligning the d-axis with the grid voltage. This method allows us to decouple the control of active and reactive power, making the control strategy more manageable. From the equation 10, we start by expressing the active and reactive powers in terms of the d-q components:

$$\begin{cases} P = \frac{3}{2}\left(e_d i_d + e_q i_q\right) \\ Q = \frac{3}{2}\left(e_q i_d - e_d i_q\right) \end{cases} \tag{11}$$

We can set the q-axis voltage component e_q to zero by applying the voltage orientation technique. This results in the following simplifications:

$$\begin{cases} e_d = v \\ e_q = 0 \end{cases} \tag{12}$$

Given this alignment, the equations for active and reactive power become:

$$\begin{cases} P_g = \frac{3}{2} e_d i_d \\ Q_g = -\frac{3}{2} e_d i_q \end{cases} \tag{13}$$

This decoupling allows for independent control of active and reactive power. The active power can be controlled by adjusting the d-axis current I_d and the reactive power can be controlled by adjusting the q-axis current I_q.

After decoupling the active and reactive power control, we examine equation (13). This formulation introduces two new control inputs: I_{dref} and I_{qref}. These inputs are essential for regulating the d-axis and q-axis currents, respectively. We can achieve a fast dynamic response and zero steady-state errors using PI-type regulators. In the diagram, K_{ip} and K_{ip} represent the proportional and integral parameters respectively; I_{ref} is the reference current signal, and I is the feedback current. This configuration is designed for the I_d and I_q control loops. Based on the diagram, the closed-loop transfer function for the I_d and I_q axis current loops is:

$$\frac{I_d}{I_{dref}} = \frac{I_q}{I_{qref}} = \frac{k_{ii}}{L_f} \frac{s + \frac{k_{ii}}{k_{ip}}}{s^2 + s\frac{k_{ip} + R_f}{L_f} + \frac{k_{ii}}{L_f}}$$

(14)The parameters of the current regulator can be designed as follows:

$$k_{ip} = 2\zeta\omega_n L_f - R_f$$

(15)

$$k_{ip} = \omega_n L_f$$

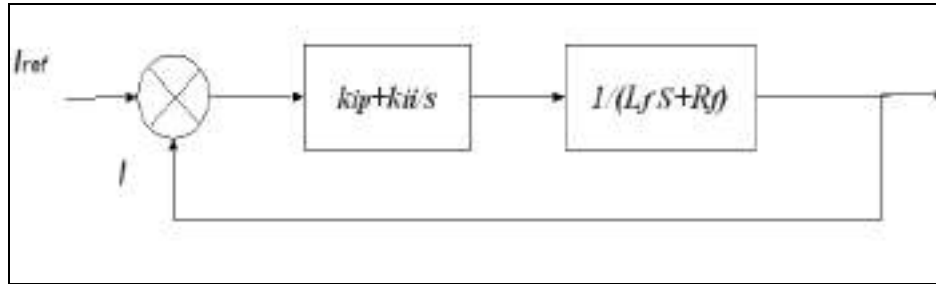(16)

Figure 8. Current loop diagram

DC Bus Voltage Control Strategy

The correct operation of the inverter also depends on good regulation of the V_{dc} voltage. The regulation of this voltage provides a reference current for the d axis (I_{dref}). As a result, the DC-link voltage's open-loop transfer function can be presented as:

$$G(s) = \frac{V_{dcref}}{I_{dref}} = \frac{3}{2} \frac{e_d}{sCV_{dc}}$$

(17)

The PI controller input is the error signal between the reference DC voltage and the actual capacitor DC link voltage, and this error shall be equal to zero to regulate the DC voltage at a fixed value. So, the closed-loop transfer function of the DC link Voltage loop after adding a PI controller will be a second-order system as expressed in equation (18) the poles of the transfer function of the closed-loop DC link voltage shall equal the poles of the reference system characteristic equation shown in equation (19) and (20).

$$G_{cl}(s) = \frac{(3K_{up}e_d s + 3K_{ui}e_d)}{2CV_{dc}s^2 + 3K_{up}e_d s + 3K_{ui}e_d}$$

(18)

Where *C* is the DC-link capacitance, K_{up} and K_{ui} are DC-link voltage controller gain values.

The damping ratio $\frac{2\xi}{\omega_n} = 3\frac{K_{up}e_d}{2CV_{dc}}$ and $\frac{1}{\omega_n^2} = 3\frac{K_{ui}e_d}{2CV_{dc}}$

Thus, the parameters of the voltage regulator can be designed as follows:

$K_{up=}\dfrac{4\xi C}{3\omega_n}$

(19)

$K_{ui=}\dfrac{2C}{3\omega_n{}^2}$

(20)
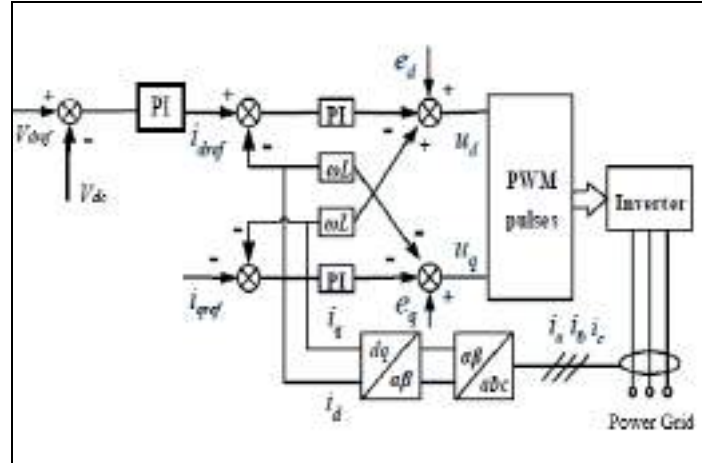
Figure 8. Control Block Diagram of the Grid tied Inverter

Results and Discussion

In this section, MATLAB/SIMULINK is used to show the validity of the proposed algorithm on the grid-tie system modeling. The system is composed of the PV array, the boost converter, and the three-phase grid, as described in Figure 1, Table 2 lists the grid-tied system simulation parameters where the characteristics of the PV array system for series modules of N_{se}=12 and parallel modules of N_p=10 are given in Table 1.

To study the importance of the proposed controller, rigorous irradiance profiles are applied to the grid-tie PV system at 25 °C ambient temperature. First, the classical IC MPPT techniques have been tested under step change irradiance.

Table 2. Parameters of electrical power system

Parameter	Description	Value
P_{pv}	Maximum PV power	25.8 KW
$E_{[RMS]}$	Terminal Voltage	230 V
f_g	Grid frequency	50Hz
V_{dc}	DC-link Voltage	620 V
L_f	Filter Inductance	6.2 mH
R_f	Filter Resistance	0.05 Ω
I_{pv}	PV array current	78.5 A
V_{pv}	PV array voltage	354.2 V
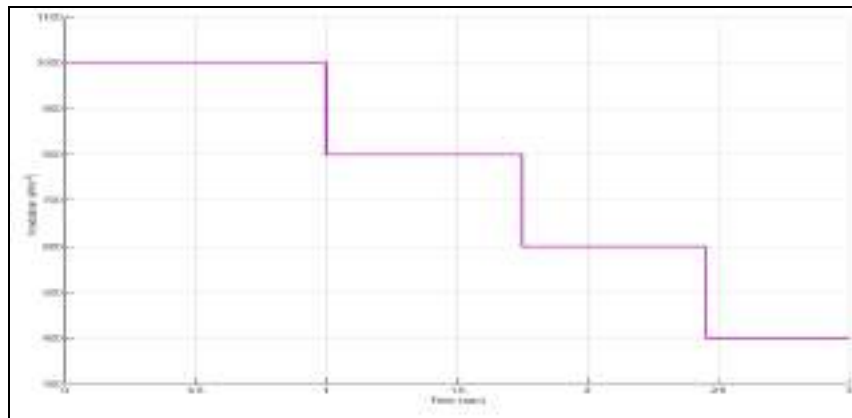
Figure 9. Irradiance levels used in a simulation for MPPT control with 25∘C temperature

The PV current dynamically adjusts as the irradiance changes to match the irradiance profile. Figure 10 displays the PV current and voltage, duty cycle, and PV power output, illustrating how the controller tracks irradiance variations over time. This tracking allows the system to consistently reach the maximum power point, ensuring optimal power delivery from the PV solar array.
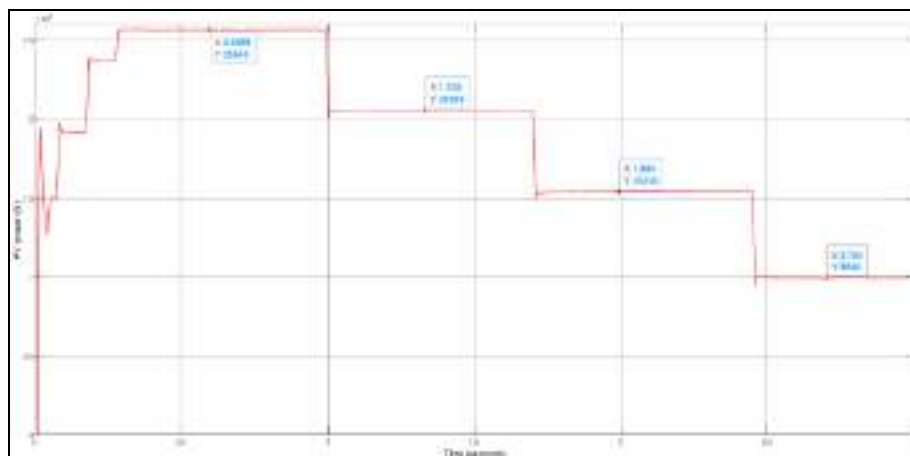

(a)
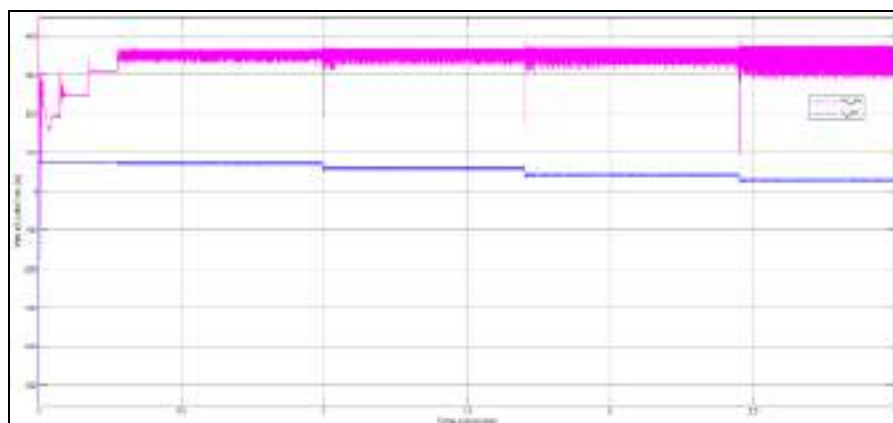
(b)
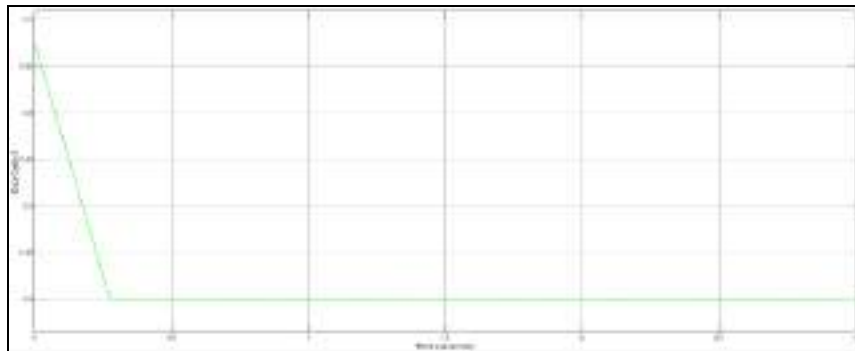
(c)

Figure 10. (a) Output power, (b) Output voltage and current, (c) duty cycle

Figure 11 shows the grid voltage and current in phase, indicating a unity power factor for the grid power. When the current and voltage are in phase, maximum active power transfer to the grid is achieved, which illustrates the active power delivered to the grid. By setting the reference I_q to zero, the reactive power component is effectively eliminated, allowing only real power to be injected into the grid. The DC link voltage is kept constant during the irradiation change.
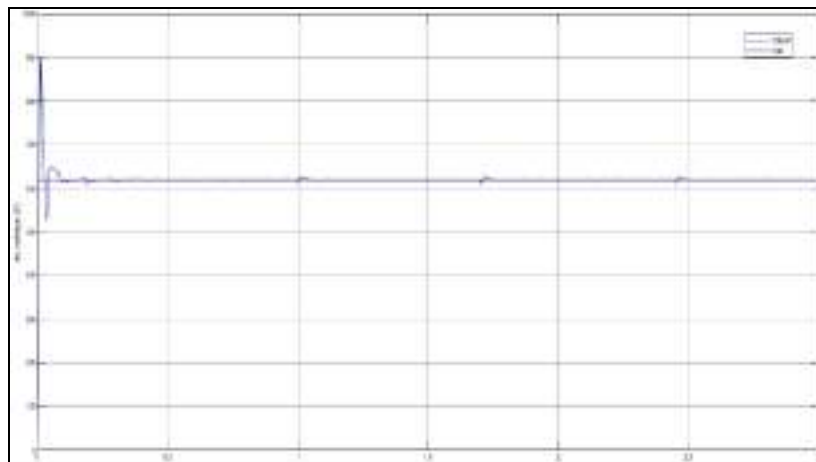
(a)
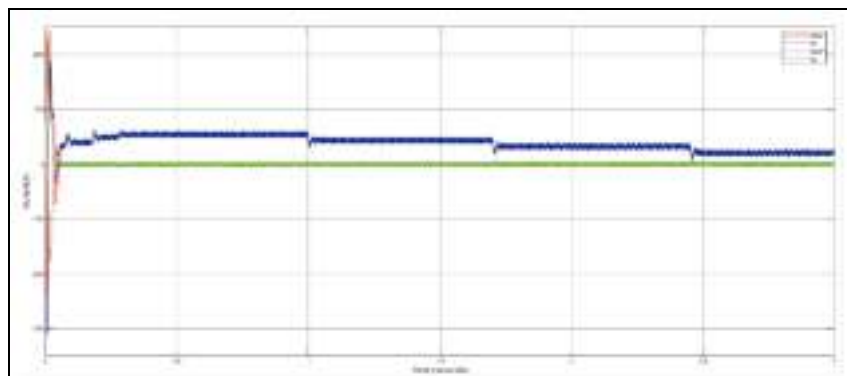
(b)
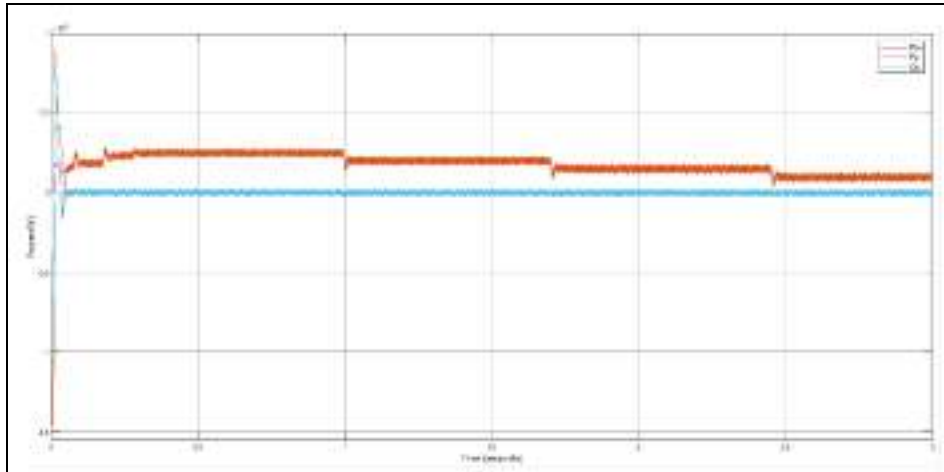
(c)
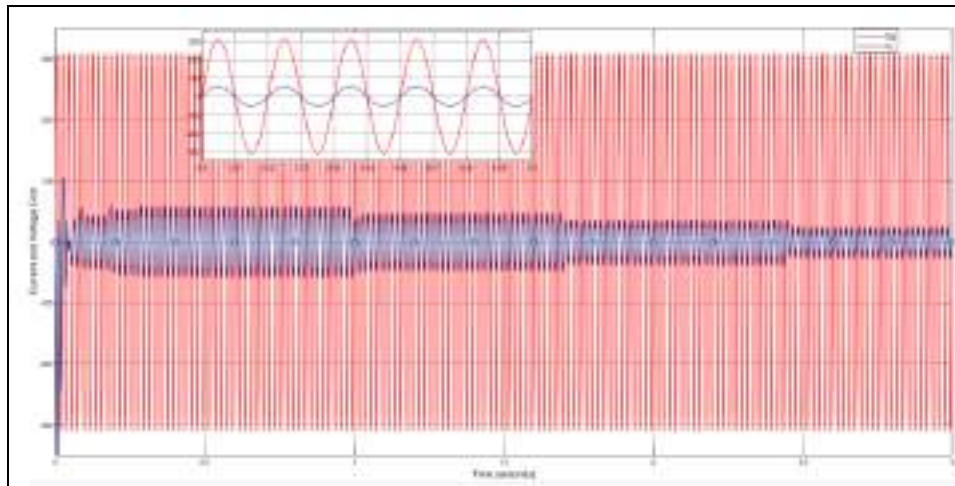
(d)

Figure 11. (a) DC-Link voltage and reference, (b) direct and quadratic currents,
(c) Active and reactive Power and (d) phase voltage and current grid

To evaluate the performance of the proposed control system, a variable load connection test was carried out on
the quality of the energy injected into the grid.

Test 1: Resistive load

To evaluate the performance of the proposed control system, a variable load connection test was carried out on
the quality of the energy injected into the grid. The system initially operates in balanced load mode. The 10 kW
three-phase resistive load is disconnected at t=1s and connected at t=2 with the same resistive load.

When disconnecting the three-phase load, the load currents decrease, and when connecting the load the currents
increase. The output voltage quality is the same against load disturbances. The load configuration chosen in this
test does not cause system instability.
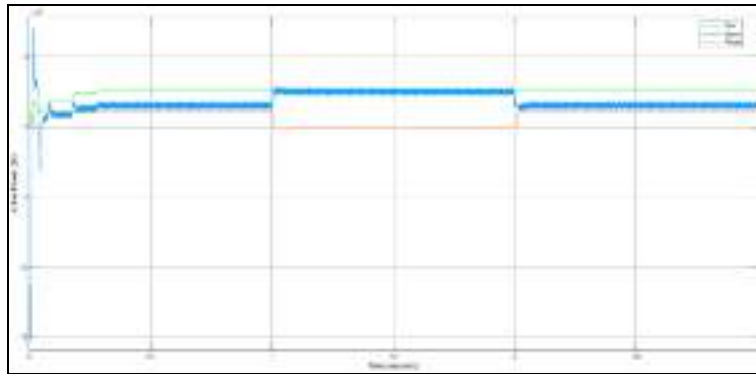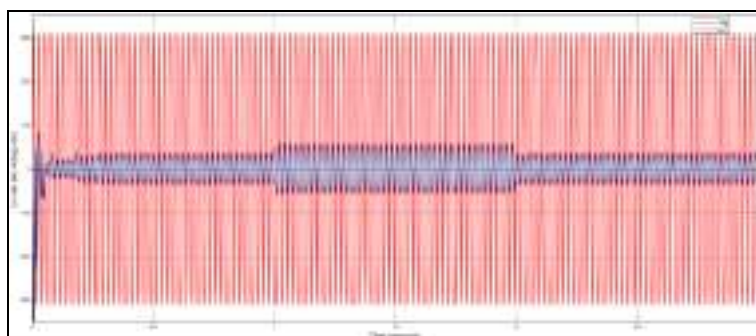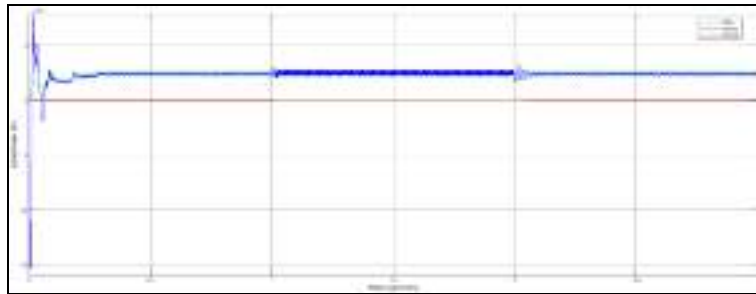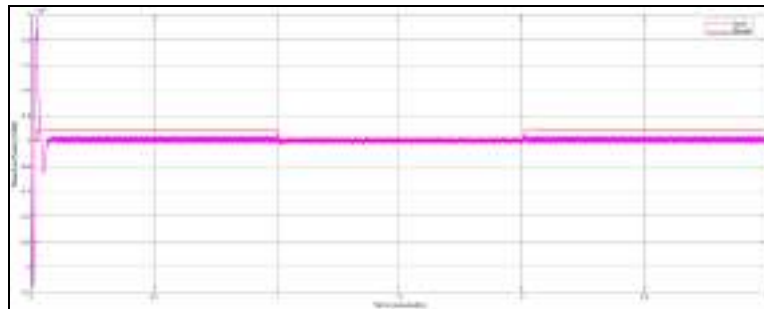
(a)
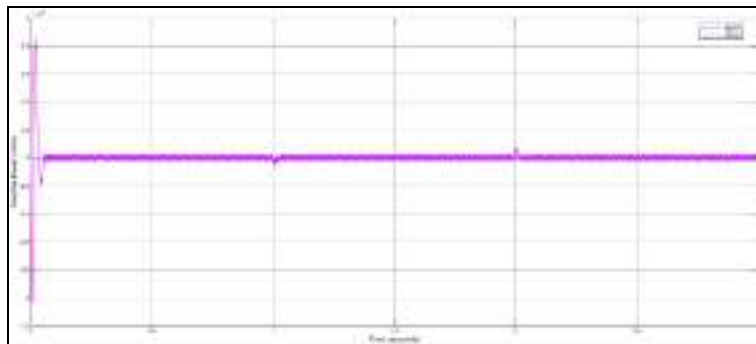
(b)
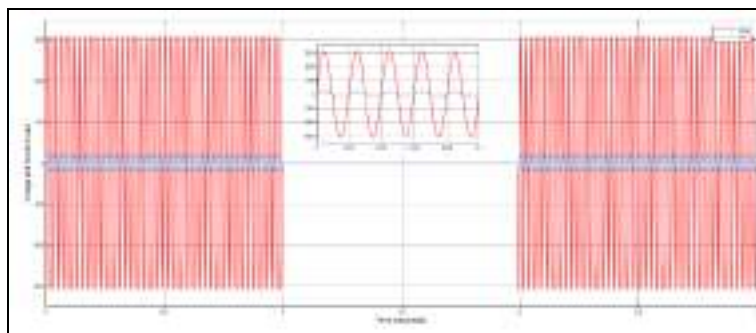
(c)

(d)

Figure 12. (a) PV, active and Load Power, (b) Reactive power, (c) Load current
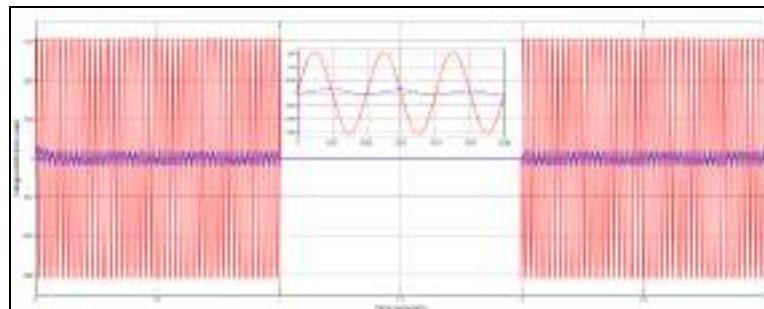
(d) Grid current

Test 2: Inductive Load

As shown in Figure 13, the system maintains its stability during connection and disconnection of the RL load. However, the load currents undergo very short transients before reaching the steady state. The generator thus provides both reactive power and active power corresponding to the grid-connected RL load power.
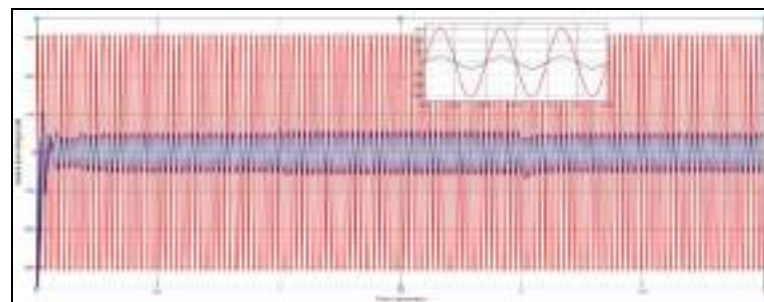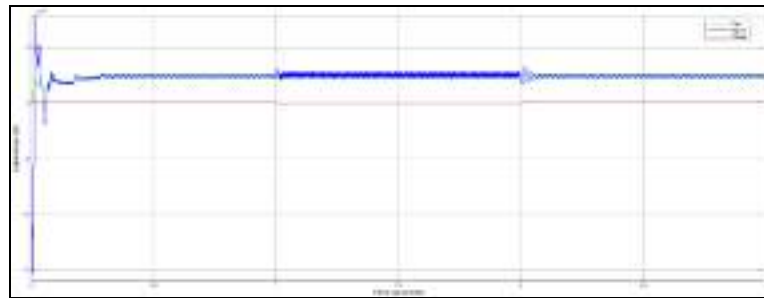

(a)

(b)

(c)

(d)

Figure 13. (a) PV, active and Load Power, (b) Reactive power, (c) Load current
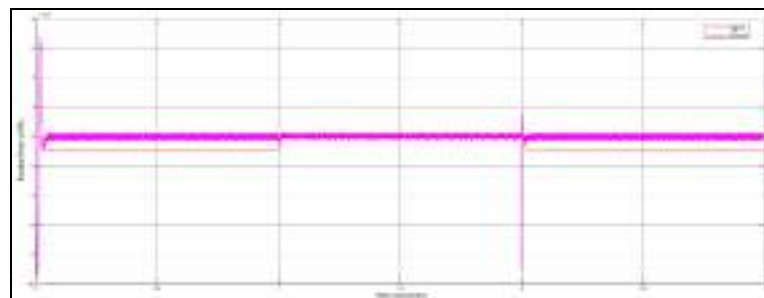(d) Grid current

Test 3: Capacitive Load

In this case study, we evaluate our results to the variations of a capacitive resistive load. An RC load with a power of 5kW and -9kVAR is disconnected at t = 1s and then connected at t = 2 s.
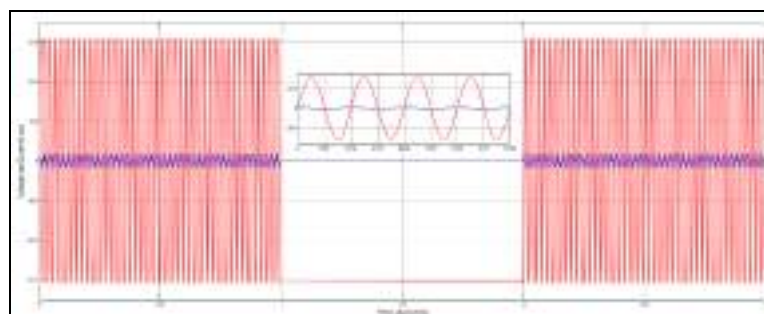
The system maintains its stability during connection and disconnection of the resistive capacitive load, the load currents undergo very short transient regimes which remain within acceptable limits.
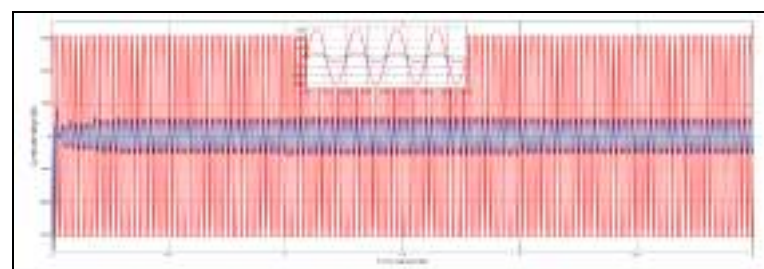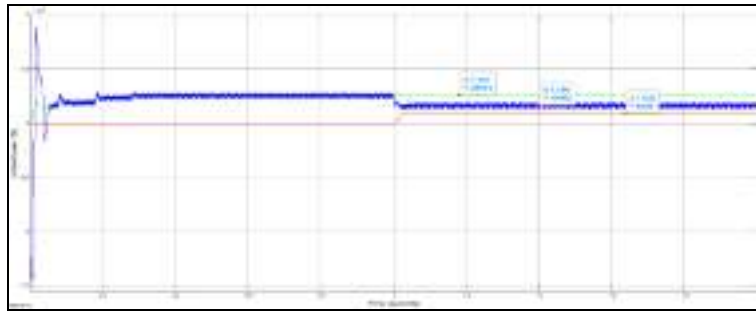
(a)

(b)

(c)

(d)

Figure 14. (a) PV, active and Load Power, (b) Reactive power, (c) Load current
(d) Grid current

Test 4: Nonlinear load

In this test, the performance of the system with a nonlinear load is studied. The system initially operates with a three-phase diode bridge rectifier on a resistive load R, that is disconnected at t=1s. The rectifier is a nonlinear load and generates harmonic currents. Figure 15(d) shows the PCC currents that are distorted after connecting the rectifier load.

(a)
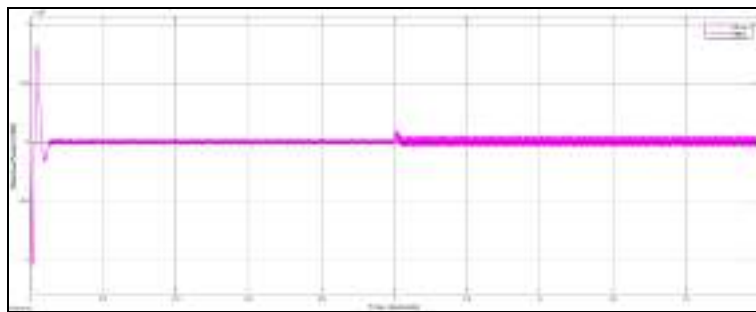
(b)

(c)
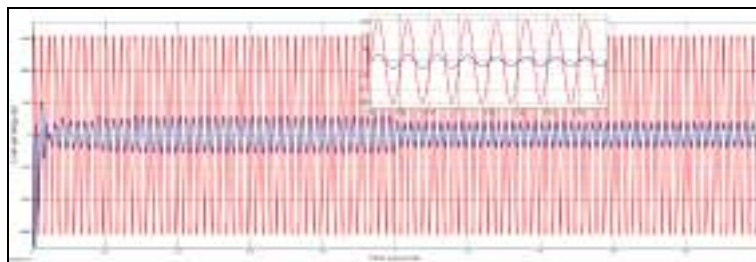
(d)

Figure 15. (a) PV, active and Load Power, (b) Reactive power, (c) Load current
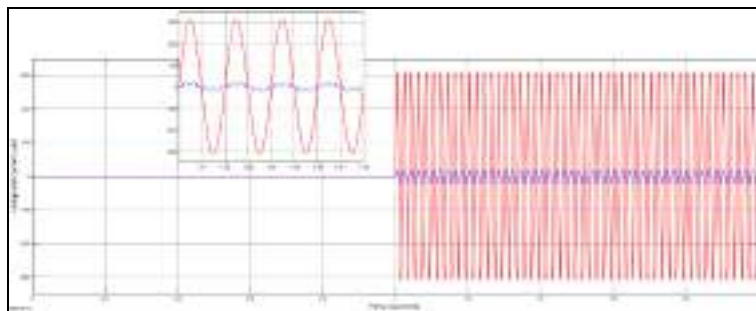(d) Grid current
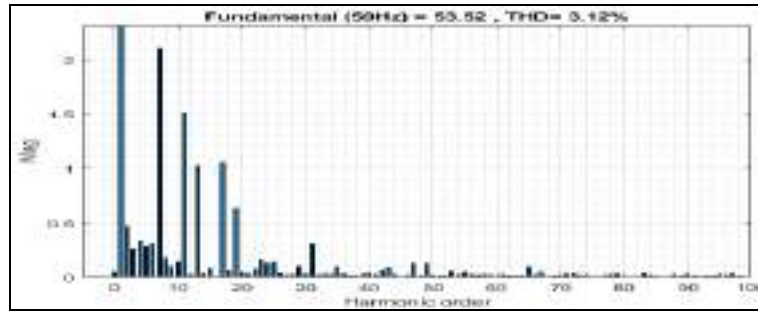
(a)
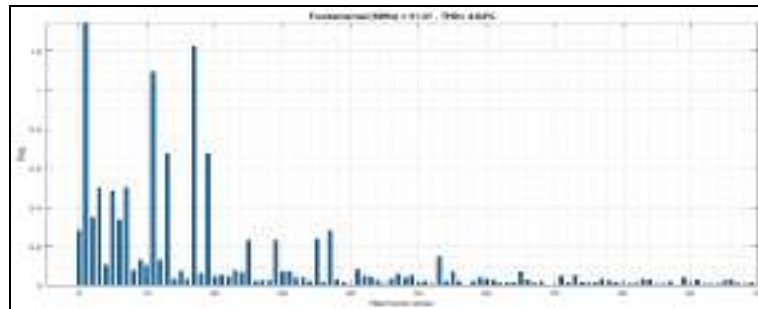
(b)

(c)
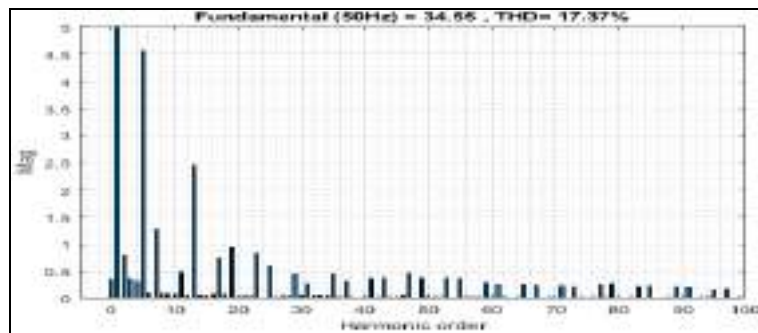
(d)

Figure 16. Grid current harmonic specter (a) with resistive load, (b) with inductive load,
(c) with capacitive load, (d) with nonlinear load

The grid current THD of the system is obtained with a PI controller during 1000 W/m² irradiation and variable loads are 3.12% with a resistive load, 4.64% with inductive load, 4.60% with a capacitive load, and 17.37% with nonlinear load. The FFT analysis of the network current during load variation is illustrated in Figure 16 with a

PI controller. A significant distortion of the THD is obtained especially when a non-linear load is connected to the network.

Conclusion

In this paper, a decoupled control of a grid-connected PV system using PI controller is presented. The Matlab/Simulink software is used to develop and simulate the system. The PI control technique has been implemented to supply PV power to a three-phase grid, providing load balancing, harmonic minimization, and power factor correction. Simulation and test results have shown that the THD of the grid current is within an acceptable range except for a non-linear load and it extracts the maximum amount of energy from a solar PV array. The proposed control has proven to be reliable and is used to connect a solar PV array to a three-phase grid. However, test results have shown that a PV array provides maximum power to the grid and the THD of the grid current is within the acceptable limit of an IEEE 519 standard except for the non-linear load.

References

Ben Si Ali, N., Benalia, N., & Zerzouri, N. (2023). Improved design of advanced controller for a step-up converter used in photovoltaic system. Energy Harvesting and Systems, aop. https://doi.org/10.1515/ehs-2022-0080.

Boopathi, R., & Indragandhi, V. (2024). Experimental investigations on photovoltaic interface neutral point clamped multilevel inverter-based shunt active power filter to enhance grid power quality. *IEEE Access*. https://doi.org/10.1109/ACCESS.2024.3405533.

Boubakir, A., Touil, S.-A., Labiod, S., & Boudjerda, N. (2023). A robust model-free controller for a three-phase grid-connected photovoltaic system based on ultra-local model. Protection and Control of Modern Power Systems. https://doi.org/10.1186/s41601-023-00315-5

Guerrero, J. M., Loh, P. C., Lee, T. L., & Chandorkar, M. (2013). Advanced control architectures for intelligent microgrids - Part II: Power quality, energy storage, and AC/DC microgrids. *IEEE Transactions on Industrial Electronics, 60*(4), 1263-1270.

Haro-Larrode, M., & Bayod-Rújula, Á. A. (2023). A coordinated control hybrid MPPT algorithm for a grid-tied PV system considering a VDCIQ control structure. *Electric Power Systems Research*, 221, Article 109426. https://doi.org/10.1016/j.epsr.2023.109426.

Khan, A., Khan, L., Khan, Q., Ullah, Z., & Latif, A. (2024). Observer based finite time sliding mode control strategies for single-stage grid-connected PV system with LCL filter. *Energy Reports*, 12, 381–401. https://doi.org/10.1016/j.egyr.2024.02.008.

Livinti, P. (2021). Comparative study of a photovoltaic system connected to a three-phase grid by using PI or fuzzy logic controllers *Sustainability, 13*(5), 2562. https://doi.org/10.3390/su13052562.

Mai, C., Zhang, L., & Hu, X. (2024). Combining dynamic adaptive snake algorithm with perturbation and observation for MPPT in PV systems under shading conditions. *Applied Soft Computing, 162*, Article

111822. https://doi.org/10.1016/j.asoc.2024.111822.

Munish Manas, Obulesu Dakka , Shivi Sharma , Sairaj Arandhakar , Rambabu Kallelapu , Satyanarayana Golla . (2023). *A novel metaheuristic-based robust unified control MPPT algorithm for grid-connected PV system* Electric Power Systems Research, Volume (221), 109389. https://doi.org/10.1016/j.epsr.2023.109389.

Prajapati, S., Garg, R., & Mahajan, P. (2024). Novel adaptive MPPT technique for enhanced performance of grid integrated solar photovoltaic system. *Computers and Electrical Engineering*, *109*, 109648. https://doi.org/10.1016/j.compeleceng.2024.109648.

Rujas, A., Landaburu, I., Lopez-Martin, V. M., & Barambones, O. (2023). Magnetic design of a 3-phase SiC-based PV inverter with DC-link referenced output filter. IEEE Access, 11, 25531-25542. https://doi.org/10.1109/ACCESS.2023.3254887.

Saleem, S., Farhan, M., Raza, S., Awan, F. G., Butt, A. D., & Safdar, N. (2023). Power Factor Improvement and MPPT of the Grid-Connected Solar Photovoltaic System Using Nonlinear Integral Backstepping Controller. Arabian Journal for Science and Engineering, 48 (6453–6470). https://doi.org/10.1007/s13369-022-07416-x.

Singh, A. K., Hussain, I., & Singh, B. (2018). *Double-Stage Three-Phase Grid-Integrated Solar PV System With Fast Zero Attracting Normalized Least Mean Fourth Based Adaptive Control*. IEEE Transactions on Industrial Electronics, 65(5), 3921–3931. https://doi.org/10.1109/TIE.2017.2758750.

Zeb, K., Ul Islam, S., Uddin, W., Khan, I., Ishfaq, M., Busarello, T. D. C., & Kim, H. J. (2021). High-performance and multi-functional control of transformerless single-phase smart inverter for grid-connected PV system. Journal of Modern Power Systems and Clean Energy, 9(6), 1386–1394. https://doi.org/10.35833/MPCE.2019.000331.

Zerzouri, N., Ben Si Ali, N., & Benalia, N. (2023). A maximum power point tracking of a photovoltaic system connected to a three-phase grid using a variable step size perturb and observe algorithm. Electrical Engineering & Electromechanics, 5, 39-45. https://doi.org/10.15407/eeletmech2023.05.039.

.

Bridging Skills Gaps: Competency-Based Learning Analytics in Omani Engineering Programs

John Regan Pillai

Military Technological College, Oman, https://orcid.org/0000-0002-5290-2597

Tariq Hussain

Military Technological College Muscat Oman, https://orcid.org/0000-0001-9975-8986

Abid Ali Khan

Military Technological College Muscat Oman, https://orcid.org/0000-0001-7763-1490

Mohamed Al Siyabi

Military Technological College, Oman, https://orcid.org/0000-0003-4898-9324

Abstract: It is becoming increasingly important to use competency-based approaches in higher education as it adopts technologies to promote student-centered learning. By shifting away from traditional, one-size-fits-all models of education, competency-based learning ensures that students not only acquire theoretical knowledge but also develop the practical abilities necessary to succeed in their chosen fields. This alignment between educational practices and individual student competencies is essential for fostering deeper engagement, improving learning outcomes, and preparing students for the complexities of the modern workforce. This study highlights the application of competency-based learning analytics to predict student motivation, individualities, and alignment with academic pathways. Focusing on the INSTITUTION "A" in Oman, where students are often assigned to disciplines that may not align with their personal preferences, this study examines the impact of this misalignment on student performance and engagement. It critically explores how learning analytics can be leveraged to assess student readiness by analysing individual profiles, considering factors such as prior academic history and personal preferences. Through this approach, the study aims to provide insights into how better alignment between students and their academic pathways can enhance their overall success. The findings of this research highlight the importance of integrating digital tools for assessment and decision-making. By implementing data-driven strategies, institutions can better match students to pathways that suit their skills and interests, ultimately enhancing academic success and operational readiness. This approach potentially offers a model for optimising educational outcomes, not only at INSTITUTION "A" but also in broader higher education contexts, where student engagement and competency alignment are increasingly crucial for achieving long-term educational and professional goals.

Keywords: Competency, Analytics, Learning, Digital Tools, Adaptive

Introduction

Higher education has always incorporated technological changes to give stakeholders an improved teaching and learning environment. Higher education's teaching practices are evolving as student-centered approaches to instruction become increasingly prevalent. Teaching and instruction need to be re-evaluated in light of the changing nature of instructors from transmitters of knowledge to facilitators and curators (Mona Mourshed et al.,2017),(van Barneveld, A et al., 2012) . Instructors can enhance their teaching practices and facilitate learning by using digital tools by redesigning courses and programs to use digital tools.

Schools, universities, and training programs for military members aim to foster technical, professional, and leadership skills. During education, students grapple with ambiguity while they reflect on the concepts they are learning. An individual's training can enhance readiness by providing opportunities to practice their knowledge, skills, and abilities and provide immediate feedback. Education and training assessment methods currently measure knowledge retention and skill proficiency. Nevertheless, operational readiness and performance differ significantly from those metrics. (Smith, Brent et al., 2019). The future learning ecosystem will require digital representations of all ways to assess an individual's ability and why learning analytics tools are a boon to the educational institution.

At INSTITUTION "A", Oman, the foundation students had to follow a procedure to indicate their preferred pathway. However, their intention does not always match what they are assigned. Students are assigned to different disciplines or pathways, considering various other criteria. Therefore, it could affect their performance over the period since they lack motivation, and their profile, such as their characteristics and prior academic history, would not match the competency requirement for that specific pathway.

This report presents a critical review of learning analytics to predict student's motivation, characteristics and traits to perform and or to indicate whether they are fit for purpose. Also, it recommends how this can be implemented to support the next generation of students to maximise student's readiness for the pathway they have chosen.

Review of Literature

Similar to any business in the world, Higher educational institutions also share the exact reason for adopting analytics. However, the reasons specific to Higher Education are mainly due to financial and operational

efficiency and responding to global and regional knowledge economy demands.

Organisational success and efficiency are being addressed by higher education in the same way that business practices are being adopted and used to prepare for organisational success.

Teaching practices is always put into two different approaches, student-centred or teacher-centred (Ravitz, Becker and Wong, 2000; Deng et al., 2014). In the student-centered approach, the teacher plays the role of a facilitator who focuses on interaction and engagement, mainly related to the constructivist social constructivist way of teaching (Mayer 2003). Whereas, in the teacher-centred approach, the teacher plays the role of content expert (Mayer 2003), mainly related to behaviourist teaching (Deng et al., 2014). The technology-centred approach deals with which uses or functions of technology used in the teaching process are the most effective in transferring knowledge or presenting data. In comparison, the learner-centred approach deals with how technology can develop learners' cognitive abilities. The learner-centred approach encourages learners to strengthen their thinking skills with E-learning digital tools (Mayer 2009). Therefore, this pandemic would push the teachers to design the curriculum appropriately, making it more learner-centric, participatory and inclusive.

Competency-Based learning and readiness

In the industrial age, traditional education was based on one-size-fits-all approaches. In order to teach a student, an instructor uses a curriculum created by course designers or course leaders. Assessing student understanding, processing, and receipt of information is part of the learning process. The instructor customises the approach based on the individual student's needs while receiving and processing information. The student is transferred to the workplace after obtaining a passing grade (certification). Throughout their employment, they learn from their own experiences, the mentorship of fellow employees, and workplace challenges. (Smith, Brent et al., 2019).

Nonetheless, these elements are only captured in periodic job reviews and employee evaluations. It may be necessary to initiate significant changes in "andragogy" or "heutagogy" after a significant operational failure occurs periodically. Training and education gaps can affect student's readiness to work on the job immediately. Figure 1 shows the schematic of traditional learning. (Smith, Brent et al., 2019).
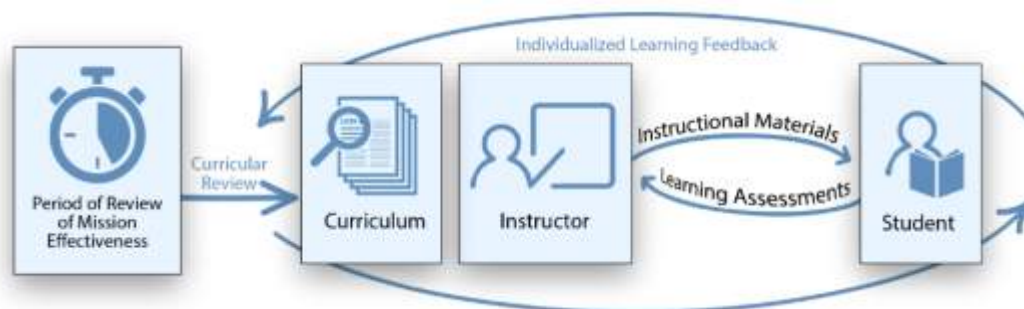

Figure 1. Traditional Training and education lifecycle. Source: Source: Smith, Brent et al. (2019)

On the other hand, in their operational environments, students need a wide range of knowledge, skills, attitudes, abilities, motivations, and traits. In contrast with competency-based education, competency-based learning recognises military training as a separate endeavor. Performance and learning data can be collected and collated so that time spent on formal training is optimised, and learning, performance, and mission effectiveness can be clearly defined. (Smith, Brent et al., 2019).

According to Natsu J. (2010), analytics can be used to improve teaching and learning. As she noted, the use of predictive analytics could encompass a wide range of activities, including improving efficiencies, improving student achievement, or even saving money. The data analytics field can be subdivided into several sub-disciplines based on the data types being analysed and the intended outcomes of the analysis. Types of analytics include text, audio, video, and social media analytics, but the most relevant analytics in higher education is predictive analytics. (Gandomi, A. et al., 2015). Predictive analytics, for example, help recruit college students, reserve classrooms, and recruit and retain college students. The importance of Predictive analytics in informing teaching and learning has attracted much attention in higher education. Despite this, its practical application has also been hindered by uncertainty and hesitation (Drachsler and Greller, 2012).

Martín Liz-Domínguez (2019), classified the analytics depending on whether they present a predictor or an early warning system. The term "predictor" refers to an application that predicts the final result of a course or degree based on input data, usually expressed in terms of grades or a passing/failing classification. In addition to performing the same tasks as a predictor, an early warning system, "EWS", alerts a teacher or student of a potential problem early enough so that action can be taken to mitigate the risk. Since EWS are required to perform analyses early in a course, they have a stricter timing requirement than predictors.

Predictors are used in a particular course or for an entire degree program to assess a student's performance. There are two types of widely used prediction goals. The first is to predict a student's final grade, and the second is to assess whether the student will succeed or fail.

Listed below are some classic examples used in various academic institutions:

Ornelas and Ordonez implemented a Naïve Bayesian classifier which was used in 13 different courses at Rio Salado Community College (Ornelas and Ordonez,2017)]. The courses were part of the degree programs in science and humanities. Data was collected for the study from student engagement activities online and each student's academic performance. The classifier predicted student success, defined as obtaining a lower grade or higher in a course. After testing this tool, the classifier achieved an accuracy of over 90% for most courses, whereas the accuracy dropped to values between 80% and 90% for three science courses. The authors explained this variation in accuracy owing to the complexity of the scientific courses compared to others. A large student population, with a training sample of 5936 students and a validation sample of 2722, was used to conduct the investigation.

Thompson deployed a classifier based on logistic regression in an introductory biology course taught during the first semester of a university major [Thompson,Bowling and Markle, 2018]. This classifier was used to predict whether the student would pass the course or not.The data set was extracted from the results of tests taken at the start of the semester to evaluate the students' scientific reasoning and mathematical abilities. The predictor was tested over a population of 413 students. The fact that success can be predicted even before the commencement of the course is intriguing. However, success depends not entirely on a student's academic ability but also on factors such as motivation and engagement.

Benablo et al. (2018) used a classifier to measure student success with student procrastination as input data (Benablo, Sarte, Dormido and Palaoag,2018). Students were surveyed about their time on social networks and playing online games to extract the dataset. Support vector machines (SVM), k-nearest neighbours (KNN), and random forest (RF) algorithms were used to evaluate the performance of each of them. The experiment was conducted with a cohort of 100 computer science students from a university in the Philippines. The SVM classifier predicted more accurately than the other two algorithms. However, a small population of 100 students is too small to predict the results accurately compared to a larger scenario.

An attempt was made by Umer et al. (2018) to estimate the earliest time at which the students' final performance could be predicted (Umer,Susnjak,Mathrani, Suriadi, 2018). This survey was conducted on 99 students enrolled in a 16-week-long introductory mathematics course taught at an Australian university. The tool collected data related to student engagement from Moodle logs and student's grades in the assignments. Four different classifier algorithms were used to predict final grades, and the predictor was evaluated on the basis of its ability to classify students into high and low performers. The RF was the best performing algorithm, but the study on the small population may be unreliable.

Early Warning Systems (EWS):

Many universities have used EWS since the late 2000s, and Course Signal is considered the first application of EWS research documented by Arnold and Pistilli (2012). Course standards are the most widely referenced system used by researchers in the community. The EWS system can use homework test performance and student-related information about the institution to assess each students risk of failing a course. The resulting risk information is presented in a multi-level format that is easy for instructors and students to understand and evaluate. After a thorough evaluation instructors can develop an intervention plan to improve student performance and retention.

Student Explorer, developed by Krumm et al. (2014), implements a similar three-level scale to assess students' risk of failing a course. Additionally, student Explorer categorises students into categories such as "encourage", "explore", and "engage".

Through the years, Student Explorer has undergone many modifications. Below are add-ons and studies based

on this EWS:

(Waddington and Nam, 2014) added information on accessing lecture notes and completing assignments to the existing input data in Student Explorer. Over the course of ten consecutive semesters, 8762 students were tracked using this system. According to the authors, using resources and getting a good grade in a course are directly related. To achieve the desired results, exam preparation played a crucial role. According to Brown et al.,(2016) the first study examined why students fall into a medium or high-risk category. An event history analysis technique determines the likelihood of a student entering one of the risk levels. It was tested on 556 first-year students from different academic programs. Second, the study examined the best ways to help struggling students recover. A study of 2169 first-year statistics students found that high-risk students benefited more from rigorous test preparation while average students sought help in planning to study more effectively. Their third study analysed the impact of co-enrollment on student achievement. Binary logistic regression was used to classify specific courses as challenging due to student's complexity and performance problems at risk. This edition of the Student Explorer was conducted with 987 students enrolled in a programming course. LADA (Learning Analytics Dashboard for Advisors) was developed by Gutierrez et al. And it enabled academic advisors to make decisions easily (Gutierrez Seipe Ochoa Chiluiza de Laet Verbert 2018). It contains special modules that predict students chances of passing a particular course. LADA assesses students risk scores on a five-point scale using the number of courses and credits the student takes as inputs. The system has been implemented in two universities one in Europe and the other in Latin America. Student advisors were satisfied with the usefulness of LADA because the tool analysed individual student issues in a shorter period of time and in turn increased their decision-making efficiency. According to Finney R et. (2017) any forecasting model can only be as good as the data provided so the analysis performed here has some limitations.

The need for Competency Based Curriculum (CBC)

INSTITUTION "A" offers diploma and bachelor's degree programs. Students must meet specific requirements to progress from the diploma to the bachelor's degree. The General Studies Department prepares students for engineering courses by improving their skills in English, math, computing, and physics. All new students take a placement test for English proficiency, and those with an IELTS score of 5.0 or higher are exempt. The program length varies based on each student's English level, with a maximum of two years. INSTITUTION "A" faces challenges recruiting students with the required IELTS score of 5.0 for the engineering foundation program. The engineering program enrollment was only 38% in 2016/2017, and although it has improved slightly, it remains a challenge for the college despite the introduction of the two-year GFP. UK-accredited engineering programs have strict requirements for degree accreditation. While diplomas lead to professional careers, performance data is lacking. Graduate transcripts are reliable but provide limited details on graduate capabilities. The UK Vocational School Assessment Standards must be met, putting pressure on students to meet international quality standards. The impact of lacking qualifications on graduates' job performance is unclear.

1.Meagre output from DipHE, who can progress to the BEng programme. In the Academic year 2021, out of

200 students, not even a single student from the Systems Engineering department progressed to the BEng programme.

2. Graduate's skills and competency – A measure of how well graduates can use their acquired skills and knowledge to complete tasks to their employer's satisfaction.

The current educational systems rely on digital technologies to supplement traditional teaching, but lack integration. By analyzing student data using statistical and machine learning models, at-risk students can be identified early and provided with targeted support to improve their learning performance. While various universities utilize predictive tools, the US Department of Defense's approach is more user-centered, making it more suitable for military institutions. The key information can be rewritten more concisely as follows: Track students from entry to BEng level 6 to provide continuous support and guide them into suitable pathways based on their abilities and interests. Create a learner profile that includes demographic, learning preference, skill, and achievement data to inform feedback and placement decisions that meet competency and graduate attribute requirements.
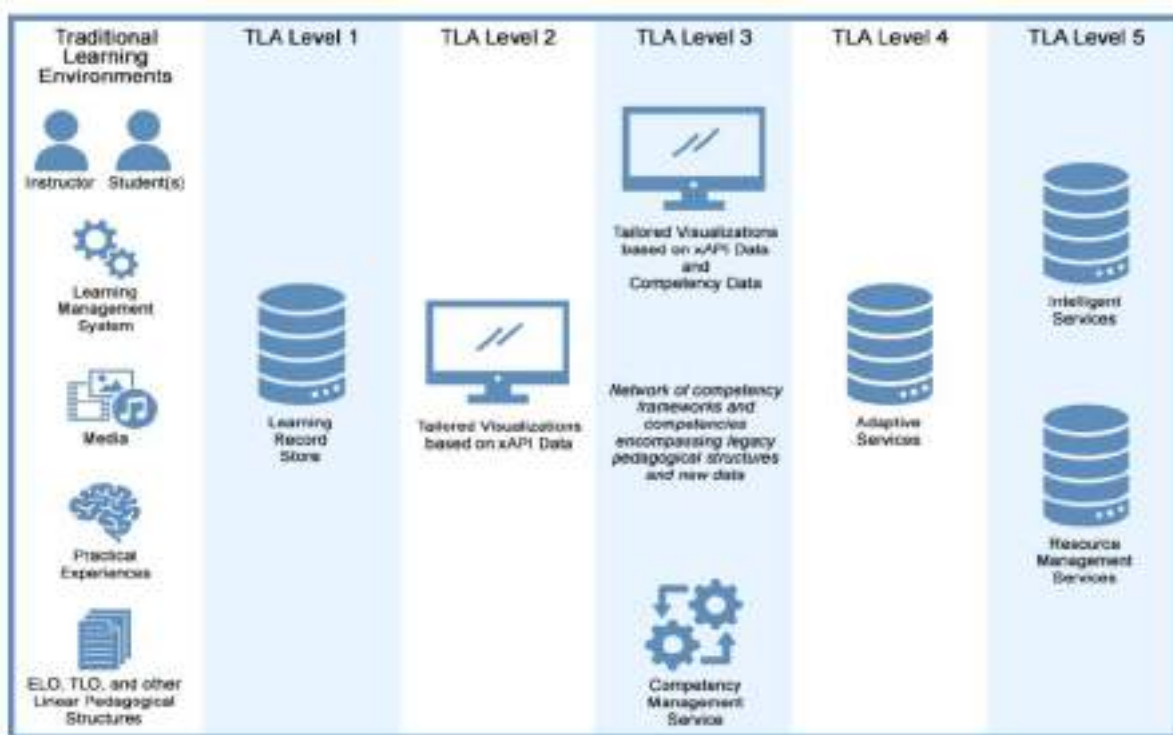
Figure 2. Total Learning Architecture Stages. Source: Smith, Brent (2019)

INSTITUTION "A" can adopt the US Department of Defense's system that uses xAPI for activity tracking and an LRS for data analysis and decision support. xAPI collects performance data from various learning activities, which can be combined in an LRS. A dashboard visualizes this data for different stakeholders to support decision-making. Performance data outside the classroom can also be used to guide interventions. Adopting the Total Learning Architecture (TLA) at level 3 can enhance instructional design based on competency goals. In a

competency-based learning system, learners can customize their learning path by completing modules instead of full courses, focusing on their weaknesses. Data-rich competency and activity tracking services enable adaptation, allowing TLAs to optimize approaches for better learner experiences. Adaptation can involve content recommenders, intelligent tutoring, and continuous-learning paths, leveraging machine learning to optimize training resources.

Model for INSTITUTION "A" to be adapted:

To adopt the above learning architecture, INSTITUTION "A" should start rolling out a comprehensive process plan to initiate and implement learning analytics effectively. This process plan should include several key steps and considerations: 1. Establish a cross-functional task force: INSTITUTION "A" should form a dedicated task force comprising representatives from various departments, including academic leadership, IT, data analytics, and student affairs. This task force will be responsible for overseeing the entire learning analytics implementation process. 2. Conduct a comprehensive needs assessment: The task force should begin by conducting a thorough needs assessment to identify the specific challenges, goals, and potential use cases for learning analytics within INSTITUTION "A". This assessment should involve gathering input from faculty, staff, and students to understand their data and analytics needs. 3. Define clear objectives and key performance indicators (KPIs): Based on the needs assessment, the task force should define clear objectives for the learning analytics initiative, such as improving student retention, enhancing academic performance, or optimizing course delivery. Additionally, they should establish a set of KPIs to measure the success and impact of the implementation. 4. Develop a data management and governance strategy: INSTITUTION "A" should create a robust data management and governance strategy to ensure the integrity, security, and ethical use of student data. This strategy should address data collection, storage, access, and privacy considerations. 5. Implement the necessary technological infrastructure:

The institution should invest in the necessary technological infrastructure, such as learning management systems, data warehouses, and analytics platforms, to support the learning analytics initiative. This may involve integrating existing systems or procuring new solutions. 6. Train and engage faculty and staff: INSTITUTION "A" should provide comprehensive training and support to faculty and staff to ensure they understand the capabilities of the learning analytics tools and can effectively utilize the insights to improve teaching and learning practices. 7. Pilot and iterate the learning analytics implementation: The task force should start with a pilot implementation, focusing on a specific program or department, to test the effectiveness of the learning analytics approach. Based on the lessons learned, the institution can then iterate and scale the implementation across the entire institution. 8. Communicate and engage the broader community: INSTITUTION "A" should develop a communication plan to keep the broader campus community informed about the learning analytics initiative, its progress, and the benefits it is delivering. This will help foster buy-in and engagement from faculty, staff, and students. By following this comprehensive process plan, INSTITUTION "A" can ensure a successful and sustainable implementation of learning analytics, leading to improved student outcomes and enhanced institutional effectiveness.

PLAN	**ENABLE**	**COLLECT & MONITOR**	**ANALYSE**	**REPORT**	**ACTION**
Plan for the information needed, the sources, the report format, stakeholders who need to receive the reports, and come up with questions	Enable data analytics, at appropriate level and stage	Collect student data through moodle / LMS system /academic Portal / laboratory, classroom	Analyse data which is collected	Report and discuss with the concerned stakeholders	Take corrective actions and modifications required.

O What information is needed?

O From where can the information be gathered?

O How might the information be analysed?

O How will the findings be reported and to whom?

Conclusion

The integration of learning analytics systems into the educational ecosystem at INSTITUTION "A" has the potential to be a game-changer in terms of student engagement and academic success. These cutting-edge tools will provide tutors with the ability to monitor student participation and performance in real-time, allowing them to identify potential issues before they escalate. By closely tracking the ebb and flow of student engagement, tutors can proactively intervene and support those at risk of dropping out or underperforming, giving them the best chance of achieving their academic and professional goals. However, the implementation of such sophisticated analytics systems is not without its challenges. Accurately measuring and assessing student competencies can be a complex endeavor, as it involves evaluating a multitude of factors, including attitude, interest, and even physical dexterity. These elements can be inherently subjective, making it difficult to establish reliable and consistent benchmarks. Nonetheless, the potential benefits of using competency-based learning (CBL) methodologies cannot be overstated. By leveraging CBL, INSTITUTION "A" can gain invaluable insights into how students are likely to perform in their future careers, allowing for more informed and targeted interventions. The adoption of learning analytics and CBL represents a crucial step forward in INSTITUTION "A" 's ongoing commitment to student success. While the road ahead may involve navigating some technical

and conceptual hurdles, the long-term payoffs in terms of improved student outcomes, enhanced institutional effectiveness, and stronger ties between academic and professional realms make this a worthwhile investment. As INSTITUTION "A" continues to explore and refine these innovative approaches, the institution stands poised to redefine the very nature of student support and success.

References

Arnold, K.E.; Pistilli,M.D.(2012). Course Signals at Purdue: Using Learning Analytics to Increase Student Success. 2nd International Conference on Learning Analytics and Knowledge (LAK '12), Vancouver, BC, Canada, 29 April–2May 2012; ACM: New York.

Benablo, C.I.P.; Sarte, E.T.; Dormido, J.M.D.; Palaoag, T (2018) Higher Education Student's Academic Performance Analysis Through Predictive Analytics. 7th International Conference on Software and Computer Applications, Kuantan, Malaysia.

Brown, M.G.; DeMonbrun, R.M.; Lonn, S.; Aguilar, S.J.; Teasley, S.D.(2016). What and when: The Role of Course Type and Timing in Students' Academic Performance. Sixth International Conference on Learning Analytics & Knowledge (LAK '16), Edinburgh, UK.

Finnie, R., Fricker, T., Bozkurt, E., Poirier, W., Pavlic, D. (2017) Using Predictive Modelling to Inform Early Alert and Intrusive Advising Interventions and Improve Retention. Toronto: Higher Education Quality Council of Ontario.

Gandomi, A.; Haider, M.(2015). Beyond the hype: Big data concepts, methods, and analytics. Int. J. Inf. Manag. 2015, 35, 137–144, doi:10.1016/j.ijinfomgt.2014.10.007

Gutiérrez, F.; Seipp, K.; Ochoa, X.; Chiluiza, K.; De Laet, T.; Verbert, K. (2018) LADA: A learning analytics dashboard for academic advising. Comput. Hum. Behav.

Krumm, A.E.; Waddington, R.J.; Teasley, S.D.; Lonn, S. A (2014). Learning Management System-Based Early Warning System for Academic Advising in Undergraduate Engineering. Learning Analytics: From Research to Practice; Larusson, J.A., White, B., Eds.; Springer: New York, NY, USA.

Mayer, R. E. (2003) 'Theories of learning and their application to technology'. in O'Neil Jr., H. F. and Perez, R. S. (Eds.) Technology Applications in Education: A Learning View. Mahwah, NJ: Erlbaum, pp. 127–157.

Mayer, R.E. (2009) Multimedia Learning. 2nd edn. Cambridge University Press.

Military Technological College, Quality Audit Portfolio, 2017. p.8. (Accessed 6 July 2022).

Mona Mourshed, Marc Krawitz, and Emma Dorn. (2017). How to improve student educational outcomes: New insights from data analytics. McKinsey & Company, 2017.

Natsu J. (2010). Advanced analytics: helping educators approach the ideal. eSN Special Report, eSchool News.

Ornelas, F.; Ordonez, C. (2017) Predicting Student Success: A Naïve Bayesian Application to Community College Data. Technol. Knowl. Learn.

Ravitz, J., Becker, H. J. and Wong, Y. T. (2000). Constructivist-compatible beliefs and practices among U. S. teachers', Center for Research on Information Technology and Organisations..

Thompson, E.D.; Bowling, B.V.; Markle, R.E. (2018) Predicting Student Success in a Major's Introductory Biology Course via Logistic Regression Analysis of Scientific Reasoning Ability and Mathematics Scores. Res. Sci. Educ.

Umer, R.; Susnjak, T.; Mathrani, A.; Suriadi (2018) learning analytics approach: Using online weekly student engagement data to make predictions on student performance. In Proceedings of the 2018 International Conference on Computing, Electronic and Electrical Engineering (ICE Cube), Quetta, Pakistan.

van Barneveld, A., Arnold, K. E., & Campbell, J. P. (2012). Analytics in higher education: Establishing a common language (Educause Learning Initiative No. 1).

Waddington, R.J.; Nam, S.(2014) Practice Exams Make Perfect: Incorporating Course Resource Use into an Early Warning System. In Proceedings of the Fourth International Conference on Learning Analytics and Knowledge (LAK '14), Indianapolis, IN, USA.

Wolfgang Greller, & Hendrik Drachsler. (2012). Translating Learning into Numbers: A Generic Framework for Learning Analytics. *Journal of Educational Technology & Society*, *15*(3), 42–57. http://www.jstor.org/stable/jeductechsoci.15.3.42.

Comparative Evaluation of PID, Fuzzy Logic and ANFIS Controllers in Automatic Voltage Regulators of Power Systems

Benalia Nadia

LEA Laboratory, Badji Mokhtar Annaba University, Annaba, Algeria, https://orcid.org/ 0000-0003-4819-5313

Bensiali Nadia

LEA Laboratory, Badji Mokhtar Annaba University, Annaba, Algeria, https://orcid.org/ 0000-0001-7248-4823

Zerzouri Nora

LEA Laboratory, Badji Mokhtar Annaba University, Annaba, Algeria, https://orcid.org/ 0000-0003-1209-4617

Abstract: Voltage control is performed to reduce network losses in power systems. Automatic Voltage Regulator (AVR) system is commonly used in power systems to keep output voltage on a constant value defined in a specified range. In order to improve dynamic response of an AVR system and minimize obtained steady state error, researchers focus on developing control schemes and designing controllers for the AVR system. In controller design process, meta-heuristic algorithms are generally preferred to optimally tune the parameters of the controller. In this comparison study, parameters of traditional Proportional-IntegralDerivative (PID) controller, utilized for the voltage control of an AVR system, are tuned using an Adaptive-Neuro-Fuzzy Inference System ANFIS and fuzzy logic control. This investigation aims to analyze the controller's behavior so that it can be used in any of the other control systems in the power system. Leveraging the power of MATLAB-SIMULINK, the PID controller undergoes meticulous tuning, while the ANFIS controllers are trained using meticulously curated data from the PID controller. The performances of the designed PID controllers are compared using Overshoot, settling time and steady-state error values.

Keywords: PID, ANFIS, Fuzzy logic control, Automatic voltage control.

Introduction

In power systems, automatic voltage regulators (AVRs) are typically utilized to maintain a generator's terminal voltage at a specific value and to provide continuous voltage control. Power systems work with high voltages, therefore any variations in the terminal voltage could have negative consequences. Because of this, the stability of the AVR determines the security of a power system. Sometimes, load fluctuations, high winding inductance, and insulation breakdown from voltage fluctuations make it difficult to provide a consistent and quick response from the AVR. Therefore, improving the AVR's performance is crucial. This can be accomplished by removing the previously mentioned issues using an efficient control algorithm.

The implementation and development of effective control Algorithms have played a crucial role in various applications like industrial processes and electrical systems. Various control algorithms, including proportional-integral-derivative (PID)(Sahib, 2015).

The main function of the electric power system is to supply electric energy to the end custom,2015; (Sahin, 2021; Soliman & Ali ,2021) , fuzzy logic (Zhang., Shi., & Liu,2013); artificial neural network (ANN), and adaptive neuro-fuzzy inference system (ANFIS), are published in the literature to control the AVR systems. Numerous closed-loop control strategies have been presented in conjunction with optimization techniques to enhance the controller's efficiency. This power system is dynamic and non linear in nature and works in a changing environment. The main control function of the excitation system is to regulate the generator terminal voltage which is accomplished by adjusting the field voltage with respect to the variation of the terminal voltage.

Power systems mainly depend on synchronous generators as a source of electrical energy. SGs are multi-input multi-output (MIMO) systems that are fast-acting, nonlinear, and constantly susceptible to load changes. The AVR design must account for both normal load and fault conditions. It appears that the system dynamics are significantly altered by these operating circumstances. The exciter provides the excitation voltage, which the AVR regulates. Artificial neural networks (ANN's) can be used as intelligent controllers to control non-linear, dynamic systems through learning, which can easily accommodate the non-linearity's and time dependencies called neurocontrollers.

Automatic Voltage Regulator

An automatic voltage regulator (AVR) is typically employed in power systems to ensure concurrent voltage regulation and maintain a generator's terminal voltage at a predetermined level. Given that electricity systems operate at elevated voltages, any variations in terminal voltage can result in significant issues. The security of a power system is contingent upon the stability of the AVR. Achieving a reliable and rapid reaction of the AVR can be challenging due to load variations, the high inductance of the generator windings, and insulation failures

resulting from voltage swings. Therefore, improving the AVR performance is crucial. This can be accomplished by employing an efficient control method to resolve the aforementioned concerns. Various control mechanisms for managing AVR systems are documented in the literature, including proportional-integral-derivative (PID) (Sahib,2015), fuzzy logic (Lin, 2013), and adaptive and predictive control (Elsisi,2021) . Various closed-loop control methodologies, in conjunction with optimization methods, have been implemented to enhance the controller's performance (Sikander.2020; Elsisi et al 2021; Tang, 2016). The fractional order PID, optimized using the cuckoo search method (Sikander, 2018) and the particle swarm optimization (PSO) algorithm (Li et al, 2017) is shown. Fuzzy logic, in conjunction with a genetic algorithm (GA), is utilized to determine the ideal parameter values of the PID controller (Al Gizi et al., 2015). Furthermore, Fuzzy logic combined with a modified Particle Swarm Optimization (PSO) is employed to determine the ideal gain values of the controller and achieve an online optimized transient response (Mukherjee, 2007; Al Gizi, 2019). Additionally, Fuzzy logic and PID controllers are employed to equilibrate the whole system generation with various loads and losses in the AVR system (Dabur, 2012). Besides PID and fuzzy logic controllers (FLCs), the adaptive neuro fuzzy inference system (ANFIS) is employed to mitigate low frequency oscillations in the system (Christy Juliet et al ; 2014). ANFIS is utilized for the online tuning of PID controllers by training the ANFIS system with optimum PID parameters (Yavarian, 2015). Additionally, model predictive control and H-infinity control paradigms are introduced to address the uncertainties in the AVR parameters (Elsisi et al., 2021). Additionally, the neural network (NN) predictive controller, improved by the imperialist competitive algorithm, is implemented to mitigate fluctuations in the terminal voltage of the AVR system (Elsisi, 2019). The feedback closed-loop response of the AVR system exhibits deficiencies regarding time-domain indices. These metrics are employed to evaluate the closed-loop responsiveness of the system. Optimally, the reaction necessitates reduced settling time, rising time, and overshoots, along with minimal steady-state error (SSE) (Pachauri, 2020). Conversely, unforeseen alterations in system characteristics jeopardize the stability and security of the power system. Moreover, system perturbations may lead to prolonged electrical oscillations, resulting in instability within the system (Yavarian et al., 2014). Therefore, in power systems, selecting an effective control approach to address unforeseen system changes and disruptions is of paramount importance.

The PID controller is recognized for its straightforward implementation and uncomplicated configuration. Nonetheless, it is susceptible to issues such as system nonlinearities and necessitates re-tuning of its parameters. The Fuzzy Logic Controller (FLC) is commonly employed due to its simplicity, efficacy, cost-effectiveness, robustness, and capacity to address nonlinearity in intricate systems. The Adaptive Neuro-Fuzzy Inference System (ANFIS) is an exceptionally effective method for modeling complex and nonlinear systems with high accuracy, integrating the precise learning and adaptive features of neural networks with the rapid learning capabilities of fuzzy logic. These three controllers—PID, FLC, and ANFIS—have been extensively utilized across various engineering applications. Moreover, these controllers are widely employed in diverse control methodologies for managing the AVR in power systems (Spoljaric, 2018). The literature is deficient in a comprehensive analysis of the three controllers regarding stability and robustness against unforeseen disruptions and variations in system parameters inside AVR systems. This research employs PID, FLC, and ANFIS controllers in a closed-loop control strategy to regulate an AVR system, assessing the performance of each

controller. The controllers' temporal response, encompassing rise time (Tr), settling time (Ts), and steady-state error (SSE), is documented and examined. Furthermore, a disturbance test is performed to assess the capability of each controller to manage unforeseen disruptions. Additionally, to evaluate the resilience of each controller to unforeseen variations in system parameters, each controller is assessed using diverse system parameters. The optimal performance controller is recommended to ensure the stability and dependability of power systems.

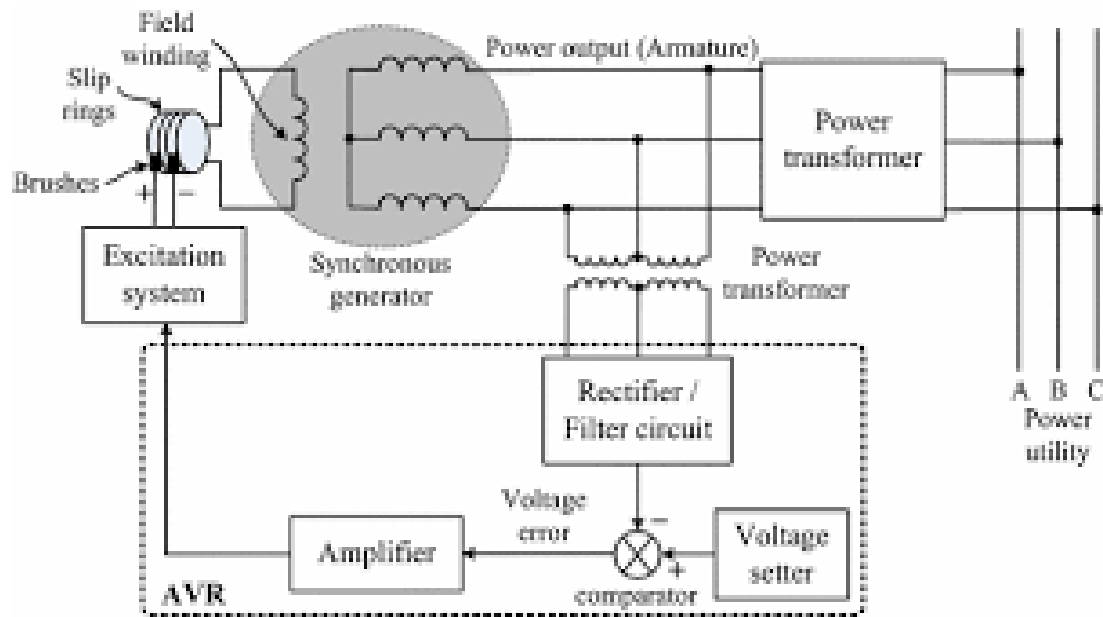**Description of the AVR system**

Figure 1. Schematic diagram of AVR.

If we keep the voltage constant, we can adjust the speed of the generator, which will keep the system's voltage constant. This sort of voltage control is referred to as an excitation control system. A voltage regulator automatically stabilizes voltage to a constant level. A voltage circuit adjusts or stabilizes voltage levels to meet certain circuit requirements Fig.1.

Thus, a voltage regulator is used for main two reasons are:

 1. To regulate or vary the output voltage of the circuit system.

2. To keep the output voltage constant at the desired value in spite of variations in the supply voltage or in the load current.

3. The generator terminal voltage Vt is compared with reference voltage Vref to obtain an error signal as This signal is applied to the exciter as a voltage function as KA/(1+STA).

The generator field can represent by a transfer function Ke/(1+STf).The total transfer is given as

$$\frac{\Delta V}{\Delta V_{ref}} = \frac{G(s)}{G(s) + 1} \qquad (1)$$

$$G(s) = \frac{K_A K_e K_F}{(1 + sT_A)(1 + sT_e)(1 + sT_F)} \qquad (2)$$

AVR Modelling

The AVR system, illustrated in Fig. 2, comprises four principal components: the amplifier, exciter, generator, and sensor. To model and find the transfer function of each component, linearization is essential, necessitating the disregard of nonlinearities and saturation effects. Additionally, the predominant time constant of each component must be taken into account (Govindan, 2019) . The transfer function of the amplifier is defined as:

$$G_a = \frac{K_a}{1 + \tau_a S} \qquad (3)$$

Here, Ka denotes the amplifier's gain, whereas τa signifies the time constant of the amplifier's model. The typical range for the gain Ka is from 10 to 400, but the conventional range for the time constant τa is from 0.02 to 0.1 seconds. The exciter's transfer function is expressed as:

$$G_e = \frac{K_e}{1 + \tau_e S} \qquad (4)$$

where Ke denotes the gain of the exciter, and τe signifies the time constant of the exciter model. The typical range for the gain Ke is from 1 to 400, but the conventional range for the time constant τe is from 0.4 to 1 second. The transfer function of a linearized generator model is similarly expressed by:

$$G_g = \frac{K_g}{1 + \tau_g S} \qquad (5)$$

where Kg represents the generator's gain, and τg represents the time constant of the generator's model. The standard range of the gain Kg is between 0.7 and 1, whereas the standard range of the time constant τg is between 1 and 2 s.

Finally, the transfer function of a sensor model is represented by:

$$G_s = \frac{K_s}{1 + \tau_s S} \qquad (6)$$

where Ks represents the sensor's gain, and τs represents the time constant of the sensor. The standard range of the gain Ks is 1, while the standard range of the time constant τs is between 0.001 and 0.06 s.
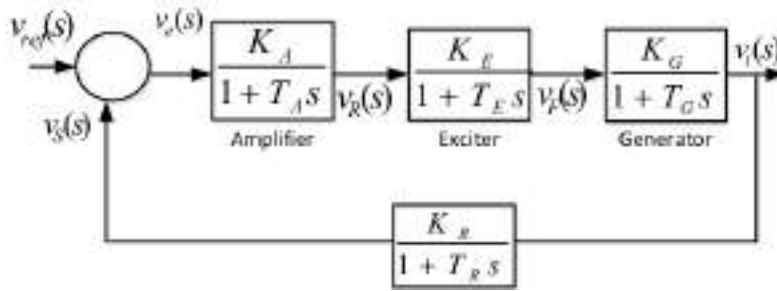
Figure.2. Basic diagram of AVR

Controllers

In this study, three alternative controllers are used with the AVR system. These include PID, PD-like Fuzzy logic, and ANFIS controllers. Each controller's performance is recorded and assessed, as described in the subsections that follow.

PID Controller

A Proportional-Integral-Derivative (PID) controller is a fundamental control mechanism utilized for system stabilization and regulation. It generates a control signal output by evaluating the difference between a specified set point and the current process value.

 The controller is comprised of three fundamental components:

- Proportional (P) Term: Generates an output proportional to the current error, reducing steady-state error and improving responsiveness.
- Integral (I) Term: Integrates the error over time, eliminating steady-state error and long-term errors or correcting for biases.
- Derivative (D) Term: Considers the error's rate of change stabilizing the system and mitigating abrupt or oscillatory changes.
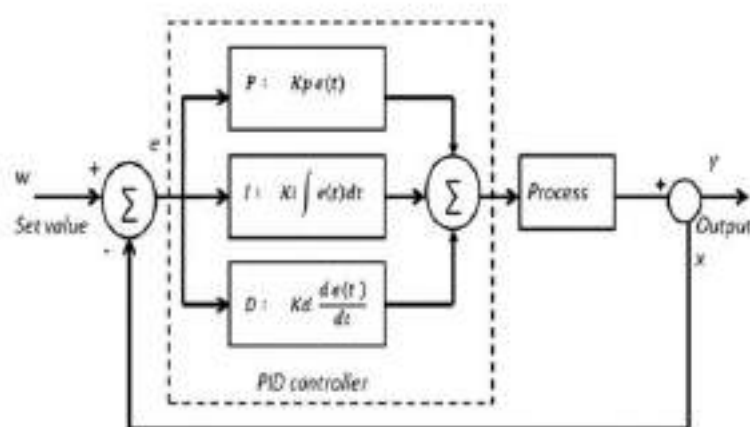

Figure. 3 Block Diagram of the PID Controller

Method

Fuzzy logic controller

Controlling extremely non-linear complex systems has shown to be exceedingly challenging using traditional control theory. The artificial intelligence, utilizing natural language, has demonstrated use in scenarios including uncertainties, so aligning more closely with human logical reasoning. Fuzzy logic was selected in the realm of artificial intelligence.

Fuzzy Logic Controller Data

In recent years, the application of fuzzy logic has garnered significant attention for its efficacy in simplifying model complexity in problem-solving, utilizing language words that address the causal relationship between input and output constraints. The fuzzy set theory was primarily inspired by the belief that conventional analytical methods were insufficient to characterize phenomena whose constraints were not governed by differential equations. This theory offers a method for conveying ambiguous concepts via the element and its affiliation with this collection.

Fuzzy set

In fuzzy logic controllers, a fuzzy set is a collection of different elements characterized by a degree of relevance or inclusion, determined by a characteristic function known as the membership function. The fuzzy set serves as a generalization of a conventional set, whereby membership is restricted to two values: {0,1}. The fuzzy set U can be expressed as an ordered pair of a generic element U and its membership function degree μF.

The Fuzzy Controller

FLC is a decision algorithm that relies on an operator's experiential knowledge rather than mathematical principles. This control method is well-suited for non-linear systems, such as the synchronous generator, which demonstrates non-linearity between the input field current and the output armature voltage . Fundamentally, FLC is a multi valued logic system that permits the specification of intermediate values between traditional binary evaluations such as true/false, yes/no, and high/low. Concepts such as relatively tall or exceedingly fast can be mathematically articulated and processed by computers, facilitating a more human-like approach in computer programming. A fuzzy system serves as an alternative to conventional concepts of set membership and logic, originating from ancient Greek philosophy.

The use of fuzzy logic has garnered significant attention in recent years due to its efficacy in simplifying model complexity in problem-solving, utilizing language words that address the causal relationship between input and output constraints. Fuzzy Logic Controllers (FLC) is swiftly emerging as a credible substitute for traditional controllers. The rationale for this is that FLC can closely replicate human control mechanisms. FLC technology

facilitates the integration of engineering expertise and empirical findings in the design of embedded systems. A primary benefit of employing an FLC technique is that it facilitates model-free estimation of the system. The designer is not required to specify the mathematical dependence of the outputs on the inputs. Fuzzy Logic Control (FLC), grounded in fuzzy set theory, serves as an effective mechanism for transforming expert linguistic control into automated control rules . Complex processes can be effectively regulated in many settings by employing fuzzy automatic rules derived from heuristic or mathematical methodologies. However, the paramount and challenging issue is determining the appropriate control rules for a specific system.

The fuzzy controller consists of four components:

1- A rule base: (A collection of If-Then rules), which encompasses a fuzzy logic representation of the expert's linguistic delineation for attaining effective control.

2- An inference mechanism, sometimes referred to as a "inference engine" or "fuzzy inference" module, simulates the expert's decision-making process in understanding and applying knowledge for optimal plant control.

3- Fuzzification interface: This component transforms controller inputs into data that the inference mechanism can readily utilize to activate and implement rules. A fuzzifier transforms a numerical variable into a verbal label. In a closed-loop control system, the error (e) is the difference between the reference voltage and the output.

FLC intelligently determines the appropriate field voltage to be applied, which is then outputted and immediately applied to the generator's field winding. Triangular membership functions were employed for the controller.

Fuzzy logic architecture: The block diagram of fuzzy controller as shown in Fig. 4.
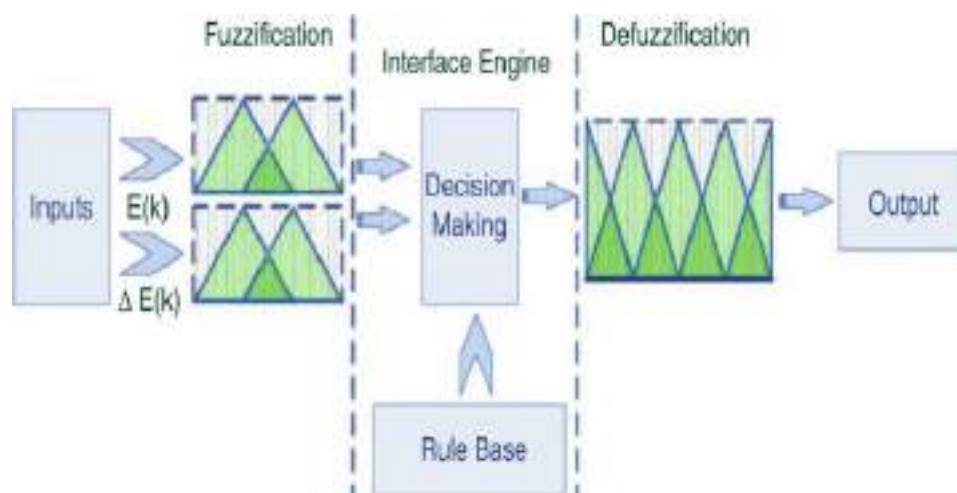

Figure 4. Schematic diagram of the FLC building blocks

Adaptive Neuro-Fuzzy Inference System (ANFIS)

The primary benefits of a fuzzy logic system (FLS) include its capacity to express nonlinear input-output interactions through a series of qualitative if-then rules. The primary benefit of an artificial neural network (ANN) is the Innate learning capacity, which allows the networks to progressively enhance their performance. The principal attributes of a neuro-fuzzy network include the precise learning and adaptive skills of neural networks, coupled with the generalization and rapid learning features of fuzzy logic systems. An adaptive neuro-fuzzy inference system (ANFIS) integrates neural networks and fuzzy systems, utilizing neural networks to ascertain the parameters of the fuzzy system.

A neural network is employed to autonomously adjust the system parameters. ANFIS is an effective method for modeling nonlinear and complicated systems, requiring minimal input and output training data while facilitating rapid learning and achieving high precision. The neuro-fuzzy system, which combines the learning capabilities of neural networks with the benefits of rule-based fuzzy systems, can greatly enhance performance and facilitate the integration of historical observations into the categorization process. The training of a neural network fundamentally constructs the system. The system is constructed using fuzzy logic concepts and further enhanced by neural network training methods within a neuro-fuzzy framework.

ANFIS Architecture

The modeling methodology employed by ANFIS resembles other system identification techniques. Initially, a parameterized model framework is proposed, linking inputs to membership functions, rules, outputs, and subsequent membership functions. Subsequently, input/output data is gathered in a format suitable for ANFIS training. ANFIS can thereafter be employed to train the FIS model to replicate the provided training data by adjusting the membership function parameters based on a selected error criterion. The operation of ANFIS resembles that of a feed-forward back propagation network. Consequent parameters are computed in a forward manner, whereas premise parameters are computed in a backward manner.

The neural part of the system employs two learning methodologies: the hybrid learning method and the back-propagation learning method. In the fuzzy part, only the zero or first order Sugeno inference system or the Tsukamoto inference system may be employed. This section presents the fundamentals of ANFIS network architecture and its hybrid learning algorithm. The Sugeno fuzzy model was introduced by Takagi, Sugeno, and Kang to establish a systematic method for deriving fuzzy rules from an input-output dataset. The ANFIS design, featuring two inputs, one output, and two rules, is illustrated in Figure 5. Predicted values, accordingly, and in the buried layers, nodes operate as membership functions (MFs) and rules. This architecture mitigates the drawback of a conventional feed forward multilayer network, wherein it is challenging for an observer to comprehend or alter the network. In this context, x and y denote inputs, f signifies the output, circles illustrate fixed node functions, and squares depict adaptive node functions.
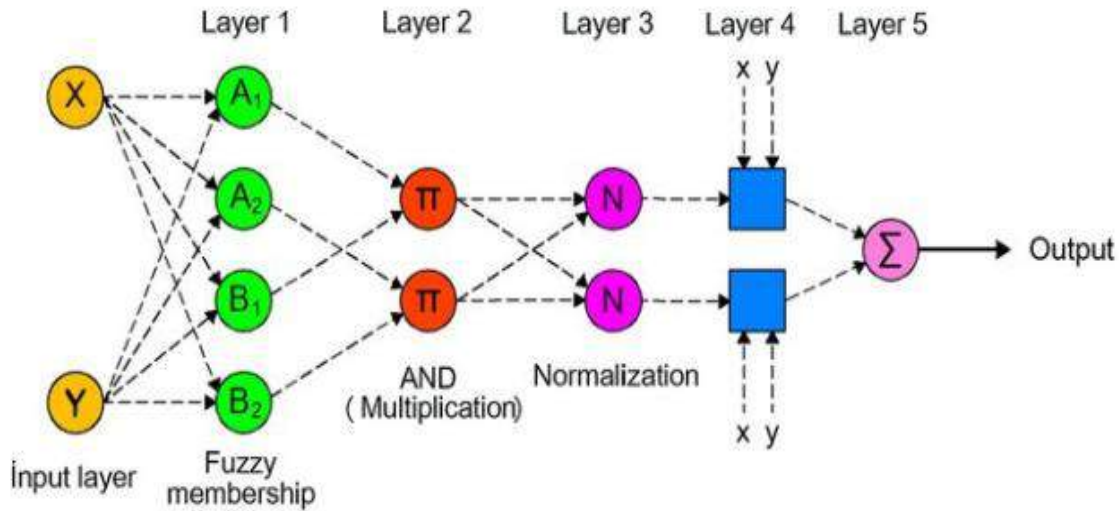
Figure 5. ANFIS architecture

Consider a first order Sugeno fuzzy inference system which contains two rules:

Rule1; if X is A_1 and Y is B_1, then $f_1 = p_1x + q_1y + r_1$

Rule2; if X is A_2 and Y is B_2, then $f_2 = p_2x + q_2y + r_2$

Where p1, p2, q1, q2, r1, and r2 are linear parameters, while A_1, A_2, B_1, and B_2 are nonlinear parameters. ANFIS is an application of a fuzzy logic inference system utilizing the design of a five-layer feed-forward network. The system architecture comprises five layers: fuzzy layer, product layer, normalized layer, de-fuzzy layer, and total output layer. In this manner, ANFIS leverages the learning capabilities of neural networks alongside the inference mechanisms akin to human cognition offered by fuzzy logic. The functionality of each layer is as follows: The output node i in layer l is represented as $l\_i\^O$. Layer 1 serves as the fuzzification layer. Each node i in this layer is an adaptive node with a node function.

$$O_{1,i} = \mu A_i(x), \qquad for\ i = 1,2$$
$$O_{1,i} = \mu B_i(x), \qquad for\ i = 3,4 \qquad (7)$$

Let x denote the input to the i-th node, and $l\_i\^O$ represent the membership grade of x in the fuzzy set A_i. The generalized bell membership function is a widely utilized approach for defining fuzzy sets due to its smoothness and succinct notation, and is defined as follows:

$$\mu_{A_i}(x) = \frac{1}{1 + \left| \dfrac{x - c_i}{a_i} \right|^{2b_i}} \qquad (8)$$

585

Here {i a, i b, i c} constitutes the parameter set of the membership function. The center and width of the membership function are modified by altering i c and i a. The parameter i b regulates the slopes at the crossover sites. This layer constitutes the antecedents of the fuzzy rules (IF component). Layer 2 constitutes the regulatory framework. Each node in this tier is a static node and encompasses a singular fuzzy rule. The output is the result of all incoming signals and indicates the activation strength of each rule.

$$O_i^2 = w_i = \mu_{A_i}(x)\mu_{B_i}(y), \quad i = 1,2 \tag{9}$$

Layer 3 serves as the normalizing layer. Each node in this layer is a static node, and the i-th node computes the ratio of the firing strength of the i-th rule to the aggregate firing strengths of all rules. The outputs of this layer are referred to as normalized firing strengths, calculated as follows:

$$O_i^3 = \overline{w_i} = \frac{w_i}{w_1 + w_2} \quad i = 1,2 \tag{10}$$

Layer 4 is the subsequent layer. Each node in this layer is an adaptive node that calculates the values of the rule consequent (THEN portion) as follows:

$$O_i^4 = \overline{w_i}f_i = \overline{w_i}(p_i x + q_i y + r_i) \tag{11}$$

Layer 5 is summation layer and consists of single fixed node which calculates the overall output as the summation of all incoming signals as:

$$O_i^5 = \sum_i \overline{w_i}f_i = \frac{\sum_i w_i f_i}{\sum_i w_i} \tag{12}$$

This ANFIS architecture contains two adaptive layers: the first layer and the fourth layer. The initial layer contains three adjustable parameters {ai, bi, ci}, associated with the input membership functions. These parameters are referred to as premise parameters. In the fourth layer, three adjustable parameters {pi, qi, ri} are associated with the first-order polynomial. These parameters are referred to as subsequent parameters (Gupta, 1994).

Learning algorithm of ANFIS

The task of the learning algorithm for this architecture is to tune all the modifiable parameters, namely {ai, bi, ci} and {pi, qi, ri}, to make the ANFIS output match the training data. When the premise parameters ai, bi and ci of the membership function are fixed, the output of the ANFIS model can be written as:

$$f = \frac{w_1}{w_1 + w_2}f_1 + \frac{w_2}{w_1 + w_2}f_2 \tag{13}$$

Substituting Eq. (5) into Eq. (8) yields:

$$f = \overline{w_1} f_1 + \overline{w_2} f_2 \tag{14}$$

Substituting the fuzzy if-then rules into Eq. (9), it becomes:

$$f = \overline{w_1}(p_1 x + q_1 y + r_1) + \overline{w_2}(p_2 x + q_2 y + r_2) \tag{16}$$

After rearrangement, the output can be expressed as:

$$f = (\overline{w_1} x) p_1 + (\overline{w_1} y) q_1 + (\overline{w_1}) r_1 + (\overline{w_2} x) p_2 + (\overline{w_2} y) q_2 + (\overline{w_2}) r_2 \tag{17}$$

This is a linear combination of the changeable consequent values p1, q1, r1, p2, q2 and r2. Easy identification of the ideal values of these parameters can be accomplished with the least squares approach. The search space grows more and the convergence of the training slows down when the premise parameters are not fixed. This problem is solved using a hybrid approach combining the gradient descent technique with the least squares method. The hybrid algorithm consists of a forward pass and a backward pass. The least squares method (forward pass) is employed to optimize the subsequent parameters while keeping the premise parameters constant. Upon identifying the ideal consecutive parameters, the backward pass commences immediately. The gradient descent approach (backward pass) is employed to optimally change the premise parameters associated with the fuzzy sets in the input domain. The ANFIS output is determined by utilizing the resultant parameters identified during the forward pass. The output error is utilized to adjust the premise parameters by a conventional backpropagation technique. This hybrid approach has been demonstrated to be particularly efficient in training the ANFIS (Yen,1995) .

Results

The closed-loop response of the AVR system devoid of a controller exhibits significant oscillations and deviates from the intended steady-state value of 1 Fig 7.
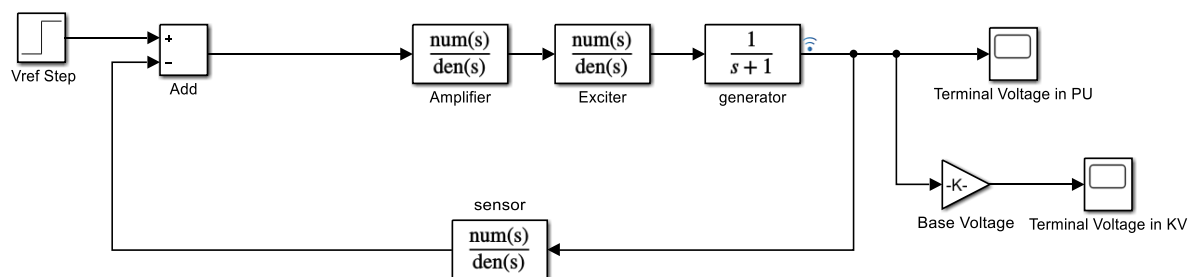

Figure.6 Diagram of an AVR without controller

The oscillatory response exhibits a peak overshoot of 1.6, a rising time of 0.26 seconds, a settling time of 28 seconds, and a steady-state value of 0.9. This oscillating behavior is unacceptable, compromising the stability and security of the system. This study employs, tests, and analyzes three distinct controllers to enhance the transient and steady-state performance of the AVR system.
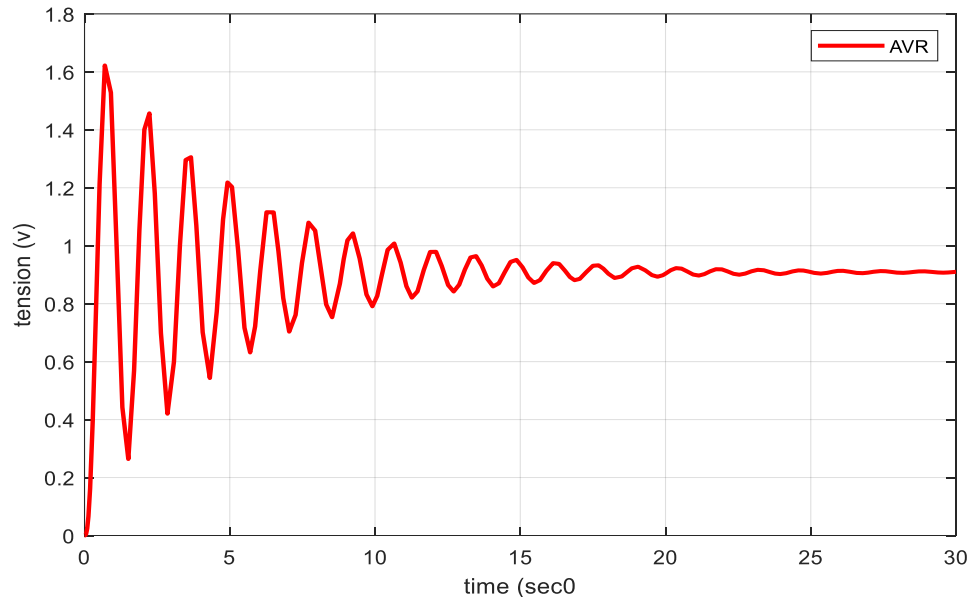

Figure. 7 Closed-loop response of the AVR without controller

The implementation of the PID controller, illustrated in Figure 3, markedly enhanced the system's response. By meticulously adjusting the controller gains (Kp, Ki, Kd), an optimal response was attained, marked by low overshoot and a decreased settling time as illustrated in Figure 4. Table 1 enumerates the optimum PID controller gains employed in this study.
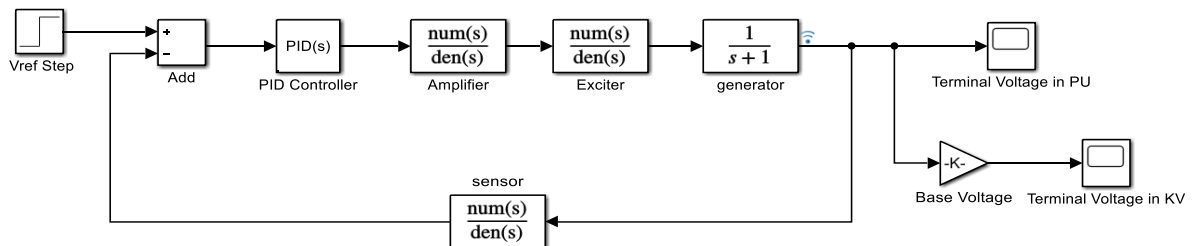

Figure .8 Diagram of AVR system with PID controller

The PID controller, when applied to the AVR system, demonstrated its capability to enhance the system's dynamic response and reduce steady-state error. Figure 9 illustrates the terminal voltage response of the AVR system, exhibiting a large overshoot and extended settling time.
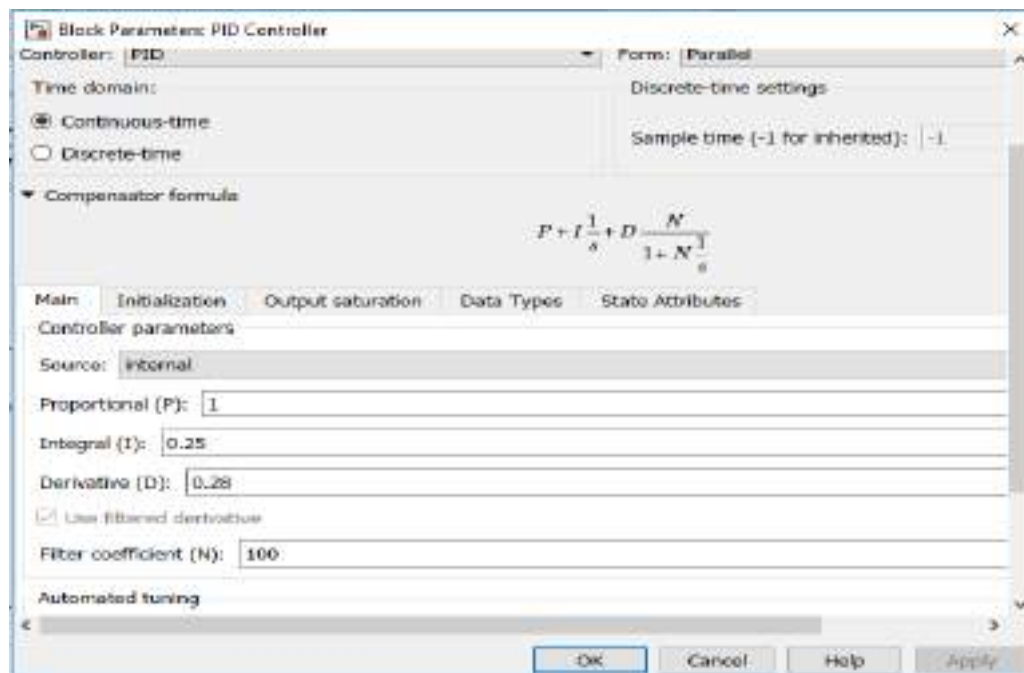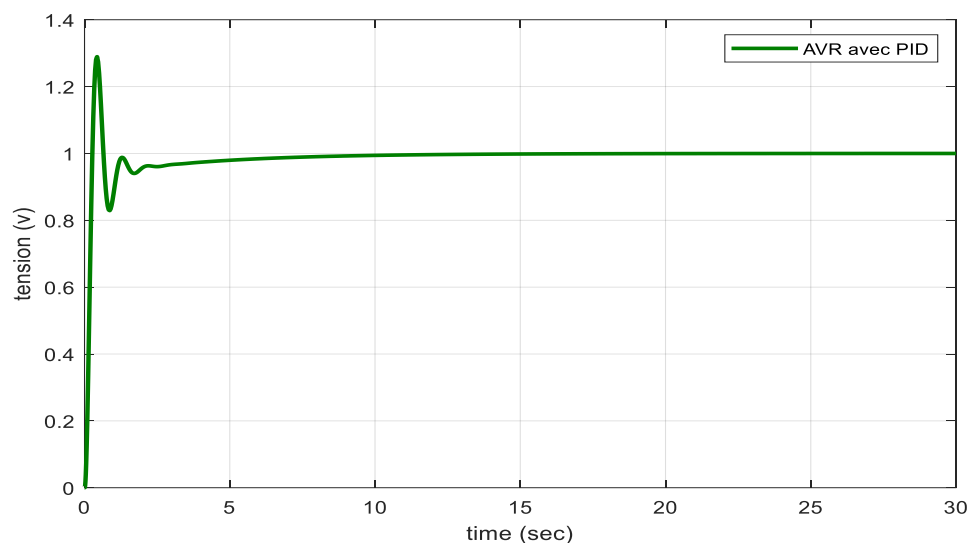
Figure. 9 Tuned value of PID Controller

Figure. 10 Terminal voltage in per unit with PID controller

In this part, the FLC controller is used to adjust the output voltage of the AVR system based on the error signal obtained by comparing a unity step reference input signal to the actual feedback output voltage. The PD-like FLC (Mamadani type) has one input and one output.

The FLC input's represent change in voltage, while the output controls the excitation system . The input and output membership functions of the FLC can be seen in Fig. 6, A standard PD-like fuzzy rule base, of 7 rules, is used as shown in Table 1, in which EL, VL, L,N, H, VH and EH denote extremely low, very low, low,normal, high, very high extremely high. The FLC closed-loop approach is presented in Fig. 8.
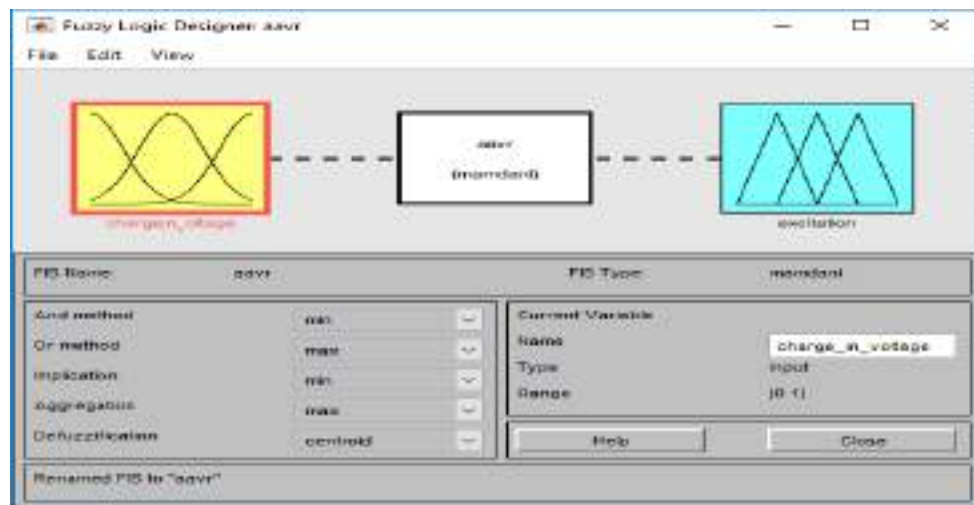
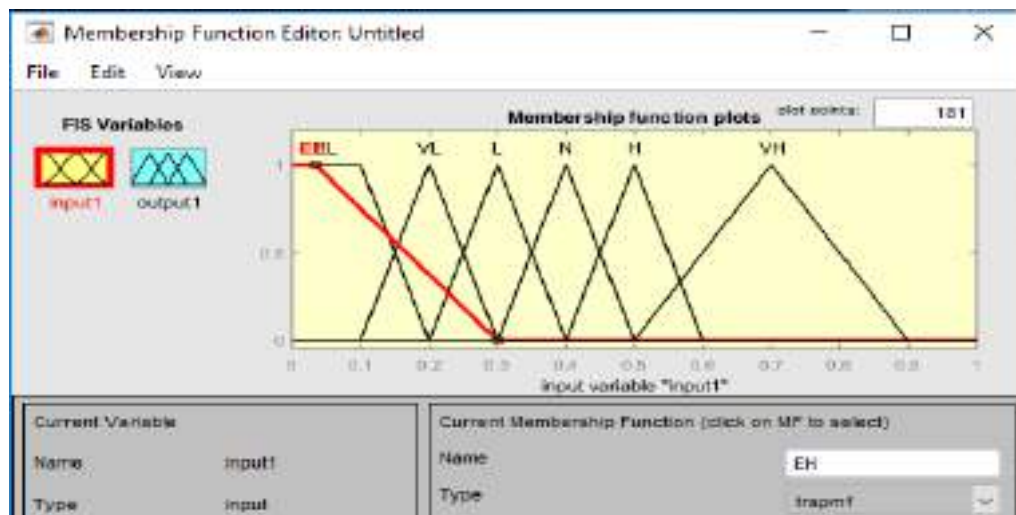Figure.11. Input /output Fuzzy logic controller

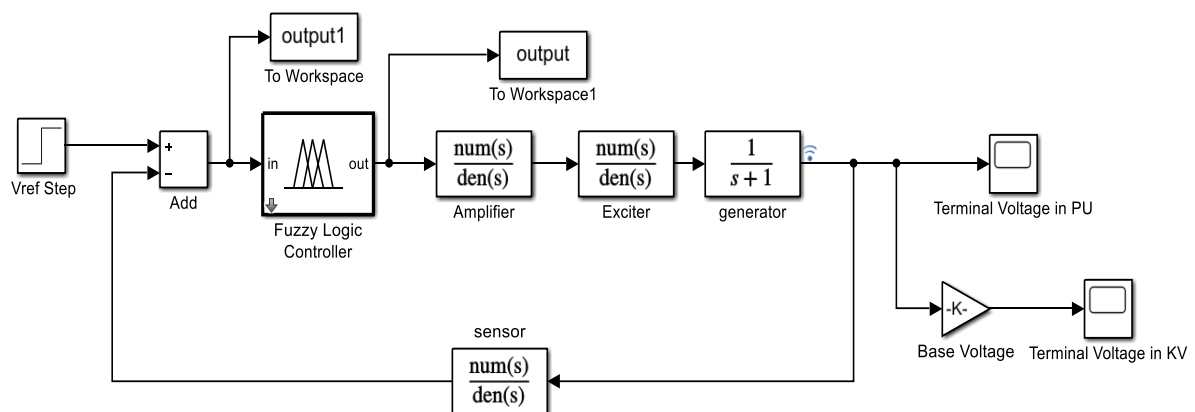Figure. 12 Input/Output membership functions of the FLC.

Figure. 13 Diagram of AVR system with FLC controller

The fuzzy logic controller, utilizing expert knowledge via linguistic rules, exhibited performance better to that of the PID controller. Figure 13 illustrates the AVR system using the integrated fuzzy controller. The system's reaction, depicted in Figure 14, demonstrated a swift settling time and minimal overshoot, validating its proficiency in managing the AVR system's nonlinearities.
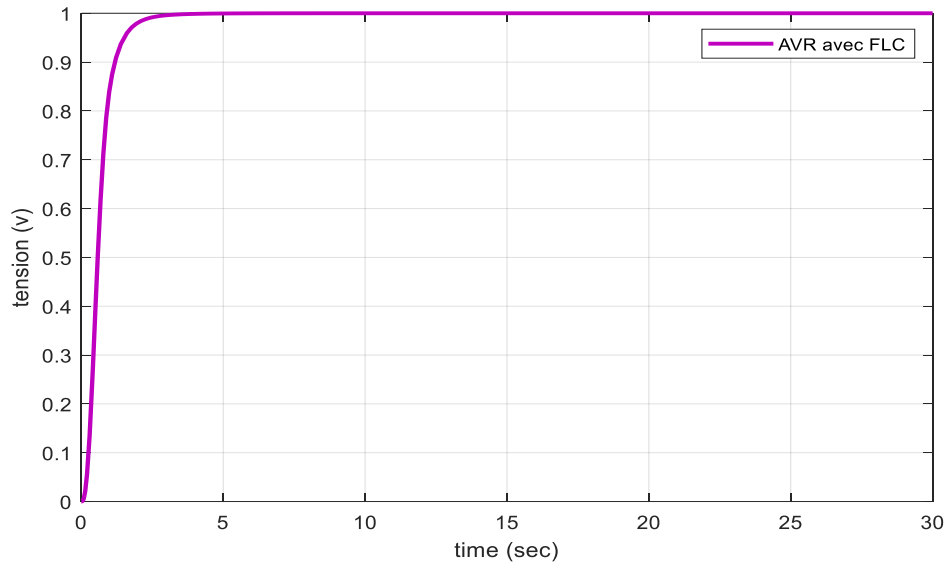
Figure. 14 Terminal voltage in per unit with FLC controller

The ANFIS controller, which integrates fuzzy logic and neural networks, shown exceptional adaptability and efficacy in managing the AVR system. Figure 15 depicts the AVR system combined with the ANFIS controller. Fig.17 illustrates that the ANFIS controller attained a rapid settling time with negligible overshoot, demonstrating its proficiency in learning and adapting to the system's dynamics.
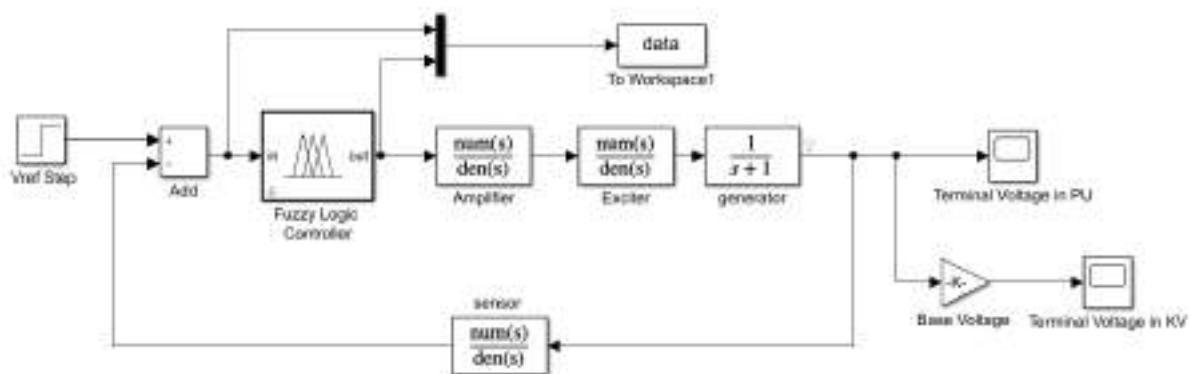
Figure .15 Diagram of AVR system with an ANFIS controller

ANFIS comprises five layers, each interconnected with the subsequent layer using weights. The data from the input layer's first levels are transformed into membership functions to determine the degree of membership of

that input. Fuzzy rules facilitate the linkage between input and output in the second layer. The output is transmitted to the fourth layer subsequent to its normalization by the third layer. The fourth layer generates the output membership function and transmits the output data. The outputs are amalgamated at the fifth layer to generate a singular output. In this inquiry, the number of membership functions is ten, and the type is 'trimf' and constant. The tasting method is designated as 'Hybrid,' and the epochs are set at 50 iterations. The input and output data for the training is derived from the PID controller.
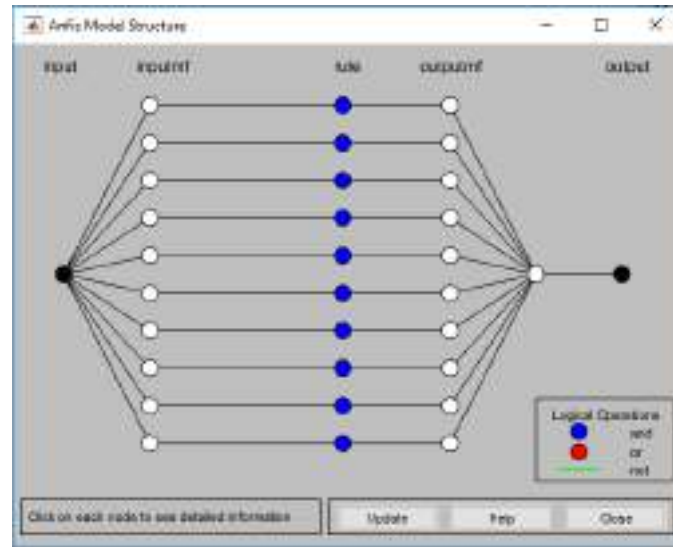

Figure. 16 The Structural Design of ANFIS

Figure 17 illustrates the response of the ANFIS controller within the system, offering significant insight into its behavior.
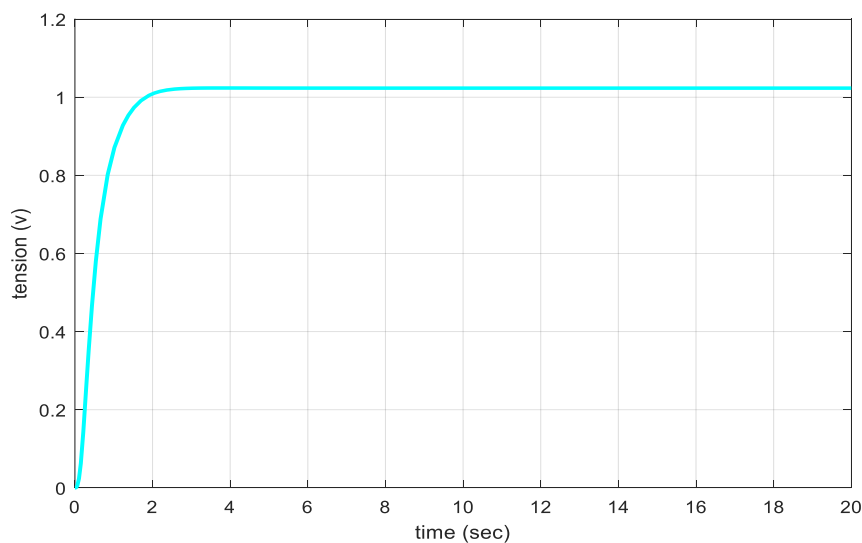

Figure. 17: Terminal voltage in per unit with ANFIS controller

The graph indicates that the system requires roughly 2.555 seconds to reach a steady state, referred to as the

steady-state condition. Throughout this process, a notable characteristic arises: the complete lack of overshoot, indicated by an exceptional 0% overshoot. This illustrates that the system achieves its intended state without surpassing the specified parameters, signifying a remarkable degree of control and precision in its operation.

Conclusion

Three distinct controllers—PID, PD-like FLC, and ANFIS—are employed in this work to control an AVR system. We analyzed and examined the three controllers' performances. The PID generated was not robust enough to disturbances as it produced fluctuations for almost 4 s , produced a 1.3 overshoot in the output and with sittling time of 8 s better than only AVR . Although the FLC was better than other controllers in terms of delay and rising times, and produced a zero overshoot in the output, the FLC produced a steady-state error of 0 V and was robust enough to disturbances as it   dont produced fluctuations s when exposed to negative disturbance signal ,with 4s of sittling time and zero overshoot. In terms of delay and rising times, the ANFIS controller was faster than the PID controller; moreover, it created zero overshoot than the PID. Comparatively to the other two controllers, the ANFIS controller shown same performance in rejecting positive and negative disturbance signals. Regarding resistance to changes in system characteristics, ANFIS and FLC both performed rather well. While the ANFIS controller managed to limit the SSE to zero with a small rise in the overshoot in some circumstances, the FLC suffered from 12.5% increase in the SSE. In several occasions the PID controller suffered from significant overshoot values. The aforementioned leads one to conclude that the ANFIS controller is better suited and dependable than PD-like FLC and PID controllers and can be applied in an AVR system.

References

Al Gizi, A. (2019). "A particle swarm optimization, fuzzy PID controller with generator automatic voltage regulator," Soft Computing, vol. 23, pp. 8839–8853, 2019.

Al Gizi,A., Mustafa, M., Al-geelani, N. Alsaedi, M. (2015). "Sugeno fuzzy PID tuning, by genetic-neutral for AVR in electrical power generation," Applied Soft Computing, vol. 28, pp. 226-236.

Ayas, M., Sahin, E. (2021)."FOPID controller with fractional filter for an automatic voltage regulator," Computers and Electrical Engineering, vol. 90, pp. 106895.

Ayas,M , & Sahin.E .(2021), "FOPID controller with fractional filter for an automatic voltage regulator," Computers and Electrical Engineering, vol. 90, pp. 106895.

ChristyJuliet, B., Vinothini, D; Vidhyashree, S. (2014). "Power system stabilisation based on Ga-Anfis in generators," International Journal of Research in Engineering and Technology, vol. 3, no. 7, pp. 758-760.

Dabur, P., Yadav, N., Avtar, R .(2012) "Matlab design and simulation of AGC and AVR for single area power system with fuzzy logic control," International Journal of Soft Computing and Engineering, vol. 1, no. 6, pp. 44-49.

Elsisi, M. (2019). "Design of neural network predictive controller based on imperialist competitive algorithm

for automatic voltage regulator," Neural Computing and Applications, vol. 31, pp. 5017–5027, 2019.

Elsisi, M., Tran, M., Hasanien, H., Turky, R., Albalawi, F., Ghoneim, S.(2021). "Robust model predictive control paradigm for automatic voltage regulators against uncertainty based on optimization algorithms," Mathematics, vol. 9, no. 22, pp. 2885.

Elsisi,M; Soliman,M.(2021) "Optimal design of robust resilient automatic voltage regulators," ISA Transactions, vol. 108, pp. 257-268.

Govindan, P.(2019)."Evolutionary algorithms-based tuning of PID controller for an AVR system," International Journal of Electrical and Computer Engineering, vol. 10, no. 3, pp. 3047-3056.

Gupta, MM., Rao, DH.(1994). Newo-control systems: theory and applications. Piscataway, NJ: IEEE Press.

Li, X., Wang,Y., Li, N., Han,M.., Tang, M., Liu , F .(2017). "Optimal fractional order PID controller design for automatic voltage regulator system based on reference model using particle swarm optimization," International Journal of Machine Learning and Cybernetics, vol. 8, no. 5, pp. 1595-1605.

Lin, Y. (2013). "Proportional plus derivative output feedback based fuzzy logic power system stabiliser," International Journal of Electrical Power and Energy Systems, vol. 44, no. 1, pp. 301-307.

Mukherjee,V., Ghoshal, S.(2007). "Intelligent particle swarm optimized fuzzy PID controller for AVR system," Electric Power Systems Research, vol. 77, no. 12, pp. 1689-1698.

Pachauri, N.(2020)"Water cycle algorithm-based PID controller for AVR," The International Journal for Computation and Mathematics in Electrical and Electronic Engineering, vol. 39, no. 3, pp. 551-567.

Sahib.M. (2015), "A, novel optimal PID plus second order derivative controller for AVR system," Engineering Science and Technology, an International Journal, vol. 18, no. 2, pp. 194-206.

Sikander, A; Thakur.P.2020. "A new control design strategy for automatic voltage regulator in power system," ISA Transactions,vol.100,pp .235-243

Sikander,A., Thakur, P., Bansal,R., Rajasek,.S. (2018). "A novel technique to design cuckoo search based (A FOPID controller for AVR in power systems," Computers and Electrical Engineering, vol. 70, pp. 261-274 .

Soliman.M., & Ali.M,.(2021) "Parameterization of robust multi-objective PID-based automatic voltage regulators: generalized Hurwitz approach," International Journal of Electrical Power and Energy Systems, vol. 133, pp. 107216.

Spoljaric,T., Lusetic, C ., Simovic, V .(2018). "Optimization of PID controller in AVR system by using ant lion optimizer algorithm," MIPRO, pp. 1522-1526.

Tang, Y., Zhao,L. , Han, Z.,X. Bi, Guan, X.(2016) "Optimal gray PID controller design for automatic voltage regulator system via imperialist competitive algorithm," International Journal of Machine Learning and 7, no. 2, pp. 229-240.

Yavarian, K., Hashemi, F., Mohammadian, A .(2014)."Design of intelligent PID controller for AVR system using an adaptive neuro fuzzy inference system," International Journal of Electrical and Computer Engineering, vol. 4, no. 5, pp. 703-718.

Yavarian,K., Mohammadian, M., Hashemi, F.(2015)."Adaptive neuro fuzzy inference system PID controller for AVR system using SNR-PSO optimization," International Journal on Electrical Engineering and Informatics, vol. 7, no. 3, pp. 394-408.

Yen J, Langari R, Zadeh LA.(1995) . Industrial applications of fuzzy logic and intelligent systems. New York, NY: IEEE Press.

Zadeh, L.(1965). " Fuzzy Sets", Informat Control, vol. 8, pp. 338-353.

Zhang, H., Shi, F., & Liu, Y.(2014). "Enhancing optimal excitation control by adaptive fuzzy logic rules," International Journal of Electrical Power and Energy Systems, vol. 63, pp. 226-235.

Comparative Analysis of Service Identification Approaches

Wafa Souiou

LISCO Laboratory, Badji Mokhtar-Annaba University, Annaba, Algeria https://orcid.org/0009-0007-8837-3221

Nora Bounour

LISCO Laboratory, Badji Mokhtar-Annaba University, Annaba, Algeria https://orcid.org/ 0000-0003-4267-5834

Abstract: Software reengineering has become essential in today's computing world, where systems need to continually evolve with new requirements and technologies. In this context, the transition to service-oriented architectures has become a popular approach to enhance the flexibility, scalability, and maintainability of Legacy systems. However, transforming a monolithic system into a service-oriented architecture presents its own challenges. It requires careful analysis, accurate service identification, and detailed reengineering planning. Various methods and tools are used to facilitate this complex transition. In this article, we perform a comparative analysis of different service identification approaches, focusing on four major methods employed in service-oriented software reengineering. Each approach provides a distinct viewpoint on how to approach service identification and the transition from monolithic systems to services.

Keywords: SOA, Service Identification, Legacy System, Reengineering, A monolithic system.

Introduction

Transitioning to service-oriented architectures (SOA) is a vital but challenging process for many companies aiming to modernize their computer infrastructures. Service-oriented architectures (SOA) present several benefits for organizations, including (Sneed, 2006):

- **Flexibility and Agility**: Service-oriented architectures enable companies to decompose their systems into independent services, making it easier to adapt to rapid market changes and new business requirements. Services can be developed, deployed, and updated independently, which enhances the company's responsiveness (Souiou & Bounour, 2013) (Krafzig & al., 2007).
- **Service Reusability**: Services created within a service-oriented architecture can be reused across various contexts and applications. This allows companies to conserve time and resources by preventing duplication of development efforts (Krafzig et al., 2007) (Almonaies et al., 2010).

- **Interoperability:** Service-oriented architecture enhances interoperability among diverse systems and applications within the company (Krafzig et al., 2007) (Sneed, 2006). Services are designed to be independent of platforms and programming languages, simplifying the integration of different systems.

- **Scalability**: Service-oriented architectures are designed to be scalable, enabling them to accommodate varying workloads by adding or removing service instances as necessary (Papazoglou, 2003).

- **Ease of Maintenance**: By partitioning systems into smaller, self-contained services, service-oriented architectures simplifie system maintenance and management. Updates and bug fixes can be applied to individual services without affecting the entire system (Krafzig et al., 2007) (Papazoglou, 2003).

-

In summary, transitioning to service-oriented architectures enables companies to enhance their flexibility, agility, and responsiveness to market changes (Sneed, 2006). It promotes reusability, interoperability, and scalability, leading to improved efficiency and competitiveness within the company (Souiou & Bounour, 2013). In the literature, various methodologies for identifying services have been proposed. In this article, we will perform a comparative analysis of these service identification strategies, focusing on the principal methods employed in service-oriented software reengineering. Each method provides a distinct viewpoint on the process of service identification and the conversion of monolithic systems into services (Abdellatif et al., 2021). We will evaluate their characteristics and weak points based on several factors, including complexity of implementation, reusability of the identified services, and dependence on specific technologies. This analysis aims to provide a comprehensive understanding of the different available approaches, assisting practitioners and researchers in making well-informed choices during software reengineering initiatives aimed at adopting service-oriented architectures.

The remainder of this paper is structured as follows: section 2 describes related work, focusing on their characteristics and weak points. The comparative analysis of the different service identification approaches is detailed in Section 3. Results and discussion are detailed in Section 4. Finally, Section 5 concludes our work and states the possible future work.

Related Work

The challenge of transitioning a legacy system to Service Oriented Architecture (SOA) has been explored by many researchers, and several service identification approaches have been reported in the literature (Souiou & Bounour, 2013). For example in (Adjoyan et al., 2014), authors proposed an automatic strategy for identifying services from object-oriented source code. The proposed approach is based on a mapping model from objects to services and a quality function that measures semantic accuracy of identified services. In (Bandara & Perera, 2020), authors proposed an automated technique to identify microservices within legacy monolithic system taking into account service quality characteristics, Using a tool that establishes a mapping model between Java classes and microservice concepts. Then, it proposes a fitness function to evaluate service quality. Initially, the method treats all service classes as a single microservice and subsequently improves the service identification

process iteratively through the fitness function. In (Shatnawi et al., 2020), authors proposed ReSIde (Reusable Service Identification): an automated approach that identifies reusable services from a set of object-oriented Software Product Variants SPVs. This method relies on analyzing the commonality and the variability across SPVs to pinpoint reusable functionality related to cloned codes enabling them to be packaged as reusable services. In (Zhang et al., 2005), authors concentrated on extracting services from existing systems and organizing them into coherent modules to facilitate the transition to a service-oriented architecture, while enhancing the system's modularity, reusability and maintainability.

To provide an in-depth comparative analysis between these different approaches, we analyze each approach individually emphasizing their main characteristics and weak points drawing comparisons among them.

Table1. Characteristics and Weak Points of Service Identification Approaches

Approach	Characteristics	Weak Points
(Adjoyan et al., 2014)	- Identification of services from Code source Java. - Based on software quality metrics such as Functionality, Composability and Self-Containment. - Based on a mapping model from objects to services. -Based on quality function that measures semantic accuracy of identified services. -Applied a hierarchical Clustering Algorithm. - Proposed an automatic approach.	-Quality metrics can be subjective and context-dependent. - Significant effort is required for the collection and analysis of metrics.
(Bandara & Perera, 2020)	- Identification of Microservices from Code source Java. - Based on software quality metrics such as Functionality, Composability, Self-Containment and Usage.	- Can be limited by the complexity of existing monolithic systems. - Often requires a deep understanding of the existing source code.

	- Provides a set of tools and techniques to evaluate monolithic systems. - Based on a mapping model between Java classes and microservice concepts. -Proposed method using two approaches as a manual approach and a semi-automated approach. -Based on quality function that measures characteristic similarity between each group of classes. -Applied a hierarchical Clustering Algorithm.	
(Shatnawi et al., 2020)	- Identification of reusable services from code source of similar software families. - Based on the analysis of the commonality and the variability between the source code of Software Product Variants (SPVs). - Based on software quality metrics such as Functionality, Composability and Self-Containment. - Proposed an automatic approach. - Applied a hierarchical Clustering Algorithm.	- Can be difficult to apply in contexts where the software is very different or heterogeneous. - Requires a good understanding of the similarities and differences between the software in the family.
(Zhang et al., 2005)	-Integrated and reused software components as services. -Adopted SADL and UML representation. -Applied a hierarchical Clustering Algorithm. - Proposed an automatic approach.	- Can be limited by the complexity of existing systems and the variability of reengineering requirements. - Requires careful management of dependencies between identified services.

After evaluating the different approaches, it's clear that each one has its characteristics and weak points depending on the nature of the system and the reengineering goals. For example, if the objective is to maximize service reuse, the ReSIde approach could be more suitable. On the other hand, if the emphasis is on improving service quality, the approach based on quality metrics may be more applicable. Meanwhile, there are some approaches that share common features, such as (Adjoyan et al., 2014) (Bandara & Perera, 2020) (Shatnawi et al., 2020) all those, identified services from code source, based on software quality metrics such as Functionality, Composability ,Self-Containment and based on quality function that measures semantic accuracy of identified services. In addition, all approaches mentioned in table1 applied a hierarchical Clustering Algorithm to group classes and create services.

Comparative Analysis

In this section, we provide a comparison of the different methods discussed earlier. The comparative study is elaborated by answering the following questions:

   Q1: What level and complexity of transformation is required?
   Q2: How reusable are the identified services?
   Q3: How the classes are regrouped to form a service?
   Q4: what is the level of dependence on specific technologies?

Table2. The Comparative Analysis

Criteria / Approach	The required level and complexity of transformation	The reusability of identified services	the method used for grouping classes	Dependence on specific technologies
(Adjoyan et al., 2014)	-High complexity due to the specific quality metrics Collected.	-Improved reusability by focusing on quality.	-A hierarchical Clustering Algorithm.	- Dependent because it focuses on source code and quality metrics.
(Bandara & Perera, 2020)	- Significant complexity due to the transformation of monolithic systems to microsevices.	- Less reusable services due to the increased granularity of microservices.	- A hierarchical Clustering Algorithm.	- Highly dependent on specific technologies for transformation into microservices

(Shatnawi et al., 2020)	- Moderate complexity, but strong dependence on similarities between software.	- Improved reusability by analysing several SPV's.	- A hierarchical Clustering Algorithm.	- Dependent because it focuses on source code and quality metrics.
(Zhang et al., 2005)	- Moderate to high complexity because it's based on service identification and service packaging processes.	- Moderate to high reusability depending on how services are packaged and designed .	- A hierarchical Clustering Algorithm.	- Highly dependent especially to technologies used for packaging and service management.

Results and Discussion

From this comparison, it is evident that each approach possesses its own strengths and weaknesses based on evaluated criteria. The selection of an approach will primarily be influenced by the characteristics of the Legacy system, the objectives of reengineering, preferences concerning reusability, complexity, and technological dependencies.

Below are some overarching conclusions that can be made:

Required Level and complexity of Transformation

The various methods differ in the complexity involved in their implementation and the level of transformation necessary to shift from Legacy system to a service-oriented architecture. Approaches that focus on quality metrics analysis may require moderate to high structural transformation due to the need to identify and measure specific quality metrics (Adjoyan et al., 2014) (Shatnawi et al., 2020), while tools for evaluating monolithic systems may demand a more profound transformation due to the deep transformation of Legacy systems (Bandara & Perera, 2020).

Service Reusability

The ReSIde approach focuses in service identification on the analysis of several Software Product Variants (SPVs) that increase the reusability of identified services, which is beneficial in environments where reusability

is significant (Shatnawi et al., 2020). However, the other approaches can also generate reusable services based on their design and implementation. Also, based on how services are packaged and designed.

Dependency on Specific Technologies

Some approaches may depend heavily on specific technologies like (Zhang et al., 2005) and (Bandara & Perera, 2020), which potentially limits their effectiveness across varied technological environments. Approaches based on quality metrics analysis (Shatnawi et al., 2020) (Adjoyan et al., 2014), may provide more flexibility in this aspect, because it focuses more on general aspects of quality.

Used technique for grouping classes

All the above approaches use the same method of class grouping, which is hierarchical clustering.

Reengineering Objectives

The selection of an approach will significantly depend on the particular aims of the Reengineering. For example, if the goal is to improve service quality, the approach centered around quality metrics may be more appropriate. However, if the emphasis is on reusability and transformation into microservices, other approaches may be more suitable.

Conclusion

In this paper, we have presented the principal methods employed in service-oriented software reengineering. Each approach provides a distinct viewpoint on how to approach service identification and the transition from monolithic systems to services. We have evaluated their characteristics and weak points depending on the nature of the system and the reengineering goals. We conducted a comparative analysis by answering the questions presented in section 3. We conclude that no solution is generally applicable to every situation. The selection of an approach will primarily be influenced by the specific needs of the project, the nature of the Legacy System, and the Reengineering objectives. A mixed approach combining elements of the various approaches or adaptation of different approaches depending on the specific context can also be a possible solution and the choice of approach will be highly impacted by the nature of the Legacy System, the Reengineering goals, and preferences concerning reusability, complexity, and technological dependencies.

References

Adjoyan, S., Seriai, A.-D., & Shatnawi, A. (2014). Service Identification Based on Quality Metrics. Proceedings of the 26 International Conference on Software Engineering & Knowledge Engineering (SEKE2014),

1–6. https://doi.org/10.13140/2.1.2980.6723.

Abdellatif, M., Shatnawi, A., Mili, H., Moha, N., Boussaidi, G. El, Hecht, G., Privat, J., & Guéhéneuc, Y. G. (2021). A taxonomy of service identification approaches for legacy software systems modernization. Journal of Systems and Software, 173. https://doi.org/10.1016/j.jss.2020.110868.

Almonaies, A. A., Cordy, J. R., & Dean, T. R. (2010). Legacy System Evolution towards Service-Oriented Architecture - Google Search. http://www.google.com.au/search.

Bandara, C., & Perera, I. (2020). Transforming monolithic systems to microservices - An analysis toolkit for legacy code evaluation. 20th International Conference on Advances in ICT for Emerging Regions, ICTer 2020 - Proceedings, 95–100. https://doi.org/10.1109/ICTer51097. 2020.9325443.

Krafzig, D., Banke, K., & Slama, D. (2007). Enterprise SOA. In Service oriented Architecture Best Practices: Vol. 5. print (p. 373).

Papazoglou, M.P. (2003). Service-oriented computing: concepts, characteristics and directions. In 0-7695-1999-7 (Ed.), Proceedings of the Fourth International Conference on Web Information Systems Engineering, 2003. WISE 2003. IEEE. https://doi.org/10.1109/WISE.2003.1254461.

Shatnawi, A., Seriai, A., Sahraoui, H., Ziadi, T., & Seriai, A. (2020). ReSIde: Reusable service identification from software families. Journal of Systems and Software, 170. https://doi.org/10.1016/j.jss.2020.110748.

Souiou, W., Bounour, N. (2013). Migration of Legacy Systems to Service Oriented Architecture. The Third International Conference on Digital Information Processing And Communications (ICDIPC 2013)_, March 2013, 1_8.

Sneed, H. M. (2006). Integrating legacy Software into a Service oriented Architecture. The Conference on Software Maintenance and Reengineering (CSMR'06). https://doi.org/0-7695-2536-9/06.

Zhang, Z., Liu, R., & Yang, H. (2005). Service Identification and Packaging in Service Oriented Reengineering. The 17th International Conference on Software Engineering and Knowledge Engineering (SEKE'05).

An Investigation of Pre-Service Social Studies Teachers' Perceptions of Technological Self-Efficacy

Özkan Akman

Süleyman Demirel University, Türkiye, https://orcid.org/0000-0002-8264-3178

Abstract The aim of this article is to examine pre-service social studies teachers' perceptions of technological self-efficacy. Technological developments significantly affect educational processes and methods, which makes it necessary for pre-service teachers to increase their competencies related to technology. It is especially important for social studies teachers to be able to use technology effectively to enrich course content and communicate more effectively with students. Technology integration is not only the addition of technological tools to the educational environment, but also the use of these tools in a student-oriented manner that is compatible with pedagogical goals. Successful integration increases efficiency and effectiveness in education and provides students with 21st century skills. The research was designed to determine how competent pre-service social studies teachers feel themselves in the use of technology. In this context, how pre-service teachers use technological tools in lesson planning, implementation and evaluation processes were discussed. A positive perception of self-efficacy towards technology can contribute to preservice teachers' managing these processes more effectively. The research data were collected from pre-service social studies teachers studying at various universities through a questionnaire. The questionnaire aimed to measure pre-service teachers' knowledge and skills related to technology and assessed their self-efficacy perceptions. The findings show that pre-service social studies teachers generally feel relatively competent in technological competence, but they need more support in some areas. In conclusion, improving pre-service social studies teachers' technological self-efficacy requires more effective integration of technology into the teacher training programs of faculties of education. This can play an encouraging role for pre-service teachers to continuously improve their competencies in the use of technology in education after graduation.

Keywords: Social Studies, Technology, Self-efficacy.

Introduction

Today, the rapid development of technology leads to significant transformations in the field of education (Cakir, Ozturk, & Unal, 2019; Ozturk, 2023). Educational technologies have brought many innovations such as

enriching course content, diversifying teaching methods and individualizing learning processes (Almaz & Ünal, 2014). In this context, the ability of pre-service teachers to use technology effectively has become one of the requirements of modern education understanding (Aydogan & Koc, 2022; Kaya, 2017; Kirbas & Bulut, 2024).

In particular, pre-service social studies teachers can offer more comprehensive and interactive learning experiences to their students by using technological tools and digital resources while teaching interdisciplinary knowledge (Akbaş & Toros, 2017; Ünlü, Kaşkaya & Coşkun, 2017). Therefore, examining pre-service teachers' technological self-efficacy perceptions is of great importance in terms of contributing to their professional development processes and improving the quality of education (Kaya, 2020). The purpose of this study is to evaluate pre-service social studies teachers' perceptions of technological self-efficacy and to analyze how these perceptions differ in terms of various variables.

Theoretical Framework

Self-efficacy theory was developed within the framework of Bandura's social cognitive theory and refers to the belief that individuals have in themselves to successfully perform a certain task or situation. Technological self-efficacy perception, on the other hand, represents an individual's belief in performing technology-related tasks effectively. In this context, it is known that individuals with high technological self-efficacy perception can integrate technology into learning and teaching processes more effectively (Bakar, & Çiftçi, 2020).

The technological self-efficacy of pre-service teachers affects their competencies in technology integration in education and their capacity to offer better educational opportunities to students (Yıldız & Seferoğlu, 2020. Technological self-efficacy also reduces individuals' anxiety levels regarding the use of technology, allowing them to adopt more innovative and flexible methods (Ünal, 2013; Akman, 2014).

This study addresses the technological self-efficacy perceptions of pre-service social studies teachers within the framework of technology acceptance model and self-efficacy theory. The technology acceptance model provides a framework for understanding the factors affecting users' adoption of new technologies (Turan & Bay, 2023). In this model, perceived usefulness and ease of use have a strong relationship with technological self-efficacy (Burmabıyık, 2014). The research aims to examine how pre-service teachers' technological self-efficacy perceptions are shaped in line with these factors

Method

The aim of this study is to examine the technological self-efficacy perceptions of pre-service social studies teachers by using descriptive analysis method. Descriptive survey model, one of the quantitative research methods, was adopted as the research design.

Participants

The participants consisted of 880 pre-service teachers enrolled in social studies teaching programs in universities located in different geographical regions of Turkey. The demographic characteristics of the participants were evaluated in the analysis phase of the study.

Data Collection Tools

A reliable and valid scale measuring technological self-efficacy perceptions was used as a data collection tool. The scale consists of questions prepared for self-efficacy perceptions about technology use. Participants' degree of agreement with each statement was measured using a Likert-type scale.

Data Collection Process

The data collection process was carried out by using face-to-face or online questionnaire applications. In the process of administering the questionnaires, the participants were informed about the purpose and scope of the study and voluntary participation was ensured. The data obtained were prepared to be analyzed with descriptive statistical techniques.

Data Analysis

The data obtained in the study were analyzed using SPSS 22.00 (Statistical Package for the Social Sciences) software. Descriptive statistics were used to determine the general trends and distributions of the data. By calculating descriptive statistics such as frequency, percentage, mean and standard deviation, a general profile of the participants' technological self-efficacy perceptions was created. In addition, it was examined whether the participants' perceptions of technological self-efficacy differed according to their demographic characteristics. For this purpose, significant differences were evaluated by applying appropriate statistical tests such as correlation and ANOVA.

This methodological framework allowed for a comprehensive examination of pre-service social studies teachers' perceptions of technological self-efficacy and revealed how these perceptions differed in the context of various variables. The results of the study aim to provide important inputs for technology integration strategies in teacher education programs.

Results

This study evaluated the technological self-efficacy perceptions of 880 pre-service social studies teachers studying at various universities in Turkey. The findings are detailed below:

Table 1. Teacher technology knowledge according to gender variable

Gender	N	Average Rank	Total of Rows	U	p
Woman	480	403.46	21824.00		
Man	400	416.52	2987.00	8896	0.6
Total	880				

The Mann-Whitney U Test was used to examine whether the technological knowledge of teacher candidates differed according to the gender variable. As a result of the analysis, it was seen that the technological knowledge of teacher candidates did not show a significant difference according to the gender variable, that is, there was no difference in technological knowledge between female and male teacher candidates (U=8896.00, p>.05). Accordingly, it can be said that the technological knowledge of female and male teacher candidates did not differ according to the gender variable.

Table 2. Technological knowledge of teacher candidates according to the frequency of technology use

Frequency of technology use	N	Average Rank	Total of Rows	sd	X	p
Few hours per day	440	413.46	21824.090	2	10.26	0.005
Few hours per week	240	416.52	2987.50			
Few hours per month	200	68	2990.60			
Total	880					

In the study, Kruskal-Wallis Test was used to examine whether the technological knowledge of the prospective teachers showed a significant difference according to the technology usage frequency variable. According to the information presented in Table 2, the technological content knowledge of the prospective teachers showed a significant difference according to the internet usage frequency variable ((2)=10.26, p<.05). Accordingly, it can be said that the technological knowledge of the prospective teachers who use the internet for a few hours a day is at a higher level than the prospective teachers who use the internet for a few hours a week and a few hours a month.

Table 3. Correlation between the prospective teacher's self-efficacy perception and technological competency knowledge

	Technology competency knowledge
Teacher self-efficacy perception	0.555*

** The correlation is significant at the 0.01 level.

Correlation analysis was used to determine the relationship between teacher self-efficacy perceptions and technology self-efficacy perceptions of teacher candidates. The analysis revealed that there was a positive and moderate relationship between teacher self-efficacy perceptions and technology self-efficacy. According to the

findings, it can be said that as teacher self-efficacy perceptions of teacher candidates increase, their technology knowledge also tends to increase.

Discussion, Conclusion and Recommendations

This study aimed to examine the technological self-efficacy perceptions of social studies teacher candidates and to reveal how these perceptions differ in the context of different demographic and educational variables. The findings of the study show that teacher candidates generally have a positive attitude towards technology and are confident in using technological tools effectively.

1. General Technological Self-Efficacy Level: Social studies teacher candidates have a high self-efficacy perception towards technology. This result shows that the candidates are ready for a meaningful integration of technology in their educational processes.

2. Demographic Differences: The gender factor did not have a significant effect on technological self-efficacy perceptions. However, it was observed that self-efficacy perceptions increased as the grade levels progressed. It is an expected result that teacher candidates approach technology more confidently as their experience increases.

3. Access to and Use of Technology: A positive relationship was found between access to technological tools and the daily use of these tools and self-efficacy perceptions. This relationship indicates that teacher candidates who actively use technology develop more self-confidence and have the potential to use these tools more effectively in their teaching processes.

The findings show that the perception of technological self-efficacy can develop further throughout the education process of prospective teachers and that this offers a significant advantage for the future of students in the information age (Burmabıyık, 2014; Turan & Bay, 2023). Educational programs should encourage candidates to use technology effectively in a pedagogical context. This should ensure that digital tools and resources are perceived not only as substitute materials but also as an integral part of the teaching process (Akman, 2014; Akbaş & Toros, 2017; Ünal, 2013; Ünlü, Kaşkaya & Coşkun, 2017).

Future research can also examine the relationship between technological self-efficacy and students' attitudes towards educational technologies in more depth. In addition, studies conducted over a longer period of time and in various cultural contexts can provide a broader perspective on this issue (Kaya, 2017).

References

Akbaş, Y., & Toros, S. (2017). Sosyal Bilgiler Öğretmen Adaylarının Mekânsal Teknolojilere Yönelik Öz Yeterlik Algılarının Bazı Değişkenler Açısından İncelenmesi. *Journal of International Social*

Research, *10*(54).

Akman, Ö. (2014). *Sosyal bilgiler öğretmenlerinin ve öğretmen adaylarının teknolojik, pedagojik ve alan bilgisi öz yeterlik algı düzeylerinin çok yönlü incelenmesi* (Doctoral dissertation, Necmettin Erbakan University (Turkey)).

Almaz, G., & Ünal, E. (2014). Öğretmen Adaylarının Yaratıcı Drama Yöntemini Kullanmaya Yönelik Öz Yeterlik Algılarının İncelenmesi. *International Journal of Languages' Education and Teaching*, *2*(3), 48-65.

Aydogan, H., & Koc, M. (2022). Junior High School Teachers' Self-Efficacy Levels for STEM Practices: A Sample of Aydin City. In P. Dankers, M. Koc, & M.L. Ciddi (Eds.*), Proceedings of ICEMST 2022--International Conference on Education in Mathematics, Science and Technology* (pp. 15-21), Antalya, TURKEY. ISTES Organization.

Bakar, M. H. D., & Çiftçi, B. (2020). Sosyal bilgiler öğretmen adaylarının 21. yüzyıl becerileri yeterlilik algılarının incelenmesi:(Nevşehir ili örneği). *Kapadokya Eğitim Dergisi*, *1*(2), 44-61.

Burmabıyık, Ö. (2014). *Öğretmenlerin teknolojik pedagojik içerik bilgilerine yönelik öz-yeterlilik algılarının çeşitli değişkenler açısından incelenmesi (Yalova İli Örneği)* (Master's thesis, Sakarya Üniversitesi).

Cakir, E., Ozturk, M.S., Unal, M. (2019). Interpainting as a Creating Method in Digital Illustration: Reinterpretations from Movie Scenes. *Science, Education, Art and Technology Journal (SEAT Journal), 3*(2), 78-88.

Kaya, K. (2017). Yüzüncü yıl Üniversitesi eğitim fakültesindeki sosyal bilgiler öğretmeni adaylarının öz-yeterlik algılarının çeşitli değişkenler açısından incelenmesi. *Uluslararası Türk Eğitim Bilimleri Dergisi*, *2017*(9), 446-454.

Kaya, R. (2020). *Eğitim fakültesi öğrencilerinin teknoloji entegrasyonu öz-yeterlik algıları ile dijital yeterlik seviyeleri arasındaki ilişkisinin incelenmesi* (Master's thesis, Balıkesir Üniversitesi Sosyal Bilimler Enstitüsü).

Kirbas, A. & Bulut, M. (2024). Investigation of the screen reading self-efficacy perceptions of Turkish Language and Literature and Turkish teacher candidates. *International Journal of Education in Mathematics, Science, and Technology (IJEMST), 12*(3), 621-641. https://doi.org/10.46328/ijemst.3958

Ozturk, O.T. (2023). Examination of 21st Century Skills and Technological Competences of Students of Fine Arts Faculty. *International Journal of Education in Mathematics, Science, and Technology (IJEMST), 11(*1), 115-132. https://doi.org/10.46328/ijemst.2931

Turan, İ., & Bay, G. D. (2023). Sosyal Bilgiler Öğretmen Adaylarının 21. Yüzyıl Becerileri Öz-yeterlik Algılarının İncelenmesi (Doğu Karadeniz Örneği). *Turkish Studies-Educational Sciences*, *18*(3).

Ünal, E. (2013). *Öğretmen adaylarının teknoloji entegrasyonu öz-yeterlik algıları ve teknolojik pedagojik içerik bilgisi yeterlikleri arasındaki ilişkinin incelenmesi* (Master's thesis, Ankara Universitesi (Turkey)).

Ünlü, İ., Kaşkaya, A., & Coşkun, M. K. (2017). Sosyal bilgiler öğretmen adaylarının teknolojik pedagojik alan bilgisi yeterliliklerinin çeşitli değişkenlere göre incelenmesi. *Erzincan Üniversitesi Eğitim Fakültesi Dergisi*, *19*(1), 214-228.

Yıldız, E., & Seferoğlu, S. S. (2020). Uzaktan eğitim öğrencilerinin çevrim içi teknolojilere yönelik öz yeterlik algılarının incelenmesi. *Manisa Celal Bayar Üniversitesi Sosyal Bilimler Dergisi*, *18*(1), 33-46.

www.istes.org

www.ijemst.net   www.ijres.net   www.ijtes.net

www.ijte.net   www.ijonse.net   www.ijonest.net   www.ijonses.net

International Conference on Studies in Engineering, Science, and Technology

istesoffice   istesoffice   istesoffice

www.icsest.net